HIGH VOLTAGE LABORATORY TECHNIQUE

TO OUR
FORMER COLLEAGUES
IN THE METROPOLITAN-VICKERS
HIGH VOLTAGE RESEARCH LABORATORY

HIGH VOLTAGE LABORATORY TECHNIQUE

J. D. CRAGGS
AND
J. M. MEEK

LONDON
BUTTERWORTHS SCIENTIFIC PUBLICATIONS
1954

BUTTERWORTHS PUBLICATIONS LTD.
88 KINGSWAY, LONDON, W.C.2

AFRICA : BUTTERWORTH & CO. (AFRICA) LTD.
DURBAN: GOODRICKE'S BUILDINGS, MASONIC GROVE

AUSTRALIA : BUTTERWORTH & CO. (AUSTRALIA) LTD.
SYDNEY: 8 O'CONNELL STREET
MELBOURNE: 430 BOURKE STREET
BRISBANE: 240 QUEEN STREET

CANADA : BUTTERWORTH & CO. (CANADA) LTD.
TORONTO: 1367 DANFORTH AVENUE

NEW ZEALAND : BUTTERWORTH & CO. (AUSTRALIA) LTD.
WELLINGTON: 49/51 BALLANCE STREET
AUCKLAND: 35 HIGH STREET

ALLAMA IQBAL LIBRARY
14019

621.314
C843H

T01
RG1
S782

CHECKED

JAMMU & KASHMIR UNIVERSITY
LIBRARY
No 14,019
Dt. 20. 12. 55.
SRINAGAR

Set in Monotype Baskerville type

Printed in Great Britain by R. J. ACFORD LTD., CHICHESTER

PREFACE

THE LACK of a book, in English, on high-voltage techniques has been apparent to us for some time, particularly for research workers beginning to use high-voltage equipment. We have usually supplied our research students in this laboratory with references to the original literature or to the books in German on the subject, notably that by Bouwers. But, with the increasing use of high voltages by electrical engineers and physicists in industrial, university and Government laboratories, we felt that a book dealing with the appropriate techniques would be of value.

Our own experience in this field is restricted to research laboratory studies, and we have therefore limited the scope of the book mainly to the techniques used in such work. We have not dealt with the many technical problems of electric power generation and transmission at high voltages, or with the high-voltage testing of electrical equipment. Further, in order to keep the book to a reasonable length, it has also been necessary to omit detailed consideration of high-voltage insulation problems, since it would then have been necessary to include several chapters on the electrical break-down of vacua, gases, liquids and solids, and on break-down over surfaces. Some of this material is contained in our book on " Electrical Breakdown of Gases " (Oxford University Press) and in the book by S. Whitehead on " Dielectric Breakdown of Solids " (Oxford University Press).

Most of the work described in this book has already been published. We have emphasized the more recent methods, especially those which, we feel, deserve further use. In general, the experimental techniques used by various workers in the solution of any given problem all differ to a greater or lesser degree and we are therefore confident that it is unlikely for any given method, as described in this book, to be used without some modification. This is desirable since techniques, from their nature, should constantly be developed and improved and can rarely be transferred without alteration from one problem to another.

We have each spent over ten years in the High Voltage Laboratory in the Research Department of Metropolitan-Vickers in Manchester. We remember with pleasure the congenial and stimulating atmosphere in which we worked, initially under the direction of Dr. T. E. Allibone, F.R.S., and latterly under Mr. F. R. Perry, and we wish to thank our many former colleagues there for the great benefits we gained from being in association with them.

We acknowledge the help that we have derived from our study of the books by Bouwers, Marx, Roth and Strigel. We are also grateful to

Mr. J. Durnford for his useful advice in the preparation of Chapter 5. Dr. L. L. Green and Dr. R. Turnock kindly read and commented on the manuscript of Chapters 1 and 10, respectively.

We wish to thank the following individuals and organizations for sending original photographs: Dr. H. Böcker, Dr. F. M. Defandorf, Dr. B. Gänger, Ferranti Limited, Metropolitan-Vickers Electrical Company Limited, Philips Electrical Limited.

Finally, we express our appreciation to the staff of Butterworths Scientific Publications for their valuable cooperation, and particularly for the care that they have taken in the redrawing of the many diagrams included in this book.

J. D. Craggs
J. M. Meek

Department of Electrical Engineering,
University of Liverpool.
November, 1953.

CONTENTS

	PAGE
PREFACE	v
1. GENERATION OF HIGH-VOLTAGE DIRECT CURRENT	1
Valve rectifier circuits (power frequencies)	1
Valve rectifier circuits (high frequencies)	10
Valve rectifier circuits (with pulse generators)	15
Cascaded rectifier circuits using valves	19
Cascaded rectifier circuits using metal rectifiers	35
Electrostatic generators using belts	37
Electrostatic generators using blown streams of charged particles	53
Miscellaneous electrostatic generators	55
2. STABILIZATION OF HIGH-VOLTAGE DIRECT CURRENT SOURCES	60
General theory	60
Stabilizing circuits using thermionic valves	67
Stabilizing circuits for electron microscopes	72
Miscellaneous stabilizing systems	76
Voltage stabilization of Van de Graaff generators ..	78
3. GENERATION OF HIGH-VOLTAGE ALTERNATING CURRENT ..	89
Cascaded transformers	89
Resonance transformers	93
High frequency transformers	101
Tesla coils	104
4. IMPULSE VOLTAGE GENERATION	111
Impulse voltage wave-shapes	111
Impulse generator circuits	112
Mathematical analysis of basic impulse generator circuits	117
Factors influencing the design of impulse generators ..	131
The general construction of impulse generators	133
Impulse generator spark gaps	139
The synchronization of the operation of impulse generators and oscillographs	144
5. GENERATION OF HIGH-CURRENT IMPULSES	152
Theoretical considerations of the design of resistance shunts for the measurement of high-current impulses ..	156
Details of typical resistance shunts for the measurement of high-current impulses	164

5. GENERATION OF HIGH-CURRENT IMPULSES—*contd.* PAGE
Measurement of high currents by magnetic links 166
The operation in sequence of high-voltage and high-current impulse generators 168

6. GENERATION OF SQUARE PULSES AT HIGH VOLTAGES .. 175
Pulse generators using pulse-forming networks 175
Rotating spark gaps 177
Triggered spark gaps operating in air 179
Sealed triggered spark gaps 192
Mercury and hydrogen thyratrons 202
Hard-valve pulse generators 205
Magnetic switching devices 207

7. MEASUREMENT OF HIGH DIRECT AND ALTERNATING VOLTAGES 211
Electrostatic voltmeters 211
Sphere gaps 224
Uniform field spark gaps 233
Rod gaps 236
Series resistance voltmeters 237
Series capacitance voltmeters 237
Series inductance voltmeters 241
Potential dividers 241
Voltage transformers 241
Generating voltmeters 241
Electronic voltmeters 250
Fixing a voltage scale by nuclear reactions 253

8. MEASUREMENT OF HIGH IMPULSE VOLTAGES 264
Sphere gaps 264
Rod gaps 283
Oscillographic measurements 286
The klydonograph or surge recorder 287

9. POTENTIAL DIVIDERS FOR HIGH VOLTAGE MEASUREMENT: D.C., A.C., AND IMPULSES 293
D.C. potential dividers 293
A.C. potential dividers 296
Potential dividers for impulse work: Burch's treatment .. 300
Potential dividers for impulse work: later investigations .. 306

10. HIGH-SPEED OSCILLOGRAPHIC TECHNIQUES 326
Recurrent surge oscillographs 326
High-speed sealed-off oscillographs 335
High-speed continuously evacuated oscillographs .. 346

PAGE

10. HIGH-SPEED OSCILLOGRAPHIC TECHNIQUES—*contd.*
Miscellaneous techniques for the recording of very short transients or ultra-high-frequency oscillations .. 354
The photography of cathode-ray oscillograph screen traces 365

11. MISCELLANEOUS HIGH-VOLTAGE APPARATUS 371
Resistors 371
Capacitors 386
Thermionic rectifiers 387
Corona rectifiers 390
Mechanical rectifiers 391
Surge protection devices 392

INDEX OF AUTHORS 397

INDEX OF SUBJECTS 402

1

GENERATION OF HIGH-VOLTAGE DIRECT CURRENT

VALVE RECTIFIER CIRCUITS (POWER FREQUENCIES)

THE theoretical treatment of simple rectifier circuits which are often used to provide high-voltage d.c. (up to say 100 kV) has been the subject of many publications in which the methods vary in complexity, due to the different assumptions made. For the present, the consideration of such matters as ripple and valve loadings will be considered and the subject of the accurate stabilization of the d.c. output voltage from rectifier sets will be considered elsewhere.

HARNWELL and LIVINGOOD[1] give an excellent elementary account of the simple half-wave and full-wave rectifier circuits which suffices for many practical cases. The ripple ΔV in the output capacitor voltage during Δt (the periodic time of the supply voltage) is given by equating the charge flow in and out of the reservoir capacitor. So if I is the mean output current then $I\Delta t = C\Delta V$ or $\frac{\Delta V}{V} = I\frac{\Delta t}{VC}$. For a 50 μA load current at 20 kV (60 c/s, 0·0042 μF capacitor) the ripple is not greater than 1 per cent. If each condenser in the full-wave circuit has the above value, then the output voltage at 50 μA for the same ripple will clearly be 40 kV.

The theory of rectifier circuits is discussed in many standard technical texts and also in papers. Recent theoretical work by SCHADE[2] includes a study of the performance of half-wave, full-wave and voltage-doubler circuits. BELL[3] has discussed the theory of rectifier circuits for high voltages, with special references to X-ray therapy and to cases where the resistance of the h.t. transformer secondary winding is appreciable. Amongst the more extensive treatments is that of MITCHELL[4] whose analysis will be followed here in some detail.

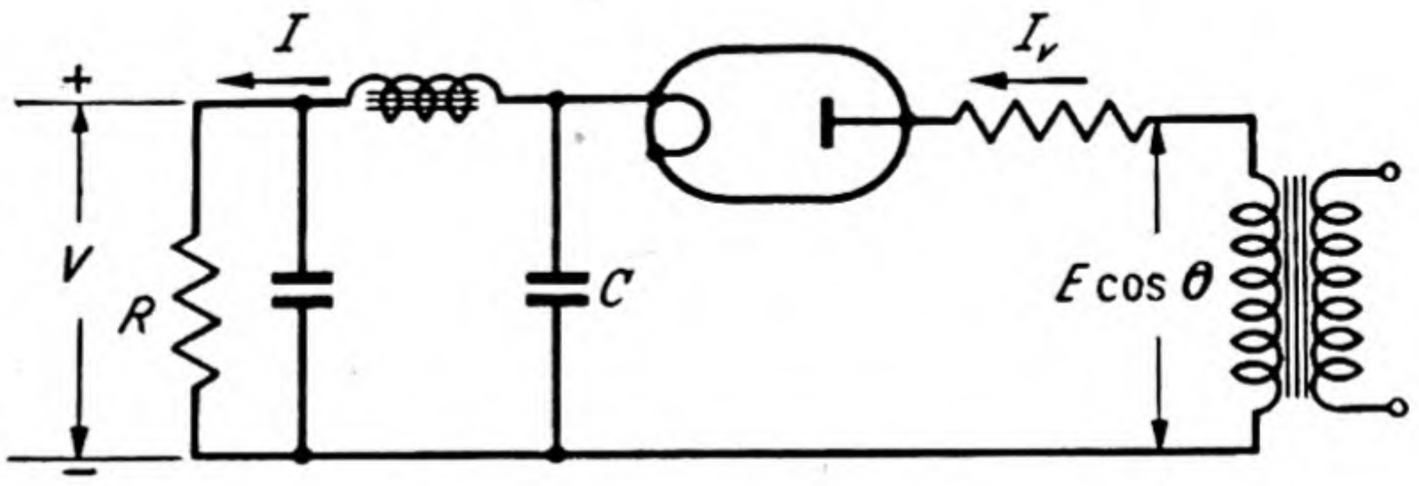

Figure 1. Single-phase half-wave circuit. (Mitchell[4], by courtesy, *Wireless Engr.*).

It is assumed that the input voltage is sinusoidal, that the transformer leakage reactance is negligible and that the ripple is small ; also, the rectifier characteristic is taken to be linear, an approximation

which is rendered legitimate in many cases because of the insertion of a current-limiting resistance in the circuit, and which is normal practice. Finally the absence of valve saturation and the linear wave-form of the reservoir capacitance voltage during the charge period are also assumed. The cases shown in *Figures 1, 2, 3, 4*, namely single-phase half-wave, bi-phase half-wave and single-phase full-wave

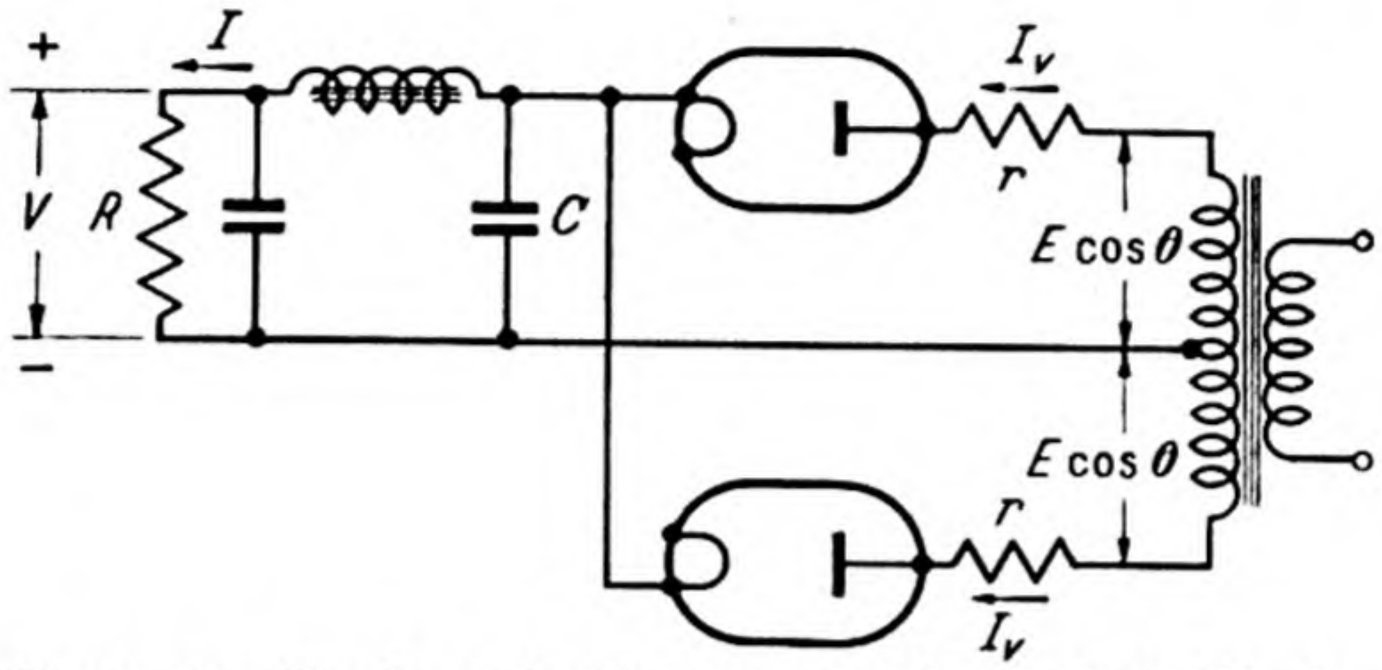

Figure 2. Bi-phase half-wave circuit (Mitchell[4], by courtesy, *Wireless Engr.*).

circuits respectively are treated. The symbols used in the figures are self-explanatory, but the treatment involves many quantities listed by Mitchell as follows.

E = peak transformer secondary voltage per phase
V = mean D.C. output voltage
η = voltage conversion ratio, V/E
δV = amplitude of ripple voltage (unsmoothed)
$K = \frac{\delta V}{V}$
I = load current
i, I_v and $\hat{\imath}$ = instantaneous, mean and peak valve currents respectively
R = load resistance
R_a = valve a.c. resistance
r = total charging resistance, including the valve resistances of which there will be two in series in the single-phase full-wave circuit, the transformer losses and any added resistances
ϕ_1 and ϕ_2 = angles between (*a*) commencement of current flow and peak input voltage and (*b*) peak input voltage and point of current cut-off (*see Figure 4a*).
$\phi = \frac{\phi_1 + \phi_2}{2}$ = half angle during which current flows through each valve, per charging cycle
t_D = discharge period of reservoir capacitor, whose capacitance is C and whose reactance is X at the supply frequency
D = anode dissipation
I_c = condenser ripple current (r.m.s.)
and i_c = instantaneous condenser current.

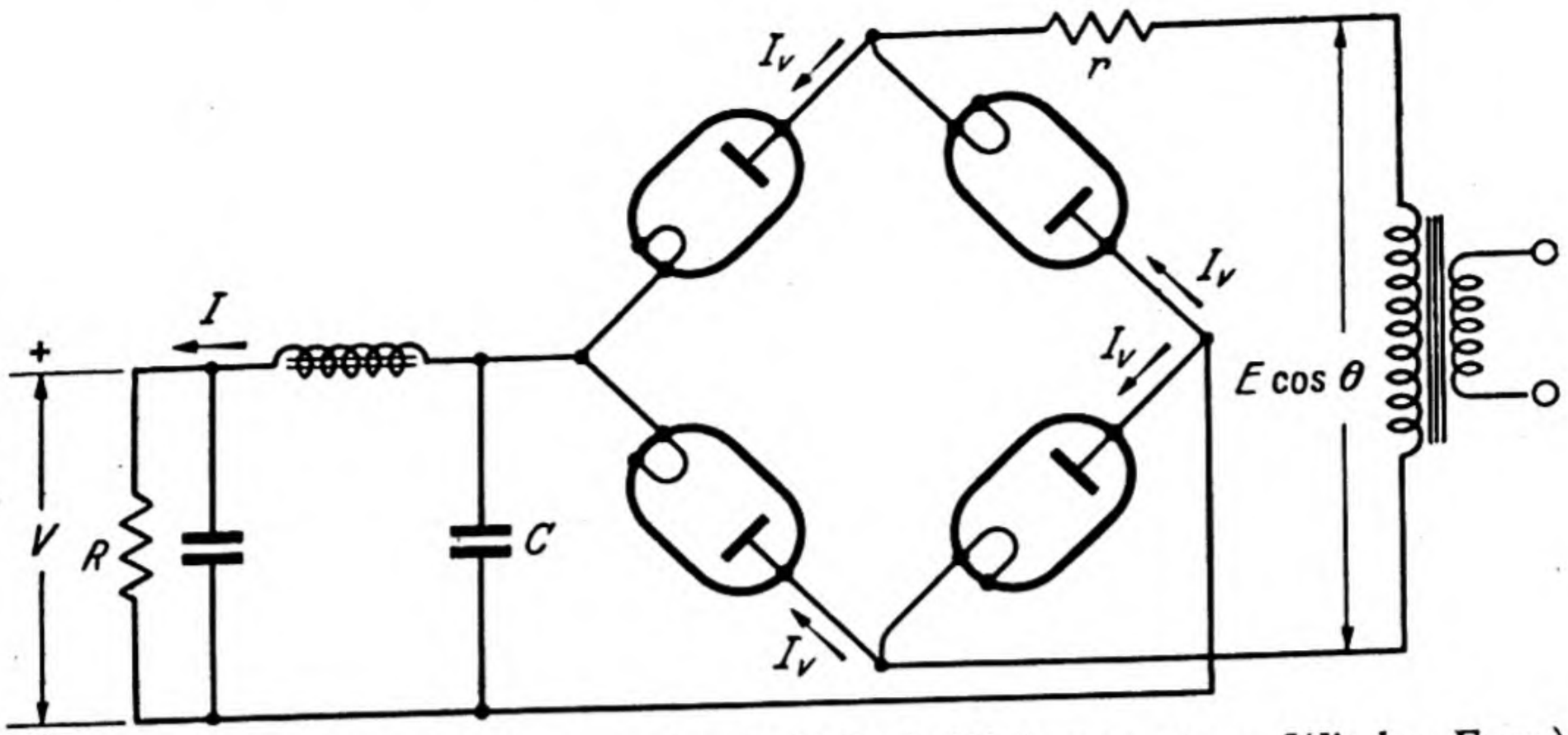

Figure 3. Single-phase full-wave circuit (Mitchell[4], by courtesy, *Wireless Engr.*).

The relevant wave-forms are shown in *Figure 4 a* and *b*. We shall deal now with a linear charging wave for which Mitchell shows that:—

$$\cos \phi_1 = n\ (1 - K)$$
$$\cos \phi_2 = n\ (1 + K)$$

so giving ϕ_1 and ϕ_2 if n and K are known.

$$I_v = \frac{E}{2\pi r}\left[2 \sin \phi \cos \frac{\phi_1 - \phi_2}{2} - (\cos \phi_1 + \cos \phi_2)\, \phi \right]$$

Also, $I = V/R = \frac{nE}{R}$ and $V = \frac{E \cos \phi_1 + E \cos \phi_2}{2}$

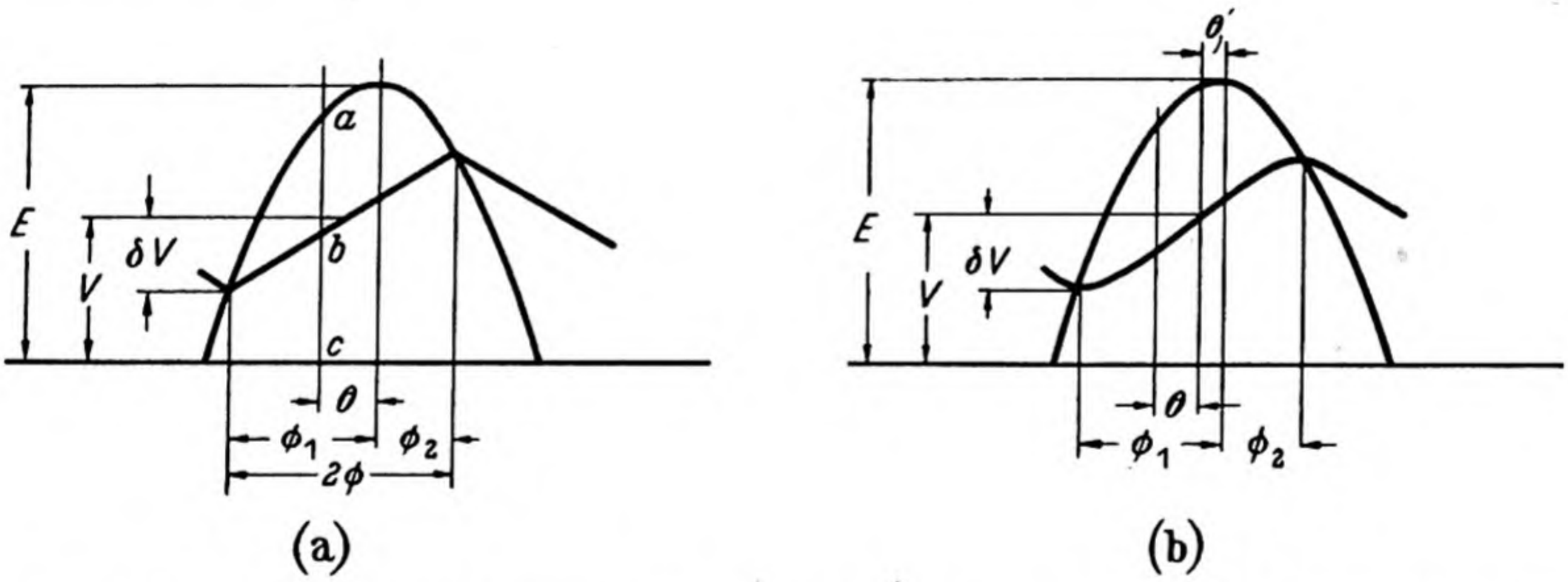

Figure 4. (a) Linear charge; (b) sinusoidal charge (Mitchell[4], by courtesy, *Wireless Engr.*).

In the case of the single-phase half-wave system, $I_v = V/R$ (the load current) but in the bi-phase half-wave and single-phase full-wave circuits the load current is $2\, I_v$

$$\text{Then, since } 2\, \delta V = \frac{I t_D}{C}, \quad \frac{\delta V}{V} = \frac{I t_D}{2CV} = \pi f t_D X/R$$

The results are concisely expressed in Mitchell's curves shown in *Figures 5–11.* In *Figures 9–12 K* is converted to a percentage of r.m.s. ripple voltage relative to V, *i.e.* $K\ 100/\sqrt{2}$. The ripple frequency for the single-phase half-wave circuit is equal to the supply frequency,

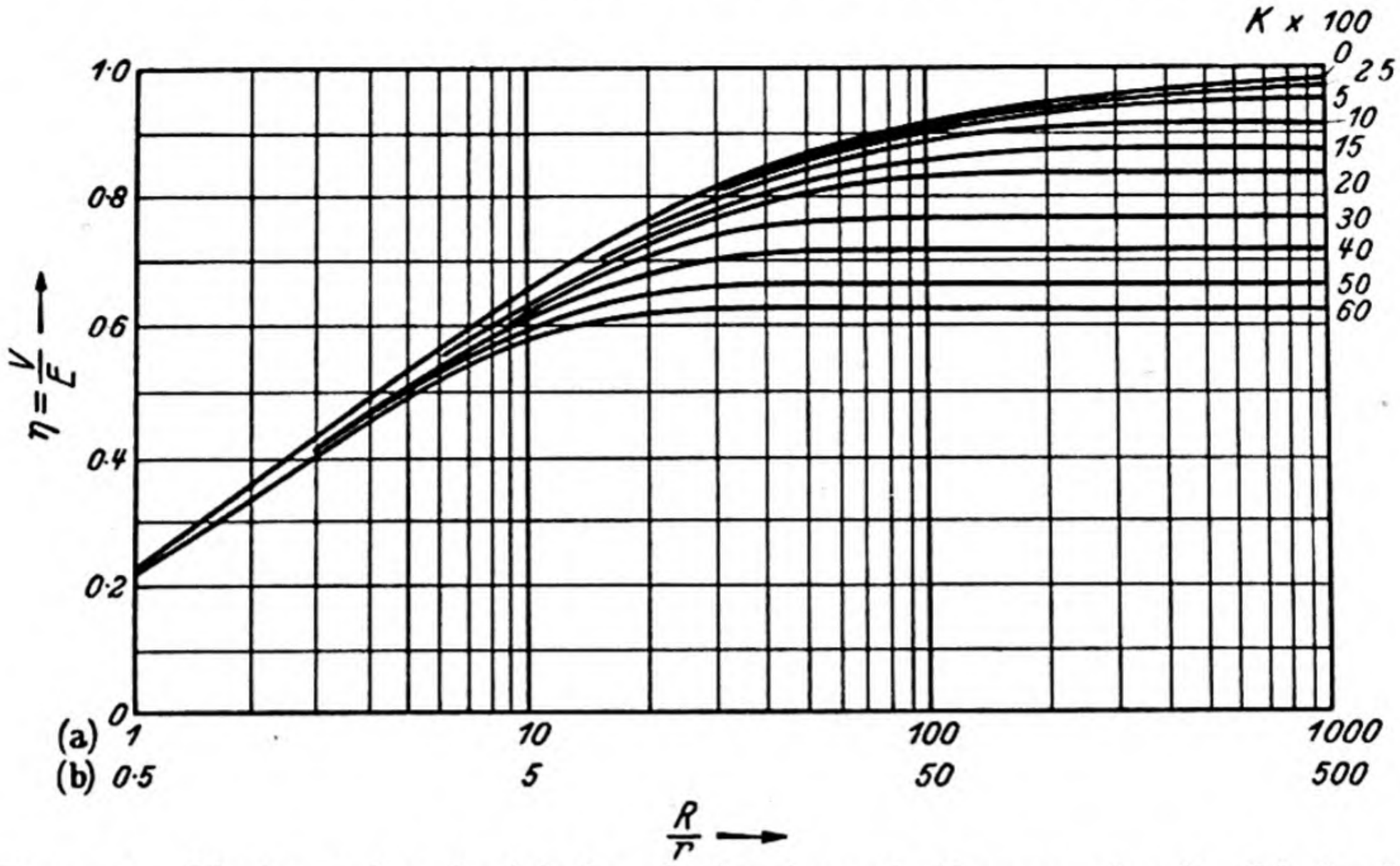

Figure 5. Horizontal scale (a) for single-phase half-wave circuit, (b) for bi-phase half-wave and single-phase full-wave circuits (Mitchell[4], by courtesy, *Wireless Engr.*).

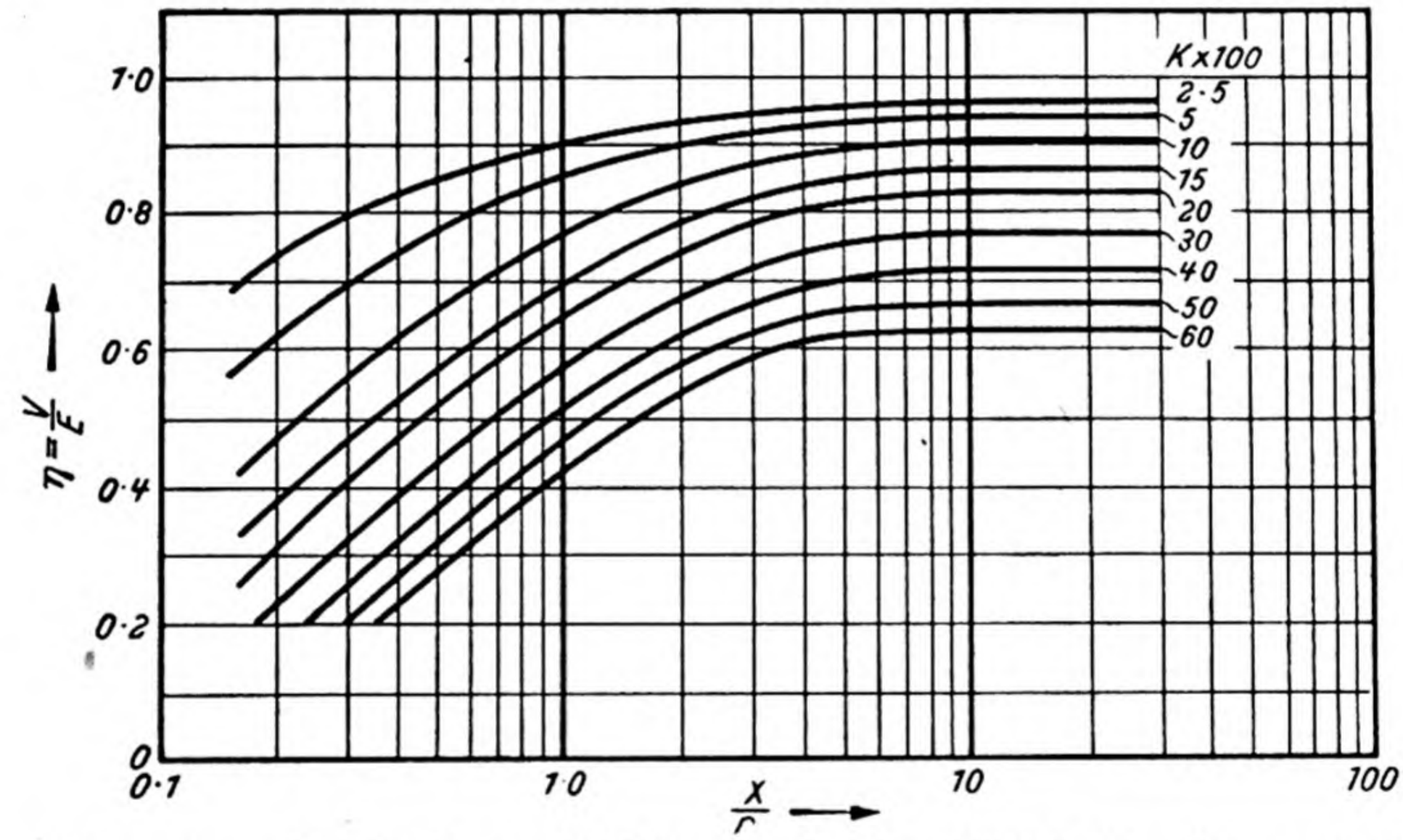

Figure 6. Single-phase half-wave circuit (Mitchell[4], by courtesy, *Wireless Engr.*).

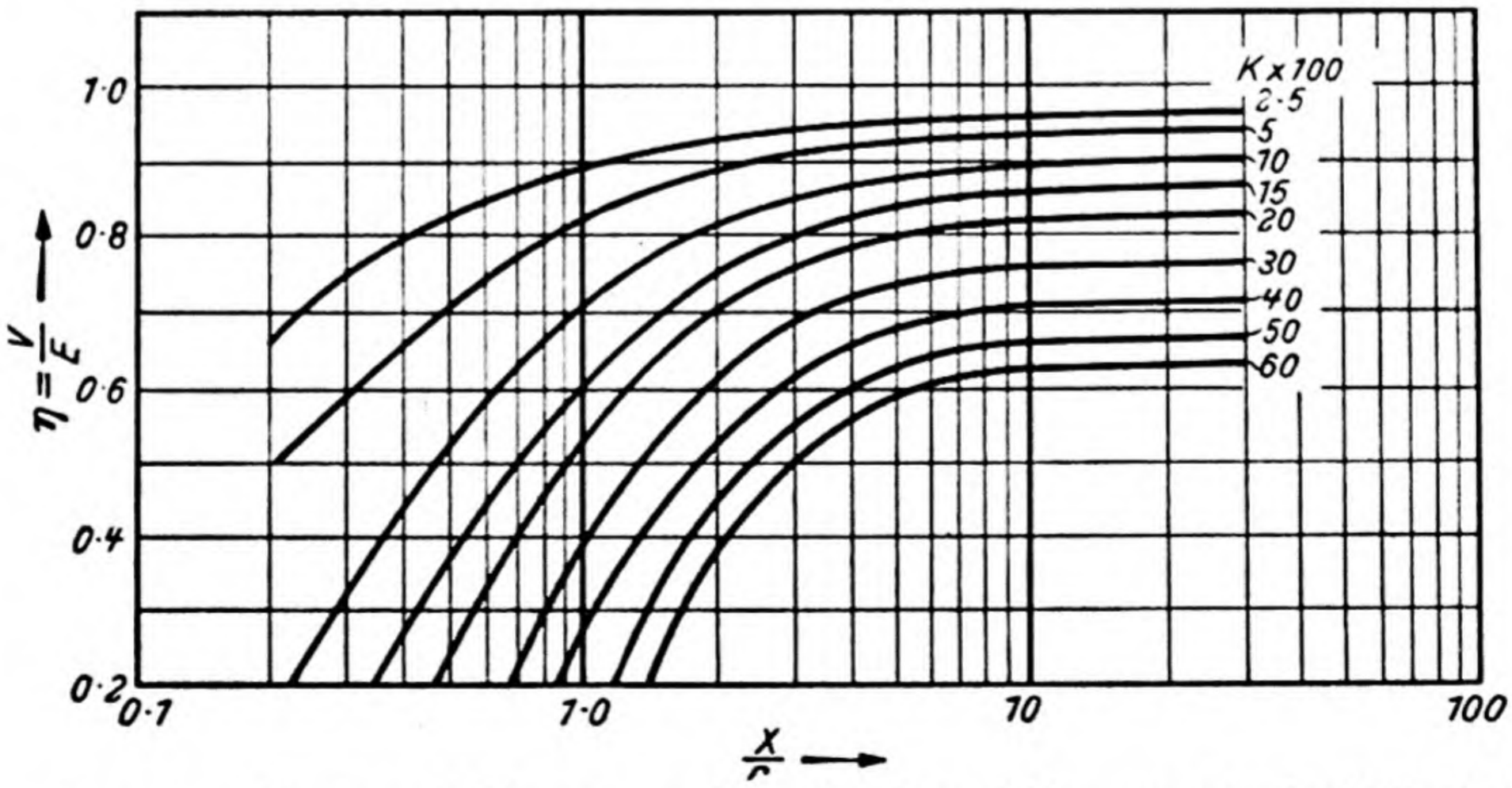

Figure 7. Bi-phase half-wave, and single-phase full-wave circuits (Mitchell[4], by courtesy, *Wireless Engr.*).

but in the other circuits is twice this value. *Figure 12* shows the relation between the peak charging current and other parameters.

Generally, values of the a.c. input, required d.c. output voltage, current and permissible ripple are known, and from these data the average current, peak valve current and transformer secondary current and reservoir capacitance must be found. The peak reverse voltages that the valves must withstand in the various circuits are given in *Table I*.

TABLE I

Circuit	*Reverse Peak Voltage*
Single-phase half-wave	$E+V$
Bi-phase half-wave	$E+V$
Single-phase full-wave	$V+(E-V)\ R_a/r$
Voltage-doubler circuit (see below)	$V+(E-\frac{V}{2})\ R_a/r$

The voltage-doubler circuit (*Figure 13*) is often valuable in practice since it enables a lower transformer secondary voltage to be used but the need for extra insulation on one of the filament heating transformers is apparent. The circuit works, for equal reservoir capacitors, as two single-phase half-wave circuits in series, as the imaginary

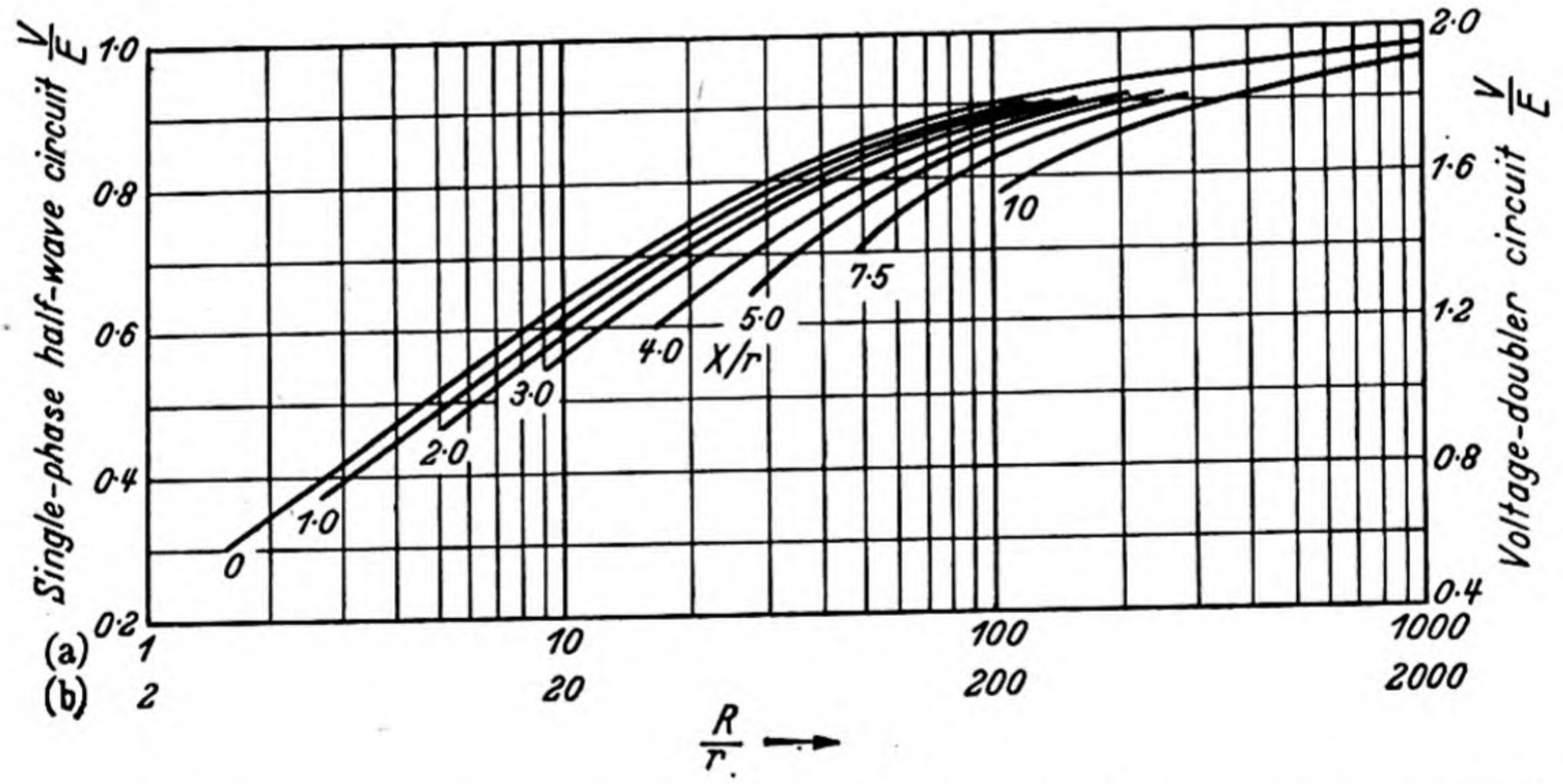

Figure 8. Horizontal scale (a) for single-phase half-wave circuit, (b) for voltage-doubler circuit (Mitchell[4], by courtesy, *Wireless Engr.*).

connection between the mid-points of R and the reservoir capacitors makes clear. The characteristics of the voltage-doubler can be determined from *Figures 8* and *9*, using $R/2$ there instead of R. The output voltage is then twice that for one section. The ripple, whose frequency is twice the supply frequency, is less than that for each section δV_s and is found to be

$$\delta V = \delta V_s \left(1 - \frac{\phi}{\pi - \phi}\right).$$

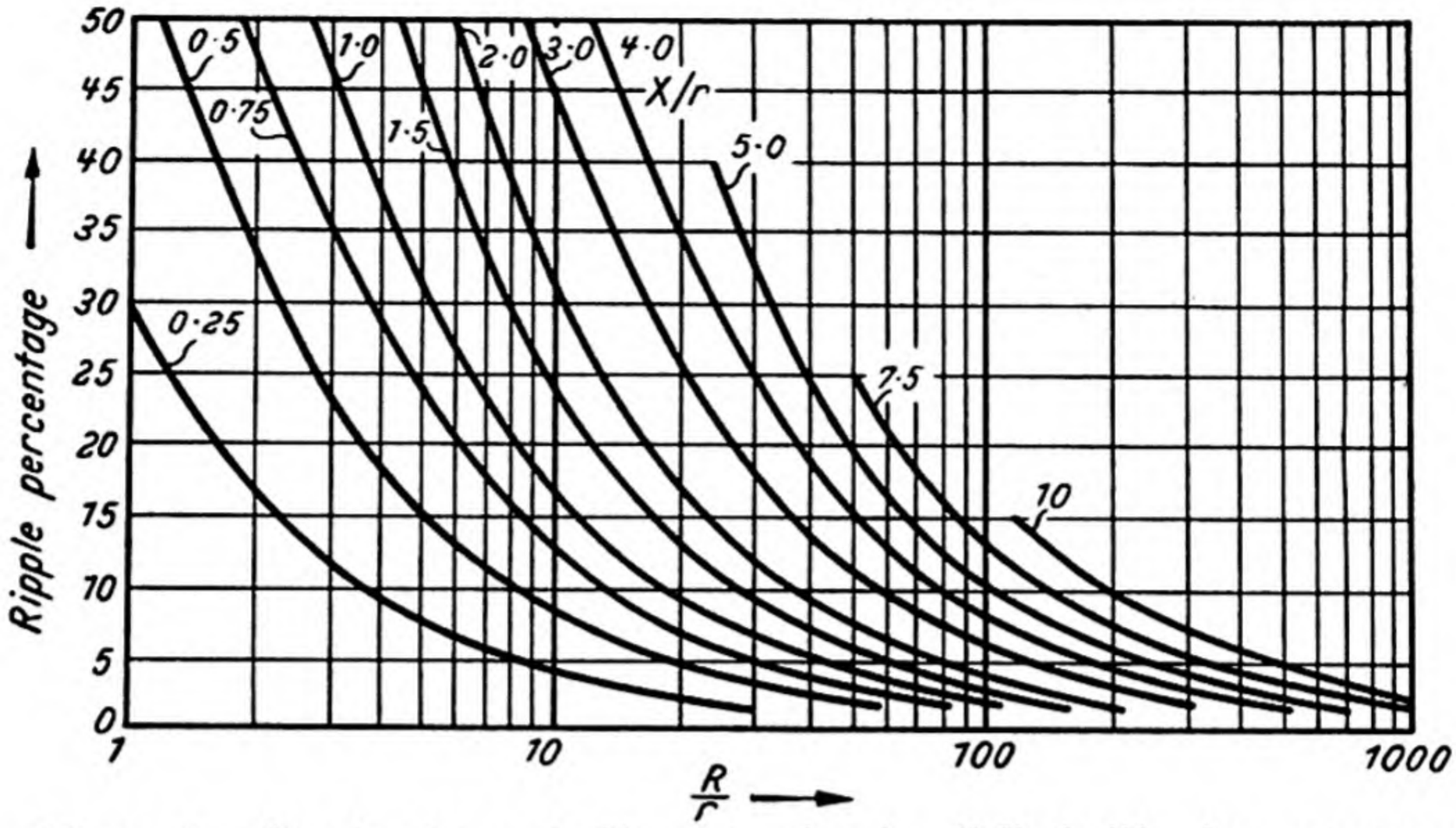

Figure 9. Single-phase half-wave circuit (Mitchell[4], by courtesy, *Wireless Engr.*).

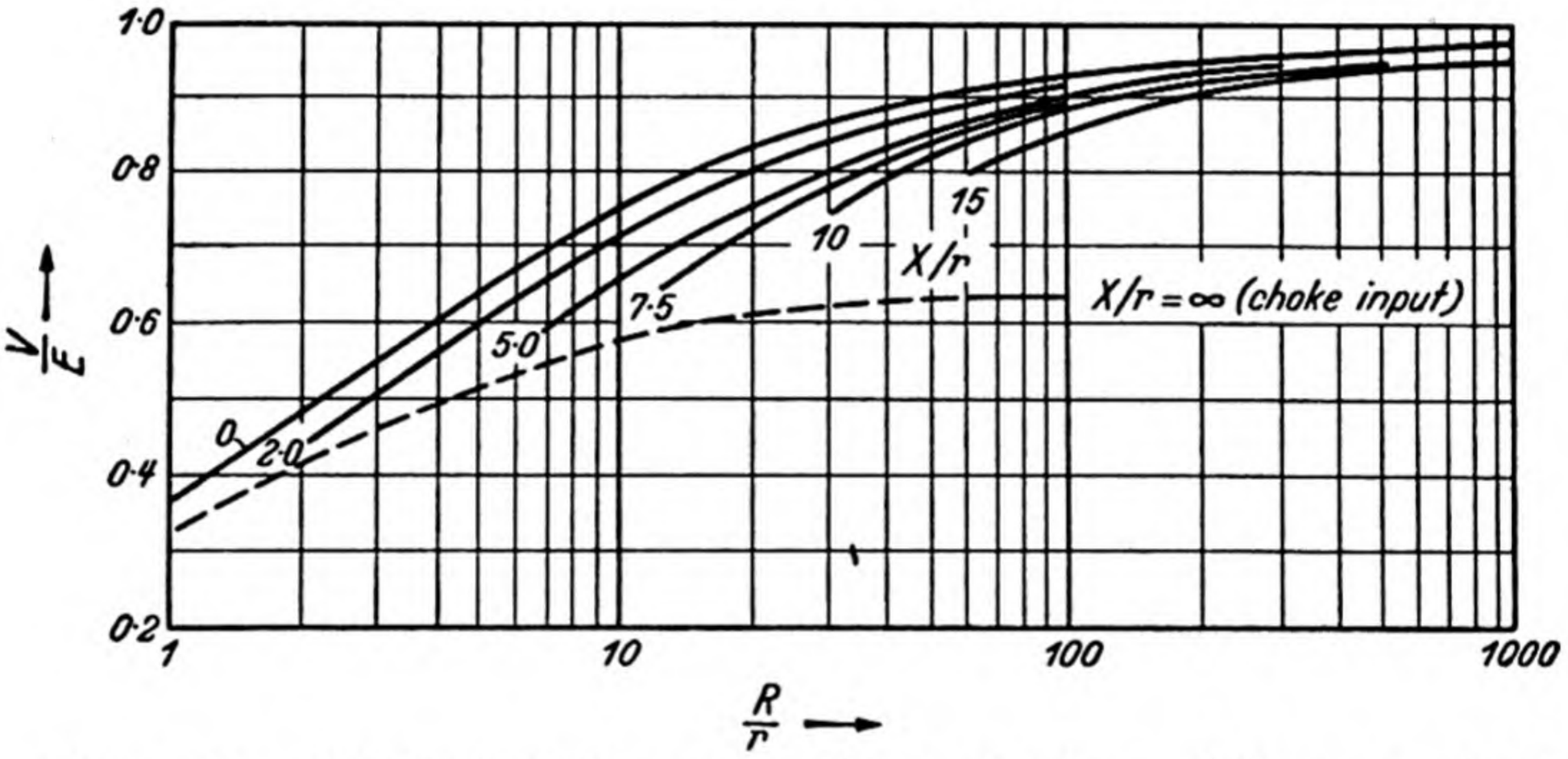

Figure 10. Bi-phase half-wave and single-phase full-wave circuits (Mitchell[4], by courtesy, *Wireless Engr.*).

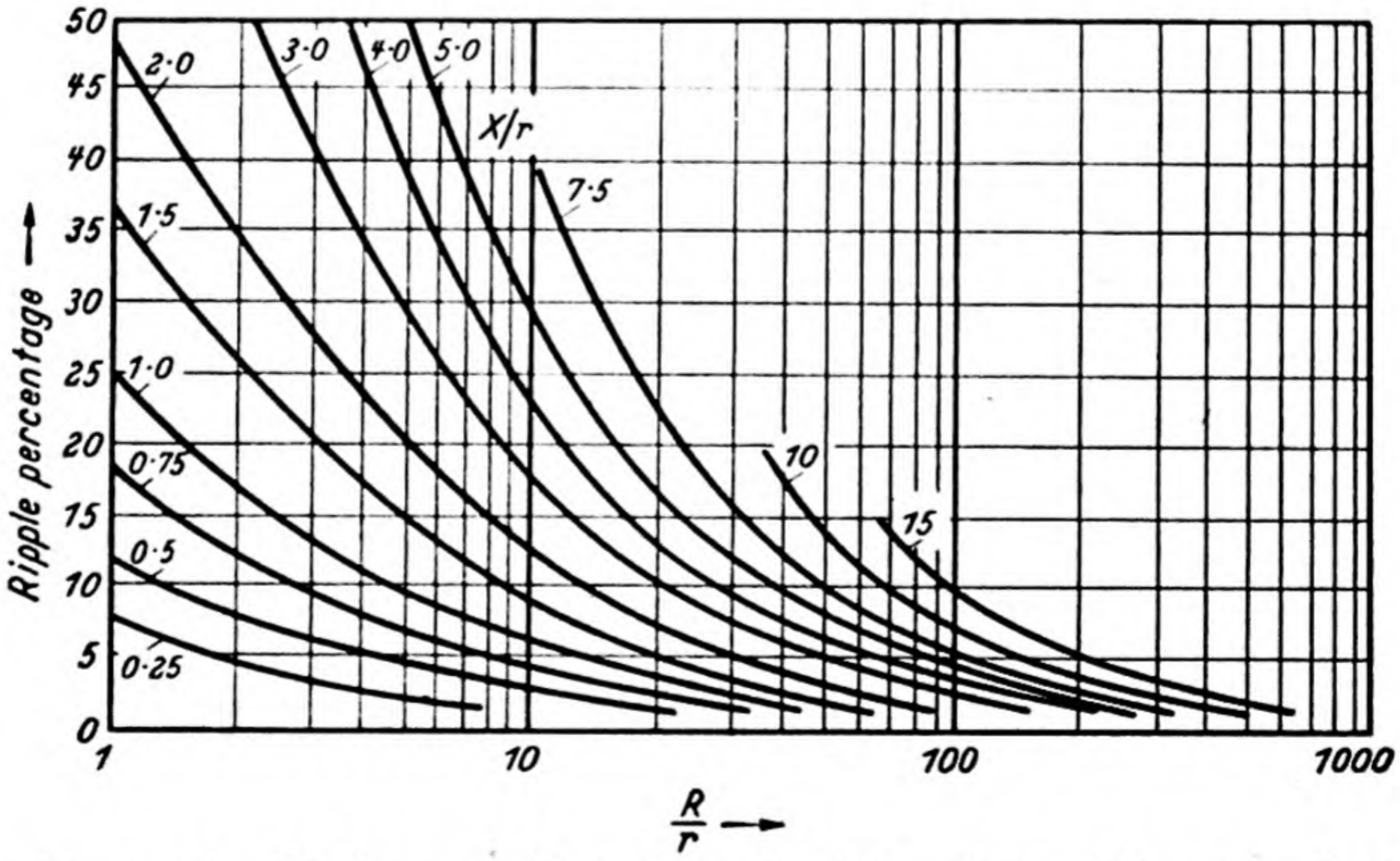

Figure 11. Bi-phase half-wave and single-phase full-wave circuits (Mitchell[4], by courtesy, *Wireless Engr.*).

Now δV_s, V and ϕ can be found as before, knowing η and K provided that R, r and C are known. Thus δV can be found and is plotted in *Figure 14*. Values of $\hat{\imath}/I_v$ may be determined by considering one half-wave section only and by the use of *Figures 8*, *9* and *12*, using $R/2$ instead of R.

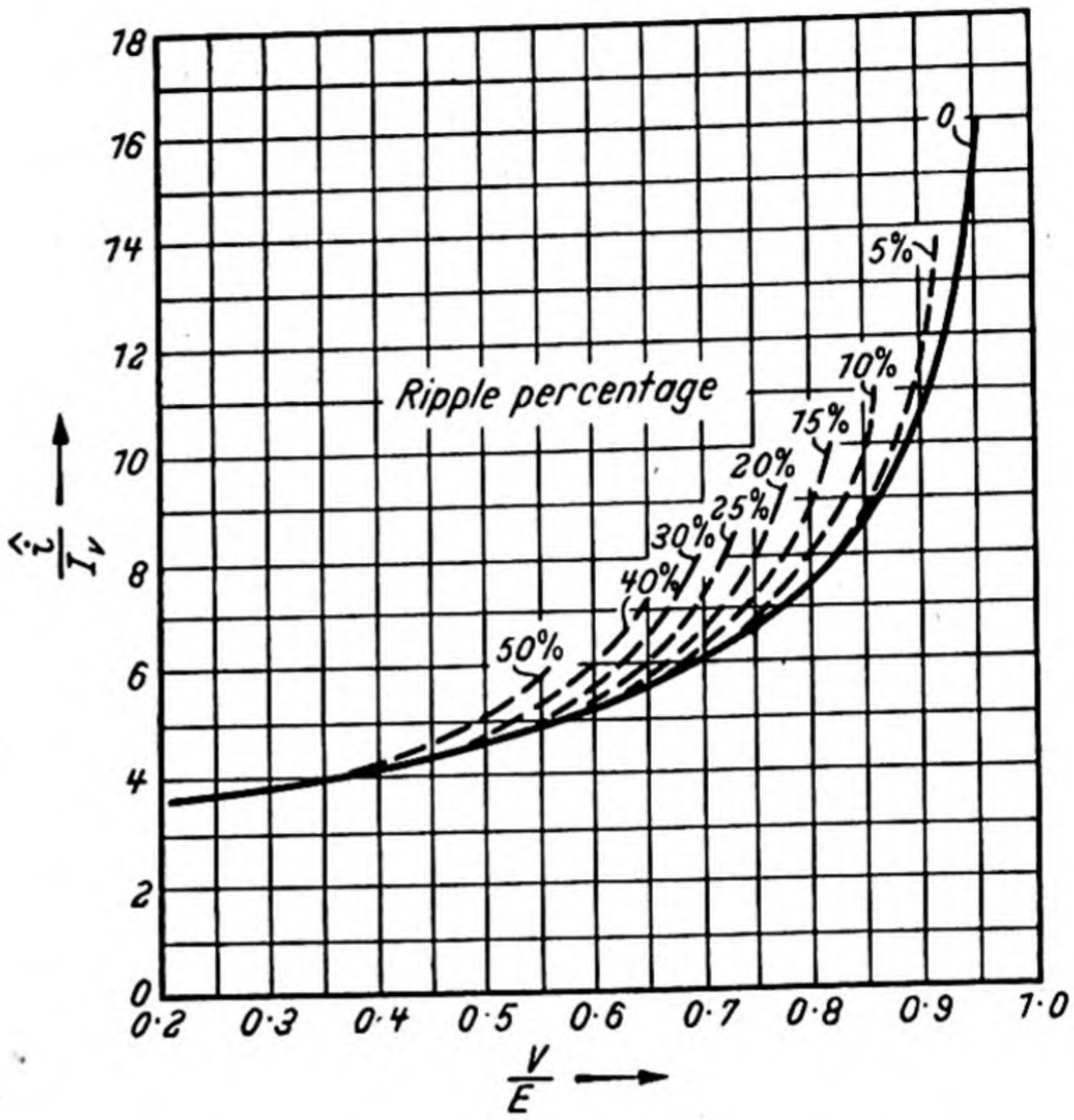

Figure 12. Relation between peak charging current and other parameters (Mitchell[4], by courtesy, *Wireless Engr.*).

The rectifier anode dissipation, assuming a half-sine wave of current, at instant θ is $i^2 R_a = \hat{\imath}^2 R_a \cos^2 [\theta\pi/2\phi]$

$$\text{since } i = \hat{\imath} \cos \left[\theta \cdot \frac{\pi}{2\phi}\right].$$

The dissipation D for a whole cycle of operation is then

$$D = \hat{\imath}^2 \frac{R_a}{\pi} \int_0^{\phi} \cos^2 \left[\theta \cdot \frac{\pi}{2\phi}\right] d\theta.$$

Finally $D = \hat{\imath}^2 Ra\phi/2\pi$.

Now as Mitchell shows, $I_v = \hat{\imath}\, 2\phi/\pi^2$ or $\hat{\imath}/I_v = 1{\cdot}57\,\frac{\pi}{\phi}$ and therefore $D = 1{\cdot}24\ I_v^2\ R_a\pi/\phi$. F_D which equals $1{\cdot}24\,\pi/\phi$ is plotted against V/E in *Figure 15*.

The transformer secondary currents are:—

(*a*) for single-phase half-wave and bi-phase half-wave circuits:—

$$I_{\text{r.m.s.}} = I_v \sqrt{rF_D}$$

In the bi-phase circuit this is the current per leg of the transformer secondary, I_r being half the load current

(*b*) single-phase full-wave and voltage-doubler circuits:—

$$I_{\text{r.m.s.}} = I_v \sqrt{2F_D}$$

I_v is half the load current in the single-phase full-wave circuit but is equal to the total load current in the voltage-doubler circuit.

The condenser ripple currents (I_c) are as follows :—

Single-phase half-wave case: $I_c = I\sqrt{1{\cdot}23\pi/\phi - 1}$. Bi-phase half-wave and single-phase full-wave cases $I_c = I\sqrt{0{\cdot}62\pi/\phi - 1}$. For the voltage-doubler circuit I_c is found by taking one half section. In reiteration, ϕ is determined from R and r which are circuit constants and which can be used in *Figure 8* (single-phase half-wave case) knowing X/r, to give η which, in turn, is used in *Figure 5* to give K. ϕ is related simply to K and η as shown above.

TABLE II

Circuit		*Single-phase half-wave, input 750V*		*Bi-phase half-wave input 1,000V*			*Voltage doubler, input 700V*		
$r\ \Omega$		800	800	800	800	800	500	500	800
$R\ \Omega$		20,000	20,000	20,000	20,000	10,000	40,000	40,000	40,000
R/r		25	25	25	25	12·5	80	80	50
$C\mu F$		8	1	8	0·5	8	4	1	1
X/r		0·5	4	0·5	8	0·5	1·6	6·4	4
DC Output Volts	*Theoretical*	824	730	1,213	1,000	1,102	1,160	975	964
	Experimental	825	718	1,202	1,045	1,105	1,155	960	940
Percentage Ripple	*Theoretical*	3·8	29	1·4	22	2·5	2·8	11·5	10
	Experimental	3·3	27	1·4	22	2·3	3·4	12·2	11·6
$\hat{\imath}/I_v$	*Theoretical*	7·2	7·0	8·8	8·6	7·2	8·6	7·5	7·2
	Experimental	7·4	7·4	9·0	9·1	7·45	9·7	9·2	8·2

To demonstrate the accuracy of his treatment, Mitchell gives tabulated experimental and theoretical data, using V15 valves at a frequency of 50 c/s for practical examples, which show excellent agreement. A selection of the data is given in *Table II*.

Various rectifier valve arrangements for the production of high-voltage d.c. are discussed by ALLIBONE, BEETLESTONE and INNES[5]. The basic rectifier circuits are given for half-wave, voltage-doubler and certain special modifications of these, including the series arrangement of two voltage-doublers shown in *Figure 16* where the second h.t.

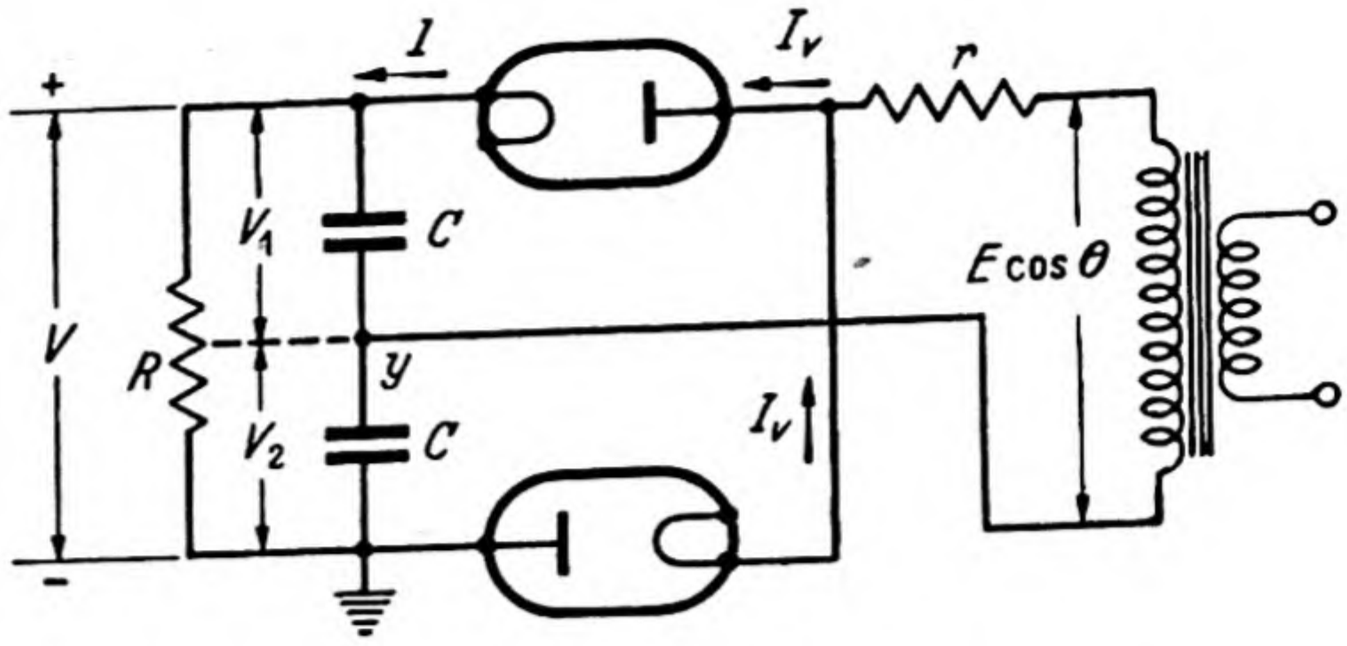

Figure 13. Voltage doubler circuit (Mitchell[4], by courtesy, *Wireless Engr.*).

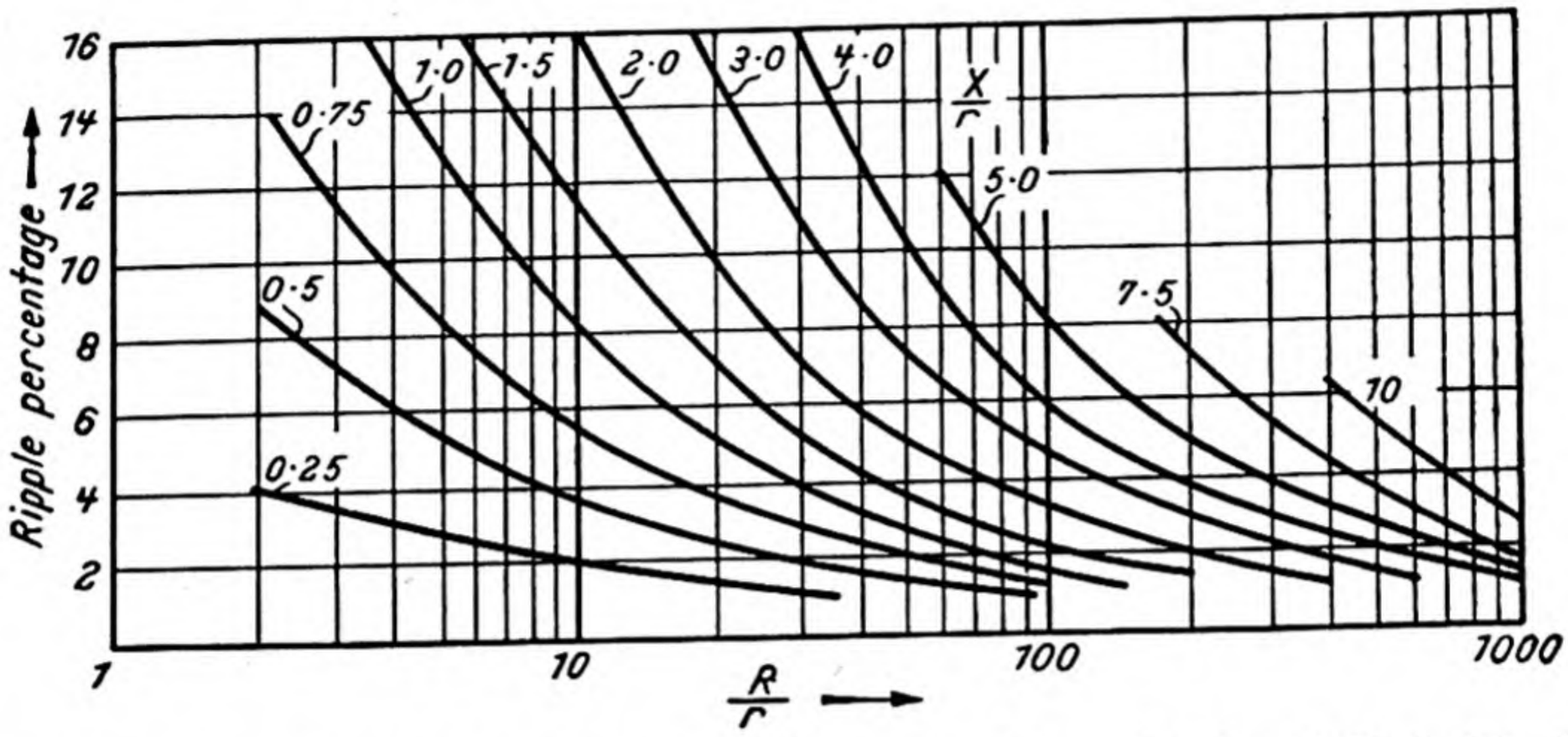

Figure 14. Characteristics of voltage doubler circuit (Mitchell[4], by courtesy, *Wireless Engr.*).

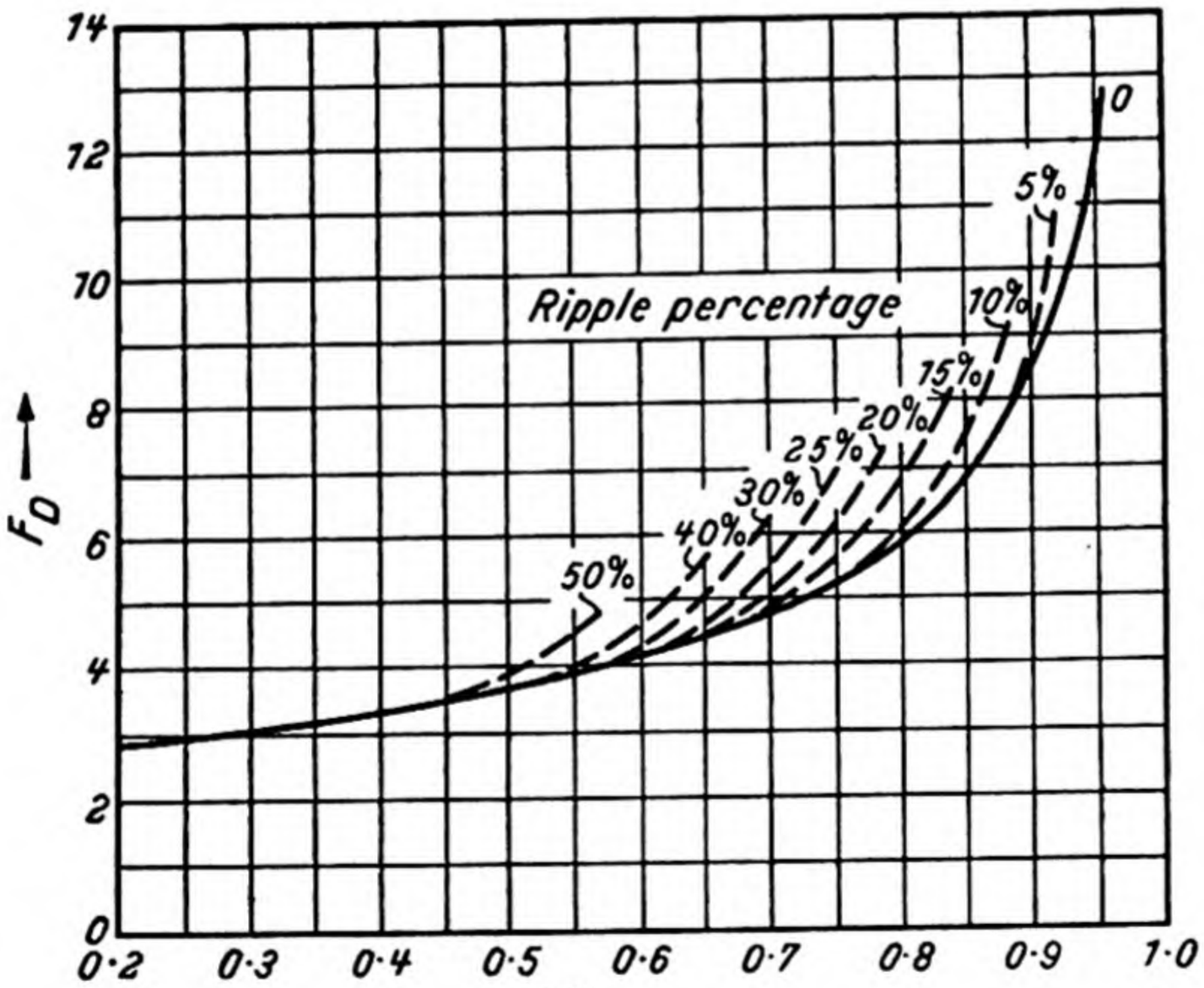

Figure 15. Characteristics of voltage doubler circuit (Mitchell[4], by courtesy, *Wireless Engr.*).

transformer V_2 is excited through a special isolating transformer. The rectifiers R_1 to R_4 are all in series and the potential distribution across them is uniform since C_1, C_2, C_3, C_4 are all equal. The valves may therefore be continuously evacuated in one column, and an arrangement of two valves, each of which may withstand 300 kV,

is used. Each valve envelope is of porcelain, 30 inches long. The anode–cathode geometry (*AC*) is very simple with the cathode recessed in a suitable electrode which gives electrostatic shielding and so

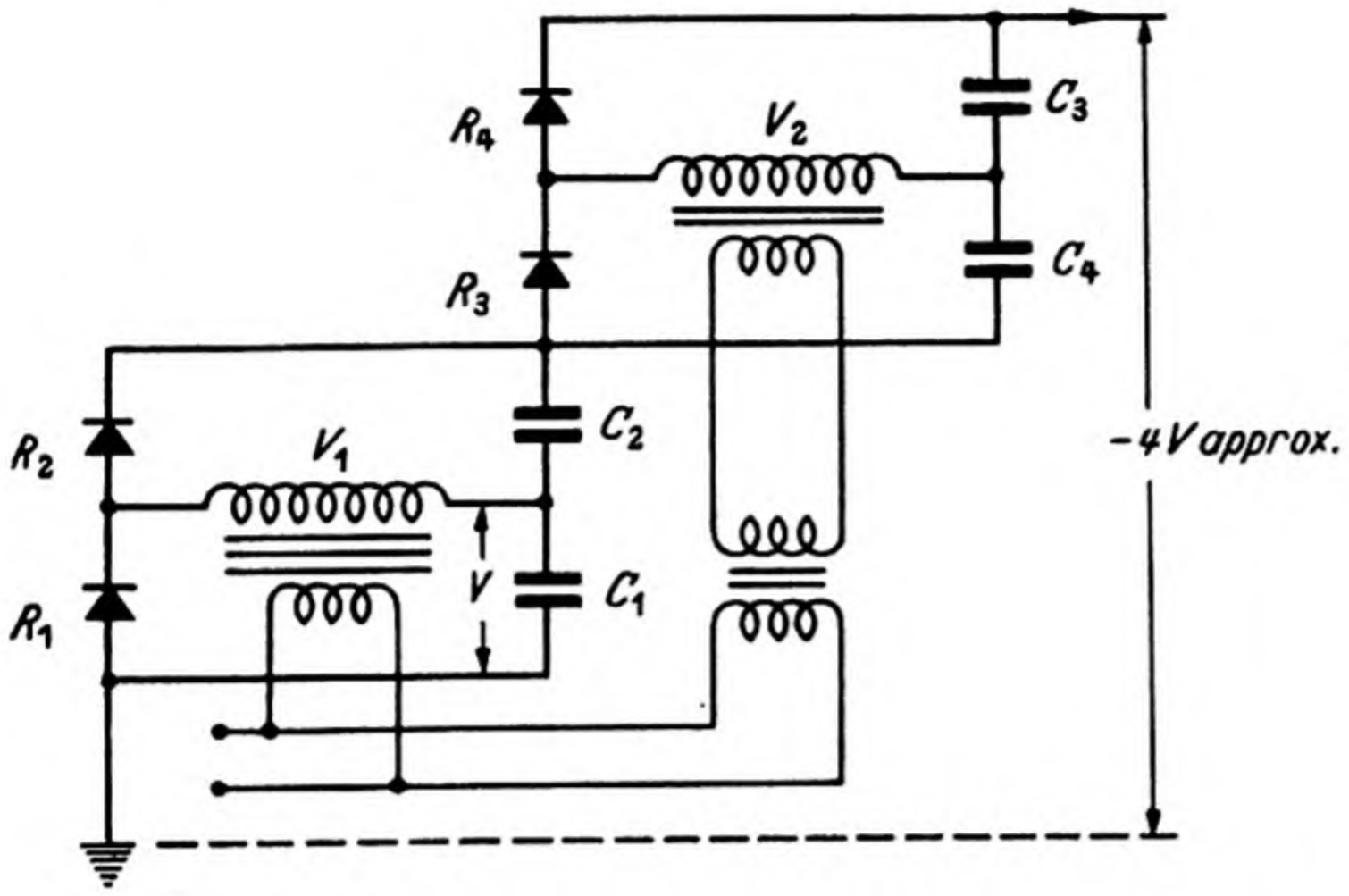

Figure 16. Voltage doubling circuits in series for very high voltages to ground (Allibone *et al*[5], by courtesy, *Brit. J. Radiol.*).

inhibits field emission from the cathode wires. The latter may be renewed through special side tubes without dismantling the whole stack.

VALVE RECTIFIER CIRCUITS (HIGH FREQUENCIES)

The technique used by Schade[2], *i.e.* the generation of high-voltage d.c. by the use of rectified h.f. currents generated with a suitable oscillator and h.f. transformer, has now been widely employed in compact h.t. units for electron microscopes, cathode-ray oscillographs and other electronic instruments. Thus HAINE, PAGE and GARFITT[6] have published details of an h.t. set of this type electronically stabilized for 25kV, 50kV, 75kV (all with 1mA maximum output current), and 100kV (0·4mA output). The circuits for the h.t. circuit, the oscillator and stabilizer are shown in *Figures 17* and *18*. Three oscillators supply power for the h.t. circuit, the h.t. rectifier valve filament and the electron gun filament in the microscope source. The respective frequencies are 30, 50 and 50 kc/s. The h.t. unit, a Greinacher voltage-doubler circuit, is contained in an oil-filled tank and stabilization is obtained by the use of negative feed-back from a high resistance potential-divider connected across the output circuit through a d.c. amplifier to the screen circuit of the oscillator valves using batteries (180V) as the standard voltage source (*see* Chapter 2).

Schade[7] points out that conventional rectifier sets, working at power frequencies, are apt to be bulky owing to the necessary size of the h.t. transformer and other components, even for voltages of a few kV. He therefore developed d.c. h.t. units in which the h.t. was generated by means of an oscillator and h.t. transformer and rectified, usually

with relatively small diodes in a cascaded arrangement if the value of the h.t. voltage rendered the latter necessary.

The above paper includes a study of h.f. oscillators and coupled circuits and it is shown there that a stable oscillation characteristic

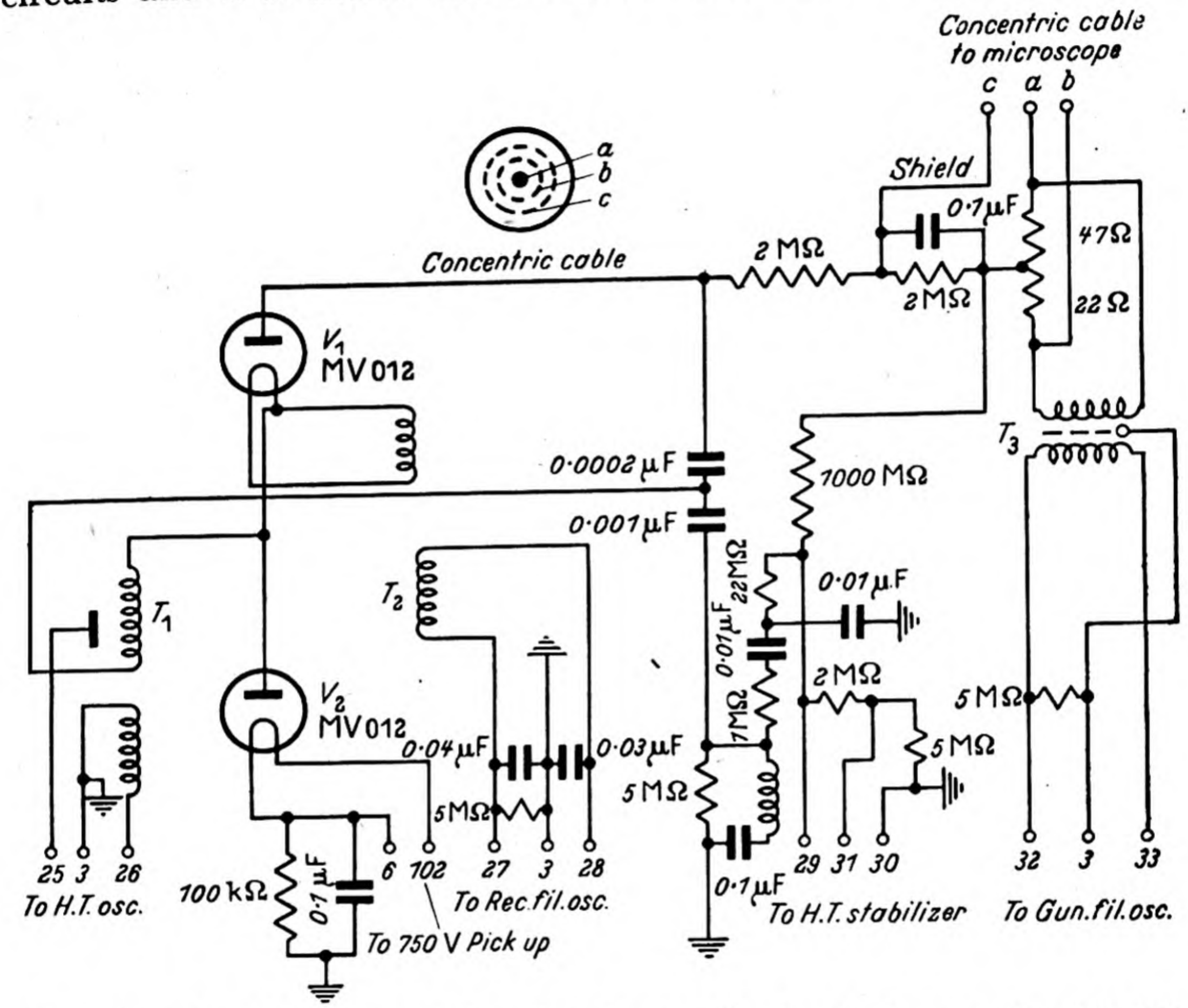

Figure 17. Circuit diagram of the oil tank assembly, in the h.t. set of a 100 kV electron microscope (Haine *et al*[6], by courtesy, *J. appl. Phys.*).

is obtained if the grid coil L_3 is coupled to L_2 the secondary coil, as shown in *Figure 19*. If the coils L_1 and L_3 are wound as for normal oscillators, ω_1 (*Figure 19*) is the resonance pulsatance but if L_1 or L_3 is reversed then ω_2 is the point of stable oscillation. The coupling factor K should[7] be $\sim 20K_c$ where the critical coupling factor K_c is $K_c = 1/\sqrt{Q_1 Q_2}$ and Q_1 and Q_2 are the Q values for the primary and secondary circuits; the latter values should thus be large in order to give high overcoupling. It is desirable that $Q_1 \geqslant 10$ and $Q_2 \geqslant 20$ with shunting respectively by the reflected plate load R_p and the equivalent rectifier load R_L. The no-load Q's will be higher perhaps by about a factor of 10, owing to circuit losses which may be ~ 10 per cent. per circuit.

$\omega L_1 \leqslant 0{\cdot}1R_p$ and $\omega L_2 \leqslant 0{\cdot}05R_L$. Also $R_L = \frac{(\hat{E}_2)^2 \overline{R}}{2\overline{E}^2}$ where $\overline{R}$ is the d.c. load resistance, $\overline{E}$ is the d.c. output voltage and $\hat{E}$ is the a.c.

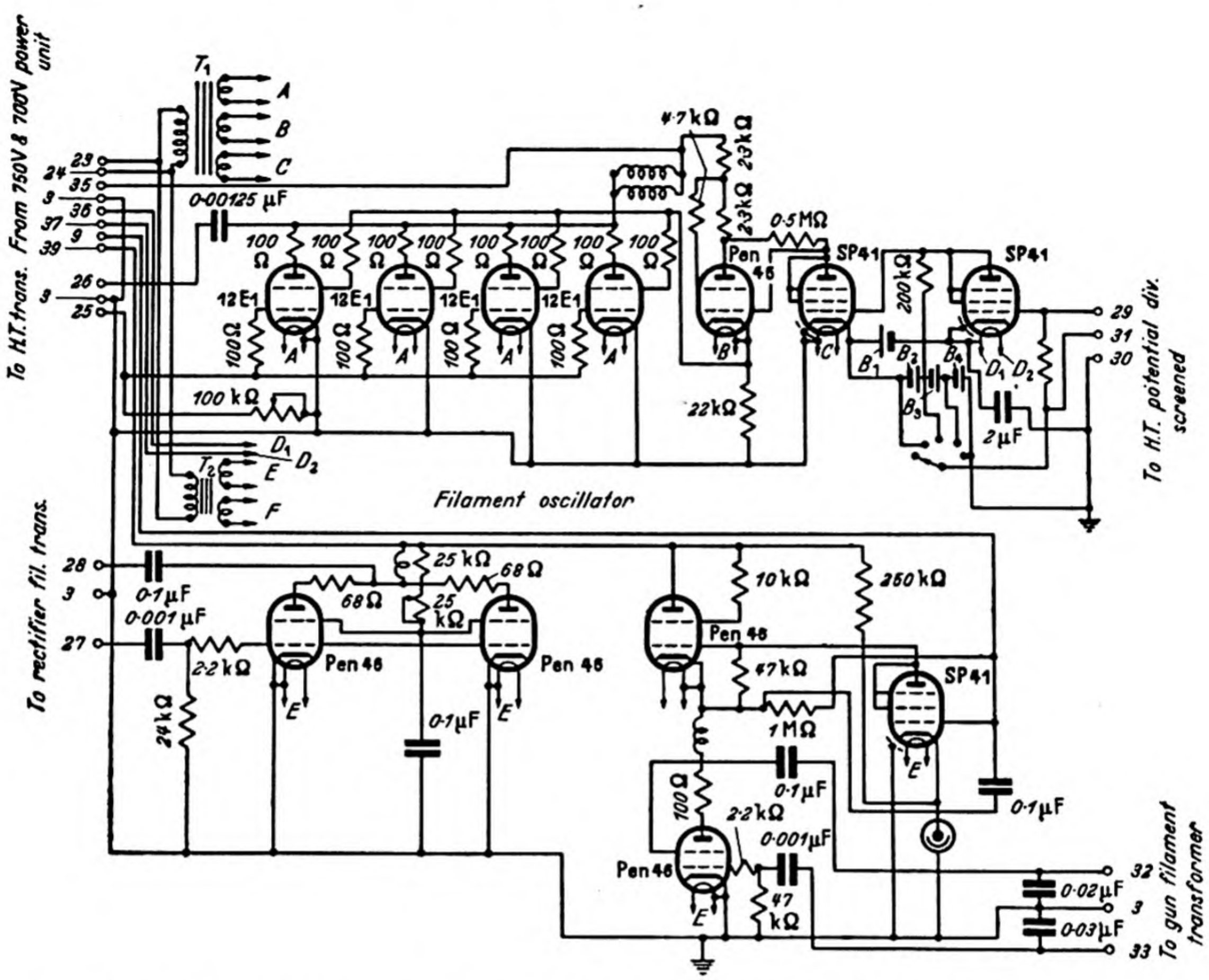

Figure 18. Circuit diagram of the H.T. oscillator and stabilizer (Haine *et al*[6], by courtesy, *J. appl. Phys.*).

peak voltage applied to the rectifier tubes. It is found that $R_L = \frac{1}{2\bar{R}}$ and $R_L = {}^1/_{8\bar{R}}$ for half-wave and voltage-doubler circuits respectively. Hence a voltage-doubler, requiring a lower circuit impedance, is more efficient. R_p from which ωL_1 may be determined, is given by $R_p = (\hat{E}_p)^2/2P$ where P is the oscillator power output and $\hat{E}_p$ is the oscillator peak voltage swing.

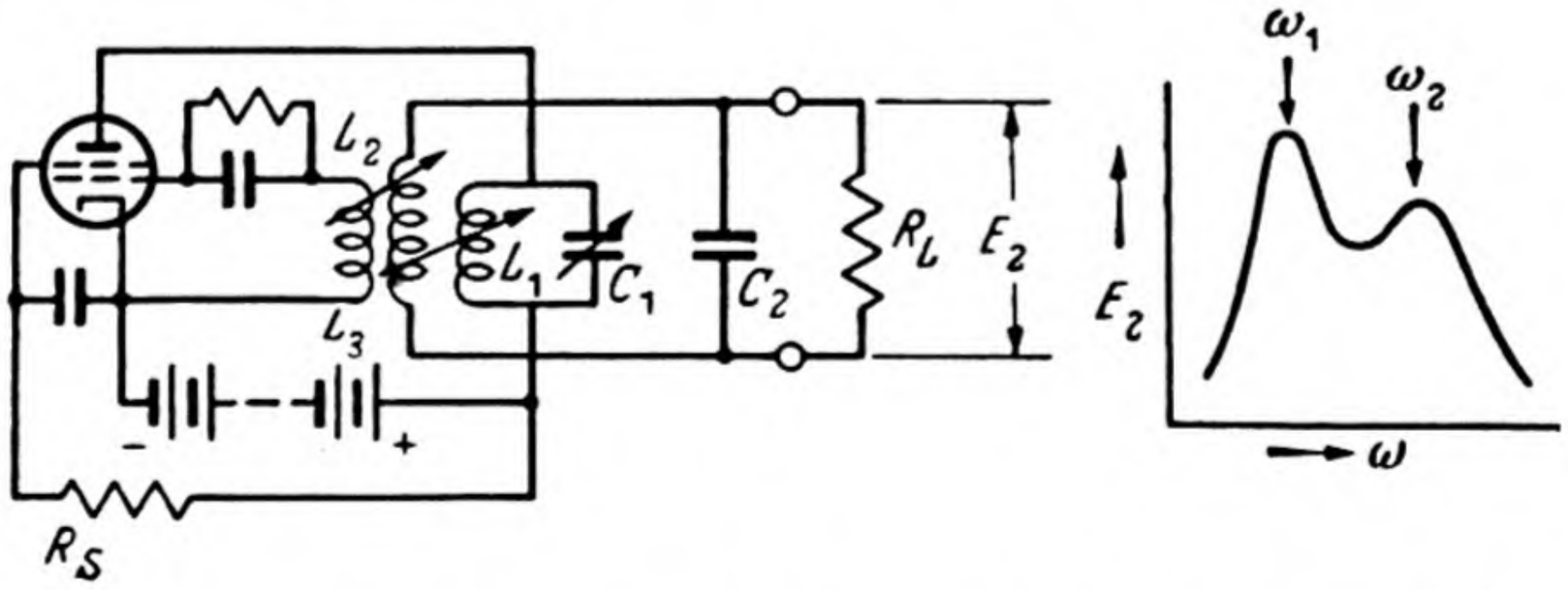

Figure 19. Oscillator circuit for all values of K, and stable characteristic when $K \gg K_c$. Stable oscillations are obtained at ω_1 or ω_2 depending on phase or feedback (Schade[7], by courtesy, *Proc. Inst. Rad. Engrs.*).

Schade[7] discusses in detail the design of coils, which should be subdivided to withstand the high voltage developed across them.

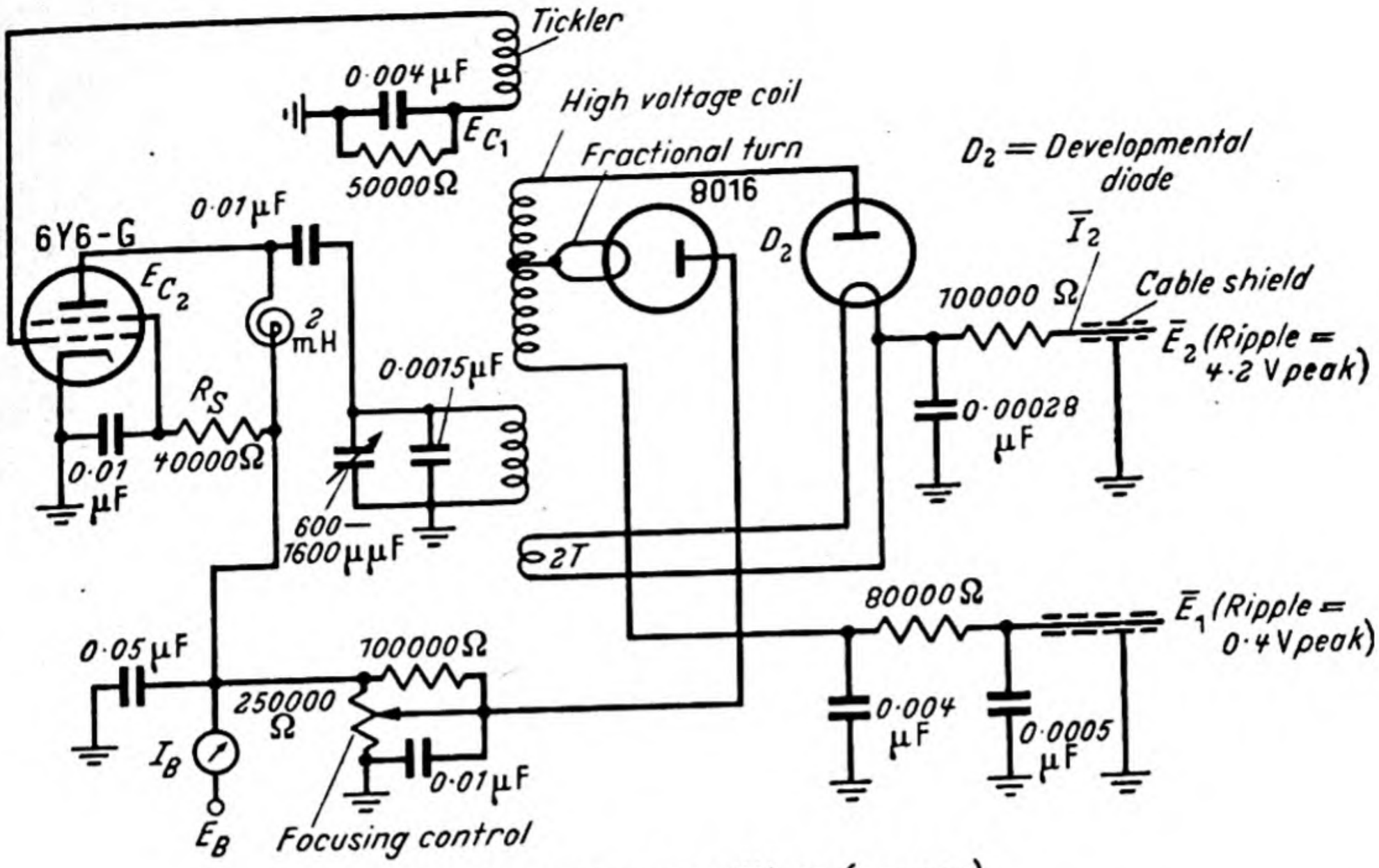

Operating conditions (approx.)

E_B Volts	I_B mA	E_{C_2} Volts	E_{C_1} Volts	$\bar{E}_1$ kV	$\bar{E}_2$ kV	$\bar{I}_2$ mA
+325	31	+68	−36	2	10·6	0
					9·4	0·95
+325	62	+115				

Figure 20. Circuit and operating conditions of a 10-kilovolt supply (Schade[7], by courtesy, *Proc. Inst. Rad. Engrs.*).

An example, for 10–15 kV, has a winding containing 4,200 strands of No. 41 wire, with $L = 387$ mH, and may be used at 96 kc/s. With 1,400 turns of 3-strand Litz wire, $L = 43$ mH, the Q is greatly increased for an operating frequency of 288 kc/s. Circuits for 10 and 30 kV h.t. units are given without coil data (the 10 kV set is shown in *Figure 20*).

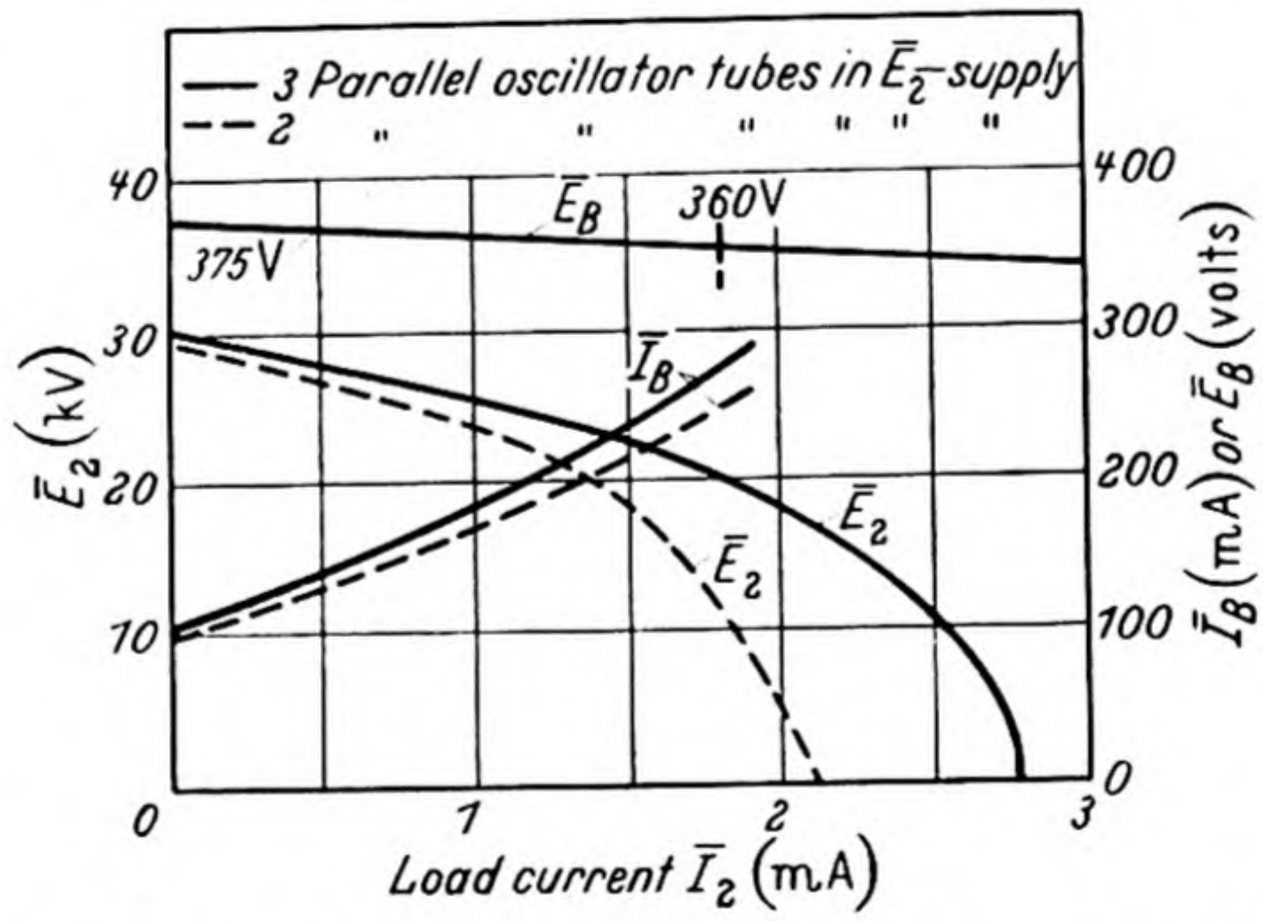

Figure 21. Regulation characteristics of a 30-kilovolt supply, on Schade's system (Schade[7], by courtesy, *Proc. Inst. Rad. Engrs.*).

The regulation characteristics of *Figure 21* for the 30 kV circuits are of interest since they are typical of this type of h.t. source.

The design of the h.f. coils is one of the most important aspects of circuits of this type and Schade gives, in great detail, a description of the coils used in his work. The coils are subdivided into pie-wound sections, in order to reduce the electrical stresses as mentioned above; details of several coils, respectively for 4, 10, 30 and 90 kV are given in the paper. MAUTNER and SCHADE[8] describe in detail the practical arrangement of sets supplying d.c. at voltages up to 90 kV, following the earlier report by Schade[7] already treated above.

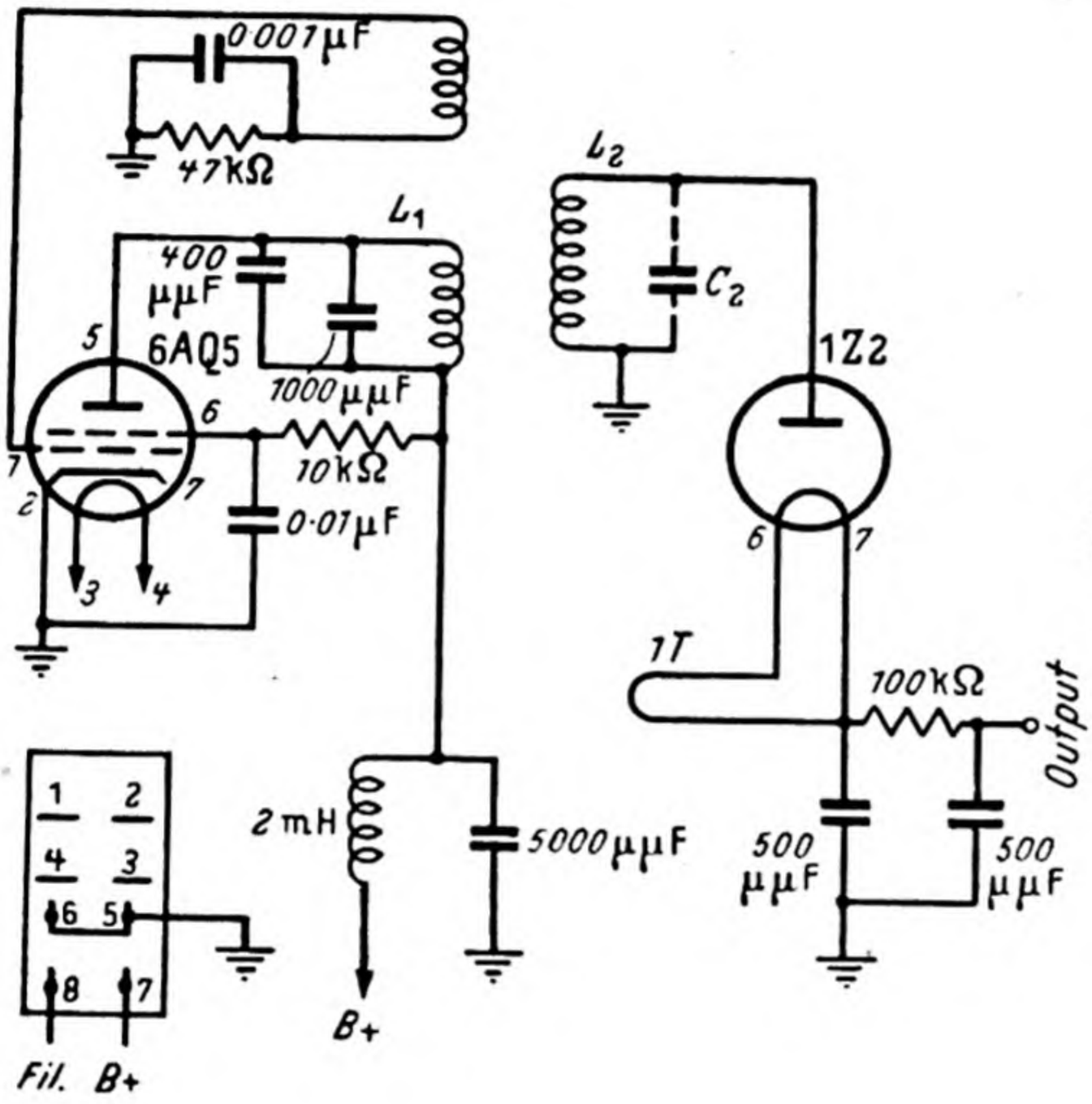

Figure 22. Circuit of 4-kilovolt supply (Schade[7], by courtesy, *Proc. Inst. Rad. Engrs.*).

The basic circuit is shown in *Figure 22*, for a 4 kV supply. L_1 is the primary (oscillator) coil and L_2 is the high-voltage tuned secondary coil, the capacitance C_2 being composed only of the circuit stray capacitances. For higher voltages, multiplier circuits are used and for 90 kV three diode valves type R6194A are used. For a 90 kV set the required area is only 24 in. × 32 in.

The rectifier circuit shunts the tuned high-voltage circuit with a load R^1 given by

$$R^1 = R/2n^2$$

Where R is the d.c. load resistance in the output circuit and n is the number of cascaded rectifier stages. For 90 kV output at 0·8 mA d.c., $R = 110\,M\Omega$ and the inverse rating of the diode (R6194A) requires that $n = 3$. This gives $R^1 = 6\,M\Omega$.

The 90 kV circuit is shown in *Figure 23*, for which the resonant frequency is 65 kc/s. The diode filaments are heated by means of small coils coupled to the transformer primary (for single rectifier

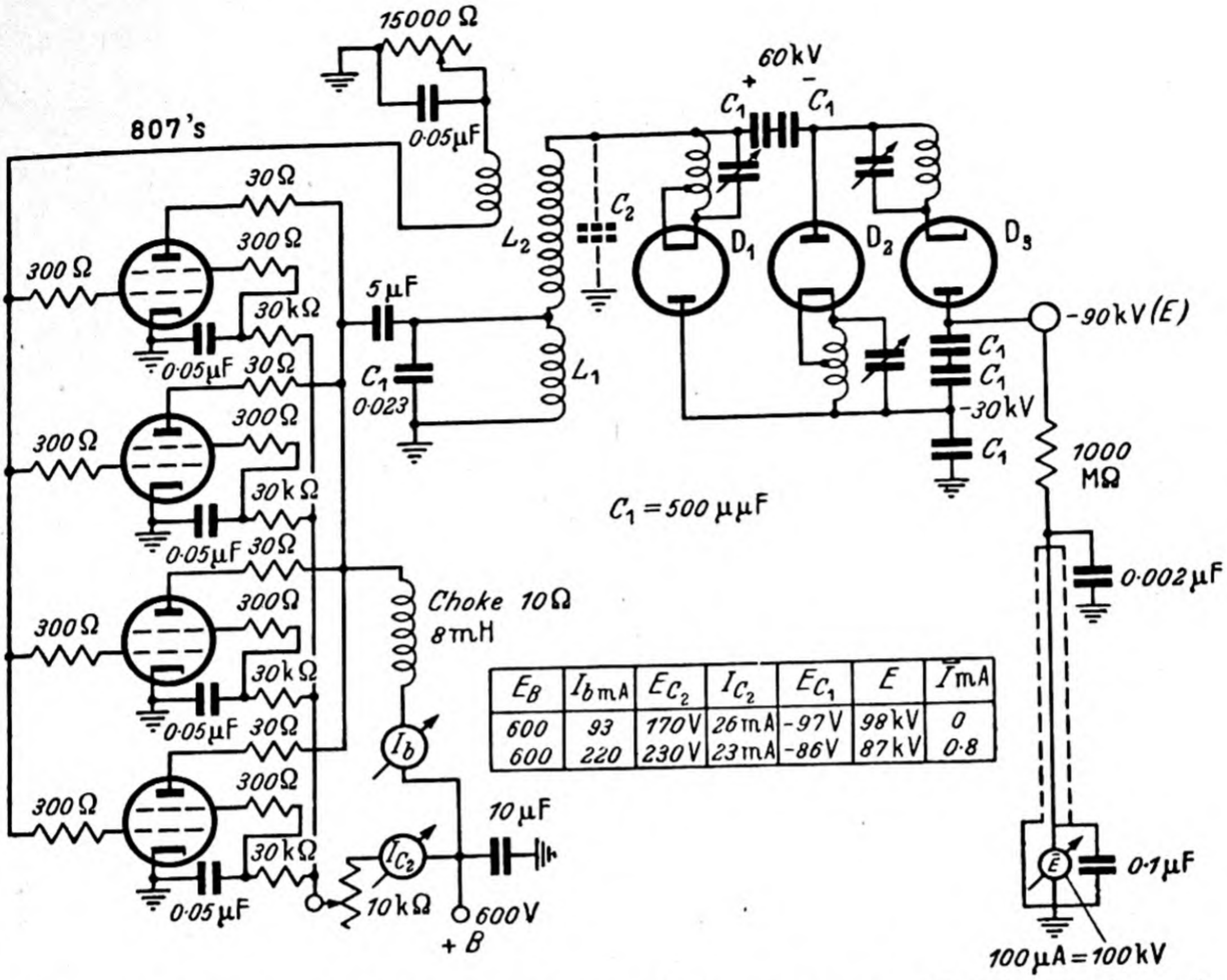

E_B	I_b mA	E_{C_2}	I_{C_2}	E_{C_1}	E	I mA
600	93	170V	26mA	-97V	98kV	0
600	220	230V	23mA	-86V	87kV	0·8

Figure 23. Circuit of 90-kV tripler. (*I* output load current. The *E's* denote voltages.) (Schade[7], by courtesy, *Proc. Inst. Rad. Engrs.*).

sets) or, as in the case of the 90 kV set, by resonating the capacity current through the diode in the primary of a step-down transformer. Schade's paper[7] is exhaustive and includes discussions of rectifier characteristics, oscillator conditions, regulation characteristics and frequency characteristics of the rectifier circuit. Details of circuits for the following rectifier sets are given: 4 kV single stage, 90 kV tripler, 30 kV tripler, 30 kV unbalanced doubler, and 10 kV two-stage.

VALVE RECTIFIER CIRCUITS (WITH PULSE GENERATORS)

It is possible to generate high-voltage d.c. by supplying cascade h.t. generators (*see* pages 19–37) from a recurrent pulse circuit and details of a 25 kV supply source for a projection television cathode-ray oscillograph using this principle, have been given by SIEZEN and KERKHOF[9]. The cascade circuit has in this case 3 stages and supplies 150 μA at 25 kV, taking 11 W from a d.c. 350 V source. The internal resistance, with no load, is about 5 $M\Omega$. The whole apparatus, excluding the d.c. supply, is extremely compact and only occupies a space 18 cm × 10 cm × 15 cm. It is claimed by Siezen and Kerkhof that this circuit tends to give less interference than the h.f. method of generating h.t. described by Schade[7] (*see* pages 10–15).

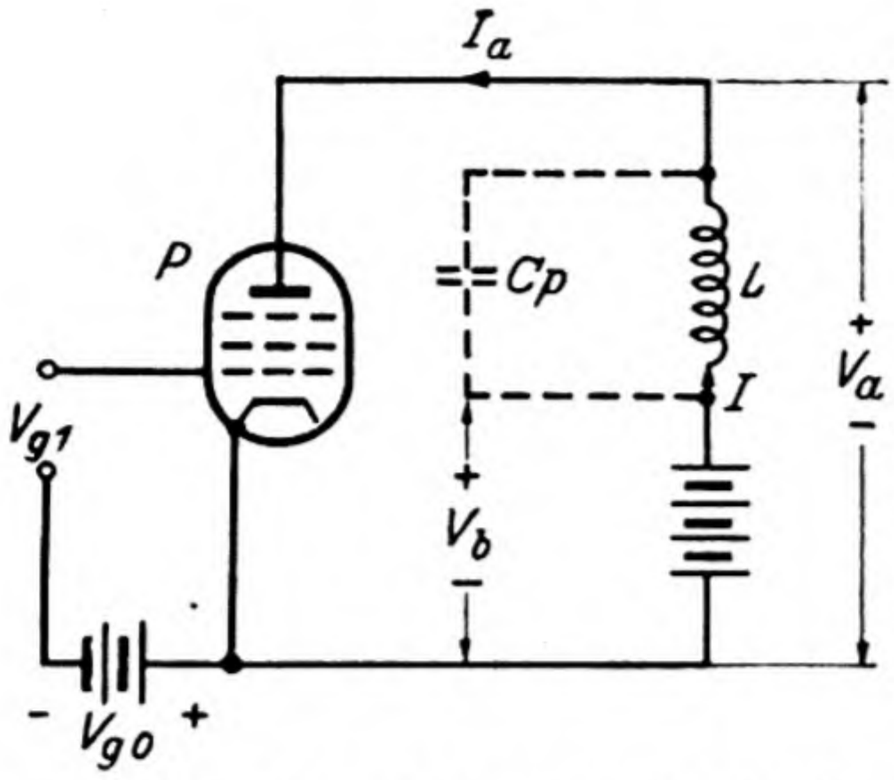

Figure 24 (*Left*). Diagram of a pulse generator. L = self-inductance of a coil (with self-capacitance C_p) in the anode circuit of a pentode P (Siezen and Kerkhof[9], by courtesy, *Philips Tech. Rev.*).

Figure 25 (*Below*). Cascade rectifier, connected to a pulse generator, (a) with even number of stages, (b) with odd number of stages. V_h = direct voltage output, R_h = load resistor through which the direct current I_h flows; i_r = current taken up by the rectifier. (c) Complete diagram of pulse generator and rectifier. T_r = triode EBC 33 for producing the sawtooth voltage P = pentode EL 38 with the coil S_1, of the transformer T in the anode circuit. S_2 S_3, S_4 = cathode current winding of the diodes D_1, D_2, D_3 (type EY 51). S_5 = winding for control voltage V_r. The circuit is fed with 350 V direct voltage (Schade[7], by courtesy, *Proc. Inst. Rad. Engrs.*).

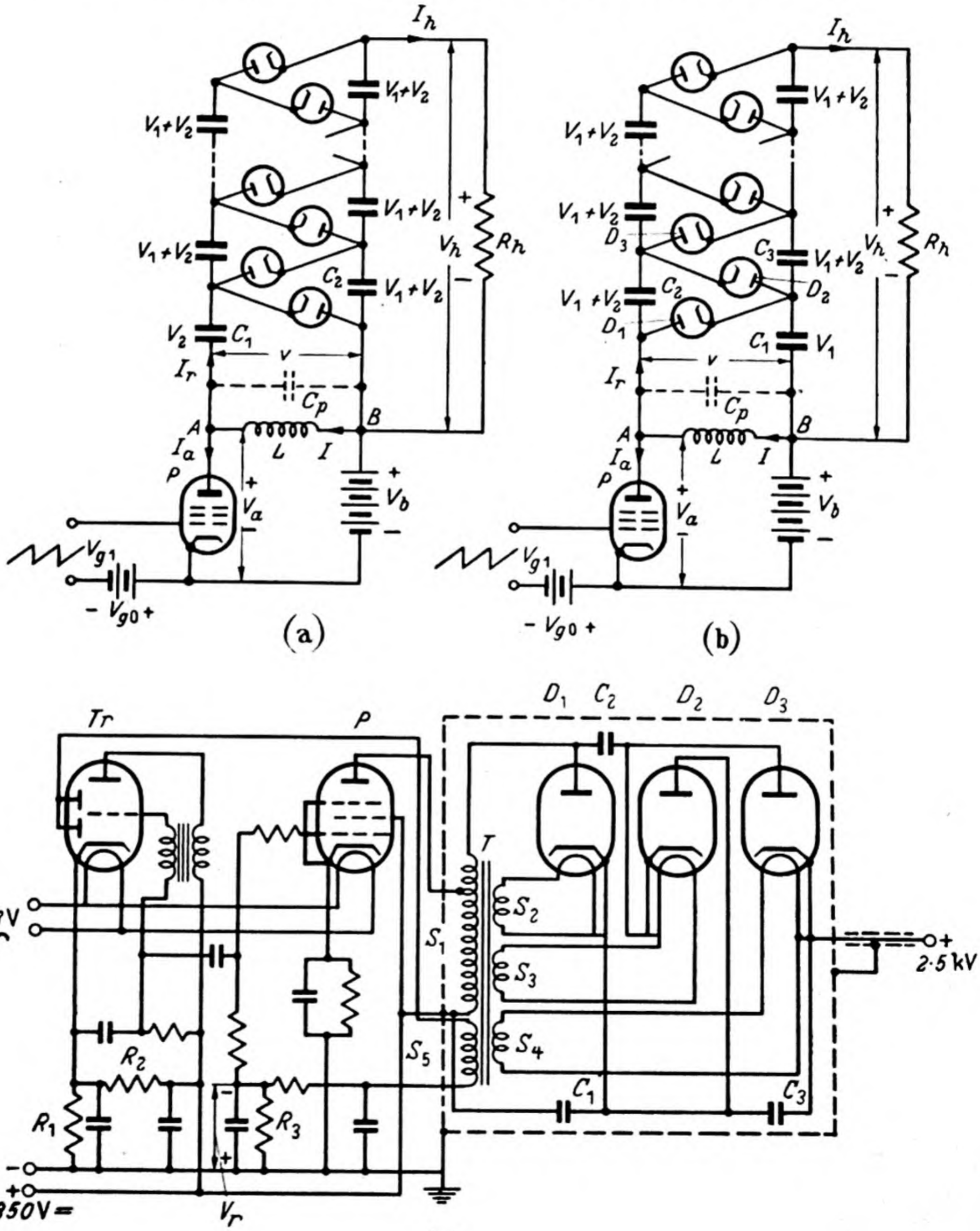

The pulses are generated in the anode circuit of a valve when the latter is suddenly cut off, a method well known in the early development of radar in Britain and described, for example, in the Institution of Electrical Engineers Radiolocation Convention (1946) by CRAGGS, HAINE and MEEK[10] and others (*see* pages 180–181 for further details). The basic circuit, as given by Siezen and Kerkhof, is shown in *Figure 24*. When the current I_{max} through the coil L, of self-capacitance C_p, is interrupted the peak value of the voltage developed across the coil is

$$V_{max} = I_{max} \sqrt{\frac{L}{C_p}} .$$

For example if $I_{max} = 120$ mA, $L = 0{\cdot}5$ H and $C_p = 50\ \mu\mu$F, then $V_{max} = 12$ kV. In *Figure 24* the anode current of the pentode P is suddenly shut off, as described also in pages 180–181, by the application of a sufficiently high negative bias.

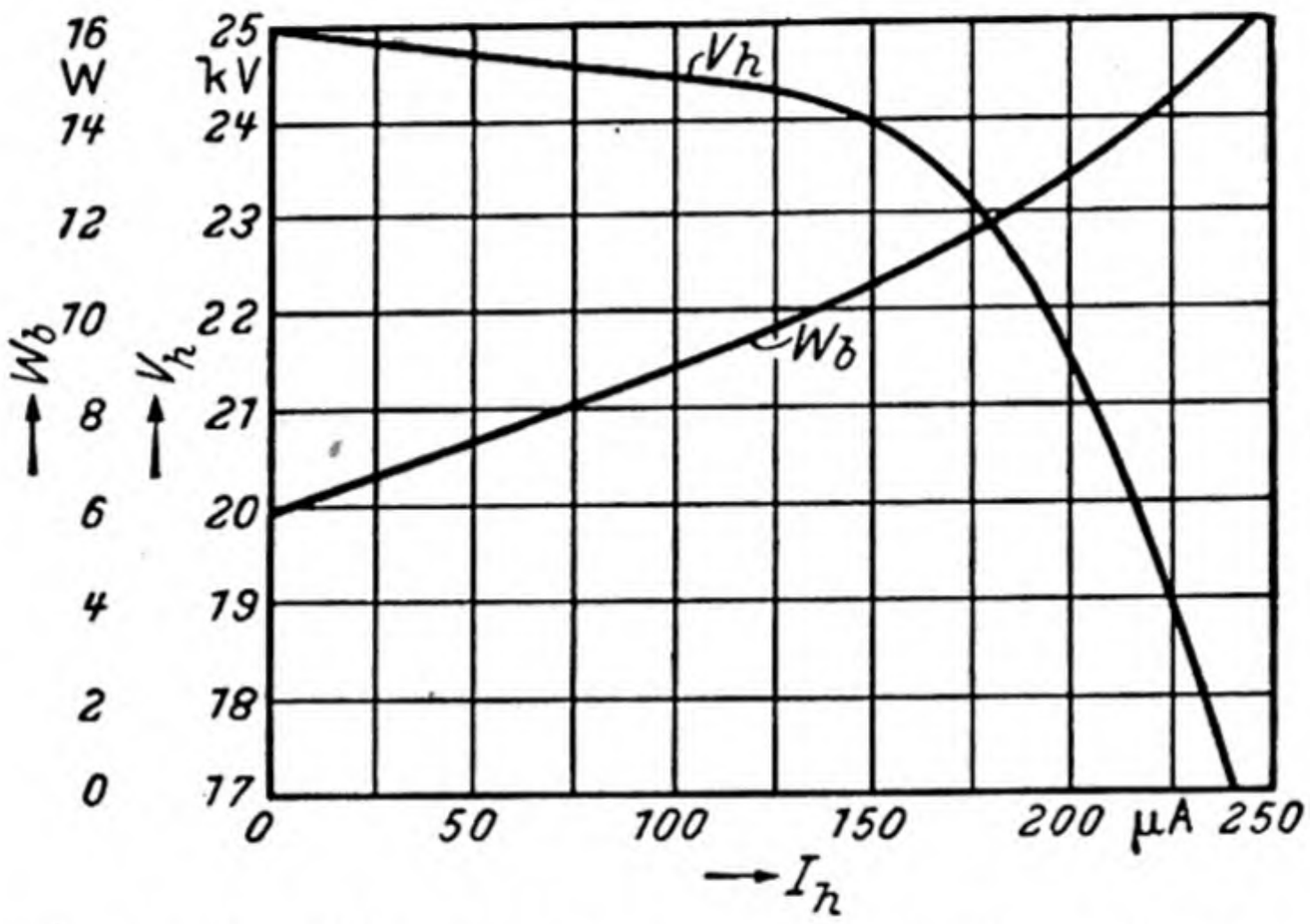

Figure 26. Direct voltage output V_h and direct current power consumption W_b as function of the direct current output I_h for pulse d.c. generator (Schade[7], by courtesy, *Proc. Inst. Rad. Engrs.*).

It is shown[9] that a sawtooth grid-bias wave-shape is advantageous; also the choice of the most suitable valve, of V_{max}, and the requisite number of voltage multiplier stages should be carefully made. The schematic circuits for complete generators of this type are shown in *Figure 25a* which includes also the pulse-forming circuits. The final 3-stage circuit for supplying 25 kV 150 μA is given in *Figure 25c*. S_1 is the h.t. anode coil of the pulse-former across which a voltage of 8·5 kV is developed and D_1, D_2 and D_3 are the rectifier valves in the cascade circuit, using condensers C_1, C_2 and C_3. The blocking-oscillator pulse-circuit (PS_1) operates at a recurrence rate of 1,000 c/s. The transformer T, with its five windings, has a Ferroxcube core and, since it is oil-immersed (with the rest of the cascade circuit), is of very small size.

The load characteristics of this d.c. source are shown in *Figure 26*, from which it is seen that the d.c. output voltage drops rapidly for load currents above 175 μA.

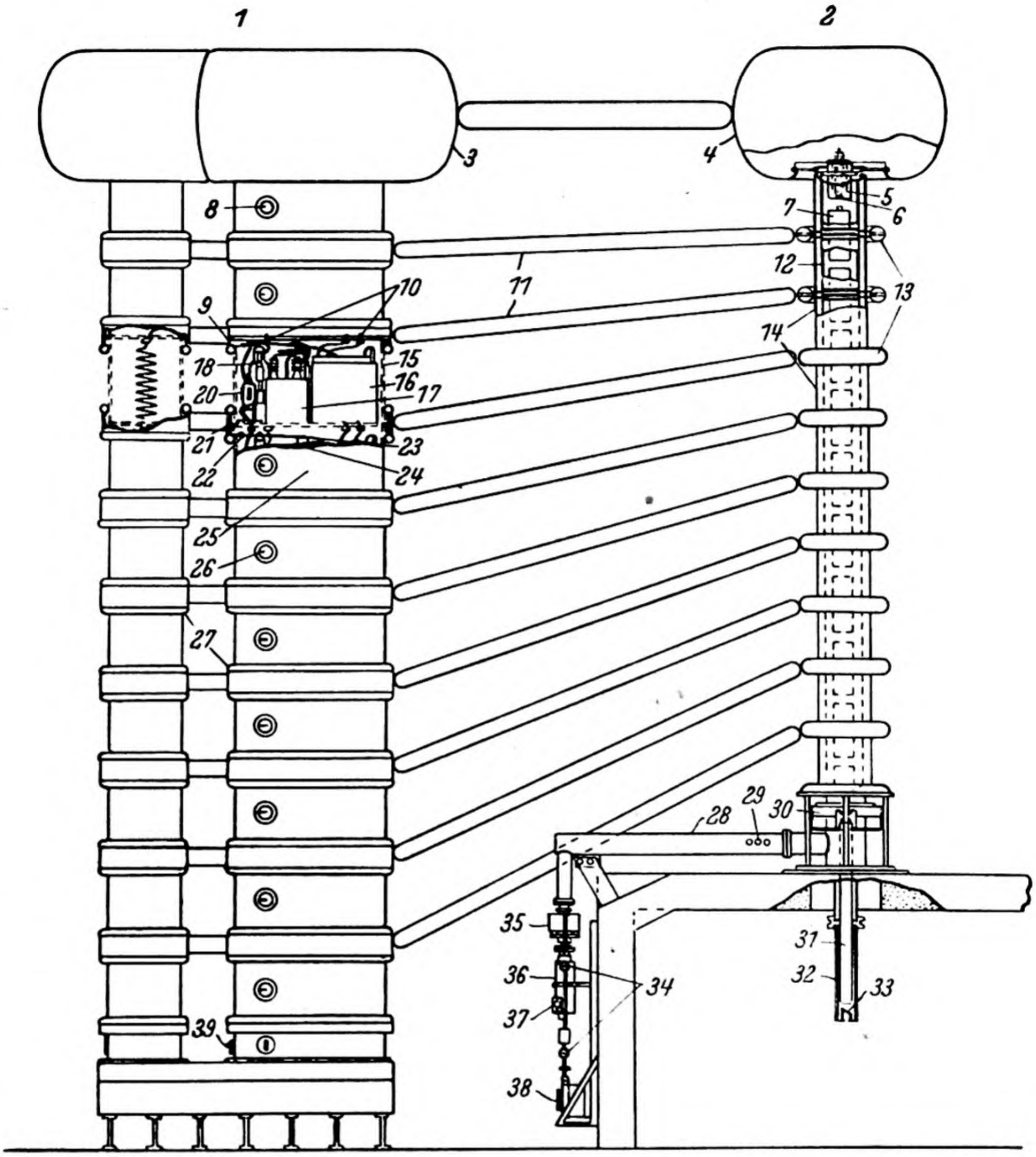

Figure 27. Assembly of the 1,400-kV constant-potential X-ray equipment (Charlton and Hubbard,[11] by courtesy, *Gen. Elect. Rev.*).

1: Ten-section cascade 1,400-kV d.c. generator.
2: Ten-section X-ray tube.
3: Top corona shield of generator.
4: Top corona shield of X-ray tube.
5: Permanent magnet to compensate effect of external magnetic field.
6: Cathode assembly.
7: First intermediate electrode.
8: Oil gauge.
9: Filling plug.
10: Spring contacts.
11: Connections to intermediate voltage taps.
12: Cylindrical glass envelope.
13: Tube corona shields on intermediate sections.
14: Herkolite protective shields.
15: Herkolite tank.
16: Plate transformers.
17: Capacitors
18: Kenotrons.
19: Herkolite stack housing high-voltage resistance potentiometer.
20: Filament transformer.
21: Drain valve.
22: Polarity-switch control.
23: Reversing polarity switch.
24: Plate resistors.
25: 140 kV unit.
26: Viewing window.
27: Corona shields for generator and resistance potentiometer stack.
28: Vacuum line.
29: Ionization gauges.
30: Magnetic focusing coil.
31: Insulated collector electrode.
32: Extension chamber with water jacket.
33: Tungsten target.
34: Vacuum shut-off valve.
35: Charcoal trap.
36: Oil-diffusion pump.
37: Hale-Pirani gauge.
38: Rough vacuum pump.
39: Filament and power-supply terminals.

CASCADED RECTIFIER CIRCUITS USING VALVES

The generation of high-voltage d.c. by the use of a cascaded series of rectifier sets, each complete in itself, has been described by CHARLTON and HUBBARD[11]. The generator was built for the National Bureau of Standards for precision work on measurement of X-rays in the range 400–1,400 kV.

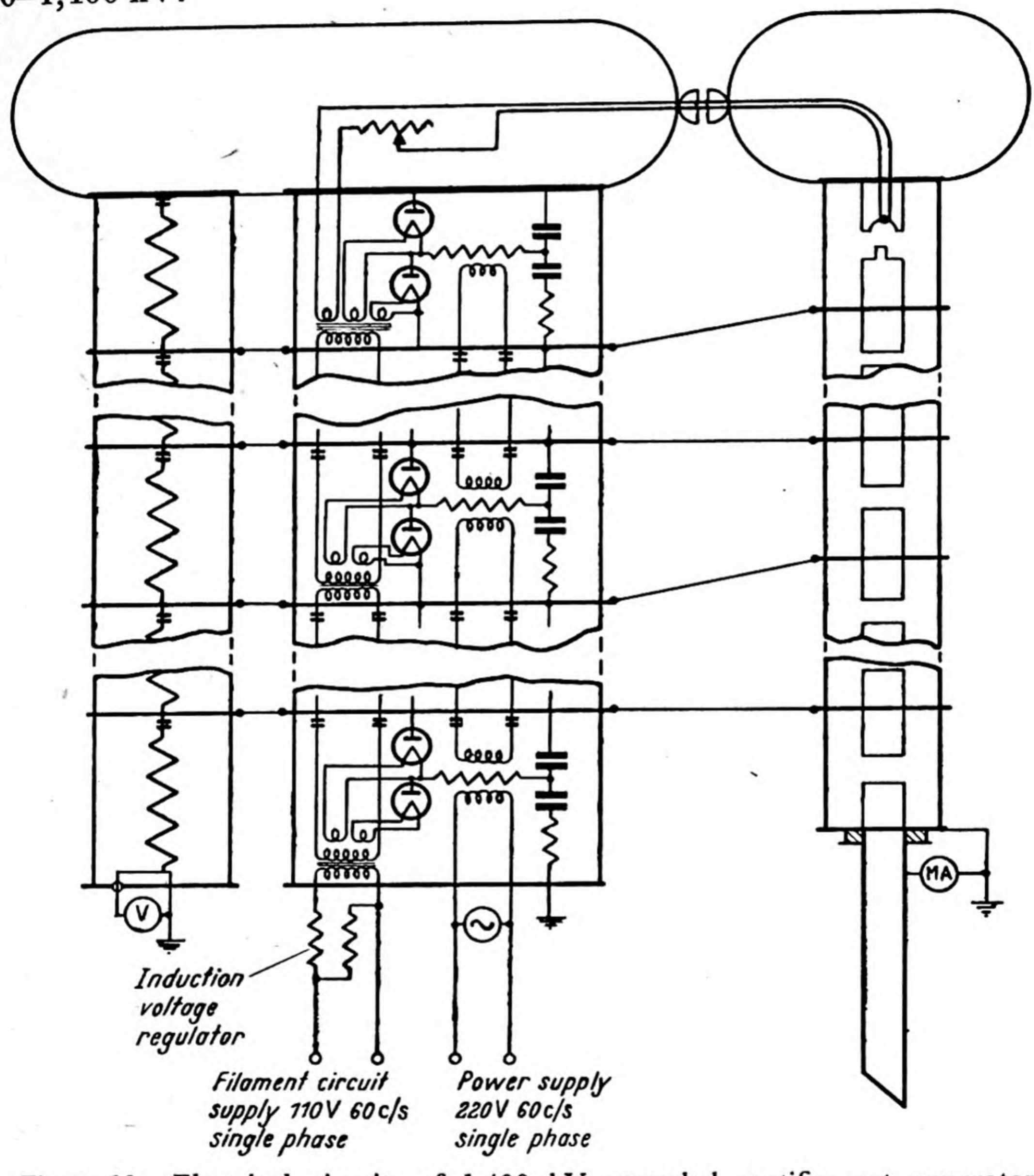

Figure 28. Electrical circuits of 1,400 kV cascaded rectifier set generator (Charlton and Hubbard[11], by courtesy, *Gen. Elect. Rev.*).

The d.c. generator (total height 30 ft. 6 in.) consists of ten 140 kV oil-filled full-wave rectifier units, using 0·1 μF condensers, arranged as shown in *Figure 27*. Each transformer has a tertiary winding linking it to the next unit. The electrical circuit is shown in *Figure 28*. The polarity can be rapidly changed by means of reversing switches in each unit. The rectifier filaments are heated by cascaded transformers and each unit contains an h.t. transformer (whose h.t. coil,

insulated for 70 kV d.c. at the capacitor end and for 140 kV d.c. at the tube end, is wound for 3 kVA at 66 kV r.m.s.) a filament transformer, two rectifiers, capacitors and resistors. The tanks, made of the insulating material Herkolite, are approximately 50 in. in diameter and $28^{5}/_{9}$ in. long and are fitted with drain-cocks and observation windows of Lucite opposite each rectifier. The filament transformers are also arranged for series excitation and are provided with four windings all insulated from each other and for 150 kV d.c. The kVA ratings are small and the exciting current is controlled with parallel capacitors across the primaries (shunt capacitors were also used across the supply terminals in each rectifier unit to provide power factor correction).

Electrical tests on the stack gave the results shown in *Figure 29* including the voltage distribution among the units in the stack and also the total voltages from ground at different points up the stack for output currents of 1, 4 and 15 mA. The regulation over this current range is seen to be extremely good.

The total corona current at 1,400 kV is only 0·16 mA, due largely to the corona shields fixed round the h.t. end of the stack (*see Figure 27*). The larger shield is formed of a spinning with a horizontal diameter of 100 in. and a depth of 48 in. A similar spinning is mounted on the top of the X-ray tube. Connections between the h.t. stack and the tube are made with aluminium tubes, $10\frac{1}{4}$ in. in diameter at the top section and 6 in. in diameter elsewhere. The corona suppression rings on the rectifier units are shown in *Figure 27*; the flanges of each pair of connected sets are covered with stainless steel bands, a simple procedure which is probably only corona-free because of the shielding effects of the circular tubes also shown in *Figure 27*.

Load characteristics are given in *Table III*.

TABLE III

Load current *mA*	*Input* *V*	*A*	*kW*	*Power factor*	*Efficiency* %
0·16	148	23·6	1·81	0·52	—
1·0	159	46·9	4·40	0·59	35
2·0	166	54	5·83	0·65	48
5·0	180·5	80	10·95	0·757	64
10·0	192	120	19·35	0·84	72·3
15	200	158	27·50	0·87	76·5

The use of the voltage-doubler circuit of *Figure 16* enables d.c. at, say, up to 300 kV to be obtained. COCKROFT and WALTON[12] describe a set using a 350 kV transformer designed and built by Metropolitan-

Vickers. Other authors (*see* Chapter 3) have worked with transformers giving even higher voltages. Even so, for voltages above 200 or 300 kV d.c. the use of multiplier circuits in which the individual capacitor and rectifier units have only to withstand a fraction of the total output voltage clearly has great advantages. Schenkel in 1919[13] followed by GREINACHER[14] and SLEPIAN[69] seem to be the early pioneers of this technique. However, its modern extensive use in nuclear and medical physics largely dates from the work of Cockroft and Walton[15] who improved on earlier cascade systems. The techniques were later developed by Dutch workers in the Philips' laboratories (*see* BOUWERS[16], and BOUWERS and KUNTKE[17]). A notable early installation was the 1 MeV X-ray tube (ALLIBONE, BANCROFT and INNES[18]) in St. Bartholomew's Hospital (*Figure 30*).

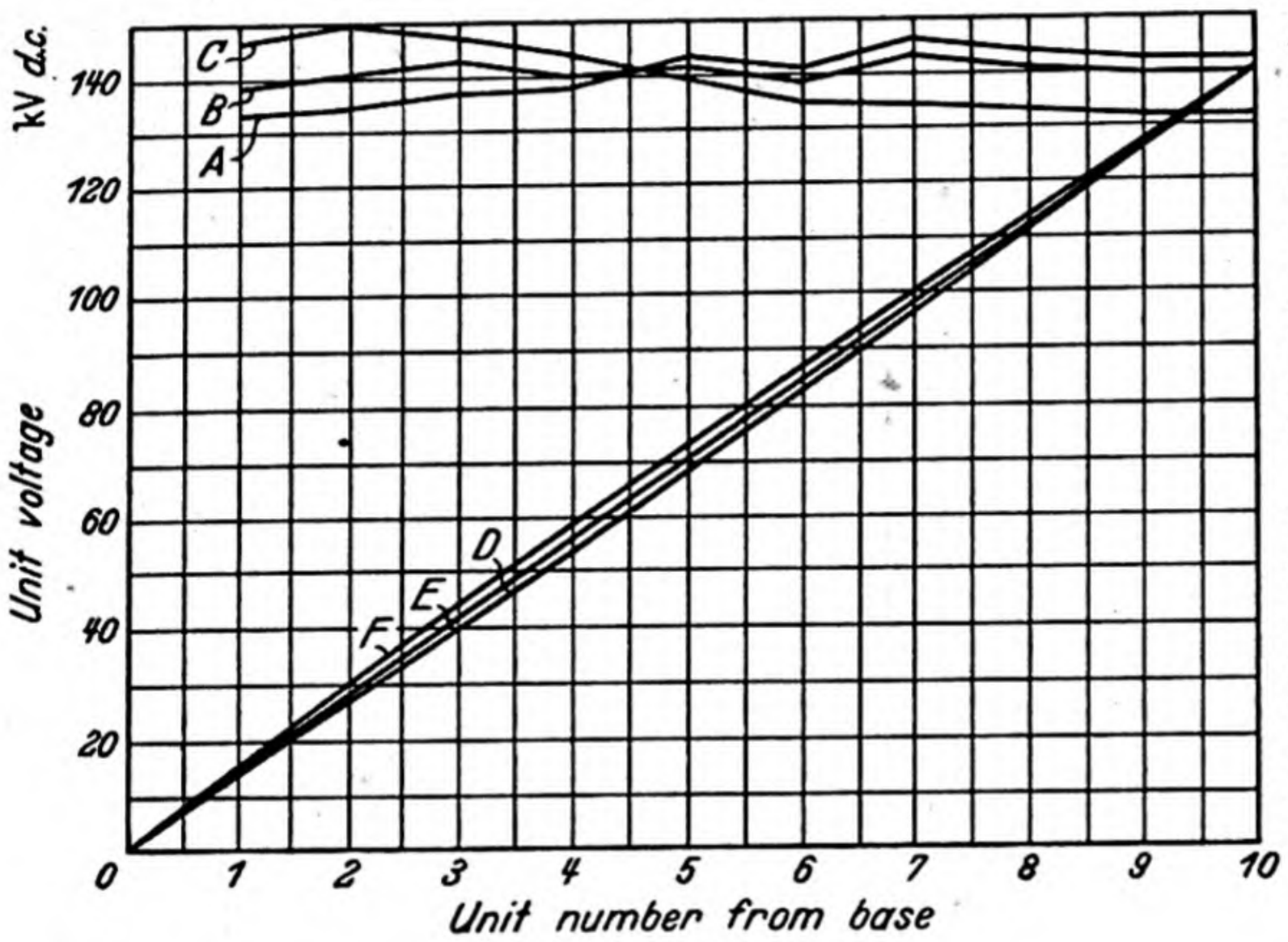

Figure 29. Curves of voltage distribution across the units when the X-ray outfit is operating at 1,400 kV (Charlton and Hubbard[11], by courtesy, *Gen. Elect. Rev.*). (There appears to be a misprint in the ordinate scale in the original diagram which has been corrected.)

Unit Distribution
A: 1-milliamp load
B: 4-milliamp load
C: 15-milliamp load

Total voltage above ground Scale voltage times 10

D: 1-milliamp load
E: 4-milliamp load
F: 15-milliamp load

The first Cambridge set (800 kV d.c.) described by Cockroft and Walton in 1932[15] operates as shown schematically in *Figure 31*. Capacitors K_1, K_2 and K_3 each of capacitance C are connected in series, with a d.c. source joined across K_3. Two other condensers X_1 and X_2 are connected into the circuit alternately by the full and dotted lines shown. This switching is carried out with rectifier valves as described later. With X_1 and X_2 connected to K_2 and K_3, X_2 will be charged to E. When the switches are as shown by the full lines X_2 will be joined to K_2 and, if of equal capacitance, each will reach a voltage $E/2$. On the next switch reversal, K_2 and X_1 are joined and charged to $E/4$ whilst X_2 is recharged to E so that finally, assuming no losses, a voltage $3E$ appears across K_1, K_2 and K_3 in series.

The circuit with rectifier valve switching is arranged as shown in *Figure 32* when the D's are diodes. The transformer supplies power at peak voltage $E/2$ and on the negative peak X_3 is charged through D'_3 to voltage $E/2$; the potential of t_3 therefore alternates between O

and E. When t_3 approaches E, K_3 will be charged through D_3. As the potential of t_3 falls again, the potential of t_2 falls below that of p_3 and X_2 is charged through D'_2. Finally K_1, K_2, K_3, X_1 and X_2 are all charged approximately to voltage E. The charge lost from K_1, if a load resistance $3R$ is connected across the system, in a cycle of

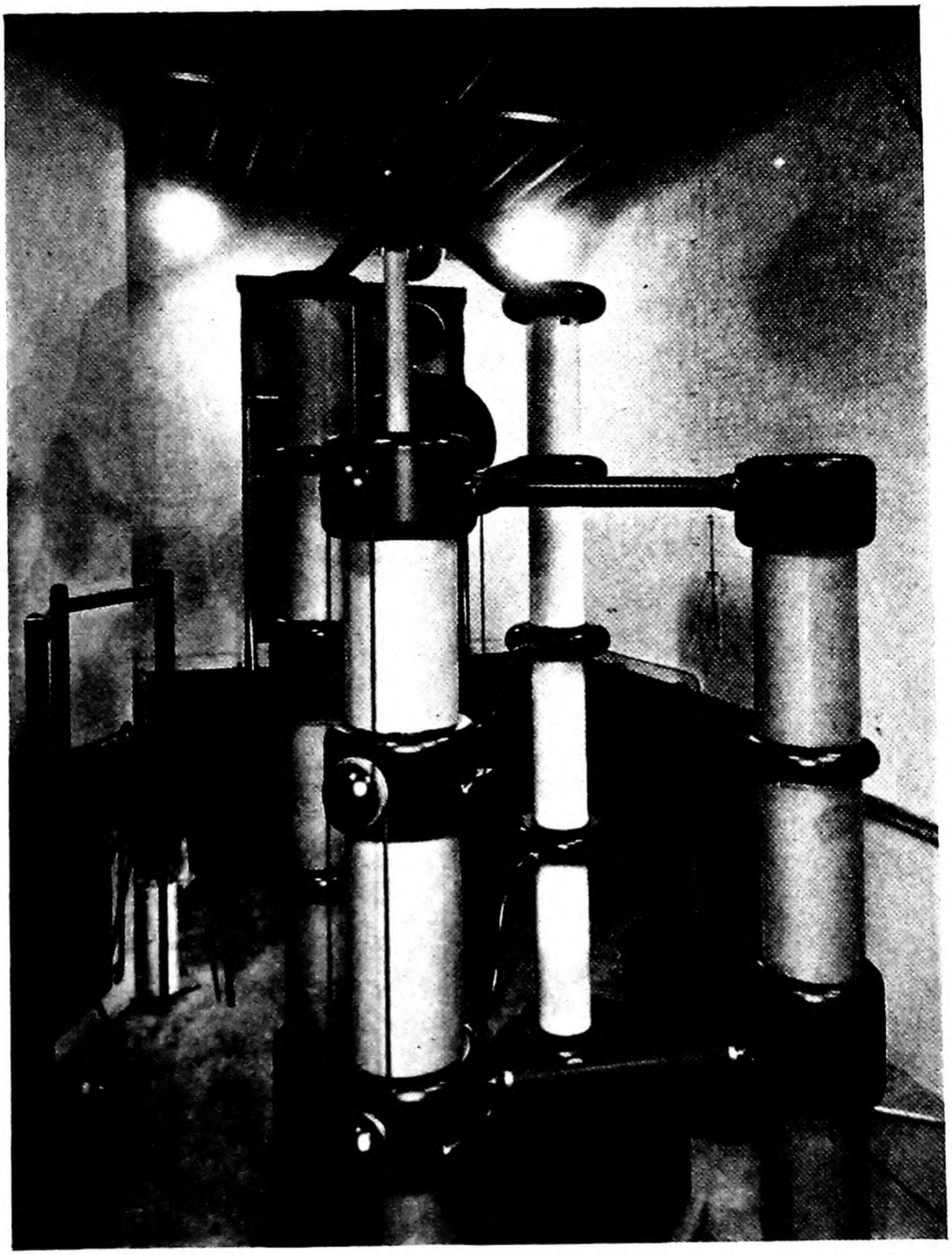

Figure 30. 500 kV d.c. generator using a Cockroft-Walton circuit (Allibone *et al*[18], by courtesy, *J. Inst. elect. Engrs.*).

duration τ is $E\tau/R$. This must be regained during the charging cycle (*Figure 32a*) when K_2 receives a charge $2Q$ (to replenish the charge lost to the load and that transferred to X_1 in the other half-cycle, termed by Cockroft and Walton the transfer half-cycle), and

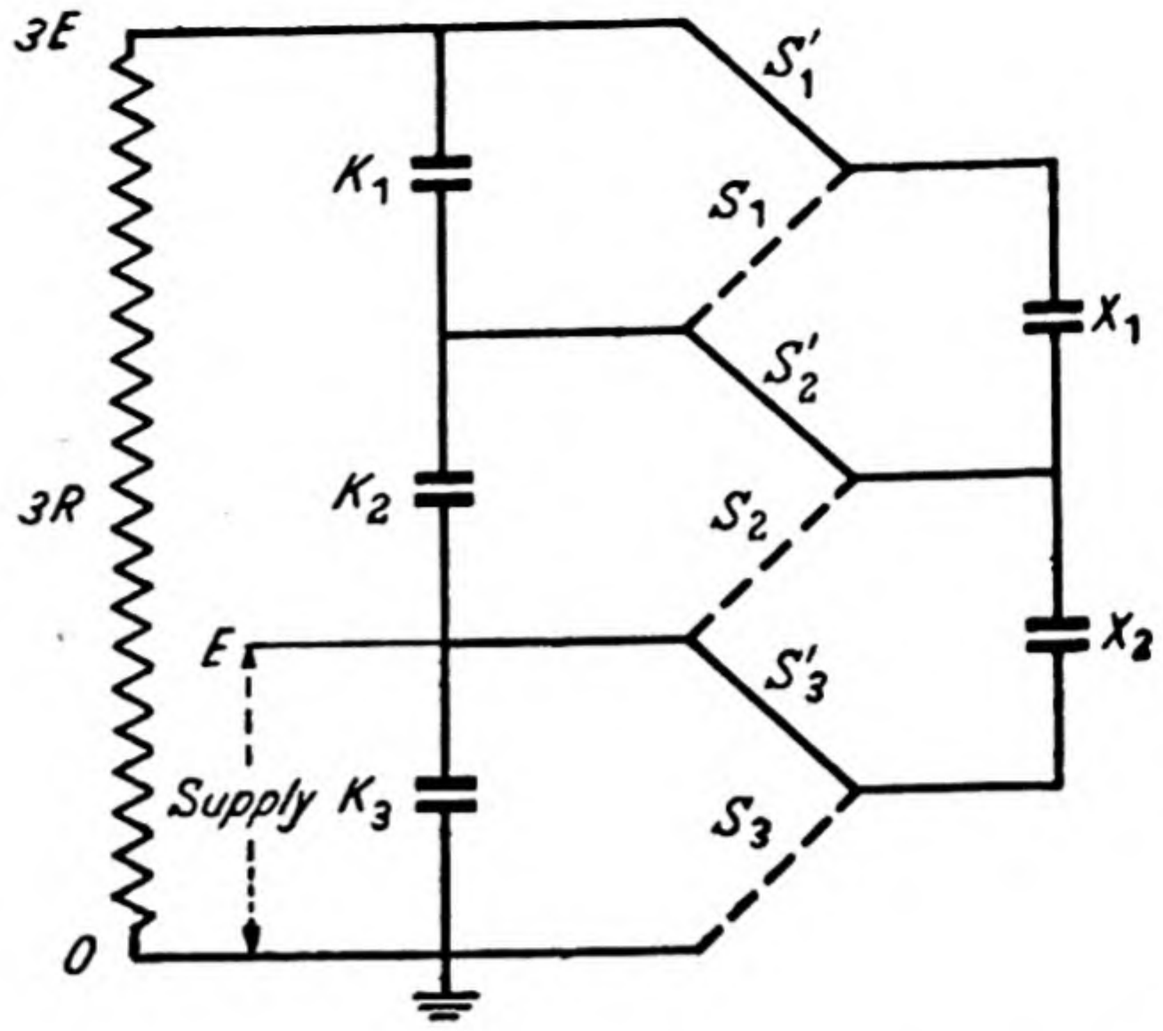

Figure 31. Circuit of Cockroft-Walton cascade generator (Cockroft and Walton[15], by courtesy, *Proc. roy. Soc.*).

K_3 receives $3Q$. The transformer supplies power during this period of value $3Q.E/2$.

The transfer half-cycle is shown in *Figure 32b* and here D'_1, D'_2, and D'_3 conduct near the negative peak of the transformer secondary voltage. K_2 transfers charge Q to X_1, K_3 transfers $2Q$ and the transformer provides charge $3Q$.

For an n-stage circuit ($2n$ voltage-multiplication) the total voltage fluctuation across the load during the charging period is

$$\delta V = \frac{Q}{C} + \frac{2Q}{C} + \ldots \frac{nQ}{C} = n\frac{(n+1)}{2} \cdot \frac{E\tau}{CR}$$

and the percentage fluctuation is given by

$$\delta V/V = \frac{n+1}{2}\tau/_{CR}$$

For $n=2$, $R=10^9\Omega$, $C=0{\cdot}001\ \mu F$, $\tau=10^{-2}$ sec and the ripple will be 1·5 per cent., for a load current of 0·4 mA at 800 kV provided that the

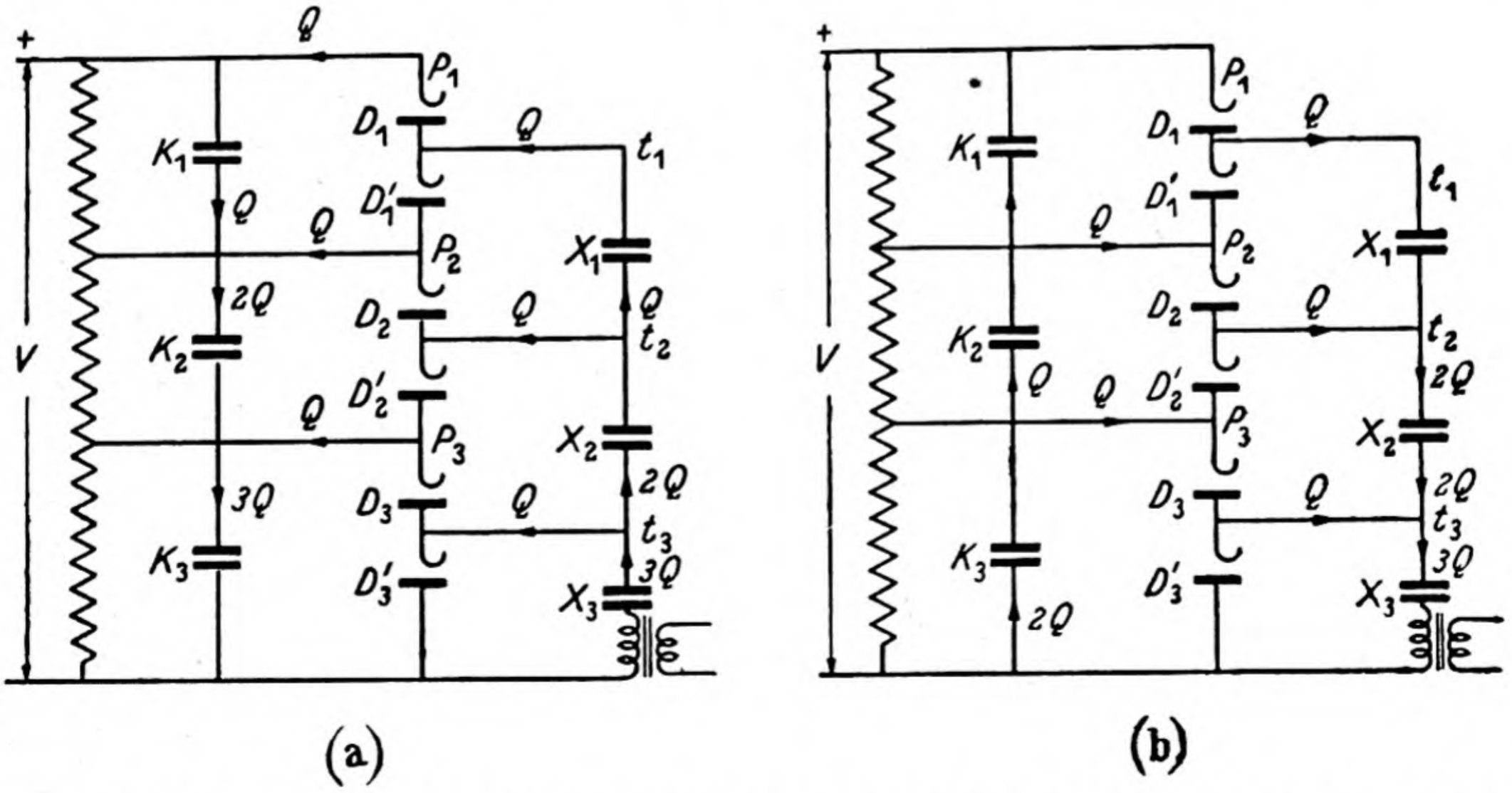

Figure 32. Cockroft-Walton circuits (Cockroft and Walton[15], by courtesy, *Proc. roy. Soc.*).

rectifier valves will pass the required charging current. Each capacitor and rectifier has to withstand twice the transformer voltage. The system therefore differs from SCHENKEL's[13] circuit in which, with a different arrangement of capacitors, some of the latter have to withstand the full output voltage.

An example of the Cockroft and Walton circuit is described by Allibone, Bancroft and Innes[18] (*see Figure 30*) for a 1 MV X-ray tube using two 500 kV, 4-stage, rectifier sets of different polarity. The circuit (*Figure 33*) includes 50 kΩ resistances in the condenser leads to minimize damage during short circuits or flashes in the rectifiers. The latter are described in Chapter 11, and, if continuously evacuated

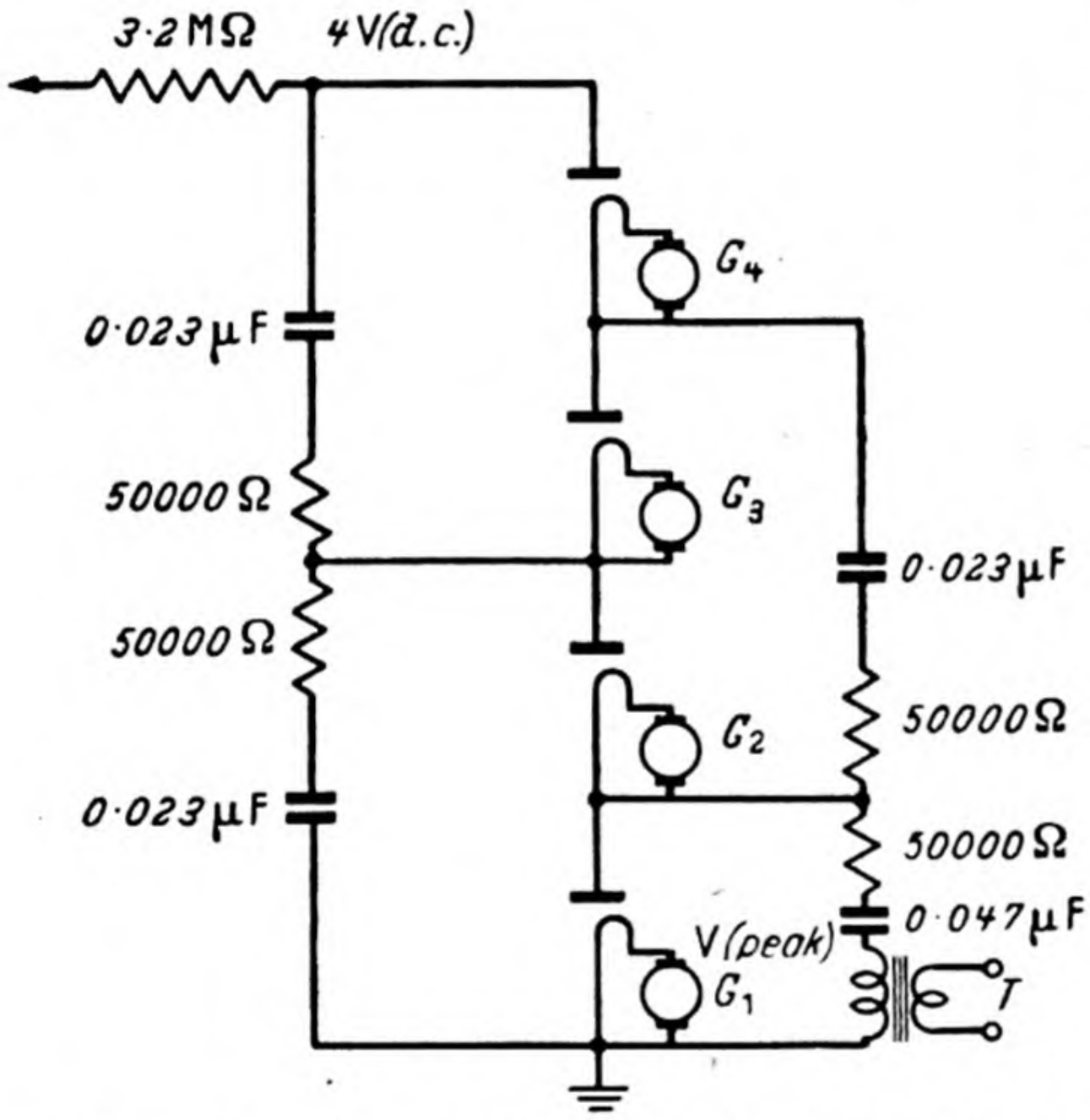

Figure 33. Circuit diagram of negative d.c. generator (St. Bartholomew's Hospital 1 MV X-ray set) (Allibone *et al*[18], by courtesy, *J. Inst. elect. Engrs.*).

as in the present case, are conveniently mounted in the same vertical stack, as shown in *Figure 30* (front stack, mounted on pump cubicle). The valve filaments are heated from belt-driven 150 W d.c. generators (G_1—G_4 in *Figure 33*). The load current is about 5 mA when the overall efficiency of the stack, at 500 kV, is about 86 per cent. An installation using a voltage-doubler circuit for 800 kV, also for the excitation of an X-ray tube, is described by CHARLTON *et al* [19].

Mitchell[20] has given a detailed analysis of the basic circuit of cascade h.t. generators from which the performance of such circuits, for various values of the important parameters, such as capacitor size, may be calculated. The treatment is based on Mitchell's earlier work on simpler rectifier sets, and uses the basic circuit for a 3-stage unit given in *Figure 34*. The rectifiers T_2, T_4 and T_6 are operative on the positive half-cycles. The current and voltage wave-forms

are shown respectively in *Figures 35* and *36*. As T_1, T_3 and T_5 and T_2, T_4 and T_6 are respectively conductive over approximately the same periods, the various pulses are additive in the condensers to which they are common, unless the ripple is appreciable when there is a progressive phase change throughout the circuit. The difference between the current pulses in the feed and load condensers should be noted; the latter, except the last unit, carry a steady discharge current in addition to the short pulse.

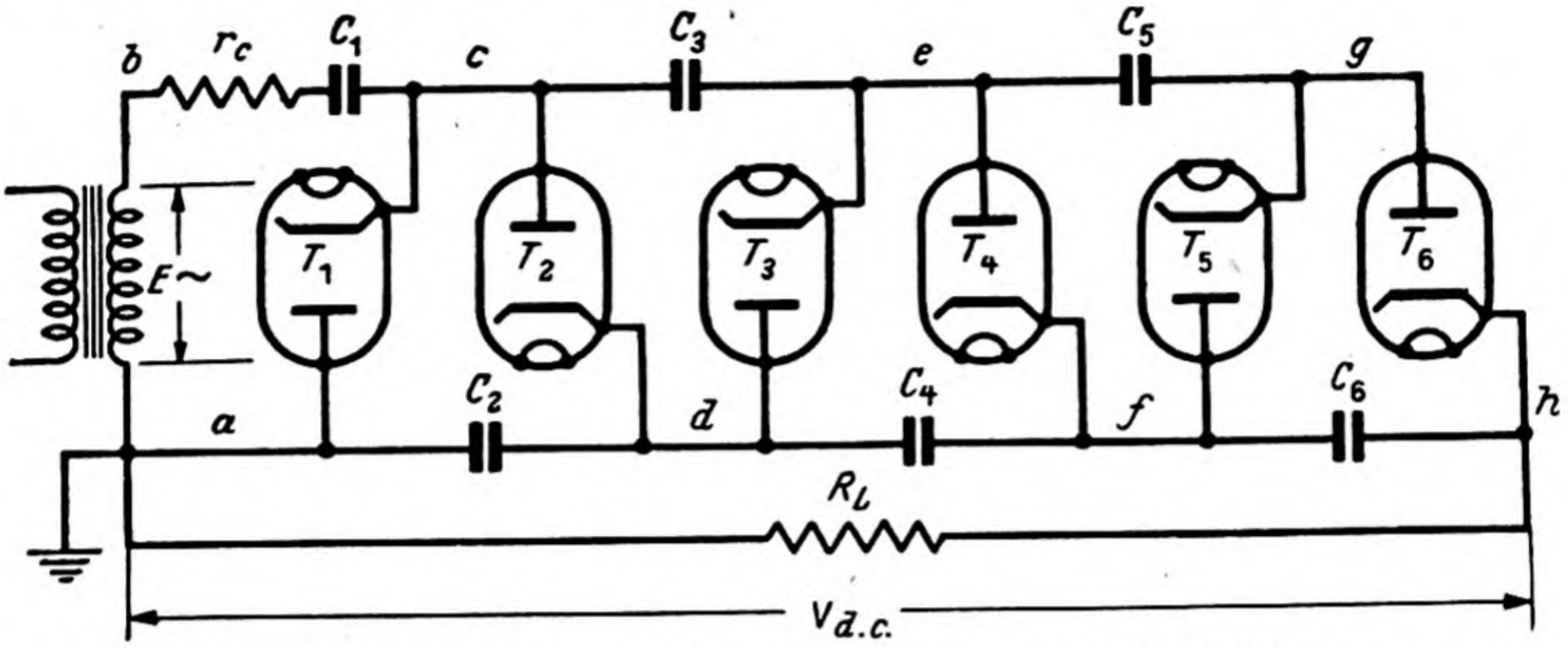

Figure 34. Schematic circuit of cascade d.c. set (Mitchell[20], by courtesy, *Wireless Engr.*).

The voltage on C_2 is the sum of E_v (the input a.c. voltage) and the voltage across C_1, and is thus the shaded part of *Figure 36a*. Vc_2, the mean voltage on C_2, is less than the positive peak value of the charging voltage $(E+V_{c1})$. The condenser voltages for the other units in the stack are derived in a similar manner, *i.e.*, by determining the difference between the voltage across the previous condenser and the charging voltage.

The condenser C_1 will charge to a value $\eta_1 E < E$ (as in a single-phase half-wave circuit) but the voltage on C_2 is $VC_2 = VC_1 + \eta E = \eta_1 E + \eta_2 E$. The charging voltage on C_3 is $Vc_3 = E(\eta_2 + \eta_3)$ and finally $V_{d.c.} = E\,(\eta_1 + \eta_2 + \cdots)$. Because of the interaction of the various stages on each other, the latter cannot be treated simply as a series of half-wave circuits and effective values r_e, X_e and R_e for feed resistance, condenser reactance and load resistance respectively must be introduced.

Mitchell shows that

$$r_e = \frac{Nr_e + r_a}{M}, \quad R_e = \frac{R_L}{NM} = \frac{V_c}{I_{st}}, \quad X_e = \frac{X}{M[(N^2 - M^2) + M]}$$

for the feed condensers and $X_e = \dfrac{X}{m(N - M + 1)\,(N + M)}$

This assumes $V_c = V_{d.c.}/N$ which is true when $\frac{X_e}{r_e}$ is small and when η is found to be constant for all the stages.

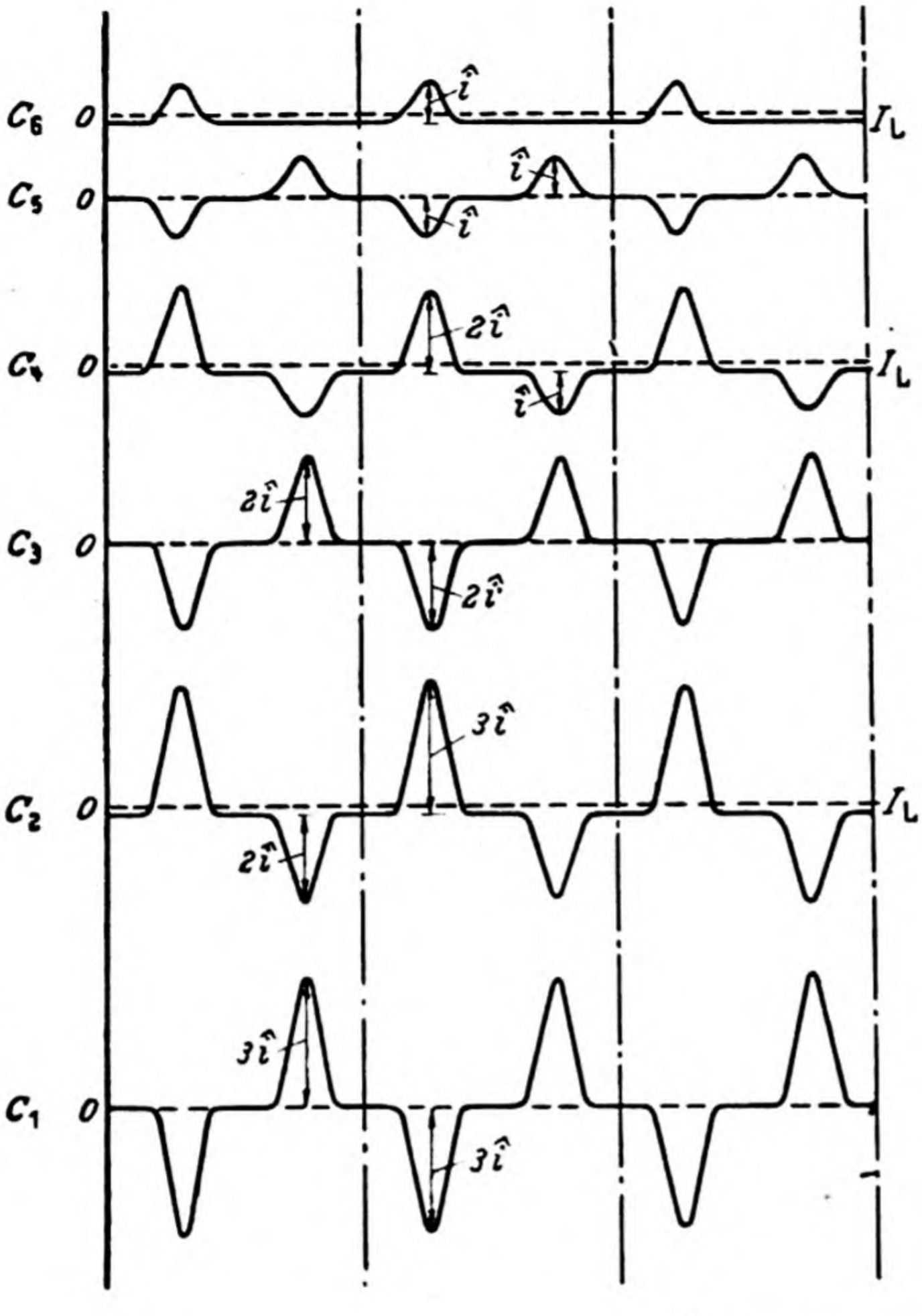

Figure 35. Current wave-forms in Mitchell's treatment of cascade d.c. sets (Mitchell[20], by courtesy, *Wireless Engr.*).

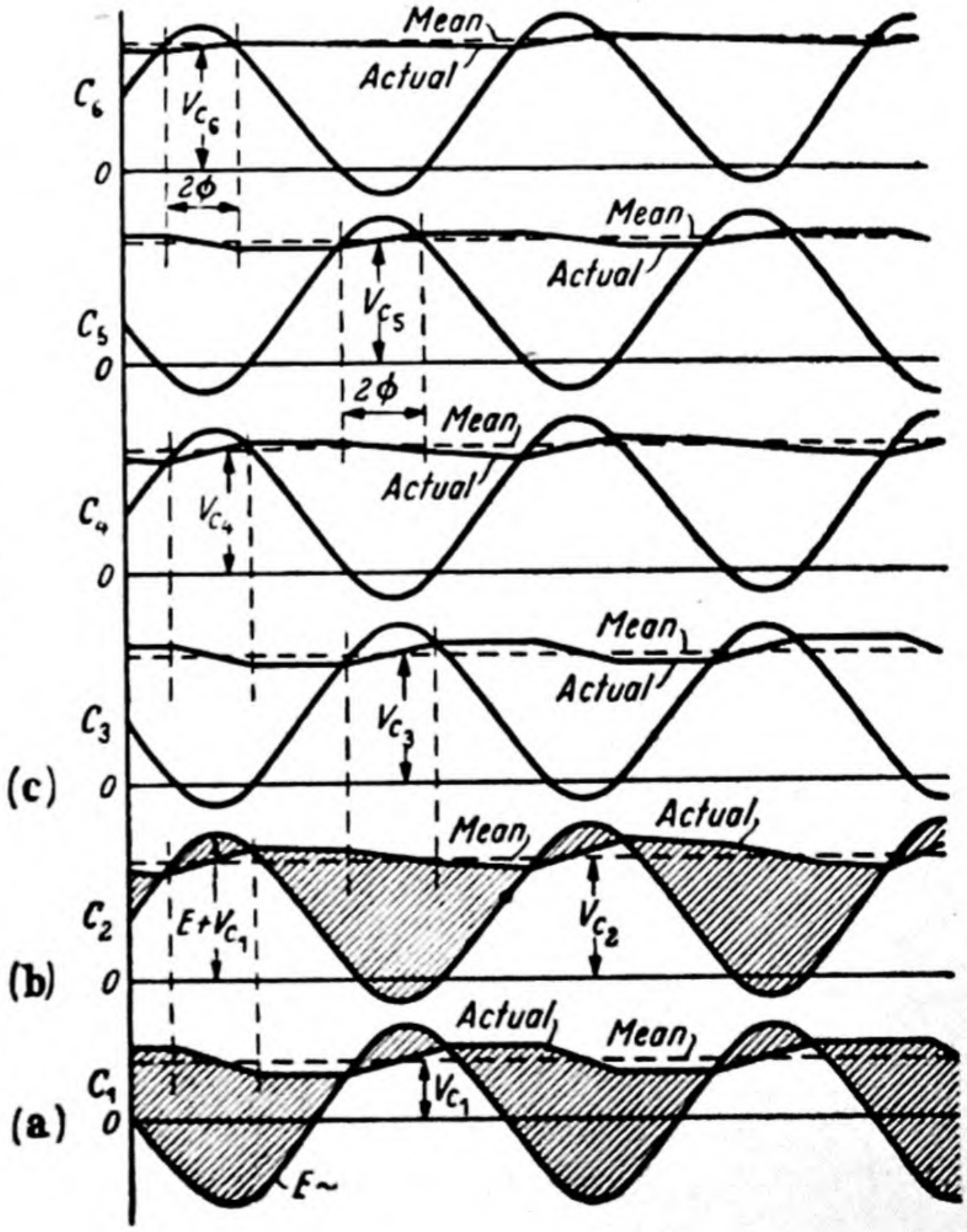

Figure 36. Voltage wave-forms in Mitchell's treatment of cascade d.c. sets (Mitchell[20], by courtesy, *Wireless Engr.*).

The symbols are defined as follows: I_{st} = stage current; $\mathcal{N}$ = number of stages; M = number of any particular stage counted from the output end of the generator; r_c = charging resistance, including the transformer a.c. resistance, common to all stages; r_a = rectifier impedance; R_L = load resistance; X = reactance of the condensers, taken as equal units, at the supply frequency; V_c = mean condenser d.c. voltage. The variation of η with $\frac{R_e}{r_e}$ for various values of X_e/r_e is given in *Figure 37*.

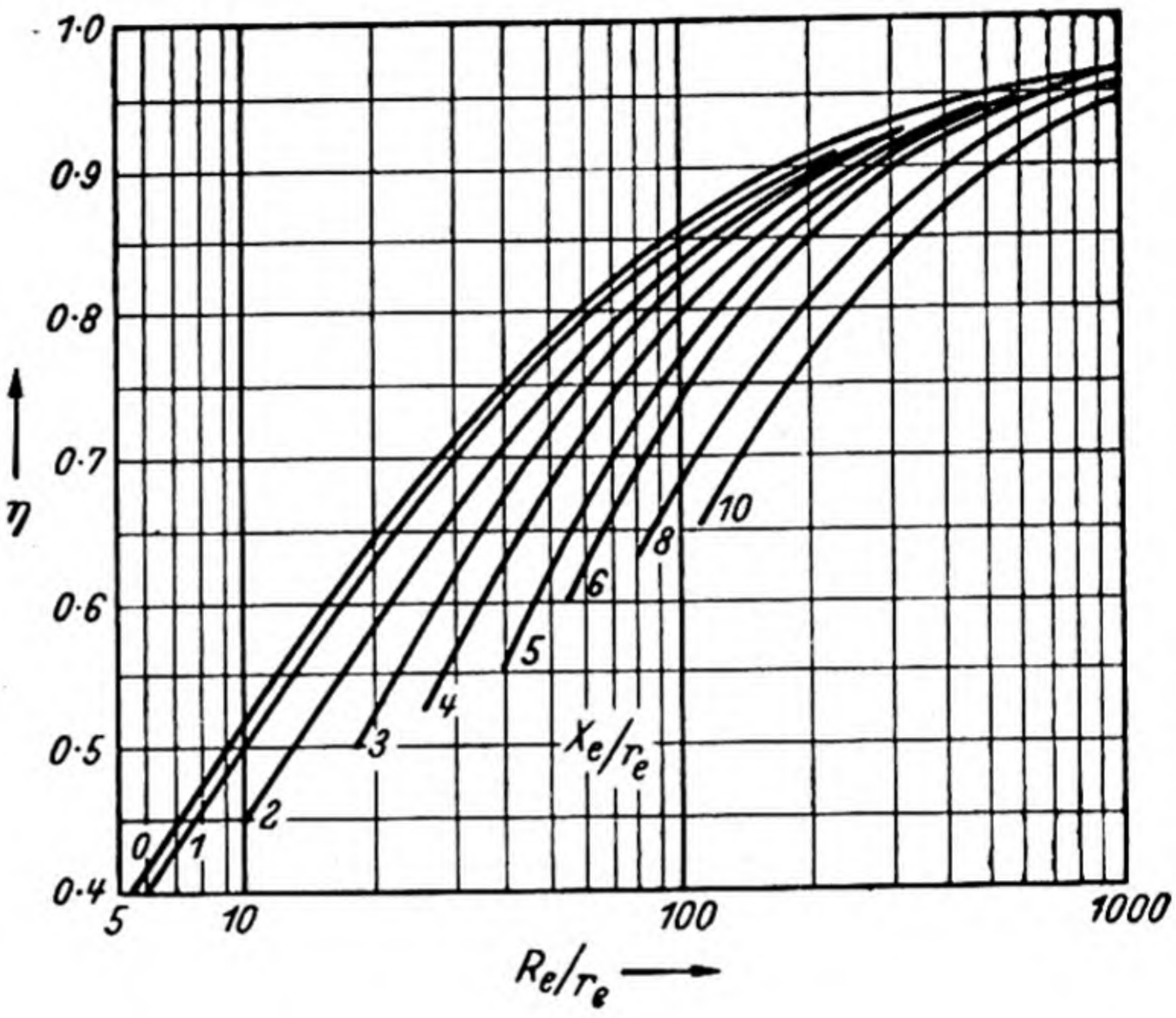

Figure 37. Illustrative of Mitchell's treatment of cascade d.c. generators (Mitchell[20], by courtesy, *Wireless Engr.*).

The overall ripple is :

$$\Sigma \frac{\delta V}{V_{d.c.}} = \pi \mathcal{N} \left[\frac{\mathcal{N}+1}{2} - \frac{\phi}{\pi} \right] \frac{X}{R_L}$$

and the percentage r.m.s. ripple is : $111\mathcal{N}(\mathcal{N}+1)\,X/R_L$ Here $\phi = \frac{\phi_1 + \phi_2}{2}$ = one-half of the angle of current flow per cycle if ϕ_1 and ϕ_2 respectively are the angles between (*1*) the point of commencement of charging current and peak input voltage and (*2*) the peak input voltage and current cut off. π/ϕ is plotted as a function of R_e/r_e in *Figure 38*. Other useful quantities are (*a*) the peak rectifier current $\hat{\imath}/I_L = \left(\frac{\text{peak charging current}}{\text{mean d.c. load current}}\right)$ (*b*) rectifier anode dissipation $D = 1{\cdot}24\ I^2{}_L r_a \pi/\phi$ (*c*) the r.m.s. current in the transformer secondary, which is the maximum condenser circulating current, *i.e.*, that in C_1, $I_{\text{r.m.s.}} = \mathcal{N} I_L \sqrt{2{\cdot}47\pi/\phi}$ (*d*) the dissipation in the feed resistance $D = I^2{}_{\text{r.m.s.}} \cdot r_c$ and, finally (*e*) the peak reverse voltage on the rectifiers $V_{P.R.} = E(1+\eta)$.

The above treatment is based on the assumption that the charging pulses through the valves are all in phase, but this is only true when the ripple is low. This covers the most useful practical cases satisfactorily,

but Mitchell discusses briefly the effect of phase differences between the charging pulses.

Mitchell[20] also deals with the circuit analysis in the case of multiple loading, *i.e.* when voltages are tapped off at points *h*, *f*, *d* and *a* in *Figure 34*, and with circuits in which the capacitances are unequal.

Bouwers[21] has given a slightly different treatment of the cascade generator, as follows :

If current I flows from d (*Figure 39*) the capacitors C_1, C_2 and C_3 are discharged and thus each capacitor voltage falls by It/c (c = capacitance, I = mean current flowing for time t). For a time $^1/f$ (f = a.c. supply frequency) the voltage drop is I/fc and the corresponding charge transfer is I/f. The end condition for stability is that each capacitor receives as much charge as it loses, and so the charge flowing

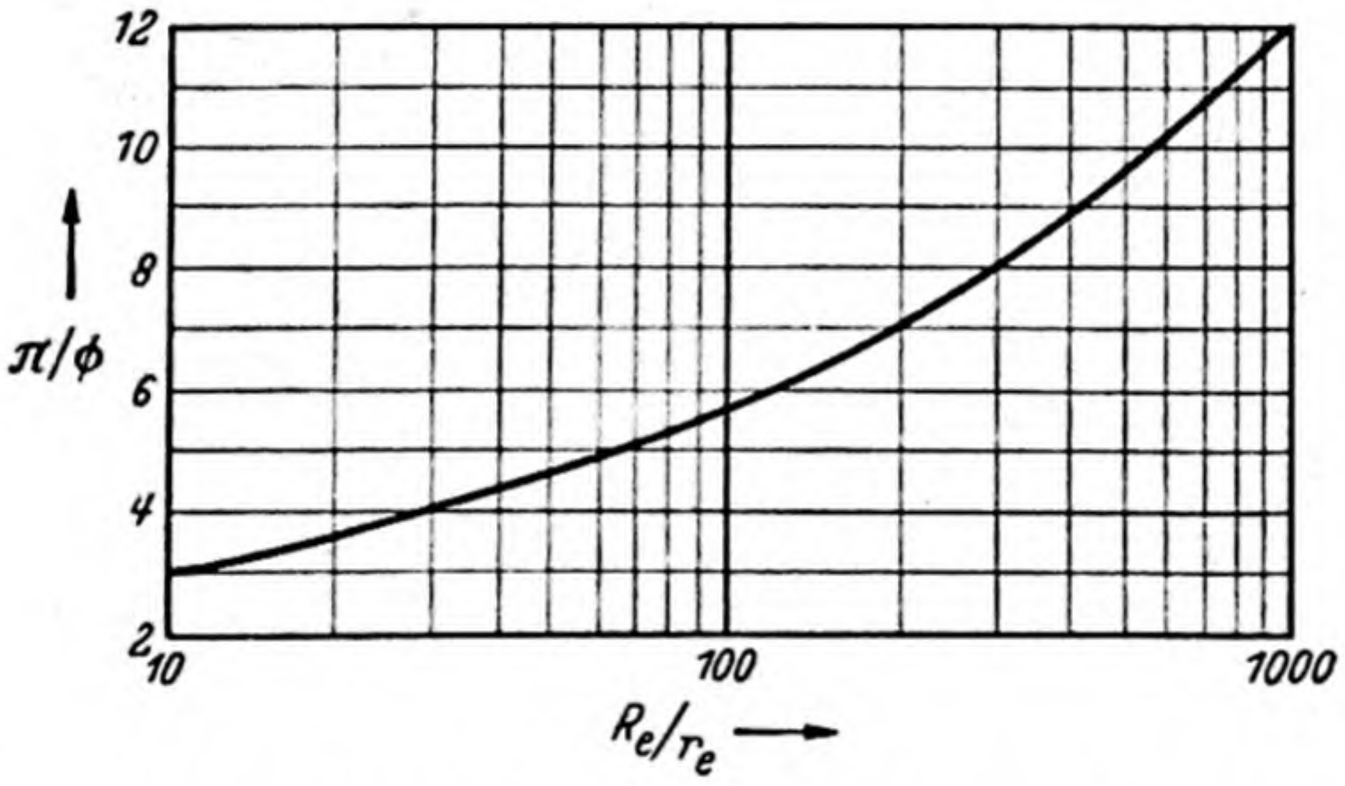

Figure 38. Illustrative of Mitchell's treatment of cascade d.c. generators (Mitchell[20], by courtesy, *Wireless Engr.*).

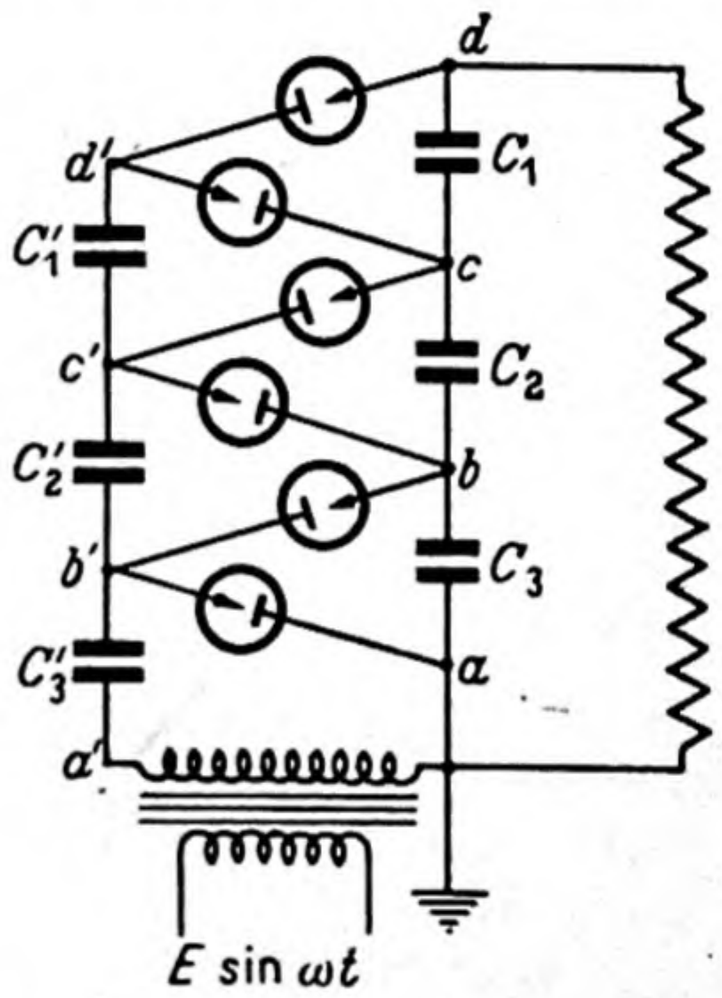

Figure 39. Bouwer's basic circuit for a cascade high voltage set (Bouwers[21], by courtesy, *Springer*).

from d must be replaced from C'_1 through the valve $d'd$, *i.e.* whilst d' is positive with respect to d. This occurs when a' has approximately the maximum positive voltage with respect to a. This charge is I/f and must, in the next half cycle, be taken from C_2 through the valve cd'. Thus the condenser C_2 loses, in one cycle, $2I/f$ through ad, and gains an equal quantity of charge from C'_1. Similarly, C'_2 loses $2I/f$ and C_3 and C'_3 are discharged and charged by $3I/f$.

The ripple on the output voltage is $\delta V = \frac{I}{f}\left(\frac{1}{C_1} + \frac{2}{C_2} + \frac{3}{C_3}\right)$. In general, for n stages where there are $2n$ capacitances (assumed equal) and $2n$ valves we have

$$\delta V = \frac{I}{fc}\ (1+2+3\ \cdots\ n) = \frac{I}{fc}\frac{n(n+1)}{2}$$

Thus the lowest condensers are responsible for most of the ripple and so it is desirable to increase the capacitances, going down the stack, appropriately. If the capacitance of the nth capacitor, counting

from the output end, is n times the value of the uppermost unit, *i.e.*, $C_n = nC$, then $\delta V = {}^{nI}/_{fc}$.

In addition to δV there is a voltage drop ΔV which is the difference between the theoretical no-load voltage and the on-load voltage. To find ΔV refer to *Figure 39* where all the capacitances are equal. Now C_3 is not charged up to the full voltage $2E$ but only to $(2E - 3I/fc)$ because of the charge given up through C'_3 in one cycle, which gives a voltage drop of $3I/fc$. The voltage drop in the transformer is assumed to be negligible. Thus C'_2 is only charged to the voltage $(2E - 3I/fc) - 3I/fc$ since the reduction in the voltage across C_3 again is $3I/fc$. C_2 attains the voltage $2E - \left(\frac{3I + 3I + 2I}{fc}\right)$. In general the respective decreases in the stage voltages for each stage in a stack of n stages are as follows.

$$\begin{aligned}
\Delta V_n &= \frac{I}{fc} n \\
\Delta V_{n-1} &= \frac{I}{fc} \left\{ 2n + (n-1) \right\} \\
\Delta V_1 &= \frac{I}{fc} \left\{ 2n + 2(n-1) + \cdots 2 \cdot 2 + 1 \right\}
\end{aligned}$$

so by summation:— $\Delta V = \frac{I}{fc} \Sigma^n_1 \, n\,(2n-1)$

and $$\Delta V = \frac{I}{fc} ({}^2/_3 n^3 + \tfrac{1}{2} n^2 - \tfrac{1}{6} n).$$

Thus the lowest capacitors contribute most to the total ΔV and so again it is advantageous to increase their capacitance in suitable steps. The extent to which this procedure should be followed depends on whether a minimum ripple or a minimum voltage drop is desirable, *i.e.* whether $(C_1 + C_2 + \cdots C_n)$ has to be small or whether the series capacitance $\frac{1}{\frac{1}{C_1} + \frac{1}{C_2} + \cdots \frac{1}{C_n}}$ has to be small, and also depends on the arrangement of the stack.

A doubling of C'_n (the lowest condenser, *i.e.* C'_3 in *Figure 39*) is easily undertaken in each case since this capacitor has to withstand only one-half of the voltage across the other condensers, *i.e.* E instead of $2E$. Considering this case in more detail, the voltage drops $\Delta V_1 \ldots \Delta V_n$ decrease progressively by the amount $(0{\cdot}5nI/fc)$ and also the voltage drop ΔV decreases, stage by stage, by an amount $(0{\cdot}5n^2 I/fc)$. Thus $\Delta V = (\frac{2}{3}n^3 - \frac{1}{6}n)\ {}^I/_{fc}$ or, since the second term in brackets is negligible when $n \geqslant 3$ we have $\Delta V = {}^2/_3 \cdot n^3 I/fc$ . . . . (1.1)

The total voltage varies between the values

$$V_{\max} = 2nE - \Delta V \qquad \ldots\ (1.2)$$

and $V_{\min} = 2nE - \Delta V - \delta V$ consequently $\delta V \sim {}^1/_n \Delta V$.

As the number of stages (n) is increased, the maximum voltage rises initially proportionally to n but the voltage cannot be increased without limit since for large values of n ΔV increases too rapidly. The highest voltage is obtained with a number of stages determined

by differentiation of Equation (1.2) with respect to n after substitution from Equation (1.1) and putting $\frac{dV_{\max}}{dn} = 0$. Thus

$$n_{\text{optimum}} = \sqrt{\frac{Efc}{I}}$$

For a generator having $E = 110$ kV, with $f = 200$ c/s and $C = 0{\cdot}02\ \mu$F and for a current of 4 mA, $n_{\text{optimum}} \doteqdot 11$.

It is desirable to use a value of n considerably less than the optimum since the dimensions, and also the voltage variation for varying load,

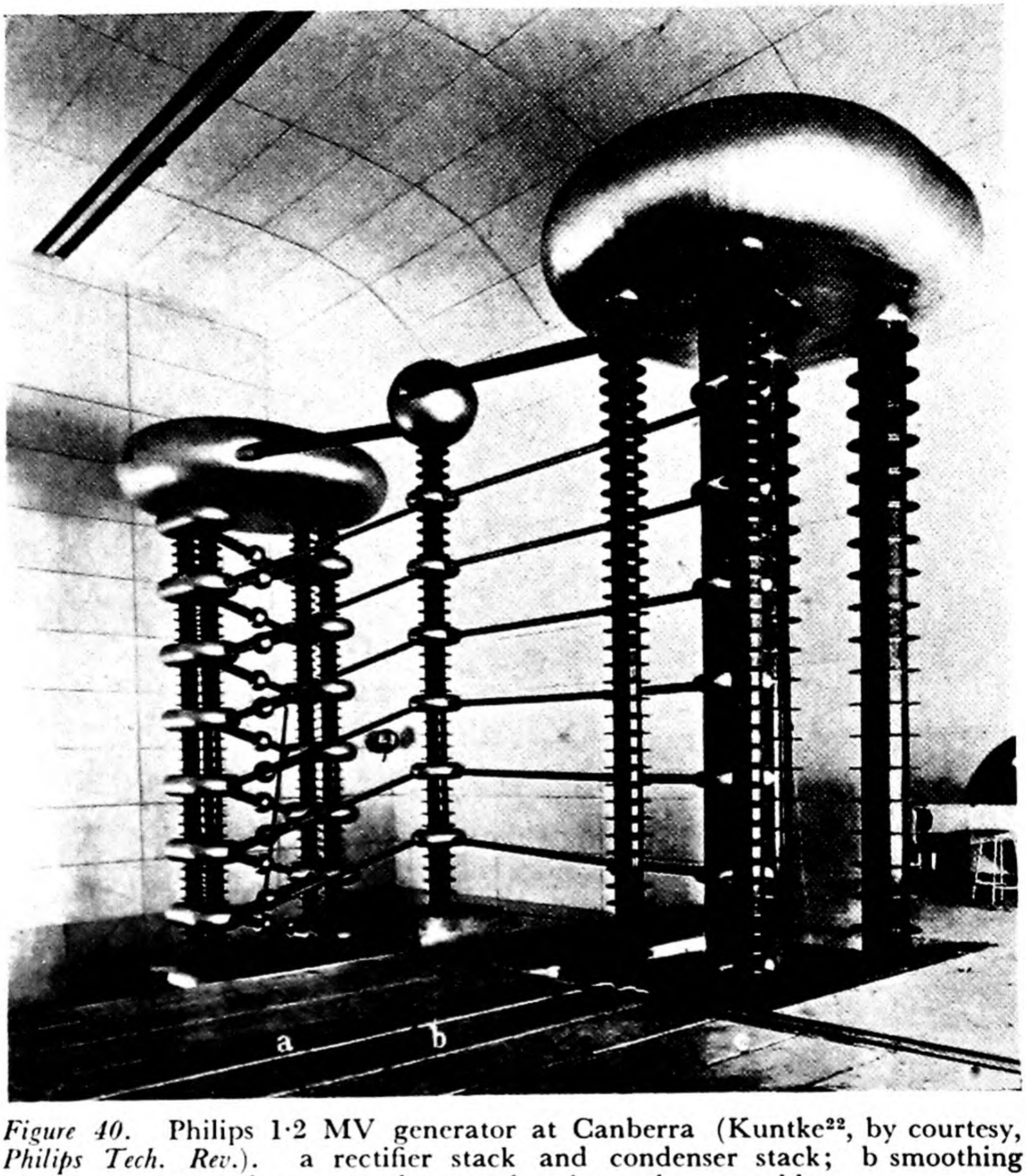

Figure 40. Philips 1·2 MV generator at Canberra (Kuntke[22], by courtesy, *Philips Tech. Rev.*). a rectifier stack and condenser stack; b smoothing condenser; and c acceleration tube assembly.

increases more than linearly with n for a very small gain in voltage. From Equation (1.1) even with $n = 8$ the voltage drop per mA in the above numerical example is $\Delta V \doteqdot 85$ kV.

Now if the capacitances are increased, going down the stage, according to the relation $C_n = nC$ then the voltage drop is

$$\Delta V = \frac{I}{fc}\,(1 + 3 + 5 \cdots 2(n-1) + 1) = \frac{n^2 i}{fc} \quad \ldots\ (1.3)$$

and the optimal number of stages is $n_{\text{optimum}} = Efc/I$. In this case,

if $E = 120$ kV, $f = 200$ c/s, $C = 0{\cdot}005\ \mu$F and $I = 4$ mA we find $n_{\text{optimum}} = 27$. The general rule, that the practical number of stages is less than this value, applies even more so here. Even for $n = 10$ we find from Equation (1.3) that the voltage drop per mA is $\Delta V = 100$ kV. The corresponding no-load voltage for 10 stages is 2,400 kV and by employing modern techniques the total stack height would be about 6 m. It can be seen from Equations (1.1) and (1.2) that ΔV can be made smaller by increasing f, but an upper limit is set to this by the high voltage appearing across inductances and the high capacity currents, which may be undesirable. This problem is made worse by the fact that the charging current flows only for a fraction of a half-cycle so that the effective frequency is a multiple of f.

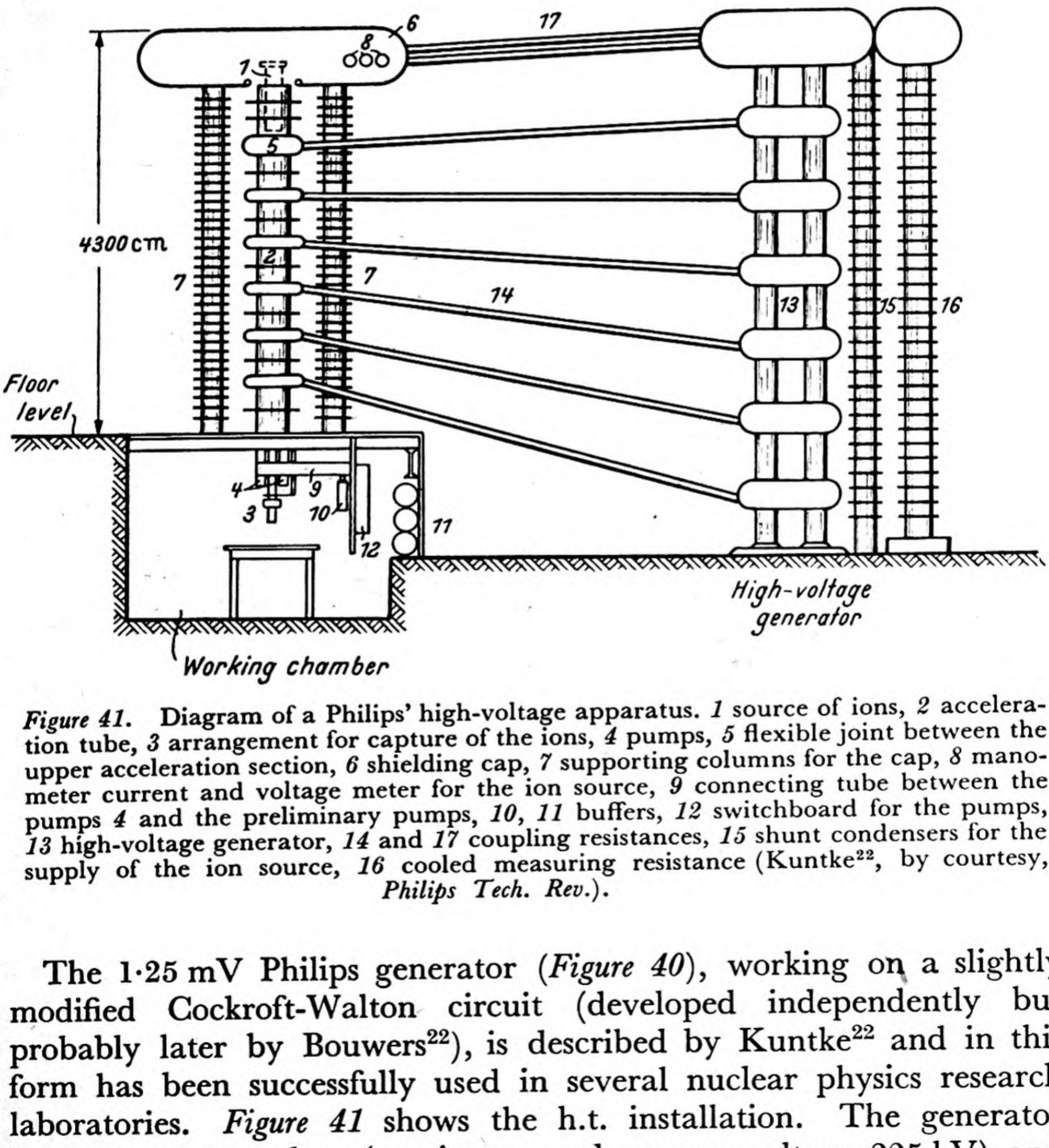

Figure 41. Diagram of a Philips' high-voltage apparatus. *1* source of ions, *2* acceleration tube, *3* arrangement for capture of the ions, *4* pumps, *5* flexible joint between the upper acceleration section, *6* shielding cap, *7* supporting columns for the cap, *8* manometer current and voltage meter for the ion source, *9* connecting tube between the pumps *4* and the preliminary pumps, *10*, *11* buffers, *12* switchboard for the pumps, *13* high-voltage generator, *14* and *17* coupling resistances, *15* shunt condensers for the supply of the ion source, *16* cooled measuring resistance (Kuntke[22], by courtesy, *Philips Tech. Rev.*).

The 1·25 mV Philips generator (*Figure 40*), working on a slightly modified Cockroft-Walton circuit (developed independently but probably later by Bouwers[22]), is described by Kuntke[22] and in this form has been successfully used in several nuclear physics research laboratories. *Figure 41* shows the h.t. installation. The generator incorporates 12 valves (maximum peak reverse voltage 225 kV) and

12 condensers (*i.e.* 6 stages). The capacitance values are as follows: C_1, C'_1, C_2, C'_2, C_3, C'_3, $= 0{\cdot}01\ \mu$F with 240 kV maximum d.c. voltage rating, C_4, C'_4, C_5, C'_5, $C_6 = 0{\cdot}02\ \mu$F with the same d.c. rating and $C'_6 = 0{\cdot}04\ \mu$F with one-half of this rating. The input voltage, 120 kV peak, is delivered at 200 c/s from a transformer and the loss in voltage in the generator (see the theoretical treatment given above) is thus reduced below that for 50 c/s. The transformer primary is supplied from a motor generator, the excitation of which is controlled in order to alter the d.c. h.t. output from the cascade generator. The loss in voltage ΔV which can be calculated as shown above, is about 40 kV/mA and the ripple δV is 7 kV/mA.

Modern practice is to connect a smoothing condenser consisting of, say, one $0{\cdot}018\ \mu$F unit per stage, to a total number of condensers equal to the number of stages in a stack across the output terminals of the generator. In this way the ripple may be reduced below the value given in the theoretical treatment above.

At the maximum output current of 4 mA the h.t. output voltage is 1·1 MV. The valve cathodes are heated with power at 500 kc/s from a high frequency generator of 250 W rating, and for this purpose a heating current of about 0·7 A passes up through the condensers (*see* page 34). The highest valve and the h.t. transformer are by-passed by a series resonant circuit which passes the h.f. heater current, and the valve heaters are fed from small transformers placed in the shields. The valves are described in Chapter 11. Another account of the same generator has been given by Bouwers and Kuntke[17].

A novel proposal for accelerating charged particles using a d.c. generator of the above type as h.t. source has recently been made by Alvarez[23] following a somewhat similar system due to Dempster[24]. Alvarez suggests that if negative hydrogen ions are accelerated to an electrode at $+V$ volts above ground potential and have two electrons removed by passage through a thin foil, in which energy loss and scattering are negligible, so that they can then be accelerated as positive ions back to ground, then the effective voltage of the accelerator would be doubled. Alvarez states that such a generator, for 4 MeV, is now (May, 1951) being designed in Berkeley.

The success which the modified Cockroft-Walton type of generator as built by Philips has achieved is described for example by Burcham[25] who has given a short history of the Philips' 1·25 MV generator installed in 1937 in the Cavendish Laboratory. A total running time of 5,700 hours has been recorded since installation, and an overall figure of 100 hours' operation per fault including minor and major break-downs (the latter being rare) has been obtained. Burcham stresses the desirability of obtaining such equipment from the electrical industry, where possible.

A recent account of the subsidiary apparatus (for nuclear physics) needed with the h.t. generator is given by HEYN and BOUWERS[26] following the earlier descriptions of the generator by Kuntke[27] and others. The ion source which is of the OLIPHANT type[28], now largely superseded by that of THONEMANN[29], needs an a.c. supply of 50 kV for a rectifier set in the h.t. terminal (at a potential of +1·25 MV with respect to earth), and this reaches the terminal through the two condensers (15 in *Figure 41*) and the resistance 17 (also in *Figure 41*).

Reference to the use of a 450 kV modified Cockroft-Walton set for a high-voltage electron microscope is made by VAN DORSTEN, OOSTERKAMP and LE POOLE[30]. In the description of the generator it is mentioned that the usual Philips' mercury vapour valves are replaced by vacuum rectifiers to eliminate possible instability in the h.t. due to variations in the firing voltages of the vapour-filled tubes.

The development of these Philips' circuits from the basic Greinacher circuit is discussed by GRADSTEIN[31] who also gives some details of the Philips' technique[70] of heating the rectifier valve filaments, by the passage up the rectifier stack of h.f. current (750 kc/s, 0·7 A) as shown in *Figure 42*). Here, condensers C_1–C_4 allow the h.f. current to pass, but block the d.c. The h.f. supply is connected across ab_1. The resistances R (20,000 Ω) limit the initial current through the valves and serve also to prevent the valves from acting as shunts for the h.f. current which is bypassed with C' and C'' from the transformer and the last valve respectively. L tunes the circuit to resonance at the h.f. and thus reduces the impedance of the h.f. circuit to a minimum.

A d.c. generator, for about 900 kV, and consisting of cascaded Greinacher rectifier circuits, was described in 1940 by BJERGE, BROSTRÖM, KOCH and LAURITSEN[32]. The original generator built by Koch and Sterzel is arranged as in *Figure 43*, where the h.t. transformers A_1–A_4, rated at 125 kV peak, are supplied by the specially insulated cascaded transformers B_1–B_4. The condensers have each a capacitance of about 0·22 F, and the Siemens-Reiniger rectifier tubes are designed for 320 kV peak reverse. The rectifier filaments are supplied by generators driven from ground through insulated shafts.

In the circuit of *Figure 43*, a_1 charges up to 125 kV through A_1 and V_1, whilst b_1 oscillates between 0 and 250 kV, charging C_1 through V_1 to 250 kV. In this way the potentials of points a_1 to c_4 on the condenser column increase to a maximum of 1,000 kV. The potential, measured with a $10^9\Omega$ oil-cooled resistance, can be varied in steps of about 5 kV by means of a variable ratio transformer across the mains supply.

It is of interest to note that this generator can be used to deliver a.c. by removal of the rectifiers, and by making the appropriate connections. Further, it can be modified to make a 2 MV impulse generator, using the Marx circuit (*see* Chapter 4).

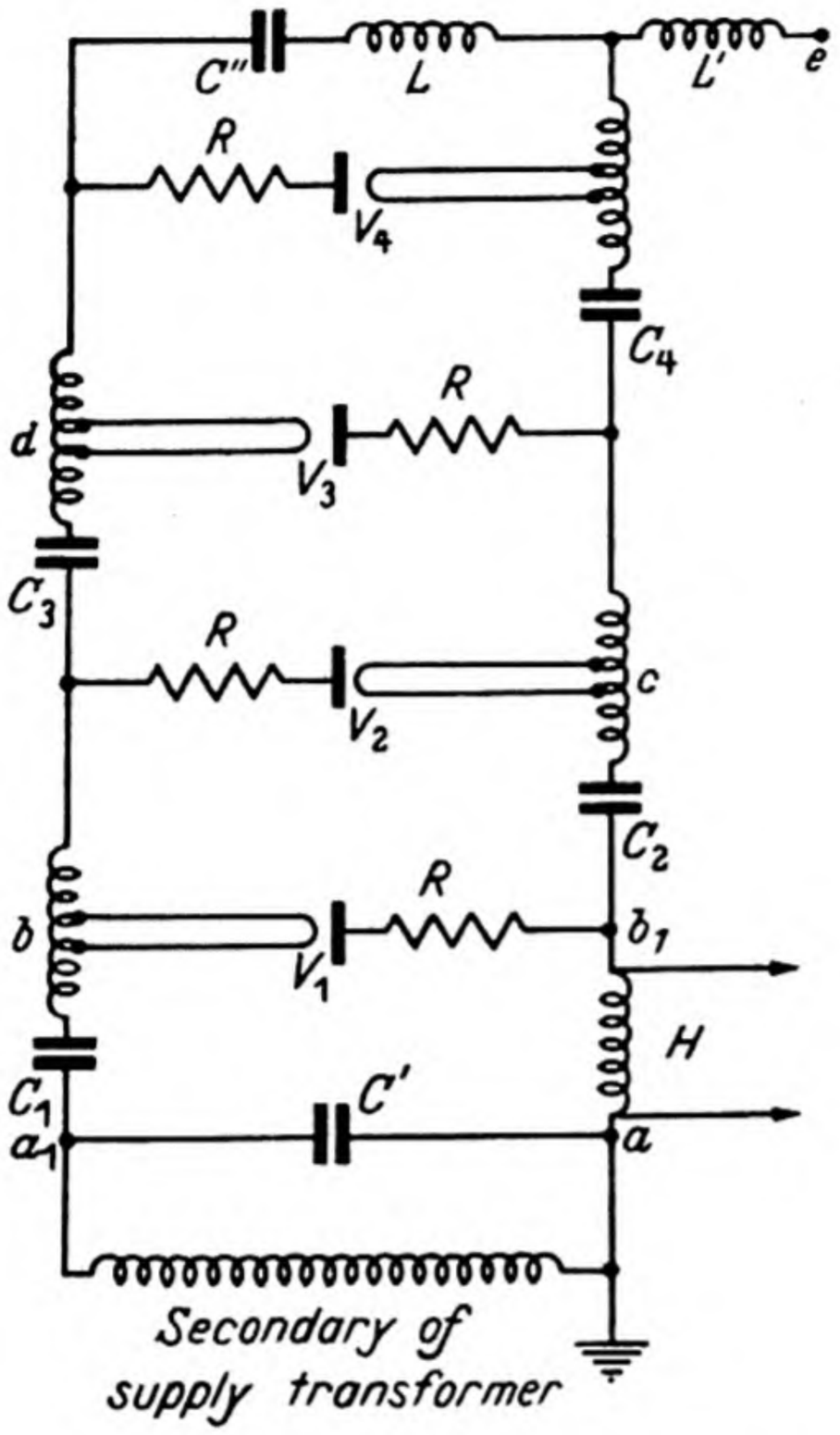

Figure 42. Circuit diagram of a cascade d.c. set, with supplementary high-frequency heating. Through the high-tension circuit there also flows a 750 kc/s current of 0·7 A; by means of specially-designed air-core transformers (at *b*, *c*, *d* and above C_1), the requisite value of 3·5 A for heating the cathodes is obtained. The functions of the supplementary components (capacities, inductances and resistances) are explained in the text (Gradstein[31], by courtesy, *Philips Tech. Rev.*).

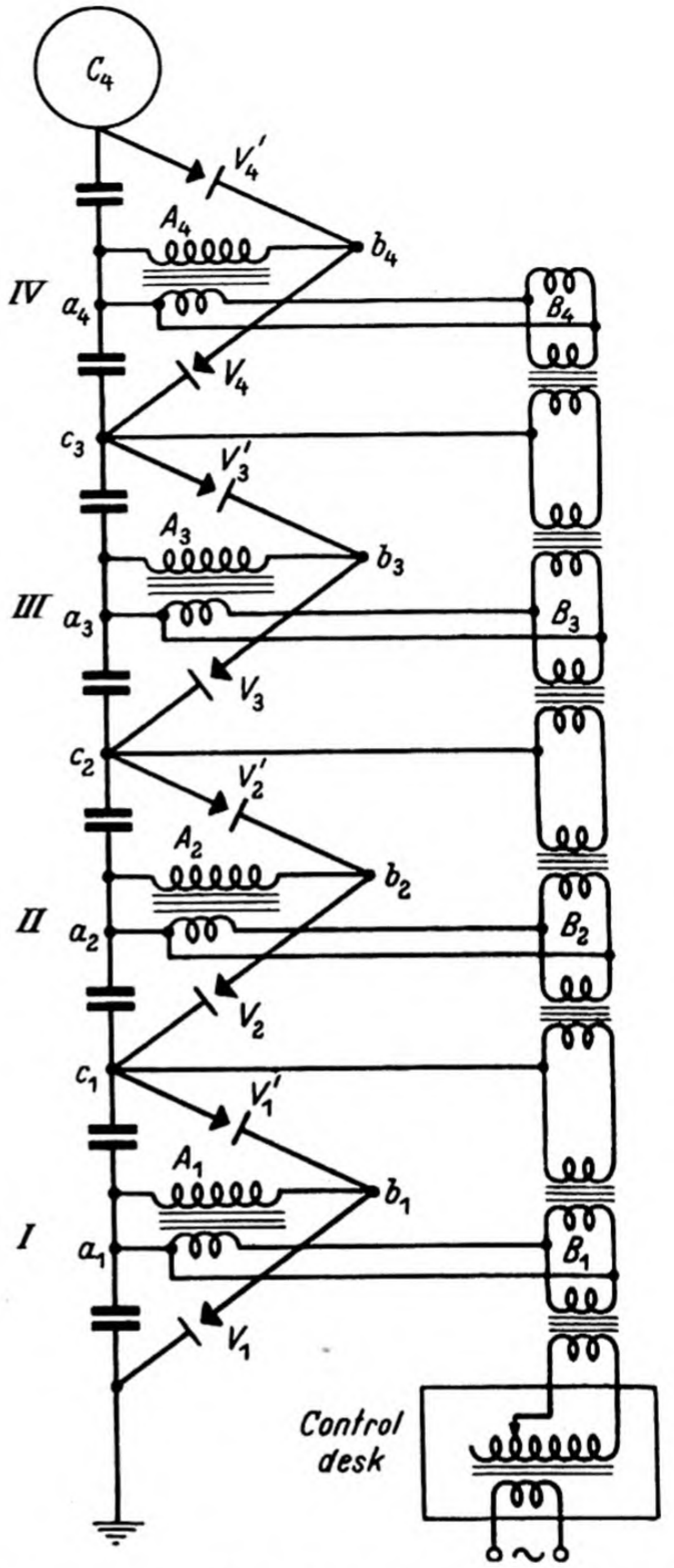

Figure 43. Electrical circuit of a high-tension generator showing four Greinacher sections (I–IV) mounted one on top of the other. A_n: High-tension transformers. B_n: Feeding transformers. V_n: Rectifier tubes (Bjerge *et al*[32], by courtesy, *Det. Kgl. Danske Videns Selskab.*).

The sealed-off rectifiers were later replaced, because of their liability to puncture and the expense of replacements, by a stack of eight continuously-evacuated rectifiers similar to those made by Metropolitan-Vickers (*see* pages 22 and 24). The rectifier valve anodes are made with hemispherical polished ends, to minimize field emission. The filaments are each arranged inside shielding cups, for the same reason. The internal resistance of the rectifiers is ~30–60 kΩ and at 9·5 A filament current provides a saturation current of ~100 mA.

The generator circuit of *Figure 43* has also been modified to include protective water resistances in the transformer connections and to provide spark-gap protection of the transformers.

CASCADED RECTIFIER CIRCUITS USING METAL RECTIFIERS

The use of small selenium rectifiers in the generation of high-voltage d.c. has been studied by ARNOLD[33] who built a multi-stage generator, following the basic Cockroft-Walton circuit, for 500 kV. It is clear that the replacement of valves, with their heater transformers, by disc type rectifiers (in this case the G.E. type 6RS5K72) can result in economy. Some details of the construction and characteristics of the small selenium rectifiers made by Philips are given by VAN AMSTEL[34]; these units may be cascaded to give very compact h.t. sources. The circuit[33] is shown schematically in *Figure 44*; 44 condensers are used in 22 stages, and each condenser is rated at 1 μF, 25 kV. Each rectifier assembly consists of 5 rectifier units in series, thus withstanding 25 kV

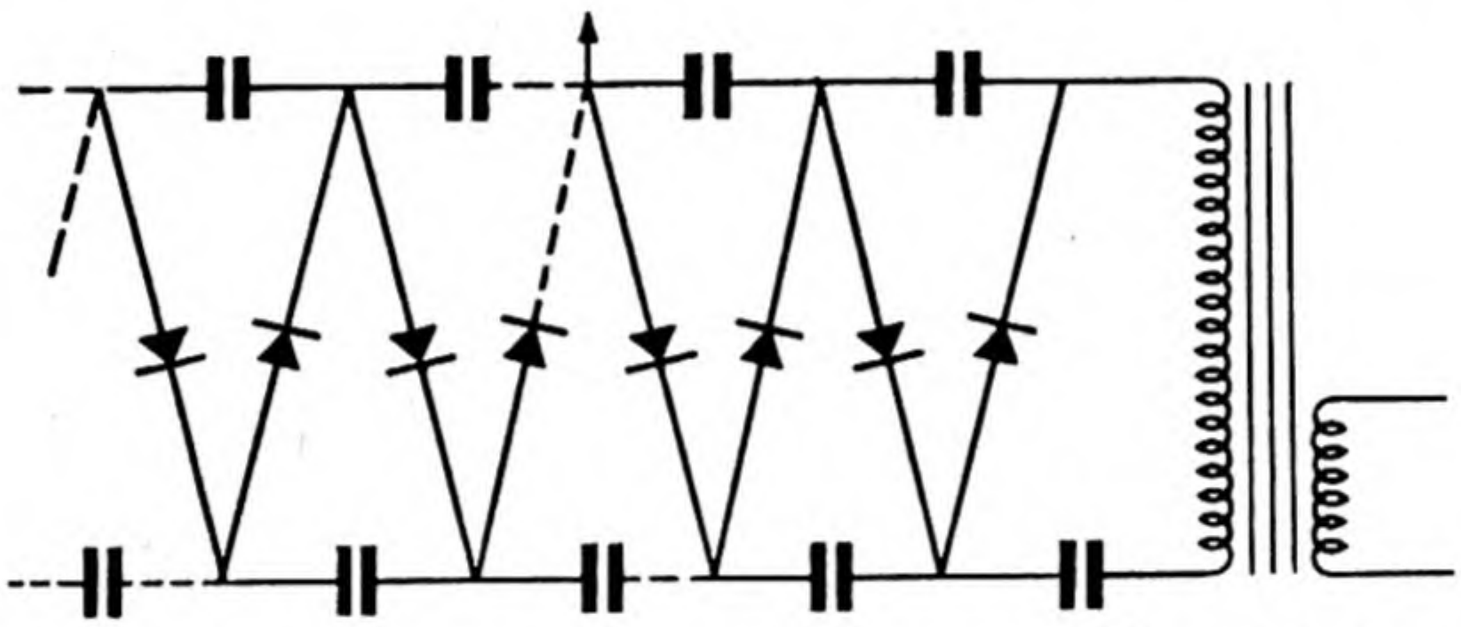

Figure 44. Voltage multiplier circuits using selenium rectifiers. The circuit below the arrow represents the usual quadrupler or two-stage multiplier (van Amstel[34], by courtesy, *Philips Tech. Rev.*).

and with a current rating of 2·5 mA. The input (750 c/s) transformer secondary is insulated for 50 kV and gives an output of 10 kV; the primary is excited from a 10 kVA, 750 c/s, alternator. The output voltage V may be expressed as (*see* pages 28–31):

$$V = 2nE - I\left[\frac{2n^3}{3} + \frac{n^2}{2} - \frac{n}{6}\right] / fc$$

where C is the capacitance of each condenser, I is the load current, f is the supply frequency and E is the peak input voltage. For large n, and in this case $n = 22$, the terms in n^2 and n may be neglected. Since $C = 10^{-6}$F, $f = 750$ c/s and $E = 12{\cdot}5$ kV for maximum input we have

$$E = (550 - 9{\cdot}5I) \text{ kV}$$

if I is in mA. Then the regulation is $9{\cdot}5I$ kV or about 25 kV/mA. By finding $\frac{dV}{dn}$, the maximum output voltage for 2·5 mA load, $C = 1\ \mu$F and $f = 750$ c/s, is obtained for $n = 61$. Also, the peak-to-peak ripple v is given by $v = I\left[\frac{n^2}{2} + \frac{n}{2}\right] / fc$. At full load for the above component values $v = 840$ V. Arnold points out that the ripple and voltage drop can be reduced by grading the capacitance values

along the stack (*see* pages 28–31) but it is convenient to use condenser units of the same size.

The condensers are mounted in 4 stacks, each containing 11 condensers, with each of the latter arranged in an aluminium cylinder 18 in. in diameter, and 9 in. high. Adjacent cylinders are insulated from each other with a 26 in. disc of Textolite insulation, 0·4 in. thick, and later with a $\frac{3}{8}$ in. annealed glass plate on which a 28 in. corona shield is fixed. The h.t. terminal of each condenser is connected, by means of an aluminium tube, to the corona shield of the appropriate condenser in the adjoining stack. The selenium rectifiers, joined in 25 kV units, as mentioned above, are fixed inside Textolite tubes, 0·5 in. internal diameter, by means of springs, and the rectifier units are attached by means of fuse clips to the aluminium tubes. Care is necessary to avoid bad contacts, with subsequent arcing between the individual rectifier discs. All four stacks are insulated from ground to allow a bias voltage, to compensate for h.t. drift, to be applied to the lower ends of the stacks. A large corona shield is mounted on the h.t. end of the stack. The generator has an overall height of 12 ft.

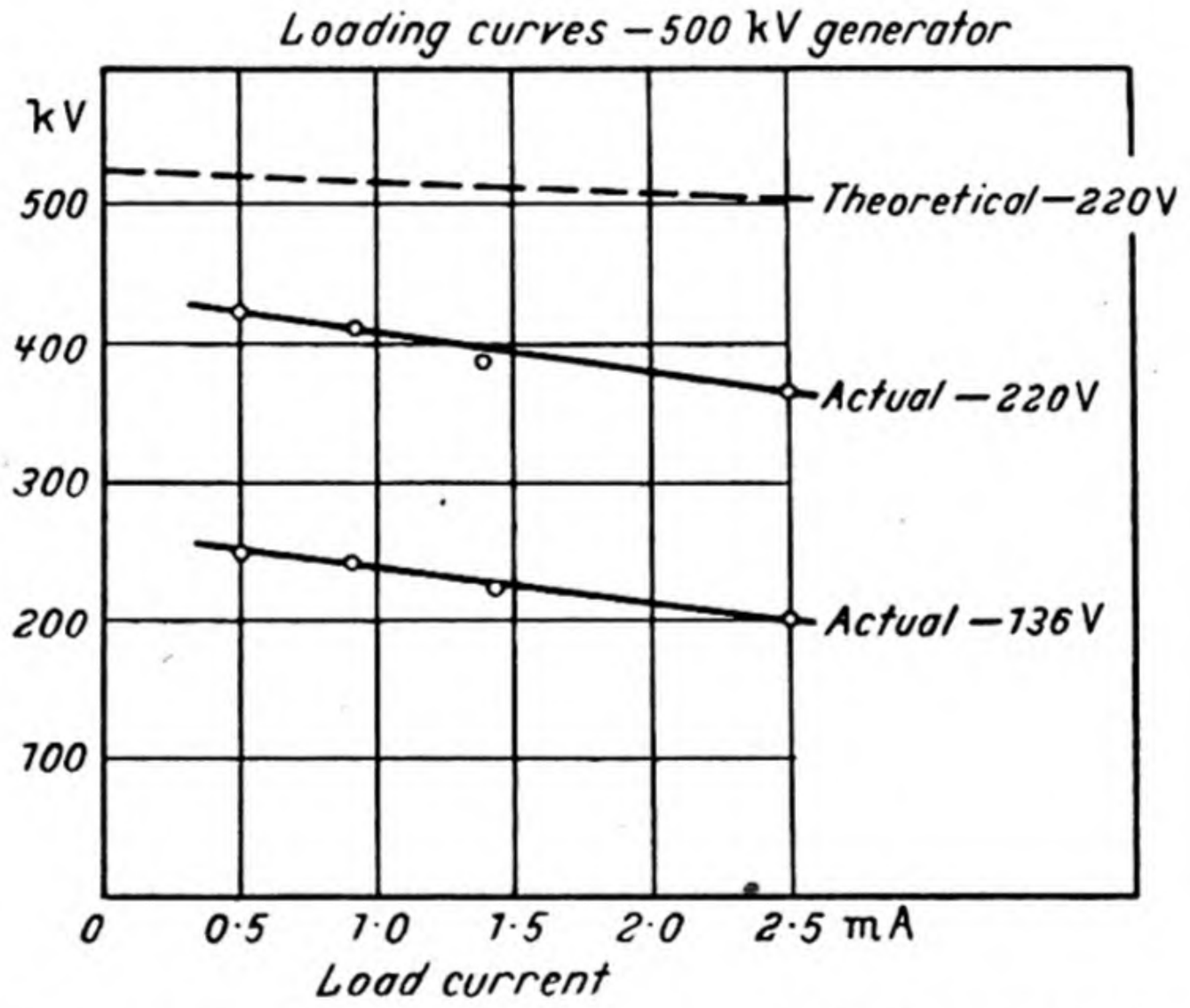

Figure 45. Output voltage vs. load curves for Arnold's[33] d.c. generator. The curves are designated by the corresponding input voltage to the supply transformer (by courtesy, *Rev. Sci. Instrum.*).

Load characteristics, shown in *Figure 45* were taken by means of a liquid resistance (NaCl/water). The output voltage was measured by the deflection of a proton beam at the lower end of an acceleration tube connected to the generator. The curves show a voltage drop, on load, of about 25 kV/mA. The generator gave an efficiency of about 7 per cent. at 350 kV, 0·5 mA. The h.t. ripple was measured with a cathode-ray oscillograph connected across a suitable resistance connected in series with the liquid load resistance.

BOUWERS and HEYN[63] describe a small d.c. generator giving 1·2 kV for Geiger counter work, in which 20 small selenium rectifiers[64] are used, connected in a cascade circuit.

ELECTROSTATIC GENERATORS USING BELTS

Earlier forms of electrostatic generators, giving high voltages, such as the Wimshurst machine, the Kelvin water dropper and many other similar devices have been largely if not entirely replaced by greatly improved devices. Amongst these the Van de Graaff generator is pre-eminent but the 'dust generators' of PAUTHENIER, MOREAU-HANOT, MORAND *et al* (see page 53) have also been successful. Van de Graaff generators, working up to 5 or 6 MeV d.c., are now in use in several nuclear physics laboratories.

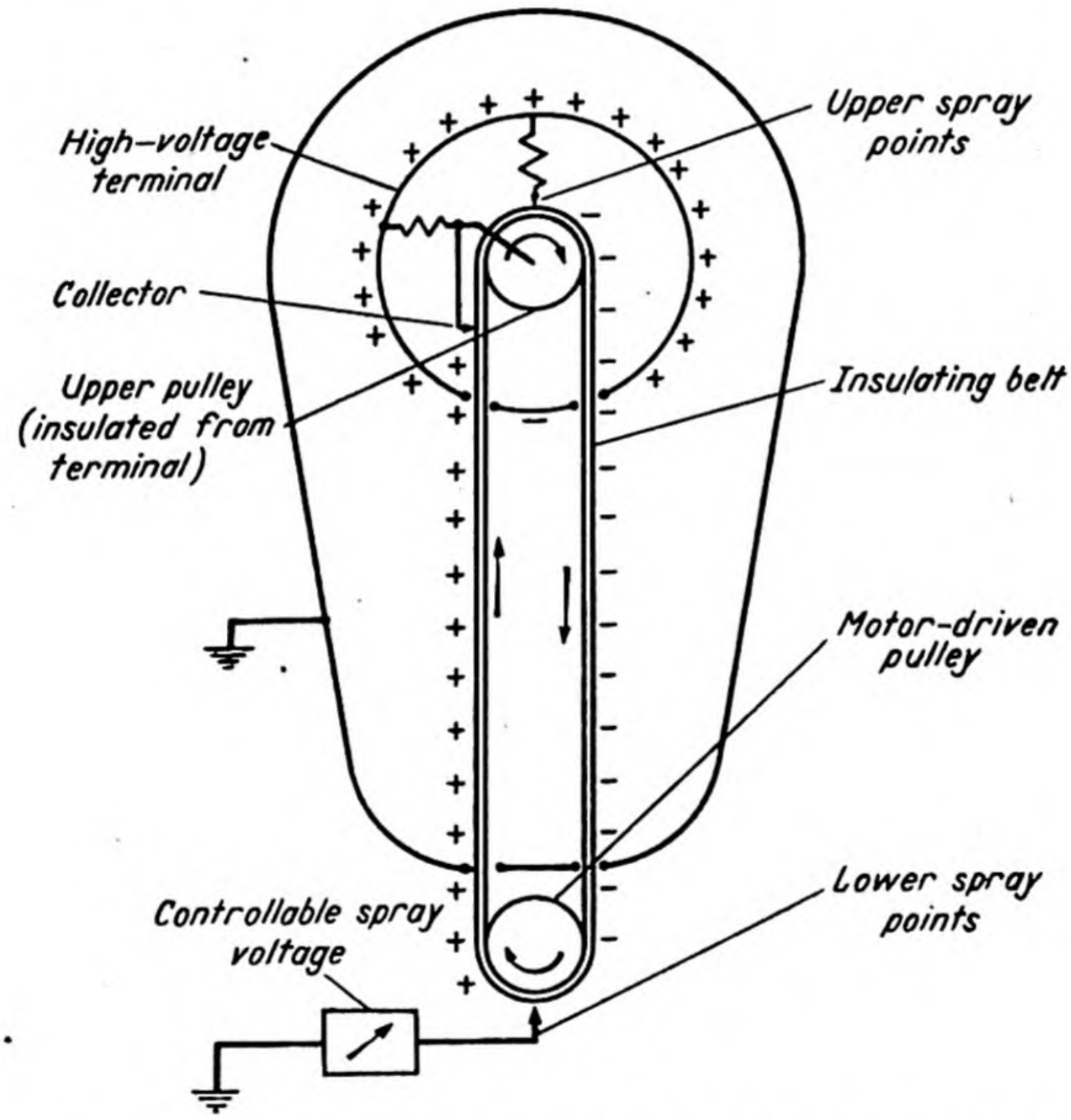

Figure 46. Schematic diagram of electrostatic belt generator (Van de Graaff *et al*[35], by courtesy, *Rep. Prog. Phys.*).

Recent review articles on Van de Graaff generators are by VAN DE GRAAFF, TRUMP and BUECHNER[35], SHIRE[36] and, most recently, FORTESCUE[37].

The basic mechanism of a Van de Graaff generator is illustrated in *Figure 46*. This shows a generator enclosed in an earthed metal tank, which is the usual modern technique. The principle of operation is the same as with the original open-air machines. Charge is sprayed on to an insulating moving belt from corona points relatively

near (perhaps 10–100 kV from) earth potential and is removed from the belt by discharging points connected to the inside of an insulated metal electrode through which the belt passes. At any instant the terminal potential is $V=Q/C$ where Q is the stored charge and C the capacitance of the high-voltage electrode to earth. The terminal potential rises at the rate $\frac{dV}{dt}={}^{I}/_{C}$ where I is the net charging current to the terminal and dV/dt may be ~ 1 MV/sec. The high-voltage terminal is a Faraday cage and its final potential would be infinite in the absence of any mechanism of charge loss. In practice equilibrium is established at a terminal potential which is such that the charging current equals the discharge current which will include corona losses, leakage currents, and load currents, due to potential dividers, X-ray or ion tubes.

The terminal shape must be such that the surface gradient of electric field is always less than the corona onset field or discharges will occur. In practice it is almost impossible (at a few MV) to avoid corona entirely. An isolated sphere is the most favourable electrode shape[35] and will maintain a voltage Er (r = sphere radius, E = breakdown or corona onset field in the surrounding medium). Thus for air at N.T.P., $E \simeq 30$ kV/cm., and with a 1 m diam. sphere the voltage would be about 1·5 MeV. In practice, because of the need to accommodate the belt system, tube, *etc.* the h.t. electrode cannot be spherical and the aperture should have re-entrant edges (as in Smee's generator, see *Figure 52*[38]). Further, the field distribution between the h.t. terminal and ground should be made as uniform as possible, to avoid local break-down at too low a voltage, by means of suitable electrode systems, some of which will be described below. The moving belt system also distorts the electric field and suitable potential grading rings are usually mounted round it.

Returning to *Figure 46*, charge is sprayed on to the belt by the lower spray points, usually a row of needles connected to a d.c. set so that a corona discharge between the points and the belt surface is maintained. A suitable point system near the point of entry into the terminal removes this charge from the belt in the h.t. terminal, thus charging the latter. A second point system, excited by a rectifier set inside the terminal or, more usually, by a self-inducing arrangement, enables the down-going belt to be charged to the polarity opposite to that of the terminal and thus the rate of charging of the latter, for a given belt speed, is doubled. The self-charging system is obtained by insulating the upper pulley and maintaining it at a potential above that of the terminal (to which it is connected by a resistor) by connecting the collector point system, already mentioned, to the pulley. Then a second row of points, connected to the inside of the h.t. terminal (*Figure 46*), and directed towards the pulley above

its point of entry into the terminal, gives a corona discharge to the belt (because of the 'live' pulley). This clearly neutralizes any remaining belt charge and leaves an excess charge, of opposite polarity to the terminal, to travel down with the belt to be neutralized at the charging points.

The relation between the electric field intensity E_d normal to the belt and the surface density of charge δ can be shown (Gauss' law for a plane) to be $E_d = 4\pi\delta$ (*see* Bouwers[21], page 39). If $E_d = 30$ kV/cm. then δ must be $< 2{\cdot}7 \times 10^{-9}$ coulombs/cm.^{2} to avoid break-down. Because of inhomogeneities and the general departure of a practical belt from the ideal case of an infinite plane, this theoretical charge

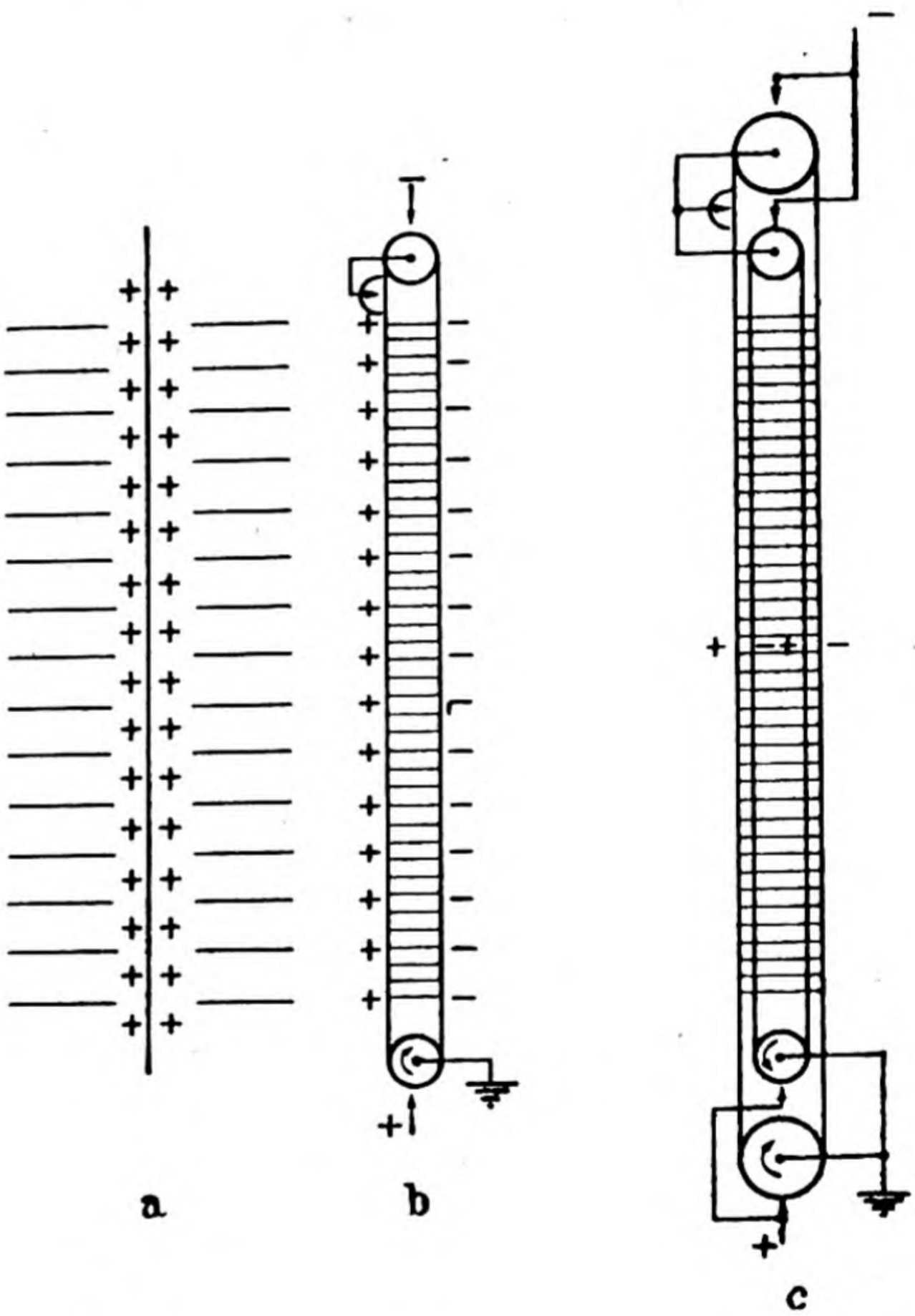

Figure 47. Lines of force in various belt arrangements in a Van de Graaff generator (Getting *et al*[40], by courtesy, *Phys. Rev.*).

density cannot be realized in practice and about 50 per cent. of this figure, say δ^1, can be reached, $\sim 1{\cdot}4 \times 10^{-9}$ coulomb/cm.^{2} for one belt surface. If the belt speed is V cm./sec. and it has a breadth b cms. then the charging current per unit surface area is $I = bv\delta^1$. For $b = 300$ cm. and $v = 2$ m/sec., $I = 8 \times 10^{-4}$ A.

Bouwers[21] shows how the terminal voltage can be related to other constants of the generator by equating the charging and discharging currents on the assumption[39] that the corona current I_2 depends on

the terminal voltage V through the relation $I_2 = a(V - V_o)^2$ where a and V_o are constants. Then if I_n represents the other current losses

$$I = bv\delta^1 = I_n + a(V - V_o)^2$$

or

$$V = V_o + \sqrt{(bv\delta^1 - I_n)/a}$$

It has been shown above that the theoretical surface density of charge on a belt in air at N.T.P. is about $2{\cdot}7 \times 10^{-9}$ coulombs/cm^2. It is now of interest to consider the charge transport in multi-belt machines where the belts may be mounted side by side[38] or sandwiched[40] as shown in *Figure 47*. If, as in *a* of *Figure 47* the whole belt (not each surface of it as on page 39) is charged with a surface density δ esu/cm.^{2}, *i.e.* with a surface gradient of potential $2\pi\delta$ then in *b* $\delta/2$ will be the maximum surface density of charge. In *c* where the belts rotate in opposite directions the outer and inner belts carry $\delta/2$ and δ esu/cm.^{2} respectively, thus giving an increase in average δ over all the belt surfaces, as compared with *b*. This arrangement with a third belt is used by GETTING *et al*[40] who give full details of the different belt currents in their paper (*see Table IV*).

SMEE[38] discusses these results and suggests that the full advantage of sandwiching is not obtained unless the belts touch or almost touch and in his own machine, with side-by-side belts (*Figure 48*) the output short-circuit current was increased from 1·7–1·8 mA with tight belts to 2·3 mA if the belts touched. Smee also considers that GETTING *et al* were incorrect in taking the inter-belt spacing at the nominal value of 0·5 in. and that, in fact, due to electrostatic forces their belts probably touched. The data of *Table IV* may be collected from Smee's paper ; the theoretical maximum belt charge density is taken as $2{\cdot}65 \times 10^{-9}$ coulombs/cm^2.

TABLE IV

Author and Reference	*Belt arrangement*	*Charge carrying efficiency (% of theoretical max.)*
Smee[38]	Tight belts	61
—	Belts slack and touching on one side only	83
Van Atta *et al*[41]	Tight belts	60
Getting *et al*[40]	Sandwiched belts: inside belt	94
	middle belt	124
	outside belt	74
Trump and Van de Graaff[42]	Single belt, field controlled (*see* below)	76

Smee suggests that the middle belt of Getting's generator touches almost completely on both sides, thus acting as a completely sandwiched belt, since its 124 per cent. efficiency is twice that of a tight

belt (about 60 per cent.); Getting's inside belt is thus considered to be partially sandwiched.

The principle of field control (*see Table IV*, last line) is to grade the potential distribution down the belts and their insulating supporting system by means of an array of tubes, wires, *etc.*, so that premature

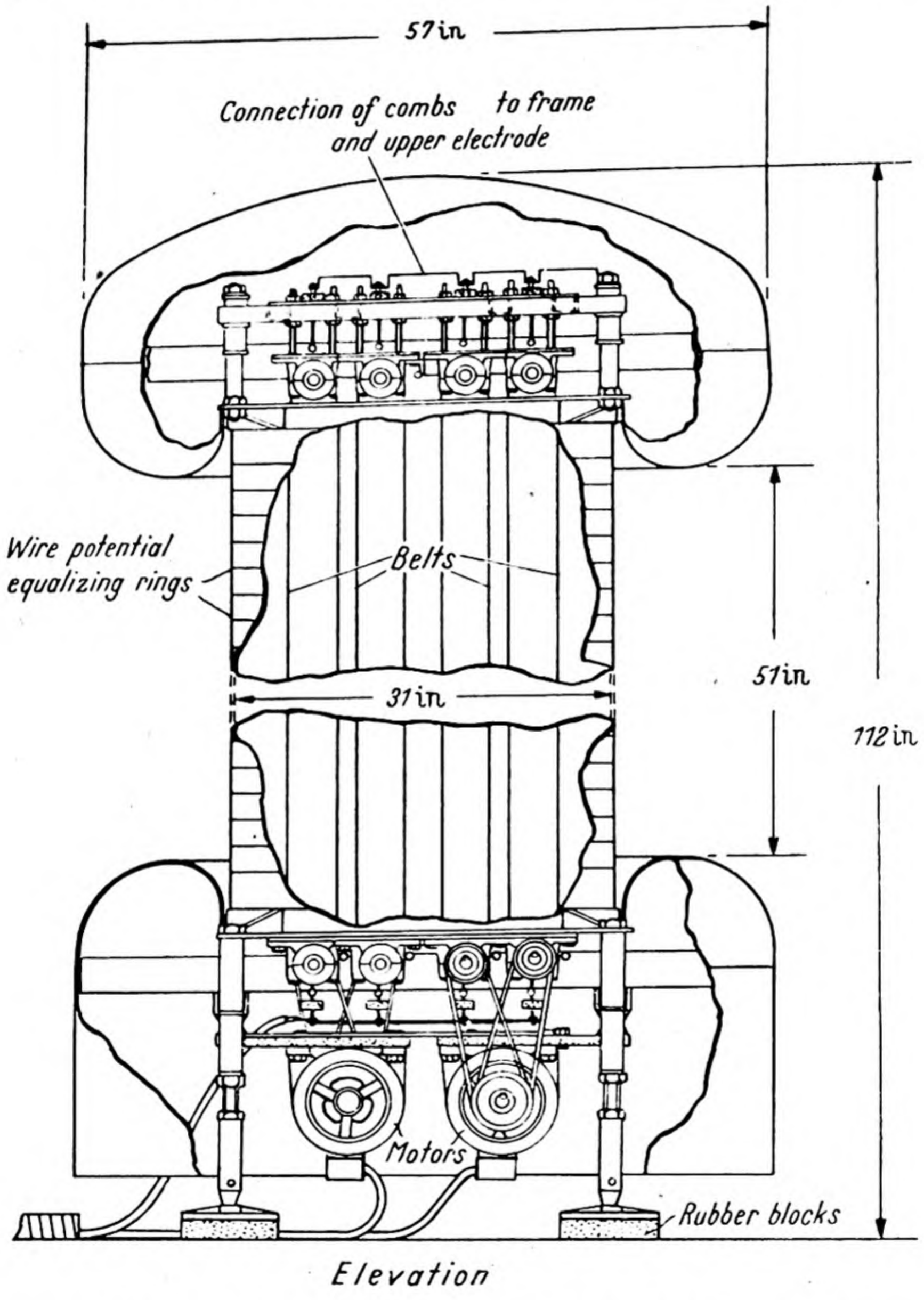

Figure 48. A 1 MV Van de Graaff generator (Smee[38], by courtesy, *J. Inst. elect. Engrs.*).

local break-down in a region of high electrostatic stress is prevented. Trump and Van de Graaff[42] describe a small generator, built for X-ray work in hospitals, in which it was important to obtain the highest possible voltage in a limited tank space. The field grading system consisted of a series of tubes fitted near the belt on both sides (*see Figure 49*[42] for a typical system of this kind).

The recent tendency has been to enclose the Van de Graaff generator in a pressure tank, since this enables relatively high voltage to be obtained in a small space. Earlier machines were operated in open air, one of the first being the famous Round Hill generator which still appears to have been the largest generator of this type. Originally[41] it consisted virtually of two separate generators, one positive

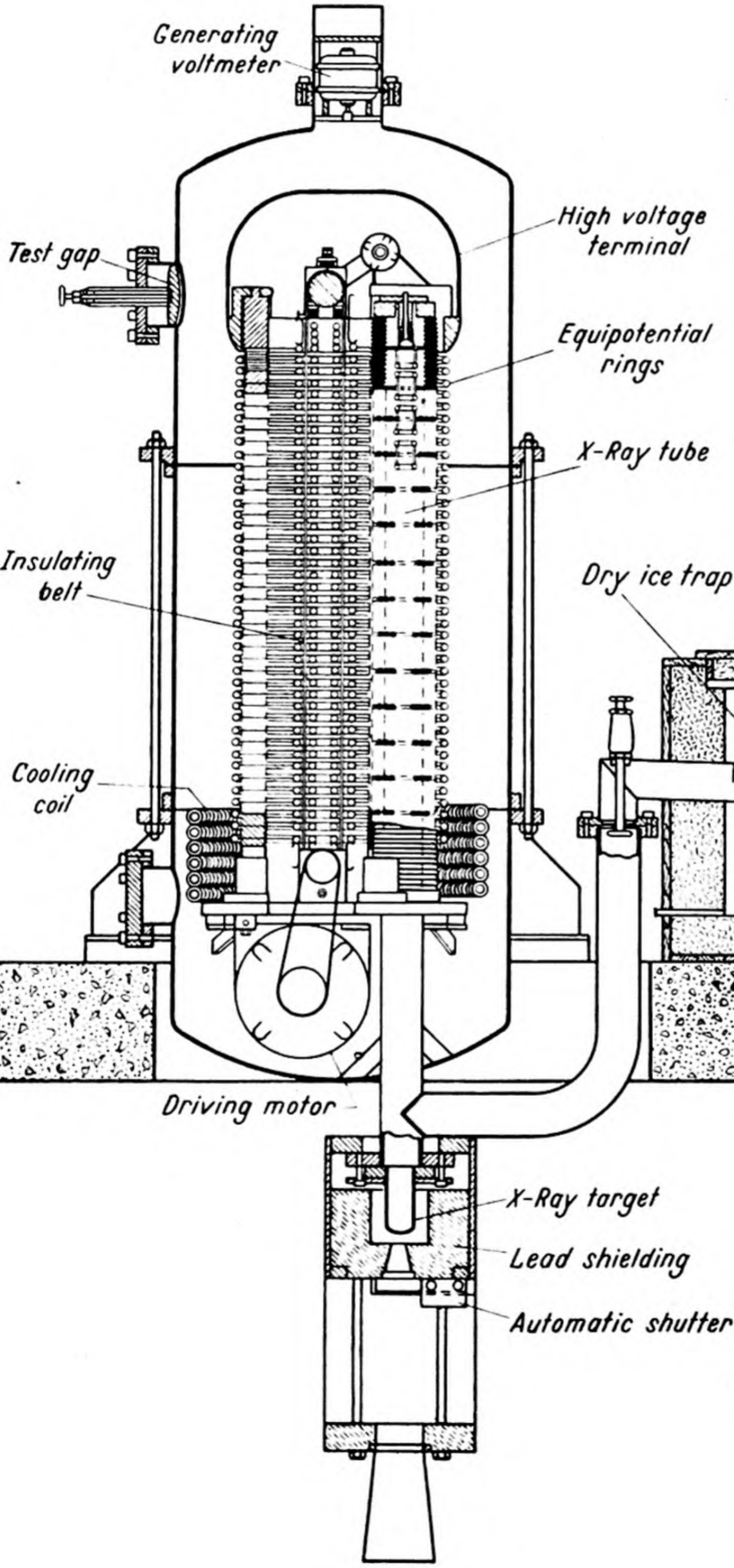

Figure 49. Sectional view of pressure-insulated X-ray generator (Trump and Van de Graaff[42], by courtesy, *Phys. Rev.*).

and one negative with respect to earth, housed in two spherical aluminium terminals, 15 ft. in diameter, mounted on Textolite cylinders, 22 ft. in length. A maximum charging current of 2·1 mA was obtained, practically independent of voltage and the highest terminal voltages were +2·4 MV and −2·7 MV, giving 5·1 MV between terminals. The generator was housed in an airship hangar. It was necessary, in order to reduce leakage losses, to control the humidity in the terminals, columns and carrying trucks on which the latter were mounted and details are given in the original paper[41]. The belts, two for each terminal, were made of electrical insulating paper 0·017 in. thick and 47 in. wide joined at the seams, which were cut in a 45° taper, and joined with a special belt cement. The pulleys, the mounting of which is critical, run at 2,880 or 3,600 r.p.m., giving belt speeds of 4,520 or 5,650 ft./min. and windage losses of 2 or 4 kW. The whole generator consumes powers of 16 and 24 kW, off load and on full load respectively.

Several open air generators, smaller than that built at Round Hill, have been described[65, 66] and brief accounts of a few of these generators will be given. Similar machines might with advantage be used in more h.t. laboratories than is the case at present, since small Van de Graaff generators can be simply and cheaply constructed.

Trump, Merrill and Safford[43] describe a 500 kV generator, giving 200 μA short-circuit current with a single 10 in. belt which is made of a three-ply rubber-fabric $^{3}/_{32}$ in. thick, driven at about 5,000 ft./min. The charge is sprayed on to the belt from corona points energized with a 10 kV half-wave rectifier set. It is found (*see also* page 40) that the short-circuit current capacity is usually 40 per cent. of the theoretical maximum discussed on page 39.

A dimensioned drawing is given in *Figure 50*, the details of which are listed in *Table V*. Attention is drawn to the use of a re-entrant spinning for the high-voltage terminal which ensures screening of the various bolts and metal pieces used in securing the upper terminal and the pulley frame. When this generator was built in 1938 its cost was $325 for material and manufacturing time, but excluding assembly and tests.

Smee's generator[38], now at Imperial College, London, is similar to that of Trump, Merrill and Safford[43] but is larger, and gives output voltages of 910 kV on positive excitation or 1,020 kV on negative excitation; load currents of about 1·5 mA and 1·7 mA respectively are available at 700 kV. The assembly of the generator is shown in *Figure 48* from which the overall height is seen to be about 9 ft. with a maximum diameter of about 5 ft. Four belts consisting of three-ply rubberized cotton, about 1·4 mm. thick, are used; two of the belts are 26 in. wide whilst the others are 18 in. wide for pulley widths

respectively of 28 and 20 in. The pulleys are 4 in. in diameter and each pair is run at 440 r.p.m. from a 2 h.p. 3-phase induction motor running at 2,800 r.p.m. The pulley adjustment, to ensure true running of the belts, are critical and are described in detail by Smee[38]. The linear belt speed is thus 2,340 cm./sec, and the area of belt entering the h.t. terminal is $5{\cdot}24 \times 10^5$ cm.^{2}/sec. The short-circuit terminal currents obtained with the machine with belts tight and with belts slack enough to touch are respectively $1{\cdot}6 \times 10^{-9}$ and $2{\cdot}2 \times 10^{-9}$ coulomb /cm.^{2}; these values are 61 per cent. and 83 per cent. of the maximum theoretical density (*see* page 39, also Getting, Fisk and Vogt[40] and Van Atta *et al* [41]) for a break-down voltage gradient in air of 30 kV/cm. These efficiency figures agree satisfactorily with those found by other authors, *e.g.* 60 per cent. for a tight belt machine[41] and the values given by Getting[40]. Other open air Van de Graaff generators have been described by Kossel and his collaborators in Danzig[44].

A load curve for operation on positive excitation for this generator is given in *Figure 51*, for voltages varying up to about 750 kV. The means which had to be adopted to obtain these data are of interest

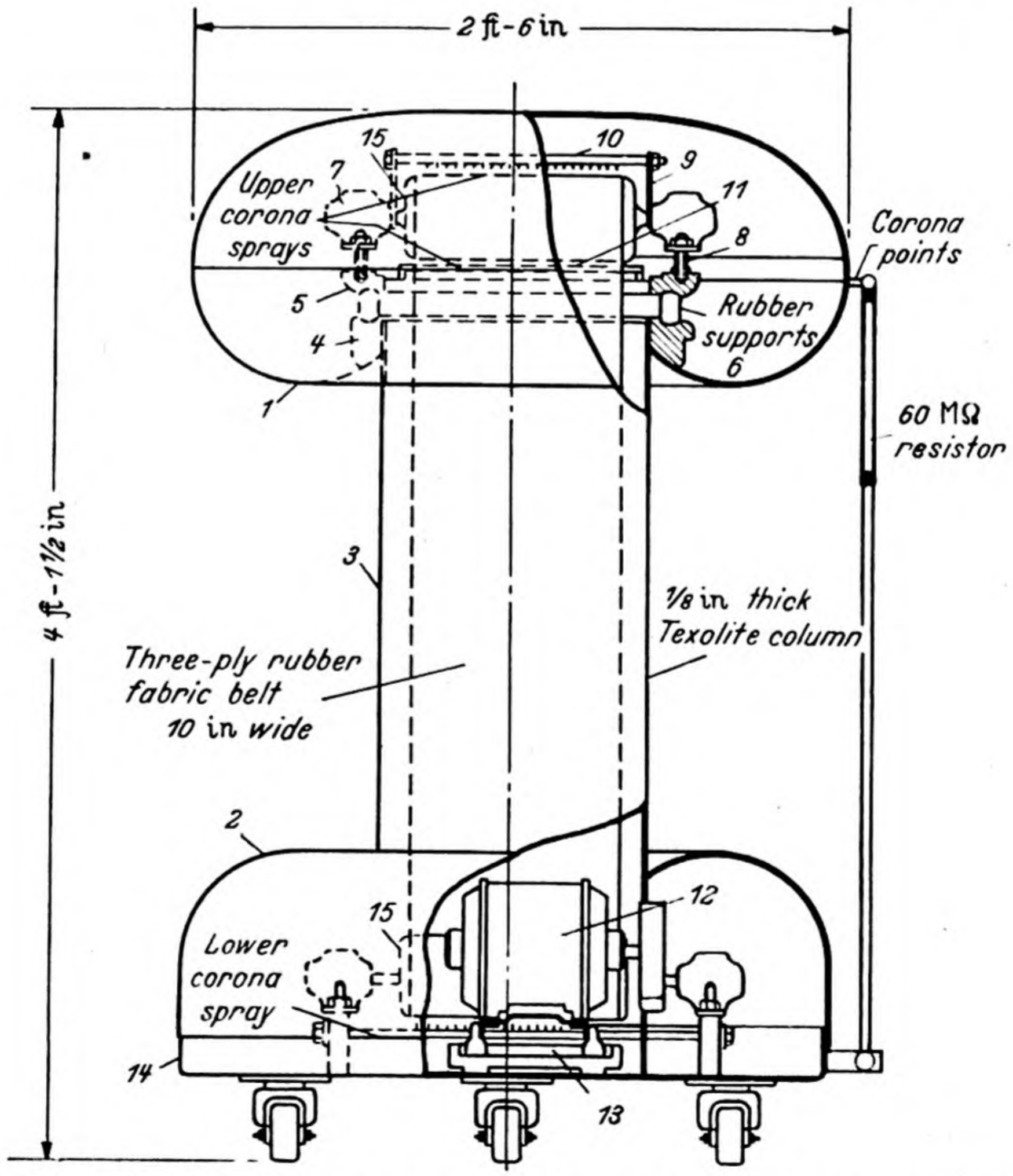

Figure 50. General arrangement of an electrostatic generator (Trump *et al*[43], by courtesy, *Rev. Sci. Instrum.*).

and will therefore be described since, also, the taking of similar load curves for other types of h.t. generator is often necessary.

A number of wire-wound resistances, of the type described on pages 374–376 and developed by WATERTON[45] to a total value of 734 MΩ, are stacked inside a long pressboard cylinder which extends some 18 in. above the upper end of the resistance stack. This cylinder serves to eliminate nearly all the corona current which flows from the stack when the latter is connected to the generator, and which is detected by comparing the voltage across the resistance, taken as $I_B \times R_L$ (*Figure 52*) with the voltage read on the sphere gap *S*. Spheres 1 m. in diameter are used. Allowance for the resistance of the pressboard cylinder, $6{\cdot}5 \times 10^9\ \Omega$, is made since this is connected in parallel with the resistance stack. Referring to *Figure 52*, *A* measures the total output current external to the machine, *B* the useful load current and *C* the input to the h.t. combs which charge the belts. *C* does not measure the true input current to the belts since it also

TABLE V

List of components shown in Figure 50

(1) High-voltage terminal, 30 in. diameter and 12 in. high made by two aluminium spinnings joined together at the equator by a brass ring.

(2) Lower grounded terminal, consisting of an aluminium spinning identical with the lower half of the h.t. terminal. A heater is placed under this spinning to prevent condensation of moisture inside the generator on insulating surfaces.

(3) Insulating column, 38 in. long, 12 in. outside diameter with $\frac{1}{8}$ in. wall thickness, made of Textolite or Micarta.

(4) Upper aluminium casting used to attach the high-voltage terminal to the top of the insulating column. The lower surface of this casting serves as a smooth continuation of the spinning surface to the column.

(5) Aluminium ring shaped casting, carrying the upper pulley frame.

(6) 4 rubber supports, $1\frac{1}{4}$ in. diameter, $1\frac{1}{2}$ in. long for mechanical and electrical insulation of the upper pulley frame from the terminal.

(7) Pillow blocks with self-aligning bearings.

(8) Pillow block mounting for adjusting the tension and running position of the main belt.

(9) Insulating supports for upper corona spray rod.

(10) Upper corona spray rod, $\frac{5}{8}$ in. brass with gramophone needles spaced $\frac{1}{2}$ in. and projecting $\frac{3}{8}$ in.

(11) Upper collector comb, as (10).

(12) $\frac{1}{2}$ h.p., 3,450 r.p.m. driving motor. For heavier belts a more powerful motor would be necessary.

(13) Adjustable hinged motor mounting for setting the belt tension.

(14) Generator base made of a standard flanged steel head $\frac{3}{16}$ in. thick and 30 in. diameter.

(15) Dynamically balanced hollow steel pulleys 4 in. diameter, 10 in. long with $\frac{1}{8}$ in. (in radius) per foot taper extending 3 in. at each end of the pulley.

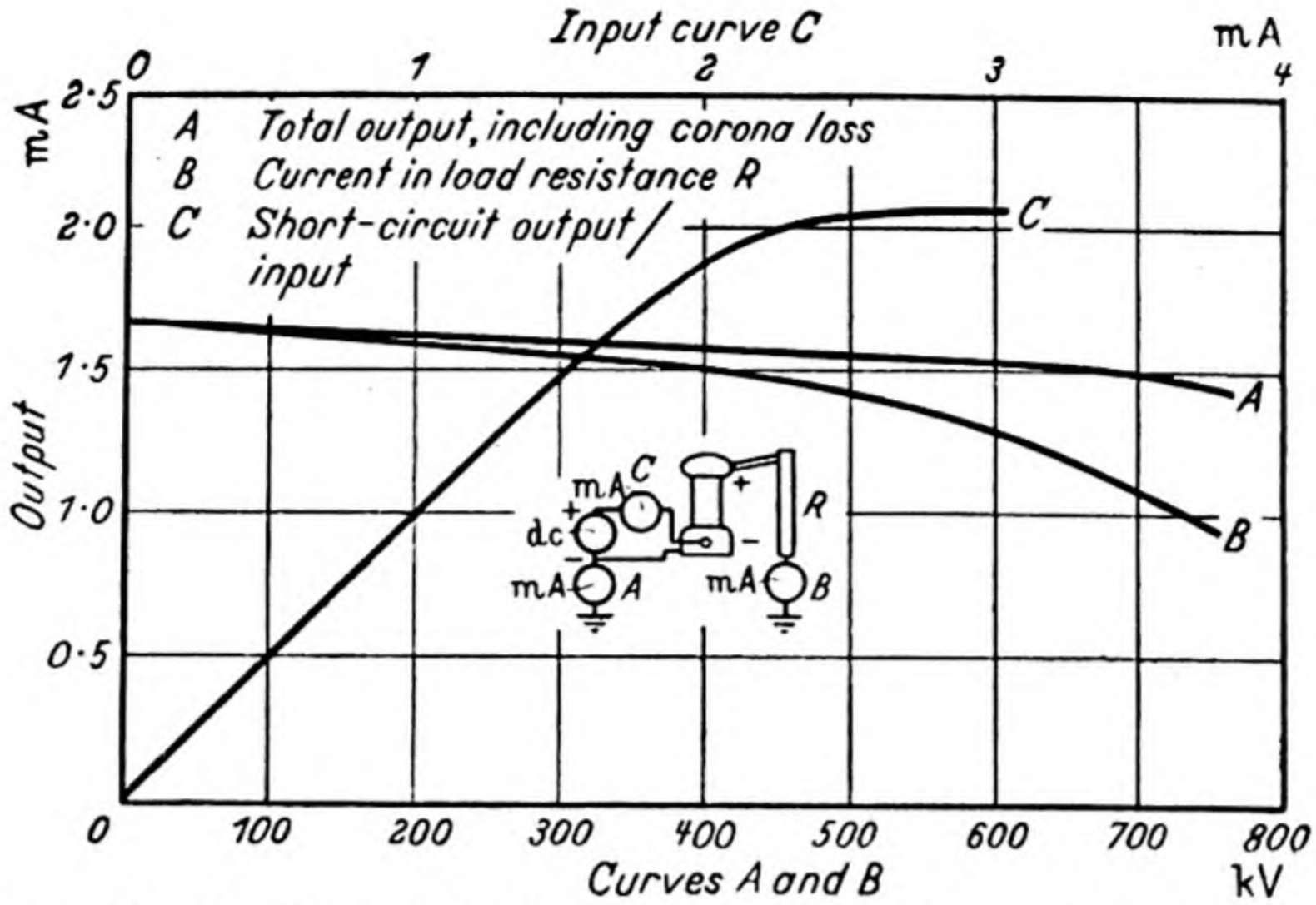

Figure 51. Positive excitation. Load curves drawn for a constant input corresponding to a short-circuit output of 1·6mA (Smee's[38] Van de Graaff generator, by courtesy, *J. Inst. elect. Engrs.*).

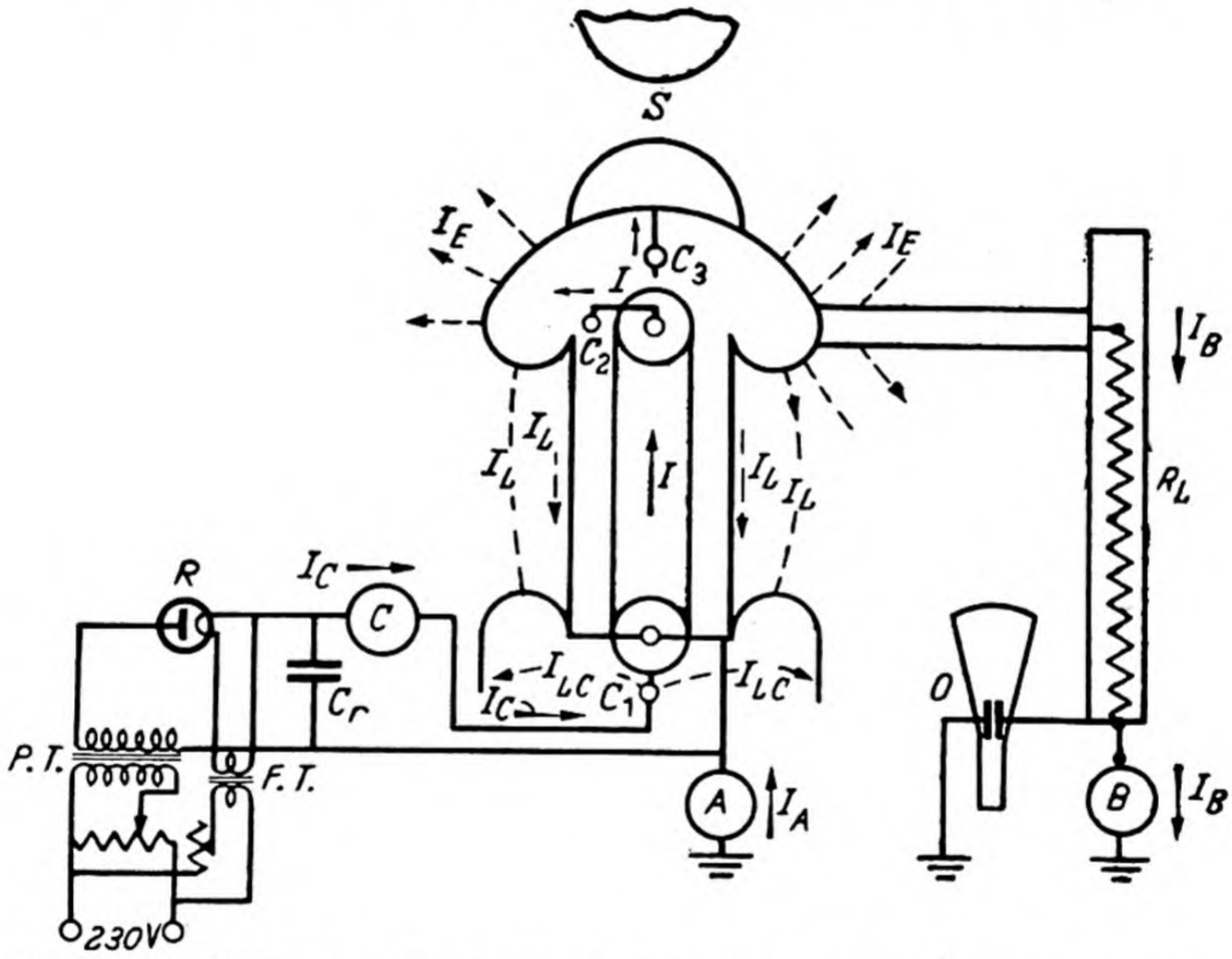

Figure 52. Diagram of test circuits, showing analysis of currents, for a Van de Graaff generator (Smee[38], by courtesy, *J. Inst. elect. Engrs.*).

PT. Potential transformer.
FT. Filament transformer.
R. Rectifier valve.
C_r. Reservoir or smoothing condenser.
C_1. Charging comb.
C_2. Upper exciting comb.
C_3. Upper charging comb.
S. Sphere gap.
R_L. Load resistance.
O. Oscillograph.
A. Total-current milliameter.
B. Load-current milliameter.
C. Charging-current milliameter.

Currents.

I_C. Charging current to C_1.
I. Belt current to upper electrode.
I_A. Total current, including all external losses by corona.
I_B. Load current in R_L.
I_{LC}. Corona leakage loss from C_1.
I_E. Corona loss direct to earth.
I_L. Corona and leakage loss to lower electrode. (Internal loss, not measurable separately.)

Analysis of Currents.

$$I_C = I + I_{LC}$$
$$I = I_A + I_L$$
$$I_A = I_B + I_E$$
$$I_C = I_B + I_E + I_L + I_{LC}$$
$$I_L + I_{LC} = I_C - (I_B + I_E) = I_C - I_A$$

includes stray corona discharges from the combs to objects near them. The readings of *A*, *B* and *C* are given in *Figure 51.* The voltage measurements with the sphere-gaps are believed to be correct to within about 2 per cent.; the resistance is known much more accurately than this (*see* Chapter 11, page 376) but the corona losses even after

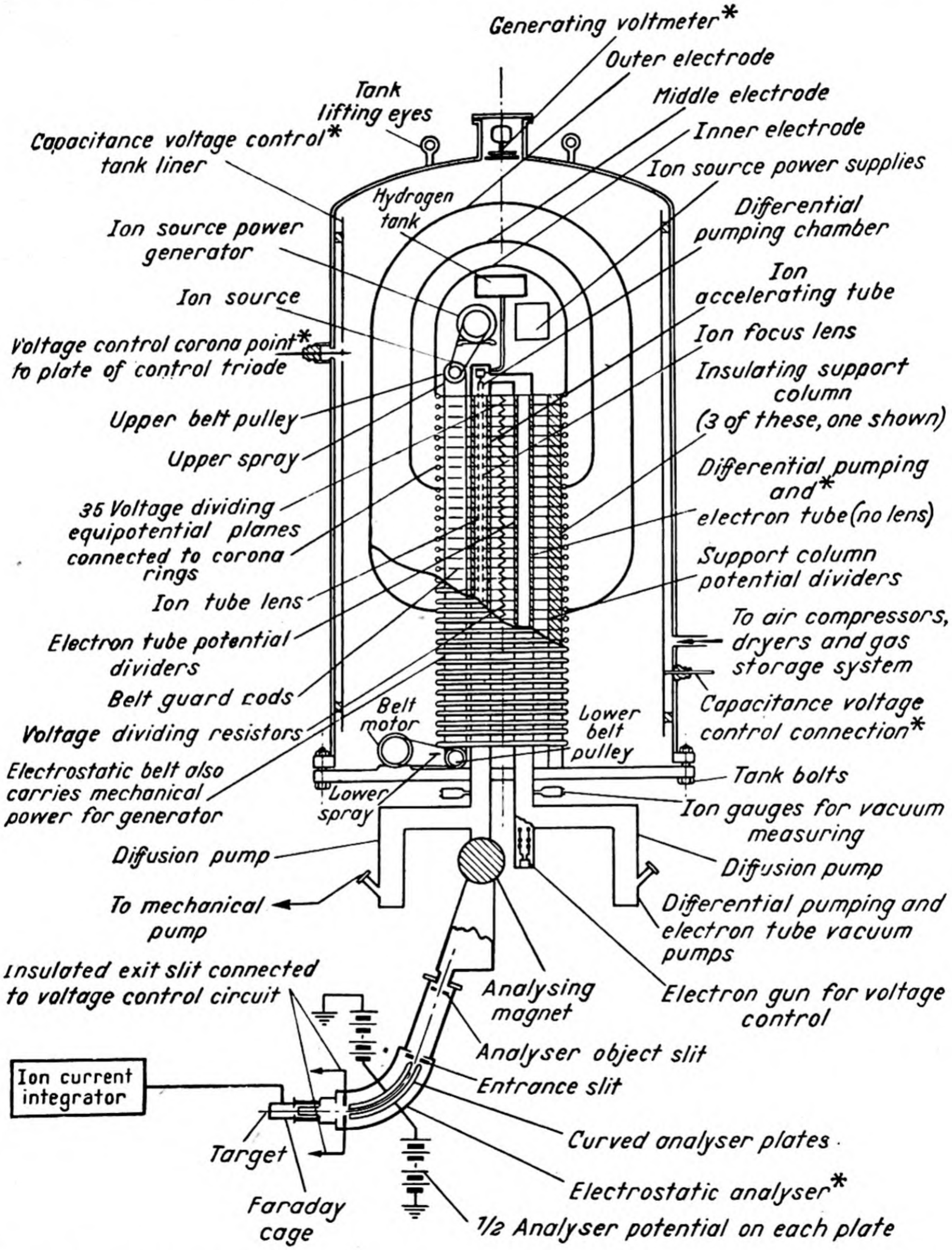

Figure 53. Schematic of an electrostatic generator, in a pressure tank (Jennings[46], by courtesy, *Proc. Inst. Rad. Eng.*). ** Items shown with an asterisk would probably not simultaneously be on any one electrostatic generator.*

the shielding cylinder was used made the voltmeter errors also about 2 per cent. R_L was varied in order to alter I_B by shorting out in turn the various units of the stack.

The enclosure of the generator in a pressure vessel enables a higher output voltage, for a given generator length, to be obtained and most if not all modern generators of this type for nuclear work are so arranged. The sparkover voltage can be increased by the use of compressed air, or better still compressed Freon 12 (CCl_2F_2) or sulphur hexafluoride (SF_6). A full schematic diagram of a pressure tank Van de Graaff generator is shown in *Figure 55*. In this latter paper, by JENNINGS[46],

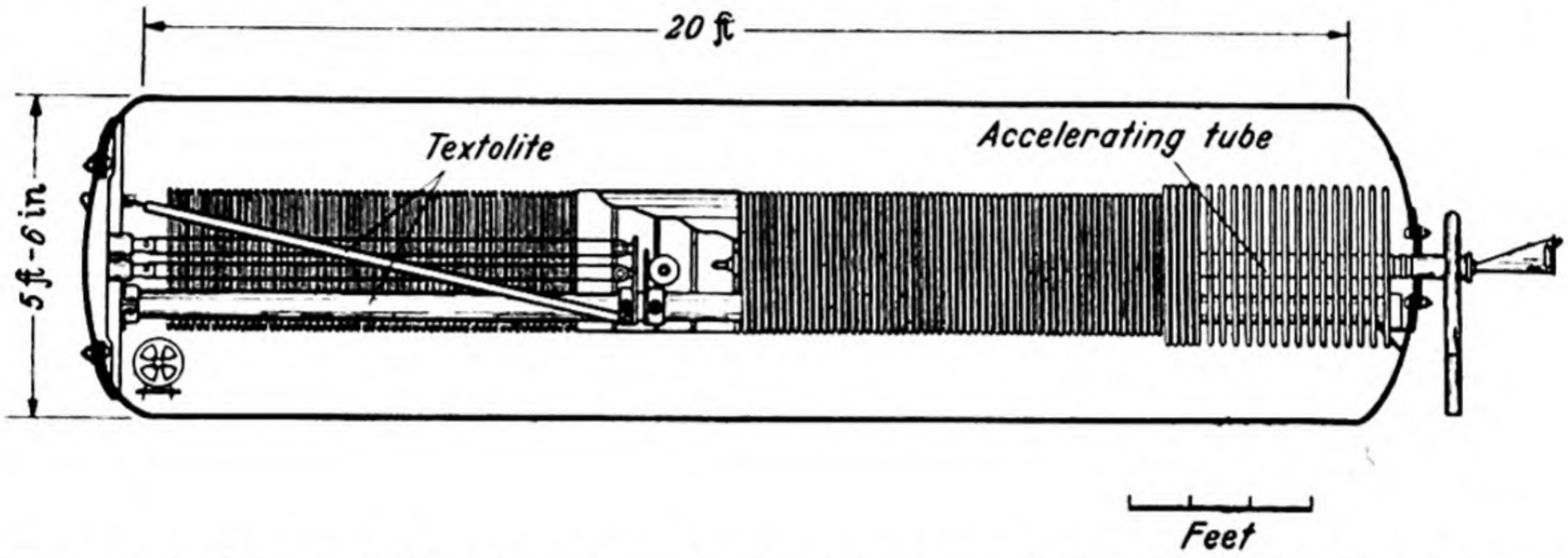

Figure 54. Electrostatic generator, in a pressure tank (Herb *et al*[48], by courtesy, *Phys. Rev.*).

there is an excellent modern review of electronic techniques as applied to such generators, including a discussion of acceleration tube problems, ion sources, beam measurement and voltage measurement and stabilization.

The maximum h.t. voltage in a tank-enclosed generator is obtained when the tank diameter is twice the terminal diameter[35] on the assumption that break-down occurs for a given voltage gradient at the terminal. It is often advantageous to grade the electric field round the terminal by means of a system of roughly concentric

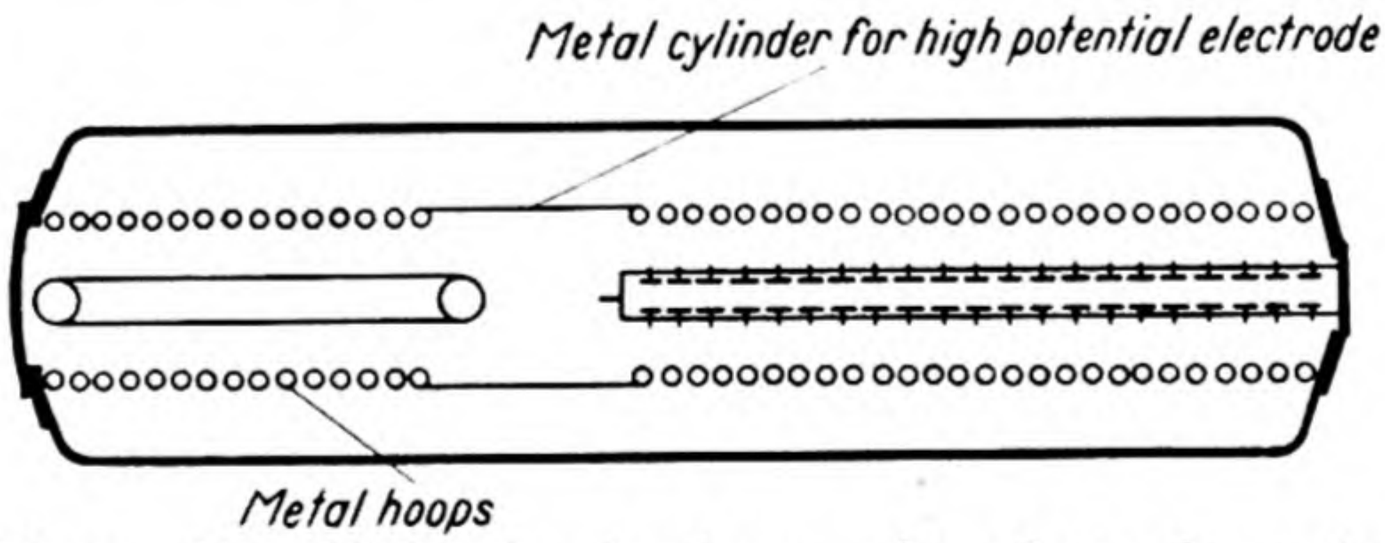

Figure 55. This sketch shows the electrode system adopted for a large Van de Graaff generator. The hoop system was thought to provide the closest practical approach to the theoretically ideal arrangement (Herb *et al*[48], by courtesy, *Phys. Rev.*).

electrodes connected to appropriate points along the potential grading ring system round the belts. This technique appears to be due to HERB and his collaborators[47] following earlier work by the same authors on pressure tank generators with a single h.t. terminal[48].

If it is assumed[35] that the flash-over of a gap in a gas is determined by the maximum gradient in the gap, then the radii and potentials of the shielding electrodes should be such as to give the same maximum gradients for each gap, *i.e.*,

$$\frac{r_1}{r_2} = \frac{r_2}{r_3} = \frac{r_{n-1}}{r_n}$$

where $r_1 \ldots r_n$ are the radii of the terminal and the intermediate electrodes respectively. The shields behave as cylinders since, it is found their hemispherical end-caps are of less importance than the cylindrical shells of the electrodes. In practice, two intermediate electrodes are found to be sufficient.

The following are brief summaries of the main characteristics of several important pressure tank Van de Graaff generators; *see* also

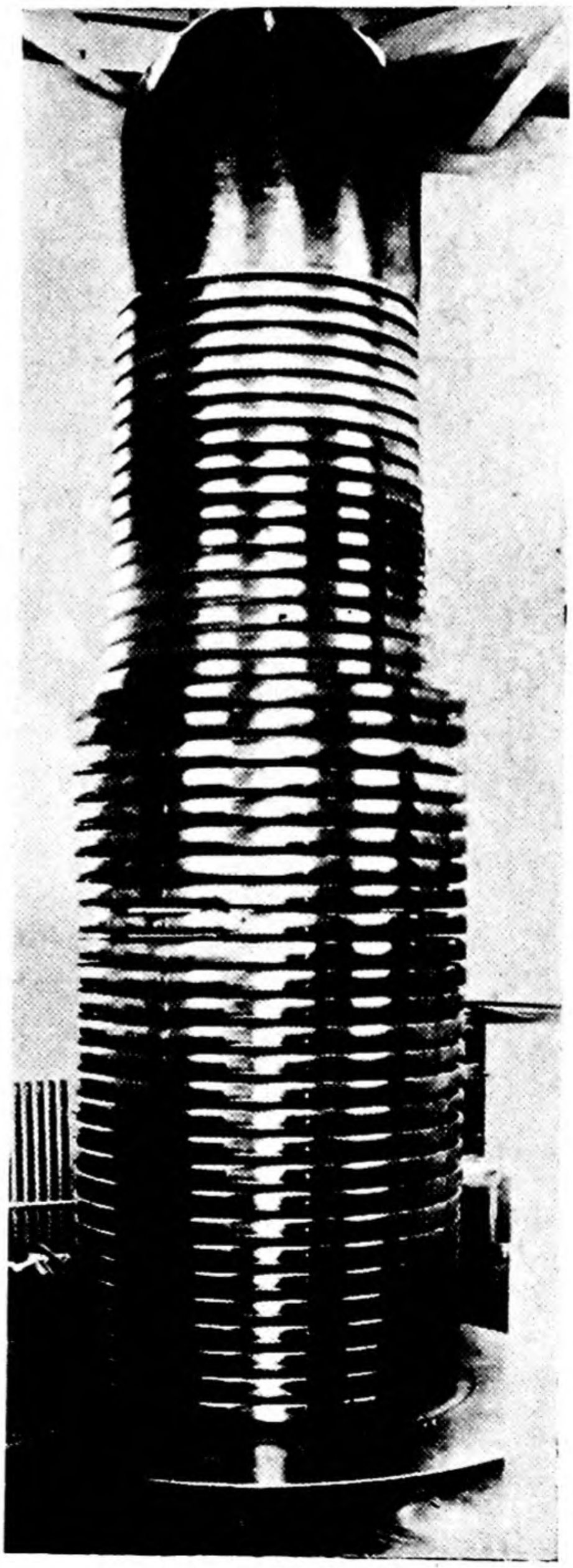

Figure 56. Potential grading rings in the 4 MV Van de Graaff generator at the AEI laboratories.

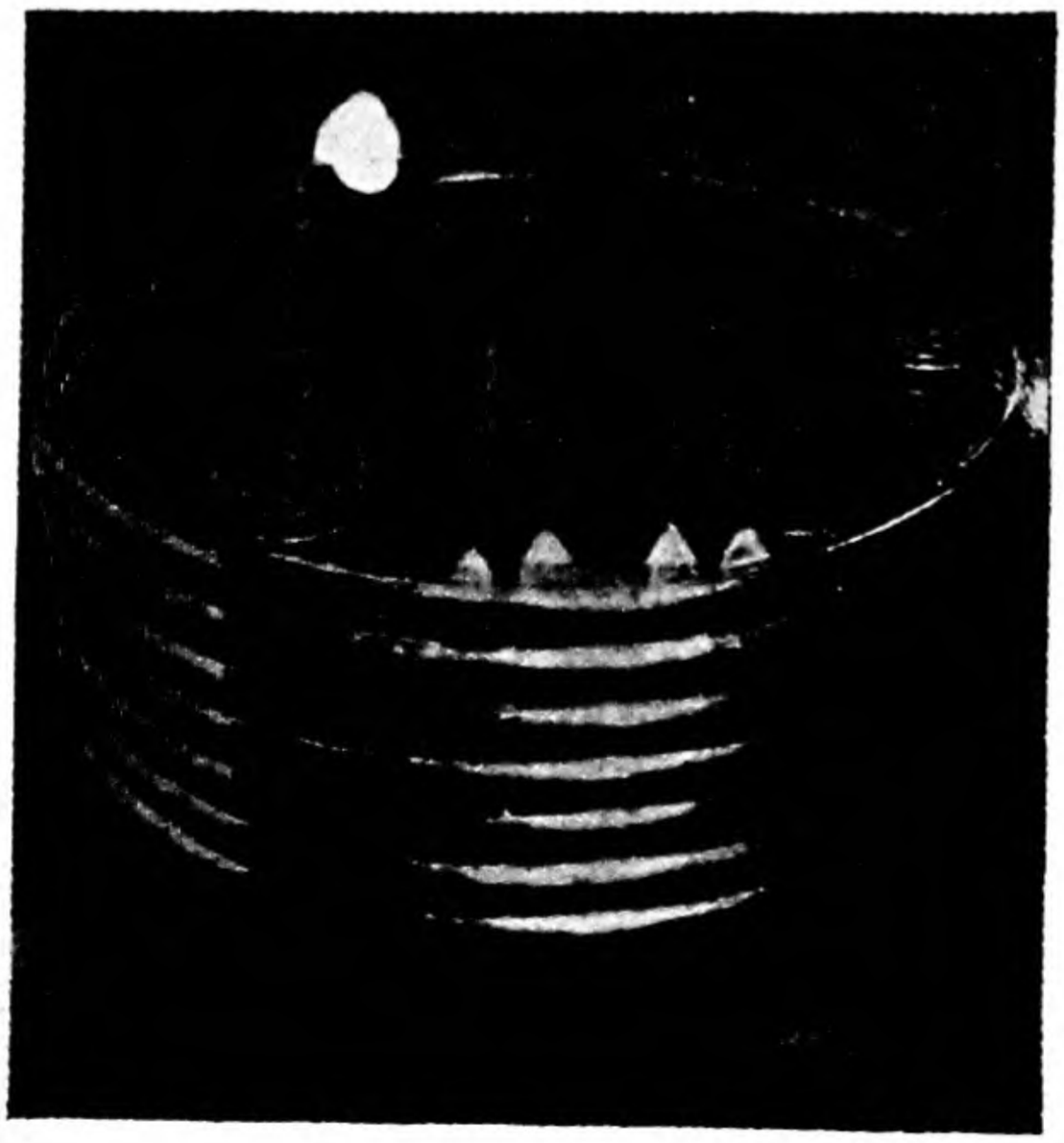

Figure 57 (*Below*). View of partially assembled generator column, for a pressure tank Van de Graaff generator (Trump and Van de Graaff[42], by courtesy, *Phys. Rev.*).

Table VI and review articles[35, 36, 37, 46] mentioned in this chapter.

(*a*) HERB, PARKINSON and KERST[48] describe a 2·2 mV generator installed in a tank, under an air pressure of 100 lb./in.^{2}, $5\frac{1}{2}$ ft. in diameter and 20 ft. long (*Figure 54*). The belt system and the positive ion accelerator tube oppose each other in the tank and both are surrounded by a system of tubular electrodes (*Figures 56* and *57*) which serves to render the voltage distribution more nearly linear. A similar system, shown in *Figure 56*, is used in the 4 mV generator at the A.E.I. Research Laboratories and is due to CHICK and his collaborators. This technique is now generally adopted in modern Van de Graaff generators. The above generator[48] did not incorporate the above-mentioned shielding electrodes round the h.t. terminal.

(*b*) A compact generator providing more than 1 mA target current of electrons at 1·25 MV is described by Trump and Van de Graaff[42] and shown in *Figure 49*. The steel tank is 34 in. in diameter and only 100 in. high. A single 14-in. belt, running at 5,000 ft./min. is used,

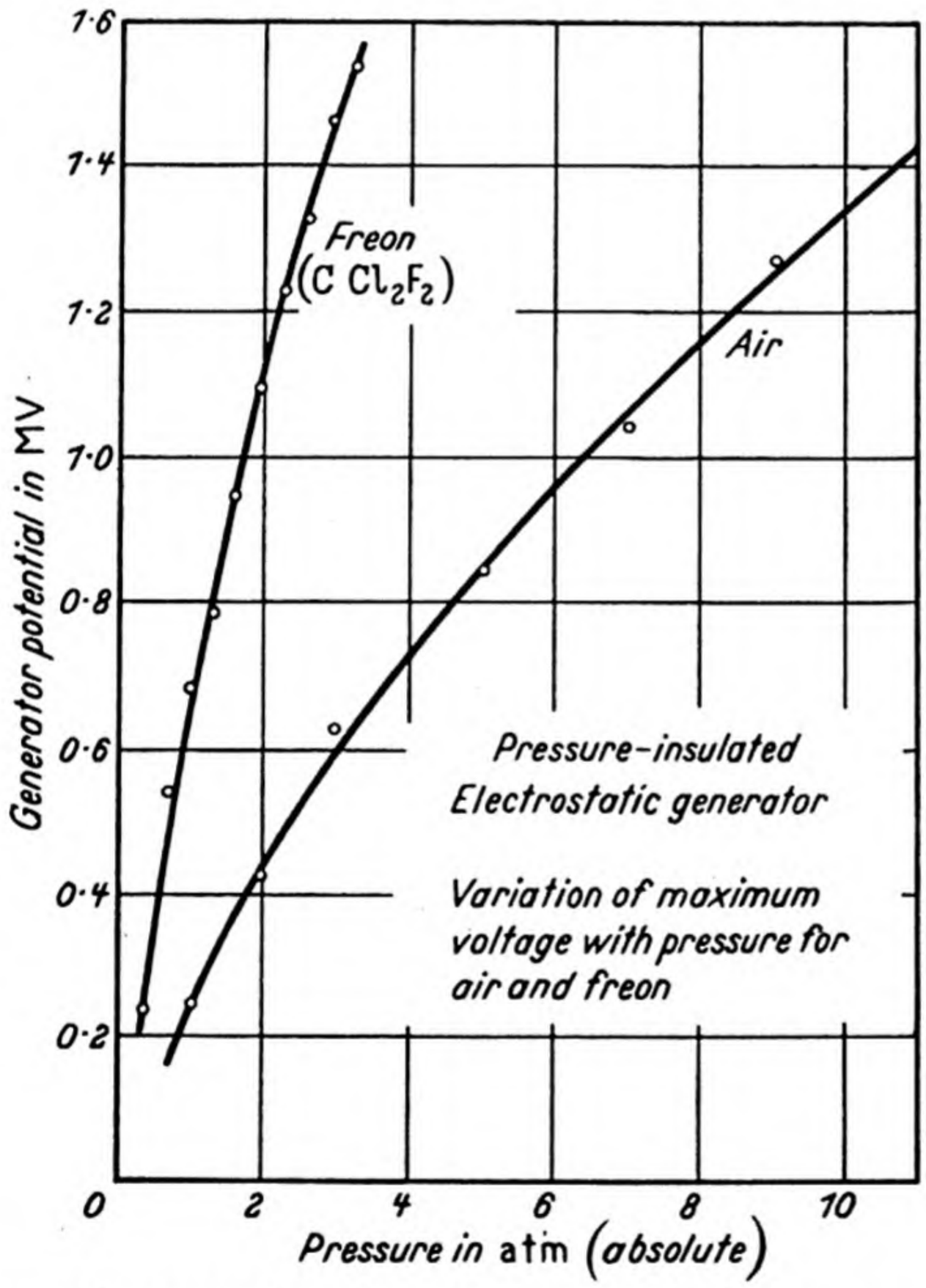

Figure 58. Increase of generator voltage with pressure for air and freon (Trump and Van de Graaff[42], by courtesy, *Phys. Rev.*).

working under the ring system shown partially constructed in *Figure 57* and which is found to reduce sparking at and over the belt even more than the earlier systems of simple circular tubes. The variations of generator current and output voltage with air or freon (CCl_2F_2) pressure are shown in *Figure 58* respectively. Generators of this size are of particular use in hospitals for X-ray therapy and Van de Graaff and his associates have devoted much effort to developing apparatus

of this kind, with a performance which should be compared with the resonant transformer sets described elsewhere, in Chapter 3.

(*c*) H.T. shielding electrodes have been used by HERB, TURNER, HUDSON and WARREN[47] in a large Van de Graaff generator, developed from their earlier 2·2 MV generator. In its new form the generator gives 4·5 MV (freon-air tank filling to a pressure of about 100 lb./in.^{2} air, with 15 lb. wt. of freon, *i.e.*, CCl_2F_2, added). TRUMP and CLOUD[49] have described the production of X-rays using an electron acceleration tube in a pressure tank system. This generator has worked steadily at 4 MV (negative) with air at 13 atmospheres pressure and up to 4·7 MV using CCl_2F_2 – air mixtures also at 13 atmospheres total pressure.

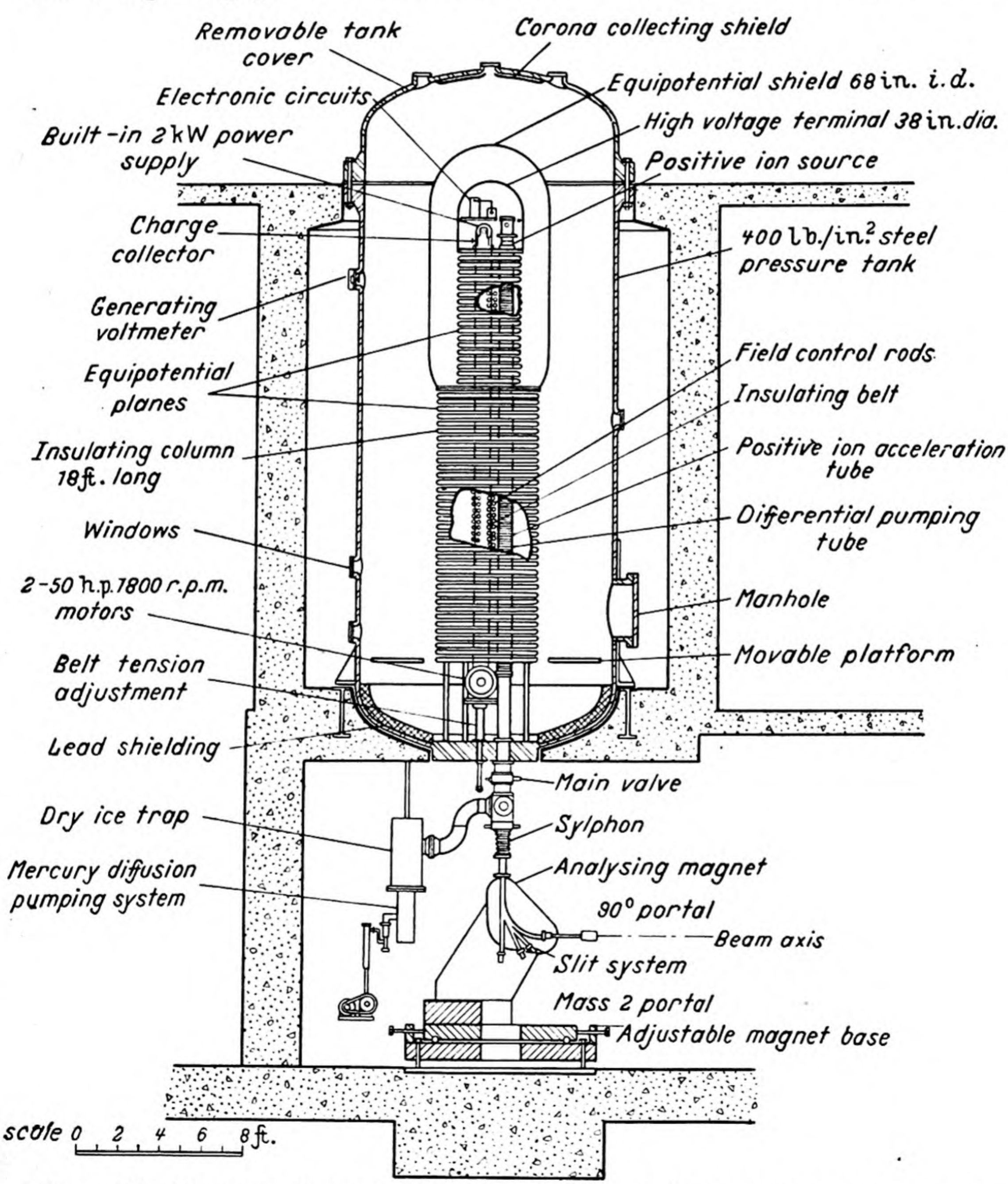

Figure 59. Diagram of the 12,000,000-volt electrostatic accelerator now nearing completion at M.I.T. (Trump[50], by courtesy, *Elect. Engng.*).

TABLE VI*

Designer	*Tuve*	*Herb*	*Williams*	*von Ardenne*	*Danforth*	*McKibben*
Insulating gas and pressure	Air, 1 atm	Air + CCl_2F_2 7 atm	Air, 6 atm	Air, 1 atm	$N_2 + CCl_2$, 5 atm	SF_6, 17 atm
Diam. of h.t. electrode (in.)	80	30	108	66	24	48
Length of insulating column to ground (in.)	70	132	250	110	60	240
Material of solid insulation	Resin, fabric base	Resin, fabric base	Porcelain	Resin, paper base	Resin, fabric base	Glass bonded mica
Max. voltage (MV) and limiting factor	1·3 belt	2·6 belt	3·5 tube	1·1 MV acceleration tube	1·75 MV tube	Estimated 12 MV
Total width of belt and belt speed	40 in. 7,200 ft./min. (?)	26 in. 2,700 ft./min.	72 in. 2,700 ft./min.	16 in. 2,400 ft./min.	14 in. 3,800 ft./min.	30 in. 5,200 ft./min.
Belt material	Paper	Rubberized fabric	Woven cotton	Rubber	Woven cotton	Probably woven cotton
Method of stabilization	Manual	Corona point current fed back to spray	Corona point current fed back to spray	Not published	Manual	Possibly electron beam
Stability obtained	±20 kV	±10 kV	±30 kV	Not published	±5 kV	No estimate

* Taken from Fortescue's review[37].

(*d*) A remarkable generator is described briefly by Van de Graaff *et al*[35] for 2 MV. Using permanent gases at 400 lb./in.^{2} pressure, a column gradient of 1 MV/ft. with a terminal–tank spacing of only 7 in. can be obtained. The 6-in. single belt travels at 4,000 ft./min. and gives a load current of 250 μA at 2 MV. *Table VI* gives preliminary data for a 12 MV generator by McKibben[37], and a similar generator is being built at M.I.T.[35] A Van de Graaff generator for 12 MV is now under construction at Los Alamos. The former is briefly described by Trump[50] in a review paper. The generator, shown in *Figure 59* has two h.t. field grading electrodes, the larger at 8 MV potential, and is to be housed in a vertical steel tank, 12 ft. in diameter and 32 ft. high, which can be filled to a pressure of 27 atmospheres ; a 20-in. belt travelling at 3,600 ft./min. will supply over 1 mA of h.t. current.

ELECTROSTATIC GENERATORS USING BLOWN STREAMS OF CHARGED PARTICLES

Charge may be transported to an isolated electrode by a stream of insulating particles, themselves charged either in an electric field or by friction in a jet. Loeb has recently summarized the present state of knowledge on contact electrification[51] and his review should be read by those interested in electrostatic generators using dust streams.

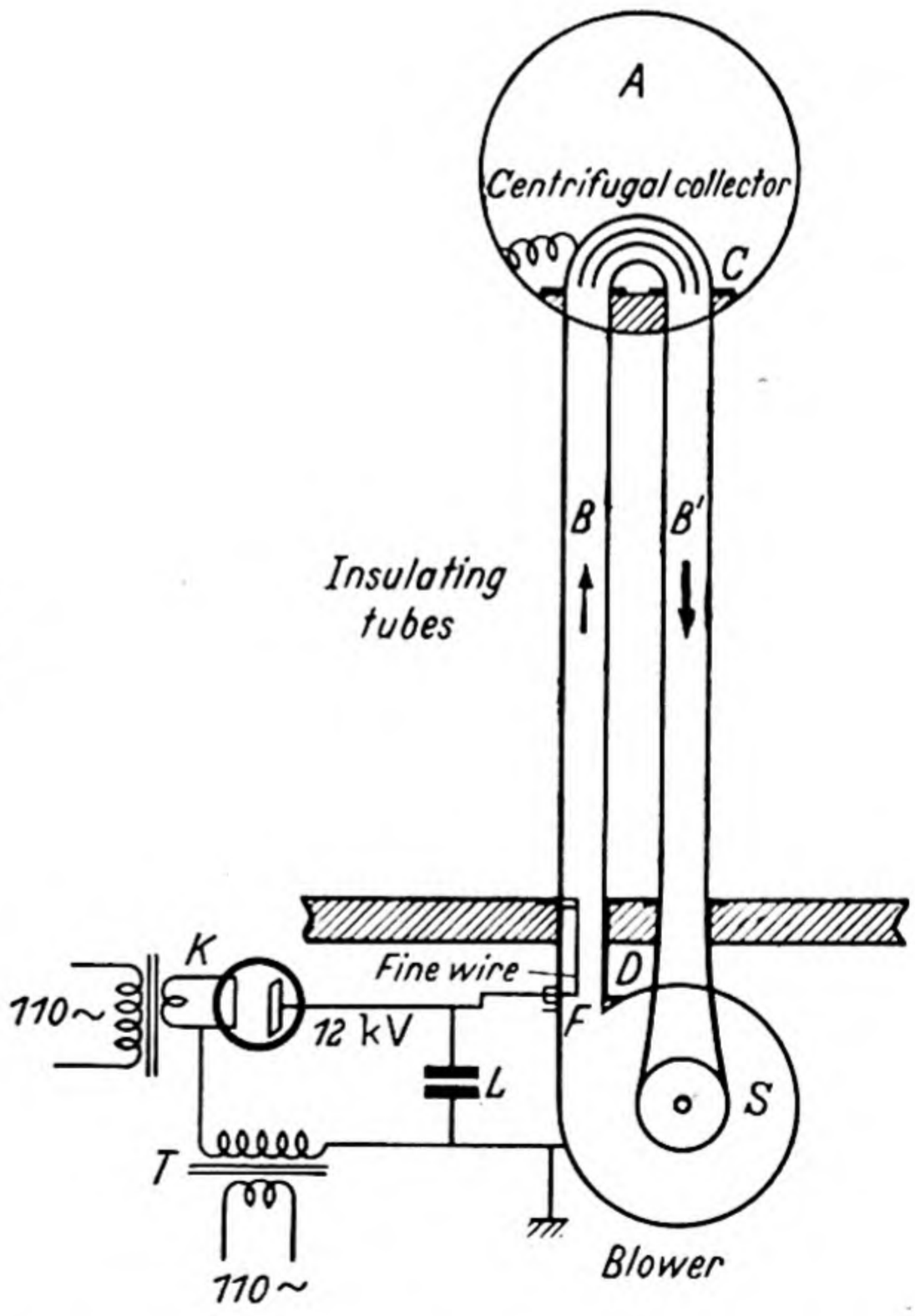

Figure 60. An electrostatic generator using a blown dust stream (Pauthenier and Moreau-Hanot, by courtesy, *J. Phys. et le Radium*).

High-voltage d.c. generators of this type have been studied mainly in France and notably by Pauthenier and Moreau-Hanot and

their associates [52, 53]. Early work in this field is due to VOLLRATH[62]. Streams of conducting particles, drops, or simple ions may also, of course, be used for charging appropriately isolated electrodes, and BABAT, for example, has described the use of mercury vapour streams for this purpose[54]. In a later paper[53] the above authors describe a 1·2 MV generator, with 75 cm. diameter spherical terminals, made to the schematic arrangement shown in *Figure 60*. Here, *TKL* is the rectifier set charging, near the wire *F*, the dust stream which is circulated by blowers *S* through the insulating tubes *BB'*. *A* becomes charged as a Faraday sphere because of charge collected from the dust particles in the electrode system *C*. The air-stream velocity was about 50 m/sec., with *BB'* some 10 cm. in diameter. Thin copper wires in the charging chamber were found to give satisfactory positive and negative charging characteristics but were found to be mechanically unsatisfactory. In a case where the corona characteristics of the charging wires are found to be appreciably different on opposite polarity, adjustments of the rectifier set would be necessary when changing polarity.

Pauthenier and Moreau-Hanot showed that spherical particles of radius a in a field E, where the charging wires pass a current I/unit length may be charged to a limit given by $\rho E a^2$ where

$$\rho = \frac{3\,\epsilon}{\epsilon + 2}$$

(ϵ = dielectric constant of the particles, a $\sim 1-10\mu$)

At a distance r from the axis, the particles take up, in time t, a fraction $t/(t+\tau)$ of their limiting charge where $\tau = 2rE/i$ is the time necessary to acquire one-half of the limiting charge. As an example, $\tau = 0{\cdot}002$ sec. at a distance of 2 cm from the axis of a cylinder where $E = 2{\cdot}4$ kV/cm. From these formulae, the length of charging wires, necessary to give virtually complete charging of the particles in their passage through the ionized region near the wires, may be deduced. The h.t. potential may be calculated as follows. The maximum electric field experienced by a particle approaching a sphere of radius R and voltage V_l is V_l/R and for a particle carrying a charge $\rho E a^2$ the force is $\rho E a^2 V_l/R$. Now, an air stream flowing with a velocity u and density δ exerts a force, on the sphere, equal to $C\pi a^2 \delta u^2/_2$ where C is an aerodynamic coefficient. The limiting voltage is thus given by

$$\frac{\rho E a^2 V_l}{R} = \frac{C}{2}\,\pi a^2 \delta u^2, \text{ so that } V_l = \frac{R c \pi \delta u^2}{2\rho E}$$

which is independent of the particle size. For example, if $R = 50$ cm., $\delta = 12 \times 10^{-4}$, $C = 0{\cdot}4$, $u = 10^4$ cm./sec., $\rho = 2$, $E = 10$ esu then $V_l \sim 60$ MV. In atmospheric air the limiting voltage gradient of about 30 kV/in. would set a much lower limit than the above value of V_l, namely

about 1·5 MV. Thus the air-stream velocity need not be greater than that necessary to maintain this voltage and in the present case this would be 20 m./sec. The above authors also have calculated the charge carried in given circumstances. If S_1 is the total surface area of all the dust particles in 1 cc. and I the current flow from 1 cm. length of wire in a tube of radius R, then

$$\Delta I/I = -\rho S_1 R/3, \text{ found by experience to be } \sim 0{\cdot}4$$

$$\text{also } \rho = \epsilon_{1\text{cc.}}\rho E a^2 = \rho S_1 E/4\pi$$

$$= \frac{0{\cdot}4 \times 3E}{4\pi R} \sim E/10R$$

For $E = 10$ C.G.S., $R = 2$ cm., $\rho = 0{\cdot}5$ C.G.S., *i.e.*, 6 litres of air will transport 1 μ coulomb. Pauthenier and Moreau-Hanot describe elsewhere[55], in great detail, the physics of the dust charging processes occurring in the ionization chamber, with a full study of the potential distribution near the charging wires. This work is of interest in relation to dust precipitation by high-voltage methods[68]. Further, but short, publications on the dust charging processes and other problems relating to generators of this type have also appeared[56] and PAUTHENIER[57] and much later, MOREL[58] have given other accounts of work in this field.

It appears that h.t. generators of this type have been little used in nuclear physics or high-voltage research but despite this their basic mechanisms present many points of interest. Van de Graaff electrostatic generators would seem to be more reliable and easier to stabilize than blown-dust generators, although a very reliable dust generator has recently been described by MORAND *et al*[67].

MISCELLANEOUS ELECTROSTATIC GENERATORS

The possibility of using other types of electrostatic h.t. generators, besides the Van de Graaff and dust-flow types, has often been considered, and both the generation of power and its conversion into mechanical effort have been discussed. Trump[59], and MOREL[58] show the potentialities of electrostatic machines, working *in vacuo*, by considering for example[59] two metallic plates, each with an area of 100 in.^{2} For a gradient of 30 kV/cm. which is about the maximum obtainable in atmospheric air, the electrostatic force of attraction would be about 0·5 lb. but, in a high vacuum, with 3 MV/cm., the force would be about 5,700 lb. and renders possible, if such gradients can be obtained, various attractive electro-mechanical machines.

Trump[59] suggests that vacuum-insulated motors and generators would be essentially variable capacitors with rotor and stator composed of interleaved plates. The current flowing in the capacitor C (Trump[59]) is

$$I = C\frac{de}{dt} + e\frac{dc}{dt}$$

and the instantaneous power input to the circuit is

$$\rho = eI = eC\,{}^{de}/_{dt} + e^2\,\frac{dc}{dt}$$

Here $\rho^1 = \frac{e^2}{2} \cdot \frac{dc}{dt}$ represents the rate at which the stored energy at voltage e is changing and an equivalent amount of work $\left(\frac{e^2}{2} \cdot \frac{dc}{dt}\right)$ must be done on or by the system at voltage e to give a rate of change of capacitance dc/dt. If the latter is positive, then electrical energy is being transferred into mechanical energy and *vice versa.*

Trump then proceeds to describe, in outline, an a.c. synchronous electrostatic machine consisting of a variable capacitor to which a periodic voltage e is applied of frequency f and which develops power as a motor when $+ dc/dt$ occurs at the larger values of e, and *vice versa.* The synchronous speed is $n = 120\ f/p$ (r.p.m.) if p is the number of cycles of capacitance change/revolution. The machine responds to increasing loads in an analogous manner to an electromagnetic synchronous motor, to a limit beyond which the motor pulls out of step. The machine can also be run as a generator. Trump also gives formulae for the power developed by such a machine in terms of its geometrical parameters, and mentions a 60 W machine with an efficiency of more than 99 per cent. which operated with a 60 c/s line voltage of 90 kV and an electric field in the capacitor of about 100 kV/cm. The average power developed by the synchronous electrostatic machine, with a sinusoidal variation of capacitance is

$$\rho_a = \frac{139 \times 10^{-15}}{d}\ E^2 f S\,(r^2{}_1 - r^2{}_2) \sin 2\theta \text{ Watts}$$

where E is the maximum value of line voltage, of frequency f
S is the number of rotor discs
r_1 and r_2 are the inner and outer radii of the rotor and
d is the rotor-stator separation (cm.).

The basic circuit of a d.c. h.t. generator of the rotating capacitor type, due to Trump, is given in *Figure 61.* Note the opposite polarities of the input and output voltages. For negative output the cycle is given by Trump as follows. When the capacitance from rotor to stator $C = C_m$ (the maximum), tube 2 ceases to conduct and the stator is at ground potential. E is then applied across tube 1 and V across C_m. As the rotor turns, C diminishes, but neither tube is now conducting and the voltage across C increases, the stator becoming more and more negative with respect to earth. When the stator reaches line potential, tube 1 conducts and further movement causes charge to flow into the line. Tube 2 now has E across it and the charge left in the generator system is then (with stator at line potential)

$$Q_o = C_o\,(E+V) + (C_s + C_v)\,E$$

where C_s = capacitance of stator to earth
C_v = capacitance of tube 2 to earth (*Figure 61*)
and C_o = minimum value of C.

The average power output is $\rho_a = 4{\cdot}63 \times 10^{-15} Knsp\ (r^2_1 - r^2_2)\ \frac{VE}{d}$ watts

$$\text{where } K = \frac{1 - C_o\,(E+V) + (C_s + C_v)\,E}{C_m V}$$

n is speed of rotation (r.p.m.), s is the number of rotor plates, d = rotor-stator separation (cm.), r_1 and r_2 are the maximum and minimum rotor radii (cm.). Practically, K may be as high as 0·75, and if the generator action can be distributed over the whole cycle for 1 MV divided equally between V and E for a gradient of 1 MV/cm., then a remarkable machine performance is possible. For example (Trump[59]), a 4,000 r.p.m. machine with 50 rotor plates, with 4 ft. maximum and 2 ft. minimum rotor diameters, and 16 rotor poles, would develop 7,000 kW. The generator size could be quite small, *i.e.*, 6 ft. in diameter and 10 ft. in length.

A detailed study of electrostatic machines as generators and motors has been made by FELICI in a series of three papers[60]. This author

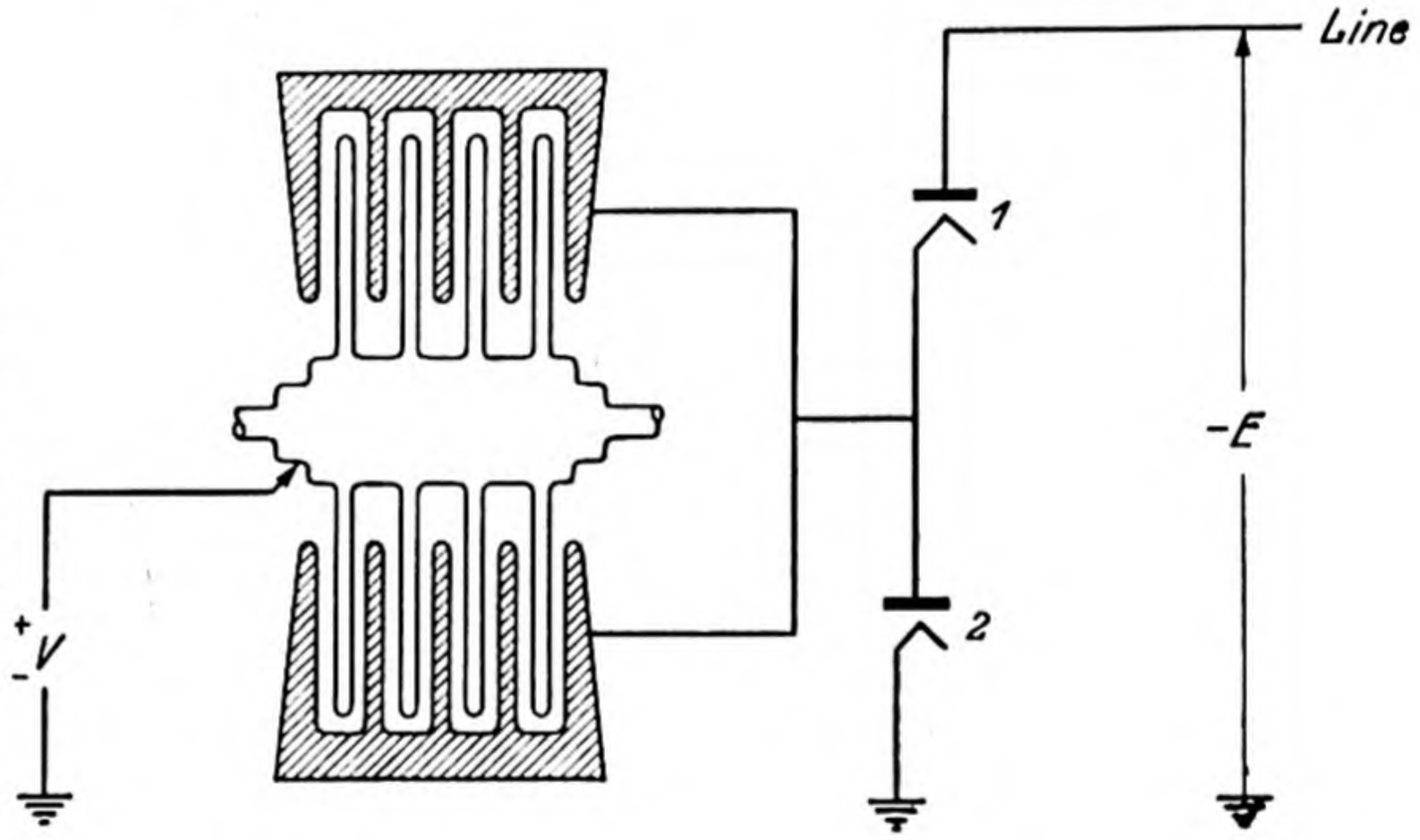

Figure 61. Schematic diagram of a variable-capacitor constant-potential electrostatic generator for operation in high vacuum. C_s = capacitance of stator to ground. C_v = capacitance of tube 2 to ground (Trump[50], by courtesy, *Elect. Engng.*).

considers machines with insulating charge transporters, such as Van de Graaff generators, and also those with conducting charge transporters, *i.e.* modern versions of the Wimshurst and other machines. This work has only an indirect bearing on h.t. generators, and so will only be considered briefly, but it is of interest and importance in showing the possibilities of electrostatic machines. Felici studied various forms of generator, such as cascaded and multi-plate types with particular attention to the field distribution near the charge-carrying plates and to the possibilities of compressed gas insulation, but seems to have little to report on finished machines. However, a modified Toepler machine (the basic electrode arrangement of general types of the latter is described in some detail in the above papers), was built in 1943 which worked with an inter-electrode

gradient of 620 kV/cm. for 2·5 mm. clearance. The importance of such results is clear from the work of Trump described above. Electrostatic rotating machines have also been studied by MALPICA[61] who worked with devices in which charge is transferred by a moving dielectric disc from one condenser to another. By suitable connections of primaries and secondaries it is possible to cascade several units, and in this way Malpica made a 300 kV 1 mA d.c. generator; 22 glass discs, each 1 m. in diameter and revolving at 268 r.p.m., were used.

REFERENCES

1 HARNWELL, G. P., and LIVINGOOD, J. J. *Experimental Atomic Physics*, *p.* 184. New York, 1933.
2 SCHADE, O. H. *Proc. Inst. Rad. Engrs.*, **31** (1943) 341.
3 BELL, G. E. *Brit. J. Radiol.*, **7** (1934) 654.
4 MITCHELL, R. G. *Wireless Engr.*, **20** (1943) 414.
5 ALLIBONE, T. E., BEETLESTONE, A., and INNES, G. S. *Brit. J. Radiol.*, **7** (1934) 83.
6 HAINE, M. E., PAGE, R. S., and GARFITT, R. G. *J. appl. Phys.*, **21** (1950) 173.
7 SCHADE, O. H. *Proc. Inst. Rad. Engrs.*, **31** (1943) 158.
8 MAUTNER, R. S., and SCHADE, O. H. *R.C.A. Rev.*, **8** (1947) 43.
9 SIEZEN, G. J., and KERKHOF, F. *Philips Tech. Rev.*, **10** (1948) 125.
— — *Proc. Inst. Rad. Engrs.*, **36** (1948) 401.
10 CRAGGS, J. D., HAINE, M. E., and MEEK, J. M. *J. Inst. elect. Engrs.*, Pt. 3A **93** (1946) 963.
11 CHARLTON, E. E., and HUBBARD, H. S. *Gen. Elect. Rev.*, **43** (1940) 272.
12 COCKROFT, J. D., and WALTON, E. T. S. *Proc. roy. Soc.* (A), **129** (1930) 477.
13 SCHENKEL, M. *Elektrotech. Z.*, **40** (1919) 333.
14 GREINACHER, H. *Bull. Schweiz. elek. Ver.*, **11** (1920) 59.
— *Z. Phys.*, **4** (1921) 195.
15 COCKROFT, J. D., and WALTON, E. T. S. *Proc. roy. Soc.* (A), **136** (1932) 619.
16 BOUWERS, A. *Radiology*, **22** (1934) 163.
17 BOUWERS, A., and KUNTKE, A. *Z. tech. Phys.*, **18** (1937) 209.
18 ALLIBONE, T. E., BANCROFT, F. E., and INNES, G. S. *J. Inst. elect. Engrs.*, **85** (1939) 657.
19 CHARLTON, E. E., HOTALING, G., WESTENDORP, W. F., and DEMPSTER, L. E. *Radiology*, **29** (1937) 329.
20 MITCHELL, R. G., *Wireless Eng.*, **22** (1945) 474.
21 BOUWERS, A. *Elektrische Höchstspannungen.* Berlin, 1939.
22 KUNTKE, A. *Philips Tech. Rev.*, **1** (1937) 46.
23 ALVAREZ, L. W. *Rev. Sci. Instrum.*, **22** (1951) 705.
24 DEMPSTER, A. J. *Phys. Rev.*, **42** (1932) 901.
25 BURCHAM, W. E. *Nature*, **160** (1947) 316.
26 HEYN, F. A., and BOUWERS, A. *Philips Tech. Rev.*, **6** (1941) 46.
27 KUNTKE, A. *Philips Tech. Rev.*, **2** (1937) 161.
28 HEYN, F. A. *Philips Tech. Rev.*, **3** (1938) 331.
29 THONEMANN, P. C., MOFFATT, J., ROAF, D., and SANDERS, J. H. *Proc. Phys. Soc.*, **61** (1948) 483.
30 VAN DORSTEN, A. C., OOSTERKAMP, W. J., and LE POOLE, J. B. *Philips Tech. Rev.*, **9** (1947) 193.
31 GRADSTEIN, S. *Philips Tech. Rev.*, **1** (1936) 6.
32 BJERGE, T., BROSTRØM, K. J., KOCH, J., and LAURITSEN, T. *Det. Kgl. Danske. Videns. Selskab.*, **18** (1940) 1.

REFERENCES

[33] ARNOLD, W. R. *Rev. Sci. Instrum.*, **21** (1950) 796.
[34] VAN AMSTEL, J. J. A. P. *Philips Tech. Rev.*, **9** (1947) 267.
[35] VAN DE GRAAFF, R. J., TRUMP, J. G., and BUECHNER, W. W. *Rep. Prog. Phys.*, **11** (1946–47) 1.
[36] SHIRE, E. S. "The Acceleration of Particles to High Energies." *Institute of Physics Symposium*, p. 30. London, 1950.
[37] FORTESCUE, R. L. *Progress in Nuclear Physics*, p. 21. London, 1950.
[38] SMEE, J. F. *J. Inst. elect. Engrs.*, Pt. 1 **91** (1944) 422.
[39] PEEK, F. W. *Dielectric Phenomena in High Voltage Engineering*. New York, 1929.
[40] GETTING, I. A., FISK, J. B., and VOGT, H. G. *Phys. Rev.*, **56** (1939) 1098.
[41] VAN ATTA, L. C., NORTHRUP, D. L., VAN ATTA, C. M., and VAN DE GRAAFF, R. J. *Phys. Rev.*, **49** (1936) 761.
[42] TRUMP, J. G., and VAN DE GRAAFF, R. J. *Phys. Rev.*, **55** (1939) 1160.
[43] TRUMP, J. G., MERRILL, F. H., and SAFFORD, F. J. *Rev. Sci. Instrum.*, **9** (1938) 398.
[44] KOSSEL, W. *Z. Phys.*, **3** (1938) 264.
[45] WATERTON, F. W. *J. Sci. Instrum.*, **19** (1942) 105.
[46] JENNINGS, B. *Proc. Inst. Rad. Engrs.*, **38** (1950) 1126.
[47] HERB, R. G., TURNER, C. M., HUDSON, C. M., and WARREN, R. E. *Phys. Rev.*, **58** (1940) 579.
[48] HERB, R. G., PARKINSON, D. B., and KERST, D. W. *Phys. Rev.*, **51** (1937) 75.
[49] TRUMP, J. G., and CLOUD, R. W. *Amer. J. Roentgenol.*, **49** (1943) 531.
[50] TRUMP, J. G. *Elect. Engng.*, **70** (1951) 781.
[51] LOEB, L. B. *Science*, **102** (1945) 573.
[52] PAUTHENIER, M., and MOREAU-HANOT, M. *Comptes Rendus.*, **201** (1935) 1332; **202** (1936) 1915.
[53] PAUTHENIER, M., and MOREAU-HANOT, M. *J. de Phys. et le Radium.*, **8** (1937) 193.
[54] BABAT, G. *J. Tech. Phys. U.S.S.R.*, **3** (1936) 786.
[55] PAUTHENIER, M., and MOREAU-HANOT, M. *J. de Phys. et le Radium.*, **3** (1932) 590; **6** (1935) 257.
[56] MOREAU-HANOT, M. *Comptes Rendus.*, **206** (1938) 1168.
[57] PAUTHENIER, M. *Rév. Gén. Elect.*, **45** (1939) 583.
[58] MOREL, R. *Ann. Univ. Grenoble*, **23** (1948) 155.
[59] TRUMP, J. G. *Elect. Engng.*, **66** (1947) 525.
[60] FELICI, N. J. *J. de Phys. et le Radium*, **8** (1947) 1; **9** (1948) 65; **10** (1949) 137.
[61] MALPICA, J. M. *Rev. Sci. Instrum.*, **22** (1951) 364.
[62] VOLLRATH, R. E. *Phys. Rev.*, **42** (1932) 298.
[63] BOUWERS, A., and HEYN, F. A. *Philips Tech. Rev.*, **6** (1941) 75.
[64] DUINKER, D. *Philips Tech. Rev.*, **5** (1940) 199.
[65] BRAMHALL, E. H. *Rev. Sci. Instrum.*, **5** (1934) 18.
[66] ANDERSON, M. W. *Rev. Sci. Instrum.*, **6** (1935) 309.
[67] MORAND, M., RASKIN, A., and WINAND, L. *Comptes Rendus.*, **234** (1952) 2450.
[68] ONSLOW, D. V. *ERA Report*, *Z/T*55.
[69] SLEPIAN, J. *U.S. Patent* 1666473.
[70] DOUMA, T., and BREKOO, H. J. P. *Philips Tech. Rev.*, **11** (1949) 123.

2

STABILIZATION OF HIGH-VOLTAGE DIRECT CURRENT SOURCES

GENERAL THEORY

A comprehensive review of different types of electronic voltage stabilizers and their elementary theory is given by HUNT and HICKMAN[1], and their important paper, which provides the basis for much of the later work on stabilizers, will now be summarized in some detail. Further extensive work on the theory of feed-back circuits is given in an exhaustive paper by BLACK[2].

In order to distinguish between the effects due to the internal resistance of the rectifier circuit, which provides the power, and the stabilizing circuit, the above authors study two quantities S_o and R_o for a stabilizer operated from a source having zero internal resistance, and two similar quantities S and R referring to the behaviour of a stabilizing circuit and a source of finite resistance. S_o and S are stabilization ratios and R_o and R are the appropriate internal resistances.

Taking the behaviour of stabilizing circuits to be such that a linear variation of output voltage with input voltage or with output current is obtained, the stabilizer circuit may be represented as in *Figure 62a*. Here R_L is the load resistance, and the internal e.m.f. E' is the open circuit output voltage which is a linear function of the input voltage E_i. We require to find E' in terms of E_i, R_o and S_o where the latter is defined (*see Figure 62a* for E_o and e) by

$$\left(\frac{\delta E_o}{\delta E_i}\right)_e = \frac{1}{S_o}$$

where e is a test voltage which is introduced to effect a convenient separation of the variables. Further we put

$$\left(\frac{\delta i_o}{\delta e}\right)_{E_i} = \frac{1}{(R_o + R_L)}$$

and

$$E_o = i_o R_L - e$$

for the output circuit.

Finally

$$E_o = \frac{(E_i + K_1)}{S_o/(1 + R_o/R_L)} - i_o R_o$$
$$= E' - i_o R_o \qquad \ldots\ldots(2.1)$$

(K_1 is a constant of integration), from which

$$E_o = \frac{E_i + K_1}{S_o} - \frac{R_o e}{R_o + R_L} \qquad \ldots\ldots(2.2)$$

Equations 2.1 and 2.2 show that the relations between the output voltage and the input voltage or output current are controlled by the parameters S_o and R_o which are therefore characteristics of any particular stabilizer circuit.

Now introduce the source resistance R_r as in *Figure 62b* where E is the rectifier e.m.f. Again a nearly linear relation can be shown to exist between output voltage and either output current or E. The

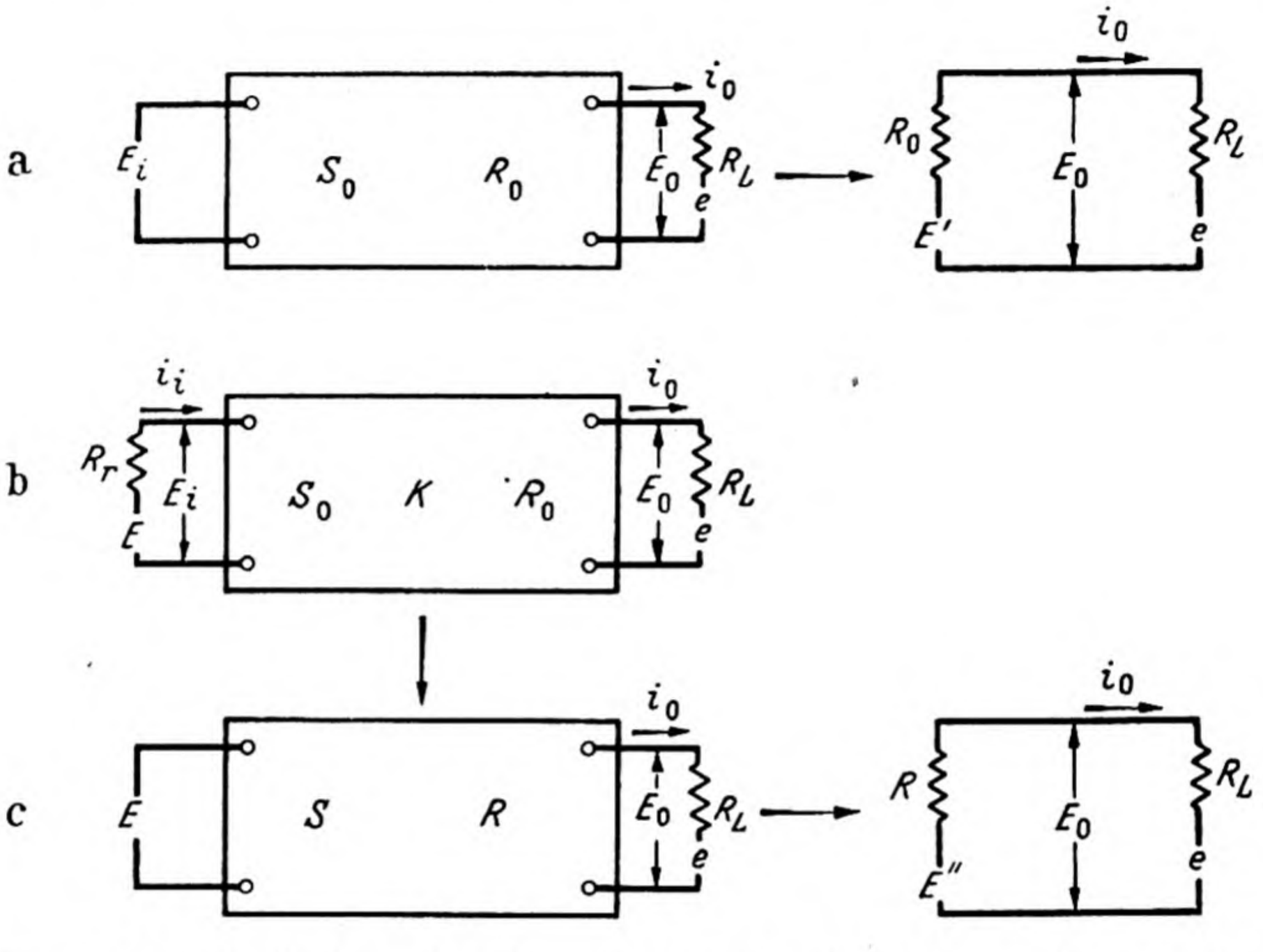

Figure 62. Equivalent circuits and notation for the analysis of the effect of source resistance on stabilizer performance (Hunt and Hickman[1], by courtesy, *Rev. Sci. Instrum.*).

equivalent circuit for the case of *Figure 62b* when we introduce the quantities S and R as explained above, is shown in *Figure 62c*. By definition

$$\left(\frac{\delta E_o}{\delta E}\right)_e = \frac{1}{S}$$

and

$$\left(\frac{\delta i_o}{\delta e}\right)_E = \frac{1}{(R+R_L)}$$

Since some (i_s) of the input current (i_i) to the stabilizer may be diverted from the output we put $i_i = i_o + i_s$ and $i_s = k\ (E_i + K_2)$ where k is an equivalent conductance and K_2 is a constant.

Finally

$$E_o = \frac{(E+K_3)}{S/\,(1 + R/R_L)} - i_o R = E'' - i_o R$$

where K_3 is a constant of integration.

If E and R_r are adjusted to produce the same input E_i as in the first case treated above, the output voltages may be stabilized knowing that

$$E_i = E - i_i R_r$$

We then obtain

$$E\left\{\frac{1}{\alpha S_o} - \frac{1}{S}\left(1+\frac{R_r}{\alpha S_o R_L}\right)\right\} - e\left\{\frac{R_o}{(R_o+R_L)} - \frac{R}{(R+R_L)} + \frac{R_r}{\alpha S_o(R+R_L)}\right\}$$
$$+\left\{\frac{K_1}{S_o} - \frac{R_r k K_2}{\alpha S_o} - \frac{K_3}{S}\left(1+\frac{R_r}{\alpha S_o R_L}\right)\right\} = 0$$

where $\alpha = 1 + kR_r$

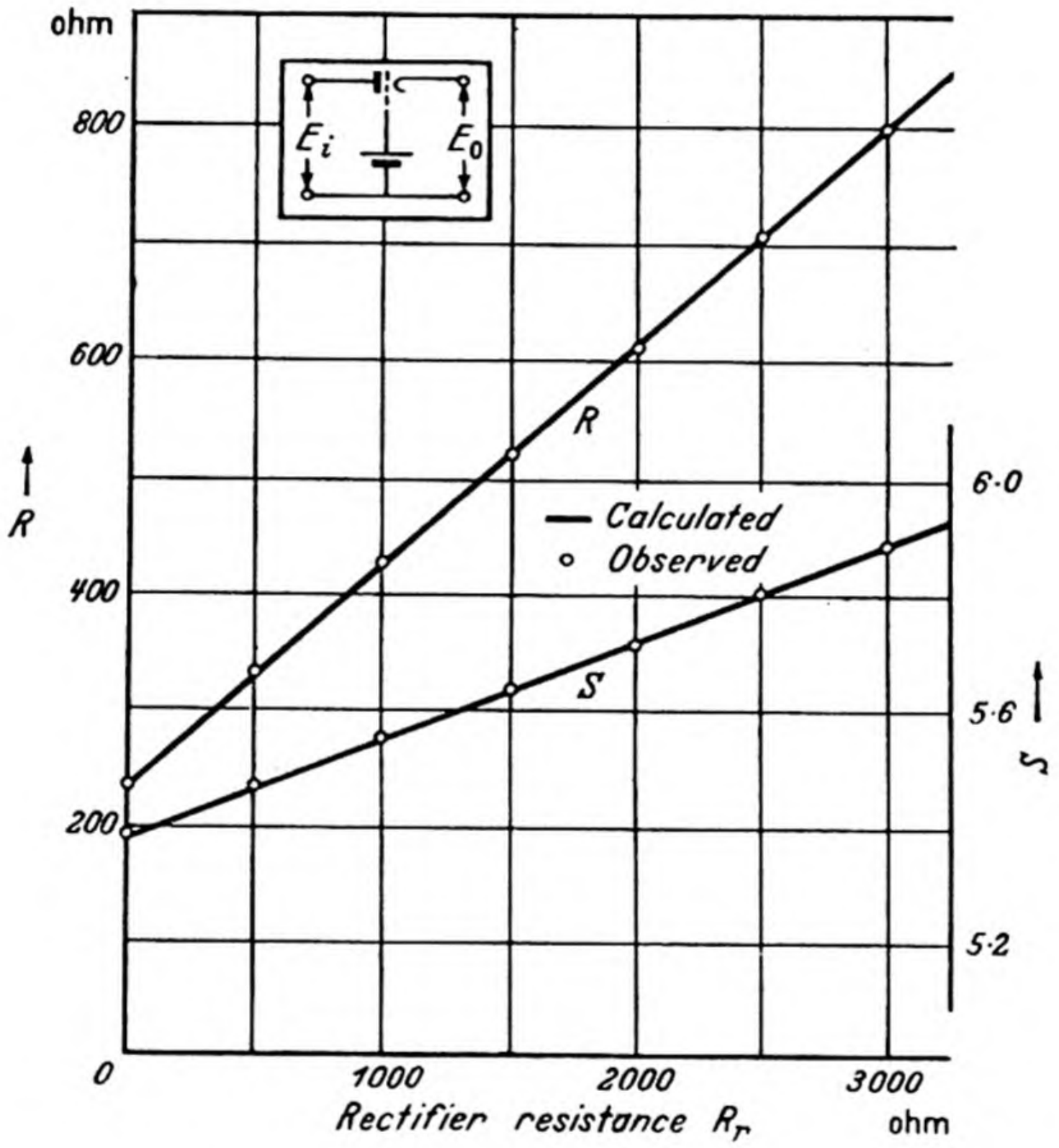

Figure 63. Data verifying the predicted variation in the performance of a simple stabilizer when the internal resistance of the source is altered (Hunt and Hickman[1], by courtesy, *Rev. Sci. Instrum.*).

In order that this expression should vanish for independent variations of E and e each bracket must vanish separately. Thus

$$S = S_o(1+kR_r) + R_r/R_L$$

$$\text{and} \quad R = R_o + \frac{R_r}{S_o} \cdot \frac{(1+R_o/R_L)}{(1+kR_r)}$$

From these expressions the effect of the rectifier-source resistance on the overall stabilizer behaviour can be predicted. The use of the above expressions for R and S is illustrated in *Figure 63* which gives a

comparison between the theory (curves) and practice (circles on the curves) for a simple circuit.

Hunt and Hickman[1] proceed to classify stabilizing circuits into four categories and their discussion will now be briefly summarized.

(1) The bridge circuit (*Figure 64*) used for measuring $\frac{\delta I_p}{\delta e_g}$ (mutual conductance) for a valve, where I_p and e_g are plate current and grid voltage respectively, may be used as a stabilizer since the circuit is arranged to keep the plate voltage e_p constant. Thus if the input, in *Figure 64*, is taken from a rectifier set, the output voltage will be

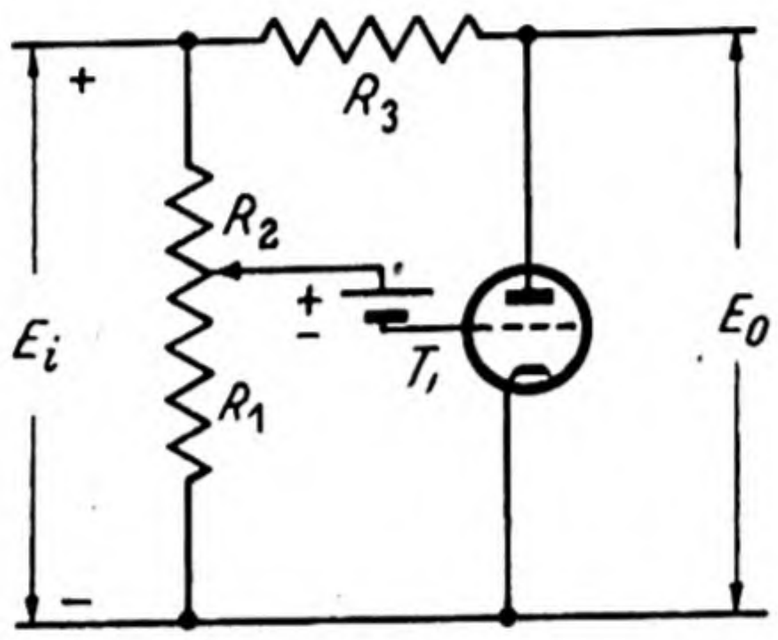

Figure 64. A modification of the *s* type stabilizer derived from the basic transconductance bridge circuit (Hunt and Hickman[1], by courtesy, *Rev. Sci. Instrum.*).

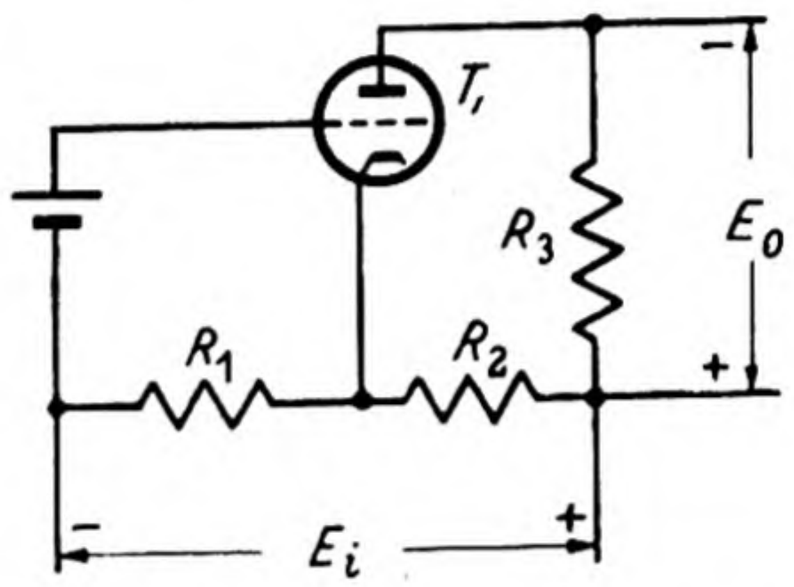

Figure 65. A modification of the *u* type stabilizer derived from the basic amplification-factor bridge circuit (Hunt and Hickman[1], by courtesy, *Rev. Sci. Instrum.*).

stabilized against variations in the input over the range of conditions for which $\delta I_p/\delta e_g$ is constant. This circuit has been described by KING[3] and KOHLER[4]. The balance condition is obtained when

$$S_m = \frac{\delta I_p}{\delta e_g} = \frac{R_1 + R_2}{R_3 R_1}$$

(2) The circuit of *Figure 65* which may be used for the measurement of $-\delta e_p/\delta e_g$ for a valve (I_p constant) may also be used to give stabilization, since the constant current flowing through a stable resistance will give a constant output voltage. This circuit, or modifications of it, have been used for providing stable h.t. supplies for Geiger counters and have been described by STREET and JOHNSON[5], EVANS[6], GINGRICH[7] and ASHWORTH and MOUZON[8]. The approximate balance condition is $u = R_2/R_1$ where $u = -\delta e_p/\delta e_g$. This circuit is specially suitable for high-voltage, low-current supplies since only a portion of the stabilized output voltage appears across the valve.

(3) The next basic form of stabilizer, shown in *Figure 66*, is based on the single-stage degenerative d.c. amplifier. Here the valve is connected in series with the rectifier circuit and the load. Changes in the output voltage tend to compensate themselves through the valve

which may be represented crudely as a series rheostat. In *Figure 66a* the bias voltage has to be almost as large as the output voltage and to avoid this, so as to make a small bias voltage adequate, the circuit of *Figure 66b* has been developed by Street and Johnson[5]. The stabilization ratio for this circuit is approximately equal to the amplification factor of the valve; the data of *Figure 63* refer to this arrangement. In the circuit of *Figure 66b* if the fraction of the output voltage appearing between the grid tap and the positive output terminal is

$$C = R_1/(R_1 + R_2)$$

then the stabilization ratio is approximately Cu (u defined as above)

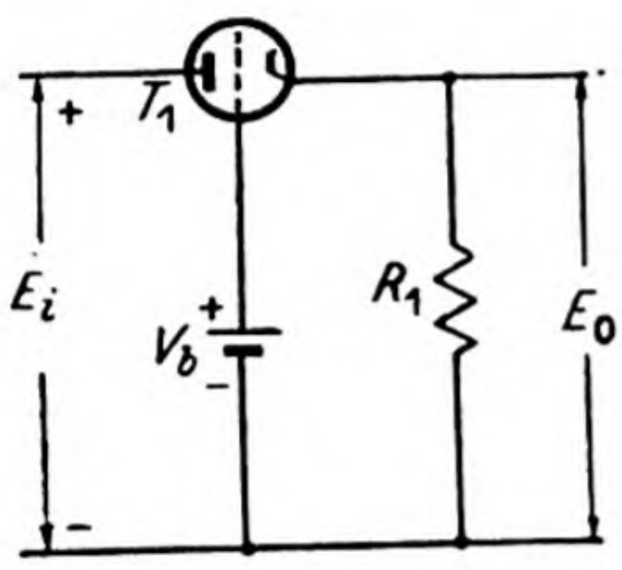

a

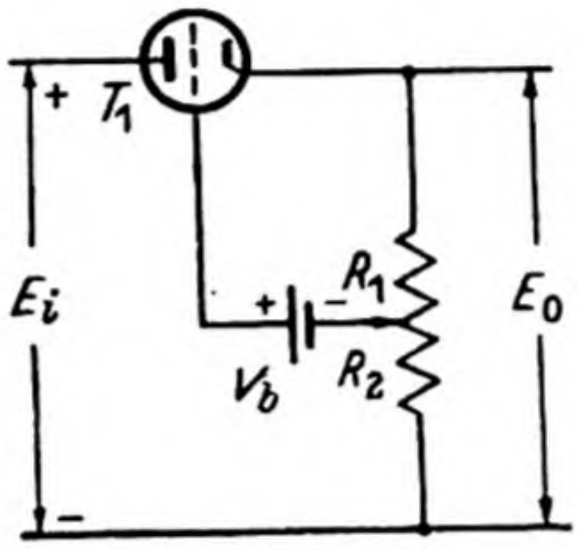

b

Figure 66. Two modifications of the basic degenerative type stabilizer circuit (Hunt and Hickman[1], by courtesy, *Rev. Sci. Instrum.*).

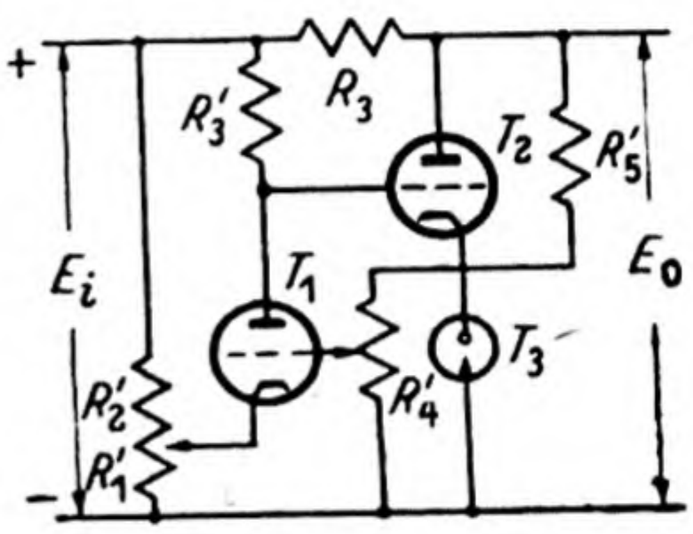

Figure 67. *s* type stabilizer circuit with a *u* circuit arranged to provide a stabilized bias voltage (Hunt and Hickman[1], by courtesy, *Rev. Sci. Instrum.*).

whilst the internal resistance is increased to

$$R_o = 1/(k_p + CS_m)$$

An advantage of this arrangement is that a wide variation in stabilized output may be obtained merely by adjustment of the grid tapping shown in *Figure 66b*.

(4) The final group of stabilizing circuits comprises more complicated arrangements built up from the preceding three groups, for example by the addition of extra amplification. Hunt and Hickman give seven examples of such improved circuits, including for example a combination of type (1) with a type (2) circuit to provide a stabilized grid bias voltage (*Figure 67*). When a variable load is needed, a degenerative stabilizer with a low internal resistance is more satisfactory and an example of this type of circuit is shown in *Figure 68*, where a circuit of type (1) is used to provide the bias. This latter circuit need not have a low impedence since no appreciable current is drawn from it. Further examples in group (4) are given, to meet various special requirements; the paper by Hunt and Hickman[1] should be consulted for a detailed discussion of them.

LINDENHOVIUS and RINIA[9] have described various circuits which may be used for the stabilization of low d.c. voltages and, since the principles of operation are equally applicable to h.t. d.c. sources, their work will be briefly summarized.

Consider again the simple triode circuit shown in *Figure 66* where V_b is a stable bias battery. If E_i increases then E_o will also increase slightly if the load current is constant, to an extent such that the increase in negative bias compensates for the effect of the increase in anode voltage. The ratio $\left(\frac{\Delta E_o}{\Delta E_i}\right)_{\Delta I=0}$ will be termed α. Next, if the load current increases for constant input voltage, the output voltage tends to fall so that the triode grid bias becomes more positive and thus the anode current is increased. The quantity $-\left(\frac{\Delta E_o}{\Delta E_i}\right)_{\Delta E_i=0}$ may be termed the internal resistance R of the system. We wish to determine α and R in terms of measurable or calculable quantities.

We have $\Delta I = S\Delta V_g + \frac{S}{\mu}\Delta V_a$ where V_g, V_a, I, S and μ are respectively the grid voltage, anode voltage, anode current, slope and amplification factor of the valve.

Also
$$\Delta V_g = -\Delta E_o, \quad \Delta V_a = \Delta E_i - \Delta E_o S_o$$
$$\Delta I = -S\left(1+\frac{1}{\mu}\right)\Delta E_o + \frac{S}{\mu}\Delta E_i$$

whence
$$\alpha = \frac{1}{\mu+1} \text{ and } R = \frac{\mu}{S(\mu+1)}$$

or more approximately
$$\alpha = \frac{1}{\mu} \text{ and } R_I = \frac{1}{S}$$

If the output load is a constant resistance R_1, then (*see Figure 66*)

$$\Delta I = \frac{\Delta E_o}{R\mu} \text{ and } \frac{\Delta E_o}{\Delta E_i} = \frac{1}{\mu+1+\frac{\mu}{R_1 S}}$$

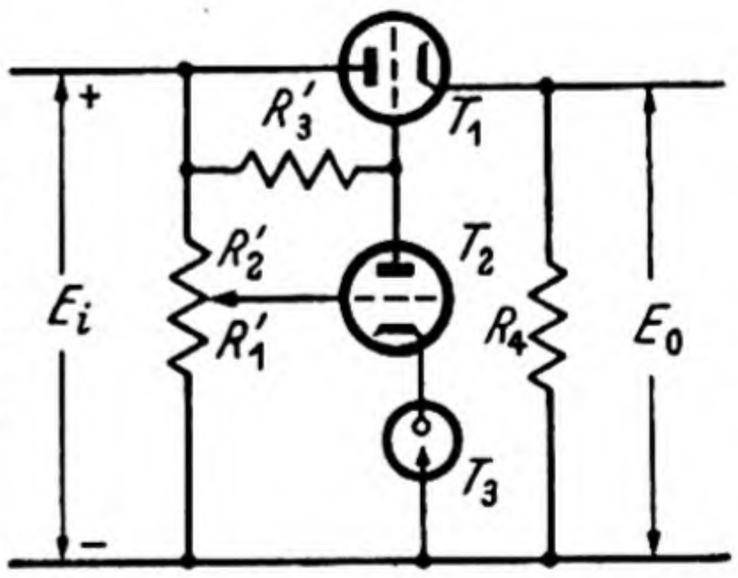

Figure 68. A modification of the simple degenerative stabilizer employing an *s* circuit to provide a stabilized bias voltage; with proper adjustment these circuits simulate the bridge circuit for measurement of negative amplification factor (Hunt and Hickman[1], by courtesy, *Rev. Sci. Instrum.*).

When the rectifier system supplying E_i has an internal resistance R_v then $\Delta E_i = -R_v\Delta I$ and

$$R_{\text{total}} = \frac{\mu}{S(\mu+1)} + \frac{R_v}{\mu+1} \qquad \ldots\ldots(2.3)$$

Here the internal resistance of the circuit is increased by an amount $R_v/(\mu+1)$ from inspection of Equation (2.3). For example with $\mu = 20$, $S = 10$ mA/V and $R_v = 500\ \Omega$ it is found that $\alpha = 0{\cdot}048$ and the internal resistance is 119 Ω.

The circuit of *Figure 66a* can be easily made to give a variable output by taking the battery V_b to the tap on a potentiometer across the output, and greater sensitivity can be achieved with another amplifier valve as in *Figure 67* which shows the circuit of *Figure 68* re-arranged.

$$\text{Here} \quad \alpha = \frac{1}{n\mu + 1} \sim \frac{1}{n\mu}$$

$$\text{and} \quad R_{\text{total}} = \frac{\mu + R_v S}{S\,(n\mu + 1)} \sim \frac{1}{nS} + \frac{R_v}{n\mu}$$

n = amplification given by valve A which is the amount by which this circuit gives an improvement in stability compared with the circuit of *Figure 69*.

To obtain complete stabilization or indeed an over-compensation for fluctuations, a circuit of the type shown in *Figure 70* may be used. For the current through B to remain constant, when the input voltage

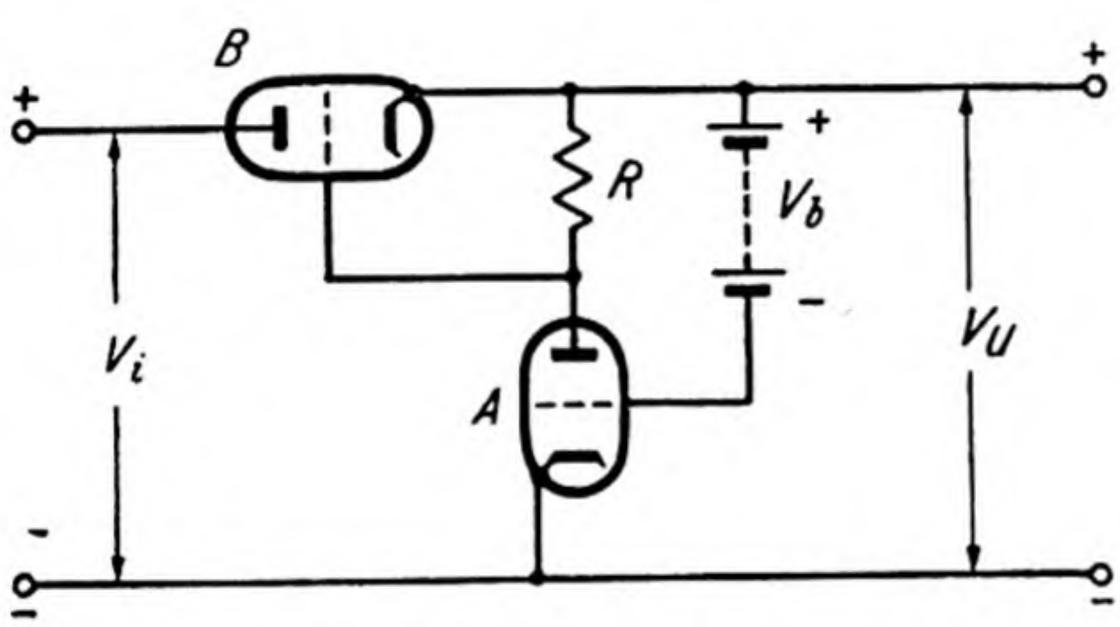

Figure 69. Stabilizer connections with increased sensitivity. The voltage variations on the control grid of the regulating valve B are amplified with the help of a second valve A (Lindenhovius and Rinia[9], by courtesy, *Philips Tech. Rev.*).

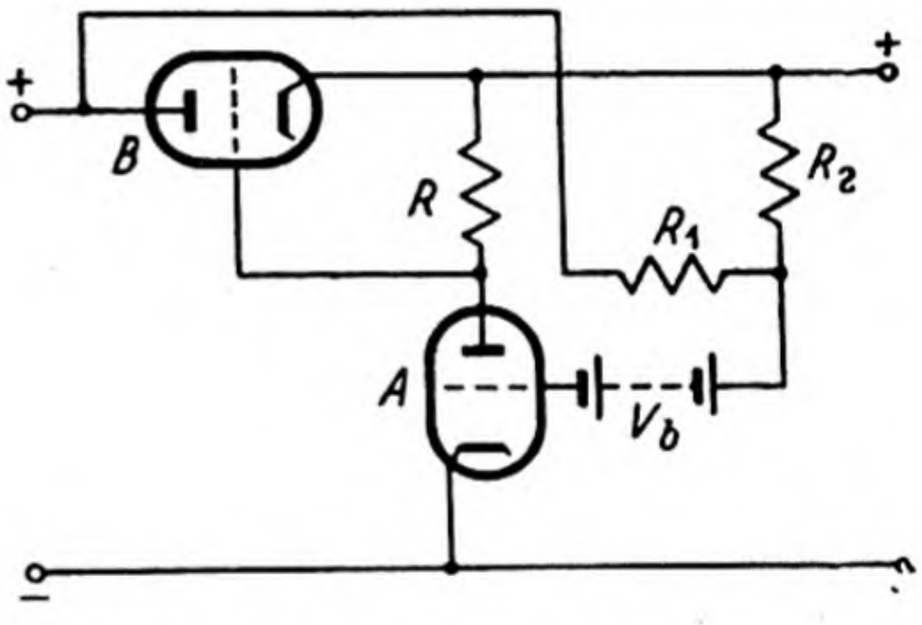

Figure 70. Connections in which the output voltage remains constant despite changes in the input voltage (Lindenhovius and Rinia[9], by courtesy, *Philips Tech. Rev.*).

varies by an amount ΔV_I the grid voltage of B must suffer a change $\Delta V_g = \frac{\Delta V_I}{\mu}$ opposite in sign to ΔV_I. If the grid voltage change for valve A is ΔV_{gA} then

$$\Delta V_{gA} = \frac{\Delta V_I}{n\mu} \qquad \ldots\ldots(2.4)$$

This equals the output voltage, assumed constant, less the bias voltage, also assumed constant, and the potential difference along R_2. The latter varies with ΔV_I the change in input voltage, thus:—

$$\Delta V_{R2} = \Delta V_I \cdot \frac{R_2}{R_1 + R_2}$$

Hence to satisfy Equation 2.4 we must have

$$\frac{R_2}{R_1+R_2} = \frac{1}{n\mu}$$

This equation cannot be exactly satisfied always, since n and μ vary with current to some extent and there is still a residual voltage variation given approximately by

$$\frac{\Delta V_u}{\Delta V_I} \sim \frac{1}{n\mu} - \frac{R_2}{R_1+R_2}$$

so that n should be as large as possible.

Various further developments of these basic circuits are also discussed by Lindenhovius and Rinia[9] who finally describe a d.c. set to supply power at 150–300 V, with a maximum output current of 100 mA. A mains voltage variation of 5 per cent causes an output voltage variation of $< 0{\cdot}004$ per cent.

STABILIZING CIRCUITS USING THERMIONIC VALVES

Examples of modern circuits, based on types illustrated briefly above, designed to supply stabilized h.t. voltages of perhaps 1–5 kV for Geiger counters, photomultiplier tubes and similar devices, are given in various books[10, 11].

Many stabilized d.c. supply sources for 50–150 kV have been built by various authors, usually to the general system described by Hunt and Hickman which can be represented also as in the outline diagram of *Figure 71*[12]. Here A is the unstabilized supply and B

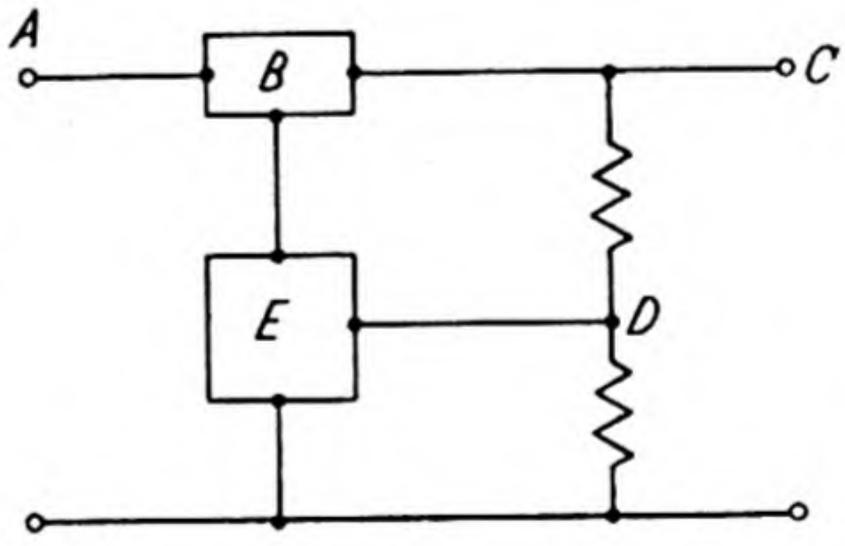

Figure 71. Block diagram of feed-back stabilizer (Haine[12], by courtesy, *J. Inst. elect. Engrs.*).

subtracts from the supply a voltage which is derived from the output of the amplifier E which in turn is controlled by a fraction of the stabilized output, taken off the potentiometer D. The stabilizing ratio S, or the reduction in voltage variations from A to C is given by

$$S = \frac{1}{1+A} \quad \text{or if } A \gg 1,\ S = \frac{1}{A}$$

where A is the overall internal amplification of the feed-back system. HAINE[12] shows clearly that in order to obtain the best possible resolution with an electron microscope the fractional variation in h.t. should not exceed approximately 0·005 per cent.

The basic circuit given in *Figure 71* can be developed further as in VAN DORSTEN's work[13] to give the circuit of *Figure 72* in which L_2 replaces B of *Figure 71*. V_2 is a stabilized d.c. supply which is opposed to the p.d. between B and C thus enabling the valve L_1 to have normal grid bias. The amplification factor of the pentode L_1 may be $\sim 3{,}000$ so that fluctuations in the voltage across BC are greatly amplified, partly by L_1 and partly by L_2 which may give a further amplification ~ 100. Thus the current through R_1 tends to remain constant because if the input voltage V_1 rises, C tends to become more negative with respect to B and the voltage across L_1 and L_2 rises thus reducing V_1. The fluctuations of voltage appear between B and D. R_1 should be a wire-wound resistance with low temperature coefficient, immersed in oil.

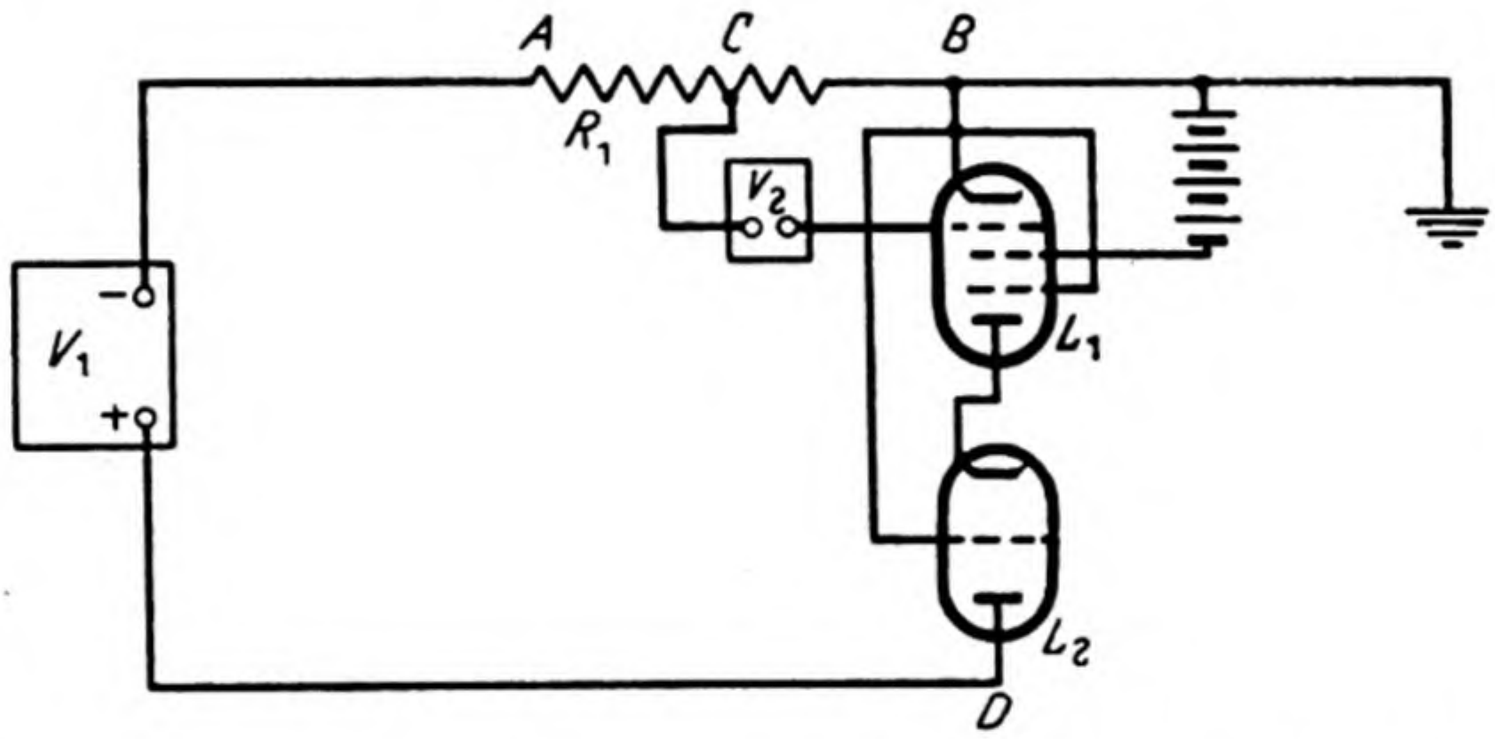

Figure 72. Circuit diagram applied for the stabilization of the constant potential for an electron microscope. V_1 = voltage supplied by the rectifier. V_2=a highly constant reference voltage ; R_1 is a high-stability resistor, L_1 a pentode and L_2 a triode. The electron microscope is shunted across the resistor between A and B (van Dorsten[13], by courtesy, *Philips Tech. Rev.*).

The more detailed development of the circuit of *Figure 72* is shown in *Figure 73* which includes the rectifier valve G and the h.t. transformer which has a stray capacitance between its h.t. terminal (E) and earth. The capacitive current through this stray impedance, which also passes through L_1 and L_2, may be higher than the stabilized load current, especially for high-voltage low-current sources for electron microscopes, perhaps even by a factor $\sim 10^5$ greater than that for low-voltage, high-output-current sets. To reduce the effect of this capacitive current the filter F (*Figure 73*) may be used, but electrostatic screening of the transformer winding is usually more effective. Similar difficulties may arise with the filament transformer for G unless appropriate measures are taken. The input capacitance of the pentode L_1 in *Figure 72* is reduced if V_2 is applied between B and the cathode of L_1. Also since the resistance AC may

be $\sim 10^8$ ohms it should be shunted with a small capacitance, to correct for the effect of the stray capacitance between C and ground which tends to slow down the response of the stabilizing circuit to rapid fluctuations in voltage. The shunt capacitor between A and C should be in series with a resistance to limit the current in case of break-down in the electron gun to which the voltage across AB is applied.

The final circuit is shown in *Figure 74*. Here the rectifiers L_3 and L_4 are used with the h.t. transformer T_1 (80 kV) in a voltage-doubler circuit; the secondary of T_2, supplying L_3, is insulated for 20 kV and

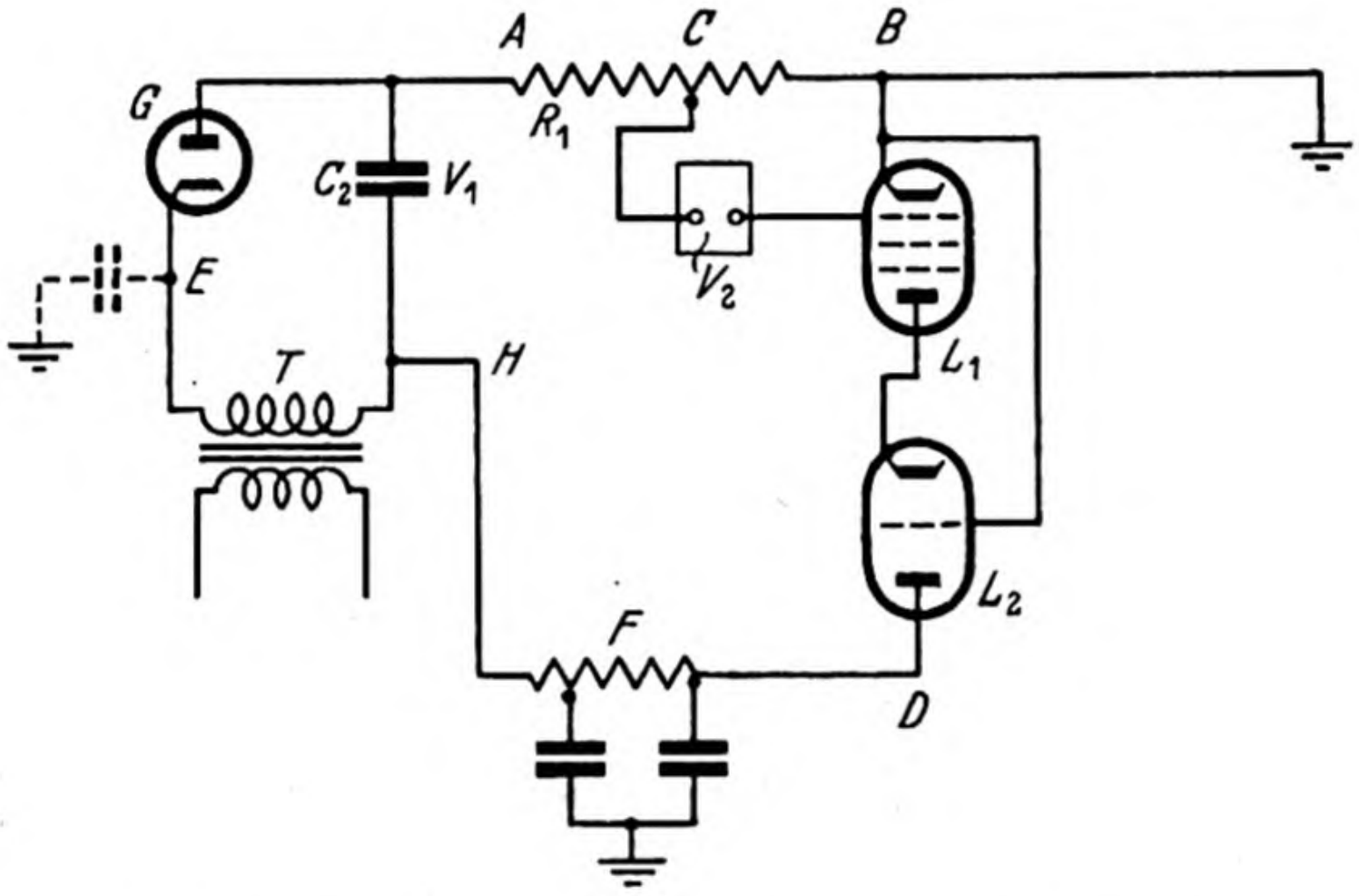

Figure 73. Diagram of the system of *Figure 72* further extended to include the high-tension transformer T and the rectifying valve G, a smoothing condenser C_2 as well as a filter F to eliminate the alternating voltage arising from the capacitive current flowing from the high-tension terminal of the transformer to earth (van Dorsten[13], by courtesy, *Philips Tech. Rev.*).

the secondary of T_3 is insulated for 180 kV. T_3 is connected on its primary side through another transformer insulated for 20 kV, whose secondary with that of T_2 is connected to the case of T_1 to bypass the capacity current. The resistance R_1, *i.e.*, the output resistance of the h.t. source, through which a constant current flows, should clearly be as stable as possible. In the present case it comprises a coil of resistance-wire wound helically on a cotton core, in a fashion similar to that used by WATERTON[14] (*see* pages 374–376), and in turn is wrapped on a glass cylinder and immersed in oil in a suitable insulating container. The length of the resistance cylinder is 1·8 m.

Van Dorsten describes how the circuit is brought into adjustment by setting B and D after which, by hand adjustment of T_o, the valve

L_2 is brought into its regulating range, taking up a voltage of about 7 kV. The high-impedance valve voltmeter M_1 indicates the fluctuations in voltage on the input side of the stabilizing circuit; these can range up to ± 5 per cent. in the mains voltage.

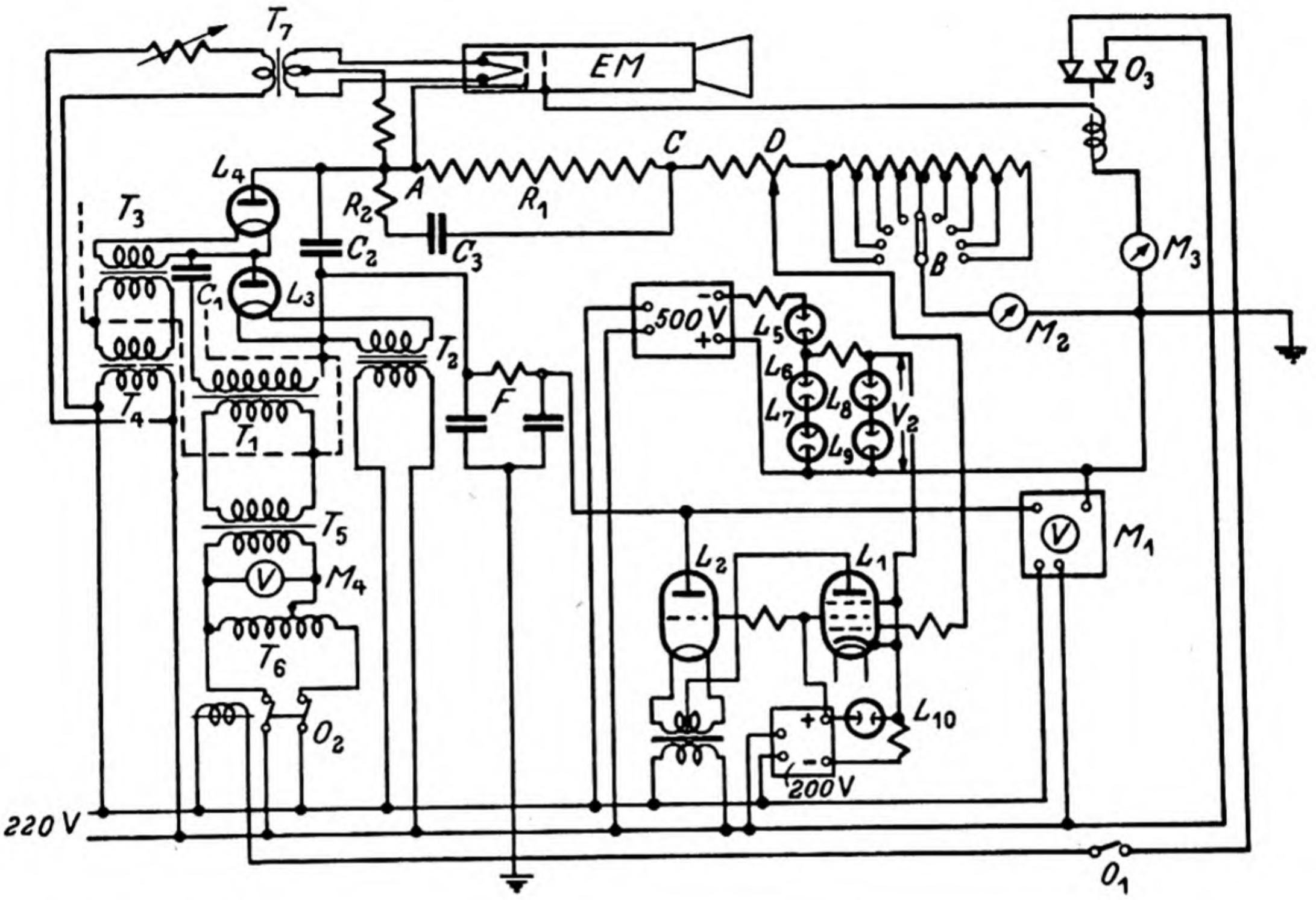

Figure 74. Circuit diagram of the high-tension installation of the experimental electron microscope for 150 kV installed in the Institute for Electron-microscopy at Delft. *EM* is the electron microscope, L_1 and L_2 are a pentode and a triode respectively, L_3 and L_4 two rectifying valves, L_5–L_{10} neon stabilizing valves, M_1–M_4 measuring instruments, O_1–O_3 switches, T_1–T_7 transformers, F a filter. The box of the high-tension transformer is represented by a dotted line. In so far as this circuit relates to the high-tension rectifier, the following is to be noted : The transformer T_1, connected on the primary side to the regulating transformer T_6 via the intermediate transformer T_5, supplies on the secondary side a voltage with a maximum peak value of 80 kV. C_1 is a condenser having a value of 0·05F. Since the load current is small (1–2 mA), at maximum voltage this condenser is charged almost up to 80 kV, the peak value of the transformer voltage via the high-tension valve L_3 (type 28122). The pulsating voltage, amplitude about 2×80 kV, across this valve causes the condenser C_2, with a value of 0·025 F, to be charged *via* the valve L_4 to a voltage of about 160 kV (van Dorsten[13], by courtesy, *Philips. Tech. Rev.*).

A circuit for stabilizing 40 kV (d.c.) to about 0·02 per cent. has been described by HANSON[15] who has used it, as described in Chapter 1, to provide a stable source for measuring the beam voltage in a Van de Graaff generator. The rectifier set (*Figure 75*) consists virtually of

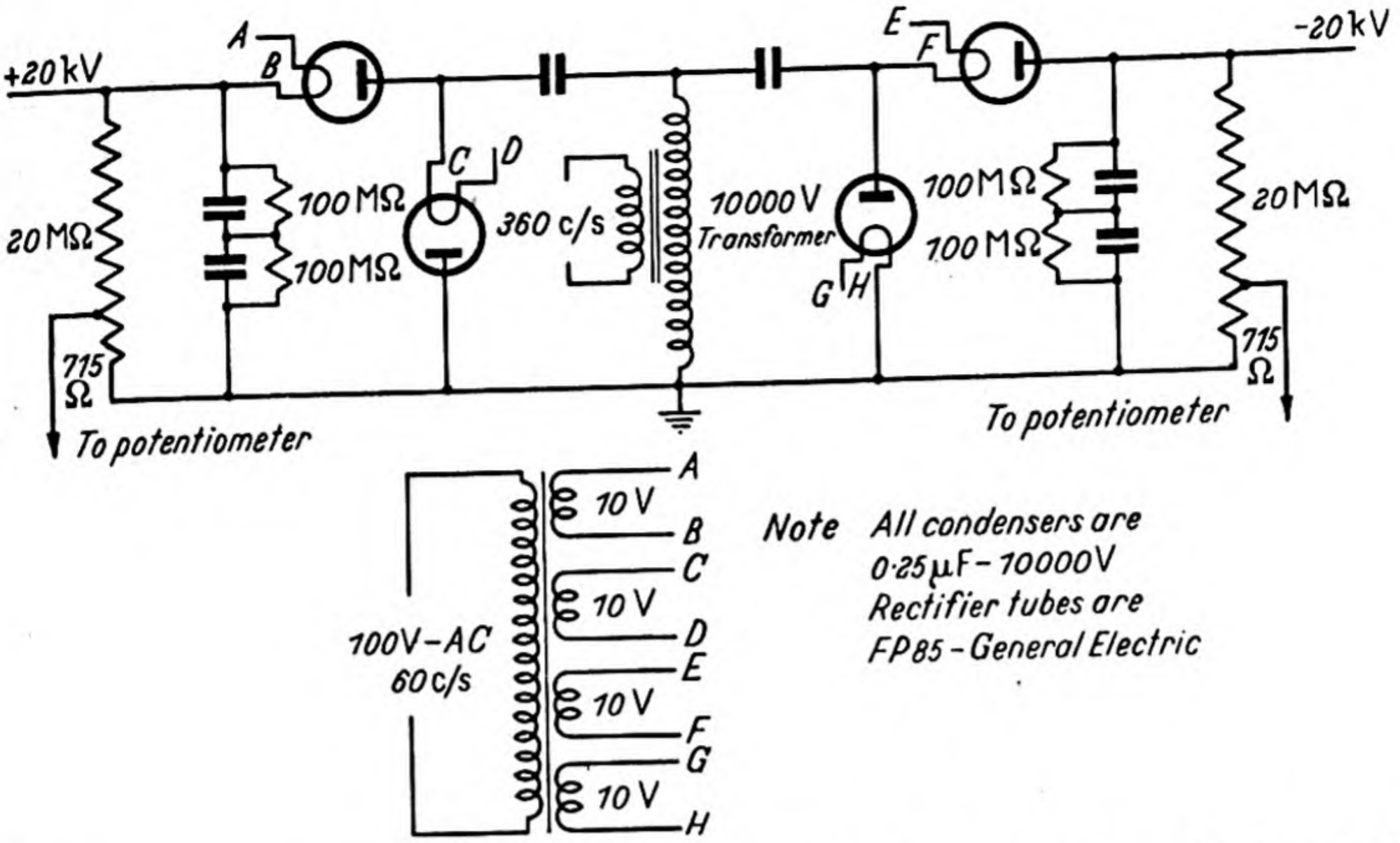

Figure 75. 40 kV supply (*see Figure 76*), (Hanson[15], by courtesy, *Rev. Sci. Instrum.*).

two voltage doublers each supplying 20 kV (one negative and the other positive), and incorporates a 10 kV 360 c/s transformer excited from an a.c. generator, which is driven by a three-phase induction motor. The latter, run below its rated power, is practically synchronous but the regulation so provided is inadequate and a degenerative regulator (*Figure 76*) was built. In this, a fraction of the total voltage from the rectifier set is balanced against a 45 V

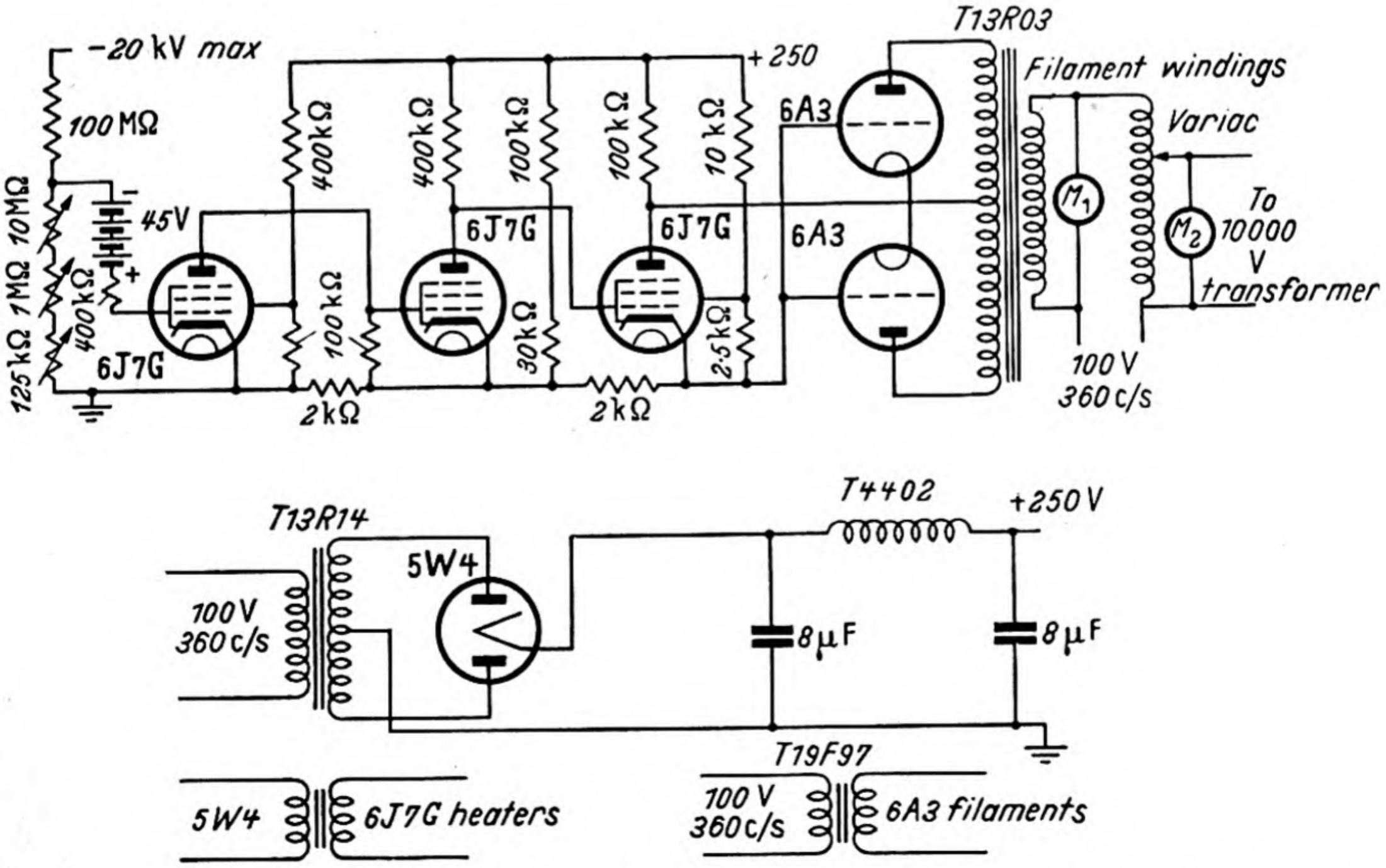

Figure 76. Regulator for 40 kV supply (Hanson[15], by courtesy, *Rev. Sci. Instrum.*).

battery and the difference voltage, amplified by the circuit shown, controls a variable impedance placed in series with the Variac, from which the a.c. input to the rectifier set is taken, in such a way that fluctuations in d.c. output tend to be minimized. The variable impedance consists of two filament windings on a radio power transformer connected in series, and their impedance is controlled by the two 6A3 tubes which energize the primary of the transformer.

The amplifier input resistance (100 MΩ) is made of ordinary 1 watt 10 MΩ resistance units which cause a drift less than 0·05 per cent. during a five-minute run. This is often not objectionable. The input capacity should be a minimum since the time constant so introduced would cause hunting. The output voltage is set as follows. First the input resistors in the regulation amplifier are set at a low value and the Variac is then adjusted until the output voltage is slightly above the desired value and the input resistors are then increased until the voltage is reduced to the required value by the stabilizer. The voltage is measured with a resistance unit, described in Chapter 11 (pp. 376–377).

STABILIZING CIRCUITS FOR ELECTRON MICROSCOPES

Recent developments in electron microscopy have made stable h.f. supplies essential. A variation of not more than about 0·007 per cent.[16] for a voltage of 20–100 kV is often required for a load current of about 1 mA or less, and for an exposure time of perhaps 30 seconds.

VANCE's simple and compact system[16] is similar to that of *Figures 75* and *76*; the h.t. voltage is derived from a voltage-doubler circuit, oil-immersed in a metal tank. Part of the h.t. is tapped off with a 10^9 Ω, 100 kV carbon resistance potentiometer, with a tapping point at 5–25 MΩ from the l.t. end of the potentiometer. Current limitation is provided by the resistance element of the h.t. output filter. The h.t. stabilization is obtained by backing-off a 500 V dry battery against the voltage tapped-off from the supply and amplifying the difference voltage, using a IN5G valve d.c. coupled to a 6L6. The latter drives two 203 A valves, which act as a variable resistance across the secondary of a transformer whose primary is connected in series with the a.c. supply to the h.t. generator. A network is used to give power factor correction, and maintains the input impedance of the generator fairly constant over a wide range of output voltages, which are obtained by coarse control of the input voltage to the fine control circuit.

This circuit should[16] reduce the input line voltage fluctuations by several thousand times, unless the changes are very rapid. The standard battery is found to maintain a voltage constant to less than 3 parts in 10^6 over 30 seconds and a similar stability is claimed for the

resistance value of the potential divider taken as a unit, although the ratio of the divider is found to change by more than this value. Drift of the d.c. amplifier is made negligible by supplying the input valve (11V5G) with special supplies (~0·1 per cent. stability) for its plate, screen and filament. The circuit ripple is about 0·0016 per cent.

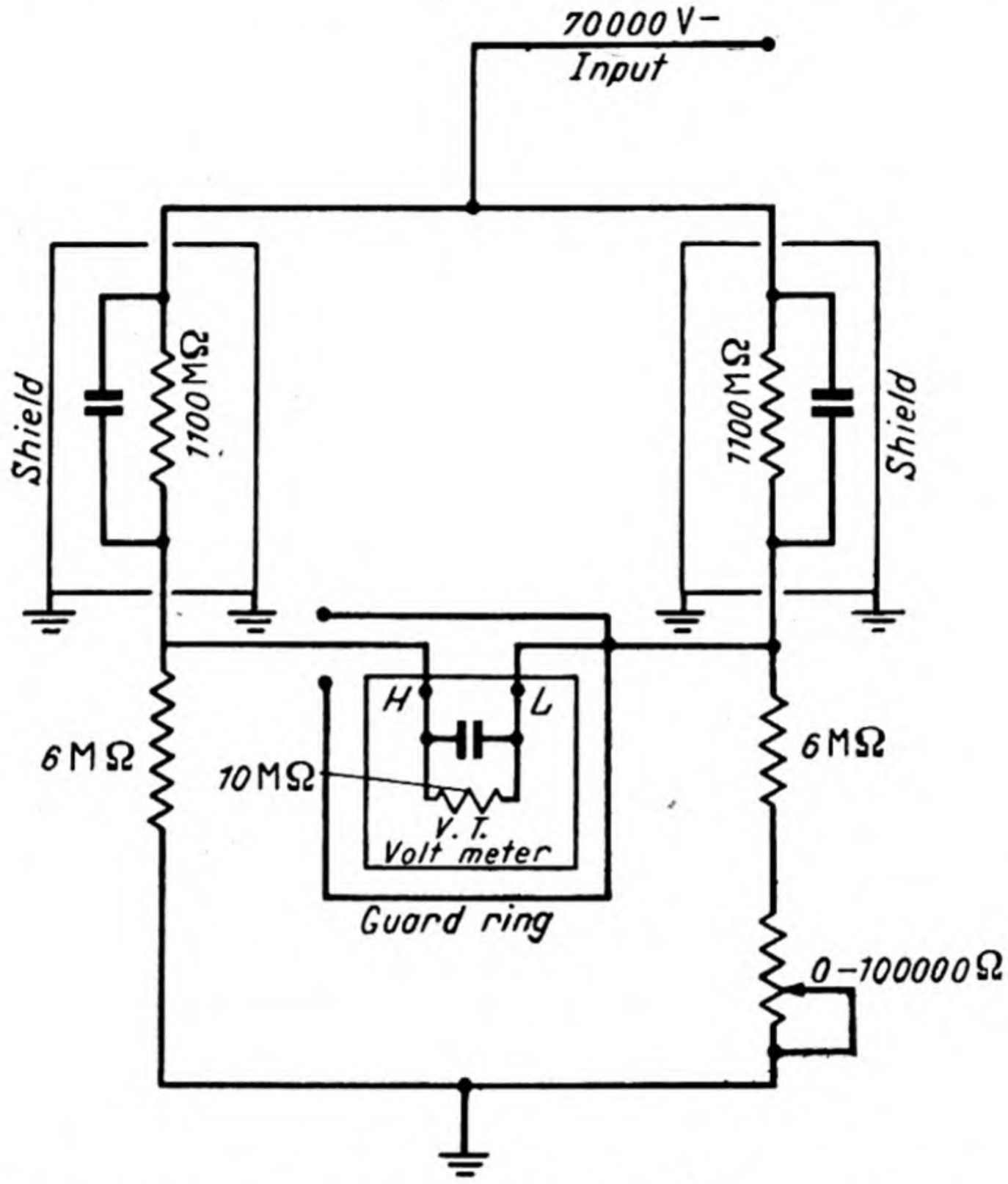

Figure 77. A bridge circuit for tests of circuit stability (Vance[16], by courtesy, *R.C.A. Rev.*).

Vance treats the measurement of the stability of his circuit in some detail, pointing out that to a first approximation the absolute value of the voltage is unimportant for the purposes of electron microscopy. The bridge circuit of *Figure 77* was made in which two identical potentiometers (1,100 MΩ, 100 kV) were used each consisting of carbon resistor chains immersed in wax with 6 MΩ wire-wound resistors for the lower arms of the bridge. Compensating condensers are mounted in the case of each high resistance unit. The detector is a valve voltmeter reading 0·1 V full scale at 10 MΩ resistance, shunted by a condenser so that the capacitance ratio of the bridge is nearly equal to the resistance ratio. The 100 kΩ resistor (*Figure 78*) is used to balance the bridge. At 70 kV input, the maximum variation in 30 seconds is 0·001 V, peak-to-peak, giving a stability for each potentiometer of 0·00026 per cent. on the assumption that the true variation in each potentiometer occurred at random. A dry battery is then used to replace one potentiometer, as in *Figure 76*, and in 20 minutes the average meter deflections during 30 seconds were 0·014,

0·007 and 0·003 V which correspond, since the dynamic ratio of the potentiometer is 294, to fluctuations of about 0·006, 0·003 and 0·0012 per cent. With the ripple, therefore, the maximum fluctuation is about 0·0075 per cent.

Van Dorsten, Nieuwdorp and Verhoeff[17] have described a different system from those described above, for the stabilization of the h.t. supply of an electron microscope working at voltages of 50–100 kV. In this case the authors did not find it necessary to allow for fluctuations in the load current provided by the h.t. source, as van Dorsten[13] had done with his feed-back circuit shown on page 70,

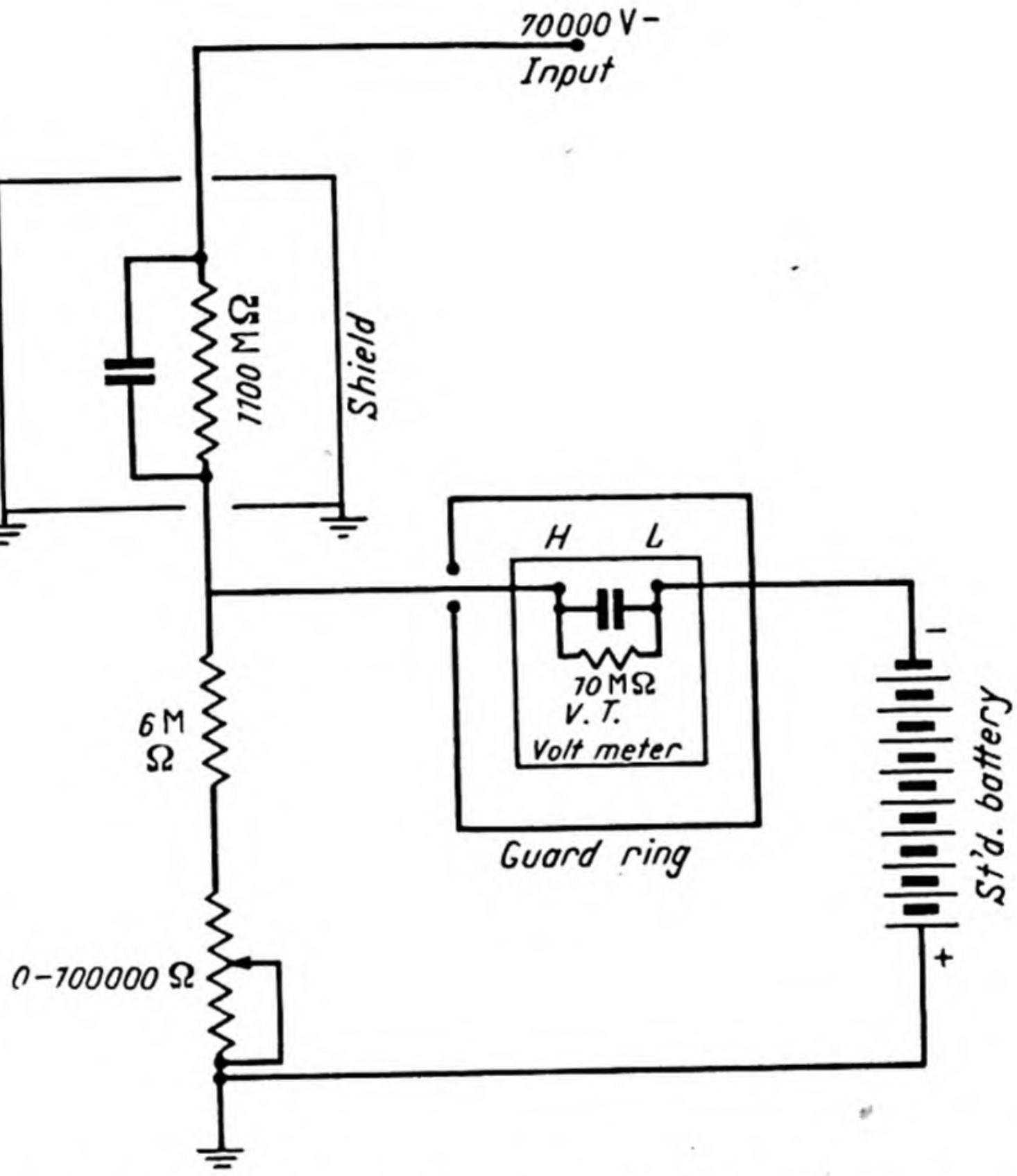

Figure 78. Illustrative of Vance's method of testing voltage stabilizing circuits (Vance[16], by courtesy, *R.C.A. Rev.*).

because in the present case[17] the electron gun in the microscope is arranged as a self biasing triode and is, to a satisfactory extent, self-stabilizing in beam current. Hence it is necessary only to compensate for input voltage fluctuations.

The basic circuit is shown in *Figure 79*. The d.c. rectifier set is oil-immersed and is supplied from a 100 c/s 20 W valve oscillator, which obtains its d.c. supply from a stabilizing circuit of the type described by Lindenhovius and Rinia[9]. The advantage is that only low-voltage d.c. need be stabilized. The other details of *Figure 79* are self-explanatory, with the exception of *G* which is a stabilized

d.c. source for the oscillator valve. The high-voltage transformer supplies power at 50 kV, multiplied by the cascade valve system $V_1 V_2$ and the output is controlled with the variable ratio transformer T_r.

The stabilization of h.t. sources for electron microscopy has been studied by many other workers, for example, MARTON[18] whose pioneer work in this field is well known. Exhaustive bibliographies of papers on electron microscope techniques have appeared.

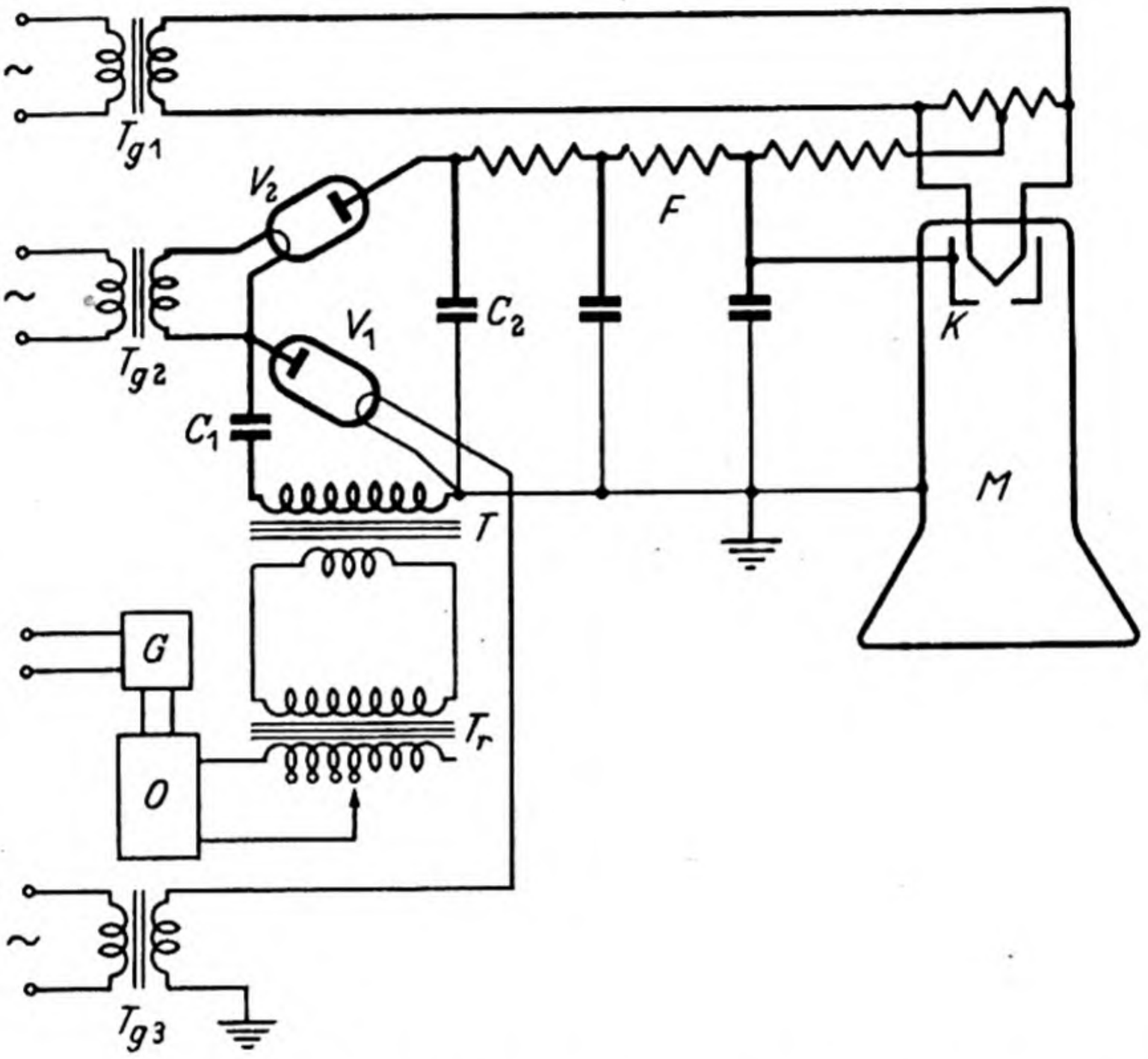

Figure 79. Circuit of a high-voltage generator. T high-voltage transformer, C_1, C_2 capacitors and V_1, V_2 valves of the cascade circuit, T_r variable-ratio transformer, T_{g1}, T_{g2}, T_{g3} filament-current transformers, F smoothing filter, M microscope tube with cathode K and earthed anode. The generator is fed from the valve oscillator O (frequency 100 c/s) which receives the necessary anode and filament voltages from the stabilized supply unit G. The high-voltage parts are drawn in heavy lines (van Dorsten[17], by courtesy, *Philips Tech. Rev.*).

MULVEY[19] has described how the stability of the h.t. supply of an electron microscope may be checked by observations of the shadow pattern of an object placed near the back focus of the final projection lens. The variation in shadow pattern due to spherical aberrations of the lens are sensitively related to changes in h.t. voltage and an accuracy of measurement considerably better than 1 V in 50 kV is readily obtained. In a particular experiment the accelerating voltage changed by less than 1 V during an exposure time of 20 seconds. The method can be used whilst the electron microscope is being

operated in the usual manner and thus variations of h.t. voltage during an exposure may be measured.

MISCELLANEOUS STABILIZING SYSTEMS

RUTHERGLEN[20] has developed a feed-back circuit to stabilize a Philips d.c. generator (about 1 MV) and his system has been used at the University of Liverpool where a stability better than 3 kV has been obtained with a similar generator.

The use of a saturated diode as a constant current device to provide a constant voltage drop along a load resistance, irrespective of the voltage input, has long been used to provide stabilized d.c. THOMSON, FINCH and others have applied this technique in electron diffraction work[21] as mentioned by THOMSON and COCHRANE[22]. Voltages of some 50–100 kV can be stabilized in this way and it would seem profitable to investigate this method again using modern valves, in view of its simplicity.

In their precise work on the measurement of small ionization currents in gases, necessary for the determination of Townsend's α and γ coefficients, LLEWELLYN JONES and PARKER[23] have used a stabilized d.c. source for ~ 100 kV of the following form. A 500 c/s motor-alternator with a carbon-pile stabilizer and driven by accumulators provides power for a voltage-doubler circuit, the smoothing circuit of which consists of ten 0·25 μF condensers in series, centre-tapped for voltage doubling and followed by a filter composed of a 1 MΩ resistor and four 0·5 μF condensers in series. No ripple is observed and the calculated amount is $< 10^{-4}$ per cent. Slow fluctuations of about 4×10^{-2} per cent., due to a certain lack of stability of the motor generator and battery, are recorded. For much experimental work of this kind, this limit is of trivial importance and the above simple system has much to commend it.

Other relatively simple circuits, for the provision of stabilized h.t. voltages, may be built with constant-voltage transformers using the non-linear characteristic of a saturated iron core. One of the basic types of magnetic stabilizers consists merely of saturated and unsaturated reactors connected in series; the output voltage is tapped off across the former and thus varies less with current than the input voltage.

A particular commercial model (Foster Type FCPF) shown schematically in *Figure 80* will give an output voltage (50 c/s) constant to within ± 1 per cent. for varying power factor and will vary by not more than 4 per cent. from no load to full load at any power factor. Standard units rated up to about 5 kVA are available and will give an output voltage, on full load, constant to $\pm 0{\cdot}5$ per cent. for $\pm 12{\cdot}5$ per cent. change in supply voltage. It is sometimes necessary to

filter harmonics from the output supply. Two such transformers, operated in cascade, may give a stability $\sim 0{\cdot}1$ per cent., adequate for many experiments in which the highest possible stability is unnecessary. For d.c. output the above transformers may be connected to suitable rectifier sets in the normal manner.

Constant-voltage transformers have been used for the stabilization of high d.c. voltages, mainly for electron microscope and spark breakdown work. Thus LIEBMANN[24] mentioned the use of a saturated-core constant-voltage transformer to reduce mains fluctuations. The transformer is connected to a two-stage negative-feed-back amplifier backed off with a dry battery and giving residual fluctuations, on constant load, of ~ 1 V in 50 kV.

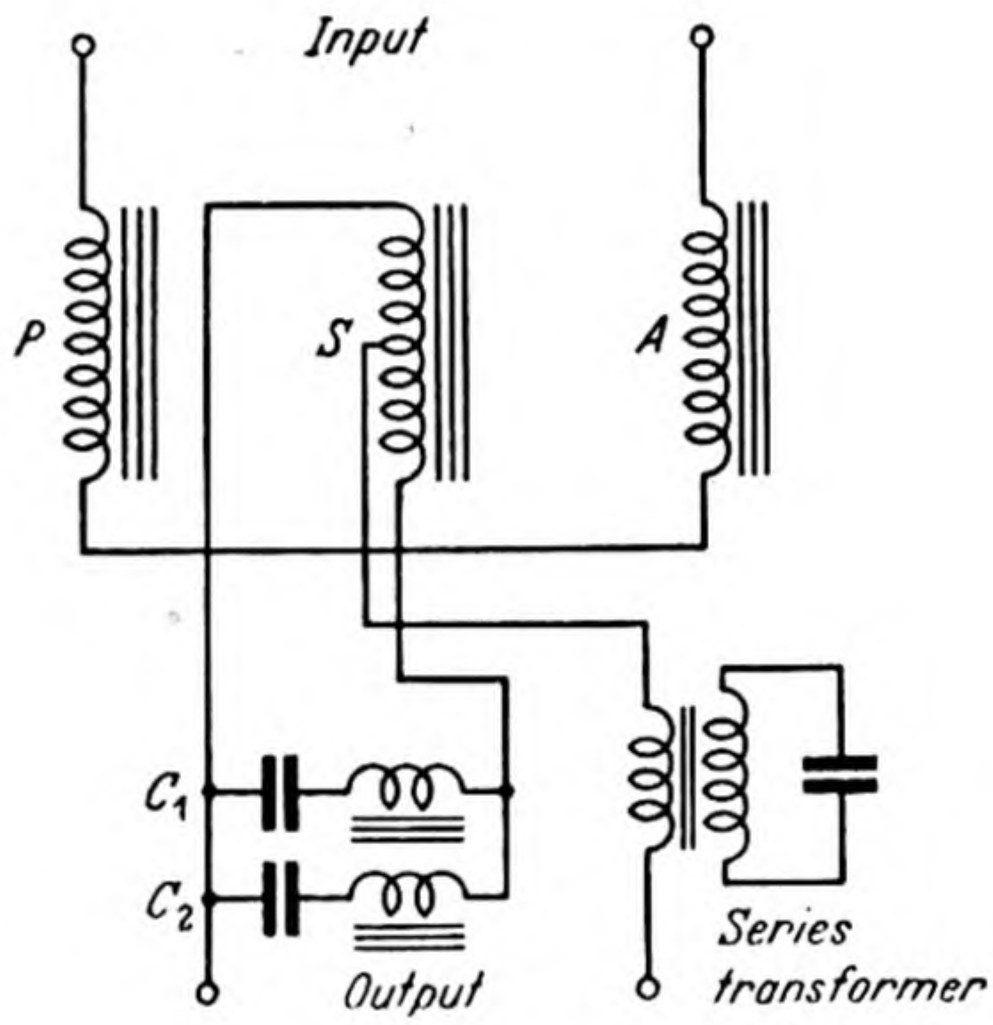

Figure 80. Foster regulator (Hafstad, Heydenburg and Tuve[29], by courtesy, *Phys. Rev.*).

Other similar arrangements have been described by BEDELL and KUHN[25] and an excellent summary is given by BENSON[26].

A magnetic amplifier with a gain $\sim 10^6$, load resistance 10 Ω, 0·5–360 watts output, has been briefly described by FAHNESTOCK[27]. With this apparatus the regulation is 0·5 per cent. in output for ± 10 per cent. change in line voltage or load current, from 0–300 mA at a d.c. output voltage of 200–300 V. It is clear that a regulation comparable with that obtained by the use of valve circuit stabilizers (*see* pages 70–72) may be obtained by cascading transductors or with magnetic amplifiers but it seems likely that the very high degree of stability (say $\sim 0{\cdot}01$ per cent.) needed in some experiments[28] is best obtained by means of valve amplifiers with appropriate feed-back devices.

BENSON's recent book on voltage stabilizers[26] gives an exhaustive treatment of many experimental methods, including the use of discharge tubes as stabilizing elements, magnetic stabilizers (for example saturated-core transformers) and many thermionic circuits. A bibliography of 292 references is included in this work.

VOLTAGE STABILIZATION OF VAN DE GRAAFF GENERATORS

A detailed study of voltage fluctuations in a 1·2 MV open-air Van de Graaff generator has been made by HAFSTAD *et al*[29]. The fluctuations in the generator voltage are measured across a tapping point on a 10^4 MΩ voltmeter resistor (described on page 376) with a suitable amplifier, and are found to be $\sim \pm 1$ per cent. or about 1·4 per cent. peak ripple. Measurements of the fluctuations in 250 equal ' voltage intervals ' gave the statistical data of *Figure 81* in which the total voltage is compounded from that inside the h.t. terminal and that outside the terminal. The latter is measured with the

Voltage in kV	*Fluctuation in kV or Per Cent*		
	RMS	$W_H/2$	W_O
468 (OUTSIDE)	1·20	3·70	5·60
105 (INSIDE)	1·20	1·20	1·90
573 (TOTAL)	1·70	3·90	5·90
FLUCTUATION %	0·29	0·68	1·03
720 (OUTSIDE)	1·9	5·5	11·1
105 (INSIDE)	1·2	1·2	1·9
825 (TOTAL)	2·24	5·7	11·2
FLUCTUATION %	0·26	0·69	1·35
800 (OUTSIDE)	3·3	8·0	16·0
105 (INSIDE)	1·2	1·2	1·9
905 (TOTAL)	3·5	9·2	16·2
FLUCTUATION %	0·39	0·89	1·8
886 (OUTSIDE)	4·6	9·7	27·7
105 (INSIDE)	1·2	1·2	1·9
991 (TOTAL)	4·7	9·8	27·8
FLUCTUATION %	0·48	0·98	2·8

ORDINATES : Instantaneous voltage from oscillograph-trace
ABSCISSAE : Total time spent at corresponding voltage.

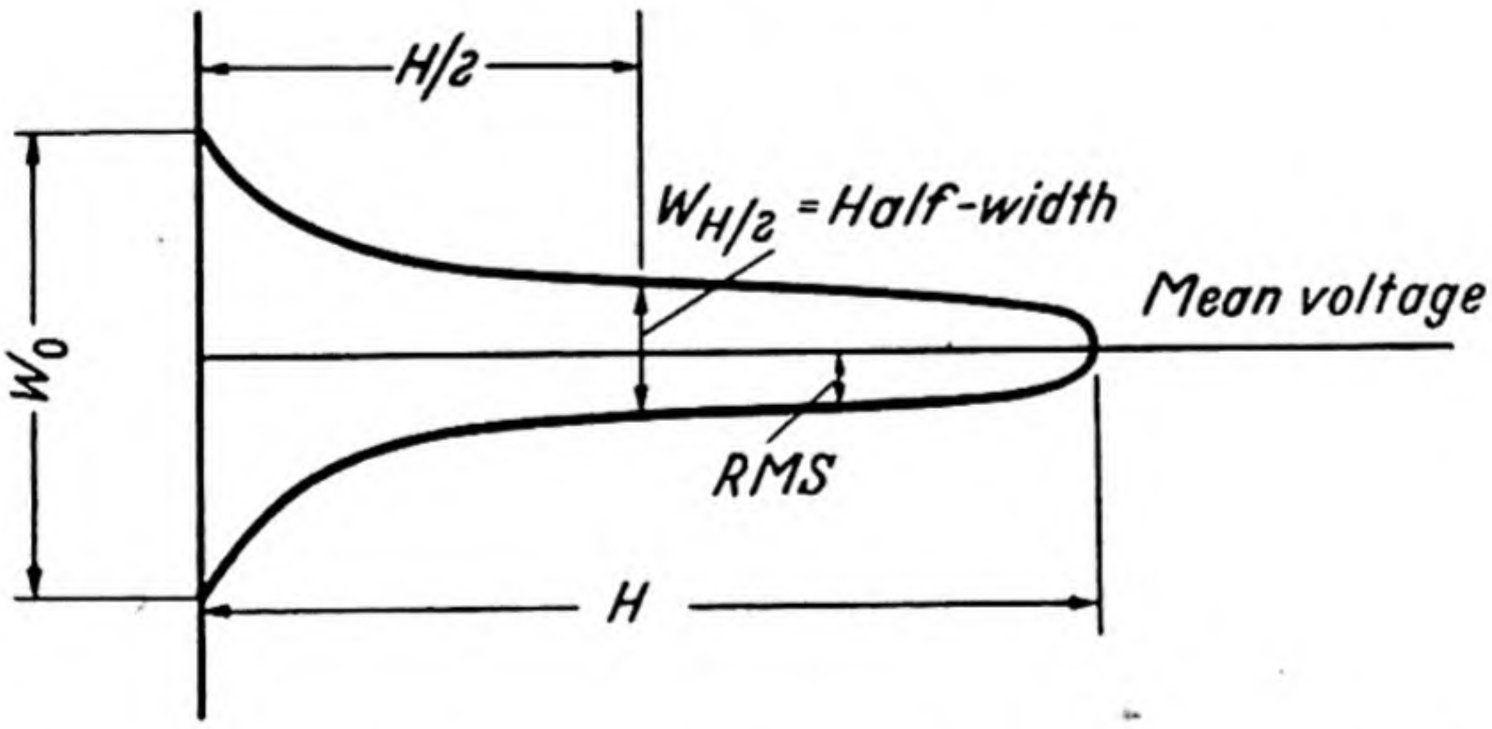

Figure 81. Analysis of voltage-fluctuations on an electrostatic generator (Hafstad, Heydenburg and Tuve[29], by courtesy, *Phys. Rev.*).

10^4 MΩ resistor mentioned above and the former with a separate voltmeter resistance. With this generator, the voltage is controlled with a corona-point assembly moved towards or away from the h.t. electrode and thus acting as a variable load. No other regulating device was used. Corona-point voltage-control systems for Van de Graaff generators are usually similar to that shown in *Figure 82*[30].

HAXBY *et al*[31] have demonstrated the probable approximate limit to be reached by manual control of the terminal voltage of a Van de Graaff generator through the corona-input set used for belt-charging.

The terminal voltage is observed with a generating voltmeter, of the type described in Chapter 7 (page 248). The best published curve for the thick target neutron yield for the Be(p,n) reaction is that of *Figure 83*. The resolving power appears to be about 0·05 per cent. Fast variations in voltage could not be read on the generating voltmeter and could only be estimated from the width (assumed to be

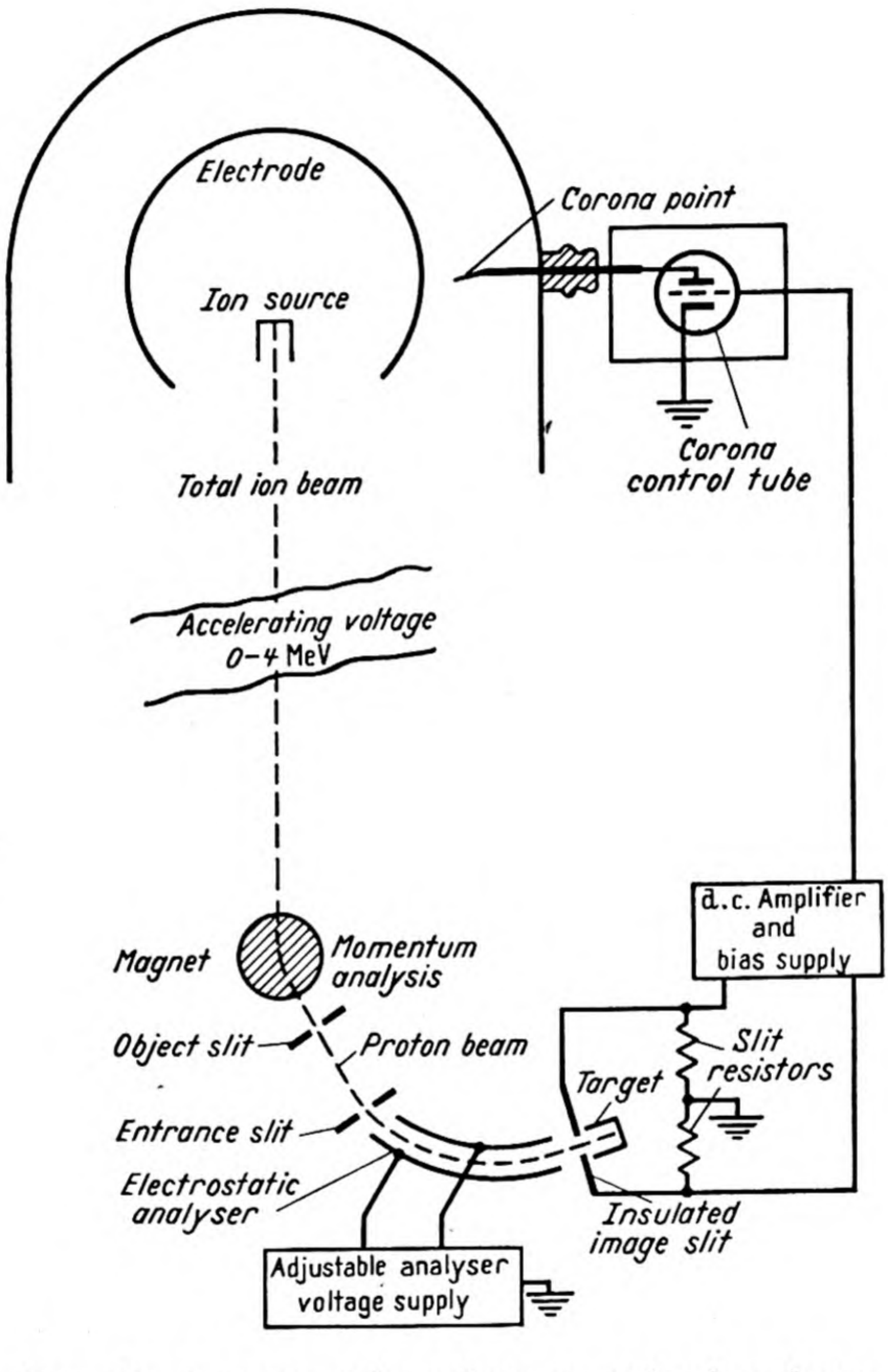

Figure 82. A corona point voltage control using electrostatic analyser (Jennings[30], by courtesy, *Proc. Inst. Rad. Engrs.*).

entirely experimental) of thin target γ-ray resonances (for example those of *Figure 84* which illustrates admirably the use of these resonances for the fixing of a voltage scale, a matter referred to again in Chapter 7). The resonance width at half-maximum intensity for a 1 kV (proton) thick target varied from about 3–10 kV. Similar results have been obtained by other workers.

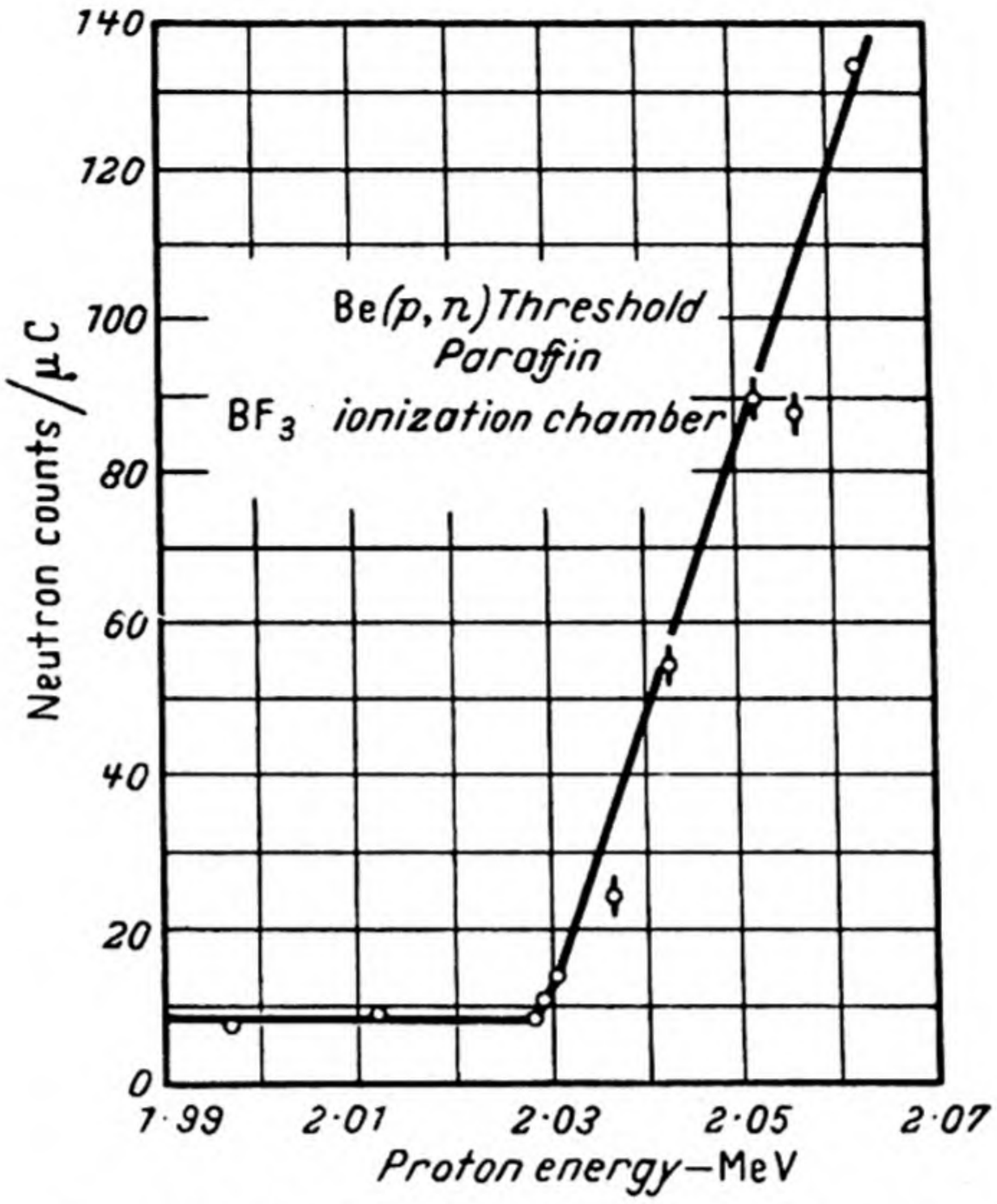

Figure 83. Thick target neutron yield curve for Be(p,n) taken with BF_3 ionization chamber in paraffin and with a generating voltmeter (Haxby *et al* [31], by courtesy, *Phys. Rev.*).

Some of the earliest experiments on the automatic stabilization of Van de Graaff h.t. voltages appear to be those of PARKINSON *et al*[35]. This technique involved the use of a two-stage amplifier, the circuit for which is given in *Figure 85*. The input is a voltage

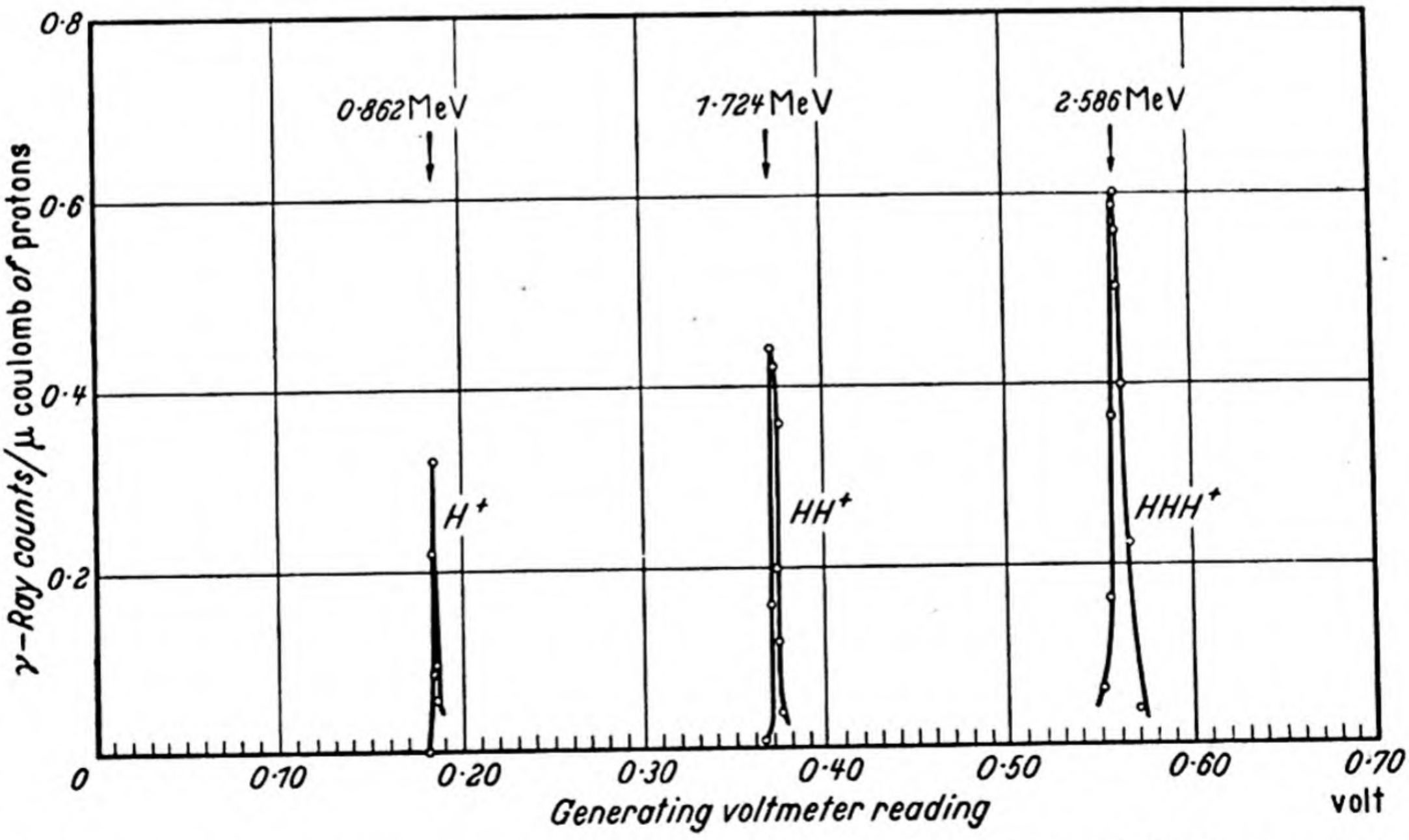

Figure 84. Thin target γ-ray yield curve for the F(γ,p) 0·862-MeV resonance taken with H^+, HH^+, and HHH^+ at $E_p = 0{\cdot}862$ MeV, 1·724 MeV, and 2·856 MeV (Haxby *et al* [31], by courtesy, *Phys. Rev.*).

derived from the corona current flowing to a needle projecting into the pressure tank of the generator opposite to the h.t. terminal. The output of the amplifier controls the current in the primary of the h.t. transformer in the belt charging set. The needle position is remote-controlled. The condenser C_2 is introduced to prevent hunting due to the lag in alterations in belt speed and to the finite generator terminal capacitance, and C_1 is used to smooth out rapid fluctuations in corona current. The time constants of all other parts of the changing circuit are kept as small as possible and no

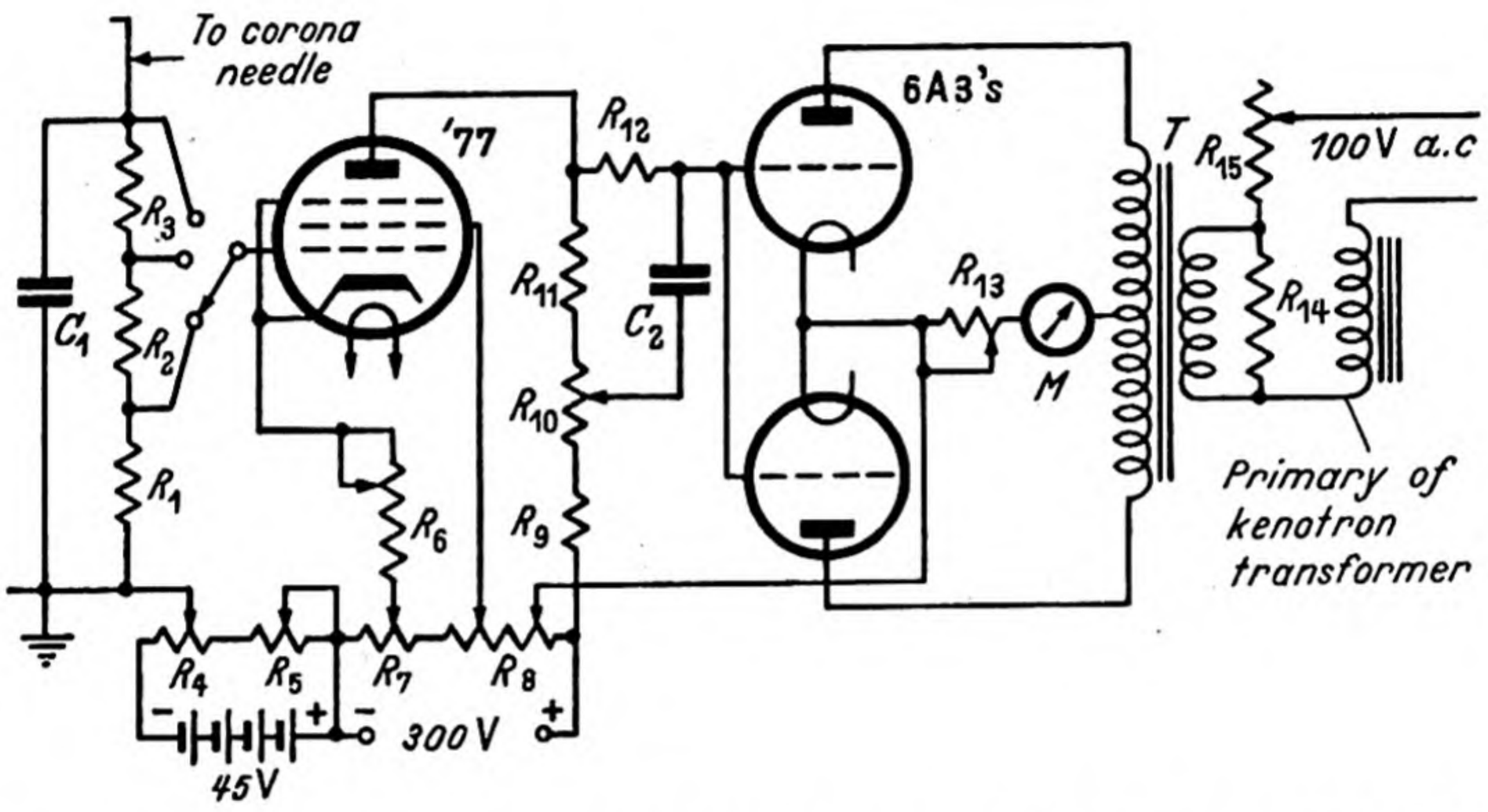

Figure 85. Circuit diagram of voltage stabilizer. $R_1 = 1\text{M}\Omega$ wire wound. $R_2 = 0{\cdot}5$ MΩ wire wound. $R_3 = 0{\cdot}5$ MΩ wire wound. $R_4 = 25{,}000\ \Omega$ potentiometer for voltage control. $R_5 = 5000\Omega$ variable for fine adjustment of voltage. $R_6 = 5000\Omega$ variable gain control. $R_7 = 1000\,\Omega$ potentiometer for balance. $R_8 = 50{,}000\ \Omega$ resistor with taps. $R_9 = 0{\cdot}5$ MΩ. $R_{10} = 9$ resistors of 50,000 Ω mounted on a selector switch. $R_{11} = 1$ MΩ. $R_{12} = 4$ MΩ. $R_{13} = 2500\ \Omega$ resistor with taps. R_{14} and R_{15} = rheostats for control of high voltage. $C_1 = 0{\cdot}5$ mF. $C_2 = 1{\cdot}5$ mF. T = Thordarson T5604 radio power transformer. M = milliammeter : 0–100 mA (Parkinson *et al*[35], by courtesy, *Phys. Rev.*).

smoothing condenser is used in the charging set. The h.t. voltage stability thus obtained is about 0·5 per cent.

The generator voltage is set roughly first with R_{15} using a coarse calibration and the needle position is set to give the best stability performance, after which R_4 and the fine control R_5 are used to set the voltage accurately. The h.t. is read on a generating voltmeter, and the latter is calibrated as described in Chapter 7. This method was later used by WILLIAMS *et al*[33] to stabilize the Minnesota 3 MV Van de Graaff generator to within 1 per cent.

HANSON[15] has described another method for stabilizing the h.t. voltage. An electron or ion beam, accelerated through the voltage to be stabilized, impinges in the middle of two small metal plates

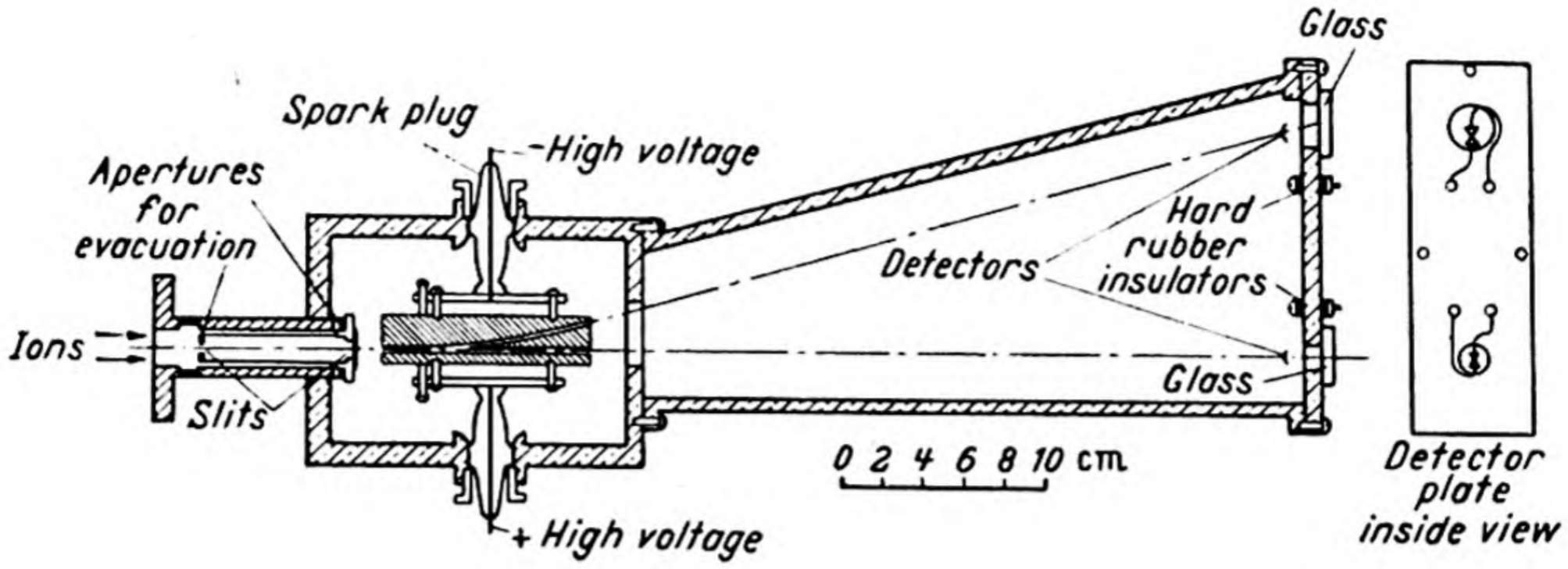

Figure 86. An electrostatic analyser (Hanson[15], by courtesy, *Rev. Sci. Instrum.*).

suitably insulated, at the required h.t.; the beam can be centred by means of an auxiliary electrostatic field (the deflection apparatus is shown in *Figure 86*). When the h.t. fluctuates, the beam no longer impinges symmetrically on the two plates and a current flow can be set up in a suitable circuit which provides feed-back to control the charging current on the Van de Graaff generator belt. The current from the detector plates is $\sim 10^{-8}$ A. The circuit is shown in *Figure 87* and incorporates a 'double electric eye tube' to show the beam position with respect to the collector plates at any constant. The average beam energy is then kept stable to about 0·1 per cent. and fluctuations of about 1 per cent. can be corrected in < 1 second.

The voltage stabilization technique due to PARKINSON *et al*[35] and described above has been modified by BROSTRÖM, HUUS and TANGEN[36]. The latter authors used a generating voltmeter arranged as shown in *Figure 88* with two vanes W_1 and W_2 moving past fixed plates P_2 and P_1. The potential of P_2 is varied for a given generator h.t.

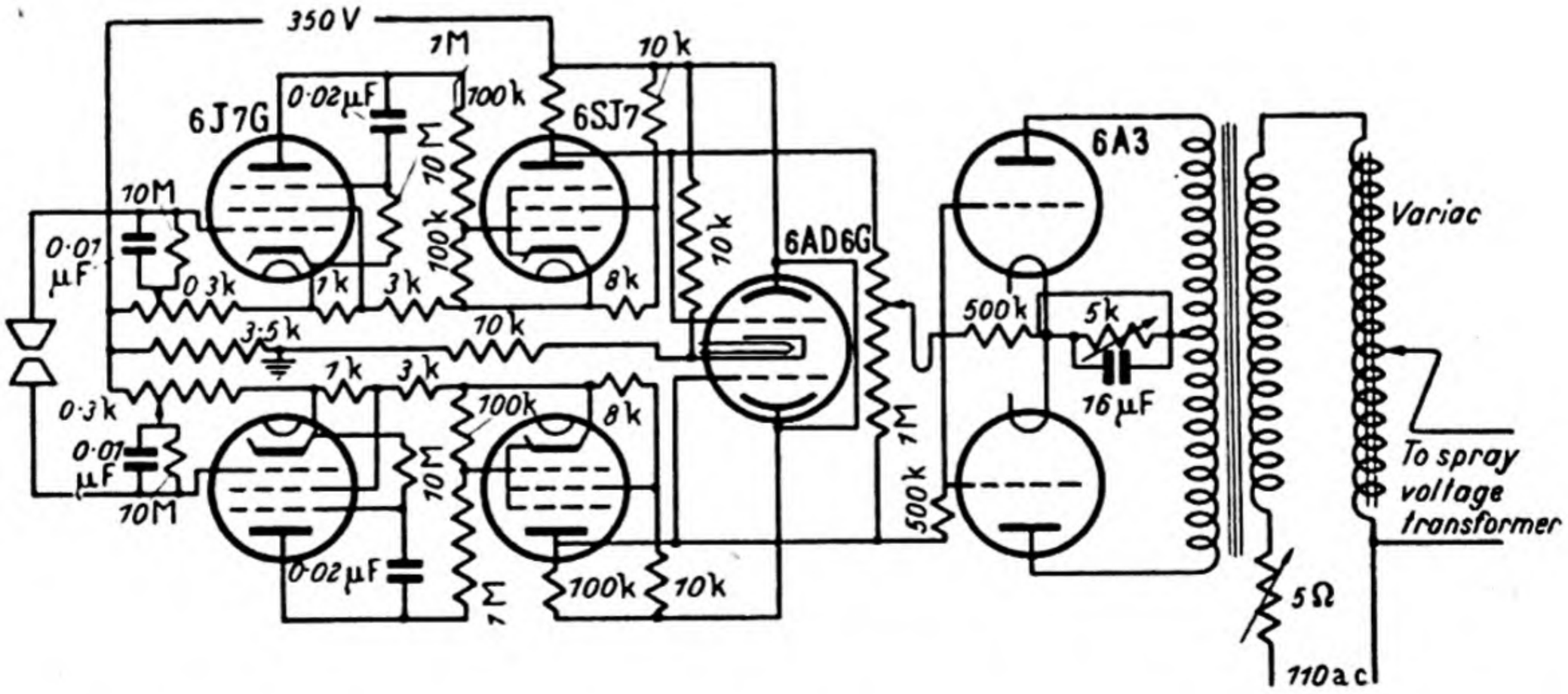

Figure 87. Regulator for electrostatic generator (Hanson[15], by courtesy, *Rev. Sci. Instrum.*).

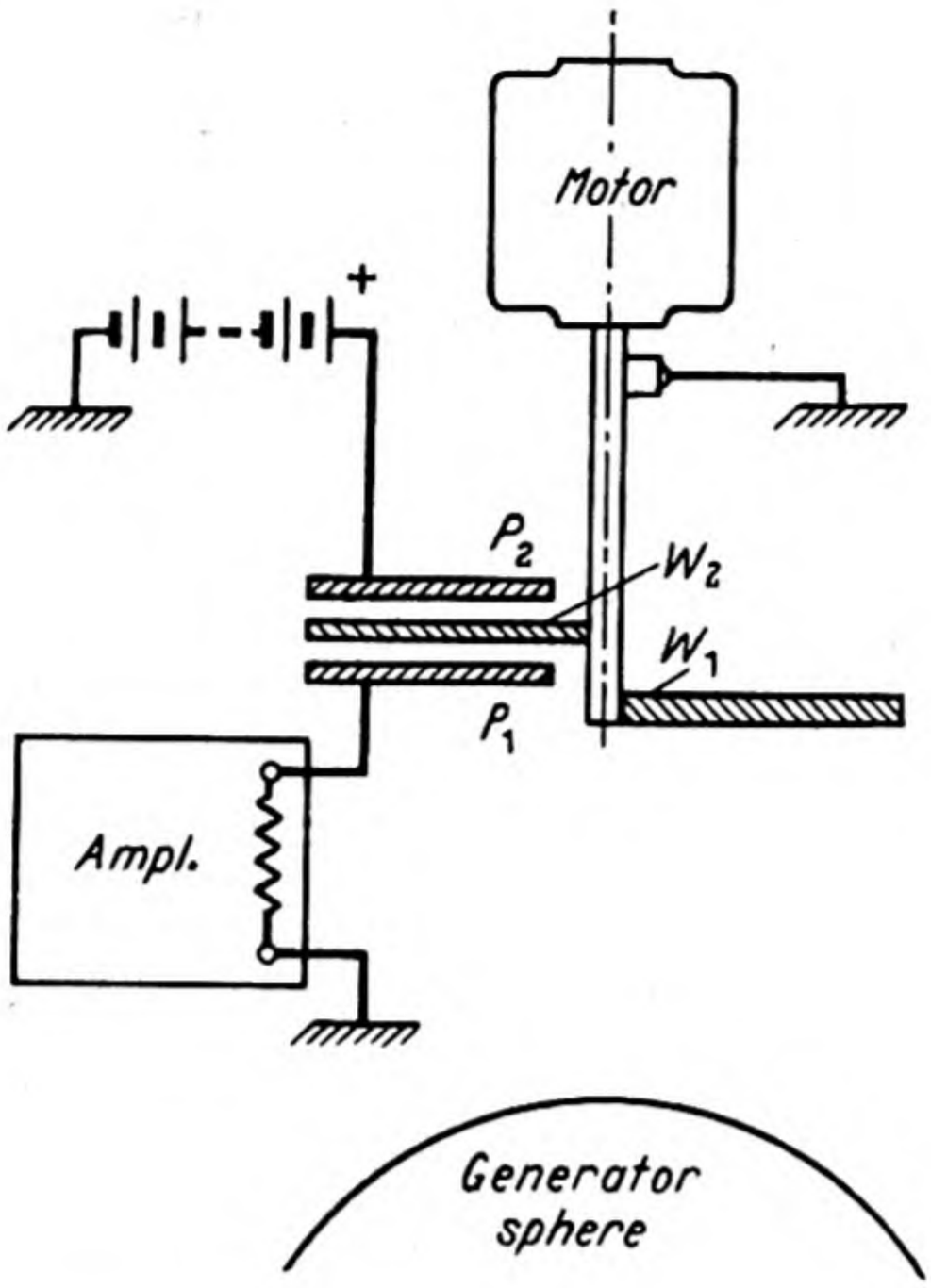

Figure 88. Rotating compensation voltmeter (Broström, Huus and Tangen[36], by courtesy, *Phys. Rev.*).

voltage, until the potential of P_1 remains constant as the vanes W_1 and W_2 rotate. If balance is not obtained, then an a.c. voltage appears on P_1. Thus conversely if P_2 remains fixed in potential, variations in the generator h.t. voltage cause such an a.c. voltage to appear, and this is amplified and fed back to the voltage stabilizer, which is of the form used by PARKINSON and his collaborators[35]. The amplified signal also causes the counter tube and the beam integrator

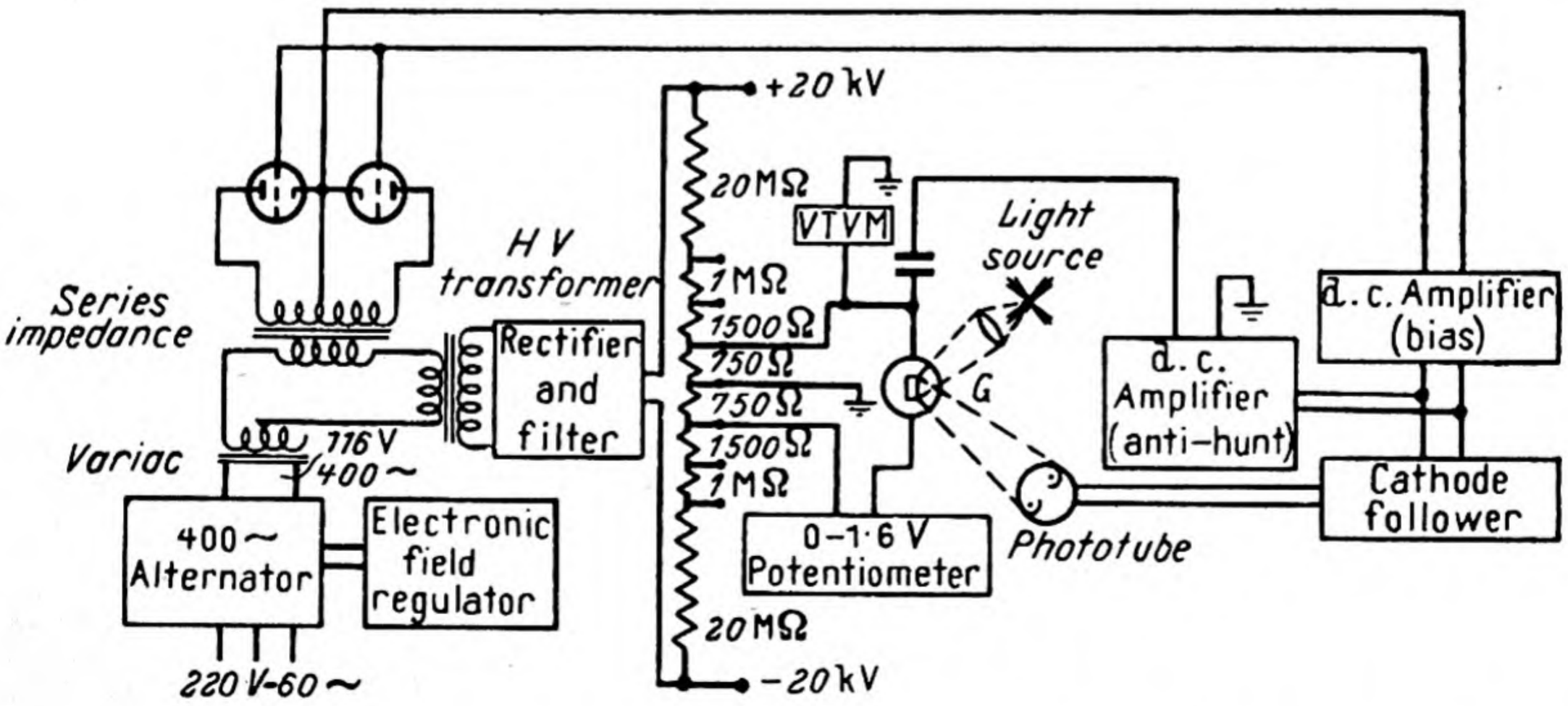

Figure 89.—Block diagram of power supply and regulator. (Henkel and Petree[28], by courtesy, *Rev. Sci. Instrum.*)

(used in the nuclear work described by BROSTRÖM *et al*[36]) to be cut off when the generator voltage fluctuates by more than a certain amount. The voltage fluctuations can be reduced to about ± 1·5 kV with a maximum h.t. voltage of about 1,800 kV.

Another system for the stabilization of a suitable voltage source, to be used as a reference standard in the correction of Van de Graaff generator h.t. fluctuations, is described by HENKEL and PETREE[28]. The source provides 5 to 50 kV d.c. with a stability within ± 0·01 per cent. and is used in connection with the electrostatic analysers described elsewhere (pages 81–82) and applied by Hanson[15], ASHBY and HANSON[37] and WARREN, POWELL and HERB[38]. It replaces a 30 kV stack of dry batteries which tend to suffer from drift and

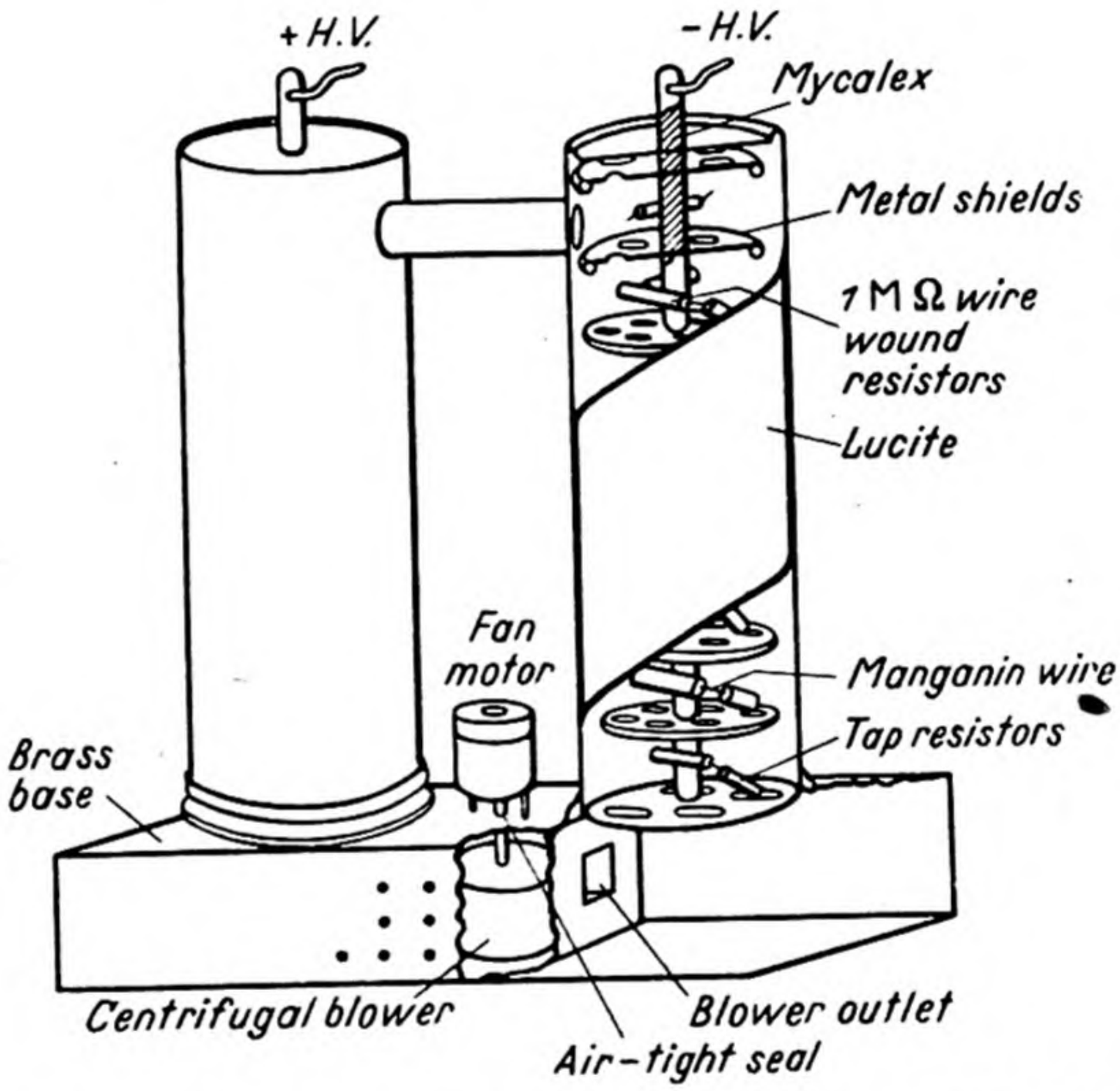

Figure 90. High voltage resistor stack (Henkel and Petree[28], by courtesy, *Rev. Sci. Instrum.*).

internal impedance changes[39]. The basic circuit is shown in *Figure 89* and operates as follows. A fraction of the voltage developed across the output potentiometer is balanced against a small standard voltage derived from another potentiometer and the error signal is amplified by means of the galvanometer photo-tube amplifier shown (see the work of VON FRIESEN[40] and GILBERT[41]). The error current passes through the galvanometer and the resulting deflection of the light beam gives a change in the output of the phototube. The feed-back voltage finally reaches the variable impedance transformer[42] in the H.V. transformer primary circuit. The power source is a 1·5 kVA, 115 V, 400 c/s generator driven by a 3-phase induction motor. Since

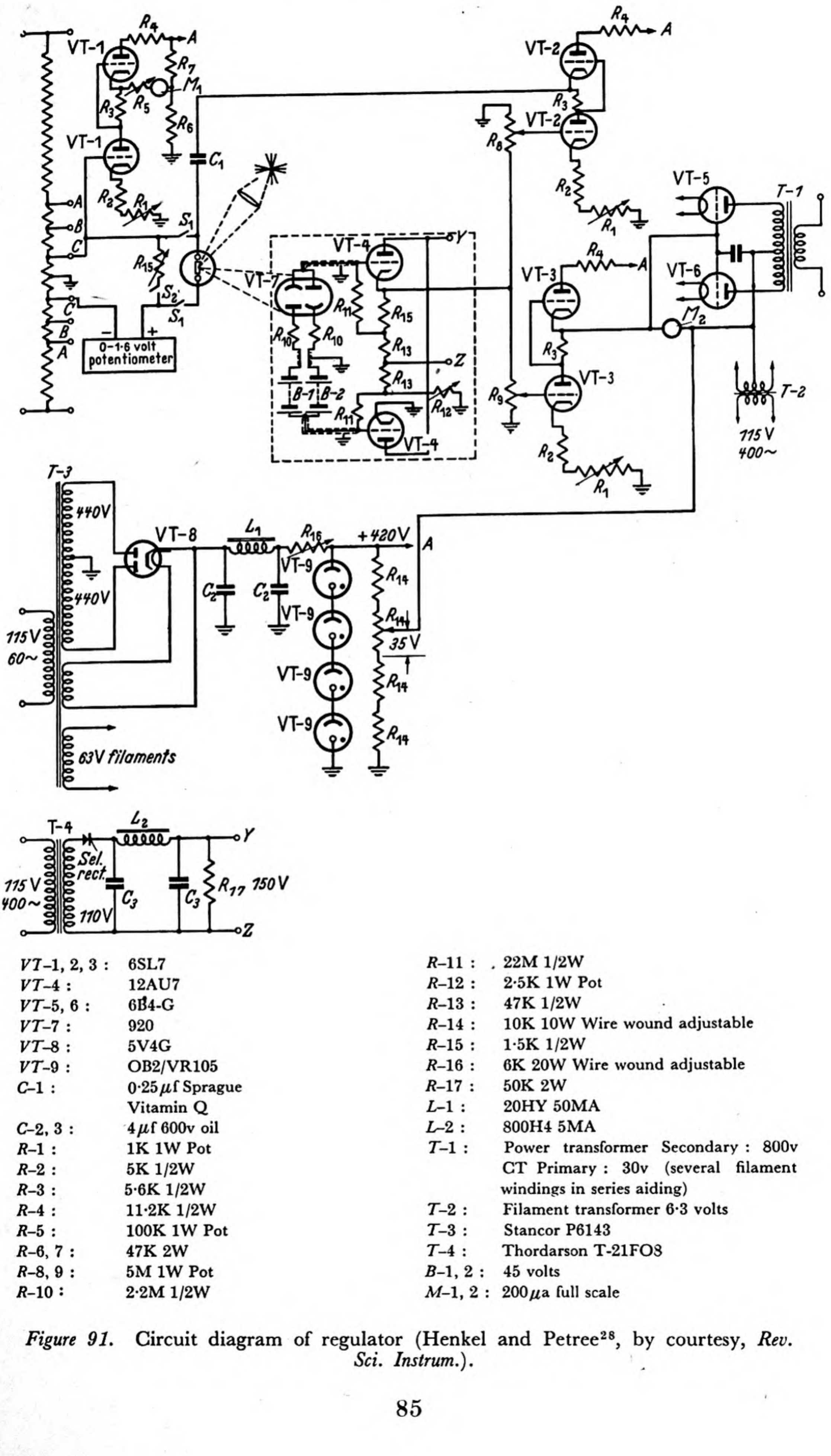

VT–1, 2, 3 :	6SL7
VT–4 :	12AU7
VT–5, 6 :	6B4-G
VT–7 :	920
VT–8 :	5V4G
VT–9 :	OB2/VR105
C–1 :	0·25 μf Sprague Vitamin Q
C–2, 3 :	4 μf 600v oil
R–1 :	1K 1W Pot
R–2 :	5K 1/2W
R–3 :	5·6K 1/2W
R–4 :	11·2K 1/2W
R–5 :	100K 1W Pot
R–6, 7 :	47K 2W
R–8, 9 :	5M 1W Pot
R–10 :	2·2M 1/2W
R–11 :	22M 1/2W
R–12 :	2·5K 1W Pot
R–13 :	47K 1/2W
R–14 :	10K 10W Wire wound adjustable
R–15 :	1·5K 1/2W
R–16 :	6K 20W Wire wound adjustable
R–17 :	50K 2W
L–1 :	20HY 50MA
L–2 :	800H4 5MA
T–1 :	Power transformer Secondary : 800v CT Primary : 30v (several filament windings in series aiding)
T–2 :	Filament transformer 6·3 volts
T–3 :	Stancor P6143
T–4 :	Thordarson T-21FO8
B–1, 2 :	45 volts
M–1, 2 :	200 μa full scale

Figure 91. Circuit diagram of regulator (Henkel and Petree[28], by courtesy, *Rev. Sci. Instrum.*).

there are two windings on this generator a degenerative regulator could be used. The circuit, due to McKibben, gives a stability of about 1 in 3,000. The high-voltage divider shown in *Figure 89* is claimed to have a value constant to better than 0·01 per cent. and consists of 40 1 MΩ Shallcross manganin wire resistors, mounted in groups of 3 between corona shields and air cooled with a fan. The assembly of the resistance stack is shown in *Figure 90*. The complete

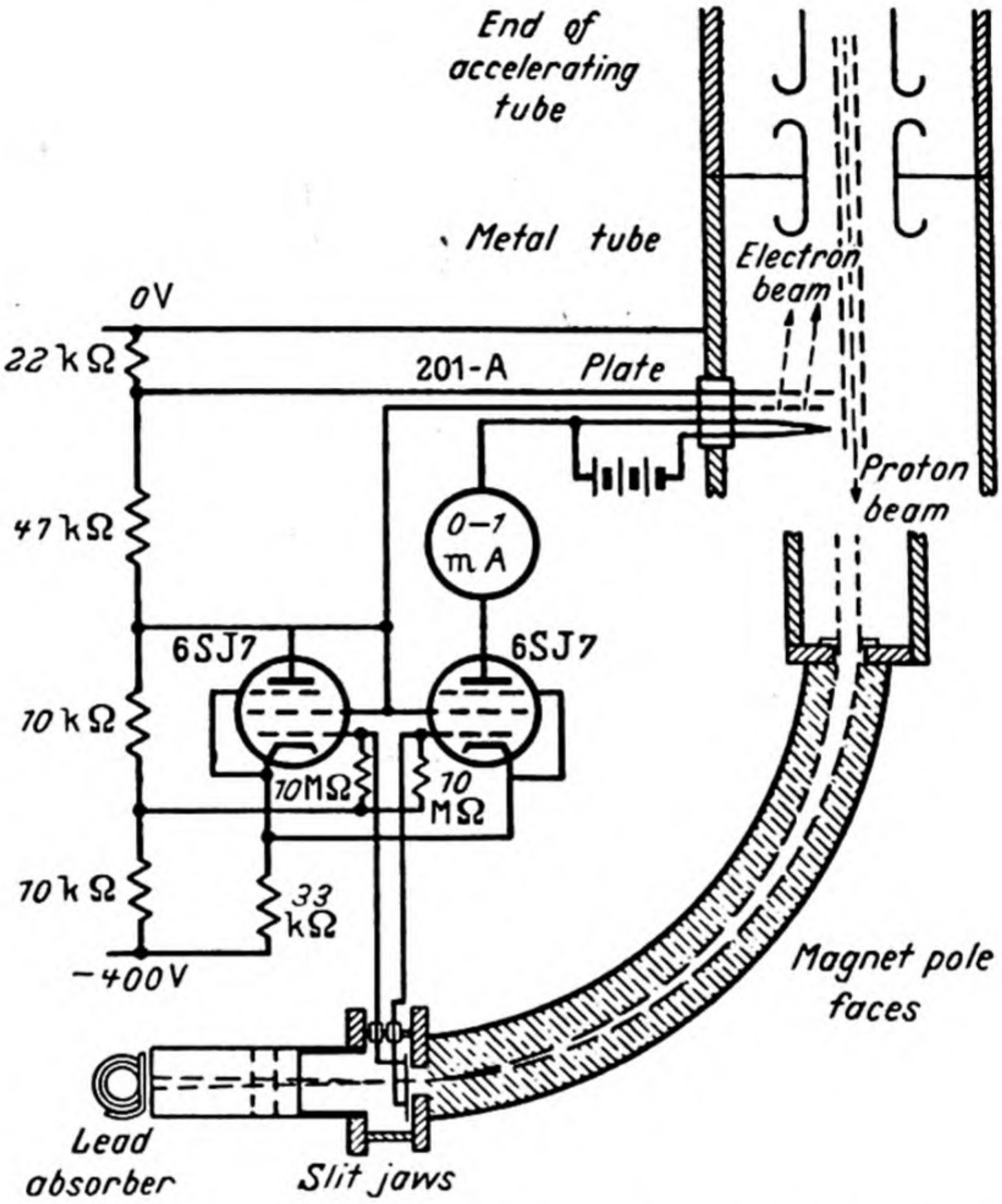

Figure 92. Diagram of the experimental arrangement showing the magnetic energy selector and the electronic potential regulator. The proton-beam passes through the two insulated jaws of the narrow slit and proceeds to the target. The modulated electron current goes up the vacuum tube in the reverse direction to that of the positive ion-current. The 0-1 milliammeter measures the modulated electron current which leaves the electron gun; the current through this meter serves as an indicator of whether the stabilizer is centred within its limits of regulation (Bennett *et al*[32], by courtesy, *Phys. Rev.*).

circuit of the regulator, on the output side of the h.t. potentiometer, is shown in *Figure 91*. Other details of the rectifier circuit and its filter system are given in the paper cited[42].

Voltage control of Van de Graaff generators by means of an insulated tank liner used as a potential probe is described briefly by Jennings[30]. The liner is shown in *Figure 53* (page 47). If the

terminal voltage changes with respect to ground (to which the beam is accelerated) the potential of the liner with respect to ground also changes and this voltage change can be used to provide stabilization of the terminal voltage against slow changes. Fast changes may be compensated by the corona or beam control methods described elsewhere in this Chapter (pages 78–86).

Probably the highest degree of stabilization, with a Van de Graaff generator, has been attained by BENNETT, BONNER, MANDEVILLE and WATT[32] in their work on nuclear resonances. Their experimental arrangement is shown in *Figure 92*. The proton beam with ~1 MV energy arriving at the lower end of the accelerating tube is deflected in a magnet system using stabilized field current and thus its energy is accurately known. The geometry of the deflection system is such that the proton energy spread over the collector slit width is about 600 V; the maximum energy spread due to the finite source voltage is about 1 kV but the received energy spread is made less than this by the use of a fine collector slit. The beam energy is stabilized by detecting beam movements (due to h.t. voltage changes) using a special slit with insulated jaws (*see also* page 255). Differential currents, due to imperfect centring of the proton beam on this slit or to beam movements across the slit after centring, are amplified and used, with appropriate circuits (*Figure 92*), to modulate an electron beam passing in the reverse direction up the acceleration tube. Thus proton beam movements are made to alter the generator load and so to stabilize its output voltage. The total delay time in the circuit is 2 μsec which sets a lower limit to the theoretical potential fluctuations of about 0·02 V. Since the beam energy spread due to the source is several hundred volts, this theoretical limit could not be reached. However the calculated fluctuations in potential using the circuit of *Figure 92* are about $\pm$150 V, a remarkable figure for a 1 MV generator.

REFERENCES

1 HUNT, F. V., and HICKMAN, K. W. *Rev. Sci. Instrum.*, **10** (1939) 6.
2 BLACK, H. S. *Bell. Sys. Tech. J.*, **13** (1934) 1.
3 KING, R. W. *Bell. Sys. Tech. J.*, **2** (1923) 31.
4 KOHLER, H. W. *Electronics*, **7** (1934) 388.
5 STREET, J. C., and JOHNSON, T. H. *J. Frank. Inst.*, **214** (1932) 155.
6 EVANS, R. D. *Rev. Sci. Instrum.*, **5** (1934) 371.
7 GINGRICH, N. S. *Rev. Sci. Instrum.*, **7** (1936) 207.
8 ASHWORTH, J. A., and MOUZON, J. C. *Rev. Sci. Instrum.*, **8** (1937) 127.
9 LINDENHOVIUS, H. J., and RINIA, H. *Philips Tech. Rev.*, **6** (1941) 54.
10 ELMORE, W. C., and SANDS, M. L. *Electronics: Experimental Techniques.* New York, 1949.
11 CURRAN, S. C., and CRAGGS, J. D. *Counting Tubes.* London, 1949.
12 HAINE, M. E. *J. Inst. elect. Engrs.*, **94** Pt I. (1947) 447.

13 VAN DORSTEN, A. C. *Philips Tech. Rev.*, **10** (1948) 135.
14 WATERTON, F. W. *J. Sci. Instrum.*, **19** (1942) 105.
15 HANSON, A. O. *Rev. Sci. Instrum.*, **15** (1944) 57.
16 VANCE, A. W. *R.C.A. Rev.*, **5** (1941) 293.
17 VAN DORSTEN, A. C., NIEUWDORP, H., and VERHOEFF, A. *Philips Tech. Rev.*, **12** (1950) 33.
18 MARTON, L. *J. appl. Phys.*, **16** (1945) 131.
19 MULVEY, T. *J. Sci. Instrum.*, **29** (1952) 149.
20 RUTHERGLEN, J. G., in course of publication.
21 FINCH, G. I., QUARRELL, A. G., and WILMAN, H. *Trans. Faraday Soc.*, **31** (1935) 1051.
22 THOMSON, G. P., and COCHRANE, W. *Theory & Practice of Electron Diffraction.* London, 1939.
23 LLEWELLYN JONES, F., and PARKER, A. B. *Proc. roy. Soc.* (A), **213** (1952) 185.
24 LIEBMANN, G. *J. Sci. Instrum.*, **25** (1948) 37.
25 BEDELL, F., and KUHN, J. *Rev. Sci. Instrum.*, **3** (1932) 20.
26 BENSON, F. A. *Voltage Stabilizers.* London, 1950.
27 FAHNESTOCK, J. D. *Electronics*, **25** (1952) 140.
28 HENKEL, R. L., and PETREE, B. *Rev. Sci. Instrum.*, **20** (1949) 729.
29 HAFSTAD, L. R., HEYDENBURG, N. P., and TUVE, M. A. *Phys. Rev.*, **50** (1936) 504.
30 JENNINGS, B. *Proc. Inst. Rad. Engrs.*, **38** (1950) 1126.
31 HAXBY, R. O., SHOUPP, W. E., STEPHENS, W. E., and WELLS, W. H. *Phys. Rev.*, **58** (1940) 1035.
32 BENNETT, W. E., BONNER, T. W., MANDEVILLE, C. E., and WATT, B. E. *Phys. Rev.*, **70** (1946) 882.
33 WILLIAMS, J. H., RUMBAUGH, L. H., and TATE, J. T. *Rev. Sci. Instrum.*, **13** (1942) 202.
34 STRAIT, E. N., and BUECHNER, W. W. *Rev. Sci. Instrum.*, **20** (1949) 783.
35 PARKINSON, D. B., HERB, R. G., BERNET, E. J., and MCKIBBEN, J. L. *Phys. Rev.*, **53** (1938) 642.
36 BROSTRÖM, K. J., HUUS, T., and TANGEN, R. *Phys. Rev.*, **71** (1947) 661.
37 ASHBY, R. M., and HANSON, A. O. *Rev. Sci. Instrum.*, **13** (1942) 128.
38 WARREN, R. E., POWELL, J. L., and HERB, R. G. *Rev. Sci. Instrum.*, **18** (1947) 559.
39 HERB, R. G., SNOWDON, S. C., and SALA, O. *Phys. Rev.*, **75** (1949) 246.
40 VON FRIESEN, S. Dissertation. Uppsala, 1935.
41 GILBERT, R. W. *Rev. Sci. Instrum.*, **7** (1936) 41.
42 RIDENOUR, L. N., and LAMPSON, C. W. *Rev. Sci. Instrum.*, **8** (1937) 162.

3

GENERATION OF HIGH-VOLTAGE ALTERNATING CURRENT

CASCADED TRANSFORMERS

The detailed literature on high-voltage transformers, from say 100 kV to higher voltages, does not appear to be extensive. However KEHSE[1] and GASTER[23] have published short papers on the insulation of such transformers and CRÄMER[2] has described a single transformer giving 1 MV, and arranged for horizontal mounting. Many of the standard books on transformer design deal to some extent with high-voltage units but usually not in great detail. References to some of the papers published in the technical press are given in the list on page 110, and in BOUWERS' book[3].

An early system of cascaded transformers for the production of high-voltage a.c. is described by SORENSEN[4] who used four 250 kVA, 250 kV Westinghouse transformers (50 c/s) arranged in the circuit shown in *Figure 93*. The transformer tanks are mounted in the manner

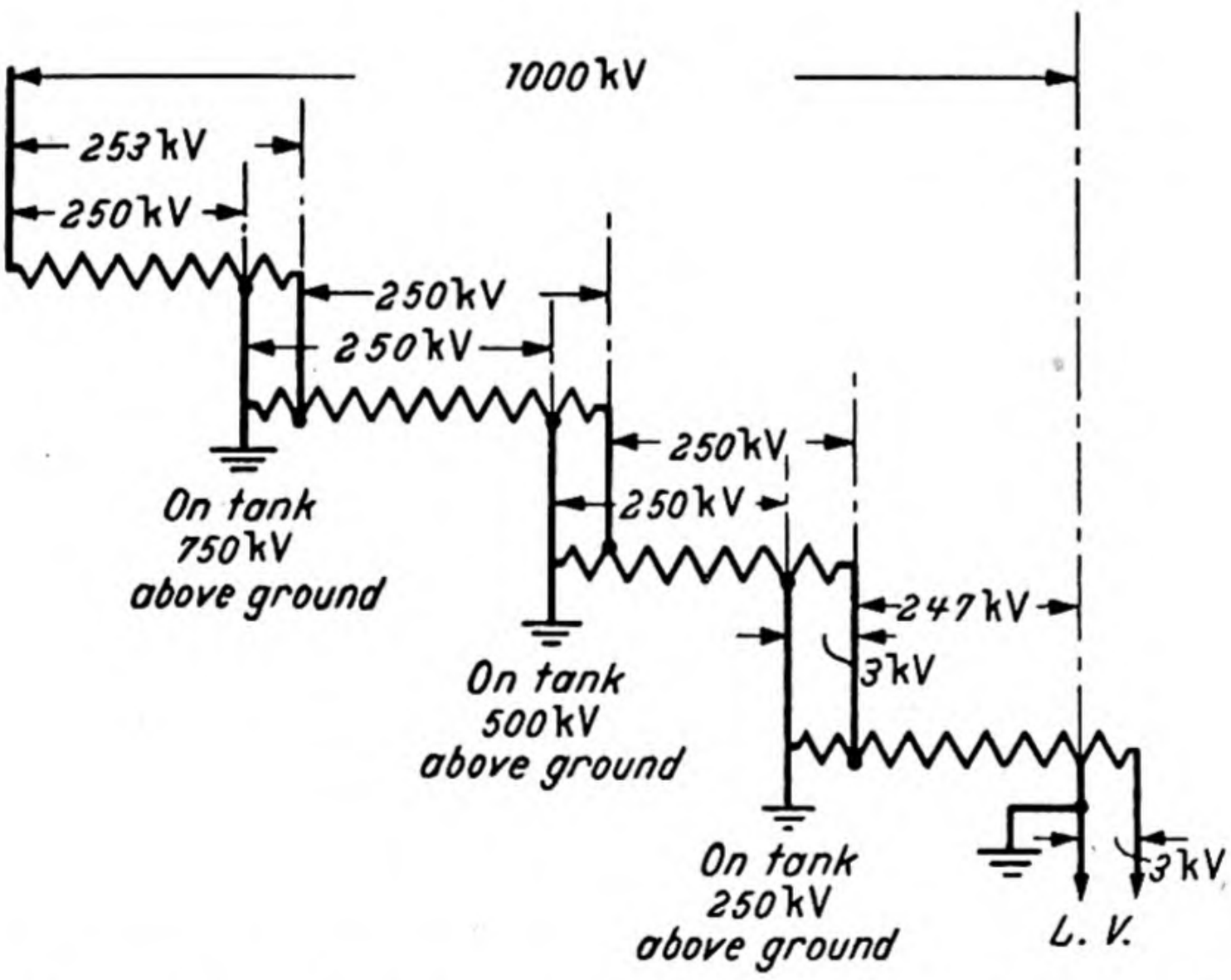

Figure 93. Diagram of transformers connected in cascade (Sorensen[4], by courtesy, *J. Amer. elect. Engrs.*).

indicated in *Figure 94* and are suitably insulated from ground. There are three windings on each transformer comprising primary (3–6 kV), secondary (247 kV) and exciting coils (3 kV); the latter are used, as shown in *Figure 93*, as taps to supply the subsequent units. A

voltmeter winding (150–300 V) is also provided on each transformer. Special regulating transformers, for the supply, were built and are briefly described in the paper by Sorensen[4], which gives details of test data, such as impedance curves for the transformer windings and voltage calibrations.

Similar installations have been described by other authors. For example, NORRIS and TAYLOR[5] deal generally with the requirements for high-voltage a.c. testing transformers and discuss the arrangement, very similar to that of Sorensen[4], shown in *Figure 95* and due to DESSAUER. Three 330 kV transformers are used together to give 1 MV; each transformer has in effect three windings, a primary t_o—t_1 (*see Figure 95*), an h.t. winding T_o—T_1 one end of which is connected to the transformer tank and the other end of which is insulated for 330 kV, and a tap at T_2 such that the voltage across

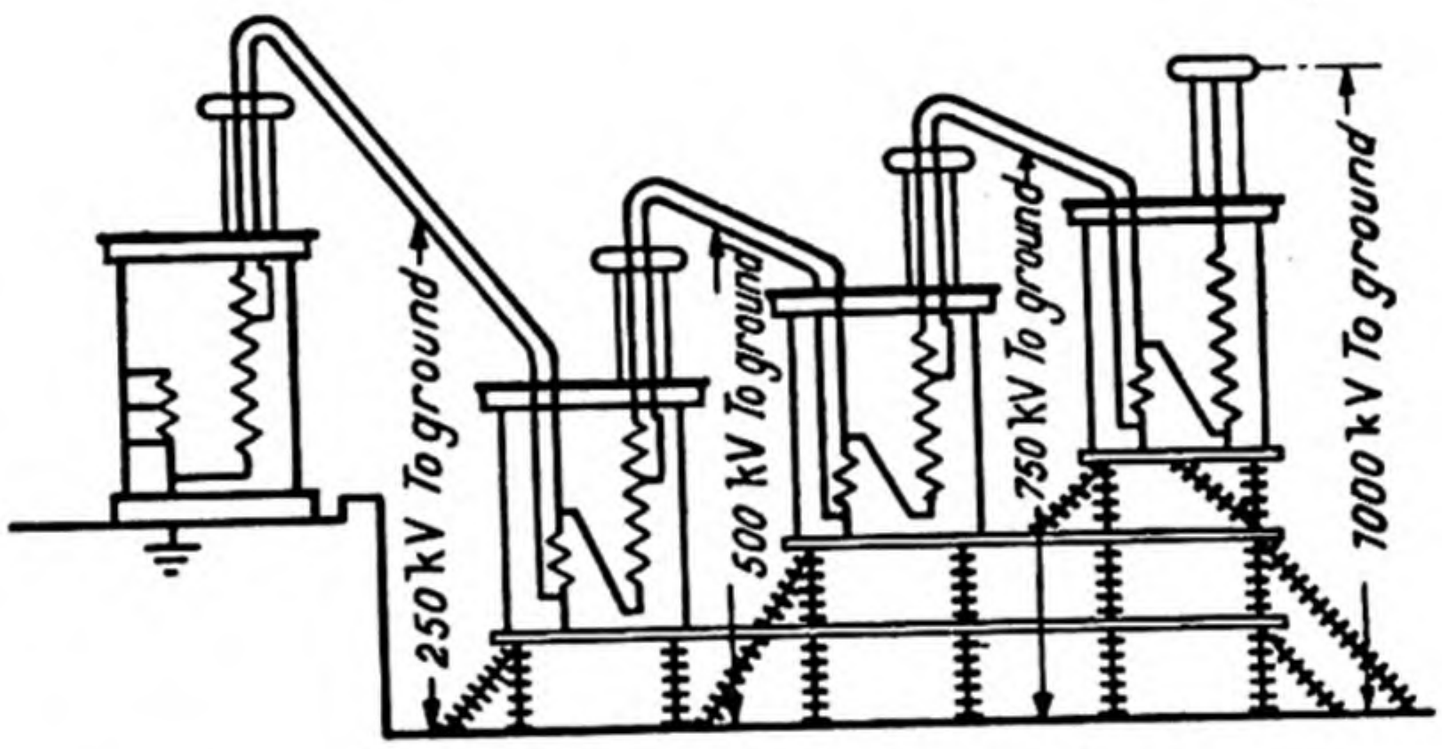

Figure 94. An arrangement of cascaded transformers (Sorensen[4], by courtesy, *J. Amer. elect. Engrs.*).

T_1T_2 equals that across t_o—t_1. The leads T_1T_2 are brought up through the h.t. bushing and are connected to the next transformer as shown in *Figure 95*. T_1T_2 is at a high potential above earth, and so the tanks of all the transformers, except No. 1, must be suitably insulated. The arrangement of *Figure 96*[5], where the h.t. windings are connected at their mid-points to the tanks, enables cheaper transformers to be used, since they now need insulation to withstand only 167 kV, although all three transformers must be insulated from earth. The small windings T_1T_2 (*Figure 95*) have to provide the excitation and load currents for the second and third transformers and since there is a high leakage reactance between T_1T_2 and the primary, additional primary or compensating windings, shown in *Figures 95* and *96*, must be provided. Transformers for such high voltages (up to 500 kV) are generally of the core type to facilitate insulation of the secondaries, and the insulation consists usually of Bakelite barriers and an oil filling. Metropolitan-Vickers constructed, many

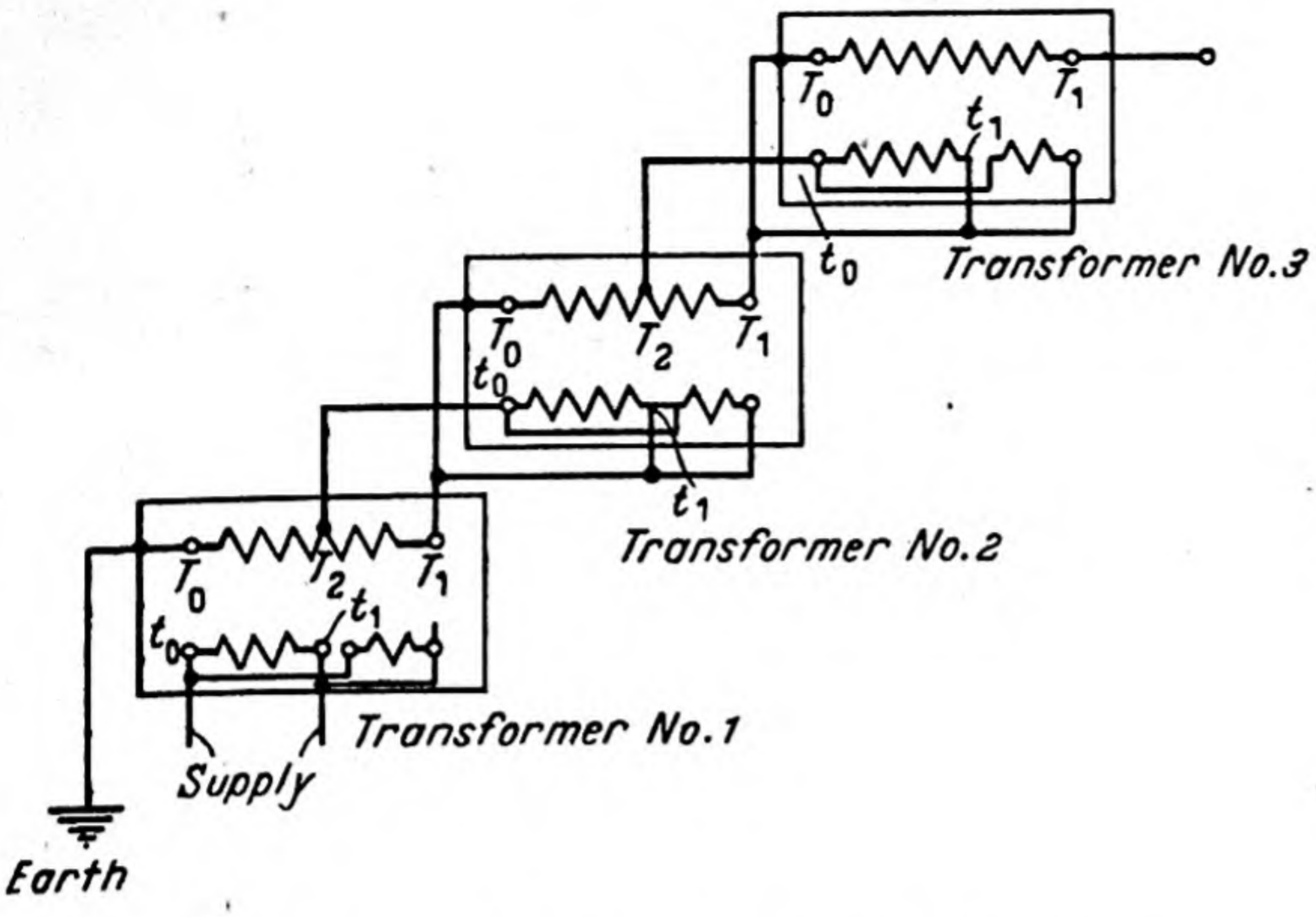

Figure 95. Cascade connection of transformers (Norris and Taylor[5] by courtesy, *J. Inst. elect. Engrs.*).

Transformer tank connected to terminal T_0 for each transformer.
Tank of transformer No. 2 insulated for 333,000 V.
Tank of transformer No. 3 insulated for 667,000 V.

years ago, two 500 kV, 500 kVA transformers for cascade operation at 1,000 kV and this installation has been used in many investigations on electrical break-down problems, such as the work of EDWARDS and SMEE[6] on sphere-gap calibrations.

One of the few detailed analyses of cascaded transformer arrangements is by WINZ[7], who has carried out a full theoretical investigation and also gives design data, *e.g.* for a 110 kV set. KÜCHLER[8] gives a brief description of an iron-cored cascade transformer for 100 kV,

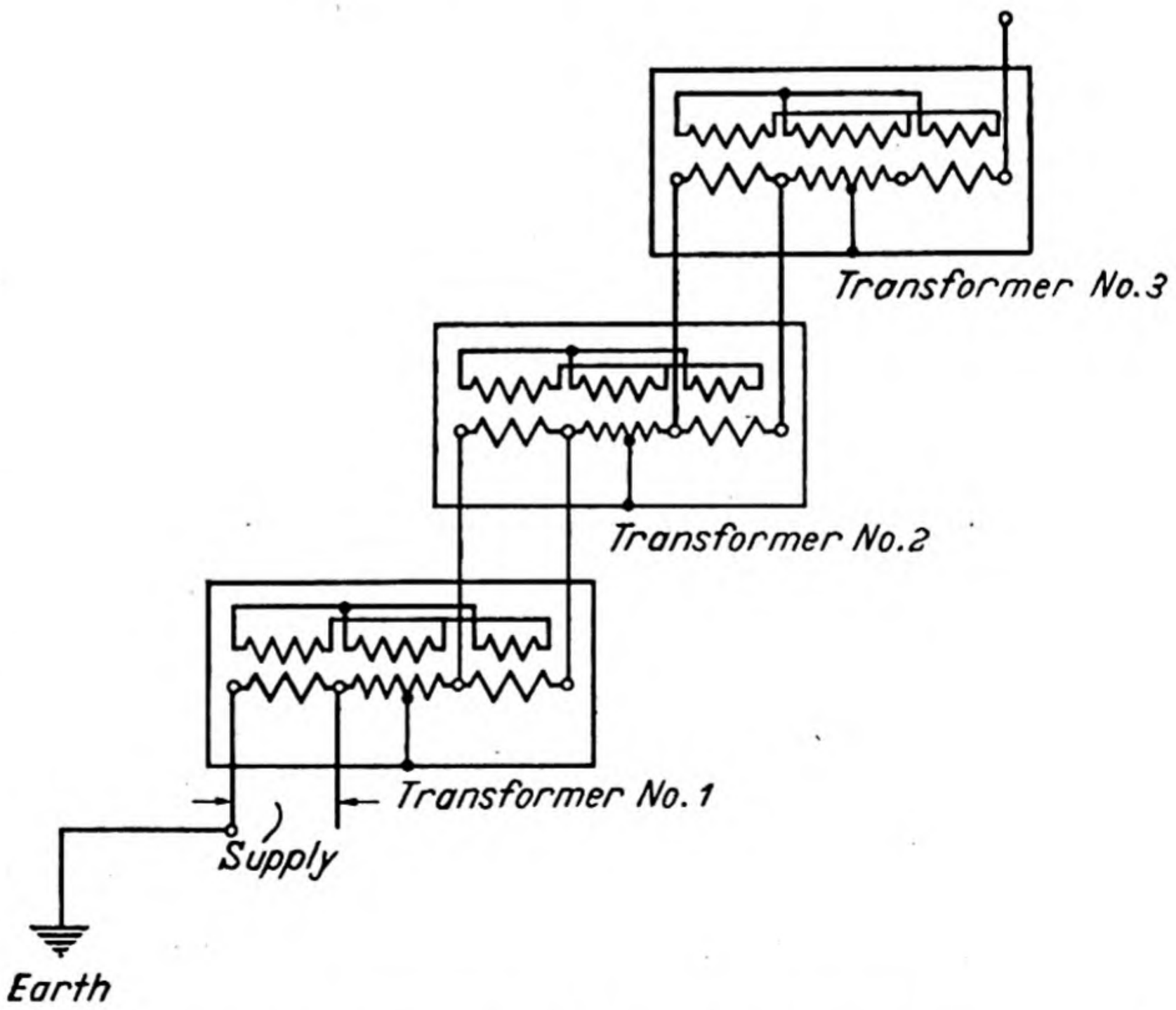

Figure 96. Cascade connection of transformers (Norris and Taylor[5], by courtesy, *J. Inst. elect. Engrs.*).

Tank of transformer No. 1 insulated for 168,000 V.
Tank of transformer No. 2 insulated for 500,000 V.
Tank of transformer No. 3 insulated for 833,000 V.

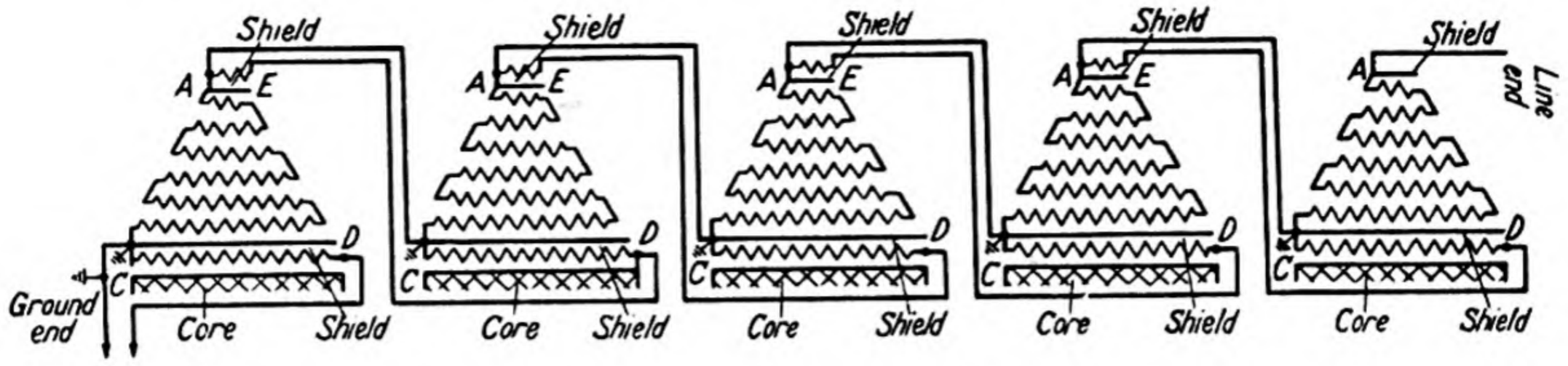

C. Beginning of low-voltage and high-voltage windings.
D. End of the low-voltage winding.
A. End of the high-voltage winding and beginning of the exciting winding.
E. End of the exciting winding.

Figure 97. Diagram of connections of a cascade-type potential transformer (Camilli[9], by courtesy, *Gen. Elect. Rev.*).

in which oil insulation is not necessary. Ten secondary windings are used in series but the design is simple and could probably be easily modified for use in many laboratory applications.

The cascaded transformers, briefly described above, have been used for the production of very high voltages largely for the purposes of testing experimental insulation, bushings and other high-voltage equipment. The cascade method for producing a.c. at fairly high voltages (~ 100 kV, for example) might also be used with advantage in laboratory apparatus. CAMILLI[9] has shown how the transformer

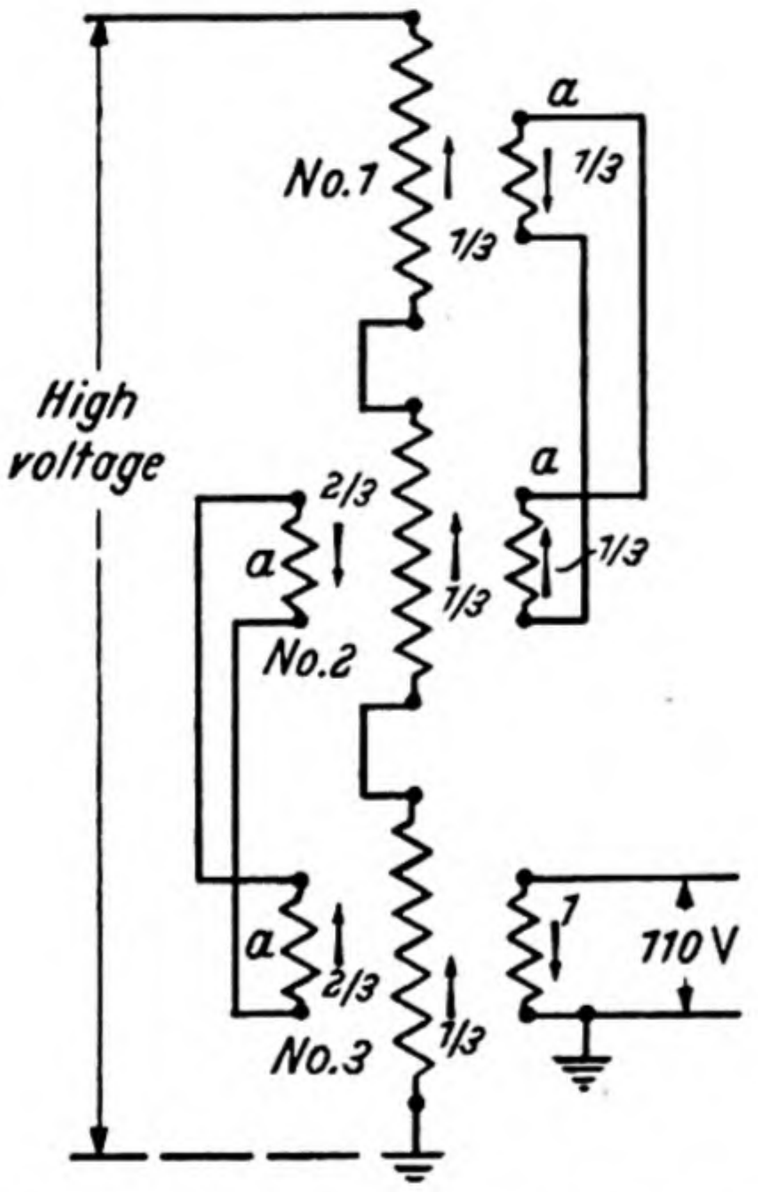

Figure 98. An arrangement of transformers to provide a non-inductive path to the load-current flow, accomplished by coupling each transformer to the next through windings *a*, thereby obtaining the advantages of cascading (Camilli[9], by courtesy, *Gen. Elect. Rev.*).

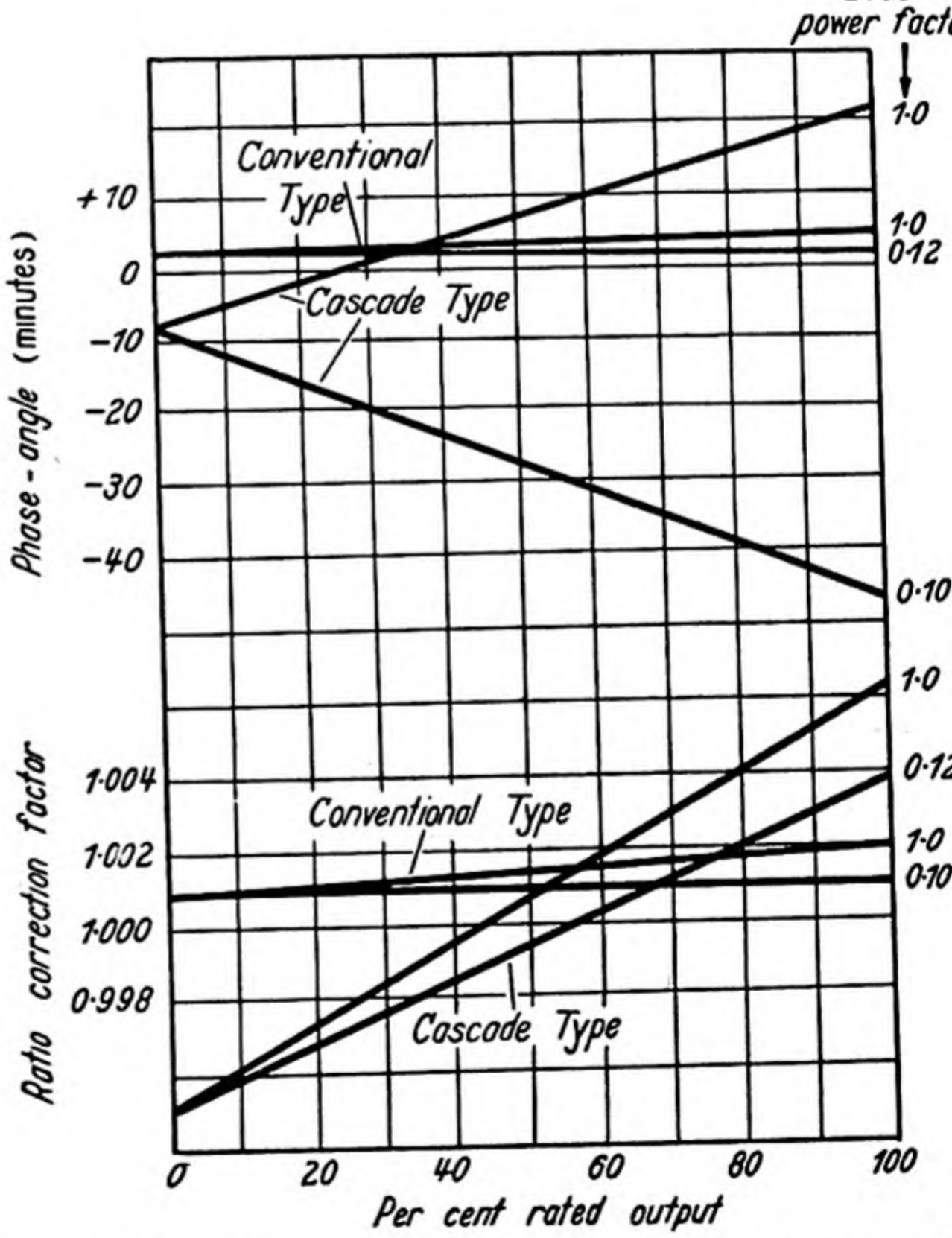

Figure 99. Comparative characteristic curves of a conventional and a cascade-type potential transformer for operation at 220 kv. (Camilli[9], by courtesy, *Gen. Elect. Rev.*).

cost for a given voltage may thus be reduced, since cascaded units need not individually possess the expensive and heavy insulation needed in single-stage transformer sets for high voltages. A cascaded set for 220 kV has windings arranged as in *Figure 97* and connections following the simplified scheme shown in *Figure 98*. Each unit in the cascade is contained in an oil-filled porcelain shell. Some characteristic curves are given in *Figure 99* and show that the present type of cascaded transformers do not compare favourably with conventional transformers in certain special respects, although the change of ratio with output, shown in *Figure 99* may be unimportant in most cases. Voltage distributions in such cascaded transformers are briefly discussed by Camilli[9].

RESONANCE TRANSFORMERS

Recently, the General Electric Laboratories in Schenectady have developed the resonance transformer method for producing a.c. at high voltages. The technique has been applied in the production

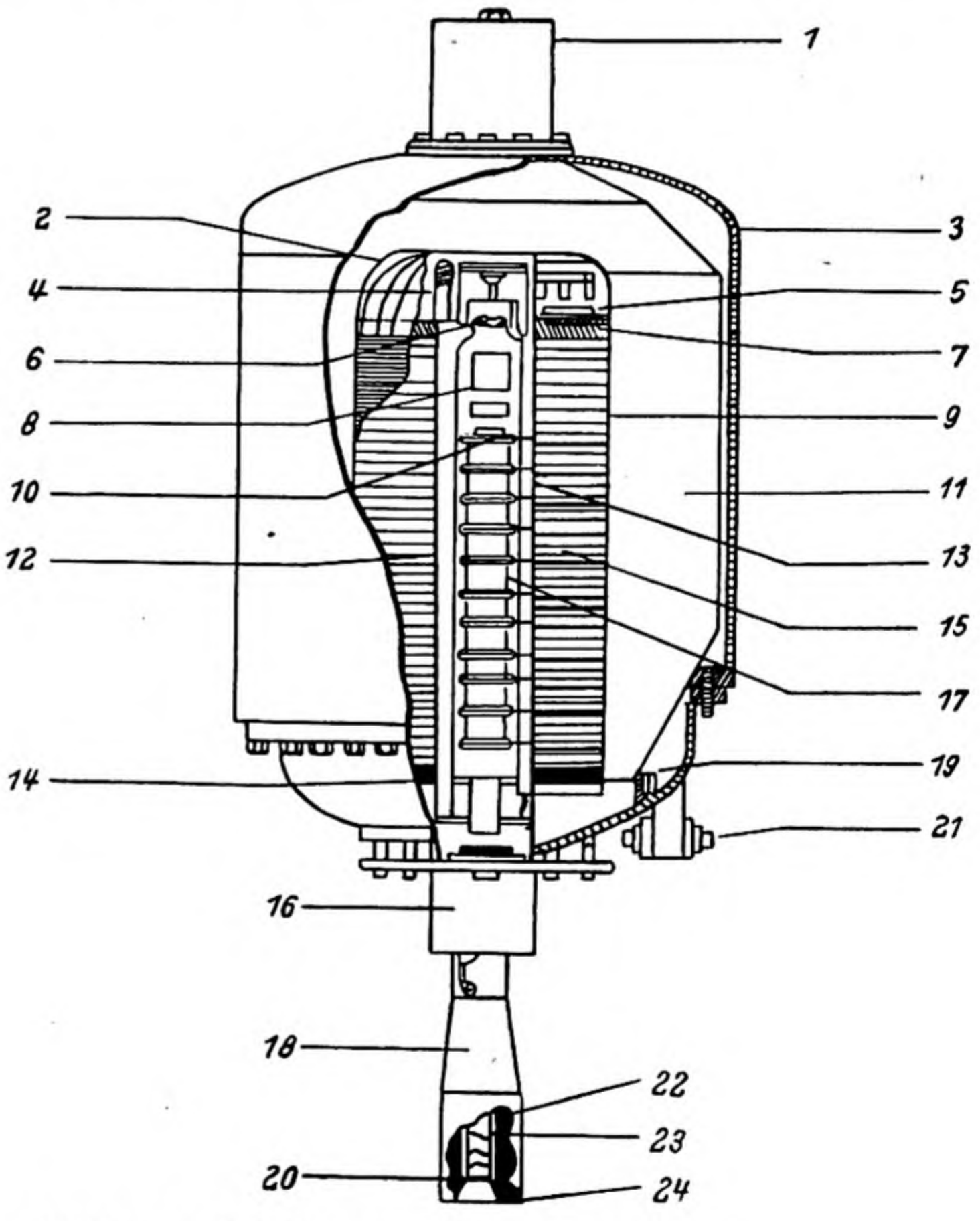

Figure 100. Principal elements of million-volt Portable X-ray unit (Charlton *et al*[11], by courtesy, *J. appl. Phys.*).

1. Cooler.
2. Slotted brass shield.
3. Steel tank.
4. Spring for tie rod.
5. Variable reactor.
6. Cathode assembly.
7. End turn filament coil.
8. First intermediate electrode.
9. Secondary coils.
10. Shields around the X-ray tube.
11. Laminated shield.
12. Glass tie rod.
13. Insulating filament-control shaft.
14. Primary winding.
15. Tap lead.
16. Focusing coil.
17. Glass envelope.
18. Lead shield.
19. Laminated steel bottom.
20. Tungsten target.
21. Filament control motor.
22. Water jacket.
23. Extension chamber.
24. Lead diaphragm.

of a self-contained X-ray unit, working at 1 MV with a sealed-off cascade X-ray tube mounted inside the transformer winding, which itself is enclosed in a steel pressure tank containing CCl_2F_2 at about 60 lb./in.^{2} gauge pressure. The whole unit is 3 ft. in diameter, 4 ft. in length and weighs 1,500 lb. (*Figure 100*) and is described with other similar units, by CHARLTON, WESTENDORP *et al*[10, 11].

It is seen from *Figure 100* that the secondary of the h.t. transformer, which is air-cored, consists of a pile of (125) thin coils. The resonant frequency of the winding is designed, by control of the number of turns, etc., to be 180 c/s and power at this frequency is supplied to the primary of the transformer from a generator. The power input circuit is shown in *Figure 101*. The formula $T = 2\pi\sqrt{LC}$ for the natural

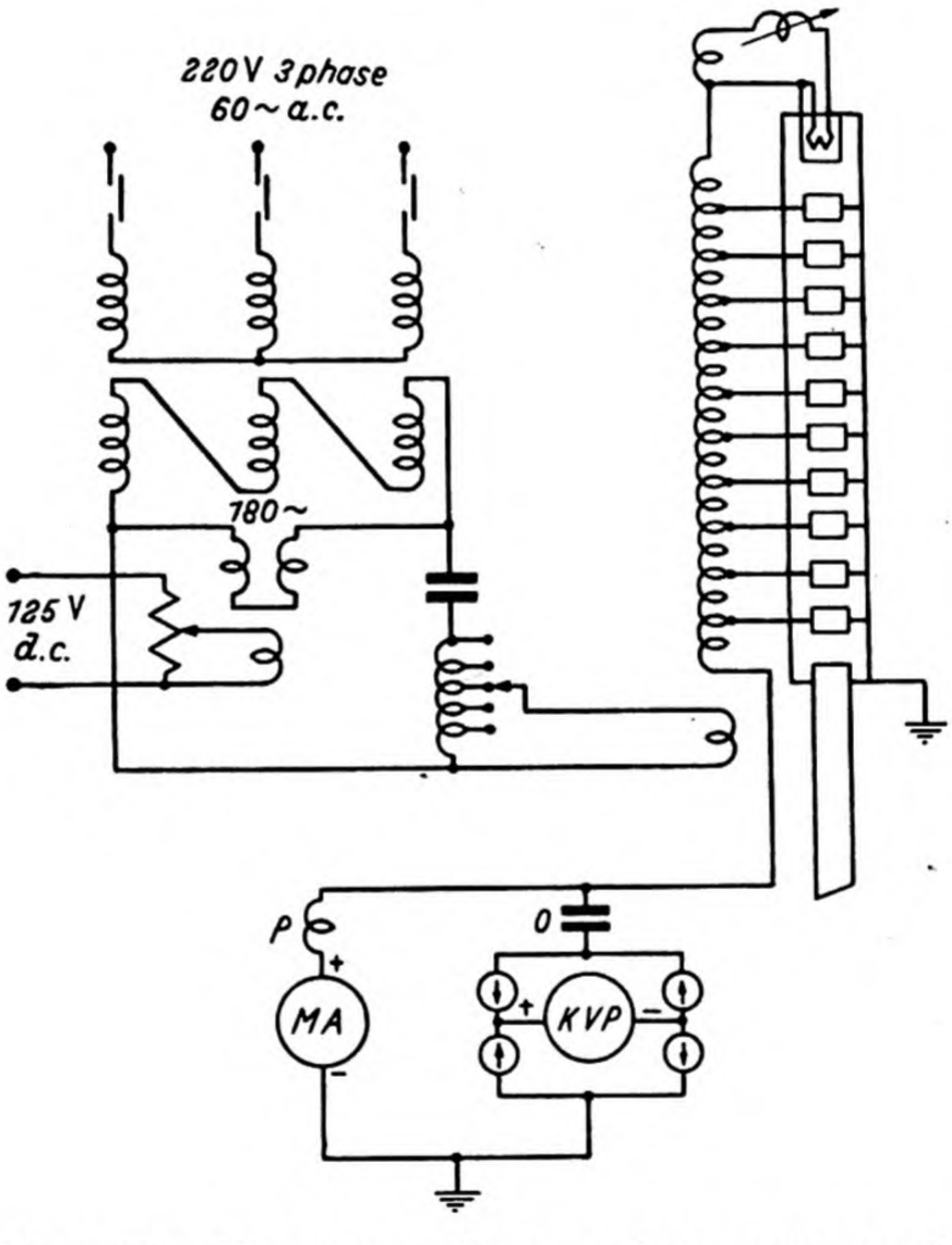

Figure 101. The circuit diagram of the power supply system for a resonant transformer X-ray set (Charlton *et al*[11], by courtesy, *J. appl. Phys.*).

period of a tuned circuit may be applied[10] provided that the correct effective values of L and C for the compound secondary are used. The above authors evaluate L and C as follows

$$L = 25n^2 \frac{D^2}{l_1 + l_2 + l_3} 10^{-9}\ H$$

where n = total number of turns
D = minimum turn diameter plus one-third of the difference between minimum and maximum diameters, in inches.
l_1 = coil stack height, in inches.
l_2 = distance from bottom coil to laminated steel disc below it, in inches.
$l_3 = 1/4\ D$, in inches.

$$C = C_1 + C_2 + C_3 + C_4 + \tfrac{1}{3}C_5$$

where C_1, C_2, C_3 and C_4 represent the component capacitances of the terminal cap in simplified terms such that they can be calculated either as parallel-plane or concentric cylinder capacitors:

C_1 = parallel-plane capacitance of terminal cap top to tank.
C_2 = cylindrical capacitance of cap to side wall.
C_3 = parallel-plane capacitance between cap and ground through the coils, putting the dielectric constants of the gas, pressboard coil cheeks and spacers, and the windings respectively as 1, 2 and ∞.
C_4 = parallel-plane capacitance from cap to ground through the inside of the coil, disregarding the effect of the tube electrodes.
C_5 = capacitance of the concentric cylinders formed by the outside copper turns on the coil and the inside of the laminated shell (*Figure 100*). This term is reduced by one-third in the formula for C because the energy stored in this space is only one-third of that with uniform voltage applied.

For the whole transformer, $C = 50\ \mu\mu$F and $L = 15{,}000$ H. Similar figures are obtained for other transformers of the same type. The secondary charging current is 55 mA r.m.s. at 1,000 kV peak. Transformer losses for a typical coil assembly are shown in *Figure 102*[11].

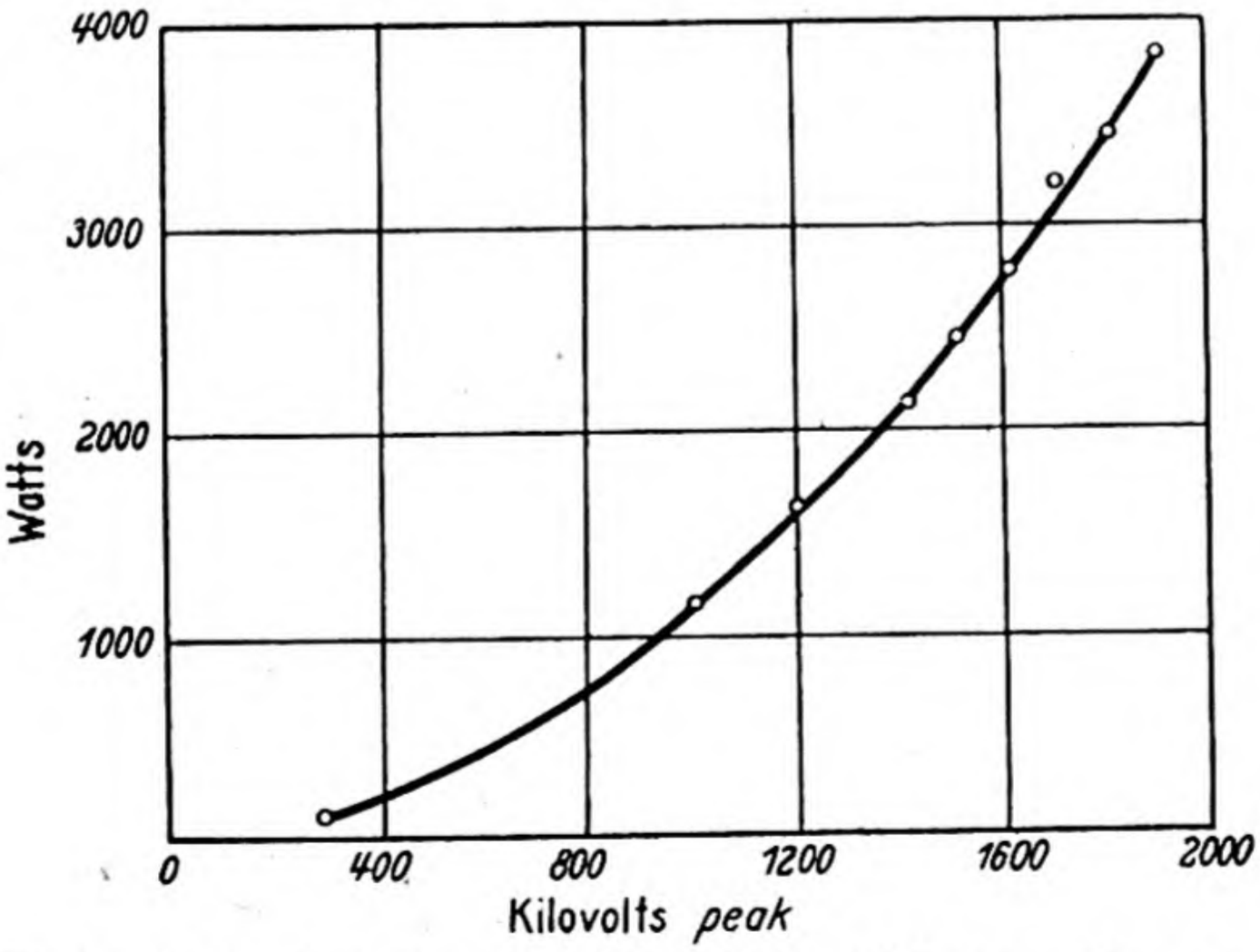

Figure 102. Losses of transformer without tube as a function of kilovolts peak (Charlton *et al*[11], by courtesy, *J. appl. Phys.*).

A 1 MV set with continuous pumping is shown in *Figure 103* where the method of tapping the stages of the X-ray tube down the coil stack to ensure uniform voltage distribution in the tube is clearly shown.

The advantages of the resonant transformer system are[10]:

(1) The absence of the iron core saves the space which would normally be required for insulation between the core and the h.t. winding.

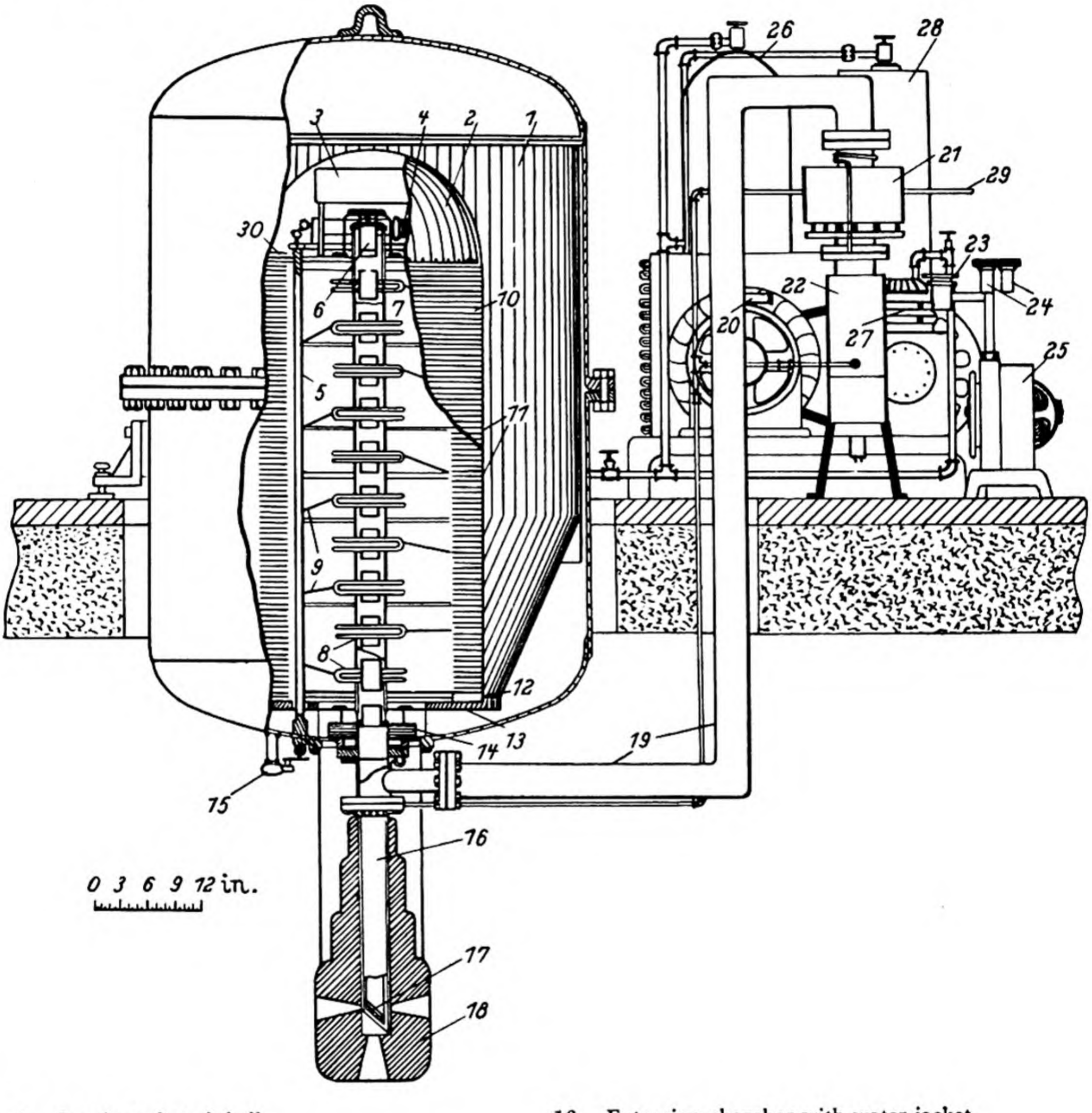

1. Laminated steel shell.
2. Slotted brass shield.
3. Lead shield.
4. Variable reactor.
5. Insulating shaft.
6. Cathode assembly.
7. First intermediate electrode.
8. Shields around the seals.
9. Tapleads.
10. Secondary coils with copper-tube shields.
11. Secondary coils.
12. Primary winding.
13. Laminated steel bottom.
14. Focusing coil.
15. Filament control motor.
16. Extension chamber with water jacket.
17. Target.
18. Lead shield.
19. Vacuum line.
20. Ionization gauge.
21. Charcoal trap.
22. Oil diffusion pump.
23. Vacuum shut-off valve.
24. Hale-Pirani gauge.
25. Rough vacuum pumps.
26. Freon supply tank.
27. Freon compressor.
28. Freon storage tank.
29. Cooling water inlet, drain omitted.
30. End-turn filament-coil.

Figure 103. Drawing of million-volt X-ray set (Charlton *et al*[11], by courtesy, *Gen. Elect. Rev.*).

(2) The wave-form in the h.t. circuit is always sinusoidal and the oscillatory current in the h.t. winding is so large, *i.e.* 55 mA r.m.s. at 1,000 kV peak, that the rated half-wave full-load current of 3 mA does not produce any measurable difference between useful and inverse voltages.

(3) The slow build-up of voltage, over a few cycles after switching on, prevents the production of unduly large voltage surges.

(4) The careful design of the coil stack and its subdivision into so many units, the spacing between which is carefully controlled, gives a very uniform voltage gradient along the stack.

The voltage distribution in a resonant transformer is as shown in *Figure 104*[11]. Special calibration methods are necessary for measuring the maximum voltage and, as used by CHARLTON *et al*[11], the principal technique is as follows. In *Figure 101* the earthy end of the

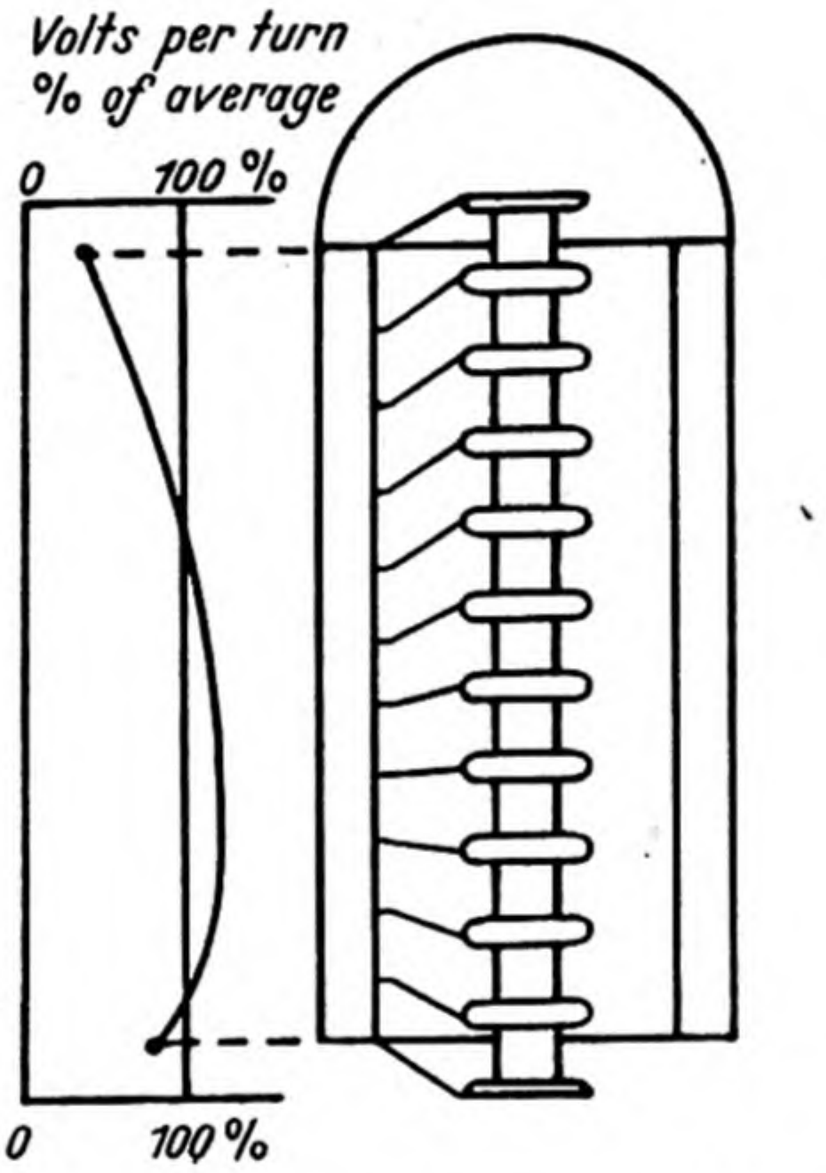

Figure 104. Voltage distribution per turn along secondary coils of resonance transformer (Charlton *et al*[11], by courtesy, *J. appl. Phys.*).

h.t. winding is connected to the branch in which *P*, a reactor, chokes out the a.c. and passes d.c. and to the parallel branch in which the capacitor *O* only passes a.c. to the valve rectifier bridge. The d.c. milliammeter connected to the bridge thus registers rectified a.c. and can be calibrated in terms of the h.t. by the use of a sphere gap, using 12·5 cm. spheres, reading up to 100 kV, temporarily mounted in the tank between the latter and the h.t. end of the resonant transformer secondary. The secondary is then tuned, at a frequency rather lower than its normal operating resonance frequency of 180 c/s, because of the additional capacitance of the sphere gap, using a motor generator set. The rectified charging current is read when the

spheres spark over at 100 kV. The experimental resonant frequency so found is 174 c/s and the rectified current is 7·85 mA. The sphere gap is then removed, so that the normal resonance is obtained at 180 c/s, when the charging current should be $\frac{174}{180} \times 7{\cdot}85 = 7{\cdot}6$ mA or 76·0 mA for 1,000 kV. The circuit inductance is here assumed to be constant, *i.e.* independent of the sphere gap. The linear extrapolation is justified since there is little iron in the circuit.

Another method of voltage calibration, the results of which confirm those obtained with the charging current method, is illustrated in *Figure 105*. Here, the ring *P* serves to pick up a voltage from the h.t. secondary winding which may be rectified as shown, thus giving a microammeter reading proportional to the h.t. voltage. This method is also of value in measuring the h.t. when, for example, an X-ray tube is connected to the transformer and allowed to pass current.

The above 1 MV set shows < 1 per cent. difference between useful and inverse peak voltage at 10 mA tube current, and the distortion of the secondary voltage is usually negligible as the typical oscillogram of *Figure 106* for 3 mA shows. Charlton *et al*, point out that at this current the half-wave load of the tube is about 2 kVA whilst the secondary coil power is about 50 kVA.

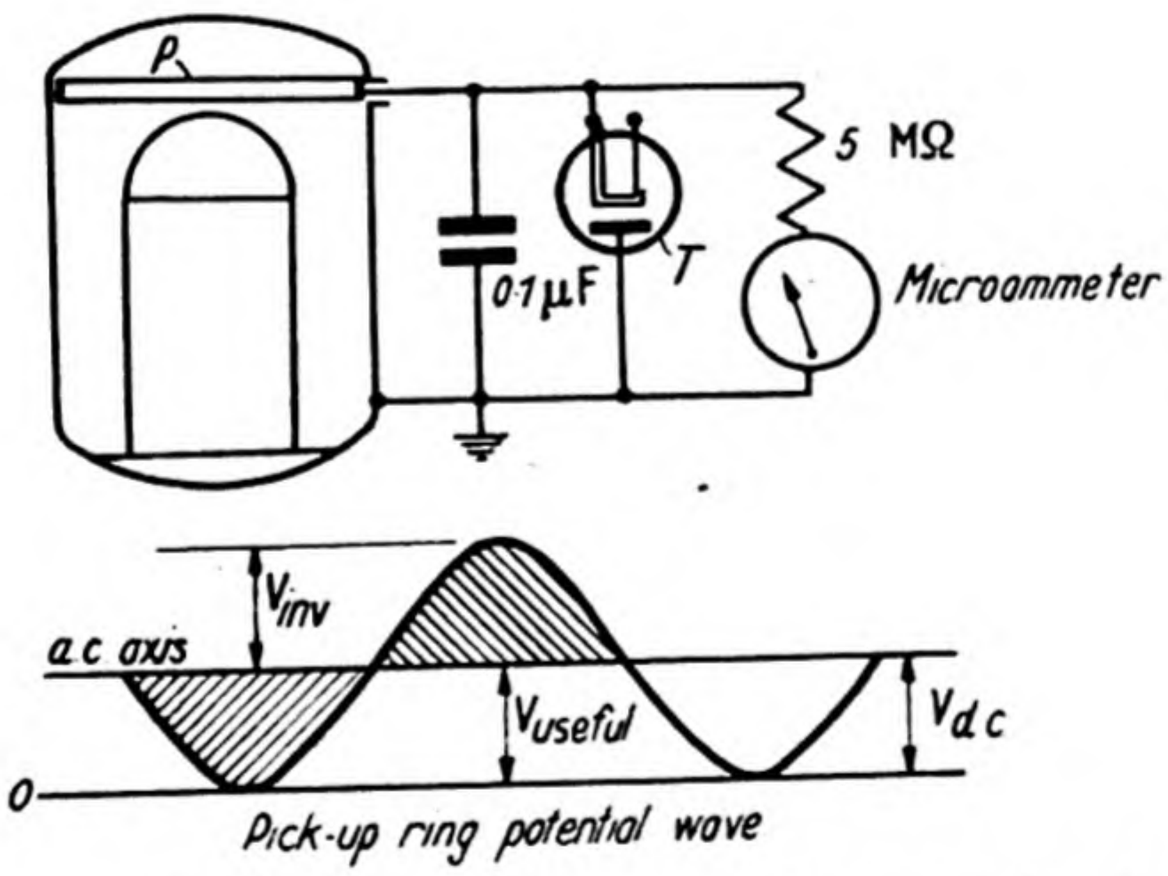

Figure 105. Circuit diagram of peak voltmeter for tests on resonant transformers (Charlton *et al*[10], by courtesy, *Gen. Elect. Rev.*).

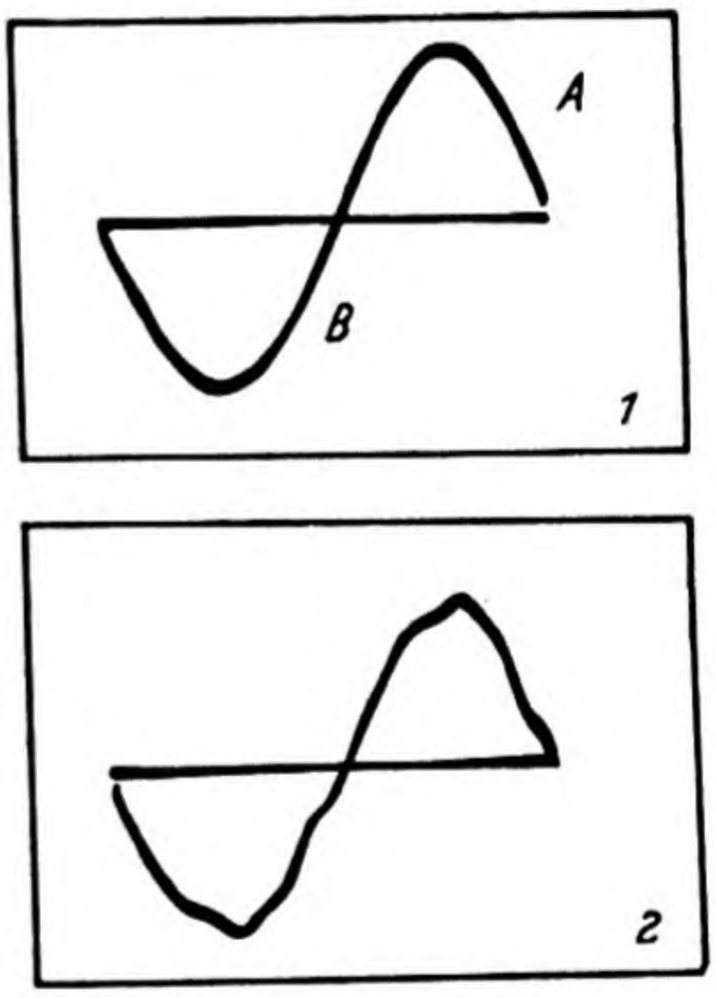

Fig. 106. Oscillographic Records of the X-ray unit operating at 1000 kV peak and 3 mA. *No. 1* secondary voltage, *A* being the useful half-cycle and *B* the inverse half-cycle. *No. 2* primary voltage (Charlton *et al.*[10], by courtesy, *Gen. Elect. Rev.*).

Power requirements are as shown in *Table VII*. The frequency-tripler on the input side, of the circuit (*Figure 107*) is designed for a continuous rating of 10 kW. Further information on frequency-triplers is available in other papers[12, 13, 14]. The secondary losses

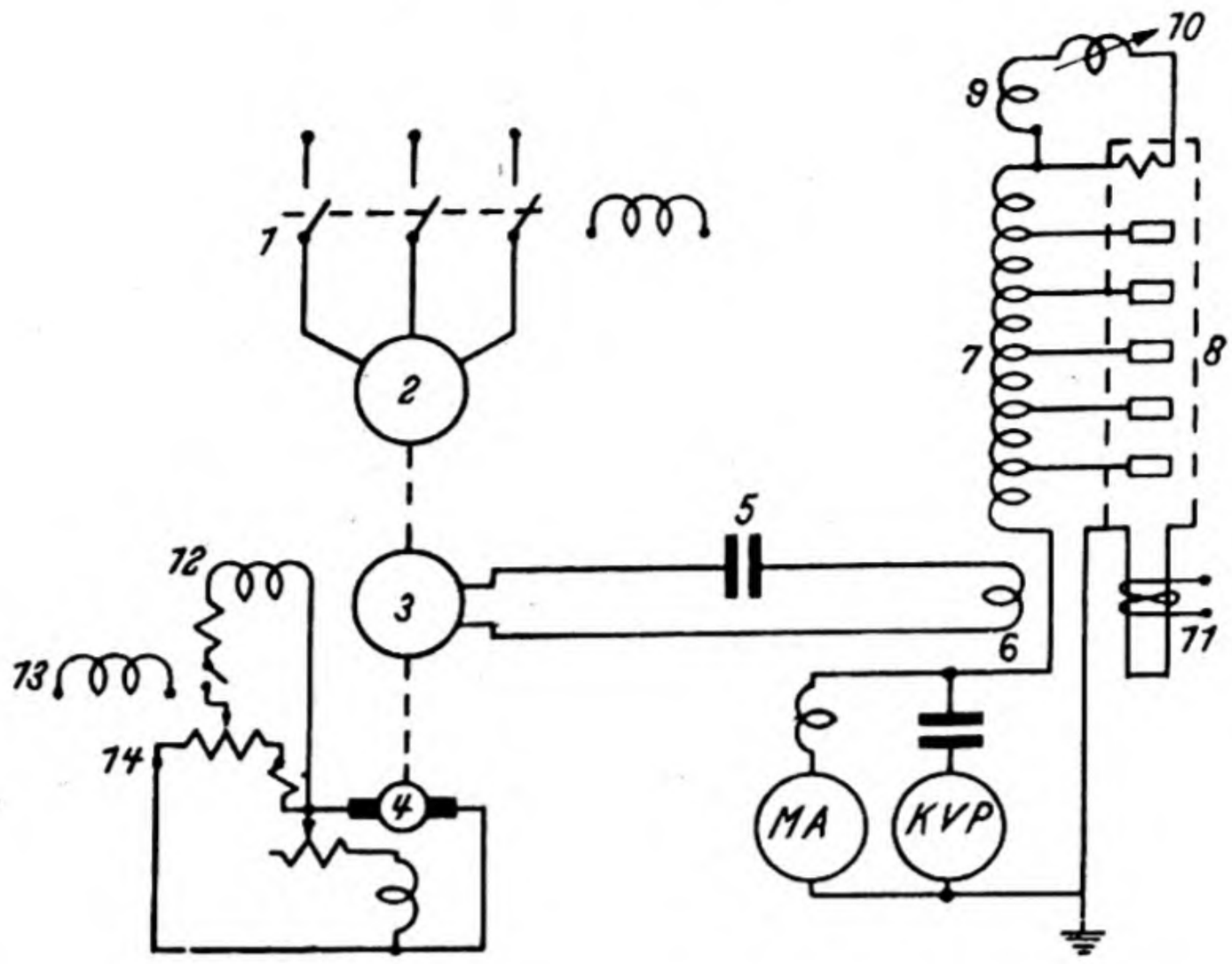

1. Three-phase 60 c/s line and motor starter.
2. Synchronous motor, self-excited.
3. Generator for 180 c/s.
4. Exciter.
5. Series capacitor.
6. Primary winding of resonance transformer.
7. Secondary winding.
8. Million-volt sealed off X-ray tube with auxiliary electrodes.
9. End turns for filament power.
10. Adjustable reactor.
11. Focus coil.
12. Generator field.
13. Starting relay.
14. Kilovoltage adjusting potentiometer.

Figure 107. Diagram of the principal circuits of the portable million-volt X-ray outfit (Charlton *et al*[10], by courtesy, *Gen. Elect. Rev.*).

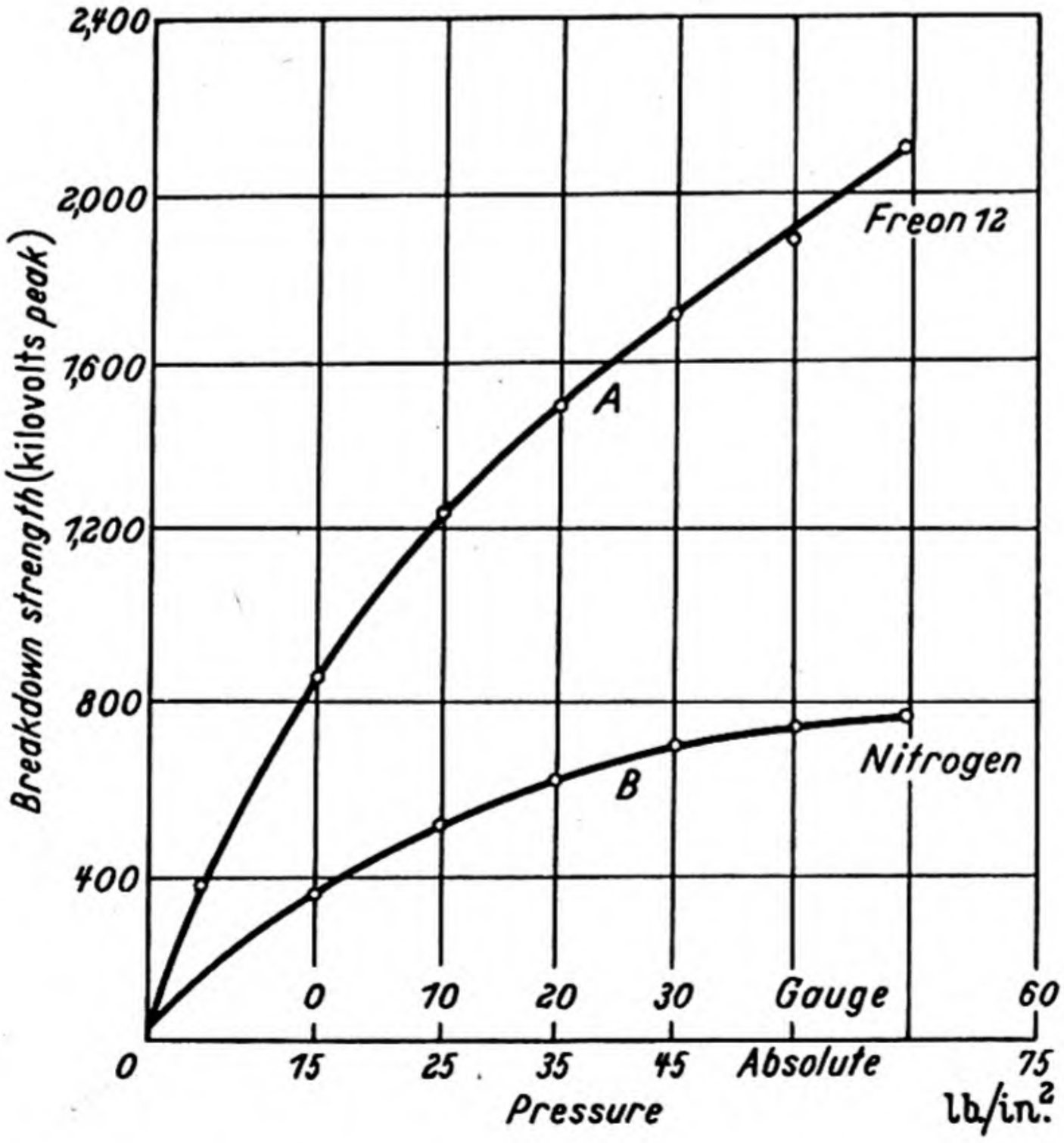

Figure 108. Break-down strength of nitrogen and freon 12 when used as insulation for the resonance transformer as a function of pressure (Charlton *et al*[10], by courtesy, *Gen. Elect. Rev.*).

are prevented from causing overheating of the coils by spacing the latter 3/32 in. apart in the 1 MV set, with a tank filling of CCl_2F_2 at 40 lb./in.^{2} gauge pressure. This gives a secondary coil break-down

TABLE VII

Input power data as a function of output power for high voltage resonant transformer unit
(1 *MV X-ray set.*)

3-PHASE 60-CYCLE LINE			
VOLTS	AMP.	KVA'	WATTS
218	40	15·0	2300
217	45	17·0	4900
216	51	19·2	6700
213	80	29·5	12300
218	41	15·5	2880
216	49	18·2	6040
215	60	22·5	8380

180-CYCLE POWER FROM TRIPLER				
VOLTS	AMP.	KVA	WATTS	*PF*%
143	8·8	1·25	1200	96
190	19·8	3·75	3600	96
220	27·2	6·00	5200	87
330	43	14·2	9800	69
172	10·5	18·0	1730	96
224	21·5	4·81	4620	96
245	30·0	7·35	6530	89

CHARGING CURRENT MA AVG	TUBE VOLTAGE KV PEAK	TUBE CURRENT MA
76·0	1000	0
81·2	1000	3
84·5	1000	5
86·6	1000	10
91·2	1200	0
96·2	1200	3
99·5	1200	5

voltage of about 1·9 MV peak (*see Figure 108*). Since the heat losses of the transformer for no load increase with the square of the voltage, forced cooling as shown in *Figure 109* becomes necessary at voltages much above 1 MV. For 1·25 MV the above-described apparatus, nominally rated at 1 MV, may be run with a blower forcing the gas through the transformer at 20 ft.^{3}/min. when a maximum temperature

of 45° C. is reached in 8 hours, whereas with no forced cooling at 1 MV a temperature of 35° C. is reached in 8 hours.

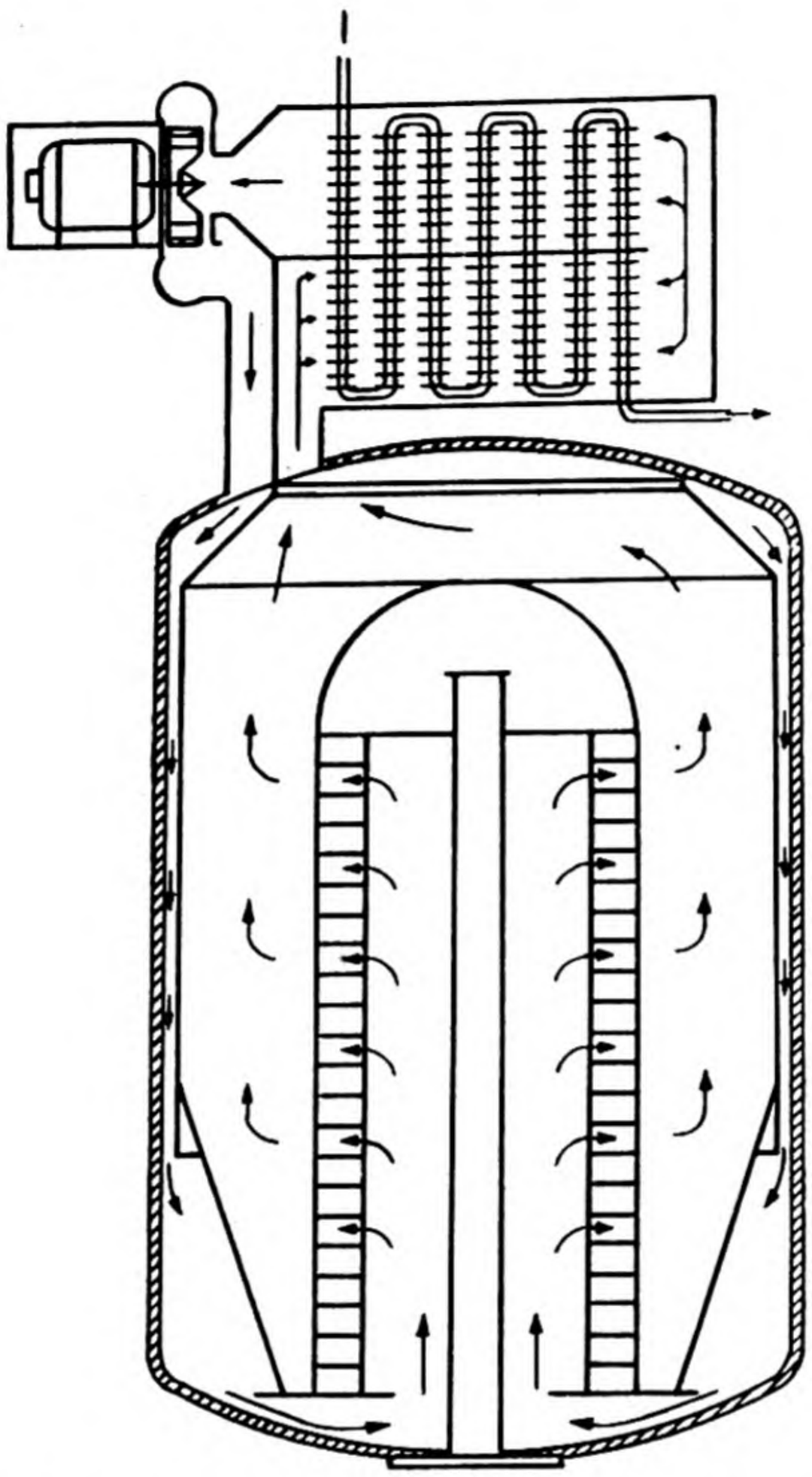

Figure 109. Forced circulation of freon gas in tank for more effective cooling of the unit when operated continuously at voltages in excess of 1000 kV peak (Charlton *et al*[10], by courtesy, *Gen. Elect. Rev.*).

The relation between the Tesla coil, which consists of two coupled tuned circuits, and the resonance transformer, later developed so successfully by Charlton and his collaborators[10, 11] is made clear by Sloan[15] in a paper describing the acceleration of electrons up to about 800 kV. The Tesla coil, driven by a self-excited oscillator tube, cannot give an efficiency higher than 50 per cent. since above this figure two stable frequencies are produced, at each of which there is an equivalent output at 50 per cent. efficiency. The critical coupling is M where

$$2\pi f M = \sqrt{R_p R_s}$$

f is the resonant frequency of the separate coupled circuits having resistances R_p and R_s. Distinction must be made between self-

excitation with a spark gap and with an oscillator tube.

The resonance transformer, Sloan[15] points out, has a single resonance frequency and an efficiency approaching 100 per cent. can be obtained.

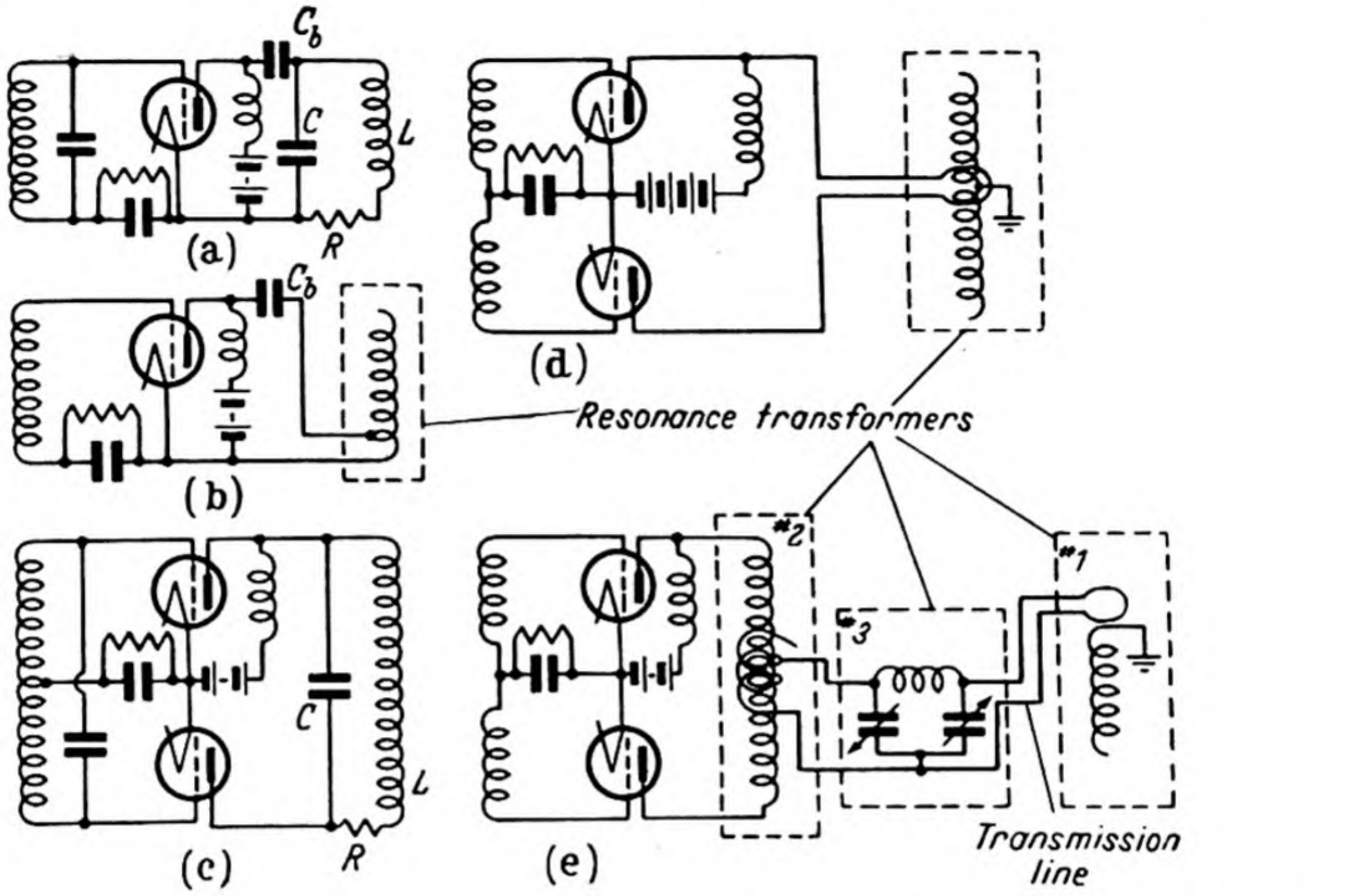

Figure 110. Resonance transformer connections to oscillator tubes (Sloan[15], by courtesy, *Phys. Rev.*).

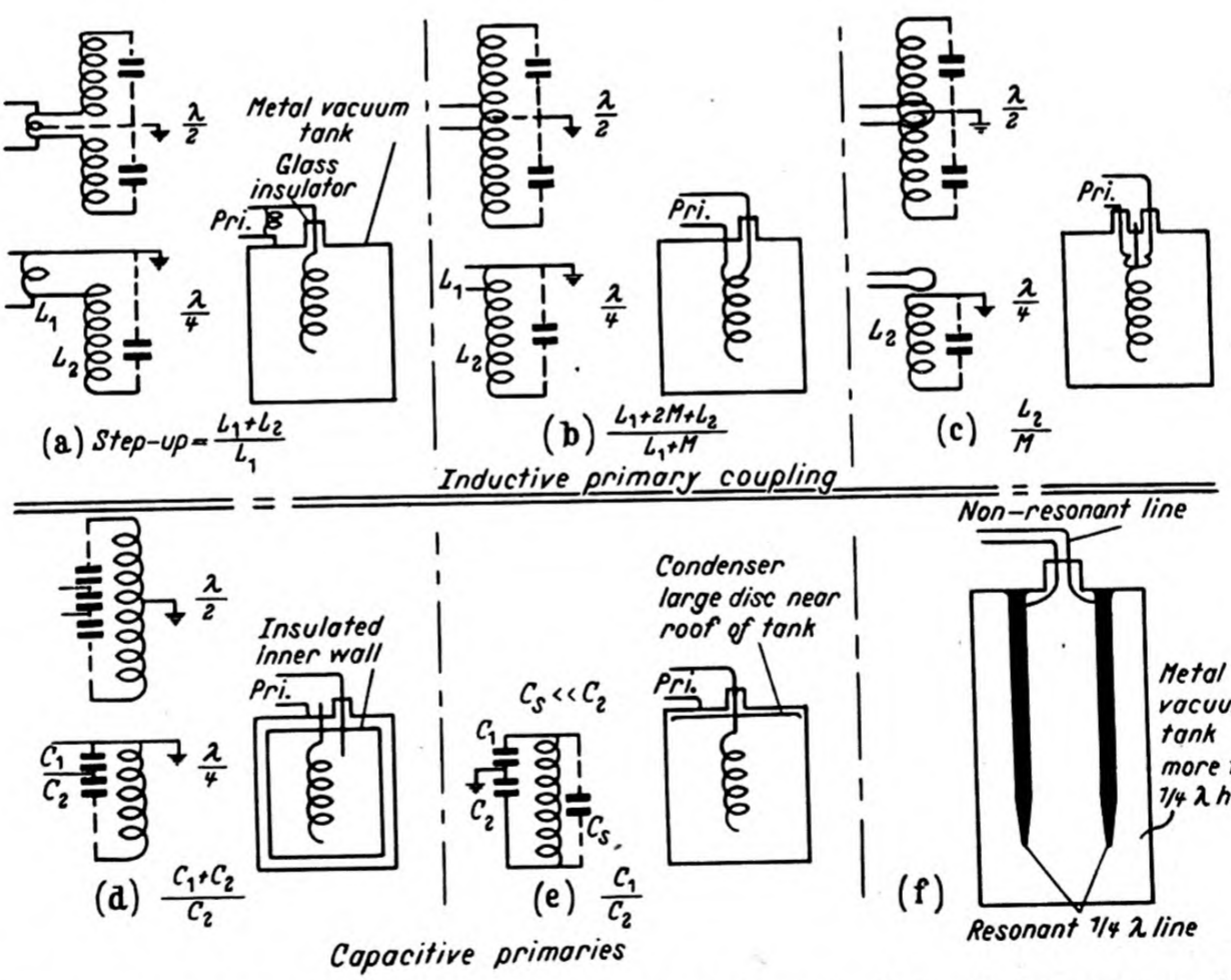

Figure 111. Types of high-voltage resonance transformers (Sloan[15], by courtesy, *Phys. Rev.*).

Circuits using valve oscillators are shown in *Figure 110*. Circuit (*c*), push-pull, is preferable to that of (*a*) where the isolating condenser C_b may become overheated. Sloan further found that parasitic oscillations are reduced if the grid circuit is tuned by coil adjustment, using as capacitance only the oscillator valve strays (circuits (*b*), (*d*) and (*e*)). The leads to the resonance transformer from the valve anodes in circuit (*d*) may be comparable with the wavelength of the oscillations and the resulting transmission line may be used to match the valves to the transformer coil. Thus in circuits (*d*) and (*e*) the intermediate transmission lines, which are essential if the resonance transformer is of the quarter-wave type (*Figure 111f*), can be used for matching.

Figure 111 shows various methods of arranging the transformer windings either as lumped circuits or with distributed constants, whose step-up ratios are given, as in *Figure 111f*, or as intermediate cases. A high shunt impedance, L/RC, necessary for high voltages is obtained by enlarged dimensions and by reduction of C to a minimum (L, R and C are the effective inductance, resistance and capacitance of the winding). The practical transformer circuits, in which the resonant circuits are neither strictly lumped or distributed, but a combination of both, are shown in *Figure 111* for $\lambda/4$ and $\lambda/2$ coils. Sloan's first full-scale arrangement, developed from circuits

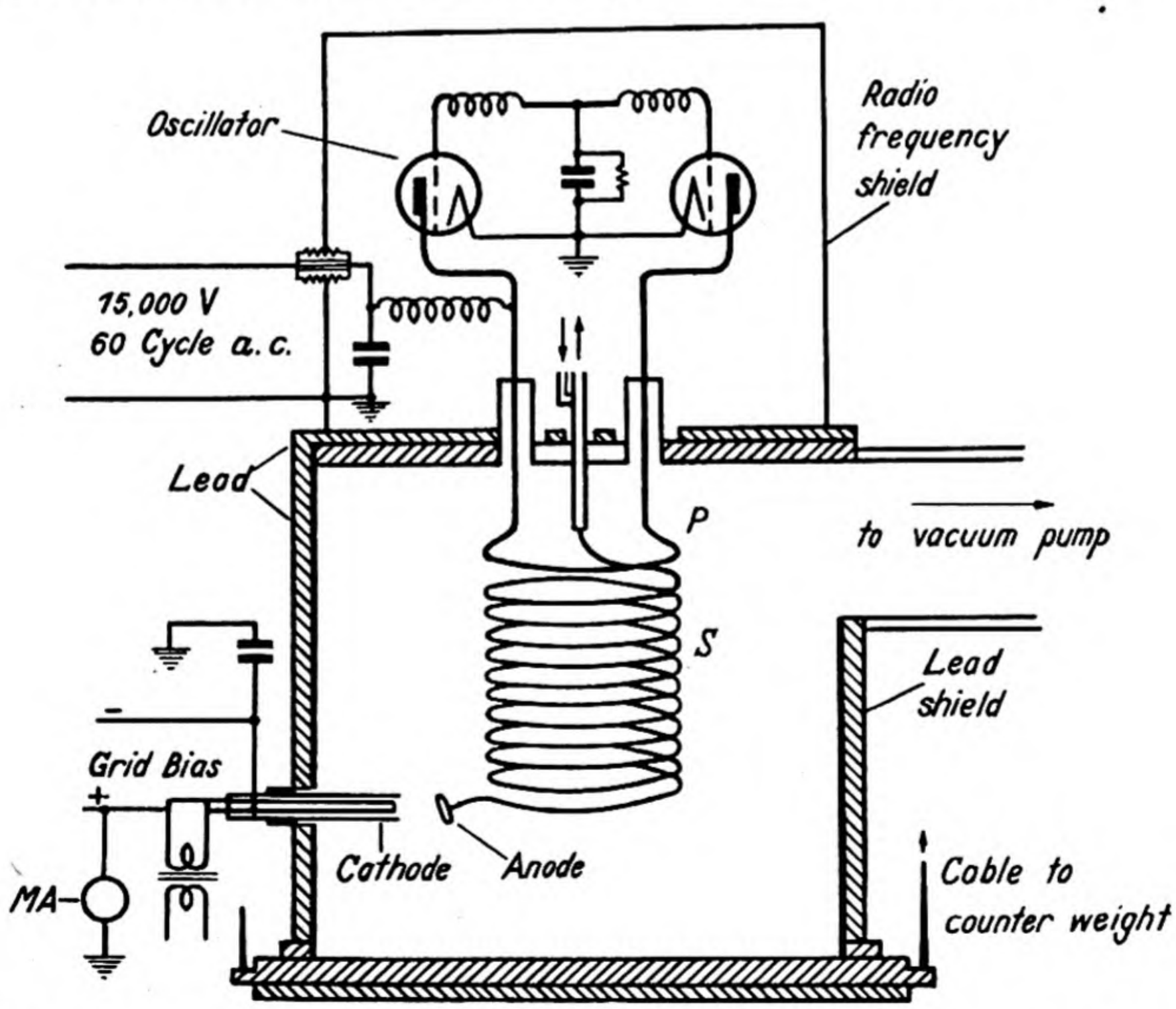

Figure 112. X-ray arrangement with inductive primary separated from the high-voltage coil (Sloan[15], by courtesy, *Phys. Rev.*).

shown in *Figures 110d* and *111c* is given in *Figure 112*. The transformer in the latter case had an impedance L/RC of 3 MΩ and would

develop 800 kV with 200 kW current input, at a resonant frequency of 6 Mc/s. Sloan's work, remarkable for 1934–1935, also involved the construction of 100, 200 and 300 kW oscillator valves and details of these tubes are given in his paper. The coil data are also given; for example, a $\lambda/4$ coil for 6 Mc/s consisted of 12 turns of 7/8 in. copper pipe wound into a helix 14 in. in diameter and 15 in. long.

The X-ray intensity at 0·7 m. from a tungsten target with 2–8 mA emission current was 20 Roentgens/min., but the circuit could supply 10 mA. This output is small compared with that from later installations such as the St. Bartholomew's 1 MV set designed by ALLIBONE and collaborators[16] and with that from betatrons or synchrotrons operating at 20 MV or more[13].

TESLA COILS

The circuit of a Tesla coil, used for the production of damped h.f. oscillations is arranged as shown in *Figure 113*[17]. A generator of this type in the Metropolitan-Vickers laboratories has an output voltage of 750 kV at 130 kc/s. In the circuit, T is a trigger gap

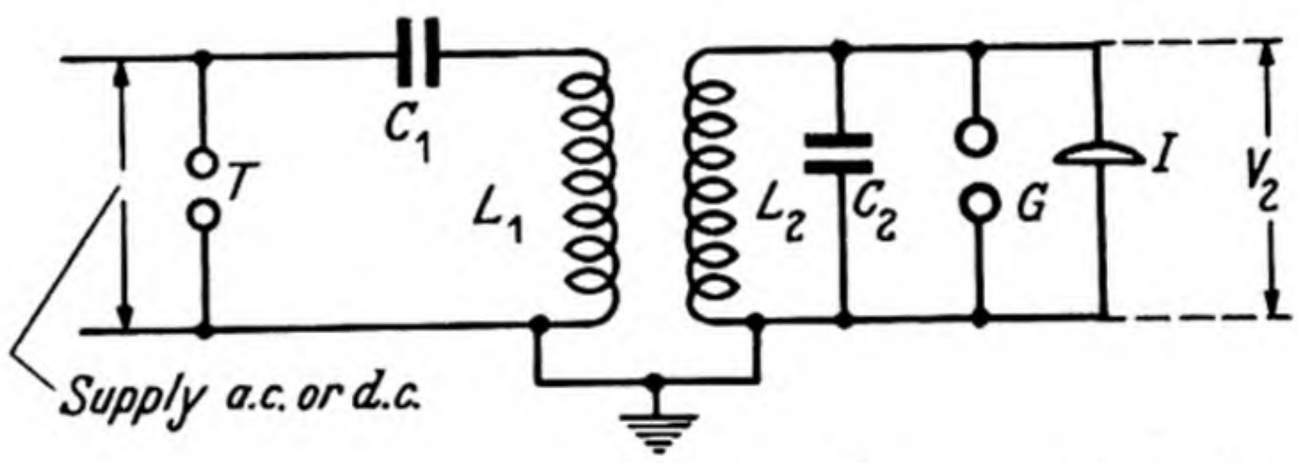

Figure 113. Diagram of connections of Tesla transformer (Perry[17], by courtesy, *Trans. S. African Inst. elect. Engrs.*).

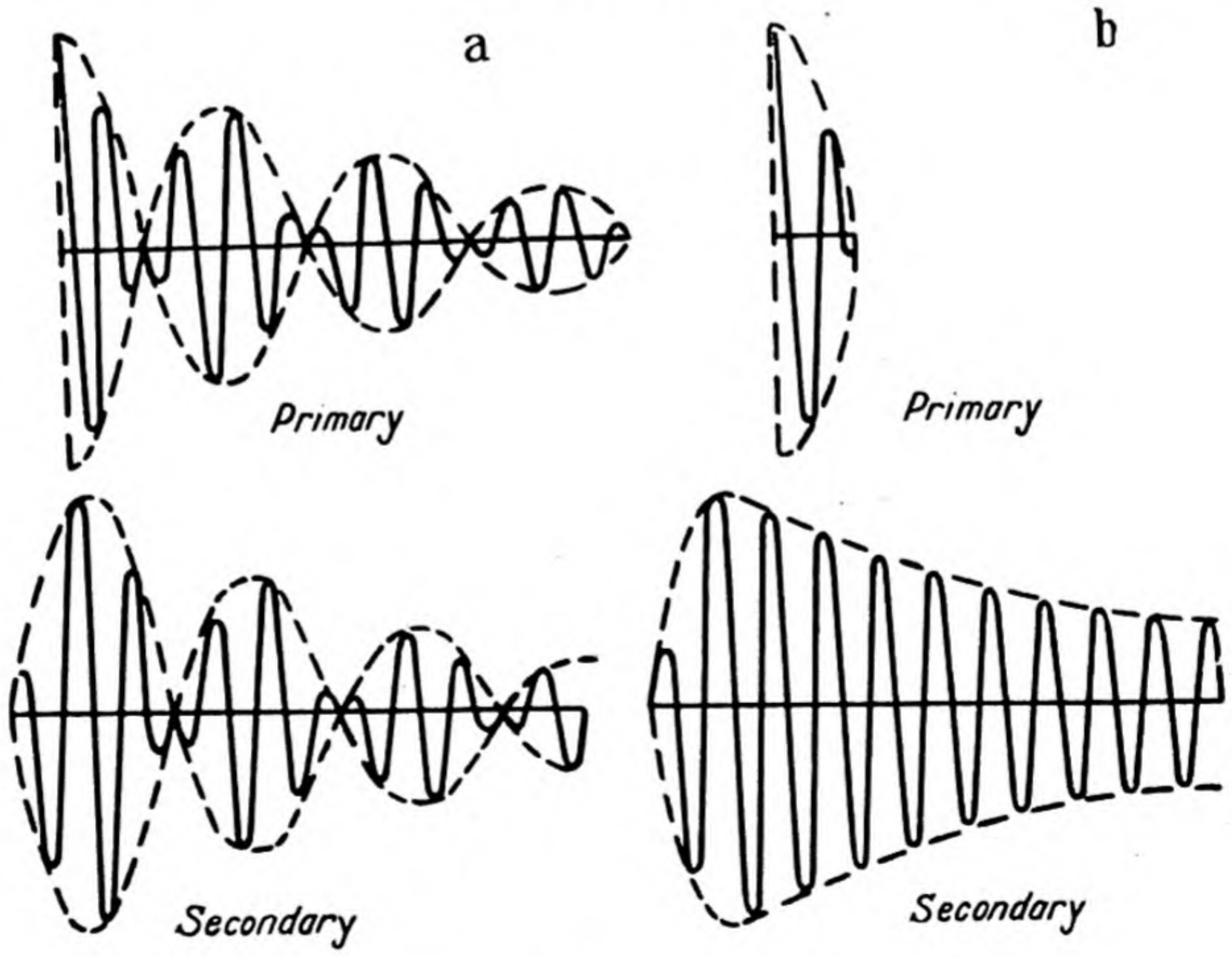

(a) No interruption to primary circuit oscillations.
(b) Primary circuit oscillations interrupted by air blast.

Figure 114. Voltage wave shapes in a Tesla transformer (Perry[17], by courtesy, *Trans. S. African Inst. elect. Engrs.*).

which sparks over when C_1, charged from an a.c. or d.c. source, reaches a given potential. The primary circuit, then closed, forms an oscillatory circuit which supplies energy to the secondary circuit L_2C_2 to which the primary coil L_1 is coupled so that the primary voltage falls and the secondary voltage rises. Eventually power is transferred in the reverse sense, *i.e.* from L_2C_2 to L_1C_1 and the process is repeated, giving damped wave trains, because of finite circuit losses in both primary and secondary circuits (*Figure 114a*). The arc in the gap T is often interrupted with an air blast after the first quarter cycle of the beat-frequency wave (*see Figure 114b*) so that the energy remains in the secondary circuit. PERRY, whose paper is quoted above[17], shows that if p^2 is the efficiency of the circuit, then $W_2 = p^2 W_1$ where $p^2 < 1$ and where W_1 and W_2, respectively equal to $\frac{1}{2} C_1 V^2_1$ and $\frac{1}{2} C_2 V^2_2$, are the amounts of energy stored in primary and secondary respectively. Thus

$$\frac{V_2}{V_1} = p\sqrt{\frac{C_1}{C_2}} \qquad \ldots\ldots(3.1)$$

In the Metropolitan-Vickers Tesla transformer, the primary circuit is supplied from a 50 c/s 50 kV transformer controlled with a variable resistor in the primary circuit. The h.t. output voltage is controlled by the setting of T.

The oscillation frequency is of the same order as that of the primary circuit, namely

$$f = \frac{1}{2\pi\sqrt{L_1C_1}}$$

where L_1 and C_1 are the primary inductance and capacitance respectively. At high frequencies the secondary voltage falls rapidly with increasing load and GOODLET[18] suggests that 100 kc/s is a practicable limit for many technical purposes.

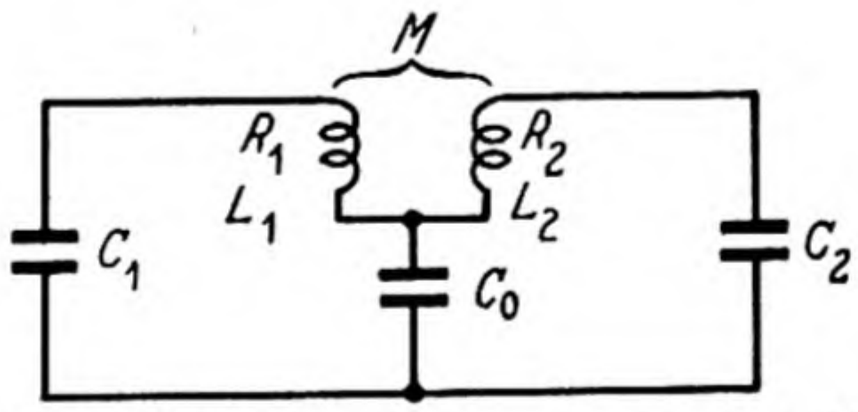

Figure 115. Basic circuit of a Tesla transformer (Goodlet[18], by courtesy, *J. Inst. elect. Engrs.*).

A theoretical treatment of the Tesla coil circuit is given in Bouwer's book[3], but the following analysis, which differs to some extent, is due to Goodlet[18].

The basic circuit of *Figure 115* is taken, where a spark gap of capacitance C_2 is connected across the load capacitor C_o, which may be a bushing, with the inclusion of self and mutual inductance as shown. If C_1 is charged to voltage E then

$$E = R_1 I_1 + L_1 \frac{dI_1}{dt} + \left(\frac{1}{C_o} + \frac{1}{C_1}\right)\int I_1 dT + M\frac{dI_2}{dt} - \frac{1}{C_o}\int I_2\, dt \qquad \ldots\ldots(3.2)$$

and $$O = R_2 I_2 + L_2 \frac{dI_2}{dt} + \left(\frac{1}{C_o} + \frac{1}{C_1}\right)\int I_2 dt + M\ \frac{dI_1}{dt} - \frac{1}{C_o}\int I_1\, dt \qquad \ldots\ldots(3.3)$$

Put $$w^2{}_1 = \frac{C_o + C_1}{C_o L C_1} \qquad \text{and } w^2{}_2 = \frac{C_o + C_2}{C_o L_2 C_2}$$

also $$K^2 = \frac{C_1 C_2}{(C_o + C_2)(C_o + C_1)} \text{ and } \sigma = 1 - \frac{M^2}{L_1 L_2}$$

The reduction of the Equations 3.2 and 3.3 above gives the auxiliary Equation

$$m^4\sigma + m^3\left(\frac{R_1}{L_1} + \frac{R_2}{L_2}\right) + m^2\left(w^2{}_1 + w^2{}_2 + \frac{R_1 R_2}{L_1 L_2} + \frac{2M}{C_o L_1 L_2}\right) \qquad \ldots\ldots(3.4)$$
$$+ m\ \left(w^2{}_1\frac{R_2}{L_2} + w^2{}_2\frac{R_1}{L_1}\right) + w^2{}_1 w^2{}_2\,(1 - K^2)\ =\ 0$$

If the roots of Equation 3.4 are m_1 m_2 m_3 and m_4 then

$$V_1 = \frac{C_1 E}{C_1 + C_2 + C_o} + A_1 e^{m_1 t} + A_2 e^{m_2 t} + A_3 e^{m_3 t} + \cdots$$

$$V_2 = \frac{C_1 E}{C_1 + C_2 + C_o} + B_1 e^{m_1 t} + B_2 e^{m_2 t} + B_3 e^{m_3 t} + \cdots$$

$$V_o = \frac{1}{C_o}\int I_1 dt - \frac{1}{C_o}\int I_2 dt$$

The V's refer to the voltages across the appropriate capacitors. The initial conditions are $t=0$, $V_1 = E$, $V_2 = 0$, $dV_1/dt = 0$ and $dV_2/dt = 0$. From Equation 3.2 the following relations are obtained

$$A_1 + A_2 + A_3 + A_4 = E - \frac{C_1 E}{C_1 + C_2 + C_0}$$

$$m_1 A_1 + m_2 A_2 + m_3 A_3 + m_4 A_4 = 0$$

$$m^2{}_1 A_1 + m^2{}_2 A_2 + m^2{}_3 A_3 + m^2{}_4 A_4 = -E/\sigma L_1 C_1$$

$$m^3{}_1 A_1 + m^3{}_2 A_2 + m^3{}_3 A_3 + m^3{}_4 A_4 = -\frac{E}{\sigma L_1 C_1}\left[\frac{R_2}{L_2} - \left(\frac{R_1}{\sigma L_1} + \frac{R_2}{\sigma L_2}\right)\right]$$

and for the B coefficients

$$B_1 + B_2 + B_3 + B_4 = -\frac{C_1 E}{C_1 + C_2 + C_0}$$

$$m_1 B_1 + m_2 B_2 + m_3 B_3 + m_4 B_4 = 0$$

$$m^2{}_1 B_1 + m^2{}_2 B_2 + m^2{}_3 B_3 + m^2{}_4 B_4 = \frac{-ME}{\sigma L_1 L_2 C_2}$$

$$m^3{}_1 B_1 + m^3{}_2 B_2 + m^3{}_3 B_3 + m^3{}_4 B_4 = \frac{ME}{\sigma L_1 L_2 C_2}\left(\frac{R_1}{\sigma L_1} + \frac{R_2}{\sigma L_2}\right)$$

The Tesla coil is a special case, studied by putting $C = \infty$ and $R_1 = R_2 = 0$ in *Figure 115*.

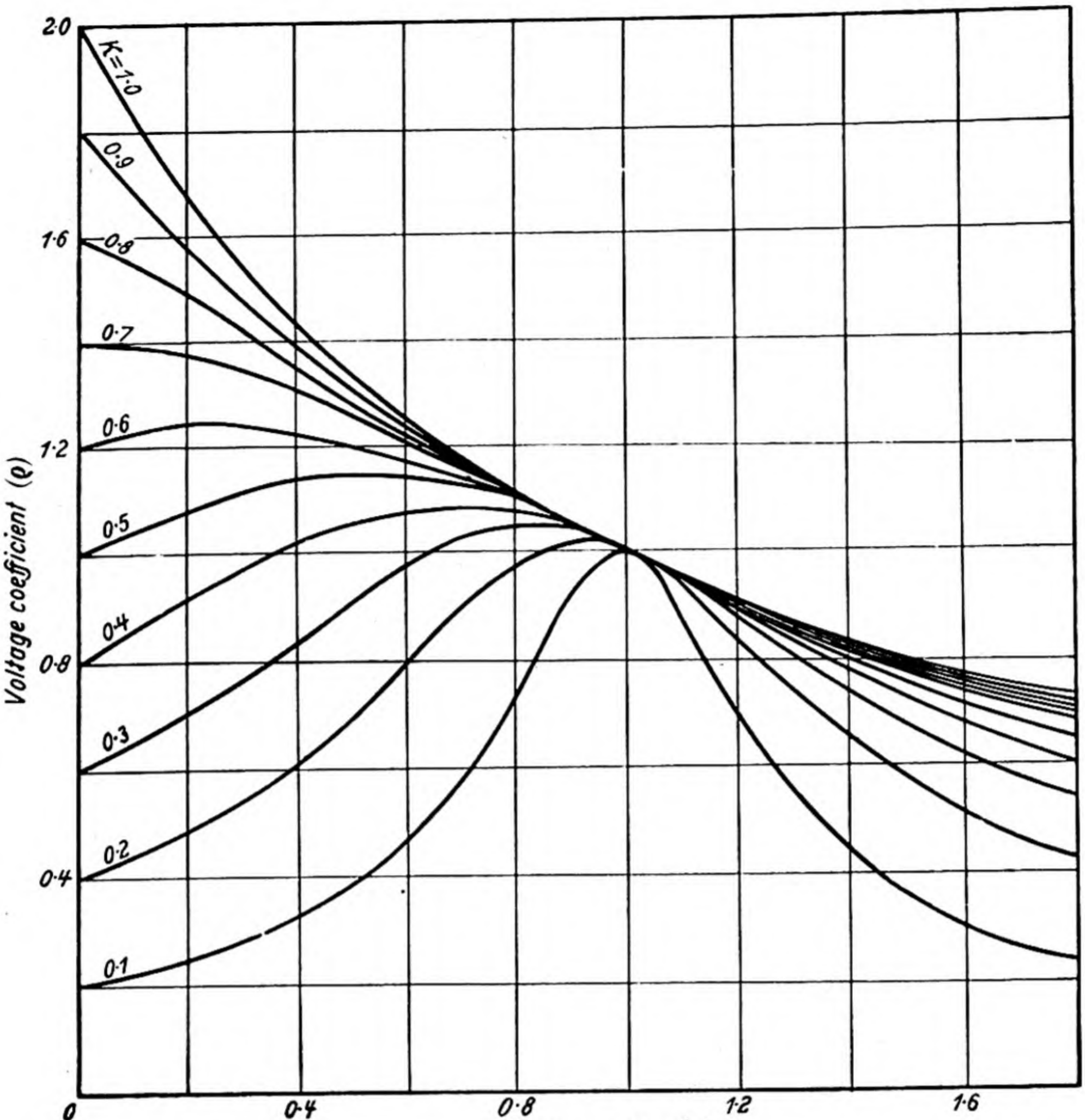

Figure 116. Parameters of a Tesla transformer (Goodlet[18], by courtesy, *J. Inst. elect. Engrs.*).

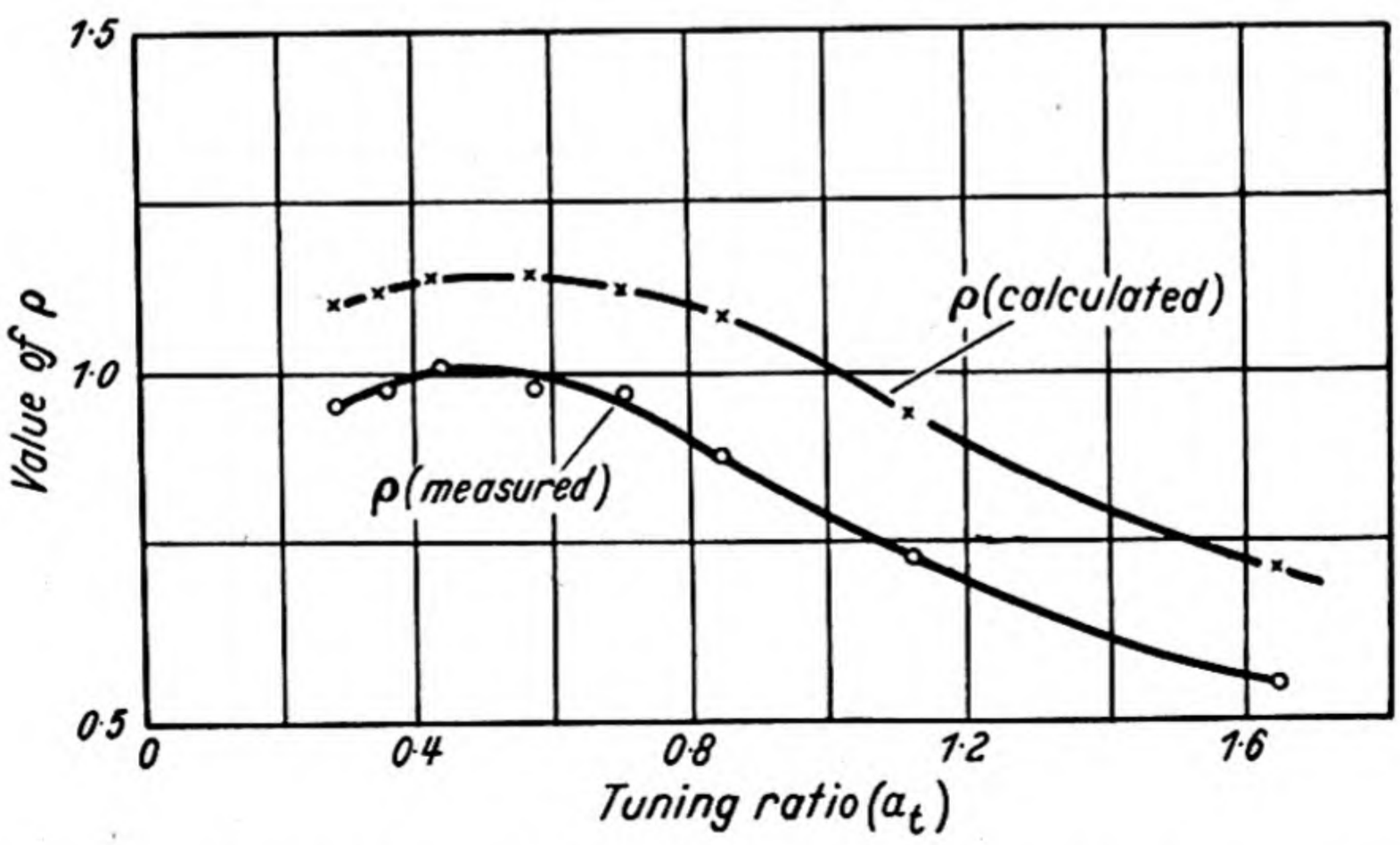

Figure 117. Data relating to Goodlet's[18] theoretical treatment of Tesla transformers (By courtesy, *J. Inst. elect. Engrs.*).

Then $$B_1 - B_2 = B_3 - B_4 = 0$$

and $$B_1 + B_2 = -(B_3 + B_4) = -\frac{ME}{\sigma L_1 L_2 C_2} \frac{1}{(\gamma^2{}_2 - \gamma^2{}_1)}$$

where $$\gamma^2{}_{1,2} = \frac{w^2{}_1 + w^2{}_2}{2} \mp \frac{\sqrt{[(w^2{}_1 + w^2{}_2)^2 - 4w^2{}_1 w^2{}_2 (1 - K^2)]}}{2}$$

so that $$V_2 = -\frac{ME}{\sigma L_1 L_2 C_2} \frac{1}{(\gamma^2{}_2 - \gamma^2{}_1)} (\cos \gamma_1 t - \cos \gamma_2 t)$$

If $$a_t = \frac{L_2 C_2}{L_1 C_1}$$ and $$\rho = \frac{2\sqrt{1-\sigma}}{\sqrt{[(1+at)^2 - 4\sigma at]}}$$

then $$V_2 = \rho \sqrt{\frac{L_2}{L_1}} \cdot E_{sin} \frac{(\gamma_2 - \gamma_1)}{2} t_{\ sin} \frac{(\gamma_2 + \gamma_1)}{2} t$$

which shows that the secondary voltage is oscillatory with a frequency $1/2\ (\gamma_2 + \gamma_1)$ and with an amplitude which is a sinusoidal time-function with frequency $1/2\ (\gamma_2 - \gamma_1)$. The voltage ratio is

$$\frac{V_{2\max}}{E} = \rho \sqrt{\frac{L_2}{L_1}}$$

Goodlet[18] has computed the data shown in *Figure 116* relating ρ to a for given values of K where

$$K = \sqrt{1-\sigma}$$

ρ is a maximum at $a_t = 1 - 2K^2$ and the no-load value of a_t should be below this. *Figure 117* shows the results of comparing calculated and measured values of ρ for different values of a_t; circuit losses which are not considered in the above treatment are considered to be responsible for the relatively trivial differences between ρ (calculated) and ρ (measured). Goodlet also shows an oscillogram (*Figure 118*) of the secondary voltage wave-form.

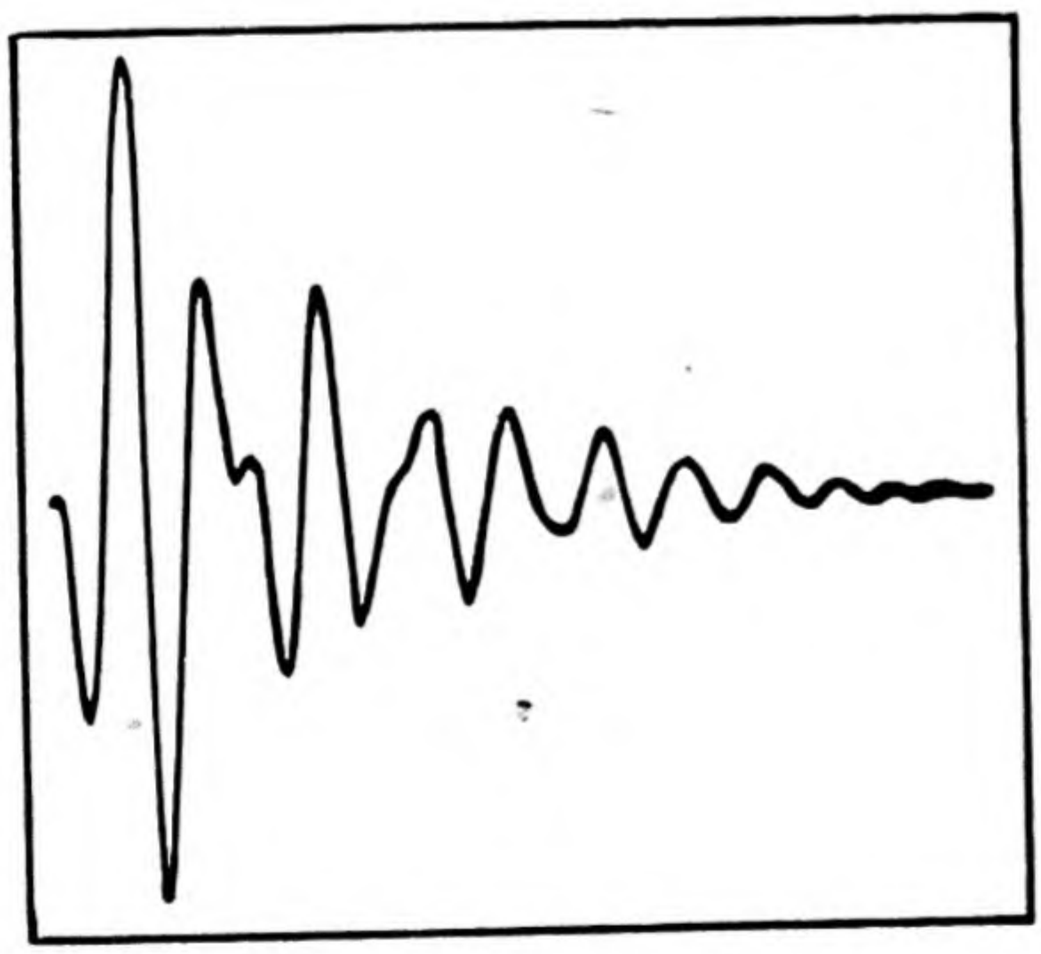

Figure 118. Tesla transformer wave-form (Goodlet[18], by courtesy, *J. Inst. elect. Engrs.*).

Goodlet[18] discusses the effect of variation in M (*see Figure 115*). The closer the coupling, the smaller is the oscillation frequency as compared with the beat frequency (*see Figure 114*) and for tight coupling the output voltage will tend to be impulsive. Similarly,

loose coupling, *i.e.* a low M, will tend to give an undamped secondary wave train so that careful control of the coupling will provide a variety of output voltage wave-forms; this possibility is now of less importance than it was in 1929 when Goodlet's work was published because the use of impulse generators (Chapter 4) has since become widely established, but HOCHHÄUSLER's study of Tesla coil wave-forms[19] is notable, and includes excellent voltage oscillograms.

One of the few detailed descriptions of high-voltage Tesla coils is due to BREIT, TUVE and DAHL[20]. At that time, 1930, the possibility of using Tesla coils for accelerating nuclear particles to high energies was being actively explored in several countries and the present work lead to the development of a Tesla transformer circuit shown schematically in *Figure 119*, resonating at about 100 kc/s., and developing about 5 MV across its secondary. The coil was oil-immersed, with a special bank of foil-coated condensers which are described in some detail by the above authors[20]. The primary of the coil consists of a few turns of copper tubing, well spaced from the secondary which has 5,000 or 7,000 turns on a Pyrex tube about 1 m. in length. Other details are given in the paper with a full account of the running-in technique and the technical difficulties encountered.

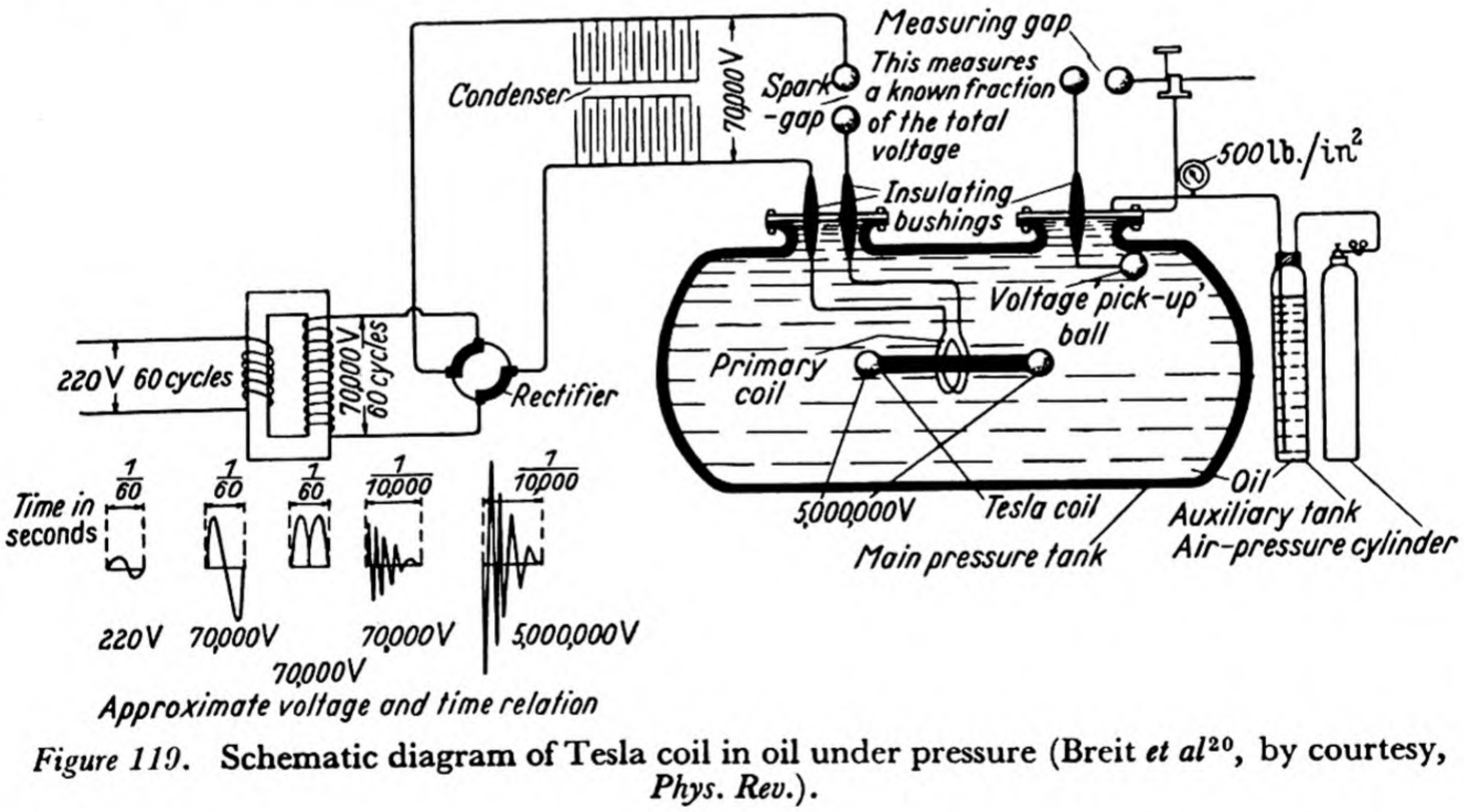

Figure 119. **Schematic diagram of Tesla coil in oil under pressure (Breit *et al*[20], by courtesy, *Phys. Rev.*).**

Tesla coils are now little used for quantitative high-voltage work since their complex wave-forms often introduce difficulties. The use of d.c., sine wave a.c. or of controlled simple pulses clearly has great advantages.

Induction coils have been the subject of a book by TAYLOR-JONES[21] and will not be described here. Recent papers are by FINCH and his collaborators[22] and GASTER[23].

REFERENCES

1 KEHSE, W. *Elektrotech. Z.*, **52** (1931) 1417.
2 CRAMER, R. *Elektrotech. Z.*, **59** (1938) 228.
3 BOUWERS, A. *Elektrische Höchstspannungen.* Berlin, 1939.
4 SORENSEN, R. W. *J. Amer. Inst. elect. Engrs.*, **44** (1925) 373.
5 NORRIS, E. T., and TAYLOR, F. W. *J. Inst. elect. Engrs.*, **69** (1931) 673.
6 EDWARDS, F. S., and SMEE, J. F. *J. Inst. elect. Engrs.*, **82** (1938) 665.
7 WINZ, E. *Arch. Elektrotech.*, **21** (1929) 563.
8 KÜCHLER, R. *Elektrotech. Z.*, 58 (1937) 203.
9 CAMILLI, G. *Gen. Elect. Rev.*, **39** (1936) 95.
10 CHARLTON, E. E., and WESTENDORP, W. F. *Gen. Elect. Rev.*, **44** (1941) 44.
11 CHARLTON, E. E., WESTENDORP, W. F., DEMPSTER, L. E., and HOTALING, G. *J. appl. Phys.*, **10** (1939) 374.
12 BRAILSFORD, F. *J. Inst. elect. Engrs.*, **73** (1933) 309.
13 KERST, D. W. *Rev. Sci. Instrum.*, **13**(1942) 387.
14 BOSLEY, W., CRAGGS, J. D., MCEWAN, D. H., and SMEE, J. F. *J. Inst. elect. Engrs.*, **95** (1948) 352.
15 SLOAN, D. H. *Phys. Rev.*, **47** (1935) 62.
16 ALLIBONE, T. E., BANCROFT, F. E., and INNES, G. S. *J. Inst. elect. Engrs.*, **85** (1939) 657.
17 PERRY, F. R. *Trans. S. African Inst. elect. Engrs.*, **27** (1936) 212.
18 GOODLET, B. L. *J. Inst. elect. Engrs.*, **74** (1934) 377.
19 HOCHHÄUSLER, P. *Arch. Elektrotech.*, **26** (1932) 518.
20 BREIT, G., TUVE, M. A., and DAHL, O. *Phys. Rev.* 35 (1930) 51.
21 TAYLOR-JONES, E. *Induction Coil. Theory and Applications.* London, 1932.
22 FINCH, G. I., and SUTTON, R. W. *Proc. Phys. Soc.*, **45** (1933) 288.
23 GASTER, W. *Elektrotech u. Maschinenb.*, **44** (1931) 809.

4

IMPULSE VOLTAGE GENERATION

IMPULSE VOLTAGE WAVE-SHAPES

The surges produced by lightning, by switching and by other such causes, can have a variety of wave-shapes. However, in most impulse testing laboratories it has become the practice to use for general purposes an impulse voltage wave which corresponds to the usual form of a travelling wave encountered on transmission lines. Occasionally other wave-shapes of more extreme characteristics are used.

The usual form of impulse voltage used in the laboratory is one having a rapid rise followed by a less rapid decay to zero. The voltage-time characteristic is defined closely by the equation

$$V = V_o(e^{-at} - e^{-bt})$$

Wave-shapes of this form can be readily produced and are described completely by defining the exponents a and b. The maximum value is called the peak value of the impulse and the impulse voltage is specified by this value.

In general it is sufficiently accurate for comparative purposes to define the wave-shape by quoting the times t_1 and t_2 in μsec, which give the wave-front and wave-tail respectively. The wave is then referred to as a t_1/t_2 wave. t_1 is the time occupied by the impulse voltage wave in rising from zero to its peak value. t_2 is the total time occupied by the impulse voltage in rising to its peak value and declining therefrom to one-half the peak value.

Exact methods of definition of the wave-front and wave-tail are specified in the British Standard Rules[1] and are such as to overcome the difficulties of determining the start of the wave and the point to be taken as the peak of the wave on the flat position of the crest. The full line *OAB* in *Figure 120* represents the impulse wave. The nominal wave-front duration t_1 is specified as $1{\cdot}25\ X_2X_3$ where OX_3 and OX_2 are the respective time intervals for the voltage wave to reach the points D and C corresponding to 10 per cent and 90 per cent of the peak voltage. The point O_1 where the line CD cuts the time axis is referred to as the nominal starting-point of the wave. The nominal wave-tail t_2 is measured between the nominal starting point O_1 and the point on the wave-tail where the voltage is one-half the peak value, *i.e.* $t_2 = O_1X_4$. The nominal steepness of the wave-front is the average rate of rise of voltage between the points on the wave-front where the voltage is 10 per cent and 90 per cent of the peak value.

The standard wave-shape specified in B.S. 923 is a 1/50 wave, *i.e.* a wave-front of 1 μsec and a wave-tail of 50 μsec. If a shorter wave is required, it is recommended that a 1/5 wave be used. A tolerance of not more than ± 50 per cent on the duration of the wave-front and ± 20 per cent on the time to half-value on the wave-tail is allowed. The 1/50 wave is also that specified by the International Electrotechnical Commission[2] and the Verband Deutscher Elektro-

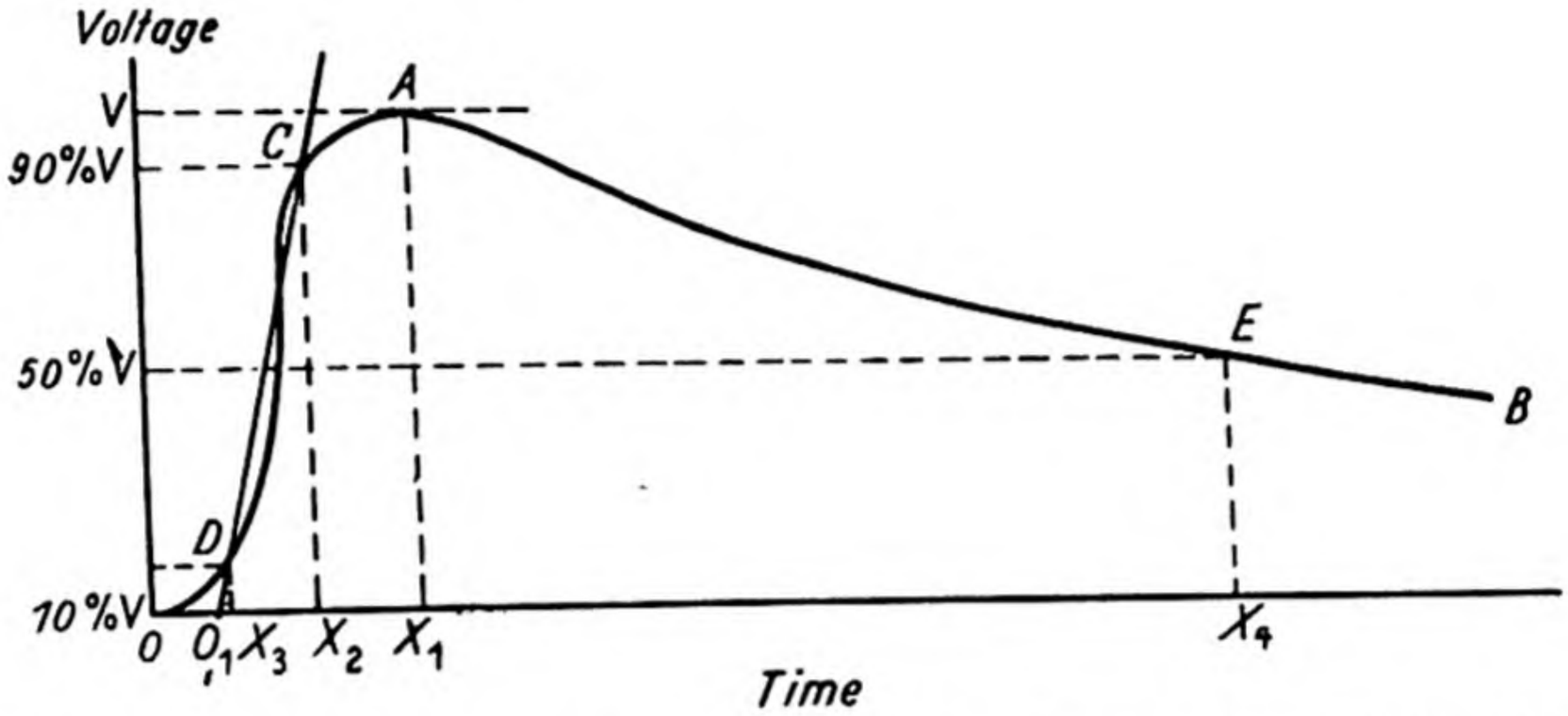

Figure 120. Impulse wave form. (The figure from B.S. 923 : 1940—Impulse voltage testing—is reproduced by permission of the British Standards Institution[1], 24–28 Victoria Street, London, S.W.1, from whom the official copies of the standard can be obtained.)

techniker[3]. The wave-shape recommended by the American Standards Association[4] is 1·5/40, with permissible variations of $\pm 0{\cdot}5$ μsec on the wave-front and ± 10 μsec on the wave-tail. Because of the given tolerances the American and British standard waves overlap. There is, however, a difference in the definition of wave-front in the American specification in that the wave-front duration t_1 is given by $1{\cdot}5\ X_2X_3$.

IMPULSE GENERATOR CIRCUITS

A diagram of the discharge circuit of an impulse generator is given in *Figure 121*[4]. In many of the practical circuits used some of the elements shown are omitted or are negligible.

A capacitance C_1 is charged from a d.c. set to a voltage which causes a discharge through a spark gap into the associated circuit. An impulse voltage then appears across the resistance R_4 to which the test object is connected.

The capacitance C_1 may consist of a single capacitance, in which case the generator is known as a single-stage generator. Alternatively, C_1 may consist of groups of capacitances which are charged in parallel and are discharged in series by means of the Marx circuit or one of its variations (page 115). The generator is then known as a multi-stage generator.

The inductance L_1 depends on the physical design of the generator and on the length of the discharge circuit, and is generally kept as small as possible. The resistance R_1 consists of the inherent series resistance of the capacitances and connections, and often includes additional lumped resistances inserted within the generator for damping purposes and for output wave-form control. Additional inductance L_2 and resistance R_2 may be connected at the generator terminal, again

R_2, R_3, L_2, C_4 and L_4 may be omitted or may be negligible compared to other constants.

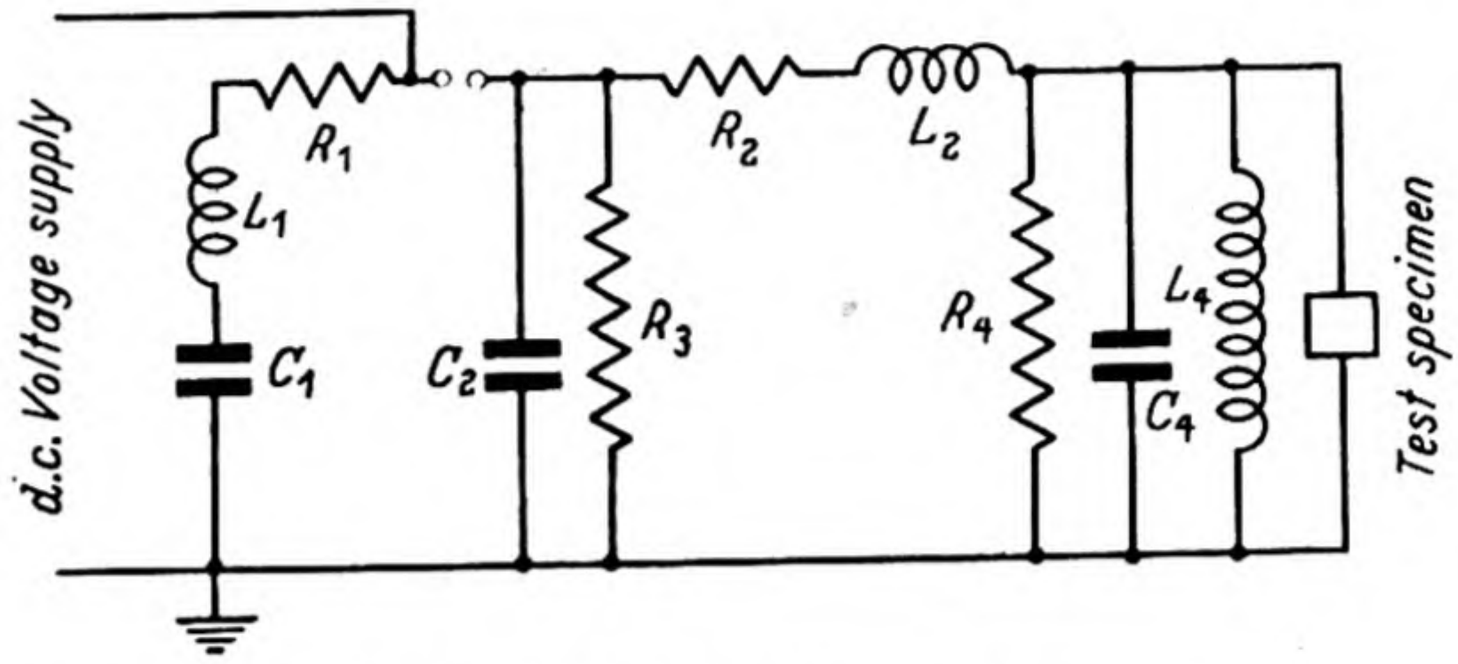

Figure 121. Surge generator discharge circuit (by courtesy, American Standards Association.[4])

for wave-form control. The function of the resistances R_3 and R_4 is mainly to control the duration of the wave. R_4 can also serve as a potential divider when a cathode-ray oscillograph is used to record the wave-shape. The capacitances C_2 and C_4 represent the capacitances to earth of the high-voltage components and leads. C_4 also includes the capacitance of the test object and of any other load capacitance which may be required for producing the required wave-shape. L_4 represents the inductance of the test object and may also affect the wave-shape appreciably.

The impulse characteristics of the test objects may vary widely, and the circuit constants may have to be altered to maintain a specified wave-shape for the impulse voltage developed across the test object. The resistances R_2, R_3 and R_4, the capacitance C_4 and, in some cases, the inductance L_2 should be capable of adjustment.

For practical reasons it is usual for one terminal of the impulse generator to be solidly earthed. The polarity of the impulse voltage is altered by changing the polarity of the output from the d.c. charging set.

Two simplified forms of impulse generator circuits are shown in *Figure 122* (*a*) and (*b*). These two circuits are widely used and differ only in the position of the wave-tail control resistance R_2. When R_2 is on the load side of R_1 the two resistances form a potential divider which reduces the output voltage, but when R_2 is on the generator side of R_1 this particular loss of output voltage is absent. *Figure 123* shows how the voltage efficiencies of the two circuits vary with the ratio of C_2/C_1 for a 0·6/5 wave, the voltage efficiency being defined

as the ratio of the peak output voltage to the initial voltage on C_1[5]. When R_2 is on the load side of R_1 the efficiency is low for small values of C_2/C_1 but when R_2 is on the generator side of R_1 the efficiency is highest when the load is zero. The circuit of *Figure 122b* should

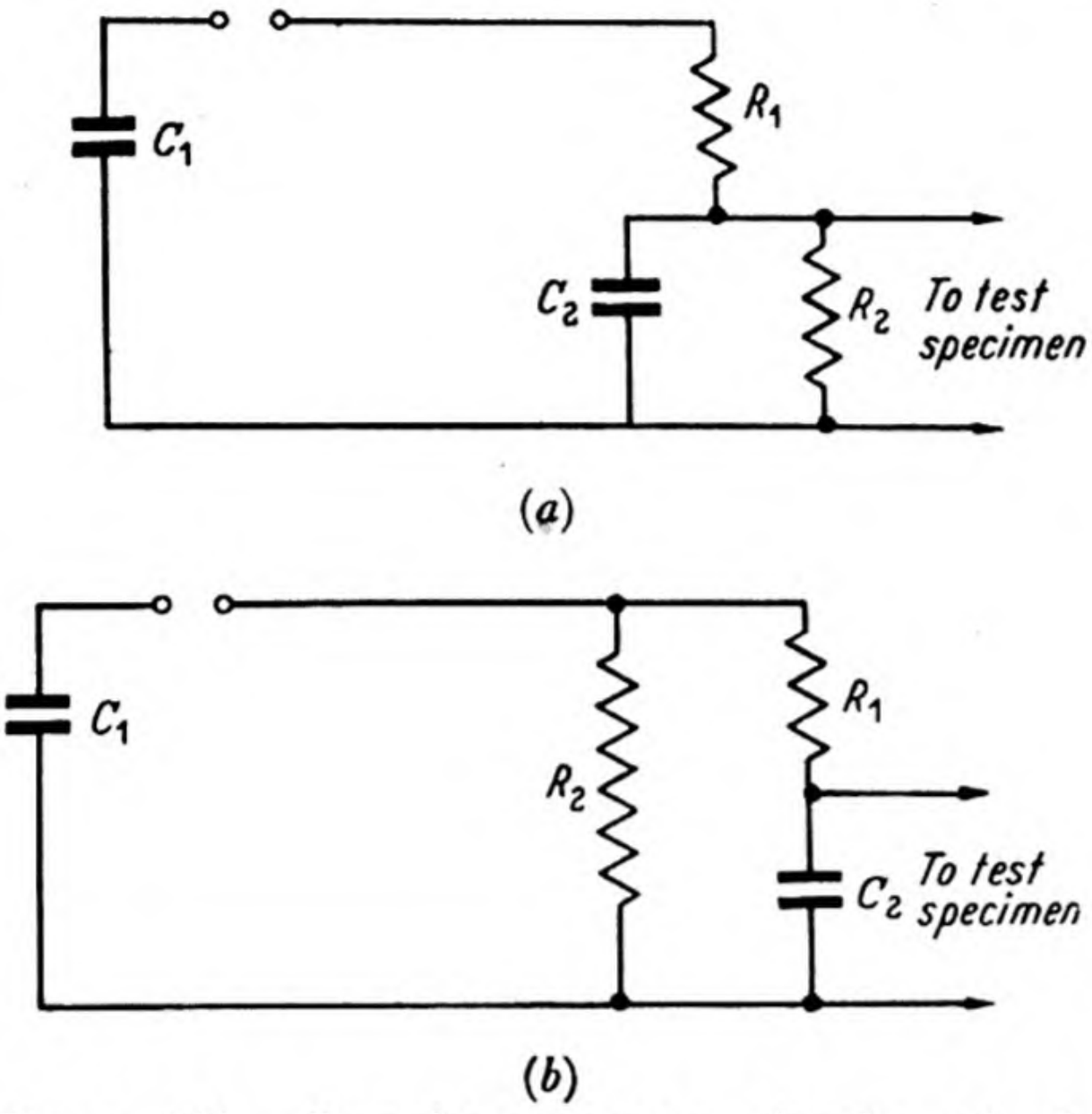

Figure 122. Impulse-generator circuits of the capacitance-resistance type (Eaton and Gebelein[23], by courtesy, *Gen. Elect. Rev.*).

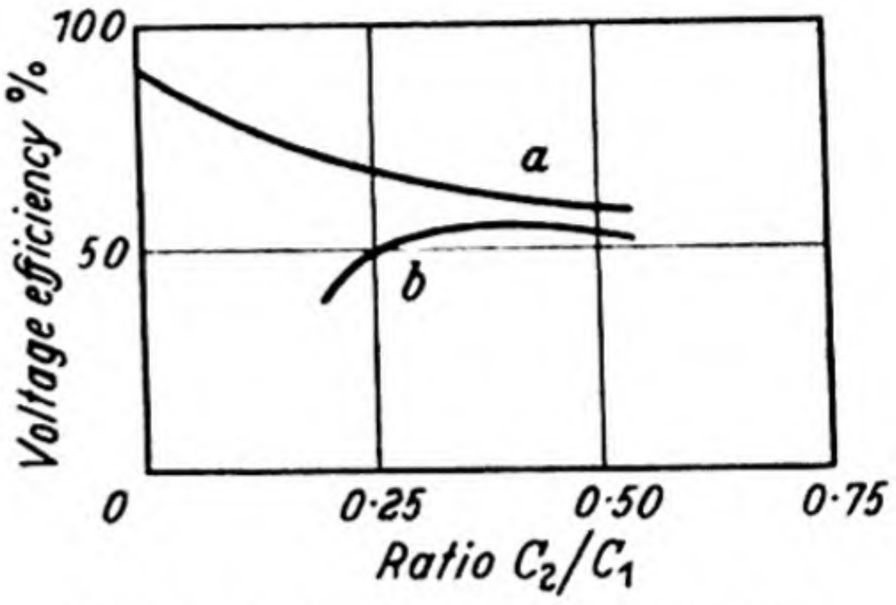

(*a*) Resistor R_2 on generator side of R_1.
(*b*) Resistor R_2 on load side of R_1

Figure 123. Effect of position of wavetail-control resistor on voltage efficiency of generator (Edwards, Husbands and Perry[5], by courtesy, *Proc. Inst. elect. Engrs.*).

therefore be used whenever possible and especially when the resistance of R_1 is not very small compared with that of R_2. The circuits of *Figure 122* are further analysed on page 121 *et seq.*

Following earlier experiments by GRÜNEWALD[6] in 1923 Marx patented a method for charging capacitances in parallel and discharging them in series for the purpose of producing high-voltage impulse waves[7, 8, 9]. This method, with modifications, forms the basis of all present multi-stage impulse generator circuits. A review of the development of such circuits is given in a paper by EDWARDS, HUSBANDS and PERRY[5].

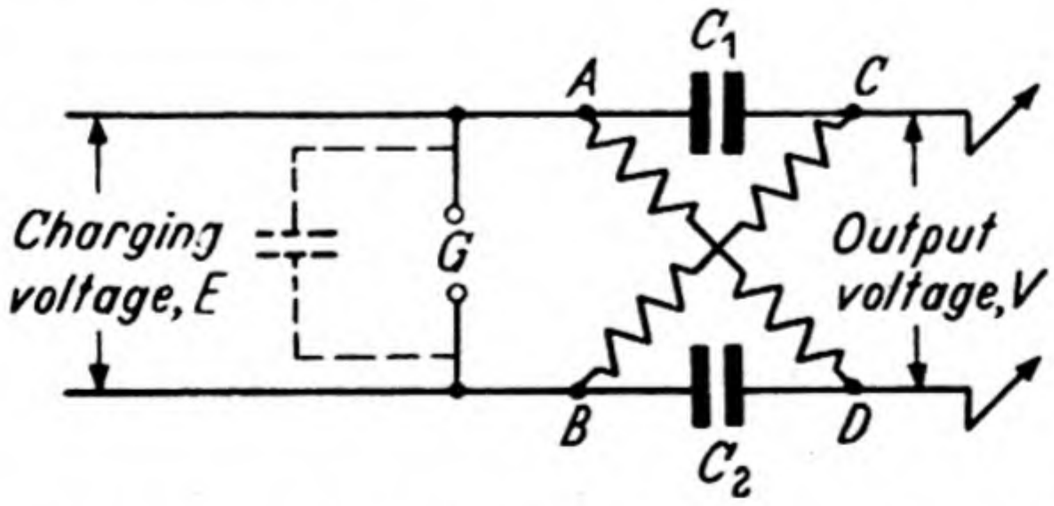

Figure 124. Marx's original voltage-doubling circuit (Edwards, Husbands and Perry[5], by courtesy, *Proc. Inst. elect. Engrs.*).

Figure 124 shows a two-stage Marx circuit. On the spark breakdown of the gap G the voltage between C and D suddenly rises from its initial value V to a value approaching $2V$ and then decays to V. The circuit has the defect that the charging voltage V is applied continuously to the load across the points C and D both before and after the appearance of the impulse wave. The purpose of the

'spark-heating' condenser, shown dotted, is to facilitate the breakdown of the gap, *G*.

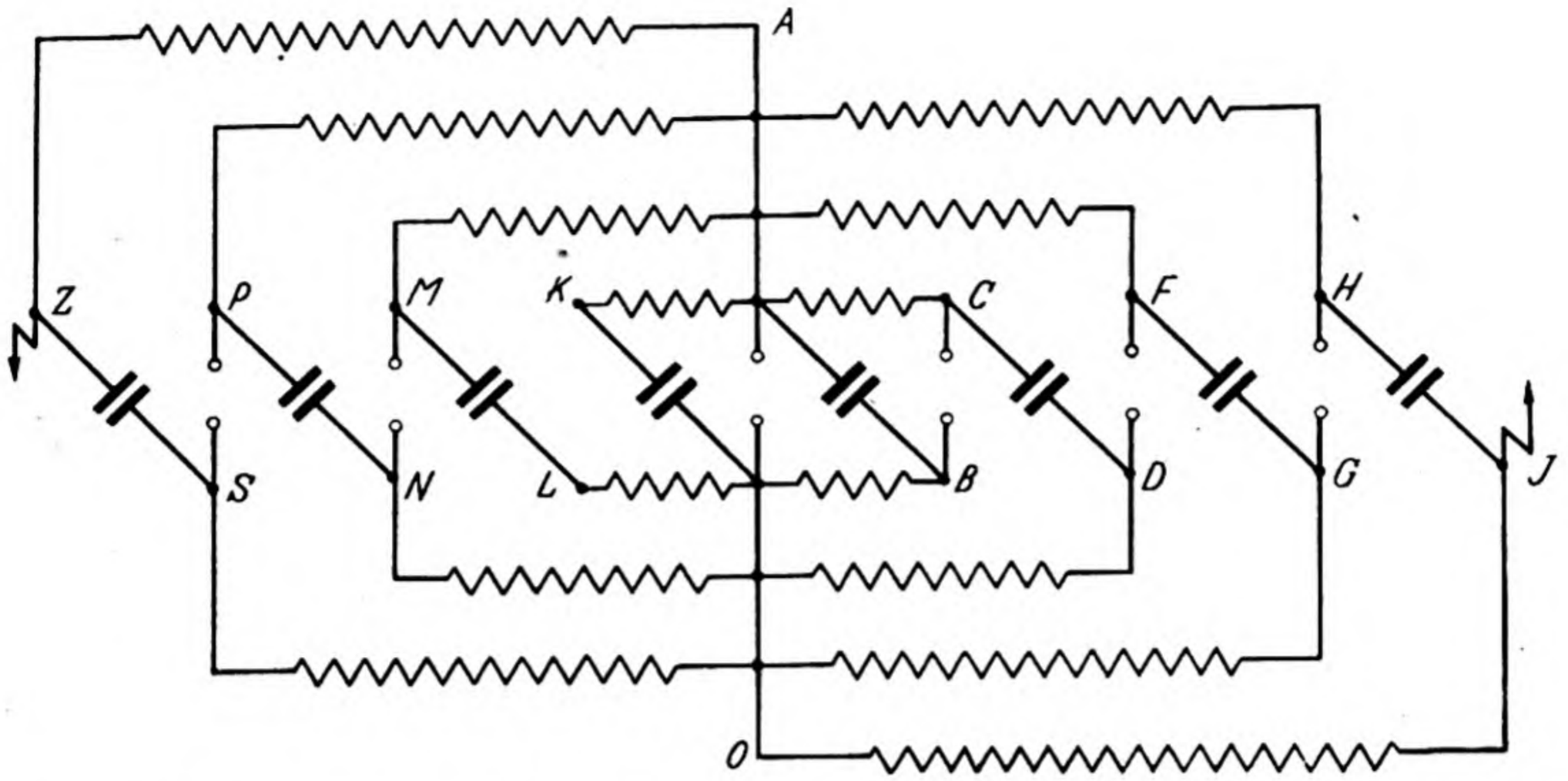

Figure 125. Marx's original multi-stage generator for eight stages (Edwards, Husbands and Perry[5], by courtesy, *Proc. Inst. elect. Engrs.*).

An eight-stage Marx circuit is drawn in *Figure 125*[5]. The charging voltage, V, is connected between A and O, the test object being between Z and J. If the point O is earthed the left-hand side of the diagram corresponds to a four-stage circuit with a steady voltage V at Z on which an impulse of $3V$ is superimposed when the spark gaps break down. The right-hand side is also a four-stage circuit, the point J being initially earthed and then suddenly subjected to an impulse of $4\ V$ when the spark gaps break down. On the simultaneous breakdown of all the spark gaps the voltage between Z and J suddenly rises from its initial steady value V to a peak value of $8V$ and then falls to V.

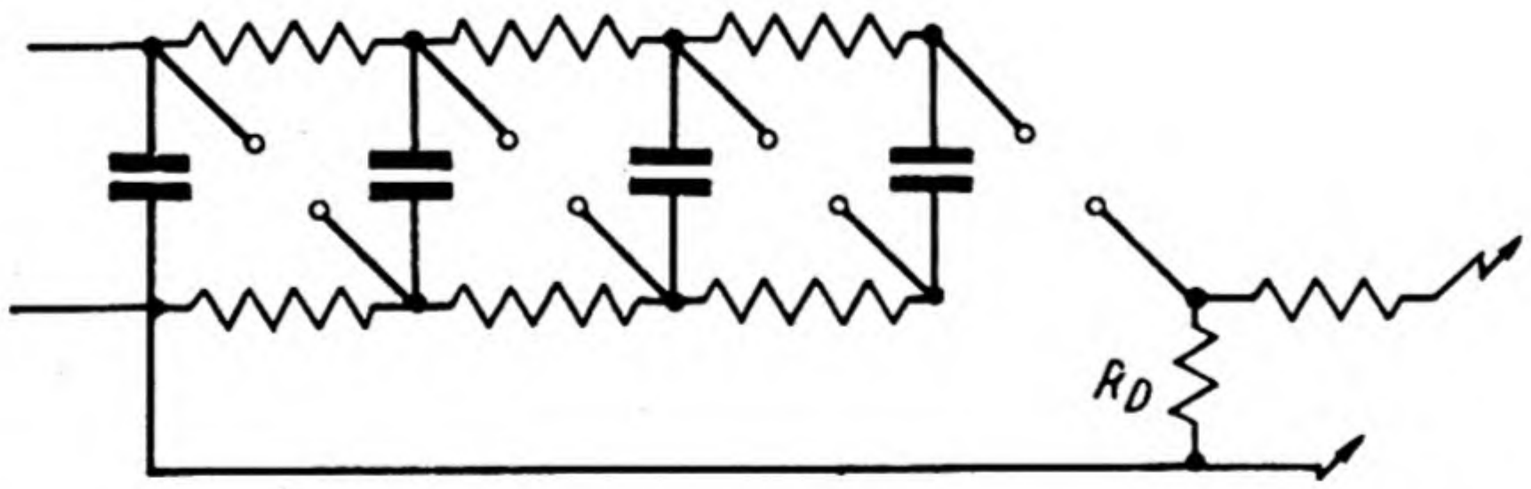

Figure 126. Marx's later multi-stage generator, with isolating gap (Edwards, Husbands and Perry[5], by courtesy, *Proc. Inst. elect. Engrs.*).

Marx's original circuit has been extended by Marx[8, 9, 10] and by other investigators[11–21]. *Figure 126* shows a circuit, given by Marx, in which the load is isolated from the generator by a sphere gap. The

load is earthed by the resistance R_D during the charging period. The occurrence of the impulse voltage at the generator terminals causes

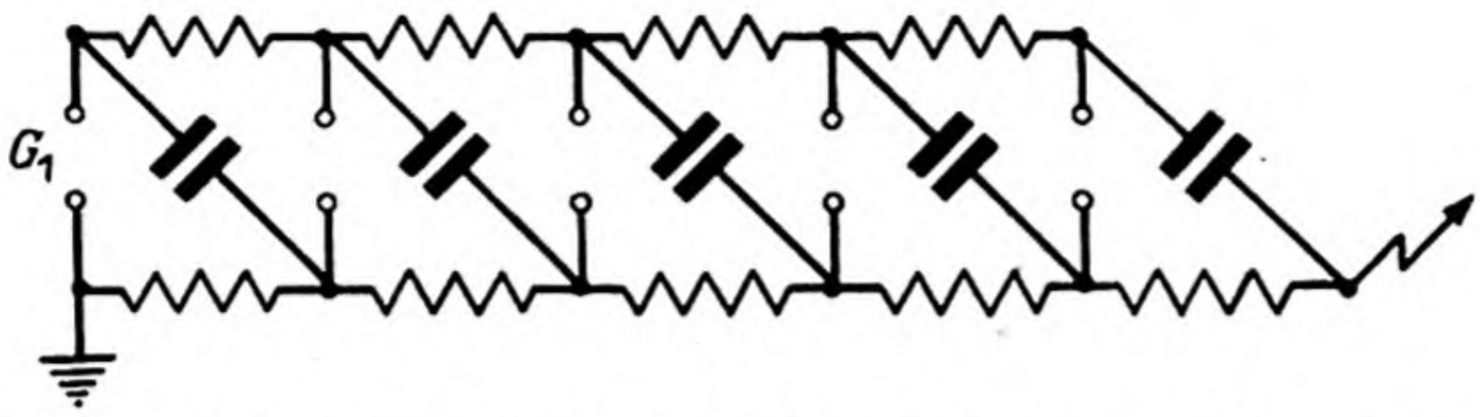

Figure 127. Goodlet's modification of Marx circuit (Edwards, Husbands and Perry[5], by courtesy, *Proc. Inst. elect. Engrs.*).

the sphere gap to break down and the impulse voltage then appears across the resistance R_D and hence across the load.

An important modification to the Marx circuit has been made by GOODLET[12] and is shown in *Figure 127*. With this circuit the load is earthed during the charging period without the necessity for an isolating gap. This circuit is now widely used. Whereas in the Marx circuit the impulse voltage is of the same sign as the charging

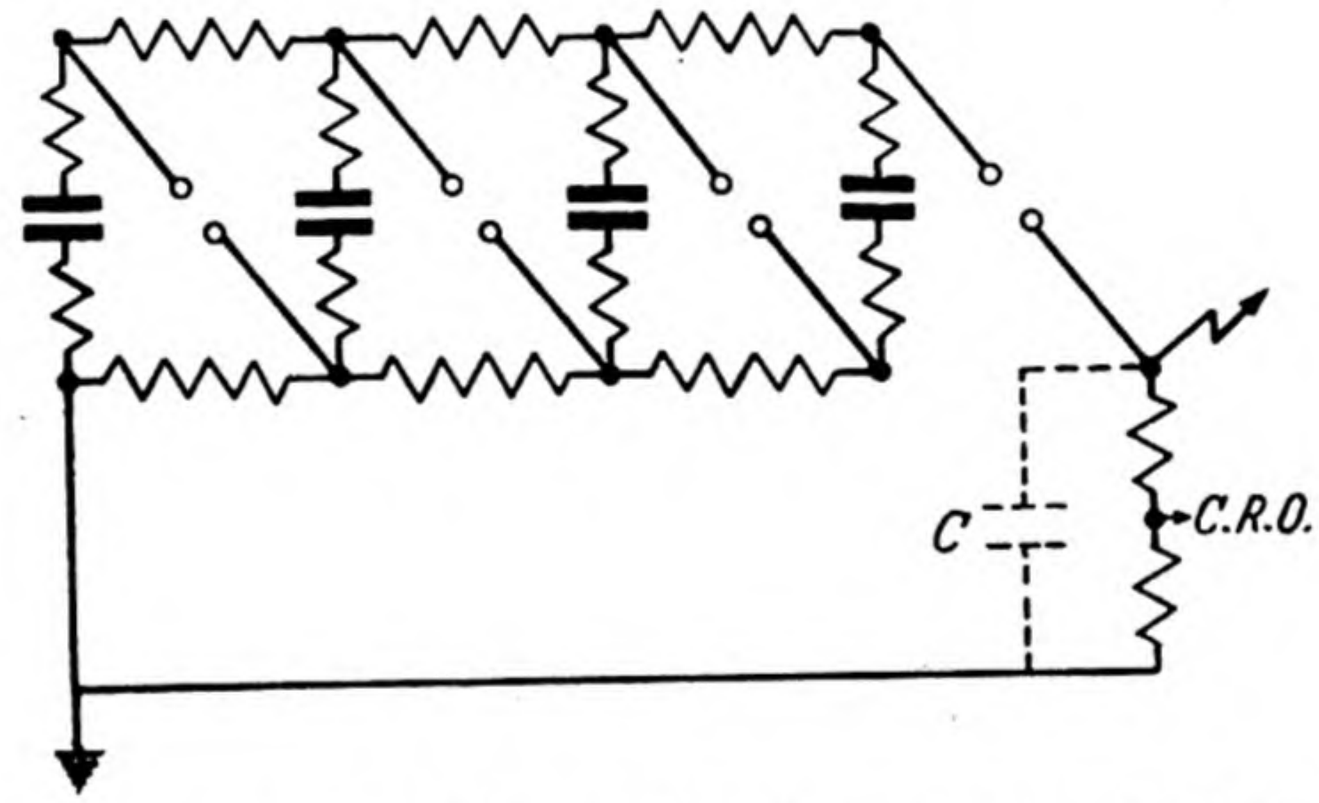

Figure 128. Multi-stage circuit, showing distributed series resistors (Edwards, Husbands and Perry[5], by courtesy, *Proc. Inst. elect. Engrs.*).

voltage, the sign is reversed in the Goodlet circuit. Another difference is that on discharge both sides of the first spark gap are raised to the charging voltage in the Marx circuit but both fall to earth voltage in the Goodlet circuit.

In many impulse generator circuits the wave-front control resistance is placed between the generator and the load. In other generators a portion of this resistance is distributed through the generator[5, 17–22]. Such an arrangement is shown in *Figure 128*. An advantage of this arrangement is that it reduces the need for an external resistor capable of withstanding the full voltage. A resistance for say 2,000 kV is

inconveniently long and may occupy useful space, so that even a small amount of internal resistance is helpful. Edwards, Husbands and Perry[5] suggest that a useful compromise is to arrange for about one-half of the total resistance to be outside the generator. It is unsatisfactory for all the series resistance to be within the generator as the inductance and capacitance of the external leads and the load form an oscillatory circuit which requires to be damped by an external resistance.

As the wave-tail current flows through the distributed resistances, if they are inserted as in *Figure 128*, it follows that the larger the discharge capacitance above a certain optimal value the lower will be the output voltage. The effect produced is essentially the same as that which results from placing the resistance R_2 of *Figure 122*, on the load side of the series resistance, the results of which are illustrated in *Figure 123*.

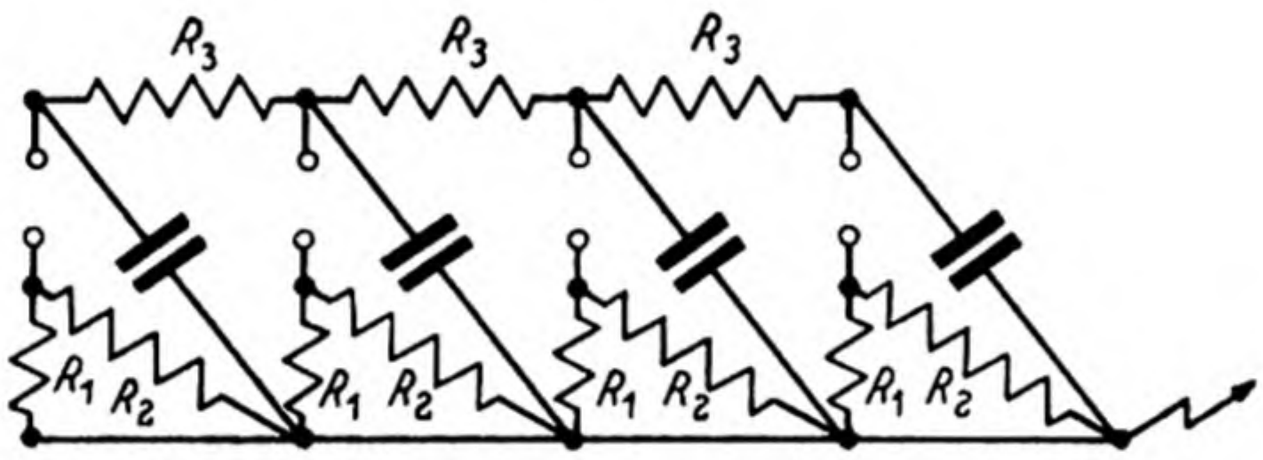

Figure 129. Modern multi-stage circuit showing distributed series resistors connected to give maximum efficiency (Edwards, Husbands and Perry[5], by courtesy, *Proc. Inst. elect. Engrs.*).

A method of using distributed wave-front resistances and also obtaining high efficiency has been developed by EDWARDS and SCOLES[20]. The circuit is given in *Figure 129*. An essential feature is that R_3 is large compared with R_1, and R_2 is made as small as is necessary to give the required wave-tail. Under these conditions the current through R_2 does not flow through R_1, and so has no effect in reducing the initial generator output voltage, no matter how small R_2 or how large R_1 may be. Edwards, Husbands and Perry[5] refer to a particular generator using this circuit in which the stage capacitance was about $0{\cdot}20\,\mu$F, R_1 was about $40\,\Omega$, and the wave-tail resistance R_2 was about $25\,\Omega$ to give a $5\,\mu$sec wave-tail. R_3 was made about $10\,\text{k}\Omega$. With this circuit less than 1 per cent. of the output voltage was lost in R_1, whereas with the normal connections about two-thirds of the voltage would have been lost in R_1. This circuit of *Figure 129* is now widely used.

MATHEMATICAL ANALYSIS OF BASIC IMPULSE GENERATOR CIRCUITS

Many theoretical analyses have been published of the various forms of impulse generator circuits[23–34, 71–73]. In this Section the most

common basic circuits are discussed. The treatment is essentially that given by EATON and GEBELEIN[23].

In the usual impulse voltage circuits the wave-form of the voltage developed across the output resistance is of the form

$$v = A\left[e^{-(\alpha-\beta)t} - e^{-(\alpha+\beta)t}\right] \quad \ldots.(4.1)$$

If the wave-form is specified in the usual manner, by the time t_1 to peak value and the time t_2 to one-half the peak value, then both α and β must have unique values irrespective of the particular circuit used.

The time-to-peak value is determined from the solution of $\frac{dv}{dt} = 0$ and is given by

$$t_1 = \frac{1}{2\beta}\log_e\left(\frac{\alpha+\beta}{\alpha-\beta}\right) \quad \ldots.(4.2)$$

The peak value of the voltage is then

$$v_1 = A\left[e^{-(\alpha-\beta)t_1} - e^{-(\alpha+\beta)t_1}\right] \quad \ldots.(4.3)$$

The voltage then decreases to half the peak value in a time t_2, so that

$$A\left[e^{-(\alpha-\beta)t_2} - e^{-(\alpha+\beta)t_2}\right] = \tfrac{1}{2}A\left[e^{-(\alpha-\beta)t_1} - e^{-(\alpha+\beta)t_1}\right] \quad \ldots.(4.4)$$

If the time t_2 is expressed in terms of t_1,

$$t_2 = kt_1 \quad \ldots.(4.5)$$

where k is a constant, then

$$A\left[e^{-(\alpha-\beta)kt_1} - e^{-(\alpha+\beta)kt_1}\right] = \tfrac{1}{2}A\left[e^{-(\alpha-\beta)t_1} - e^{-(\alpha+\beta)t_1}\right] \quad \ldots.(4.6)$$

For defined values of t_1 and k it is clear that Equation 4.2 and Equation 4.6 enable unique values of α and β to be determined. It follows therefore that if a voltage surge is of the form given by Equation 4.1, the specification of the time-to-peak value and the time to one-half peak value determine the quantities α and β. Some simplification of the calculations is enabled by the fact that in practice the second term on the left-hand side of Equation 4.6 is usually much smaller than the first term and can therefore be neglected. If this second term is omitted, and the value of t_1 from Equation 4.2 is inserted in Equation 4.6, it follows that

$$\exp\left[-\frac{\alpha-\beta}{2\beta}k\log_e\left(\frac{\alpha+\beta}{\alpha-\beta}\right)\right] = \tfrac{1}{2}\exp\left[-\frac{\alpha-\beta}{2\beta}\log_e\left(\frac{\alpha+\beta}{\alpha-\beta}\right)\right] - \tfrac{1}{2}\exp\left[-\frac{\alpha+\beta}{2\beta}\log_e\left(\frac{\alpha+\beta}{\alpha-\beta}\right)\right] \quad \ldots.(4.7)$$

We may write

$$b = \frac{\alpha+\beta}{\alpha-\beta} \quad \ldots.(4.8)$$

Then $\frac{\alpha-\beta}{2\beta} = \frac{1}{b-1}$ and $\frac{\alpha+\beta}{2\beta} = \frac{b}{b-1}$

Consequently Equation 4.7 may be written as

$$\exp\left[-\frac{k}{b-1}\log_e b\right] = \tfrac{1}{2}\exp\left[-\frac{1}{b-1}\log_e b\right] - \tfrac{1}{2}\exp\left[-\frac{b}{b-1}\log_e b\right] \quad \ldots.(4.9)$$

Equation 4.9 enables a curve to be plotted relating k with $\log_e b$, as shown in *Figure 130*. Then for any given wave-form, in which

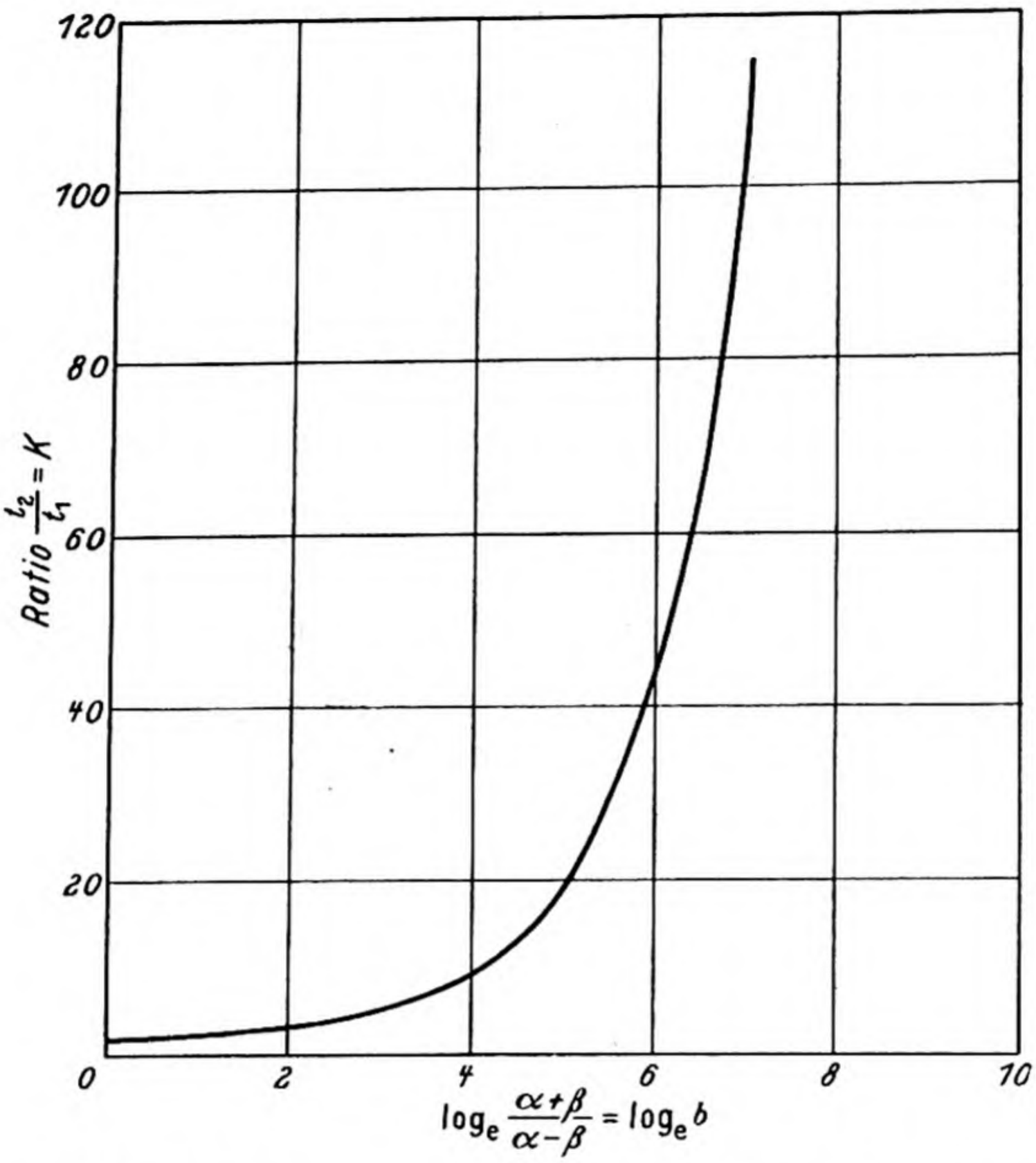

Figure 130. Reference curve for the evaluation of circuit constants (Eaton and Gebelein[23], by courtesy, *Gen. Elect. Rev.*).

t_1 and t_2 and therefore $k = \frac{t_2}{t_1}$ are specified, the value of β can be evaluated, as, from Equation 4.2,

$$\beta = \frac{1}{2t_1}\log_e b \qquad \ldots\ldots(4.10)$$

α can now be evaluated from the relation

$$\log_e b = \log_e\left(\frac{\alpha+\beta}{\alpha-\beta}\right) \qquad \ldots\ldots(4.11)$$

However, the accuracy of computation is not always satisfactory particularly as the quantities $(\alpha-\beta)$ and $(\alpha^2-\beta^2)$ enter into the circuit calculations, and slight errors in either α or β may result in large errors in these differences. In such a case a higher degree of precision is obtained by a further development of Equation 4.6. If the second term on the left-hand side is again omitted we obtain

$$e^{-(\alpha-\beta)kt_1} = \tfrac{1}{2}\left[e^{-(\alpha-\beta)t_1} - e^{-(\alpha+\beta)t_1}\right]$$

which may be rewritten as

$$2\,e^{-(\alpha-\beta)(k-1)t_1} = 1 - e^{-2\beta t_1}$$

Then

$$\alpha - \beta = \frac{1}{t_1(k-1)} \log \left[\frac{2}{1 - e^{-2\beta t_1}} \right] \quad \ldots\ldots(4.12)$$

If $2\beta t_1 > 4$, it follows that, within 2 per cent error

$$\alpha - \beta = \frac{0{\cdot}70}{t_1(k-1)} \quad \ldots\ldots(4.13)$$

The values of α and β corresponding to the most generally used wave-forms are given in *Table VIII*[23]

TABLE VIII[23]

Wave	α	β	$\alpha^2 - \beta^2$
0·5/5	4·080	3·922	1·2682
1/5	1·557	1·366	0·556
1/10	2·040	1·961	0·317
1·5/40	1·776	1·757	0·0641
1/50	3·044	3·029	0·0862

Capacitance-inductance-resistance circuit

The performance of this circuit, as shown in *Figure 131*, is described mathematically by the equation

$$\frac{1}{C}\int I dt + L\frac{di}{dt} + RI = O$$

It follows from the solution of this equation that the voltage v_R across the resistance R is

$$v_R = V\frac{\alpha}{\beta}\left[e^{-(\alpha-\beta)t} - e^{-(\alpha+\beta)t}\right] \quad \ldots\ldots(4.14)$$

where V is the initial voltage to which the capacitance C is charged.

$$\alpha = \frac{R}{2L} \quad \ldots\ldots(4.15)$$

$$\beta = \sqrt{\frac{R^2}{4L^2} - \frac{1}{LC}} \quad \ldots\ldots(4.16)$$

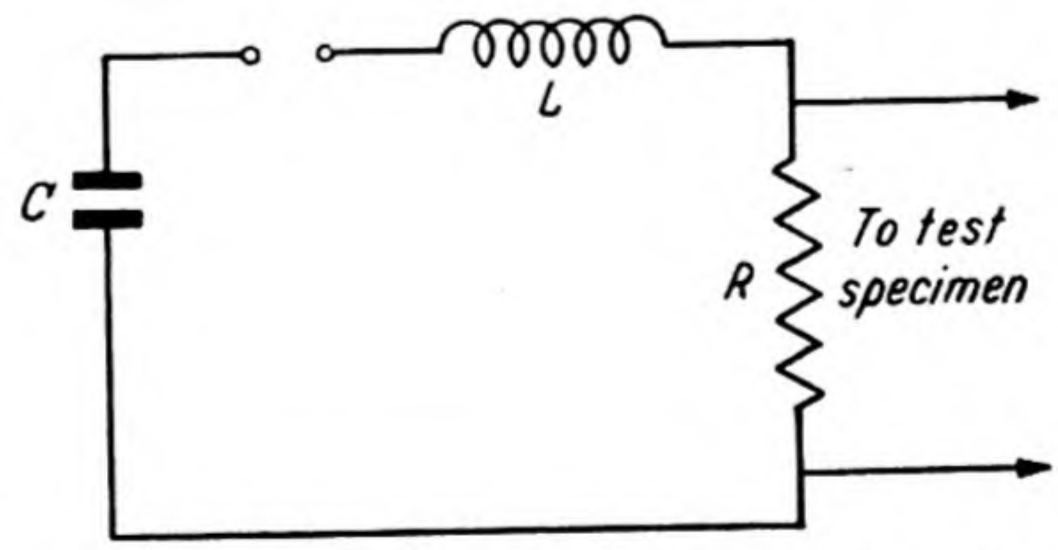

Figure 131. Impulse-generator circuit of the capacitance-inductance-resistance type (Eaton and Gebelein[23], by courtesy, *Gen. Elect. Rev.*).

For a defined wave-form α and β are fixed. Therefore, with an impulse generator having a given output capacitance C, the values

required for R and L can be calculated from Equation 4.15 and Equation 4.16. The relations between R, L and C for certain wave-forms are given in *Table IX*[23], which includes also the voltage efficiency of the circuit, *i.e.* the ratio of the peak value of the surge voltage to the initial voltage on C.

TABLE IX[23]

Wave	$M=RC$	$N=LC$	*Voltage efficiency*
1·5/5	6·43	0·788	0·954
1/5	5·60	1·80	0·881
1/10	12·9	3·16	0·954
1·5/40	55·4	15·6	0·978
1/50	70·6	11·6	0·988

(The above values apply where time is expressed in μsec. capacitance in μF, and inductance in μH)

Capacitance-resistance circuit (*Figure 122a*)

The performance of this circuit is described mathematically, in operational form, by the equations

$$\left(\frac{1}{pC_1}+R_1+R_2\right)I_1+R_2I_2 = 0$$

$$R_2I_1+\left(\frac{1}{pC_2}+R_2\right)I_2 = 0$$

The solution of these equations gives, for the voltage across C_2,

$$v = V_oC_1R_2\,\frac{\alpha^2-\beta^2}{2\beta}\left[e^{-(\alpha-\beta)t}-e^{-(\alpha+\beta)t}\right] \qquad \ldots\ldots(4.17)$$

where V_o is the voltage to which C_1 is initially charged, and

$$\alpha = \frac{R_2C_2+R_1C_1+R_2C_1}{2\,C_1C_2R_1R_2} \qquad \ldots\ldots(4.18)$$

$$\beta = \tfrac{1}{2}\left\{\left(\frac{R_2C_2+R_1C_1+R_2C_1}{C_1C_2R_1R_2}\right)^2-\frac{4}{C_1C_2R_1R_2}\right\}^{\frac{1}{2}} \qquad \ldots\ldots(4.19)$$

If we write $Y = C_1/C_2$, we can obtain from Equations 4.18 and 4.19

$$R_2 = \frac{1}{C_1}\left[\frac{\alpha\pm\sqrt{\alpha^2-(Y+1)(\alpha^2-\beta^2)}}{\frac{Y+1}{Y}(\alpha^2-\beta^2)}\right] = \frac{P}{C_1} \qquad \ldots\ldots(4.20)$$

where, for a given wave-shape P is a function of Y only. Also we have, from Equations 4.18 and 4.19

$$R_1 = \frac{1}{C_1}\left[\frac{Y+1}{\alpha\pm\sqrt{\alpha^2-(Y+1)(\alpha^2-\beta^2)}}\right] = \frac{Q}{C_1} \qquad \ldots\ldots(4.21)$$

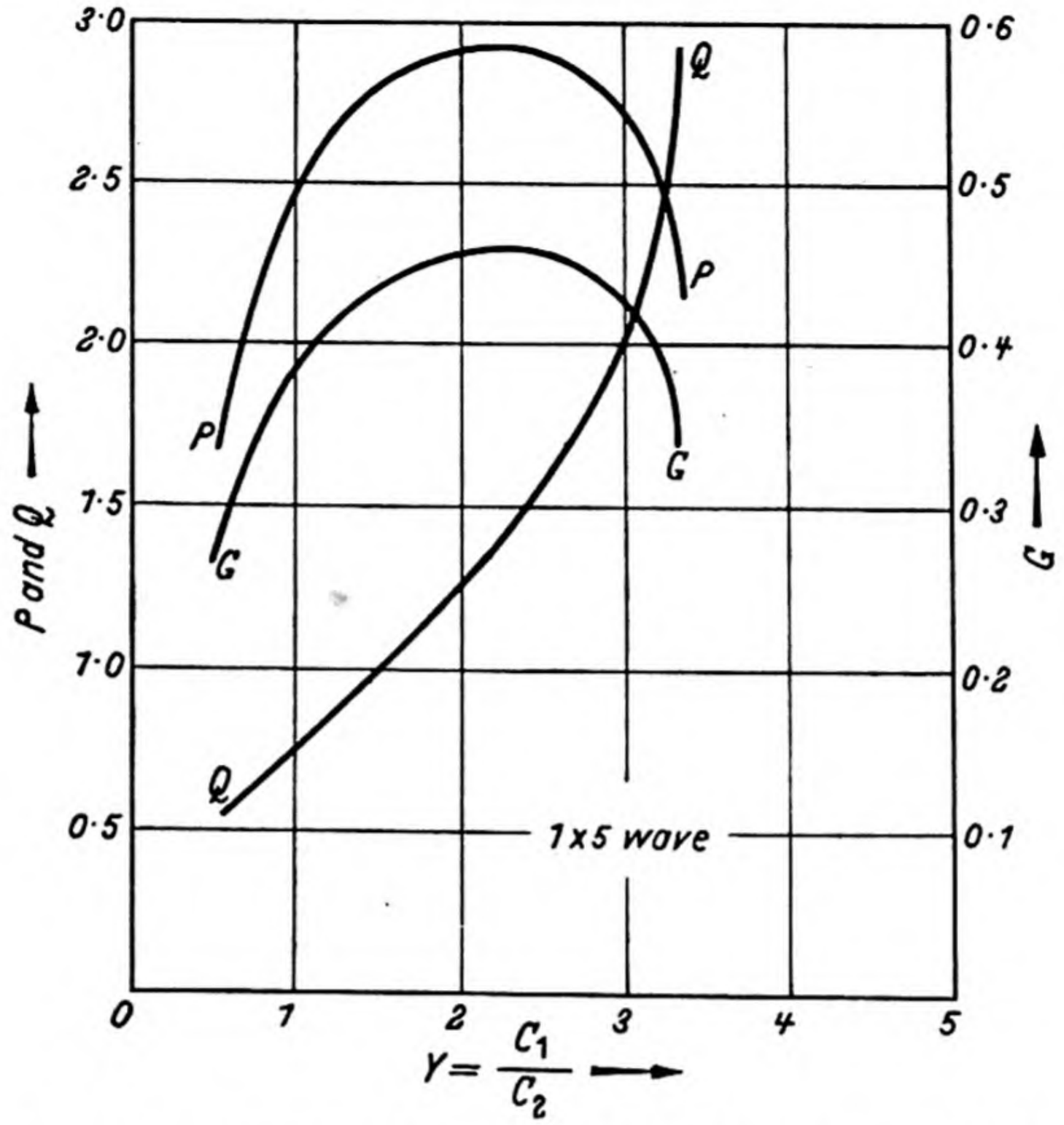

Figure 132. Circuit constants for the capacitance-resistance circuit shown in *Figure 122* (*a*). 1/5 wave (Eaton and Gebelein[23], by courtesy, *Gen. Elect. Rev.*).

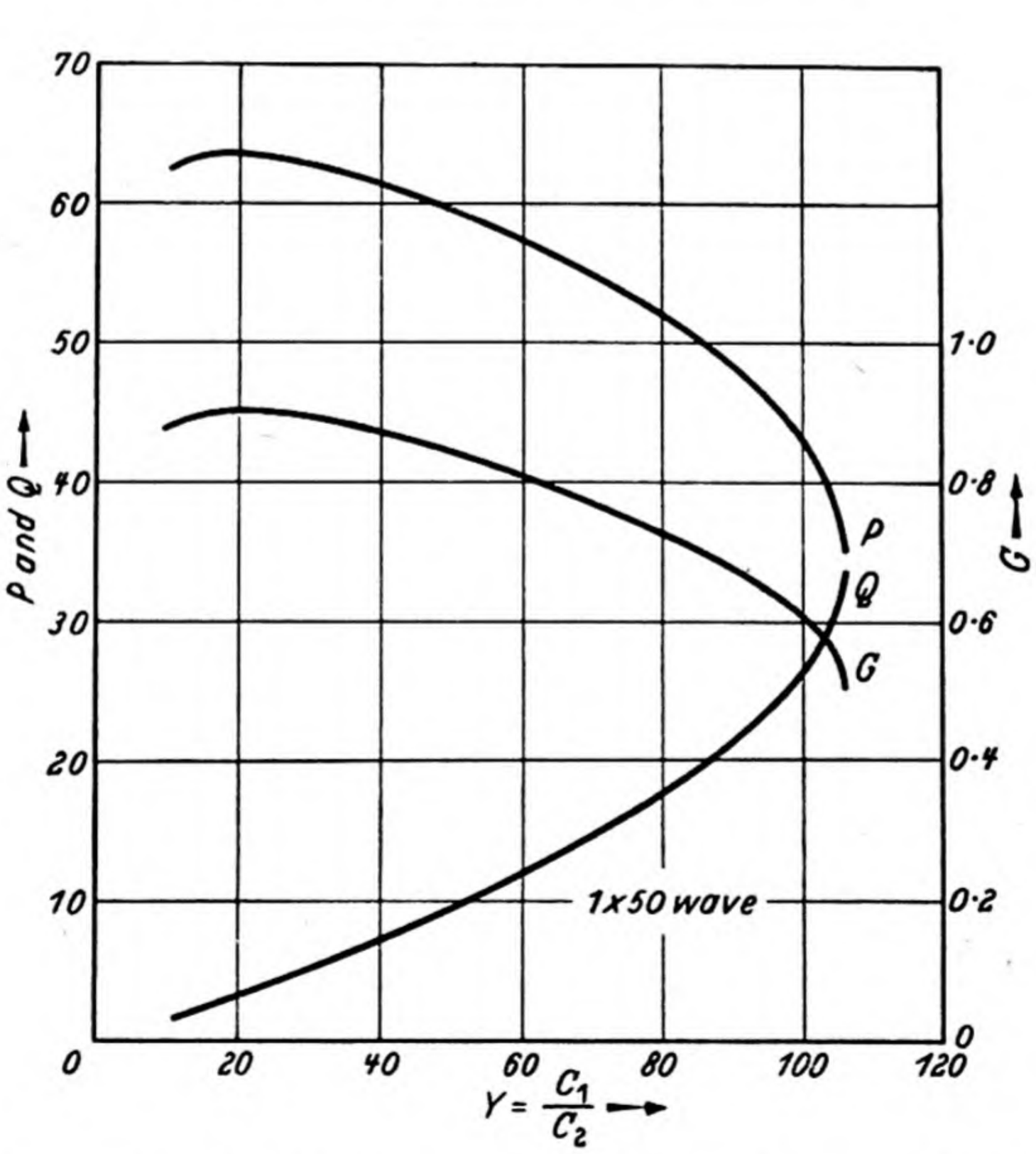

Figure 133. Circuit constants for the capacitance-resistance circuit shown in *Figure 122* (*a*). 1/50 wave (Eaton and Gebelein[23], by courtesy, *Gen, Elect. Rev.*).

where for a given wave-shape, Q is a function of Y only. Clearly from Equations 4.20 and 4.21 R_1 and R_2 have real values only if

$$\alpha^2 > (Y+1)(\alpha^2-\beta^2) \qquad \ldots.(4.22)$$

It follows therefore that Y has an upper limit which is

$$Y_1 = \frac{\beta^2}{\alpha^2-\beta^2} \qquad \ldots.(4.23)$$

If the value of R_2 from Equation 4.20 is substituted into Equation 4.17, then, at $t=t_1$, we get

$$v_{\max} = V_o P\left[\frac{\alpha^2-\beta^2}{2\beta}\left(e^{-(\alpha-\beta)t_1}-e^{-(\alpha+\beta)t_1}\right)\right] \qquad \ldots.(4.24)$$

For a given wave-shape the expression within the brackets is constant and we may write

$$v_{\max} = V_o PM = V_o G \qquad \ldots.(4.25)$$

where G is a function of Y only.

It is clear from the above relations that the terms P, Q and G can be plotted in terms of Y, the ratio of C_1 to C_2, for a given wave-shape. Such curves for a 1/5 and a 1/50 wave are given in *Figures 132* and *133*.

From Equation 4.23 it follows that for a given wave-shape, Y has an upper limit. If Y exceeds this limit it is not possible to choose values for R_1 and R_2 to obtain the given wave-shape. The values for this upper limit for various wave-shapes are given in *Table X*[23].

TABLE X[23]

Wave	*Max value of* $Y=\frac{C_1}{C_2}$
0·5/5	12·12
1/5	3·35
1/40	12·12
1·5/40	48·2
1/50	106·5

Capacitance-resistance circuit (*Figure 122b*)

The performance of this circuit is described mathematically, in operational form, by the equations

$$\left(\frac{1}{pC_1}+R_2\right)I_1 + R_2 I_2 = 0$$

$$R_2 I_1 + \left(\frac{1}{pC_2}+R_1+R_2\right)I_2 = 0$$

The solution of these equations gives, for the voltage v across C_2,

$$v = \frac{V_o}{2C_2R_1\beta}\left[e^{-(\alpha-\beta)t} - e^{-(\alpha+\beta)t}\right] \quad \ldots\ldots(4.26)$$

where V_o is the voltage to which C_1 is initially charged, and

$$\alpha = \frac{R_2C_2 + R_1C_2 + R_2C_1}{2\,C_1C_2R_1R_2} \quad \ldots\ldots(4.27)$$

$$\beta = \tfrac{1}{2}\left\{\left(\frac{R_2C_2 + R_1C_2 + R_2C_1}{C_1C_2R_1R_2}\right)^2 - \frac{4}{C_1C_2R_1R_2}\right\}^{\frac{1}{2}} \quad \ldots\ldots(4.28)$$

If we write $Y = \dfrac{C_1}{C_2}$ we can obtain from Equations 4.27 and 4.28

$$R_2 = \frac{1}{C_1}\left[\frac{\alpha \pm \sqrt{\alpha^2 - \dfrac{1+Y}{Y}(\alpha^2-\beta^2)}}{\dfrac{1+Y}{Y}(\alpha^2-\beta^2)}\right] = \frac{H}{C_1} \quad \ldots\ldots(4.29)$$

where, for a given wave-shape, H is a function of Y only. Also we have, from Equations 4.27 and 4.28

$$R_1 = \frac{1}{C_1}\left[\frac{1+Y}{\alpha \pm \sqrt{\alpha^2 - \dfrac{1+Y}{Y}(\alpha^2-\beta^2)}}\right] = \frac{J}{C_1} \quad \ldots\ldots(4.30)$$

where, for a given wave-shape, J is a function of Y only.

If Y is large, Equations 4.29 and 4.30 simplify approximately to

$$R_2 = \frac{1}{C_1} \cdot \frac{1}{\alpha-\beta} \quad \ldots\ldots(4.31)$$

$$R_1 = \frac{1}{C_1} \cdot \frac{1+Y}{\alpha+\beta} \quad \ldots\ldots(4.32)$$

From Equations 4.29 and 4.30 it is clear that R_1 and R_2 have real values only when

$$\alpha^2 > \frac{1+Y}{Y}(\alpha^2-\beta^2) \quad \ldots\ldots(4.33)$$

It then follows that Y has a lower limit given by

$$Y_2 = \frac{\alpha^2-\beta^2}{\beta^2} \quad \ldots\ldots(4.34)$$

If the value for R_1 from Equation 4.30 is substituted into Equation 4.26, we obtain for the peak value of the voltage wave, at time $t = t_1$,

$$v_{\max} = V_o\frac{Y}{J}\left[\frac{1}{2\beta}\left(e^{-(\alpha-\beta)t_1} - e^{-(\alpha+\beta)t_1}\right)\right] \quad \ldots\ldots(4.35)$$

For a given wave-shape the expression within the brackets is a constant and therefore

$$v_{\max} = V_oW \quad \ldots\ldots(4.36)$$

where W is a function of Y only.

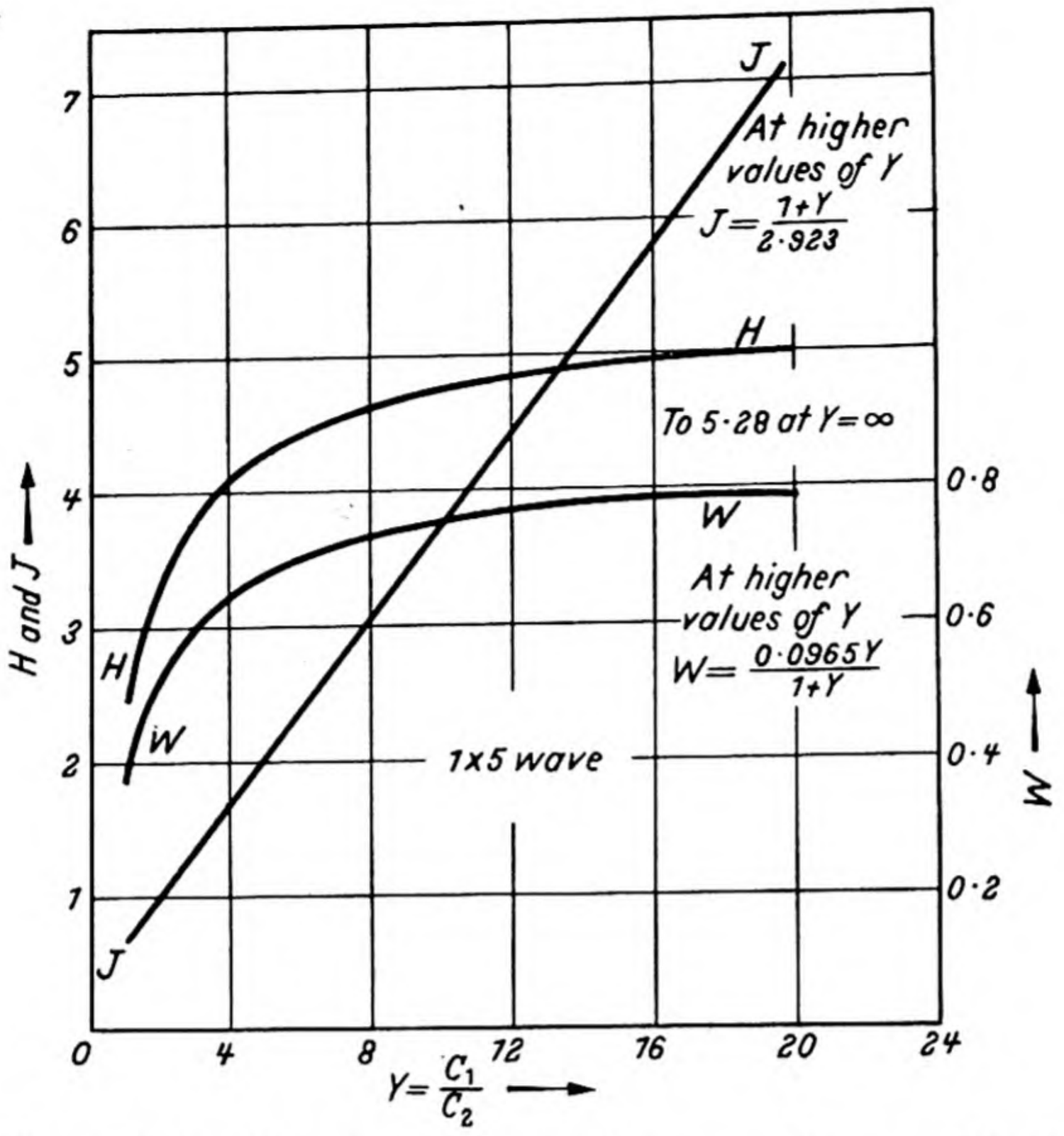

Figure 134. Circuit constants for capacitance-resistance circuit shown in *Figure 122* (*b*). 1/5 wave (Eaton and Gebelein[23], by courtesy, *Gen. Elect. Rev.*).

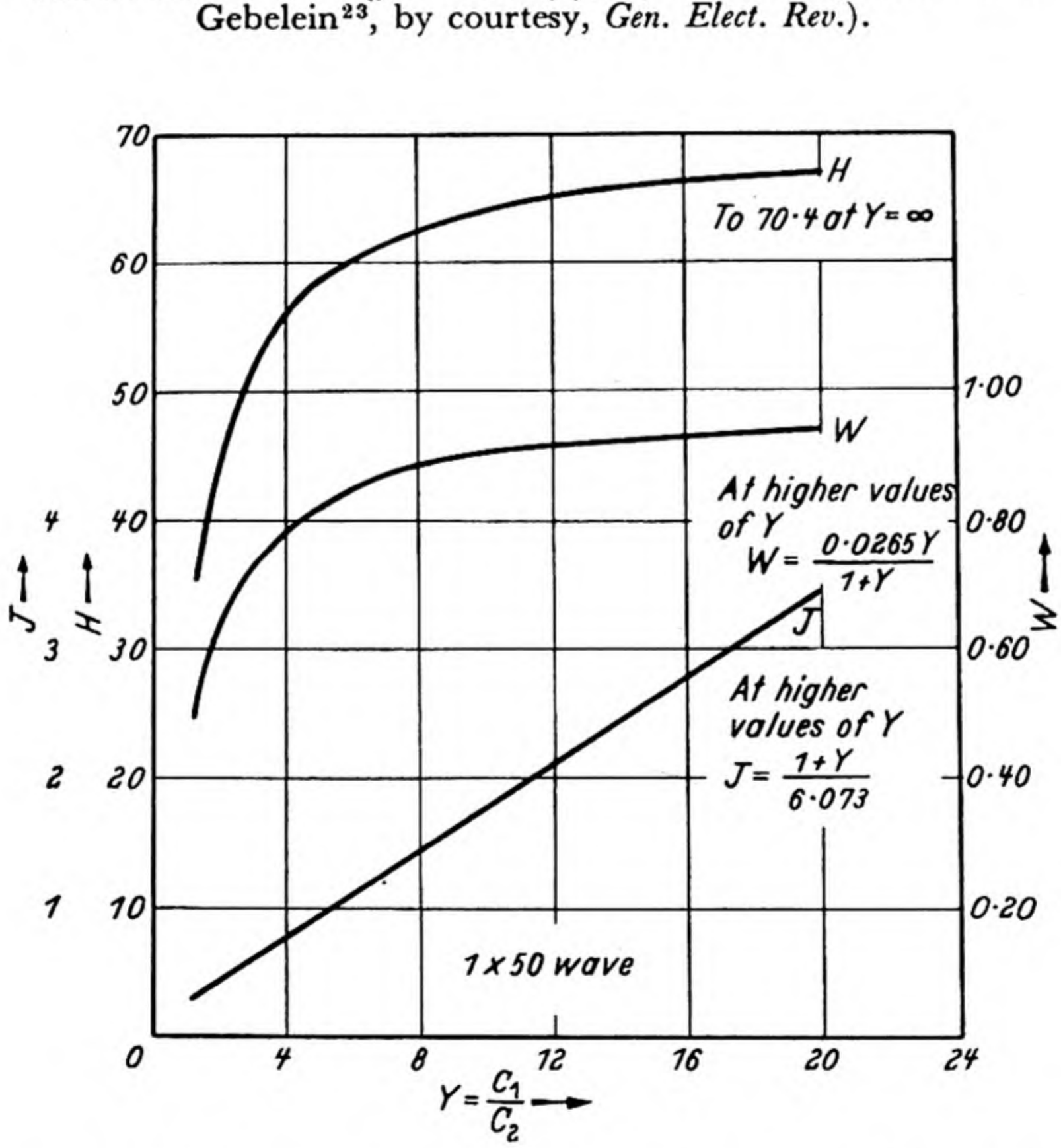

Figure 135. Circuit constants for capacitance-resistor circuit shown in *Figure 124* (*b*). 1/50 wave (Eaton and Gebelein[23], by courtesy, *Gen. Elect. Rev.*).

Curves relating the above quantities H, J and W with Y, the ratio of C_1 to C_2, are plotted in *Figures 134* and *135* for a 1/5 and 1/50 wave. From these curves the necessary values of R_1 and R_2 to produce the particular wave-shape can be calculated.

It is not possible to choose values for the resistances R_1 and R_2 to obtain a given wave-shape unless Y exceeds the minimum value given by Equation 4.34. The minimum values for Y for several wave-shapes are given in *Table XI*[23].

TABLE XI[23]

Wave	*Minimum value of* $Y = \frac{C_1}{C_2}$
0·5/5	0·082
1/5	0·296
1/10	0·082
1·5/40	0·021
1/50	0·009

Capacitance-resistance circuits with inductance

In practice the circuits of *Figures 122a* and *122b* are complicated by the presence of inductance and also by stray capacitance and mutual couplings between the circuit elements. The effect of induct-

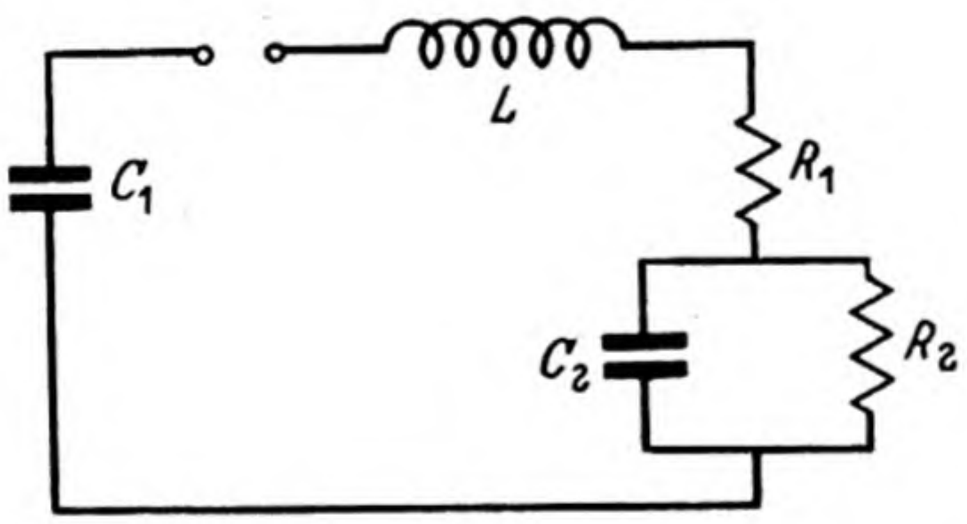

Figure 136. Impulse generator circuit of the capacitance-resistance type with inductance in one branch (Eaton and Gebelein[23], by courtesy, *Gen. Elect. Rev.*).

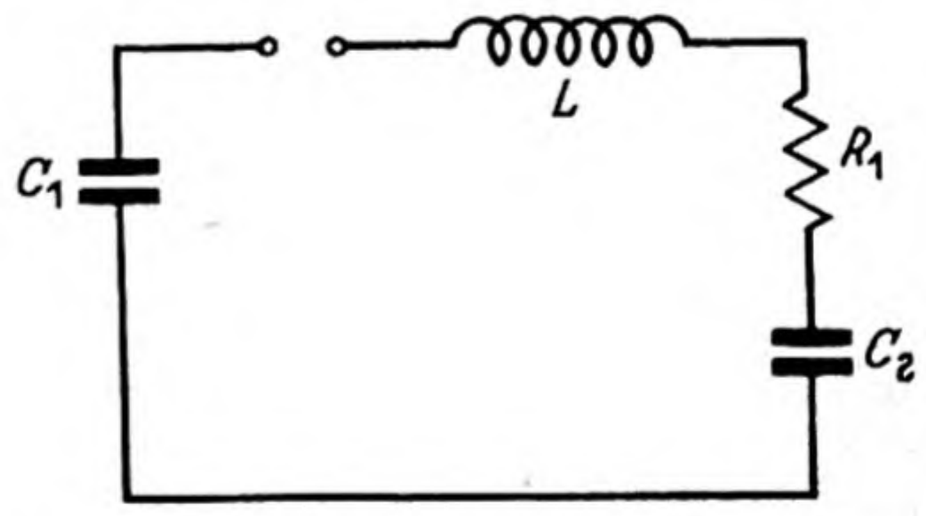

Figure 137. Impulse generator circuit of the same type as that shown in *Figure 136* but simplified for study of oscillation characteristics (Eaton and Gebelein[23], by courtesy, *Gen. Elect. Rev.*).

ance in the circuit of *Figure 122a* may be represented approximately by the circuit shown in *Figure 136*. The presence of L may result in oscillations on the wave-front. THOMASON[24, 25] has shown that this circuit can be analysed, so far as the wave-front is concerned, with inappreciable error by consideration of the circuit of *Figure 137* in which the resistance R_2 is omitted. Because of this omission the

results of the calculations are slightly pessimistic as R_2 will absorb energy and will therefore tend to prevent oscillations.

The circuit of *Figure 137* is non-oscillatory if

$$R_1 > 2\sqrt{\frac{L}{C}} \qquad \ldots\ldots(4.37)$$

where $C = \frac{C_1C_2}{C_1+C_2} = \frac{C_1}{1+Y}$ From Equation 4.37 it follows that

$$L < \frac{R^2_1}{4} \cdot \frac{C_1}{1+Y} \qquad \ldots\ldots(4.38)$$

or, as $Q = C_1R_1$ from Equation 4.21,

$$L < \frac{Q^2}{4C_1(1+Y)} \qquad \ldots\ldots(4.39)$$

Equation 4.39 may be rewritten as

$$L < \frac{S}{C_1} \qquad \ldots\ldots(4.40)$$

where S is a function of Y only.

The time constant of the circuit is

$$T_1 = \frac{2L}{R_1} \qquad \ldots\ldots(4.41)$$

and, therefore, if the circuit is non-oscillatory, from Equations 4.39 and 4.41,

$$\left.\begin{aligned} T_1 &< \frac{Q^2}{2C_1R_1(1+Y)} \\ \text{or} \quad T_1 &< \frac{Q}{2(1+Y)} \\ \text{or} \quad T_1 &< T \end{aligned}\right\} \qquad \ldots\ldots(4.42)$$

where T is a function of Y only.

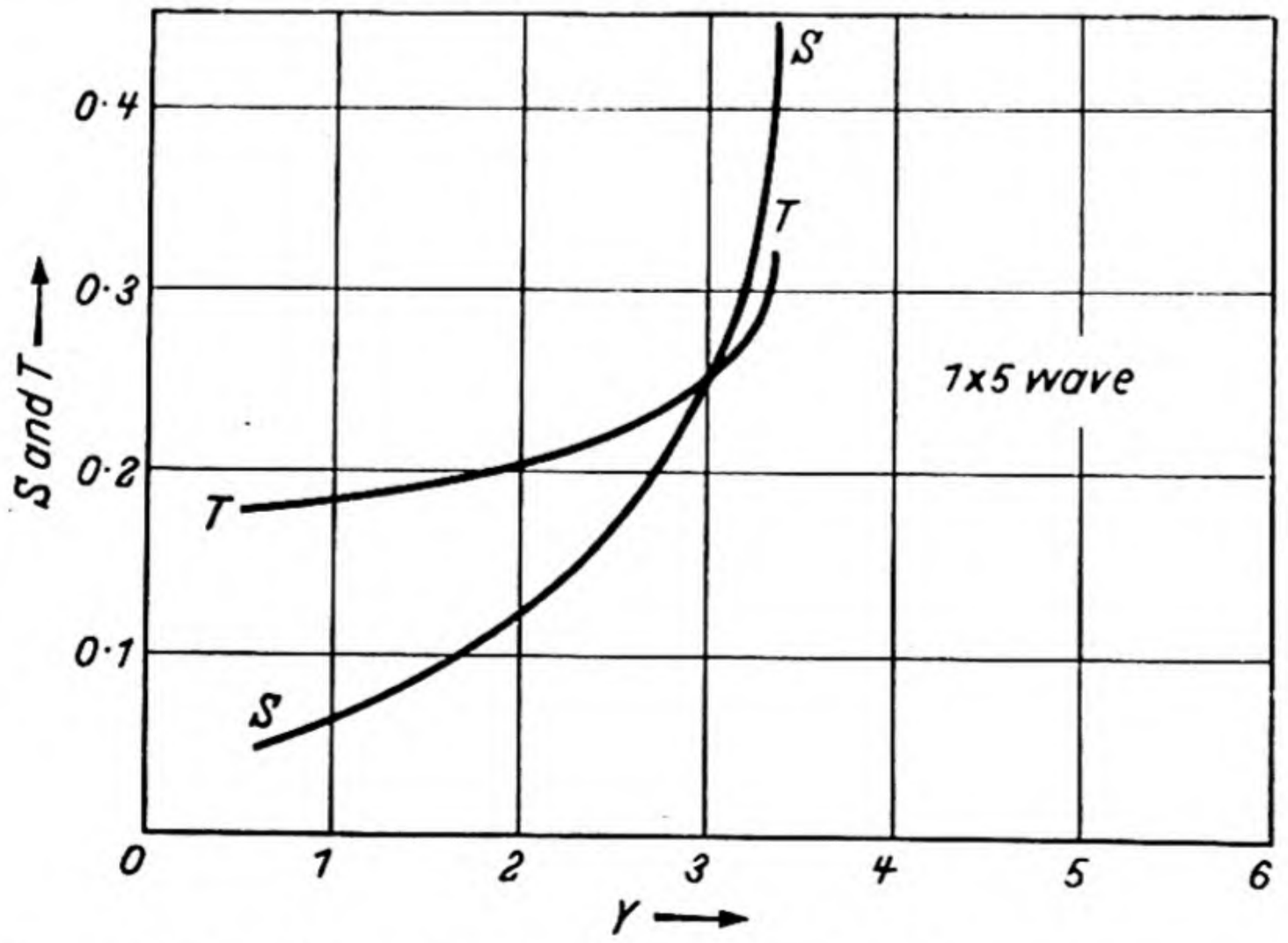

Figure 138. Wave-front characteristics for circuit shown in *Figure 122a.* 1/5 wave (Eaton and Gebelein[23], by courtesy, *Gen. Elect. Rev.*).

Curves showing the variations of S and T with Y for a 1/5 and a 1/50 wave are given in *Figures 138* and *139*. In building a circuit from the components given by *Figure 132* or *Figure 133* it is then possible by reference to *Figure 138* or *Figure 139*, with a knowledge of the circuit inductance, to determine whether the circuit is oscillatory or not. If the circuit is non-oscillatory and the time constant is appreciably less than the time-to-crest value, the circuit will be satisfactory. If, however, the circuit is oscillatory, or if the time constant is of the same order as the time-to-peak value, alterations in the circuit components are necessary. These oscillatory cases are discussed further by Thomason[24, 25].

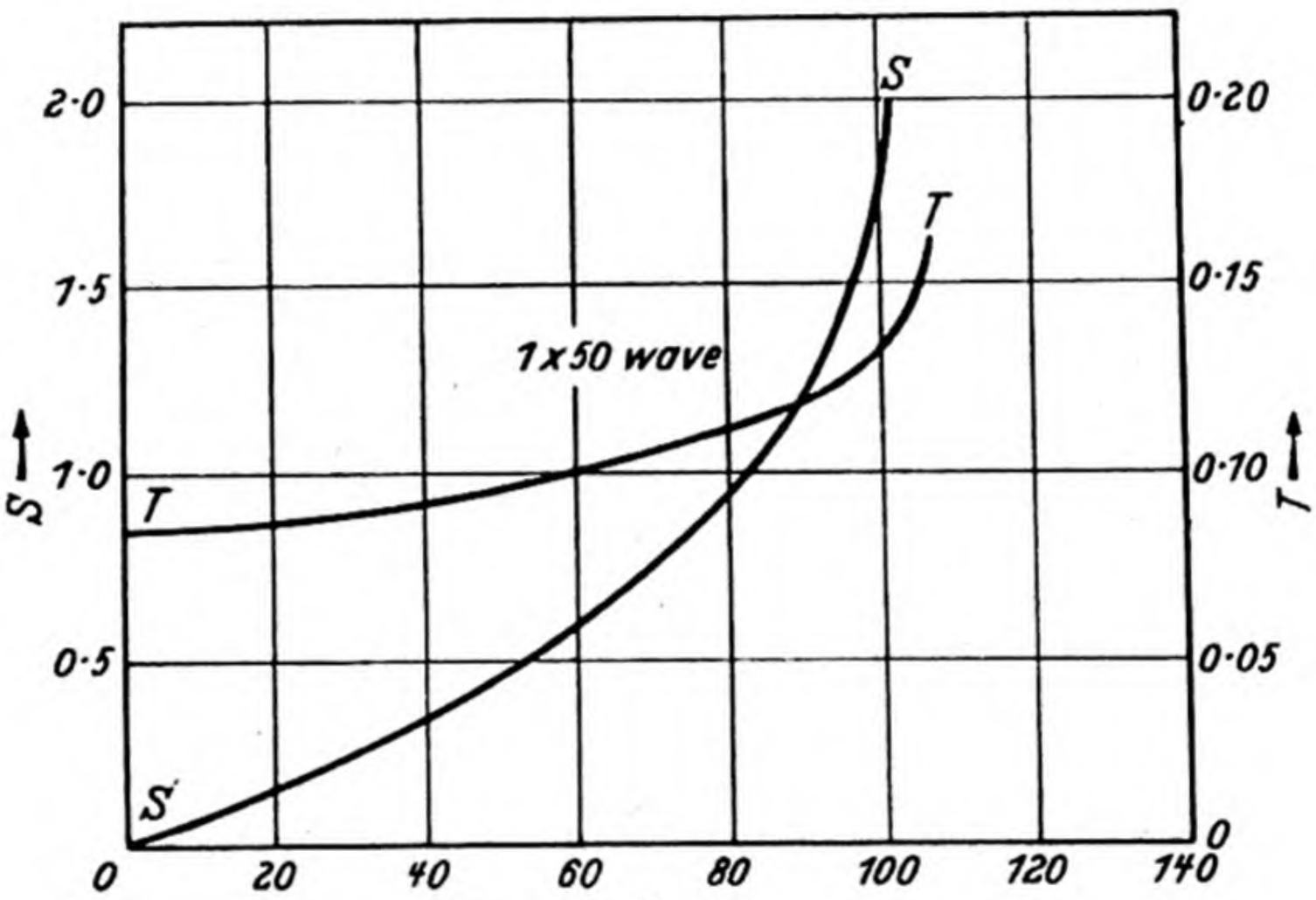

Figure 139. Wave-front characteristics for circuit shown in *Figure 122a*. 1/50 wave (Eaton and Gebelein[23], by courtesy, *Gen. Elect. Rev.*).

The influence of stray inductance in the circuit of *Figure 122b* can also be considered approximately, as regards wave-front oscillations, by reference to the circuit of *Figure 137*. As shown in Equation 4.38 this circuit is non-oscillatory if

$$L < \frac{R_1^2}{4} \cdot \frac{C_1}{1+Y}$$

For the circuit of *Figure 122b* it has been shown in Equation 4.30 that

$$R_1 = \frac{J}{C_1}$$

and therefore the circuit is non-oscillatory if

$$\left.\begin{aligned} L &< \frac{1}{C_1} \cdot \frac{J^2}{4(1+Y)} \\ \text{or} \quad L &< \frac{1}{C_1} \cdot U \end{aligned}\right\} \qquad \ldots\ldots(4.43)$$

where U is a function of Y only.

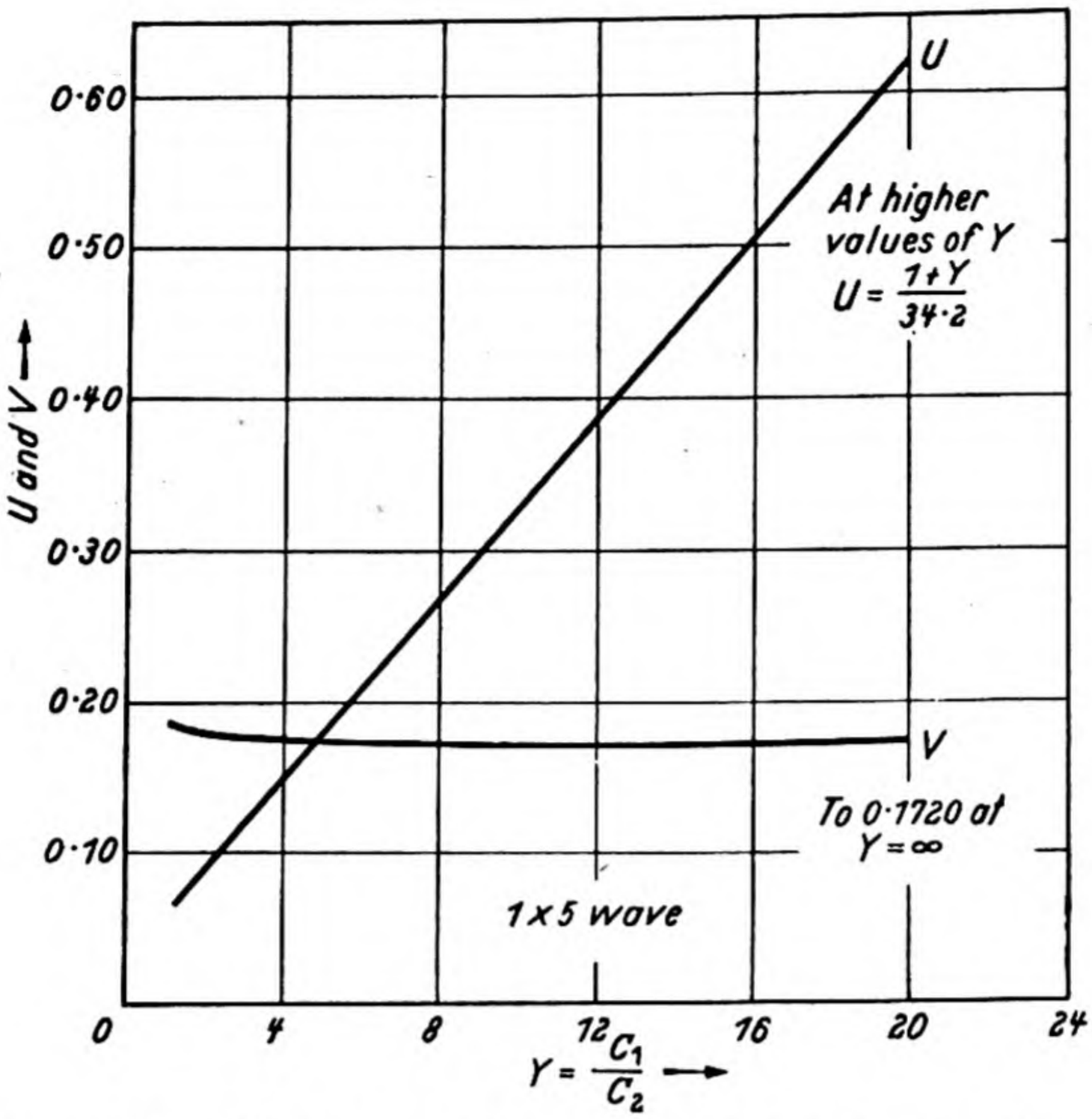

Figure 140. Wave-front characteristics for circuit shown in *Figure 122b*. 1/5 wave (Eaton and Gebelein[23], by courtesy, *Gen. Elect. Rev.*).

If the circuit of *Figure 122b* is non-oscillatory the time constant will be

$$\left.\begin{aligned} T_1 &< \frac{J}{2(1+Y)} \\ \text{or} \quad T_1 &< V \end{aligned}\right\} \qquad \ldots\ldots(4.44)$$

where, for a given wave-shape, V is a function of Y only.

Curves of U and V for the 1/5 and 1/50 waves are given in *Figures 140* and *141*.

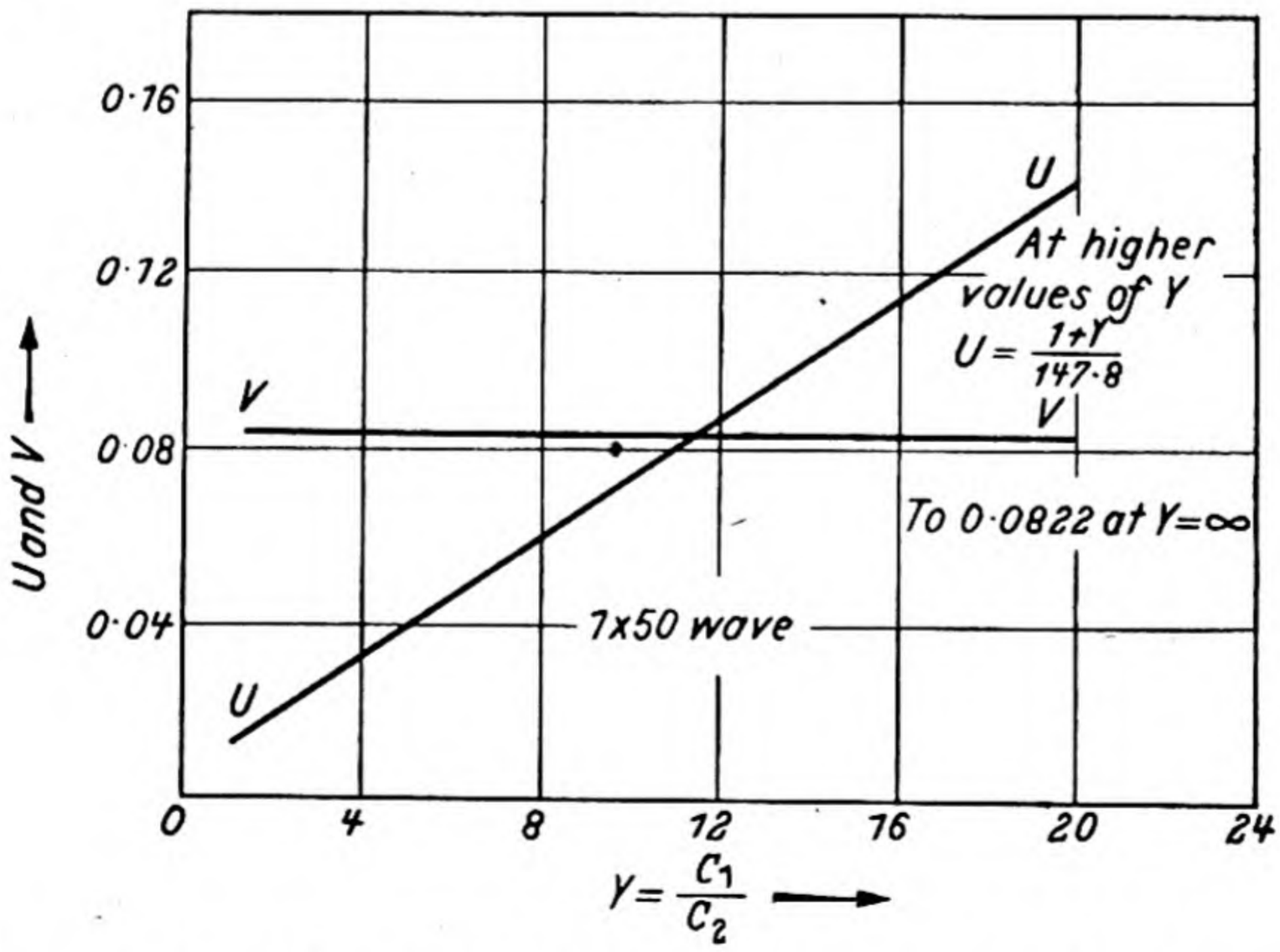

Figure 141. Wave-front characteristics for circuit shown in *Figure 122b*. 1/50 wave (Eaton and Gebelein[23], by courtesy, *Gen. Elect. Rev.*).

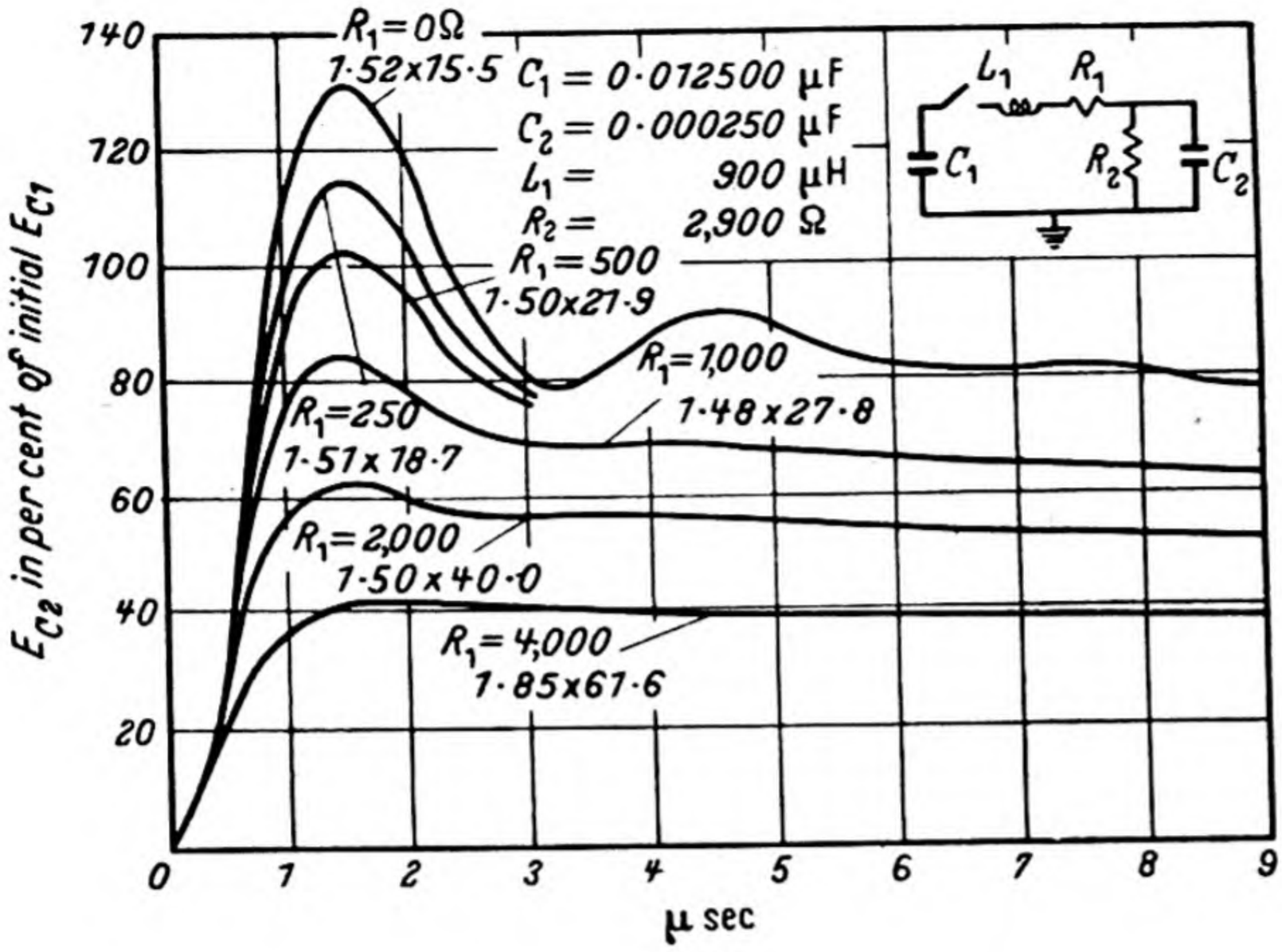

Figure 142. Effect of varying R_1 on wave shape (Thomason[24], by courtesy, *Trans. Amer. Inst. elect. Engrs.*).

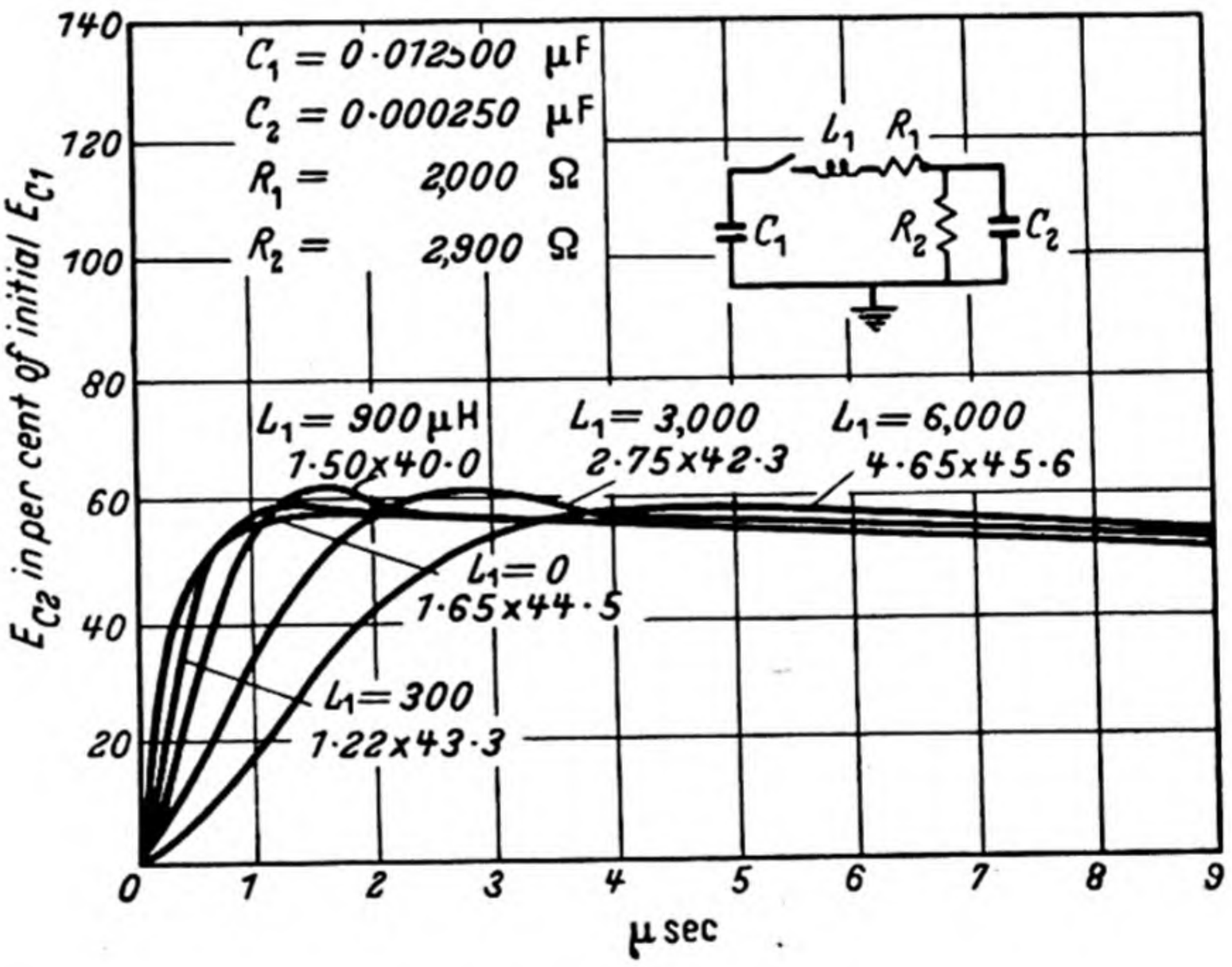

Figure 143. Effect of varying L_1 on wave shape (Thomason[24], by courtesy, *Trans. Amer. Inst. elect. Engrs.*).

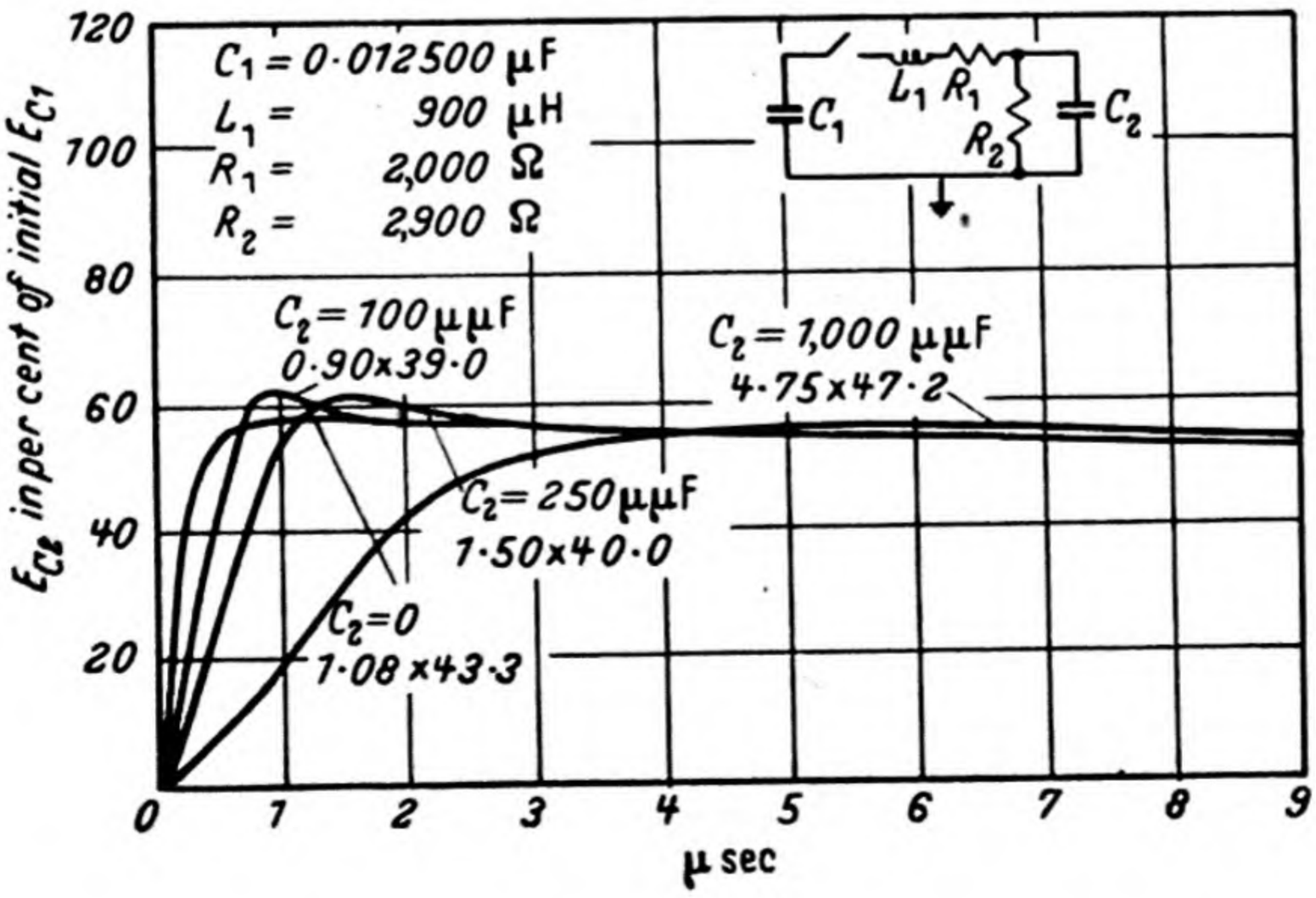

Figure 144. Effect of varying C_2 on wave shape (Thomason[24], by courtesy, *Trans. Amer. Inst. elect. Engrs.*).

The influence of the wave-front resistance, the series inductance, and the load capacitance on the wave-shape for the form of impulse generator circuit of *Figure 136* has been analysed by Thomason[24, 25] and is shown in *Figures 142*, *143* and *144*. In *Figure 142*, as the series resistance is increased the oscillations are damped out and the magnitude of the peak value of the wave is decreased; the wave-front first decreases until a critical value of series resistance is reached after which it increases. With varying series inductance, as in *Figure 143*, both the wave-front and the duration (time to half-value) of the wave have minimal values for slightly different values of inductance, but the magnitude of the peak value varies little for the chosen range of inductance. With varying load capacitance, both the wave-front and the duration of the wave have minimal values at about the same value of load capacitance, as shown in *Figure 144*.

FACTORS INFLUENCING THE DESIGN OF IMPULSE GENERATORS

The practical factors involved in the design of impulse generators have been summarized in the recent paper by Edwards, Husbands and Perry[5].

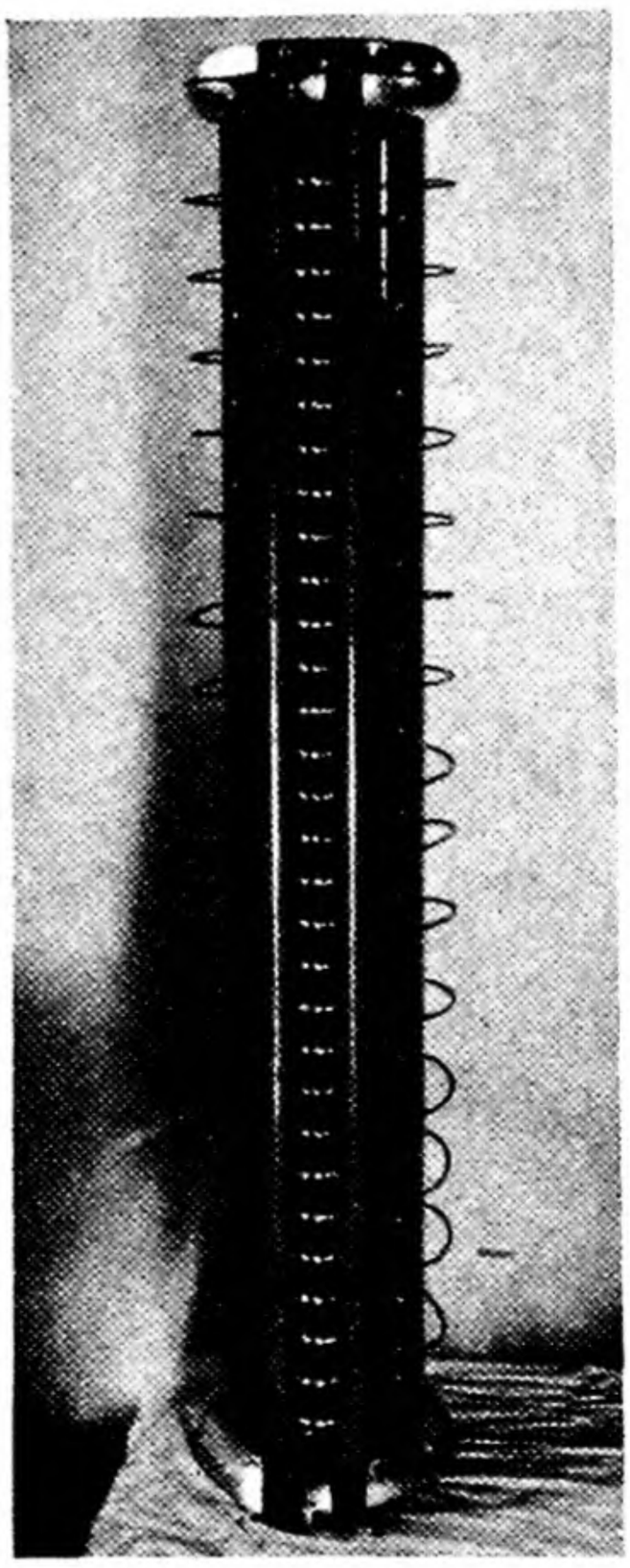

Figure 145. 600 kV portable impulse generator (by courtesy, Metropolitan-Vickers Electrical Company).

According to these authors the charging voltage selected should be about 10–15 per cent less than the open circuit voltage of the d.c. set used if the time of charging is to be kept down to a reasonable value. For the larger generators, with an output voltage of 1,000 kV

or more and a discharge capacitance of 0·01 to 0·03 μF, the most suitable charging voltage is stated to be ~170kV. With smaller impulse generators, for several hundred kilovolts and a discharge capacitance of 0·002 to 0·008 μF, the charging voltage may conveniently be 20–25 kV.

Clearly, for a given output voltage, the lower the d.c. charging voltage the greater must be the number of stages in the generator. A decision regarding the best arrangement is governed partly by economic considerations. In the 600 kV generator shown in *Figure 145*, 30 stages are used and all the condensers are assembled in one container. For generators of higher output voltage and capacitance fewer stages may be employed, as for the 2,000 kV, 12-stage generator illustrated in *Figure 146*.

With the development of new forms of rectifier sets for voltages of 1 or 2 MV or more, single-stage high-voltage impulse generators are practicable. The use of a generator with one, two or three stages has attractions because of its simplicity and the fact that, in certain laboratories, the high-voltage d.c. set can be used for other purposes. However, the higher the charging voltage the greater is the difficulty and cost of suppressing corona discharges from the leads during the charging period. Further, the multi-stage generator has a greater flexibility as, by the rearrangement of the connections between stages, large variations in output voltage and capacitance are possible for the same charging voltage. For example, with a twelve-stage generator and a d.c. charging voltage of 175 kV, variations of the interconnections enables a generator which normally delivers 2,100 kV with 0·01 μF discharge capacitance to produce 175 kV with 1·44 μF discharge capacitance.

For a given discharge resistance the duration of the wave-tail is proportional to the generator discharge capacitance C_1 plus the load capacitance C_2. If the resistance is designed to give the specified wave-tail when $C_2 = 0{\cdot}5\,C_1$, then the wave-tail will vary by ± 33 per cent about the specified amount for values of C_2 ranging from zero to C_1. The permissible variation for the impulse-testing of equipment, according to B.S. 923:1940, is ± 20 per cent in the wave-tail, and therefore at least two sets of resistance may be required if large changes occur in the load capacitance.

As the ratio of C_1 to C_2 is increased the open-circuit voltage required for a given output voltage across C_2 decreases and the circuit characteristics become less dependent on the external load. However, for economic reasons, it is desirable to limit the ratio. B.S. 923:1940 specifies a minimum ratio of 5 to 1.

If V is the open-circuit output voltage of the generator, of output capacitance C_1, and V_c is the crest voltage (assumed to be non-oscil-

latory) reaching the load, then Edwards, Husbands and Perry[5] point out that approximately

$$V = V_c\left(1+\frac{C_2}{C_1}\right) \qquad \ldots.(4.45)$$

From this equation it is clear that an increase in C_1/C_2 from 1 to 2 causes a reduction in V/V_c of 0·5. An increase from 2 to 3 causes a further reduction in V/V_c of 0·17. For successive equal increments in C_1/C_2 the corresponding reductions in V/V_c are extremely small when C_1/C_2 exceeds 5, and in practice this ratio is rarely exceeded when C_2 is the maximum load expected.

A practical example is quoted by Edwards, Husbands and Perry of a generator which was to be designed to produce $V_c = 1{,}500$ kV across a load $C_2 = 5{,}000$ $\mu\mu$F. At first, from considerations of the largest condensers available, it was proposed to construct a generator with $C_1 = 0{\cdot}01$ μF and $V = 2{,}400$ kV. Charge-sharing between C_1 and C_2 and the voltage loss on the wave-front, for a 1/50 wave, would be expected to bring the load voltage V_c down to about the specified value. With the wave-tail resistances adjusted to produce a 50 μsec wave-tail with a load of 2,500 $\mu\mu$F the wave-tails at zero and full-load would have been just within the tolerated limits. As the available building was not high enough to contain the above-designed unit the stage capacitance was increased by 50 per cent and the number of stages decreased by 15 per cent with a resultant increase in discharge capacitance of 75 per cent. The energy-storage in the generator was thereby increased by 30 per cent, but the saving in accessories, because of the reduced number of stages, and the saving in the necessary clearance caused by the reduced height of the generator and in the voltage for which the clearance to the roof was required tended to offset the extra cost.

THE GENERAL CONSTRUCTION OF IMPULSE GENERATORS

The method of construction of impulse generators is largely governed by the type of capacitors involved. Most of the recently built impulse generators[35–59, 68–70] use oil-impregnated capacitors in insulating containers. These capacitors have the dielectric assembled in an insulating cylinder of porcelain or varnished paper with plane metal end-plates. An advantage of this form of capacitor is that successive stages of capacitors can be built up in vertical columns, each stage being separated from the adjacent one by supports of the same form as the capacitors but without the dielectric. This method of construction is used in the generators shown in *Figures 146–149*. Oil-impregnated capacitors in metal tanks are occasionally used; they require an insulating framework and have the disadvantage that the voltage for which they are designed is usually low so that two or more capacitors may have to be connected in series for each stage.

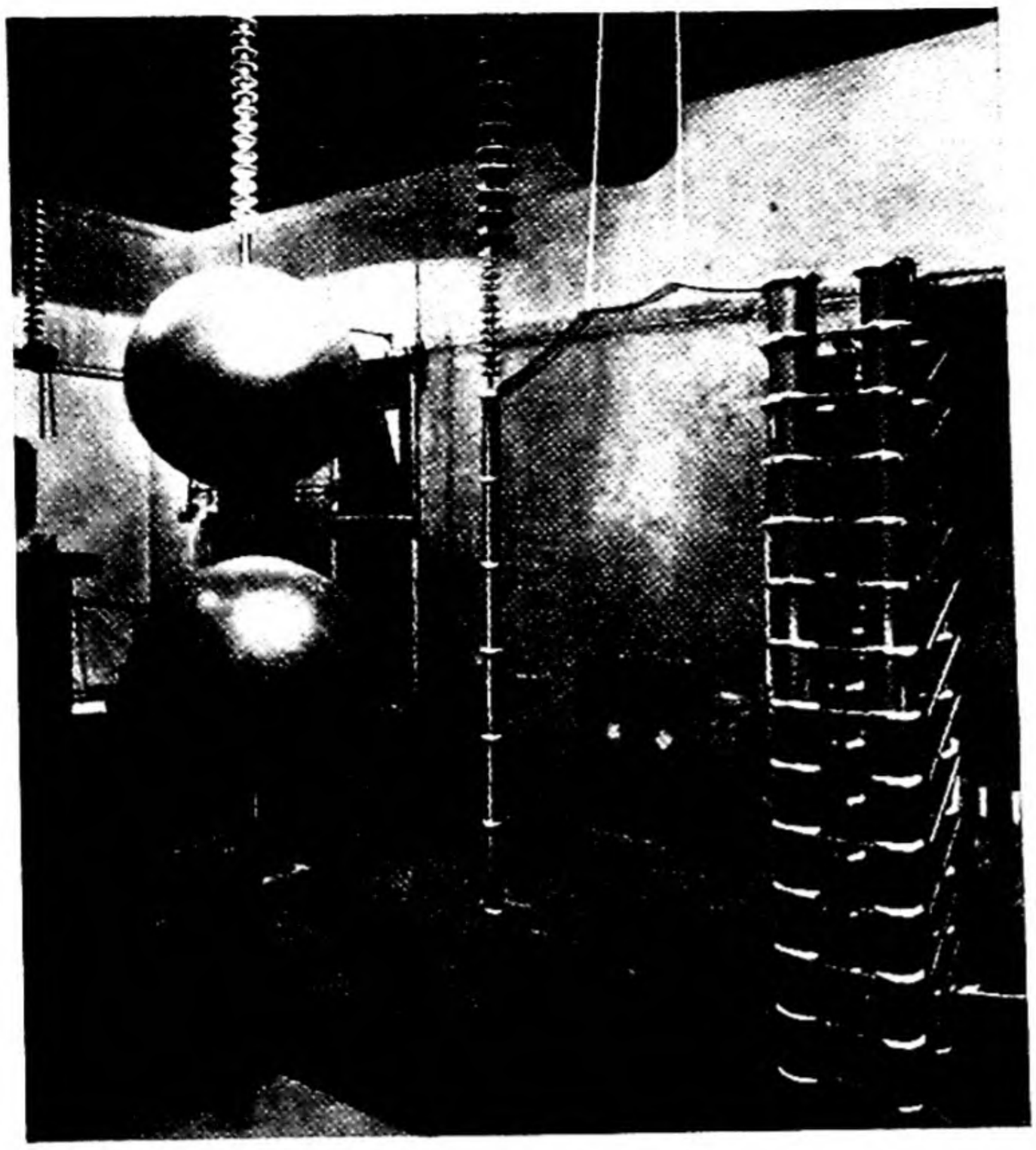

Figure 146

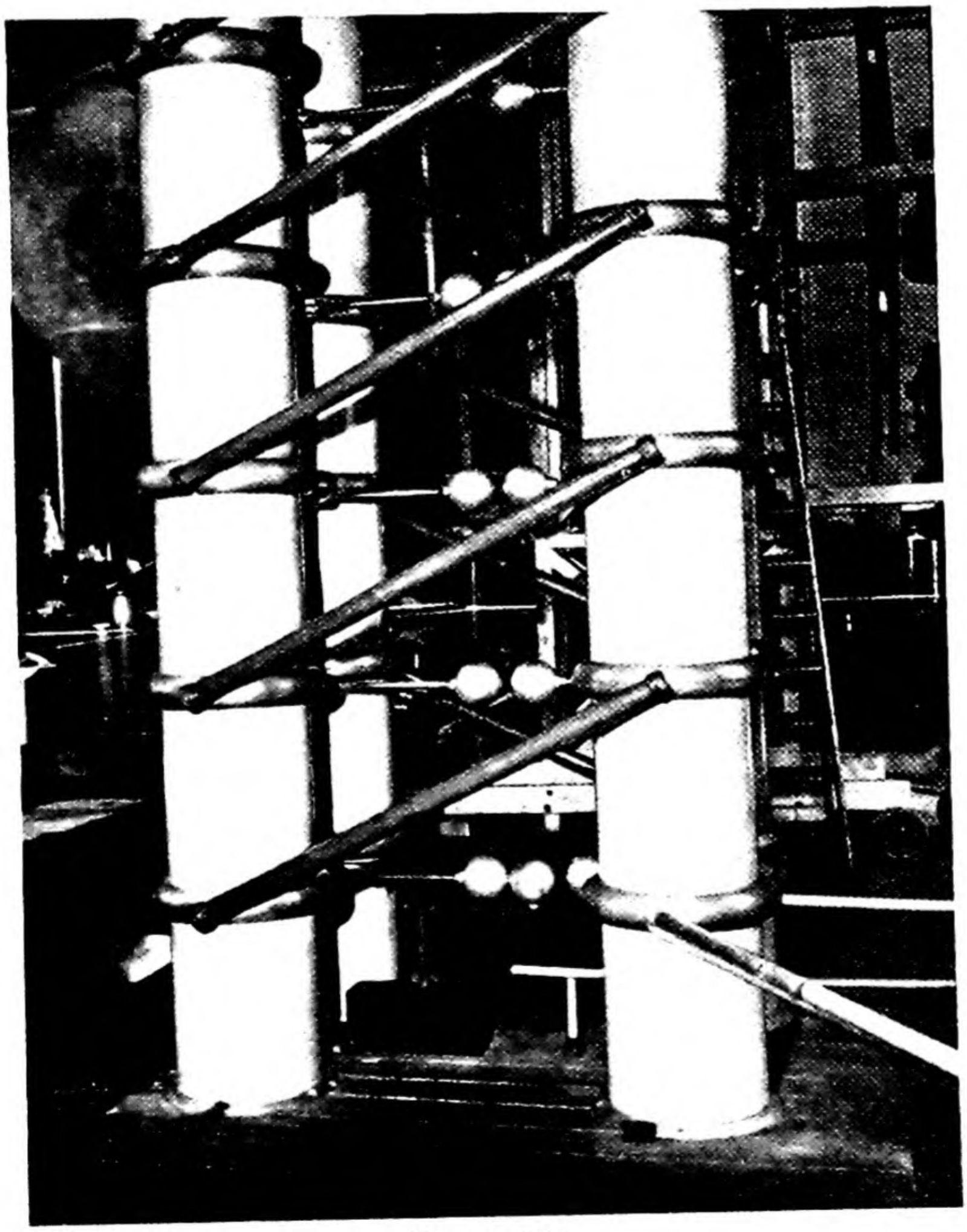

Figures 146 and 147. 2,000 kV, 12-stage impulse generator (by courtesy, Metropolitan-Vickers Electrical Company).

Figure 147

The wave-front control resistances may be composed of wire, liquids, or solids in the form of pellets or rods. The use of wire may be unsatisfactory because of inductive effects and low heat capacity. Liquids have a high heat capacity but their resistance is unstable. Solid materials are now frequently used (*see* page 322).

The wave-front resistors can be placed outside the generator, partly within and partly outside, or entirely within it. As the inductance is distributed all round the circuit, the third method is not wholly satisfactory because the external leads, the load and the stray earth capacitance form an oscillatory circuit which needs to be damped by an external resistor. An important practical reason for distributing the wave-front resistors within the generator is that the need is then diminished for an external resistor capable of withstanding the full voltage (*see* page 116).

Wave-tail control resistances can also perform the function of charging resistances and, in this case, are distributed throughout the generator. However, it is usual to arrange for part of the wave-tail resistance to be placed outside the generator as then it can be used also to serve the purpose of a potential divider. With the latter arrangement, as the wave-tail resistance is on the load side of the wave-front control resistance, there is a loss in the output voltage reaching the load (*see* page 114).

A 2,000 kV impulse generator built by the Metropolitan-Vickers Electrical Company is shown in *Figures 146* and *147*. This generator has 12 stages, each of 0·12 μF capacitance. The discharge capacitance is therefore 0·01 μF and the discharge energy is 20,000 joules. The d.c. charging voltage is 167 kV.

Each stage of the above generator consists of two capacitors each of 0·06 μF capacitance, connected in parallel. The capacitors are of the oil-impregnated type and are contained in varnished-paper cylinders with metal end-caps. Each capacitor is 21 in. long and has an overall diameter of 18 in. and a weight of 190 lb. The capacitors are stacked in four columns, each capacitor being separated from those in adjacent stages by means of insulating supports. These supports are identical with the containing-units used for the capacitor. The metal plates used for aligning the capacitors form a frame on which the central spark gaps are mounted. All the spark gaps are mechanically coupled so that the gap settings can be adjusted to a suitable value for the desired charging voltage by means of a single mechanical control. The charging and discharging resistances are all of the same length and serve also as bracing rods. The overall height of the generator is 23 ft.

Edwards[37] has described another similar impulse generator for 1,300 kV, with 12 stages and an output capacitance of 0·01 μF. This

generator has several special features as it has to be transportable for use outdoors and requires to be weatherproof. For the latter reason the capacitors are enclosed in porcelain casings.

A 2,100 kV impulse generator built by Ferranti Ltd., is shown in *Figure 148*. This generator contains twelve stages, the maximum d.c. charging voltage being 175 kV. Each stage consists of two 0·16 μF capacitors connected in parallel.

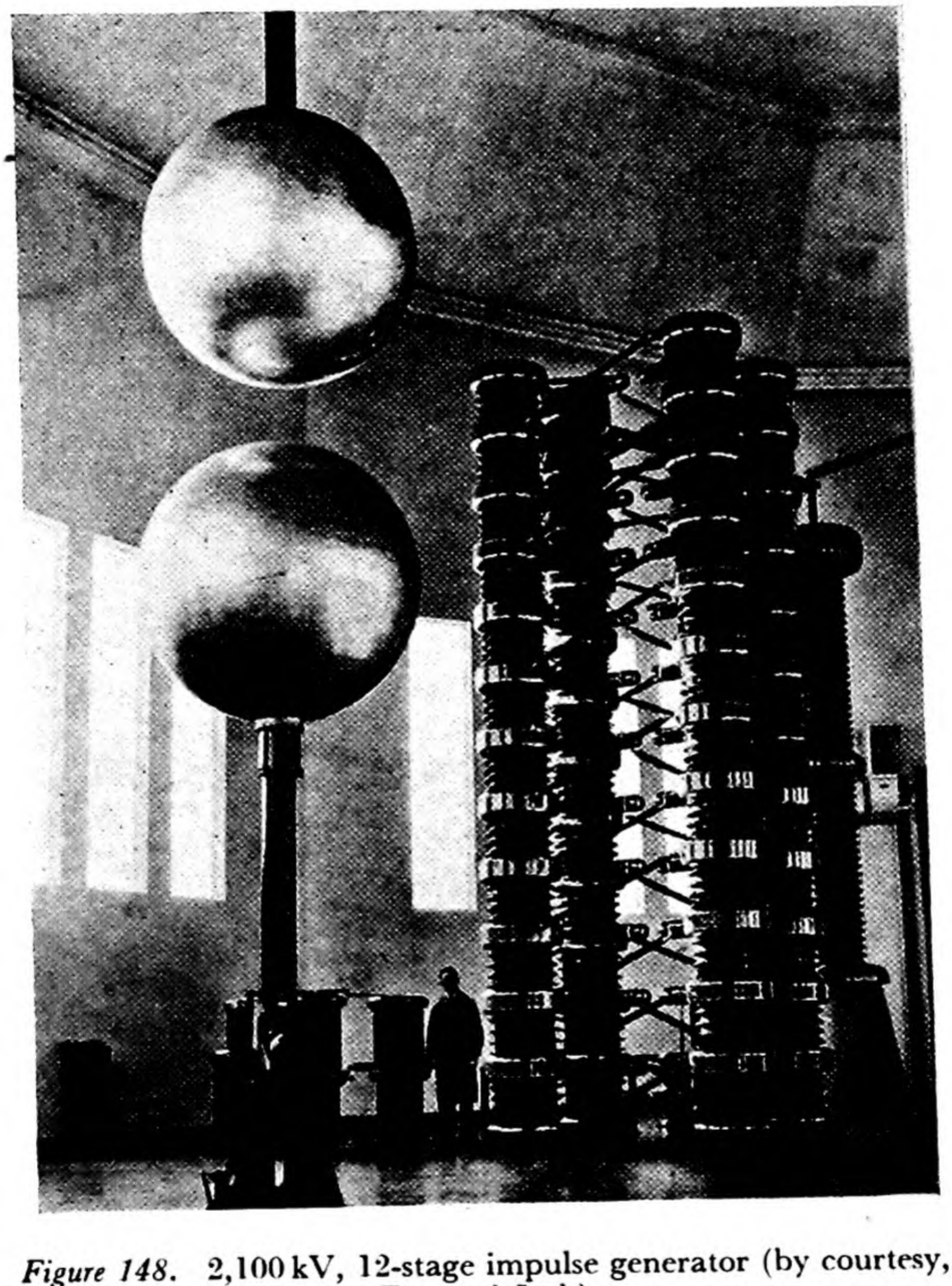

Figure 148. 2,100 kV, 12-stage impulse generator (by courtesy, Ferranti Ltd.).

Figure 149 shows an impulse generator, with a maximum output voltage of 2,100 kV, built by the Philips Electrical Company. The capacitors and insulators are mounted alternately one above the other, in four columns, and are connected through resistances and switch-arms in a spiral manner. There are 16 stages, each of 0·125 μF capacitance, and the maximum d.c. charging voltage used is 175 kV.

By means of a commutation mechanism controlling the switch-arms connecting the capacitors, resistances, and spark gaps, the 16 capacitors can be connected singly to give 12 stages, in pairs to give 6 stages, and in multiple pairs to give either 3 stages or a single stage. In this way the maximum energy of 24 kW/sec can be discharged at 2,100, 1,050, 525 or 175 kV. The overall height of the generator is about 18 ft. Similar types of generator have been built for 1,400, 2,800 and 3,500 kV.

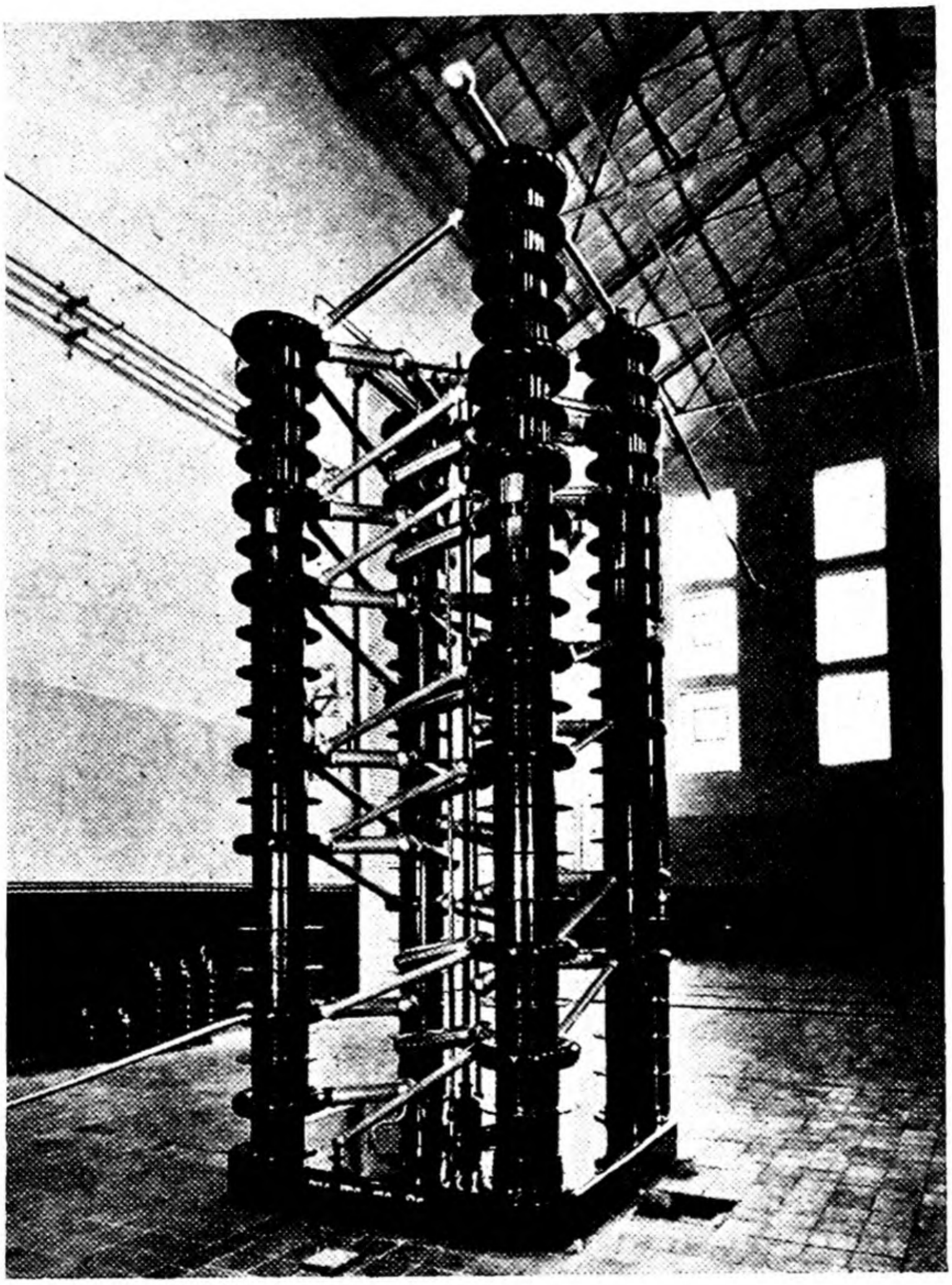

Figure 149. 2,100 kV, 16-stage impulse generator (by courtesy, Philips Electrical Company).

An impulse generator for 5,000 kV, using 20 stages each of 0·1 μF, has been described by LIECHTI[22]. This generator consists of two columns each containing five two-stage oil-immersed capacitors and a third column which serves as a support for the series-damping resistances and for the fixed spheres of the spark gaps. The movable spheres are mounted on two shafts alongside the column. The overall height is about 54 ft.

The production of impulse voltages up to 10,000 kV is described by HAGENGUTH[68] and by HENDRICKS, HUBBARD and VALLIN[38]. In this case two impulse generators are used, each giving a maximum discharge voltage of 5,000 kV at opposite polarities, the neutral point being earthed. Each generator consists of 51 capacitors assembled in 6 vertical columns. The capacitors are arranged in 17 stages, each consisting of 3 capacitors connected horizontally. Each capacitor is rated at 100 kV, 0·33 μF. A diagram showing the connections and principles of operation is given in *Figure 150*. The generator

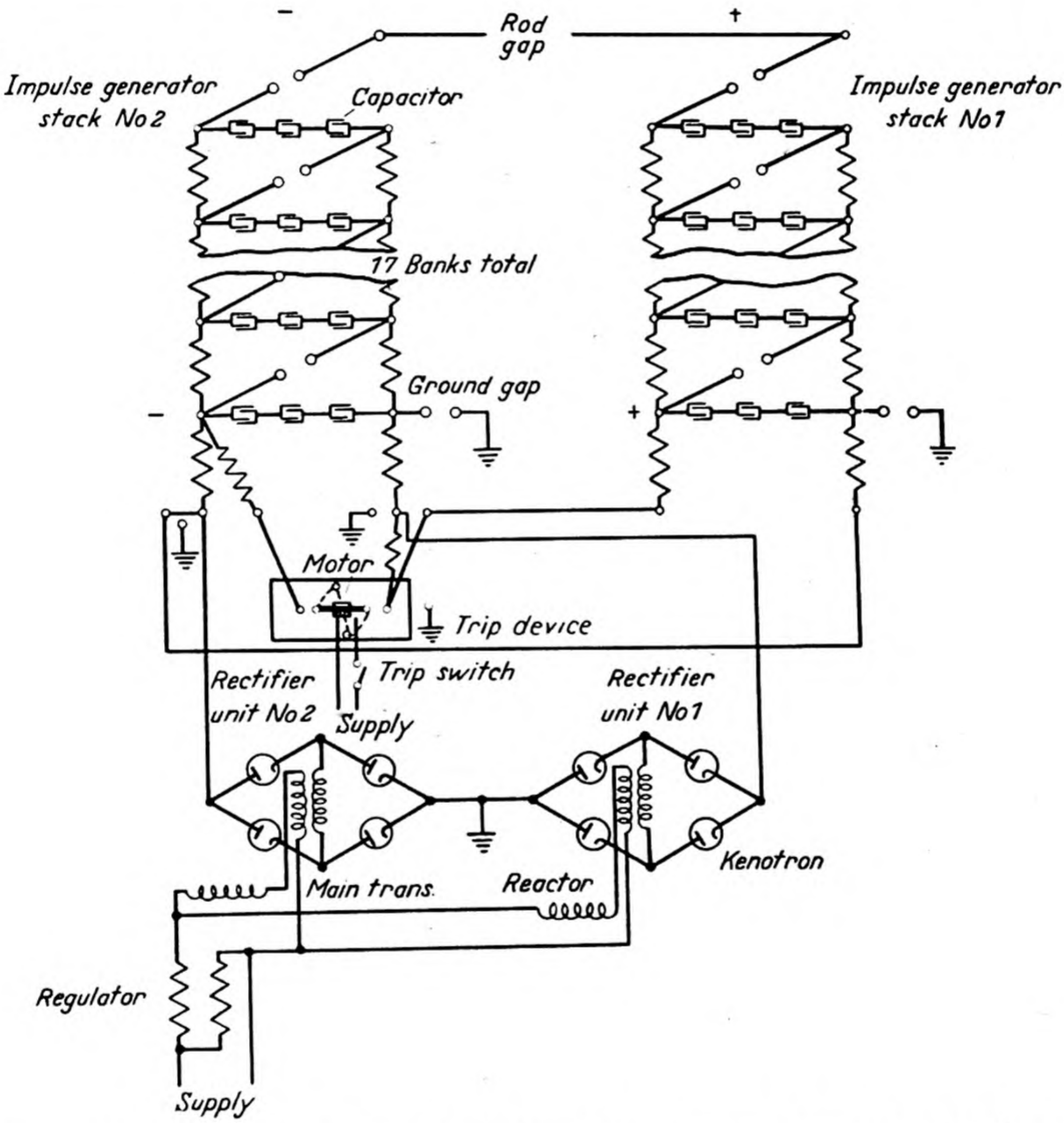

Figure 150. Connection diagram of the impulse generator and its associated equipment (Hendricks *et al*[38], by courtesy, *Gen. Elect. Rev.*).

is charged from a 300 kV d.c. source with its mid-point earthed, and the voltage of each capacitor group is therefore limited to 150 kV during the charging period. Each of the three-unit banks of capacitors at the earthed ends of the separate stacks are normally isolated from earth by a sphere gap, and when fully charged the voltage across

this gap is 150 kV. When the trip-gap is closed the voltage across the earth-gaps is raised to 300 kV, and with the break-down of these gaps the terminal voltage of capacitances immediately changes from 150 kV to 300 kV on one stack with an equal change in voltage, of opposite sign, on the second stack. An increase in voltage then occurs across the connecting spark gaps between the banks of each stack and causes the break-down of these gaps and the simultaneous development of impulse voltages on the two stacks.

A completely oil-immersed impulse generator for the production of voltages up to 3,000 kV has been described by ALLIBONE, EDWARDS and MCKENZIE[39]. The spark gaps are enclosed in a separate compressed-gas tube within the outer container, which is 5 ft. in diameter and 10 ft. in length. An advantage is that the construction of the capacitors and supports is cheaper than in the more conventional designs as the containers for the individual capacitors can either be omitted or constructed in a much lighter manner, and also the cost of provision of insulators between successive capacitors is practically eliminated.

A modification which allows a reduction in the total size is to enclose the capacitor stack in a single insulating container and to arrange the resistances and spark gaps on the outside of this container, the connexions to the capacitors being made by leads through the cylinder wall. CRÄMER[40] has described several impulse generators built on this principle, one with an output voltage of 1 MV with an output capacitance of 5,000 $\mu\mu$F.

A portable form of impulse generator for 240 kV with an output capacitance of 2,500 $\mu\mu$F has been described by Edwards[36], and is of the type illustrated in *Figure 145*. Twelve stages are used, the d.c. charging voltage therefore being 20 kV. The capacitors are arranged inside a varnished paper cylinder 37 in. long and $6\frac{3}{4}$ in. in diameter. The charging resistances consist of two ebonite tubes filled with water, the sphere spark gaps being mounted on shanks screwed into the tubes. One tube is fixed and the other can be rotated so that the gaps between the spheres can be altered. The total weight of the apparatus is 80 lb.

Several impulse generators have been built using lengths of high-voltage cable to form the stage capacitances[42, 43]. A two-stage impulse generator of this type described by BUSS[43] gives an output voltage of 1,400 kV with a discharge capacitance of 0·115 μF.

IMPULSE GENERATOR SPARK GAPS

For the larger impulse generators, where the d.c. charging voltage is ~170 kV, the spark gaps are generally in the form of spheres of 12·5 cm. in diameter. The arrangement of such spark gaps is clearly

shown in *Figure 147*. Where lower charging voltages are used, spheres of smaller diameter are satisfactory. The generator of *Figure 145*, which has a d.c. charging voltage of 20 kV, uses spheres of 1·3 cm. diameter. It is usual to arrange for the spheres forming the spark gaps to be of such a size that the spacing for the maximum voltage required does not exceed a sphere diameter. An important consideration is that corona discharge should be absent from the spark gaps, to avoid unnecessary drain on the d.c. set during the charging period, and for this reason sphere gaps with their nearly uniform field distributions are more satisfactory than more asymmetrical forms of gaps.

Figure 151. Circuit for synchronization of the tripping of the impulse generator with the crest value of an a.c. voltage (Edwards and Scoles[35], by courtesy, *Engineering*).

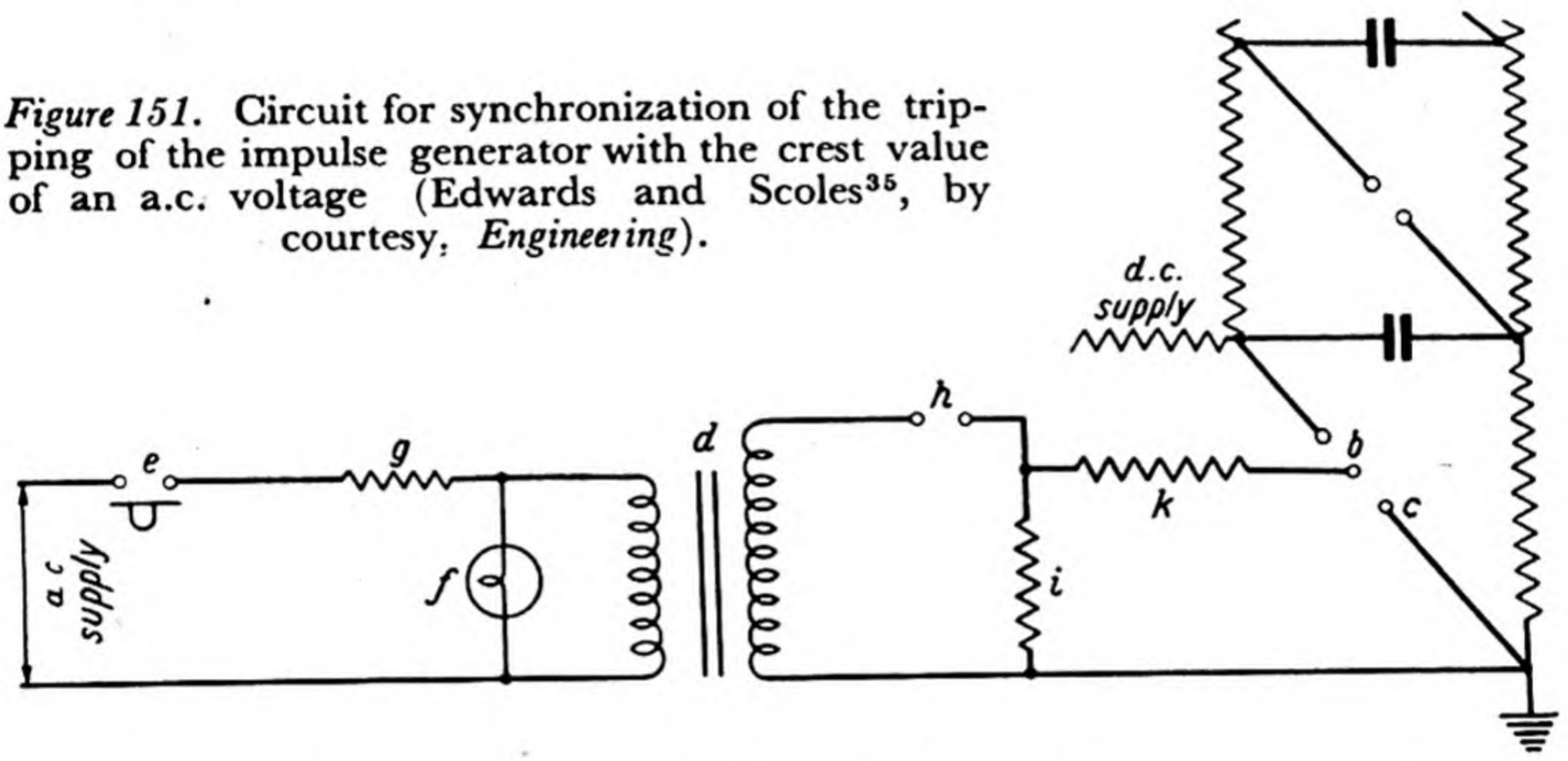

The setting of the spark gaps has to be adjusted according to the output voltage required. In the early forms of generators the gaps were adjusted manually, but in the more recent forms of the larger generators it is usual for the gaps to be driven by a remotely controlled motor[35].

A simple method for tripping the impulse generator to give a specified output voltage is to set the lowest gap to break down at a pre-determined value and then to charge the generator until break-down of this gap occurs with operation of the generator as a whole. The accuracy of the system depends on the reliability with which the first gap breaks down and some variation in voltage may be expected. Also the instant of the discharge is not precisely defined.

An electrical tripping circuit which is widely used involves a three-electrode gap connected to form the first spark gap of the generator. Usually each electrode is a sphere and the centres of the spheres are coaxial. The full charging voltage is applied between the two outer spheres. The central electrode may be earthed, normally through a high resistance, or may be biased at some voltage intermediate between those of the outer electrodes. The electrode system is adjusted to withstand the charging voltage by a small margin, and triggering of the charged generator is obtained by applying an unbalancing

voltage to the central electrode. Further details of the gap arrangement and circuits used are given on page 146. The tripping voltage may be a short pulse, in which case the timing of the generator operation is precisely controlled. Alternatively it is possible to synchronize the operation of the generator with the crest of the a.c. supply by the application of an a.c. voltage to the tripping electrode. A circuit for this purpose has been developed by EDWARDS and SCOLES[35] and is shown in *Figure 151*. The upper gap *b* of the three-electrode gap is set to a spacing equal to the other gaps of the generator and the lower gap *c* to a spacing too great for it to be broken down by the transformer *d*. The generator is first charged to a voltage just insufficient to break down *b*, after which it is tripped in the following way. When the switch *e* is closed the transformer *d* is excited, but, as the metal filament lamp *f* is cold and therefore of low resistance, the voltage drop in *g* is sufficient to prevent *h* from sparking over. The lamp *f* rapidly warms up and after a few cycles *h* breaks down. A large voltage then appears suddenly across *i* and is transferred through *k* to the three-electrode gap. If this voltage happens to be of opposite polarity to that with which the generator is charged, *b* at once breaks down and is followed by *c* and the other gaps of the generator. If it is of the same polarity the impulse occurs one half-cycle later. In either case, as the voltage across the primary of *d* builds up comparatively slowly, the break-down of *h* will occur almost exactly on the crest of the wave. This circuit is of value in the impulse testing of transformers under excitation conditions.

Other tripping techniques, and the synchronization of oscillographic measurements, are discussed on page 144.

Magnitude of over-voltage on second and subsequent gaps when first gap breaks down

In general it is assumed that the rapid break-down of the spark gaps of the generator, following the break-down of the initial spark gap, is caused by the over-voltage which is suddenly applied to the second and subsequent gaps. This matter has been examined in some detail by Edwards, Husbands and Perry[5]. According to the traditional theory for the circuit of *Figure 152* (in the absence of the dotted lines), when the first gap G_1 breaks down at a voltage of say $-V$ the potential at Z becomes zero and the voltage at Y rises to $+V$. A voltage of $2V$ appears across G_2 which will therefore break down if set to do so for some value between V and $2V$. Similarly voltages of $3V$ and $4V$ appear across G_3 and G_4 and so on.

Although in practice it has been found possible to operate a 50-stage impulse generator, it has been noted that G_2 must usually be set to break down at a voltage only slightly greater than that at which G_1

breaks down, otherwise it does not operate. This fact can be explained by the incompleteness of the above theory of operation. When the point Y attains a potential of $+V$ the potential at X does not remain at $-V$ in the absence of stray capacitance and, if the resistance between X and Z is assumed infinite during a short interval after the break-down of G_1, there is no reason why X should be at any particular potential.

Edwards, Husbands and Perry[5] point out that to explain the operation it is necessary to take account of the stray capacitances, as shown in dotted lines in *Figure 152*, and that these stray capacitances control the initial potential-distribution immediately after the break-down of G_1. For the purpose of calculation of the initial potential distribution the resistors may be assumed as open circuits; also it may be assumed that the stray capacitances are negligible in comparison with the stage capacitances.

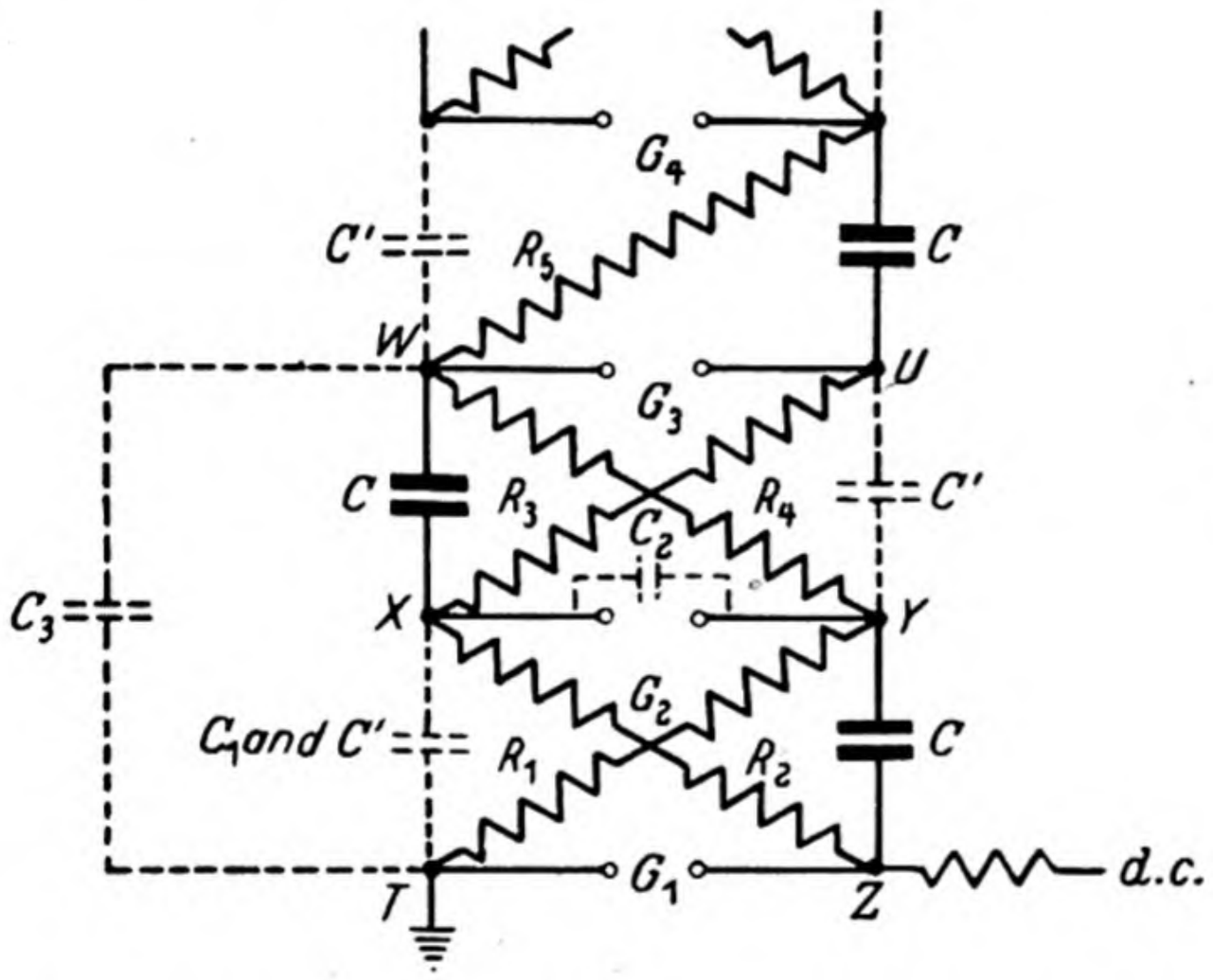

Figure 152. Diagram of multi-stage circuit showing stray capacitances (Edwards, Husbands and Perry[5], by courtesy, *Proc. Inst. elect. Engrs.*).

Consider now the circuit when Z, initially at a potential $-V$, is suddenly earthed by the break-down of the gap G_1. The point Z, initially at earth potential, assumes the potential $+V$ but the potential at X is fixed by the relative magnitudes of C_1, C_2 and C_3. If the potential at X after the transients have died away but before the resistances have begun to affect the voltage distribution is $-V_x$, then

$$V_x = V\left(\frac{C_1+C_3}{C_1+C_2+C_3}\right) \qquad \ldots\ldots(4.46)$$

Hence the voltage V_y across C_2, *i.e.* across the gap G_2, is

$$V_y = V\left(1+\frac{C_1+C_3}{C_1+C_2+C_3}\right) \qquad \ldots\ldots(4.47)$$

If C_2 is equal to zero, V_y will reach its maximum value of $2V$. If C_1 and C_3 are both zero, V_y will equal V, its minimum possible value. It is apparent, therefore, that the most favourable conditions for the operation of the generator occur when the capacitance C_2 of the

sphere gap G_2 is small and the stray capacitances C_1 and C_3 are large.

The above deductions have been confirmed experimentally by Edwards, Husbands and Perry. However, these authors also point out that the theory is still incomplete and does not account for the erratic behaviour of some impulse generators when the wave-tail resistances have been made small in order to produce a short wave. They quote the example of a 1,000 kV 8-stage generator of 0·025 μF discharge capacitance which could not be made to work consistently at charging voltages in excess of about 60 kV when arranged to give a 1/5 wave but was satisfactory for a 1/50 wave. This may be explained by consideration of the effect of the circuit resistance. The condition represented by Equation 4·47 is only transient as the stray capacitances C_1, C_2 and C_3 immediately begin to lose or gain charge so that the overvoltage $V_y - V$ across G_2 is quickly reduced to zero. As the values of C_1, C_2 and C_3 are normally of the order of 10 to 100 $\mu\mu$F the time-constants of the corresponding circuits are likely to be small. In the 1,000 kV generator mentioned above the wave-tail control resistances were $\sim 100\ \Omega$ so that the time constants were about 10^{-2} to 10^{-1} μsec.

In practice R_2 is large compared with R_4 and after the initial potential redistribution caused by the break-down of G_1 has been effected the subsequent events can be calculated on the assumption that R_4 is then connected between W and Y. The variation of the voltage across the gap G_2 is then given by

$$V_{G_2} = V\left(\frac{C_1+C_3}{C_1+C_2+C_3}\right) e^{-t/R_4(C_1+C_2+C_3)} \qquad \ldots\ldots(4.48)$$

If $C_1+C_3 \gg C_2$, this becomes

$$V_{G_2} = V e^{-t/R_4(C_1+C_3)} \qquad \ldots\ldots(4.49)$$

so that after a time $3R_4\ (C_1+C_3)$ the voltage across G_2 is only 0·05 V volts. The time constant can be lengthened, so as to maintain the enhanced voltage across G_2 by increase of C_1+C_3 or of R_4. R_4 is fixed by the stage capacitance and by the specified wave-tail. C_1 and C_3 depend upon the construction of the generator but can be increased artificially.

Experiments were carried out by Edwards, Husbands and Perry on a 12-stage generator of 0·12 μF stage capacitance, in which R_4 was varied from 100 Ω to 10,000 Ω, and both with and without an additional capacitance of $C' = 230$ $\mu\mu$F connected between X and T, in parallel with C_1 as shown in *Figure 152*. The voltages developed across the gaps G_2 and G_3 following the break-down of G_1 were recorded oscillographically. A feature of the results is the extremely short duration of the overvoltage across G_2 which never exceeds 100 per cent. A great decrease in the duration of the overvoltage occurs

with the reduction in R_4 from 10,000 Ω to 100 Ω, and at $R_4 = 100$ Ω the overvoltage persists for only 0·1 μsec. Because of the short duration of the overvoltage the need for adequate irradiation of the gaps to ensure reliable operation of the generator is apparent (*see* page 265).

Influence of dust and of irradiation on regularity of break-down of generator spark gaps

The presence of dust can cause irregular operation of a multi-stage generator. As the available overvoltage is small and of brief duration, the second and subsequent gaps cannot be set to break down at a voltage much higher than that at which the first gap breaks down. But the dispersion of the d.c. break-down voltage in the presence of dust may be so great that if the difference in settings is small any one of the gaps may fail irregularly at less than the intended voltage. Edwards, Husbands and Perry quote a case where each of the ten gaps broke down singly on ten successive tests.

To overcome this difficulty, experiments have been made with each gap enclosed in a cylindrical shroud made of pressboard and greased on the inside[5]. The first gap then broke down with great regularity and with inappreciable deviations from the mean value, but none of the other gaps broke down. The latter result may be attributed to the fact that the ultra-violet illumination from the spark in the first gap was prevented from reaching the other gaps, and consequently there were insufficient electrons present in these gaps to initiate break-down during the brief period when the gaps were subjected to overvoltage. Narrow slits were then introduced at the top and bottom of each shroud so that the irradiation from the first gap fell on the second one and so on. With this arrangement the performance of the generator was usually satisfactory. However, it was found that, although the axes of the gaps were in one vertical plane, a slight horizontal displacement of alternate gaps reduced the intensity of the illumination reaching them from the adjacent gaps, and this sometimes resulted in irregularity of firing. With the gaps later arranged in a vertical line the performance became reliable.

THE SYNCHRONIZATION OF THE OPERATION OF IMPULSE GENERATORS AND OSCILLOGRAPHS

Impulse generators are usually operated in conjunction with cathode-ray oscillographs or other apparatus for measuring the characteristics or the effects of the impulse waves[67]. Because of the short duration of the waves it is necessary that the operation of the generator and the oscillograph should be synchronized accurately and, if the wave-front is to be recorded satisfactorily, the oscillograph

time sweep has to be initiated at a time slightly before the impulse wave reaches the deflecting plates. If there is no control over the instant of operation of the generator, the time sweep must be initiated by the generator. It is then necessary to connect a delay line between the generator, or the potential divider, and the deflecting plates, so that the impulse wave reaches the plates at a controlled time after the sweep has been tripped. However, the use of a delay line considerably affects the choice of a potential divider and leads to inaccuracies in the recording. For this reason tripping circuits have been developed in which the generator is tripped at a controlled time following the tripping of the oscillograph time sweep[60–64]. This time is usually about 0·1 to 0·5 μsec.

One method for synchronizing the generator and the oscillograph involves the use of a three-sphere gap in the first stage of the generator (*see* page 140). *Figure 153* shows a circuit described by WHITE[61];

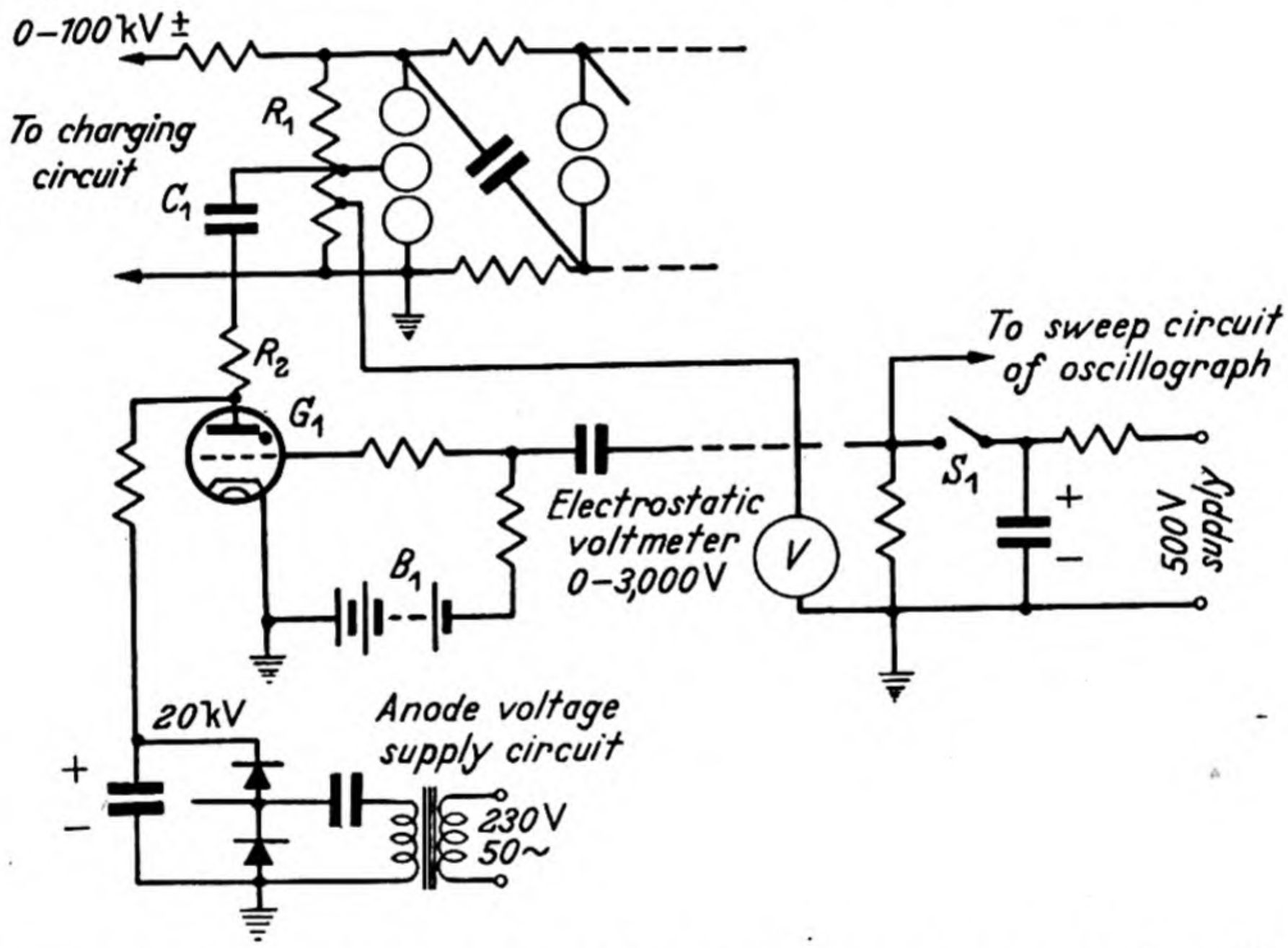

Figure 153. Circuit for synchronizing impulse generator and oscillograph (White[61], by courtesy, *J. Sci. Instrum.*).

the mechanical details are given in *Figure 154.* The spheres are arranged so that the two series gaps are sufficient to withstand the charging voltage of the impulse generator. The central sphere is insulated and is mounted on a lever system which ensures that as the right-hand sphere is moved the air-gaps remain equal. A high resistance R_1 is connected between the outer spheres, and its centre point is connected to the central sphere so that the voltage between the outer spheres is equally divided between the two gaps. If the generator is now charged to a voltage slightly below the break-down voltage of the gaps, break-down can be caused at any desired instant by applying a suitable impulse voltage to the central sphere. According

to White it is found that an impulse of either polarity and of a peak voltage not less than one-fifth of the charging voltage can be relied upon to initiate break-down of the spark-gaps.

The tripping impulse is applied through a small capacitor C_1 which, as shown in *Figure 154*, is a porcelain pin-type insulator. The cap of

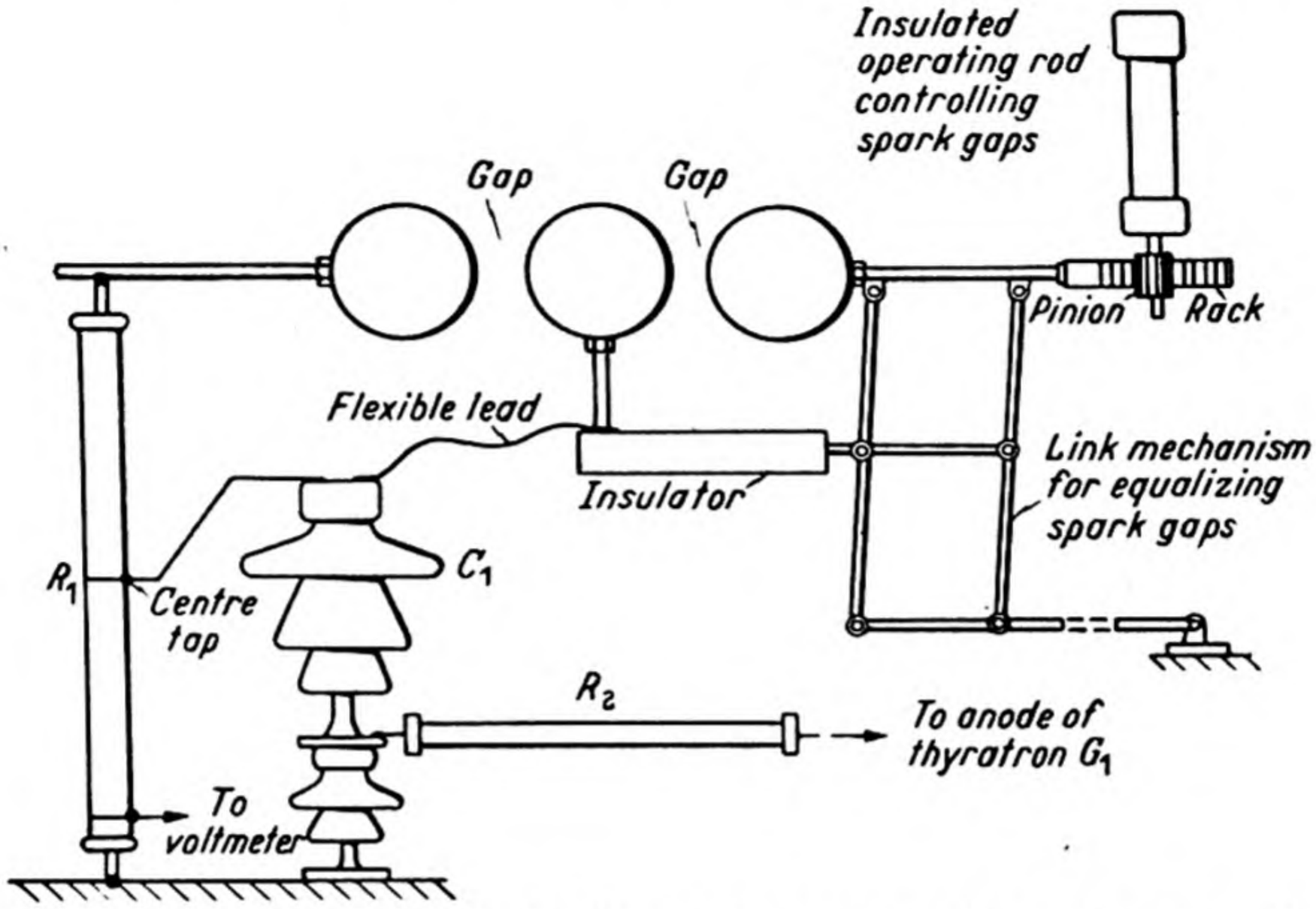

Figure 154. Mechanical details of first stage of spark gaps. R_1, 90 MΩ ; R_2, 2600 Ω (White[61], by courtesy, *J. Sci. Instrum.*).

the insulator is connected to the central sphere and the pin is connected to the anode of the thyratron G_1, through a resistor R_2. During the charging period of the generator the anode of G_1 is maintained at a positive potential of 20 kV, a suitable negative voltage being applied to the grid by means of the battery B_1. On the application of a trigger pulse to the grid the thyratron becomes ionized and a negative impulse of 20 kV is generated at the anode.

The oscillograph sweep circuit is initiated on closing the switch S_1 by the application to its own tripping circuit of an impulse of several hundred volts. This same impulse, provided that it is positive, can be applied to the grid of G_1 to trip the generator. The inherent time-delay of the thyratron ensures that the sweep circuit begins to operate before the start of the high-voltage impulse. A further delay can be introduced if required by means of a capacitance-resistance circuit to flatten the wave-front of the voltage applied to the thyratron grid.

With the above system the generator is tripped at a voltage below the normal break-down voltage of the spark gaps. The output voltage is controlled by the application of the tripping voltage, by means of the hand-operated switch S_1, when the voltage of the first stage has reached a pre-determined value. This voltage is read on an electrostatic voltmeter V connected across a suitable portion of the

resistor R_1. White has also described a simple thyratron circuit which enables the output voltage of the generator to be controlled automatically.

HUSBANDS and HIGHAM[60] have described several circuits involving three-sphere gaps, illuminated gaps and 'Trigatron' gaps[65], for the control of the operation of impulse generators in conjunction with cathode-ray oscillographs or rotating-mirror cameras.

Figure 155 illustrates a 'Trigatron' gap which has been used to form the first gap of a twelve-stage 2,000 kV generator. The high-voltage electrode is a sphere. The earthed electrode consists of a

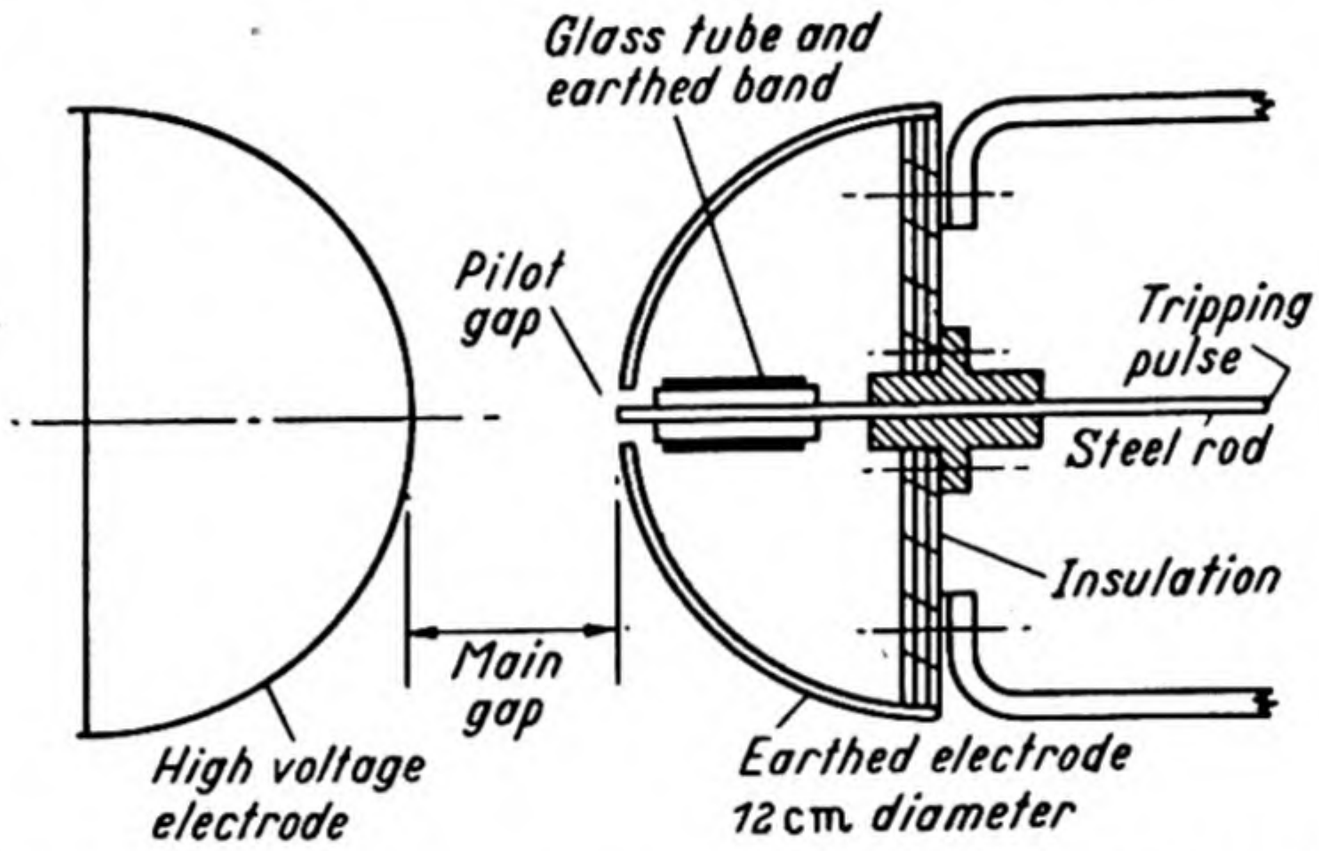

Figure 155. Triggered gap assembly (Husbands and Higham[60], by courtesy, *J. Sci. Instrum.*).

hemisphere in which is drilled a small hole into which projects a metal rod. The annular gap between the rod and the surrounding hemisphere is about 1 mm. A glass tube is fitted over the rod electrode and is surrounded by a metal foil which is connected to the earthed hemisphere. When a tripping pulse is applied to the rod the field is distorted in the main gap and the latter breaks down at a voltage appreciably lower than that required to cause its break-down in the absence of the tripping pulse. The function of the glass tube is to promote corona discharge round the rod as this causes photo-ionization in the annular gap and the main gap and consequently facilitates their rapid break-down. Further details concerning the mechanism of operation of 'Trigatrons' and their applications, have been given by CRAGGS, HAINE and MEEK[65] and are described in Chapter 6.

An impulse generator can then be charged to a particular voltage, less than that required to cause break-down of the main gap, and its operation produced by the application of a tripping pulse to the central rod. The gap of *Figure 155* has been used successfully in an impulse generator with charging voltages up to 167 kV, of either polarity. The tripping voltage required is only about 5 kV.

A circuit using the gap of *Figure 155* has been described by Husbands and Higham and is shown in *Figure 156*. The generator is used

together with a 50 kV continuously-evacuated oscillograph with a time-sweep circuit incorporating a three-sphere gap operating at 6 kV. When the time-sweep is initiated the voltage on one sphere falls rapidly from 6 kV to zero, and this provides a suitable pulse for the controlled tripping of the impulse generator. The application of this pulse directly to the first gap of the impulse generator may cause oscillations in the time-sweep circuit because of the large impulse currents, and therefore the intermediate single-stage impulse generator is introduced. This pulse generator is charged to 6 kV by the oscillograph time-sweep supply and is tripped through the gap G_2 by the illumination from the three-sphere gap of the time-sweep circuit. The gap G_2 is formed of two $\frac{1}{2}$ in. diameter spheres placed about $\frac{3}{4}$ in. from the time-sweep gap. The tripping pulse generator and the time-sweep circuit are therefore isolated from each other except for the connection of high resistances for charging purposes. It was found that the time lag, inherent in the break-down of the various gaps, provided insufficient delay in the tripping of the impulse generator, so the delay cable of *Figure 156* was introduced. This consisted of a 100 yd. length of cable, terminated at the first gap of the main generator by a matching resistance for the purpose of preventing successive reflections after the first gap of the main generator had broken down.

The above system makes use of the fact that the break-down voltage of a gap can be lowered below its normal value by intense illumination with ultra-violet light, as from a nearby spark. Measurements are recorded in which a gap with a normal break-down voltage of 10 kV has been caused to break down at 8 kV when illuminated (*see* page 279). This effect has been applied also by STEKOLNIKOV in the synchronization of an impulse generator and an oscillograph[66].

With the circuit of *Figure 156* the delay in the start of the wave-front on the oscillograms was about 0·5 μsec. This interval varied by 0·1 μsec over a long period when using a single-stage generator

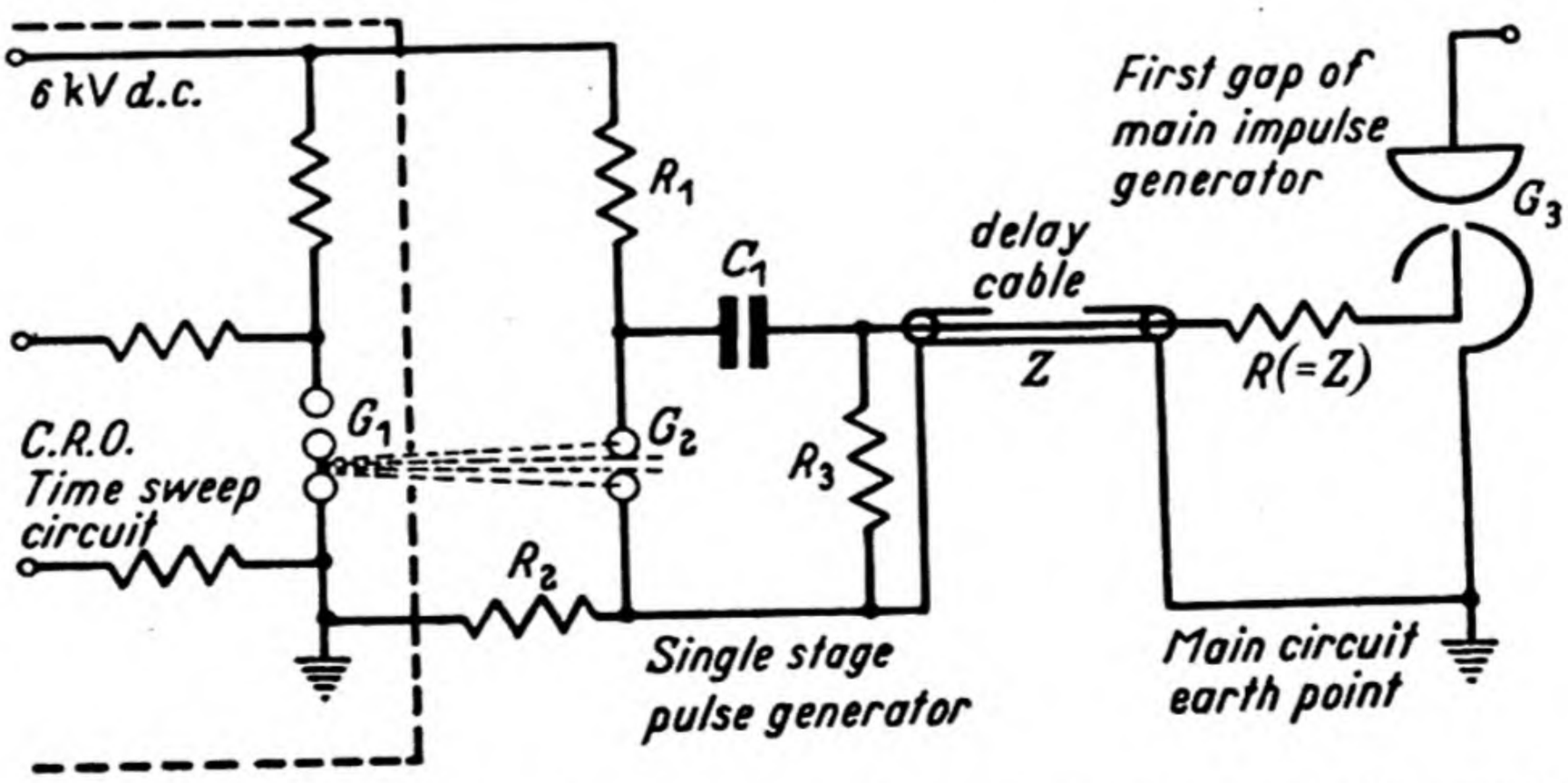

Figure 156. Circuit to trip an impulse generator from the oscillograph time-sweep circuit. $R_1 = 5\ M\Omega, R_2 = \cdot 05\ M\Omega, R_3 = 1\ M\Omega, C_1 = 0.001\ \mu F$. (Husbands and Higham[60], by courtesy, *J. Sci. Instrum.*).

operated at 100 kV, but over daily periods the delay was more consistent. With a multi-stage generator the total delay time, and its fluctuations, are influenced by the break-down characteristics of the multiple spark gaps. A twelve-stage 2,000 kV generator was tripped with an accuracy of $\pm 0{\cdot}5\ \mu$sec in synchronism with a 50 kV cathode-ray oscillograph. An eight-stage 1,000 kV generator was much more erratic until it was modified so that all its spark gaps were in line, as in the larger generator, and each gap was therefore irradiated from its neighbour (*see* page 144).

Circuits for synchronizing the operation of an impulse generator with a rotating-mirror camera are described by Husbands and Higham[60] and by PRIME and SAXE[62]. Both these circuits derive an initial tripping pulse from a photo-multiplier which is illuminated by a collimated light-beam reflected by the mirror once in each

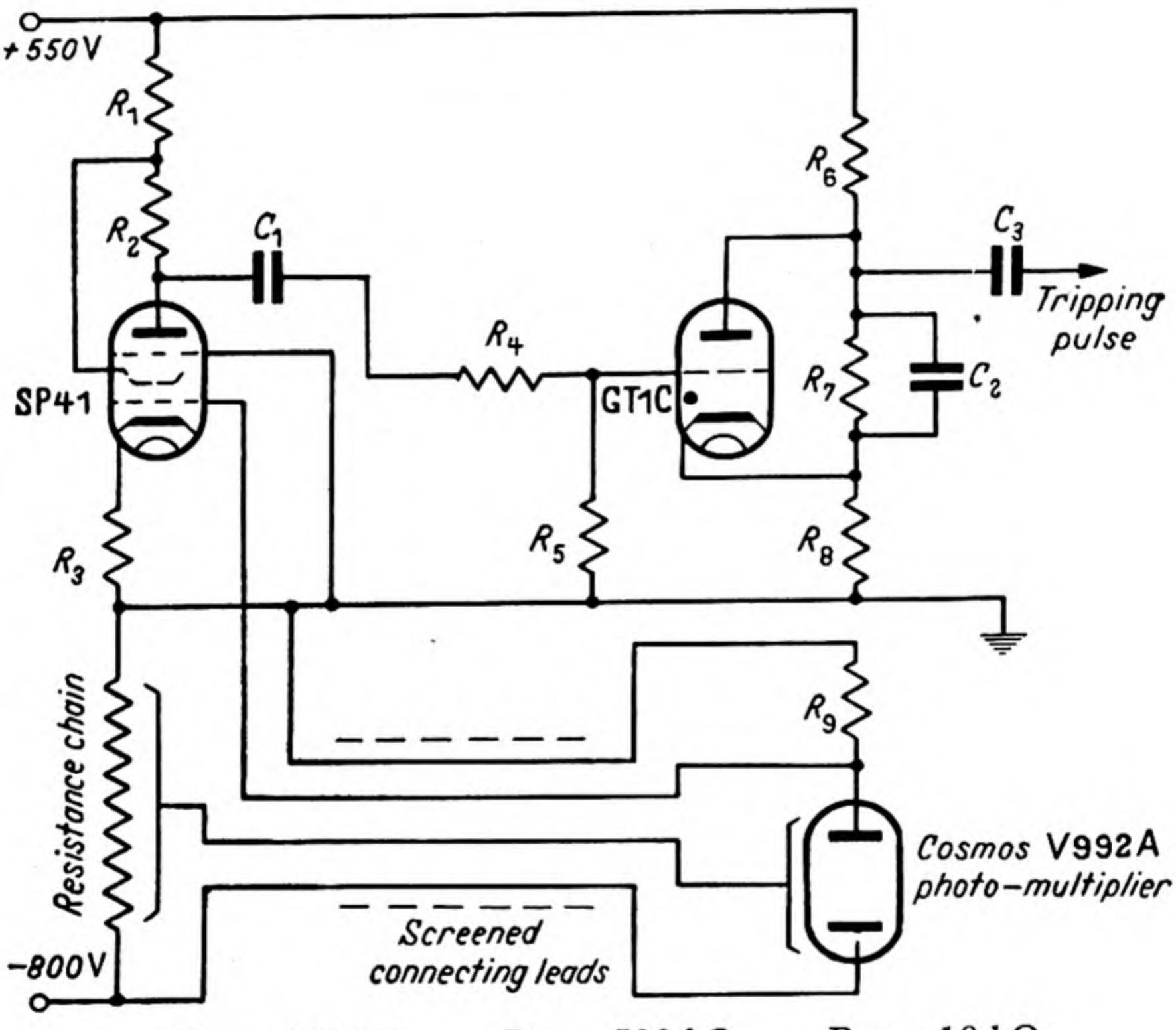

$R_1 = 100\ k\Omega$ $R_5 = 500\ k\Omega$ $R_9 = 10\ k\Omega$
$R_2 = 1{\cdot}1\ k\Omega$ $R_6 = 22\ k\Omega$ $C_1 = 0{\cdot}1\ \mu F$
$R_3 = 100\Omega$ $R_7 = 50\ k\Omega$ $C_2 = 0{\cdot}01\ \mu F$
$R_4 = 20\ k\Omega$ $R_8 = 4\ k\Omega$ $C_3 = 0{\cdot}01\ \mu F$ (7 kV)

Figure 157. Tripping circuit for use with a rotating-mirror (Husbands and Higham[60], by courtesy, *J. Sci. Instrum.*).

revolution. In this way the generator is tripped, and a spark is produced, when the rotating-mirror is in a suitable position to enable the growth of the spark to be photographed. The circuit used by Husbands and Higham is given in *Figure 157*.

REFERENCES

[1] BRITISH STANDARD No. 923–1940. "Impulse voltage testing."
[2] INTERNATIONAL ELECTROTECHNICAL COMMISSION: Publication 60, 1938.

[3] VERBAND DEUTSCHER ELEKTROTECHNIKER: Specification 0450, 1939.
[4] AMERICAN STANDARDS ASSOCIATION: Specification C.68.1, 1942.
[5] EDWARDS, F. S., HUSBANDS, A. S., and PERRY, F. R. *Proc. Inst. elect. Engrs.*, **98** (1951) 155.
[6] GRÜNEWALD, F. *Elektrotech. Z.*, **42** (1921) 1377.
[7] MARX, E. Deutsches Reichspatent No. 455933.
[8] MARX, E. *Elektrotech. Z.*, **45** (1924) 652.
[9] MARX, E. *Mitteilungen der Hermsdorf-Schomburg-Isolatoren G.M.B.H.*, **17** (1925) 466.
[10] MARX, E. *Hochspannungspraktikum.* Berlin, 1941.
[11] GOODLET, B. L. *J. Inst. elect. Engrs.*, **67** (1929) 1177.
[12] GOODLET, B. L. British Patent No. 344862.
[13] PEEK, F. W. *Dielectric Phenomena in High-Voltage Engineering.* New York, 1929.
[14] MINER, D. F. *Elect. J.*, **23** (1926) 596.
[15] MINER, D. F. *Insulation of Electrical Apparatus.* New York, 1941.
[16] BOUWERS, A. *Elektrische Höchstspannungen.* Berlin, 1941.
[17] ACKERMANN, O. *Elect. J.*, **29** (1932) 61.
[18] ELSNER, R. *Fachberichte des Verbandes Deutscher Ingenieure*, **8** (1936) 159.
[19] EDWARDS, F. S. *C.I.G.R.E. Paper* No. 305, 1939.
[20] EDWARDS, F. S., and SCOLES, G. J. British Patent No. 498021.
[21] NEWMAN, M., and KEMPPAINEN, O. *Proc. Inst. Rad. Engrs.*, **34** (1946) 247.
[22] *Micafil News*, December, 1939, page 21.
[23] EATON, J. R., and GEBELEIN, J. P. *Gen. Elect. Rev.*, **43,** (1940) 322.
[24] THOMASON, J. L. *Trans. Amer. Inst. elect. Engrs.*, **53** (1934) 169.
[25] THOMASON, J. L. *Trans. Amer. Inst. elect. Engrs.*, **56** (1937) 183.
[26] MCAULEY, P. H., and BENEDICT, F. R. *Elect. J.*, **30** (1933) 326.
[27] RAWCLIFFE, G. H. *Phil. Mag.*, **34** (1943) 353.
[28] FISHER, E. *J. appl. Phys.*, **14** (1943) 341.
[29] ANGELINI, A. M. *C.I.G.R.E. Paper* No. 335, 1950.
[30] BELLASCHI, P. L. *Trans. Amer. Inst. elect. Engrs.*, **51** (1932) 936.
[31] FOREST, C. M., KUEHNI, H. P., and ROHATS, N. *Gen. Elect. Rev.*, **35** (1932) 358.
[32] BRITISH ELECTRICAL AND ALLIED INDUSTRIES RESEARCH ASSOCIATION. *Surge Phenomena.* London, 1941.
[33] LEWIS, A. B. *J. Res. Nat. Bur. Stand.*, **17** (1936) 585.
[34] GOODLET, B. L. *J. Inst. elect. Engrs.*, **74** (1934) 377.
[35] EDWARDS, F. S., and SCOLES, G. J. *Engineering*, **144** (1937) 222.
[36] EDWARDS, F. S. *J. Sci. Instrum.*, **14** (1937) 361.
[37] EDWARDS, F. S. *Metropolitan-Vickers Gaz.*, September, 1935.
[38] HENDRICKS, A. B., HUBBARD, H. S., and VALLIN, G. L. *Gen. Elect. Rev.*, **42** (1939) 420.
[39] ALLIBONE, T. E., EDWARDS, F. S., and MCKENZIE, D. B. *Nature*, **131** (1933) 129.
[40] CRÄMER, R. *Elektrotech. Z.*, **57** (1936) 1227.
[41] BOLDINGH, H. *Philips Tech. Rev.*, **3** (1938) 302.
[42] BERGER, K., and SCHNEEBERGER, E. *Bull. Assoc. Suisse Elect.*, **24** (1933) 325.
[43] BUSS, K. *Elektrotech Z.*, **59** (1938) 437.
[44] CRÄMER, R. *A.E.G. Mitt.*, 1938, page 85.
[45] BELLASCHI, P. L. *Elect. J.*, **115** (1935) 500.
[46] BELLASCHI, P. L. *Trans. Amer. Inst. elect. Engrs.*, **56** (1937) 1253.
[47] SMUROFF, A. *Elektrichestvo*, **58** (1937) 18.
[48] SMUROFF, A. *Elektrotech. Z.*, **58** (1937) 384.
[49] ROKKAKU, H., and SHINGU, Y. *Elektrotech J., Tokyo*, **1** (1937) 75.
[50] METRAUX, A. *Bull. Assoc. Suisse Elect.*, **30** (1939) 343.
[51] SCHMIDT, K. *Elektrotech. Z.*, **62** (1941) 93.
[52] GOREV, A. A., and MASCHKILLEISON, L. E. *Elektrichestvo*, **58** (1937) 18.

[53] GOREV, A. A., and RABOV, B. *Elektrichestvo*, May, 1941, page 31.
[54] CIVILETT, J. A. *Elect. J.*, **35** (1938) 449.
[55] TRACHMANN, H. *A.E.G. Mitt.*, 1938, page 529.
[56] REBHAN, J. *Elektrotech. Z.*, **56** (1935) 1041.
[57] REBHAN, J. *Siemens Z.*, **15** (1938) 505.
[58] ROHATS, N. *Gen. Elect. Rev.*, **37** (1934) 296.
[59] LUSIGNAN, J. T., and RORDEN, H. L. *Trans. Amer. Inst. elect. Engrs.*, **53** (1934) 1255.
[60] HUSBANDS, A. S., and HIGHAM, J. B. *J. Sci. Instrum.*, **28** (1951) 242.
[61] WHITE, E. L. *J. Sci. Instrum.*, **25** (1948) 307.
[62] PRIME, H. A., and SAXE, R. F. *Proc. Inst. elect. Engrs.*, **96** (1949) 662.
[63] SNODDY, L. B., and STREET, J. C. *Gen. Elect. Rev.*, **34** (1931) 258.
[64] ROHATS, N. *Electronics*, **19** (1946) 135.
[65] CRAGGS, J. D., HAINE, M. E., and MEEK, J. M. *Proc. Inst. elect. Engrs., Pt. 3a* **93** (1946) 963.
[66] STEKOLNIKOV, I. S. *C.I.G.R.E. Paper* No. 129, 1937.
[67] ALLIBONE, T. E., HAWLEY, W. G., and PERRY, F. R. *J. Inst. elect. Engrs.*, **75** (1934) 670.
[68] HAGENGUTH, J. H. *Gen. Elect. Rev.*, September, 1949.
[69] SPRAGUE, C. S. *Trans. Amer. Inst. elect. Engrs.*, **54** (1935) 1100.
[70] GUGEL, H. *C.I.G.R.E. Paper* No. 122, 1939.
[71] PAASCHE, P. *Elektrotech. Z.*, **64** (1943) 295.
[72] MARGUERRE, W. *Elektrotech. Z.*, **59** (1938) 1205, 1234.
[73] MARGUERRE, W. *Elektrotech. Z.*, **60** (1939) 837.

5

GENERATION OF HIGH-CURRENT IMPULSES

High-current impulse generators usually consist of a number of capacitors connected in parallel to the common discharge path. The equivalent circuit is given in *Figure 158* and approximates to that of a capacitance C charged to a voltage V which can be considered to discharge through an inductance L and a resistance R. In practice both L and R are effectively distributed throughout the circuit, in the leads and in the capacitors themselves as well as in the test object.

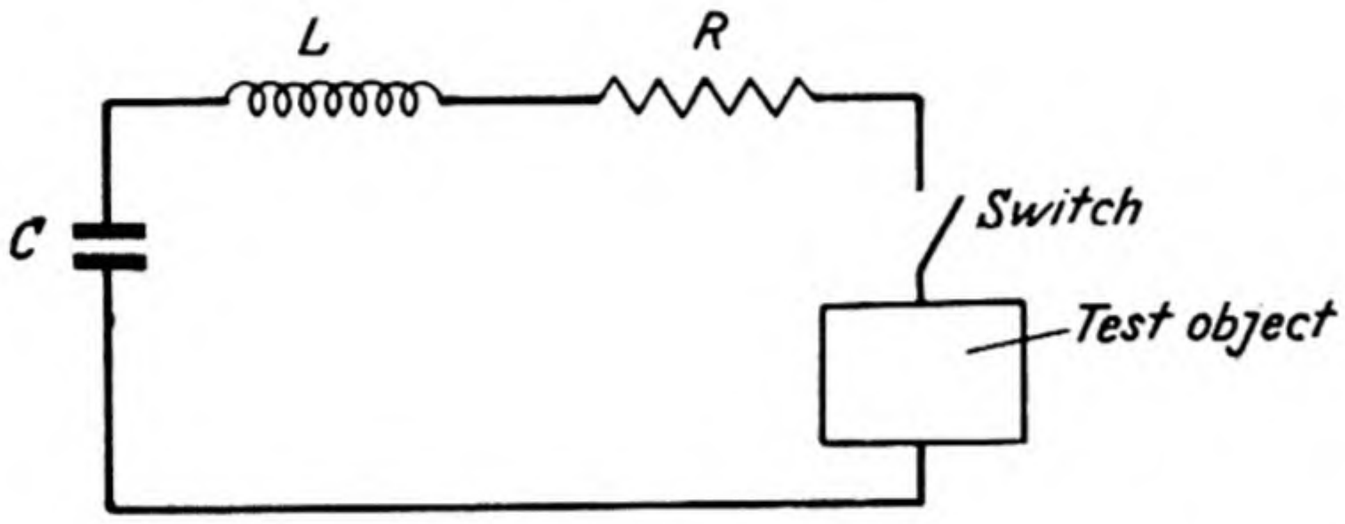

Figure 158. Equivalent circuit for a high-current impulse generator (McEachron and Thomason[5], by courtesy, *Gen. Elect. Rev.*).

In the oscillatory case, where $R < 2\sqrt{\frac{L}{C}}$, the current impulse wave is

$$I = \frac{V}{\omega L} e^{-\alpha t} \sin \omega t \qquad \ldots\ldots(5.1)$$

where $$\omega = \left[\frac{1}{LC}\left(1 - \frac{C^2R^2}{4L}\right)\right]^{\frac{1}{2}}$$

and $$\alpha = \frac{R}{2L}$$

The time for the current to rise from zero to its first maximum value I_m is

$$t_m = \sqrt{LC}\,(1-r^2)^{-\frac{1}{2}} \sin^{-1}(1-r^2)^{\frac{1}{2}} \qquad \ldots\ldots(5.2)$$

where $$r = \frac{R}{2}\sqrt{\frac{C}{L}}$$

The magnitude I_m of the first current peak is given by

$$I_m = V\sqrt{\frac{C}{L}} \exp\left[\frac{-r\sin^{-1}(1-r^2)^{\frac{1}{2}}}{(1-r^2)^{\frac{1}{2}}}\right] \qquad \ldots\ldots(5.3)$$

$$= V\sqrt{\frac{C}{L}} f(r) \qquad \ldots\ldots(5.4)$$

$$= \sqrt{\frac{2W}{L}} f(r) \qquad \ldots\ldots(5.5)$$

where $W = \frac{1}{2}CV^2$, the initial energy.

From Equation 5.5, I_m is nominally independent of the individual values of V and C for a given initial energy W and effective inductance L. To obtain the maximum value of I_m for a given initial energy W the main requirement is that L should be small. In circuits of normal construction, without added damping, the factor $f(r)$ is usually between 0·85 and 0·95.

Unidirectional impulses can be produced by damping with additional resistance. This results in a large reduction in the value of I_m, *e.g.* for critical damping I_m falls to 0·368 times the loss-free value of $V\sqrt{\frac{C}{L}}$. Foitzik[10] has shown, however, that an approximately unidirectional wave-form can be obtained by the use of a non-linear damping resistance in the circuit with a reduction in I_m to only about 0·7 times the loss-free value.

By the sub-division of C into groups of smaller units the value of the effective inductance L can be reduced. Durnford and Reynolds[15] point out that, if there are n_1 equal groups of capacitors each consisting of n_2 equal capacitor units, and if L_0 is the inductance of the common discharge path, L_1 that of each group lead and L_2 that of each unit, then the total inductance L is given by

$$L = L_0 + \frac{L_1}{n_1} + \frac{L_2}{n_1 n_2} \qquad \ldots\ldots(5.6)$$

The extent to which it is necessary to subdivide C depends on the relative values of L_0, L_1, and L_2. In generators such as that described by Durnford and Reynolds, where L_0 is of the order of 0·1 μH, it is not always practicable to reduce L_1 and L_2 and to increase n_1 and n_2 sufficiently for the contribution of these quantities to be negligible. It is then important that the $L\,C$ products of the various groups should be about equal, as obtains with a ring arrangement of capacitors round a central discharge conductor, in order that all groups should supply currents in phase.

Impulse current generators have been constructed by a number of investigators. Some details of these generators are listed in *Table XII.*

The generator developed by Durnford and Reynolds[15] contains 114 capacitor units, each of 0·5 μF, which can be charged up to a maximum voltage of 25 kV. The units are connected in parallel in 38 equal groups and are arranged in columns of six units to form the sides of a square with one column omitted to give access to the central spark-gap assembly. This arrangement favours a low inductance and also gives an approximately uniform distribution of current round the coaxial shunt. Short lengths of coaxial cable connect each group to the central spark gap. The choice of 38 groups is a compromise between practical considerations of construction and the need for a low inductance.

This particular generator is being used primarily to produce high-current spark discharges across gaps in air and other gases so that certain features of high-current discharges in gases can be studied[18].

TABLE XII

DATA ON HIGH-CURRENT GENERATORS

	C	*V*	*W*	*I*	*L*	$2\pi/\Omega$	**Circuit resistance*	*Shunt resistance*
Investigator	μF	kV	kWsec	kA	μH	μsec	Ω	Ω
Bellaschi[1]	14·9	75	41·9	100	—	~50	—	—
Rohats[2]	14·4	10	7·2	120	0·58	58	0·0073	0·01
Bellaschi[3]	16	100	80	150	3·5	45	—	—
McEachron and Thomason[5]	53	150	60	265	1·47	17·6	0·0463	0·0053
Foitzik[10]	48	52	65	330	1·12	44	—	0·003
Stekolnikov[13]	34·3	61·5	65	438	0·67	30	0·0054	0·002
Durnford and Reynolds[15]	58·5	25	18·2	470	0·104	15·5	0·0068	0·0018

* Resistance of capacitors and leads but excluding resistance of shunt.

The spark-gap assembly is shown in *Figure 159* and includes the coaxial shunt which is supported from the lower plate. The resistive element of the shunt lies in the radial path of the current outward

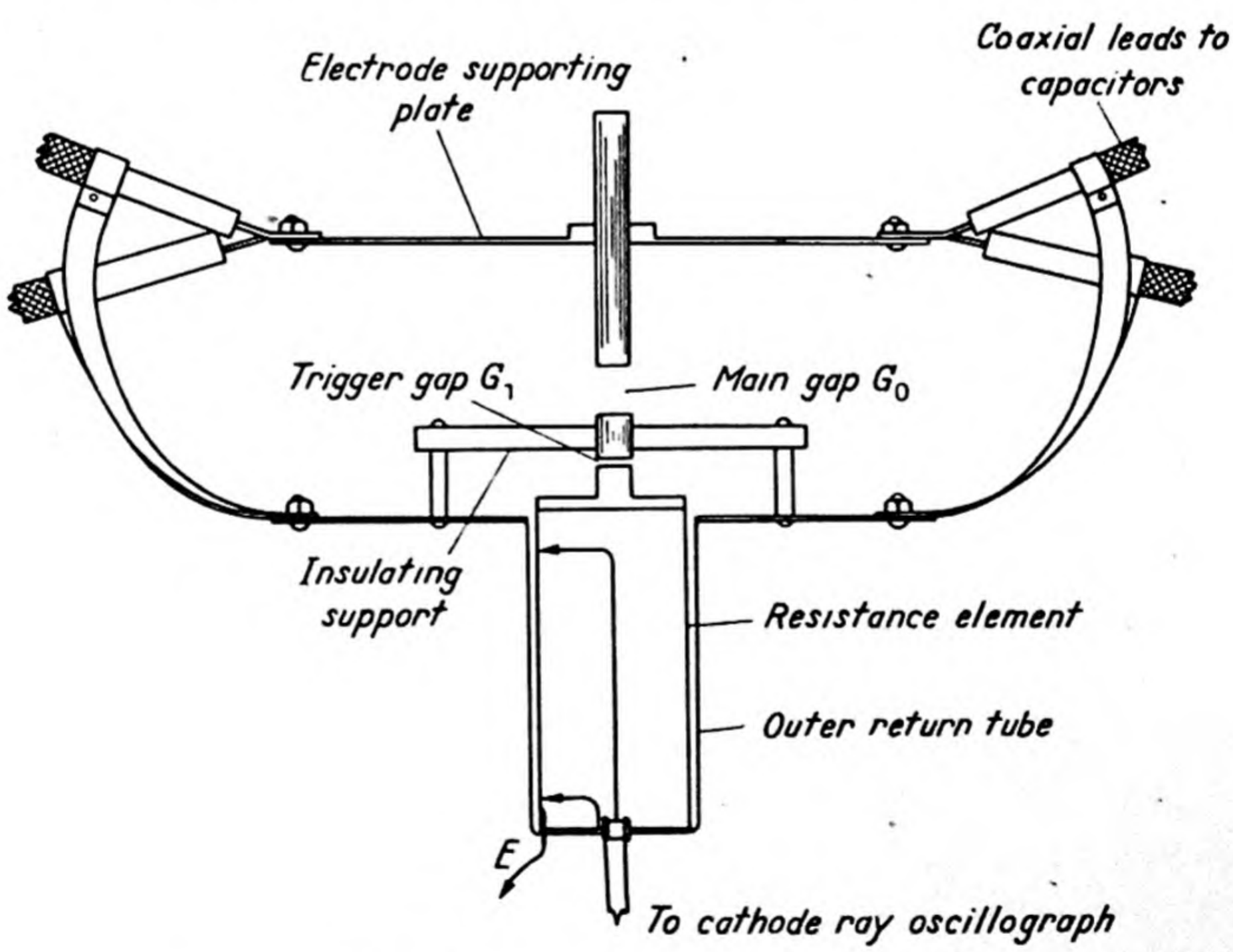

Figure 159. Spark-gap assembly and coaxial shunt.

from the bottom electrode. The voltage developed between the tapping points is taken through a coaxial lead to a cathode-ray oscillograph.

The generator and measuring circuits are connected to the main laboratory earth by a single path. The choice of the point of connection of this earth lead to the generator is of importance in relation to the reduction of interference in the measuring circuit by the currents that flow through the stray capacitance between different parts of the circuit and to earth (*see* page 162). In the above generator the earth lead is connected to the bottom of the shunt at a point close to the low-voltage tapping-point, *i.e.* at *E* of *Figure 159*. This has the object of keeping down the difference in voltage between *E* and the measuring circuit due to the main current and minimizes the flow of current in the measuring circuit leads and to earth through stray capacitances. The metal cases of the capacitor units are separately connected, also by a single lead, to the laboratory earth. As the mean voltage of the units changes by 0·5 V with respect to the point *E* when the main discharge is initiated, circulating currents flow through the stray capacitance between the units and their cases and round the loop completed by the group leads and the leads to earth from *E* and from the cases.

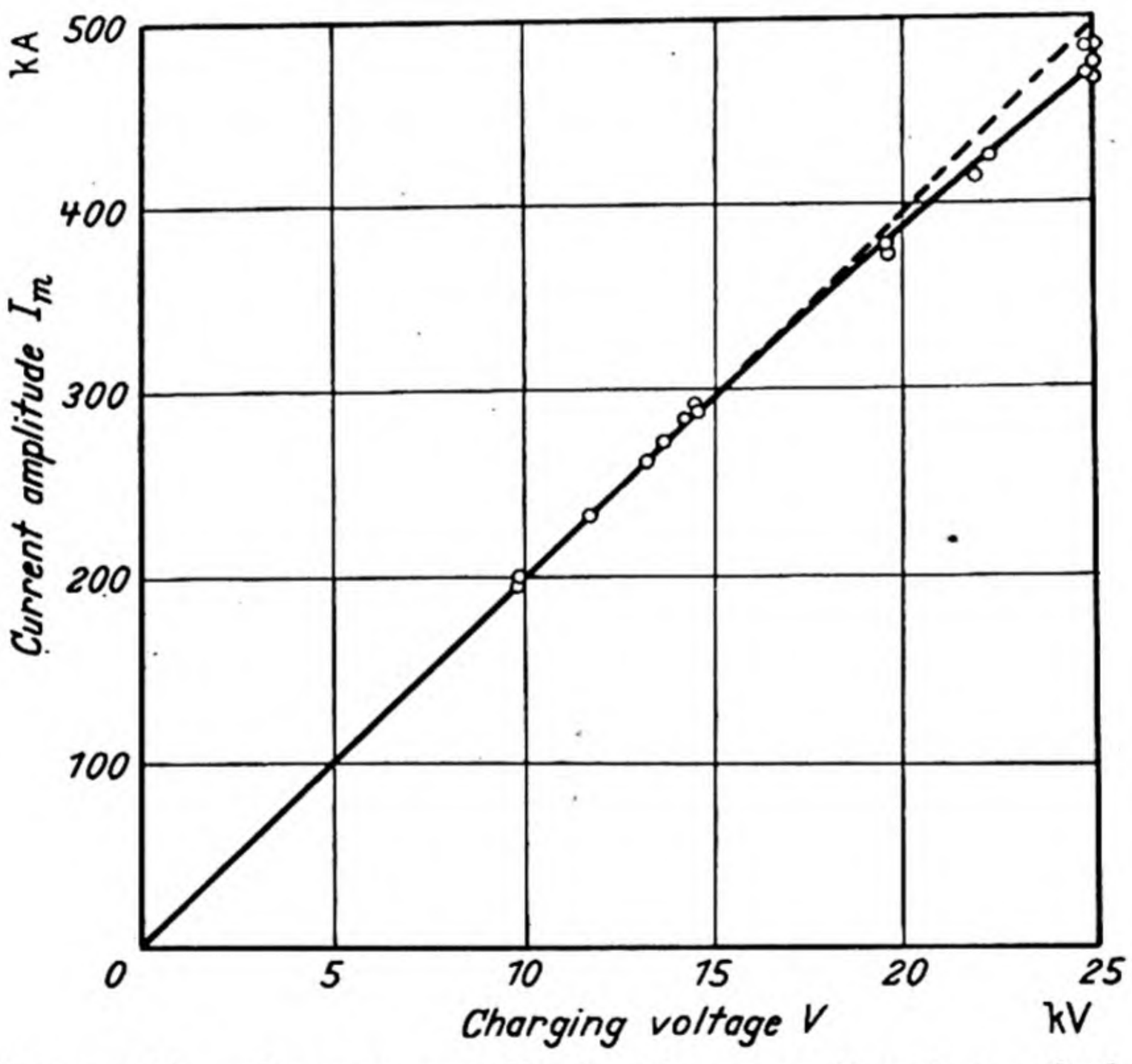

Figure 160. Current amplitude I_m as a function of the charging voltage *V*.

Although these currents are small in magnitude, relative to the main discharge current, it has been necessary for certain experiments to insert a damping resistance of several hundred ohms in each of the two leads to earth. Further consideration of these effects is given on page 162.

The discharge of the generator is initiated by applying a trigger voltage, from a small auxiliary impulse generator, to an electrode in

series with the main gap. The arrangement is shown in *Figure 159*. The trigger voltage increases the voltage across the main gap G_o above V and causes the break-down of G_o and G_1 in sequence. With a trigger voltage of up to V in magnitude the length of G_o may be increased beyond that corresponding to V and up to a limit slightly less than $2V$ provided that G_1 withstands the trigger voltage but breaks down after G_o.

The value of I_m, as measured with the low-resistance shunt described on page 164, is plotted in *Figure 160* as a function of the charging voltage V for a 3·5 in. spacing between the plates of the gap assembly. The slight loss of proportionality between I_m and V results mainly from the increase in the total resistance R of the current circuit both with gap length and with current.

Oscillograms of the current wave-form, with a discharge voltage of 25 kV, have shown that a current $I_m = 466$ kA is attained in 4·2 μsec with an initial rate of rise of 167 kA/μsec. The wave-form mainly follows Equation 5.1 but appreciable variations occur in the period and decrement of the oscillatory discharge and can be attributed to the varying non-linear impedance of the spark discharge. The value of I_m decreases with increasing spacing between the plates and falls from 466 kA at 3·5 in. spacing to about 310 kA at 15·5 in. spacing.

THEORETICAL CONSIDERATIONS OF THE DESIGN OF RESISTANCE SHUNTS FOR THE MEASUREMENT OF HIGH-CURRENT IMPULSES

The usual method of measuring impulse currents is to record oscillographically the wave-form of the voltage developed across a low-resistance shunt. The shunt is required to have an effective impedance that is essentially equal to the d.c. resistance between the tapping-points and is constant over the required frequency range. Further, its form and manner of connection should minimize interference with the measuring circuit by the main impulse current.

The basic forms of shunt used derive from the low-resistance standards of low time-constant as used for the measurement of power-frequency currents[19, 20]. Two forms widely used consist of a number of elements of thin wire[1, 40] or strip[9, 19, 20] connected in parallel, with each element folded to reduce its inductance. More recently tubular forms, which give improved screening of the measuring circuit from interference, have been developed[21, 15].

The design of shunts for the measurement of high-current impulses has been discussed in some detail by PARK[21] whose analysis is followed in close detail in this section. Park points out that three important factors need to be considered, namely, (1) the effective impedance of the shunt must be constant over as great a frequency-range as possible, (2) inductive effects of parts of the current circuit, other

than the shunt, upon the voltage-lead circuit of the shunt should be a minimum, and (3) it must be possible to connect the sheath of the cable joining the shunt to the cathode-ray oscillograph to ground at or near the shunt without causing induced voltages in the shunt voltage circuit (this is necessary to minimize the flow of ground currents in the sheath of the cable as this may cause induced voltages on the oscillograph plates).

To meet requirement (1) it is desirable that the impedance of the shunt, including skin effect, can be calculated for all frequencies within the required range. Two types of shunt construction for which calculations are possible are the coaxial tubular form and the folded flat strip. These are illustrated in *Figure 161*, which also

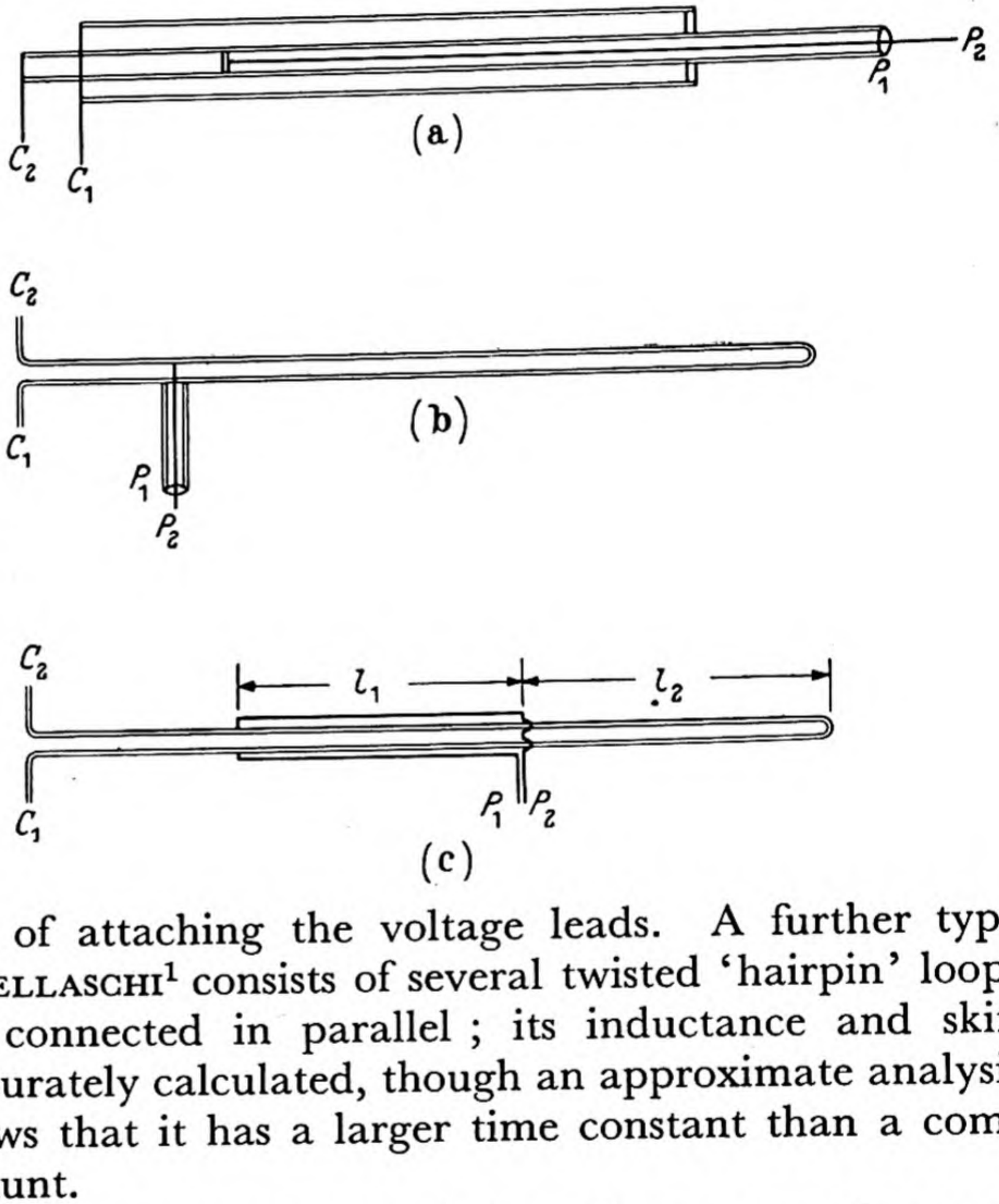

Figure 161. Three types of shunts whose inductance and skin effect can be computed. *a*, Coaxial tube shunt; *b*, flat strip shunt; *c*, flat strip shunt with potential leads arranged to give minimum inductance (Park[21], by courtesy, *J. Res. Nat. Bur. Stand.*).

shows the method of attaching the voltage leads. A further type of shunt used by BELLASCHI[1] consists of several twisted 'hairpin' loops of resistance wire connected in parallel; its inductance and skin effect cannot be accurately calculated, though an approximate analysis by BROWNLEE[9] shows that it has a larger time constant than a comparable flat strip shunt.

Park[21] has compared the constancy of the effective impedance of tubular and flat strip shunts for a range of frequencies. Two typical designs of shunt are assumed and their inductance and skin effect are calculated from the above formulae. One design is a coaxial tube shunt in which the resistance material is a copper-nickel alloy ($\rho = 22{\cdot}9 \times 10^{-6}\ \Omega$/cm.) tube with an outer diameter of 0·25 in. and a wall thickness of 0·008 in. The second design is a strip shunt, again with a wall thickness of 0·008 in. and with a width the same as the

circumference of the tube; the separation between the strips is taken to be 0·01 in. The shunt length does not affect the calculations provided it is several times the largest transverse dimension. The time constants for the shunts are calculated to be $L/R = 0{\cdot}0365 \times 10^{-6}$ for the tubular shunt and $L/R = 0{\cdot}218 \times 10^{-6}$ for the strip shunt. The skin effects at $f = 1$ Mc/s are calculated by Park from formulae given by SILSBEE and yield $R/R_{dc} = 0{\cdot}959$ for the tubular shunt and $R/R_{dc} = 0{\cdot}955$ for the strip shunt. These values are incorrect at frequencies above 1 Mc/s as the skin effect then causes a non-uniform distribution of current density over the thickness of the tube or strip. The calculations therefore show that the tubular shunt has a much lower time constant than the strip shunt which means that its reactance is negligible over a wider frequency range. The skin effect is about the same but the formula used for the calculation for the strip shunt neglects edge effects that are known to increase the skin effect at higher frequencies[21]. The tubular shunt has no edge effects and therefore its effective resistance may be expected to change less than that of the strip shunt at the higher frequencies. A decrease in both inductance and skin effect can be obtained by a reduction in the thickness of the material used but improvement in this manner is limited because of the temperature rise of the shunts. From the above considerations it would appear that the tubular shunt is preferable to the strip shunt as regards its frequency characteristics, but it is more difficult to construct.

Formulae for computing the inductance (assuming uniform distribution of current) of the folded strip shunt have been given by Silsbee[19, 20] and by Brownlee[9]. Silsbee's formula is as follows:—

$$L = 4l\left[\frac{\pi}{3}(3\beta-\delta) - \frac{25}{12}\beta^2 - \frac{\beta^4}{12} - \frac{\beta^2\delta^2}{12} + \frac{1}{12\delta^2}\left\{\alpha^4\log\alpha - 2\beta^4\log\beta - \gamma^4\log\gamma - 2\delta^4\log\delta\right\}\right] \times 10^{-3} \quad \mu H/\text{cm} \qquad \ldots\ldots(5.7)$$

where $\alpha = \dfrac{2b+g}{w}$, $\beta = \dfrac{b+g}{w}$, $\gamma = \dfrac{g}{w}$, $\delta = \dfrac{b}{w}$

and w cm. is the strip width, b cm. is the strip thickness and g cm. is the gap between the adjacent sides of the folded strip.

Corrections for non-uniform current distribution at high frequencies are complicated by edge effects[19, 20, 39]. For strips that are wide in relation to their separation, *i.e.* $w \gg g$, Silsbee quotes for the ratio of the high-frequency resistance R_{ac} to the d.c. resistance R_{dc}

$$\frac{R_{ac}}{R_{dc}} = 1 + \frac{m^4 d^4}{45} - \frac{m^8 d^8}{4725} \qquad \ldots\ldots(5.8)$$

where $m = 2\pi\sqrt{\dfrac{2f}{\rho}} \times 10^{-9}$

d is the conductor thickness in centimetres and ρ is the resistivity in Ω/cm cube.

ARNOLD[40] has pointed out that for low-current shunts a smaller time-constant is obtainable with bifilar elements made of twisted, enamel-covered wire than with folded strips.

The coaxial form of shunt has been considered in detail for power frequency purposes by Silsbee[19, 20]. With the connections of *Figure 161a* the inductance, for uniform current distribution, is

$$L = \frac{d}{3a} \times 10^{-3} \ \mu\text{H/cm} \qquad \ldots.(5.9)$$

where a cm. is the inner radius of the shunt tube and d cm. is the thickness of the shunt-tube wall.

Park[21] gives the derivation of a formula previously developed by Silsbee (unpublished) that enables the impedance of a coaxial shunt to be calculated for frequencies up to 10^9 c/s or higher. According to Silsbee's calculations the impedance of the coaxial tubular shunt is given by

$$Z = R_{dc} \frac{(1+j)\,\delta}{sinh\,(1+j)\,\delta} \qquad \ldots.(5.10)$$

where

$$\delta = 2\pi d \sqrt{\frac{f\mu}{\rho}}$$

d is the thickness of the tube wall, f is the frequency, ρ is the resistivity of the tube material and μ is the magnetic permeability.

Actual values of R/R_{dc}, $\omega L/R_{dc}$ and $|Z|/R_{dc}$ as functions of δ are shown in the continuous-line curves of *Figure 162*. The broken-line curves are calculated from formulae applicable to lower frequencies, L' being given by Equation 5.9 and R' by the following formula as derived by Silsbee[20]

$$R' = R_{dc}\,(1 - \tfrac{7}{90}\delta^4) \qquad \ldots.(5.11)$$

For $\delta < 1$ the continuous-line and broken-line curves coincide, but for $\delta > 1$ the values obtained from Equations 5.9 and 5.11 exhibit rapidly increasing errors as is to be expected from the simplifying assumptions made in their derivation.

The inductive effects of the current-carrying leads other than the shunt upon the voltage-lead circuit of the shunt depend on the mutual inductance between the current-carrying leads and any loop in the voltage lead circuit, and also upon the maximum rate of change of the current. The maximum rate of change of current for a capacitance discharging through a resistance and inductance occurs at the instant the circuit is closed and is equal to the voltage V to which the capacitance is initially charged divided by the total inductance L of the circuit. With $L = 2\mu$H and $V = 100$ kV, the maximum rate of change of current is 5×10^{10}A/sec. This would induce 50 V in the voltage circuit of the shunt if the mutual inductance M between the two circuits is 0·001 μH. As a loop in the voltage-lead circuit of 1 cm^2

area placed close to a current-carrying part may have $M = 0{\cdot}002\ \mu$H the importance of minimizing the mutual inductance is apparent. If the surge generator discharge circuit is fairly long, and $L > 2\mu$H the maximum rate of change of current will not be correspondingly reduced as the stray capacitance across the discharge circuit will effectively short out the added inductance at the instant of initiation of the impulse.

The voltage leads of a tubular shunt, as shown in *Figure 161a* can be considered as an extension of the coaxial cable from the oscillograph ending in a short circuit between the central conductor and the sheath. Because of axial symmetry the mutual inductance between the voltage circuit and any current-carrying parts is the lowest obtainable. If the sheath of the cable is earthed, and earth currents flow in the

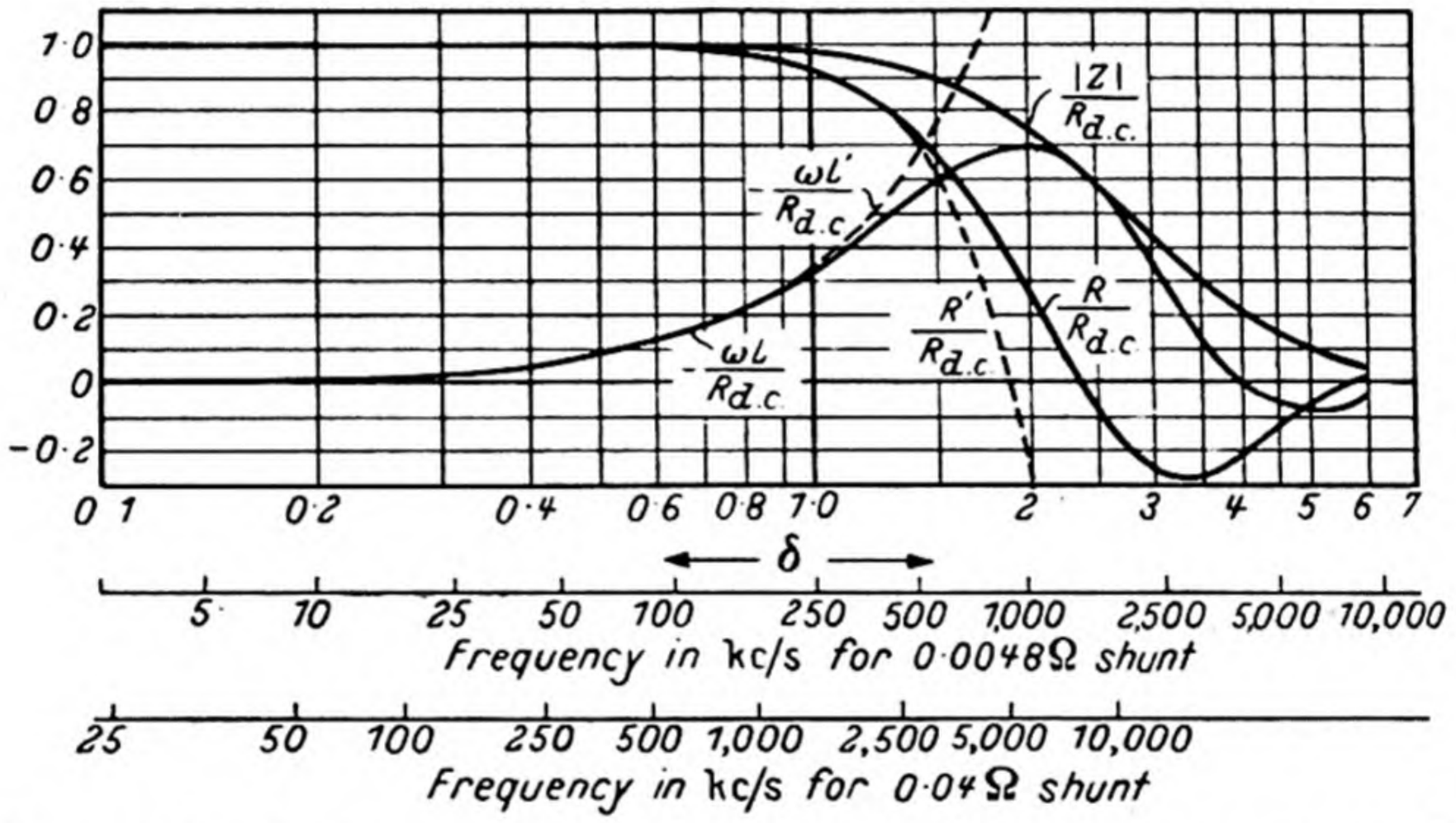

Figure 162. Curves showing ratios of a.c. resistance R, reactance ωL, and impedance Z, to d.c. resistance R_{dc}, plotted as ordinates against the parameter, δ, as abscissa. Abscissa scales in frequency are also shown for two tubular shunts. The continuous-line curves were obtained from Equation 5.10 and the broken-line curves from Equation 5.11 (Park[21], by courtesy, *J. Res. Nat. Bur. Stand.*).

sheath and in the outer current-return tube of the shunt, the earth currents will not induce voltages in the voltage circuit of the shunt provided the density of such currents is symmetrical around the axis of the shunt. End effects, or concentration of the current along one side of the shunt axis, can be largely eliminated by extending the two current-carrying tubes of the shunt several diameters beyond the end of the central conductor that serves as a voltage lead.

To reduce mutual inductance in the voltage circuit of a strip shunt the voltage leads can be taken off the strip as a central conductor and coaxial tube, as shown in *Figure 161b*. There still remains the small loop formed by the resistance material in the voltage lead and this makes possible inductive pick-up from any currents flowing in the sheath and one of the current leads to the voltage circuit. It is

not possible to separate the voltage circuit from end effects arising from such currents in a strip shunt. Although a strip shunt could be built with a low inductive pick-up between its voltage circuit and the current-carrying parts, the tubular shunt is the only design offering the possibility of entirely eliminating such inductive effects.

In the schematic diagram of an impulse-current generator given in *Figure 163* the heavy lines show the path of the impulse current from the capacitor *C* through the tripping gap, test object, measuring shunts and connecting leads. An earth connection is not essential but it is usual to connect the circuit to earth at some point between the low-voltage terminal of the capacitor and the test object in order to

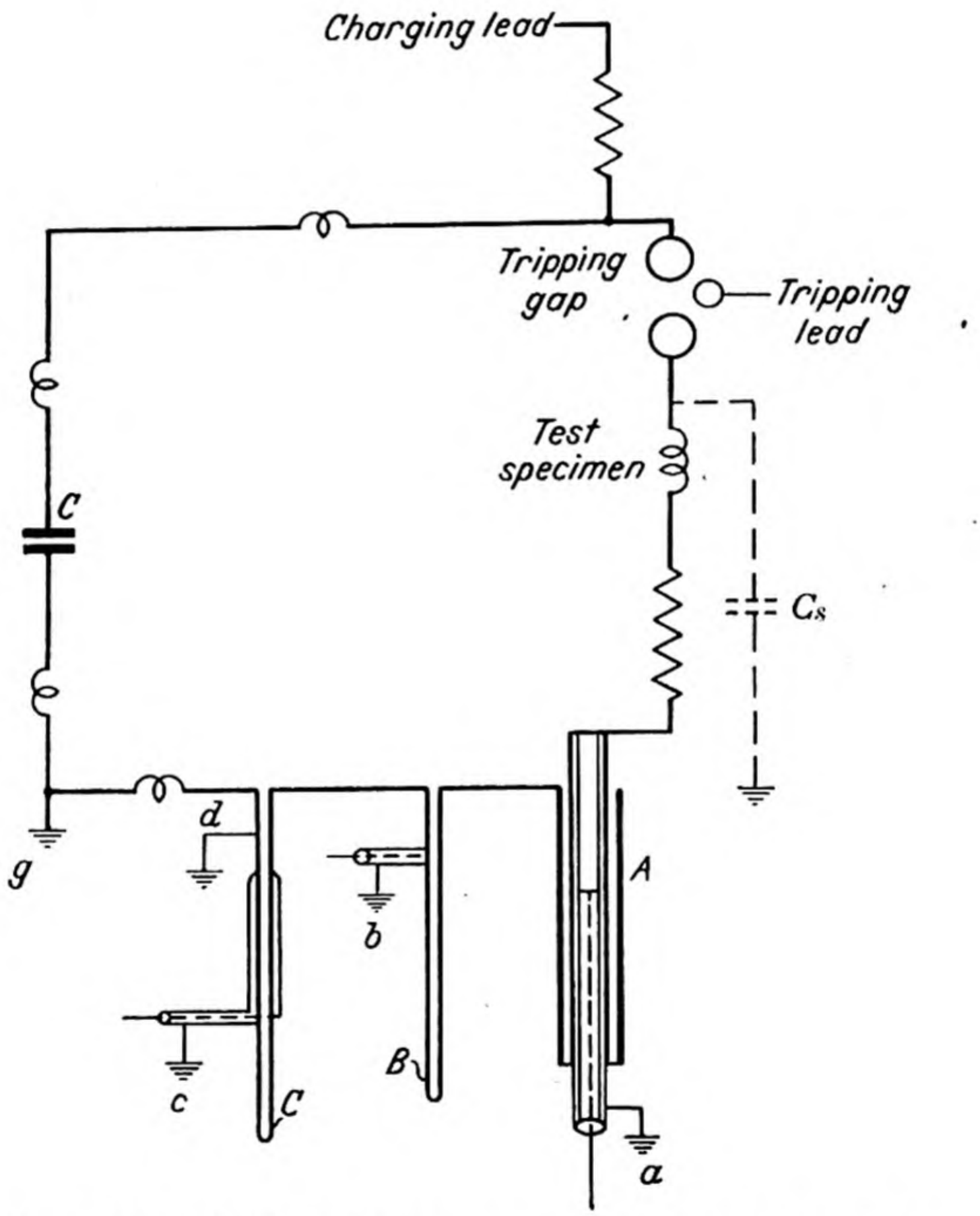

Figure 163. Wiring diagram of surge-current generator showing method of connecting shunts, their potential lead arrangement, and several possible ground connections (Park[21], by courtesy, *J. Res. Nat. Bur. Stand.*).

complete the charging circuit and to fix the voltages of the various parts of the discharge circuit with respect to earth. Assuming the connecting leads to be of round cross-section 0·5 in. in diameter their inductance is 0·01 μH per cm. length for a return at a considerable distance. For a maximum rate of change of current of 5×10^{10} A/sec the maximum voltage difference between two points 1 cm. apart in

the circuit is 500 V. Thus if the circuit is earthed at point *g* in *Figure 163* a shunt located only 10 cm. from *g* would be 5,000 V above earth at the instant of initiation of the discharge. This voltage tends to cause current to flow in the cable-sheath from the shunt to the oscillograph through the earth connection at the oscillograph and back to *g* through the laboratory earthing system. Because of the stray capacitance C_s from the lower ball of the tripping gap and from parts of the discharge circuit to earth, this voltage will be of a high-frequency oscillatory type occurring when the main current is initiated and any currents so caused will induce voltages of the same character in any coupled circuit. To minimize such effects at the oscillograph it is necessary that the cable from the shunt to the oscillograph should have its sheath earthed at or near the shunt. The influence of the stray capacitance C_s can be reduced by earthing other points in the discharge circuit, such as *g*, in addition to the cable-sheath. The best type of shunt would be one which would allow any or all of these earth connections to be made and still have minimum pick-up due to induced voltages from earth currents.

In *Figure 163* all the three shunts of *Figure 161* are included in order to assist the explanation of the effects of earth currents on each. The earth currents most likely to cause inductive pick-up are those due to the high-frequency oscillations arising from the effect of the stray capacitance C_s. In the case of the type *C* strip shunt, consideration of the possible earth connections in addition to the cable-sheath earth at the oscillograph leads to the following conclusions[21]:

(*a*) A single additional earth connection to the sheath at *c* would not be suitable, as then earth currents from C_s would flow in one potential lead of the shunt and induce high voltages in the loop formed by the voltage leads.

(*b*) A single additional earth connection at *g* would still permit sheath currents, which flow to earth at the oscillograph end of the cable, to flow through one of the shunt voltage leads.

(*c*) Two additional earths, one at *g* and one at *c*, would introduce a combination of the two above effects without the elimination of either.

(*d*) A single additional earth at *d* would reduce the inductive effects of earth currents but would not eliminate them entirely.

Thus the use of the type *C* shunt precludes the experimentally desirable flexibility in earth connections.

The above conclusions for the type *C* shunt also hold for the type *B* shunt except that all inductive effects are much less because the arrangement of the voltage leads ensures a lower mutual inductance between the voltage circuit and the current-carrying parts.

With the type *A* tubular shunt the earth current for any combination of earth connections is symmetrically distributed around the axis of the coaxial voltage circuit and theoretically eliminates any pick-up due to these earth currents.

From the above considerations it is clear that the coaxial tubular shunt design is superior to other designs for the measurement of high-current impulses. To summarize its advantages, it has a greater constancy in impedance over a wide range in frequency, it can be constructed to ensure minimum pick-up, and it offers the greatest freedom in the location of earth connections.

The cross-sectional area A and the length l of the tubular shunt are related by the expressions

$$V = lA \quad : \quad R = \frac{\rho l}{A}$$

where V is the volume of the resistance material, R is its resistance and ρ is the volume resistivity. These expressions may be rewritten as

$$A = \sqrt{\frac{V\rho}{R}} \qquad \ldots\ldots(5.12)$$

$$l = \sqrt{\frac{VR}{\rho}} \qquad \ldots\ldots(5.13)$$

The value of R is determined by the maximum current to be measured and the maximum voltage that can be recorded at the oscillograph. The volume V is governed by the largest amount of energy that must be absorbed by the resistance material during a single discharge. It is preferable to choose a material with as high a value of ρ as possible. Values of A and l can then be calculated from Equations 5.12 and 5.13. The tubing with the thinnest wall to give the above value of A should then be chosen, as the thinner the wall the slower the change in effective impedance as the frequency is increased. The limit on the thinness of the wall is set by the mechanical forces caused by magnetic effects.

With the passage of the high-current impulse through the coaxial tube shunt mechanical forces are produced by magnetic and thermal effects and these require to be considered in the design of the shunt[15, 21]. The magnetic field surrounding the inner tube produces a ' pinch effect ' tending to cause the tube to collapse.

The force on the outer tube acts outwards and is the resultant of that due to its own current and to the repulsion of the inner tube. Assuming a uniform current density the pressure between the tubes is given approximately[15] by

$$p = \frac{4{\cdot}76 \times 10^{-9}(a+2b)}{a(a+b)^2} I_m^2 \simeq \frac{3{\cdot}57 \times 10^{-9}}{a^2} I_m^2 \text{ lb./in.}^2 \qquad \ldots\ldots(5.14)$$

where a and b are the inner and outer radii of the tube in inches. The sudden change in shunt temperature during the discharge tends

to increase the length of the tube, but as it occurs so rapidly the tube does not have time to expand and is temporarily put into compression. Calculations are made on this basis by Park[21] who concludes that if the stress is to be kept within reasonable limits the allowable temperature rise is $\sim 100\,°C$. Experiments are described by Park in which a tube is stressed by successive discharges of increasing energy until a small amount of bending and crinkling of the tube is observed.

At high rates of change of current, Park has shown that the distributed capacitance and inductance of the current circuit will cause variations in the r.m.s. values of the high-frequency components along the length of a tubular shunt, *i.e.* the instantaneous value of the current along the length of the shunt may differ from the value at the current terminals. For shunts up to 100 cm. long the maximum variation in current is < 10 per cent. for frequencies up to 21·5 Mc/s.

DETAILS OF TYPICAL RESISTANCE SHUNTS FOR THE MEASUREMENT OF HIGH-CURRENT IMPULSES

Park[21] has given details of two coaxial tubular shunts, one for measuring up to about 50 kA and the other up to about 200 kA.

TABLE XIII

CONSTANTS OF TWO TUBULAR SHUNTS

	Shunt A	*Shunt B*
Four-terminal resistance	0·04 Ω	0·0048 Ω
Over-all length	39 in.	$38^1/_4$ in.
Length of resistance tube	$26^7/_{16}$ in.	$24^7/_{16}$ in.
Diameter of outside tube	$^7/_8$ in.	2 in.
Diameter of resistance tube	$^1/_4$ in.	1 in.
Wall thickness of resistance tube	0·008 in.	0·0246 in.
Cross-sectional area of resistance tube	0·0392 cm^2	0·469 cm^2
Resistance tube material	German silver	80% Cu, 20% Ni
Resistivity of resistance tube (micro-ohm cm.)	23·33	36·3
Ratio of a.c. impedance to d.c. resistance, at:		
$f=0{\cdot}25$ Mc/s	1·00	0·98
$f=0{\cdot}50$ Mc/s	1·00	0·92
$f=1{\cdot}0$ Mc/s	0·99	0·76
$f=2{\cdot}0$ Mc/s	0·96	0·48
$f=5{\cdot}0$ Mc/s	0·86	0·15
Allowable temperature rise—computed from stress due to thermal expansion	133 °C.	133 °C.
Allowable energy input	1320 joules	14,500 joules
Current limit due to magnetic force	87,600 A	223,000 A
Total inductance of current circuit	0·202 μH	0·106 μH
Maximum voltage drop at current terminals $-L\ di/dt$ for $di/dt=5\times10^{10}$ amp/sec	10,000 V	5,300 V

The principal characteristics of these shunts *A* and *B* are given in *Table XIII.* The ratio of the a.c. impedance to the d.c. resistance is that calculated from Equation 5.10.

Durnford and Reynolds[15] have described a coaxial tube shunt which has been used successfully to measure impulse currents up to 466 kA. The shunt construction is illustrated in *Figure 164.* The resistive inner tube, $3^{9}/_{16}$ in. in diameter, is 8×10^{-3} in. thick, and is formed from 'Ferry' sheet which has a resistivity of $49 \times 10^{-6}\ \Omega$/cm. cube and a temperature coefficient of resistance of 4×10^{-3} per cent./°C. The copper outer tube is formed of sheet, 0·014 in. thick, and is separated from the inner tube by mica sheet, 0·005 in. thick. The contacts are made to the inner surface of the resistive element through the Bakelite-impregnated paper supporting tube and are spring-loaded sufficiently to prevent contact bounce under the forces that result from the impulsive contraction of the outer tube when current flows.

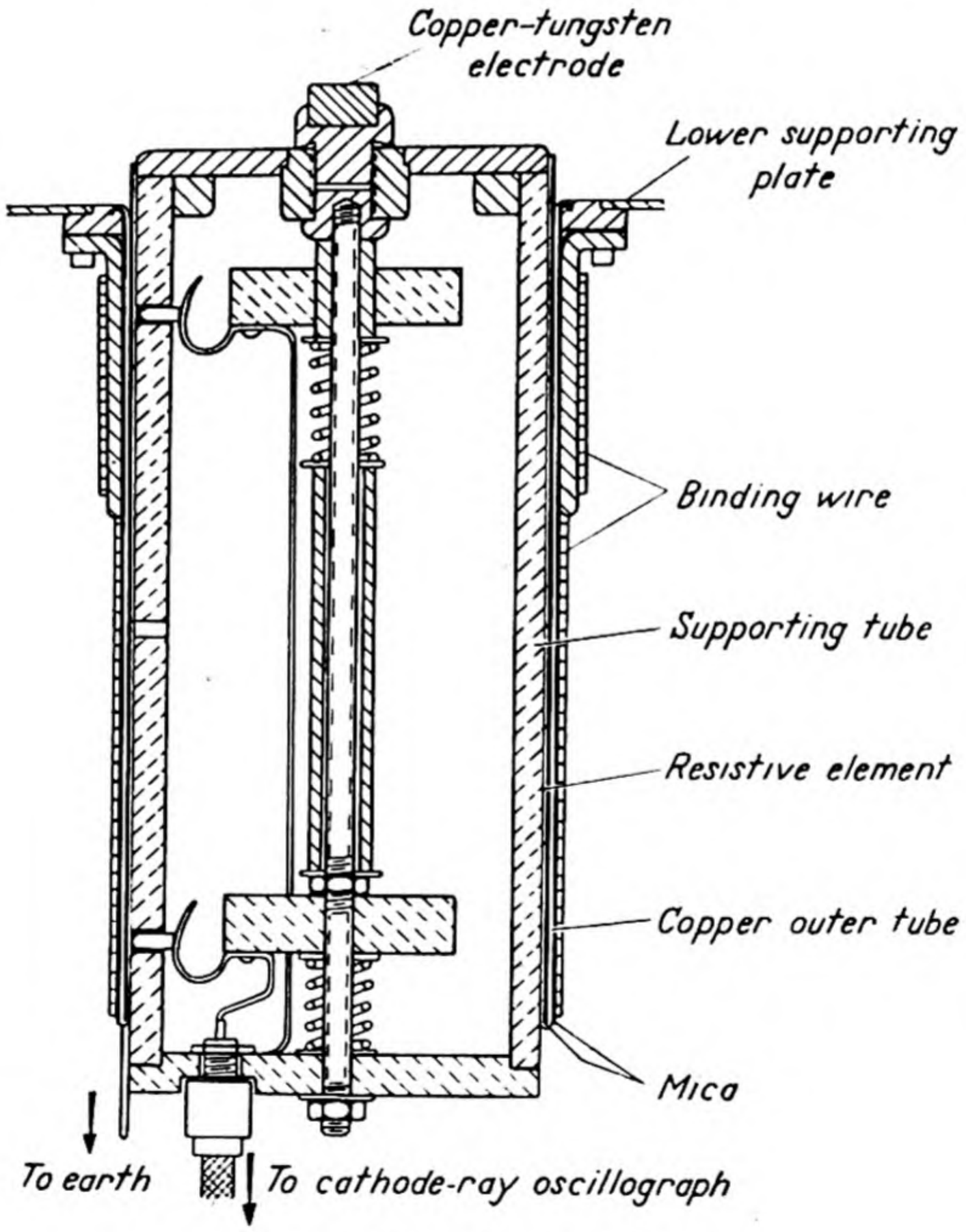

Figure 164. Coaxial shunt.

This shunt has a nominal resistance of $1{\cdot}2 \times 10^{-3}\ \Omega$; a tapping at $0{\cdot}6 \times 10^{-3}\ \Omega$ is also available. The effective impedance, as calculated from Equation 5.10 is constant, within 2 per cent., up to a frequency of 3 Mc/s when $\delta = 1$; the calculated time-constant at this frequency is 0·0136 μsec.

The maximum energy liberated in the shunt per impulse is about 3,300 joules, which is roughly 18 per cent. of the discharge energy of the generator used. The final temperature rise is about 75°C. but is only 20 per cent. of this value at the first current maximum for the current wave-form used. The pressures developed on the tubes, for $I_m = 466$ kA, are about 240 lb./in.^{2} as calculated from Equation 5.14. The outer pressure is taken up by an insulated binding of steel wire 0·04 in. in diameter.

A tubular shunt of a different form has been used by STEKOLNIKOV[13] for the measurement of currents up to ~500 kA. The resistance element is a constantan tube 8·0 cm in diameter and 0·25 mm. in thickness. The tube is 25·25 cm. long and has a resistance of $2 \times 10^{-3}\ \Omega$. There is no surrounding coaxial tube, and the main current leads are connected to the top and bottom of the resistance tube. The result is that the external inductance of the shunt is higher than that of a similar coaxial tube arrangement as used by Park[21] and by Durnford and Reynolds[15]. The screened leads to the oscillograph are connected to tapping-points inside the resistance tube.

MEASUREMENT OF HIGH CURRENTS BY MAGNETIC LINKS

A method for the measurement of peak magnitude of the current flowing in a conductor has been developed by FOUST and KUEHNI[22], and FOUST and GARDNER[23]. Its essential feature is a 'magnetic link', which consists of a small number of short steel strips of high retentivity. The link is mounted at a known distance from the conductor through which the current is expected to pass. Experiments show that the remanent magnetism of the link after the passage through the conductor of the current impulse, which may rise to its peak value in 0·5 μsec and fall to half-value in 5 μsec is the same as that caused by a direct current of the same peak value. Measurement of the remanence possessed by a link after a current impulse then enables the peak value of the current carried by the neighbouring conductor to be calculated. For accurate measurements it is usual to mount two or more links at different distances from the same conductor[22–24, 32, 33, 36, 41]. Because of its relative simplicity the technique has been widely applied in the measurement of lightning currents[22–38, 41].

While the magnetic link enables the peak current to be determined it gives no information concerning the variation with time of the current pulse. For this purpose WAGNER and MCCANN[37] have developed an instrument called the fulchronograph which consists of an aluminium wheel round the rim of which are slots containing magnetic links of sufficient length to project on both sides of the wheel. As the wheel is rotated, the links pass successively through a

pair of narrow coils through which flows the current to be measured. The current at the instant during which a particular link traverses the coil can be determined by a subsequent measurement of the residual flux in the link, and therefore a curve relating the variation of current with time can be obtained. The time scale is governed by the speed of rotation of the wheel. A considerable amount of data on lightning currents has been collected with these relatively simple instruments, which have been installed on a number of high buildings and transmission lines.

Among other devices used in the measurement of lightning currents is the surge integrator[37] which records the total charge which has flowed in a current surge. It consists of a non-inductive resistance shunt, which carries the main surge current, in parallel with an inductive coil. If the resistance of the coil is neglected the current in it at any instant is equal to the integral of the main surge current, and provided that the impulse is non-oscillatory the final maximum value of the coil current is the total integral of the main surge current. Magnetic links are placed adjacent to the coil to record the peak current flowing in it.

In many experiments on high-current surges it is useful to know the wave-form of the rate of change of current. This can be computed from an oscillogram of the current obtained by using a resistance shunt, but this involves the inaccuracy of measuring the slope of the current wave at a number of points and plotting a curve from the measured slopes. Also the high-frequency component of the current wave-form, as recorded in the oscillogram obtained with the shunt, may be highly distorted and may lead to an erroneous value of the rate of change of current, especially at the maximum rate of change.

A more accurate measurement of the rate of change can be obtained by inserting the primary of a mutual inductor in the high-current discharge circuit in place of the shunt and by connecting the secondary of the inductor to the oscillograph. The oscillograph then records $M\frac{di}{dt}$ where M is the mutual inductance of the inductor. Park[21] has discussed the requirements of such mutual inductors and describes three types which have been built. With a tubular form of inductor a frequency range up to 70 Mc/s is obtained.

A wave-front recorder using magnetic links has been developed by Wagner and McCann[37]. It consists of three circuits, containing resistance and inductance and having different time-constants, which are connected across an inductance carrying the main impulse current. Magnetic links are placed within the field of the inductance in the three circuits and enable their peak currents to be recorded. From the values of these peak currents and a knowledge of the circuit constants the mean rate of rise of current in the main circuit can be

estimated approximately. The rate of rise of voltage in a surge can also be measured by the use of magnetic links[31, 38]. In this case a capacitor is connected between the circuit and ground, and magnetic links are used to record the peak current through the capacitor; this peak current is directly proportional to the maximum rate of change of capacitor voltage.

THE OPERATION IN SEQUENCE OF HIGH-VOLTAGE AND HIGH-CURRENT IMPULSE GENERATORS

The voltage required to cause the break-down of a discharge gap is large compared with the voltage drop across the gap after a discharge has been established. Because of the relatively low voltage ($\sim$10 to 100 kV) to which the impulse current generator is initially charged the length of the discharge gap which can be broken down is limited. For this reason techniques have been developed in which the gap is first broken down by a separate high-voltage impulse generator and the high current is then produced through the pre-ionized discharge path by the high-current impulse generator. These techniques are of value in the simulation of lightning discharge conditions and in studies of high-current spark discharges.

One method for the operation in sequence of impulse voltage and current sources has been developed by Bellaschi[6, 7, 8]. The usual

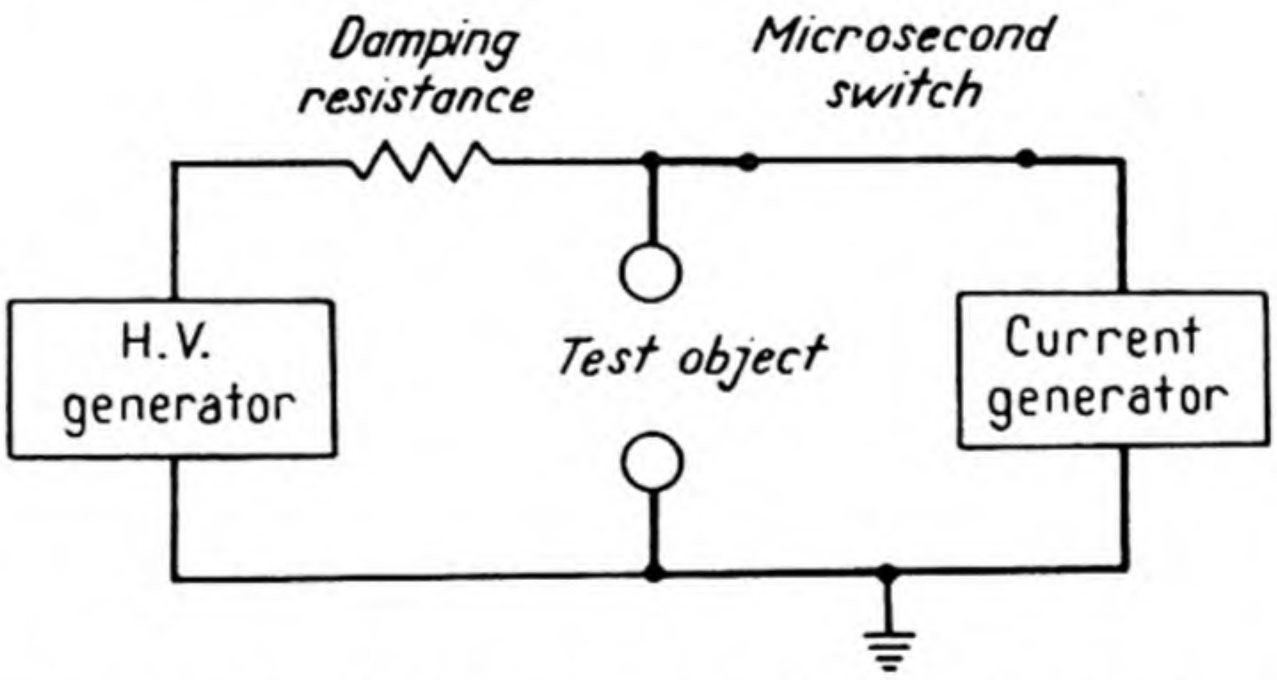

Figure 165. High-current discharge circuit using the microsecond switch for initiation (Durnford and McCormick[16], by courtesy, *Proc. Inst. elect. Engrs.*).

arrangement is shown in *Figure 165*. An isolating impedance in the form of a thin resistance wire, known as the 'microsecond switch', is connected between the test object and the current generator. On the operation of the high-voltage generator the high-voltage impulse causes the break-down of the test object and simultaneously fuses the resistance wire. The current generator then begins to discharge through the resistance wire and the test object and within a few μsec the effective impedance of the wire has fallen from several hundred ohms to a low value.

The method has certain disadvantages in that :—

(*a*) the wire has to be renewed after each discharge,

(*b*) because of the relatively low resistance of the wire, if its length is not to be excessive, only a proportion of the available impulse voltage can be used for break-down of the test object,

(*c*) the additional impedance introduced into the current circuit by the wire path may, in high-current circuits, result in a considerable reduction in the maximum current amplitudes,

(*d*) a delay of 5 to 10 μsec occurs between the initiation of the break-down and the effective start of the current impulse.

Durnford and McCormick[16] have described another method in which the initial isolation between the test object and the current source is provided by a chain of spark gaps whose break-down follows that of the test object. The process is essentially an extension of that occurring in the series form of three-electrode gap commonly used in impulse work when a controlled initiation of break-down is required. The method does not suffer from the limitations (*a*) and (*b*) above, and enables limitations (*d*) and possibly (*c*) to be reduced. A similar technique has been developed independently by Solomonov[14].

Durnford and McCormick[16] preface their description of their multiple-gap method of initiation by a brief analysis of the three-electrode gap. The latter is shown in *Figure 166* for the conditions in which, before break-down, the centre electrode is maintained respectively at

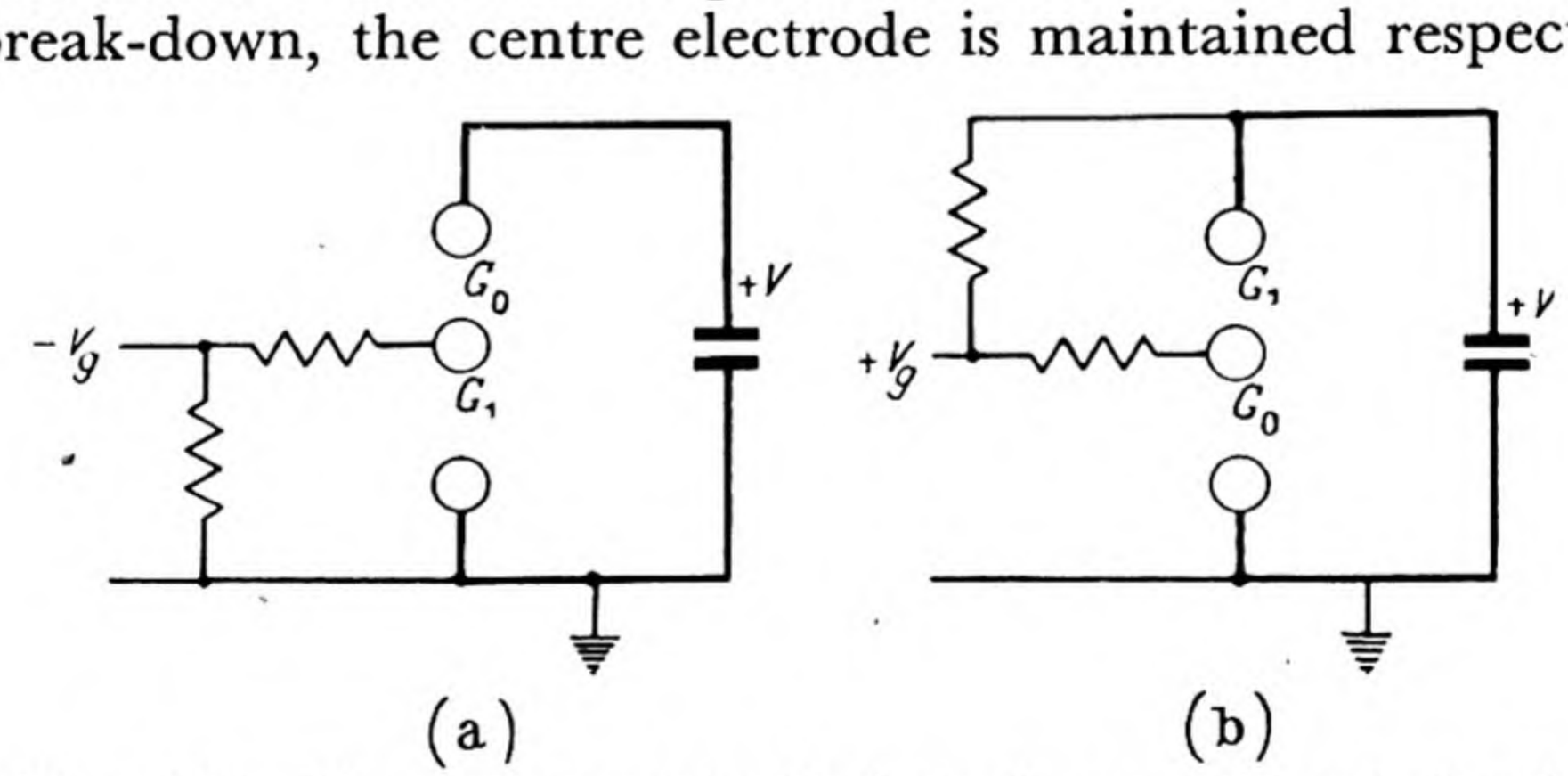

Figure 166. Two arrangements of 3-electrode gaps (Durnford and McCormick[16], by courtesy, *Proc. Inst. elect. Engrs.*).

earth potential and at the potential of the high-voltage electrode. In each case G_o represents the main gap, whose break-down is primarily required, and G_1 is the auxiliary gap. To initiate break-down a trigger voltage V_g is applied to the centre electrode such that the voltage across G_o is increased above its initial value V. This results in the break-down first of G_o and then of G_1, if the lengths of the gaps are correctly chosen, *i.e.*, if

$$V_g + V \geqslant V_o \geqslant V \quad \text{for gap } G_o$$

$$\text{and} \qquad V \geqslant V_1 \geqslant V_g \quad \text{for gap } G_1$$

where V_o and V_1 are the minimum break-down voltages for gaps G_o

and G_1 respectively. In practice V_o should exceed V by a margin sufficient to avoid spurious break-down and V_g should exceed $(V_o - V)$ to an extent that depends on the need for a short break-down time lag of G_o. If V_g is increased the length of the gap G_o can be increased with a resultant increase in V_o; this may be continued until V_o reaches a limit slightly less than $2V$ as V_g approaches V in magnitude. Simultaneously it is necessary to increase the length of G_1 sufficiently so that, on the application of V_g, its break-down does not occur before that of G_o.

The same principle can be used to break down a gap G_o subjected to a voltage $(V_g + V)$ that is greater than $2V$ if the auxiliary gap G_1 is replaced by a series of gaps which are graded in their spacings and electrode voltages so that they break down successively after G_o.

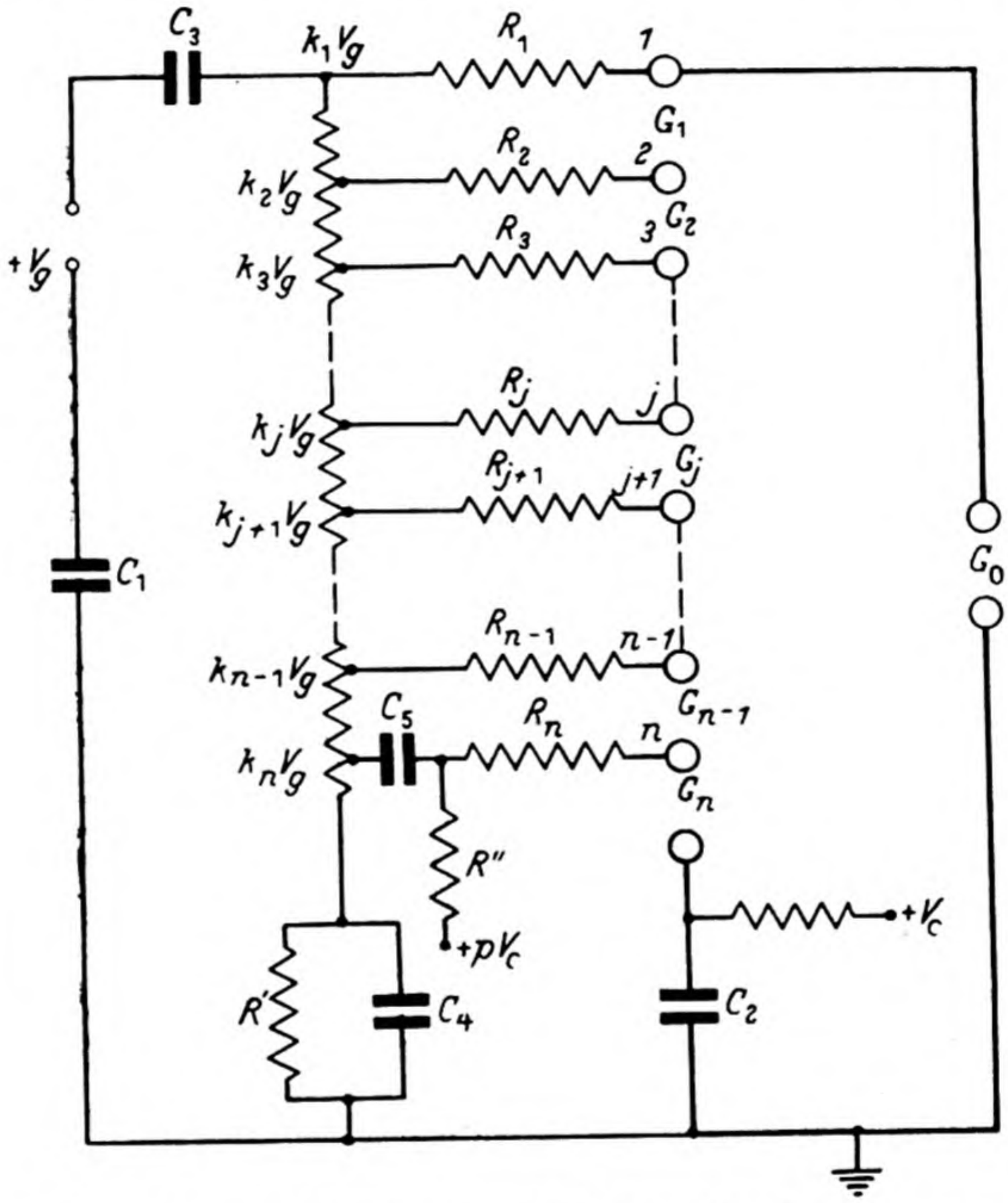

Figure 167. Multiple-gap initiating circuit for current source C_2 (Durnford and McCormick[16], by courtesy, *Proc. Inst. elect. Engrs.*).

It is usual to require that one electrode be held at or near earth potential, as in *Figure 166b*, and this condition is satisfied in the multi-gap initiating circuit given in *Figure 167*. This circuit differs from that of Solomonov in that the electrodes of the series of gaps—with the exception of the *n*th electrode—are maintained at earth potential; the break-down of G_o therefore occurs under the initiating voltage V_g alone.

The electrodes of the auxiliary gaps $G_1 \ldots\ldots G_n$ in *Figure 167* are connected through isolating resistors $R_1 \ldots\ldots R_n$ to corresponding tapping-points on the voltage divider R, which is effectively connected directly across the output terminals of the impulse-voltage source C_1 (the capacitor C_3 and the parallel connection of R' and C_4 in series with R, are inserted for protective purposes and are chosen so that the respective voltages developed across them under correct operating conditions are small). An initial direct voltage pV, where $0 < p < 1$, is also applied to the nth electrode, and the associated gaps G_{n-1} and G_n are set to withstand the resulting voltages; this arrangement is necessary in order that G_{n-1} and G_n together can withstand the voltage V of the current-source, but G_n can be set to break down under the voltage V that is developed across it after G_{n-1} has broken down.

When the impulse voltage V_g is applied, nominal maximum potentials $k_1 V_g \ldots\ldots k_n V_g$ are developed at the corresponding tapping-points on R and—neglecting the effects of stray capacitance—also on the gap electrodes. The auxiliary gaps are set to withstand the voltages that result should G_o not break down under $k_1 V_g$. If G_o breaks down, the voltage across the next gap, G_1, changes from $(k_1 - k_2)\ V_g$, where $k_2 < k_1$, to $k_2 V_g$; break-down then follows if the setting of this gap is less than $k_2 V_g$. This procedure is repeated for $G_2 \ldots\ldots G_{n-2}$ in succession, and in a similar manner for G_{n-1} under combined direct and impulse voltages; the breakdown of G_n under the voltage V then initiates the discharge of the current source C_2.

In the alternative circuit described by Solomonov, the low-voltage end of the voltage-divider R—at the junction with R' and C_4 in *Figure 167*—is connected directly to the current source; as mentioned above, all the gap electrodes are thereby initially maintained at the potential V, which augments the impulse voltage for the break-down of each gap, including G_o. The importance of this is limited and the absence, in the circuit of *Figure 167*, of voltage on the electrodes of $G_1 \ldots\ldots G_n$ and also across G_o until V_g is applied, normally makes this circuit preferable from the point of view of safety of operation.

A detailed mathematical analysis of the initiating circuit is given by Durnford and McCormick and enables the number and settings of the auxiliary gaps to be determined when account is taken of the various factors that affect the electrode voltage. The causes of incorrect operation are considered and means of preventing the discharge of the current source under the conditions are discussed.

When the above technique is used in high-current circuits, where the energy associated with the current-source can be large, *e.g.* of the order of 50,000 joules, it may be desirable to prevent the discharge of the source which can occur should the initiating circuit not operate correctly. Consideration of the circuit of *Figure 167* shows that if

any one of the auxiliary gaps breaks down inadvertently before G_o, when V_g is applied, break-down extends in both directions; when it includes G_n the current source can discharge through the initiating network. If, however, the resistor R' is made sufficiently large, *e.g.* of the order of 10 MΩ, then, for $V = 20$ kV, the discharge can be inhibited after C_3 and C_4 have become charged up to about V.

Durnford and McCormick describe experimental results obtained with an initiating circuit with five gaps. An impulse voltage up to 150 kV for the initial break-down of the gap G_o was used; the current generator was charged to an initial d.c. voltage of 25 kV. The values of the circuit constants (*see Figure 169*) were as follows: $C_1 = 0{\cdot}002\,\mu$F, $C_2 = 0{\cdot}5\,\mu$F, $C_4 = 0{\cdot}01\ \mu$F, $R = 25$ kΩ, $R_2 = R_3 = R_4 = R_5 = 70$ kΩ, $R' = 10$ MΩ; C_3 was omitted as it was found to be unnecessary. Each gap was adjusted in turn, starting with G_5, so that when G_o did not break down it would just withstand the actual voltage developed with V_6 and V both about 10 per cent. greater than the required operating values.

Consistent initiation of the discharge of C_2 was obtained with a total break-down time of $G_1 \ldots . G_5$ of about $1{\cdot}2\,\mu$sec as recorded oscillographically. Irradiation of G_1 and the adjacent gaps by radioactive cobalt, equivalent to 6 mg. of radium, reduced the break-down time by only about 10 per cent. The break-down times recorded in successive operations varied by only about ± 10 per cent. about the mean value. Approximately the same total break-down time was obtained with the resistance R increased to 50 kΩ.

In a discussion of their technique Durnford and McCormick point out that before the break-down of the test object the isolating impedance is infinite and, therefore, apart from the effect of the loading imposed by the voltage divider R, the full output of the impulse generator is available for break-down purposes. Whereas the proportion normally obtainable with the microsecond switch system appears, from Bellaschi's data[6, 7, 8] to be about 75 per cent. or less. This follows from the practical limitations to the maximum resistance of the microsecond switch and to the minimum value of the generator damping and wave-front resistor.

The current which flows from the voltage source through the test object after break-down is determined primarily by the first isolating resistor R_1 and, except where the capacitance of the test object requires this resistance to be small, the current may normally be expected to be about 0·001 of that obtained with the microsecond switch. This, together with the short delay time of about 1 μsec between break-down and the initiation of the current discharge may be important when the technique is being used to produce long high-current spark discharges in G_o for the purpose of investigations of the characteristics

of such discharges. It is less important for lightning simulation tests on electrical equipment. Under these conditions it should normally be possible to use an impulse voltage source of relatively low capacitance and energy.

No experimental comparison has been made between the values of the respective impedances of the microsecond switch and of the multi-gap arrangement after initiation but Durnford and McCormick consider that some reduction should be obtained with the latter. For a test object with a break-down voltage of 2 MV Bellaschi has used a wire-length of 110 in. For the equivalent multi-gap arrangement the sum of the gap lengths excluding the electrodes would be about 30 in., assuming a reasonably uniform stress in each gap. With the electrodes taken into account the total length might be 60 to 90 in. The increase in the current magnitude due to the shorter path-length for the multiple-gap arrangement would probably not be great as the current is approximately proportional to the reciprocal of the square-root of the inductance for an oscillatory discharge. The shorter gaseous discharge path—although through an ionized gas and not, as in the microsecond switch, through an ionized metal vapour—might, however, be significant but no comparative data have been obtained.

The multiple-gap arrangement is relatively complex to design and adjust compared with the microsecond switch, but, once adjusted, it will normally operate over a moderate range of voltage of both the voltage and current sources.

REFERENCES

1 BELLASCHI, P. L. *Trans. Amer. Inst. elect. Engrs.*, **53** (1934) 86.
2 ROHATS, N. *Gen. Elect. Rev.*, **37** (1934) 296.
3 BELLASCHI, P. L. *Elect. J.*, **32** (1935) 237.
4 BELLASCHI, P. L., and ROMAN, W. G. *Elect. J.*, **31** (1934) 96.
5 MCEACHRON, K. B., and THOMASON, J. L. *Gen. Elect. Rev.*, **38** (1935) 126.
6 BELLASCHI, P. L. *Trans. Amer. Inst. elect. Engrs.*, **56** (1937) 1253.
7 BELLASCHI, P. L. *Trans. Amer. Inst. elect. Engrs.*, **58** (1939) 466.
8 BELLASCHI, P. L. *Elect. J.*, **33** (1936) 273.
9 BROWNLEE, T. *Trans. Amer. Inst. elect. Engrs.*, **53** (1934) 481.
10 FOITZIK, R. *Elektrotech. Z.*, **6** (1939) 89, 128.
11 FLOWERS, J. W. *Phys. Rev.*, **64** (1943) 225.
12 NORINDER, H., and KARSTEN, O. *Arkiv. för Math. Astr. o Fysik*, **36** (1949) 1.
13 STEKOLNIKOV, I. S. *Comptes Rendus (Doklady) Acad. Sci. U.R.S.S.*, **52** (1946) 413.
14 SOLOMONOV, N. M. *Zhur. Tekh. Fiz.*, **18** (1948) 395.
15 DURNFORD, J., and REYNOLDS, P., to be published.
16 DURNFORD, J., and MCCORMICK, N. R. *Proc. Inst. elect. Engrs.*, **99** (1952) 27.
17 BROWNLEE, T. *Trans. Amer. Inst. elect. Engrs.*, **61** (1942) 539.
18 ALLEN, J. E. *Research*, **3** (1950) 527.
19 SILSBEE, F. B. *J. Res. Nat. Bur. Stand.*, **13** (1916) 375.
20 SILSBEE, F. B. *J. Res. Nat. Bur. Stand.*, **4** (1930) 73.
21 PARK, J. H. *J. Res. Nat. Bur. Stand.*, **39** (1947) 191.

[22] FOUST, C. M., and KUEHNI, H. P. *Gen. Elect. Rev.*, **35** (1932) 644.
[23] FOUST, C. M., and GARDNER, G. F. *Gen. Elect. Rev.*, **37** (1934) 324.
[24] FOUST, C. M., and HENDERSON, J. T. *Trans. Amer. Inst. elect. Engrs.*, **54** (1935) 373.
[25] ZADUK, H. *Arch. tech. Messen*, **5** (1935) 155.
[26] GRÜNEWALD, H. *C.I.G.R.E. Paper* No. 326, 1935.
[27] BERGER, K. *Bull. Ass. Suisse Elect.*, **27** (1936) 145.
[28] BELL, E. *Trans. Amer. Inst. elect. Engrs.*, **59** (1940) 822.
[29] HANSSON, E., and WALDORF, S. K. *Trans. Amer. Inst. elect. Engrs.*, **63** (1944) 251.
[30] GROSS, I. W., and LIPPERT, G. D. *Trans. Amer. Inst. elect. Engrs.*, **64** (1945) 76.
[31] LEWIS, W. W., and FOUST, C. M. *Trans. Amer. Inst. elect. Engrs.*, **64** (1945) 107.
[32] PERRY, F. R. *J. Inst. elect. Engrs.*, Pt II **88** (1941) 69.
[33] PERRY, F. R., WEBSTER, G. H., and BAGULEY, P. W. *J. Inst. elect. Engrs.*, Pt II **89** (1942) 185.
[34] DAVIS, R. *The Engineer*, **180** (1945) 435.
[35] STEKOLNIKOV, I. S., and VALEEV, C. *C.I.G.R.E. Paper* No. 330, 1937.
[36] LEWIS, W. W. *Protection of transmission systems against lightning.* New York, 1950.
[37] WAGNER, C. F., and MCCANN, G. D. *Trans. Amer. Inst. elect. Engrs.*, **59** (1940) 1061.
[38] GROSS, I. W., and LIPPERT, G. D. *Trans. Amer. Inst. elect. Engrs.*, **61** (1942) 178.
[39] ARNOLD, A. H. M. *J. Inst. elect. Engrs.*, **80** (1937) 395.
[40] ARNOLD, A. H. M. *Proc. Inst. elect. Engrs.*, **97** (1950) 280.
[41] BRITISH ELECTRICAL AND ALLIED INDUSTRIES RESEARCH ASSOCIATION, *Surge Phenomena*. London, 1941.

6

GENERATION OF SQUARE PULSES AT HIGH VOLTAGES

PULSE GENERATORS USING PULSE-FORMING NETWORKS

Techniques for the production of recurrent high-voltage square pulses have been widely developed during recent years, largely because of the need for such pulses in the anode modulation of magnetron oscillator valves, as used in radar transmitters. Details of much of the British work in this field are described in papers presented at a Convention held by the Institution of Electrical Engineers in 1946[1–8]. American work has been summarized in the book entitled *Pulse Generators*, edited by GLASOE and LEBACQZ[9]. However, the need for high-voltage square pulses is not confined to radar, and an increasing number of applications are being found, as for example in the control of electro-optical shutters[10–13], in X-ray technique[14], in the study of certain aspects of electrical discharges[15] and in some types of nuclear physics apparatus, such as high-energy linear accelerators[16].

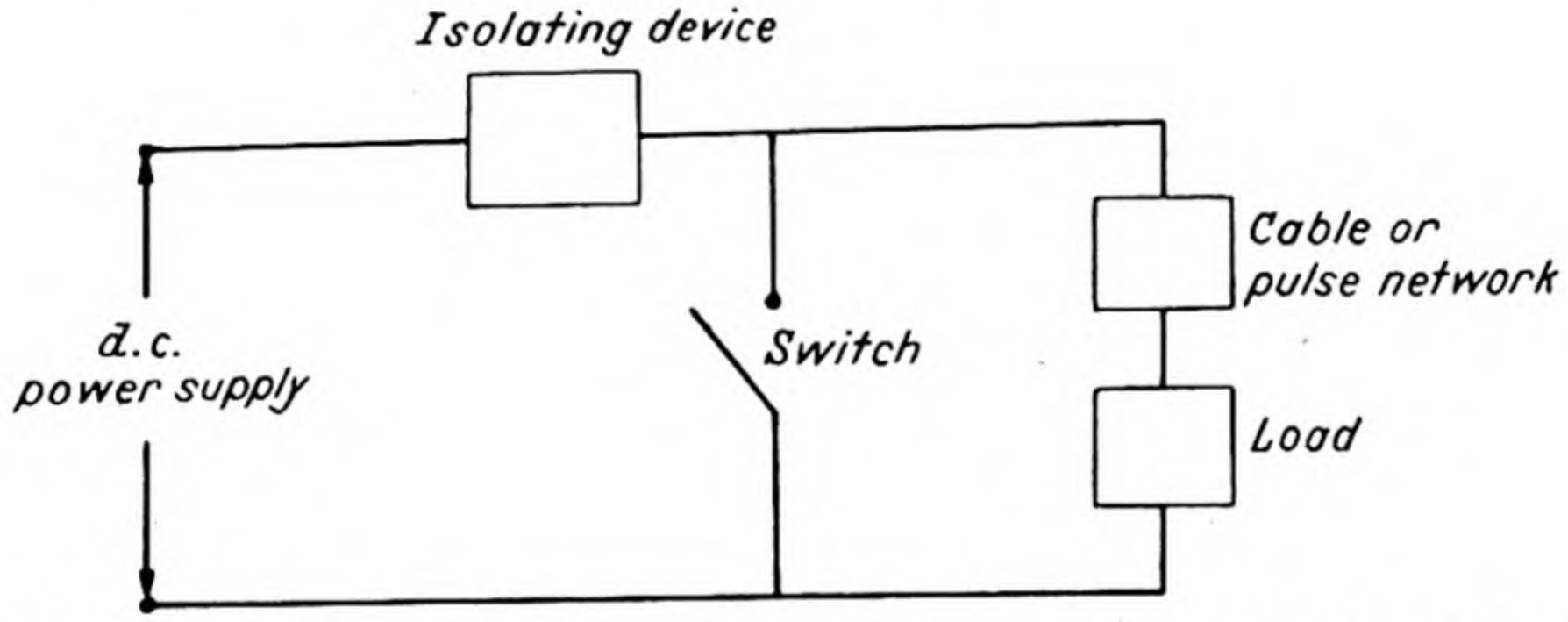

Figure 168. Basic circuit of square-pulse generator using a pulse-forming network.

Probably the most widely applied type of high-voltage square-pulse generator is that involving the use of a cable or pulse-forming network. The basic features of the circuit for this type of generator are shown in *Figure 168*. A length of cable, or equivalent pulse-forming network, is charged from a power supply, either a.c. or d.c., until its voltage reaches a chosen value. The switch is then closed and the cable discharges through the resistance load. If the value of the resistance is chosen correctly in relation to the surge-impedance of the cable a square pulse of voltage is developed across the load.

To produce a square pulse a length of coaxial single-core cable may be used. The surge impedance of the cable is $Z_o = \sqrt{(L_o/C_o)}$ where L_o is the inductance of the cable and C_o is the capacitance of the cable.

If the cable is charged to a voltage V and is discharged through a resistance R a current $I = \frac{V}{R+Z_o}$ flows through R and the pulse voltage developed across R is $\frac{RV}{R+Z_o}$. The pulse current is sustained by a voltage wave $V-RI$ which travels into the cable with velocity $\frac{l}{\sqrt{(L_oC_o)}}$ where l is the length of the cable. This wave, after reflection at the far open-circuited end of the cable, returns after time $t=2\sqrt{(L_oC_o)}$ in such a sense as to reduce the current in the load R. When the load resistance is matched to the cable, $R=Z_o$, and the reflected wave terminates the pulse current. For the matched condition the pulse voltage is equal to $V/2$.

In practice, the coaxial cable is frequently replaced by a pulse-forming network, known also as an artificial transmission line[17, 18]. The pulse network consists of a series of lumped capacitances and inductances connected as shown, for example, in the diagrams of

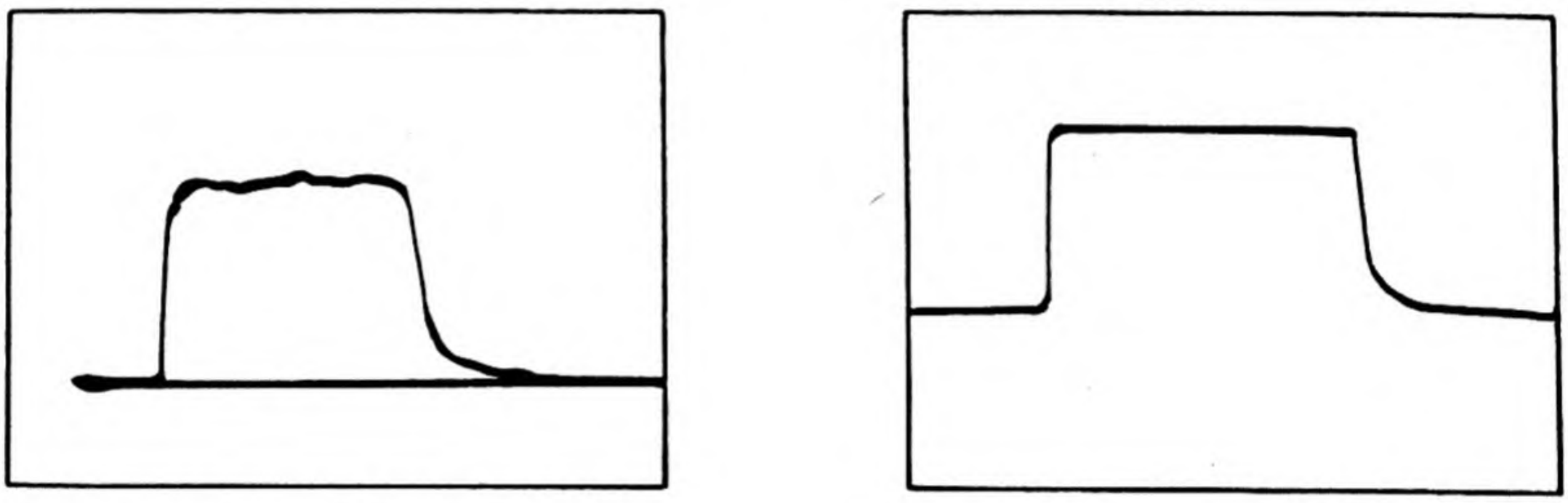

(a) (b)

Figure 169. (*a*) Artificial line, 4 units each containing 18 sections. $Z_o=77\,\Omega$, 14 kV d.c. Pulse length, along top of pulse, about 3·6 μsec. (*b*) Coaxial cable. $Z_o=52\,\Omega$, 20 kV d.c. Pulse length, along top of pulse, 3·5 μsec (different time base from (a)).

Figures 171 and *172*. It is found that six or more equal sections of capacitance and inductance are sufficient to give a good approach to the ideal cable condition. In the circuit of *Figure 171* the pulse network, or artificial line, consists of 9 stages each of 200 $\mu\mu$F connected by inductances of 50μH.

Oscillograms showing pulses obtained with a coaxial cable and with a pulse network are reproduced in *Figure 169*.

The switch shown in *Figure 168* may consist of a rotating spark gap, a triggered spark gap or a thyratron. In this chapter attention has been given mainly to the use of circuits involving spark gaps, but it is possible for the spark gaps to be replaced by thyratrons in many of the applications described. Thyratrons have an advantage in that a lower trigger voltage is required.

It is not always possible to generate the power and deliver it to the load, *e.g.* a magnetron, at voltage and impedance levels suitable for

direct application. In this case pulse transformers can be used to match the impedances of adjacent units to each other. A pulse transformer may couple directly the pulse generator and the load. Alternatively, two pulse transformers may be used, particularly if the system requires remote operation of the generator and the load ; then one transformer is arranged to match the generator to the cable impedance and the second transformer steps up the voltage to the required value at the load.

Full details of the design and operation of pulse transformers have been given by MELVILLE[7] and by BOSTICK[19]. Pulse transformers have been built for pulse powers up to 10 MW. Bostick refers to a pulse transformer for 0·5 μsec pulses which has operated successfully with an output voltage of 100 kV supplying a load of 20,000 Ω ; the step-up ratio is 5·5.

ROTATING SPARK-GAPS

Figure 170a shows the essential features of the circuit for a modulator using resonant charging[2]. G is the rotating spark-gap element. The value L of the charging choke is chosen in relation to the capacitance C_o of the pulse network so that

$$f = \frac{1}{\pi\sqrt{(LC_o)}} \qquad \ldots.(6.1)$$

where f is the required rate of pulses per second and is therefore also the frequency at which the fixed electrodes of the gap G are bridged by

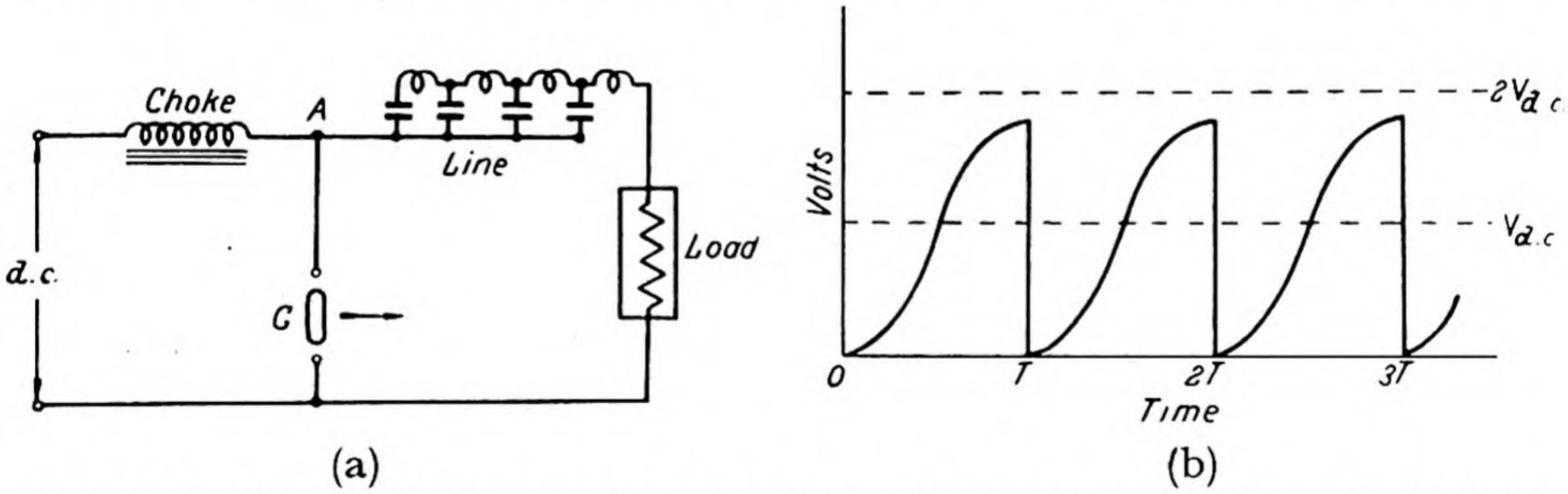

Figure 170. (*a*) Circuit diagram for a modulator using resonant charging. (*b*) Voltage wave-form at point *A* in *Figure 170a* (Craggs, Haine and Meek[2], by courtesy, *J. Inst. elect. Engrs.*).

the moving electrode. The load consists of a resistance R chosen to equal the impedance Z_o of the pulse network

$$R = Z_o = \sqrt{\frac{L_o}{C_o}} \qquad \ldots.(6.2)$$

where L_o is the total inductance of the pulse network. The waveform of the voltage at the point A in the circuit is shown in *Figure 170b*. The line is discharged when the voltage reaches a maximum value V_m given by $V_m = nV_{dc}$, where V_{dc} is the d.c. input voltage. Ideally the

factor n is equal to 2, but because of losses in the charging inductance n is nearer to 1·8 under normal conditions of resonant charging. By the use of linear charging, described on page 182, the factor n may be increased to 1·9 or more.

With a resistive load, as in *Figure 170a*, a square voltage pulse is produced across the load. The peak magnitude of this voltage, when the load resistance matches the impedance of the pulse network, is one-half of the voltage to which the line is initially charged and is therefore about 0·9 V_{dc} for resonant-charging conditions.

Craggs, Haine and Meek[2] describe several rotating spark-gap modulators developed for radar purposes. In these gaps rod-shaped electrodes are inserted through equally-spaced holes round a Bakelite disc which is rotated between two parallel Bakelite discs on which similar electrodes are mounted. The pulse network is discharged through one or more pairs of gaps. Tungsten and molybdenum are found to be the most suitable electrode materials.

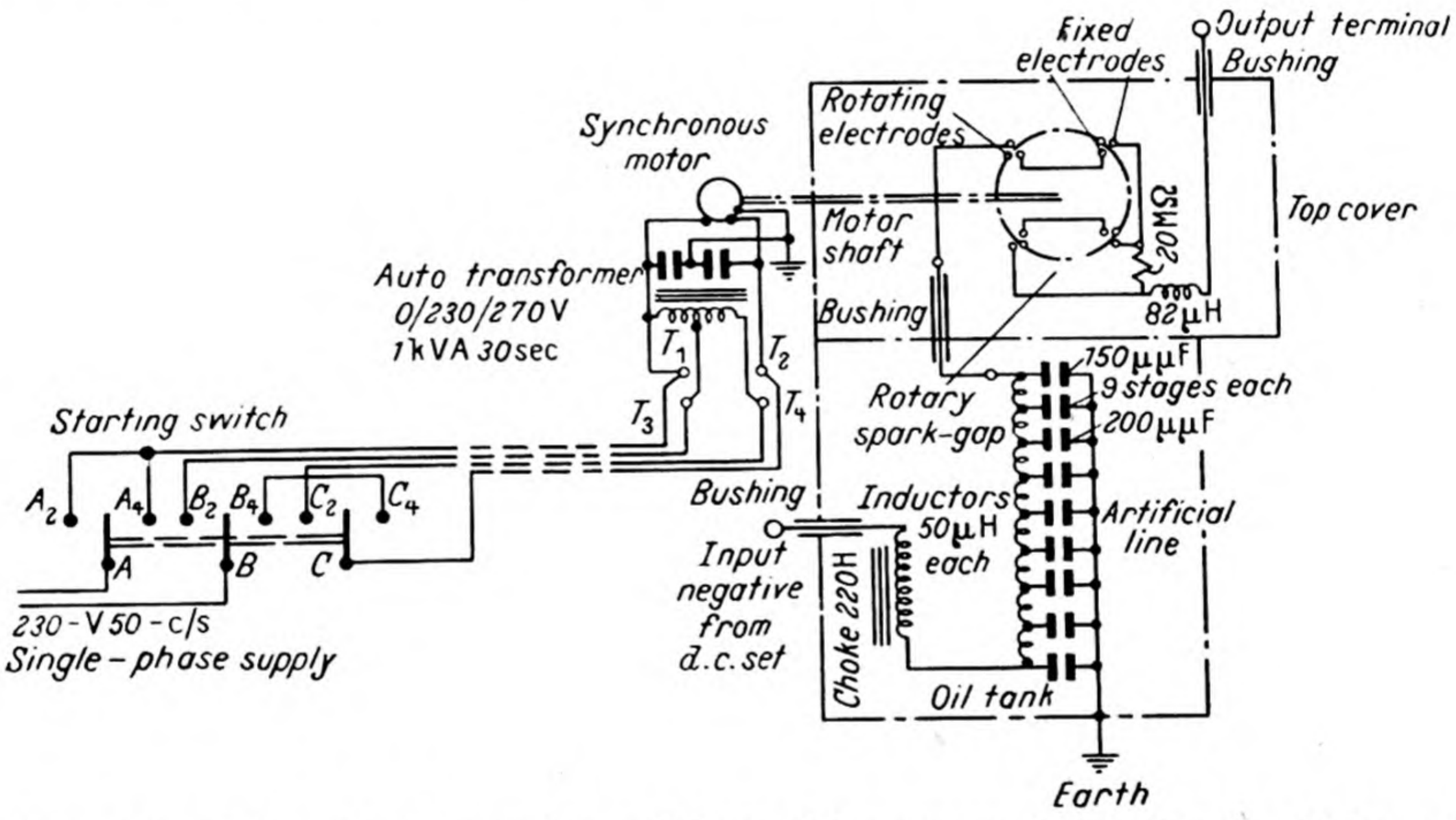

Figure 171. Schematic diagram for modulator with rotary spark gap (Craggs, Haine and Meek[2], by courtesy, *J. Inst. elect. Engrs.*).

A diagram of connections for a modulator of this type is shown in *Figure 171.* This modulator produces 30 kV, 2 μsec pulses across a resistance load of 500 Ω at a pulse recurrence rate of 500 pulses/sec. The pulse power is 1·8 MW.

For pulse voltages above 35 kV Craggs, Haine and Meek describe a method of connection of two pulse networks which are charged in parallel through suitable inductances and are discharged in series through one rotary gap and one stationary gap. The circuit is given in *Figure 172.* The stationary gap consists of two tungsten rods spaced several centimetres apart. With one particular set designed to

produce 0·8 μsec pulses discharging into a 500 Ω load at 380 pulses/sec the peak magnitude of the pulse voltage could be varied from 35 to 62 kV, corresponding to pulse powers of 2·4 and 7·7 MW respectively, by alteration of the d.c. charging voltage from 19 to 36 kV.

The development of rotating spark gaps in the U.S.A. has been described by GOUCHER, HAYNES, DEPP and RYDER[20] and by LEBACQZ and WHITE[21].

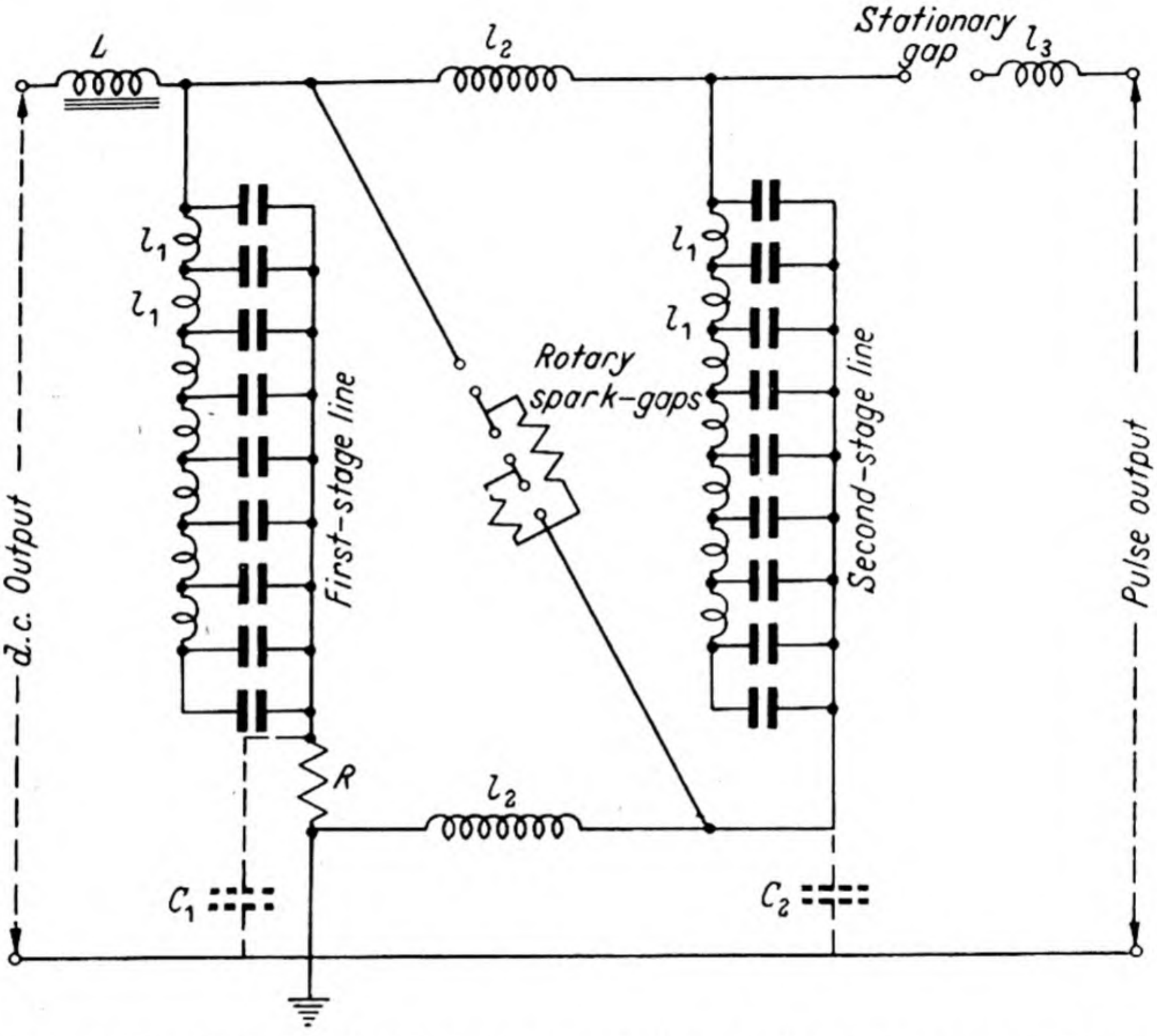

Figure 172. Circuit diagram for a modulator using a rotary spark gap in series with a stationary spark gap (Craggs, Haine and Meek[2], by courtesy, *J. Inst. elect. Engrs.*).

Although rotating spark gaps have been used in various applications they have a number of defects. Considerable jitter is observed in the time intervals between successive sparks, also the time of occurrence of individual pulses cannot be synchronized accurately with an incoming locking pulse and it is necessary therefore to lock all the associated equipment to synchronize with the rotating gap. This disadvantage is overcome by the use of triggered spark gaps which have now largely replaced rotating spark gaps.

TRIGGERED SPARK GAPS OPERATING IN AIR

The development of triggered spark gaps, known as Trigatrons, has been described by Craggs, Haine and Meek[2]. The Trigatron consists essentially of three electrodes, arranged as shown in *Figure 173*, and is connected in the circuit so that the undrilled electrode is negative

with respect to the drilled electrode and the trigger electrode. The latter two electrodes are normally at the same potential and are connected by a high resistance. When a voltage pulse is applied to the trigger electrode spark break-down is caused to occur between the two main electrodes and the connected circuit is then discharged. For the optimum operating characteristics to be obtained the trigger pulse should be positive with respect to the surrounding electrode. Molybdenum is used for the sparking surfaces of the two main electrodes and tungsten for the trigger wire.

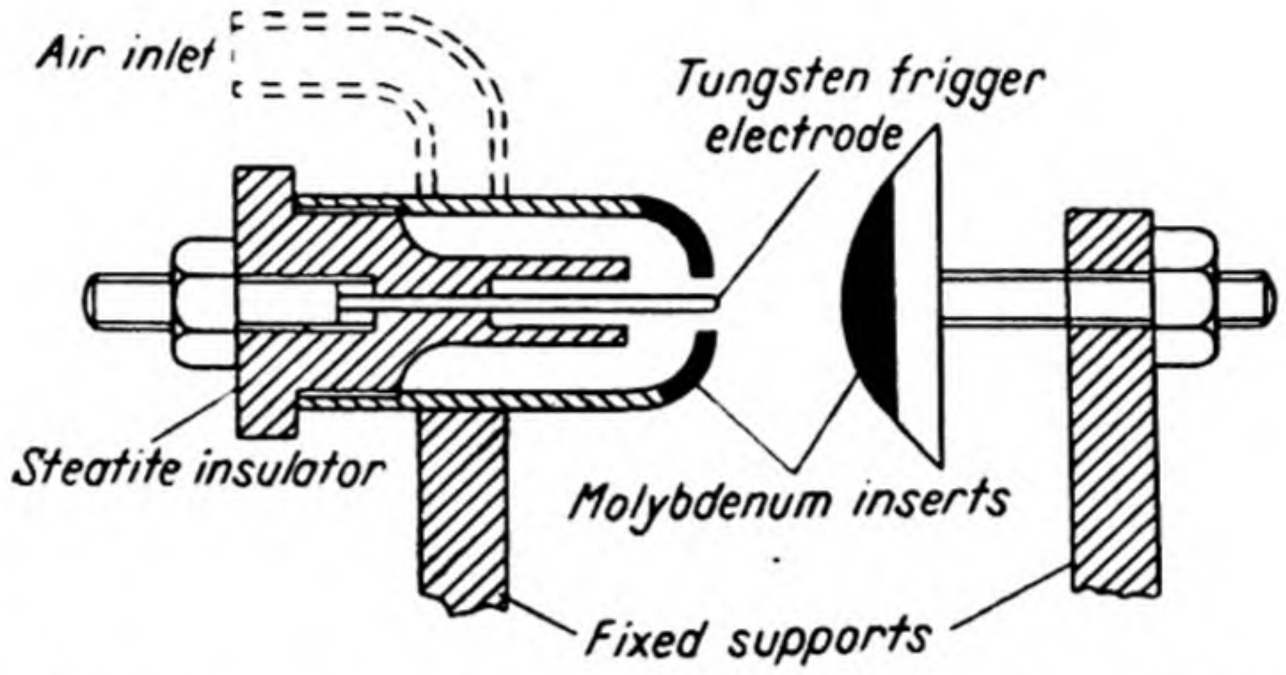

Figure 173. General arrangement of the electrodes in an open-air Trigatron (Craggs, Haine and Meek[2], by courtesy, *J. Inst. elect. Engrs.*).

Other forms of electrode arrangement including the well-known three ball gap (*see* page 145), have been investigated[2], but the operating characteristics are less satisfactory than those of the Trigatron. Three-electrode gaps similar to the Trigatron have been developed by MÜLLER-HILLEBRAND[22] and by STRIGEL[23] for use in surge diverters where, on the arrival of a voltage surge at the gap, the break-down of the gap is facilitated by the presence of the third electrode.

The Trigatron requires a pulse of 3–6 kV to trigger the discharge. This pulse, which is applied to the trigger electrode, has to supply sufficient energy to charge a capacitance of about 10 $\mu\mu$F. The method generally used[2] to provide the pulse employs a 'break valve' with a high peak-emission and good anode insulation. The circuit is given in *Figure 174*. A positive voltage pulse of a few hundred volts is applied to the grid of the valve which is normally biased beyond cut-off. The duration of the pulse is between 5 and 20 μsec and has a short cut-off. During the pulse current builds up in the small inductance connected in the anode circuit. The end of the pulse causes the cessation of current flow and a voltage is produced across the stray capacitance at the valve anode. For a current of 1 A, an inductance of 10 mH and a stray capacitance of 100 $\mu\mu$F the peak voltage developed is 10 kV in a time of about 1·5 μsec. The coupling arrangement between the trigger-valve anode and the trigger electrode is usually a capacitor shunted by a high-resistance leak of about 100 kΩ. A

resistance of about 1,000 Ω is connected in series with this capacitor and the trigger wire to suppress oscillations occurring immediately after break-down.

If the break-down voltage of the gap between the two main electrodes of the Trigatron in the absence of the trigger voltage pulse is V_{max}, then the breakdown can be caused to occur at any lower voltage V down to a value V_{min} on the application of the trigger pulse. The voltage V may be maintained indefinitely across the gap until the trigger pulse is applied. The reduction in the normal break-down voltage is thought to be caused by the increase in the voltage gradient in the region of the trigger wire on the application of the trigger pulse. While the magnitude of the trigger pulse has some effect

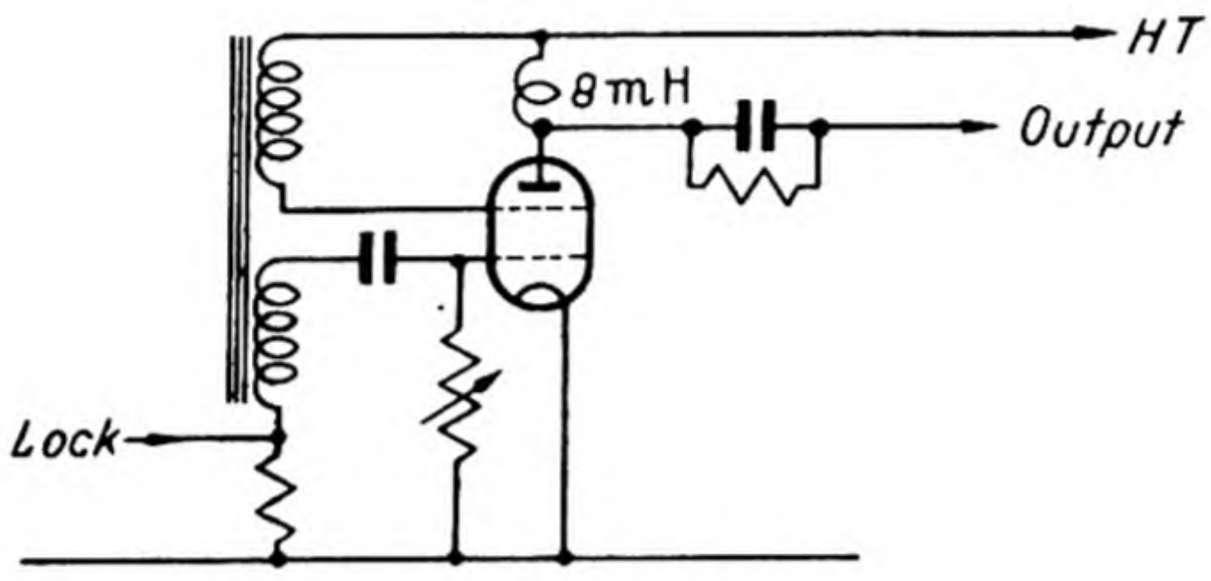

Figure 174. "Break-valve" circuit for trigger pulse (Craggs, Haine and Meek[2], by courtesy, *J. Inst. elect. Engrs.*).

on the amount of lowering of the break-down voltage the observed lowering is much greater than that given by the direct addition of the trigger voltage to the voltage between the main electrodes. For short gaps oscillographic studies show that, over part of the operating range, the voltage on the trigger wire has dropped to about that of the surrounding electrode before break-down of the main gap takes place. In this case the lowered break-down voltage may be caused by field distortion in the gap caused by space charges resulting from the photo-ionizing effects of the trigger spark[2, 15].

For satisfactory operation irradiation of the gap seems to be required in order to provide primary electrons to initiate the discharge at the instant the trigger pulse is applied[2, 15]. This irradiation is provided by corona discharge which is formed around the central wire. By the insertion of an insulating cylinder usually of glass between the wire and the surrounding anode, as shown in *Figure 173*, the gas near the wire is more highly stressed and the corona discharge thereby intensified.

While the operating voltage range of the Trigatron when used to control single discharges lies between the voltages V_{max} and V_{min} the operating range for recurrent pulses is affected both by the pulse energy and the pulse-recurrence rate. This is because the dielectric strength of the gap has not fully recovered from the effect of one spark

before the next occurs. For this reason the maximum operating voltage decreases with increasing pulse energy and with increasing recurrence rate.

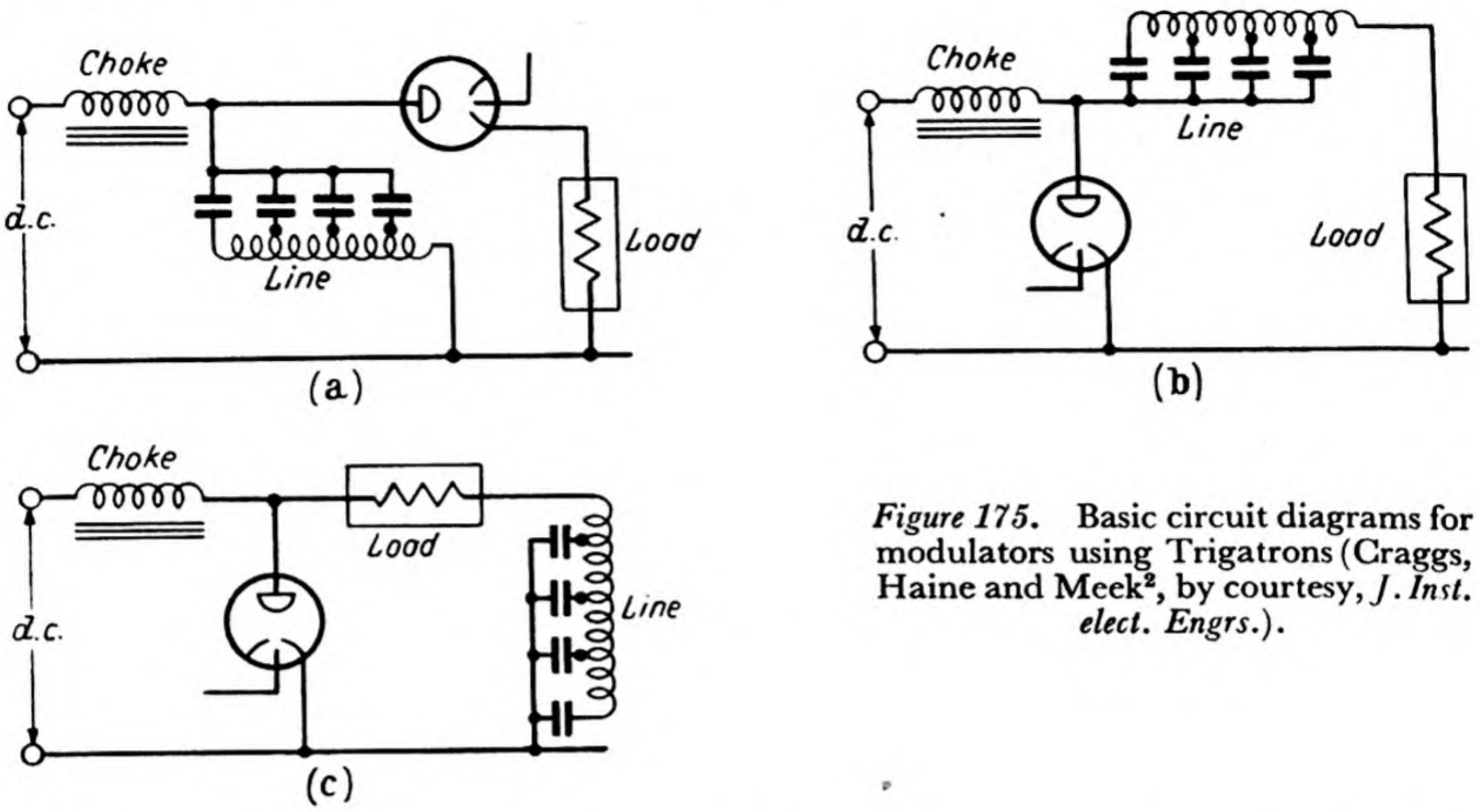

Figure 175. Basic circuit diagrams for modulators using Trigatrons (Craggs, Haine and Meek[2], by courtesy, *J. Inst. elect. Engrs.*).

Diagrams of several modulator circuits involving Trigatrons are given in *Figure 175*. Craggs, Haine and Meek[2] point out that in their initial experiments the value of the charging inductance was chosen in relation to the capacitance of the pulse network and the pulse-recurrence rate so that the successive discharges took place at the crest of the sinusoidal charging wave, as shown in *Figure 170b*. However it was found that with fixed values of charging inductance and network capacitance the Trigatron continued to operate for recurrence rates higher than the resonant value. The pulse recurrence rate can

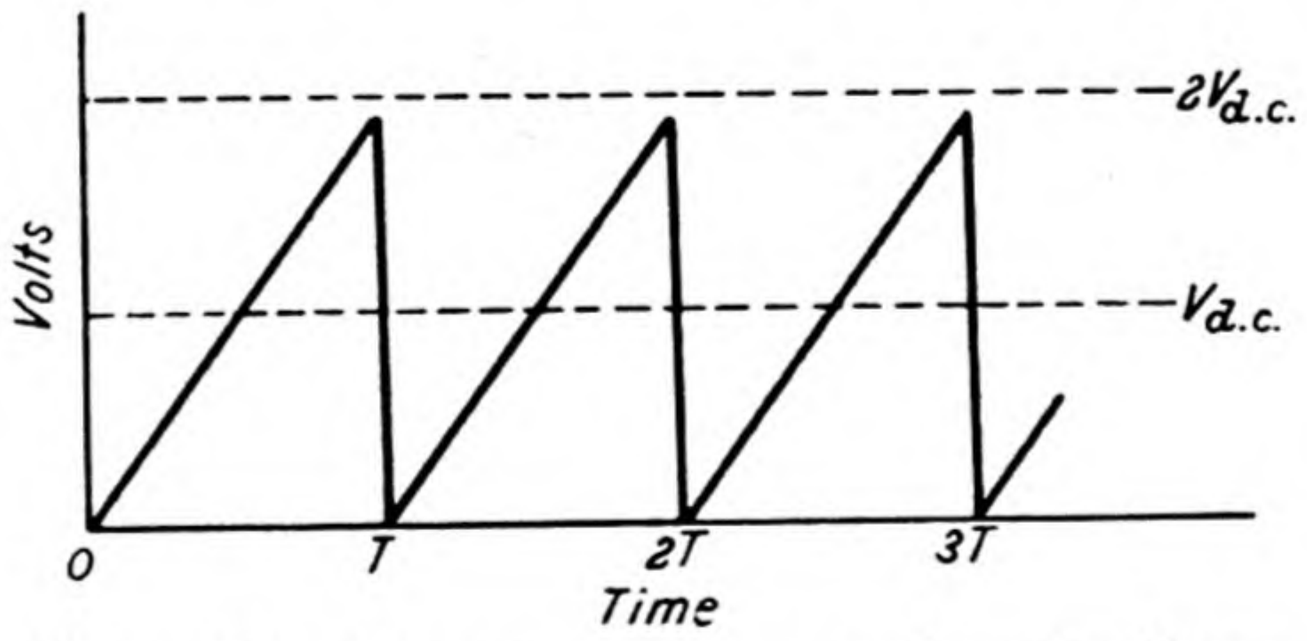

Figure 176. Charging voltage waveform for linear charging (Craggs, Haine and Meek[2], by courtesy, *J. Inst. elect. Engrs.*).

therefore be varied over a wide range by alteration of the frequency of the incoming trigger pulse. Under such conditions the charging waveform becomes closely linear, as shown in *Figure 176*, and the current flow during the charging cycle is maintained at a nearly uniform value. Because of the reduction in the a.c. component of current in the

charging choke, the iron losses are greatly reduced, with a consequent improvement in the doubling factor n and economy in the choke design.

The advantages of linear-charging have led to its adoption in most of the circuits using Trigatrons. An exception occurs in the case of alternator-charging, as shown in *Figure 177*, where the pulse network is charged from an a.c. supply. In this case the trigger pulse is synchronized with the frequency of the alternating supply, so that the discharge occurs at the crest of each charging cycle, as in *Figure 170b*. WILKINSON[8] has made use of a series peaking transformer for this purpose (*see* page 188).

In the circuits of *Figures 175b*, *175c* and *177* the charging current for the artificial line is required to pass through the load. If the load is a valve oscillator it is clearly necessary to shunt the latter with an inductance or resistance the impedance of which is so large that an inappreciable current is diverted during the pulse and yet small compared with the impedance of the charging choke. An

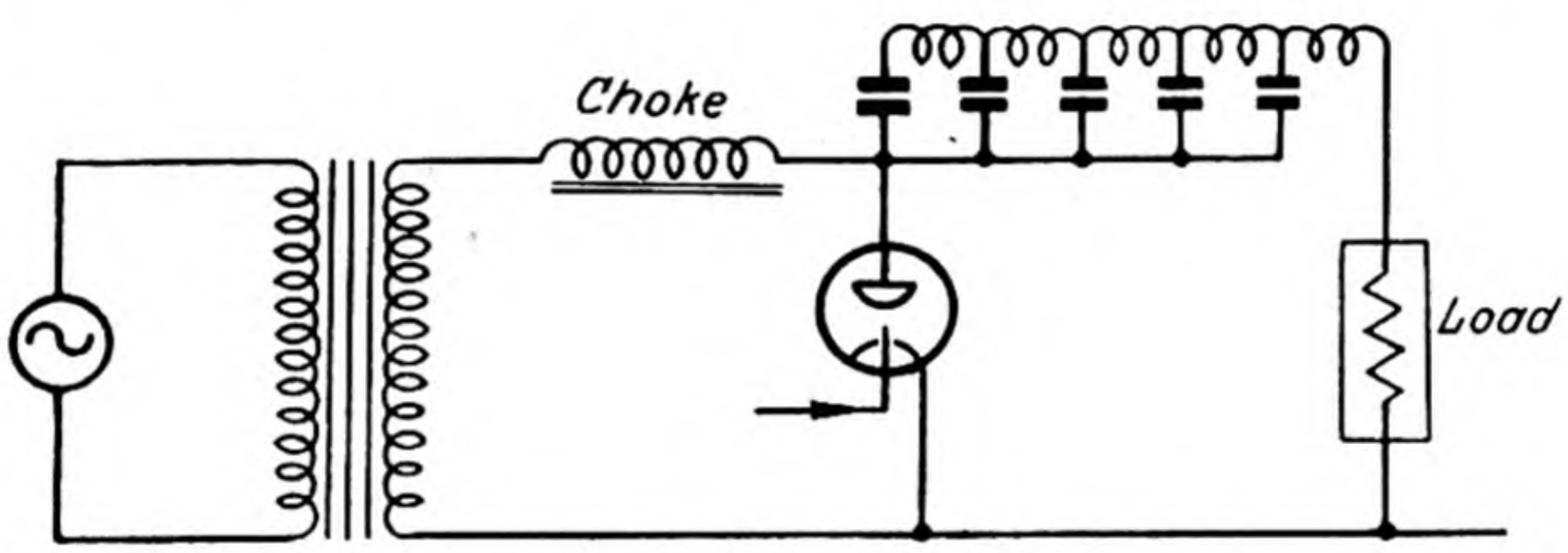

Figure 177. Basic circuit diagram for Trigatron modulator using alternator charging (Craggs, Haine and Meek[2], by courtesy, *J. Inst. elect. Engrs.*).

inductance of about 10 mH is suitable for most applications. In any of these circuits a pulse transformer[7, 19] can be connected in place of the load.

The curves of *Figure 178* show some results[2] obtained with a Trigatron of the type illustrated in *Figure 173* when discharging a line of capacitance 0·005 μF and pulse duration 1·2 μsec at 400 pulse/sec. The Trigatron operates satisfactorily at any voltage within the limits bounded by the two curves corresponding to the upper and lower operating voltages. The upper operating limit is defined as the peak voltage at which pre-firing (*i.e.* break-down without the application of the trigger voltage) occurs at a rate of not less than one per second. The lower operating limit is that at which steady operation is obtained with a jitter of $< 0{\cdot}2$ μsec. Under normal operating conditions the jitter is so small, $< 0{\cdot}1$ μsec, that it is not observed[2]. The starting voltage is set essentially by the maximum lowering of break-down voltage caused

by the incidence of the trigger pulse and is defined as the lowest steady d.c. voltage at which break-down of the main gap occurs when the trigger voltage is regularly applied.

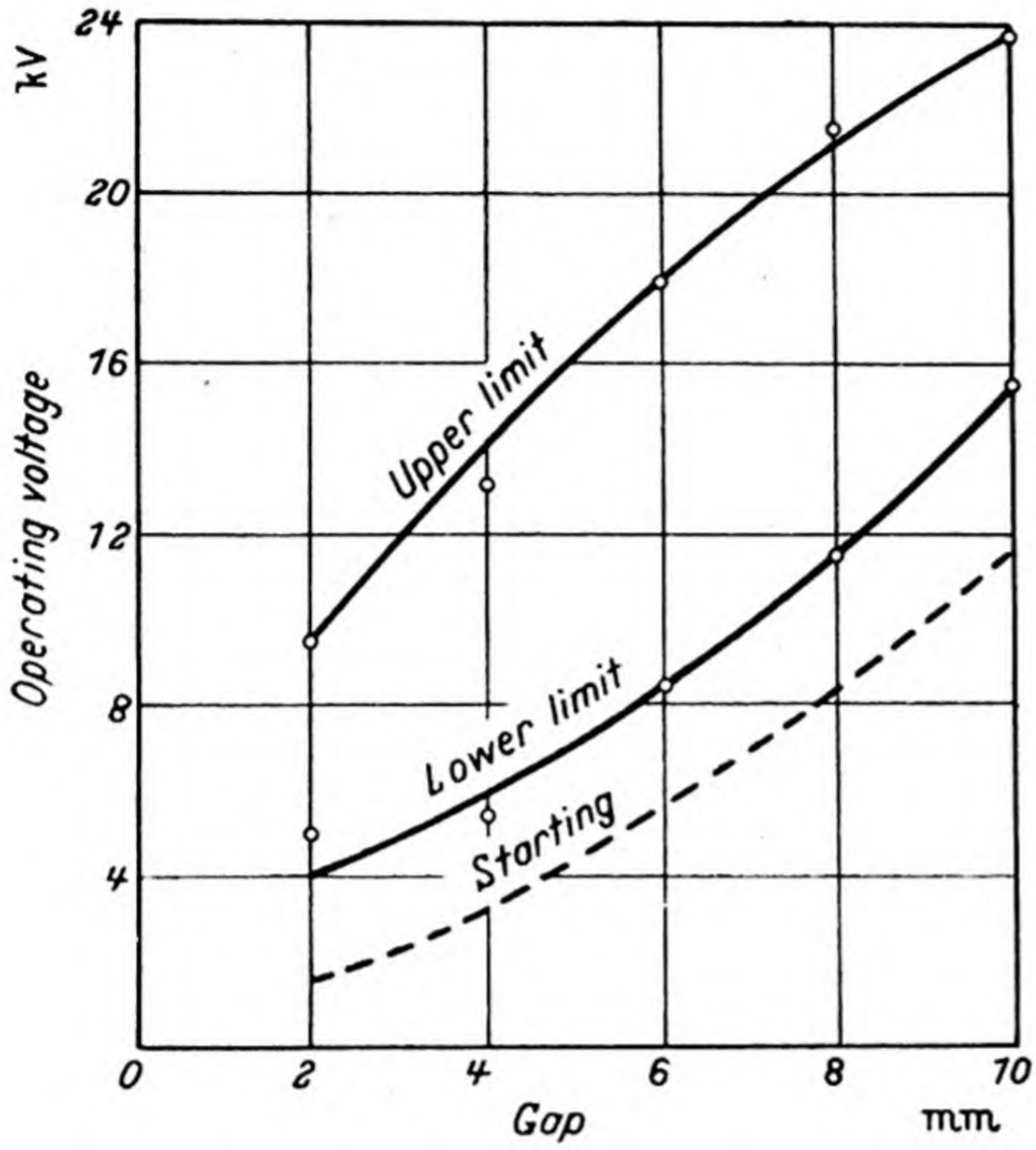

Figure 178. Operating characteristics of a typical open-air Trigatron (Craggs, Haine and Meek[2], by courtesy, *J. Inst. elect. Engrs.*).

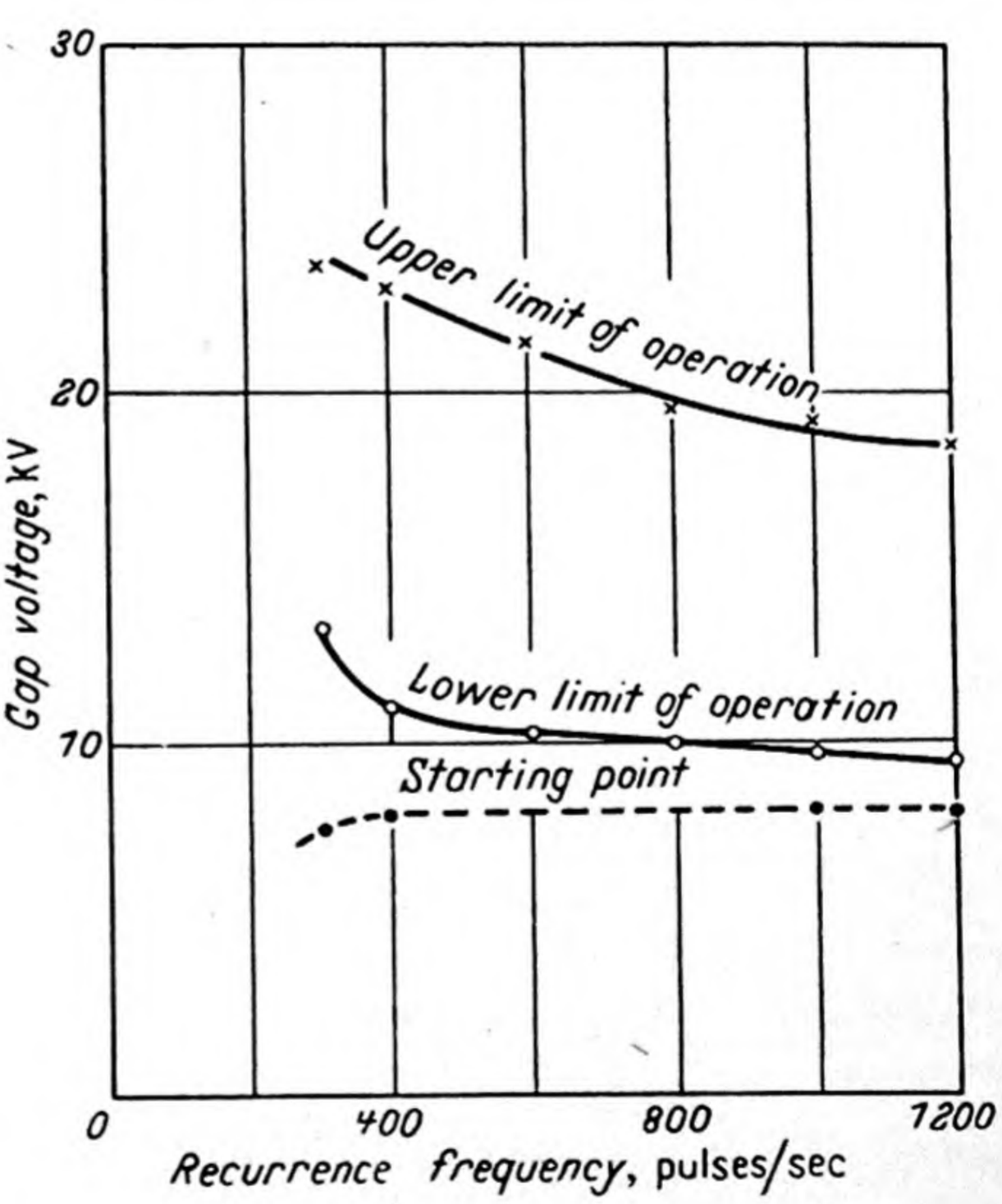

Figure 179. Operating characteristics of a typical open-air Trigatron (Craggs, Haine and Meek[2], by courtesy, *J. Inst. elect. Engrs.*).

For a given gap between the cathode and the trigger wire the operating range is little affected by the projection of the trigger wire beyond the anode, within reasonable limits. With a 5 mm. gap and a projection of 1 mm. the upper and lower operating limits are 17·7 kV

and 6·7 kV respectively for a line capacitance of 0·005 μF discharging into a 125 Ω load at 300 pulses/sec. For the same gap with no projection the upper limits are 17·4 kV and 7·8 kV. A projection of about 0·5 mm. is generally used.

With increasing pulse-recurrence rate the operating range of the Trigatron decreases, as shown in *Figure 179*, which refers to a 0·005 μF pulse network discharging into a 125 Ω load. A considerable improvement in the performance, for high pulse energies at increased recurrence rates, is obtained by the use of an air blast entering the gap through the trigger hole, as illustrated in *Figure 173*. The Trigatron has been used in this way to control 2 MW, 1 μsec pulses recurring at 1,000 pulses/sec.

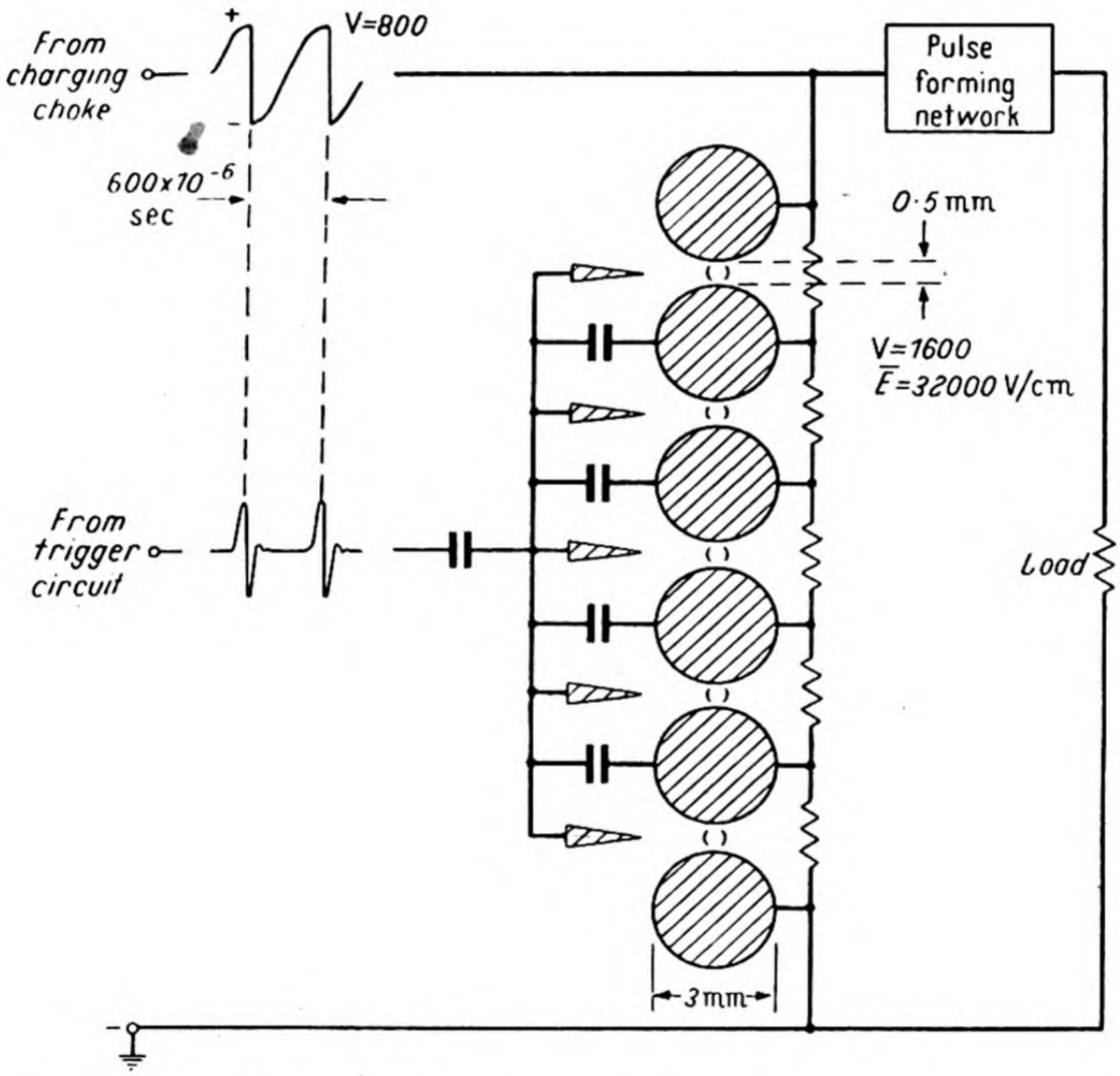

Figure 180. Line modulator circuit with fixed gap switch composed of five 0·5 mm. air gaps triggered electrically (Goucher *et al*[20], by courtesy, *Bell System tech. J.*).

A six-electrode gap operating in air, as described by Goucher *et al*[20], is shown diagrammatically in *Figure 180*. Six tungsten pins, 3 mm. in diameter, are spaced to give five 0·5 mm. gaps. The main voltage is divided by means of equal resistances connected across the gaps. The trigger pulse is applied to the four middle pins through capacitance-coupling. Corona points are also connected in such a way that the gaps are irradiated to reduce spark initiation time. By a suitable adjustment of the circuit elements the series of gaps can be broken down by the application of the trigger pulse. The operation of the

device is essentially similar to that of the three-ball gap (*see* pages 145, 169), but because of the greater number and shorter length of the gaps, for a given main charging voltage, the de-ionization is more rapid.

A Trigatron type of gap developed by COLLINS[2] for operation in compressed air at a pressure up to 3 atm. is shown in *Figure 181*. Air is blown through the trigger hole at a rate of about 6 cu. ft./min. The operating voltage ranges for three different gap lengths when the Trigatron is discharging a 0·008 μF, 1 μsec pulse network at 2,000

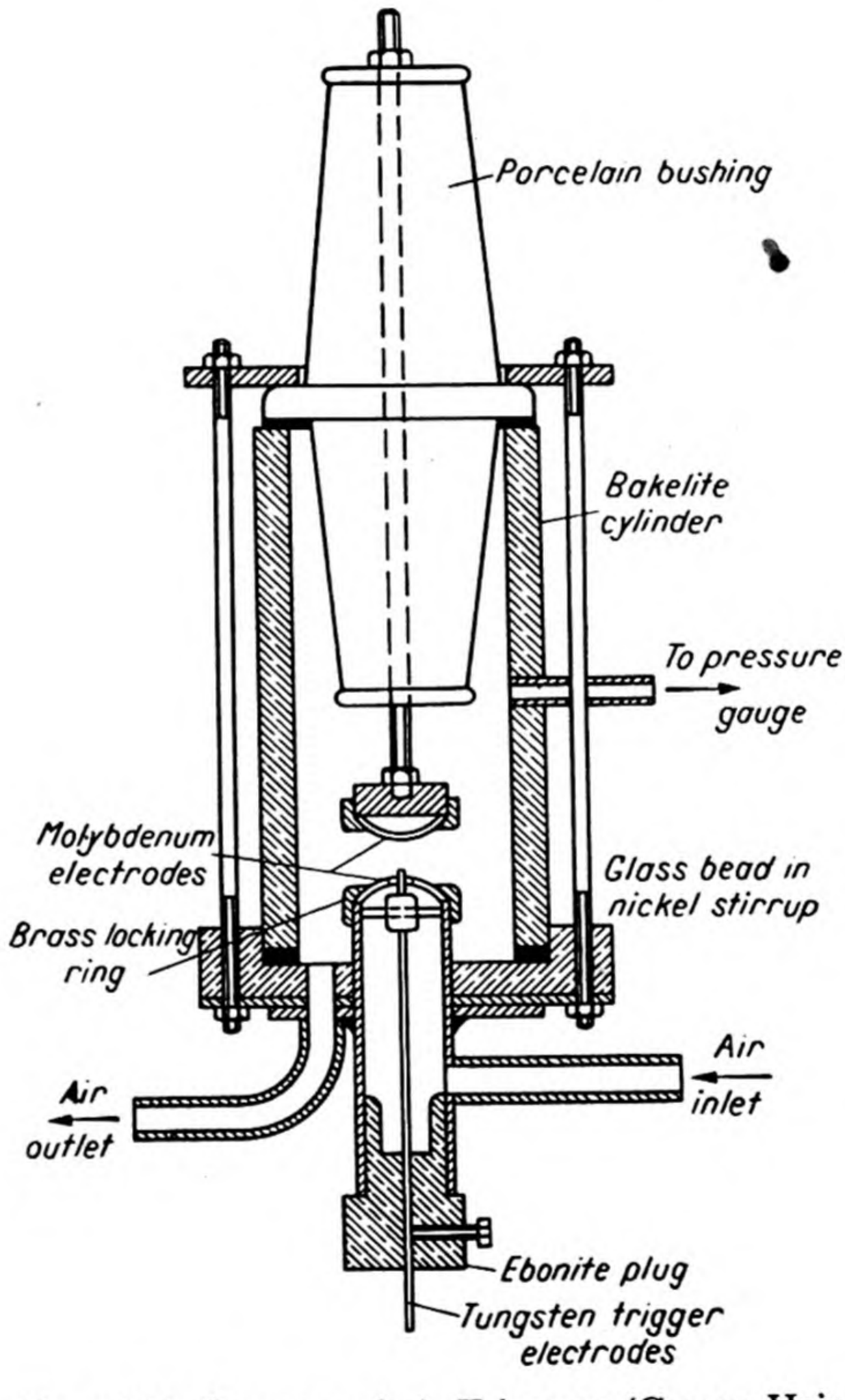

Figure 181. Compressed-air Trigatron (Craggs, Haine and Meek[2], by courtesy, *J. Inst. elect. Engrs.*).

pulse/sec, are given in *Figure 182* as a function of the air pressure in the gap. In measurements of electrode wear, when the gap was discharging a 0·012 μF, 1 μsec network at 18 kV and 2,000 pulse/sec little wear was observed in the molybdenum anode after 100 hours' operation, but the cathode, of molybdenum 0·05 in. thick, was worn through after 65 hours.

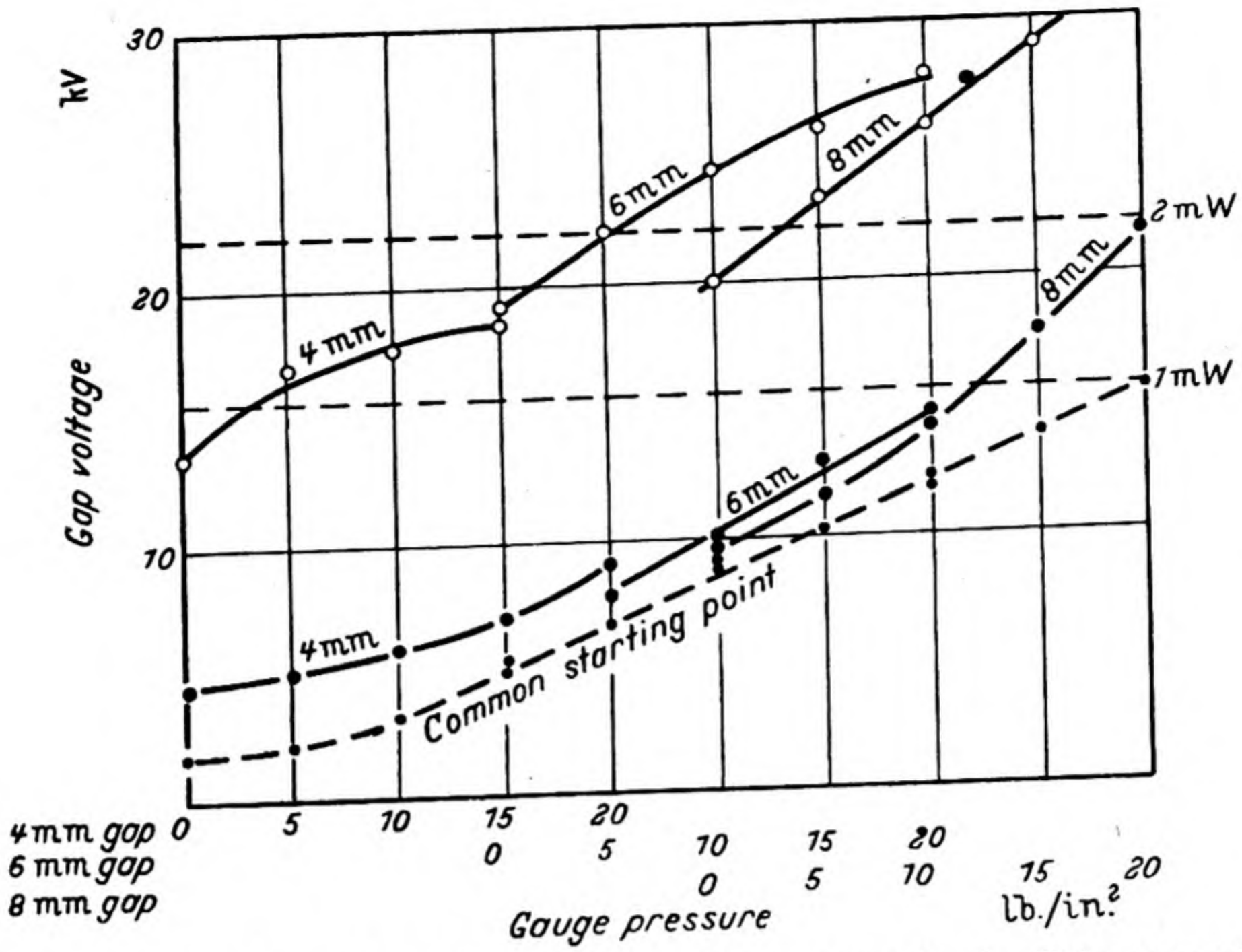

Figure 182. Operating characteristics of compressed air Trigatron of *Figure 181*, plotted as a function of air pressure (Craggs, Haine and Meek[2], by courtesy, *J. Inst. elect. Engrs.*).

Another air-blown triggered spark gap operating in compressed air has been described by WILKINSON[8]. A sectional view of one form of this gap is shown in *Figure 183.* The electrode arrangement is the same as

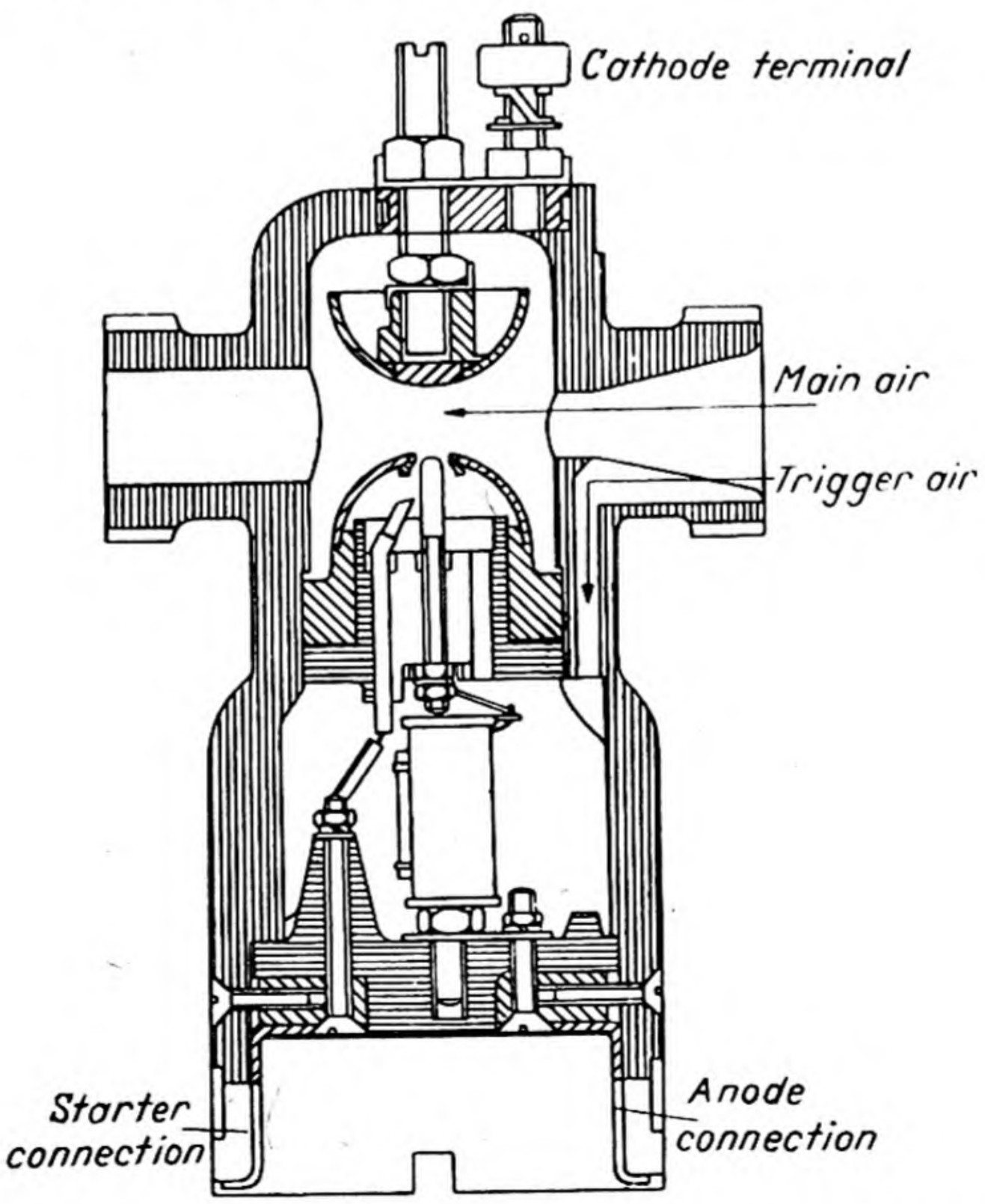

Figure 183. Sectional view of air-blown triggered four-electrode spark gap (Wilkinson[8], by courtesy, *J. Inst. elect. Engrs.*).

that in the Trigatron described above with the exception that in place of the insulator surrounding the trigger wire an auxiliary electrode, known as a starter electrode, is provided (shown to the left in the lower hemispherical electrode of *Figure 183*). The trigger voltage is applied to the starter electrode and causes spark break-down to occur between this electrode and the central trigger electrode. The starter spark irradiates the main gap through the trigger orifice and thereby reduces jitter. A stream of air is blown across the main gap, and through the trigger orifice, to ensure sufficiently rapid de-ionization of the gap.

In the modulators described by Wilkinson[8] alternator charging, as illustrated in *Figure 177*, is used. With this arrangement the gap is triggered when the charging current to the pulse network is zero, and this instant can be defined by a series peaking transformer. The trigger voltage is obtained directly from the peaking transformer using the circuit of *Figure 184*. The peak voltage is applied to a 20 $\mu\mu$F capacitor and to the starter electrode. The voltage on the latter then builds up in about 10 μsec until break-down occurs to the trigger electrode, when the 20 $\mu\mu$F capacitor discharges through the 1 mH inductance into the trigger circuit by way of the starter spark. This causes the trigger voltage to rise at a suitably high rate and leads to the break-down of the main gap.

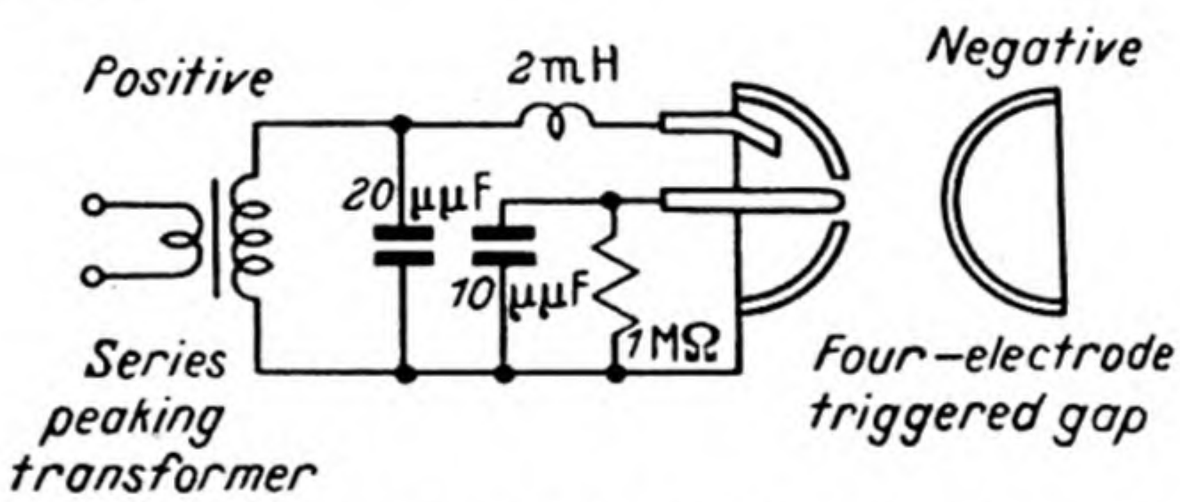

Figure 184. Method of firing the four-electrode gap directly from a peaking transformer (Wilkinson[8], by courtesy, *J. Inst. elect. Engrs.*).

If the upper and lower limits of the voltage range over which the triggered gap can be operated are respectively V_{max} and V_{min} then Wilkinson gives a figure of merit η for the gap where

$$\eta = (V_{max} - V_{min})/(V_{max} + V_{min}).$$

Curves illustrating the performance of a gap when discharging a 87 Ω, 1 μsec line at 500 pulse/sec are given in *Figure 185*. The gap is blown with 5 cu. ft./min. of air. Three curves are given for three degrees of jitter. With a mean gap voltage of 20 kV an operating range in voltage of 1·8/1 is obtained with a jitter 0·1 μsec.

A voltage-doubler circuit, developed by BLUMLEIN, is described by RATSEY[1] and Wilkinson[8]. Two cables or pulse networks, each of impedance Z_o, are connected as in *Figure 186*. Both networks are charged in parallel to a voltage $+V$. A triggered spark gap is connected across the end of one network. On the break-down of this gap a current wave

of magnitude $I = V/Z_o$ flows in the network, discharging all the capacitors and building up a current I in the inductors. When the current wave reaches the junction of the two networks, because the magnetron load is an open-circuit at that instant, the wave is reflected and tends to charge all the capacitors of the left-hand network to $-V$. The voltages then add to give an effective voltage 2 V, which is divided equally between the series networks and the matching load, and therefore a voltage $-V$ across the load for twice the transit time of the

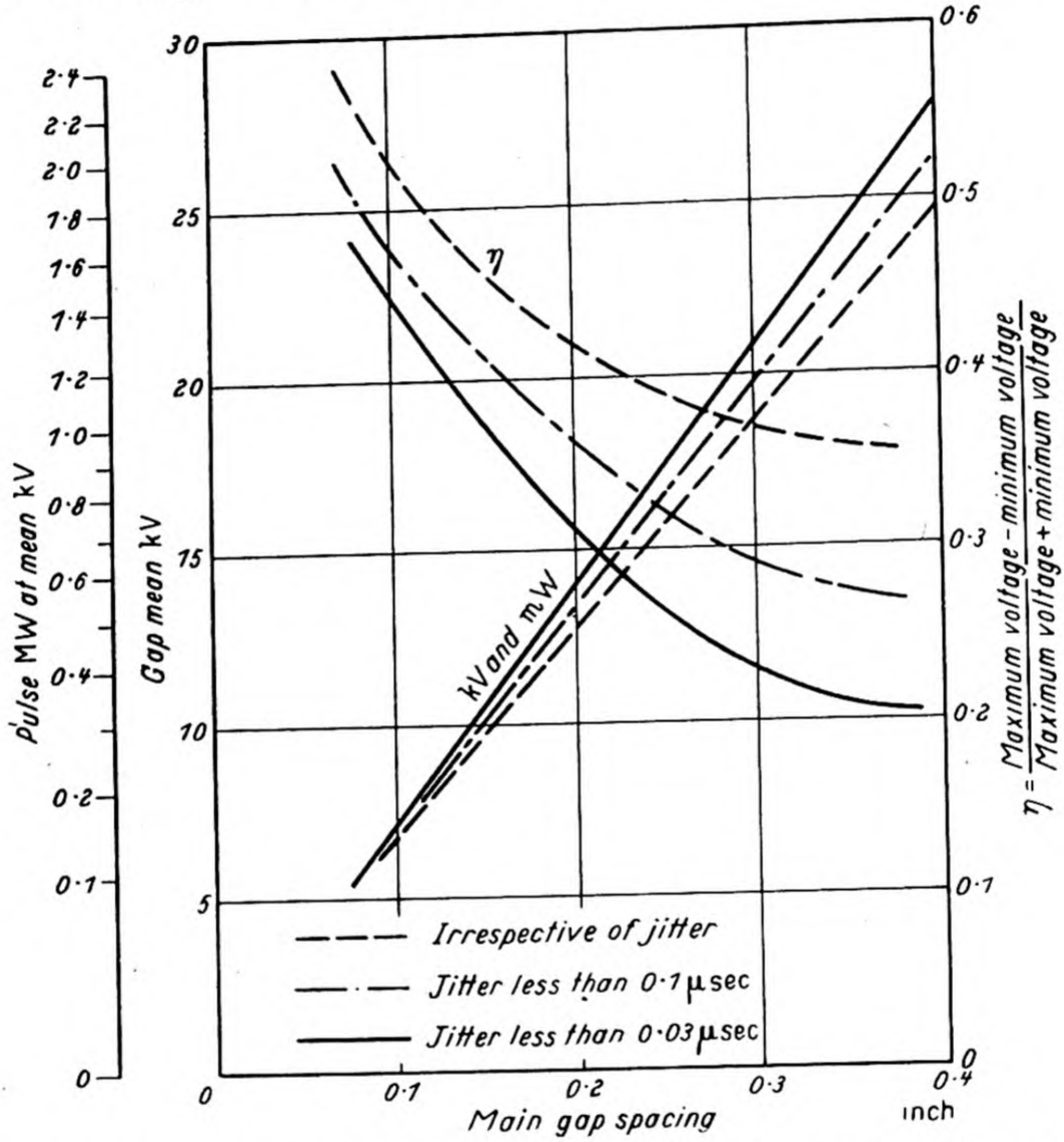
Pulse MW at mean kV
Gap mean kV
kV and mW
η
Maximum voltage − minimum voltage / Maximum voltage + minimum voltage
Irrespective of jitter
Jitter less than 0·1 μsec
Jitter less than 0·03 μsec
Main gap spacing
inch

Figure 185. Characteristics of a four-electrode blown triggered spark gap showing voltage range when discharging an 87 Ω cable at 500 pulse/sec in 1 μsec pulses (Wilkinson[8], by courtesy, *J. Inst. elect. Engrs.*).

networks. With this arrangement there is a delay of half the pulse length before the pulse is generated in the load. A full analysis of the operation of the Blumlein circuit is given by Wilkinson[8].

A four-stage Marx-connected impulse-generator circuit has been used in one of the modulators described by Wilkinson[8]. The four stages, each consisting of a pulse network, are connected by inductances in place of the resistances used in the normal Marx circuit (*see* page 115). With this arrangement pulses of 50 kV, 100 A, 5 μsec, recurring at 500 pulse/sec are obtained.

A ten-stage impulse generator incorporating pulse networks and using resistance-charging has been developed by CLAYTON[14] for use as a voltage source in the production of recurrent X-ray pulses. The

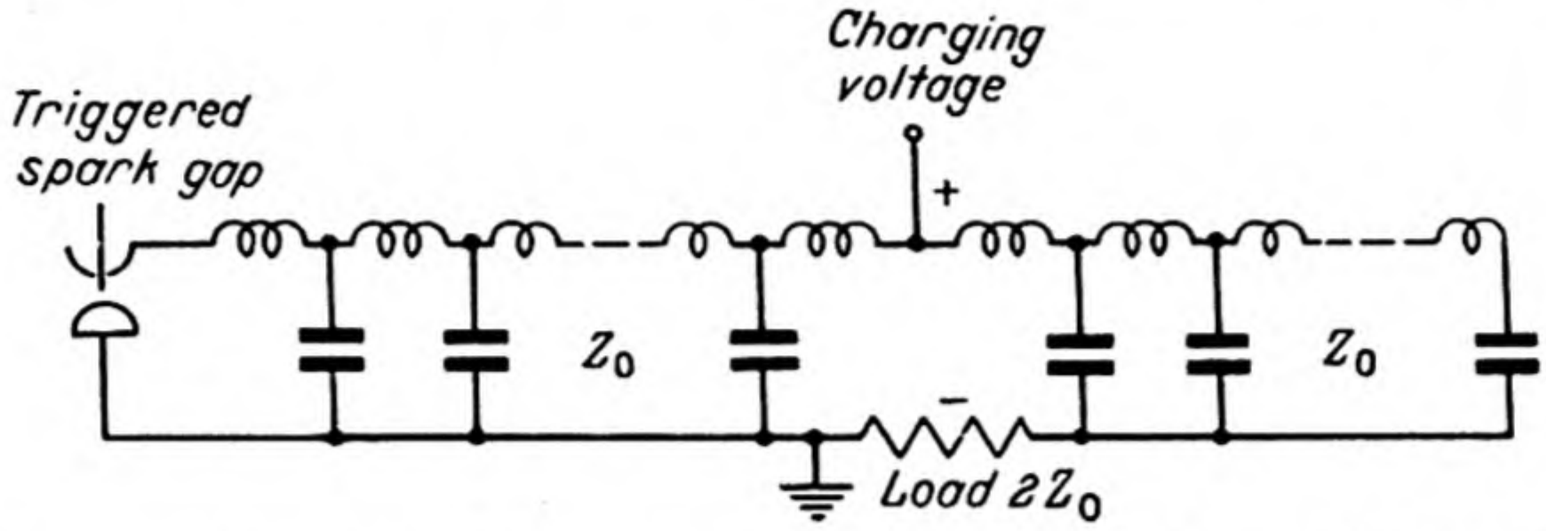

Figure 186. Blumlein voltage-doubler circuit (Wilkinson[8], by courtesy, *J. Inst. elect. Engrs.*).

spark gaps in this generator consist of sphere gaps operating in open air. The first sphere gap of the generator is triggered by the application of a 10 kV pulse to a point electrode which is directed at one of the spheres. The charging voltage is 8 kV so that the output pulse voltage is 40 kV. This generator has operated satisfactorily in the production of 1 μsec pulses at a recurrence rate of about 10 pulse/sec.

A method for the production of single current pulses by means of a chopped discharge is described by DURNFORD and MCCORMICK[24], and has been used to obtain pulses up to 500 A in amplitude and up to 10 μsec in duration with a fall-time of $< 0{\cdot}25$ μsec. The circuit given in *Figure 187* demonstrates the principle of the method. A d.c. voltage V_c is applied across the capacitance C. If a spark is caused to occur in

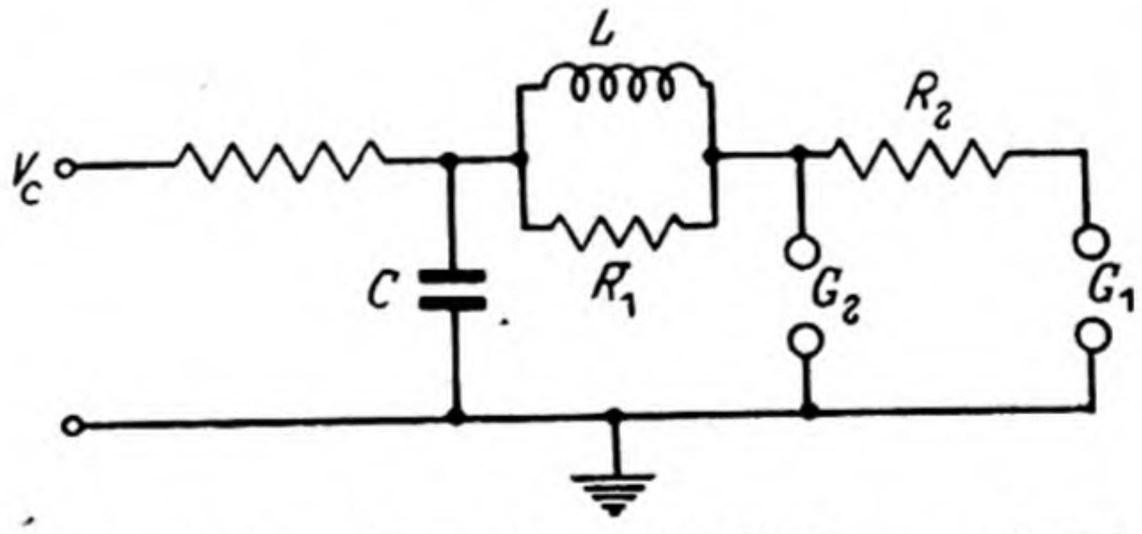

Figure 187. Compensated discharge circuit (Ratsey[1], by courtesy, *J. Inst. elect. Engrs.*).

the gap G_1 the initial current flowing through the resistance R_2 and the gap G_1 is V_c/R where $R = R_1 + R_2$. The subsequent rise of current through the inductance L may be made to compensate closely for the effect of the reduction in the voltage across the capacitance C as the latter discharges with the result that the current in G_1 can be maintained within a few per cent. of its initial value for a time that depends upon R_1/R and L. If the chopping gap G_2 is then caused to break down the current through R_2 and G_1 falls rapidly. In this way an approximately square current pulse is obtained through R_2 and G_1 ; the times of rise and fall in a practical circuit are determined only by the time

constants associated with R_1 and R_2 and the residual inductances (not shown in *Figure 187*). To obtain a short fall-time it is essential that the compensating inductance L should be connected across R_1 and not across R_2. The energy stored in L by the end of the pulse is then released mainly through G_2 and affects the fall of current in G_1 only to the extent that the impedance of G_2 cannot be neglected in comparison with that of the parallel path consisting of R_2, G_1 and of their connecting leads.

The practical form of the circuit used by Durnford and McCormick is given in *Figure 188* and shows the method for obtaining a given delay between the times of break-down of G_2 and G_1. The chopping gap G_2

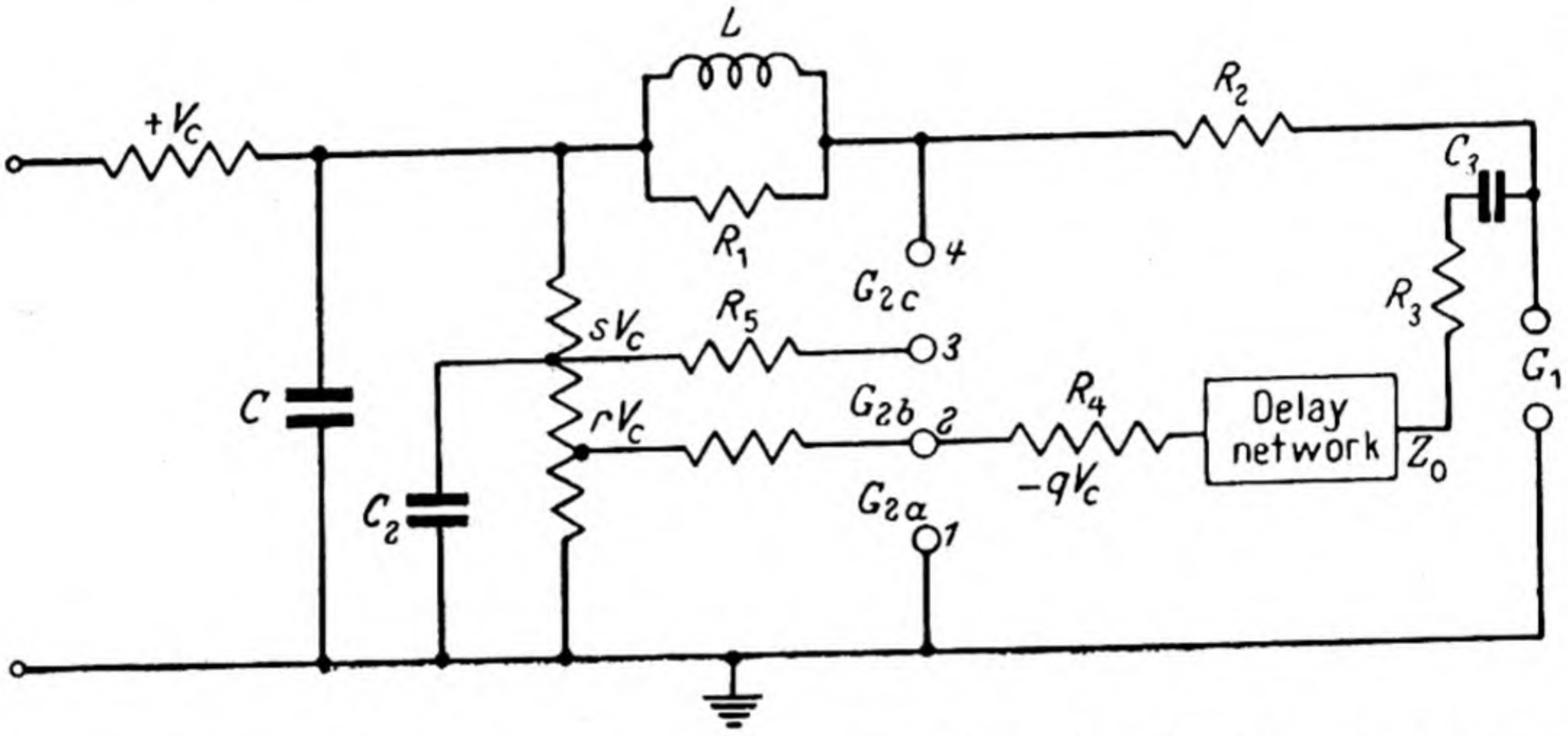

Figure 188. Chopped-discharge pulse-forming circuit (Durnford and McCormick[24], by courtesy, *Proc. Inst. elect. Engrs.*).

consists of a four-electrode triggered gap, but the Trigatron type of gap (*see* page 180) is also suitable. G_2 has to withstand the voltage V_c initially across C and to break down under the voltage of approximately $\frac{R_2}{R_1+R_2} V_c$ which is developed across R_2 during the current pulse in G_1. The trigger voltage for G_2 is obtained, as shown in *Figure 188*, by delaying in the artificial line network Z_o the proportion $\frac{Z_o}{R_3+Z_o}$ of the voltage to which C_3 is charged and which is developed across $R_3 + Z_o$ when G_1 breaks down.

With $C = 0{\cdot}5$ μF and $R_1 + R_2 = 50$ Ω, pulses of up to 500 A in amplitude and 11·2 μsec in duration have been obtained with the circuit given in *Figure 188* for initial d.c. voltages across C up to 25kV. An oscillogram of a typical pulse is shown in *Figure 189a*. If the linear resistance R_2 is replaced by a non-linear resistance material, Metrosil, of suitable characteristics a pulse with a greatly reduced fall-time is obtained as shown in *Figure 189b*. The measured reduction in fall-time for the two cases is from 0·7 μsec to 0·2 μsec. The change in pulse shape is otherwise small except that there is a slight increase in the wave-front with the Metrosil resistance.

Durnford and McCormick[24] point out that the maximum pulse-length, of about $0{\cdot}5\,C\,(R_1 + R_2)$ that can be obtained with the chopped-discharge method, for moderate variations in current amplitude, is one-half of that given by an artificial line network of the same capacitance and charging voltage and operating into its characteristic impedance to give the same current. If pulses of different durations are required a corresponding number of networks Z_o are necessary ; alternatively the network can be replaced by an RC or a valve delay-circuit in conjunction with an auxiliary trigger-voltage source. In order to maintain a given flatness of the top of the pulse the value of L should be increased directly with the pulse duration when the latter is

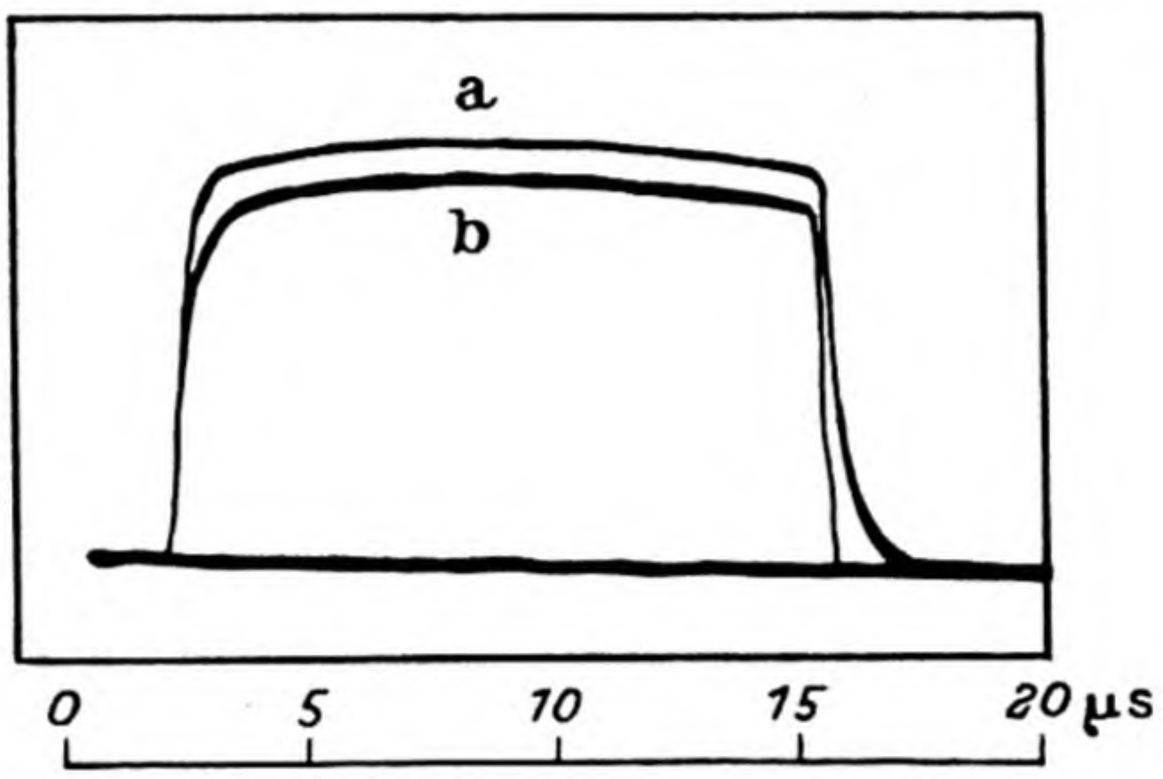

Figure 189. Current pulse. (*a*) When R_2 is linear. (*b*) When R_2 is non-linear (Durnford and McCormick[24], by courtesy, *Proc. Inst. elect. Engrs.*).

varied by means of C, keeping the charging voltage and nominal pulse current constant. This procedure, however, is limited by the resistance of L which tends to reduce the rise of the compensating current.

The voltage developed across R_2 is clearly of the same pulse-shape as the current pulse and the circuit can therefore be used to produce square voltage pulses. In this case R_2 can be placed on the earthed side of the gap G_1. At low voltages, for which G_1 and G_2 can be replaced by gas-filled relays, the rise- and fall-times obtainable are comparable with those produced by hard-valve circuits[3].

SEALED TRIGGERED SPARK GAPS

With the development of modulators for use in aircraft flying at high altitudes the need arose for triggered spark gaps to operate in sealed containers. Air was found to be unsatisfactory as the operating medium because of the formation of ozone and oxides of nitrogen which adversely affected the gap performance. The operation of Trigatrons in several other gases was therefore investigated[2].

Among the gases studied were nitrogen, hydrogen and the rare gases. Nitrogen proved to be unsatisfactory because of excessive electrode wear and the fact that the operating range decreased rapidly

with increasing frequency. Hydrogen-filled gaps had a good frequency response and a wide operating range, even at frequencies up to 3,000 pulse/sec for certain low power ratings. However, the use of hydrogen was impracticable because of the rapid wear of the electrodes and the large jitter in the time-interval between the application of the trigger pulse and the break-down of the main gap. Satisfactory operation was finally obtained with Trigatrons operating in argon containing a small amount of oxygen. Trigatrons in argon alone gave a poor performance, particularly at the higher pulse frequencies because of the slow rate of de-ionization of the gap due partly, it is thought, to the persistence of metastable argon atoms between discharges and partly to other mechanisms[15]. The addition of oxygen, which is a known quenching agent for metastable argon atoms, caused a marked improvement in the operation.

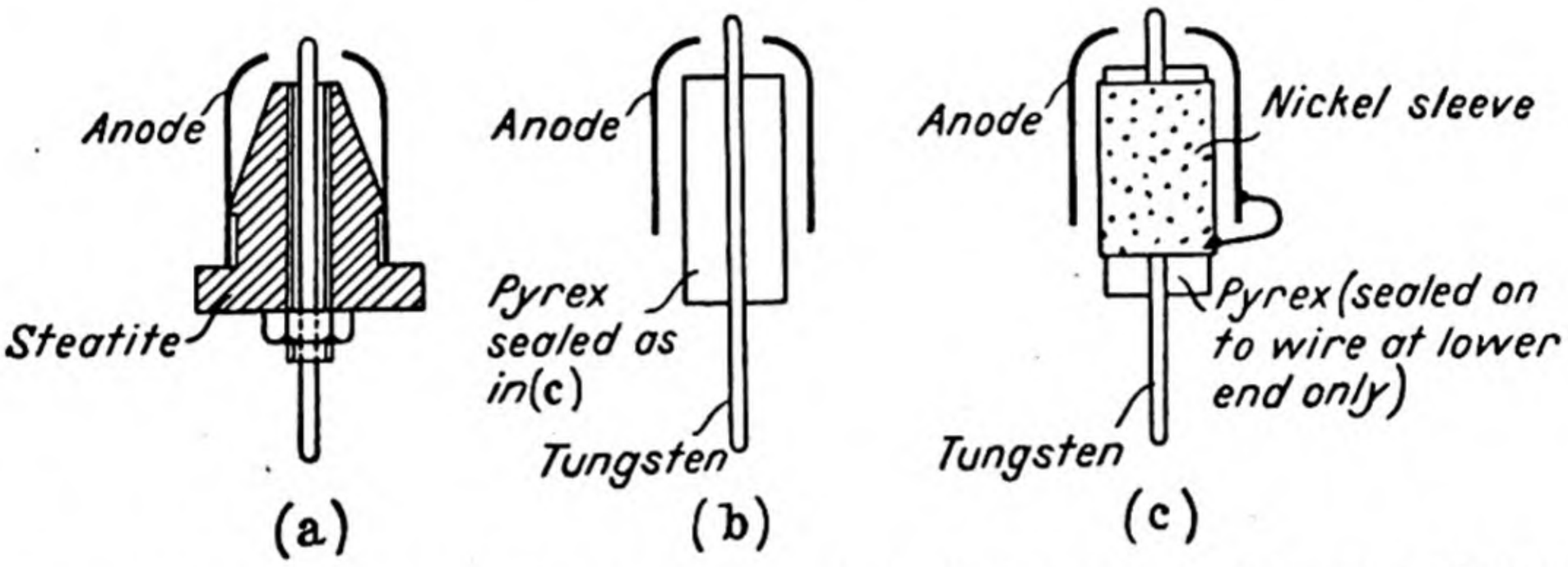

Figure 190. Trigger beads used in sealed-off Trigatrons (Craggs, Haine and Meek[2], by courtesy, *J. Inst. elect. Engrs.*).

In the final form of the sealed Trigatron developed by Craggs, Haine and Meek[2] the gap is contained in a glass bulb filled with an argon-oxygen mixture at a total pressure of several atmospheres. The operating life of a sealed Trigatron depends on the pulse power and recurrence rate but lives over 1,000 hours are obtained in many applications. The life is generally terminated by clean-up of the oxygen.

Typical arrangements of the insulating beads surrounding the trigger wire are shown in *Figure 190*. Glass proved to be the most satisfactory material of those tried, and its effect on corona production round the trigger wire was improved by the addition of a metal strap as illustrated in *Figure 190c*. With this arrangement the trigger voltage was always < 6 kV and was frequently as low as 2·5 kV.

Curves showing the upper and lower limits of the operating voltage range and the starting voltage, as a function of pulse recurrence frequency, are given in *Figure 191* for a Trigatron with a 0·5 cm. gap containing 15 cm. Hg of oxygen and filled to a pressure of 55 and 115 lb./in.^{2} abs. respectively with argon. The results were obtained for the Trigatron discharging a 0·0075 μF, 1 μsec network. A pronounced

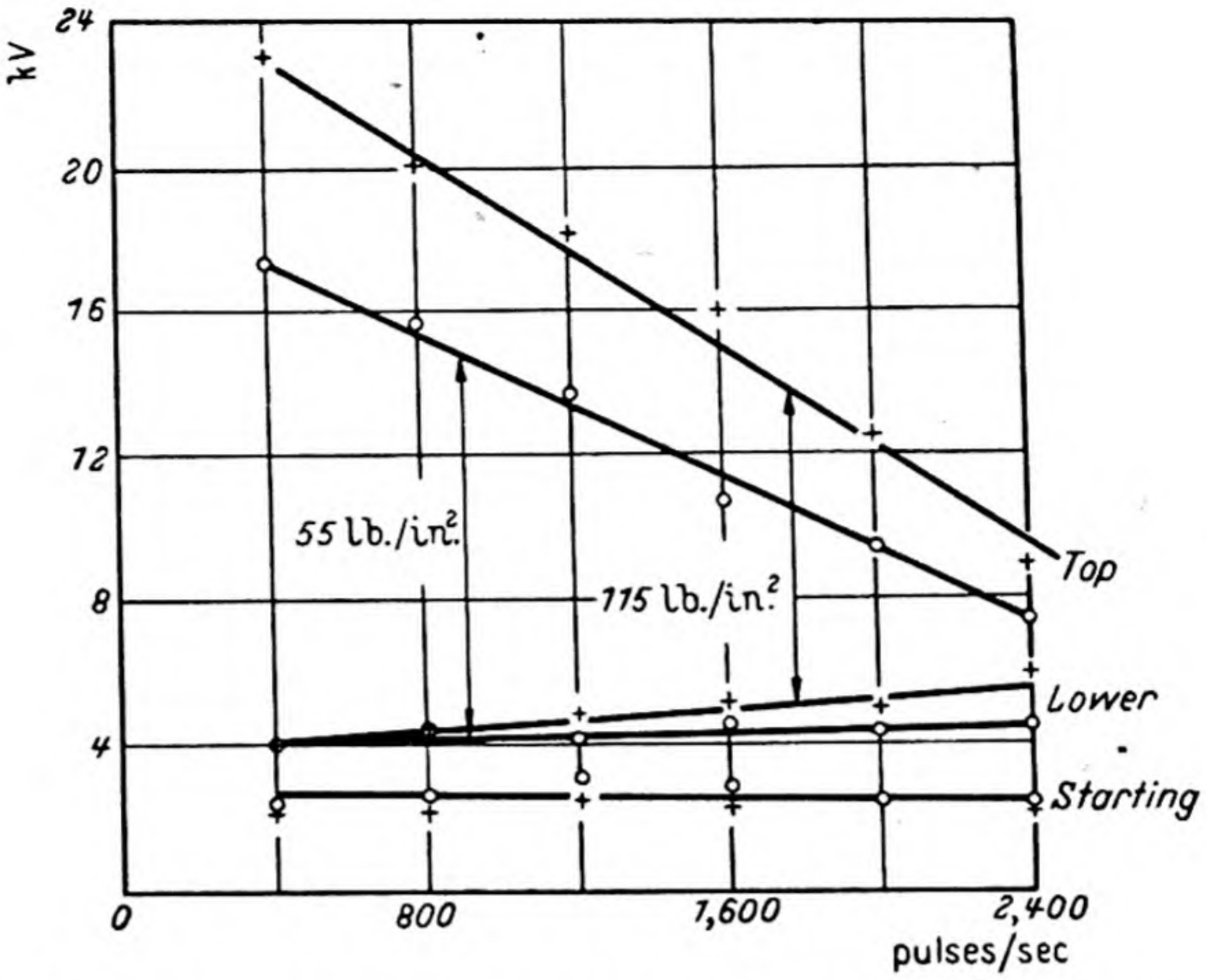

Figure 191. Curves for the upper and lower limits of operating voltage and the starting voltage as a function of pulse-recurrence frequency (Craggs, Haine and Meek[2], by courtesy, *J. Inst. elect. Engrs.*).

fall occurs in the operating range as the pulse recurrence frequency is increased.

Trigatrons may be connected in series as shown in *Figure 192* in order to control higher voltages than are possible with a single Trigatron. The external trigger pulse is applied to one Trigatron only, and the circuit is so arranged that a pulse is applied to the second Trigatron on the break-down of the first. With correctly chosen circuit components the system operates with negligible jitter, $< 0{\cdot}1$ μsec. The arrangement can be extended to include additional Trigatrons in series.

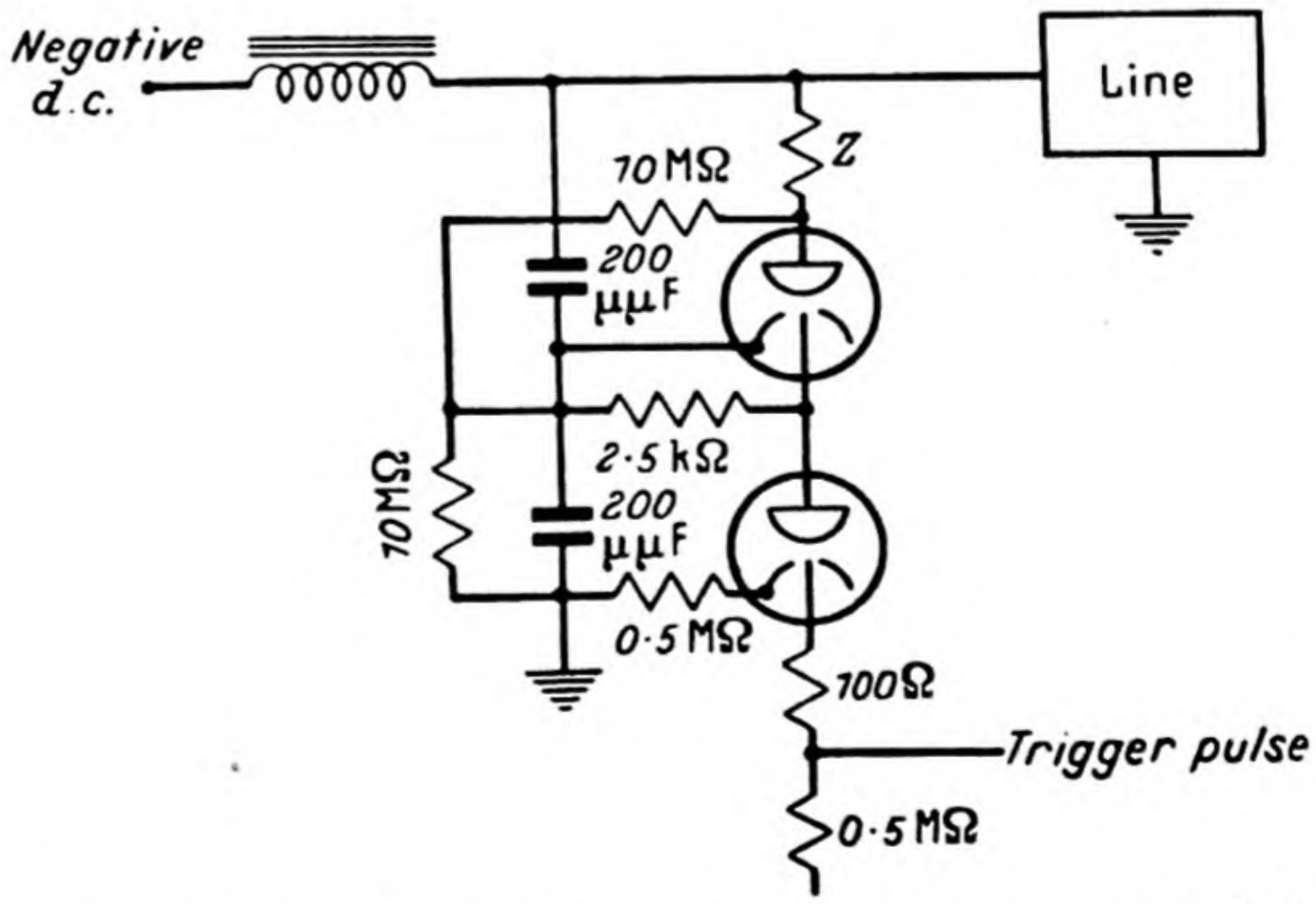

Figure 192. Circuit diagram for series operation of Trigatrons (Craggs, Haine and Meek[2], by courtesy, *J. Inst. elect. Engrs.*).

For high-power applications two or more Trigatrons may be connected in parallel, as shown for example in *Figure 193* where two pulse networks are discharged by separate Trigatrons. One Trigatron is triggered by a pulse from the external trigger circuit, and the second Trigatron by a pulse produced by the break-down of the first Trigatron.

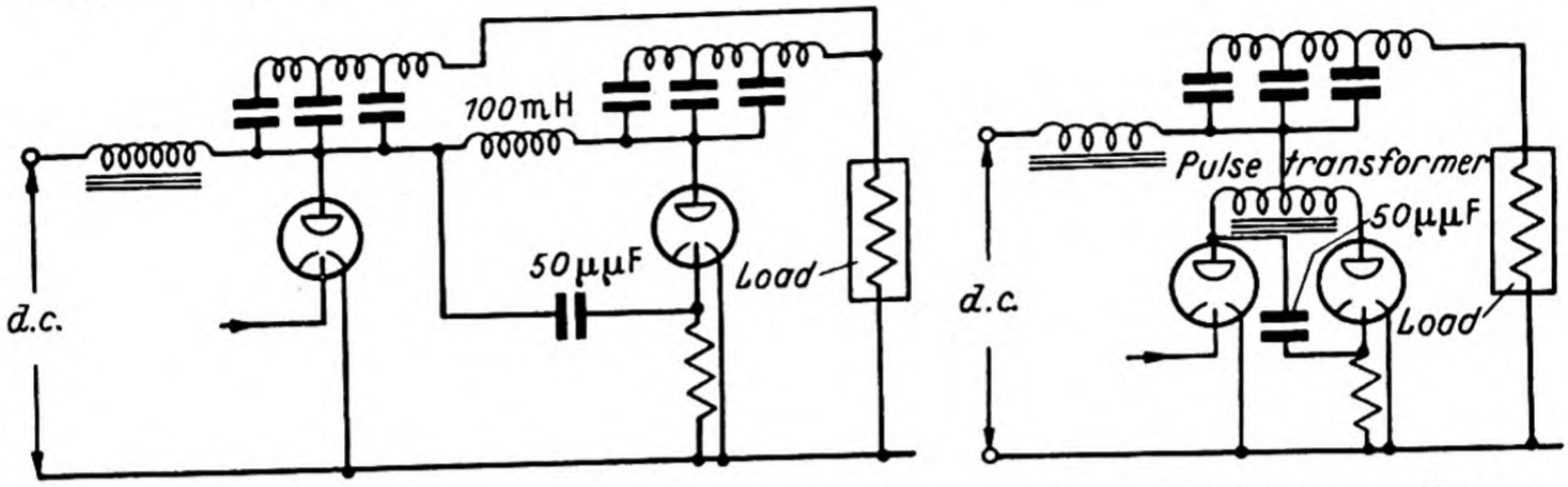

Figures 193 and 194. Circuit diagrams for parallel operation of Trigatrons (Craggs, Haine and Meek[2], by courtesy, *J. Inst. elect. Engrs.*).

An arrangement with two Trigatrons discharging a single network through a centre-tapped pulse transformer is illustrated in *Figure 194*. One Trigatron is triggered by a pulse from an external source, and the second by a pulse from the first. After break-down the currents are equalized automatically by the transformer. As the two halves of the transformer winding are in opposition the transformer offers a low impedance to the discharge.

Trigatrons may be operated in parallel using a bi-phase trigger circuit. This circuit, which may be arranged to synchronize with an incoming locking pulse or to self-oscillate, gives an output of two trigger

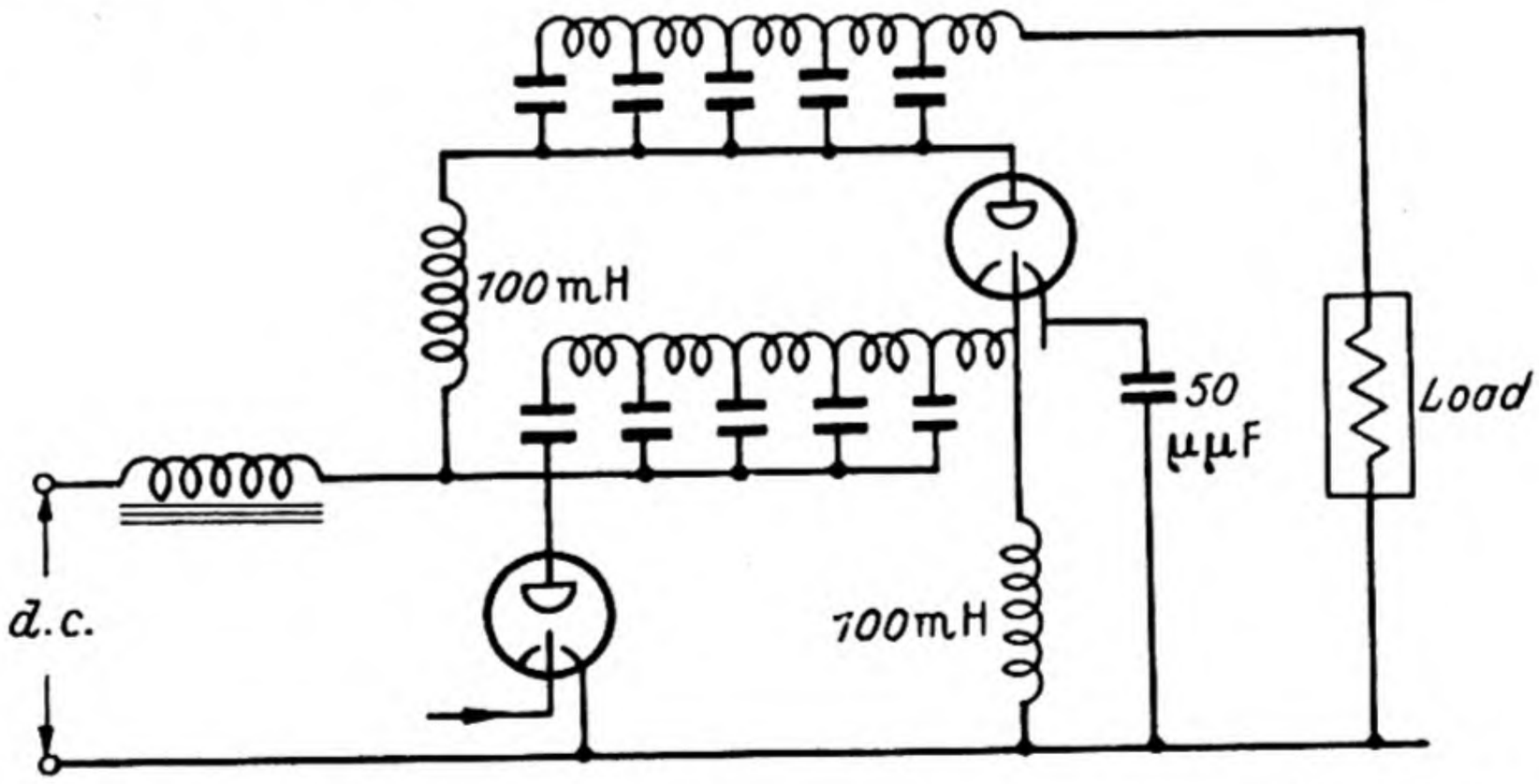

Figure 195. Circuit diagram for cascade operation of Trigatrons (Craggs, Haine and Meek[2], by courtesy. *J. Inst. elect. Engrs.*).

pulses each recurring at half the required pulse-recurrence frequency. Two Trigatrons are separately triggered by the two pulses and discharge two pulse networks through a common load, so that pulses are produced at the full frequency. Pulses of 500 kW, 1 μsec, recurring at 2,000 pulses/sec, and of 625 kW, 0·2 μsec, recurring at 3,000 pulses/sec, have been produced with Trigatrons connected in this manner.

A circuit for the operation of Trigatrons in cascade, as in an impulse generator circuit, is given in *Figure 195*. One incoming trigger pulse only is required to trigger the first Trigatron. The circuit can be extended to include three or more Trigatrons.

Other types of sealed-off spark-gaps operating in glass tubes have been developed by Goucher *et al.*[20]. In their initial experiments hydrogen was used as the gas-filling because of its high de-ionization rate. However, it proved to be unsatisfactory in that the spark in hydrogen terminated as a glow discharge with a high cathode-drop rather than the low drop required for efficient switching. This was corrected by the addition of ~25 per cent. of argon to the hydrogen. Although this gas mixture gave satisfactory operation, cathode erosion or sputtering was found to be excessive. The sputtered material was deposited on all surfaces in the form of a fine powder which eventually destroyed the insulation. With aluminium electrodes, however, it was observed that some of the sputtered material was deposited on the anode opposite the cathode from which it was removed, and for this reason tubes were finally designed with the anode surrounded by the cathode. Although in general the deposit on the anode was found to be reasonably compact and smooth the growth of spikes on the anode was observed and led to the limitation of the useful operating life of the gap. The growth of spikes in hydrogen is also recorded by Craggs, Haine and Meek[2].

A drawing of one of the gaps developed by Goucher *et al.*[20] is shown in *Figure 196*. The central anode consists of an aluminium rod surrounded by a hollow cylindrical aluminium cathode. The gas filling is 75 per cent. hydrogen and 25 per cent. argon, at a pressure of about two-thirds of an atmosphere. The inside diameter of the cathode is enlarged near its open end and the sparking is therefore confined to the deeper position of the cathode. To ensure consistent break-down irradiation of the gap is provided by corona points mounted on the cathode, opposite the anode, and a small quantity of radium is also introduced. The gap shown in *Figure 196* is designed to operate in series with a similar gap for the discharge of a pulse network charged at 4 kV and giving pulses of 67 A of 0·75 μsec duration at pulse recurrence rates up to 1,000 pulse/sec. Other similar gaps for higher pulse powers have also been developed.

A different form of gap described by Goucher *et al.*[20] has a molybdenum anode with a cathode consisting of a sintered iron sponge saturated with mercury, as shown in *Figure 197*. The gas-filling is again a hydrogen-argon mixture at a total pressure of nearly 1 atm. These tubes are capable of switching higher peak powers than the aluminium cathode gaps, and have a wider operating range and less jitter. Gaps of this type have been developed with a range approaching 3 to 1 in a two-gap circuit, capable of switching 10 MW peak power and with a time jitter < 0·02 μsec.

The operation of switching circuits using gaps of the form developed by Goucher *et al.*[20] is illustrated in *Figure 198* and is essentially similar to that of the three-ball gap described on page 169. In the two-gap circuit of *Figure 198a* if the first half-cycle of the trigger pulse and the switch voltage are both positive, gap 1 will break down when the potential at the mid-point, due to the sum of the switch voltage and that of the trigger, is equal to the gap break-down voltage. This effectively shorts gap 1 and throws the full switch voltage across gap 2 which then breaks down provided the switch voltage is equal to or greater than the break-down voltage of one gap. The gaps will operate for all switch voltages up to a value equal to twice the break-down voltage of one gap, when both gaps break down without the application of the trigger voltage. This is then the maximum operating voltage and the ratio of maximum to minimum operating voltage is two to one on the basis of this simple picture.

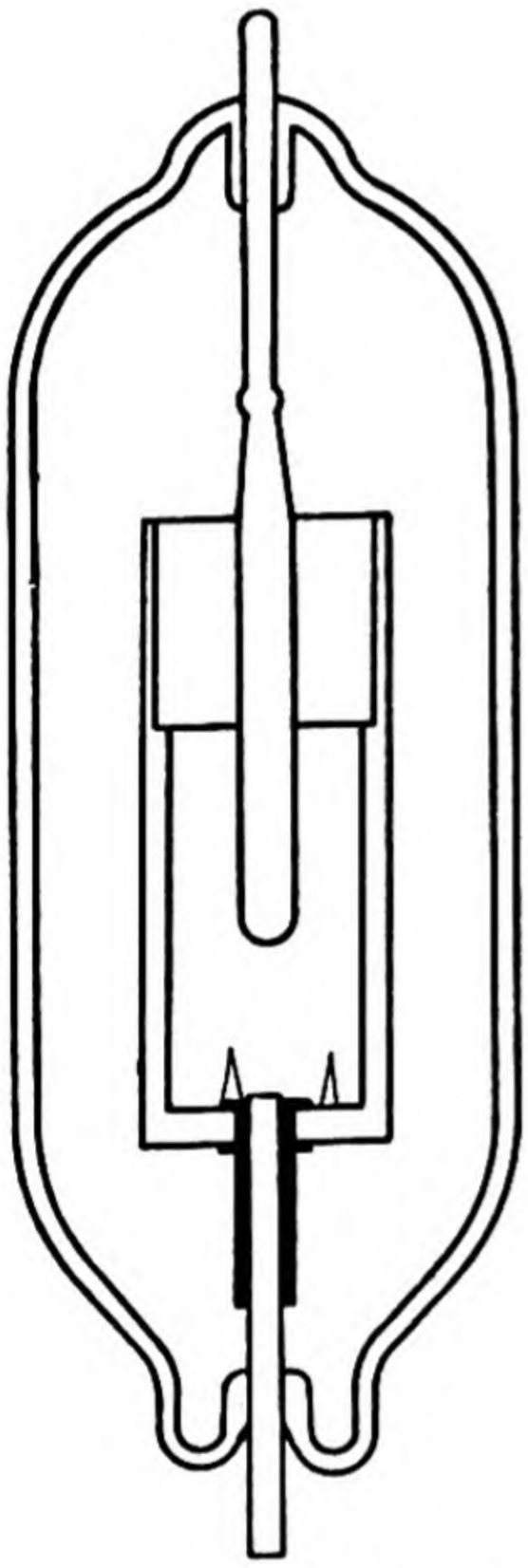

Figure 196. 1B22 spark gap tube (Goucher *et al.*[20], by courtesy, *Bell System tech. J.*).

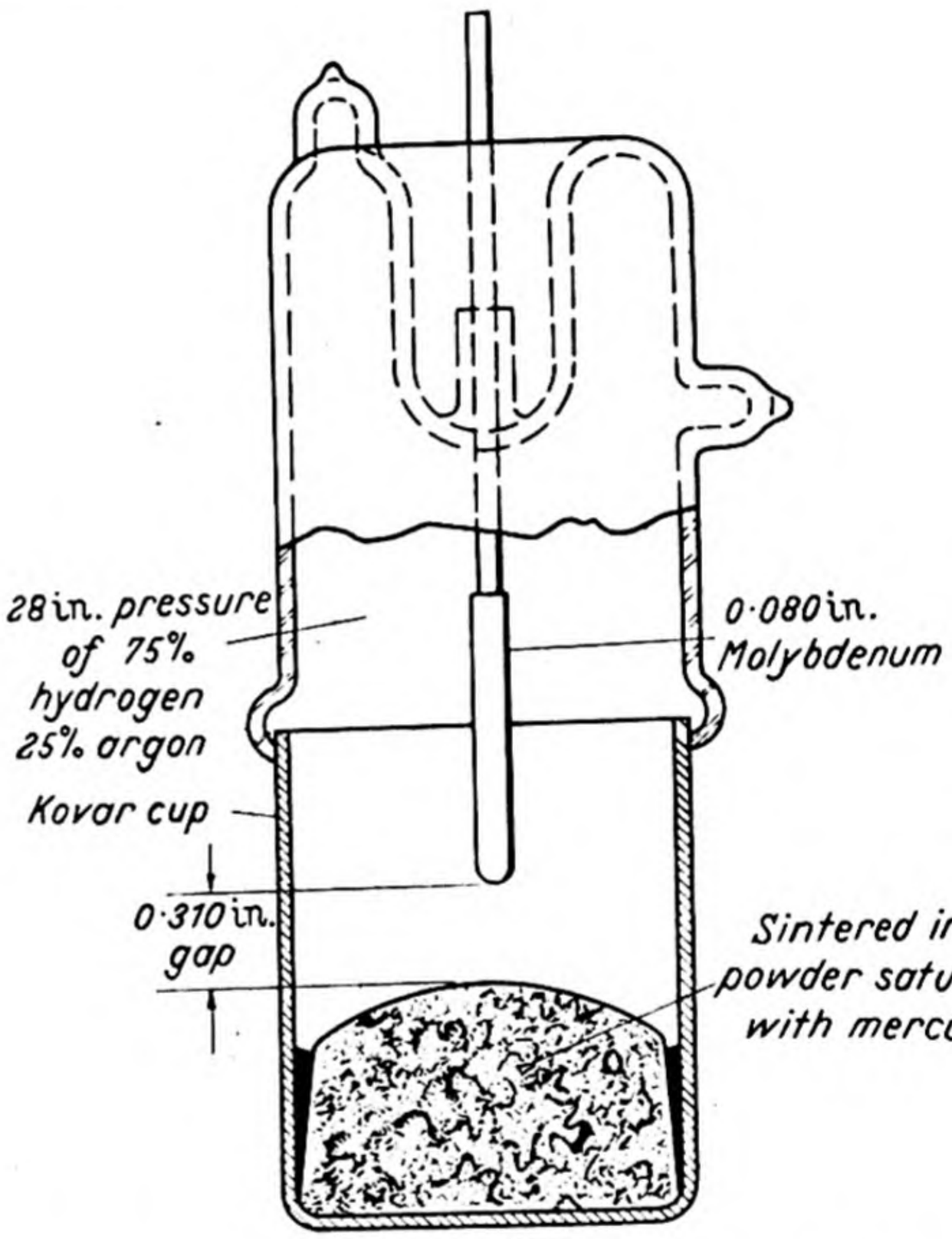
28 in. pressure of 75% hydrogen 25% argon
Kovar cup
0·310 in. gap
0·080 in. Molybdenum
Sintered iron powder saturated with mercury

Figure 197. Schematic drawing of an iron-sponge mercury cathode unit gap (Goucher *et al.*[20], by courtesy, *Bell System tech. J.*).

Goucher *et al.* next describe the three-gap circuit of *Figure 198b* where gaps 1 and 2 may be broken down by the simultaneous application of a trigger pulse. The circuit elements can be chosen so that gap 1 breaks down first and leaves enough trigger voltage on gap 2, above that supplied by the switch voltage, to break it down. The full switch

voltage is then applied across gap 3 and it will break-down for values of switch voltage in excess of the single gap break-down voltage. The switch voltage may therefore be increased to a value three times that of the break-down of one gap before the three gaps can break down without the addition of the trigger voltage. Thus the ratio of maximum to minimum operating voltage is three to one. Ideally this ratio may be increased by the addition of more gaps. However, the operating

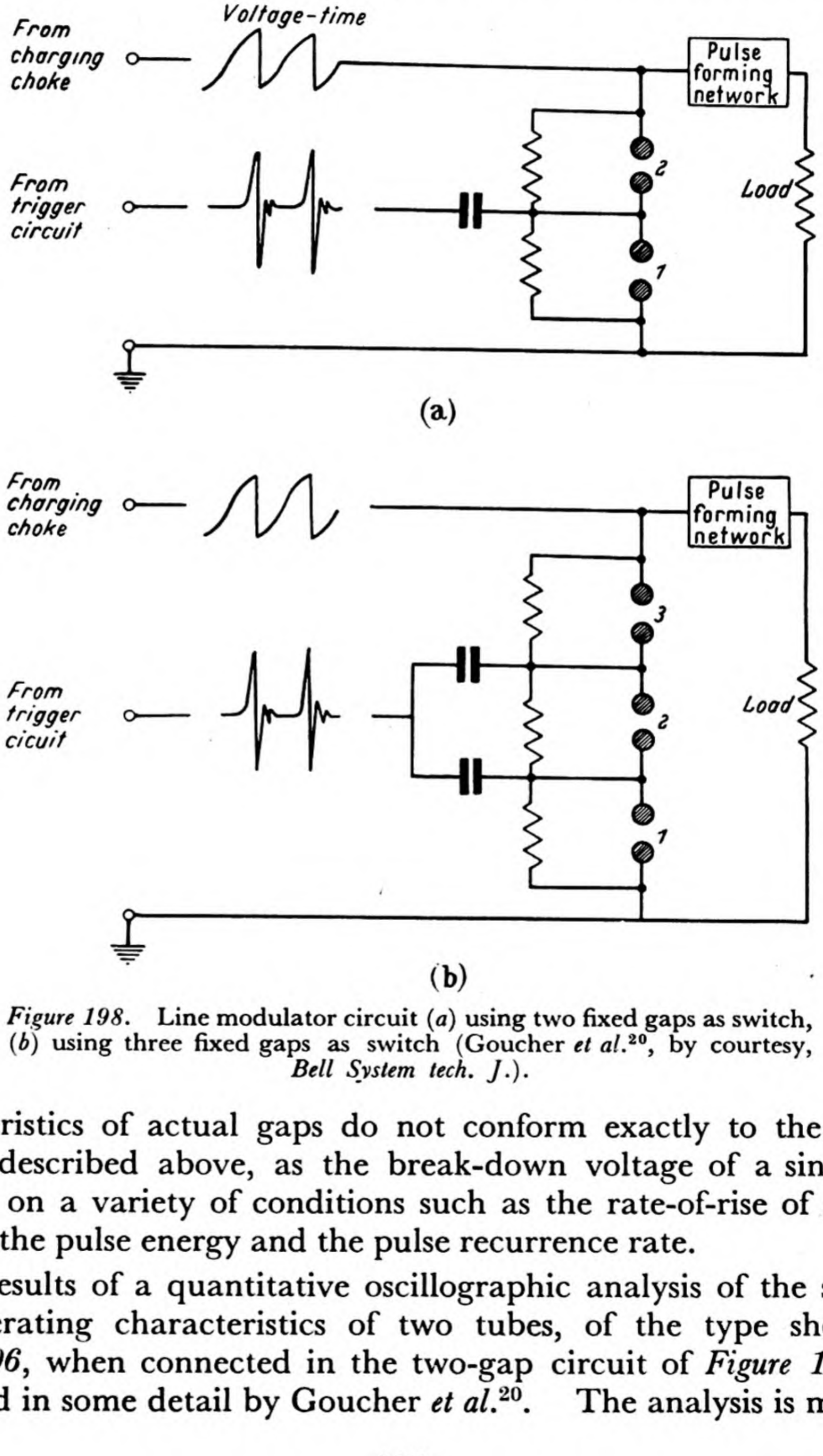

Figure 198. Line modulator circuit (*a*) using two fixed gaps as switch, (*b*) using three fixed gaps as switch (Goucher *et al.*[20], by courtesy, *Bell System tech. J.*).

characteristics of actual gaps do not conform exactly to the simple picture described above, as the break-down voltage of a single gap depends on a variety of conditions such as the rate-of-rise of applied voltage, the pulse energy and the pulse recurrence rate.

The results of a quantitative oscillographic analysis of the starting and operating characteristics of two tubes, of the type shown in *Figure 196*, when connected in the two-gap circuit of *Figure 198a* are described in some detail by Goucher *et al.*[20]. The analysis is made by

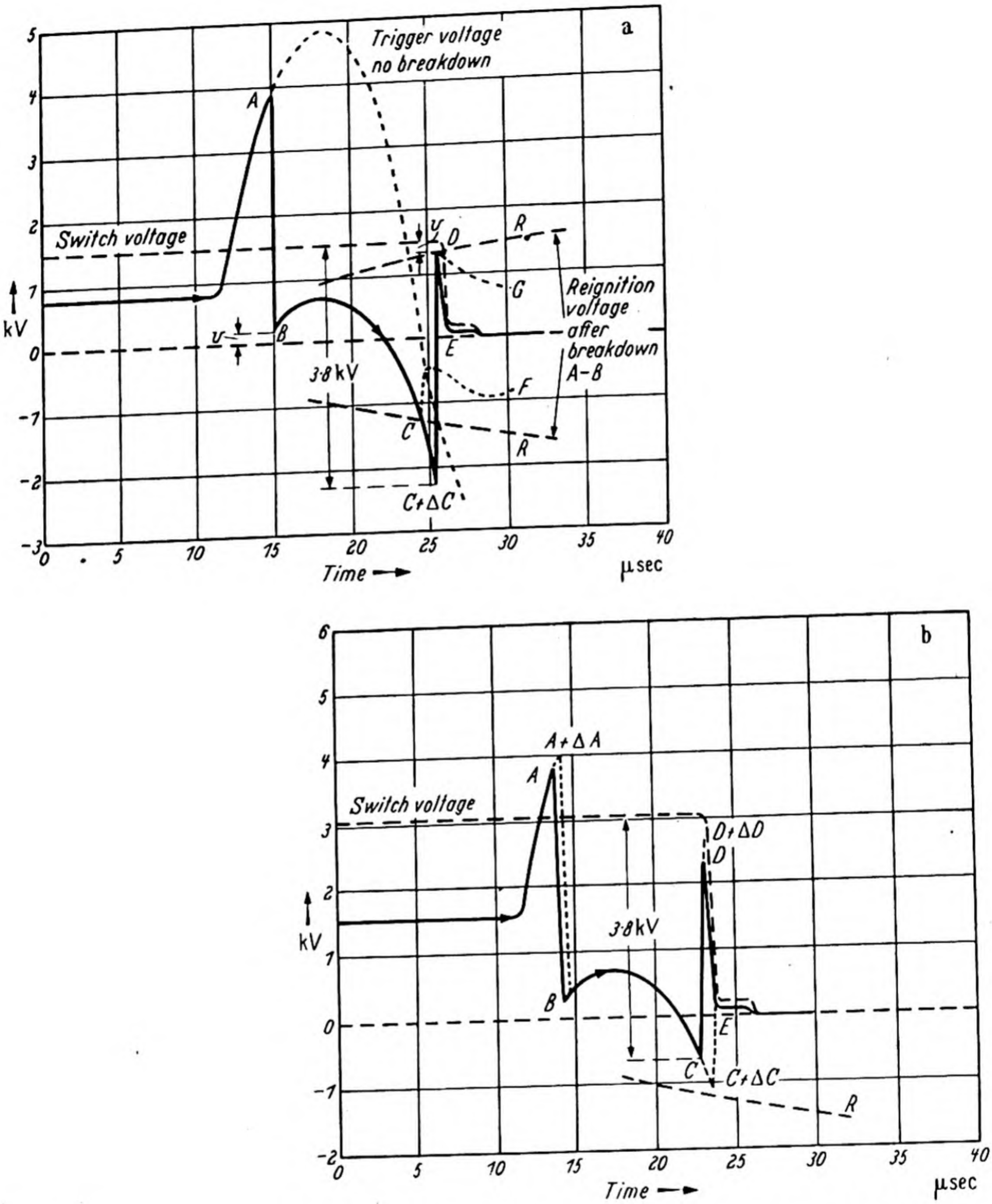

Figure 199. Oscillographic traces of voltage vs. time as measured at the mid-point of a two-gap circuit during break-down of 1B22 tubes, (*a*) for starting, (*b*) for operation at minimum switch voltage (Goucher *et al.*[20], by courtesy, *Bell System tech. J.*).

an examination of the voltage-time wave at the mid-point of the two gaps. The oscillographic traces are drawn in *Figure 199*. The voltage across gap 1 is the voltage shown on the oscillogram with respect to ground zero voltage, while the voltage across gap 2 is the voltage on the oscillogram with respect to the switch voltage.

The sequence for starting is shown in *Figure 199a*. Just before the application of the trigger pulse the voltage at the mid-point of the gaps is one-half the d.c. voltage. When the trigger pulse is applied the

voltage rises to A, 3·8 kV, which is the minimum break-down voltage for these tubes with voltage rates of rise encountered in the trigger pulse. Gap 1, therefore, may break down at A by passing a low-energy spark supplied by the trigger circuit. The voltage then drops sharply to B and the discharge stops as the voltage v remaining is insufficient to maintain the discharge. This voltage—the extinguishing voltage—is about 0·2 kV. Gap 1 is now ionized and has the independently measured re-ignition voltage characteristics R as shown. Under the action of the trigger voltage the voltage then proceeds to $C + \Delta C$ when gap 2 may break down since it has the minimum required voltage of 3·8 kV across it. When break-down occurs the voltage rises sharply to D, which falls short of the switch voltage by the amount v, the extinguishing voltage. At this point gap 1 may re-ignite. If this occurs both gaps are simultaneously conducting and the switch voltage drops to E while passing the high-current pulse of energy from the network. This sequence occurs relatively infrequently.

Because of spark delay-times arising from lack of irradiation, instead of breaking down at A, gap 1 may break down at some higher voltage, or not at all. Then, instead of gap 2 breaking down at $C + \Delta C$, gap 1 may break down in the reverse direction at any voltage higher than C, its re-ignition voltage, and is only prevented from doing so by spark delay times. Also, because of this time lag, gap 1 will usually fail to re-ignite at D, its re-ignition voltage, and since D is also the extinguishing voltage v for gap 2, the potential will drop to G. If any of these things occur the gaps will not start on that particular application of trigger pulse, but as the trigger pulses are applied at the rate of several hundred per second it is usually only a fraction of a second before operation occurs.

From the conditions necessary for starting it follows that the starting switch voltage V_{dc} must be equal to $A - (R + \Delta C)$ or $v + R$, whichever is the greater. As R increases with time, $A - (R + \Delta C)$ decreases and $v + R$ increases. A minimum for V_{dc} is obtained when the period of the trigger voltage wave is such that when gap 2 breaks down

$$A - (R + \Delta C) = v + R$$

As also for this minimum

$$V_{dc} = A - (R + \Delta C)$$

we get

$$V_{dc} = \frac{A - \Delta C + v}{2}$$

Substitution of the observed values of A, ΔC, and v in the expression for V_{dc} gives $V_{dc} = 1{\cdot}5$ kV.

After the tubes have started to operate the switch voltage is nearly double the d.c. voltage and the tubes will operate continuously provided the switch voltage is above the minimum break-down voltage.

The sequence of events near the minimum operating voltage is shown in *Figure 199b*. During operation, the spark delay time is much less than during starting.

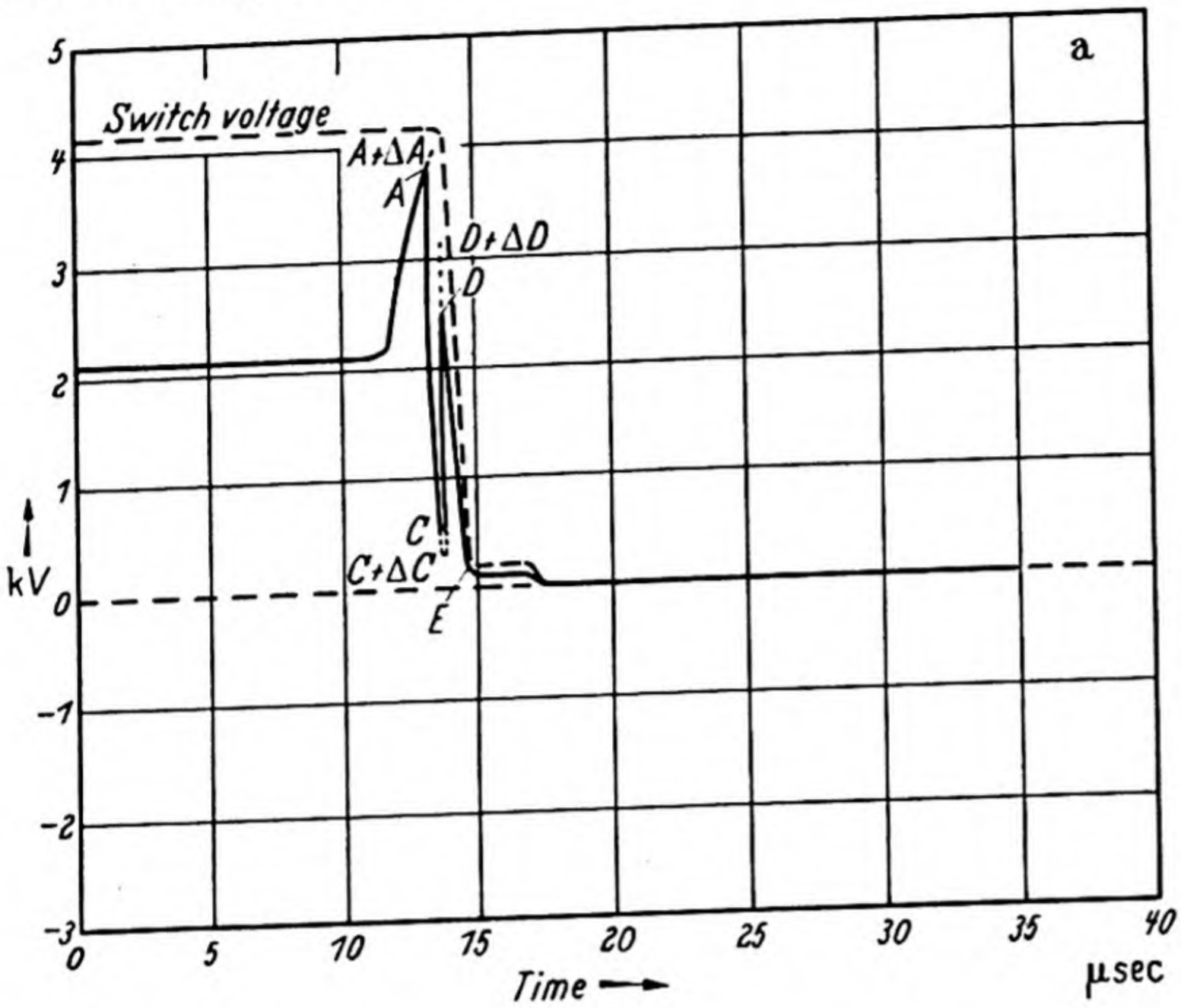

Figure 200. Oscillographic traces of voltage vs. time as measured at the mid-point of a two-gap circuit during break-down of 1B22 tubes (*a*) for normal operating switch voltage, (*b*) for operation at maximum switch voltage (Goucher *et al.*[20], by courtesy, *Bell System tech. J.*).

In practice, tubes are operated well above their minimum operating voltages. The characteristics of tubes with a switch voltage at a practical operating value are shown in *Figure 200*. Gap 1 breaks down between A and $A + \Delta A$, and before gap 1 is extinguished gap 2 breaks down between C and $C + \Delta C$. In this case both gaps are conducting

simultaneously and the main pulse passes without re-ignition of gap 1. The voltage at the mid-point of the two discharges rises to a value between D and $D + \Delta D$ due to the rapid change of spark impedance.

If the switch voltage is increased to a value near the maximum operating voltage the voltage time characteristic given in *Figure 200b* results. With a slightly higher voltage than that shown the gaps can break down spontaneously during the network-charging cycle before the application of the trigger pulse even though the value of A is some 20 per cent. greater than the charging voltage applied to the gap.

The above characteristics were obtained by Goucher *et al.*[20] using a current pulse of 0·75 μsec duration at a rate of 1,000 pulse/sec with a 30 Ω resistance load. The minimum operating voltage is then about 6·1 kV. If the pulse recurrence rate is increased to 2,000 pulse/sec the maximum operating voltage falls to 5·4 kV.

MERCURY AND HYDROGEN THYRATRONS

In most of the circuits described earlier in this chapter the triggered spark-gaps may be replaced by thyratrons, which have the advantage that a lower trigger voltage is required.

GRIFFITHS[25] refers to the use of mercury thyratrons in radar modulators and mentions the B.T.H. types CV 13 and CV 22 (or BT 45) and the GEC–MOV type CV 12. These are rated for 16 kV, 120 A pulses, 20 kV, 65 A pulses, and 15 kV, 200 A pulses respectively. A disadvantage of mercury thyratrons is the need for careful temperature control and the long warming-up time. Another disadvantage is the slow rate of de-ionization, which limits their application to pulse recurrence rates of not more than about 500 pulse/sec.

Details of the development of mercury thyratrons are given by KNIGHT and HERBERT[26] and later by KNIGHT[27]. An average life of about 900 hours is obtained for the BT 45 thyratron when operating at 20 kV and passing 100 A pulses of 1 μsec duration at 500 pulses/sec. Knight quotes an upper limit of about 600 A/μsec for the rate of current rise in mercury thyratrons. Rates of rise up to 1,000 A/μsec are obtainable but are inadvisable because of the resulting severe bombardment suffered by the cathode. Because of this limit on the rate of rise of current mercury thyratrons are unsatisfactory for use in modulators designed for the production of pulses lasting a fraction of 1 μsec.

By the use of hydrogen thyratrons some of the difficulties inherent in the use of mercury thyratrons have been overcome. Knight[27] and KNIGHT and HOOKER[28] describe two types of hydrogen thyratrons, the BT 79 and the BT 83, for operation at 3 kV and 10 kV respectively. Details of the operation of these two tubes in modulator circuits are given in *Table XIV*. In the case of the BT 83 alternative ratings are possible, the permitted peak current being inversely proportional to the

pulse frequency, though with a maximum value of 200 A. Rates of current rise up to over 2,500 A/μsec are possible but these high rates are inadvisable as they shorten the life of the tubes.

TABLE XIV

	BT 79	*BT 83*	
Anode current { peak, A	35	120	75
Anode current { mean, mA	45	100	100
Rate of current rise, A/μsec	750	1,500	1,500
Maximum frequency, pulse/sec	2,500	1,500	2,500

The hydrogen filling enables operation at frequencies much higher than is possible with mercury vapour, but it entails a higher voltage drop, in the region of 50 to 70 V as compared with 10 to 15 V. The gas pressure used is about 300 to 600 micron. Clean up of the hydrogen occurs but is counteracted by the use of a hydrogen reservoir comprising a capsule in which a quantity of titanium hydride is heated to an appropriate temperature. A suitable grid-firing voltage is one rising to at least 250 V in < 1 μsec. The hydrogen thyratron fires with great precision and the jitter between consecutive pulses is $< 0{\cdot}01$ μsec.

The development of hydrogen thyratrons in the United States is described by GERMESHAUSEN[29] who gives details of three types, the 3 C 45, 4 C 35 and 5 C 22, for operation at 3, 8 and 16 kV respectively. The corresponding peak pulse currents for these tubes are 35, 90 and 325 A. The permissible maximum pulse duration in each case is 6 μsec. Operating lives of 500 hours are quoted for these tubes operating at their maximum rating.

Ignitrons have been used in high-power pulse generators, and some details concerning experiments at the B.T-H. Company, Rugby, have been communicated to the authors by Mr. W. S. Melville. One type of ignitron used, the BK.108, has been developed from low-voltage industrial type ignitrons, such as the BK.24 and BK.44, which require only minor modifications to enable them to withstand voltages in excess of 20 kV. With the BK.108 ignitron operating lives in excess of 1,000 hours have been obtained for the following operating conditions:

Peak Pulse Power Output	:	5 Megawatts.
Max. Anode Voltage	:	25 kV
Typical Pulse Current	:	500 A.
Pulse Duration	:	2 μsec
Repetition Frequency	:	750 c/s.
Peak Ignitor Break-down Voltage	:	400–500 V.
Peak Ignitor Current	:	200–250 A.
Approx. duration of ignitor current pulse	:	3 μsec
Cooling water temperature	:	18°–23°C.
Type of Charging Circuit	:	A.C. Resonant.

The BK.108 ignitron is found to perform satisfactorily only when the temperature of the cooling liquid is closely controlled. Failures are in general due to "sludging" caused by particles of graphite, from the anode block, which become intimately mixed with the mercury and form a froth on the mercury surface. This eventually prevents the formation of an ignitor arc.

To obtain still higher powers a multi-electrode ignitron, the BK.56, has been developed in the B.T-H. Laboratories by Mr. H. de B. Knight. It is similar in design to the GL.5630 and GL.506, developed earlier by the General Electric Company in the U.S.A. and originally intended for use as inverters at 60 c/s and 20 kV. The mechanism of triggering, for output pulses of 2 μsec, is briefly as follows:

1. A voltage pulse is applied to the ignitor.
2. The ignitor strikes and a semi-sinusoid of current flows.
3. At the crest of this current a pulse of voltage is applied to the holding anode.
4. The holding anode arc is established and a semi-sinusoid of current flows.
5. At the crest of this current a voltage pulse is applied to the control grid.
6. The main anode arc is established.
7. During the main anode pulse of current, the control grid remains around earth potential.
8. After the main anode pulse, ionization persists for about 100 μ sec during which time the control grid remains at earth potential; it then returns exponentially with a time constant of about 100 μsec to the bias line. The ignitor and holding anode arcs extinguish themselves respectively about 3 and 5 μsec after the main pulse.

Typical operational conditions are given below.

Peak Pulse Power Output	:	about 20 Megawatts.
Max. Anode Voltage	:	60 kV.
Typical Anode Current	:	1,000 A.
Pulse Duration	:	2 μsec.
Repetition Frequency	:	750 c/s.
Ignitor Conditions	:	as for BK.108 (see above).
Holding Anode voltage	:	200 V.
Peak Holding Anode Current	:	30 A.
Control grid bias voltage	:	-100 V.
Control grid pulse voltage	:	$+500$ V.
Screen grid voltage	:	0
Grading Anode voltage	:	$0{\cdot}5 \times$ Main Anode Volts.
Cooling Water Temperature	:	$45°C. \pm 1°C.$
Anode Seal	:	Externally heated.
Type of Charging Circuit	:	A.C. Resonant.
Mean Output Power	:	about 25 Kilowatts.

A modulator operating under these conditions has shown no sign of deterioration after several hundred hours of service.

HARD-VALVE PULSE GENERATORS

The design of hard-valve modulators for the production of high-voltage pulses has been discussed by JOHNSON[6]. There are two principal forms of circuits used. In one the load is in series with the modulating valve, as in *Figure 201*, while in the other it is parallel-fed by a capacitor or transformer, as in *Figure 202*.

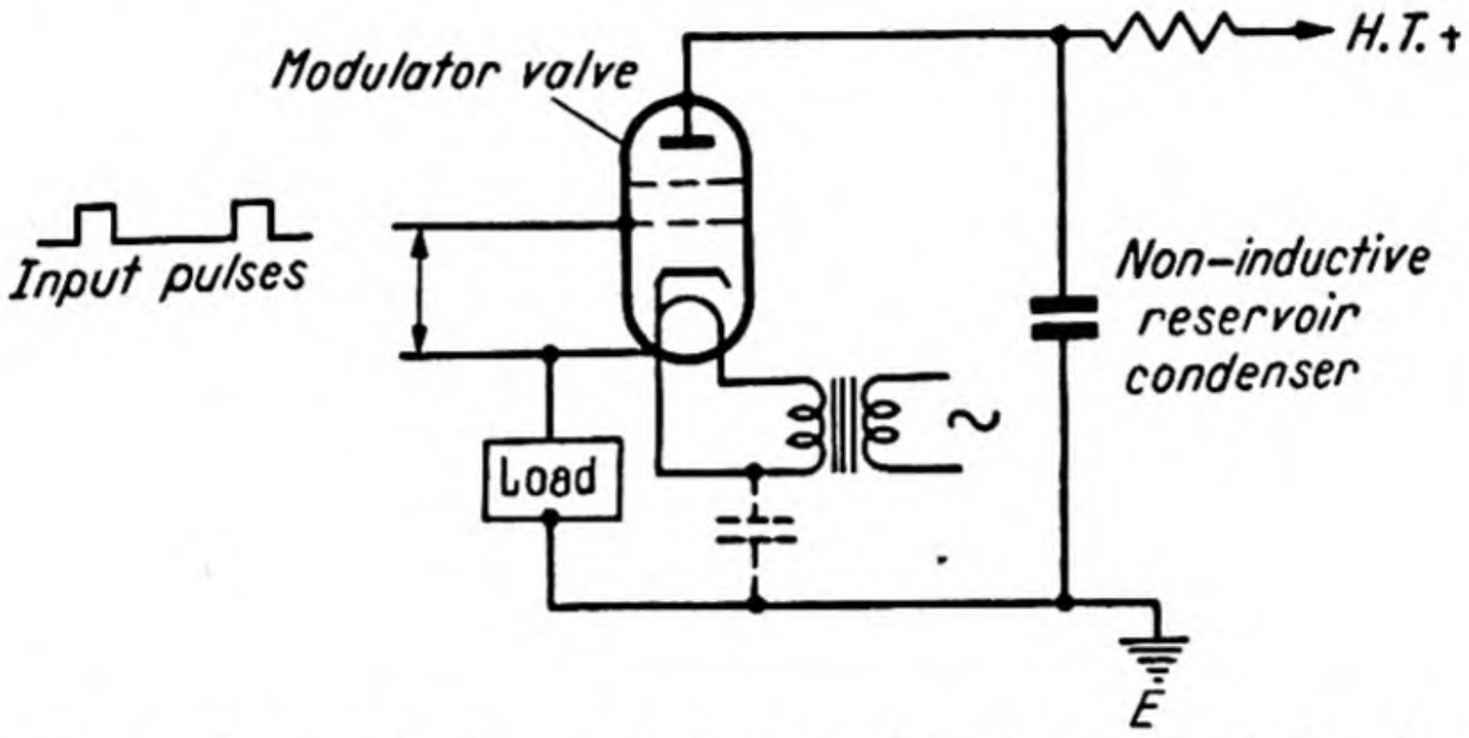

Figure 201. Series modulation circuit (Johnson[6], by courtesy, *J. Inst. elect. Engrs.*).

The output from the circuit of *Figure 201* is in the form of positive-going pulses. In this circuit the stray capacitances to earth of the filament-heater winding and the grid circuit shunt the load and this seriously affects the pulse shape for pulses of short duration. It is also difficult to drive the modulator valve, as part of the drive circuit has to be insulated to pulse potential. This can be overcome by the use of a suitable pulse transformer. In practice a tetrode could be used, with a separate screen supply, as too much power would be wasted by a potential divider across the main h.t. supply. The pulse current is taken from the reservoir condenser.

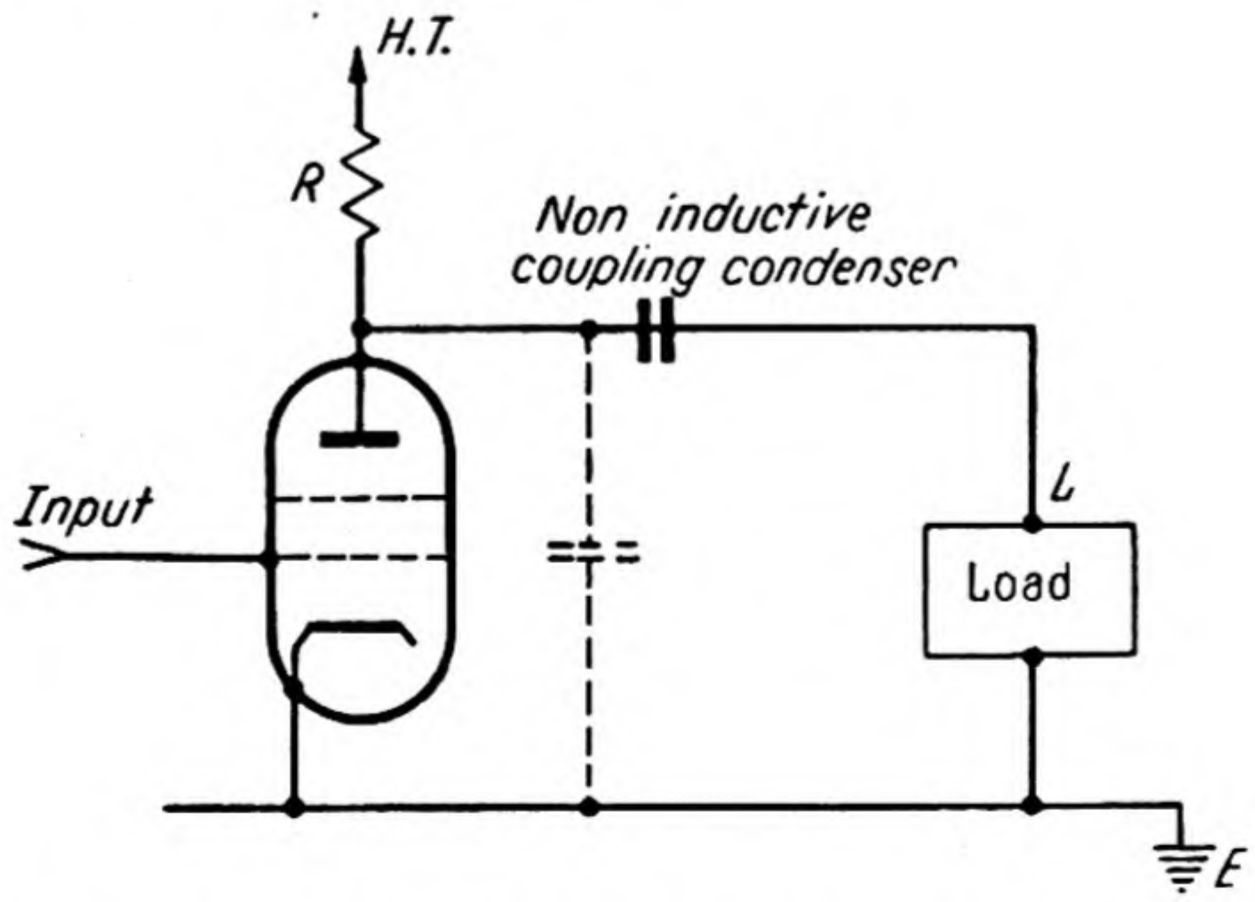

Figure 202. Parallel-feed modulator (Johnson[6], by courtesy, *J. Inst. elect. Engrs.*).

The circuit of *Figure 202* yields negative pulses. The capacitances shunting the load are the anode-earth capacitance of the modulator valve and the capacitance to earth of the coupling condenser, which has to be insulated to the full pulse potential. This circuit is that most commonly used as it is the most flexible and only one component has to be highly insulated.

Another method of feeding the load is through a pulse transformer in place of *R* in *Figure 202*. Owing to the difficulties of maintaining the characteristics of the pulse transformer, and of providing insulation for the full h.t. voltage, it is better to supply the pulse transformer as shown in the position *L* of *Figure 202*. The transformer can be phase-reversing or otherwise according to the output required.

Johnson gives details of a hard-valve modulator yielding approximately square pulses of 10 A at 10 kV. The pulse width is continuously variable from less than 0·1 to 2 μsec and the pulse recurrence rate can be varied up to 5 kc/s. Another hard-valve modulator described by Johnson produces square pulses of 50 A at 20 kV, with pulse duration continuously variable from 0·2 to 2 μsec and pulse recurrence rates up to 5 kc/s.

The advantages of hard-valve modulators, as compared with modulators using pulse-forming networks, have been summarized by Johnson as follows:

(1) The repetition frequency can be varied continuously from zero, the upper limit being governed by the mean power rating and the dissipation of the valves.

(2) The pulse duration can be made to vary over a wide range and may be altered when the modulator is operating.

(3) The pulse can have an almost perfectly flat top as there is no lumped pulse-forming network and not necessarily a pulse transformer.

(4) The output is easily controlled at any value from zero upwards.

Disadvantages are :

(1) The minimum time of rise of the pulse is limited but can be reduced to $< 0{\cdot}1$ μsec.

(2) There is a long time of fall of the voltage pulse, when operating into a magnetron load, because the load impedance becomes high after the voltage has fallen below that required to pass current through the magnetron. In practice this can be reduced to < 1 μsec, and as the magnetron is not then passing current, its operation is not normally affected. When the modulator is feeding a resistive load the time of fall is only a little longer than the time of rise.

(3) The energy stored in the reservoir condenser is many times that required for a single pulse, and the possibility of damage to the load is therefore greater than with a generator using a pulse network.

Details of American hard-valve pulse modulators are given by GLASOE[30].

MAGNETIC SWITCHING DEVICES

MELVILLE[31, 32] has developed a completely different system for the production of square pulses in which use is made of saturable reactors, known as pulsactors, with cores of materials having rectangular B–H characteristics and saturating at low values of the magnetizing force H.

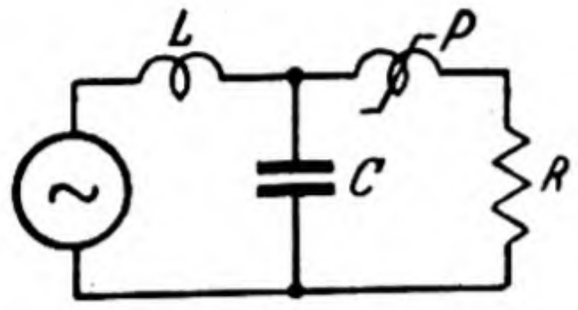

(a) *Simple pulsactor pulse generator*

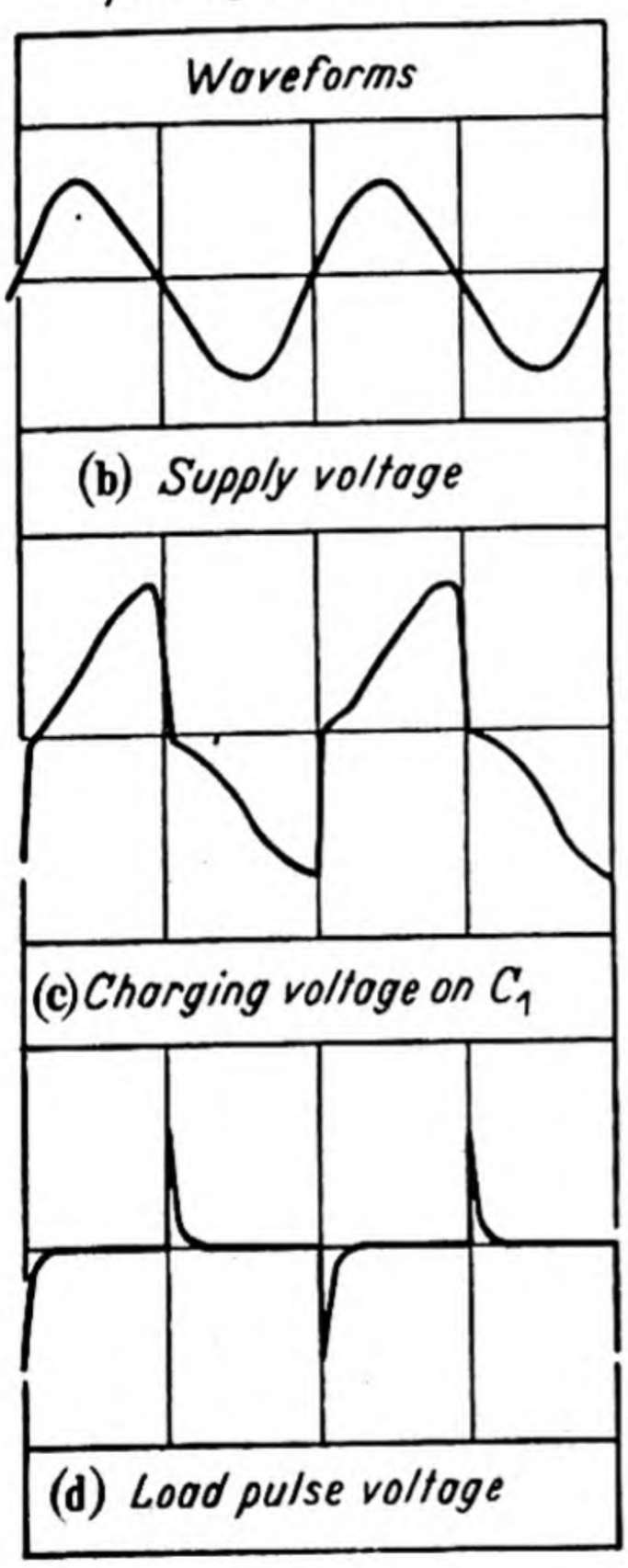

Figure 203. Operation of simple pulsactor pulse generator (Melville[32], by courtesy, *B.T.H. Activities*).

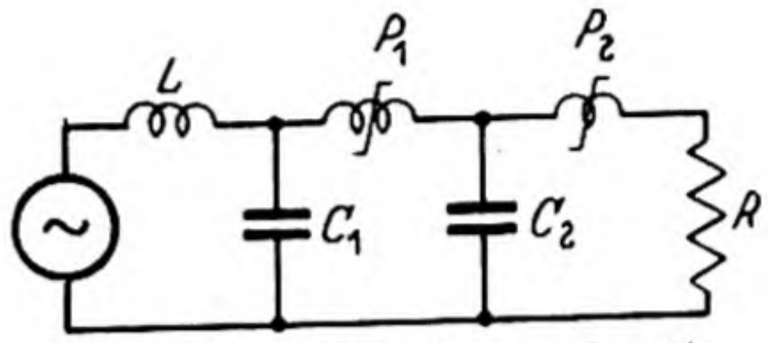

(a) *Cascade discharge circuit*

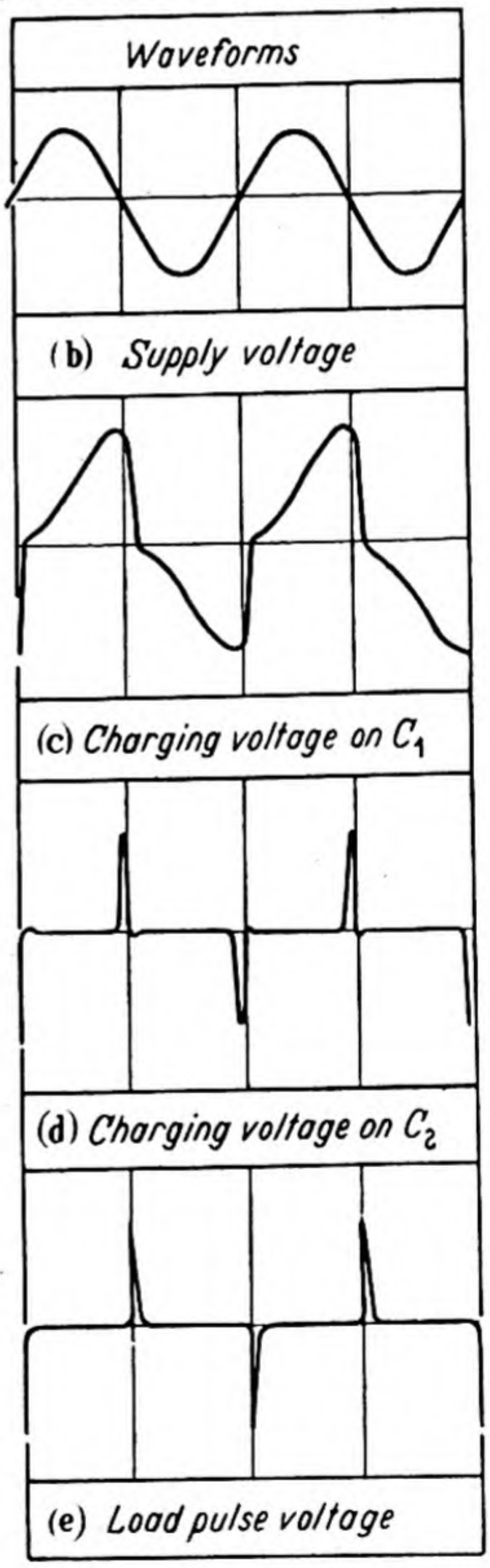

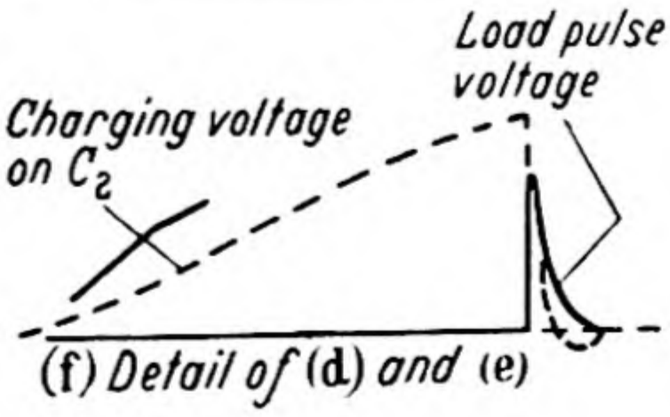

Figure 204. Operation of two-stage cascade pulsactor circuit (Melville[32], by courtesy, *B.T.H. Activities*).

For small values of H the pulsactor has a high impedance ; when the magnetic material saturates the impedance falls to a low value. Because of the large change in impedance the pulsactor may be used as a switching device (*see* references [26] and [27] of Chapter 11). The special suitability of rectangular loop materials, such as H.C.R. metal or Mumetal, as compared with orthodox materials for duty as switches is due to the small change in flux density at the knee of the B–H characteristic which is necessary to cause a sharp transition between the two impedances, the ratio of which may be many thousands to one.

A simple form of magnetic pulse generator is shown in *Figure 203*. The inductor L and capacitor C, together with the unsaturated inductance of the pulsactor P, are made resonant at the frequency of the sinusoidal supply voltage. The pulsactor is designed so that the change in flux induced in its core by the charging voltage on the capacitor causes saturation to occur when the voltage on the capacitor is at a maximum value. The capacitor then discharges through the saturated inductance of the pulsactor to produce a current pulse in the load resistance R. This cycle is repeated for each half-cycle of the supply and identical pulses of opposite polarity are produced alternately.

By polarizing the core of the pulsactor so that saturation of the magnetic material takes place in one direction only, the discharge may be caused to occur once per cycle of the supply and to generate a pulse of either polarity depending on the direction of polarization.

The circuit of *Figure 203* cannot be used to produce any desired pulse as the design of the pulsactor is completely determined by the charging circuit requirements. Consequently the saturated inductance is similarly prescribed and, only in exceptional cases, is the saturated inductance of a single stage sufficiently low to allow direct discharge into the load to take place. This difficulty is overcome by the use of cascade operation, the principle of which is illustrated by *Figure 204*. Instead of discharging into the load the capacitor C_1 is discharged into an equal capacitor C_2. As the discharge rate corresponds with the saturated inductance of the pulsactor P_1, C_2 is charged much more rapidly than was C_1. At the half-period of the oscillatory discharge all the energy which was stored in C_1 has been transformed to C_2, and a suitably designed pulsactor P_2 can be arranged to discharge C_2 at the instant of maximum charge. As the time taken to charge C_2 is much less than that to charge C_1 the saturated inductance of P_2 is much less than that of P_1. The impedance of the discharge circuit for the two stage case is much less than that for a single stage, and an output pulse of higher peak power and shorter duration can therefore be obtained as shown in the waveforms of *Figure 204*. The process can be repeated in

a cascaded arrangement of as many stages as are necessary to reduce the inductance of the final discharge circuit to a permissible value.

The circuit shown in *Figure 205a* is that used in a marine radar modulator producing 150 kW, 13 kV, 12·5 A pulses of 0·25 μsec duration recurring at 1,500 pulses/sec. It consists of a single-phase resonant a.c.-charged system in which energy to supply losses in the circuit and to develop the required output pulse is stored in C_1. This capacitor is discharged through a polarized pulsactor P_1 to charge capacitor C_2. Two further cascade-pulsactor stages P_2, C_3, P_3, are interposed between C_2 and the pulse-forming network. The final stage consists of the pulse-forming network, pulsactor P_4, pulse transformer and magnetron.

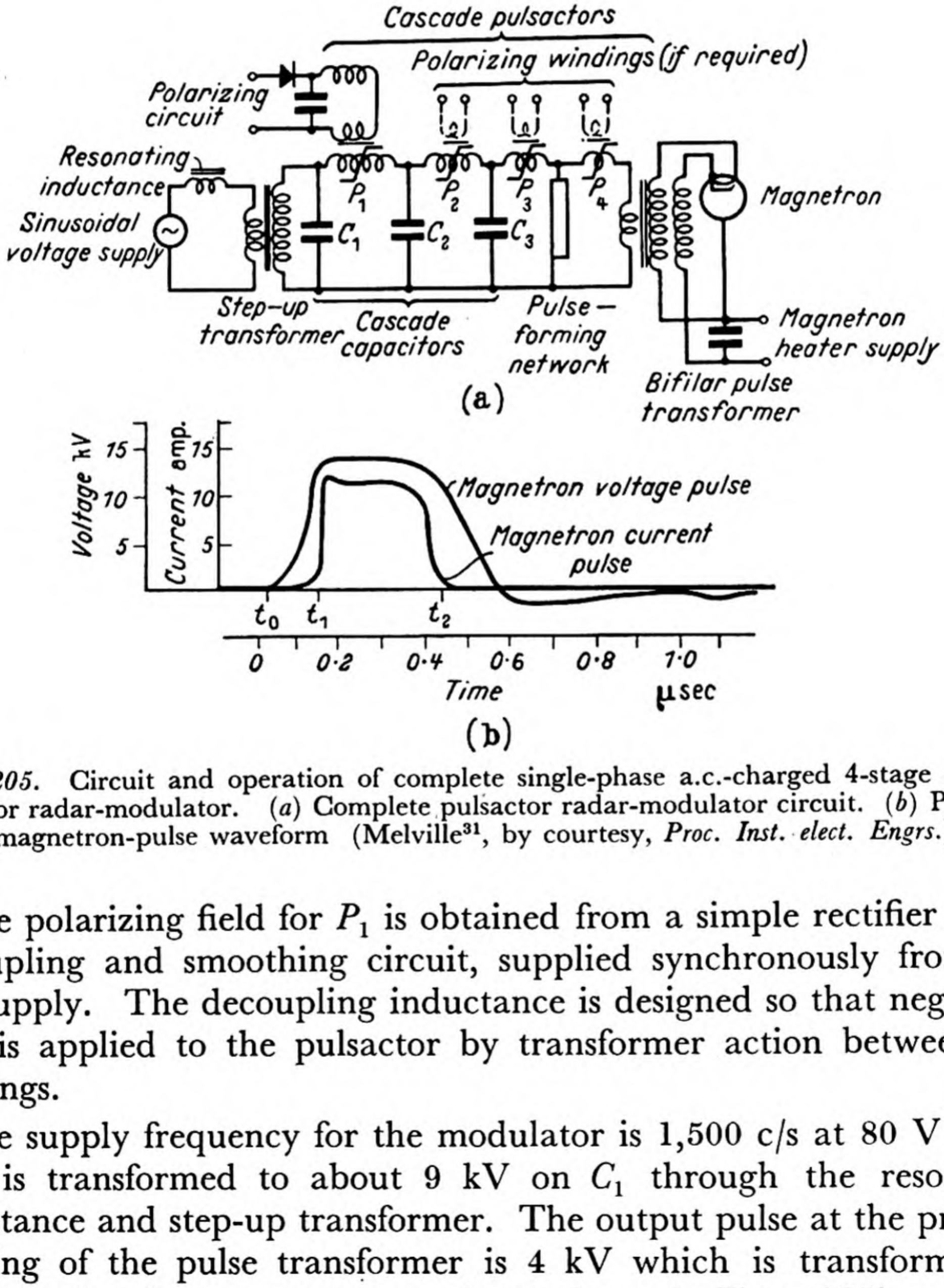

Figure 205. Circuit and operation of complete single-phase a.c.-charged 4-stage cascade pulsactor radar-modulator. (*a*) Complete pulsactor radar-modulator circuit. (*b*) Practical magnetron-pulse waveform (Melville[31], by courtesy, *Proc. Inst. elect. Engrs.*).

The polarizing field for P_1 is obtained from a simple rectifier and a decoupling and smoothing circuit, supplied synchronously from the a.c. supply. The decoupling inductance is designed so that negligible load is applied to the pulsactor by transformer action between the windings.

The supply frequency for the modulator is 1,500 c/s at 80 V r.m.s. This is transformed to about 9 kV on C_1 through the resonating inductance and step-up transformer. The output pulse at the primary winding of the pulse transformer is 4 kV which is transformed to 13 kV to give the magnetron waveforms shown in *Figure 205b*.

REFERENCES

1 RATSEY, O. L. *J. Inst. elect. Engrs.*, Pt. IIIA., **93** (1946) 245.
2 CRAGGS, J. D., HAINE, M. E., and MEEK, J. M. *J. Inst. elect. Engrs.*, Pt. IIIA., **93** (1946) 963.
3 DODDS, J. M., and LUDLOW, J. H. *J. Inst. elect. Engrs.*, Pt. IIIA., **93** (1946) 1007.
4 ENGLAND, T. S. *J. Inst. elect. Engrs.*, Pt. IIIA., **93** (1946) 1016.
5 WHELPTON, R. V. *J. Inst. elect. Engrs.*, Pt. IIIA., **93** (1946) 1027.
6 JOHNSON, R. H. *J. Inst. elect. Engrs.*, Pt. IIIA., **93** (1946) 1043.
7 MELVILLE, W. S. *J. Inst. elect. Engrs.*, Pt. IIIA., **93** (1946) 1063.
8 WILKINSON, K. J. R. *J. Inst. elect. Engrs.*, Pt. IIIA., **93** (1946) 1090.
9 GLASOE, G. N., and LEBACQZ, J. V. *Pulse Generators*, New York, 1948.
10 KAYE, W., and DEVANEY, R. *J. appl. Phys.*, **18** (1947) 912.
11 FROOME, K. D. *J. Sci. Instrum.*, **25** (1948) 371.
12 ZAREM, A. M., and MARSHALL, F. R. *Rev. Sci. Instrum.*, **21** (1950) 514.
13 HOLTHAM, A. E. J., and PRIME, H. A. *Proc. Phys. Soc. B.*, **63** (1950) 561.
14 CLAYTON, C. G. *Proc. Inst. elect. Engrs.* Pt. I, **99** (1952) 206.
15 MEEK, J. M., and CRAGGS, J. D. *Electrical breakdown in gases*, London, 1953.
16 FRY, D. W., and WILKINSHAW, W. *Rep. Prog. Phys.*, Vol. XII, 1949.
17 GUILLEMIN, E. A. *Communication Networks*, New York, 1946.
18 WHITE, H. J., GILLETTE, P. R., and LEBACQZ, J. V. *Pulse Generators*, pp. 175–224, New York, 1948.
19 BOSTICK, W. H. *Pulse Generators*, pp. 499–660, New York, 1948.
20 GOUCHER, F. S., HAYNES, J. R., DEPP, W. A., and RYDER, E. J. *Bell System Tech. J.* **25** (1946) 563.
21 LEBACQZ, J. V., and WHITE, H. J. *Pulse Generators*, pp. 275–294, New York, 1948.
22 MÜLLER-HILLEBRAND, D. *Siemens Z.*, **14** (1934) 281.
23 STRIGEL, R. *Arch. Electrotech.*, **28** (1934) 586.
24 DURNFORD, J., and MCCORMICK, N. R. *Proc. Inst. elect. Engrs.*, Pt. II, **99** (1952) 33.
25 GRIFFITHS, J. H. E. *J. Inst. elect. Engrs.*, Pt. IIIA., **93** (1946) 173.
26 KNIGHT, H. DE B., and HERBERT, L. *J. Inst. elect. Engrs.*, Pt. IIIA., **93** (1946) 949.
27 KNIGHT, H. DE B. *Proc. Inst. elect. Engrs.* Pt. III., **96** (1949) 361.
28 KNIGHT, H. DE B., and HOOKER, O. N. *B.T.H. Activities*, **20** (1949) 47.
29 GERMESHAUSEN, K. J. *Pulse Generators*, pp. 335–354, New York, 1948.
30 GLASOE, G. N. *Pulse Generators*, pp. 21–89, New York, 1948.
31 MELVILLE, W. S. *Proc. Inst. elect. Engrs.* Pt. III, **98** (1951) 185.
32 MELVILLE, W. S. *B.T.H. Activities*, **23** (1952) 169.

7

MEASUREMENT OF HIGH DIRECT AND ALTERNATING VOLTAGES

ELECTROSTATIC VOLTMETERS

In the electrostatic voltmeters which have been developed for use at high voltages the electrode arrangements usually follow the design originally suggested by KELVIN[1]. This consists of a movable plane disc, surrounded by a fixed plane guard-ring, and placed opposite a parallel plane electrode. In some instruments spherically-shaped electrodes are used.

Under uniform-field conditions, if the surface of the disc and the guard-ring are coplanar and if the clearance between the disc and the guard-ring is small, the force on the disc is given by

$$F = \frac{d^2}{32\,l^2} V^2 \text{ dyne} \qquad \ldots\ldots(7.1)$$

where d cm. is the diameter of the disc, l cm. is the gap length and V is the potential between the electrodes in e.s.u. If V is expressed in kV, Equation 7.1 can be rewritten as

$$F = \frac{d^2}{2825\,l^2} V^2 \text{ gm wt} \qquad \ldots\ldots(7.2)$$

The magnitude of the force on the disc is sufficient to enable it to be used to determine the applied voltage. In many electrostatic instruments the movement of the disc is indicated by mechanical, electrical or optical methods to give a steady record of the voltage on an instrument scale. Alternatively, the force can be measured mechanically and the result used to give an absolute measurement of the applied voltage.

In the various high-voltage voltmeters and electrometers which have been developed, the restoring force required to balance the electrostatic attraction is provided in the following ways:

(*a*) Suspension of the moving electrode on one arm of a balance[1, 9, 15].

(*b*) Suspension of the moving electrode on a spring[8, 18].

(*c*) Pendulous suspension of the moving electrode[24, 26].

(*d*) Suspension of the moving electrode on a metallic membrane[9, 10, 11].

(*e*) Torsional suspension of the moving electrode[3, 7].

(*f*) Combination of torsional suspension with the torque provided by a current-balance arrangement of coils which permits adjustment of the restoring force by a change in current[7].

The higher the attractive force the greater is the precision that can easily be obtained with the instrument and it is clear therefore that in the measurement of a given voltage V it is desirable to increase the disc diameter d and to decrease the gap length l as far as possible. If uniformity of the field is to be maintained an increase in d must be

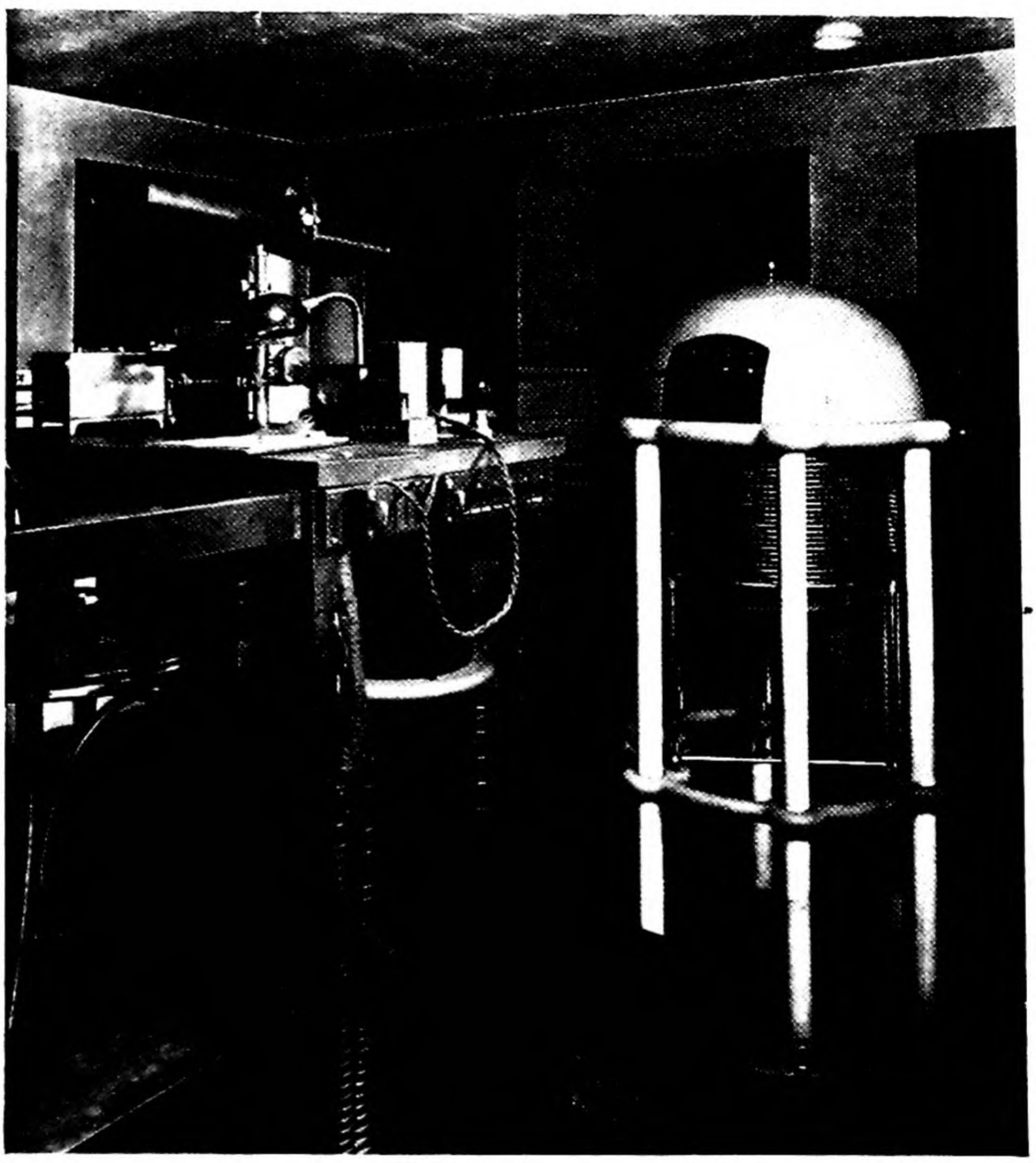

Figure 206. Absolute voltmeter constructed by Brooks, Defandorf and Silsbee for the measurement of voltages up to 275 kV peak (by courtesy, Nat. Bureau of Standards).

accompanied by an increase in the diameter of the surrounding guard-ring and of the opposing plate, and the electrodes may therefore become unreasonably large, especially for higher voltages. Reduction in the gap l is limited by the need to work well below the break-down gradient for the gap. Gradients up to 5 kV/cm. are

possible for voltmeters operating in open air, but much higher operating gradients are possible with other insulating media such as compressed gas[9–13] or vacuum[14].

An absolute electrometer of the attracted disc type, for the measurement of voltages up to 275 kV peak, has been built by BROOKS, DEFANDORF and SILSBEE[15, 16]. An external view of the instrument is shown in *Figure 206*. The basic features can be described by reference to *Figure 207*. The hemispherical metal dome *C* encloses a sensitive balance *D* which measures the force of attraction between the movable disc, which hangs from one of its arms, and the lower plate *B*. The disc hangs with a small clearance, ~0·01 cm., in a central opening in the upper plate, which serves as a guard-ring. The diameter of each of the plates is 100 cm. Two sizes of discs are used, of diameter 10 cm. and 16 cm. respectively. Light reflected

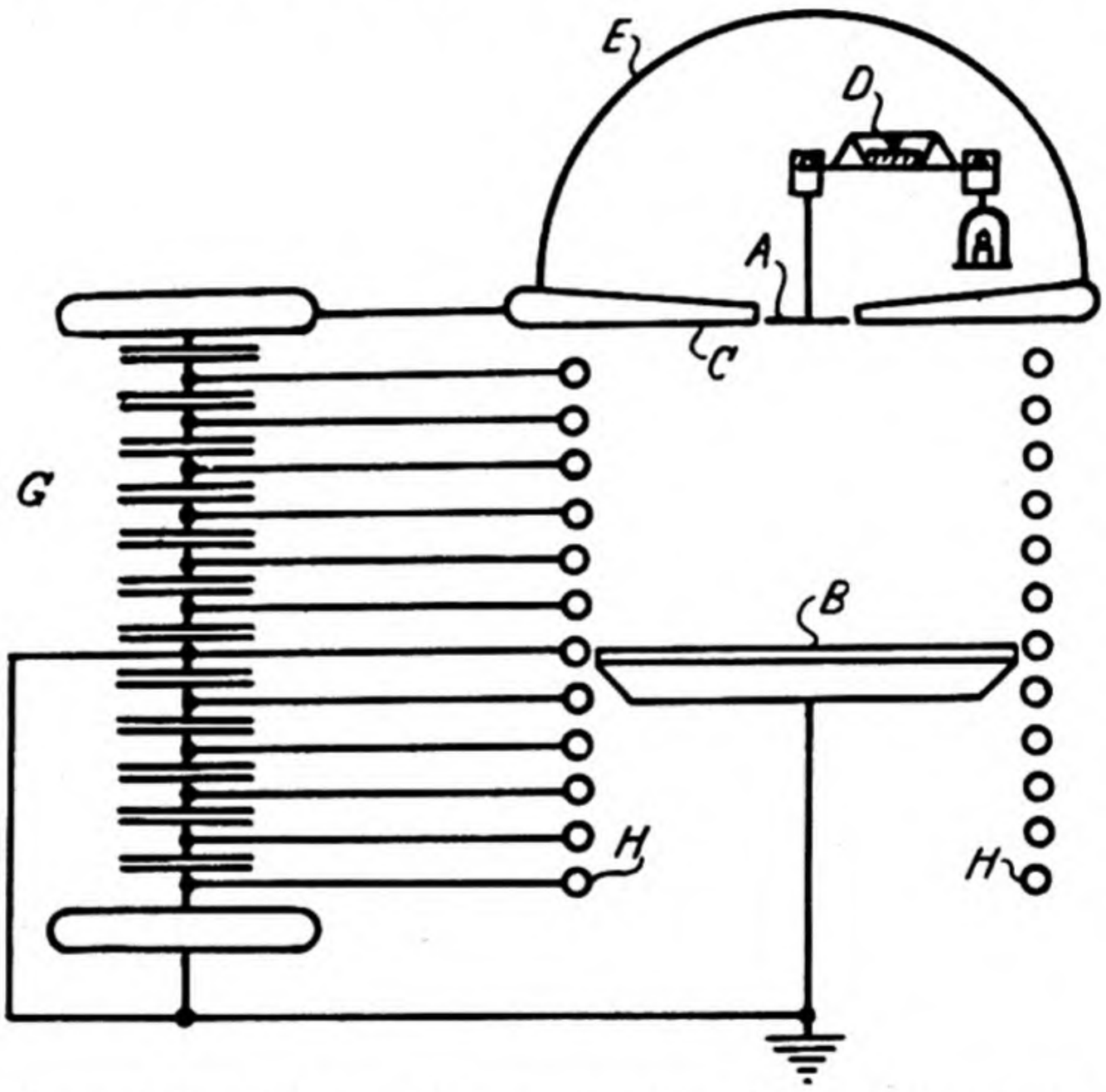

Figure 207. Schematic cross-section of absolute electrometer (Brooks *et al*[15], by courtesy, *J. Res. Nat. Bur. Stand., Wash.*).

The attracted disc at *A* is suspended with its lower surface in the same plane as that of the guard ring *C* which is at the same potential. The electrostatic attraction is measured by the sensitive balance *D*. The horizontal hoops are each connected to a tap from the capacitance potential divider *G*. The two cross-sections of each hoop appear as circles as at *H-H*. The capacitor units and hoops below the particular location at which the lower plate is used for a given voltage are short-circuited and grounded.

from a mirror carried by the balance beam serves to magnify its motion and to indicate to the operator at a safe distance when a condition of equilibrium is reached. It also serves to indicate the height of the disc relative to the surrounding guard-ring. At the spacing of 100 cm. required between the plates for an applied voltage of 275 kV, the field in the gap is kept uniform by the provision of equally spaced 'guard-hoops' which enclose the cylindrical space

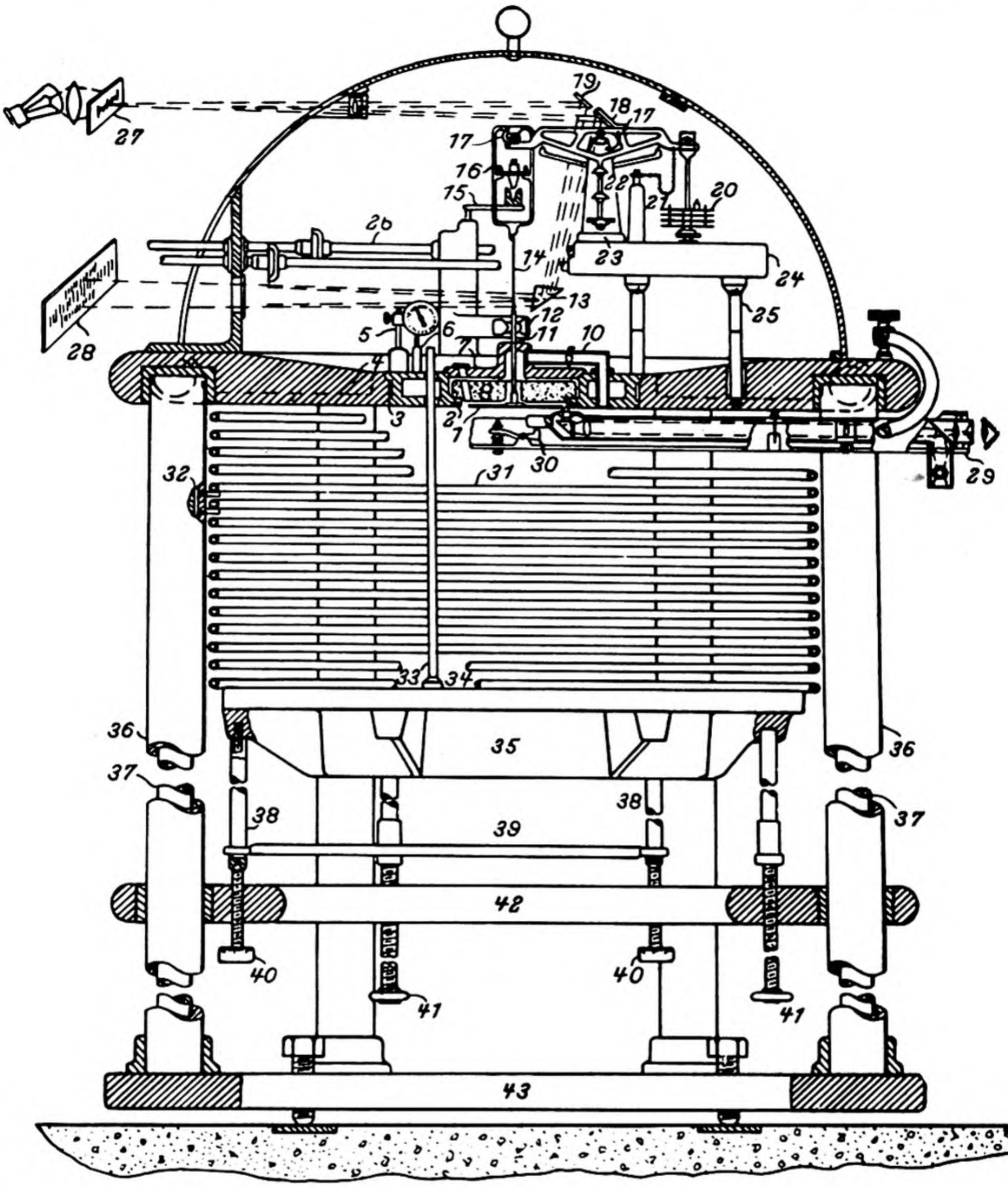

Figure 208. Schematic cross-section of electrometer and accessory equipment (Brooks *et al.*[15], by courtesy, *J. Res. Nat. Bur. Stand., Wash.*).

1 Disc.
2 Stainless -steel insert.
3 Bushing.
4 Upper plate.
5 Surface gauge.
6 Gauge block.
7 Cover above disc.
8 Balsa-wood filter.
9 Perforated plug in gauge hole.
10 Air duct.
11 Disc stem.
12 Stem clamp.
13 Prism*.
14 Suspension strip.
15 Weight lifter.
16 Weight pan.
17 Gold ligaments.
18 Beam mirror.
19 Fiducial mirror.
20 Counterpoise.
21 Chainomatic chain.
22 Stabilizing rod.
23 Balance column.
24 Balance base.
25 Balance-base legs.
26 Control rods*.
27 Vernier reticule.
28 Ground-glass electrometer scale.
29 Coplanarity microscope and mounting.
30 Pin guiding microscope objective.
31 Guard hoops.
32 Maple pegs.
33 Gauge rod.
34 Segmental gauge block.
35 Lower plate.
36 Silica pillars.
37 Micarta inner pillars.
38 Invar rods.
39 Aluminium cross brace.
40 Micrometer screws.
41 Jackscrews.
42 Intermediate ring.
43 Base.

* In the actual instrument prism (13) is at 90° from the position here drawn so that the reflected rays to the scale (28) are at right angles to the plane of the figure. The path of the incoming beam of light and the location of the control rods (26) are also different from those shown.

between the plates *B* and *C*. These hoops *H*—*H* are maintained at equally spaced voltages by means of the capacitance divider *G*. In general the distance between the plates is chosen to give a voltage gradient of about 2,500 V/cm. Further details of the construction of the instrument are given in *Figure 208*.

As the operation of the electrometer depends essentially on a balance between the electrostatic and the mechanical forces acting on the disc, its sensitivity and stability are vitally affected by the manner in which these forces vary with the position of the disc. The various factors involved are discussed in detail by Brooks, Defandorf and Silsbee[15] following the earlier theoretical treatment by Snow[17]. In particular the influence of the voltage distribution in the guard-hoops on the uniformity of the field in the gap is thoroughly examined. The authors also describe experimental tests, and mathematical analyses, of other possible sources of error, including (*a*) tilt of the disc plates, (*b*) flatness of the disc and plates, (*c*) width of aperture

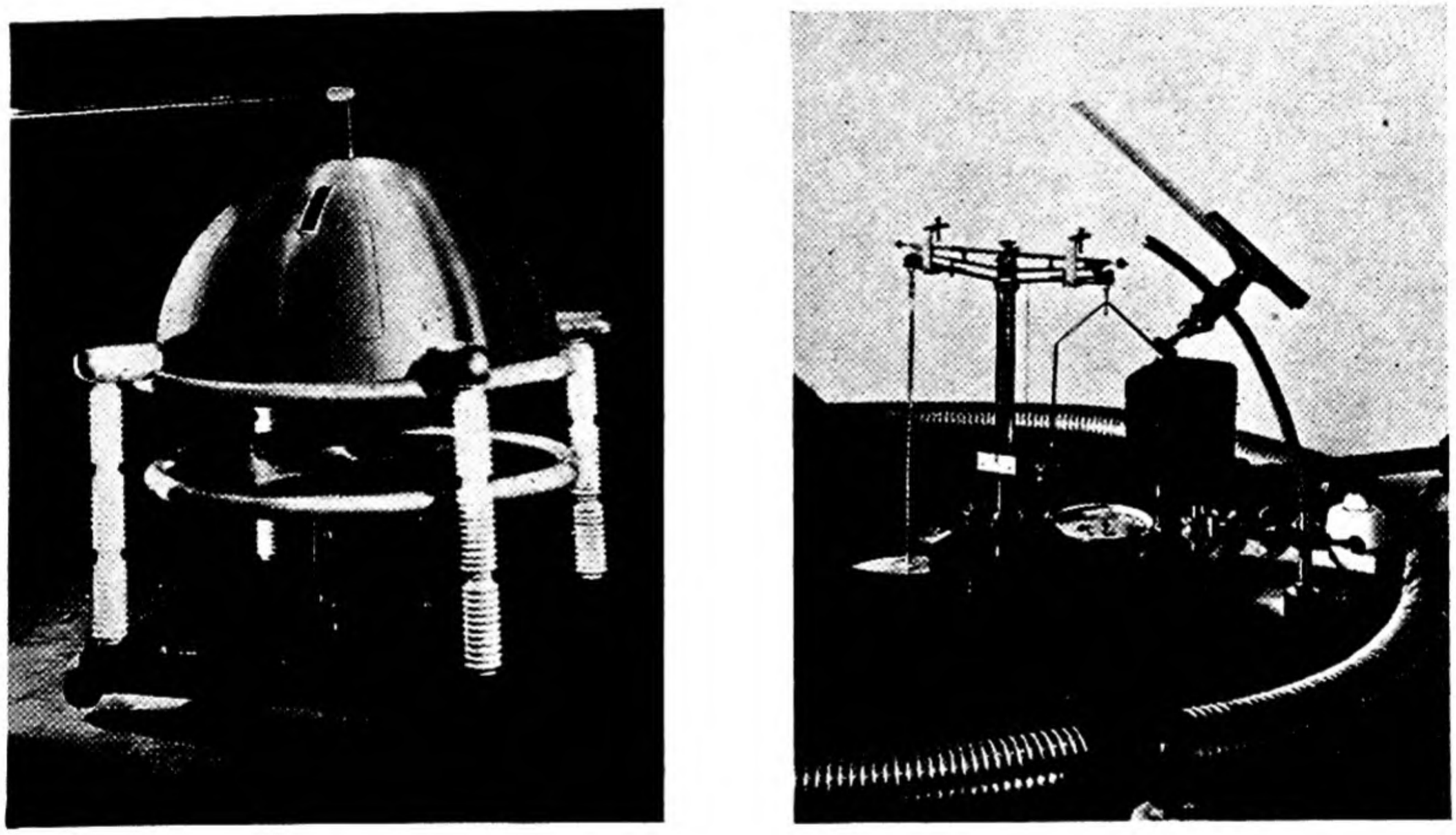

(*a*) (*b*)

Figure 209. Absolute electrometer constructed by Böcker[9] for the measurement of voltages up to 100 kV peak. (*a*) External view; and (*b*) view of mechanical balance attached to moving disc in the upper electrode (by courtesy, *Arch. Elektrotech.*).

between the disc and the plate, (*d*) eccentricity of the disc in the aperture, (*e*) temperature effects, (*f*) vibration, (*g*) air convection currents, (*h*) electrical corona discharges.

Experimental trials of the instrument under various conditions, for voltages ranging from 10 kV to 100 kV, indicate that the probable error of the values obtained with it is about 0·01 per cent., and that this error will not be greatly increased when the instrument is used at 275 kV.

In another absolute electrometer, described by Böcker[9], the main

electrodes are parallel plates of 100 cm. diameter. A plane disc, 14·97 cm. in diameter, is suspended from the arm of a balance and can move freely through a hole of 15 cm. diameter at the centre of the upper plate. For an applied voltage of 100 kV and a spacing of 20 cm. between the plates the force on the disc is 1·998 gm. Photographs of the apparatus are shown in *Figure 209*.

A number of similar voltmeters have been built in which the movement of the disc in the applied field is restrained by a spring or similar control device[3, 4, 5]. The amount of movement, which depends on the magnitude of the applied field, is amplified by a suitable mechanism to produce the deflection of a pointer on a scale. Alternatively, an optical method can be used to amplify the disc movement. These direct reading instruments have been developed to measure voltages up to 1,000 kV.

In other attracted-disc voltmeters the pull on the disc is balanced by a dynamometer method. The arrangement used by NACKEN[6, 7] is shown in *Figure 210* and includes two pairs of current-balance coils

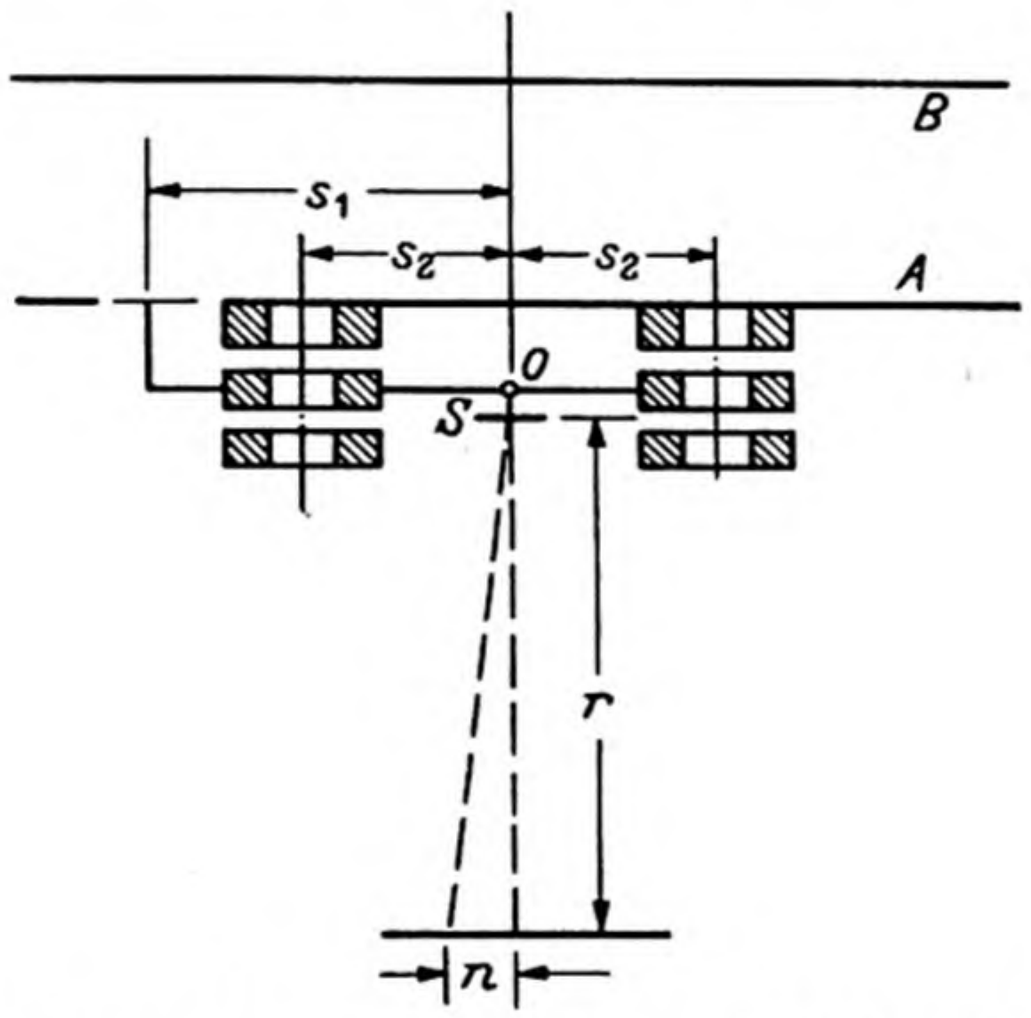

Figure 210. Arrangement of balancing coils in Nacken's[6] attracted-disc voltmeter (by courtesy, *Arch. Elektrotech.*).

connected in a manner that permits adjustment of stability as well as of sensitivity. The restoring force is produced partly by the torsional suspension carrying the disc and partly by the balance-coils. One pair of field coils, carrying a current I_f is connected in series aiding, with one moving coil, and provides a torque proportional to I_f for balancing the electrostatic force on the disc; the other pair of coils, carrying a current I_m, is connected in series opposing so that by adjustment of the value of I_m relative to the current in the moving coil the restoring force of the suspension toward the coplanar position of the disc may be either opposed or aided. The stability of the system can then be altered by the adjustment of the current in the

latter pair of coils, and this arrangement permits higher sensitivity at large spacings of the electrodes where the deflecting force decreases. An accuracy of within 0·01 per cent. is claimed by Nacken for this instrument.

In a recent form of attracted disc voltmeter described by GÄNGER[25] the disc is controlled in the manner shown schematically in *Figure 211*. Three springs F attach the disc M to the three fixed points A_1, A_2 and A_3 on the surrounding guard-ring P. A metal plate K_1 is mounted on insulators behind the disc M and faces a parallel plate K_2 which is fixed related to the guard-ring P. The plate K_1 is made of steel and K_2 of non-magnetic material. A force can then be exerted on K_1 by the action of an electromagnet mounted over the spindle S to the left of K_2. When a high voltage is applied to the voltmeter the disc M is attracted to the right, in *Figure 211*, by an electrostatic

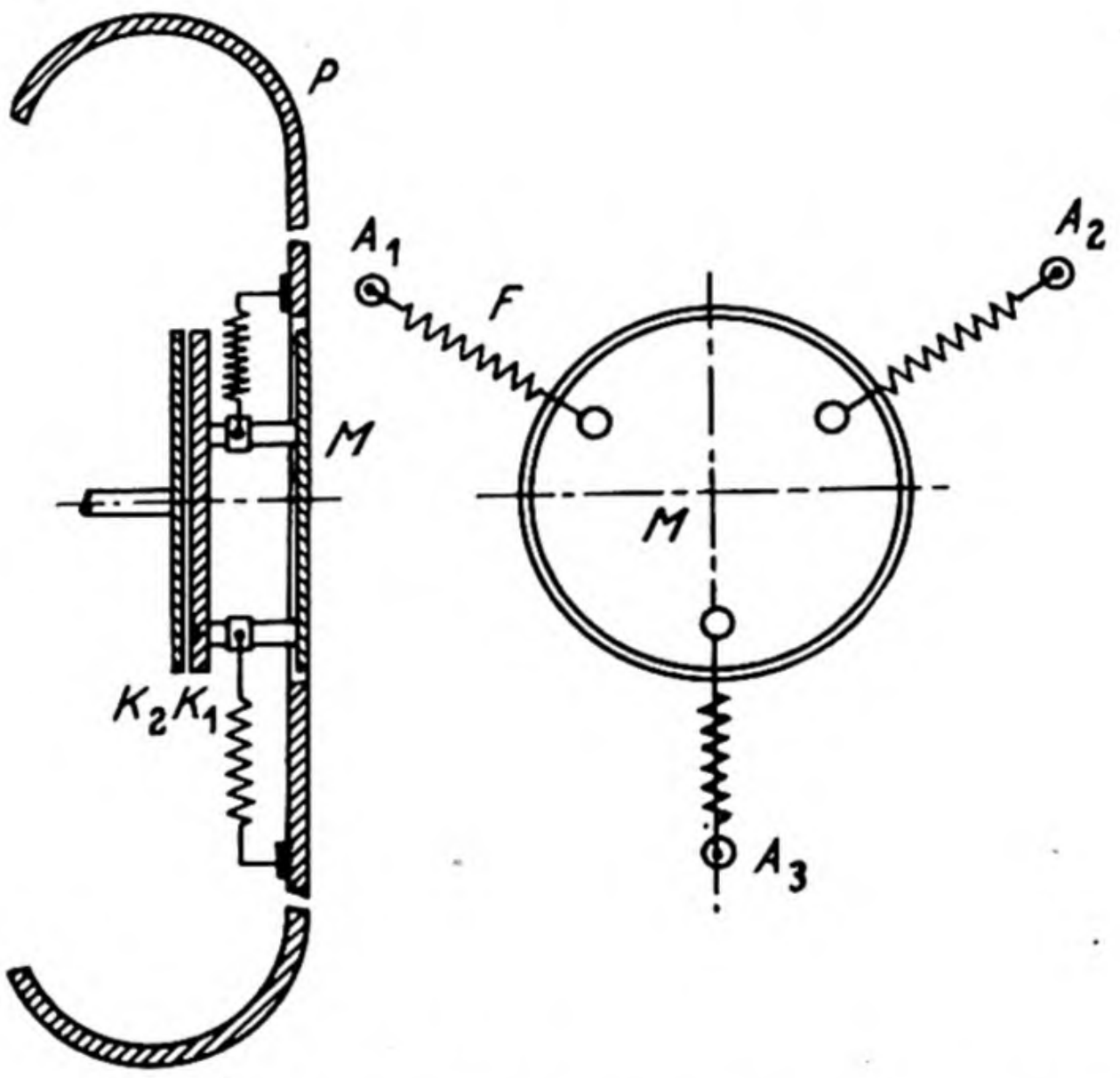

Figure 211. Method of suspension and control of moving disc in Gänger's[25] attracted-disc voltmeter (by courtesy, *Arch. Elektrotech.*).

force. Then, by variation of the magnetic force on K_1 as caused by adjustment of the current in the coil of the electromagnet behind K_2, the disc can be restored to the position coplanar with the guard-ring. A direct relation can therefore be established between the applied high voltage and the coil current for balance. The capacitance between K_1 and K_2 is used to form part of a high-frequency circuit and, if the system is suitably adjusted initially, affords a method for determining when coplanarity exists between the disc and the guard-ring.

A photograph of the complete instrument is given in *Figure 212*. The voltmeter can be calibrated against a standard voltmeter or it can

be used as an absolute instrument. For the latter purpose a mechanical force is applied to pull the disc away from K_2 and the current in the coil of the electromagnet is adjusted until M and P are coplanar. In this way a relation is obtained between the coil-current and the mechanical force. The latter can then be expressed in terms of an equivalent electric field by the expression given in Equation 7.2, so that a direct calibration is obtained between the coil-current and the applied field when balance occurs.

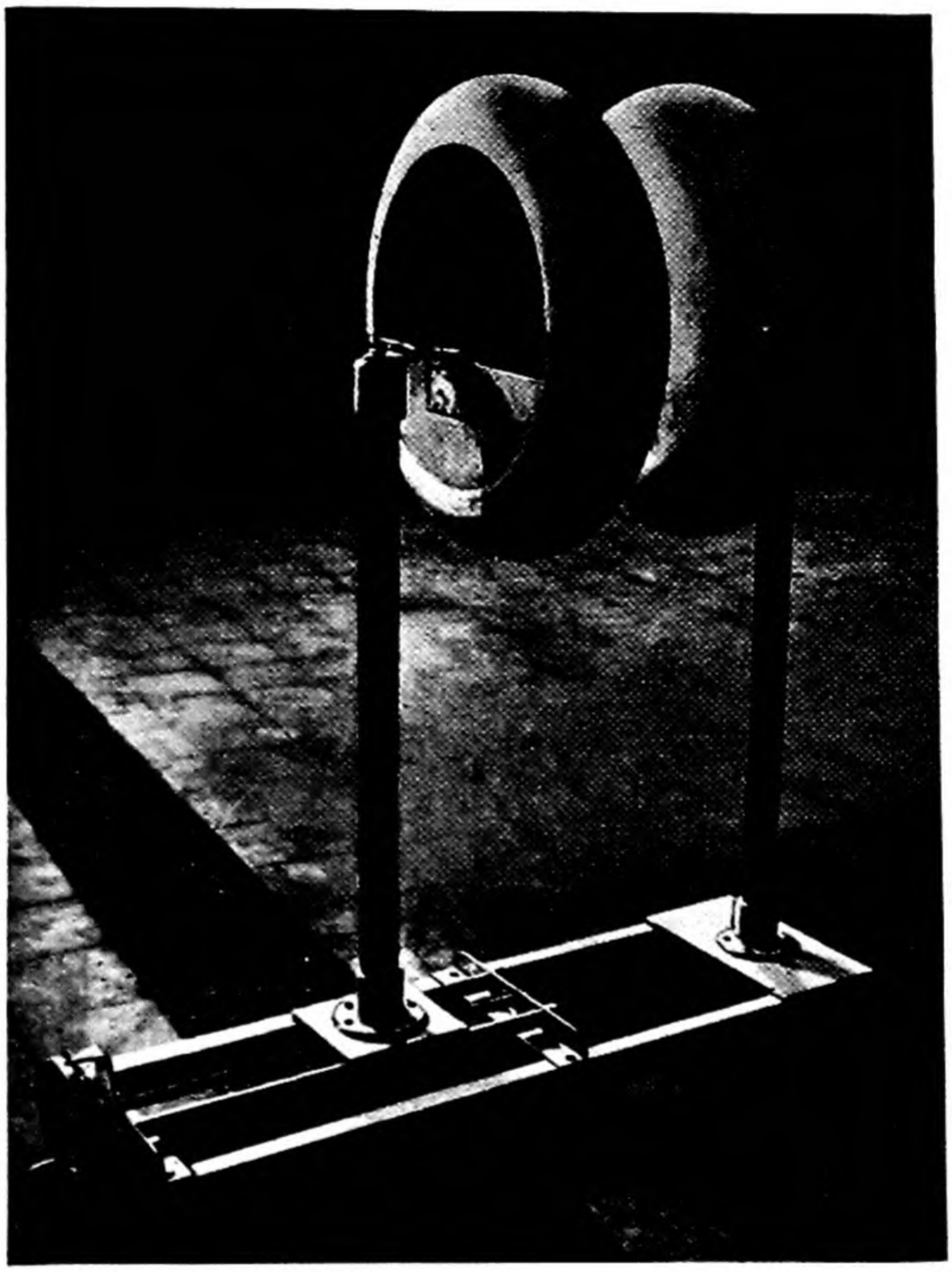

Figure 212. Attracted-disc voltmeter constructed by Gänger[25] (by courtesy, *Arch. Elektrotech.*).

Investigations have been made by HUETER[18] of the possibility of using the electrostatic attractive force between a pair of spheres, of 100 cm. diameter, in the measurement of the voltage applied to the spheres. The spheres are arranged with a vertical axis and at a spacing slightly greater than the sparking distance for the particular voltage to be measured. The upper high-voltage sphere is supported on a spring, and the extension of the spring caused by the electrostatic force is magnified by a lamp-mirror-scale arrangement. The weight of the upper sphere is 60 kg. and for a 75 cm. gap the electrostatic attraction

is approximately 800 gm. at 1,000 kV. To minimize effects of changing gap length only small displacements, of $< 0{\cdot}5$ per cent. of the gap length, of the spring-suspended sphere are used. Similar studies have been made by SORENSON *et al.*[20, 21] with spheres of 50 cm. and 100 cm. diameter, the axis between the spheres being horizontal. They conclude that the system merits consideration as a standard method for the measurement of high voltages. DEFANDORF[19] considers that an accuracy approaching 0·5 per cent. is possible with Hueter's system.

Electrostatic voltmeters using compressed gas as the insulating medium have been developed by PALM[12, 13] and by ROGOWSKI and BÖCKER[9–11]. Because of the higher operating voltage gradient which is possible between the electrodes in compressed gas as compared with open air, the attractive force between the electrodes is appreciably higher and greater mechanical precision can easily be obtained. Further, for a given applied voltage, the shorter gap length enables the required uniformity of the field to be maintained with electrodes of smaller diameter and a more compact system can therefore be arranged.

In the compressed gas voltmeter described by Rogowski and Böcker[11] nitrogen at 15 atm. is used. The voltmeter is of the attracted-disc type and can be applied to the measurement of voltages up to 300 kV. A diagram illustrating the mechanism is shown in *Figure 213*[19]. The movable disc electrode is mounted on a thin metallic diaphragm *D* which provides the restoring force. The diaphragm supports an iron-cored coil *M* above a similar fixed iron-cored coil *N*. Small changes in the air-gaps between the moving and fixed cores are sufficient to cause deflections of an ammeter connected across the moving coil, and this ammeter is calibrated to read the high-voltage applied to the instrument. The fixed coil is supplied from a regulated alternating voltage supply. A coil *K* is also suspended from the diaphragm and moves in a solenoid arrangement which enables the attractive force to be measured in terms of the solenoid current. The voltmeter can be calibrated directly before it is placed in the compressed gas chamber, by placing known weights on the disc and measuring the current in the solenoid against deflections of the diaphragm as shown by the ammeter.

An improved form of this voltmeter, for voltages up to 600 kV, has been developed by BÖCKER[9–10]. A sectional drawing is given in *Figure 214*. The gas used is carbon dioxide at 15 atm. The overall height of the instrument is 2·9 m. From comparative measurements with another voltmeter Böcker concludes that the accuracy of his instrument is within 1 per cent.

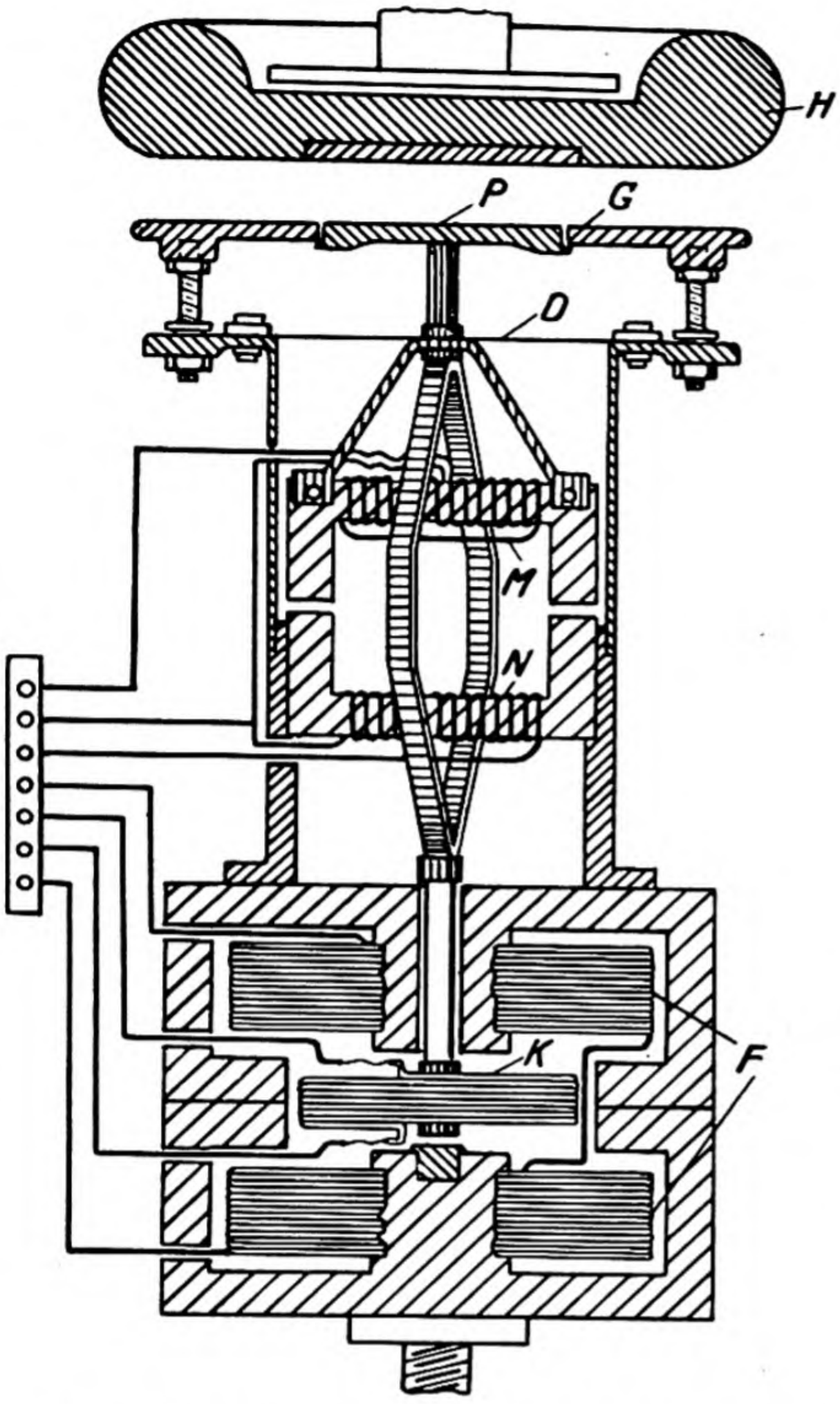

Figure 213 (*above*). Control mechanism for moving disc in the compressed-gas attracted-disc voltmeter constructed by Rogowski and Böcker (Defandorf[19], by courtesy, *J. Wash. Acad. Sci.*).

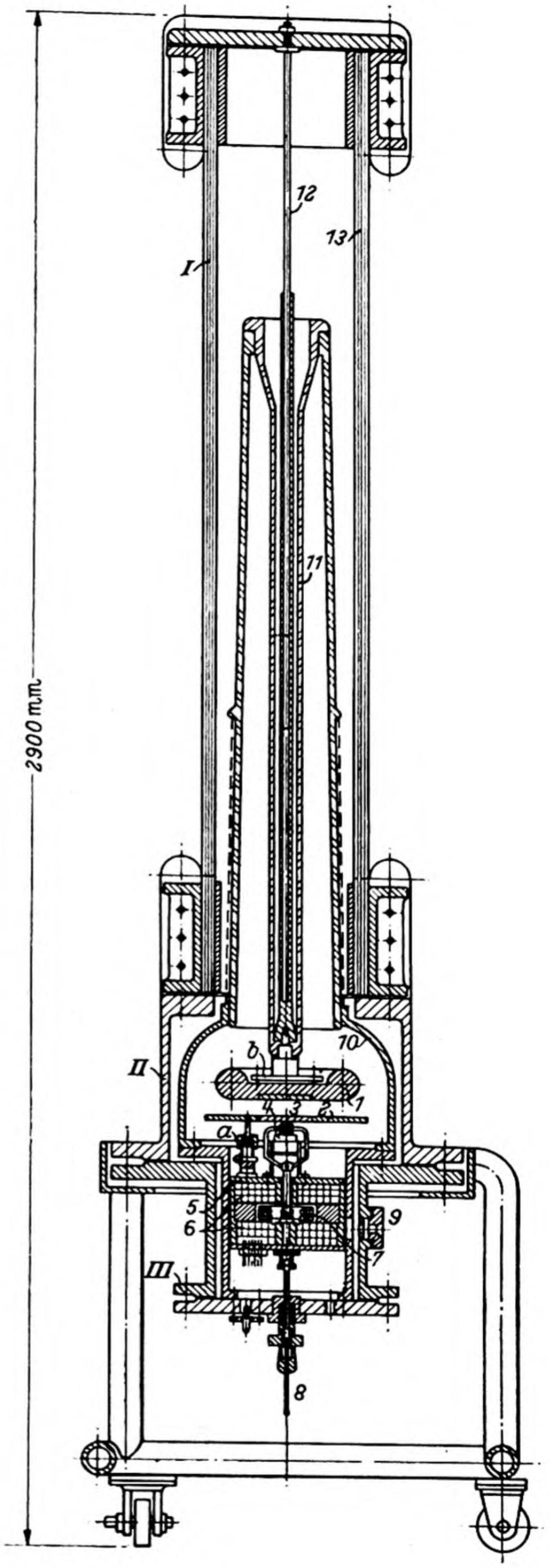

Figure 214 (*on right*). Cross-sectional diagram of the compressed-gas attracted-disc voltmeter constructed by Böcker[10], for voltages up to 600 kV (by courtesy, *Arch. Elektrotech.*).

I Insulating tube.
II Measuring chamber.
III Instrument can.
2, 3 Guard ring electrode system.
4 Electrode support.
5, 6, 7 Magnetic coil balancing system.
8 Adjusting spindle.
9 Observation window.
10 High-voltage electrode support.
11 Insulating tube.
12 High-voltage lead.
13 Insulating tube.
a, b Adjusting devices for the measuring-plate system.

MEEK and WATERTON[14] have drawn attention to the advantages of enclosing electrostatic voltmeters in vacuum. The working voltage gradient between plane electrodes can then be increased to 100 kV/cm. or more. An attractive force of 4·5 gm./cm.^{2} of electrode area can then be obtained as compared with 0·011 gm./cm.^{2} at a working gradient of 5 kV/cm. in open air. On account of the large deflecting force available the instrument can be made of more robust construction than one operating in air, and an improved accuracy and greater reliability of indication can be obtained. There is an absence of convection currents which is one of the causes of difficulty in the operation of the open-air type of instrument. Also there is freedom from interference by dust and humidity.

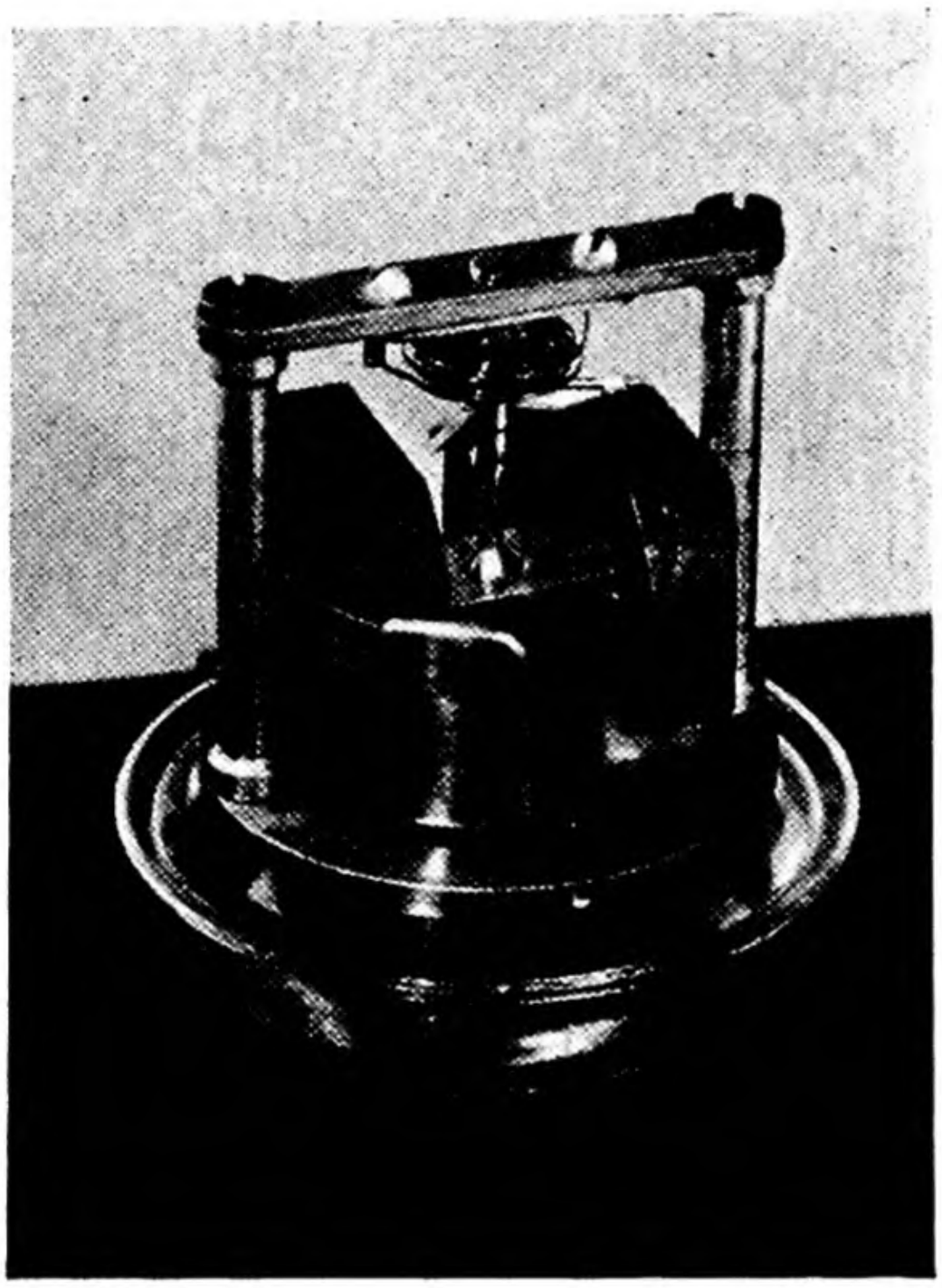

(*a*)

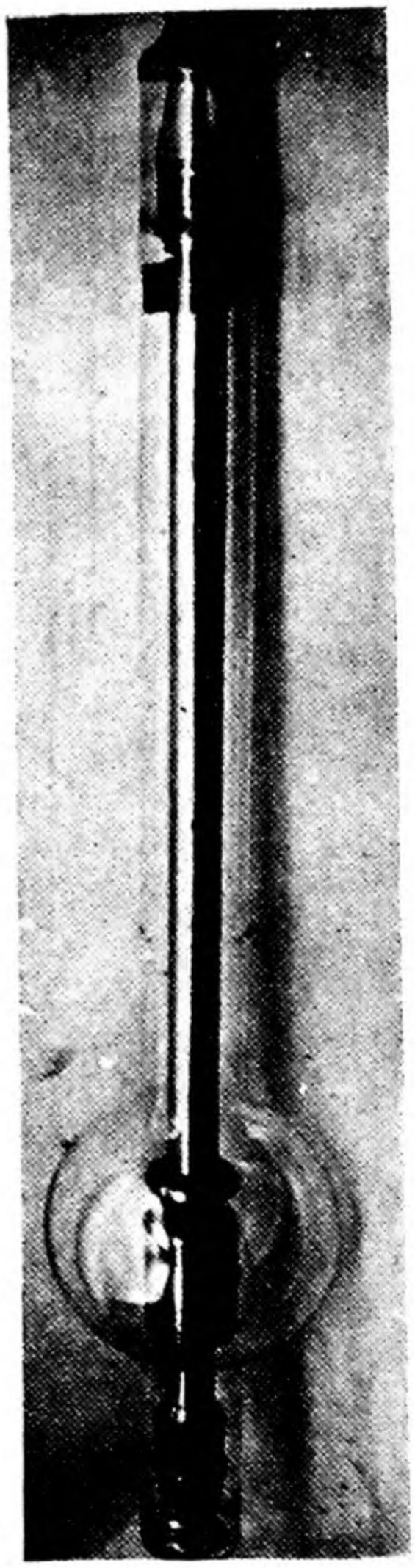

(*b*)

Figure 215. (*a*) Mechanism of a 12 kV electrostatic voltmeter for operation in vacuum. (*b*) 200 kV electrostatic voltmeter sealed in vacuum (by courtesy, Metropolitan-Vickers Electrical Co.).

Several experimental instruments operating in vacuum have been constructed for various voltage ranges. A photograph of the mechanism used in a 12 kV instrument is shown in *Figure 215a*. The moving and fixed vanes consist of sections of co-axial aluminium cylinders. The

radial portion of the moving vane passes between the poles of a magnet, and the eddy currents so generated are used to damp the movement, which is closely aperiodic. The movement is spring-controlled. The complete mechanism is sealed-off in a glass vacuum tube, and the relative movement between the vanes is indicated on a scale by the reflection of a light beam from a mirror mounted on the spindle supporting the moving vane. Another vacuum-type instrument, which has been used experimentally at voltages up to 200 kV, is shown in *Figure 215b*. The deflecting portion consists of a disc surrounded by a guard-ring. These electrodes are both earthed, and the gap between them and the high-voltage electrode can be adjusted to alter the range of the instrument.

A variety of different electrode arrangements, other than the attracted disc form, have been used in the construction of other electrostatic voltmeters[22–24, 26–28]. A repulsion type of instrument, for the measurement of voltages up to 80 kV, is described by ZDRALIK[22]. The moving system consists of a horizontal bar suspended at its centre by a torsion wire. Two similar spheres are supported on insulators adjacent to the moving spheres. Repulsion between the two pairs of spheres occurs when the voltage to be measured is applied to both fixed and moving parts. A similar form of instrument has been constructed by STEUBING[23]. In another repulsion type of voltmeter described by ROGOWSKI[24] and WINGEN[26] one electrode is a fixed plate and the other an adjacent plate hinged to the first. Voltages up to 70 kV have been measured in this manner, with a stated accuracy of within 1 per cent. A simple repulsion type of voltmeter, with fixed and moving vanes, has been built by MACNEICE[28] for voltages up to 8 kV. The moving vanes are supported by a phosphor-bronze suspension to which a mirror is attached to indicate the angular position.

An electrostatic voltmeter using a capacitance divider, for the measurement of d.c. voltages up to 100 kV, has been constructed by ALFVÉN and EKLUND[29]. The principle is illustrated in *Figure 216*. A plane electrode *A* is connected to the high-voltage source and is arranged parallel to a plane electrode *B* which is connected to a low-voltage electrostatic voltmeter *M*, the other pole of which is earthed. An earthed shield *S* can be inserted between *A* and *B* so that *B* is completely shielded from the field produced by *A*. The shield is provided with a device whereby it earths the electrode *B* when in the inserted position. When the shield is removed *M* shows a deflection the magnitude of which depends on the voltage of *A*. Provided that the insulation of the voltmeter *M* and the electrode *B* is adequate the deflection recorded on *M* remains unchanged for a time much longer than that required for a reading. After the

reading has been made S is reinserted between A and B earthing the voltmeter M. If C_1 is the capacitance between A and B, and C_2 is the capacitance between B and earth, then the voltage V on the electrode A is given by

$$V = \frac{C_2}{C_1}\left(1+\frac{C_1}{C_2}\right)V_2 \qquad \ldots\ldots(7.3)$$

where V_2 is the voltage recorded on the voltmeter M. Different ranges of measurement can be obtained by changing the distance between A and B and therefore the capacitance C_1. In order that the method may be practicable it is essential that the voltmeter deflection should not vary appreciably, *e.g.* 1 per cent., during the time required for a measurement, *e.g.* 5 sec. The insulation should therefore be such that the time-constant is not less than 500 sec.

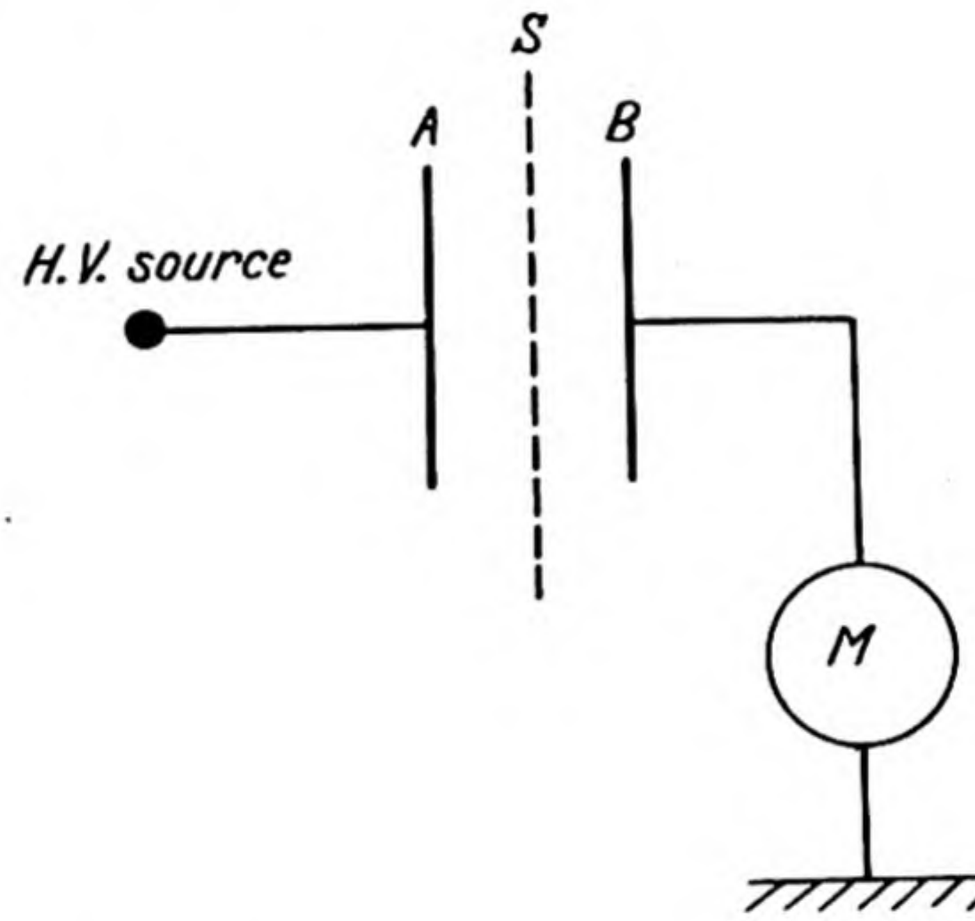

Figure 216. Diagram illustrating the principle of the electrostatic voltmeter developed by Alfvén and Eklund (by courtesy, *Rev. Sci. Instrum.*).

An alternative electrostatic method for the measurement of high voltages has been described by THORNTON and THOMPSON[30] and has been developed to a high degree of precision by BRUCE[31]. In this method the voltage gradient in a uniform electrostatic field is measured in terms of the periodic time of a conducting ellipsoid freely suspended in that field. For oscillations of small amplitude about the line of the field, the field strength is given by

$$E = k\,(f^2 - f_o^2)^{\frac{1}{2}} \qquad \ldots\ldots(7.4)$$

where f and f_o are the frequencies of oscillation in the field E and in zero field respectively, and k is a constant which is determined entirely by the dimensions of the ellipsoid and can be calculated. In Bruce's instrument the uniform field is formed between two parallel plates, each of 145 cm. in diameter with rolled edges 7 cm. in diameter. The plates are supported in parallel vertical planes; one plate is earthed and the other plate is connected to the high-voltage supply. The spacing between the plates is 45 cm. The ellipsoid is suspended between the plates on a length of 120 cm. of unspun silk fibre. The

periodic time of the ellipsoid is measured by observing the motion through a telescope. As a result of his investigations Bruce concludes that the error in the measurement of voltage with his instrument is less than $\pm 0{\cdot}03$ per cent.

The characteristics of the ellipsoid voltmeter and of other oscillating electrode systems have been considered by BRADSHAW and others[32] who also describe some preliminary experiments with two of these systems. In one case a sphere is suspended from a fixed point and oscillates above a similar fixed sphere; in the other case a sphere is suspended from a fixed point and oscillates along the line joining the centre of two similar fixed spheres. The investigators have derived the operating laws for the two cases and show that the relations between the applied voltages and the frequency are of the same form as that given in Equation 7.4.

General surveys of the different types of electrostatic voltmeters and of their performance as compared with other high-voltage voltmeters have been presented by PALM[34], DREWNOWSKI[35] and Defandorf[19].

THORNTON, WATERS and THOMPSON[33] have developed an instrument known as an ' ionic wind ' voltmeter with which high voltages may be measured to an accuracy of ± 2 per cent. An earthed, heated filament is placed in the region of a high-voltage sphere, but at such a distance from it that corona does not occur. Ionic motion in the gap results in an increase in the cooling effect on the filament, above that occurring when the electric field is absent. The consequent variation of the filament resistance, as observed by a bridge method, can then be used to give an indication of the high voltage applied to the instrument.

SPHERE GAPS

The experimentally-determined calibration curves relating break-down voltages with gap lengths between spheres enable sphere gaps to be used as a standard method for the determination of the peak value of a.c., d.c. and impulse voltages and for the checking of volt-meters and other voltage-measuring devices used in high-voltage tests. Standard specifications for the use of sphere gaps, with calibration tables for different sizes of spheres, have been issued in Great Britain[36], the United States[37] and Germany[38], and are based on the results of numerous investigations in the different countries concerned[39–63].

In the British Standard Rules, No. 358:1939, calibrations are given for the variation of break-down voltage with spacing between spheres of various diameters up to 200 cm., and for voltages ranging from 2 to 2,500 kV. These calibrations are reproduced in *Tables XV*, *XVI* and *XVII*. *Tables XV* and *XVI* correspond to the case when the high voltage is applied to one sphere and the other sphere is earthed, *Table XV* then giving the power-frequency alternating, the negative unidirectional

and negative impulse break-down voltages and *Table XVI* the positive unidirectional and impulse break-down voltages. *Table XVII* corresponds to the symmetrical condition, when both spheres are insulated and equal voltages of opposite sign are applied to the spheres. As there is some doubt about the accuracy of the B.S.358 tables for spheres of 2 cm. diameter, a recent calibration for this size of sphere is given in *Table XVIII*[64].

TABLE XV

SPHERE-GAP BREAK-DOWN VOLTAGES IN kV (PEAK) IN AIR AT 20°C AND 760 MM. Hg FOR POWER-FREQUENCY ALTERNATING, NEGATIVE IMPULSE AND NEGATIVE UNIDIRECTIONAL VOLTAGES; ONE SPHERE EARTHED

Gap in cm.	*Sphere diameter in cm.*										
	5	6·25	10	12·5	15	25	50	75	100	150	200
0·5	17·3	17·1	16·9	16·7	16·5						
1	32·0	31·9	31·6	31·5	31·3	31					
1·5	45·7	45·9	45·6	45·6	45·5	45					
2	57·4	58·2	59·1	59·2	59·2	59	58	58			
2·5	67·2	69·6	72·0	72·0	72·6	72			71		
3	75·4	79·1	84·1	85·2	85·5	86					
4	(88·4)	94·8	105	109	110	112	112	112			
5	(98)	(107)	123	129	132	137	137	137	137	137	137
6		(116)	138	146	152	161	164	164	164		
7			150	162	169	184	178	178			
8			(160)	174	185	205	214	215			
9			(169)	186	198	225	238	240			
10			(177)	(196)	209	243	262	265	266	267	265
12				(212)	(229)	275	308	313			
14					(245)	302	352	360			
16						•325	392	406			
18						345	428	450			
20						(363)	461	492	503	508	510
25						(396)	532	586	611	626	630
30							591	670	709	739	745
35									797	846	858
40							(679)	806	876	947	965
50							(738)	904	1010	1130	1180
60								(983)	1120	1280	1360
70								(1040)	1210	1420	1530
80									(1280)	1530	1680
90									(1330)	1630	1810
100									(1370)	1710	1930
120										(1850)	2120
140										(1950)	2280
160											(2410)
180											(2500)
200											(2580)

The manner in which the data from the experimental investigations in various countries have been analysed in the preparation of the final calibration tables has been described by WEICKER and HÖRCHER[48] and by WHITEHEAD[49]. *Figure 217* shows a comparison between the results of different investigators, the results being expressed as the

mean break-down voltage gradient (*i.e.* break-down voltage V divided by gap length S) as a function of sphere diameter D for different values of the ratio S/D. According to Whitehead the great majority of the experimental results are contained within limits differing by < 10 per cent. and frequently < 5 per cent. To determine the final calibrations it was agreed that the values chosen should be as consistent as possible between different sizes of spheres, and that the voltage-spacing curves should be smooth. Whitehead has analysed in detail the polarity effect in sphere gaps with one sphere earthed and puts forward reasons why the negative impulse break-down curve should coincide with the power-frequency break-down curve. The positive impulse break-down voltage is derived from the negative impulse break-down voltage by multiplication by a mean factor, as

TABLE XVI

SPHERE-GAP BREAK-DOWN VOLTAGES IN kV (PEAK) IN AIR AT 20°C AND 760 MM. HG FOR POSITIVE IMPULSE AND POSITIVE UNIDIRECTIONAL VOLTAGES; ONE SPHERE EARTHED

Gap in cm.	*Sphere diameter in cm.*										
	5	6·25	10	12·5	15	25	50	75	100	150	200
0·5	17·5	17·2	16·9	16·7	16·5						
1	32·0	31·9	31·6	31·6	31·3	31					
1·5	46·1	45·9	45·6	45·6	45·5						
2	59·4	60·0	59·1	59·2	59·2	59	58	58			
2·5	71·0	72·3	72·8	72·5	72·6	72·5					
3	81·0	83·4	85·6	85·7	85·6	86					
4	(97·5)	103	109	111	111	112	112	112			
5	(109)	(117)	130	134	136	138	138	138	137	137	137
6		(128)	148	154	158	162	164	164			
7			163	172	178	187	189	189			
8			(176)	188	196	210	214	215			
9			(186)	202	212	232	238	240			
10			(195)	(214)	226	252	262	265	266	267	265
12				(232)	(249)	290	310	313			
14					(269)	321	356	360			
16						348	401	407			
18						372	440	452			
20						(393)	478	499	505	509	510
25						(430)	558	602	616	626	
30							625	694	719	740	745
35									816	850	
40							(721)	841	900	957	967
50							(785)	949	1050	1150	1180
60								(1030)	1160	1310	1380
70								(1100)	1260	1460	1560
80									(1330)	1580	1710
90									(1390)	1680	1850
100									(1430)	1770	1980
120										1920	2180
140										(2020)	2350
160											(2480)
180											(2580)
200											(2650)

determined in the U.S.A., though it is pointed out by Whitehead that considerable divergences exist between the results obtained by different investigators.

For spheres of a particular diameter the *Tables XV*, *XVI* and *XVII* give values of break-down voltage for spacings up to a sphere diameter only. The recommendation is made in B.S. 358 that the spacing should not exceed a sphere-radius if accurate measurements are required. The size of the spheres used is therefore governed by the magnitude of the voltage which is to be measured. The possible error incurred by the use of sphere gaps in the measurement of power-frequency alternating voltages is stated in British Standards[36] to be ±3 per cent. The same possible error applies to impulse voltage

TABLE XVII

SPHERE-GAP BREAK-DOWN VOLTAGES IN kV (PEAK) IN AIR AT 20°C AND 760 MM. Hg FOR POWER-FREQUENCY ALTERNATING, IMPULSE AND UNIDIRECTIONAL VOLTAGES; SYMMETRICAL GAP

Gap in cm.	*Sphere diameter in cm.*										
	5	6·25	10	12·5	15	25	50	75	100	150	200
0·5	17·5	17·2	16·9	16·7	16·5						
1	32·2	32·0	31·6	31·5	31·3	31					
1·5	46·1	46·0	45·8	45·7	45·5	45					
2	58·3	59·0	59·3	59·4	59·2	59	58	58			
2·5	69·4	70·9	72·4	72·6	72·9	72			71		
3	79·3	81·8	84·9	85·4	85·8	86					
4	(96·4)	101	107	110	111	113	112	112			
5	(111)	(117)	128	132	134	138	138	138	137	137	137
6		(131)	146	152	155	162	164	164			
7			163	170	175	185	189	190			
8			(177)	187	194	207	214	215			
9			(191)	203	211	228	239	240			
10			(203)	(217)	227	248	263	265	266	267	267
12				(241)	(256)	286	309	314			
14					(280)	320	353	362			
16						352	394	408			
18						381	434	452			
20						407	472	495	504	511	511
25						(463)	558	596	613	628	632
30							638	689	714	741	747
35									812	848	860
40							(767)	856	902	950	972
50							(874)	997	1070	1140	1180
60								(1120)	1210	1320	1380
70								(1220)	1340	1490	1560
80									(1460)	1640	1730
90									(1560)	1780	1900
100									(1660)	1910	2050
120										(2140)	2330
140										(2330)	2580
160											(2800)
180											(3000)
200											(3180)

measurements, provided that the impulse wave has a wave-front $>1\ \mu$sec and a wave-tail $>5\ \mu$sec. The error is probably greater in the range of sparking distances between $0{\cdot}5\,D$ and $0{\cdot}75\,D$. In the range from $0{\cdot}75\,D$ to D the break-down voltages given in *Tables*

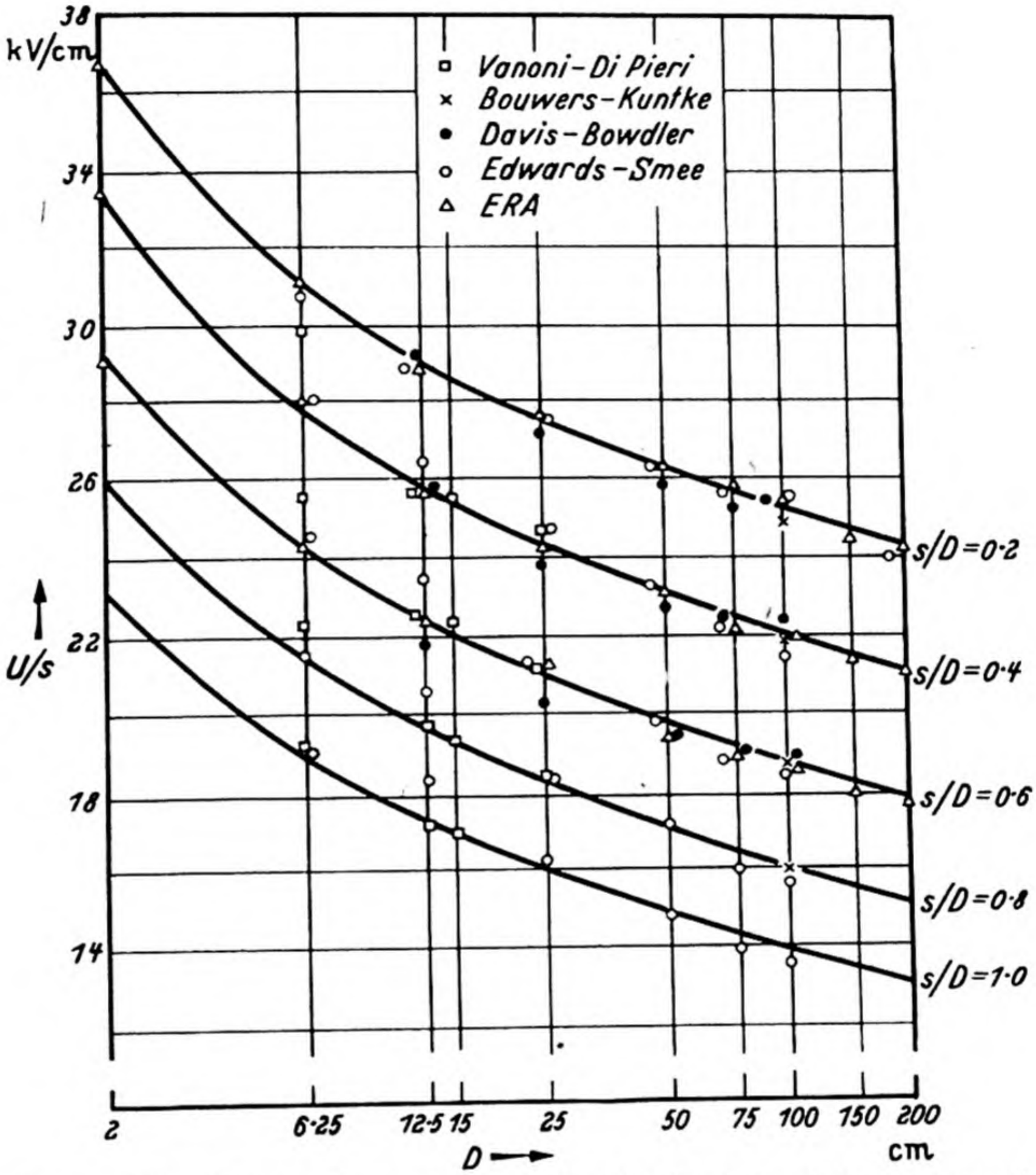

Figure 217. Comparison of the results obtained by different investigators of the mean break-down voltage gradient as a function of sphere diameter for different values of the ratio of spacing to diameter (Weicker and Hörcher[48], by courtesy, *Elektrotech. Z.*).

XV to *XVII* are regarded as of doubtful accuracy and for this reason are given in brackets. A possible error of ± 5 per cent. is given for the measurements of continuous unidirectional voltages. This larger error is attributable to the fact that the calibration tables are based entirely on measurements with power-frequency alternating voltages and impulse voltages. Little data has been obtained for the d.c. break-down of gaps between spheres though the available evidence

TABLE XVIII

CALIBRATION OF 2 CM. DIAMETER SPHERE GAP IN AIR AT 760 MM. HG AND 20°C

Gap length in cm.	0·05	0·1	0·2	0·3	0·4	0·5	0·6	0·7	0·8	0·9	1·0
Breakdown kV	2·8	4·6	8·0	11·1	14·1	17·1	20·0	22·7	25·3	27·8	30·2

shows that there is close agreement between the d.c. and a.c. break-down voltages. According to MEEK[65] the difference between the negative and positive d.c. break-down voltages is negligible (< 1 per cent.) for gaps up to a radius spacing between 6·25 and 12·5 cm. diameter spheres, and there is some doubt as to whether *Table XVI* should apply to positive d.c. break-down characteristics at gaps for which divergences occur between *Tables XV* and *XVI*.

The break-down voltage for a given spacing is generally higher for spheres of larger diameter than for spheres of smaller diameter. However, at short spacings it appears from *Tables XV* to *XVIII* that a slightly higher voltage is required to break down a given gap between spheres of small diameter than for the same gap between larger spheres. This may be the result of inadequate irradiation of the gap in the experiments on which the results of the Tables are based. Irradiation becomes increasingly necessary as the gap length and sphere size are reduced because of the decrease in sparking area[65, 74] (*see* Chapter 8).

TOEPLER[69, 70] has shown that the measured break-down curve for a sphere gap can be matched by two empirical curves and that there is a discontinuity in the slopes of the two curves at their meeting-point. For gap lengths shorter than that at which the discontinuity occurs the break-down voltage is independent of the sphere diameter. The critical gap lengths d_k as measured by CLAUSSNITZER[58] for different sphere diameters are given in *Table XIX*. For gaps up to $0{\cdot}5\,d_k$ Claussnitzer finds that the a.c. break-down voltage corresponds closely to that for the uniform field. Between $0{\cdot}5\,d_k$ and d_k the break-down voltage is higher than that for the same gap between spheres of larger diameter, the deviation reaching a maximum at about $0{\cdot}8\,d_k$. For gaps greater than d_k the break-down occurs at a voltage lower than that for the larger spheres. An increase in the scattering of the measured break-down voltages for gaps in the region between $0{\cdot}5\,d_k$ and d_k is also observed by Claussnitzer[58] and by Hueter[41] and DATTAN[45, 46]. A detailed analysis of the effect is given by JØRGENSEN[71]. Possible reasons for the effect have been discussed by Meek[72, 73, 74].

TABLE XIX

Sphere diameter in cm.	2	5	10	15	25	50	75	100
d_k cm.	0·90	2·05	3·65	5·00	7·15	11·00	14·15	17·00

Specifications are made in British Standards[36] regarding the profile of the spheres and it is stated that measurements of the curvature should be made with a spherometer at various positions over an area enclosed by a circle of radius $0{\cdot}3\,D$ about the sparking point, where D is the sphere diameter. The readings of the spherometer should not differ from the value which would be obtained with a perfect

sphere of the correct diameter by more than 0·001 D. The distance between the feet of the spherometer must not be less than 0·125 D or greater than 0·25 D. It is also specified that the length of any diameter should not differ from the correct value by more than 1 per cent. for spheres of diameter < 100 cm. or by more than 2 per cent. for larger spheres.

In general the spheres are mounted with the axis of the sphere gaps vertical, and the lower sphere is earthed, though with the smaller sphere diameters the arrangement with a horizontal axis is frequently preferred. The latter arrangement also has advantages when both spheres are to be insulated for the measurement of symmetrically applied voltages. In all cases it is important that the sphere gap should be situated in a space comparatively free from external electric fields and from bodies and surfaces which may distort the electric field between the spheres.

When one sphere is earthed the distance from the sparking point of the high-voltage sphere to the equivalent earth plane to which the earthed spheres is connected is required by B.S. 358:1939 to fall within the limits given in *Table XX*. These limits are subject to the provision that, when the sparking distance S exceeds 0·5 D, the distance of the sparking point of the high-voltage sphere from the earth plane above that sphere, *e.g.* a ceiling, shall exceed the distance of the sparking point of the earthed sphere from the earthed plane to which it is connected. If $S < 0{\cdot}5\ D$ it is sufficient if the two distances mentioned above are within the limits given in columns 2 and 3 of *Table XX*.

TABLE XX

HEIGHT OF SPARKING POINT OF HIGH-VOLTAGE SPHERE ABOVE THE EQUIVALENT EARTH PLANE

Sphere diameter D	$S < 0{\cdot}5D$		$S > 0{\cdot}5D$	
	Minimum height	*Maximum height*	*Minimum height*	*Maximum height*
Up to 25 cm.	10S	7D	5D	7D
50	8S	6D	4D	6D
75	8S	6D	4D	6D
100	7S	5D	3·5D	5D
150	6S	4D	3D	4D
200	6S	4D	3D	4D

The shanks supporting the spheres should be free from sharp edges and corners so that corona discharges are reduced. No conductor, except the shanks supporting the spheres, should be nearer the sparking point of the high-voltage sphere than the distance given by the expression $(25 + \frac{V}{3})$ cm., where V is the peak voltage in kV which is

to be measured. When large spheres are used for the measurement of low voltages the limiting distance should not be less than a sphere diameter. In the case of high-voltage conductors, particularly if they are discharging, the above limits must be regarded as absolute minima. As S/D is increased these precautions become increasingly important. The use of an earthed metal cage surrounding the sphere gap, to minimize the effect of external fields, has been examined experimentally by Hueter[41].

No difference appears to have been observed, within the limits of experimental error, in the break-down voltage calibrations of sphere gaps when spheres of different metals are used. B.S. 358:1939 states that the spheres may be made of brass, bronze, steel, copper, aluminium or light alloys. The surfaces of the spheres should be cleaned immediately before use and should be free from grease films, dust or deposited moisture. Care should be taken to keep the gap as free as possible from floating dust particles, fibres, etc. (*see* page 144).

In order to limit the discharge current and to prevent high-frequency oscillations, a protective resistance with a value of about 1 Ω/V should be used for power-frequency tests. The interval between successive discharges should be of sufficient duration to prevent any appreciable heating of the spheres and, if the surfaces of the spheres become severely pitted, they should be replaced. B.S. 358:1939 recommends that a number of preliminary discharges should be made before test readings are taken. It is advisable, where possible, to repeat the preliminary discharge until the break-down voltage for a given spacing between the spheres becomes constant as shown by some other voltage indicator, *e.g.* a peak voltmeter (*see* page 297).

TABLE XXI

ρ	0·70	0·75	0·80	0·85	0·90	0·95	1·0	1·05	1·10
k	0·72	0·76	0·81	0·86	0·90	0·95	1·0	1·05	1·09

The break-down voltage of a sphere gap decreases with decreasing air pressure and increasing temperature. The values given in *Tables XV* to *XVIII* correspond to a standard pressure of 760 mm. Hg and a temperature of 20°C. For the usual range of variation of atmospheric conditions the break-down voltage is closely proportional to the air density. However, a more accurate relation between the break-down voltage V at a relative air density ρ and the break-down voltage V_n at 760 mm. Hg and 20°C is given by

$$V = kV_n \qquad \ldots\ldots(7.5)$$

where k is a factor depending on ρ. Values for k are given in *Table XXI*; ρ is related to the air pressure p and temperature t°C by the expression

$$\rho = \frac{p}{760} \cdot \frac{293}{273 + t} \qquad \ldots\ldots(7.6)$$

According to B.S. 358:1939 the break-down voltage of a sphere gap is independent of atmospheric humidity, though deposited dew on the sphere surfaces lowers the break-down voltages. However, LEWIS[68] has recorded an increase in the break-down voltage with humidity for a 0·4 cm. gap between spheres of 2 cm. diameter, the break-down voltage increasing by ~0·1 per cent. per mm. Hg increase of water vapour in the atmosphere (*see* page 236).

When voltages of less than 50 kV are being measured it is suggested in British Standards[36] that irradiation by radio-active or other ionizing media should be used. In the American Standards[37] ultra-violet irradiation is recommended for sphere-gaps of 6·25 cm. diameter or less when arranged at spacings of one-third the sphere diameter or less; a quartz-mercury arc lamp of specified characteristics is proposed for the irradiating source, to be placed at a distance from the sphere surfaces of not less than five times the gap length. Experiments

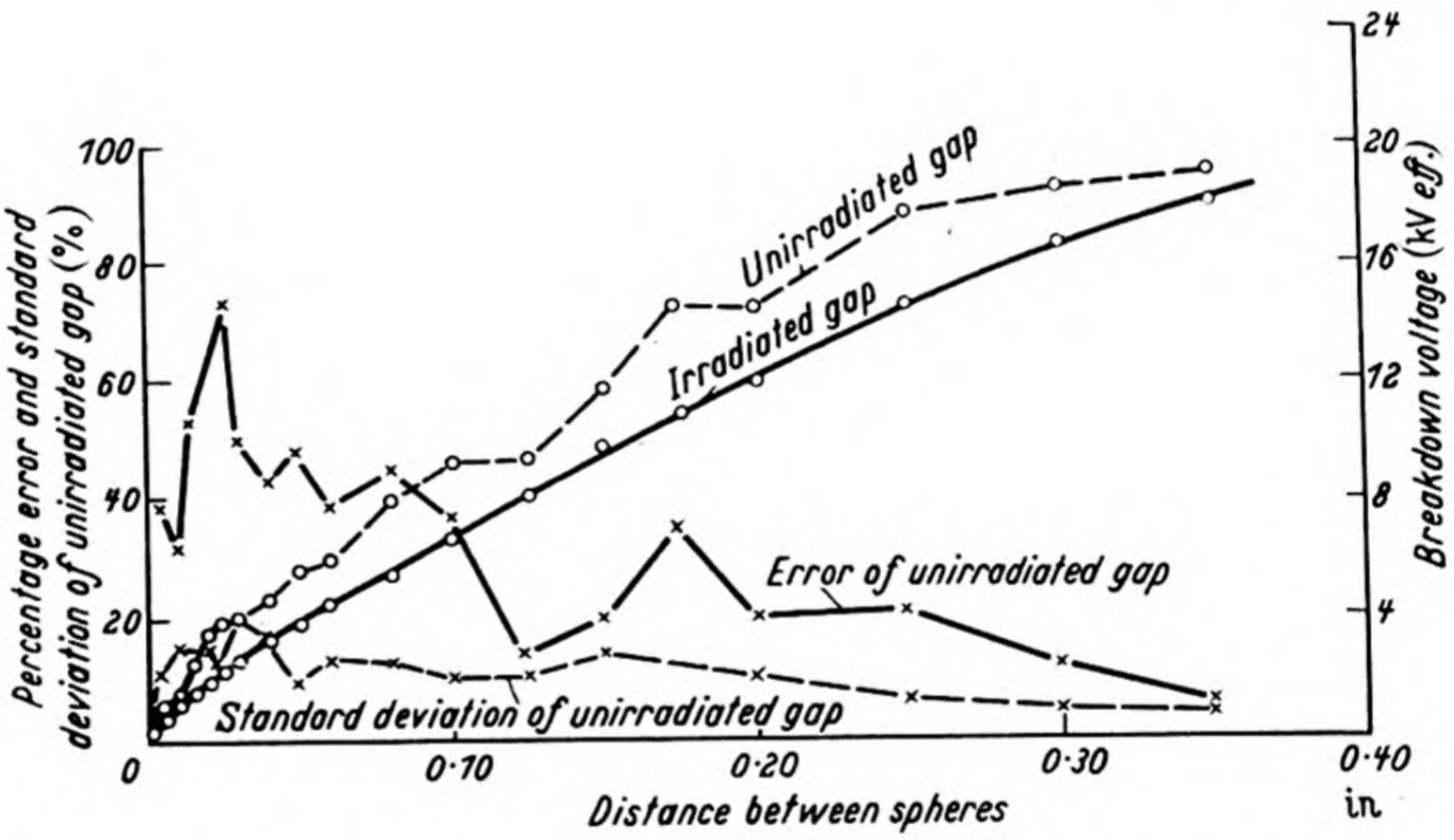

Figure 218. Break-down voltage curves and error curves obtained for gaps between spheres of 13 mm diameter when unirradiated and when irradiated by 0·5 mg of radium (Edwards and Smee[39], by courtesy, *J. Inst. elect. Engrs.*).

concerning the influence of irradiation on the behaviour of short gaps between spheres are reported by EDWARDS and SMEE[39]. These investigators have studied the break-down of gaps between spheres of 1·3, 1·6 and 6·25 cm. diameter, and have used an arc lamp and also 0·2 and 0·5 mg. of radium as irradiating sources. The radium, in the form of a capsule, is inserted in the high-voltage sphere and is held against the back of the sparking surface, which is about 1 mm. thick (*see* page 269). Curves showing the break-down voltage as a function of gap length for a 1·3 cm. diameter sphere gap, when unirradiated and when irradiated with 0·5 mg. of radium, are given in *Figure 218*, which includes also curves for the percentage errors

involved. In the case of larger gaps, a slight improvement in the consistency of the power-frequency break-down of a 50 cm. diameter sphere gap subjected to ultra-violet illumination is reported by SPRAGUE and GOLD[52] who found the break-down voltage of the illuminated gap to be 1 to 2 per cent. lower than the unirradiated value, for gaps up to 15 cm.

UNIFORM-FIELD SPARK GAPS

The use of uniform-field spark gaps for the measurement of a.c., d.c. and impulse voltages has been suggested by Bruce[75, 76] who has investigated the characteristics of such gaps for power-frequency a.c. voltages ranging from 9 to 315 kV. The results of his studies lead Bruce to conclude that the accuracy of the gaps when used for a.c. voltages is within 0·2 per cent., an appreciable improvement as compared with the equivalent sphere-gap arrangement.

The electrodes used by Bruce have plane sparking surfaces with edges of gradually increasing curvature, the contour following that

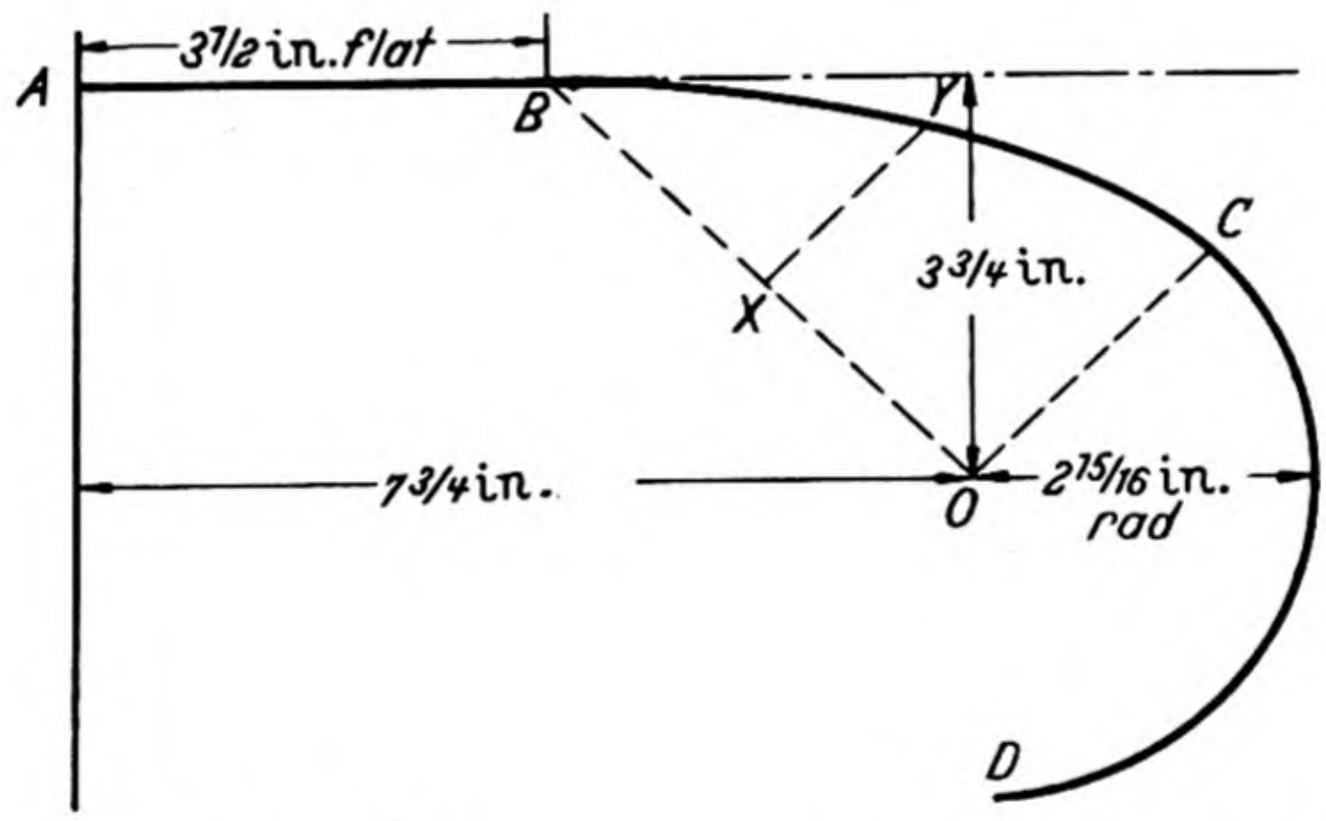

Figure 219. Half-contour of uniform-field electrode; working-range up to 420 kV peak (Bruce[75], by courtesy, *Proc. Inst. elect. Engrs.*).

suggested by STEPHENSON[77]. *Figure 219* shows a half-contour of one of the electrodes used. The portion $A\,B$ is flat, the total diameter of the flat portion being not less than the maximum spacing at which the electrodes are to be used. The portion $B\,C$ consists of a sine curve, based on the axes OB and OC, and given by $XY = CO \sin\left(\frac{BX}{BO} \cdot \frac{\pi}{2}\right)$. The portion CD is an arc of a circle centre O. It is not necessary that the design be strictly followed to close limits, but the flat portion should be as true as possible, and each portion should merge smoothly into the next. In Bruce's electrodes the estimated deviations from the true flat, for the portion AB, was $< 0{\cdot}003$ cm. With increasing gap length the size of the electrode has to be increased to maintain uniform-field conditions and three pairs of electrodes were used in

the investigations, the diameter of the flat surfaces being 2·25, 4·4 and 7·8 in. respectively. The corresponding overall diameter of the electrodes are 4·5, 9·0 and 15·0 in. These electrodes were designed to measure voltages up to 140, 280 and 420 kV respectively. For all three sizes of electrodes, and for a range of gaps covering break-down voltages from 9 to 315 kV, Bruce shows that the break-down voltage V of a gap of length S cm. in air at 20°C and 760 mm. Hg is within 0·2 per cent. of the value given by the empirical relation

$$V = 24{\cdot}22\,S + 6{\cdot}08\sqrt{S} \qquad \ldots\ldots(7.7)$$

The break-down voltages measured by Bruce[75] are compared with those obtained by other investigators[79, 80, 83, 89] in *Table XXII*, which includes also the break-down voltages for sphere gaps when the gap length is small compared with the sphere radius so that the field is nearly uniform[36].

TABLE XXII

BREAK-DOWN VOLTAGES OF UNIFORM-FIELD SPARK GAPS IN AIR AT 20°C AND A PRESSURE OF 760 MM. HG

Gap length	*Break-down voltage according to*					*Break-down voltage of sphere-gap*
	Schumann	Ritz	Holzer	Fisher	Bruce	
cm.	kV	kV	kV	kV	kV	kV
0·1	4·5	4·54	—	—	—	4·6
0·2	8·0	7·90	—	—	7·56	8·0
0·3	11·3	11·02	—	—	10·60	11·1
0·4	14·4	14·01	—	14·1	13·54	14·1
0·5	17·4	17·00	—	16·9	16·41	17·0
0·6	20·3	19·90	—	19·6	19·24	19·8
0·7	23·2	22·80	—	22·3	22·04	22·7
0·8	26·1	25·70	—	24·9	24·81	25·8
0·9	28·9	28·50	—	27·5	27·57	28·6
1·0	31·7	31·35	31·66	30·3	30·30	31·0
2	59·6	58·7	61·20	55·7	57·04	58
3	87·0	85·8	86·94	—	83·19	85
4	114·0	112·0	113·04	—	109·0	112
5	140·0	138·5	137·8	—	134·7	137
6	166·2	163·8	163·44	—	160·2	164
7	191·8	189·9	187·74	—	185·6	190
8	216·8	215·0	212·88	—	211·0	215
9	241·2	240·0	237·78	—	236·3	240
10	266·0	265·0	263·0	—	261·4	265
11	290·4	290·0	288·2	—	286·6	288
12	—	315·5	313·2	—	311·6	312
13	—	—	338·1	—	—	336
14	—	—	363·2	—	—	362
15	—	—	387·7	—	—	388
16	—	—	412·6	—	—	412

In measurements of the variations of break-down voltage observed in successive readings for a given gap Bruce records a mean deviation of 0·06 per cent. This compares with a mean deviation of 0·2 per cent. for a 25 cm. diameter sphere gap in similar conditions.

Bruce has examined the various errors which may be introduced by faulty alignment of the electrodes and by neighbouring conductors and corona discharges. To confirm that spark break-down is occurring under the required conditions it is preferable that the spark path should be viewed by two observers, with lines of sight at right angles. Lack of parallelism or the presence of dust will cause the spark paths to congregate in small areas on the electrode surfaces, and the proximity of nearby objects may cause spark break-down near the edges of the electrodes and distortion of the spark path. Bruce recommends that the clearance between the edges of the electrodes and the nearest earthed conductor in the plane of the gap should be not less than four times the maximum gap spacing. The clearance between the edges of the electrodes and a corona-discharging conductor should be not less than ten times the maximum spacing.

Other measurements of uniform-field break-down have been made by HOLZER[79] and RITZ[80] whose results for various gap lengths are listed in *Table XXII*. The relation between the break-down voltage V and the sparking distance S is given by Ritz as

$$V = 24{\cdot}55\,S + 6{\cdot}66\sqrt{S} \qquad \ldots\ldots(7.8)$$

and that given by Holzer is

$$V = 23{\cdot}85\,S + 7{\cdot}85\sqrt{S} \qquad \ldots\ldots(7.9)$$

The gaps used by Holzer and Ritz have electrodes with plane sparking surfaces, the edges being curved to a profile specified by ROGOWSKI and others[81, 82]. This profile is determined from considerations of the electrostatic field due to a finite plane plate parallel to an infinite plane plate and is chosen to correspond closely to an equipotential surface. Curves enabling the profile to be readily calculated are given by STOERK[82]. In Ritz's measurements three pairs of electrodes were used, with diameters of 8·5, 18 and 45 cm. for gaps up to 2, 5 and 12 cm. respectively. Holzer used electrodes of 60 cm. diameter. An accuracy within 0·5 per cent. is quoted by Ritz.

Break-down voltages obtained by FISHER[83] for the d.c. break-down of uniform-field gaps are also given in *Table XXII*. Fisher's values agree closely with those of Ritz for gaps up to 0·6 cm. but for longer gaps Fisher's results fall below Ritz's values. Fisher attributes this fall to the influence of the walls of the surrounding glass chamber on the field of the discharge-gap, the effect becoming more important as the gap length is increased.

The influence of gas density on the break-down voltage is such that the break-down voltage Equations 7.7, 7.8 and 7.9 require to be modified as follows:—

$$V = A\rho S + B\sqrt{\rho S} \qquad \ldots\ldots(7.10)$$

where ρ is the gas density.

Holzer and Ritz have noticed that a change in humidity causes a measurable change in the break-down voltage. For example, with a 2·0 cm. gap, the break-down voltage is increased by about 3 per cent. when the absolute humidity is changed from 5 to 15 mm. Hg (*see* page 232). According to Ritz the influence of humidity may be included in the break-down relationship as follows:

$$V = 6{\cdot}66\sqrt{\rho S} + [24{\cdot}55 + 0{\cdot}41\,(0{\cdot}01e - 1)]\,\rho S \qquad \ldots\ldots(7.11)$$

where e is the absolute humidity in mm. Hg. The break-down voltages given by Ritz in *Table XXII* refer to a standard humidity of 10 mm. Hg.

ROD GAPS

A rod gap may be used to measure the approximate peak value of a power-frequency alternating voltage. The gap usually consists of two one-half inch square (or five-eighth inch square) rod electrodes which are cut off squarely at their ends and are mounted on insulating supports so that a length of rod equal to or greater than one-half of the gap spacing overhangs the inner edge of the support[37, 84]. Break-down voltage data for rod gaps, as given in the American Standards[37] are reproduced in *Table XXIII*. They refer to gaps in air at 25°C and 760 mm. Hg, with a water-vapour pressure of 15·5 mm. Hg.

The rod gap break-down voltage increases with increasing relative air density, the relation being a closely proportional one over the normal variations in atmospheric pressure. The break-down voltage also increases with increasing relative humidity, the standard humidity being taken as 15·5 mm. Hg for the values given in *Table XXIII*. If the humidity departs from the standard value it is necessary to adjust the break-down voltages of *Table XXIII* by the percentage correction factor H given in *Table XXIV*[37]. The values in *Table XXIV* apply to voltages above 141 kV peak; for lower voltages the correction H has to be reduced to H_1 where $H_1 = H \times \frac{\text{kVpeak}}{141}$. Different correction factors apply in the case of the impulse voltage break-down of rod gaps[84] (*see* page 284).

The corrections for humidity are based largely on the measurements by FIELDER[85, 86]. In later work by LEBACQZ[87] on the break-down voltages for gaps ranging in length from 6 in. to 30 in., it is found that while the break-down voltage increases with increasing humidity the percentage increase per mm. Hg vapour pressure is not constant

TABLE XXIII

POWER FREQUENCY BREAK-DOWN VOLTAGES FOR GAPS BETWEEN HALF-INCH SQUARE RODS[37] IN AIR AT 25°C AND 760 MM. HG, WITH WATER VAPOUR PRESSURE 15·5 MM. HG

Gap length in cm.	*Break-down kV peak*	*Gap length in cm*	*Break-down kV peak*	*Gap length in cm.*	*Break-down kV peak*
2	26	30	172	100	537
4	47	35	198	120	642
6	62	40	225	140	744
8	72	50	278	160	847
10	81	60	332	180	950
15	102	70	382	200	1054
20	124	80	435	220	1160
25	147	90	488		

and attains a maximum of 1·2 per cent. per mm. Hg for spacings between 18 in. and 24 in. Reference values for temperature, pressure and humidity have been discussed by BELLASCHI and MCAULEY[88].

TABLE XXIV

HUMIDITY CORRECTIONS FOR ROD GAP BREAK-DOWN VOLTAGES[37]

Vapour pressure in mm. Hg	*Correction factor H %*
2·54	− 16·5
5·0	− 13·1
10·0	− 6·5
15·0	− 0·5
20·0	+ 4·4
25·0	+ 7·9
30·0	+10·1

SERIES RESISTANCE VOLTMETERS

A method widely used in high-voltage d.c. measurements is to connect a high resistance, R, in series with a sensitive ammeter having an impedance negligible compared with R. The value of the indicated current I then gives the high voltage $V = RI$.

Details of the design and characteristics of resistors built for this purpose are fully discussed on pages 371–385.

SERIES CAPACITANCE VOLTMETERS

High alternating voltages can be determined by measurement of the current flowing through a capacitor connected to the high-voltage source, the current being measured with a rectifier-milliammeter

combination[19, 39, 90–95]. The principles of the method are discussed on page 298. Both peak and r.m.s. voltages can be recorded in this way.

The method has been used by Edwards and Smee[39] for the measurement of voltages up to 1,000 kV (r.m.s.). The high-voltage testing circuit shown in *Figure 220* consists of two 500 kV transformers con-

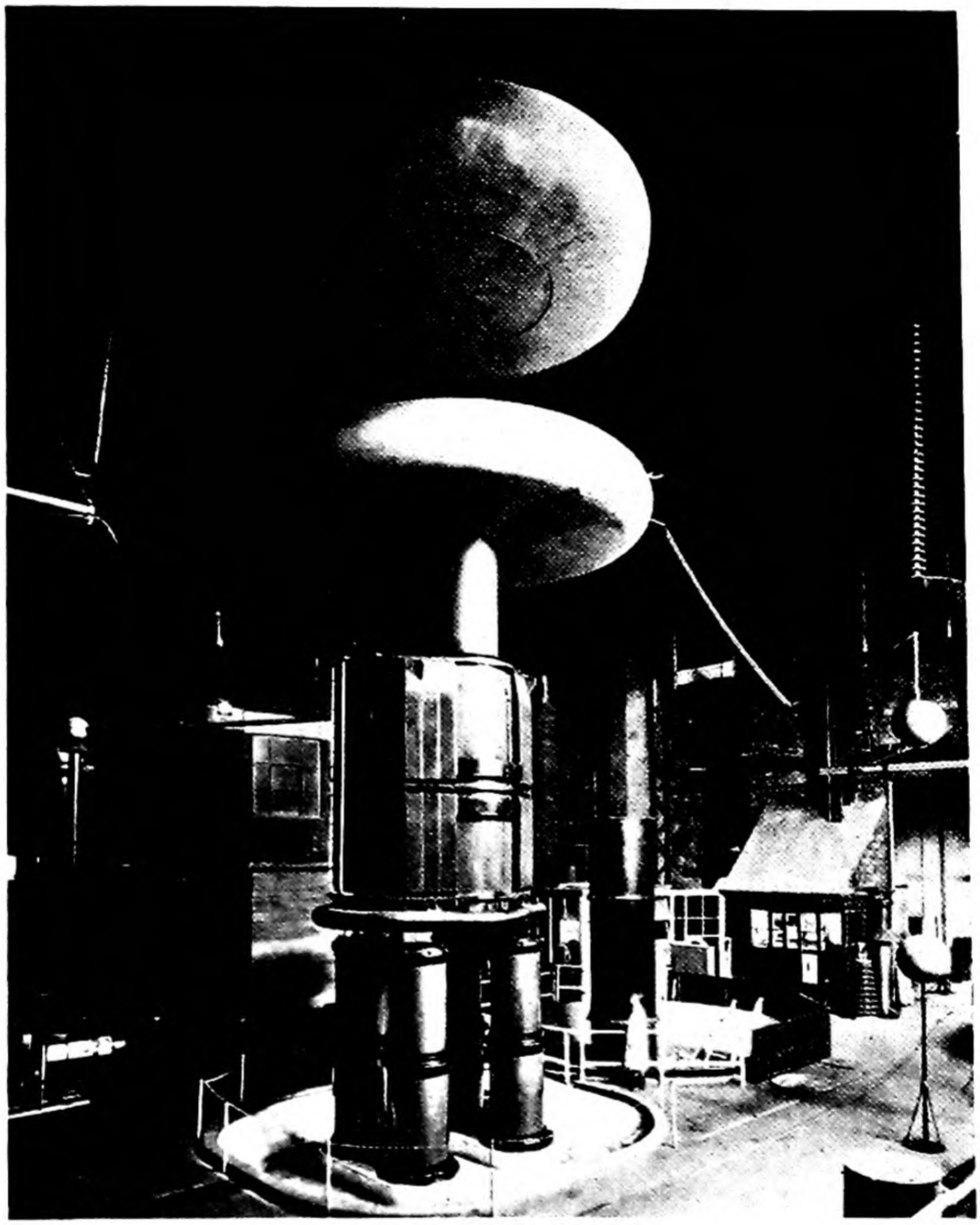

Figure 220. 1,000 kV air capacitor mounted on a 500 kV transformer which is insulated from earth and connected in cascade with a similar transformer (by courtesy, Metropolitan-Vickers Electrical Co.).

nected in cascade, the tank of the second transformer being insulated from earth for 500 kV on Bakelite-impregnated paper columns. Each transformer is provided with a condenser-type terminal bushing with a buried low-voltage foil insulated from earth and which can be used for connection to a crest-voltmeter circuit if required. The standard

air condenser is mounted above the terminal bushing of the second transformer, and consists of two horizontal flat discs, of 20 ft. in diameter, with rounded edges of 2 ft. radius. One electrode is connected to the transformer output, and the other electrode is supported from the roof directly over the lower electrode. The arrangement is clearly shown in *Figure 220*. The distance between the discs is 11 ft. The discs are constructed of expanded metal, mounted on an angle-iron framework, and coated with plaster, rubbed down and then treated with conducting paint. The upper electrode is in two parts, and consists of a central disc of 10 ft. diameter which is insulated from the outer, rounded portion which forms the guard-ring and is earthed. The central disc is connected by a screened lead to the rectifier-milliammeter system. The rectifier used is of the mechanical type, with negligible voltage drop. The milliammeter reads up to 1 mA full scale and is shunted by a resistance of such value to enable it to read 0 to 1,000 kV directly.

Edwards and Smee[39] give a detailed account of the methods of measurement of the capacitance of the air condenser. For this purpose the capacitance of each terminal bushing was measured on a Schering bridge, using a compressed-gas condenser as a standard, for voltages up to 225 kV. Measurements were then made of the capacitance of the parallel-plate air condenser under three conditions:

(*a*) With the second 500 kV transformer used for excitation, its tank being earthed;

(*b*) With the transformers in cascade, so that the tank of the second transformer was at half the voltage impressed on the condenser;

(*c*) With the first (*i.e.* permanently earthed) 500 kV transformer used for excitation, the second transformer being short-circuited, with its tank at the test voltage.

Three practically straight parallel lines connecting capacitance with voltage were obtained in this way. They showed an increase in capacitance of about 0·25 per cent. as the voltage was raised from 100 to 225 kV. The capacitance at any one voltage increased with the voltage on the tank of the second transformer, being lowest under condition (*a*), 1 per cent. higher under condition (*b*), and 2 per cent. higher under condition (*c*).

The next step followed by Edwards and Smee was to arrange crest-voltmeter circuits on each transformer. For the first transformer this presented no difficulty, but for the second the instrument and rectifiers had to be mounted on the tank, the readings being taken through a telescope. With the transformers connected in cascade readings were taken of the individual transformer voltages and of the total voltage to earth up to 1,000 kV. The two individual 500 kV

crest voltmeters were compared with the 1,000 kV crest voltmeter so that the true voltage to earth and hence the capacitance of the plate condenser could be calculated up to 450 kV, which was the limit beyond which no direct knowledge was available of the component voltages.

Measurements were next made of the bushing capacitances against the air condenser as a standard up to 500 kV and it was now possible to calibrate the two crest voltmeters up to 450 kV and thence to calculate the plate condenser up to 900 kV. Two other calculations, *viz.* calibration of the two crest voltmeters up to 500 kV and thence the calculation of the plate condenser capacitance up to 1,000 kV, complete the work.

Small discrepancies arising from the results obtained and from cross-checks were traced to the influence of the temporary high-voltage leads which had to be used and allowance had to be made for their effects.

Edwards and Smee point out that their method avoids the necessity for the extrapolation of any curve except (1) the capacitance-voltage curve of the compressed-gas condenser, for which strong evidence exists as to its linear nature, and (2) the plate condenser capacitance-voltage curve from 225 to 500 kV for the conditions (*a*) and (*c*) above. Here the variation of the capacitance with voltage was known for condition (*b*), and as the capacitance under this condition was a linear function of voltage up to 450 kV, and as the capacitance-voltage curves under the conditions (*a*) and (*c*) were straight lines close to and parallel to the line for condition (*b*) over the range 0 to 225 kV, it was assumed that a linear extrapolation could be made. It had also to be assumed that the capacitance of the bushing of the second transformer was unaffected by the tank voltage.

Other possible errors are:

(1) The earth capacitance of the screened lead from the top plate of the air condenser to the rectifier is about 1,600 $\mu\mu$F. The maximum voltage on this lead is 5 V and at 50 c/s this corresponds to a shunted current of 2·5 μA in quadrature with the current of ~ 5 mA flowing through the rectifier. This shunted current can therefore be entirely neglected. The error due to this cause from high harmonics might be serious but such harmonics were not present to affect the results in Edwards and Smee's measurement.

(2) Any difference in phase between the voltages of the two cascade-connected transformers would make the apparent capacitance of the air condenser too small and the instrument would therefore read high. This phase difference was, however, so small that the error due to this cause was $< 0{\cdot}1$ per cent.

(3) Errors in frequency result in a proportional voltmeter error. In Edwards and Smee's investigations the frequency was indicated by a vibrating-reed instrument capable of showing variations of $\pm\frac{1}{4}$ c/s, or $\pm 0{\cdot}5$ per cent., and the frequency was controlled within these limits.

SERIES INDUCTANCE VOLTMETERS

A high inductance in series with a current-measuring instrument can be used to determine high voltages[19, 96]. As pointed out by Defandorf[19] the system has the drawback that the inductor used requires an iron core at lower frequencies if the inductance is to be large compared with the resistance of the windings. Stray and distributed capacitances also cause complications with the result that series inductors have been little used in high-voltage measurement.

POTENTIAL DIVIDERS

Potential divider methods for the measurement of high voltages are described in Chapter 9.

VOLTAGE TRANSFORMERS

The use of transformers of known ratio in the measurement of high alternating voltages has been briefly reviewed by Defandorf[19]. With a suitable type of construction such transformers may have ratios constant to about 0·01 per cent. Silsbee and Defandorf[16] have described the use of a resistance bridge to measure transformer ratios. A capacitance bridge has been used for the same purpose by Bousman and Ten Broeck[97]. The former authors also describe how extrapolation methods can be used for transformers with multiple high-voltage windings to enable voltages up to 250 kV to be measured to an accuracy within 0·1 per cent. Small cascaded transformers[98–101] or transformers with tapped secondary windings[102] or with separate tertiary windings[103] may similarly be used. Alternative methods make use of a high-voltage resistor[104], reactor[105] or capacitor[106, 107] in series with a small transformer.

GENERATING VOLTMETERS

The generating voltmeter has often been used for the measurement of high d.c. voltages and in its simplest form consists essentially[108] of an electrostatic alternator excited by the field to be measured. *Figure 221* shows a simple type of generating voltmeter in which the fixed insulated quadrants *B* are exposed to the h.t. terminal whose voltage is to be measured, and are then covered by the rotating vanes twice in each revolution. The vanes are mounted on the

shaft *A* (*Figure 221*) and move behind the quadrant-shaped openings in the front of the voltmeter case. The induced charges on *B* leak to earth through the resistance shown (*Figure 221*) thus giving a series of voltage pulses which are amplified in a suitable manner.

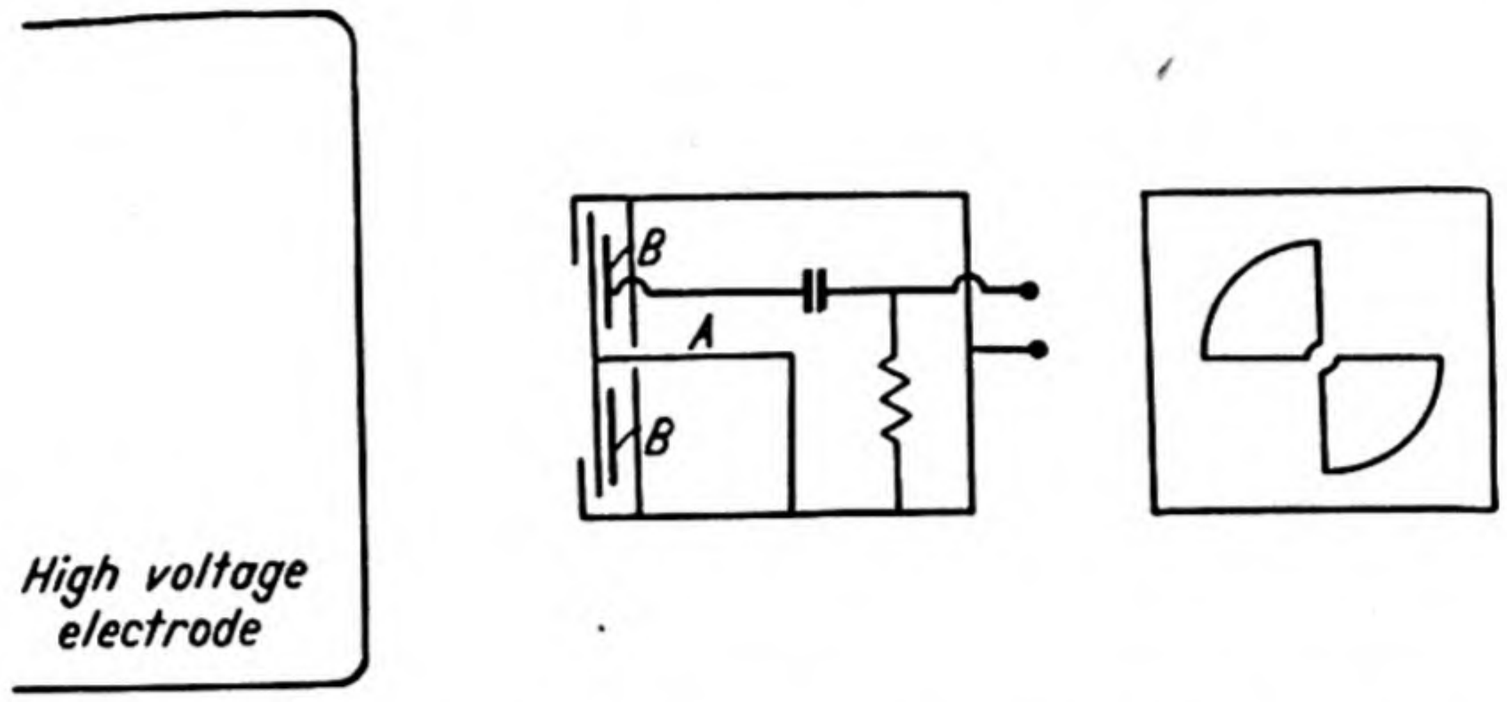

Figure 221. Schematic diagram of generating voltmeter.

If C is the capacitance of the system between the h.t. terminal and the pick-up plate and if V is the terminal potential then the charge Q on C is at any instant $Q=CV$ so that $\frac{dQ}{dt}=I=V\frac{dC}{dt}$. The mean value of $\frac{dC}{dt}$ is zero but assuming perfect rectification of the induced pulses on B, the r.m.s. voltage across the resistor (*Figure 221*)

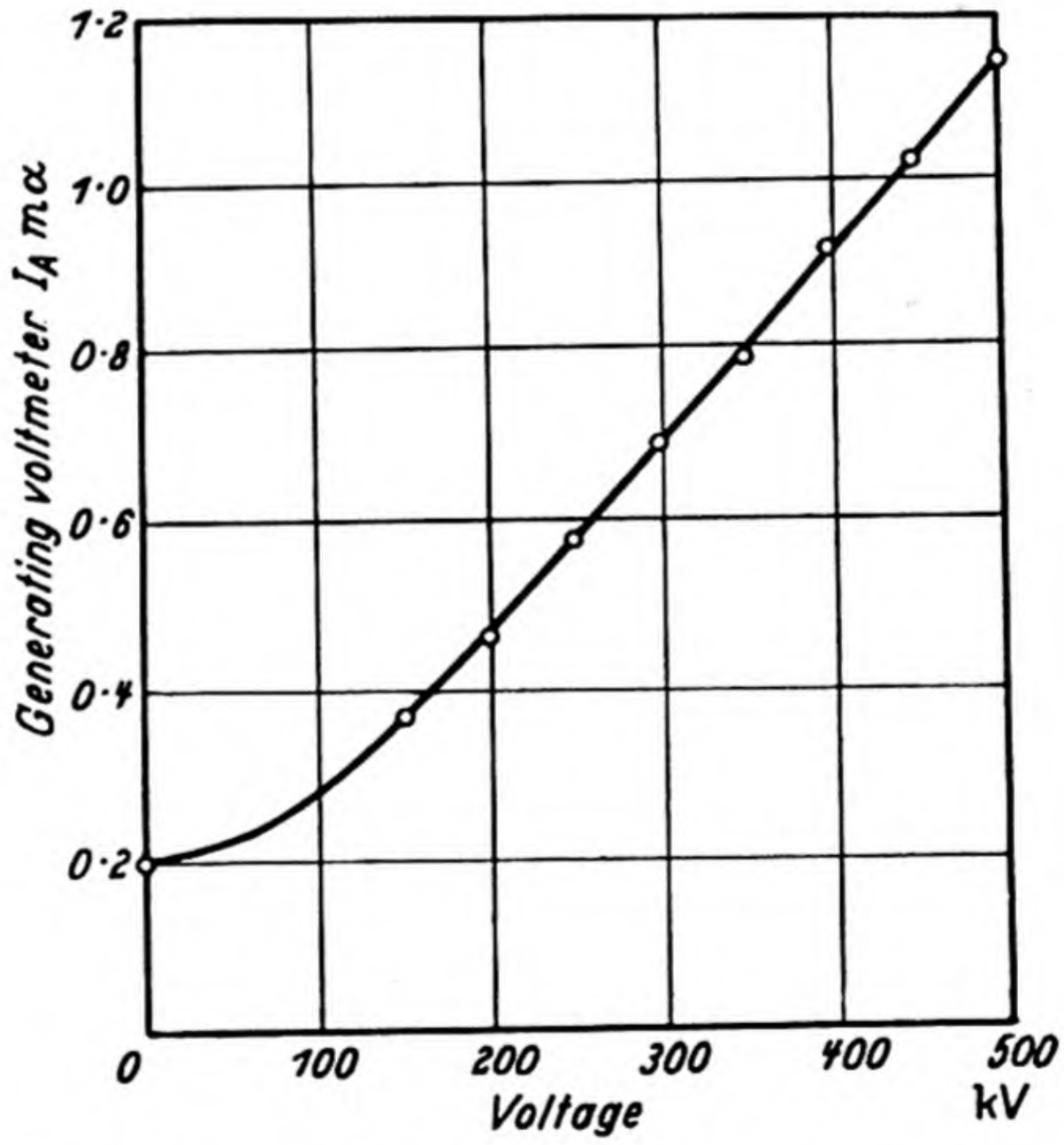

Figure 222. Calibration of generating voltmeter using 75 cm. diameter spheres as standard.

is $E=3{\cdot}93\times10^{-10}\ FASR$ millivolts where F is the field strength in V/cm. at the voltmeter, A is the exposed area of charged plate in cm.^{2}, S is the motor speed in r.p.s. and R is the resistance in ohms. If S is 25 r.p.s. $A=157$ cm.^{2}, $F=4$ kV/cm. then $E=62$ volts if $R=10\text{M}\Omega$.

The instrument was built at a cost of a few pounds in 1939 from $\frac{1}{8}$ in. aluminium sheet. The box dimensions were $10 \times 10 \times 14$ in. and the quadrants cut out in the front of the box had a radius of 10 cm. The spinning vane consisted of two quadrants with a radius of 10·5 cm. and had clearances to the insulated plate and the box front of 1·5 cm. The insulated pick-up plate was shielded by an earthed plate as shown in *Figure 221*. A $\frac{1}{8}$ h.p. motor was adequate for the driving of the spinning vane. Using a simple valve circuit connected to the generating voltmeter a sphere-gap calibration gave the generating voltmeter a response curve as shown in *Figure 222* and the accuracy obtained was 2 or 3 per cent. If great care is taken to avoid fringing fields, edge effects, etc., a calibration may be made with a low-voltage plate placed near to the voltmeter to give values of F comparable to those obtained in the h.t. condition. It is also possible to make the calibration in an absolute manner from a knowledge of the capacitance between the charging plate and the h.t. terminal but this is difficult and apparently is rarely if ever carried out.

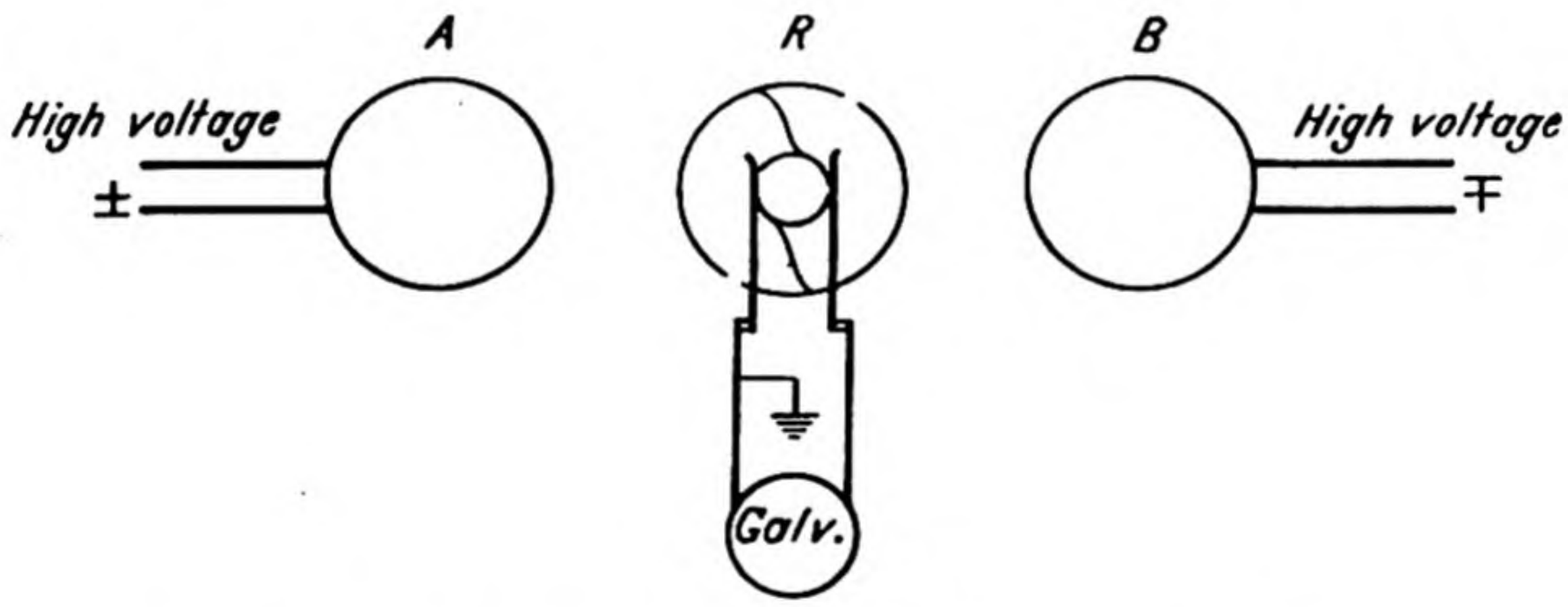

Figure 223. Schematic diagram of a generating voltmeter (Kirkpatrick and Miyake[112], by courtesy, *Rev. Sci. Instrum.*).

Generating voltmeters have been made for use with pressure-tank Van de Graaff generators and typical examples are described by PARKINSON *et al.*[109], TRUMP *et al.*[110], HAXBY *et al.*[111] and others. However the earliest work on generating voltmeters appears to be due to KIRKPATRICK and MIYAKE[112], KIRKPATRICK[113] and GUNN[114]. Kirkpatrick and Miyake show the schematic diagram of *Figure 223* in which A and B are conducting spheres, at equal positive and negative potentials with respect to earth and with a total voltage difference, between A and B of V. The rotor, R, consists of two insulated hemicylinders and a commutator, connected to a galvanometer. If C is the maximum capacitance between either side of the rotor and one of the spheres then each half-turn of the rotor results in a charge Q, where $Q=CV$, flowing through the galvanometer. If the rotor is driven at n r.p.s. the average galvanometer current is $I=2\,CVn$.

An early generating voltmeter[112] had a rotor 18 cm. long and 18 cm. diameter mounted midway between two spheres each 18 cm. in diameter, with a clearance of 10 cm. on each side of the rotor which was driven at 1,800 r.p.s. The calibration of the voltmeter is shown in *Figure 224* and it is interesting to note that this could be checked absolutely if C were known accurately. The latter measurement is seldom accurate because of stray capacitances which are often difficult to measure.

An oil-immersed generating voltmeter has been used by THOMAS[115] in which the rotor which revolves between two long stator plates, is made of two hemicylinders, insulated from each other. It is 6 in. long and 1 in. in diameter and with a rotor-stator separation approximately equal to the rotor diameter. Voltages up to about 100 kV peak could be measured. The advantages of oil-immersion are the same as those obtained with the compressed-gas or vacuum electro-

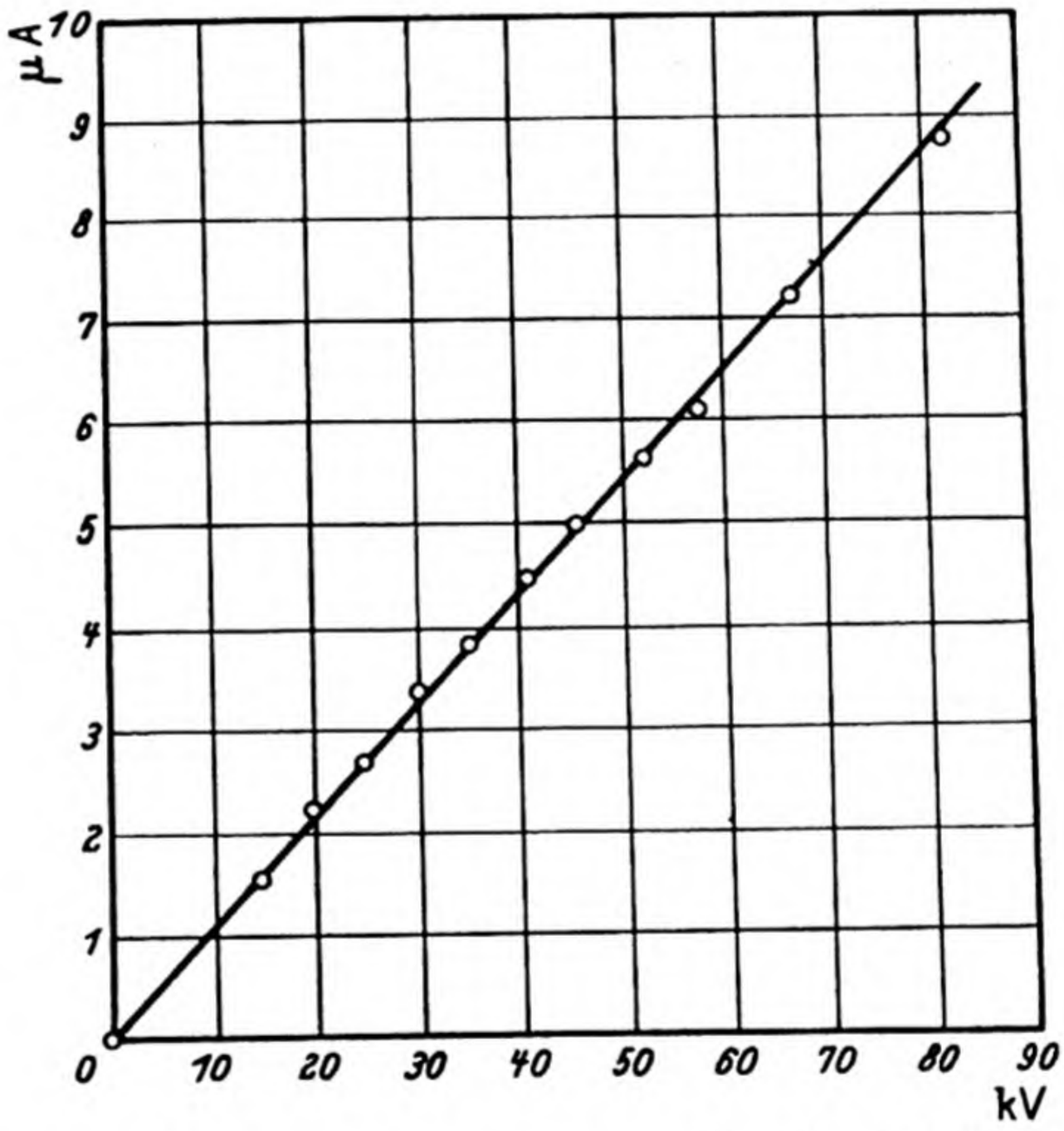

Figure 224. Generating voltmeter calibration (Kirkpatrick and Miyake[112], by courtesy, *Rev. Sci. Instrum.*).

static voltmeters (*see* pages 219–222), namely small size for a given voltage and a greater current output, enabling relatively insensitive measuring instruments to be used. Thomas calibrated his voltmeter against sphere gaps.

Generating voltmeters have been used also in measurements of electrical potential gradients in the atmosphere by WORKMAN and HOLZER[116].

Kirkpatrick's later paper[113] describes a generating voltmeter for use up to 100 kV, with a cylindrical rotor having a diameter of 5 in.

and a length of 12 in. The rotor projects through the side of a screening box which also contains the fixed electrodes between which the rotor turns and to one of which the h.t. is applied. The rotor is mounted on a $\frac{1}{6}$ h.p. synchronous motor. This arrangement is, indeed, little different from that described above but the calibration, given in *Figure 225*, which extends from 1 to 10^5 V is of interest in that it indicates the validity of a low-voltage calibration in corona-free h.t. measurements with this type of instrument. Further, since $I = 2CVn$ (where I is the galvanometer current, n is the number of revolutions of the motor shaft/sec, V is the applied voltage and C is the maximum capacitance between either electrode and the rotor), it is possible to calculate C from *Figure 225*. Kirkpatrick thus found

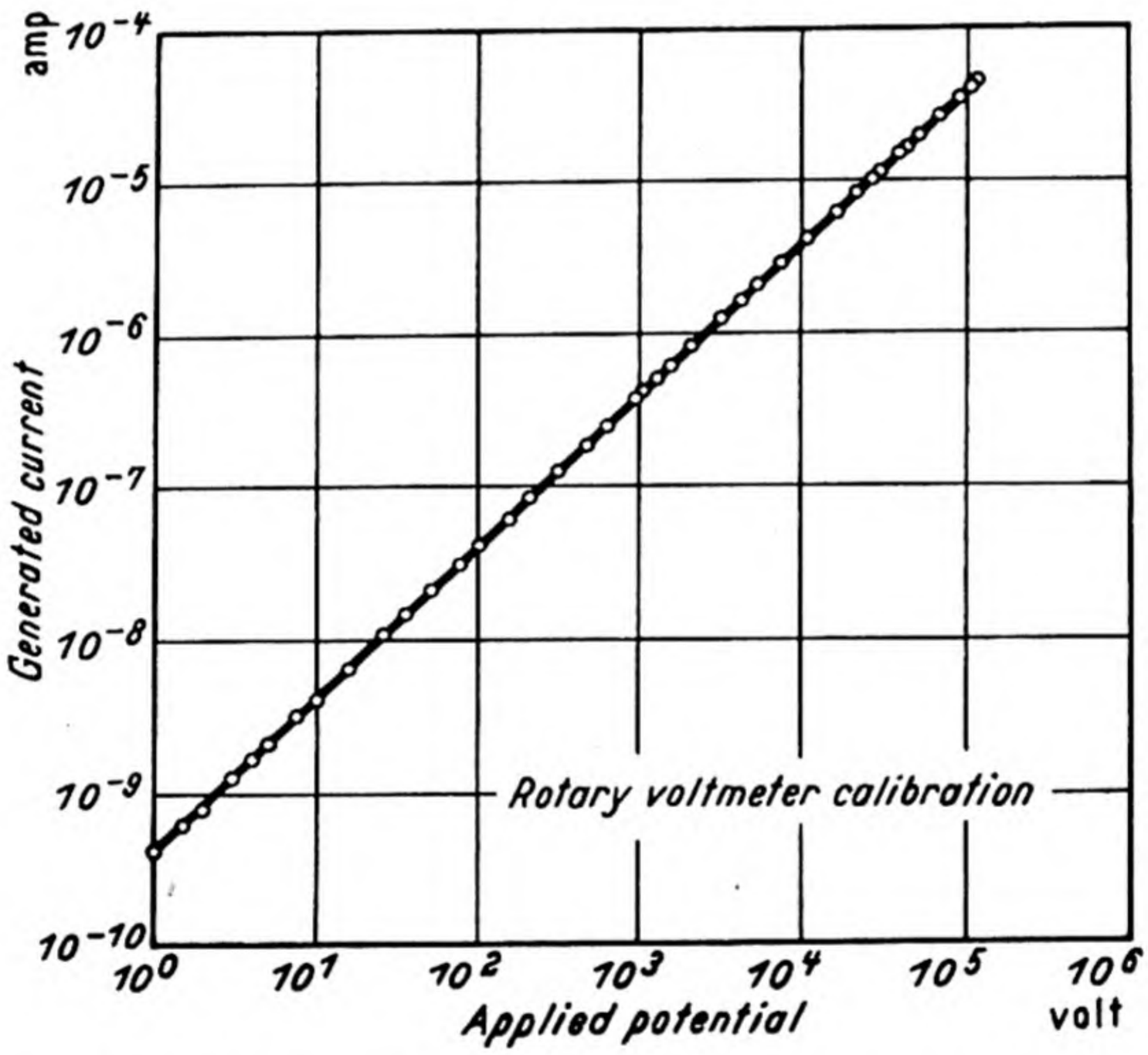

Figure 225. Kirkpatrick's[113] high-voltage calibration of a generating voltmeter (by courtesy, *Rev. Sci. Instrum.*).

$C = 6{\cdot}63 \pm 0{\cdot}02\,\mu\mu$F, in excellent agreement with the measured value of $6{\cdot}64 \pm 0{\cdot}02\,\mu\mu$F. This latter quantity was measured in a simple circuit[113] which is of some interest since it may be used, according to Kirkpatrick, for the measurement of capacitances as low as 1 $\mu\mu$F, provided adequate insulation is provided. This procedure cannot easily be carried out when the generating voltmeter is, for example, mounted in the wall of the pressure tank of a Van de Graaff generator, when the nuclear methods described elsewhere (*see* page 253) would appear to be the most suitable. Generating voltmeters are relatively simple and cheap, however, and their use in general h.t. work might advantageously be increased. Then the above calibration method becomes of considerable interest.

HENDERSON, GOSS and ROSE[117] have used a generating voltmeter to examine the output wave-form of a cascade rectifier set (830 kV maximum) used with an X-ray tube. The voltmeter has a rotor

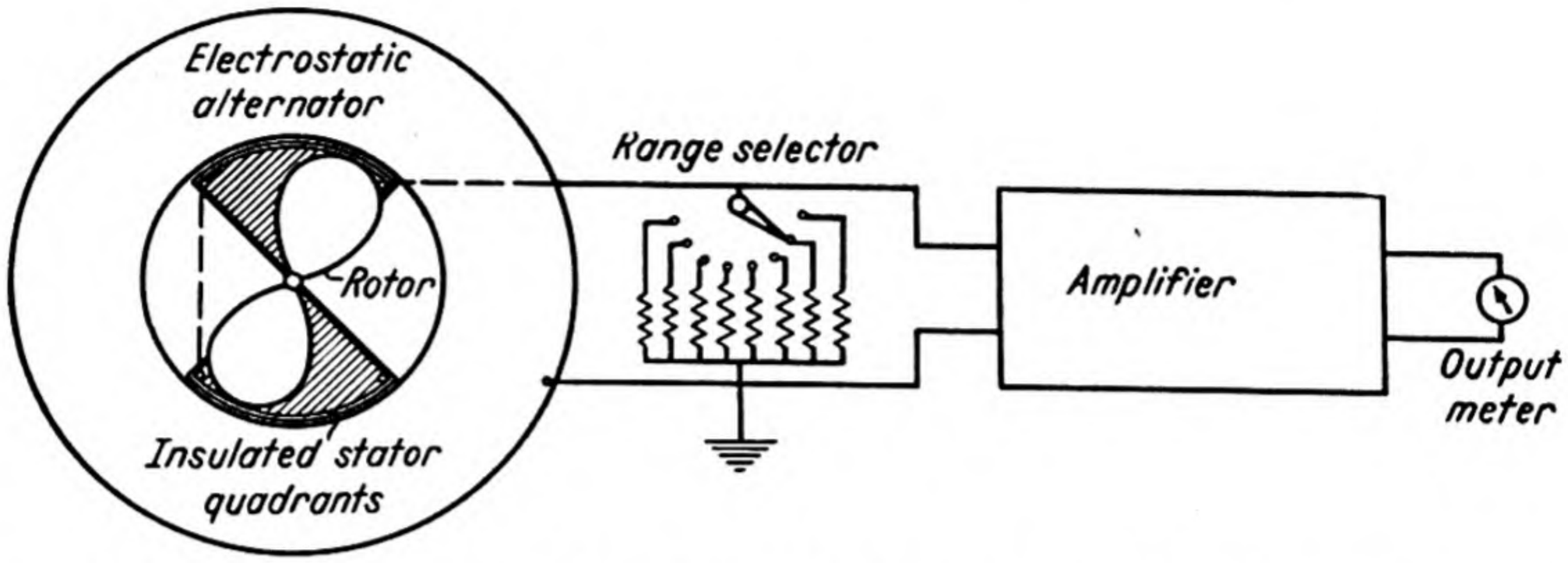

Figure 226. Component parts of the Round Hill generating voltmeter (Van Atta *et al*[108], by courtesy, *Phys. Rev.*).

diameter of 15 cm., and a length of 30 cm. following the design due to Kirkpatrick[113]. The meter is mounted in bearings so that it can be rotated as a single unit and thus used to measure wave-forms when driven from the same source as the h.t. transformer of the rectifier set. The current generated by the rotary voltmeter varies from 10–20 μA.

The generating voltmeter is calibrated at 8 kV with d.c. applied to the sphere gap normally attached to the output end of the cascade generator, and measured with a potential divider and a normal voltmeter. The calibration of the rotary voltmeter is taken as linear, on the assumption that corona and surface charging effects (*see* page 247) are negligible. This is not always a justifiable procedure although in the present case the wall behind the voltmeter was covered with a metal sheet.

TABLE XXV

Sparking distance cm.	*Rotary voltmeter measurement kV (peak)*	*AIEE Standard kV (peak)*	*Meador's value kV (peak)*
19·3	468	480	466
25	561	593	568
31·9	670	708	670
38·1	752	797	750
42·6	801	855	798
45	831	884	823

Table XXV shows break-down voltages for 75 cm. diameter spheres, as measured by the generating voltmeter using the extrapolation

method described above, and also as given by the AIEE Standards (No. 4) and by MEADOR[118].

VAN ATTA and his collaborators[108] have used the simple generating voltmeter system shown in *Figure 226* with a resistance load R varying from 300 Ω to 10^6 Ω. The rotor blades are shaped to give a sinusoidal output current from the voltmeter at a frequency of 120 c/s (3,600 r.p.m.). The linearity was checked with a large test sheet, to which known voltages were applied, mounted near the voltmeter. Thus the h.t. voltage V of a conductor is given by $V = k_2\ I/R$, where I is the output current from the amplifier. If the voltmeter is exposed also to other charged surfaces (*e.g.* insulating columns) the latter may cause an output current $\pm I_o$ so that $V = k_2\ (I \pm I_o)/R$. Van Atta *et al.*[108] show how k_2 varies with the terminal voltage for two arbitrary positions of their Round Hill voltmeter (*Figure 227*). They have also investigated

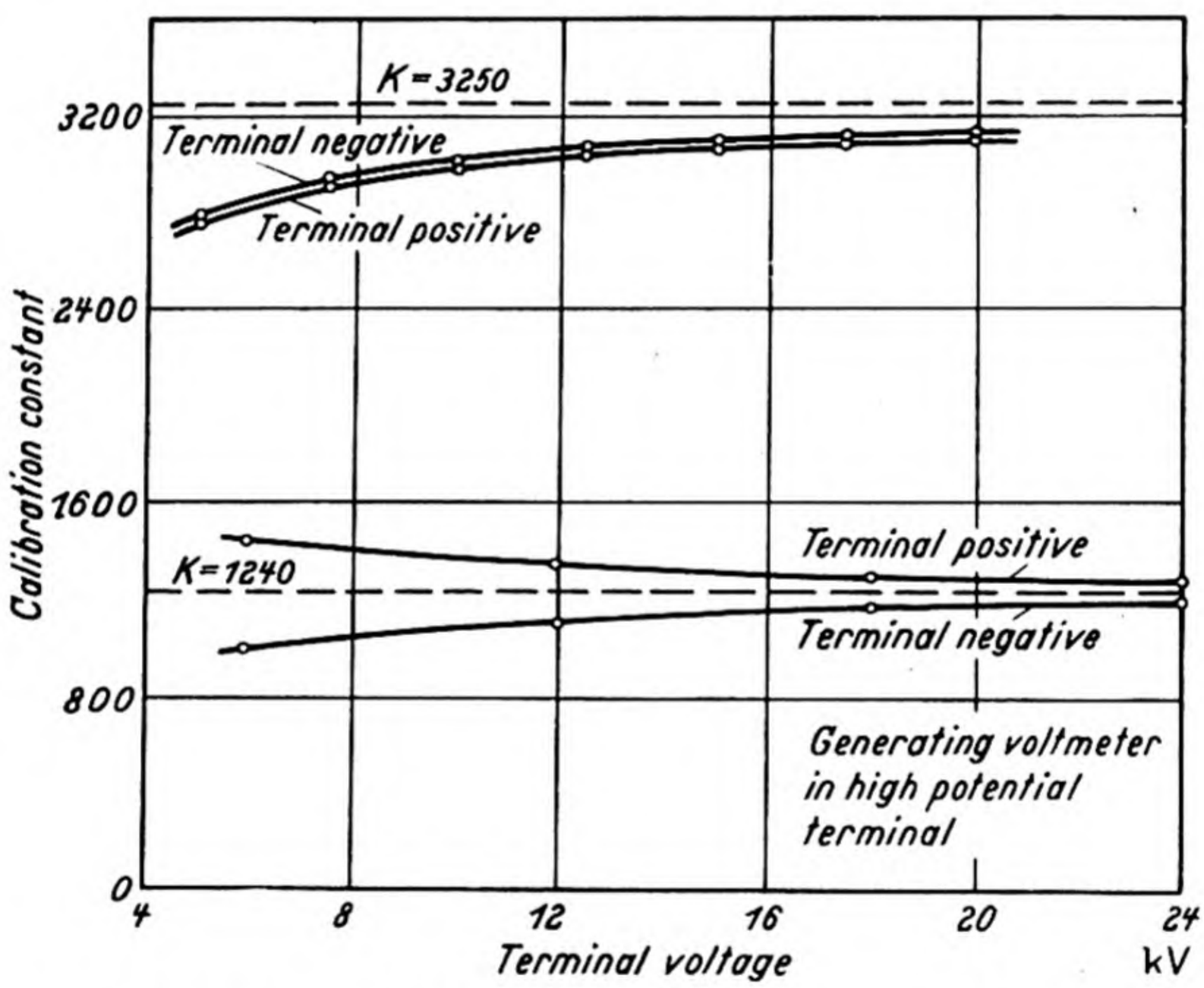

Figure 227. Uncorrected calibration curves for the Round Hill generating voltmeter, obtained with low calibrating voltages (Van Atta *et al*[108], by courtesy, *Phys. Rev.*).

the space charge effects caused by corona discharges and show that, in general, insulator-charging effects would probably be more serious. The effect of space charges may sometimes be detectable in a nearly symmetrical electrode system, such as two spheres mounted some distance from ground, by changing the voltmeter from one electrode to the other, since the sign of the space charge will be different for each electrode. In systems where the field is widely different at the two electrodes it may not always be easy to detect the effect in the above way since the space charge density may be much greater at one electrode than at the other.

The generating voltmeter used by PARKINSON *et al.*[109] in their pressure-tank Van de Graaff generator is shown in *Figures 228* and *229*. The former shows the mechanical details of the voltmeter and the method of mounting it, flush with the inner wall of the

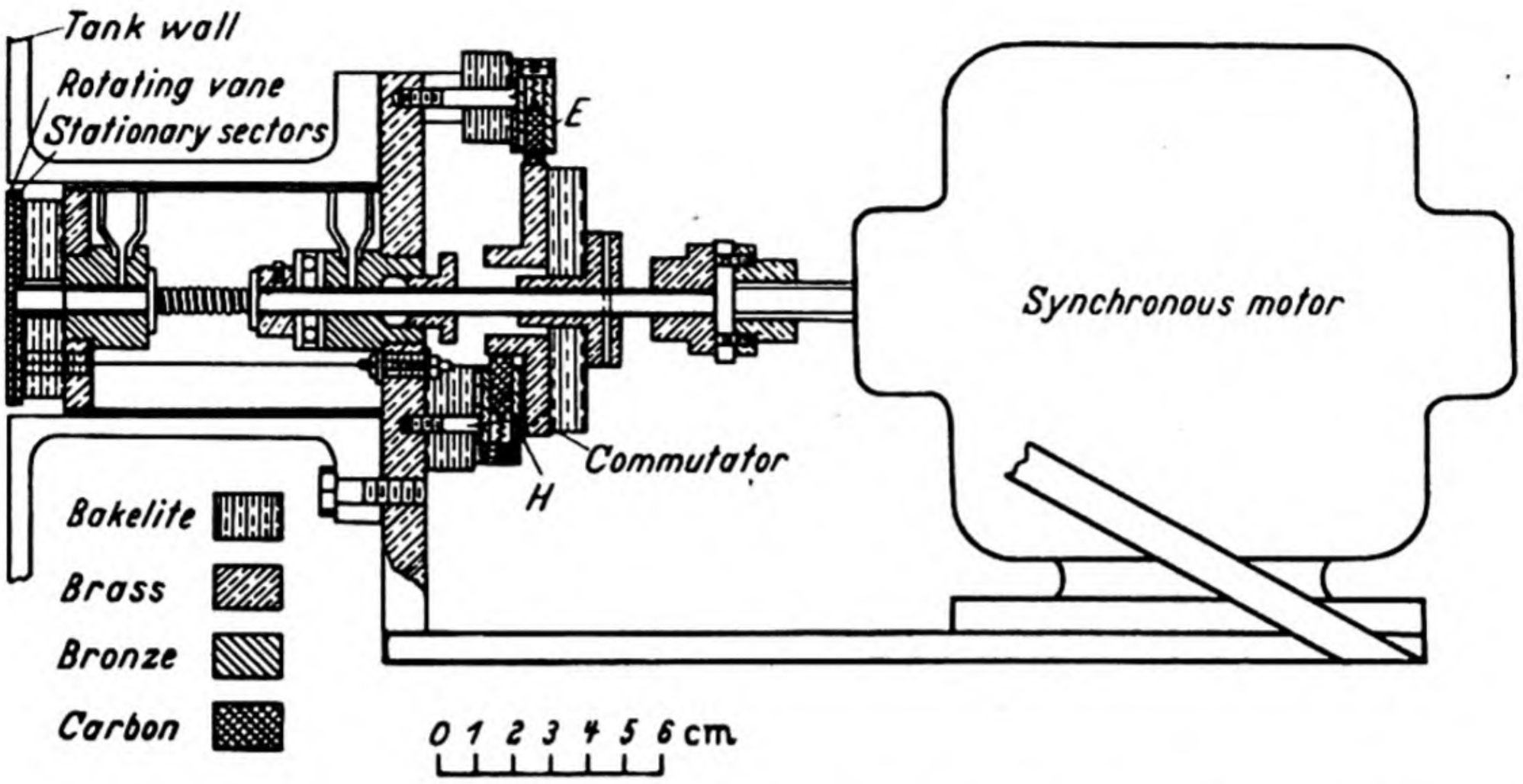

Figure 228. Cross-sectional view of a generating voltmeter (Parkinson *et al* [109], by courtesy, *Phys. Rev.*).

pressure tank, and facing the h.t. electrode, and the latter shows the electrical connections. The rotating vane is grounded, and as it revolves, a.c. is fed to the commutator and so to the galvanometer, whose sensitivity was $2{\cdot}99 \times 10^{-9}$ A/mm. The above authors found it important to avoid short-circuiting of the galvanometer circuit by any

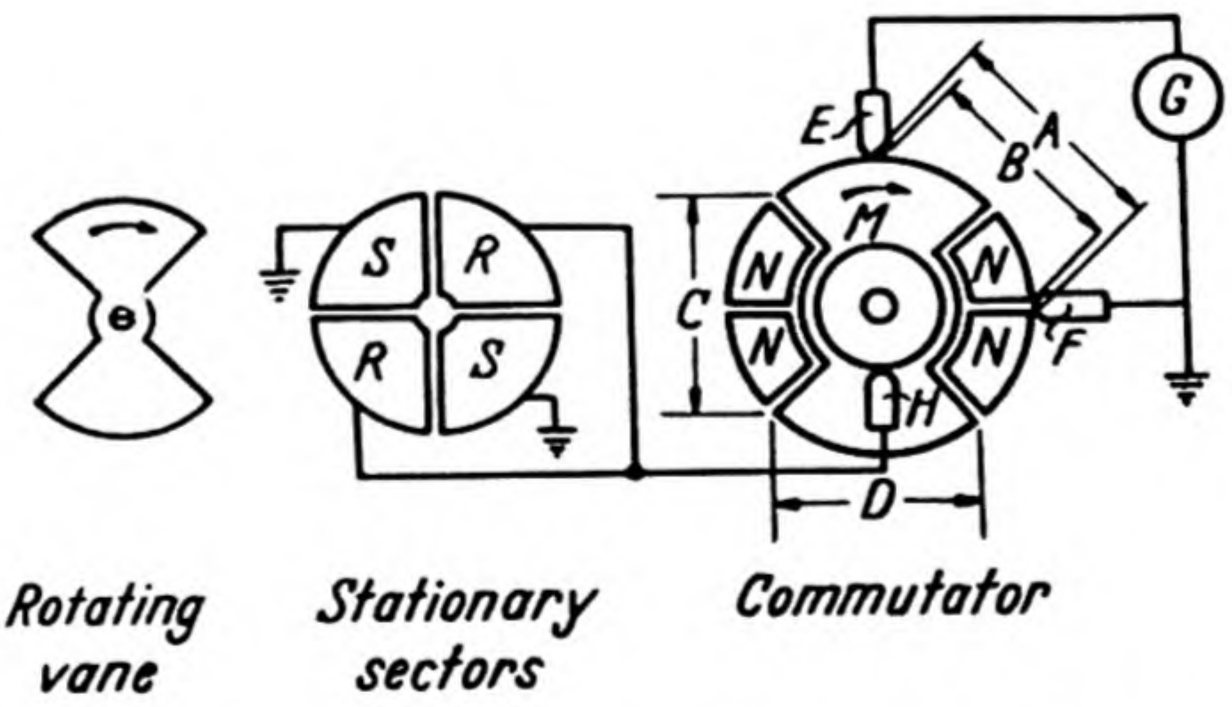

Figure 229. Schematic diagram of voltmeter circuit (*see Figure 228*) (Parkinson *et al*[109], by courtesy, *Phys. Rev.*).

part of the commutator since the thermal e.m.f.'s so generated gave a current which also passed through the galvanometer. Thus, in *Figure 229*, the sectors M and N for a given arrangement of the brushes E and F must be such that $B > D$ and $C > A$. The voltmeter

was calibrated with X-ray resonances, particularly with that (due to *Li,p*) occurring at about 440 kV (*see* pages 253–260).

TRUMP, SAFFORD and VAN DE GRAAFF[110] describe a slightly different form of generating voltmeter, developed for use with pressure tank

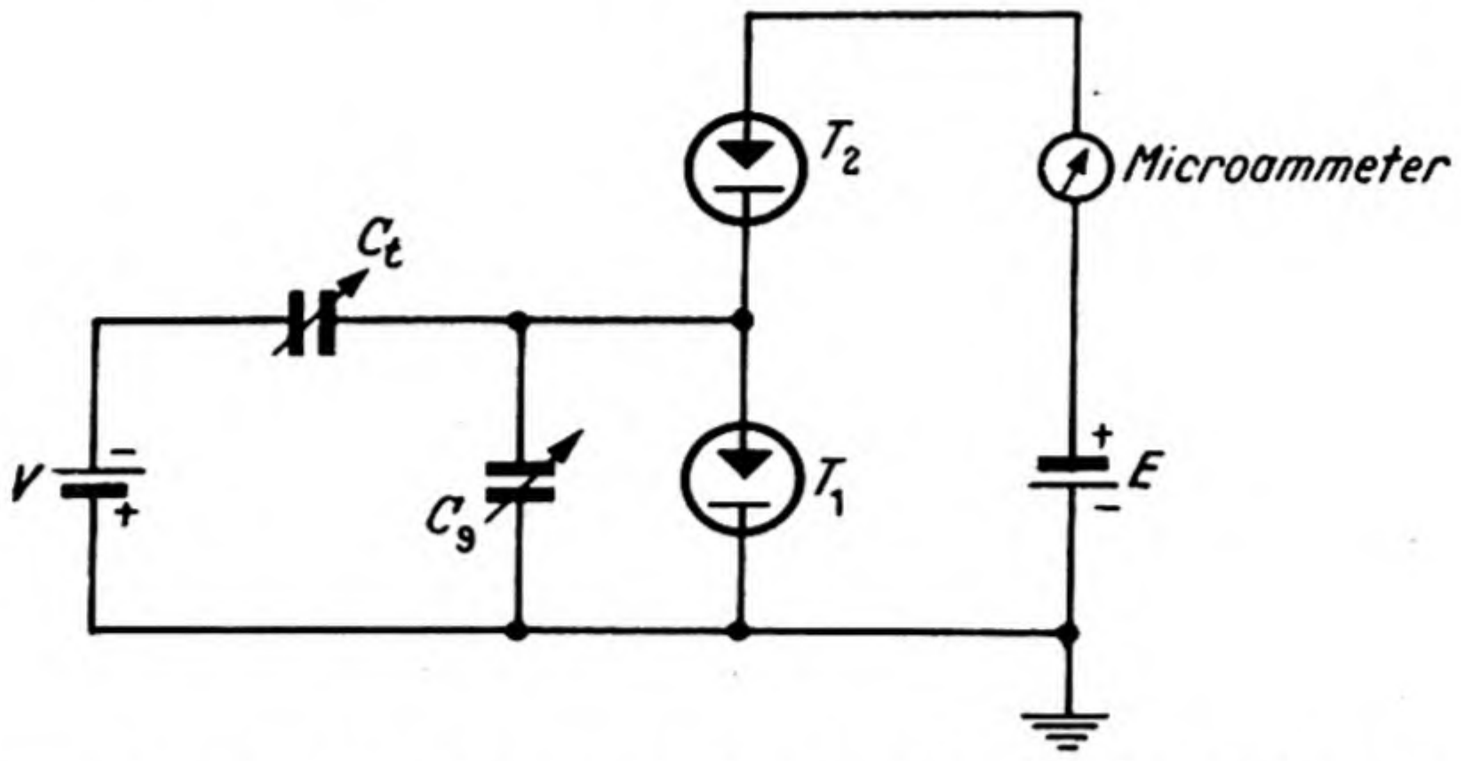

Figure 230. Simplified circuit of a generating voltmeter (Trump *et al*[110], by courtesy, *Rev. Sci. Instrum.*).

Van de Graaff generators, in which neither amplifier nor mechanical commutator is used. The circuit, shown in *Figure 230* comprises mainly a simple valve-rectifier system in which V represents the potential to be measured, C_t is the periodically-varying capacitance between the h.t. terminal and the stator of the generating voltmeter. The maximum value of C_t is C_v. C_g is the capacitance between stator and ground and has fixed and varying components; C_s is the value of C_g when $C_t = C_v$. f is the effective frequency of variation of C_t, and I/f should be long compared with the time constant of the measuring circuit. E in *Figure 230* is the biasing voltage applied to the rectifiers and prevents current flow in the non-conducting part of the cycle.

As C_t increases from its minimum value, the stator charges through T_1 until $C_t = C_v$ after which, as C_t decreases, the stator discharges

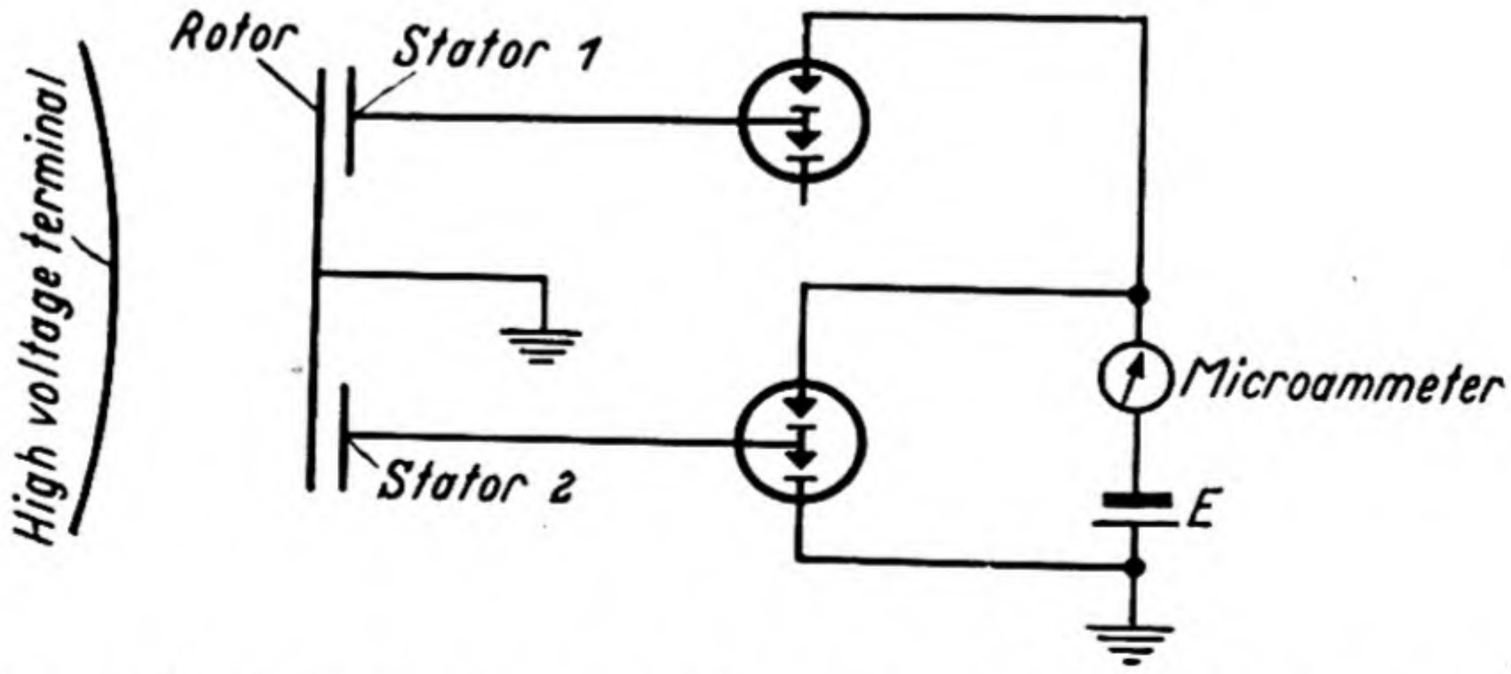

Figure 231. Circuit for generating voltmeter having two stators (Trump *et al*[110], by courtesy, *Rev. Sci. Instrum.*).

through T_2 and the microammeter until C_t reaches its minimum value. The current in the meter, neglecting voltage drop in the

rectifiers, is $I = f(C_v V - C_s E)$. Thus, for linearity, C_s should be as small as possible. The use of two stators, as in *Figure 231*, doubles the output current and also gives a substantially constant rectified current in the microammeter circuit.

ELECTRONIC VOLTMETERS

The use of the generating voltmeter with pressure-tank Van de Graaff generators (*see* Chapter 1) does not enable the voltage on any but the outermost h.t. electrode to be measured. The measurement of the total h.t. voltage, *i.e.* that on the innermost electrode (*see Figure 53*) must therefore be carried out by some indirect means and

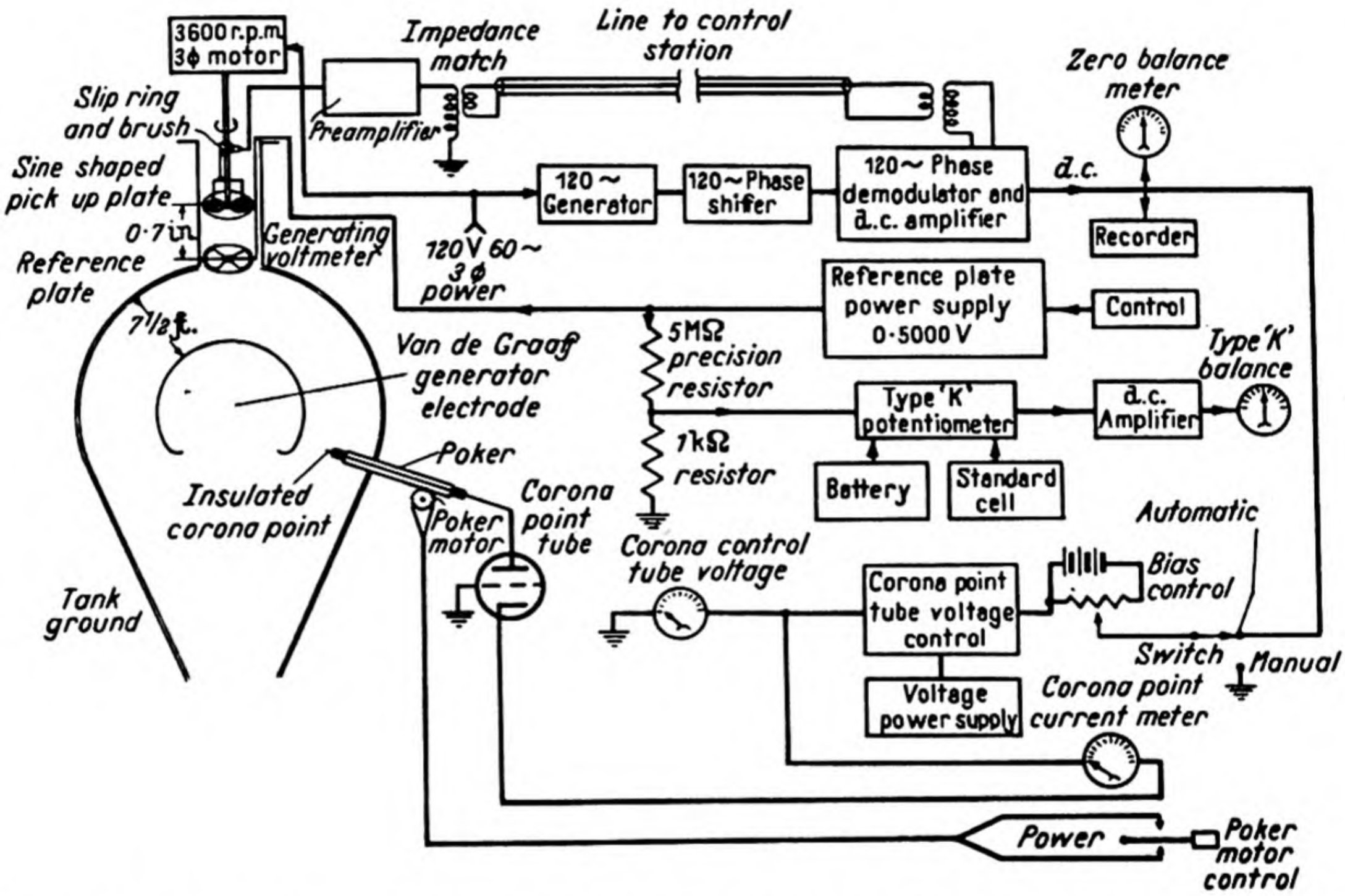

Figure 232. Westinghouse Van de Graaff generator ; generating voltmeter comparison and control circuits (Jennings[136], by courtesy, *Proc. Inst. Rad. Engrs.*).

the method of determining the voltage by accelerating a beam of charged particles through it and then deflecting the beam in a known subsidiary field has been described by HANSON[119], HANSON and BENEDICT[120] and others (*see* Chapter 2). Generating voltmeters are, however, often used (*see* also Chapter 2) for the stabilization of Van de Graaff generator output voltages using a scheme similar to that shown in *Figure 232*.

Various authors have described the use of electronic voltmeters in which the deflection by means of the unknown voltage, of a beam of electrons of known energy is measured. Thus MESSNER[121] has developed what is essentially the system of a continuous-evacuated high-voltage cathode-ray oscillograph, for the measurement of voltages ~ 100 kV.

No potential divider is used; the deflector plate chamber, to which the unknown voltage is applied, is shown in *Figure 233*. *Figure 234* shows the deflected beam positions for different sensitivities, obtained by varying the distance between the deflector plates. BINDER[122] has

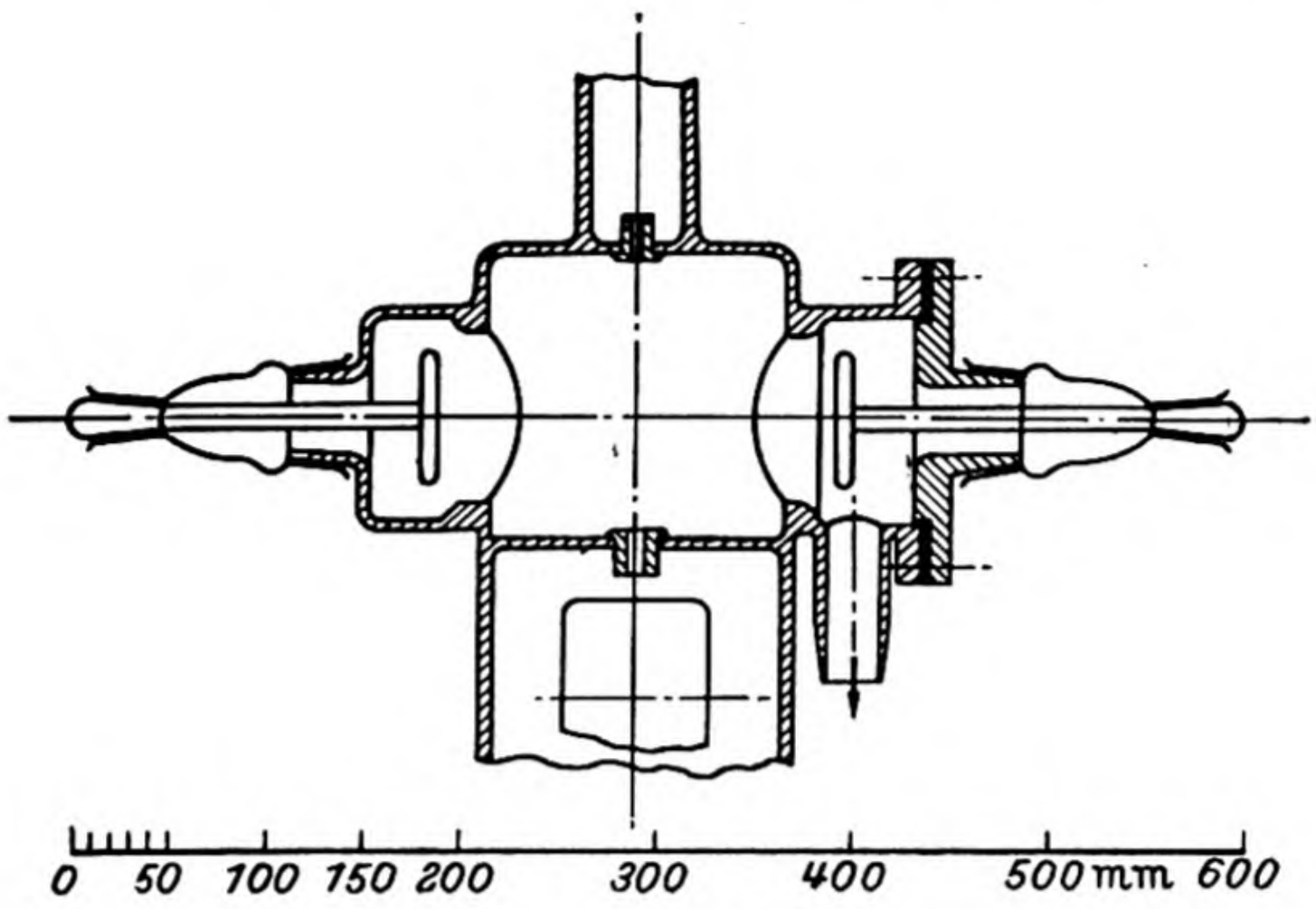

Figure 233. The deflection chamber in Messner's[121], high-voltage cathode-ray oscillograph (by courtesy, *Arch. Elektrotech.*).

described another oscillograph system, for deflector voltages varying up to 200 kV. The accuracy of the continuously evacuated, high-voltage, oscillograph when used specifically for voltage measurement has been studied by VIEHMANN[123], and other references to the

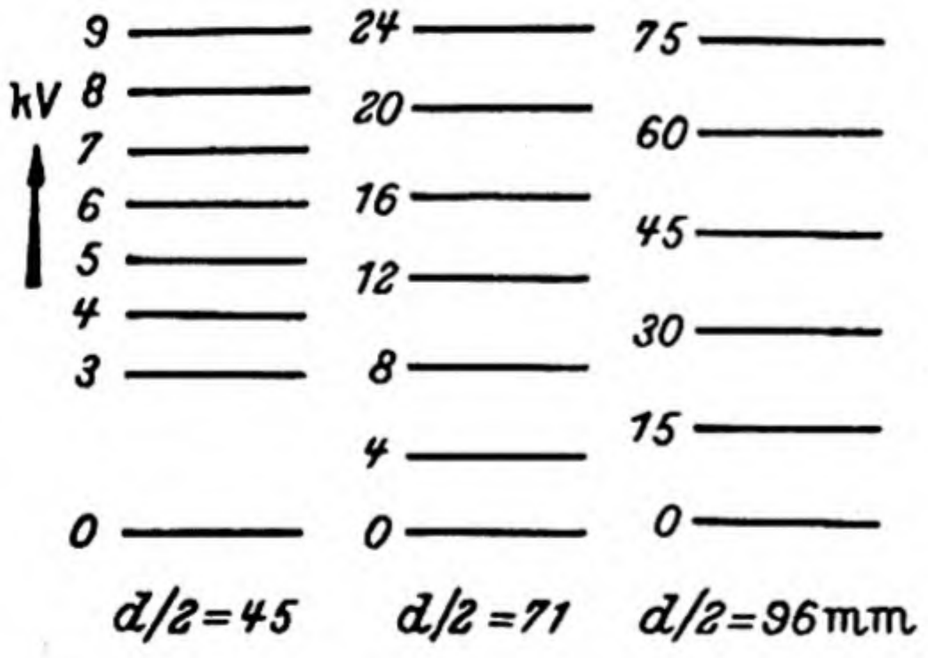

Figure 234. Calibrations of the oscillograph of *Figure 233* (by courtesy, *Arch. Elektrotech.*).

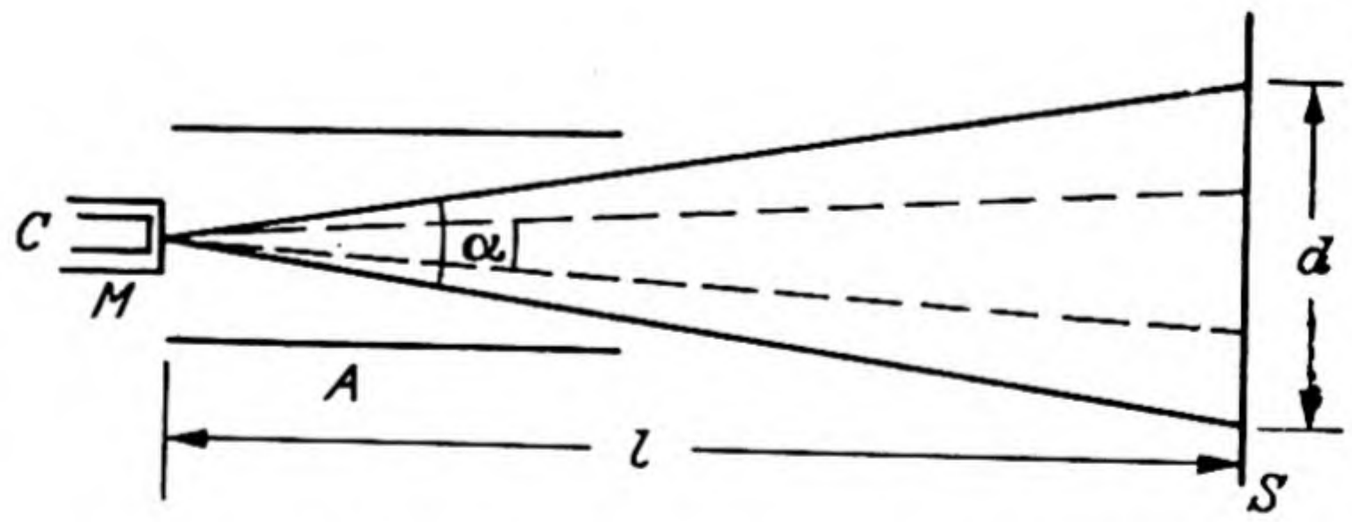

Figure 235. The electrode arrangement in Jacob's[124] electronic voltmeter (by courtesy, *J. Inst. elect. Engrs.*).

use of cathode-ray oscillographs for voltage measurement are given in Chapters 9 and 10.

JACOB's[124] electron-optical voltmeter has been used for the measurement of peak voltages between 2 and 20 kV, for d.c. or a.c., and operates in a manner different from that of the beam deflector voltmeters. The electrode system of the voltmeter is shown schematically

in *Figure 235*, and is used essentially as follows. For a fixed (high) voltage on the accelerator electrode *A*, the angular spread of the electron beam from the cathode, *C*, is set by the voltage on the modulator electrode, *M*; the beam spread decreases with an increasingly

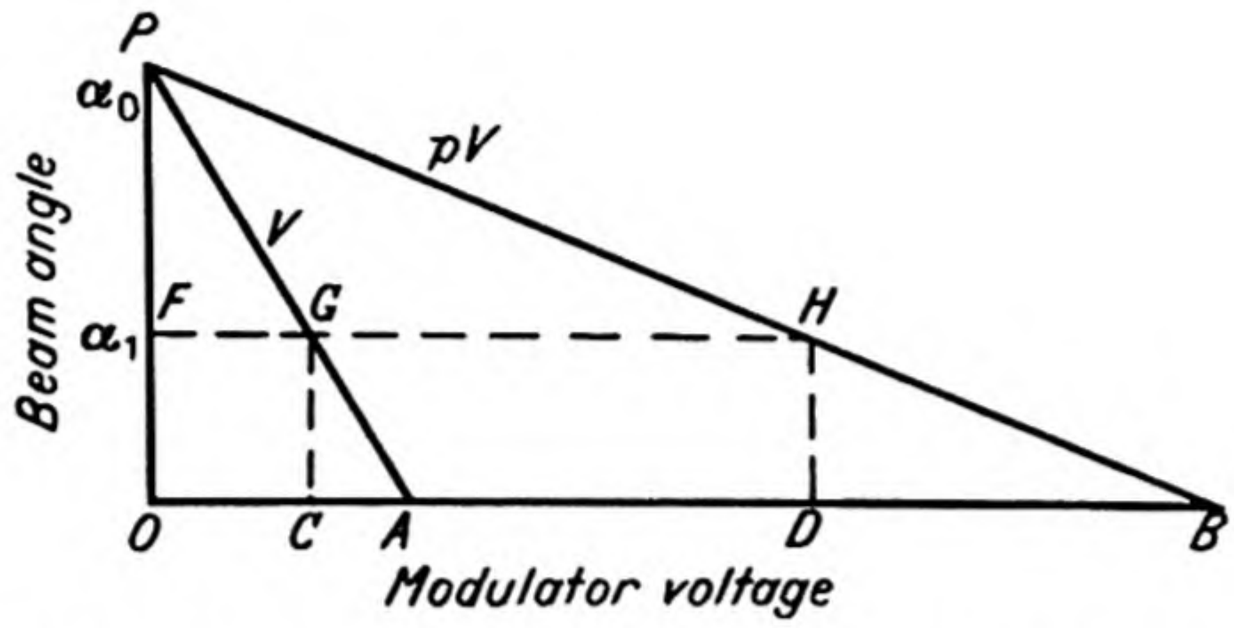

Figure 236. Illustrative of the calibration of the electronic voltmeter of *Figures 235* and *237* (Jacob[124], by courtesy, *J. Inst. elect. Engrs.*).

negative voltage on *M* and, with a sufficiently high negative voltage, can be cut-off at a sharply defined voltage which is a function of the anode voltage, as shown in *Figure 236* for anode voltages *V* and pV. Theory predicts the linear relation shown, as Jacob describes in his paper, so that $OB = pOA$ and calibration with a known value of *V* is possible. The point of disappearance of the electron beam on a suitable fluorescent screen, placed at *S* (*Figure 237*), can be judged accurately by eye or with a Faraday cylinder.

The second method of using this apparatus is to work at a constant, finite, beam angle and to obtain this at different values of anode voltage by adjusting the modulator voltage. Thus measurement of the

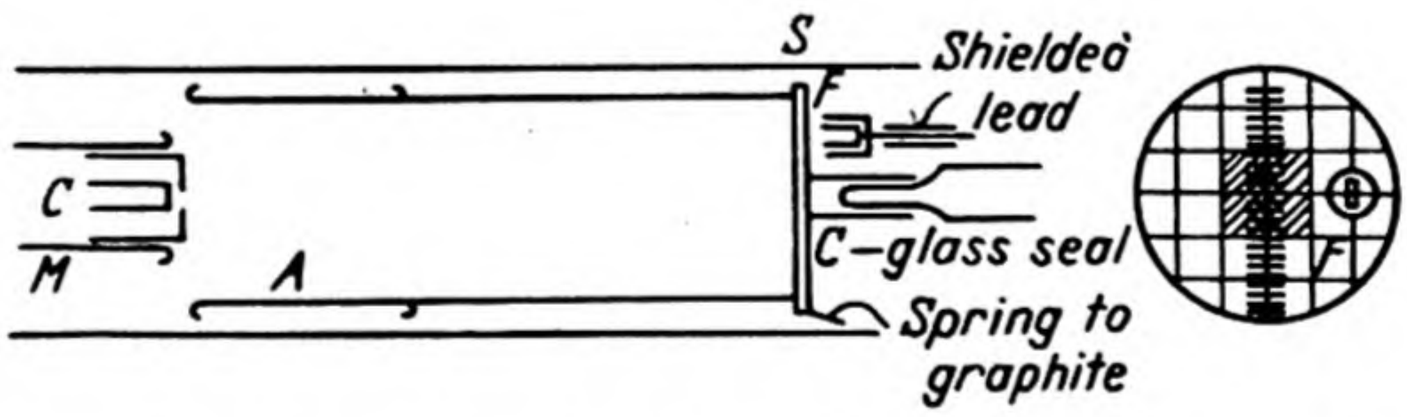

Figure 237. Experimental electronic voltmeter (Jacob[124], by courtesy, *J. Inst. elect. Engrs.*).

intercept voltage *DB* (*Figure 236*) which equals pCA enables p to be found. The apparatus in detail is shown in *Figure 237*. The modulator hole is 1 mm. in diameter and the anode cylinder is 60 mm. long with a diameter of 37 mm., screened inside a gauze cylinder *S*. The screen, shown in detail in the separate diagram of *Figure 237*, has engraved lines and a mm.-scale which are filled with fluorescent powder and viewed through a side window. *F* is a Faraday cylinder.

The errors of measurement are estimated at about ±3 per cent. Jacob also suggests that since the input capacitance of the voltmeter is 8·8 cm., it should be capable of use at frequencies varying up to perhaps 1 Mc/s or even more.

Another form of electronic voltmeter, working with voltages up to 50 kV, has been described by EHRENBERG and HIRSCH[125]. In this instrument an electron-optical image of a fine wire, placed in appropriate fashion across an electron beam, is thrown on to a fluorescent screen and the movement of this image along a scale is used to measure voltages.

FIXING A VOLTAGE SCALE BY NUCLEAR REACTIONS

The fact that certain nuclear reactions, involving transitions between different sharply defined energy levels in nuclei, have very sharply defined threshold energies for thick targets, and sharp resonance peaks for thin targets, has led to their use in setting voltage scales

TABLE XXVI

Nuclear Reaction	*Critical Voltage keV*	*Half width keV*
$Li^7(p,\gamma)Be^8$	441*	11—14
$Be^9(p,\gamma)B^{10}$	998±4	94
———	1087±2	4
$B^{11}(p,\gamma)C^{12}$	163	4·5±1·5
———	162	5·3±1
$C^{12}(p,\gamma)N^{13}$	456±2	35
———	1697±12	74±9
$C^{13}(p,\gamma)N^{14}$	554±2	40
$N^{14}(p,\gamma)O^{15}$	277±3	—
$F^{19}(p,\gamma)Ne^{20}$	340*	1·7
———	873*	5·2
———	935	80
———	1176	~130
———	1380	15

for h.t. nuclear physics. It seems, so far, that this technique has not been used to check d.c. voltage calibrations of large sphere gaps referred to on page 229. Examples of these nuclear reactions have already been given in illustration of the stability obtainable with Van de Graaff generators (Chapter 2). They can be observed by bombarding suitable targets and arranging to detect, for example with a Geiger or scintillation counter, the nuclear particles emitted at resonance. Thus, WILLIAMS *et al.*[126] use the γ-ray resonances obtained by bombardment of various light elements with protons. The reaction with fluorine (a target of CaF_2 *etc.*) occurs at 0·862 MeV,

or with molecular hydrogen ions at 1·724 MeV, since the binding energy of the molecules is negligible here and each molecule on striking the target breaks up into 2 atoms each with half the energy of the incident molecular ion. A list of some other resonances of this type is given in *Table XXVI*, where reactions marked * are particularly efficient. These data are taken from the review paper by HORNYAK *et al.*[127] who also give many references.

WILLIAMS *et al.*[126] have also used the threshold for neutron production in Be under proton bombardment as a standard voltage point, taken as 2·03 MeV.

The careful work of BENNETT *et al.*[128] on the $F(p,\gamma)$ reactions has shown resonances (γ ray or pair) at several accurately determined voltages listed in *Table XXVII*.

TABLE XXVII

DATA CONCERNING RESONANCES IN THE EMISSION OF GAMMA-RAYS AND PAIRS

Type of resonance (γ-ray or pair)	*Proton energy at resonance keV.*	*Half-width keV.*	*Relative peak intensity*	*Relative intensity* (peak × width)*
γ	820	7·6	0·8	6·1
π	832	28·	0·08	2·2
γ	862	5·2	29·	150·
γ	890	4·8	1·0	4·8
γ	927	8·0	10·	80·
γ	1076	< 1·9	0·5	1·0
π	1100	≈ 70·	0·06	≈ 4·
γ	1107	≈ 30·	0·8	≈ 24·
γ	1122	4·1	0·9	3·7
γ	1161	≈ 50·	0·8	≈ 40·
π	1220	85·	0·2	17·
γ	1274	19·	2·2	42·
γ	1335	4·8	9·0	43·
π	1362	36·	0·6	22·
γ	1363	15·	22·	330·

* The relative intensities of pair as compared to γ resonances may be in error by as much as a factor of two or more, because of the unknown angular distribution of the pairs and because of errors in the relative efficiencies of counting pairs and gamma-rays.

The successful use of nuclear reactions, *i.e.* their thresholds and resonances, for fixing a voltage scale is due to the efforts of many workers. HAFSTAD, HEYDENBURG and TUVE's[129] determination against a resistance voltmeter standard (*see* page 376) of the *Li* (p,γ) resonance of 440 keV is one of the earliest precision measurements and it is considered correct to within 1 per cent. by comparison with the $C(p,n)$

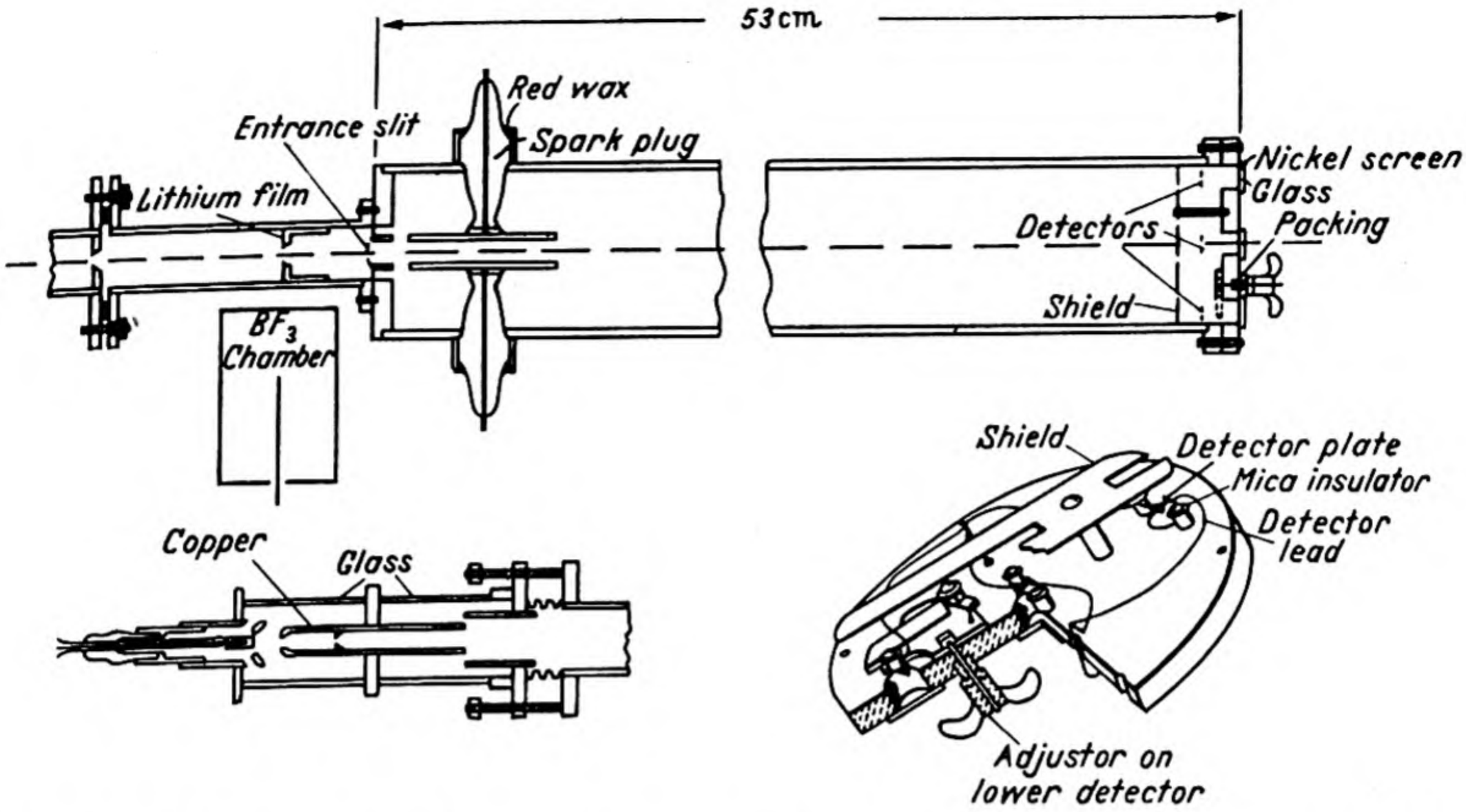

Figure 238. Electrostatic deflector (Hanson and Benedict[120], by courtesy, *Phys. Rev.*).

threshold studied by HAXBY *et al.*[111]. The later work of Hanson and Benedict[120] is more accurate; in this experiment the energy of a proton beam used to give the various nuclear thresholds or resonances (detailed below) is measured at the same time with an electrostatic deflecting system. The latter is calibrated with an electron beam and a further check is obtained by measurements of the geometry

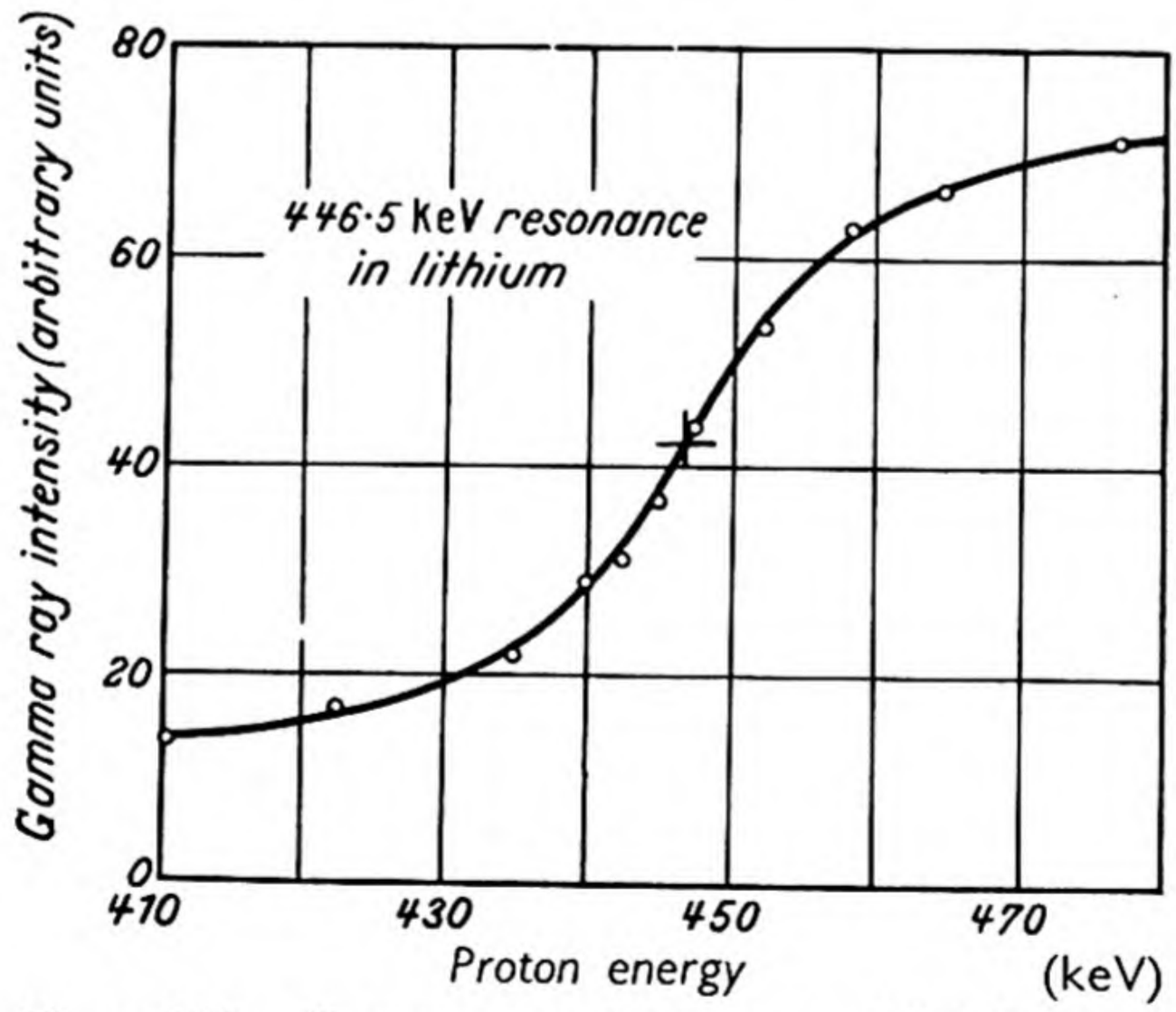

Figure 239. Gamma-ray yield from a thick lithium target using a diatomic beam (H_2^+ ions) (Hanson and Benedict[120], by courtesy, *Phys. Rev.*).

of the deflecting system. The electron beam, for calibration, had an energy in the range 8–20 kV and the requisite deflector voltage varied from about 150 to 360 V. These voltages were measured with normal

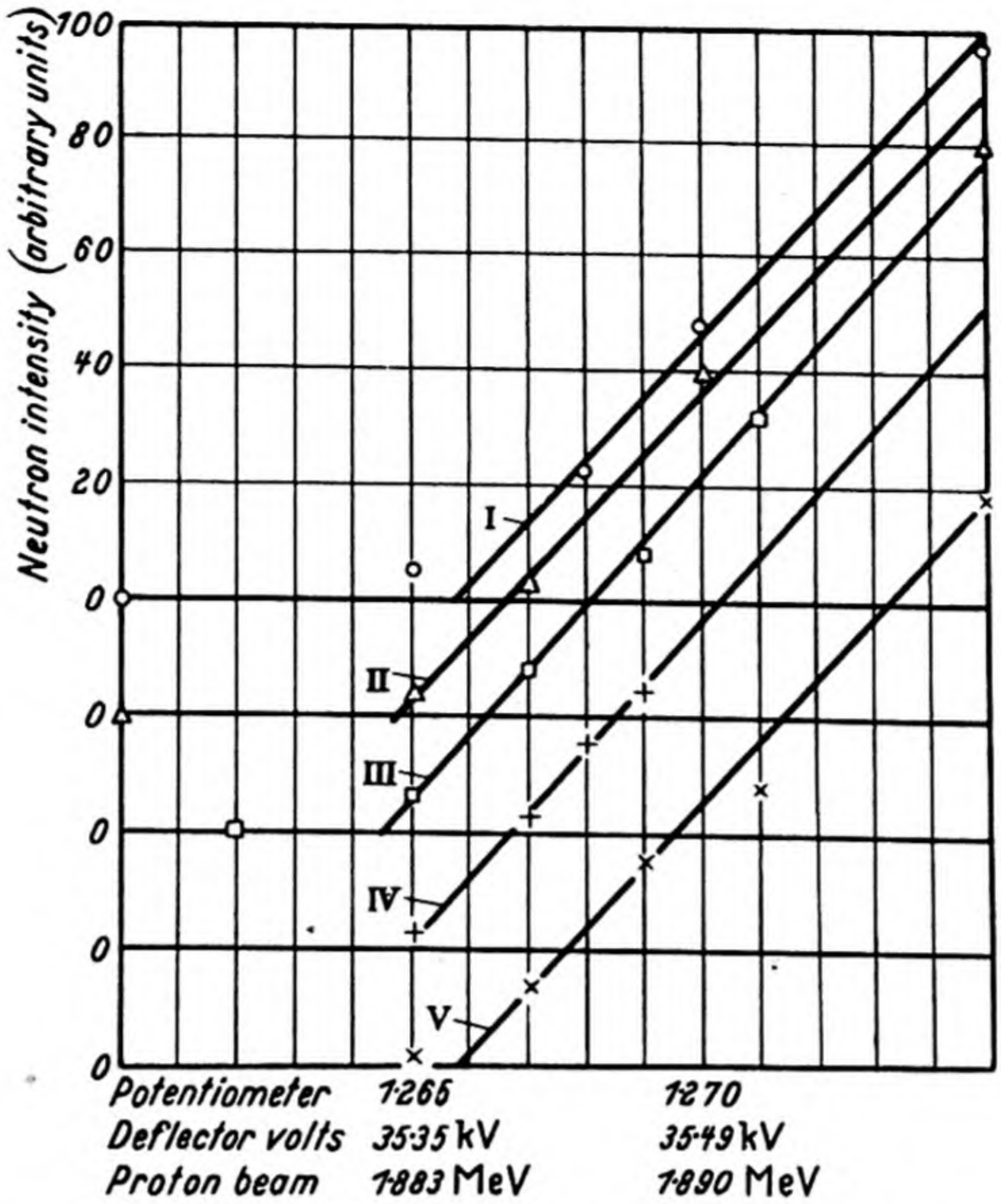

Figure 240. Neutrons from the Li(p, n) reaction. Different experimental runs are shown (Hanson and Benedict[120], by courtesy, *Phys. Rev.*).

techniques to about 0·2 per cent. accuracy. The deflector, as set up for the *Li* (p, n) experiments, was as shown in *Figure 238* using a BF_3 ionization chamber for detection of the neutrons.

TABLE XXVIII

Reaction	*Previous values based on the 440 keV Li resonance (MeV)*	*Values found by Hanson and Benedict[120] (MeV)*	*References to previous work*
Li (p, n)	1·856	1·883	[111]
Be (p, n)	2·028	2·058	[111]
F (p, γ)	0·862	0·877	[130]
—	0·867	—	[129]
Li (p, γ)	0·440	0·4465	[129]

Some results for the *Li* (p, n) threshold and for the thick target production of γ rays from *Li* (p, γ) and *F* (p, γ) are shown in *Figures 239, 240* and *241* respectively. The final values for the standard voltages were considered correct to within 0·3 per cent. (absolute) and 0·1 per cent. (relative) and are given in *Table XXVIII.*

It is therefore possible to determine a voltage scale absolutely by observations of the onset of nuclear reactions whose thresholds can be

calculated from a knowledge of mass defects. For example the photo-disintegration reactions of deuterium and beryllium have thresholds respectively of $2{\cdot}183 \pm 0{\cdot}012$ MeV and $1{\cdot}62 \pm 0{\cdot}010$ MeV (MYERS and VAN ATTA[131]) and the X-rays required could be produced by electron beams whose energies could thus be accurately measured at the above voltages. Further work is described by WIEDENBECK and MARHOEFER[132] and by COLLINS, WALDMAN and GUTH[133], the latter working also on the disintegrations produced in beryllium by electrons.

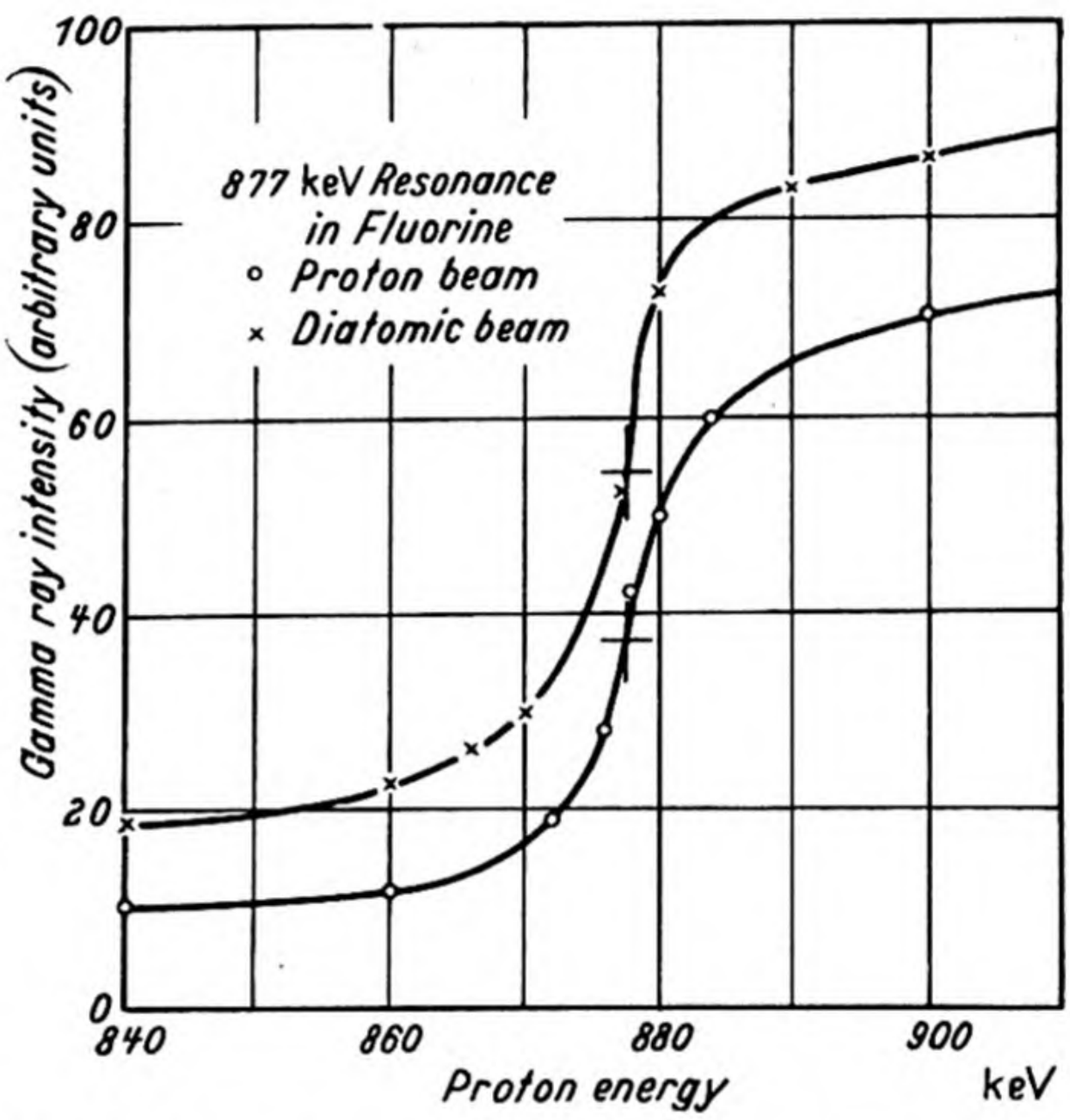

Figure 241. Gamma-ray yield from a thick target of potassium fluoride (Hanson and Benedict[129], by courtesy, *Phys. Rev.*).

The setting of a voltage scale by nuclear thresholds (critical potentials of nuclear reactions) thus often necessitates the reference to a standard deflecting field, such as that provided in an electrostatic analyser of the type described above (pages 255–256) although it is sometimes possible to calculate thresholds from purely nuclear constants. Further examples of precise work with electrostatic analysers are due to HERB, SNOWDON and SALA[134] and to WARREN, POWELL and HERB[135]. JENNINGS[136] summarizes this and other work in a comprehensive review of Van de Graaff generator electronic techniques. The electrostatic analyser technique can also, clearly, be used to provide the basis of a method of stabilizing the output voltage of such a generator. This method is discussed in pages 81–82 and is shown schematically in *Figure 242*[136].

Beam voltages may also be measured absolutely by the u.h.f. cavity method used by ALTAR *et al.*[137, 138]; see also the work of SHOUPP, JENNINGS and JONES[139], and the review by Jennings[136] from which this

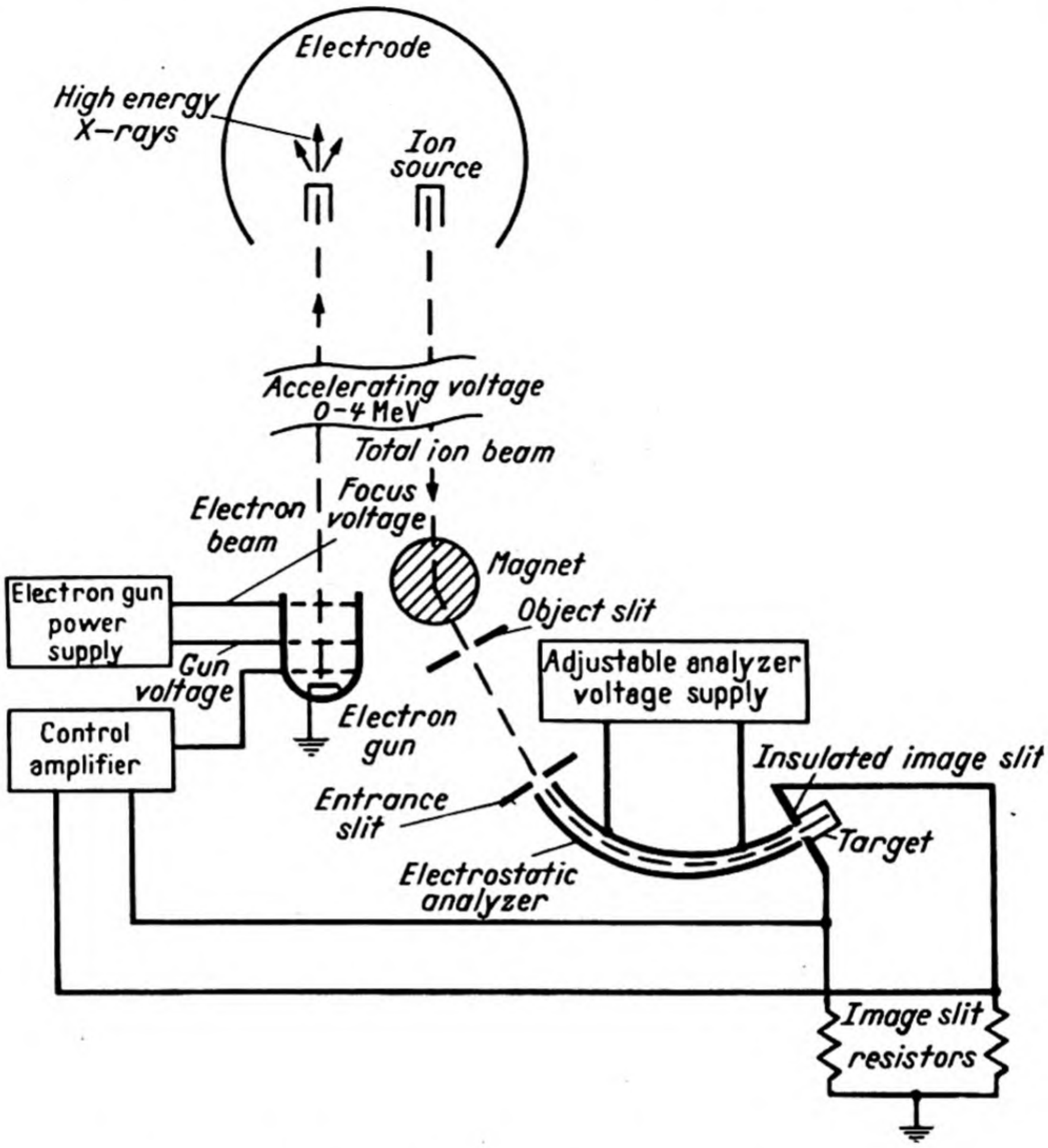

Figure 242. An electron beam voltage control using electrostatic analyser (Jennings[136], by courtesy, *Proc. Inst. Rad. Engrs.*).

account is largely drawn. In this method the kinetic energy of a particle is measured in terms of its known mass and charge, a length and a frequency. The generator ion beam is intensity-modulated at the source by means of a 70 Mc/s crystal-controlled oscillator and the resulting beam after acceleration passes through a momentum analyser. The beam of ions of required mass then passes through the cavity shown in *Figure 243*, which is tuned to resonate at the beam modulation frequency. The cavity has a high Q, so the two gaps in it are tightly coupled and the sum or difference of the voltages across them (measured by a suitable instrument) depends on the phase difference of the 70 Mc/s modulation cycle between the two gaps. There will be a minimum resultant signal when the transit angle $\Delta\theta = n\pi (n \text{ odd})$ Whence $\Delta\theta = n\pi = 2\pi f \Delta t$

$$\Delta t = n/2f = L/v$$

where Δt is the transit time of a group of particles of velocity v for the distance L between the cavity gaps, and f is the modulation

frequency. The ion velocity is $v = 2fL/n$ and the voltage V of a beam of particles of velocity v and mass/charge ratio M_o/e is

$$V = 2M_o f^2 L^2/en^2$$

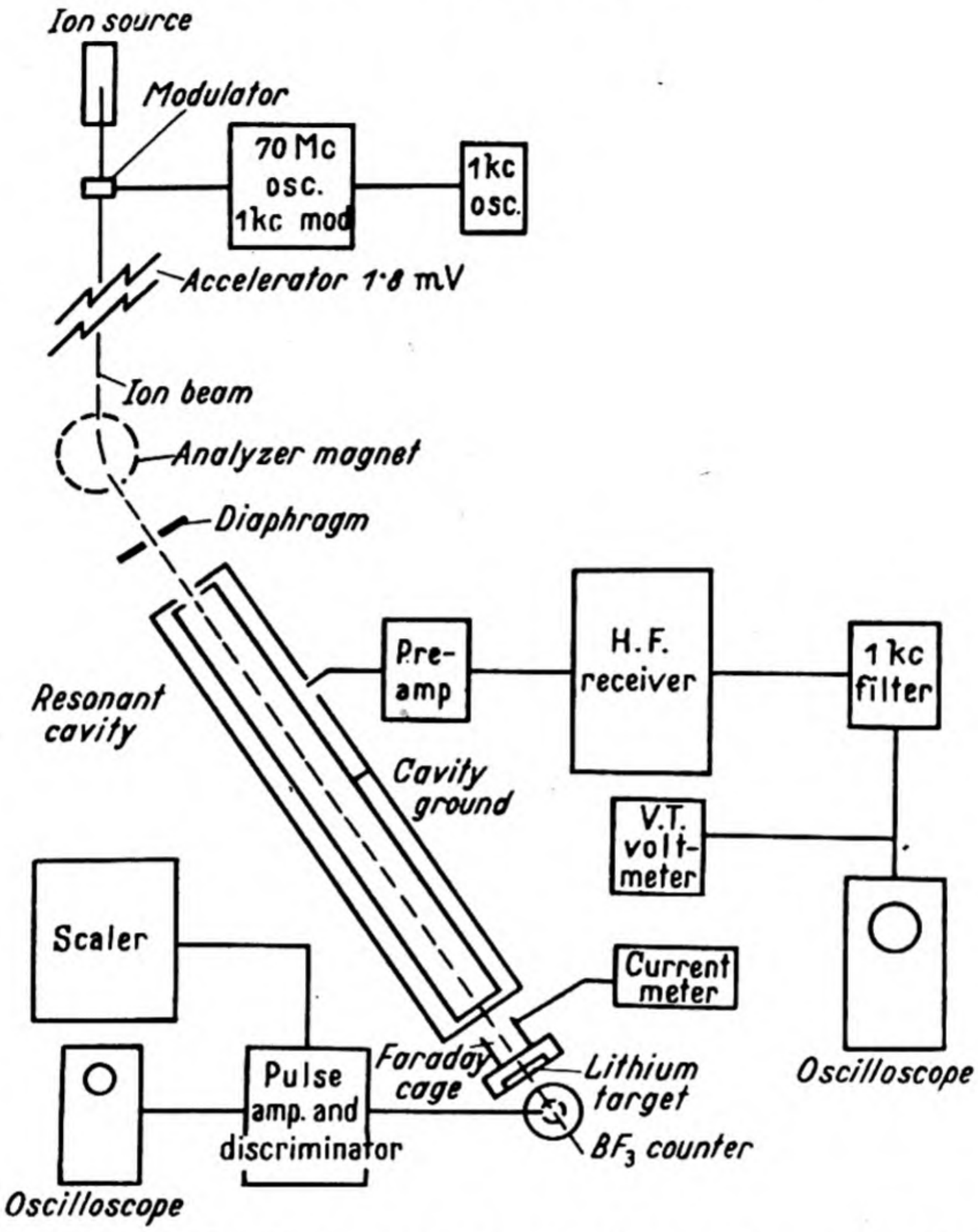

Figure 243. Radio-frequency ion speed gauge assembly. The magnetic analyser permits rapid switching from the proton beam used for threshold measurement to the mass 2 beam used for the speed measurement, the mechanical geometry remaining fixed (Jennings[136], by courtesy, *Proc. Inst. Rad. Engrs.*).

Insertion of the necessary relativity correction gives

$$V = 2M_o f^2 L^2/en^2 \cdot \left(1 + \frac{3f^2L^2}{n^2C^2}\right)$$

where $C =$ velocity of light. For fixed f and L, several voltage minima corresponding to different values of n may be found along the nuclear voltage scale to an accuracy of about 0·1 per cent. A measurement of the $Li\ (p,n)$ threshold made in this way gave $1{\cdot}8812 \pm 0{\cdot}002$ MeV, to be compared with the value $1{\cdot}8820 \pm 0{\cdot}0002$ MeV obtained with an electrostatic analyser.

Some of the most recent and exact data on nuclear resonances at lower voltages, *i.e.* at less than 500 kV, are due to Hunt[140]. A selection of his results are shown in *Table XXIX*. An absolute electrostatic analyser was used, of the general form adopted by various workers[119, 120].

TABLE XXIX

Reaction	*Resonance Energy keV*	*Reaction*	*Resonance Energy keV*
$Li^7(p,\gamma)Be^{8*}$	$441{\cdot}5 \pm 0{\cdot}5$	$Mg^{26}(p,\gamma)Al^{27*}$	$314{\cdot}2 \pm 0{\cdot}6$
$F^{19}(p,\gamma)Ne^{20*}$	$340{\cdot}4 \pm 0{\cdot}4$		$338{\cdot}5 \pm 0{\cdot}4$
$F^{19}(p,\gamma)Ne^{20*}$	$483{\cdot}1 \pm 0{\cdot}5$		$389{\cdot}4 \pm 0{\cdot}5$
$F^{19}(p,\gamma)Ne^{20*}$	$224{\cdot}4 \pm 0{\cdot}4$		$436{\cdot}5 \pm 0{\cdot}5$
$B^{11}(p,\gamma)C^{12}$	$163{\cdot}8 \pm 0{\cdot}2$		$454{\cdot}2 \pm 0{\cdot}5$
$C^{12}(p,\gamma)N^{13}$	$456{\cdot}5 \pm 1{\cdot}0$		$483{\cdot}7 \pm 0{\cdot}5$
$Be^9(p,\gamma)B^{10}$	336 ± 3	$Mg^{24}(p,\gamma)Al^{25}$	$417{\cdot}3 \pm 0{\cdot}5$
—	492 ± 3	$Al^{27}(p,\gamma)Si^{28}$	$226{\cdot}3 \pm 1{\cdot}5$
			$294{\cdot}1 \pm 0{\cdot}5$
			$325{\cdot}6 \pm 0{\cdot}4$
			$404{\cdot}7 \pm 0{\cdot}4$
			$438{\cdot}5 \pm 0{\cdot}5$
			$504{\cdot}0 \pm 0{\cdot}6$

REFERENCES

1 Lord Kelvin, Papers on electrostatics and electromagnetism. London, 1884.
2 Abraham, H., and Villard, P. *J. Phys.*, **1** (1911) 525.
3 Starke, H., and Schroeder, R. *Arch. Elektrotech.*, **20** (1928) 115.
4 Starke, H., and Schroeder, R. *Arch. Elektrotech.*, **26** (1932) 239.
5 Imhof, A. *Arch. Elektrotech.*, **23** (1929) 258.
6 Nacken, M. *Arch. Elektrotech.*, **33** (1939) 60.
7 Nacken, M. *Arch. Elektrotech.*, **36** (1942) 678.
8 Winkelbrandt, H. *Arch. Elektrotech.*, **31** (1937) 672.
9 Böcker, H. *Arch. Elektrotech.*, **33** (1939) 801.
10 Böcker, H. *Elektrotech. Z.*, **61** (1940) 729.
11 Rogowski, W., and Böcker, H. *Arch. Elektrotech.*, **32** (1938) 44.
12 Palm, A. *Z. tech. Phys.*, **1** (1920) 137.
13 Palm, A. *Z. tech. Phys.*, **14** (1933) 390.
14 Meek, J. M., and Waterton, F. W. *Nature*, **156** (1945) 422.
15 Brooks, H. B., Defandorf, F. M., and Silsbee, F. B. *J. Res. Nat. Bur. Stand. Wash.*, **20** (1938) 253.
16 Silsbee, F. B., and Defandorf, F. M. *J. Res. Nat. Bur. Stand. Wash.*, **20** (1938) 317.
17 Snow, C. *J. Res. Nat. Bur. Stand. Wash.*, **1** (1928) 1513.
18 Hueter, E. *Elektrotech. Z.*, **55** (1934) 833; **56** (1935) 1319.
19 Defandorf, F. M. *J. Wash. Acad. Sci.*, **38** (1948) 33.
20 Sorenson, R. W., Hobson, J. E., and Ramo, S. *Trans. Amer. Inst. Elect. Engrs.*, **54** (1935) 651.
21 Sorenson, R. W., and Ramo, S. *Trans. Amer. Inst. Elect. Engrs.*, **55** (1936) 444.
22 Zdralik, O., *Arch. Elektrotech.*, **24** (1930) 305.
23 Steubing, W. *Phys. Z.*, **37** (1936) 32.
24 Rogowski, W. *Arch. Elektrotech.*, **25** (1931) 521.
25 Gänger, B. *Arch. Elektrotech.*, **39** (1949) 443.
26 Wingen, H. *Elektrotech. Z.*, **53** (1932) 1034.
27 Bialous, A. J., and Malpica, J. T. M. *Gen. Elect. Rev.*, **41** (1938) 446.
28 MacNeice, G. G. *J. Sci. Instrum.*, **25** (1948) 189.
29 Alfvén, H., and Eklund, S. *Rev. Sci. Instrum.*, **17** (1946) 353.

REFERENCES

30 THORNTON, W. M., and THOMPSON, W. G. *J. Inst. elect. Engrs.*, **71** (1932) 1.
31 BRUCE, F. M. *J. Inst. elect. Engrs.*, Part II, **94** (1947) 129.
32 BRADSHAW, E., HUSSAIN, S. A., KESAVAMURTHY, N., and MENON, K. B. *J. Inst. elect. Engrs.*, Part II, **95** (1948) 636.
33 THORNTON, W. M., WATERS, M., and THOMPSON, W. G. *J. Inst. elect. Engrs.*, **69** (1931) 533.
34 PALM, A. *C.I.G.R.E., Paper* No. 135 (1937).
35 DREWNOWSKI, K. *C.I.G.R.E., Paper* No. 121 (1937).
36 'Rules for the measurement of voltage with sphere gaps', *British Standard* 358 (1939).
37 'Measurements of test voltage in dielectric tests', *A.I.E.E. Standards*, No. 4 (June, 1940).
38 'Regeln fur Spannungsmessungen mit der Kugelfunkenstrecke', VDE 0430/39.
39 EDWARDS, F. S., and SMEE, J. F. *J. Inst. elect. Engrs.*, **82** (1938) 655.
40 DAVIS, R., and BOWDLER, G. W. *J. Inst. elect. Engrs.*, **82** (1938) 645.
41 HUETER, E. *Elektrotech. Z.*, **57** (1936) 621.
42 ELSNER, R. *Elektrotech. Z.*, **56** (1936) 1405.
43 WHITEHEAD, S., and CASTELLAIN, A. P. *J. Inst. elect. Engrs.*, **69** (1931) 898.
44 BELLASCHI, P. L., and MCAULEY, P. H. *Elect. J.*, **31** (1934) 228.
45 DATTAN, W. *Arch. Elektrotech.*, **31** (1937) 342.
46 DATTAN, W. *Elektrotech. Z.*, **57** (1936) 377, 412.
47 WEICKER, W. *Elektrotech. Z.*, **60** (1939) 97.
48 WEICKER, W., and HÖRCHER, W. *Elektrotech. Z.*, **59** (1938) 1029, 1064.
49 WHITEHEAD, S. *J. Inst. elect. Engrs.*, **84** (1939) 408.
50 JACOBI, W. *Z. tech. Phys.* **5** (1938) 159.
51 BINDER, L., and HORCHER, W. *Elektrotech. Z.*, **59** (1938) 161.
52 SPRAGUE, C. S., and GOLD, G. *Trans. Amer. Inst. elect. Engrs.*, **56** (1937) 594.
53 MEADOR, J. R. *Trans. Amer. Inst. elect. Engrs.*, **53** (1934) 942, 1652.
54 VER PLANCK, D. W. *Trans. Amer. Inst. elect. Engrs.*, **60** (1941) 99.
55 MCMILLAN, F. O., and STARR, E. C. *Trans. Amer. Inst. elect. Engrs.*, **49** (1930) 859.
56 MCMILLAN, F. O. *Trans. Amer. Inst. elect. Engrs.*, **58** (1939) 56.
57 MCMILLAN, F. O., and STARR, E. G. *Trans. Amer. Inst. elect. Engrs.*, **50** (1931) 23.
58 CLAUSSNITZER, J. *Elektrotech. Z.*, **57** (1936) 177.
59 NORD, G. L. *Trans. Amer. Inst. elect. Engrs.*, **54** (1935) 107.
60 BOUWERS, A., and KUNTKE, A. *Z. tech. Phys.*, **18** (1937) 209.
61 PUGNO VANONI, E., and DI PIERI, C. *Elettrotechnica*, **22** (1935) 834; **24** (1937) 390.
62 PUGNO VANONI, E., and DI PIERI, C. *Elektrotech. Z.*, **57**, (1936) 377, 412; **58** (1937) 609, 1323.
63 KLEMM, A. *Arch. Elektrotech.*, **12** (1923) 553.
64 COOPER, R., GARFITT, D. E. M., and MEEK, J. M. *J. Inst. elect. Engrs.*, Part II, **95** (1948) 309.
65 MEEK, J. M. *J. Inst. elect. Engrs.*, **93** (1946) 97.
66 FRANCK, S. *Messentladungstrecken.* Berlin, 1931.
67 FRANCK, S. *Arch. Elektrotech.*, **23** (1926) 226.
68 LEWIS, A. B. *J. appl. Phys.*, **10** (1939) 573.
69 TOEPLER, M. *Elektrotech. Z.*, **53** (1932) 1219.
70 TOEPLER, M. *Arch. Elektrotech.*, **30** (1936) 669.
71 JØRGENSEN, M. O. *Elektrische Funkenspannungen.* Copenhagen, 1943.
72 MEEK, J. M. *J. Franklin Inst.*, **230** (1940) 229.
73 LOEB, L. B., and MEEK, J. M. *The mechanism of the electric spark.* California, 1941.

[74] MEEK, J. M., and CRAGGS, J. D. *Electrical Breakdown of Gases.* London, 1953.
[75] BRUCE, F. M. *Proc. Inst. elect. Engrs.*, Part II, **94** (1947) 138.
[76] BRUCE, F. M., *Proc. Inst. elect. Engrs.*, Part II, **98** (1951) 363.
[77] STEPHENSON, J. D. *J. Inst. elect. Engrs.*, **73** (1933) 69.
[78] MEEK, J. M. *Proc. Inst. elect. Engrs.*, Part II, **98** (1951) 362.
[79] HOLZER, W. *Arch. Elektrotech.*, **26** (1932) 865.
[80] RITZ, H. *Arch. Elektrotech.*, **26** (1932) 219.
[81] ROGOWSKI, W., and RENGIER, H. *Arch. Elektrotech.*, **16** (1926) 73.
[82] STOERK, C. *Elektrotech. Z.*, **52** (1931) 43.
[83] FISHER, L. H. *Phys. Rev.*, **72** (1947) 423.
[84] ALLIBONE, T. E. *J. Inst. elect. Engrs.*, **81** (1937) 741.
[85] FIELDER, F. D. *Elect. J.*, **29** (1932) 459.
[86] FIELDER, F. D. *Elect. J.*, **32** (1935) 543.
[87] LEBACQZ, J. V. *Trans. Amer. Inst. elect. Engrs.*, **60** (1941) 44.
[88] BELLASCHI, P. L., and MCAULEY, P. H. *Trans. Amer. Inst. elect. Engrs.*, **59** (1940) 669.
[89] SCHUMANN, W. O. *Elektrische Durchbruchfeldstärke von Gasen.* Berlin, 1923.
[90] CHUBB, L. W., and FORTESCUE, C. *Trans. Amer. Inst. elect. Engrs.*, **32** (1913) 739.
[91] CHUBB, L. W. *Trans. Amer. Inst. elect. Engrs.*, **35** (1916) 121.
[92] PALM, A. *Elektrotech. Z.*, **47** (1926) 873, 904.
[93] KÖNIG, H. *Helv. Phys. Acta.*, **2** (1929) 357.
[94] VAN CAUWENBERGHE, R. *Soc. Belge. elect. Bull.*, **43** (1929) 142.
[95] DAVIS, R., BOWDLER, G. W., and STANDRING, W. G. *J. Inst. elect. Engrs.*, **68** (1930) 1222.
[96] KEINATH, G. *Die Technik elektrischer Messgerate*, **2** (1928) 17.
[97] BOUSMAN, H. W., and TEN BROECK, R. L. *Trans. Amer. Inst. elect. Engrs.*, **62** (1943) 541.
[98] PFIFFNER, E. *Elektrotech. Z.*, **47** (1926) 44.
[99] KEINATH, G. *Siemens Z.*, **8** (1928) 629.
[100] WIRG, E. *Arch. Elektrotech.*, **21** (1929) 563.
[101] CAMILLI, G. *Gen. Elect. Rev.*, **39** (1936) 95.
[102] HENDRICKS, A. B., HUBBARD, H. S., and VALLIN, G. L. *Gen. Elect. Rev.*, **42** (1939) 420.
[103] HENDRICKS, A. B. *Gen. Elect. Rev.*, **46** (1943) 477.
[104] IMHOF, A. *Schweiz. Electr. Ver. Bull.*, **19** (1928) 741.
[105] KUCHLER, R. *Elektrotech. Z.*, **58** (1937) 203.
[106] WELLINGS, J. G., MORTLOCK, J. R., and MATHEWS, P. *J. Inst. elect. Engrs.*, **79** (1936) 577.
[107] PROBST, G. *Elektrotech. Z.*, **28** (1924) 750.
[108] VAN ATTA, L. C., VAN ATTA, C. M., NORTHRUP, D. L., and VAN DE GRAAFF, R. J. *Phys. Rev.*, **49** (1936) 761.
[109] PARKINSON, D. B., HERB, R. G., BERNET, E. J., and MCKIBBEN, J. L. *Phys. Rev.*, **53** (1938) 642.
[110] TRUMP, J. G., SAFFORD, F. J., and VAN DE GRAAFF, R. J. *Rev. Sci. Instrum.*, **11** (1940) 54.
[111] HAXBY, R. O., SHOUPP, W. E., STEPHENS, W. E., and WELLS, W. H. *Phys. Rev.*, **58** (1940) 1035.
[112] KIRKPATRICK, P., and MIYAKE, I. *Rev. Sci. Instrum.*, **3** (1932) 1.
[113] KIRKPATRICK, P. *Rev. Sci. Instrum.*, **3** (1932) 430.
[114] GUNN, R. *Phys. Rev.*, **44** (1932) 307.
[115] THOMAS, H. A. *Rev. Sci. Instrum.*, **8** (1937) 448.
[116] WORKMAN, E. J., and HOLZER, R. E. *Rev. Sci. Instrum.*, **10** (1939) 160.
[117] HENDERSON, J. E., GOSS, W. H., and ROSE, J. E. *Rev. Sci. Instrum.*, **6** (1935) 63.
[118] MEADOR, J. R. *Elect. Engng.*, **53** (1934) 942.

119 HANSON, A. O. *Rev. Sci. Instrum.*, **15** (1944) 57.
120 HANSON, A. O., and BENEDICT, D. L. *Phys. Rev.* **65** (1944) 33.
121 MESSNER, M. *Arch. Elektrotech.*, **27** (1933) 335.
122 BINDER, L. *Elektrotech. Z.*, **23** (1931) 735
123 VIEHMANN, H. *Arch. Elektrotech.*, **24** (1930) 349.
124 JACOB, L. *J. Inst. elect. Engrs.*, Pt. II **91** (1944) 512.
125 EHRENBERG, W., and HIRSCH, H. *J. Sci. Instrum.*, **20** (1943) 161.
126 WILLIAMS, J. H., RUMBAUGH, L. H., and TATE, J. T. *Rev. Sci. Instrum.*, **13** (1942) 202.
127 HORNYAK, W. F., LAURITSEN, T., MORRISON, P., and FOWLER, W. A. *Rev. Mod. Phys.*, **22** (1950) 291.
128 BENNETT, W. E., BONNER, T. W., MANDEVILLE, C. E., and WATT, B. E. *Phys. Rev.*, **70** (1946) 882.
129 HAFSTAD, L. R., HEYDENBURG, N. P., and TUVE, M. A. *Phys. Rev.*, **50** (1936) 504.
130 BERNET, E. J., HERB, R. G., and PARKINSON, D. B. *Phys. Rev.*, **54** (1938) 398.
131 MYERS, F. E., and VAN ATTA, L. C. *Phys. Rev.*, **61** (1942) 19.
132 WIEDENBECK, M. L., and MARHOEFER, C. J. *Phys. Rev.*, **67** (1945) 54.
133 COLLINS, B. G., WALDMAN, B., and GUTH, E. *Phys. Rev.*, **56** (1939) 876.
134 HERB, R. G., SNOWDON, S. C., and SALA, O. *Phys. Rev.*, **75** (1949) 246.
135 WARREN, R. E., POWELL, J. L., and HERB, R. G. *Rev. Sci. Instrum.*, **18** (1947) 559.
136 JENNINGS, B. *Proc. Inst. Rad. Engrs.*, **38** (1950) 1126.
137 ALTAR, W., GARBUNY, M., and COLTMAN, J. W. *Phys. Rev.*, **72** (1947) 528.
138 ALTAR, W., and GARBUNY, M. *Phys. Rev.*, **76** (1949) 496.
139 SHOUPP, W. E., JENNINGS, B., and JONES, W. *Phys. Rev.*, **76** (1949) 502.
140 HUNT, S. E., and JONES, W. *Phys. Rev.* **89** (1953) 1283.

8

MEASUREMENT OF HIGH IMPULSE VOLTAGES

SPHERE GAPS

The sphere gap is recognized as the standard method for the measurement of the peak value of impulse voltages, and full calibration data are given in the various Standard Specifications which have been issued[1-4]. If one of the spheres is earthed, the calibration curve of the sphere gap for a negative impulse voltage is stated to be the same as that for a power-frequency alternating voltage, as given in *Table XV* on page 225. A separate calibration is necessary for positive impulse voltages and is given in *Table XVI* on page 226.

The appropriate tables may be used for the measurement of impulse voltages of either polarity provided that the impulse is of the standard wave-form (*see* page 112) with a front of at least 1 μsec and a tail of at least 5 μsec. The gap length between the spheres should not exceed a sphere radius (*see* page 227). If these conditions are fulfilled, and the various specifications regarding the mounting, shape, etc. of the spheres are met (*see* page 230), the results obtained by the use of sphere gaps should be accurate within $\pm$ 3 per cent. The minimum break-down voltage is taken as the voltage which causes break-down on 50 per cent. of the applications of the impulse voltage to the gap.

The same conditions for air density are required when using sphere gaps for the measurement of impulse voltages as for power-frequency alternating voltages (*see* page 231). No correction is necessary for changes in humidity, according to B.S. 358 : 1939 (*see* page 232).

Investigations of the calibration curves for sphere gaps, of diameters varying from 12·5 to 100 cm., have been made by Davis and Bowdler[5]. The peak value of the impulse wave is measured by means of an oscillograph and a resistance potential divider. The estimated probable error of their values is reduced to about 1 per cent. by averaging the results of a sufficient number of records. Most of the tests were made with a 0·5/20 wave. From their measurements Davis and Bowdler conclude that, contrary to the calibrations given in B.S. 358, the power-frequency break-down voltage is always less than the negative impulse break-down voltage, the difference being about 5 per cent. at a spacing equal to a sphere-radius. The positive impulse break-down voltage exceeds the power-frequency value by an amount between 6 per cent. and 10 per cent. at a spacing equal to a sphere-radius (*see* page 227).

Little attention is given in the various Standards to the amount of pre-ionization which is required in the gap in order to ensure consistency of results with impulse voltages. B.S. 358 : 1939 includes the statement : 'It is suggested that in localities where the random ionization between the spheres is likely to be low, irradiation of the gap by radioactive or other ionizing media should be used when voltages of less than 50 kV peak are being measured.' A statement made in the American Institute of Electrical Engineers Standards[2] recommends ultra-violet irradiation as necessary for sphere gaps of 6·2 5cm. diameter or less for spacings up to one-third the sphere diameter, and suggests the use of a quartz mercury-arc lamp within a specified distance of the sphere gap.

The above recommendations are well supported by experimental evidence and precautions are usually taken to irradiate sphere gaps when used to measure impulse voltages less than about 50 kV. However, recent experiments by MEEK[6, 7] show that irradiation is required also for sphere gaps used to measure much higher voltages if accurate results are to be obtained.

In order to understand the need for irradiation of a gap it is necessary to consider the time-lag required in the development of a spark. This time-lag consists of two components (*1*) the statistical time-lag, caused by the need for an electron to appear in the gap during the period of application of the voltage in order to initiate the break-down, and (*2*) the formative time-lag, corresponding to the time required for the spark process, once initiated, to grow across the gap.

The statistical time-lag depends on the irradiation of the gap. A gap subjected to an impulse voltage may break down if the peak voltage exceeds the d.c. break-down value provided that the gap is sufficiently irradiated so that an electron is present in the gap to initiate the spark process when the peak voltage is reached. With lower irradiation the voltage must be maintained above the d.c. break-down value for a longer period before an electron appears. To cause break-down of a gap with an impulse voltage of defined wave-shape, increasing values of peak voltage are required as the amount of irradiation is decreased, so that the voltage is maintained above the d.c. break-down value for increasingly long time-intervals.

Various methods of irradiation have been used, and include radioactive materials[6–14] and ultra-violet illumination as supplied by a mercury-arc lamp[7, 15–22] or by spark[6, 7, 9, 23–28] or corona[3, 4, 29, 30, 31] discharges. The statistical time-lag has also been reduced by the use of small insulating particles scattered on the electrode surface[32–34]. The experimental results obtained with the different methods of irradiation are summarized in the following sections.

Irradiation by light from mercury-arc lamps

Many measurements have been made by STRIGEL and others[15–22] to observe the relation between the statistical time-lag and the over-voltage applied to a gap when the gap is illuminated by a mercury-arc lamp. The results of these measurements have been summarized in a book by Strigel[16]. Some curves showing the statistical time-lag as a function of over-voltage for a 0·11 cm. gap between spheres of 5 cm. diameter are given in *Figure 244*. For a given over-voltage the

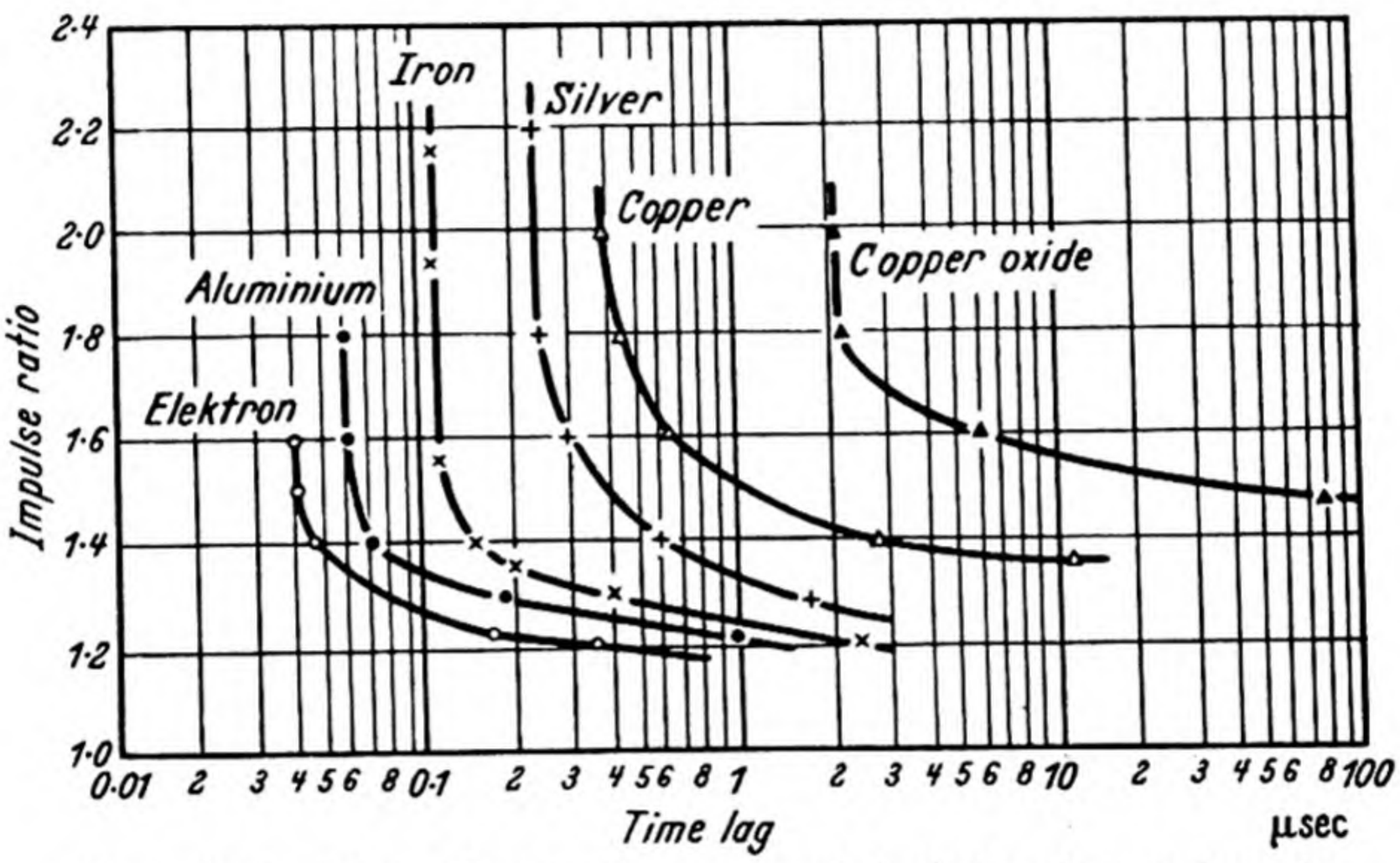

Figure 244. Dependence of mean statistical time lag on impulse ratio for different electrode materials. (The impulse ratio denotes the ratio of the peak value of the applied impulse voltage to the peak value of the a.c. break-down voltage). (Strigel[16], by courtesy, Messrs. Springer.)

statistical time-lag varies with the sphere material because of the differences in work functions and, therefore, of the photocurrent from the cathode. The distribution of the statistical time-lags, and the mean value, also varies with repeated sparking between the electrodes because of gradual changes in the nature of the electrode surfaces. From considerations of the mean photocurrent flowing in a gap Strigel has deduced that, for a 0·11 cm. gap subjected to an 80 per cent. over-voltage, the mean statistical time-lag corresponds closely to the calculated mean time-interval between the release of successive individual electrons from the cathode of the gap.

Investigations by NORD[19] for longer gaps show that illumination from a mercury-arc lamp causes a reduction of 4 per cent. in the break-down voltage of a 40 kV gap between spheres of 6·25 cm. diameter, but that it has no noticeable effect for gaps requiring more than about 70 kV to cause break-down. Larger differences are obtained for shorter gaps, for which time-lags up to 100 μsec are recorded when the gap is not illuminated.

Curves showing the influence of illumination on the transition between no break-down and 100 per cent. break-down have been

obtained by Meek[7] for a 3·0 cm. gap between 12·5 cm. diameter spheres when subjected to 1/5 and 1/500 impulse waves. These curves are given in *Figure 245*. The illumination is produced by a 125 W quartz mercury-arc lamp at a distance of 30 cm. from the gap. When the gap is illuminated a sharp transition occurs and the effect is closely equivalent to that obtained when the gap is illuminated by light from the impulse generator spark-gaps or by 0·5 mg. of radium.

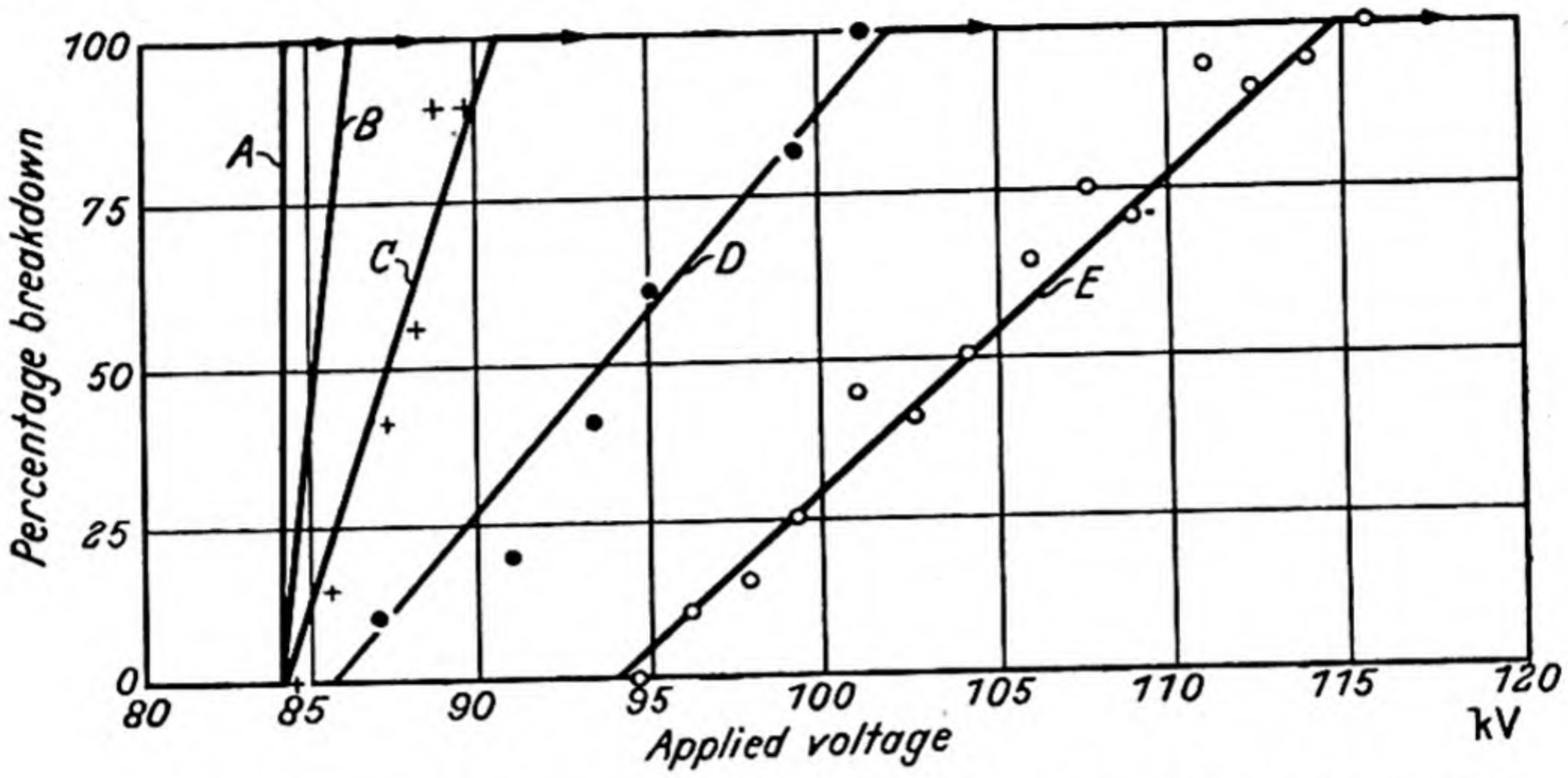

Figure 245. 3·0 cm. gap between 12·5 cm. diameter spheres (Meek[7] by courtesy *J. Inst. elect. Engrs.*)

A. Positive 1/5 wave. Gap irradiated by light from impulse-generator spark-gaps or by radium.
B. Positive 1/5 wave. Gap irradiated by light from mercury-arc lamp, at a distance of 30 cm.
C. Positive 1/5 wave. Gap irradiated by light from mercury-arc lamp, at a distance of 100 cm.
D. Positive 1/500 wave. Gap unirradiated.
E. Positive 1/5 wave. Gap unirradiated.

Measurements have been made by HARDY and CRAGGS[35] of the photocurrents emitted by different cathode materials in air when the cathodes are illuminated by a mercury-arc lamp. The results show that the currents vary widely for different cathode materials and that, for a given cathode, the current decreases rapidly with time. The method of cleaning the cathode surface also has a large influence on the current. Curves showing the variation of photocurrent for various cathodes, with a given illumination, as a function of time are given in *Figure 246*. To obtain the curves of *Figure 246* (*a*) the electrodes were polished with a fine emery paper immediately after they had been removed from the lathe. They were then illuminated for several hours and measurements of the photocurrent were made at intervals. After the curves of *Figure 246* (*a*) had been obtained the electrodes were repolished in the same manner as before and further measurements were made which resulted in the curves of *Figure 246* (*b*). Comparison of these figures clearly shows that for the same electrodes with nominally the same surface treatment there is an appreciable variation in the resultant photocurrents observed. It follows therefore that large variations can occur in the statistical time-lag characteristics of a gap,

when illuminated by a specified light source, unless the cathode conditions are also precisely defined. It appears that more satisfactory results can be obtained by the use of radioactive materials as the resultant irradiation is then independent of the cathode material.

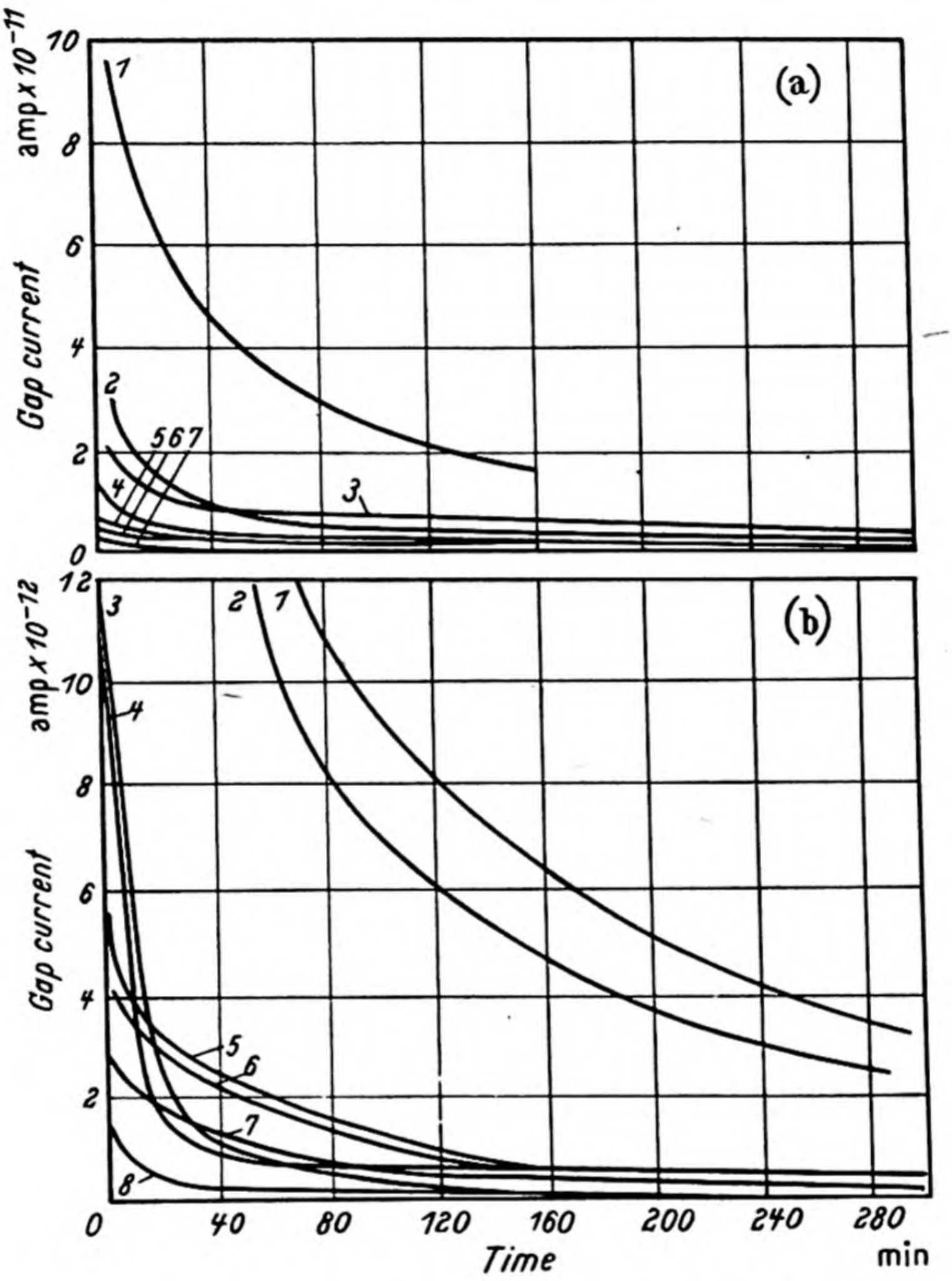

Figure 246. Photoelectric fatigue of electrodes (Hardy and Craggs[35], by courtesy, *Trans. Amer. Inst. elect. Engrs.*)

(a) After initial polish with emery paper. Curve 1. Zinc electrode; Curve 2. Magnesium electrode; Curve 3. Tin electrode; Curve 4. Copper electrode; Curve 5. Brass electrode; Curve 6. Aluminium; electrode; Curve 7. Steel electrode.

(b) After repolish with emery paper. Curve 1. Zinc electrode; Curve 2. Aluminium electrode (polished emery paper and powder); Curve 3. Magnesium electrode; Curve 4. Tin electrode; Curve 5. Brass electrode; Curve 6. Copper electrode; Curve 7. Aluminium electrode (polished with emery paper, powder, and liquid polish.)

Irradiation by radioactive materials

The influence of radioactive materials on the impulse break-down characteristics of sphere gaps has been widely examined[6–14]. They have the advantages that they can form a stable source of irradiation and that they produce an amount of ionization in the gap which is largely independent of the gap voltage and of the surface conditions of the electrodes. In some experiments the radioactive material is

placed in the region of the gap but, following a suggestion by VAN CAUWENBERGHE[8] it is now usual for the material to be placed inside one of the electrodes close behind the sparking surface[6, 7, 9]. Other investigations have been made in which the radioactive material forms the sparking surface[6, 9, 35, 36].

Figures 247 and *248* show the results observed by GARFITT[9] for the break-down of gaps between brass spheres of 0·50 inch in diameter,

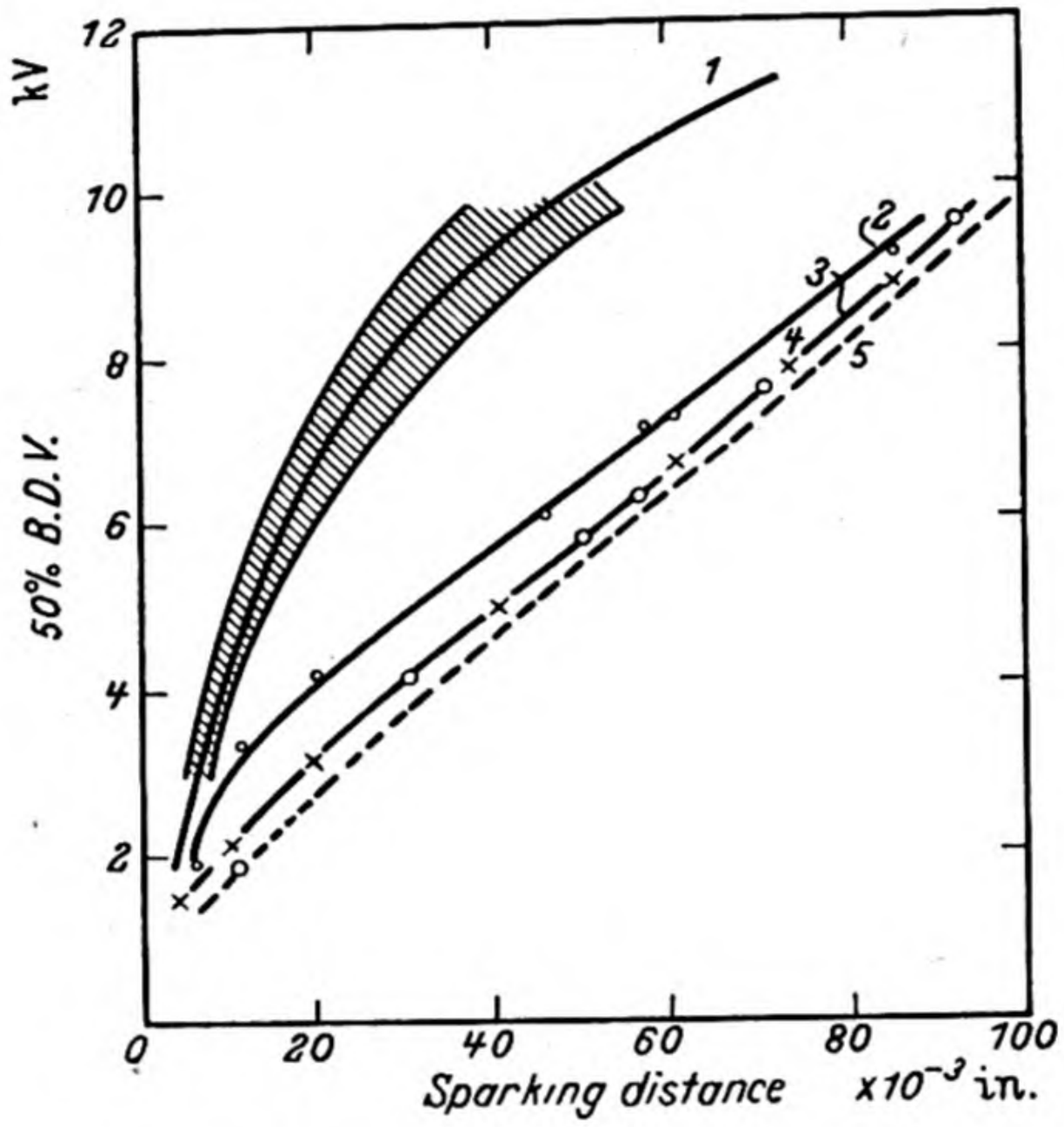

Figure 247. Calibration of 0·5-in diameter sphere-gap with d.c. and impulse voltages. Brass spheres, 0·15/4·5 μsec negative impulse voltage. For Curve 4 the gap is illuminated by a spark across an 0·04-in gap between 0·5-in diameter brass spheres at a distance of 12-in and connected across a capacitance of 0·05 μF without series resistance. (Garfitt[9], by courtesy, *Proc. Phys. Soc.*)

when subjected to 0·15/4·5 impulse waves and for different conditions of irradiation. Curve 1 is for the unirradiated gap, the hatched area indicating the spread of results obtained on different occasions. Because of the wide fluctuations in results the unirradiated gap is clearly unsatisfactory when used for the purposes of measurement of voltage. Curve 2 corresponds to the condition when 0·5 mg. of radium, contained in a Monel-metal capsule 0·2 cm thick, is inserted in one of the brass spheres which is drilled out to give a wall thickness of 1 mm. of metal between the capsule and the gap. Absorption in the metal eliminates all but γ-radiation, which can be considered as solely responsible for the observed improvement in the performance of the gap. The capsule is equally effective when placed in either the anode or the cathode. Though the curve shows that the break-down voltage

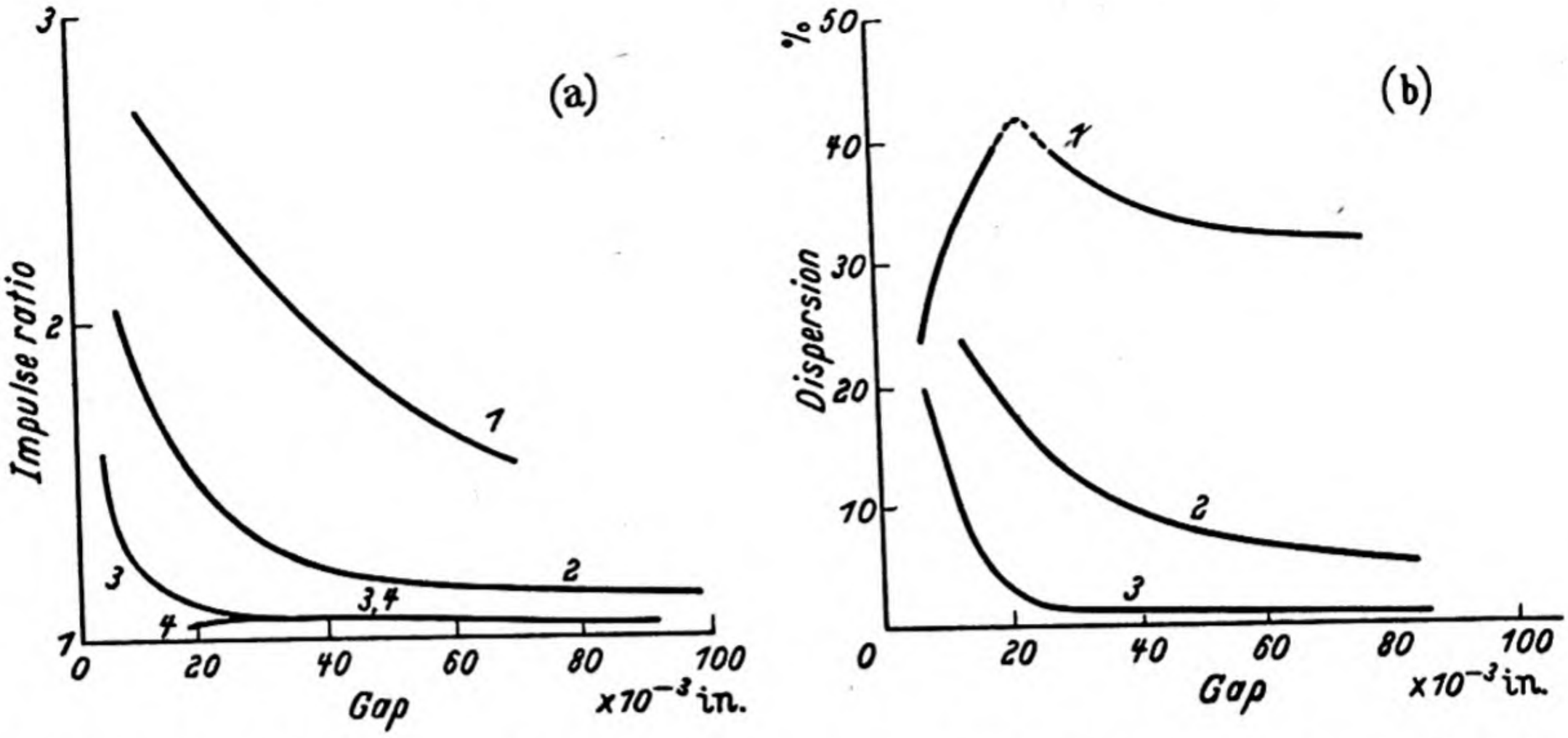

Figure 248. (a) Impulse ratio and (b) dispersion of break-down voltages (Garfitt[9], by courtesy, *Proc. Phys. Soc.*)

1. Gap not irradiated.
2. With 0·5 mg radium.
3. With polonium-coated sphere.
4. With radiation from another spark-gap.

of the gap is reduced, individual points deviate by 4 per cent. from the mean curve. At spacings of 0·050 in. or less the dispersion was of the order of 10 per cent. and the determinations of the 50 per cent. break-down voltage required a lengthy series of readings. Curve 3 is for silver-plated brass spheres, one of which is also coated with a thin film of radioactive polonium, for which the emission consists of α-particles with a range of 3 cm. For gaps of 0·030 in. or more the dispersion is less than 1 per cent. and the impulse ratio is nearly unity. Curve 4 is obtained with the gap illuminated from a spark gap (*see* page 275). Curve 5 gives the break-down voltage calibration for a d.c. voltage applied to the gap.

Other curves given by Garfitt for gaps irradiated by radium and by polonium, when subjected to impulses of different wave-forms, are given in *Figure 249*. The dispersion and impulse ratio increase as the wave-tail becomes shorter, as expected, because of the decreased time for which the voltage is applied to the gap. The dispersion and impulse ratio also increase, at low spacings, when the wave-front becomes longer, possibly because the more slowly rising voltage tends to sweep electrons from the gap before the wave reaches its peak value.

From the preceding curves it is apparent that the use of radioactive polonium causes a considerable improvement in the behaviour of the gap. However, its use has certain disadvantages in that it has a relatively short half-life, of 136 days, and also successive sparking causes the volatilization of the polonium from the sphere surfaces. The possible use of a radioactive polonium alloy for spark-plug electrodes has been investigated by DILLON[10] and by EVANS[11]. Hardy and Craggs[35, 36] have drawn attention to the advantages of

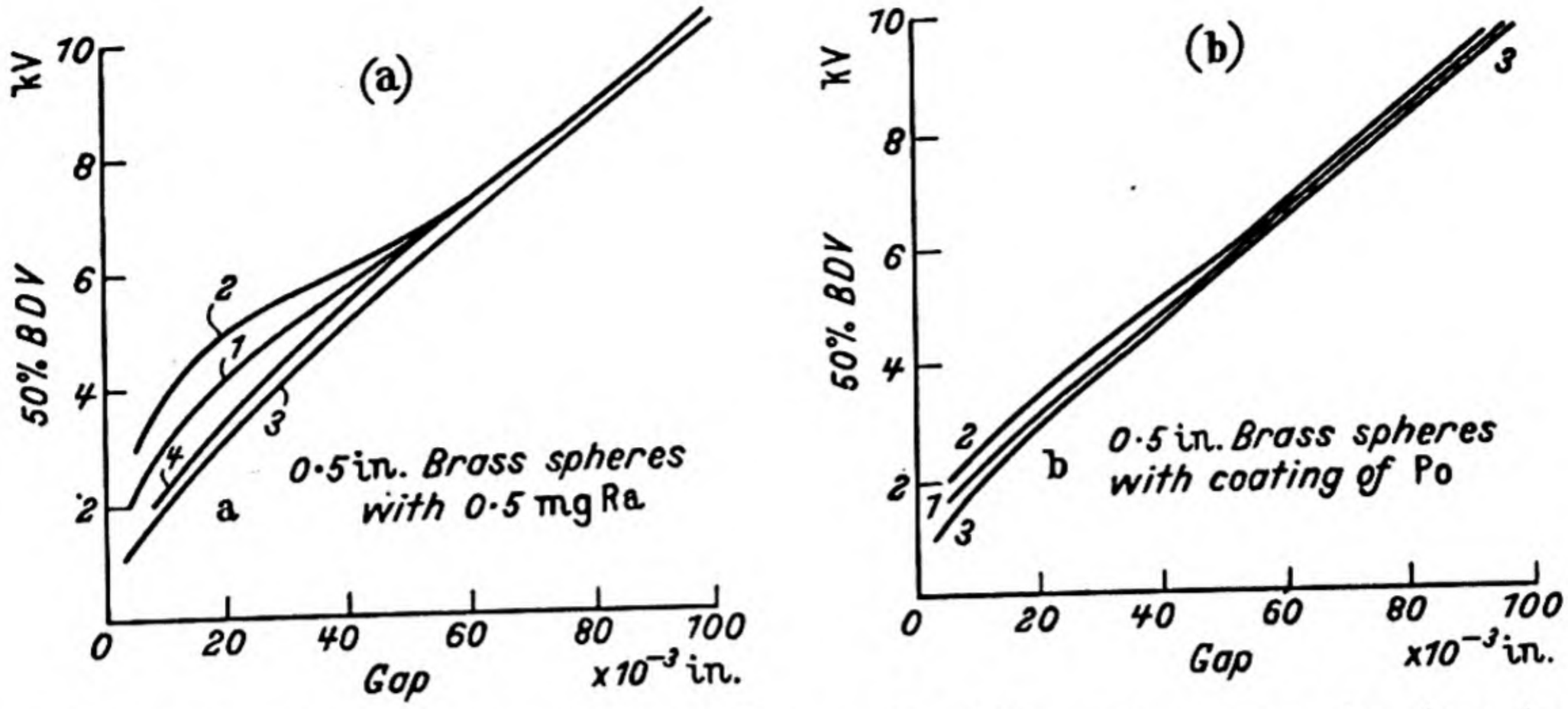

Figure 249. Comparison of break-down of 0·5-in sphere gap for impulse voltages of different shapes. (Garfitt[9], by courtesy, *Proc. Phys. Soc.*)

1. 0·15/4·5 μsec impulse voltage.
2. 0·63/4·5 ,, ,, ,,
3. 0·15/100 ,, ,, ,,
4. 0·63/100 ,, ,, ,,

radioactive cobalt either as the electrode material or as an insert in an electrode.

While the use of small amounts of radium, of 1 mg. or less, is not satisfactory for small gaps of the order of 1 mm. it is found to give excellent results for gaps of 1 cm. or more[6, 7]. This is because of the increased gap volume and the resultant increased ionization occurring in the gap, so that there is a greater chance of a suitably placed electron appearing in the gap at the instant the impulse voltage is applied.

Figure 250 shows the transition curves between no break-down and 100 per cent. break-down obtained by Meek[7] for a 12·5 cm. gap between spheres of 25 cm. diameter, when the gap is unirradiated and when the gap is irradiated by 0·5 mg. of radium. The radium is contained in a small metal capsule and is inserted in the high-voltage sphere close behind the sparking surface, the thickness of which was of the order of 2 mm. The mean break-down voltage of the unirradiated gap, for positive impulses applied to the gap, is 311 kV, with a scatter of $\pm$ 8 kV between the zero and 100 per cent. break-down voltage. When the gap is irradiated with 0·5 mg. of radium the mean break-down voltage is 291 kV, with a scatter of less than 1·5 kV. The break-down voltage is therefore lowered by about 7 per cent. by irradiation and is also much more sharply defined. The corresponding reduction in the negative impulse break-down voltage is from 285 kV to 281 kV.

Similar results are quoted by Meek[6, 7] for gaps ranging from 1 to 20 cm., between spheres of 6·25, 12·5 and 25 cm. diameter. Meek concludes that the most effective method of irradiation, for the longer gaps, is by radioactive materials placed in the high-voltage sphere. For the range of gaps studied the results obtained with 0·5 mg. of radium give a

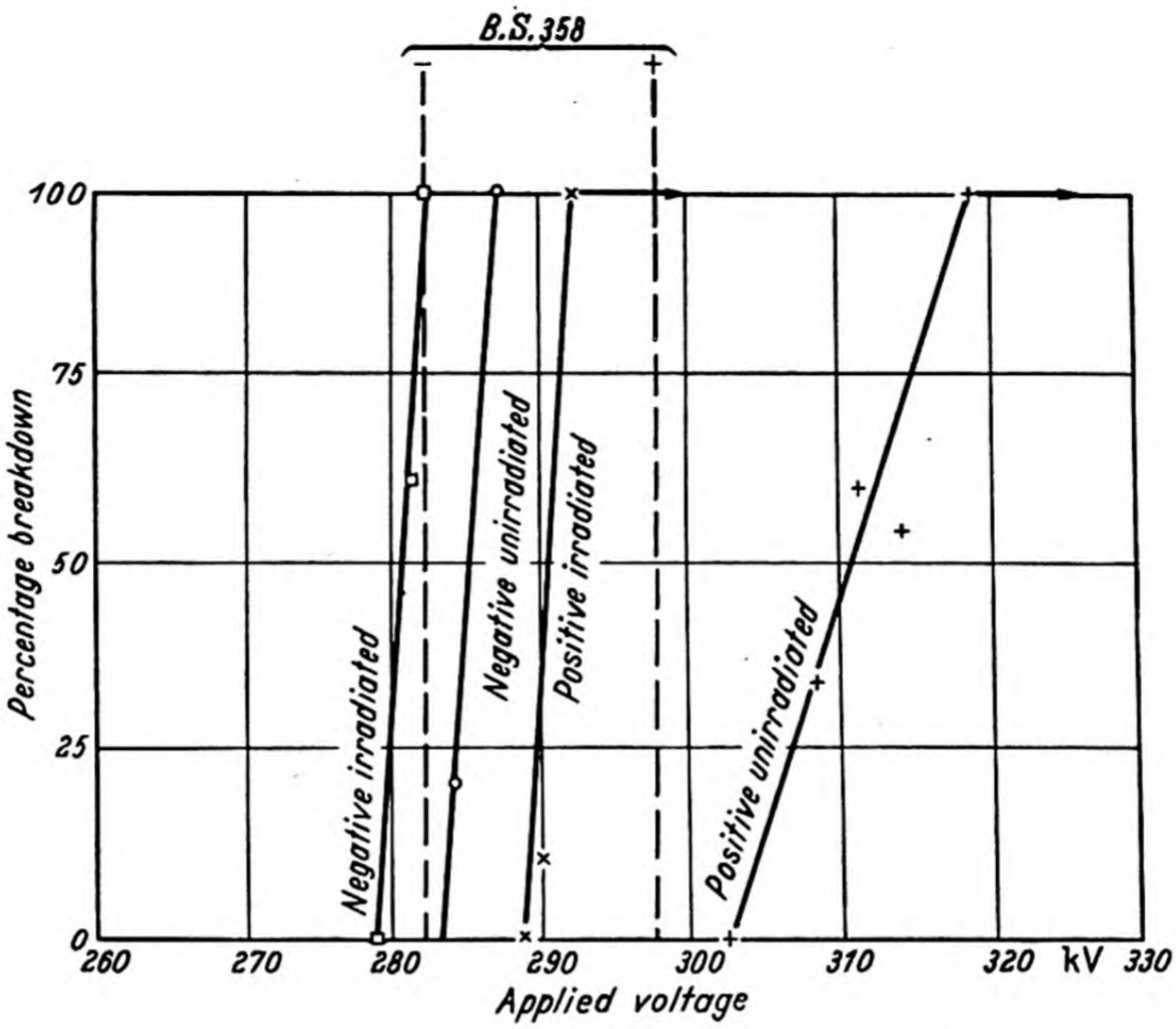

Figure 250. 12·5 cm gap between 25 cm diameter spheres: 1/50 wave. (Meek[7], by courtesy, *J. Inst. elect. Engrs.*)

○ ○ ○ Negative impulse. Gap unirradiated.
□ □ □ Negative impulse. 0·5 mg radium in high-voltage sphere.
+ + + Positive impulse. Gap unirradiated.
× × × Positive impulse. 0·5 mg radium in high-voltage sphere.

sharply defined break-down voltage. The values for the impulse break-down voltage with the gap irradiated in this matter are in close agreement with the values given in the B.S. 358 tables, for gap lengths up to that at which a polarity difference is recorded. For longer gaps the negative impulse break-down voltage for an irradiated gap agrees with the B.S. 358 tables, but the positive impulse break-down voltage is appreciably lower than that given in the tables (*see* page 282). Meek suggests that some revision of the tables for positive impulse break-down may be necessary.

Hardy and Craggs[35, 36] have investigated the ionization produced in gaps irradiated by radioactive materials. Some curves obtained for gaps between spheres of 2 cm. diameter and between plates of 2 cm. diameter are given in *Figure 251.* The curves show that 1 mg. of radium produces a current of the order of 10^{-11} A for a gap of 1 cm. and a voltage of 100 V. This current is equivalent to approximately 1 electron per 0·016 μsec. These electrons appear at random throughout the gap but, in uniform fields, only an electron appearing near the cathode is likely to initiate an electron avalanche leading to a spark when the gap is subjected to a voltage just sufficient to cause break-down[37]. If it is assumed that 10 per cent. of the electrons are produced in a region close

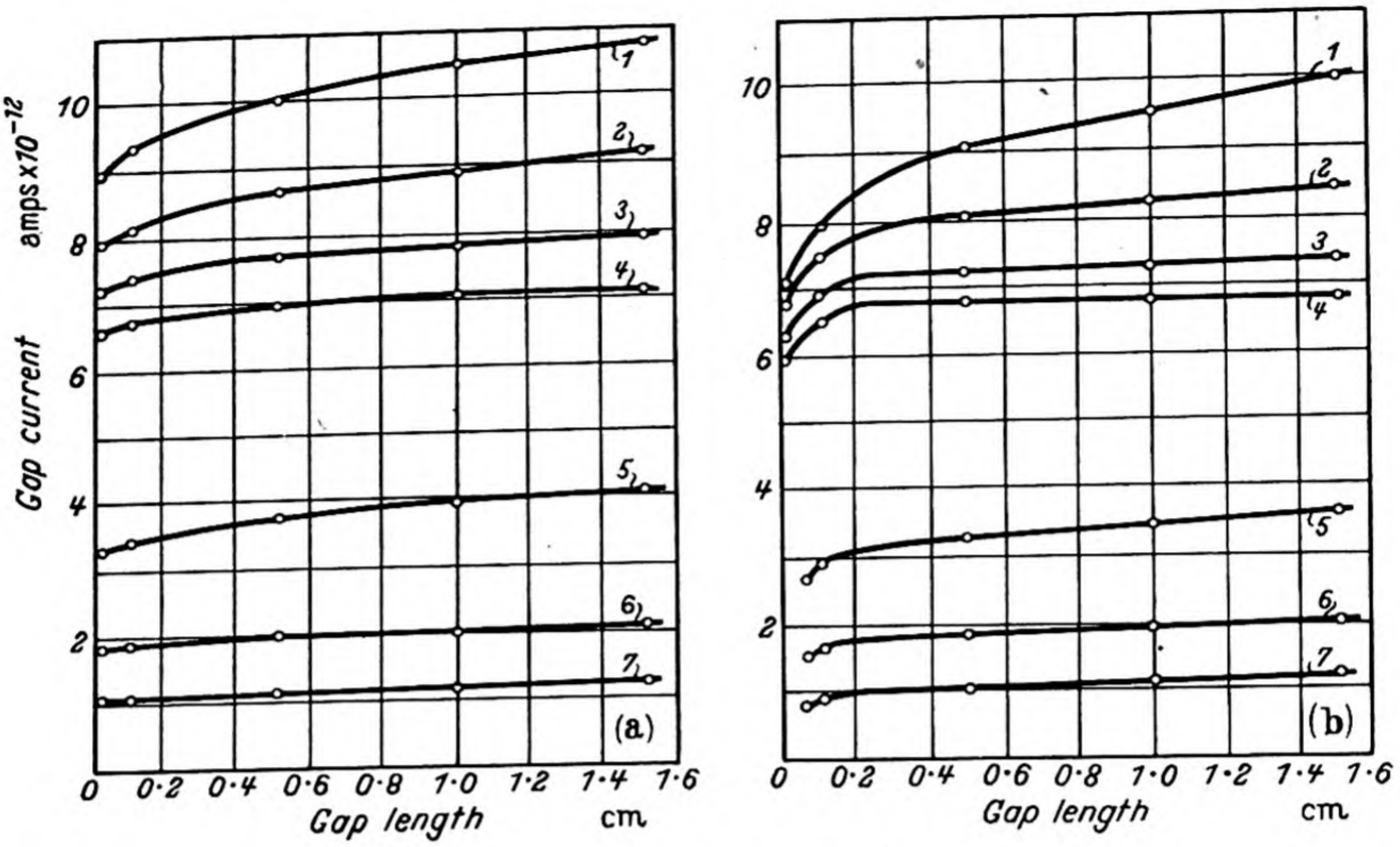

Figure 251. Variation of gap current with gap length (radium irradiation). (Hardy and Craggs[35], by courtesy, *Trans. Amer. Inst. elect. Engrs.*)

(a) 2 cm. diam. spheres.
Material—brass, gap voltage 100 volts.
Curve 1.–1 mg. radium. Depth of radium in electrode (anode) 0·030 cm.
Curve 2.–1 mg. radium. Depth of radium in electrode (anode) 0·112 cm.
Curve 3.–1 mg. radium. Depth of radium in electrode (anode) 0·288 cm.
Curve 4.–1 mg. radium. Depth of radium in electrode (anode) 0·318 cm.
Curve 5.–0·5 mg. radium. Depth of radium in electrode (anode) 0·030 cm.
Curve 6.–0·2 mg. radium. Depth of radium in electrode (anode) 0·030 cm.
Curve 7.–0·1 mg. radium. Depth of radium in electrode (anode) 0·030 cm.

(b) 2 cm. diam. flat plates.
Material brass, gap voltage 100 volts.
Curve 1.–1 mg. radium. Depth of radium in electrode (anode) 0·038 cm.
Curve 2.–1 mg. radium. Depth of radium in electrode (anode) 0·170 cm.
Curve 3.–1 mg. radium. Depth of radium in electrode (anode) 0·277 cm.
Curve 4.–1 mg. radium. Depth of radium in electrode (anode) 0·338 cm.
Curve 5.–0·5 mg. radium. Depth of radium in electrode (anode) 0·038 cm.
Curve 6.–0·2 mg. radium. Depth of radium in electrode (anode) 0·038 cm.
Curve 7.–0·1 mg. radium. Depth of radium in electrode (anode) 0·038 cm.

enough to the cathode to be effective in initiating break-down of the gap then the number of such initiating electrons is one per 0·16 μsec for the above conditions. Consistent behaviour of this gap when subjected to impulse voltages of magnitude slightly greater than the d.c. break-down voltage may therefore be expected when the duration of the impulse voltage is about 1 μsec for flat plate electrodes. The corresponding duration is about 10 μsec for spherical electrodes as only about 10 per cent. of the projected area of the spherical electrode is effective for sparking.

Radioactive cobalt can be used for irradiation and has certain advantages in that electrodes can be machined from it and then irradiated in a uranium pile. The half-life is 5·3 years. The current produced in a gap by radioactive cobalt has been studied by Hardy and Craggs[35] and results are shown in *Figure 252*. An effect equivalent to about 10 mg. of radium is obtained.

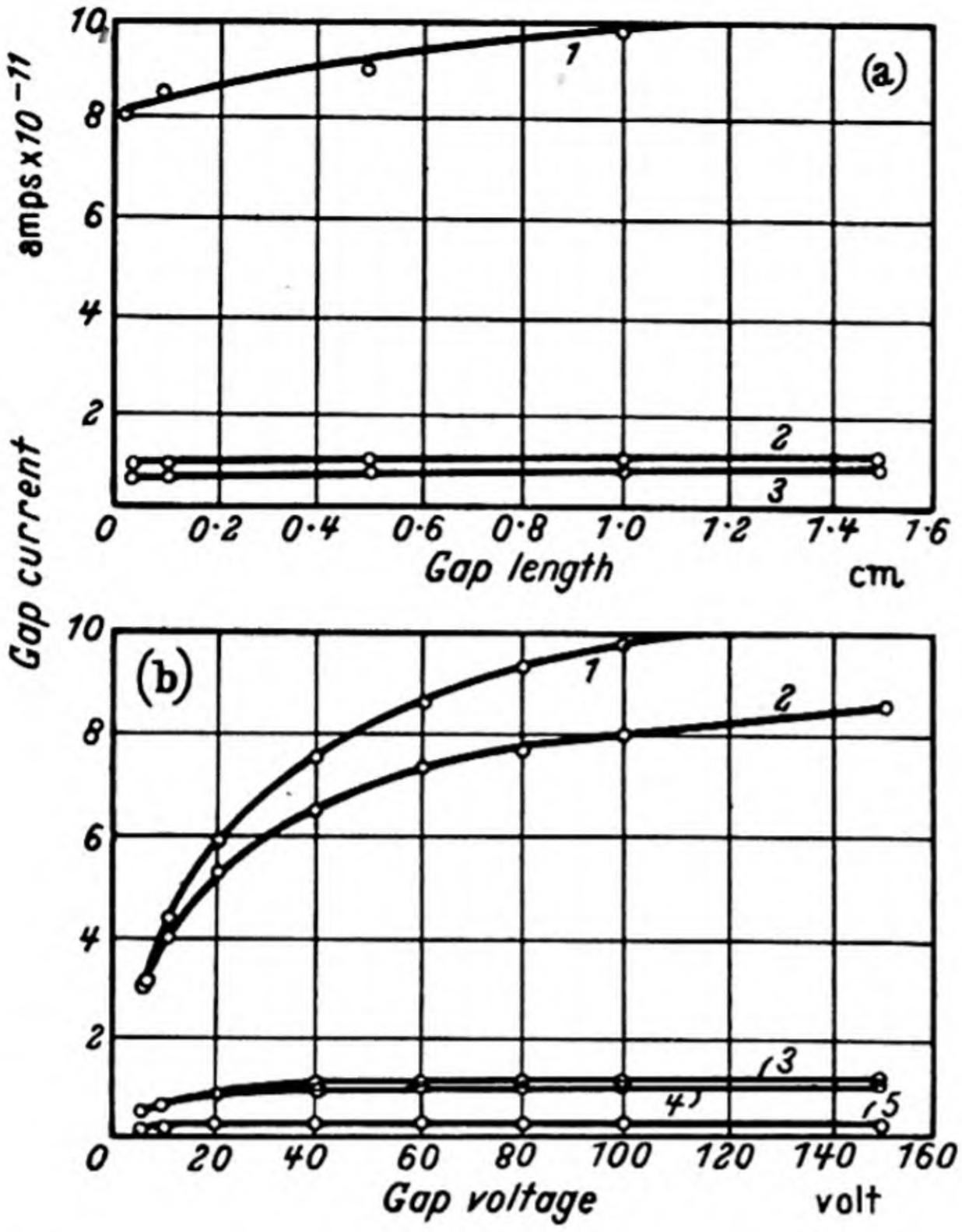

(a) Flat plate electrodes. Brass anode 2 cm diameter. Gap voltage 100 volts. Curve 1. Radioactive cobalt cathode 1·08 cm diameter. Curve 2. Cobalt cathode 1·22 cm diameter, 1 mg radium in cathode. Depth of radium in electrode 0·068 cm. Curve 3. Cobalt cathode 1·22 cm diameter, 1 mg radium in anode. Depth of radium in electrode 0.038 cm.
(b) Flat plate electrodes. Brass anode 2 cm diameter. Curve 1. Radioactive cobalt cathode 1·08 cm diameter. Gap length 1·0 cm; Curve 2. Radioactive cobalt cathode 1·08 cm diameter. Gap length 0·1 cm; Curve 3. Cobalt cathode 1·22 cm diameter, 1 mg radium in cathode. Depth of radium in electrode 0·068 cm. Gap length 1·0 cm; Curve 4. Cobalt cathode 1·2 cm diameter, 1 mg radium in cathode. Depth of radium in electrode 0·068 cm. Gap length 0·1 cm; Curve 5. Cobalt cathode 1·22 cm diameter 0·1 mg radium in cathode. Depth of radium in electrode 0·068 cm. Gap length 0·1—1·0 cm.

Figure 252. Variation of gap current with gap length and gap voltage. (Hardy and Craggs[35], by courtesy, *Trans. Amer. Inst. elect. Engrs.*)

Irradiation by light from spark and corona discharges

The ultra-violet radiations emitted from spark or corona discharges may be used to irradiate a sphere gap with pronounced effectiveness. STREET and BEAMS[23] found that a voltage equal to 16 times the minimum break-down value could be applied to an unirradiated gap for 1 μsec without break-down, whereas break-down occurred at the minimum voltage when the gap was illuminated by the light from a nearby spark. Similar results have been recorded by WYNN-WILLIAMS[29] who also established that the light provided by a corona discharge is sufficient to reduce the statistical time-lag to a low value. Later experiments by BERKEY[31] on enclosed spark gaps, as used in lightning arresters, confirm Wynn-Williams' findings and show the importance of corona discharges as a factor in the production of low impulse ratios in such gaps. In Berkey's measurements an insulating spacer separates the two electrodes, which are separated by a gap of about 2 mm. The corona discharge occurring at the insulator-electrode contacts is found to produce sufficient radiation to cause ionization in the gap and to reduce the statistical time-lag. When the gap is mounted without an insulating spacer long time-lags and high impulse ratios are recorded. The lowest impulse ratios occur with a spacer of rutile ceramic, a

material of high dielectric constant, because of the greater intensity of corona then produced.

Meek[6,7] and Garfitt[9], have shown that the behaviour of a sphere gap subjected to impulse voltages is greatly influenced by the illumination from the impulse-generator spark gaps. The position of a sphere gap relative to an impulse-generator may therefore affect the results obtained (*see* page 277).

In experiments described by Meek[6] for a 1/1000 wave applied to a 0·079 cm. gap between spheres of 1·3 cm. diameter, break-down of the gap occurred on 50 per cent. of the applied impulses, of 4·4 kV peak value, when the gap was screened from irradiation. No break-down occurred for peak impulse voltages of 3·9 kV, and break-down occurred on every impulse for peak voltages > 5·0 kV. When the gap was illuminated by light from the impulse-generator spark gaps, at a distance of 50 cm. from the sphere gap, break-down of the gap occurred regularly for applied voltages of 4·0 kV.

Some curves obtained by Garfitt are given in *Figure 253* and show the influence of illumination from a spark on the impulse break-down

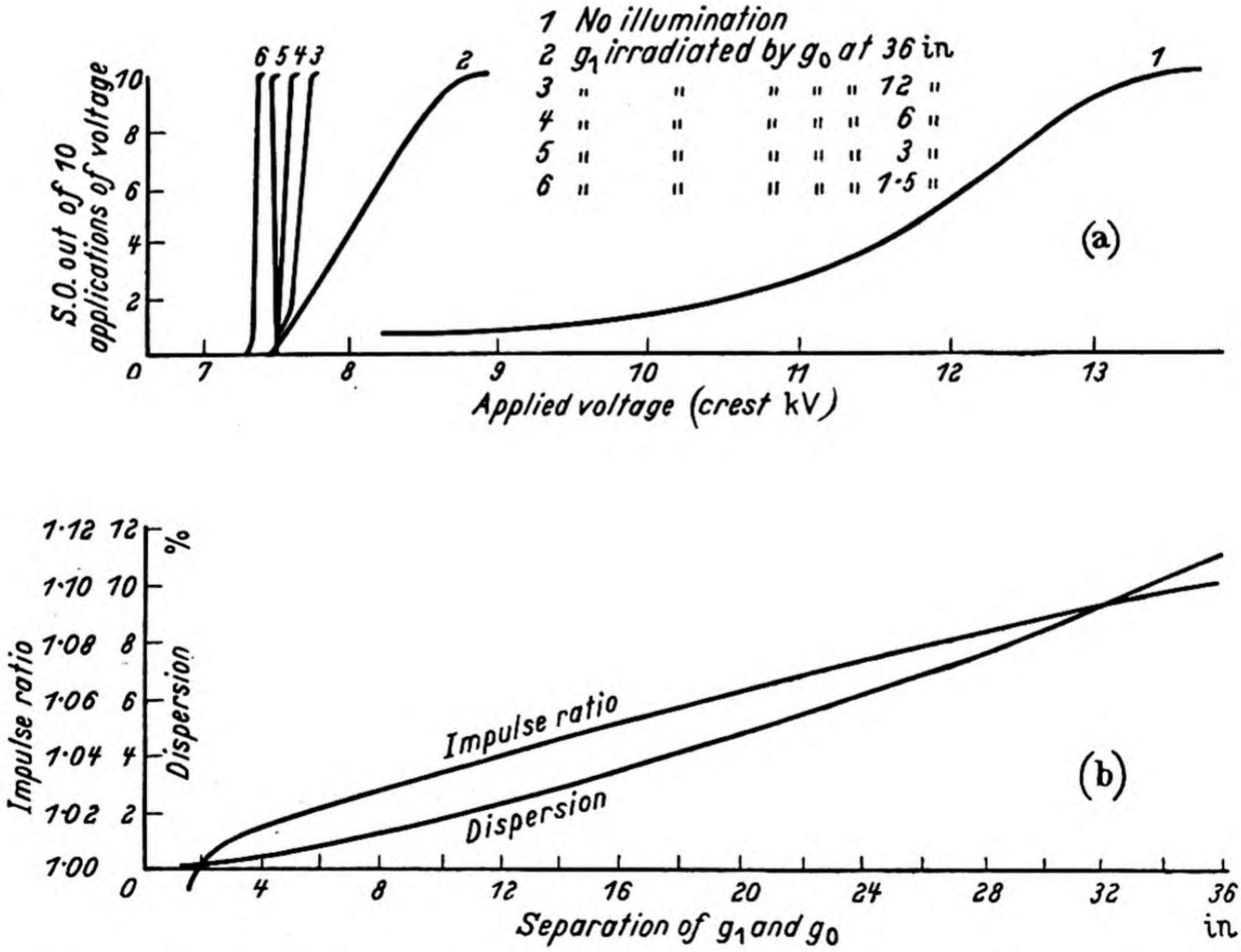

Figure 253. Break-down of 0·5-in diameter spheregap g_1 under illumination from another spark g_0. Variation of intensity of illumination by adjustment of distance between sparks. $g_1 = 0{\cdot}07$-in. (Garfitt[9], by courtesy, *Proc. Phys. Soc.*).

of a 0·070 in. gap between 0·5 in. diameter spheres, for a 0·15/4·5 wave. The impulse-generator spark gap g_o is used as the illuminating gap.

Figure 253b illustrates the effect of variation of the distance between g_o and the test-gap g_1. The influence of the angle of incidence of the illumination on the test-gap, for a given total illumination, has also been studied by Garfitt. Results for a 0·030 in. gap subjected to 0·63/100 waves are given in *Figure 254*. The illuminating gap g_o is at a fixed distance of 12 in. from the test-gap. The angle ϕ gives the direction of the illumination and is zero when the illumination is directed perpendicularly to the axis of the test-gap. *Figure 254* shows that the illumination is most effective when ϕ is $\sim -18°$; this is approximately the angle

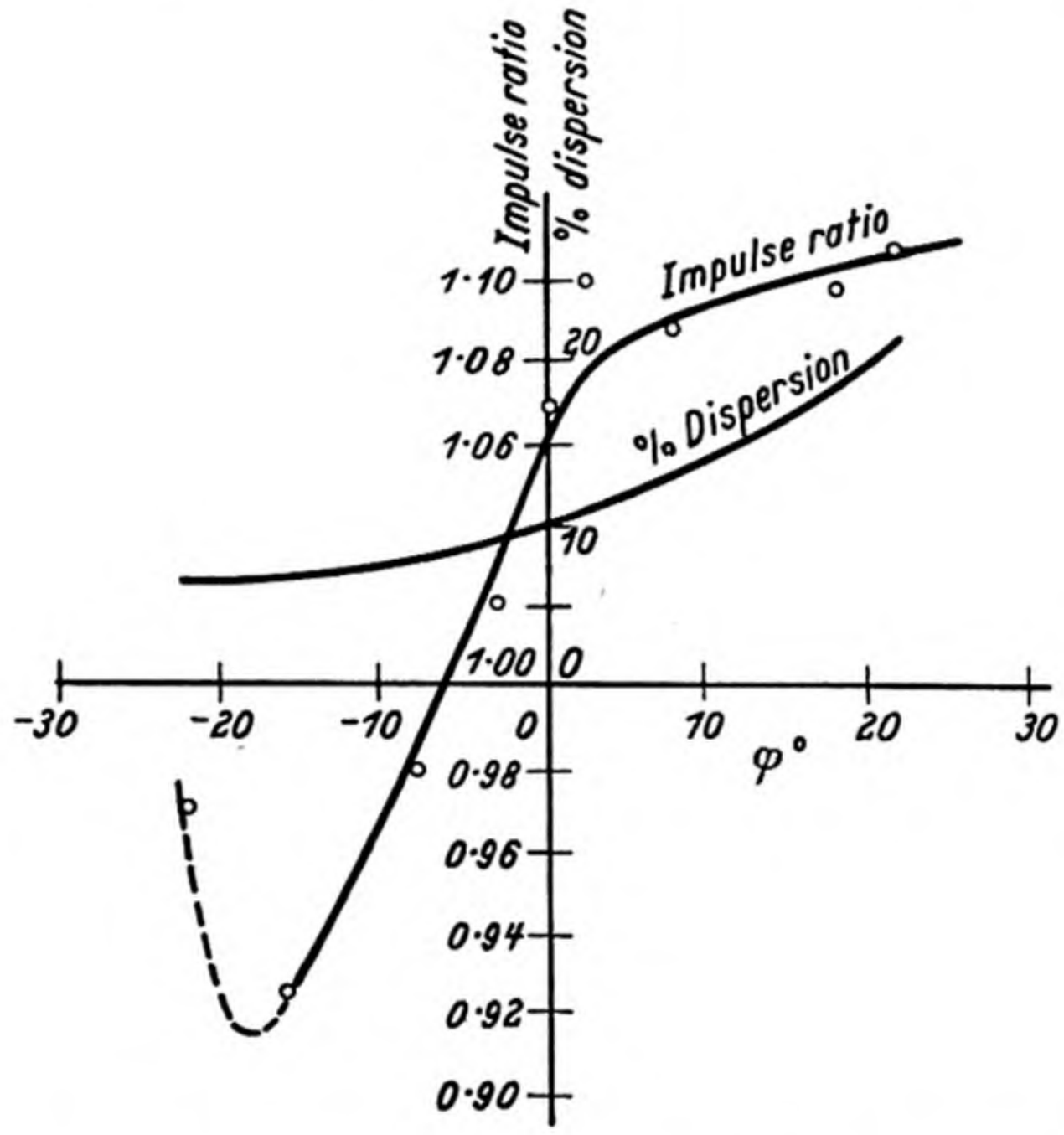

Figure 254. Break-down of 0·5-in sphere-gap under illumination from another spark. Variation of the angle of illumination. (Garfitt[9], by courtesy, *Proc. Phys. Soc.*)

at which the path of light is along the common tangent to the two spheres, *i.e.*, when the cathode receives maximum illumination.

Garfitt's measurements have been made on gaps up to ~2 mm. in length, with impulse waves of 0·15/4·5 or longer duration. Under these conditions, Garfitt concludes that illumination from a spark source is more satisfactory in producing consistent break-down than radioactive irradiation (*see* page 269).

The influence of the light from the impulse-generator spark gaps on the operation of sphere gaps has been examined by Meek[6, 7] for gaps up to about 20 cm. between spheres of several sizes. In these measurements a series of ten or more impulses of the same peak value is applied to the gap and the number causing break-down is counted. The range of voltages required to produce the transition from no break-

down to 100 per cent. break-down is then established. *Figure 255* shows the results obtained for a 1·0 cm. gap between 12·5 cm. diameter spheres. No polarity effect is recorded as the field is nearly uniform. When the gap is unirradiated the transition from no break-down to 100 per cent. break-down is a gradual one for both the wave-forms of 1/5 and 1/500 used. The 50 per cent. break-down voltage, *i.e.* the minimum break-down voltage as defined in B.S. 358, is 47 kV for the 1/5 wave and is appreciably higher than the 38 kV for the 1/500 wave. This is to be expected because of the greater length of time for which

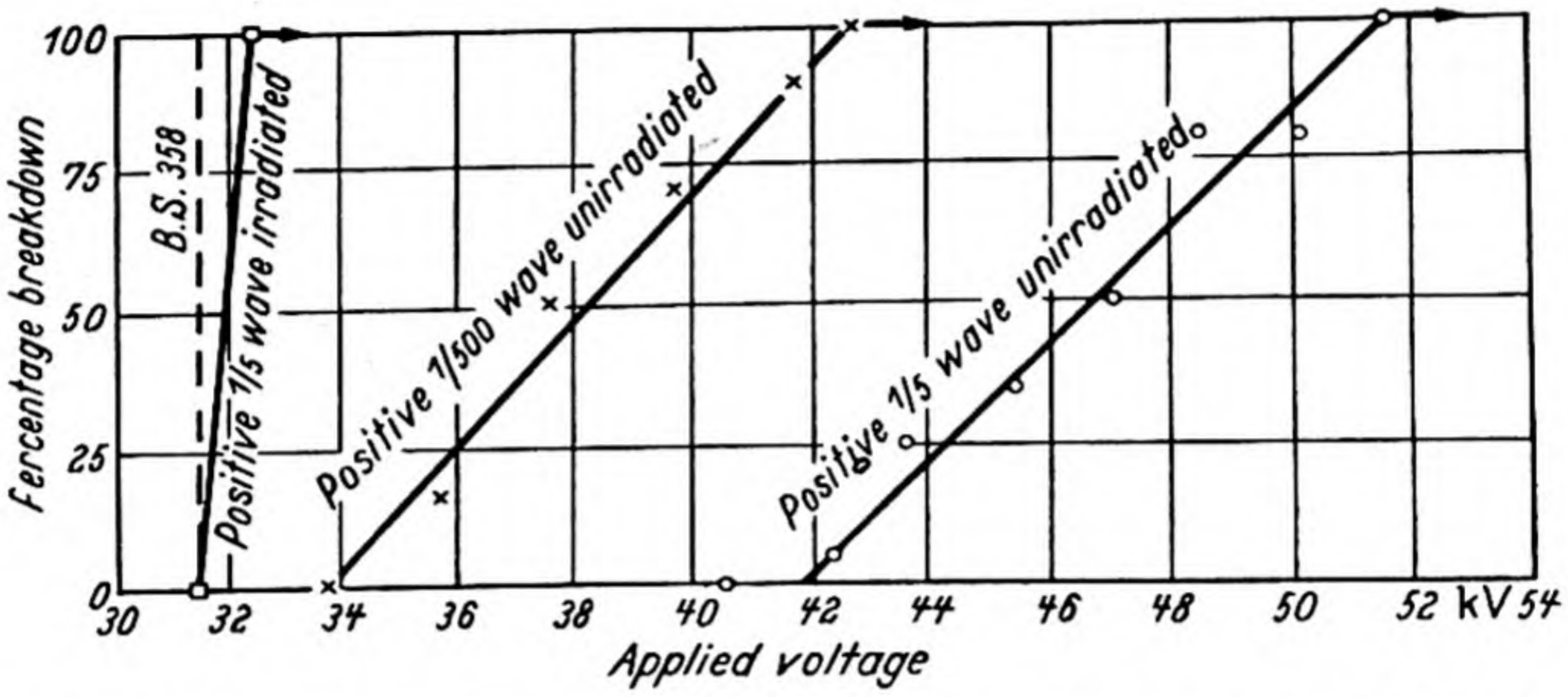

Figure 255. 1·0 cm gap between 12·5 cm diameter spheres. (Meek[7], by courtesy, *J. Inst. elect. Engrs.*).

□ □ □ Positive 1/5 wave. Gap irradiated by light from impulse generator spark-gaps.
× × × Positive 1/500 wave. Gap unirradiated.
○ ○ ○ Positive 1/5 wave. Gap unirradiated.

the voltage remains within a given percentage of its peak value. When the gap is illuminated by the light from the impulse-generator spark gaps, at a distance of 5 ft., the break-down voltage is sharply defined at a value slightly below 32 kV for both the 1/5 and 1/500 waves.

Figure 256 shows some further results given by Meek for a 1/5 wave is applied to a 3·0 cm. gap between spheres of 6·25 cm. diameter. In this case the field is less uniform and a polarity effect is observed (*see* page 281). With the unirradiated gap the transition from no break-down to 100 per cent. break-down is a gradual one for both polarities, and the 50 per cent. break-down voltages are appreciably higher than the B.S. 358 values. When the gap is illuminated by light from the impulse-generator spark gaps the break-down voltage of the gap becomes sharply defined, no noticeable difference being recorded between the positive and negative break-down voltages.

The results obtained with a 1/5 impulse wave for various gaps between spheres of 6·25 cm. diameter are given in *Figure 257*. The curve for the unirradiated gap is drawn through the points corresponding to the 50 per cent. break-down values, and the scatter between the 1 per cent. and 99 per cent. values is indicated by the vertical

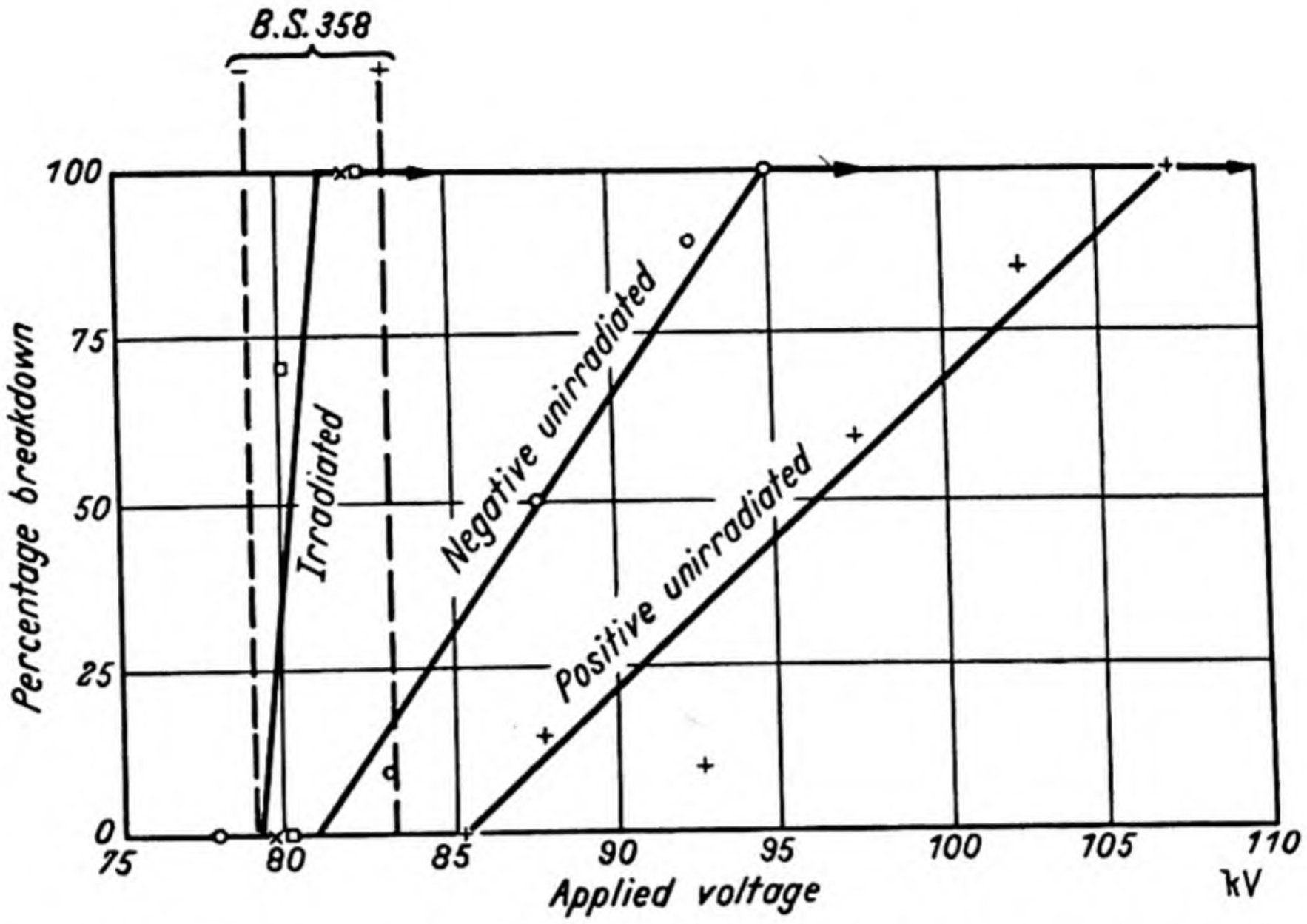

Figure 256. 3·0 cm gap between 6·25 diameter spheres: 1/5 wave. (Meek[7], by courtesy, *J. Inst. elect. Engrs.*)

+ + + Positive impulse. Gap unirradiated.
○ ○ ○ Negative impulse. Gap unirradiated.
× × × Positive impulse. Gap irradiated by light from impulse generator spark gaps.
□ □ □ Negative impulse. Gap irradiated by light from impulse generator spark gaps.

intense lines. The negative impulse break-down voltage of the unirradiated gap becomes more sharply defined as the gap length is increased and tends to that obtained when the gap is illuminated by the impulse-generator spark gaps. At about 5 cm. spacing the two

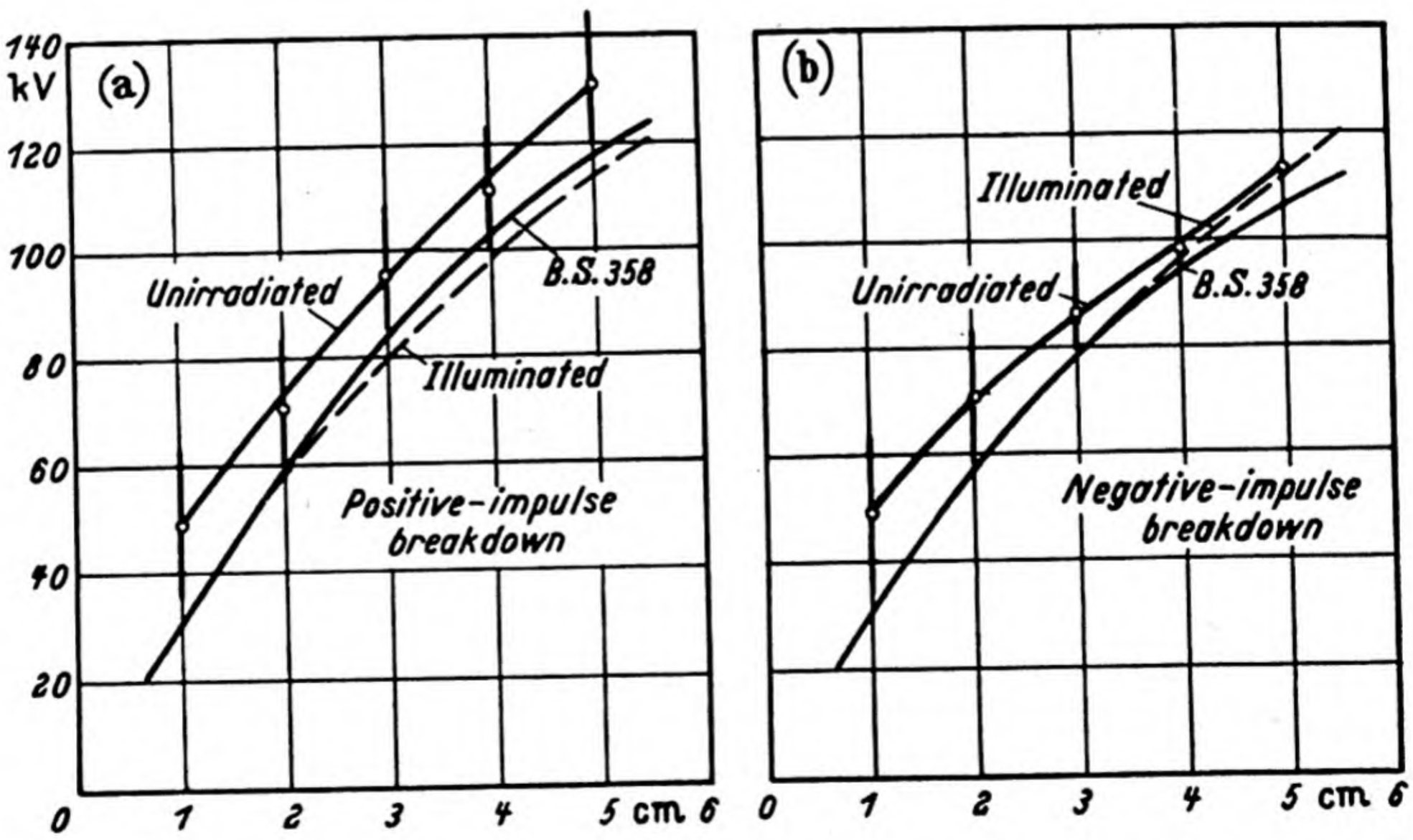

Figure 257. The variation of impulse break-down voltage with gap length for a 6·25 cm diameter sphere gap. (Meek[7], by courtesy, *J. Inst. elect. Engrs.*)

The circled points denote the 50% break-down voltages of an unirradiated gap, for a 1/5 wave; the vertical lines through the points denote the corresponding spreads between the 1% and 99% break-down voltages.
The broken-line curve gives the break-down voltage of the same gap for the same conditions, but illuminated by the light from the impulse-generator spark gaps.

curves are about the same. On positive polarity the difference between the unirradiated and the illuminated break-down voltages remains at a large value for the full range of gaps studied, and the transition from no break-down to complete break-down continues to be a gradual one. The impulse break-down voltages of the illuminated gaps agree closely with the B.S. 358 values for spacings up to 3 cm. Above this spacing the negative impulse break-down voltages exceed those given in B.S. 358, whereas the positive impulse break-down voltages fall below the B.S. 358 values. In all the measurements with the gap illuminated, the difference between the positive and negative impulse break-down voltages was < 3 per cent., whereas B.S. 358 gives a difference of 9·3 per cent. at 5 cm. spacing. This polarity effect, and its dependence on irradiation, is discussed further on page 282.

An advantage of the use of light from the impulse-generator spark-gaps is that the illumination is intense and occurs at the exact instant when it is required, namely, at the instant of application of the voltage wave to the sphere gap. However, in the measurement of impulse voltages with a sphere gap it is not always possible to arrange the spheres in a position such that they are illuminated by the light from the impulse-generator spark gaps. For this reason the use of radio-active materials is usually to be preferred (*see* page 271).

The break-down voltage of a sphere gap is not appreciably affected by ultra-violet radiations when these produce photoelectric currents at the cathode of less than about 10^{-11} A/cm.^{2}, corresponding to 1 electron per 0·016 μsec./cm^2. Any illuminating source producing photocurrents of this order may therefore be expected to reduce the statistical time-lag and to ensure consistent break-down for impulses lasting 1 μsec or more without causing a reduction in the break-down voltage. However, if a gap is exposed to intense illumination the photocurrents produced lead to distortion of the field in the gap by space-charge effects, and the break-down voltage of the gap can be lowered below its normal d.c. break-down value. Many measurements of this effect have been made[6, 17, 37–53]. BRINKMAN[17] has observed a lowering of 5 per cent. in the break-down voltage of a 10 kV gap between aluminium spheres, when the gap is illuminated by a mercury-arc lamp at 5 cm. distance from the gap. The lowering is more pronounced when the illuminating source is a nearby intense spark. The break-down voltage of a 0·2 cm. gap is lowered by 10 per cent. when it is illuminated by a spark produced by the undamped discharge of a 0·1 μF capacitance initially charged to 10 kV, the distance between the gap and the illuminating spark being 20 cm[43]. With longer gaps between spheres, when the field is sufficiently non-uniform, illumination of the gap has been observed to cause an increase in the break-down voltage[54, 55].

Influence of cathode surface

When a gap is illuminated by a mercury-arc lamp, or by any other ultra-violet source, the photocurrent from the cathode will clearly depend on the material and condition of the cathode surface (*see* page 267). However, the nature of the cathode surface can influence the impulse characteristics of a sphere gap, or other form of gap, even in the absence of illumination.

Investigations have been made by SLEPIAN and BERKEY[32] of the break-down of gaps of several mm. in length when small particles of insulating materials, including porcelain, silicon carbide, alumina or rutile, are placed on the electrode surfaces. The statistical time-lag of the gaps is then reduced considerably and the impulse ratio of the gap can be brought close to unity by a suitable choice of particle material and size. Provided that the particle size is sufficiently small, between about 0·002 and 0·015 cm., the impulse characteristics of the gap are improved without any appreciable change in the alternating break-down voltage of the gap. There appear to be two possible reasons for the observed influence of the particles. Localized field distortions in the region of each particle may cause an increase in the electron emission from the cathode, with a resultant reduction in the statistical time-lag. Alternatively, the particles may break down under the increased field and so provide the necessary electrons to initiate the growth of a spark across the gap.

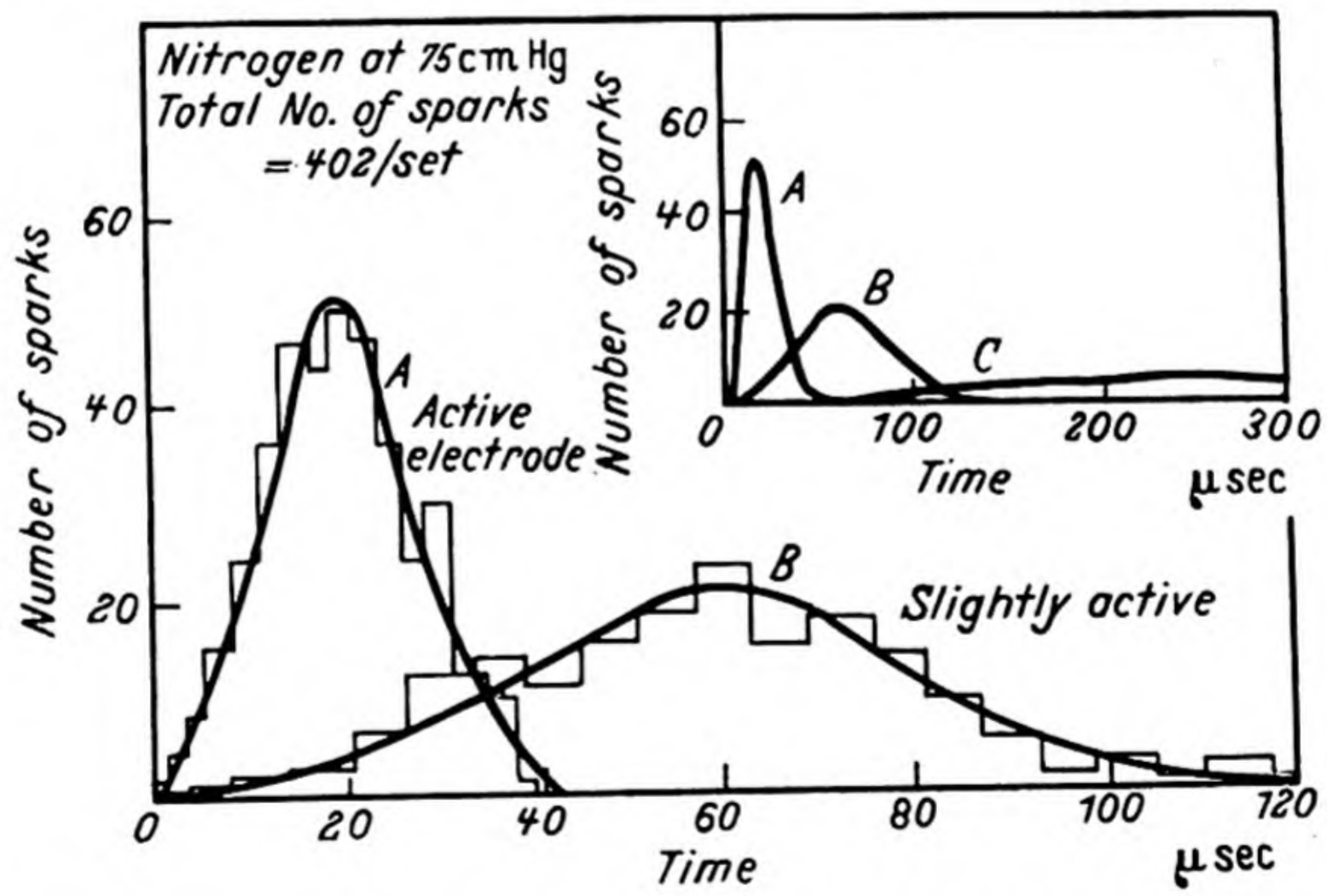

Figure 258. Distribution of spark lags about mean lag. (Llewellyn Jones[33], by courtesy, *Proc. Phys. Soc.*)

LLEWELLYN JONES and his colleagues[33, 34, 56] have investigated the influence of oxide layers on tungsten electrodes for short gaps in air. Some results are shown in *Figure 258*, which gives the number of break-downs recorded as a function of the observed time-lags[33]. Curve *A* is for heavily oxidized tungsten, curve *B* for slightly oxidized

tungsten and curve *C* for clean electrodes. No external form of irradiation was used in the investigations. From these and other experiments Llewellyn Jones and his colleagues conclude that the oxide layer enhances the yield of electrons by field emission from the cathode.

The influence of the surface condition of the electrodes becomes very pronounced at pressures above atmospheric[56–58].

Difference between positive and negative characteristics of sphere gaps

Many observations have been made of the difference between the positive and negative impulse calibration curves for sphere gaps but there is still appreciable divergence between the results obtained by the various investigators.

In 1930, McMillan and Starr[59] made a study of the 6·25 cm. and 25 cm. diameter sphere gaps, with one sphere earthed, when subjected to impulse and to power-frequency voltages. For short spacings the break-down curves coincided but with increasing spacing the positive impulse curve rose above the negative impulse curve, which was found to agree with the power-frequency curve. The difference between the positive and negative impulse curves, for a spacing of 15 cm. between 25 cm. diameter spheres, amounted to 20 per cent. The investigations were continued by McMillan[60] who explained the results in terms of space-charges. No measurements were made of the influence of irradiation on the behaviour of the gaps.

Subsequent experiments by Fielder[61], Meador[62], Bellaschi and McAuley[63], Dattan[64], and Davis and Bowdler[5] showed that similar results obtained for larger spheres, up to 200 cm. diameter. The measurements were checked by oscillographic observations. It was noticed that the 6·25 and 12·5 cm. diameter spheres behaved more erratically than spheres of larger diameter, and the suggestion is made by Meador[62] that this may be an indication of time-lag but the effects of irradiation were not studied. In the measurements by Davis and Bowdler[5], with impulse voltages up to 1,000 kV, it was found that the negative impulse break-down voltage may exceed the power-frequency break-down voltage by up to about 8 per cent., for spacings of a sphere radius. The corresponding difference for the positive impulse break-down voltage may be as great as 10 per cent. The difference between the positive and negative impulse break-down voltages, at a spacing of a sphere radius, was not more than 4 per cent. as compared with a difference of up to 8 per cent. in Meador's results[62]. The difference between the positive and negative values given by Dattan[64] varies up to 15 per cent.

Experiments have been made by Meek[7] to observe the influence of irradiation on the polarity effect. *Figure 250* shows the results obtained with a 12·5 cm. gap between spheres of 25 cm. diameter, when un-irradiated and when irradiated with 0·5 mg. of radium in the high

voltage sphere. The 50 per cent. break-down voltage is reduced by irradiation from about 311 to 291 kV for a positive impulse and from about 285 to 281 kV for a negative impulse. Similar results are obtained by Meek for the break-down of gaps between spheres of 6·25 cm. and 12·5 cm. diameter. These results may be expressed in the manner shown in *Figure 259*, which gives the percentage difference between the

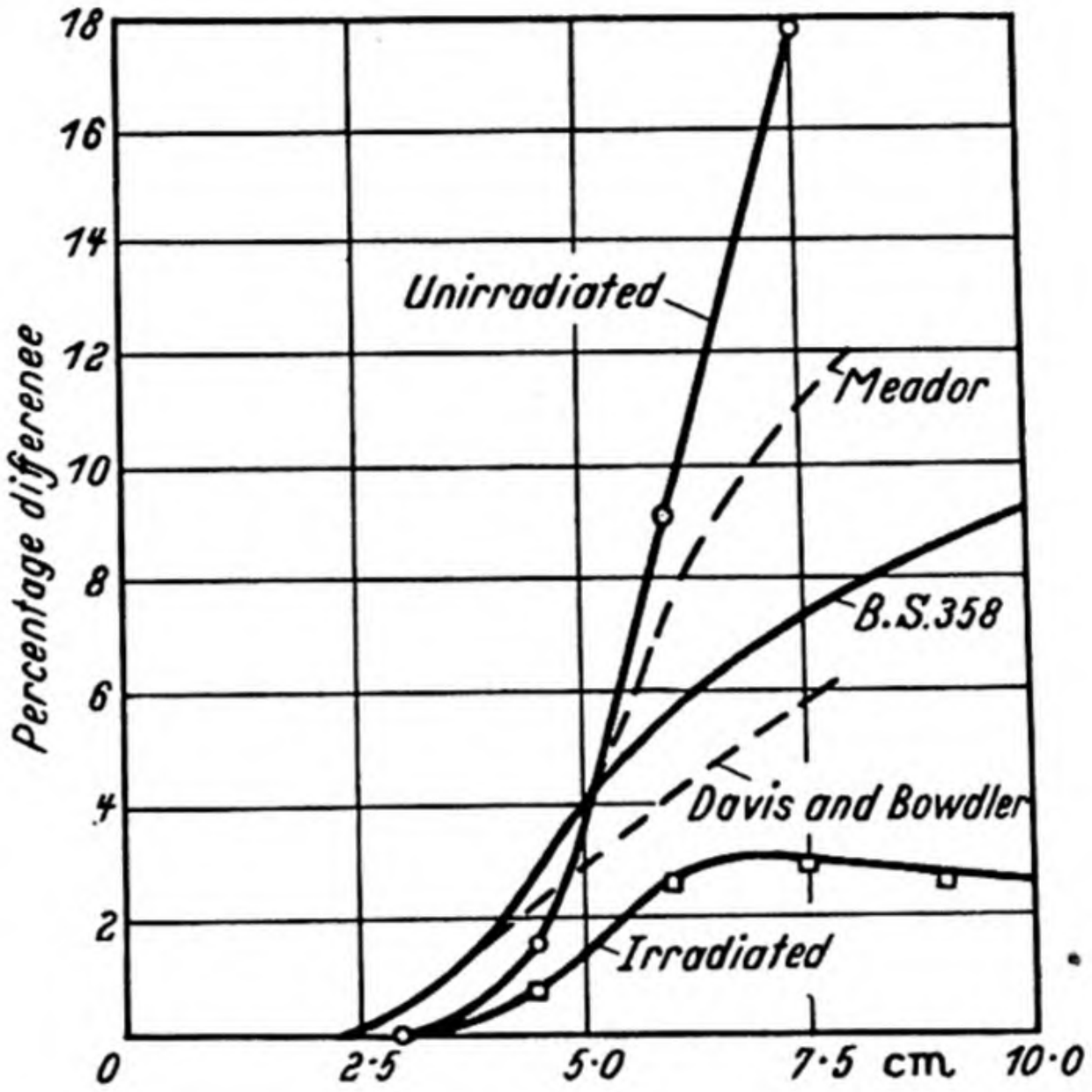

Figure 259. Variation with gap length of the difference between the positive and negative impulse break-down voltages (50% values), expressed as a percentage of the negative value, for a 12·5 cm diameter sphere gap. The curves marked "irradiated" and "unirradiated" were obtained with a 1/50 impulse wave. (Meek[7], by courtesy, *J. Inst. elect. Engrs.*)

positive and negative impulse break-down voltages as a function of the gap length between spheres of 12·5 cm. diameter. The curves obtained by Meek for the unirradiated and the irradiated gaps roughly enclose the earlier measured values[1, 5, 62].

Curves showing the percentage difference between the positive and negative impulse break-down voltages as a function of the ratio of the spacing S to the sphere radius R are given in *Figure 260*, where they are compared with the corresponding B.S. 358 values. No polarity difference is observed for an irradiated 6·25 cm. sphere-gap up to $S/R = 1$. For $1 < S/R < 1{\cdot}6$ the positive impulse break-down voltage exceeds the negative value by a small amount, but for $S/R > 1{\cdot}6$ the positive value falls below the negative value. At $S/R = 2{\cdot}0$ the positive impulse break-down voltage is 6 per cent. less than the negative value, whereas B.S. 358 shows the positive value to exceed the negative value by 10·4 per cent. The curves for the irradiated gaps tend towards the B.S. 358 curves for the larger sphere sizes.

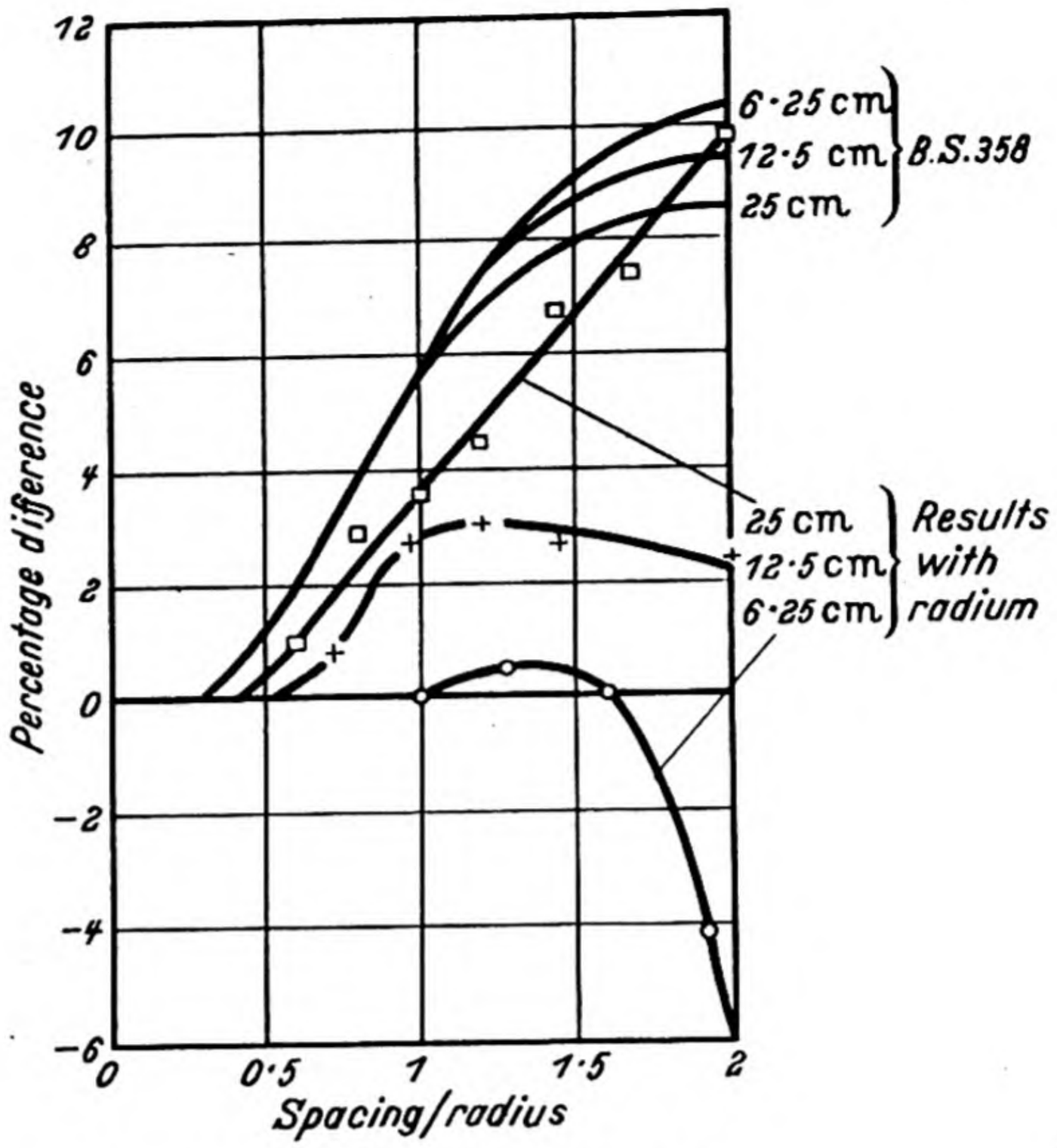

Figure 260. Percentage difference between the positive and negative impulse break-down voltages as a function of the ratio of spacing to sphere radius, for spheres of 6·25 cm, 12·5 cm and 25 cm diameter. (Meek[7], by courtesy, *J. Inst. elect. Engrs.*)

Meek's results clearly show that the positive impulse calibration of sphere gaps is influenced by irradiation and that there is therefore a need for a revision of the values given in B.S. 358. More precise specifications concerning irradiation are also needed to reduce the scatter between the results obtained in different laboratories.

ROD GAPS

The break-down of a rod gap may be used to measure the approximate peak value of an impulse voltage, and calibration data for this purpose has been issued in the American Standards[2]. The subject has been considered in detail by ALLIBONE[65] who has compared the results obtained in European and American laboratories[65–79].

In the European measurements, which were made under the auspices of the International Electrotechnical Commission[65] the electrodes are supported horizontally in the same straight line and at a distance above ground between 1·5 and 2 times the spacing. The electrodes are usually mounted on porcelain pedestal insulators and overhang from their supports by a distance of not less than one-half the electrode spacing. One electrode is earthed and the other is connected to the high-voltage

source. Both 1/5 and 1/50 impulse waves are used, and adjustment of the peak voltage of the wave is made until break-down occurs for about 90 per cent. of the applied impulses. The voltage is measured by a sphere gap. A similar procedure is followed in the American calibrations, except that a 1·5/40 wave is used instead of a 1/50 wave, and also the minimum impulse break-down voltage is defined as that at which 50 per cent. of the applied impulses cause break-down to occur. This minimum impulse break-down criterion has now been adopted by the I.E.C.

The break-down voltage of a rod gap depends upon the relative air density, in the same manner as for a sphere gap (*see* page 236). It also varies with the humidity and corrections have to be made accordingly[2, 65–67, 69, 74]. The correction factors are based on the data given by FIELDER[66] and vary with the polarity and wave-form of the applied impulse, as shown in *Figure 261*. Conversion curves from relative

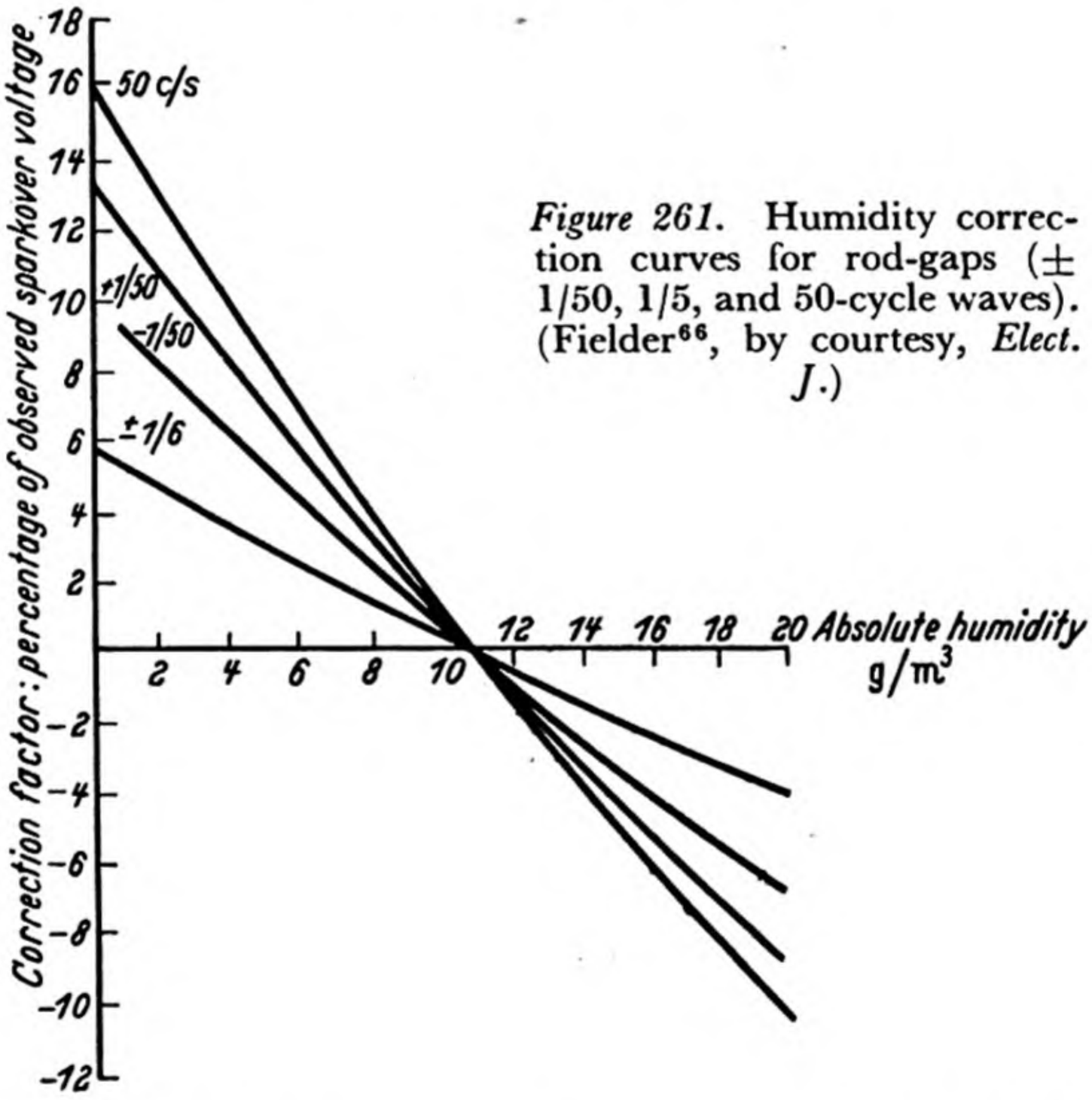

Figure 261. Humidity correction curves for rod-gaps (± 1/50, 1/5, and 50-cycle waves). (Fielder[66], by courtesy, *Elect. J.*)

humidities at various temperatures to absolute humidities are given in *Figure 262*. The I.E.C. standard humidity is 11 gm. per m.^{3}, corresponding to a relative humidity of 64 per cent. at 20° C. There is some doubt as to the accuracy of Fielder's curves, as shown by the subsequent measurements by LEBACQZ[67].

In his analysis of the results from eight European laboratories, Allibone[65] points out that there is a maximum deviation of 10 per cent. for the ± 1/50 waves and of 7 per cent. for the ± 1/5 waves. It is possible that the wide dispersion may be caused partly by differences in the circuits and in the discharge capacitances of the impulse generators

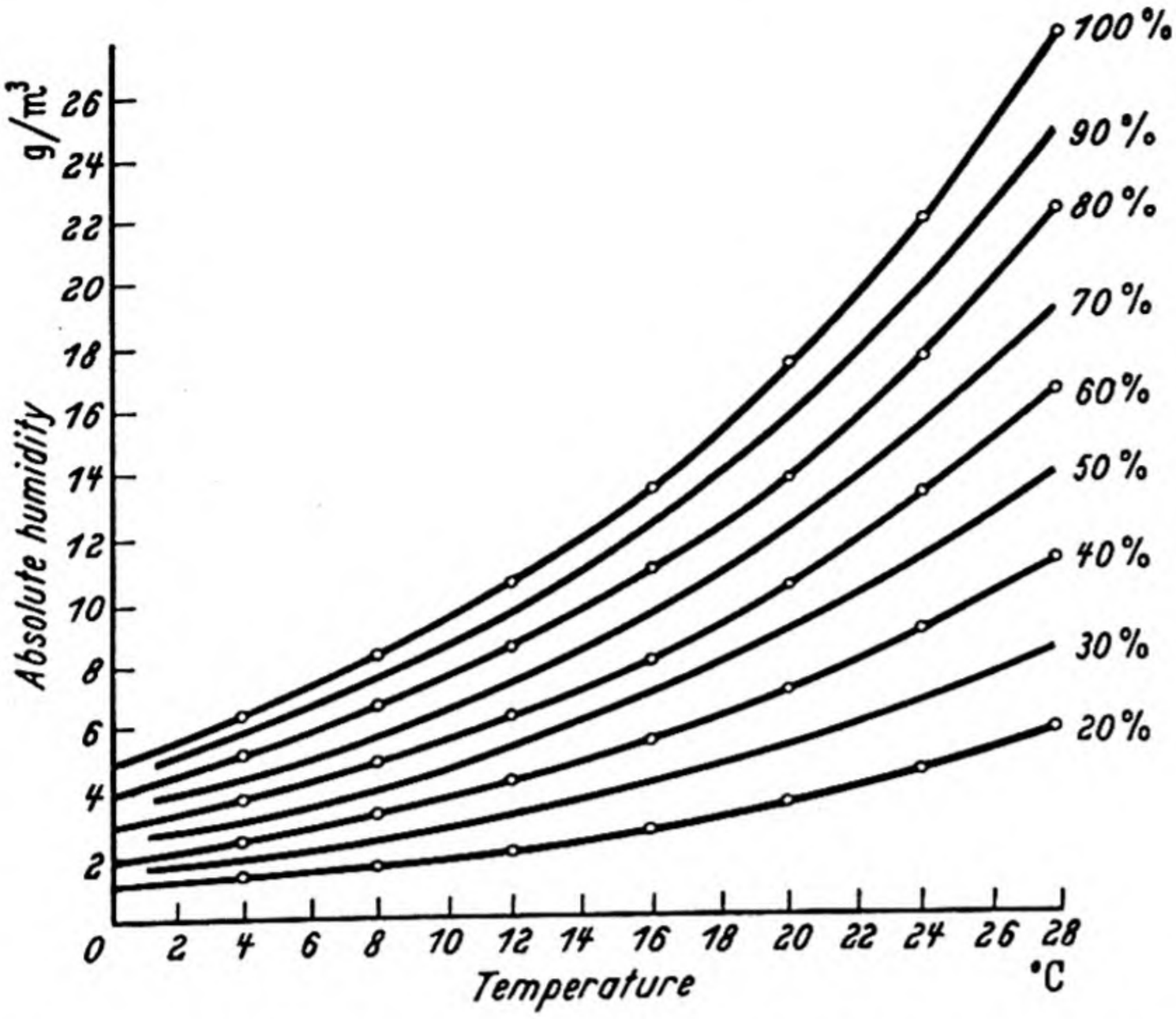

Figure 262. Relation between percentage humidity and absolute humidity at various temperatures. (Fielder[66], by courtesy, *Elect. J.*)

used[68]. Errors may also have been introduced by the sphere gap techniques used in the voltage measurements[7]. The maximum deviation in the results from five American laboratories is 5 per cent. for both the + 1/5 and the + 1·5/40 waves.

Values of the break-down voltages of rod gaps, for several gap lengths, as given by the mean I.E.C. and the mean U.S.A. calibration, are listed in *Table XXX*[65]. The I.E.C. values have been corrected from the

TABLE XXX. IMPULSE BREAK-DOWN OF ROD GAPS

Comparison between I.E.C. values and U.S.A. values[65]. Values quoted are for gaps in air at 20°C., 760 mm. Hg., with a humidity of 11 gm. per m.³

Gap length in cm.	I.E.C. + 1/50	U.S.A. + 1·5/40	I.E.C. − 1/50	U.S.A. − 1·5/40	I.E.C. + 1/5	U.S.A. + 1/5	I.E.C. − 1/5	U.S.A. − 1/5
5	56	57	61	60	60	59	66	61
10	90	88–92	97	99	101	96	111	102
15	129	121–132	135	136	139	140	155	143
20	160	153–160	178	175	179	183	208	184
25	195	185	221	217	217	230	257	230
30	226	217	262	254–265	256	271	301	269
40	279	279	339	315–350	348	355	392	351
50	334	338	407	391–401	431	433	475	435
60	393	397	470	463	513	510	557	520
80	511	515	585	590	657	670	701	695
100	629	627	703	715	820	825	855	860
120	752	745	807	850				

90 per cent. break-down criterion to the 50 per cent. break-down criterion so as to conform with American practice; this correction is made by reducing all the observed values by 4 per cent.[70]. The U.S.A.

values are corrected to the I.E.C. standards of temperature and humidity. In the U.S.A. calibration[2, 69] an uncertainty range is given for gaps between 8 and 20 cm. for a + 1·5/40 wave and between 30 and 50 cm. for a − 1·5/40 wave. Allibone[65] has concluded that in any experiments involving rod-gaps a considerable latitude of ± 8 per cent., should be made in the application of the existing calibration data.

OSCILLOGRAPHIC MEASUREMENTS

Accurate records of the wave-form are necessary in most impulse voltage measurements, and it is usual therefore to record the wave by means of a cathode-ray oscillograph which is connected to the circuit through a potential divider. Full details of typical oscillographs and potential dividers are given in Chapters 9 and 10.

Knowledge of the wave-form is essential if a sphere gap is being used to measure the peak value of the impulse. As stated in B.S. 358, the sphere gap calibration tables are satisfactory for impulse voltages having wave-fronts > 1 μsec and times-to-half-value > 5 μsec. Consequently, when the sphere gap is connected in parallel with a test object which is breaking down on the wave-front of the impulse, the sphere gap cannot be relied upon to give an accurate measurement of the peak break-down voltage. Again, it is necessary for accurate sphere gap measurements to ensure that the crest of the wave is free from superimposed high-frequency oscillations which may lead to spurious results.

The oscillographic technique can be used to measure the peak value of an impulse voltage. It has the advantage over the sphere gap in that the peak value of a single impulse can be recorded whereas 10 or more impulses of the same peak value must be applied to a sphere gap if a reliable measurement is to be obtained. The oscillographic technique can also be used to measure break-down voltages when break-down is occurring on the wave-front or when the peak voltages of impulse waves are of shorter duration that the minimum value of 1/5 specified in B.S. 358.

Davis and Bowdler[5] have made a careful study of the accuracy of measurement of the peak value V of an impulse voltage by means of a resistance potential divider and a cathode-ray oscillograph. In these investigations the voltage v applied to the oscillograph plates is kept approximately constant by varying the value of R_2, the resistance of the low-voltage section of the divider. The resistance R_1 of the high-voltage section of the divider is kept constant. In order to determine the voltage from the oscillographic record it is necessary to measure two deflections, one corresponding to the crest of the wave and the other to the calibrating voltage. Each of these deflections can be measured to an accuracy of within 0·5 per cent. If 0·5 per cent. is allowed for error in the setting of the calibrating voltage and of the accelerating

voltage, the possible error in the determination of v is about 2 per cent. The possible error in deriving V from v, from a knowledge of the ratio of R_1 to R_2, is less than 1 per cent., and therefore the total possible error, neglecting any uncertain systematic errors, is less than 3 per cent. Davis and Bowdler conclude that the probable error in the determination of the break-down voltage of a sphere-gap, as measured by their oscillographic technique, can be reduced to about 1 per cent. by averaging the results of a sufficient number of observations. Other experiments relating to the comparative accuracies of sphere-gaps and of oscillographic techniques for voltage measurement are described by Berger and Robinson[80] and by Goossens and Provoost[81].

THE KLYDONOGRAPH OR SURGE RECORDER

Because of the random nature of lightning and its relative infrequency of occurrence it is necessary to instal a large number of suitable recording devices in order to obtain a reasonable amount of data concerning the voltage and current surges produced on transmission lines and associated electrical apparatus. Some fairly simple devices have been developed for this purpose. Among these is the klydonograph[82–92], in which use is made of the patterns, known as Lichtenberg figures, which are produced on a photographic film or plate by a surface corona discharge[93–99]. The klydonograph may be used with a resistance shunt

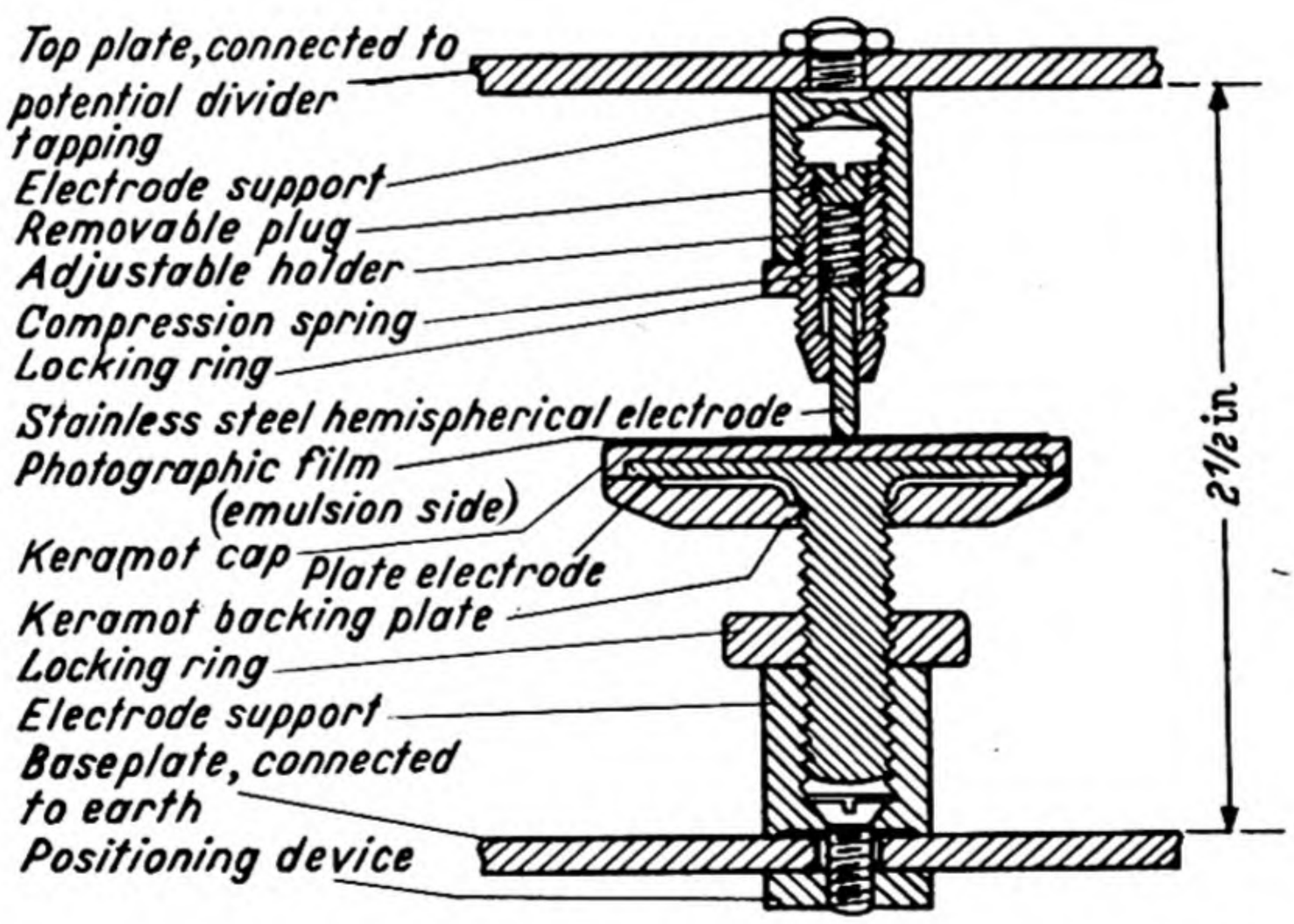

Figure 263. Sectional view of normal electrode pair in klydonograph. (Candler[89], by courtesy, *J. Inst. elect. Engrs.*)

to measure a current surge or with a potential divider to measure a voltage surge. In each case the resultant surge voltage is applied between two electrodes which are placed on opposite sides of a photographic film. A typical electrode arrangement is shown in *Figure 263*[89].

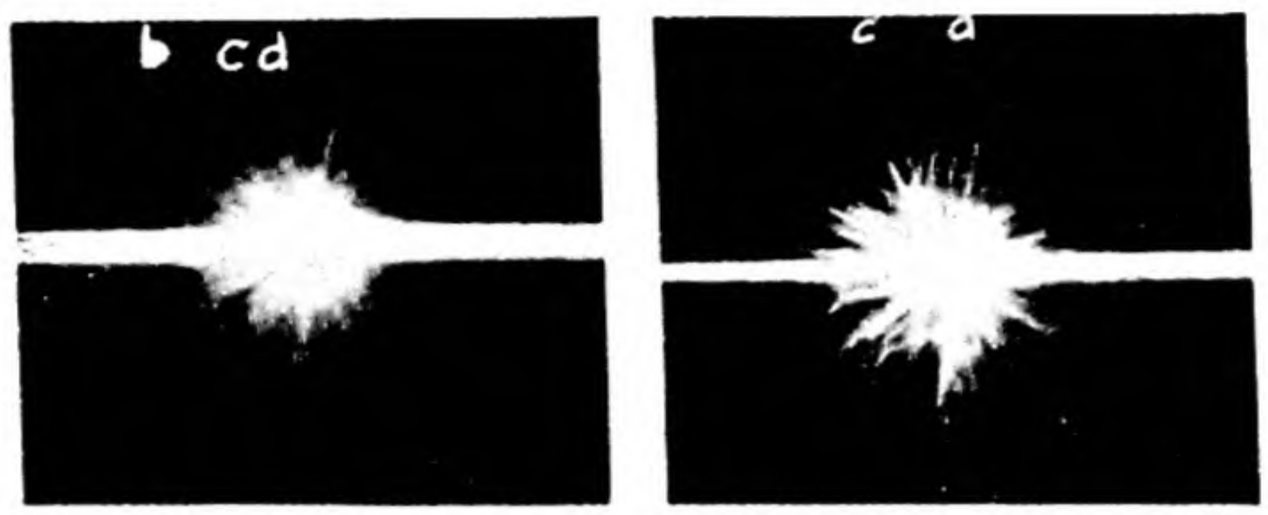

Figure 264. Klydonograms of voltages on transmission-line conductors, due to direct lightning strokes to the transmission line. (Perry, Webster and Baguley[91], by courtesy, *J. Inst. elect. Engrs.*)

Right : reverse film, *i.e.* plane electrode at high voltage-point electrode earthed.

Left : normal film, *i.e.* point electrode at high voltage-plane electrode earthed.

From the nature of the figure which appears on the film after development the polarity of the voltage surge can be deduced. *Figure 264* shows some figures obtained with positive and negative surges applied to the smaller electrode[91]. The mean size of the figure depends mainly on the peak value of the applied voltage, but it is influenced also by the wave-shape. Even for a fixed wave-shape and a given peak voltage considerable fluctuations occur in the size of the figure produced. *Figure 265* shows some curves obtained by CANDLER[89]

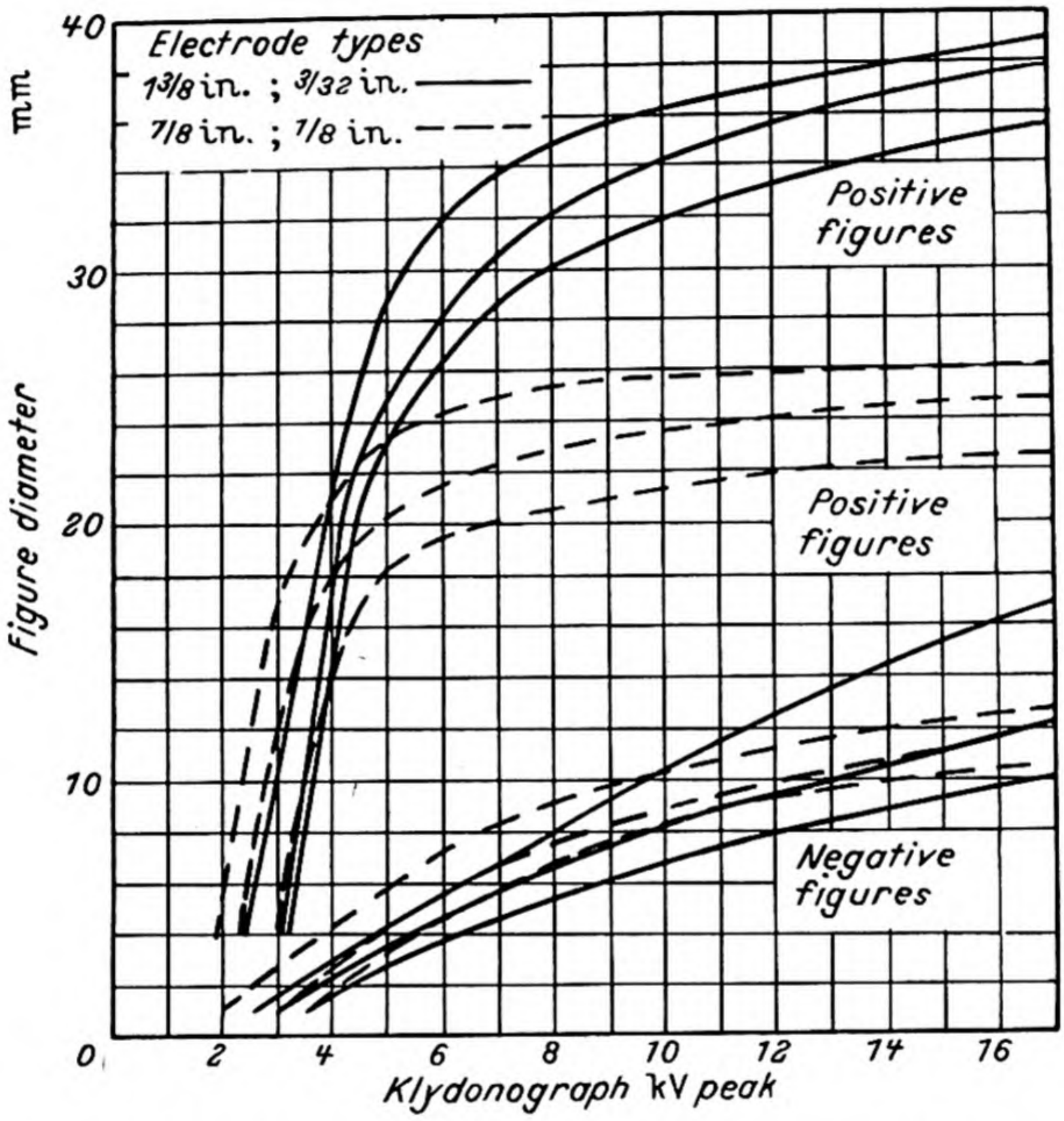

Figure 265. Impulse calibration curves, connecting figure size with probable, maximum and minimum voltages. Two types of electrodes; positive 1/50μ sec impulses (Candler[89], by courtesy, *J. Inst. elect. Engrs.*).

for the variation of figure diameter with peak voltage for 1/50 waves applied to an electrode arrangement of the form shown in *Figure* 263. Three curves are given for each condition and correspond to the probable, minimum and maximum peak voltages required to produce a pattern of given diameter.

Instruments have been built with several elemnets for recording a number of surge voltages simultaneously and a moving film is used between the electrodes to enable successive surges to be measured[89–91]. The accuracy of the technique is generally considered to be no better than about ± 25 per cent. for peak voltage measurement. It is usual

for pairs of electrodes to be connected in parallel, one pair with a high-voltage point and an earthed plate, and the other pair with a high-voltage plane and an earthed point. In this way both a positive figure and a negative figure are produced for each surge voltage, as shown in *Figure 264*. Because of its greater size the positive figure is generally used to determine the surge voltage. This is particularly necessary in the measurement of surges on transmission lines, or other such apparatus, where the continuously-applied alternating voltage gives a black band along the centre of the film caused by the superposition of positive and negative figures produced on each half-cycle. A negative figure resulting from a surge voltage of peak value up to twice the line voltage may then be marked by the band, the width of which is governed largely by the positive figures formed by the line voltage.

MISCELLANEOUS METHODS

A circuit has been described by BOWDLER[101] for the measurement of the peak value of impulse voltages by the use of a potential divider and a ballistic galvanometer. The results obtained agree within 2 per cent. with those measured oscillographically, even with voltages lasting for times of the order of 10^{-7} sec.

An electronic peak voltmeter for the measurement of impulse voltages has been developed by BRYANT and NEWMAN[102]. It consists of ten electronic units biased in such a way that the application of an impulse voltage causes the operation of a number of the units, the number depending on the peak value of the impulse. The voltage range can be covered in 10 per cent. steps and when the voltage has been determined to within 10 per cent. the instrument can be switched to cover any required 10 per cent. range in steps of 1 per cent. Accuracies within 1 per cent. are claimed for the measurement of 1/5 waves.

REFERENCES

1 *Rules for the measurement of voltage with sphere-gaps*, British Standard No. 358, 1939.
2 *Measurement of test voltage in dielectric tests*, A.I.E.E. Standards No. 4, 1940.
3 *Rules for the measurement of voltage with sphere gaps*, Verband Deutscher Elektrotechniker : Specification 0430, 1939.
4 *Elektrotech. Z.* **60** (1939) 1309.
5 DAVIS, R., and BOWDLER, G. W. *J. Inst. elect. Engrs.*, **82** (1938) 645.
6 MEEK, J. M. *J. Inst. elect. Engrs.*, **89** (1942) 335.
7 MEEK, J. M. *J. Inst. elect. Engrs.* **93** (1946) 97.
8 VAN CAUWENBERGHE, R. *Bull. Soc. Franc Elect.*, **7** (1937) 1005.
9 GARFITT, D. E. M. *Proc. Phys. Soc.* **54** (1942) 109.
10 DILLON, J. H. *J. appl. Phys.*, **11** (1940) 291.
11 EVANS, R. D. *J. appl. Phys.*, **11** (1940) 561.
12 BERKEY, W. E. *Elect. J.*, **31** (1934) 101.
13 VAN CAUWENBERGHE, R., and MARCHAL, G. *Rev. Gen. Elect.*, **27** (1930) 331.
14 BERGER, K. *Assoc. Suisse des Elect. Bull.*, **24** (1933) 17.
15 STRIGEL, R. *Arch. Elektrotech.*, **27** (1933) 137.

[16] STRIGEL, R. *Elektrische Stössfestigkeit.*, Berlin, 1939.
[17] BRINKMAN, C. *Arch. Elektrotech.*, **33** (1939) 1, 121.
[18] STRIGEL, R. *Arch. Elektrotech.*, **27** (1933) 379.
[19] NORD, G. *Trans. Amer. Inst. elect. Engrs.*, **54** (1935) 955.
[20] SPRAGUE, C. S., and GOLD, G. *Trans. Amer. Inst. elect. Engrs.*, **56** (1937) 594.
[21] STRIGEL, R. *Arch. Elektrotech.*, **26** (1932) 803.
[22] STRIGEL, R. *Wiss. Veroff. Siemens-Werk.*, **11** (1932) 52.
[23] STREET, J. C., and BEAMS, J. W. *Phys. Rev.*, **38** (1931) 416.
[24] WHITE, H. J. *Phys. Rev.*, **46** (1934) 99.
[25] WILSON, R. R. *Phys. Rev.*, **50** (1936) 1082.
[26] SNODDY, L. B. *Phys. Rev.*, **40** (1932) 409.
[27] FLOWERS, J. W. *Phys. Rev.*, **48** (1935) 954.
[28] WHITE, H. J. *Phys. Rev.*, **49** (1936) 507.
[29] WYNN WILLIAMS, C. E. *Phil. Mag.*, **1** (1926) 353.
[30] MORGAN, J. D. *Phil. Mag.*, **4** (1927) 91.
[31] BERKEY, W. E. *Trans. Amer. Inst. elect. Engrs.*, **59** (1940) 429.
[32] SLEPIAN, J., and BERKEY, W. E. *J. appl. Phys.*, **11** (1940) 765.
[33] LLEWELLYN JONES, F. *Proc. Phys. Soc. B.*, **62** (1949) 366.
[34] LLEWELLYN JONES, F., and MORGAN, C. G. *Phys. Rev.*, **82** (1951) 970.
[35] HARDY, D. R., and CRAGGS, J. D. *Trans. Amer. Inst. elect. Engrs.*, **69** (1950) 584.
[36] HARDY, D. R., and CRAGGS, J. D. *Nature*, **164** (1949) 356.
[37] MEEK, J. M., and CRAGGS, J. D. *Electrical Breakdown in Gases.* London, 1953.
[38] ROGOWSKI, W., and WALLRAFF, A. *Z. Phys.*, **97** (1935) 758.
[39] ROGOWSKI, W., and FUCKS, W., *Arch. Elektrotech.*, **29** (1935) 362.
[40] ROGOWSKI, W., and WALLRAFF, A. *Z. Phys.*, **102** (1936) 183.
[41] ROGOWSKI, W. *Z. Phys.*, **114** (1940) 1.
[42] WALLRAFF, A., and HORST, E. *Arch. Elektrotech.*, **31** (1937) 789.
[43] BRINKMAN, C. *Z. Phys.*, **111** (1939) 737.
[44] FUCKS, W., and SCHUMACHER, G. *Z. Phys.*, **112** (1939) 605.
[45] FUCKS, W., and BONGARTZ, H. *Z. tech. Phys.*, **20** (1939) 205.
[46] FUCKS, W. *Z. Phys.*, **98** (1936) 11.
[47] FUCKS, W., and SEITZ, W. *Z. tech. Phys.*, **17** (1936) 387.
[48] WHITE, H. J. *Phys. Rev.*, **48** (1935) 113.
[49] ROGOWSKI, W., and WALLRAFF, A. *Z. Phys.*, **106** (1937) 212.
[50] ROGOWSKI, W., and WALLRAFF, A. *Z. Phys.*, **108** (1938) 1.
[51] TOEPLER, M. *Phys. Z.*, **40** (1939) 206.
[52] ARNOLD, M. *Phys. Z.*, **40** (1939) 687.
[53] MEEK, J. M. *Proc. Phys. Soc.*, **52** (1940) 547, 822.
[54] JØRGENSEN, M. O. *Elektrische Funkenspannungen.* Copenhagen, 1943.
[55] CLAUSSNITZER, J. *Phys. Z.*, **34** (1933) 791.
[56] LLEWELLYN JONES, F. J., and DE LA PERRELLE, E. T. *Nature*, **168** (1951) 160.
[57] HOWELL, A. H. *Trans. Amer. Inst. elect. Engrs.*, **58** (1939) 193.
[58] FELICI, N., and MARCHAL, Y. *Rev. Gen. Elec.*, **57** (1948) 155.
[59] MCMILLAN, F. O., and STARR, E. C. *Trans. Amer. Inst. elect. Engrs.*, **48** (1929) 246 ; **50** (1931) 23.
[60] MCMILLAN, F. O. *Trans. Amer. Inst. elect. Engrs.*, **53** (1934) 942 ; **58** (1939) 56.
[61] FIELDER, F. D. *Elect. World*, **102** (1933) 433.
[62] MEADOR, J. R. *Trans. Amer. Inst. elect. Engrs.*, **53** (1934) 942.
[63] BELLASCHI, P. L., and MCAULEY, P. H. *Elect. J.*, **31** (1934) 228.
[64] DATTAN, W. *Elektrotech. Z.*, **57** (1936) 377, 412.
[65] ALLIBONE, T. E. *J. Inst. elect. Engrs.*, **81** (1937) 741.
[66] FIELDER, F. D. *Elect. J.*, **32** (1935) 543.
[67] LEBACQZ, J. V. *Trans. Amer. Inst. elect. Engrs.*, **60** (1941) 44.

[68] HAGENGUTH, J. H. *Trans. Amer. Inst. elect. Engrs.*, **60** (1941) 803.
[69] EEI-NEMA Report on "Flashover Characteristics of rod-gaps and insulators". *Elect. Engng.*, **56** (1937) 712.
[70] JACOTTET, P. *Elektrotech. Z.*, **58** (1937) 628.
[71] BELLASCHI, P. L., and TEAGUE, W. L. *Elect. J.*, **32** (1935) 56.
[72] BELLASCHI, P. L., and TEAGUE, W. L. *Trans. Amer. Inst. elect. Engrs.*, **53** (1934) 1638.
[73] FIELDER, F. D. *Elect. J.*, **29** (1932) 459.
[74] BELLASCHI, P. L., and MCAULEY, P. H. *Trans. Amer. Inst. elect. Engrs.*, **59** (1940) 669.
[75] WANGER, W. *Bull. Assoc. Suisse Elect.*, **34** (1943) 193.
[76] BELLASCHI, P. L., and EVANS, P. *Trans. Amer. Inst. elect. Engrs.*, **63** (1944) 236.
[77] ALLIBONE, T. E., HAWLEY, W. G., and PERRY, F. R. *J. Inst. elect. Engrs.*, **78** (1936) 257.
[78] GOREV, A. A., ZALESKY, A. M., and RIABOV, B. M. *C.I.G.R.E. Paper* No. 142, 1948.
[79] ALLIBONE, T. E., and PERRY, F. R. *J. Inst. elect. Engrs.*, **78** (1936) 257.
[80] BERGER, K., and ROBINSON, B. C. *Bull. Assoc. Suisse Elect.*, **31** (1940) 157.
[81] GOOSSENS, R. F., and PROVOOST, P. G. *Bull. Assoc. Suisse Elect.*, **37** (1946) 175.
[82] PETERS, J. F. *Elect. World.*, **83** (1924) 769.
[83] COX, J. H., and LEGG, J. W. *Trans. Amer. Inst. elect. Engrs.*, **44** (1925) 857.
[84] LEE, E. S., and FOUST, C. M. *Trans. Amer. Inst. elect. Engrs.*, **46** (1927) 339.
[85] MCEACHRON, K. B. *Trans. Amer. Inst. elect. Engrs.*, **45** (1926) 712.
[86] COX, J. H., MCAULEY, P. H., and HUGGINS, L. C. *Trans. Amer. Inst. elect. Engrs.*, **46** (1927) 315.
[87] LEWIS, W. W. and FOUST, C. M. *Trans. Amer. Inst. elect. Engrs.*, **49** (1930) 389.
[88] BERGER, K. *Bull. Assoc. Suisse Elect.*, **27** (1936) 145.
[89] CANDLER, J. H. *J. Inst. elect. Engrs.*, **87** (1940) 597.
[90] PERRY, F. R. *J. Inst. elect. Engrs.*, Part II, **88** (1941) 69.
[91] PERRY, F. R., WEBSTER, G. H., and BAGULEY, P. W. *J. Inst. elect. Engrs.*, Part IIA, **89** (1942) 185.
[92] WAGHORNE, J. H. *Trans. Amer. Inst. elect. Engrs.*, **66** (1947) 1114.
[93] JØRGENSEN, M. O. *Ingenioevidenskabelige Skrifter*, A. No. 37 (1934).
[94] KROEMER, H. *Arch. Elektrotech.*, **28** (1934) 703.
[95] PEDERSEN, P. O. *On Lichtenberg figures*. Copenhagen, 1919.
[96] MERRILL, F. H., and VON HIPPEL, A. *J. appl. Phys.*, **10** (1939) 873.
[97] PLEASANTS, J. G. *Elect. Engng.*, **53** (1934) 300.
[98] MAGNUSSON, C. E. *Trans. Amer. Inst. elect. Engrs.*, **49** (1930) 756 ; **51** (1932) 117.
[99] PRAETORIUS, G. *Arch. Elektrotech.*, **34** (1940) 83.
[100] ROGOWSKI, W., MARTIN, O., and THIELEN, H. *Arch. Elektrotech.*, **35** (1941) 421.
[101] BOWDLER, G. W. *J. Instn. elect. Engrs.*, **89** (1942) 555.
[102] BRYANT, J. M., and NEWMAN, M. *Trans. Amer. Inst. elect. Engrs.*, **59** (1940) 807.

9

POTENTIAL DIVIDERS FOR HIGH VOLTAGE MEASUREMENT : D.C., A.C. AND IMPULSES

D.C. POTENTIAL DIVIDERS

The measurement of high voltages, d.c., has been discussed in Chapter 7 where for example a description is given of the use of resistance voltmeters in which the measurement of the current flowing through a known resistance serves to measure the voltage. These devices are analytically indistinguishable from potential dividers, to be described here, although usually with the latter a low voltage is measured by means of an electrostatic voltmeter or potentiometer tapped across part of the resistance chain. Hence the resistances mentioned in Chapter 7 can be made up as d.c. potential dividers, in obvious ways. Certain special developments of d.c. resistance potential dividers will now be discussed.

Some recent measurements on a precision high-voltage resistance potentiometer for d.c. are due to RYMER and WRIGHT[1] who worked with potentials of the order of 50 kV and were able to obtain an

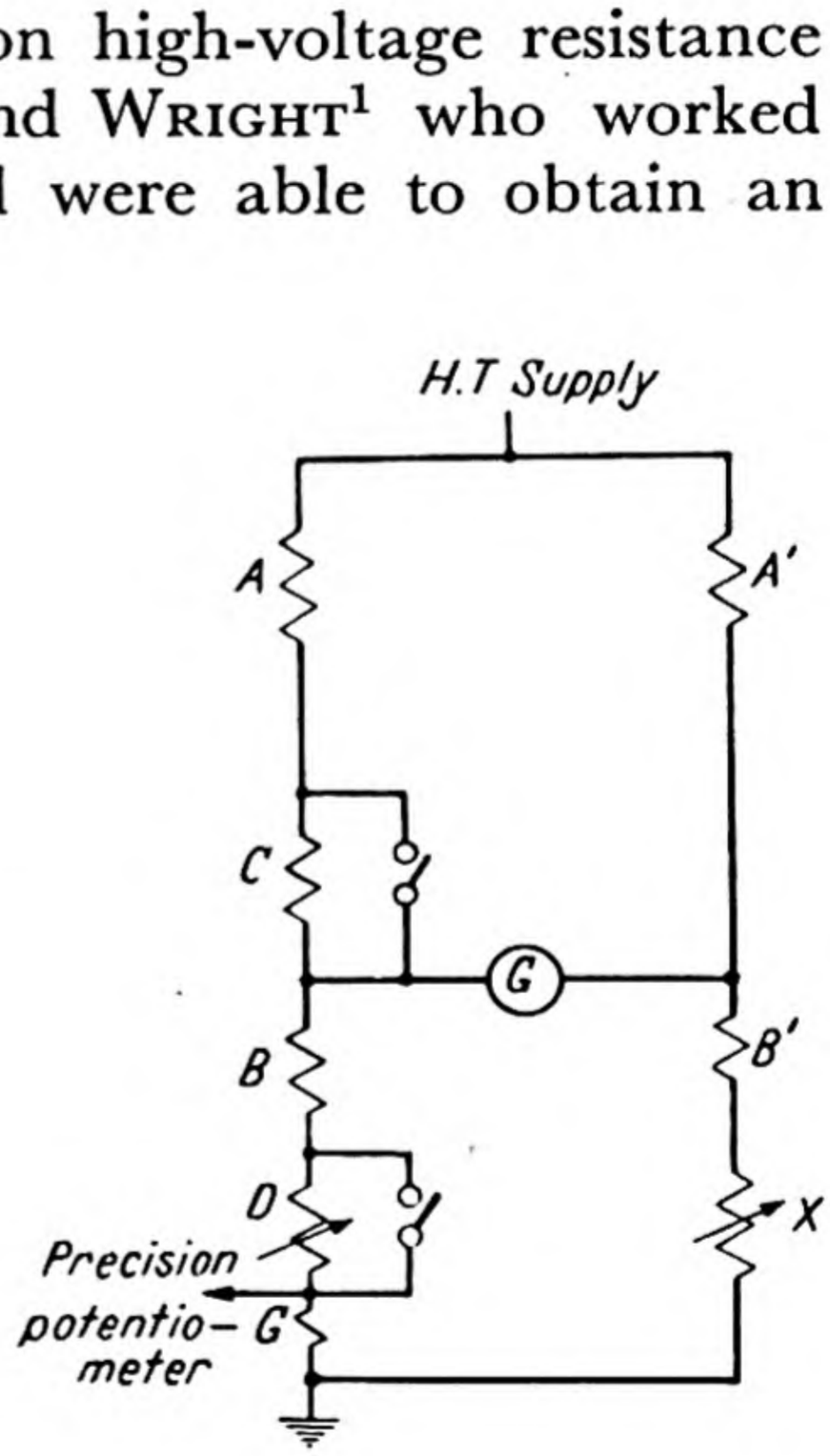

Figure 266. Simplified circuit of potentiometer (Rymer and Wright[1] by courtesy, *J. Sci. Instrum.*).

accuracy of 0·01 per cent. The method enables the potentiometer ratio to be measured whilst the h.t. is applied, thus eliminating non-linear leakage effects. The basic circuit is shown in *Figure 266*. With *C* and *D* shorted, the p.d. across *G*, which is about 3 V, is measured with

a precision potentiometer reading to 10 μV and so, in order to find the h.t. voltage the ratio

$$(A+B+G)/G = (A+B+G)/(B+G) \times (B+G)/G$$

must be found. Since $(B+G) \sim 1$ MΩ, with a voltage drop of only about 500 V, corona and leakage difficulties do not arise and B and G can be measured with an ordinary bridge. However, the ratio $(A+B+G)/(B+G)$ must be measured with the h.t. applied and Rymer and Wright used the circuit of *Figure 267* for this purpose. The Wheatstone

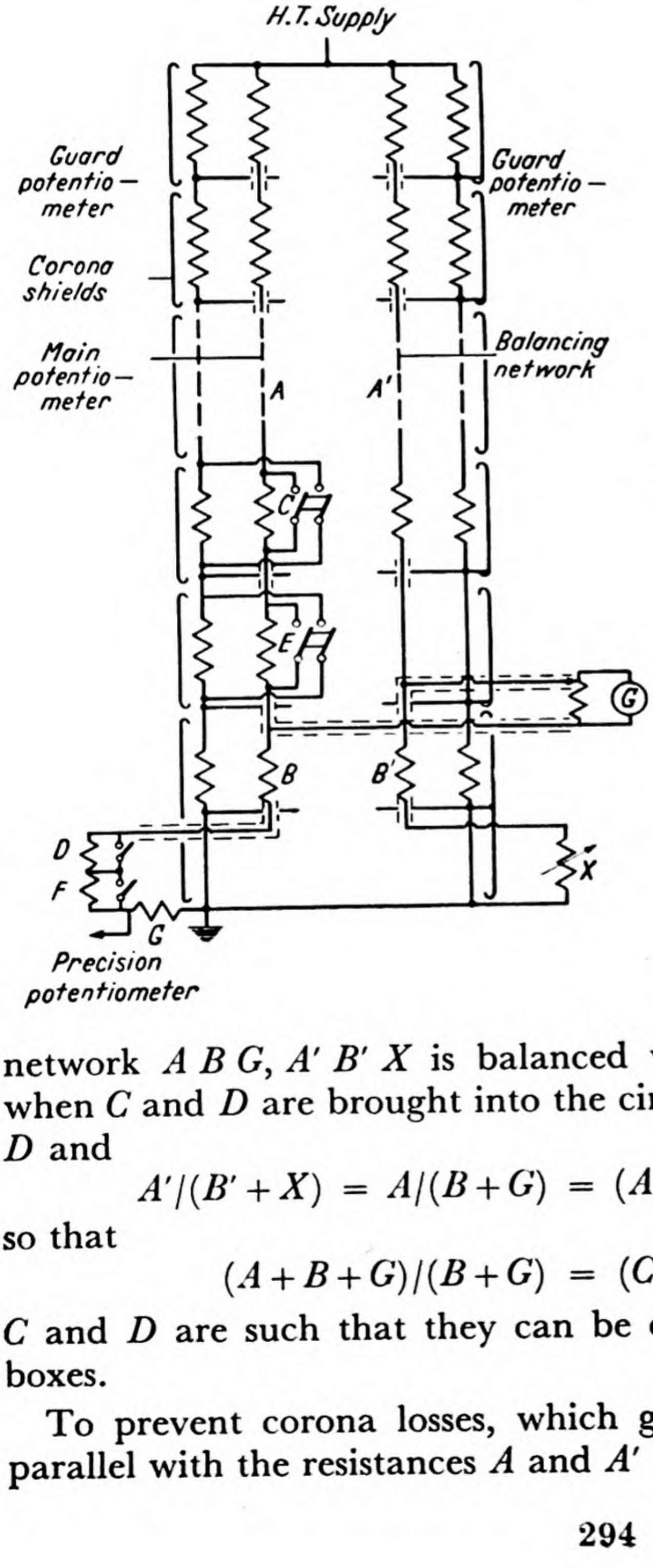

Figure 267. Complete potentiometer circuit (Rymer and Wright[1], by courtesy, *J. Sci. Instrum.*).

network $A\ B\ G$, $A'\ B'\ X$ is balanced with X, C and D shorted but when C and D are brought into the circuit the bridge is balanced with D and

$$A'/(B'+X) = A/(B+G) = (A+C)/(B+D+G) = C/D$$

so that

$$(A+B+G)/(B+G) = (C+D)/D$$

C and D are such that they can be composed of ordinary resistance boxes.

To prevent corona losses, which give leakage currents flowing in parallel with the resistances A and A' Rymer and Wright use a system

of metal shields, surrounding the various sections of A and A', the potential of each being made equal to that of the low potential end of the appropriate unit of A or A'. For this purpose a separate voltage divider, which supplies the corona losses, is used.

The above authors discuss the stability requirements for the various resistance units, and find that if the potentiometer ratio $(A+B+G)/(B+G)$ is to be measured within a fraction $\pm e$ then D must be determined to within $\pm eD$. This is also the accuracy to which $(B+D+G)$ must be capable of adjustment. Further the resistances must possess temporal variations not exceeding ep of their mean value where p is the maximum allowable fraction of the h.t. voltage to appear across C. In the case quoted by Rymer and Wright where it was required to measure 50 kV to $\pm$ 0·01 per cent., and where the maximum voltage across C was 1 kV ($e = 10^{-4}$, $p = 0{\cdot}02$), it was necessary for the resistances to have a stability of 1 in 5×10^5 for, say, 3 mins. Also, the requisite galvanometer sensitivity was about 10^{-9} A and a photocell relay stabilized by negative feed-back was used[2]. Great care was taken to ensure adequate insulation between the resistor units in the potentiometers and the corona shields. The complete circuit, including the potentiometers used to apply the appropriate potentials to the corona shields as described above, is given in *Figure 267*, and details of one of the potentiometer elements are shown in *Figure 268*. The separate units are stacked in piles. The resistances A and A' (*see Figure 268*) are wire-wound and operate in conditions such that temperature variations are negligible.

The procedure for measuring the h.t. voltage is as follows : C, D, E and F are shorted (*Figure 267*) and the galvanometer circuit is balanced by varying X after which C and D are brought into circuit and balance is then obtained with D. Then with E and F in circuit, F is used to give balance and finally with E and F shorted the output from G is measured on a potentiometer. B, C, D, E, F and G are then measured on a precise Wheatstone bridge.

The above authors found, for example, that

$B = 416{,}225\,\Omega$ $\quad E = 977{,}790\,\Omega$ $\quad$ output from $G = 3{\cdot}41718$ V
$C = 895{,}580\,\Omega$ $\quad F = 10{,}036{\cdot}4\,\Omega$
$D = 9{,}192{\cdot}0\,\Omega$ $\quad G = 2{,}999{\cdot}0\,\Omega$

Hence $(C+D)/D = 98{\cdot}43_0$ and $(E+F)/F = 98{\cdot}42_4$ giving a mean value of $98{\cdot}42_7$ Also $(B+D+G)/G = 142{\cdot}85_3$ so that the h.t. was $98{\cdot}42_7 \times 142{\cdot}85_3 \times 3{\cdot}41718 = 48{\cdot}04_8$ kV.

This work probably represents the most recent precision measurement of D.C. voltages $\sim$ 50 kV. For many purposes, however, it is sufficient to determine the fluctuations in a stable supply as distinct from the more difficult measurements of *total* voltage, such as those described above.

The 1·25 MV Philips d.c. sets incorporate a potential divider system for measurement of the output voltage[3]. The resistance unit, which is shown at 16 in *Figure 41* (page 31), is oil-immersed, has a value of 1,500 MΩ and is composed of 2,000 carbon resistances of 0·75 MΩ each. A tap on the resistance near the earthed end of the unit leads

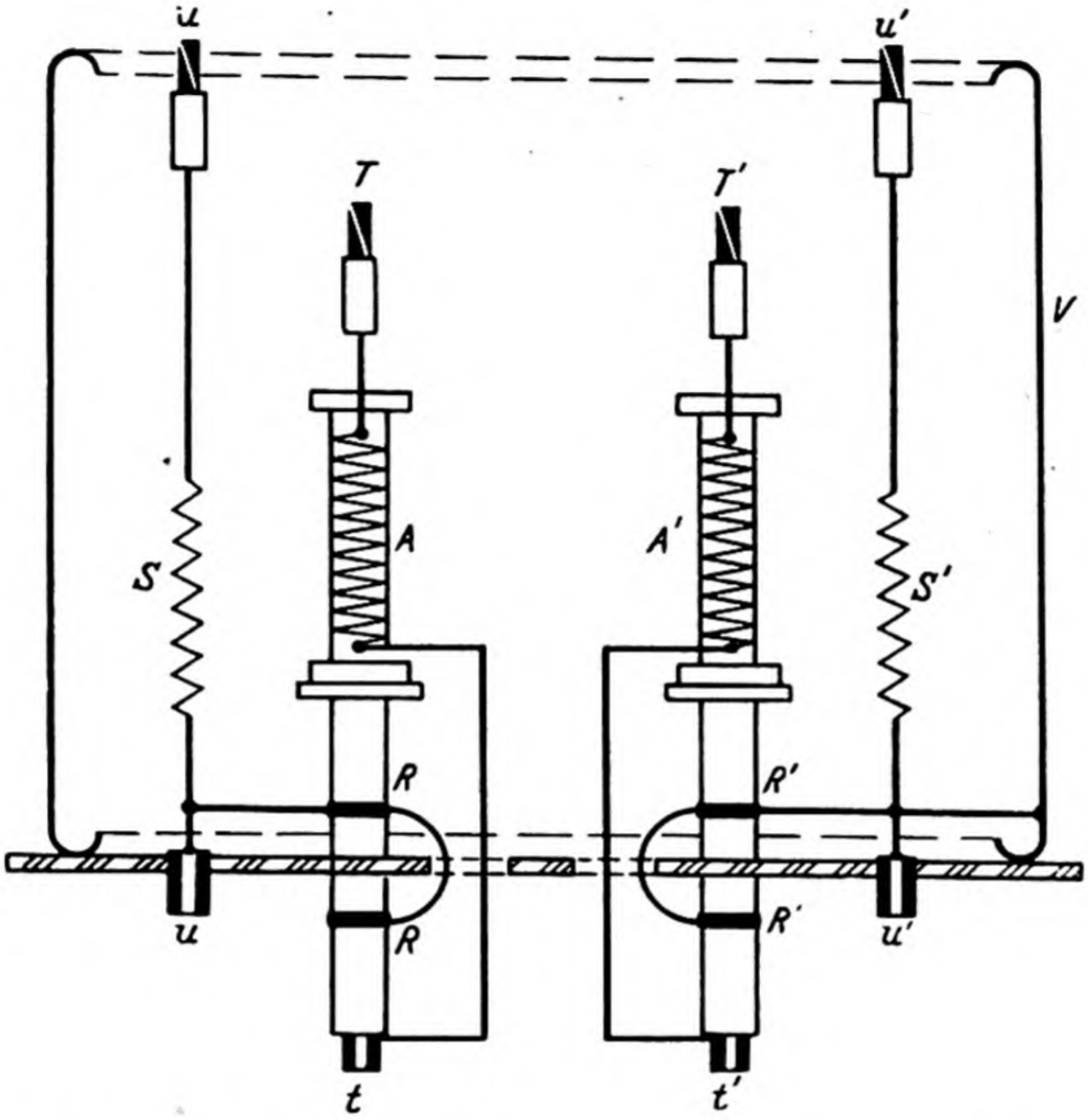

Figure 268. Section of high resistance arm of potentiometer (Rymer and Wright[1], by courtesy, *J. Sci. Instrum.*).

A,A′ = resistance of main and balancing networks.
R,R′ = guard electrodes on insulating supports.
S,S′ = guard circuit resistances.
T,t;T′,t′;U,u;U′,u′ = plug/socket connectors for joining successive sections.

to an electrostatic voltmeter and so the large temperature change in resistance (about 1·5 per cent) is of no consequence since it has negligible effect on the resistance ratio.

A.C. POTENTIAL DIVIDERS

DAVIS, BOWDLER and STANDRING[4] have carried out a detailed study of potential divider methods, for the measurement of high a.c. voltages ($\sim 10^5 - 10^6$ V). They describe the errors that may be caused by residual charges on the components of capacity dividers when the output voltage is measured electrostatically; the error may be removed by the use of a suitable high resistance leak connected across one arm of the divider.

The use of thermionic rectifiers in peak voltmeters[4] has often been described (*see* the work of EDWARDS and SMEE[5] discussed below) since the time of SHARPE and DOYLE's paper[6] and the basic circuit is given

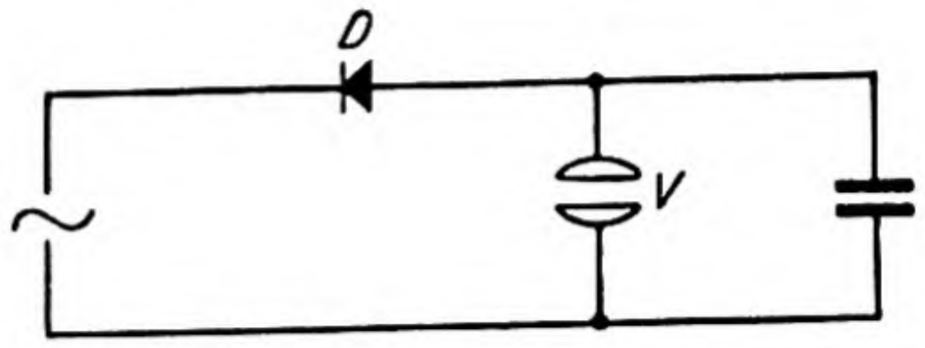

Figure 269. Basic circuit of a peak voltmeter (Davis *et al.*[4], by courtesy, *J. Inst. elect. Engrs.*).

in *Figure 269*. With a.c., the rectifier must withstand twice the peak voltage, and so the use of a potential divider is often necessary. Davis *et al.*[4] studied the circuit of *Figure 270* where R' is used to short circuit residual charges on C_2. Then if V and V_2 are respectively the input and output voltages, for the divider part $(C_1 - C_2)$ of the circuit of *Figure 270*, and if $\omega = 2\pi \times$ supply frequency,

$$\frac{V}{V_2} = \frac{C_1 + C_2}{C_1}\left[1 - \frac{1}{2\{\omega R'(C_1 + C_2)\}^2}\right]$$

If $V = 10^6$ V, $C_1 = 10\,\mu\mu$F and $C_2 = 105\,\mu\mu$F then the error introduced by $R' = 1$ MΩ, with reference to the simple expression

$$\frac{V}{V_2} = \frac{C_1 + C_2}{C_1}$$

will be < 3 in 10^4 at 50 c/s. For the simpler condition, without R', the

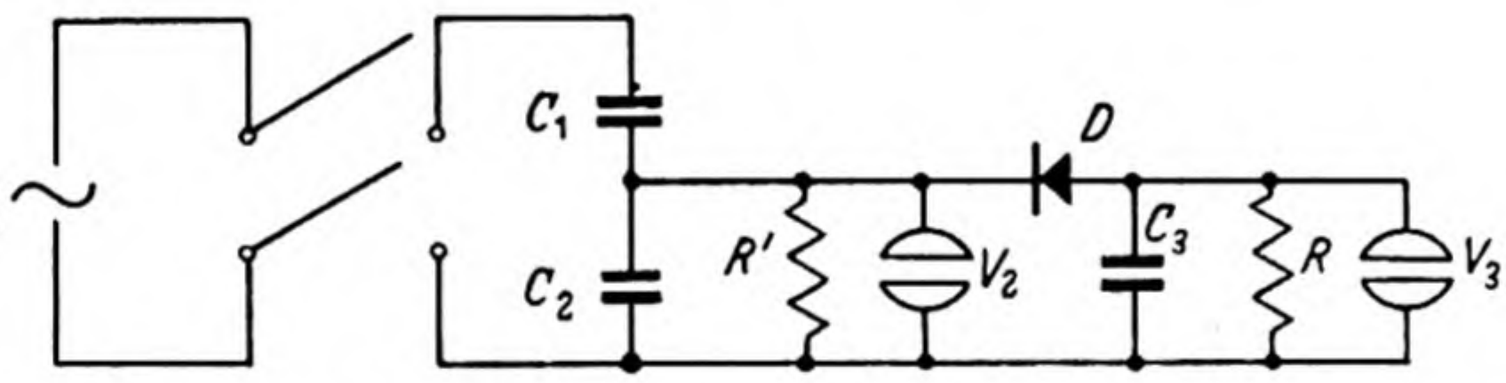

Figure 270. Peak voltmeter with capacitance potential divider (Davis *et al.*[4], by courtesy, *J. Inst. elect. Engrs.*).

output voltage V_3 read across C_3 by an electrostatic instrument is given by

$$V_3 = \frac{aV\,C_1}{C_1 + C_2 + C_3}$$

where aV is the peak input voltage.

The error caused by the effective capacitance (K) of the valve can be estimated from the following equation for the r.m.s. value of V_3:—

$$Vrms = V_m \frac{C_1}{C_1 + C_2}\left(1 - K/C_3 - K/(C_1 + C_2)\right)$$

where V_m is the maximum value of V. Davis *et al.*[4] have studied also the effects due to undesirable valve characteristics, such as contact potentials giving currents flowing with a negative rectifier anode, imperfect insulation of C_3, and non-sinusoidal wave-forms.

The errors may be summarized as

(1) the shunting effect of R' on C introduces an error

$$-V_3 \frac{1}{2\,[R'\,\omega\,(C_1+C_2)]^2}$$

(2) the effective valve capacitance K introduces errors

(i) $-V_3\,K/(C_1+C_2)$ and (ii) $-V_3\,K/C_3$

(3) the leakage resistance R (*see Figure 270*) introduces an error $-V_3\,R'/R$ but, if R is too great, the time constant RC_3 may affect the response of the measuring circuit to varying voltages.

To reduce the errors 2 (ii) and 3, both R and C_3 should be large, and for each error to be 1 in 10^3, then $C_3 \geqslant 1{,}000\,K$, $(C_1+C_2) \geqslant 1{,}000\,K$, $R \geqslant 1{,}000\,R'$ and $2\,[R'\,\omega\,(C_1+C_2)]^2 \geqslant 1{,}000$. Unsuitable valves

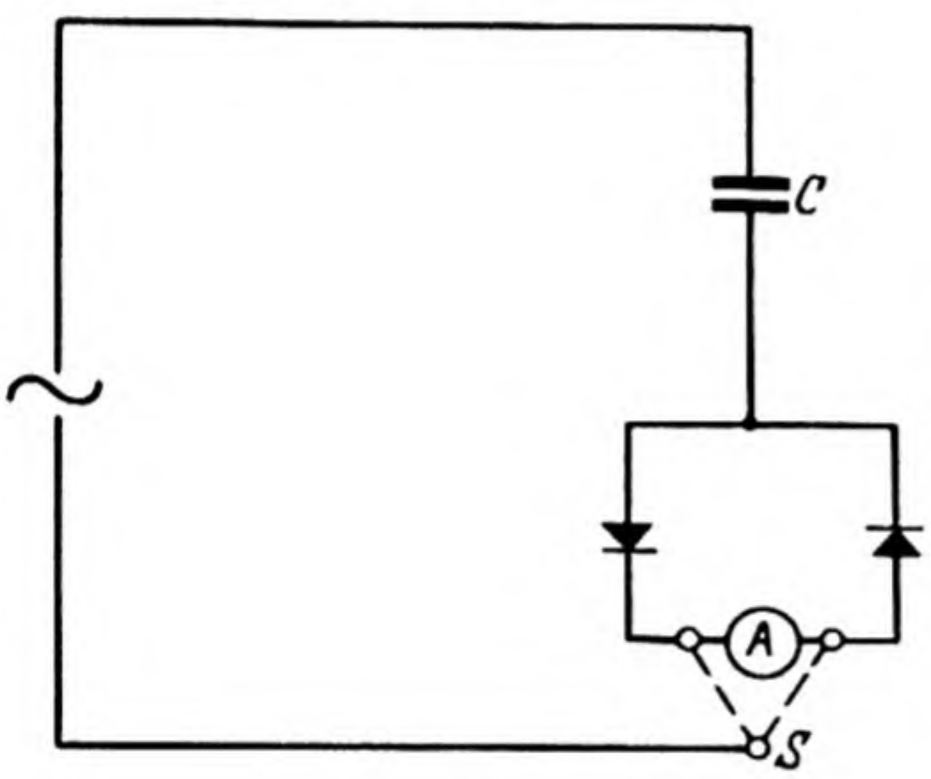

Figure 271. Peak voltmeter circuit (Chubb and Fortescue[7], by courtesy, *Trans. Amer. Inst. elect. Engrs.*).

may cause much greater errors, so care must be taken in their choice. Typical constants used in the work by Davis *et al.*[4] were :—

$$C_1 = 10 - 45\,\mu\mu\text{F},\quad C_2 = 0{\cdot}2\,\mu\text{F},\quad C_3 = 0{\cdot}2\,\mu\text{F}$$
$$K \simeq 100\,\mu\mu\text{F},\ R = 6 \times 10^9\,\Omega,\ R' = 10^6\,\Omega$$

giving a total error, including that due to valve characteristics, ~ 2 in 10^3.

The circuit of *Figure 271*, due to Chubb and Fortescue[7] can also be used[4] to measure peak voltages. S is a polarity switch. If the rectifier impedance is small compared with that of the condenser the instantaneous current is $I = C\,de/dt$ where e is the instantaneous voltage and C is the capacitance, as shown in *Figure 271*. The total charge flowing through each rectifier per cycle is

$$\int I\,dt = C\int de = 2\,\pi\,f\,CE\int_{\frac{3}{4}f}^{\frac{1}{4}f} \cos\,2\,\pi\,ft\,\,dt.$$
$$= 2\,CE$$
$$\text{if}\quad e = E\sin\,2\,\pi\,ft$$

The mean current is then $2\,CEf$, and the instrument must correctly measure mean currents for this relation to be satisfied. Errors due to imperfect valve characteristics, and to voltage drop in the rectifiers

can also arise. The former errors are due to the valve current being finite at zero valve voltage (*see Figure 272*). Davis *et al.*[4] consider this error in detail and show, for the data of *Figure 272* and for mean galvanometer currents exceeding 2·7 μA that the error will be about 1 in 10^3. The latter current is easily exceeded and, for example, 10^6 V will give a current of about 140 μA at 50 c/s through 1 $\mu\mu$F.

Since the charge flowing through the rectifier = $\int Cde$ where the integration is taken during the cycle when de/dt has no change of sign,

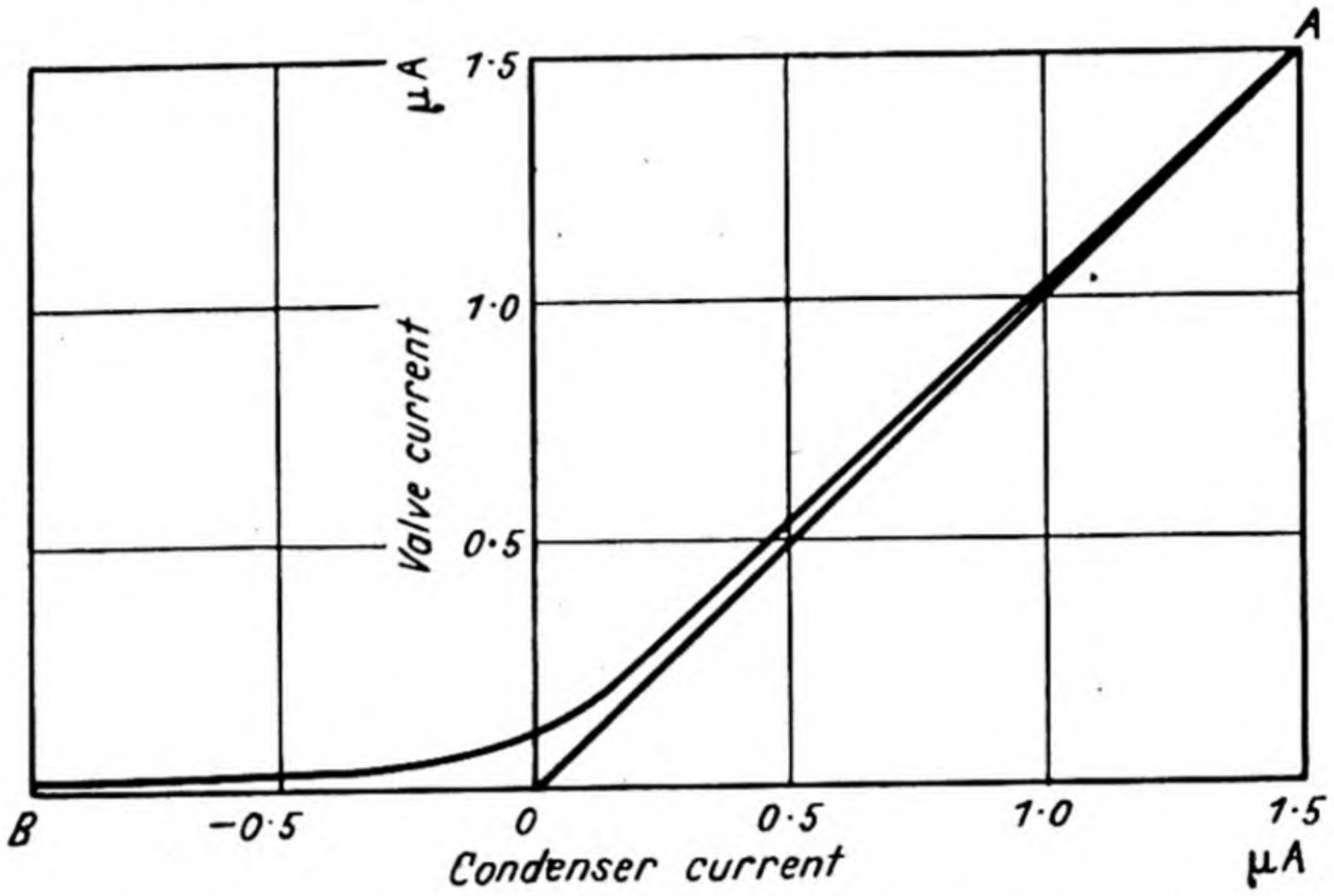

Figure 272. Curve showing relation between current through one valve and condenser current (*see Figure 270*) (Davis *et al.*[4], by courtesy, *J. Inst. elect. Engrs.*).

but is + *ve* or − *ve* for each valve, the peak voltage cannot be measured in this way if there are subsidiary peaks on either or both half cycles. The method cannot be used when the + *ve* and − *ve* peak heights are unequal.

The extraordinary consistency and accuracy obtainable by the use of the above methods of voltage and current rectification in careful hands is illustrated by the data of Davis *et al.*[4] and given in *Table XXXI.*

Capacitance potential dividers for a.c. work (low frequencies) may incorporate a single high-voltage capacitor, of the type described by Palm[8], Bousman and Ten Broeck[9] and earlier by Churcher and Dannatt[10] (*see* Chapter 11). These capacitors are usually made for Schering bridge measurements. Alternatively the high-voltage capacitor may consist of a chain of low-voltage capacitors, when its cost is likely to be less than that of a precision compressed-gas condenser but at the expense of larger inductance and losses. Corona discharges may also be more difficult to eliminate with a chain of units unless expensive metal shields are provided. Churcher and Dannatt[10] deal in great detail with the use of air (normal-pressure) condensers in precision measurements at voltages up to 300 kV. The capacitances

of their condensers could be calculated to about 1 in 10^4; their phase errors were less than 0·00001 up to their rated voltages. Particulars are given by Edwards and Smee[5] of the methods of measurement of the capacitance of a parallel-plate air condenser for use at voltages up to 1,400 kV, particular attention being given to the variation of capacitance with voltage (*see* page 237).

TABLE XXXI.

Capacitance of high voltage condenser $\mu\mu F$	*Capacitance of low voltage condenser* μF	*Peak voltage measured by*	
		Voltage rectification	*Current rectification*
45·30	0·2011	$213._2$	$213._4$
29·91	0·2011	$279._0$	$278._5$
25·51	0·2011	$426._3$	$426._5$
18·52	0·2011	$694._5$	$695._0$
10·07	0·2011	101_9	101_9
10·07	0·2011	118_4	118_1

The above technique[4] has been extended by Edwards and Smee[5] to the measurement of voltages up to 1,400 kV peak, 50 c/s (*see* page 238).

POTENTIAL DIVIDERS FOR IMPULSE WORK : BURCH'S TREATMENT

A classical paper on surge potential dividers for oscillographs is that by BURCH[11] following earlier work by GÁBOR[12], who first introduced the technique which uses a delay cable between the potential divider and the oscillograph, and by NORINDER[13]. Burch first stresses the need for high impedance potential dividers, to minimize the drain on the

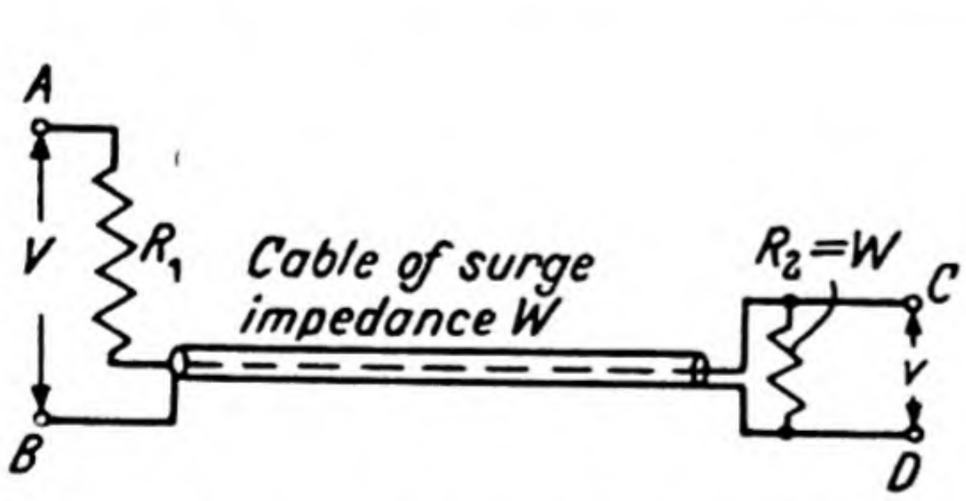

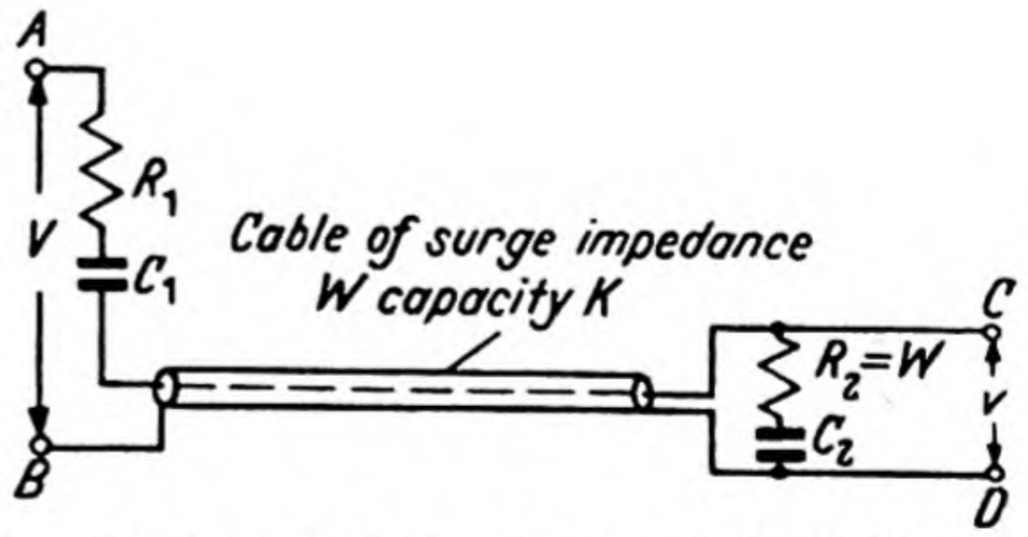

Figures 273 and 274. Gábor's potential divider circuits (Burch[11], by courtesy, *Phil. Mag.*).

source, especially when long transients are being recorded; and proceeds to discuss the errors introduced by the various circuits shown in *Figures 273* to *278*.

Figures 273 and *274* are due to Gábor. In the former, a voltage wave, caused by the application of a sudden transient across A B, charges the cable, of surge impedance W, to a voltage $W/(R_1+W)$ and this

Figure 275

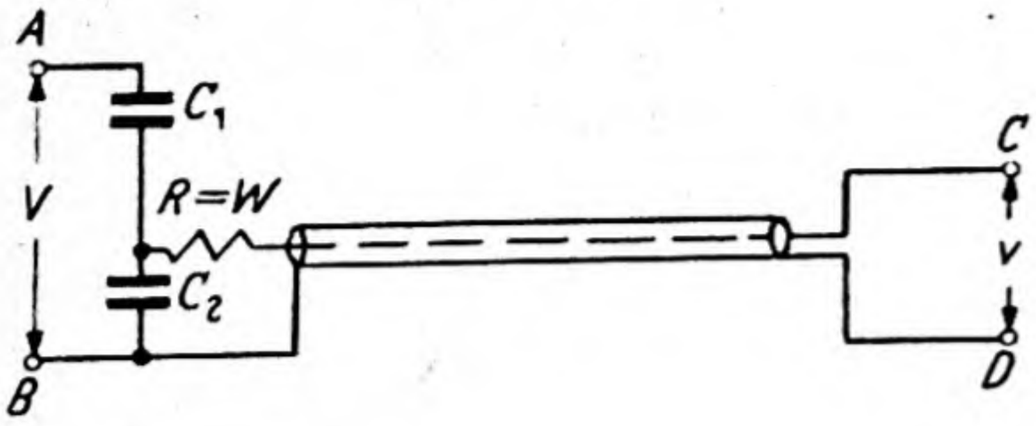

Figure 276

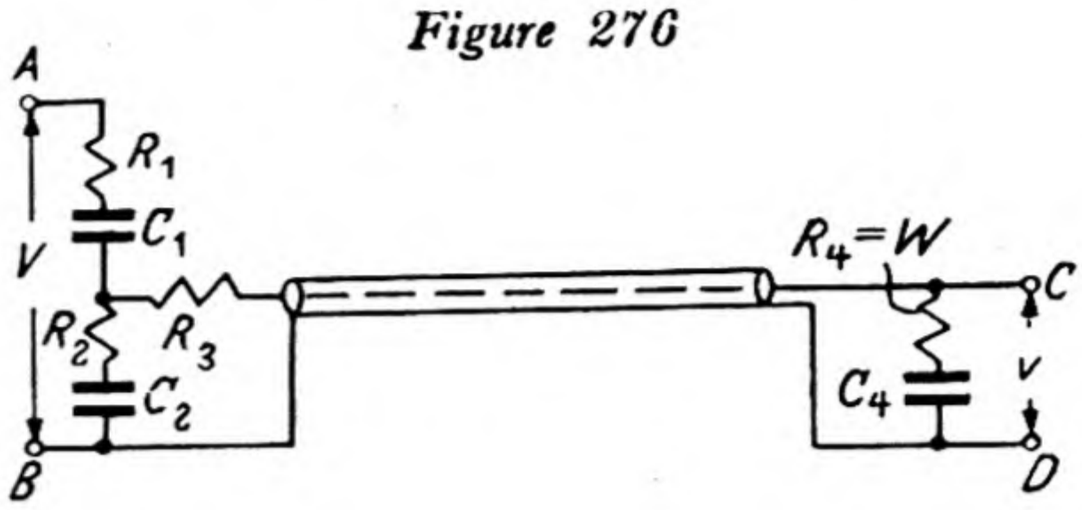

Figure 277

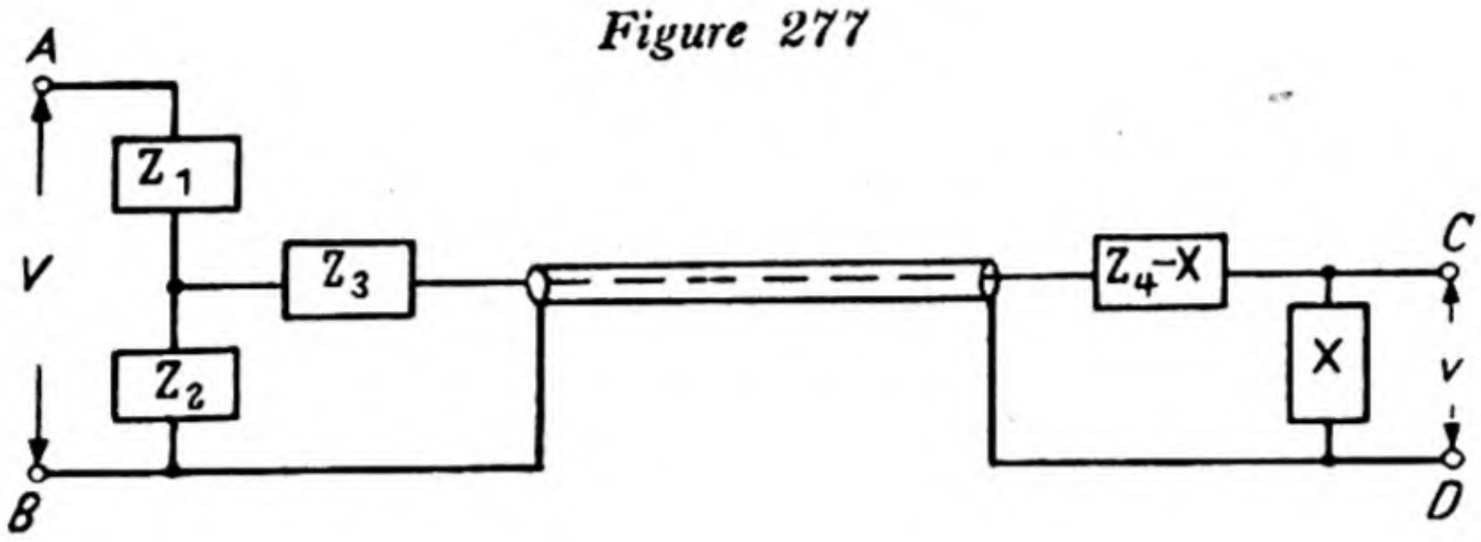

Figure 278

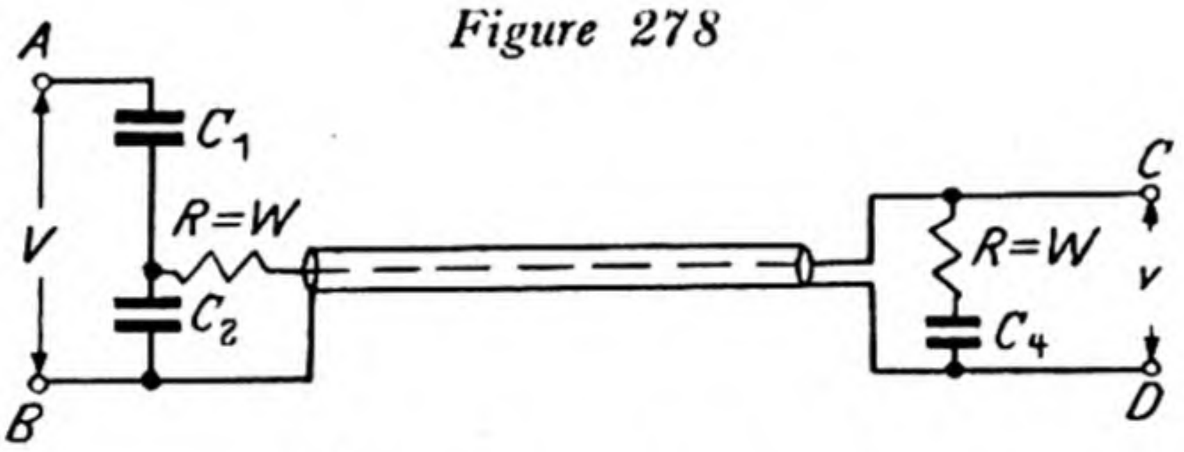

Figures 275–278. Potential divider circuits (Burch[11], by courtesy, *Phil. Mag.*).

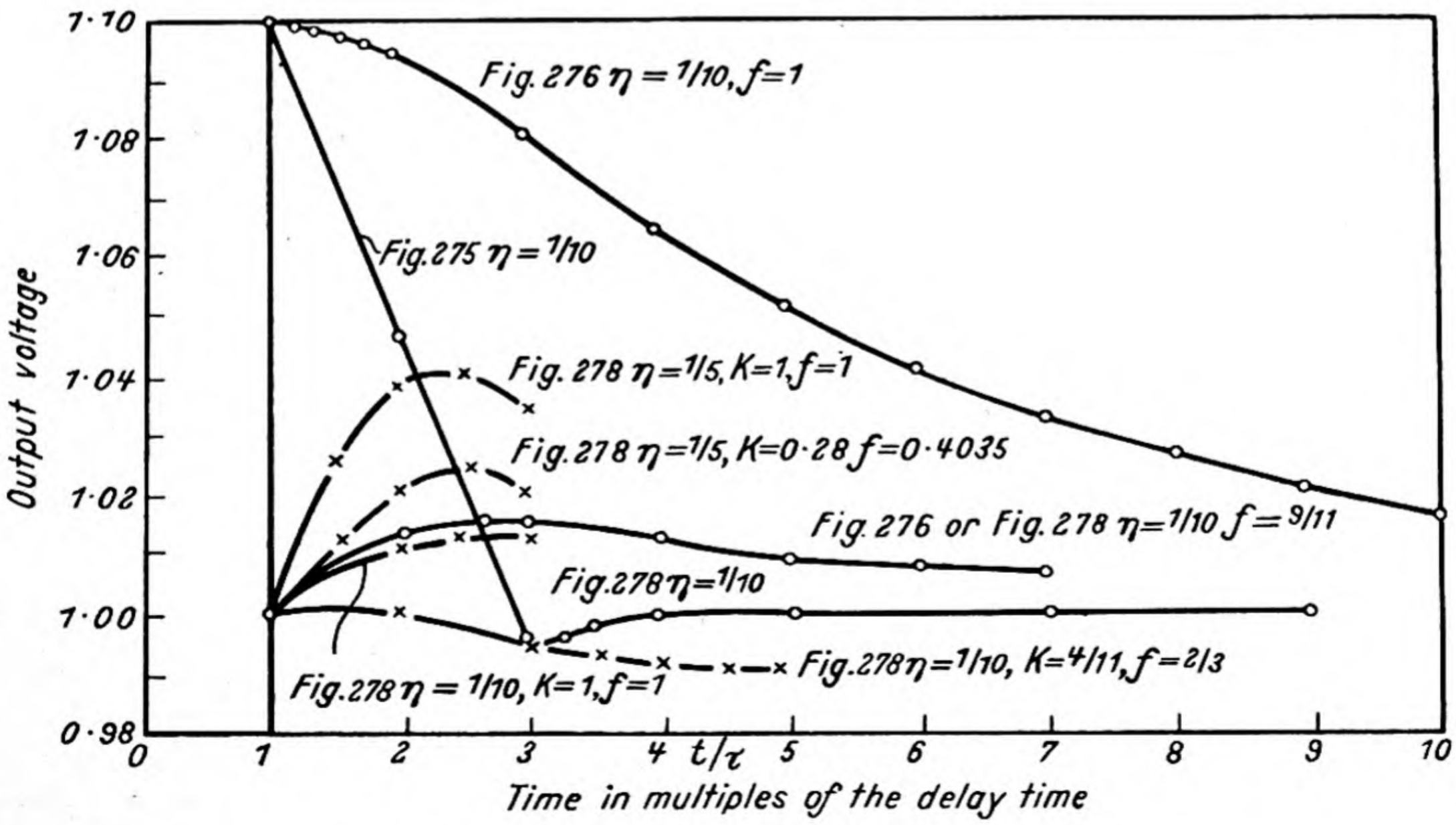

Figure 279. Response of potential divider circuits of *Figures 275–278.* Constant voltage suddenly applied (Burch[11], by courtesy, *Phil. Mag.*).

is also the voltage developed across $C\ D$ since the cable is matched by the resistance R. Gábor's circuit shown in *Figure 274* with capacitances needs $C_2 \gg K$ for faithful recording, with an error $\sim K/C_2$. Gábor showed that, if $\tau = WK =$ time taken for the wave to travel from end to end of the delay line, the voltage falls to $m_0\ (1\text{-}\eta)$ at $t = 3\tau$, passes through a minimum between $t = 3\tau$ and $t = 5\tau$ and returns to $m_0(1\text{-}\eta)$ at $t = 5\tau$ with negligible subsequent oscillations, thus giving a maximum error η where $m_0 =$ initial voltage $= W/(R_1 + W)$ (assumed to be small) and $R_1C_1 = WC_2$. The final voltage is $m_0/(1+\eta)$ where $\eta = K/(C_1 + C_2)$. Further, if $R_1C_1 = WC_2\ (1+\eta)$ the initial value of voltage is the same as the final value and the voltage at $t = 3\tau$ is approximately

$$m_0 \left[1 - \eta \frac{(1-\eta)}{1+\eta} \right]$$

The best result obtainable with the circuit of *Figure 274* is a minimum total fluctuation roughly equal to η.

Burch analysed the circuits of *Figures 275* to *278* using Carson's treatment of delay lines, based on Heaviside calculus, and applied for example to the general case of *Figure 277* using a non-dissipative cable. Here the output voltage, for input V, is given by

$$v = \frac{S\, e^{-p\tau}}{1 - \mu_1\mu_2\, e^{-2p\tau}} \cdot V \qquad \ldots\ldots(9.1)$$

where

$$S = X/Z_4 \cdot \frac{Z_2}{Z_1 + Z_2} \cdot \frac{(1+\mu_1)(1-\mu_2)}{2}$$

$$\mu_1 = \frac{W\ (Z_1 + Z_2) - (Z_1Z_2 + Z_2Z_3 + Z_3Z_1)}{W\ (Z_1 + Z_2) + (Z_1Z_2 + Z_2Z_3 + Z_3Z_1)}$$

$$\mu_2 = \frac{W - Z_4}{W + Z_4}$$

$X_1\ Z_1\ Z_2\ Z_3$ and Z_4 and in general also V, are functions of the Heaviside operator $p = d/dt$.

Equation 9·1 may be written

$$v = V \cdot S\{ e^{-p\tau} + \mu_1\mu_2\, e^{-3p\tau} + (\mu_1\mu_2)^2\, e^{-5p\tau} \ldots . \}$$

with a solution

$$v = v_0\,(t-\tau) + v_1\ (t-3\tau) + v_2\ (t-5\tau) + \ldots .$$

where $v_0\,(t)$, $v_1\,(t)$ *etc.* are solutions of the operational equations

$$v_0 = S.V$$

$$v_1 = \mu_1\mu_2\ S.V$$

$$v_2 = (\mu_1\mu_2)^2\ S.V\ \textit{etc.}$$

corresponding to the original and the reflected waves.

This analysis was next applied by Burch to the circuits of *Figures 275*, *276* and *277* for the case of an input voltage of unit function shape, *i.e.*, $V = 0$ when $t < 0$ and $V = 1$ when $t > 0$.

For the circuit of *Figure 275*, a purely capacitive divider, where a voltage wave $\frac{C_1}{2(C_1+C_2)}$ enters the cable and is doubled by reflection so that the voltage at CD jumps initially to $C_1/(C_1+C_2)$, putting

$$\frac{1}{2\,W\,(C_1+C_2)} = \frac{K}{2\,(C_1+C_2)}\,\frac{1}{\tau} = a$$

and $m=C_1/(C_1+C_2)$ we have $S=m.\ p/(p+a)$, $\mu_1 = \dfrac{-a}{p+a}$, $\mu_2=-1$ and the response terms are

$$v_0\,(\xi_0) = m\,e^{-a\,\xi_0}$$
$$v_1\,(\xi_1) = m\,(a\xi_1)\,e^{-a\,\xi_1}$$
$$\cdots\cdots\cdots$$
$$v_n\,(\xi_n) = \frac{m\,(a\xi_n)^n}{\mathrm{n}!}\,.\,e^{-a\,\xi_n}$$

where $\xi_n=t-(2n+1)\ \tau$. The terms are zero for negative ξ_n. For the practical case of $K/(C_1+C_2)=\eta=0{\cdot}1$ the response is shown in *Figure 279* for a final output voltage $C_1/(C_1+C_2+K)=1$. As in *Figure 274* the error is, if $C_1 \ll C_2$, K/C_2 and this led Burch to consider the circuit of *Figure 276*, where both ends of the delay line are shunted (cf. Gábor's circuit of *Figure 274*) and where the surge impedance of the line is again W. If, Burch pointed out, $C_1+C_2=C_4+K$ the initial and final output voltages will be the same, and an improvement in the fidelity of recording, as compared with that obtained with the circuit of *Figure 275*, is expected.

The simplest case of *Figure 276* is obtained by putting $C_4/(C_1+C_2)=f=1$ Putting

$$\frac{1}{2\,W\,(C_1+C_2)} = \frac{1}{2\,W\,C_4} = \frac{K}{(C_1+C_2+C_4)\tau} = a$$

$$m_o = \frac{C_1}{C_1+C_2}$$

then

$$S = \frac{m_o}{2}\,.\,p\,\frac{(p+2\,a)}{(p+a)\,2} \qquad \mu_1=\mu_2=\frac{-a}{p+a}\,.$$

and the response terms are, if $\xi_n=t-(2n+1)\ \tau$.

$$v_o\,(\xi_o) = \frac{m_o}{2}\,e^{-a\,\xi_0}(1+a\xi_0)$$
$$v_1\,(\xi_1) = \frac{m_o}{2}\,\frac{a\,(\xi_1)^2}{2!}\,e^{-a\,\xi_1}\left(1+\frac{a\xi_1}{3}\right)$$
$$\cdots\cdots\cdots$$
$$v_n\,(\xi_n) = \frac{m_o}{2}\,\frac{(a\xi_n)^{2n}}{2\mathrm{n}!}\,\cdot e^{-a\,\xi n}\left(1+\frac{a\xi_n}{2n+1}\right).$$

The response wave is shown in *Figure 279* for $\eta = \frac{1}{10}$, $f = 1$. For the general case

$$\frac{C_4}{C_1 + C_2} = f \neq 1$$

where

$$\frac{1}{2W(C_1 + C_2)} = a \quad \text{and} \quad \frac{1}{2WC_4} = b$$

so that

$$S = \frac{m_o}{2} \cdot p \frac{(p + 2b)}{(p + a)(p + b)}, \quad \mu_1 = \frac{-a}{p + a}, \quad \mu_2 = \frac{-b}{p + b}$$

If $C_1 + C_2 = C_4 + K$, to correct overshooting, then if

$$\eta = K/(C_1 + C_2 + C_4)$$

$$a = \frac{\eta}{(1 + \eta)\tau} \qquad b = \frac{\eta}{(1 - \eta)\tau} \qquad f = \frac{1 - \eta}{1 + \eta}$$

and the response terms, too lengthy for inclusion here, give the results shown again in *Figure 279*, for $\eta = \frac{1}{10}$ where the maximum error is now only 1·6 per cent. If this error were to be obtained with the circuit of *Figure 275* a total capacitance 6·2 times larger than that required for *Figure 276* would be needed.

In the circuit of *Figure 278* the inclusion of extra resistances modifies the response, as compared with that obtained from the circuit of *Figure 276*. The condition

$$R_3 + \frac{R_1 R_2}{R_1 + R_2} = W$$

is taken, so that reflexion of very high frequency waves is zero. In this case, if

$$\frac{1}{R_1 C_1} = \alpha \qquad \frac{1}{R_2 C_2} = \beta \qquad \frac{1}{WC_4} = \gamma$$

$$\frac{R_2}{R_1 + R_2} = m_0 \qquad 1 - \frac{R_3}{W} = \mathrm{K}$$

$$\frac{K}{C_1 + C_2 + C_4} = \eta$$

it is found, for $m_0 \ll 1$ that

$$S \simeq \frac{m_0}{2} \cdot \frac{p(p + \beta)(p + \gamma)}{(p + d)\ (p + \frac{\kappa\beta}{2})\ (p + \gamma/_2)}$$

If $\alpha = \beta$, the response is the same as for *Figure 276*. Results for other conditions are also given, *e.g.* for the case $\mathrm{K} = 1, f = 1$ for either $\eta = \frac{1}{10}$ or $\frac{1}{5}$ in *Figure 279*. The maximum errors here may be only 1·4 per cent. for $\eta = \frac{1}{10}$. For $\eta = \frac{1}{10}$, $\mathrm{K} = \frac{4\eta}{1 + \eta} = \frac{4}{11}$ and $f = \frac{2}{3}$ the error is never more than $-1{\cdot}1$ per cent. (*see Figure 279*) when $t \simeq 5\tau$.

A practical example given by BURCH[11] is as follows. If a potential divider is used to step down from 1 MV to 500 V, with $W = 50\ \Omega$ then *Figure 274* gives a resistance $R_1 = (1 - V)W/V = 99{,}950\ \Omega$ whilst *Figure 278* for $K = 0{\cdot}28$, gives $R_1 = KW/2V = 14{,}000\ \Omega$ which is still high enough if, say, the surge impedance of the high-voltage circuit is $500\ \Omega$. For $0{\cdot}5\ \mu$sec delay the cable capacitance $K = \tau/W = 0{\cdot}01\ \mu$F, and for corrected initial overshooting the circuit of *Figure 274* for a maximum error of 2·5 per cent. necessitates $\eta = \frac{1}{40}$, $C_1 \simeq 200\ \mu$F whilst, for *Figure 278*, $\eta = \frac{1}{5}$, $C_1 = 25\ \mu$F. Burch suggests that if a high R_1 is required, $K = f = 1$ for preference, and the initial overshooting should be under corrected.

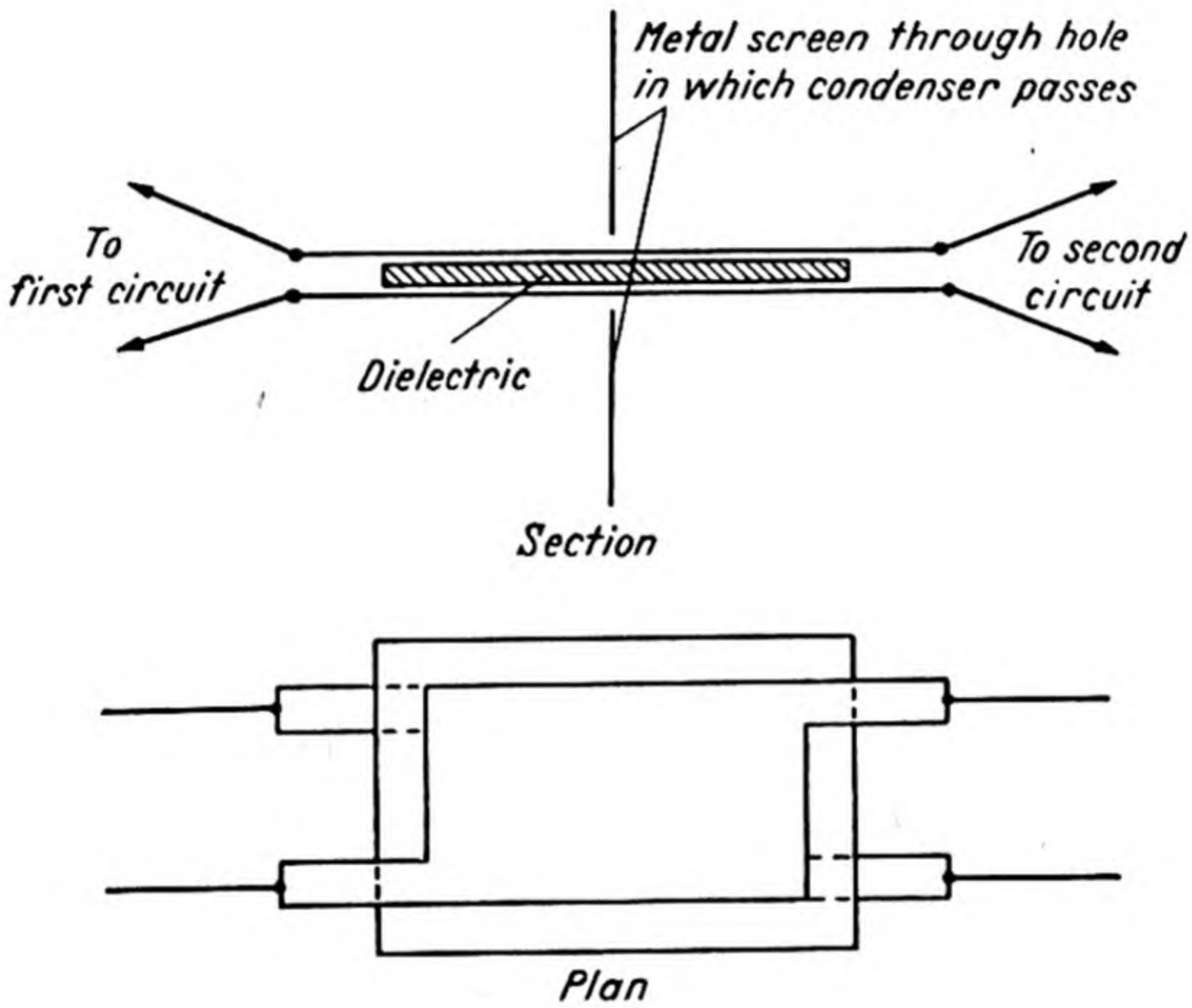

Figure 280. Capacitor giving purely capacitative coupling between two circuits (From *Surge Phenomena*, by courtesy, British Electrical and Allied Industries Research Association).

Further consideration of the circuit of *Figure* 275 above has been given in the E.R.A. book on "Surge Phenomena"[14] since it was used with the E.R.A. high speed oscillograph. The recording of pulses with rise times as short as $0{\cdot}25\ \mu$sec was satisfactory if $C_1 \not< 10K$, if C_2 is purely capacitative and if stray resistances were minimized. Then the initial and final voltage ratios m_o and m_α are substantially equal, since $m_o = \frac{C_1}{C_1 + C_2}$ and $m_\alpha = \frac{C_1}{C_1 + C_2 + K}$. The cable used had a capacitance of $0{\cdot}1\ \mu$F/100 yds. and $W \simeq 65\Omega$. Values of C_2 down to $0{\cdot}1\ \mu$F could be used without appreciable distortion. A design for C_2 in which stray inductance is minimized is shown in *Figure 280*. The leads are thus brought close to the capacitor plates, the current must flow through the plates in passing from the high-voltage source to the cable, and the stray inductive couplings are minimized by the use of metal screens

placed above and below the capacitor. Earth loops in the wiring must be kept as short as possible.

If C_2 is kept low, then C_1, the high-voltage capacitor, may also be low thus reducing costs. The E.R.A. used a 100 $\mu\mu$F condenser for C_1 in work on 132 kV transmission lines, rated to withstand 450 kV (r.m.s.) a.c. and 1,300 kV with a 1/5 μsec positive impulse. The capacitor was built in 4 sections, each consisting of a 2 ft. porcelain container with external corrugations, with the capacitor units in series in each container, and oil immersed. Many other designs of suitable high-voltage capacitors exist ; *see* Bouwer's book[15], and papers by KOHLRAUSCH[16], Palm[17] and SCHERING and VIEWEG[18]. The design of precision compressed air condensers for high voltages has been discussed by CHURCHER and DANNATT[19] amongst others and their capacitors have been used at voltages up to 500 kV, notably in the Metropolitan-Vickers Research Laboratories.

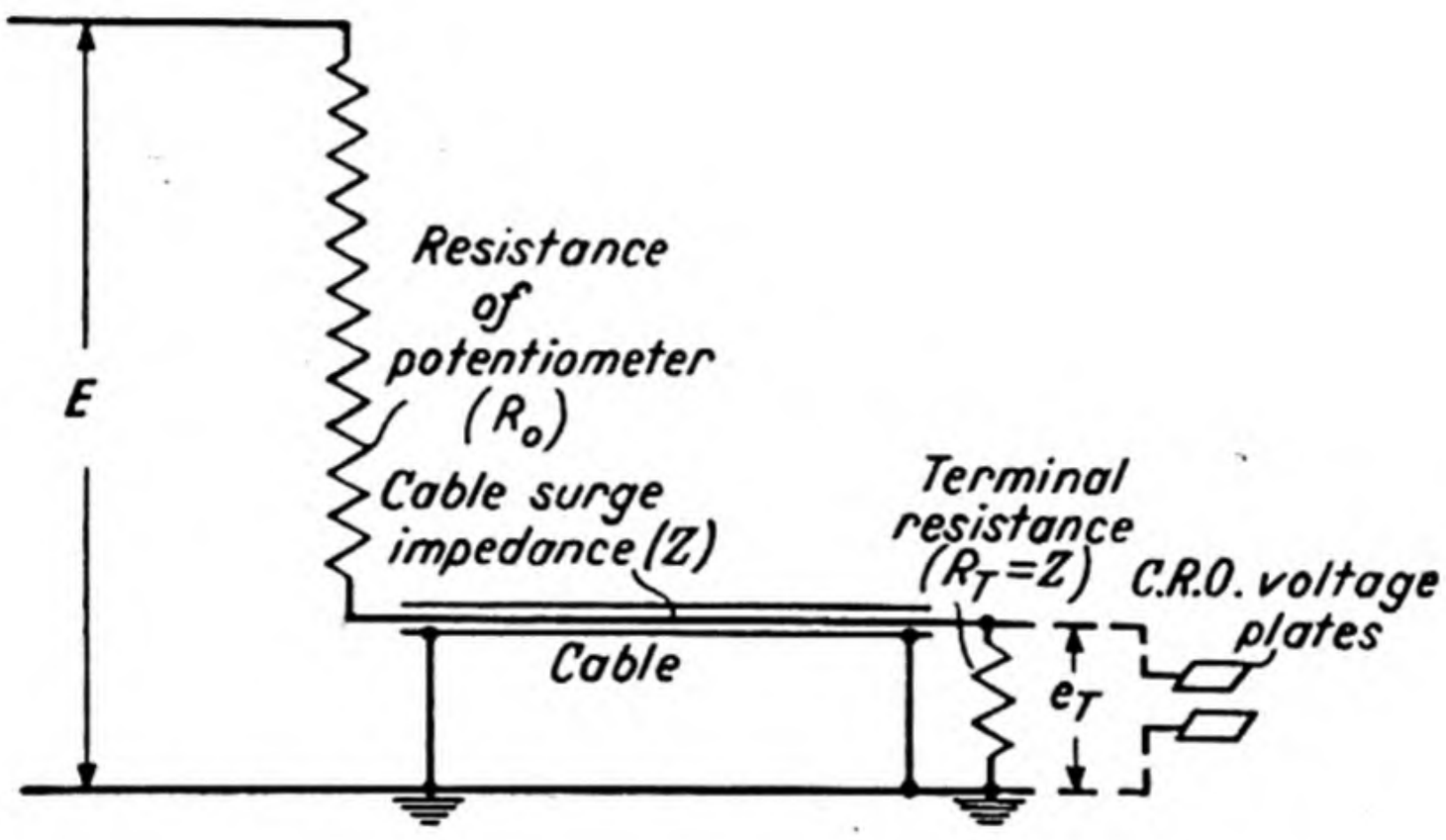

Figure 281. Plain resistance potentiometer connected to cable (Bellaschi[21], by courtesy, *Trans. Amer. Inst. elect. Engrs.*).

POTENTIAL DIVIDERS FOR IMPULSE WORK : LATER INVESTIGATIONS

Subsequent to Gábor's early experimental and theoretical work and Burch's treatment, many other authors have published accounts of potential dividers for high-voltage impulses. Thus, DOWELL and FOUST[20] describe experimental work with resistance and resistance-capacitance potential dividers for about 1 MV surges. For example, a 20,000 Ω high-voltage resistance in series with a 50 Ω cable, terminated with 50 Ω at the oscillograph terminals, was tested with 0·5/5 and 1·5/40 impulses and the effect of cable mis-match was experimentally investigated.

BELLASCHI[21] carried out similar but more detailed tests on resistance and capacitance dividers and preferred the latter because of the ease with which time delays could be eliminated despite the difficulties of

screening. The effect of distributed capacitance on the plain resistance divider of *Figure 281* was theoretically studied, as an approximation to the more practical case of uneven distribution of stray capacitances.

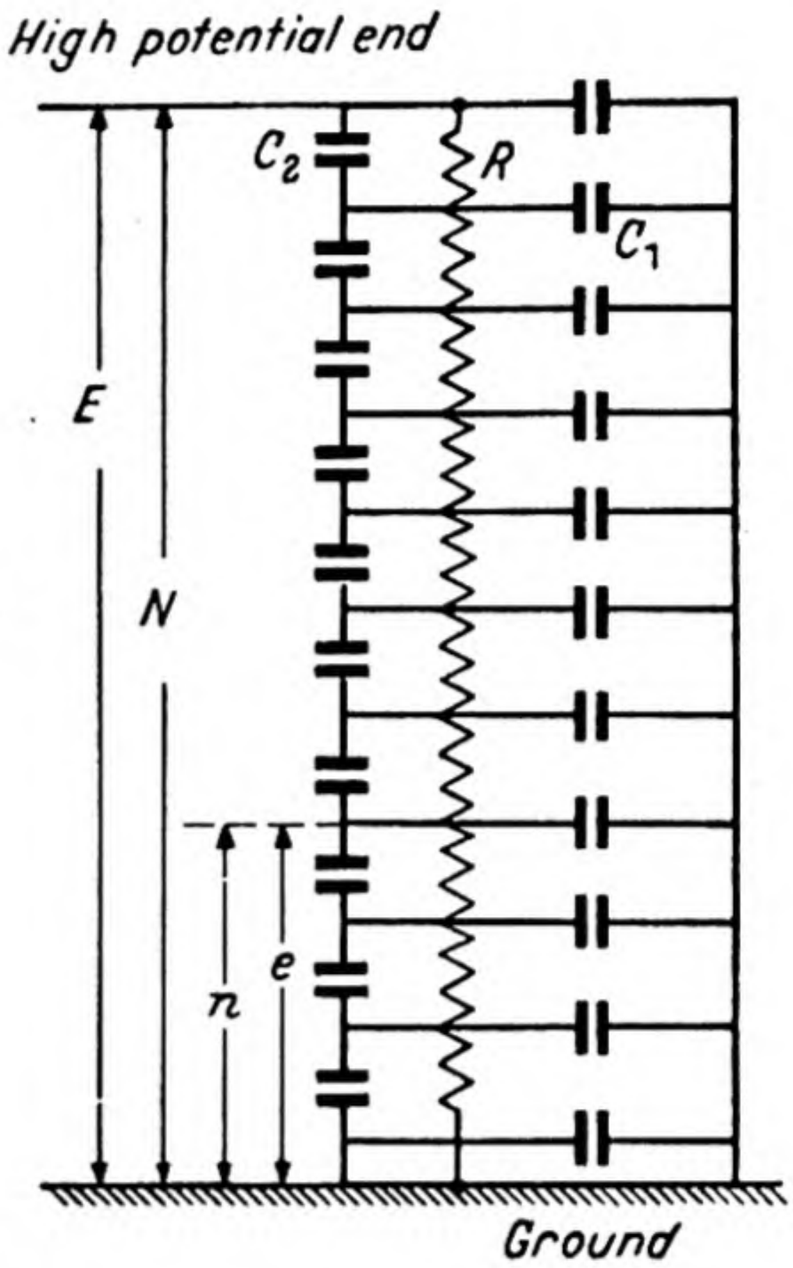

Figure 282. Circuit of resistance potentiometer (Bellaschi[21], by courtesy, *Trans. Amer. Inst. elect. Engrs.*).

The circuit including distributed capacitance is that of *Figure 282* where

$\mathcal{N}$ = total number of resistance elements, each of resistance R
C_1 = capacitance of each element to ground
C_2 = capacitance across each element
$C_g = \mathcal{N}C_1$; $C_c = C_2/\mathcal{N}$; $R_0 = \mathcal{N}R$.
E = rectangular surge voltage applied at time $t = o$
n = number of resistance elements from ground across which a voltage e appears

It is found that

$$e = \frac{n}{\mathcal{N}}E + \frac{E}{\pi}\sum_{k=1}^{k=\infty} \frac{2\sin(k\pi n/\mathcal{N})}{k\cos(k\pi)} \times e^{\frac{-R_0(C_g+k^2\pi^2C_c)}{\left(1+k^2\pi^2\frac{C_c}{C_g}\right)}}$$

and, with the substitution of typical values for the circuit constants the data of *Figure 283* can be calculated. *Figure 284* shows the calculated response for two arbitrary short impulses. The need for low resistance and low stray capacitances to ground is clear. Bellaschi used $R_o = 34{,}000\ \Omega$ (in *Figure 281*) with a cable impedance $Z = 44\ \Omega$. His capacitance potential divider was arranged as in *Figure 285* where r is a $400\ \Omega$ resistance to damp out oscillations caused by the lead inductance resonating with the stray capacitances to ground. R is inserted to prevent charging of the deflection plates of the oscillograph.

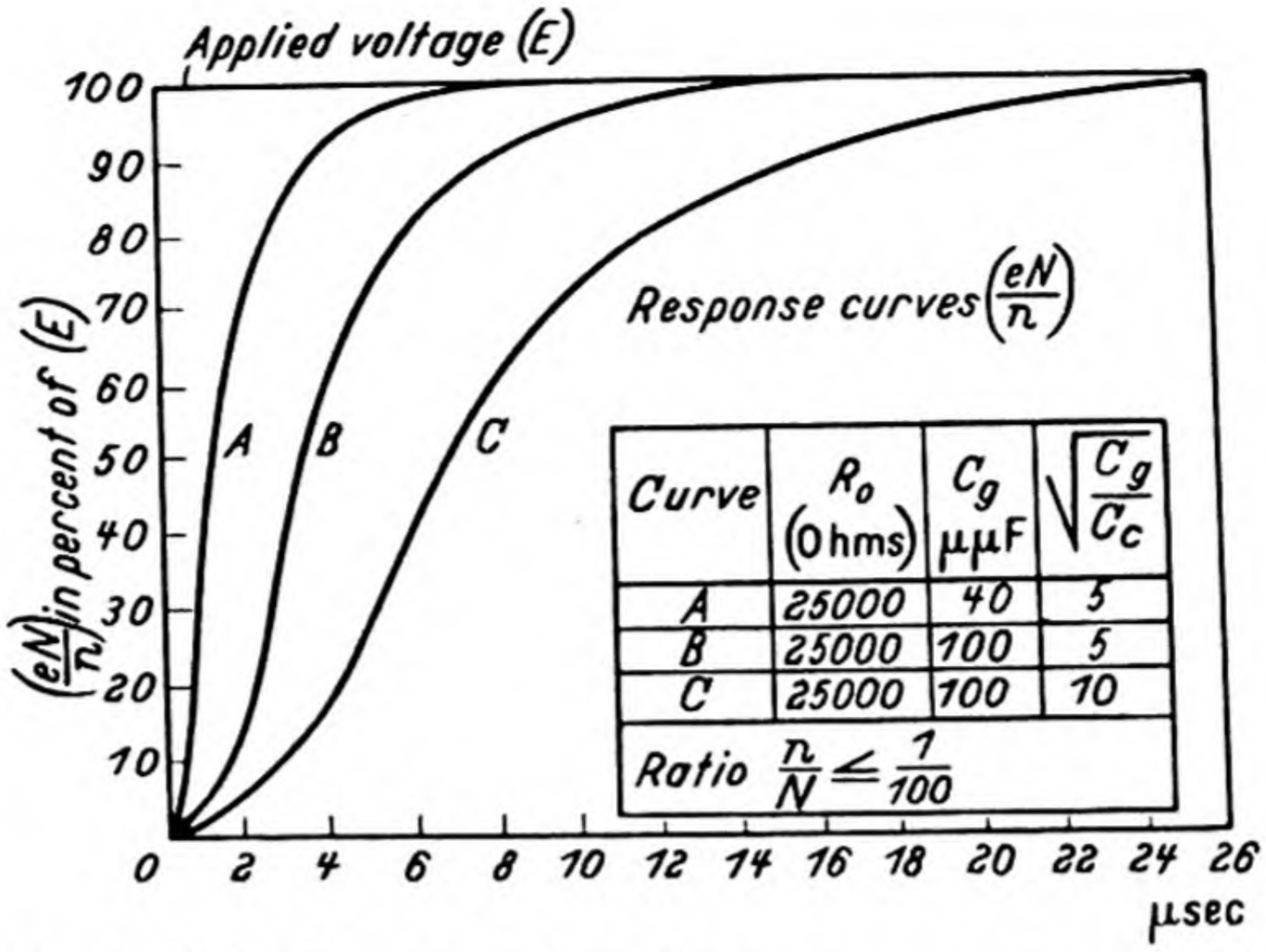

Figure 283. Response of resistance-capacity network to rectangular surge (Bellaschi[21], by courtesy, *Trans. Amer. Inst. elect. Engrs.*).

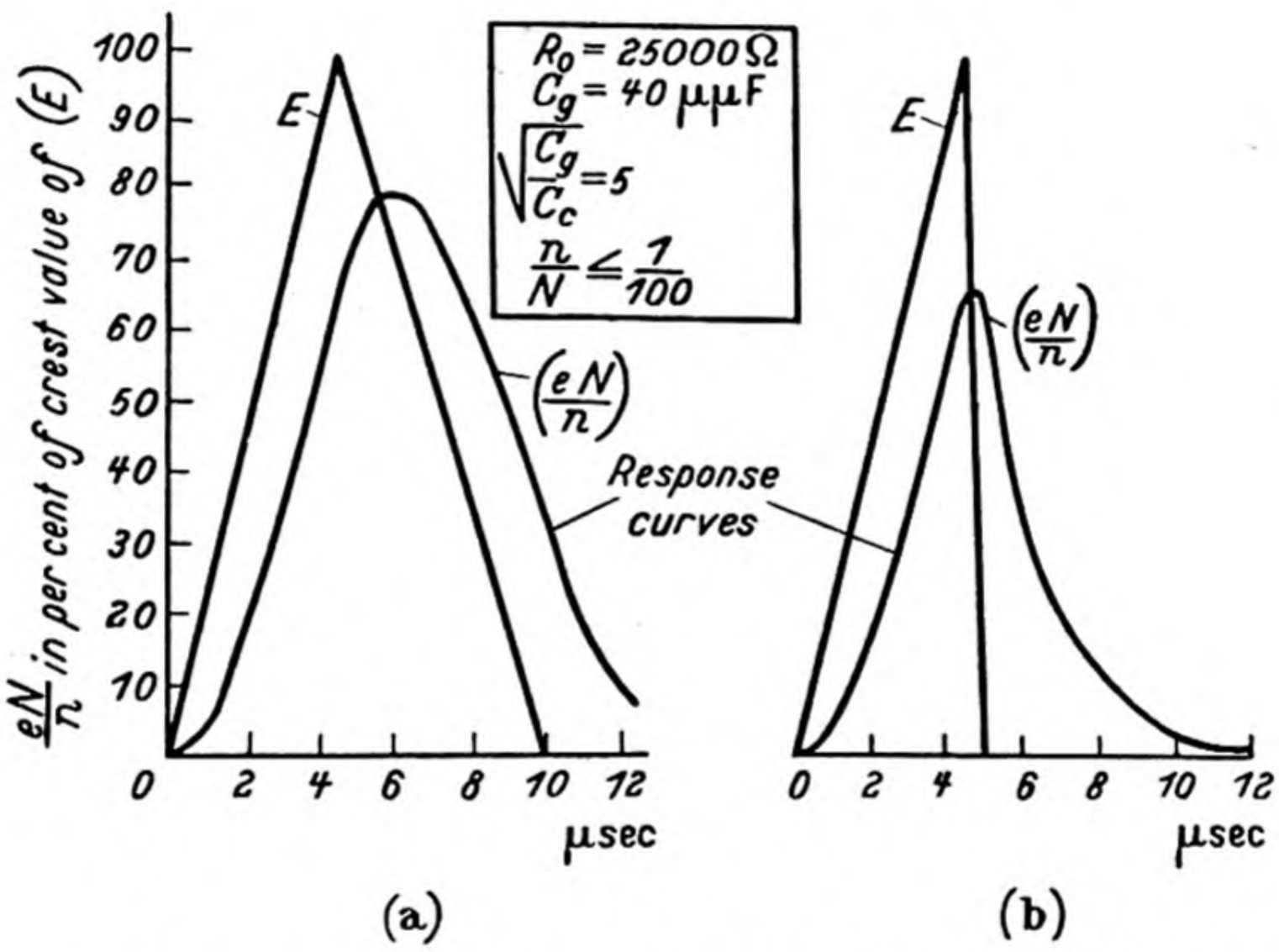

Figure 284. Response of resistance-capacity network to steep-fronted and abrupt tail surges (*see Figure 283*) (Bellaschi[21], by courtesy, *Trans. Amer. Inst. elect. Engrs.*).

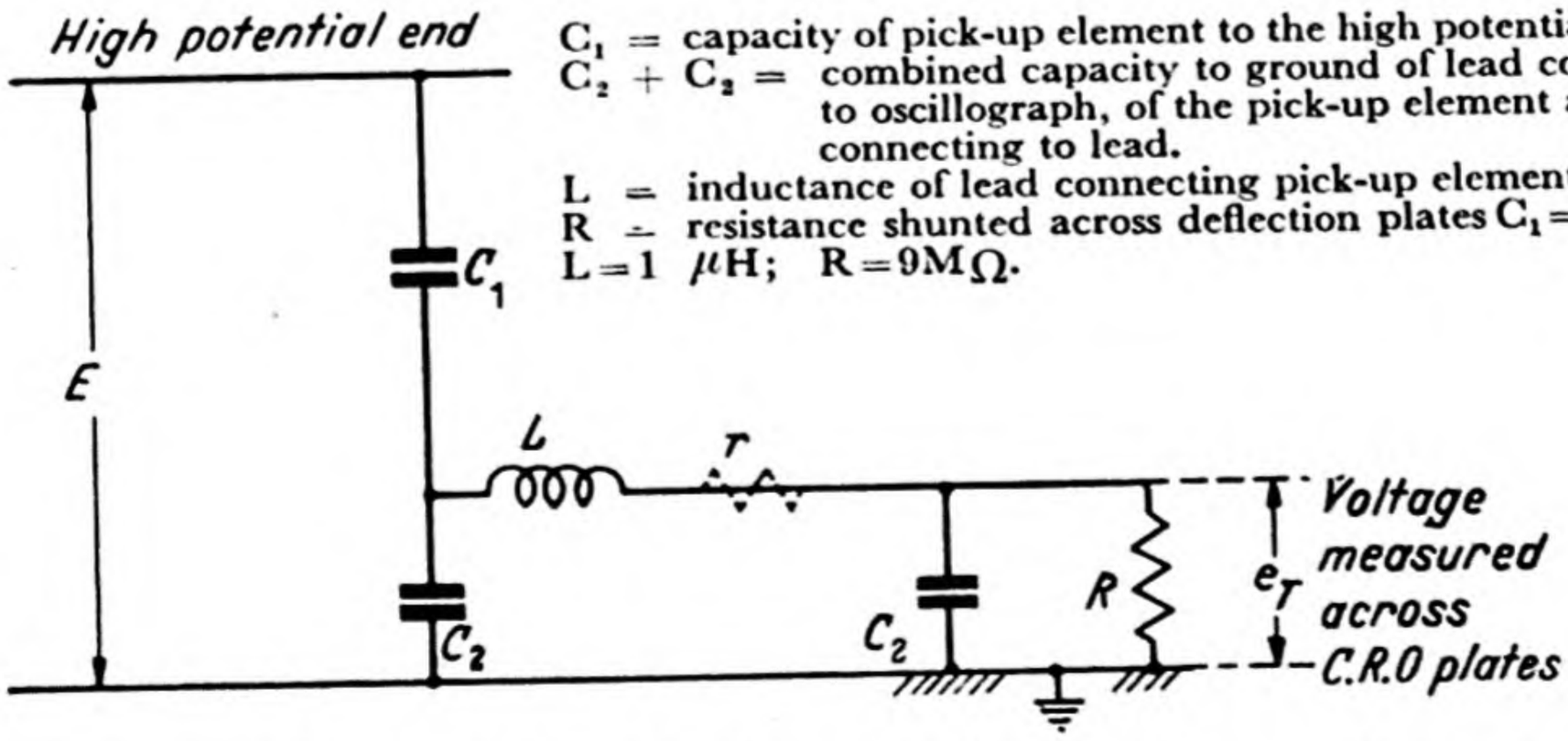

C_1 = capacity of pick-up element to the high potential end or electrode.
$C_2 + C_2$ = combined capacity to ground of lead connecting pick-up element to oscillograph, of the pick-up element and of the deflection plate connecting to lead.
L = inductance of lead connecting pick-up element to oscillograph.
R = resistance shunted across deflection plates $C_1 = 0{\cdot}06$ μμF; $C_2 = 40$ μμF: L = 1 μH; R = 9MΩ.

Figure 285. Equivalent circuit of capacity potentiometer (Bellaschi[21], by courtesy, *Trans. Amer. Inst. elect. Engrs.*).

The discussion of Bellaschi's paper includes detailed contributions by BEWLEY and CLEM to the study of potential dividers. HAGENGUTH[22] has discussed the use of potential dividers in connection with impulse work, in this case a study of short-time sparkover of various forms of discharge gaps. Strigel also gives a treatment of potential dividers, for impulse work, in his book[23] on high-voltage impulse techniques.

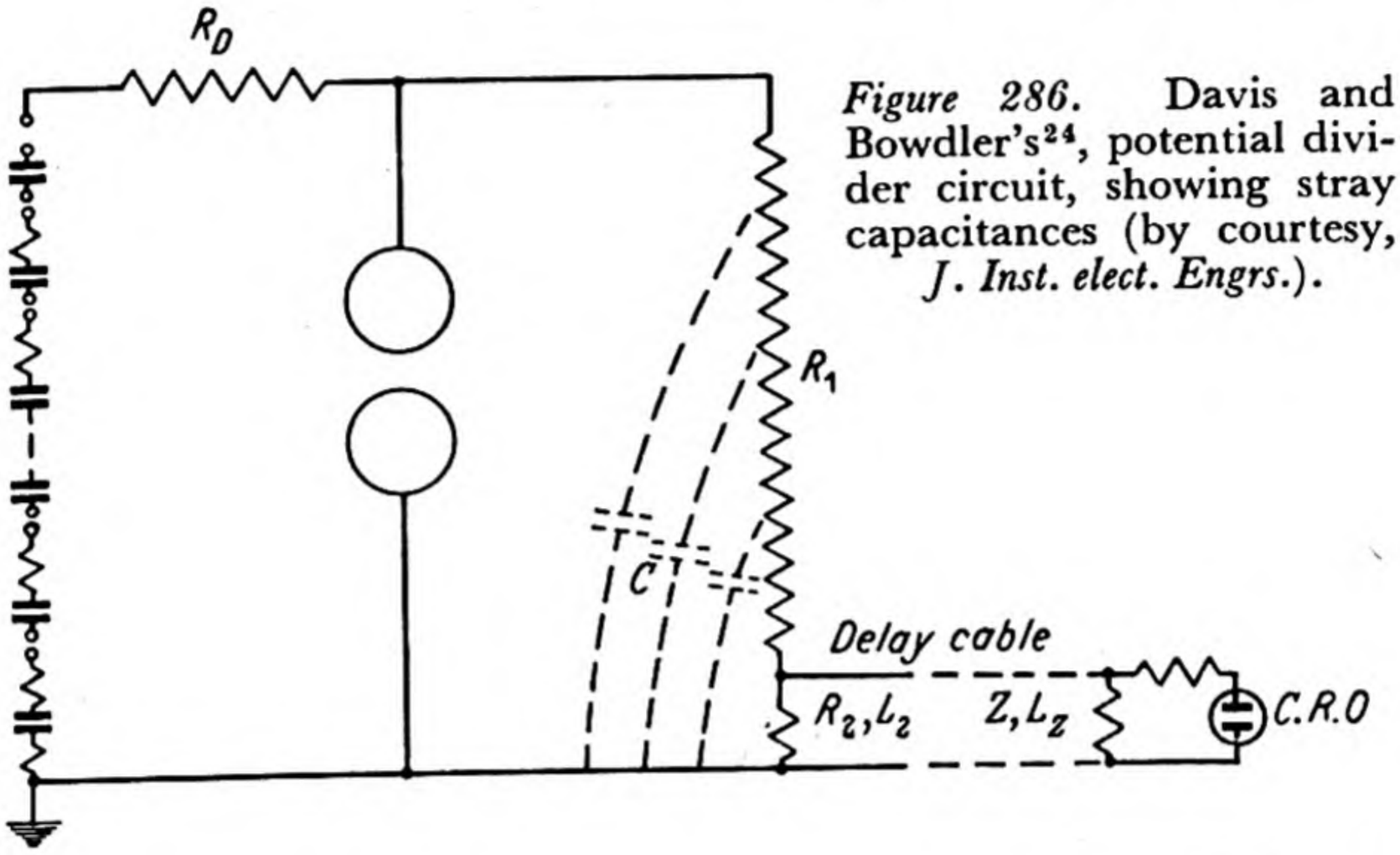

Figure 286. Davis and Bowdler's[24], potential divider circuit, showing stray capacitances (by courtesy, *J. Inst. elect. Engrs.*).

An extension of the above studies is due to Davis and Bowdler[24] who worked with the resistance divider circuit of *Figure 286*, on surges. The stray capacitance, C, of R_1 to ground, is assumed to be uniformly distributed. Then, the authors show, for unit rectangular voltage applied to the potential divider, the current $I(t)$ entering the low-voltage arm is given by

$$I(t) = F_1(t) = \frac{1}{R_1}\left[\,1 + 2\sum_{m=1}^{m=\infty}(-1)^m e^{-\frac{m^2\pi^2 t}{CR_1}}\,\right]$$

and, more generally, if the applied voltage V is of the form $F_2(t)$ then

$$I(t) = F_1(o)\,F_2(t) + \int_0^t F'_1(\lambda)\,F_2(t-\lambda)d\lambda$$

$$= \int_0^t F'_1(\lambda)\,F_2(t-\lambda)\,d\lambda$$

For the practical general case of a double exponential impulse wave where

$$F_2(t) = V(e^{-\alpha t} - e^{-\beta t})$$

$$I(t) = \frac{2\pi^2 V}{CR_1^2}\left[\sum_{m=1}^{m=\infty}\frac{(-1)^{m+1}\,m^2\,e^{-\frac{m^2\pi^2 t}{CR_1}(\beta-\alpha)}}{\left(\alpha-\frac{m^2\pi^2}{CR_1}\right)\left(\beta-\frac{m^2\pi^2}{CR_1}\right)}\right.$$

$$\left. - \sum_{m=1}^{m=\infty}(-1)^{m+1}\left(\frac{e^{-\alpha t}}{\alpha-\frac{m^2\pi^2}{CR_1}} - \frac{e^{-\beta t}}{\beta-\frac{m^2\pi^2}{CR_1}}\right)\right] \qquad \ldots\ldots(9.2)$$

Graphical integration gave the results of *Figure 287* for various impulse wave shapes, from which the importance of reducing CR_1 is apparent.

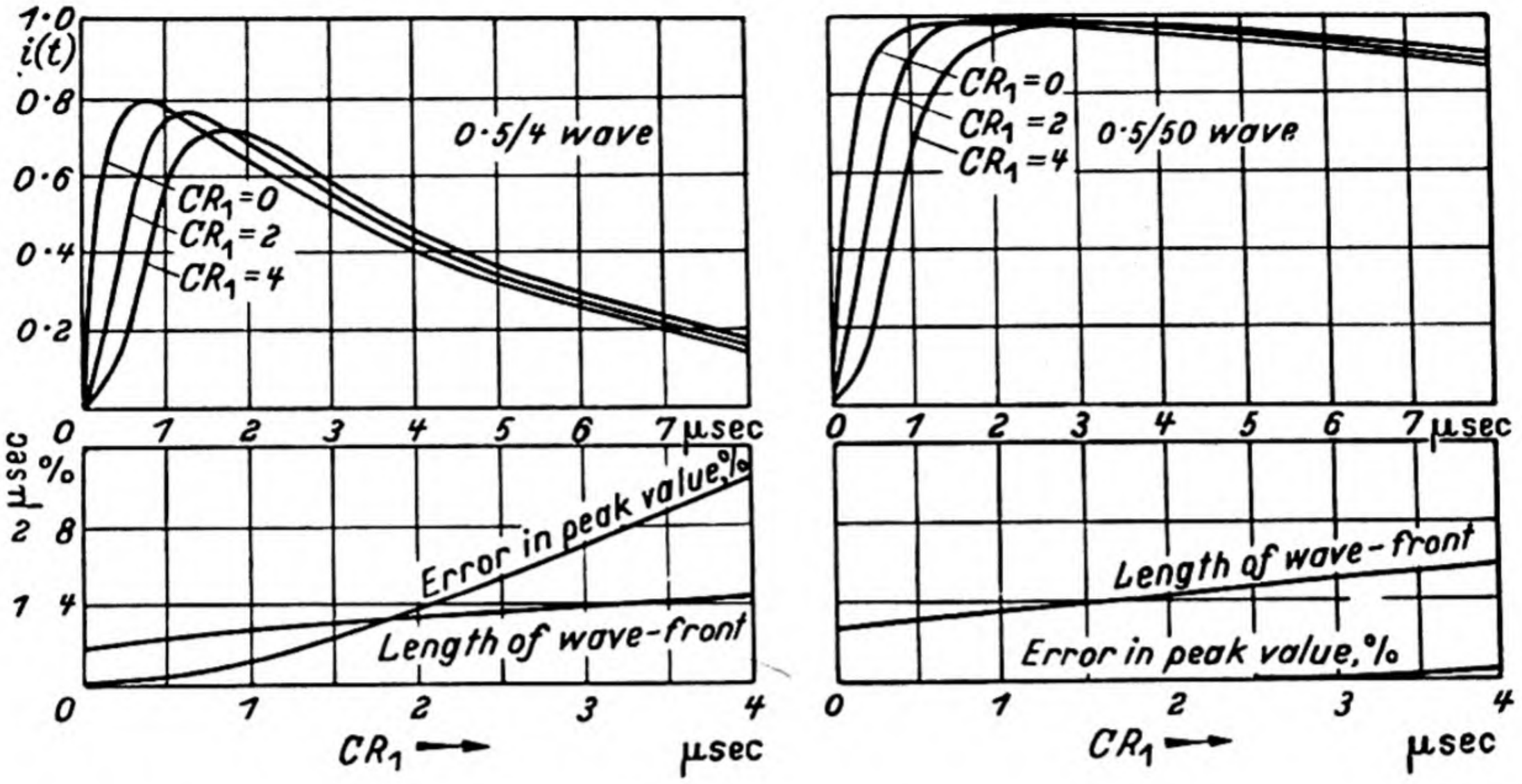

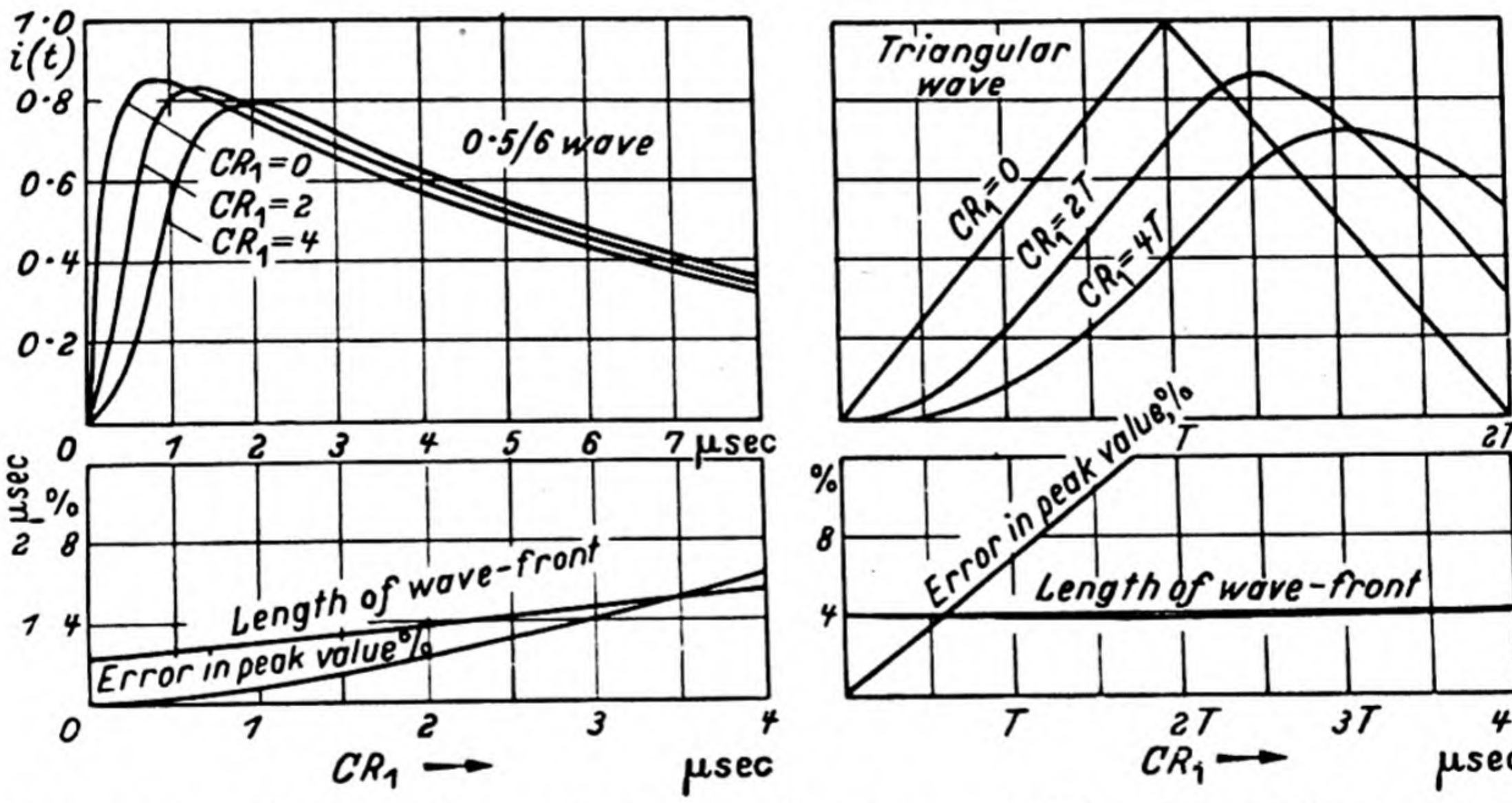

Figure 287. Theoretical response curves of resistance divider, derived from equation

$$i(t) = \int_0^t F'_1(\lambda)\, F_2(t-\lambda)\, d\lambda$$

$$\text{where } F_1(t) = \frac{1}{R_1}\left[1 + 2\sum_{m=1}^{m=\infty}(-1)^m e^{-\frac{m^2\pi^2}{CR_1}\cdot}\right]$$

$$F_2(t) = e^{-\alpha t} - e^{-\beta t}$$

(Davis and Bowdler[21], by courtesy, *J. Inst. elect. Engrs.*).

Top left-hand curve: $\alpha = 0{\cdot}23,\ \beta = 4$
Top right-hand curve: $\alpha = 0{\cdot}014,\ \beta = 4$
Lower left-hand curve: $\alpha = 0{\cdot}014,\ \beta = 4$
$\times\ 10^6$

Experimental work by Davis and Bowdler was carried out with R_1 in the form of a liquid resistance. R_2 and Z were wound non-inductively. The latter, the terminating resistance of the cable, was 121·5 Ω, equal to the impedance of the cable which consisted of a 300 m. length of

coaxial tube, respectively 6·4 mm. and 49·2 mm. in diameter, spaced off at intervals of 1 m. by ebonite pieces, each $\frac{1}{4}$ in. thick. The response of the divider to an 0·5/5 μsec wave was found for R_1 varying from 6,000 to 55,000 Ω and stressed to about *3* kV/cm. R_2 was varied to obtain a suitable output voltage.

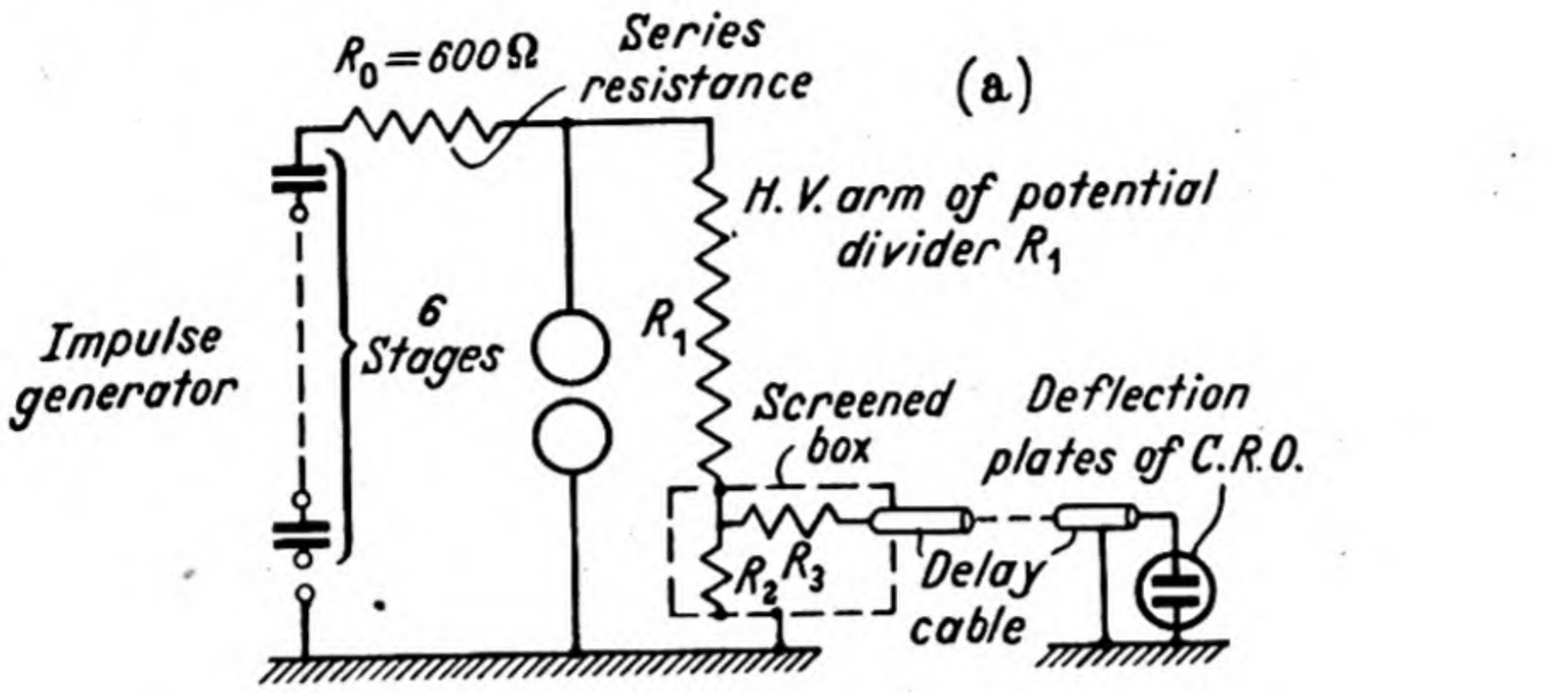
$R_0 = 600\,\Omega$
Series resistance
(a)
H.V. arm of potential divider R_1
Impulse generator
6 Stages
R_1
Screened box
Deflection plates of C.R.O.
R_2 R_3
Delay cable
Ratio of potential divider $m = \frac{R_2}{R_1 + R_2}$
Condition for matching $Z = R_3 + \frac{R_1 R_2}{R_1 + R_2}$ (Z = Surge impedance of delay cable)
(b)
(c)
R_1
R_2
R_4
R_3
Damping resistance
$Z = R_4$ $m = \frac{R_2 Z}{R_1 R_2 + Z(R_1 + R_2)}$
(1) $Z = R_4$ (2) $Z = R_3 + \frac{R_1 R_2}{R_1 + R_2}$
$m = \frac{0.5\,R_2}{R_1 + R_2}$

Figure 288. Tropper's[25] potential divider circuits (by courtesy, British Electrical and Allied Trades Research Association).

Tropper[25] has also studied the response of resistance potential dividers to impulses in a very recent paper. Particular reference is made to the errors introduced by various circuit parameters. The basic idealized treatment due to Burch[11] which is treated above at length, and which deals with loss-free lines and lumped circuit constants, is extended in detail to include a study of the effects of stray capacitance of the divider and cable losses. The circuits are shown in *Figure 288*. For a unit rectangular voltage pulse, Tropper derives the current $I(t)$ in the earthed end of the line, as had Davis and Bowdler[24] (*see* Equation 9·2), and finds

$$I(t) = \frac{1}{k}\left[1 + 2\sum_{m=1}^{m=\infty}(-1)^m e^{-\lambda m^2 t}\right]$$

Then for a voltage impulse given by

$$V(e^{-\alpha t} - e^{-\beta t})$$

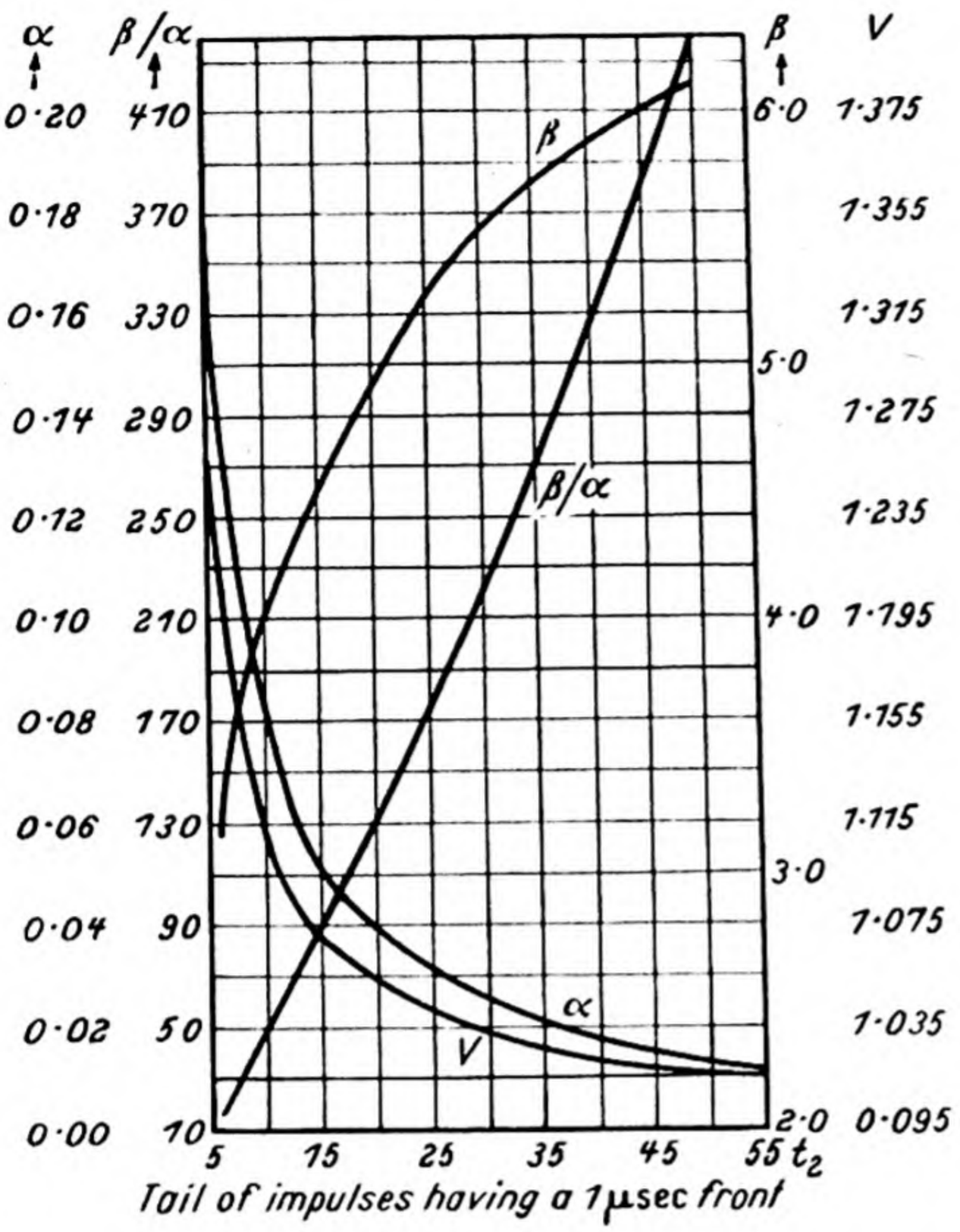

Figure 289 (*above*). α, β, β/α and V as functions of the wave-tail t_2. (Tropper[25], by courtesy, British Electrical and Allied Trades Research Association).

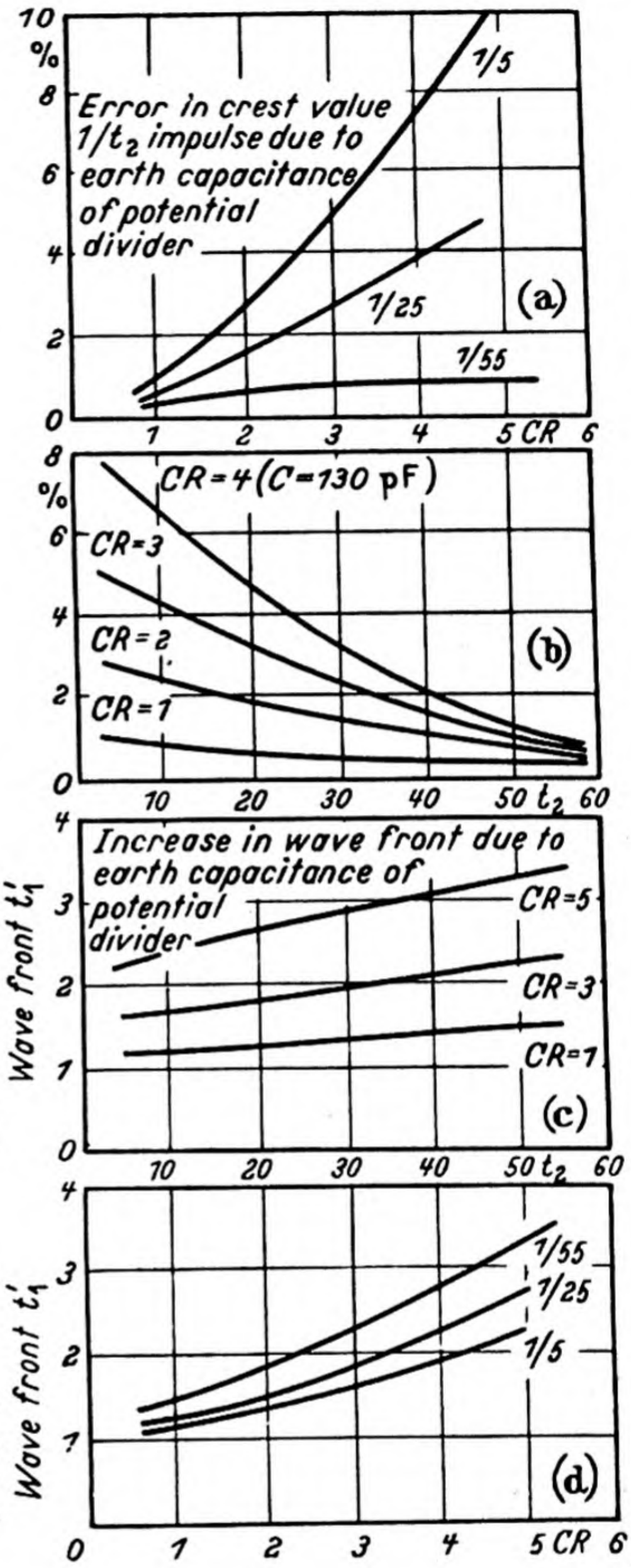

Figure 290 (a–d) (*right*). Error in the crest value due to the earth capacitance of the divider, in Tropper's[25], treatment of potential dividers (by courtesy, British Electrical and Allied Research Association).

Tropper shows, again following Davis and Bowdler,

$$I(t) = \frac{2V}{R}\left[\sum_{m=1}^{m=\infty}\frac{(-1)^{m+1}\,\lambda\, m^2\, e^{-\lambda m^2 t}\,(\beta-\alpha)}{(\alpha-\lambda m^2)(\beta-\lambda m^2)}\right.$$

$$\left. -\sum_{m=1}^{m=\infty}(-1)^{m+1}\,\lambda\, m^2\left(\frac{e^{-\alpha t}}{\alpha-\lambda m^2}-\frac{e^{-\beta t}}{\beta-\lambda m^2}\right)\right] \quad \ldots\ldots(9.3)$$

where C is the total capacitance, assumed evenly distributed, of the divider to earth, R is the total divider resistance, and $CR=\pi^2/\lambda$.

The practical specification of an impulse includes V_o, the peak voltage, the wave-front t_1, the time taken for V_o to be reached, and the wave-tail t_2, which is the time taken for the voltage to decrease to 50 per cent of crest value. t_2 is usually measured from the time when

$0{\cdot}1\,V_0$ is reached in the front. From V_0, t_1 and t_2 the parameters V, α and β can be found, preferably by graphical methods, and, using techniques described by RORDEN[26], the data of *Figure 289* may be obtained. In *Figure 289*, t_2 is plotted as a function of α, β and V for an impulse front of 1 μsec.

Tropper has shown how Equation 9·3 can be transformed in order to facilitate numerical computation. The final equation, derived in detail in the paper[25] by two methods, for $I(t)$ is :—

$$I(t) = \frac{V}{R}\left[2\sum_{m=1}^{m=\infty}\frac{(-1)^{m+1}\cdot\lambda m^2 e^{-\lambda m^2 t}(\beta-\alpha)}{(\alpha-\lambda m^2)(\beta-\lambda m^2)} + \frac{e^{-\alpha t}\sqrt{\frac{\alpha}{\lambda}\cdot\pi}}{\sin\sqrt{\frac{\alpha}{\lambda}\cdot\pi}} - \frac{e^{-\beta t}\sqrt{\frac{\beta}{\lambda}\cdot\pi}}{\sin\sqrt{\frac{\beta}{\lambda}\cdot\pi}}\right]$$

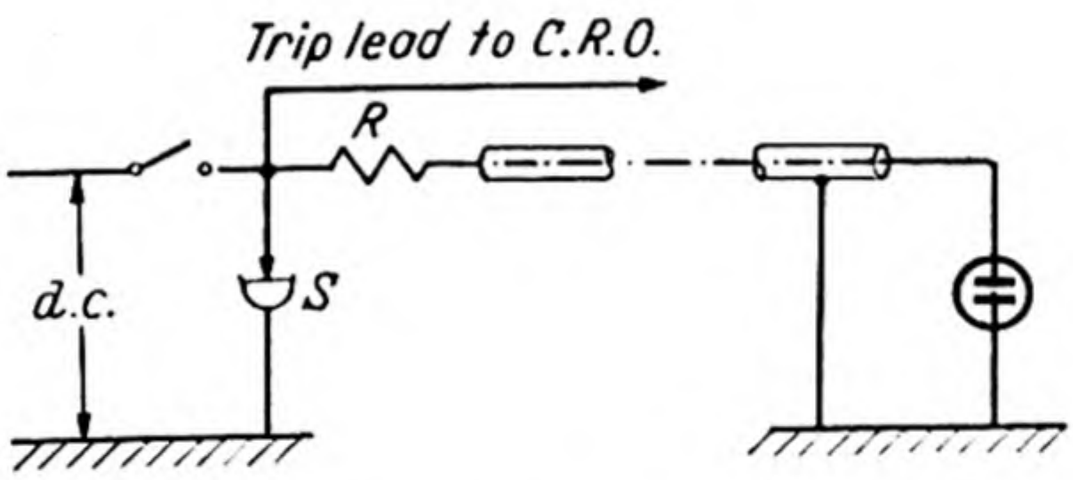

Figure 291. Circuit for the experimental determination of the surge impedance (Tropper[25], by courtesy, British Electrical and Allied Trades Research Assotion).

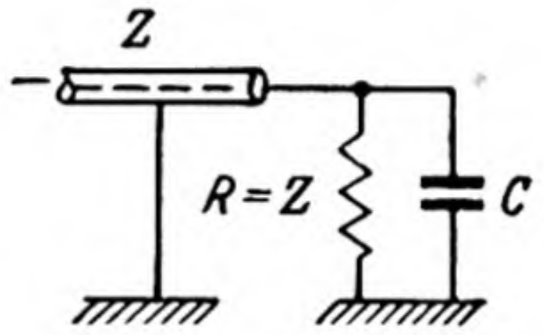

Figure 292. Matched line-end, terminated by a capacitance (Tropper[25], by courtesy, British Electrical and Allied Trades Research Association).

The last two terms are of the form ($\frac{x}{\sin x}$ × exponential term) and can be computed from tables ; thus the practical use of the equation 9·3 is greatly facilitated. In this way the recording errors due to a finite C can be calculated and are given in *Figure 290* a-d. *Figure 290* a shows the error in the peak voltage for various impulse wave-tails, as a function of CR and the data are replotted in *Figure 290* b. In *Figure 290* c and d the spurious lengthening of the front from 1 μsec to t_1 is shown.

Tropper next studied[25] the matching of delay cables in the simple circuit of *Figure 291* where S is a shorting switch. This circuit gives oscillographic records disagreeing with the simple theory of matched lines, for the case where R = cable surge impedance, in that the cable discharge pulses are not simply rectangular, but show small subsidiary waves following the main discharge. Tropper therefore extended the simple theory to include the effects of the deflector plate capacitance in the oscillograph, and stray reactance of the matching resistance. In *Figure 291* if E is the input voltage, Z the line impedance and K the oscillograph input capacitance, it may be shown that the voltage V and

current I at any point in the cable for incident unit function voltage 1 are given by

$$v = \left(A e^{\frac{xp}{v}} + B e^{\frac{-xp}{v}} \right) \cdot 1$$

$$I = \left(-\frac{A}{Z} e^{x/v \cdot p} + \frac{B}{Z} \cdot e^{-x/v \cdot p} \right) \cdot 1$$

where $$A = E \left[\frac{1}{(1-\beta) + e^{2lp/v} \cdot \frac{\alpha+p}{\alpha-p}(1-\beta)} \right] \cdot 1$$

and $$B = E \left[\frac{e^{2lp/v} \cdot \frac{\alpha+p}{\alpha-p}}{(1-\beta) + e^{2lp/v} \cdot \frac{\alpha+p}{\alpha-p}(1-\beta)} \right] \cdot 1$$

$$\alpha = \frac{1}{WK} \text{ and } \beta = \frac{R}{W}, \quad W = \sqrt{\frac{L}{C}}, \quad v = \frac{1}{\sqrt{LC}}$$

Also Z = surge impedance operator $= \sqrt{\frac{R+pL}{G+pC}} = \sqrt{\frac{L}{C}} \cdot \sqrt{\frac{p+R/L}{p+G/C}}$ where R, L, C and G are, respectively, the resistance, inductance capacitance and leakage , all per unit length of line.

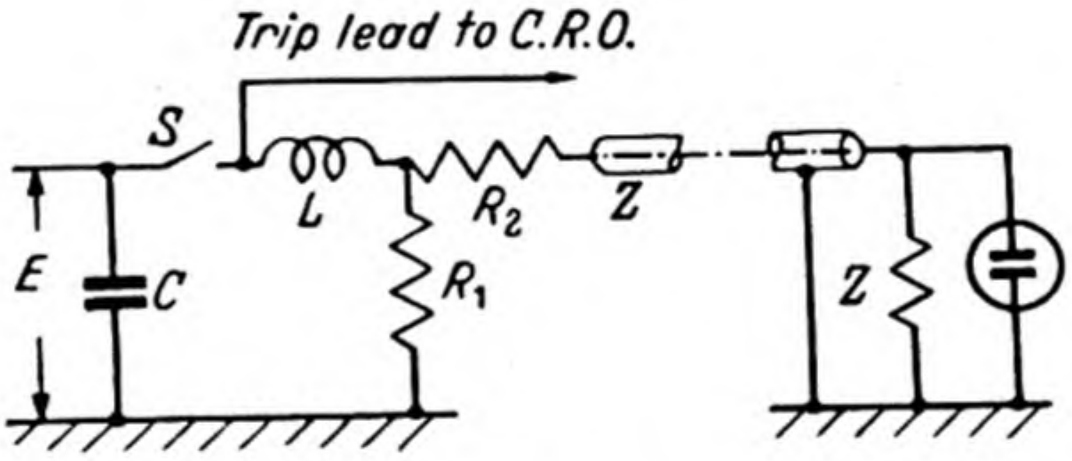

Figure 293. Circuit for the experimental determination of the attenuation of the delay cable (Tropper[25], by courtesy, British Electrical and Allied Trades Research Association).

Finally, the voltage V across the deflector plates is

$$V_l = E \cdot \frac{2\alpha}{p+\alpha} e^{-l/v \cdot p} \cdot \frac{1}{(1+\beta) - (1-\beta)\frac{p-\alpha}{p+\alpha} \cdot e^{-2l/v \cdot p}} \cdot 1$$

When $R=0$, the variation of V_l with time is complex but when $R=W$, *i.e.*, in the matched case, it is found that the only effect introduced when $K=0$ is a reduction in the initial rate of rise of voltage which is governed by the time constant $\frac{1}{\alpha} = WK$.

Study of the effect of stray capacitance across the terminating resistance (*Figure 292*) shows that reflected waves are thereby produced but the use of a matching resistance at both ends of the line (*Figure 288* c) reduces the reflected wave amplitude considerably. Tropper gives oscillograms from which it can be seen that double-matching,

even with a wave-front resistance in the generator of only 600 Ω, virtually removes the spurious waves.

Attenuation losses in the cable may sometimes be appreciable; they can be measured, for example, with the circuit of *Figure 293*. R_1 and R_2, which determine the tail of the impulse, must together equal W, the surge resistance of the cable, for double-matching. L determines the wave-front, and the impulse is obtained by discharging C through R_1 R_2 Z by means of the switch S.

If, first, $R_2 = 0$ and if R is the total circuit resistance comprising R_1 and W in parallel then the output voltage when C is discharged into the cable is given by

$$v(t) = -E\left(\frac{p_1+p_2}{p_1-p_2}\right)(e^{p_1 t} - e^{p_2 t}) = V_o(e^{p_1 t} - e^{p_2 t})$$

where

$$p_1 = \frac{-R}{2L} + \sqrt{\frac{R^2}{4L^2} - \frac{1}{LC}} \quad \text{and} \quad p_2 = \frac{-R}{2L} - \sqrt{\frac{R^2}{4L^2} - \frac{1}{LC}}$$

For a 1/60 wave, using the data plotted in *Figure 289*, $-p_1 = \alpha = 0{\cdot}009$ $\beta = -p_2 = 6{\cdot}2$ so $V_0 = -E \cdot \frac{p_1+p_2}{p_1-p_2} = 1{\cdot}018E$ thus relating E, measured statically, to V_o, the peak value of $v(t)$ where V_0 refers to the voltage wave entering the cable when $t=0$. For the 1/60 wave the crest value is $\frac{1}{1{\cdot}015} \cdot V_o$, *i.e.* is approximately equal to E, the condenser charging voltage. The attenuation in the cable is thus found by comparing V_o with the peak voltage measured on the oscillograph.

When $R_2 \neq 0$, then R is given by R_1 in *Figure 293* in parallel with $(R_2 + W)$ and the cable input in the voltage is

$$v(t) \cdot W/(R_2 + W).$$

The attenuation for the particular rubber insulated cable used in Tropper's experiments was thus found to be 6·8 per cent. Observations on the damping of natural oscillations of the line gave 7 per cent.

LIECHTI[27] has also given a full analysis of resistance, capacitance and resistance—capacitance voltage dividers. The effects of screening, either with resistive or capacitive screens are also discussed, following earlier work by KRUTZSCH[28] and RASKE[29].

Liechti gives the voltage ratio V_n/V_N, where V_N is the voltage across the whole capacitive divider of N stages (*Figure 294*) and V_n is the voltage at stage n as

$$\frac{V_n}{V_N} = \frac{n}{N} \cdot \frac{1 + \frac{1}{3!} \cdot \frac{C_0}{K_0}\left(\frac{n}{N}\right)^2 + \frac{1}{5!}\left(\frac{C_0}{K_0}\right)^2\left(\frac{n}{N}\right)^4 + \cdots}{1 + \frac{1}{3!}\frac{C_0}{K_0} + \frac{1}{5!}\left(\frac{C_0}{K_0}\right)^2 + \cdots\cdots}$$

where C_0 is the total leakage capacitance to earth, K_o is the

total capacitance, $C_0 = Nc_0$, $K_0 = k_o/N$. If $\frac{C_o}{K_o} \leqslant 0{\cdot}06$, for $\frac{n}{N} \geqslant 1$, then the ratio $\frac{V_n}{V_N}$ differs by $\gtrless 1$ per cent. from its nominal value $\frac{n}{N}$. This shows the importance of the stray earth capacitances.

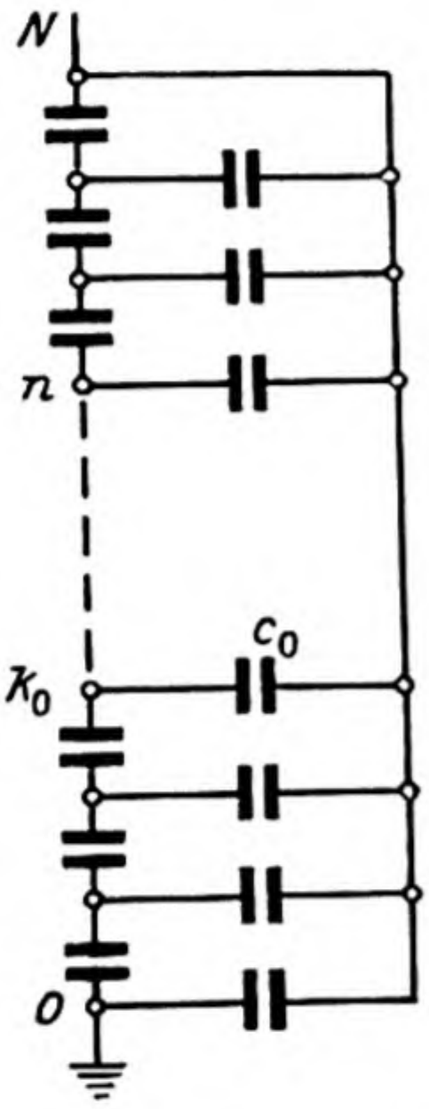

Figure 294. Basic diagram of a capacitative divider (Liechti[27], by courtesy, *Micafil News*).

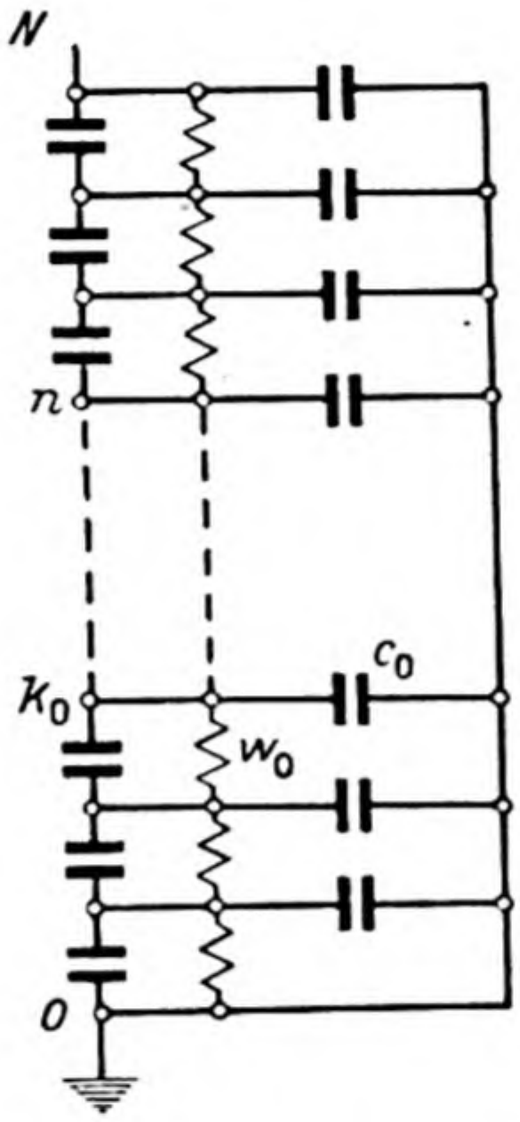

Figure 295. Basic diagram of a combined voltage divider (Liechti[27], by courtesy, *Micafil News*).

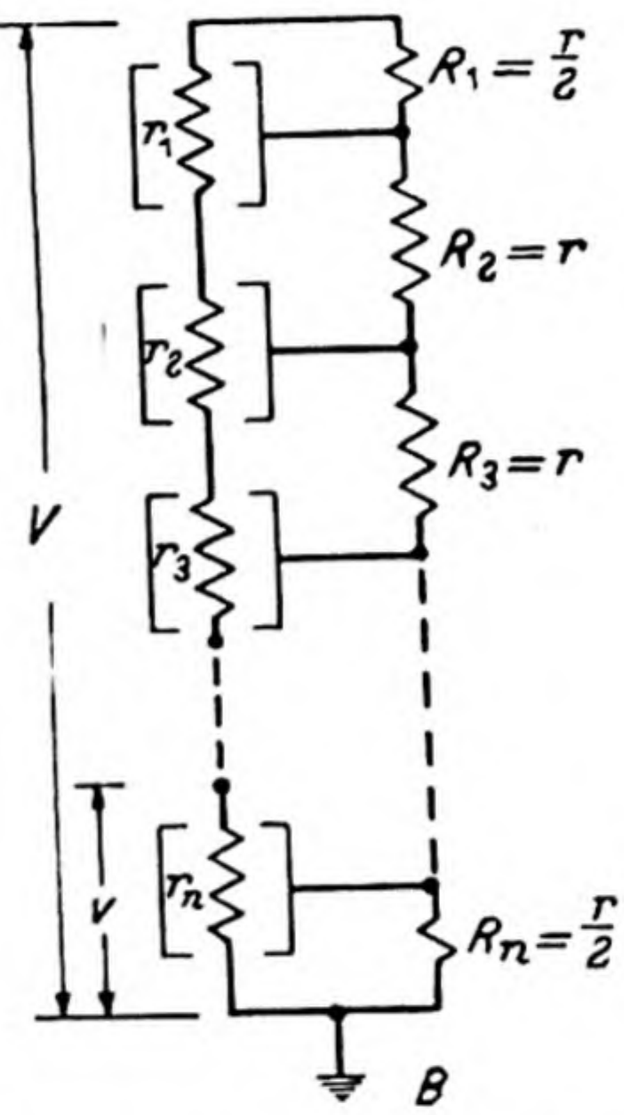

Figure 296. A.C. shielded resistor (Defandorf[34], by courtesy, *J. Washington Acad. Sci.*).

For the combined divider of *Figure 295*, which includes resistances and capacitances in parallel, with leakage capacitances to ground, Liechti also states that the departure of V_n/V_N from the value at zero frequency is $\gtrless 6$ per cent. if $C_o/K_o \leqslant 0{\cdot}36$ (*see* ELSNER[30]). For the resistive divider the self-capacitance can usually be neglected but the leakage capacitance C_o per stage (resistance w_o) is often important. If $W_o = Nw_o$ and $C_o = Nc_o$ then

$$\frac{V_n}{V_N} = \frac{n}{N} \cdot \frac{1 + \frac{1}{3!} \cdot j\omega W_o C_o \left(\frac{n}{N}\right)^2 - \frac{1}{5!}(\omega W_o C_o)^2 \left(\frac{n}{N}\right)^4 + \cdots}{1 + \frac{1}{3!} j\omega W_o C_o - \frac{1}{5!}(\omega C_o W_o)^2 + \cdots}$$

and V_n/V_N does not differ by more than 1 per cent. from its nominal value n/N if

$$1 + \frac{1}{3!} j\omega W_o C_o \leqslant 0{\cdot}1$$

i.e., when $\omega W_o C_o \leqslant 0{\cdot}84$ so long as $n/N \ll 1$.

The effects of capacitive and resistive screens are even more complicated and reference to the above mentioned papers of Krutzsch and Raske should be made. Liechti's article provides a useful summary[27].

The principle of using a guard resistor for low frequency a.c. potential divider work has also been investigated by SILSBEE[31], DAVIS[32], WELLER[33] and others (*see* DEFANDORF[34]). A shielded resistive divider with guard resistor chain R_1—R_n is shown in *Figure 296*. Here the guard resistor supplies the current, taken by the stray capacitances of the shields, that would otherwise flow through the measuring chain of resistors r_1—r_n. Defandorf[34] reports that such a shielded resistor is in use at the National Bureau of Standards for measurements of phase angles and ratios of voltage transformers up to about 30 kV, above which the effects of the stray capacitances across the guard resistors begin

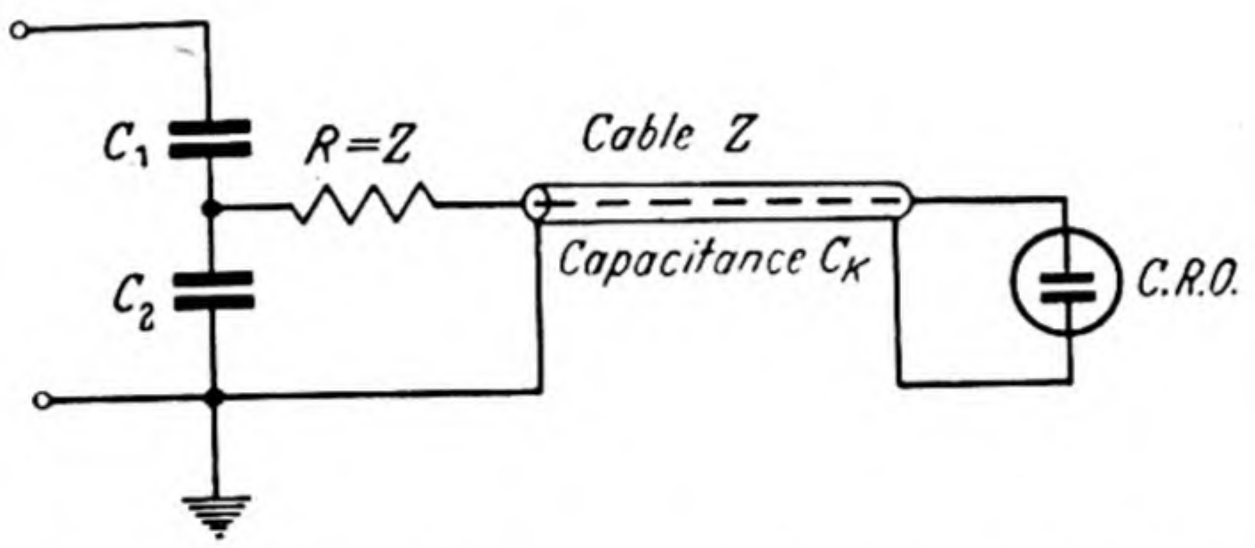

Figure 297. Raske's[37] capacitance potential divider (By courtesy, *Arch. Elektrotech.*).

to be important when voltage measurements to about 0·01 per cent. accuracy are required. In this resistor, each chain (*see Figure 296*) is of 500,000 Ω, is rated at 0·05 A, and is composed of manganin units wound on mica cards.

Very recently, HARRIS[48] has described a precision 1MΩ resistor, wire-wound with manganin in 100 units and oil immersed, for use with d.c. The resistor is rated to withstand 5 kV continuously and oil circulation enabled a stability of a few parts in 10^6 to be achieved. The paper[48] gives full details of the resistor and its characteristics.

Dividers of this type cannot in general be used for surge measurements because of the high stray capacitances due to the shields. Liechti's work, mentioned above, gives a treatment of such cases, and data on resistance dividers with graded capacitance arms have also been given by ELSNER[35] and HÖHL[36].

Raske[37] followed Bellaschi[38] and others in studying capacitance potential dividers for impulse work, and stressed the advantages of such systems for very high voltages and high source impedances in that capacitance dividers can be made of high impedance so that loading of the source may be negligible.

The basic circuit is that of *Figure 297* and, as Burch[11] pointed out, it is important that C_K, the cable capacitance, shall be negligible if the divider ratio for slow impulses *i.e.* $\frac{C_1}{C_1+C_2+C_K}$ shall be sensibly equal to that for rapidly changing voltages where the ratio is $\frac{C_1}{C_1+C_2}$. In view of the expense involved in making the high-voltage capacitance C_1 large, C_K should be small. Consider the equivalent circuit of *Figure 298*, where the earth capacitance of the h.t. terminal of the divider is C_3. The total earth capacitance is $C_e = \frac{C_1C_2+C_1C_3+C_2C_3}{C_1+C_2}$. With unit function input voltage pulse, of peak value V, the voltage u_k at the oscillograph terminals b and c is

$$u_k = V \frac{C_1}{C_1+C_2} (1 - e^{-t/Tm})$$

when the time constant $T_m = C_eZ$ (Z = surge impedance of the line feeding the impulse to a in *Figure 298*). Both C_e and Z should be made

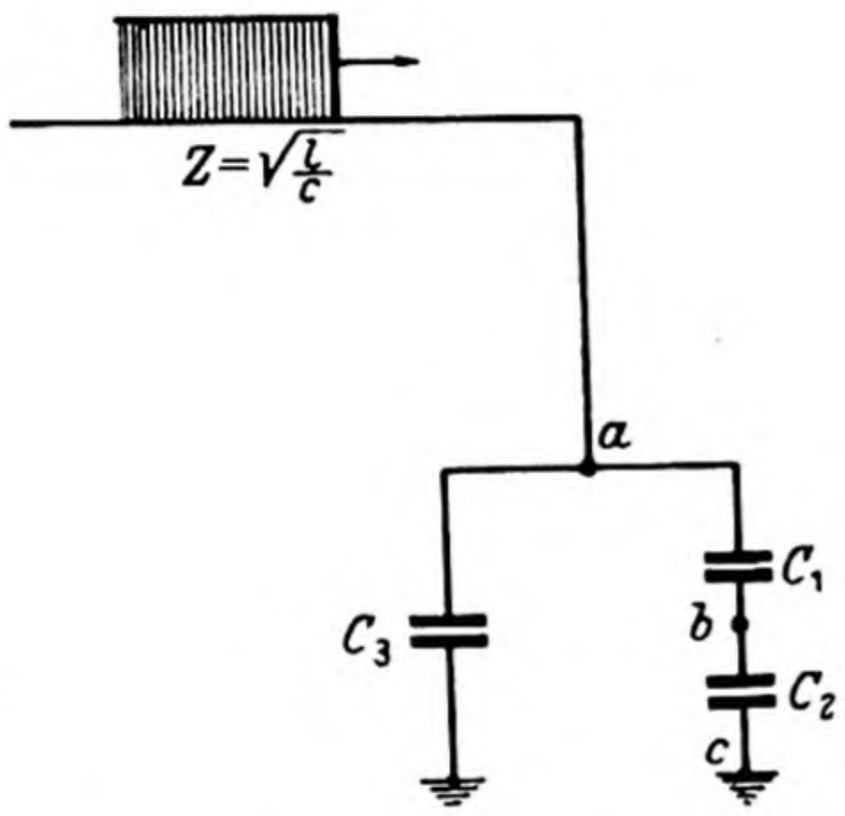

Figure 298. Basic circuit of Raske's potential divider of *Figure 297*, introducing stray capacitance C_3 (Raske[37], by courtesy, *Arch. Elektrotech.*).

small to avoid excessive flattening of the front of the impulse. If the input voltage impulse to the divider is put as

$$u = V (e^{-at} - e^{-bt}) \text{ for } t > 0$$

then the voltage at the oscillograph terminals will be

$$u_k = V \frac{C_1}{C_1+C_2} \cdot \frac{1}{1-aT_m} (e^{-at} - e^{-t/T_m}) - \frac{1}{1-bT_m} (e^{-bt} - e^{-t/T_m})$$

The response of a divider having $T_m = 16$ μsec to a very fast impulse is shown in *Figure 299* where the input wave is

$$u = 1{\cdot}02 (e^{-1{\cdot}2\times10^6 t} - e^{-0{\cdot}52\times10^9 t})$$

The reduction in the peak voltage is 5·9 per cent., due to the effect of T_m.

Bellaschi[38] has used a capacitance potential divider, *see Figure 285*, in which C_1 is the stray capacitance between the h.t. source and, say, an exposed plate connected to the oscillograph terminals (suitably shunted by a very high resistance). This arrangement is liable to disturbance due to pick-up and to the large effect on C_1, which is often

then only of a few $\mu\mu$F, of movable objects in the neighbourhood. Thus BINDER[39], MESSNER[40], NUTTALL[41] and others have adopted systems, suggested also by Rogowski[37] in which the capacitance divider is mounted inside a high-voltage cathode-ray oscillograph, of the continuously-pumped type (*see* pages 346–354). Raske[37] describes such

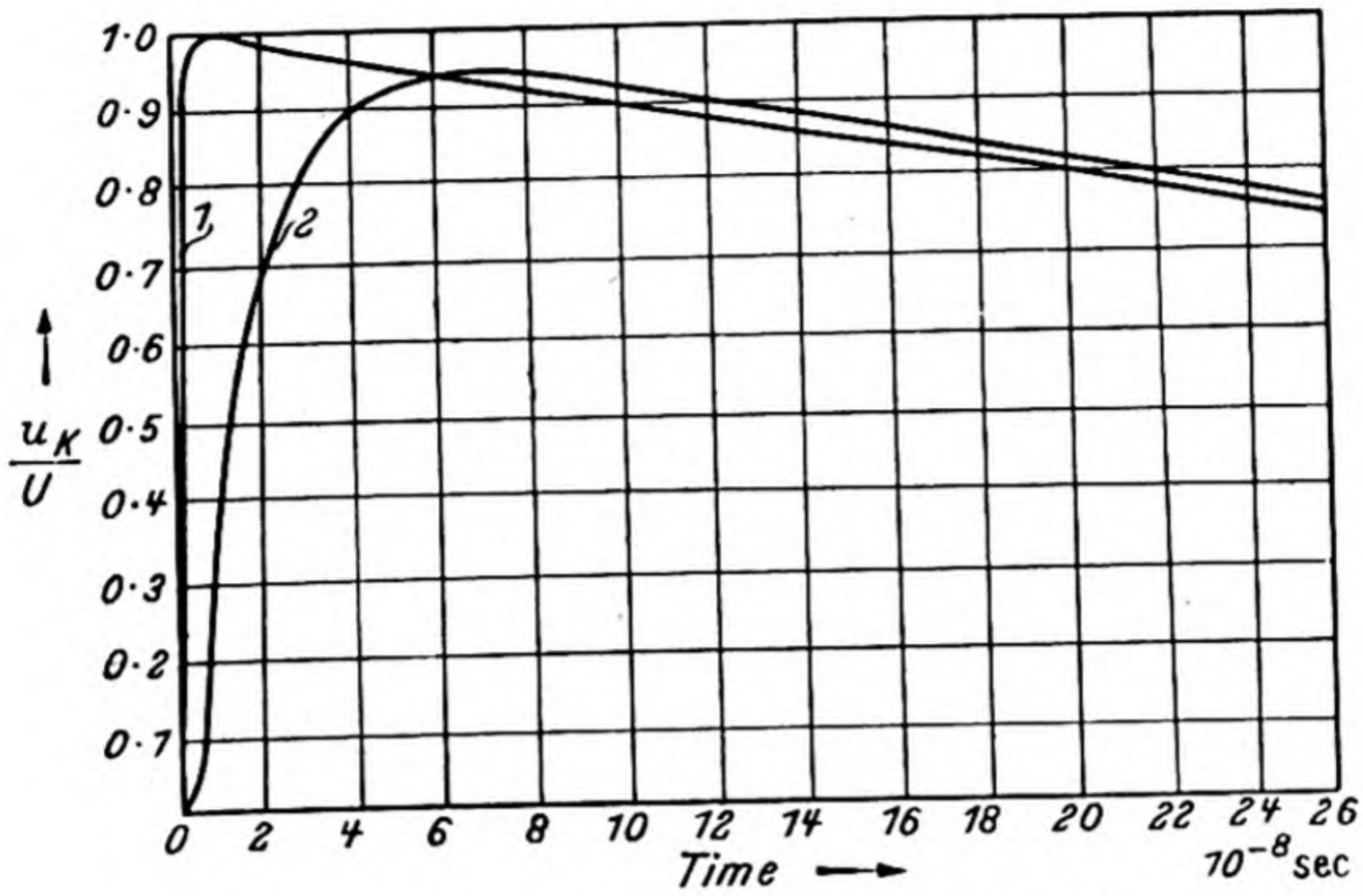

Figure 299. Response of Raske's potential divider. 1 and 2 are respectively the input and output wave-forms (Raske[37], by courtesy, *Arch. Elektrotech.*).

a system in detail. In general this technique is limited to, perhaps, 150–200 kV impulses.

Potential dividers, as built into cathode-ray oscillographs, have often been arranged with a variable ratio by means of adjustable screens which in effect alter the high-voltage capacitance. For example, Raske's system uses a variable iris diaphragm so that the capacitance between the high-voltage electrode and the deflector plate is adjustable. This gives an almost uniform field between the deflector plates in the region traversed by the electron beam. Raske has measured, with an electrolytic field plotting tank, the potential variations throughout the electrode system from which the electron trajectory can easily be computed. For voltages ~100 kV, the high-voltage electrode must be mounted in a suitable bushing.

Many similar devices are practicable. NUTTALL's[41] system for 100 kV is described elsewhere (page 352).

Höhl's work[36] on high-voltage potential dividers, using cathode-ray oscillographs, is noteworthy. The limit of recording times was ~10^{-8}sec. Capacitive, resistive and capacitive-resistance potential dividers were used and the voltage wave system set up in a 400 m. cable was measured. Höhl claimed that the resistive dividers could be used over the frequency range 0–10^7c/s and other types at least over the 0–10^9c/s.

The relative merits of resistance and capacitance potential dividers have been briefly summarized by MILLER and ROBINSON[42]. Resistance dividers are difficult to shield and their use is almost restricted to the measurement of terminal voltage, but they may in general give less loading of a delay cable than a capacitance divider. Their frequency response is limited but often adequate. Capacitance dividers, assumed to be shielded, generally impose less load on the high-voltage circuit and tend to act merely as an extra stray capacitance to ground, although when used with a delay cable the total divider capacitance requires to be increased, to limit distortion, as shown above. Capacitance dividers tend to be bulky, but Miller and Robinson[42] suggest that the possible use of compressed gas, liquid or solid dielectrics for the high-voltage capacitor has not been fully explored.

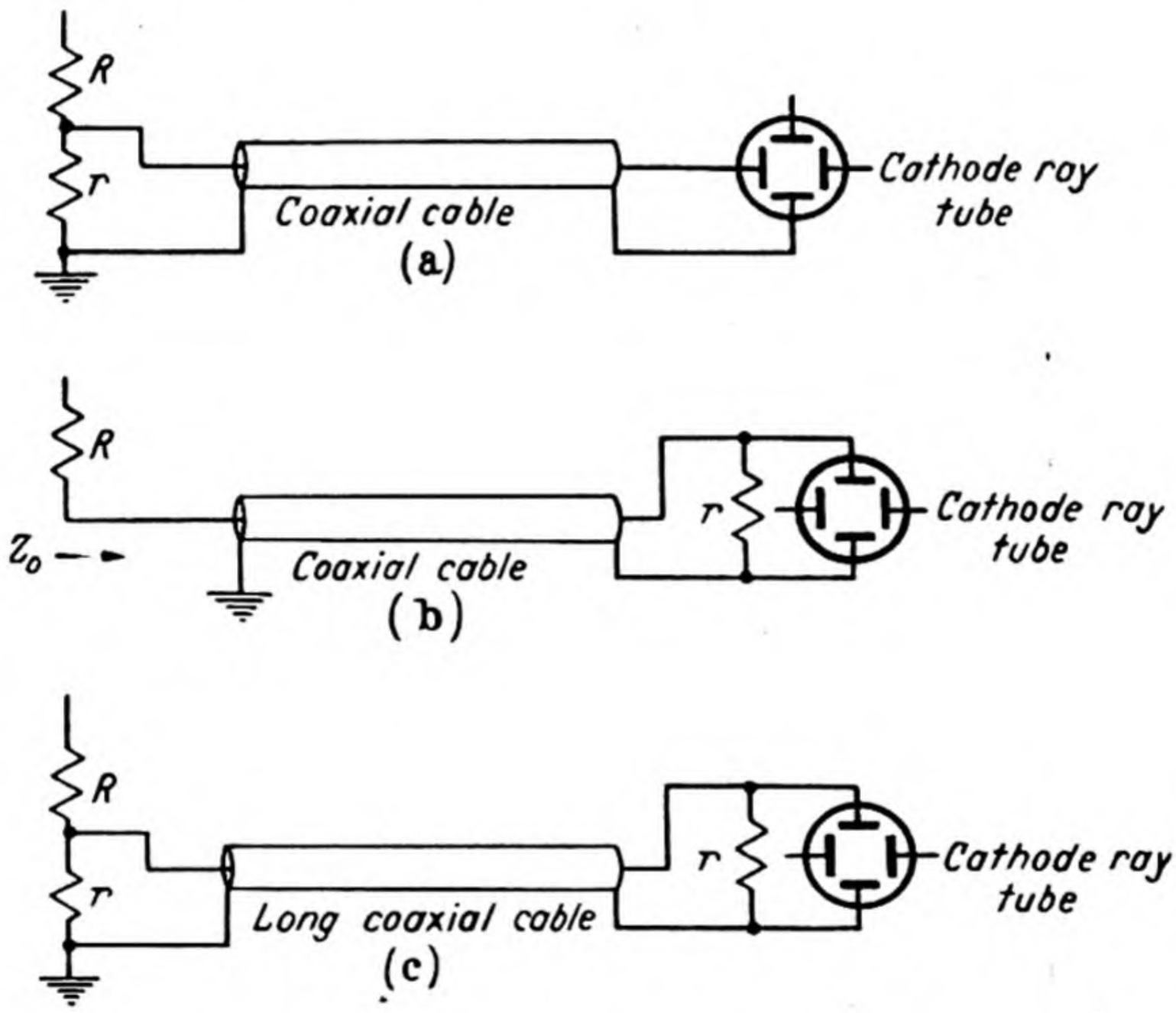

Figure 300. Resistive potential divider circuits (Cooper[45], by courtesy).

Measurements on the transient behaviour of resistance potential dividers have also been made by Raske[29] who made a special study of the effect of stray capacitances shunted across the divider. Raske carried out exhaustive tests on liquid resistances for high-voltage work, and investigated their variation with voltage and with the nature of the applied voltage. In view of the complex behaviour of such resistances their use in precision measurements is restricted, but as current-limiting devices where great stability is often not required they may be convenient. Liquid resistances for high-voltage d.c. work have been described by GRAY and READ[43], CRAGGS[44] and others.

More recent work on the measurement of unidirectional impulse voltages with resistive potential dividers is due to COOPER[45], who studied impulses of durations varying from 0·1 to 4 μsec, 20 kV, repeated at rates up to 3,000 per second. The pulses were of negative polarity. A 5 kV cathode-ray oscillograph was used with the potential dividers for the measurement of voltage, in the circuit of *Figure 300* which is self-explanatory. The cable impedance was 74·6 Ω.

Preliminary tests with 1 μsec pulses were made with the circuits of *Figure 300* a and b where r was made equal to the cable impedance, and no differences were found with a sphere gap used as standard. The arrangement of *Figure 300* was adopted because of its greater convenience but it was found necessary with 0·1 μsec pulses to modify the circuit, by the introduction of a 50 ft. length of 75 Ω delay line (*Figure 300* c) in order to allow the oscillograph time base to be tripped in good time for observation of the pulse.

For the measurement of voltage on the oscillograph screen, Cooper used D.C. bias on the Y-plates to bring the peak of the observed pulse back to a standard base-line marked across the screen, and to which the time sweep, with no Y-voltage applied, had originally been set. The bias voltage was measured in a normal fashion.

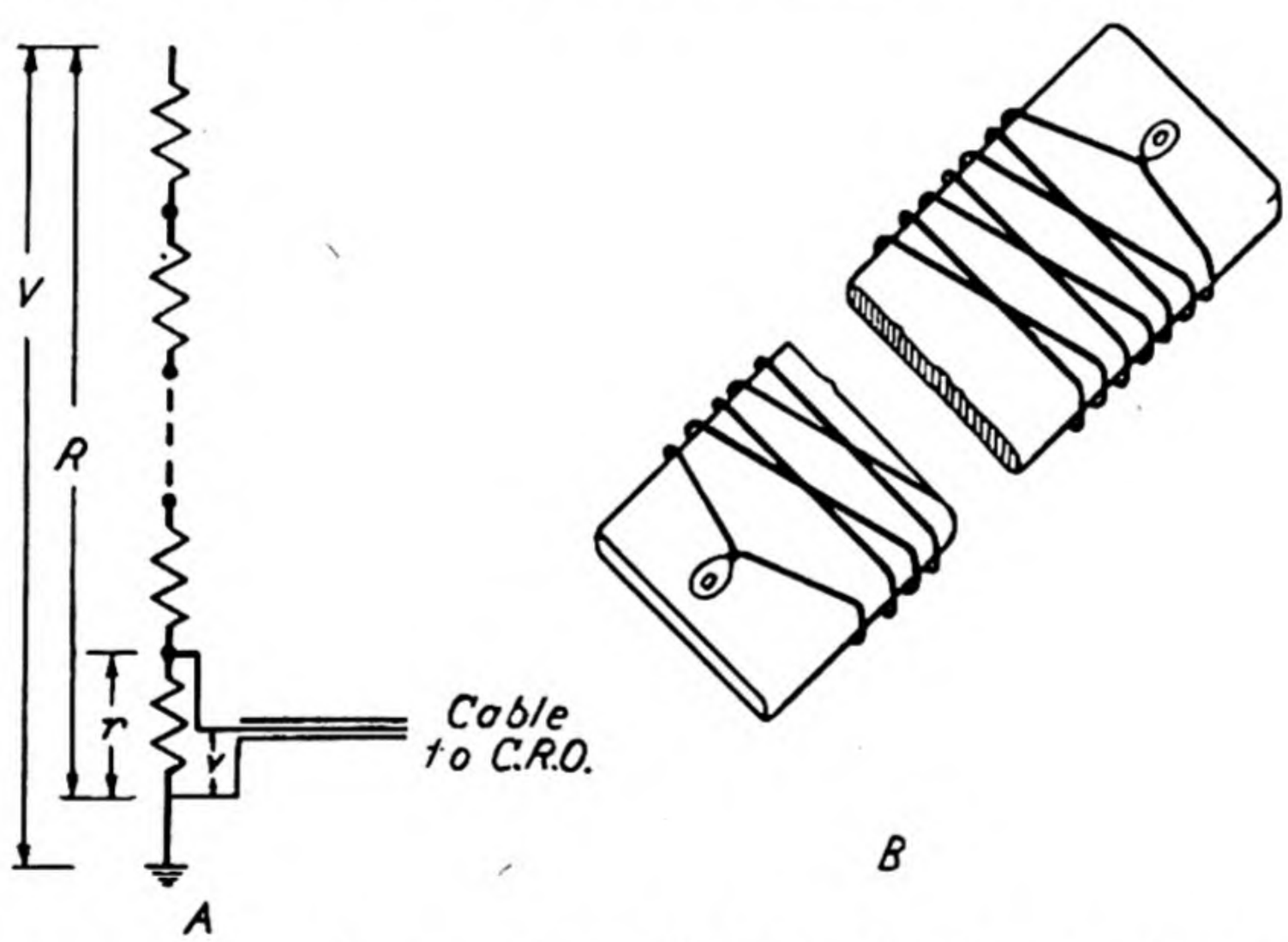

Figure 301. Surge resistor (Defandorf[34], by courtesy, *J. Washington Acad. Sci.*).

The tapping resistance r was made from about 2 m. of d.s.c. Eureka wire-wound non-inductively by doubling the wire on itself and winding it on to a thin mica sheet as shown in *Figure 301* (Defandorf[34]). Cooper states that the inductance (L) was $< 1\,\mu$H and the quantity L/r could be made $< 10^{-8}$ so that even with 0·1 μsec pulses the time constant of r was negligible. However, no direct measurement of L was made in this work. HOWARD[49] also discusses the low-voltage resistance arm, and deals with an N.P.L. pattern.

The high-voltage resistance R introduces more problems. For example, the stray capacitance of the resistor to ground must be made small to avoid spurious results. Cooper shows that if u is defined as $u = \frac{\pi^2}{RCl^2}$ where R and C are the resistance and stray capacitance to earth per unit length of the potential divider, of length l then, if t be the time, a value $ut = 6$ will give approximately the zero error due to the RC time-constant effect. This is shown by plotting the quantity

$$\tfrac{1}{2} + f(ut) = [\tfrac{1}{2} + \{ - e^{-ut} + e^{-4ut} - e^{-9ut} + e^{-16ut} \}]$$

as a function of ut. This quantity can be shown, by considering a square pulse to be the resultant of two Heaviside unit functions, of opposite sign and applied at time $t = 0$ and $t =$ pulse length $(+ve)$, to be the current flowing in the earthed end of the resistance if the square pulse voltage is applied at the h.t. end of the resistor. For the carbon resistance unit, described below, the total stray capacitance was 8·5 $\mu\mu$F and with $ut = 6$, this gives $t = 0{\cdot}06$ μsec at the time in which the recorded pulse height reaches its true value. This time was less than that of the shortest pulses used in Cooper's work.

The resistors used to form the high-voltage resistance R consisted of both wire-bound and carbon types. The wire-wound unit was composed of No. 44 S.W.G. wire rated at 5 mA, although at 20 kV only 2 mA flowed. Units of this type, in air, are liable to give corona discharges (see, however, the details given in Chapter 11). The carbon resistance unit was constructed from fifteen 3 W 700 Ω units mounted on a polystyrene sheet. Some care was needed in allowing for the temperature coefficient of resistance since r is a metallic resistance. The temperature variation of resistance for the carbon resistors used is given in *Figure 302* and using this curve, the potentiometer readings can be corrected to give an accuracy of rather better than 1 per cent.

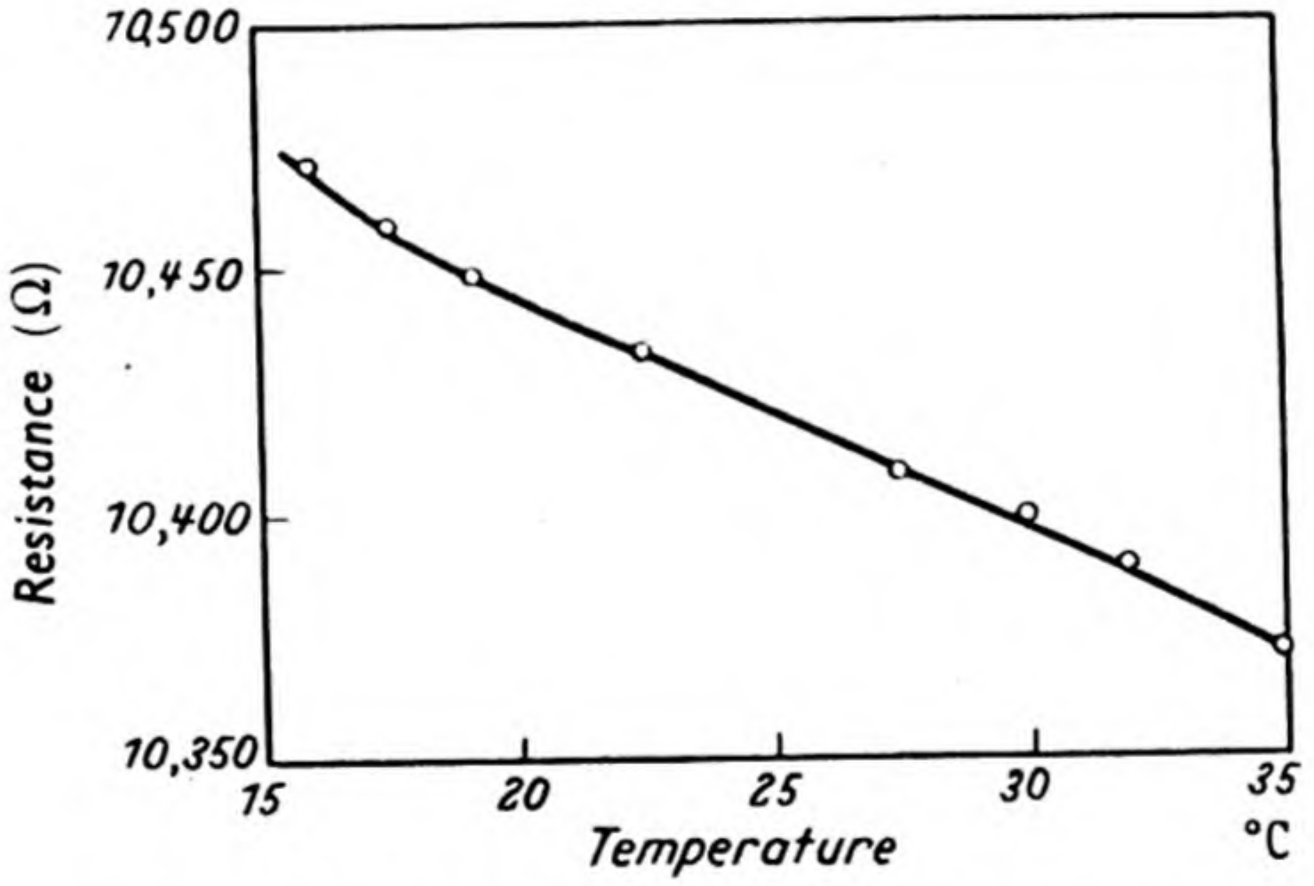

Figure 302. Thermal characteristic for a carbon base resistance (Cooper[45], by courtesy).

Cooper[45] also tested an electrolytic resistance for the h.t. element of the potentiometer but abandoned this work because of the high temperature-coefficient of resistance.

A 1 μsec voltage pulse was measured with the wire-wound and carbon resistors described above, over the range 6–22 kV and the readings agreed always to within 3 per cent. with a smaller average error. Cooper claimed an accuracy of about ± 2 per cent. which included the errors of reading the bias voltmeter for the oscillograph and the finite line thickness on the screen of the latter, and of measuring the resistances of the potentiometer elements.

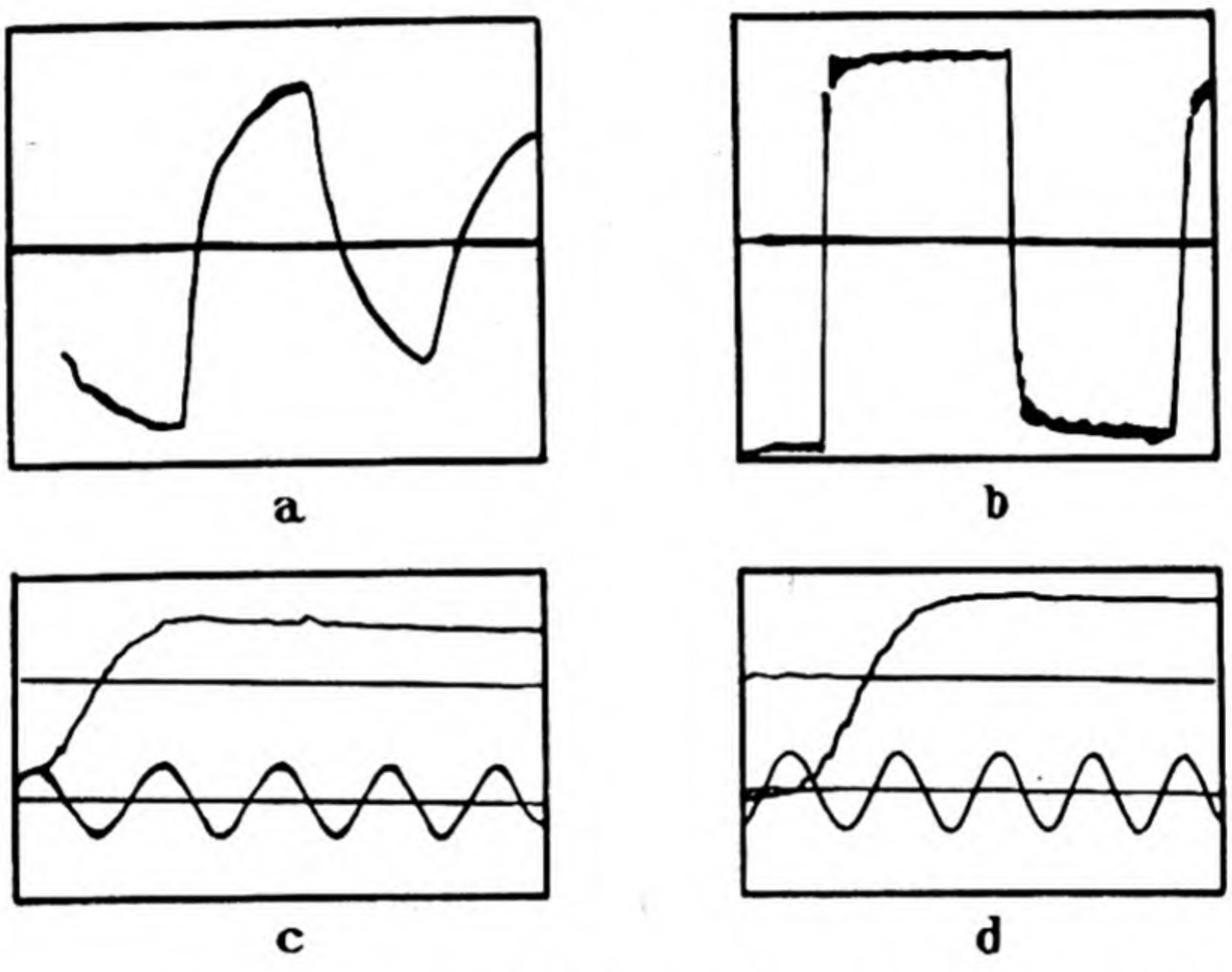

Figure 303. Comparison of a rubber-insulated delay cable (A) with an air-insulated delay cable (B). (Allibone *et al.*[46], by courtesy, *J. Inst. elect. Engrs.*).
(a), (b) = reflected waves on cables A and B respectively.
(c), (d) = 1μsec wave-front recorded on cables A and B respectively.

Allibone, Hawley and Perry[46], in the course of certain oscillographic studies of impulse phenomena, used, for work at ~ 1 MV, a resistance potential divider with 50 yards of rubber-insulated, lead-sheathed, cable. They found the attenuation in this cable to be appreciable, and therefore constructed a 100 m air-insulated cable with a surge impedance of 170 Ω. The relative behaviour of these two cables may be assessed from the oscillographic records of *Figure 303* in which a 1 μsec wave-front is shown. This comparatively slow-fronted wave is recorded with little error in both cases but the attenuation is obviously greater with the rubber-covered cable. The high impedance of the air-covered cable is also an advantage in that it enables a higher resistance potentiometer to be used. The circuit of *Figure 304* where $(R_2 + R_3) = 170\,\Omega$ was used by Allibone, Hawley and Perry[46]. R_1 was a water-tube resistance of fixed value and R_2 was

varied to give the required step-down ratio, subject to the above requirement for the value of $(R_2 + R_3)$. The above authors[46] show that recording errors can be introduced if insufficient attention is given to earthing.

A non-linear resistive potential divider for the measurement of impulse voltages has been used by HIGHAM and MEEK[47] in a study of voltage gradients in long spark channels. The high-resistance element R_1 was in series with a low resistance R_2 of 65 Ω, which matched the

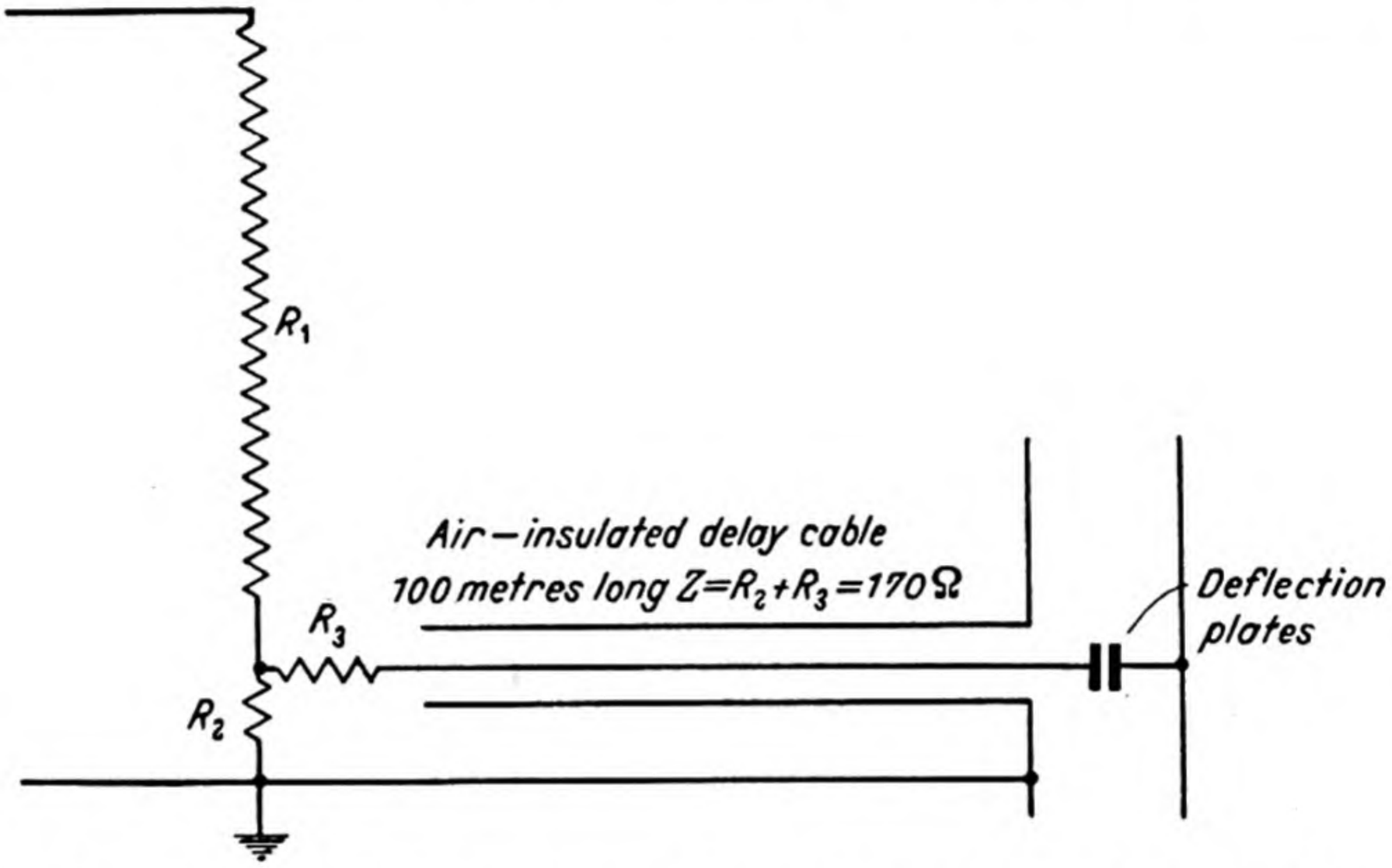

Figure 304. Arrangement of resistance potential-divider for cathode ray oscillograph measurements (Allibone *et al.*, by courtesy, *J. Inst. elect. Engrs.*).

surge impedance of the cable leading to the oscillograph, and across R_2 was shunted a block of the semi-conducting material Metrosil (Metropolitan-Vickers). The characteristic of the block was $V = KI^{\beta}$ (V = voltage across the block for a current I through it). K and β are constants ($\beta \simeq 0{\cdot}25$). Thus the potential divider was less sensitive for high voltages. The divider was used to prevent the application of excessive voltages to the oscillograph deflector plates, whilst leaving the low-voltage sensitivity virtually unaltered.

A very recent review of potential divider techniques for impulse measurements has been published by HOWARD[49]. Resistance, capacitance and mixed dividers are fully discussed and great emphasis is given to the errors involved. Consequently, the paper is of great value to experimental workers, and it is unfortunate that it appeared too late for detailed consideration in this Chapter.

REFERENCES

1 RYMER, T. B., and WRIGHT, K. H. R. *J. Sci. Instrum.*, **29** (1952) 139.
2 PRESTON, J. S. *J. Sci. Instrum.*, **23** (1946) 173.
3 KUNTKE, A. *Philips Tech. Rev.*, **2** (1937) 161.

REFERENCES

4 DAVIS, R., BOWDLER, G. W., and STANDRING, W. G. *J. Inst. elect. Engrs.*, **68** (1930) 1222.
5 EDWARDS, F. S., and SMEE, J. F. *J. Inst. elect. Engrs.*, **82** (1938) 655.
6 SHARP, C. H., and DOYLE, E. D. *Trans. Amer. Inst. elect. Engrs.*, **35** (1916) 99.
7 CHUBB, L. W., and FORTESCUE, C. *Trans. Amer. Inst. elect. Engrs.*, **32** (1913) 739.
8 PALM, A. *Z. Tech. Phys.*, **14** (1933) 390.
9 BOUSMAN, H. W., and TEN BROECK, R. L. *Trans. Amer. Inst. elect. Engrs.*, **62** (1943) 541.
10 CHURCHER, B. G., and DANNATT, C. *J. Inst. elect. Engrs.*, **69** (1931) 1019.
11 BURCH, F. P. *Phil. Mag.*, **13** (1932) 760.
12 GÁBOR, D. *Forschungshefte der Studiengesellschaft für Höchstspannungsanlagen. I.* 1927.
13 NORINDER, H. *Z. Phys.*, **63** (1930) 672.
14 ELECTRICAL RESEARCH ASSOCIATION. *Surge Phenomena.* London, 1941.
15 BOUWERS, A. *Elektrische Höchstspannungen.* Berlin, 1939.
16 KOHLRAUSCH, F. *Praktische Physik.* Leipzig, 1939.
17 PALM, A. *Elektrotech. Z.*, **47** (1926) 904.
18 SCHERING, H., and VIEWEG, R. *Z. Tech. Phys.*, **9** (1928) 442.
19 CHURCHER, B. G., and DANNATT, C. *World Power*, **5** (1926) 238.
20 DOWELL, J. C., and FOUST, C. M. *Trans. Amer. Inst. elect. Engrs.*, **52** (1933) 537.
21 BELLASCHI, P. L. *Trans. Amer. Inst. elect. Engrs.*, **52** (1933) 544.
22 HAGENGUTH, J. H. *Elect. Engng.*, **56** (1937) 67.
23 STRIGEL, R. *Elektrische Stossfestigkeit.* Berlin, 1939.
24 DAVIS, R., and BOWDLER, G. W. *J. Inst. elect. Engrs.*, **82** (1938) 645
25 TROPPER, H. *E.R.A. Report L/T* 168 (1946).
26 RORDEN, H. L. *Trans. Amer. Inst. elect. Engrs.*, **51** (1932) 824.
27 LIECHTI, A. *Micafil News*, 1945, p. 25.
28 KRUTZSCH, J. *Elektrotech. Z.*, **57** (1936) 439.
29 RASKE, W. *Arch. Elektrotech*, **31** (1937) 653.
30 ELSNER, R. *Arch. Elektrotech*, **33** (1939) 23.
31 SILSBEE, F. B. *Bur. Stds. Sci. Papers*, **20** (1925) 489.
32 DAVIS, R. *J. Inst. elect. Engrs.*, **69** (1931) 1028.
33 WELLER, C. T. *Trans. Amer. Inst. elect. Engrs.*, **48** (1929) 312.
34 DEFANDORF, F. M. *J. Washington Acad. Sci.*, **38** (1948) 33.
35 ELSNER, R. *Arch. Elektrotech.*, **36** (1942) 329.
36 HÖHL, H. *Arch. Elektrotech.*, **35** (1941) 663.
37 RASKE, W. *Arch. Elektrotech.*, **31** (1937) 732.
38 BELLASCHI, P. L. *Trans. Amer. Inst. elect. Engrs.*, **52** (1933) 553.
39 BINDER, L. *Elektrotech. Z.*, **52** (1931) 735.
40 MESSNER, M. *Arch. Elektrotech.*, **27** (1935) 335.
41 NUTTALL, A. K. *J. Inst. elect. Engrs.*, **78** (1936) 229.
42 MILLER, J. L., and ROBINSON, J. E. L. *J. Inst. elect. Engrs.*, **74** (1934) 511.
43 GRAY, L. H., READ, J., and WYATT, J. G. *Brit. J. Radiol.*, **13** (1940) 82.
44 CRAGGS, J. D. *J. Sci. Instrum.*, **19** (1942) 62.
45 COOPER, R. D. Ph.D. Thesis. Manchester, 1946.
46 ALLIBONE, T. E., HAWLEY, W. G., and PERRY, F. R. *J. Inst. elect. Engrs.*, **75** (1934) 670.
47 HIGHAM, J. B., and MEEK, J. M. *Proc. Phys. Soc. B.*, **63** (1950) 633.
48 HARRIS, J. N. *Rev. Sci. Instrum.*, **23** (1952) 409.
49 HOWARD, P. R. *Proc. Inst. elect. Engrs.*, **99** (1952) 371.

10

HIGH-SPEED OSCILLOGRAPHIC TECHNIQUES

RECURRENT SURGE OSCILLOGRAPHS

The great importance of the impulse testing of large transformers and other apparatus for power transmission lines, where lightning surges may cause heavy and expensive damage, has been emphasized in many establishments. In particular the surge voltage distribution in transformer windings has been studied with a view to improving the h.t. insulation. To avoid risk of damage to the windings during test, and to reduce the cost of test apparatus, the use of low-voltage test impulses, having the same wave-form as the standard high-voltage surges, and to which transformers respond in practically a linear fashion, has been advocated by various workers. Such low-voltage impulses may conveniently be synchronized with the recurrent time base of a suitable cathode-ray oscillograph so that, for example, the variations of voltage along a transformer winding may rapidly be studied. WHITE and NETHERCOT[1] have stressed the convenience of

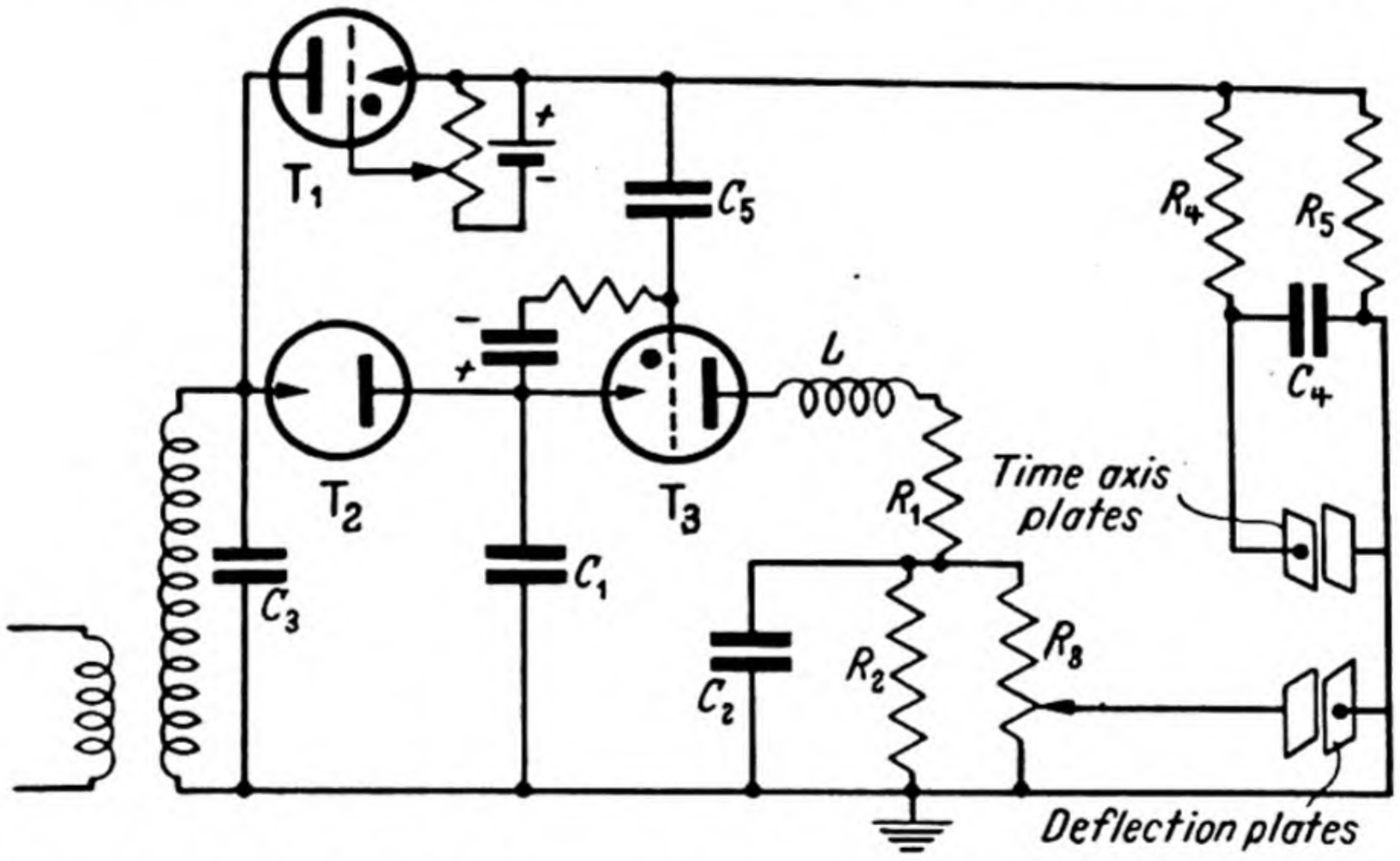

Figure 305. Circuit diagram of an oscillograph transient analyser (Rohats[2], by courtesy, *Gen. Elect. Rev.*).

recurrent test pulses in that the oscillograph trace is more easily examined than with single strokes of the time base. Modern sealed-off 10 kV cathode-ray tubes (*see* pages 338, 341) will provide easily photographed single traces for sweep times $\sim 10^{-7}$sec or less, but visual examination cannot often be made quantitative in such conditions.

ROHATS[2] appears to have been one of the first to use such a recurrent surge oscillograph. The schematic circuit of the latter is shown in *Figure 305* where the low-voltage impulse generator is shown in heavy

lines ; T_1 and T_3 are thyratrons. At the crest of each positive half-cycle from C_3, T_1 fires, and C_4 begins to charge through R_4, thus giving a deflection on the time axis of the cathode-ray tube. At the same time a positive impulse is fed through C_5 to the grid of T_3, which fires. Then C_1, previously charged in the negative half-cycle through the rectifier diode T_2, begins to discharge through the network $L\ R_1\ R_2\ R_3\ C_2$ from which the test impulse is taken and displayed on the oscillograph screen. The time-base speed may be adjusted by variation of R_4. Various standard wave shapes (*see* Chapter 4), *e.g.* the 1/5 wave, can be obtained by selection of suitable values of the above-mentioned network. L is used to inject a timing oscillation from an external source for the purpose of calibrating the time base.

Rohats describes various uses of this apparatus, such as the investigation of voltage distribution in machine windings and in transformers, and shows a series of 36 oscillograms illustrative of the passage of a travelling wave along a 20-section artificial line. Each section of this line comprises a 370 μH inductance and a 0·0023 μF capacitance. The effect of various terminations is easily and quickly shown by this method.

The next authors to use similar techniques appear to be WILKINSON[3] and SCOLES[4]. The former, following his earlier paper of 1936, gives a more detailed description of a later apparatus in 1938[5] with a higher sweep recurrence rate which enables fast transients to be photographed in a shorter time than was possible in the earlier work.

Wilkinson[3] shows that Rohats' rectifier circuit for the isolation of the thyratron impulse generator may be replaced by that shown in *Figure 306*. *Figure 307* gives circuit values for a 1/50 impulse wave (this is the normal method of describing an impulse having a wave-front, *i.e.* time to peak, of 1 μsec and a wave-tail falling to one-half of the peak value in 50 μsec). The ratio e_m/E is the quotient (crest value of the output pulse) $\div$ (crest applied voltage – thyratron tube voltage drop). A suitable value of R_2 is 30 Ω, since low impedance circuits have often to be tested. The time base and impulse generator are synchronized and may be operated at a recurrence frequency of 1,000 c/s, with a time-sweep velocity of 30 mm./μsec and a minimum time sweep duration of about 5 μsec. The synchronized circuits are given in *Figure 308*. The circuit (*A*) provides electromagnetic scanning of the oscillograph screen by the discharge of C_1 through the thyratron and scanning coils L_2. The charging circuit $L_1\ R_1$ provides negative grid bias to the thyratron during the recharging cycle and so reduces the tendency to restrike. It is also important, for the purpose of obtaining rapid de-ionization of the thyratron and a high maximum recurrence rate, to arrange that the recharging current through $L_1\ R_1$ is insufficient to prevent current reversal in the thyratron from L_2 so that a negative

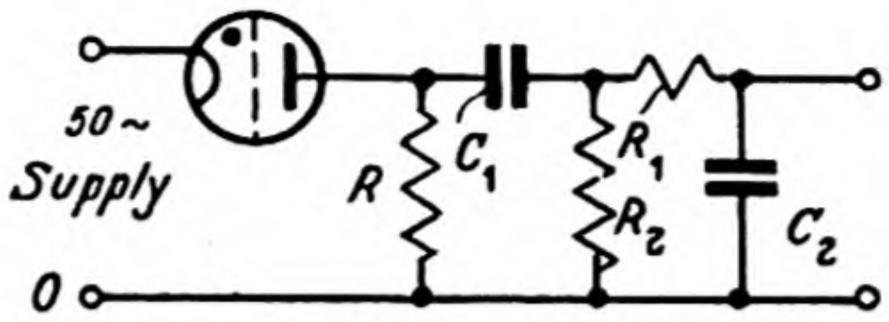

Figure 306. Wilkinson's[3] impulse generator circuit for a recurrent surge oscillograph (*see Figure* 307) (by courtesy, *B.T.H. Activities*).

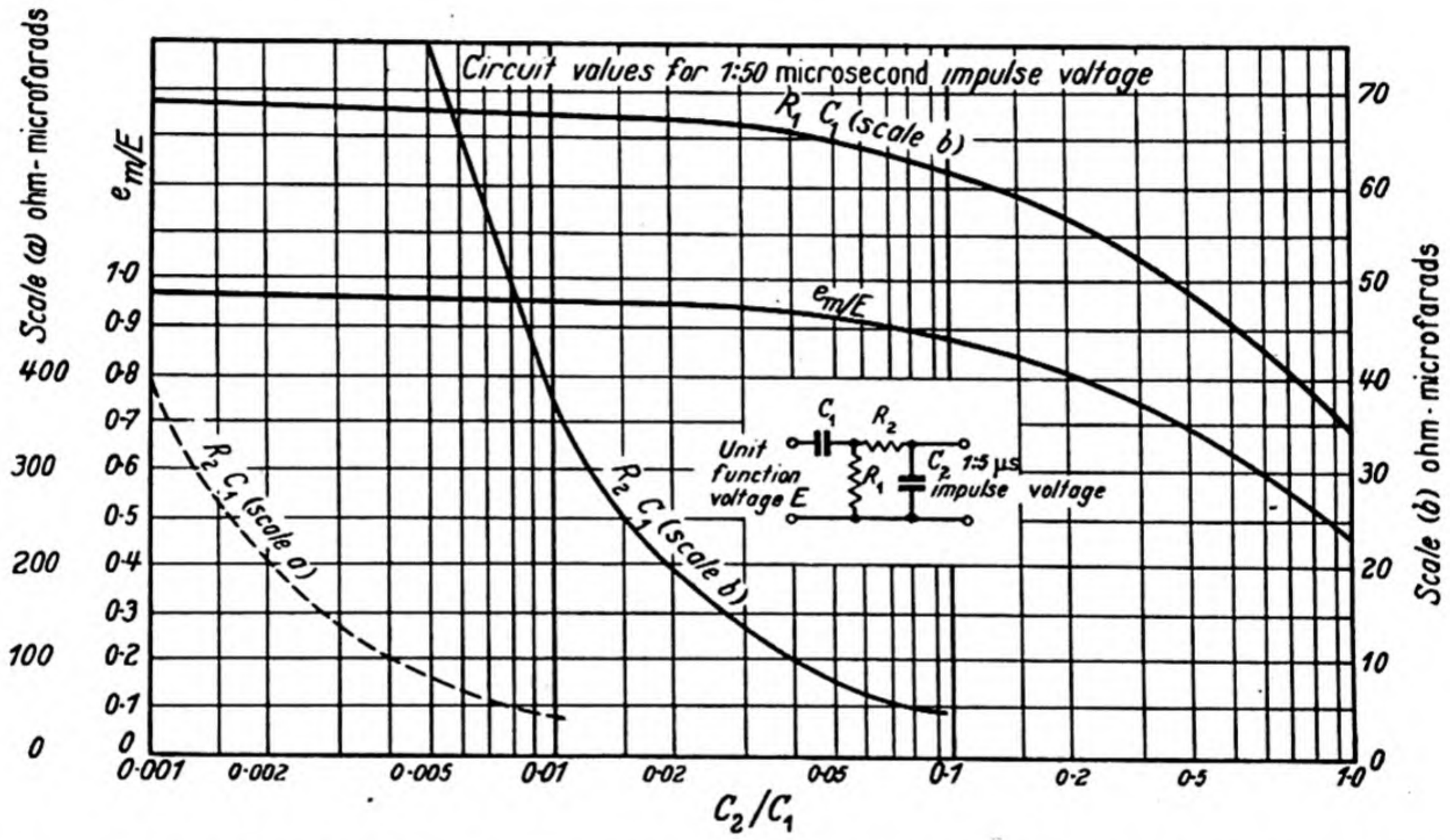

Figure 307. Circuit values for the generation of 1/50μsec impulse-voltage wave-shapes from unit-function voltage, for a recurrent surge oscillograph (*see Figure* 306) (Wilkinson[3], by courtesy, *B.T.H. Activities*).

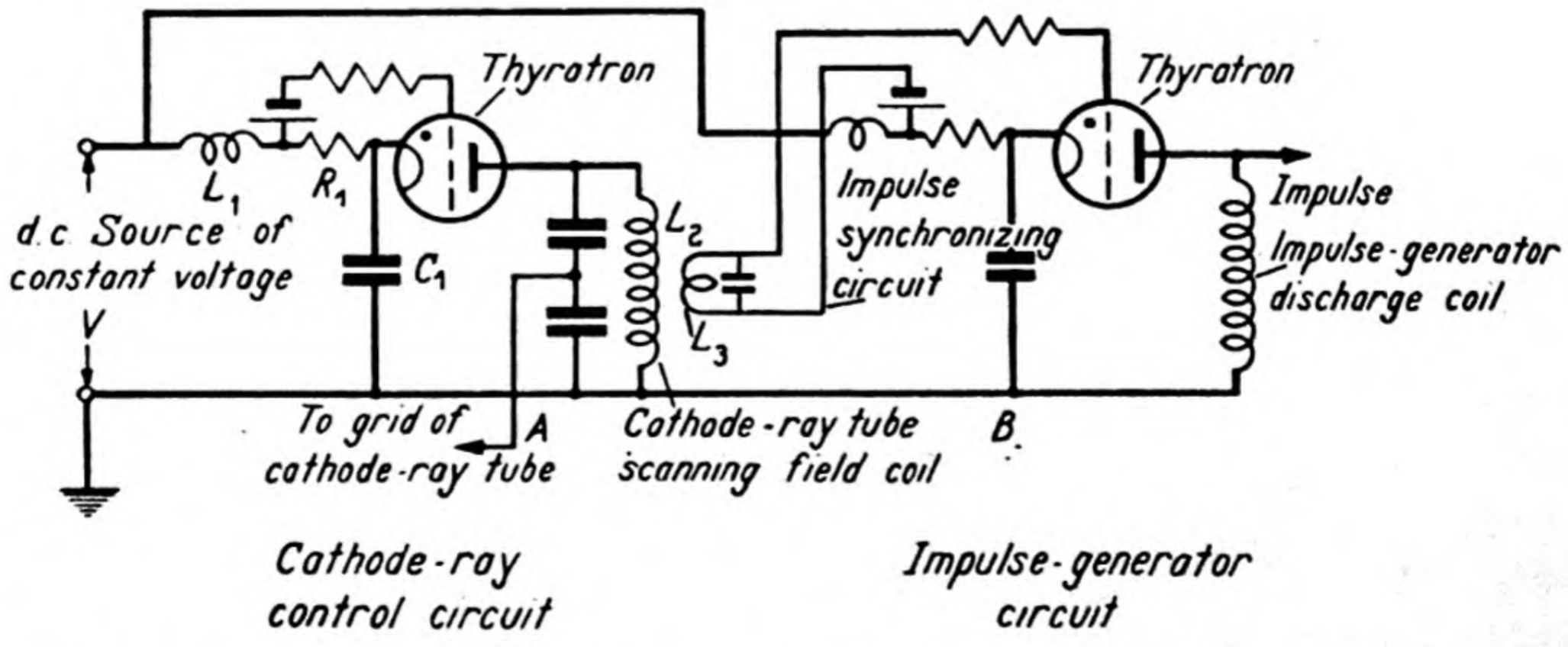

Figure 308. A circuit for electromagnetic scanning, and for synchronized impulse generation or high audio recurrence frequencies (Wilkinson[3], by courtesy, *B.T.H. Activities*).

anode voltage on the thyratron is obtained, which assists in the de-ionization process. For this purpose the natural period of oscillation of C_1 L_1 must be large compared with that of C_1 L_2.

The circuit develops a voltage E_d on C_1 in excess of that given by the source (V). Wilkinson shows that

$$E_d = -[V + (E_c + V)\, e^{-a_1\pi/b_1}]$$

where E_c is the residual voltage on C_1 after discharge, and

$$a_1 = R_1/2L_1 \quad \text{and} \quad b = \sqrt{[1/L_1C_1 - R^2{}_1/4L^2{}_1}$$

In a typical case, C_1 was 0·22 μF, L_2. was 420 μH and for $V = -220$ V, E_d was -610 V. An initial scanning speed of 24 mm./μsec was obtained, without appreciable change in 5 μsec, with a peak current of 14 A. The linearity of the sweep was ensured by choosing values of C_1 and C_2 so that one-quarter of the oscillatory period is long compared with the sweep time.

Figure 308 also shows how the impulse generator circuit B is tripped by means of a coil L_3 coupled to L_2 after a delay determined by the

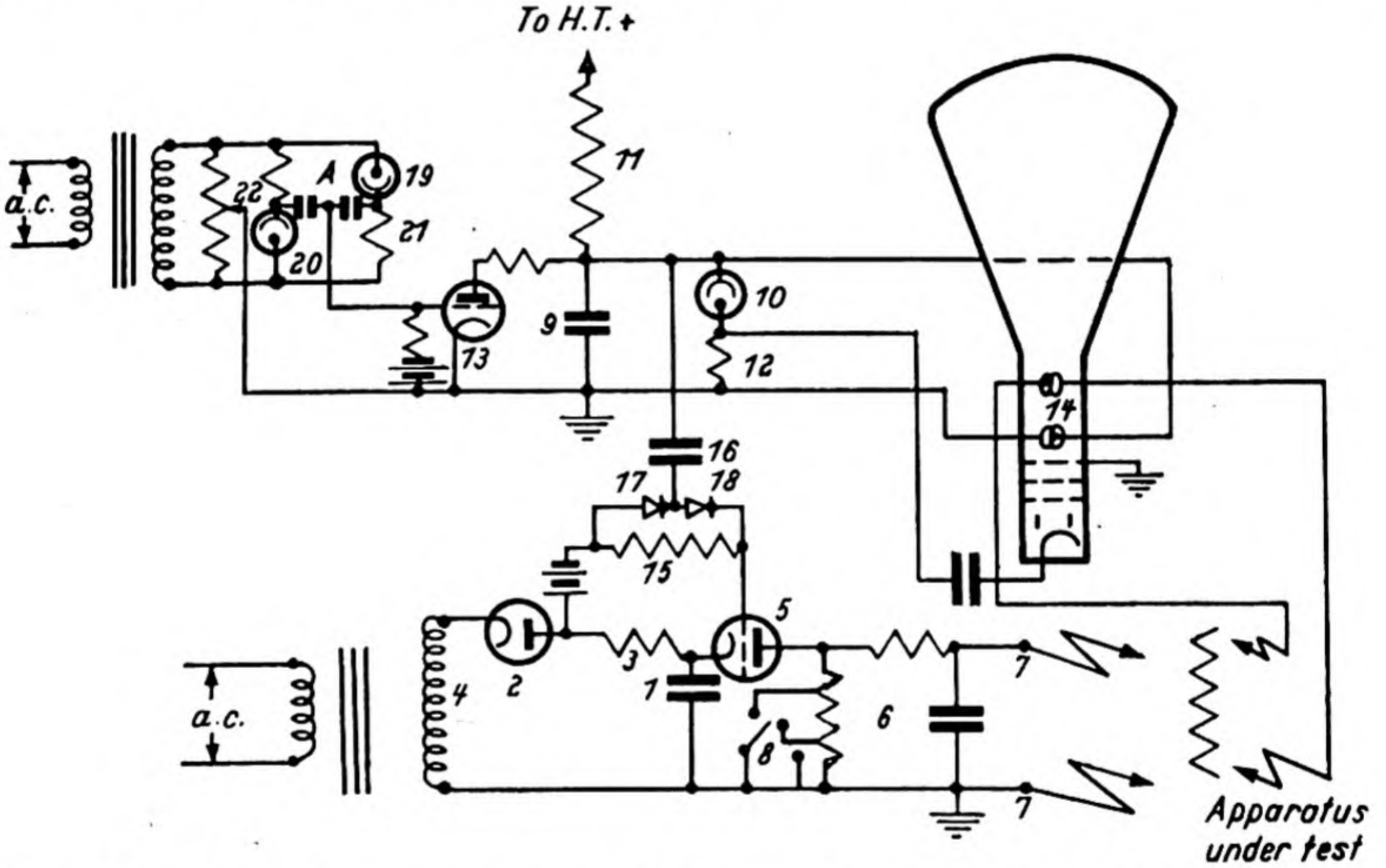

Figure 309. Circuit diagram for Scoles' recurrent surge oscillograph (Scoles[4], by courtesy, *J. Sci. Instrum.*).

ionization time of the impulse generator thyratron and by the capacitance shown. Biasing coils excited with d.c. enable the time sweep axis to be displaced vertically in order to allow the full oscillograph screen to be used.

Scoles[4] has described a similar recurrent surge oscillograph with which impulses varying from 1/50 to 1/500 μsec and time-base durations variable between 50 and 2,000 μsec are obtained.

Scoles' circuit, which differs in certain respects from those already described, is shown in *Figure 309*. The impulse generator circuit

comprises the rectifier 2, the thyratron 5 and the pulse-forming network 6. A switch 8 controls the wave-tail duration. The 100 pulse/sec time sweep is derived from the combination 9, 10 and 11 as follows. Condenser 9 is charged from the h.t. source to a value set by the neon lamp 10 and the resistance 12. When the thyratron 13 is tripped, in a manner to be described, 9 is discharged, the voltage on 12 disappears, the bias is removed from the cathode of the cathode-ray oscillograph and the spot appears on the screen, moves rapidly to the left and then, when the thyratron de-ionizes, moves to the right at a rate set by the values of 9 and 11. The impulse generator is tripped from the time base circuit through the network 15, 16, 17 and 18; the latter are copper oxide rectifiers. The mode of operation is as follows. Whilst 9 is discharging current flows through 17 from 16 so that the grid of thyratron 5 only receives a small negative charge, but when 9 charges, as it does during the time sweep, 17 does not conduct and current flows through 15 and 18, giving a positive tripping pulse on the grid of 5, thus firing it and producing the test impulse. The time base is tripped from a neon tube-condenser bridge circuit 19, 20, 21 and 22, shown at *A*, and which is fed from a small transformer. As the bridge voltage rises, one of the neon tubes will strike, feeding a pulse to 13 and to the other neon lamp which strikes, thus rebalancing the bridge. There are therefore two peaks produced per cycle, *i.e.* 100 pulse/sec. The circuit is arranged to give two positive pulses per cycle, by allowing the lamps alternately to strike first, in order to provide alternate zero lines and impulses on the oscillograph screen, and the slight difference between negative and positive striking voltages ensures this. The thyratron 5 is prevented from striking during alternate half-cycles because of the large negative potential then applied to the grid of 5, and derived from the charging current of 1 flowing through 3. The circuit can also be arranged to provide impulses only, without alternate zero lines.

Thus, to summarize, the tripping pulses from the neon lamp bridge circuit which occur at the rate of 100/sec activate the time base which in turn trips the impulse generator.

Scoles[4], in common with other authors, discusses the uses of recurrent surge oscillographs and extends the field of application by the use of chopped impulses with durations varying up to several hundred μsec. The latter are obtained by means of a characteristically simple and ingenious circuit, which is shown in *Figure 310*. This circuit is connected to the output of the impulse generator, with the anode of the thyratron *V* positive. In the initial state, with no voltage across the circuit, the voltage on *C* is that of *B*. When the impulse is applied, a current flows through *R*, applying a positive pulse to the grid of *V* which fires *V* and chops the wave. The length of the chopped wave may be controlled by alteration of *C*, *R*, or the voltage of *B*. Another chopping circuit using thyratrons[6] is shown on page 332.

It is next necessary to describe two further recurrent surge oscillographs due to WHITE[6] and to White and Nethercot[1]. In the former, thyratrons are used although the circuits differ from those due to Scoles[4] and Wilkinson[3, 5]. The latter circuit[1] uses hard valves and appears to be the most highly developed yet described in the literature.

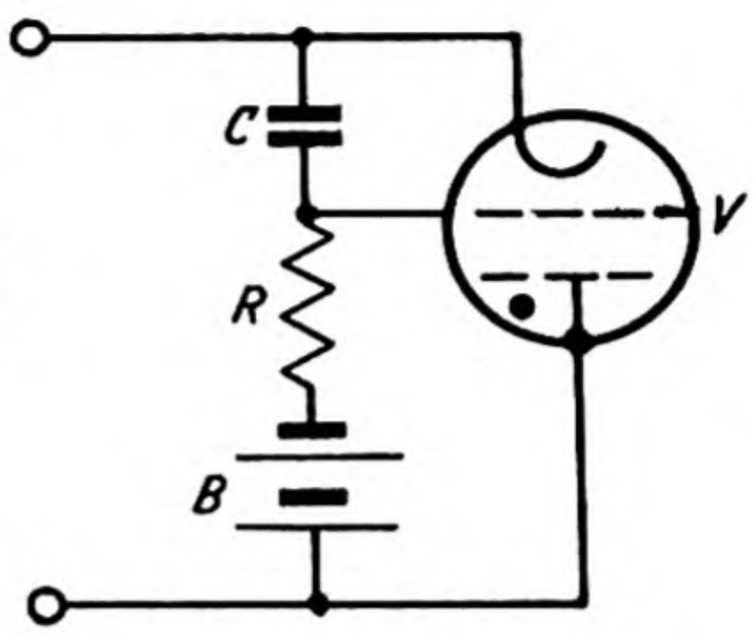

Figure 310. Circuit for producing chopped impulse waves (Scoles[4], by courtesy, *J. Sci. Instrum.*).

White's[6] earlier oscillograph has a recurrence pulse frequency of 100 pulse/sec with a time sweep variable down to less than 1 μsec and could also be used to record single or repeated transients from an external source.

The impulse generator gives negative 1/5 or 1/50 surges. A timing calibration, at frequencies of 100 kc/s, 500 kc/s, or 1 Mc/s selected by switch S, is obtained by shock-exciting the primary winding of transformer T_1, T_2 or T_3 (*Figure 311*) with the discharge of condenser C_8 through the thyratron G_5, which gives a damped oscillation in the appropriate secondary coil. It is necessary to arrange for the tripping of the impulse generator to be delayed with respect to the tripping of the time base, so as to allow inspection of the full surge on the oscillograph screen ; this delay is provided by the use of R_{10}, which, combined with the input capacitance of G_3 ensures that the latter fires after the time base has started.

By charging condensers C_7 and C_8 from 50 c/s voltages respectively in phase with and in phase opposition to the mains, G_3 and G_5 are ionized during alternate sweeps, thus generating alternate impulses and timing oscillations. The circuit, *Figure 311*, shows the necessary arrangement of connections.

The fly-back of the spot on the oscillograph screen may either be invisible, when the spot on the forward strike must be brightened by the application of a positive pulse obtained from the cathode of G_2 to the modulating electrode of the tube (after MCGILLEWIE[7]), or may be used as a zero line by raising the bias on the tube. Alternatively, the forward stroke may be used as a zero line by earthing the Y_1 deflector plate with the switch S_1. The switch S_2 enables direct comparison of the impulse applied to the test circuit with that obtained on the output side of the latter.

A 5 kV oscillograph tube (Type 4063 YB Standard Telephones & Cables Ltd.) as described by McGillewie[7] is used, with balanced deflection on the time sweep plates. The time base sweep voltage is derived from the equal condensers C_1 and C_2 which charge through R_3 and R_4 to $\pm 2{\cdot}25$ kV from A and B respectively. The current flow

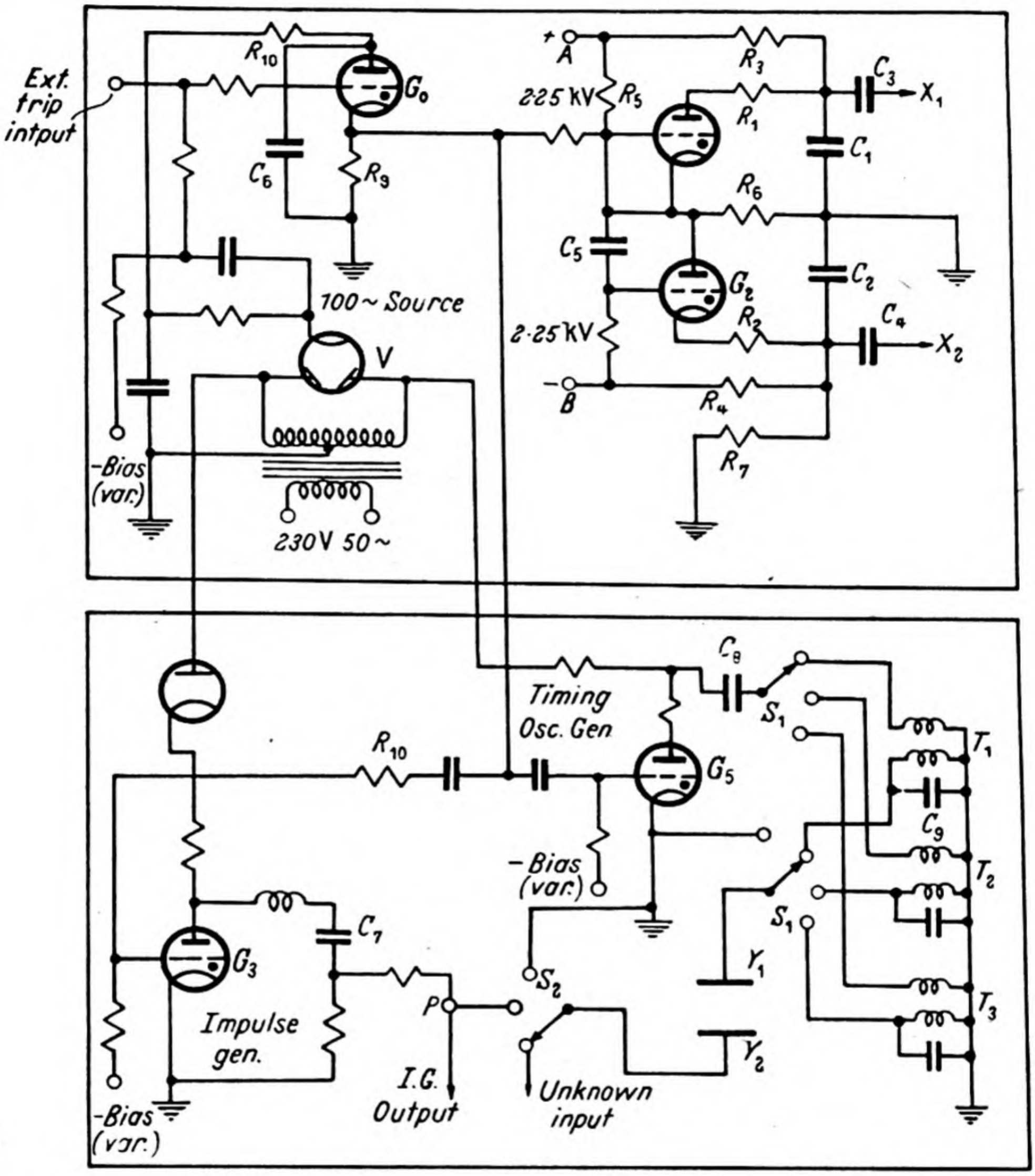

Figure 311. Time base (above), impulse and timing oscillation generators (below) of White's oscillograph (White[6], by courtesy, *J. Sci. Instrum.*).

G_0, G_5 GTIC
G_1, G_2, G_3 BT35 or BT5
C_1, C_2 0·001 μF, 0·005 μF or 0·01 μF
C_3, C_4, C_8 0·01 μF
C_5 0·0005 μF
C_6 0·002 μF
C_7 0·1 μF for 1/5 μsec surge; 1·0 μF for 1/50 μsec surge
C_9 0·001 μF

R_1, R_2 1,000, 10,000 or 50,000 Ω
R_3, R_4 300,000 Ω
R_5 9 MΩ
R_6 500,000 Ω
R_7 10 MΩ
R_9 5,000 Ω
R_{10} 3 MΩ
R_{11} 5,000 Ω

through (R_5 + R_6) and through (R_4 + R_7) supplies negative bias for the grids of G_1 and G_2 which are then non-conductive. A single sweep is obtained by firing G_o, normally biased back with the negative voltage source shown in *Figure 311*, with a positive pulse. C_6 then discharges through G_o and R_9, firing G_1, with a positive grid pulse and so C_1, begins to discharge through R_1 and R_6. The latter is large compared with R_1 and the large voltage rise across R_6 is applied to the grid of G_2 through C_5 so that G_2 fires, and together with G_1 discharges C_1 and C_2 in series through R_1 and R_2, and thus provides the sweep voltage to the deflector plates. When C_1 and C_2 are nearly discharged the thyratrons are extinguished and re-charging commences. C_6 re-charges after the

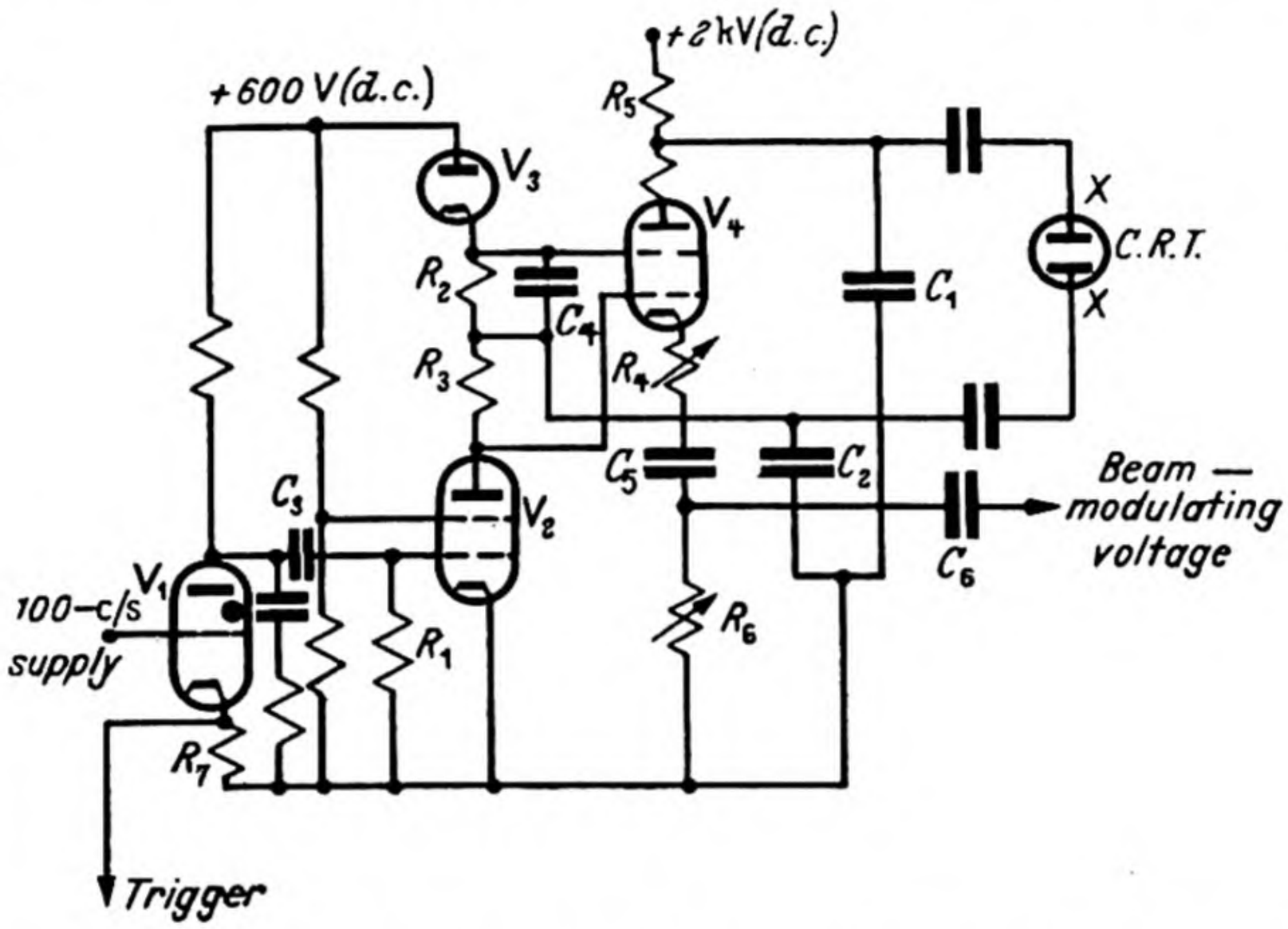

Figure 312. Sweep circuit of recurrent-surge oscillograph using hard valves (White and Nethercot[1], by courtesy, *J. Inst. elect. Engrs.*).

removal of the positive tripping pulse from the grid of G_o. Use of the external trip enables a maximum recurrence rate of about 200 pulse/sec to be reached, but this is halved when the recurrent impulse generator shown in the lower half of *Figure 311* is used ; the tripping pulses are then obtained from the positive peaks of the frequency-doubling full-wave rectifier *V*.

The hard valve time base of White and Nethercot[1] is shown in *Figure 312* ; the following details of its mode of operation are taken from the paper.

V_1, an argon-filled thyratron, supplies negative pulses (100 pulse/sec) to the grid of V_2 which remains blocked by these pulses for the duration of the longest sweep required, since the time constant $C_3 R_1$ is adequate for this purpose. When V_2 is conducting the anode current flowing through R_2 and R_3 gives voltages which are applied to the screen and grid of V_4. When V_2 is blocked the screen voltage of V_4 is maintained,

because of the discharge time constant of C_4 R_2, whilst the grid voltage of V_4, *i.e.* that across R_3, rapidly falls and V_4 fires. This causes C_1 to discharge into C_2, at a rate set by the value of R_4 so that variation of the latter, or of C_1 and C_2, sets the time-base speed. The voltage changes across C_1 and C_2 are equalized by balancing the stray capacitances across them. The diode V_3 prevents current flow back into the 600 V supply. C_2 is discharged through R_3 when V_2 becomes conducting and V_4 is also cut off. C_1 recharges to 2 kV through R_5. The combination C_5 R_6 shunted across C_2 differentiates the voltage across C_2 and so feeds a constant positive voltage to the modulator electrode of the cathode-ray tube. Finally, positive voltage pulses developed across R_7 are used to trip the impulse generator, which is of the type shown in *Figure 311* but which incorporates argon or hydrogen-filled thyratrons. A wave-front of less than 0·1 μsec was obtained, as compared with 0·5 μsec which was the value obtained with mercury thyratrons.

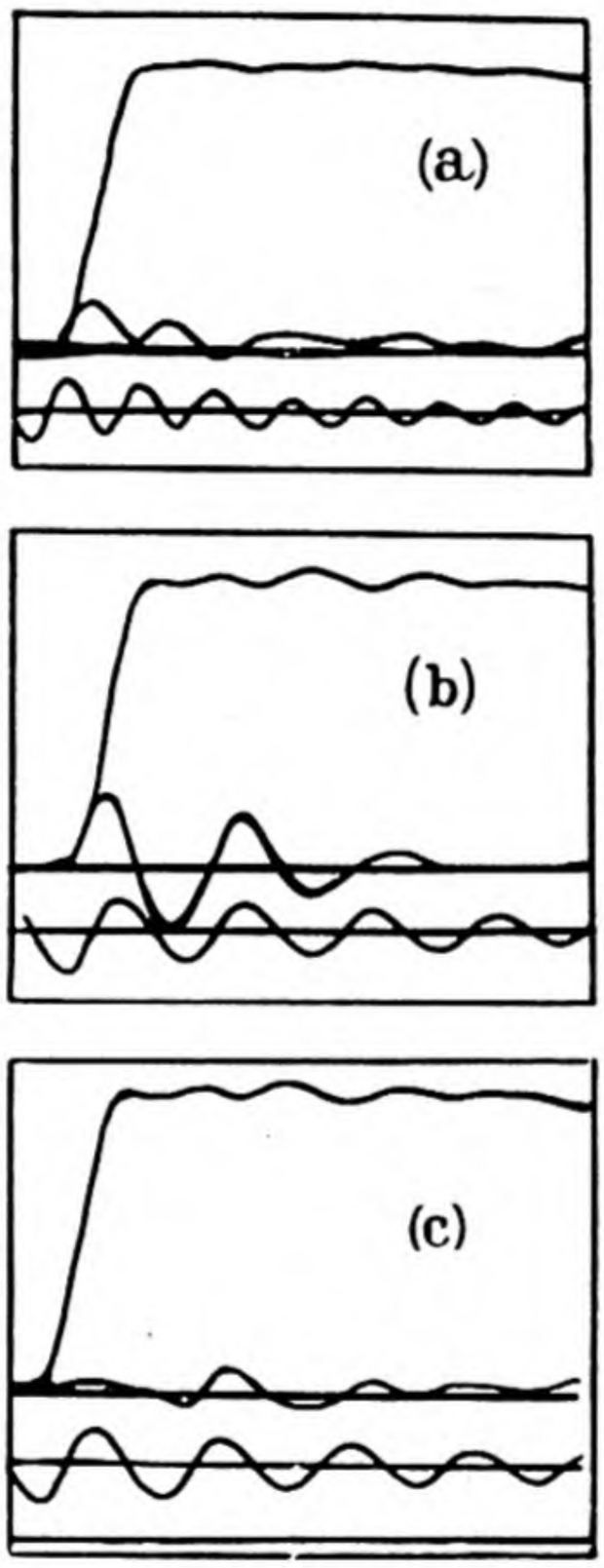

Figure 313. Inter-tapping voltages in reinforced coil of transformer winding: (a) Top trace—applied impulse. Middle trace—voltage across first layer (9 turns of reinforced coil). Timing oscillation 10 Mc/s. (b) Top trace—applied impulse. Middle trace—voltage across first three turns of reinforced coil. Timing oscillation 10 Mc/s. (c) Top trace—applied impulse. Middle trace—voltage across last two turns of reinforced coil. Timing oscillation 10 Mc/s. (White and Nethercot[1], by courtesy, *J. Inst. elect. Engrs*).

Other representative results are given in *Figure 313* which shows a series of impulses obtained in experiments on the voltage distribution in transformer coils. The cathode-ray tube voltage varied from 2–6 kV and an f/2·9 lens was used which, with orthochromatic film of speed 30° Scheiner, enabled exposure times varying from 0·5–5 sec to be used. The use of the newer high-voltage cathode-ray tubes such as the G.E.C. 908, or the post-deflection-acceleration tube (G.E.C. 1608) enable faster recurrent sweeps to be used, and details of such circuits are given later in the next section.

HIGH-SPEED SEALED-OFF OSCILLOGRAPHS

PRIME and SAXE[8] have developed a successful high-speed transient recording oscillograph, using the G.E.C. 908 PW 10 kV tube. In this tube the third anode A_3 and the four deflector plates are brought out to side-contacts on the neck of the tube so that stray reactances are minimized. Thus, if one Y-plate is connected to A_3 and earthed, then the capacitance of the other Y-plate to earth is about 7·5 $\mu\mu$F. The tube gives an excellent focus and at 10 kV a spot size not greater than 0·2 mm. is obtained. The screen diameter is about 9 cm. The time base circuit, which is shown in *Figure 314* can be triggered by either

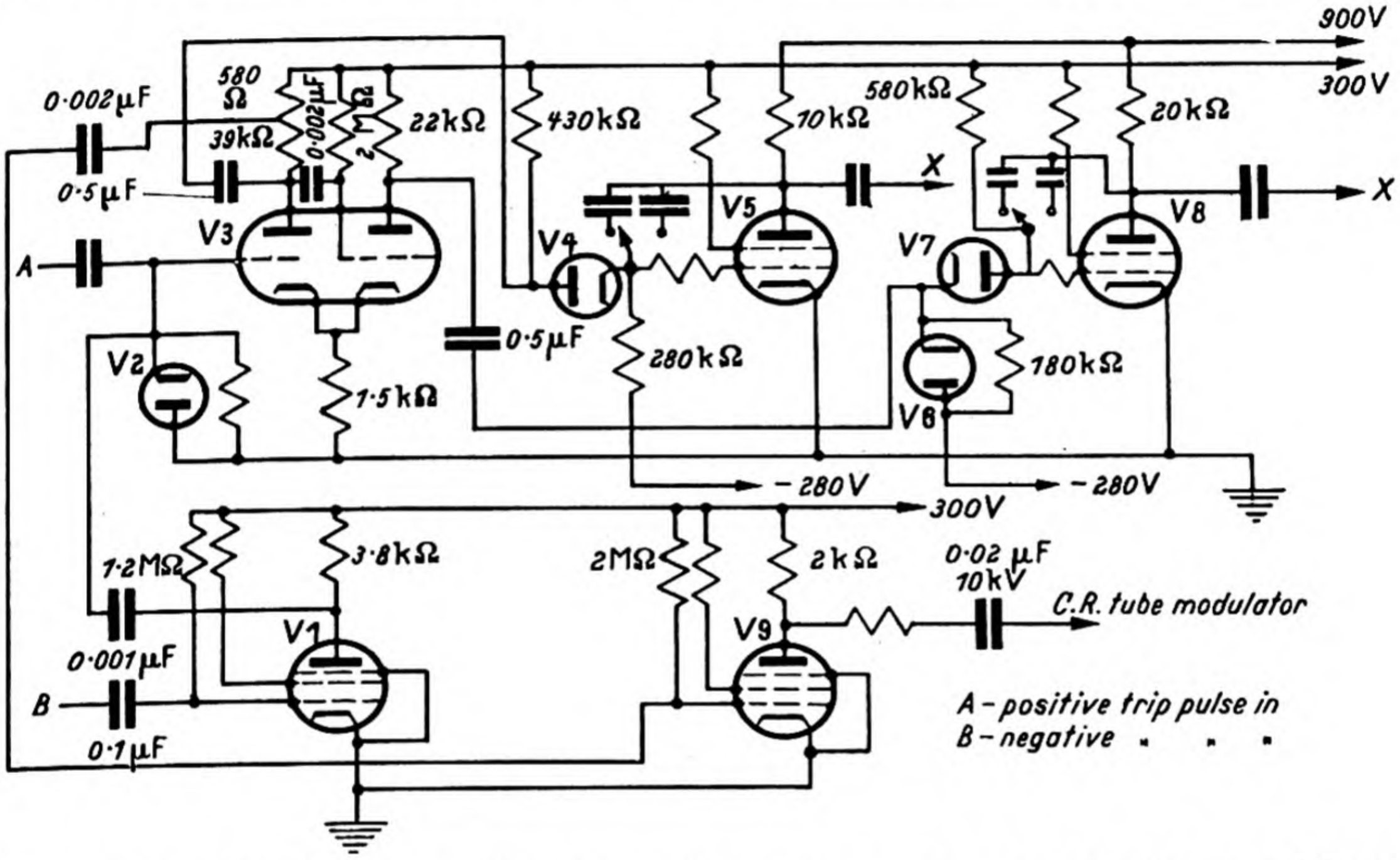

Figure 314. Circuit diagram of oscillograph time-base unit, as used by Prime and Saxe[8] (by courtesy, *Proc. Inst. elect. Engrs.*).

a positive or negative pulse applied respectively to A or B ; V_1 acts as phase-reverser for pulses applied to B. A symmetrical deflection system is used in order to minimize deflection defocusing and the sensitivity of the 908 tube is such that about 800 V per X-plate are required for full deflection. The circuit includes two Miller time base stages, V_5 and V_8 (*Figure 314*), following the work of WILLIAMS[9], thus enabling the two deflection voltages, needed for the push-pull system, to be generated separately. This allows short leads from the valves to the X-plates to be used and, further, no more amplification is needed. If the symmetrical deflection is to be obtained from a single voltage, divided either by a phase-splitting or a phase-reversing stage, then cross modulations between X and Y plates becomes more likely and, for phase-splitting, a valve capable of withstanding 1,600 V would be required. However, with the double Miller stage circuit, one of the valves must pass a heavy current in the quiescent state.

V_3 is in a cathode-coupled flip-flop stage which produces square switching pulses for the triggering of V_5 and V_8 and for the pulse-brightening valve V_9, which provides a short positive square pulse, applied to the grid of the cathode-ray tube, in order to brighten the spot trace on the forward stroke. Six time-base speeds are provided by switching of the anode-grid coupling condensers of V_5 and V_8.

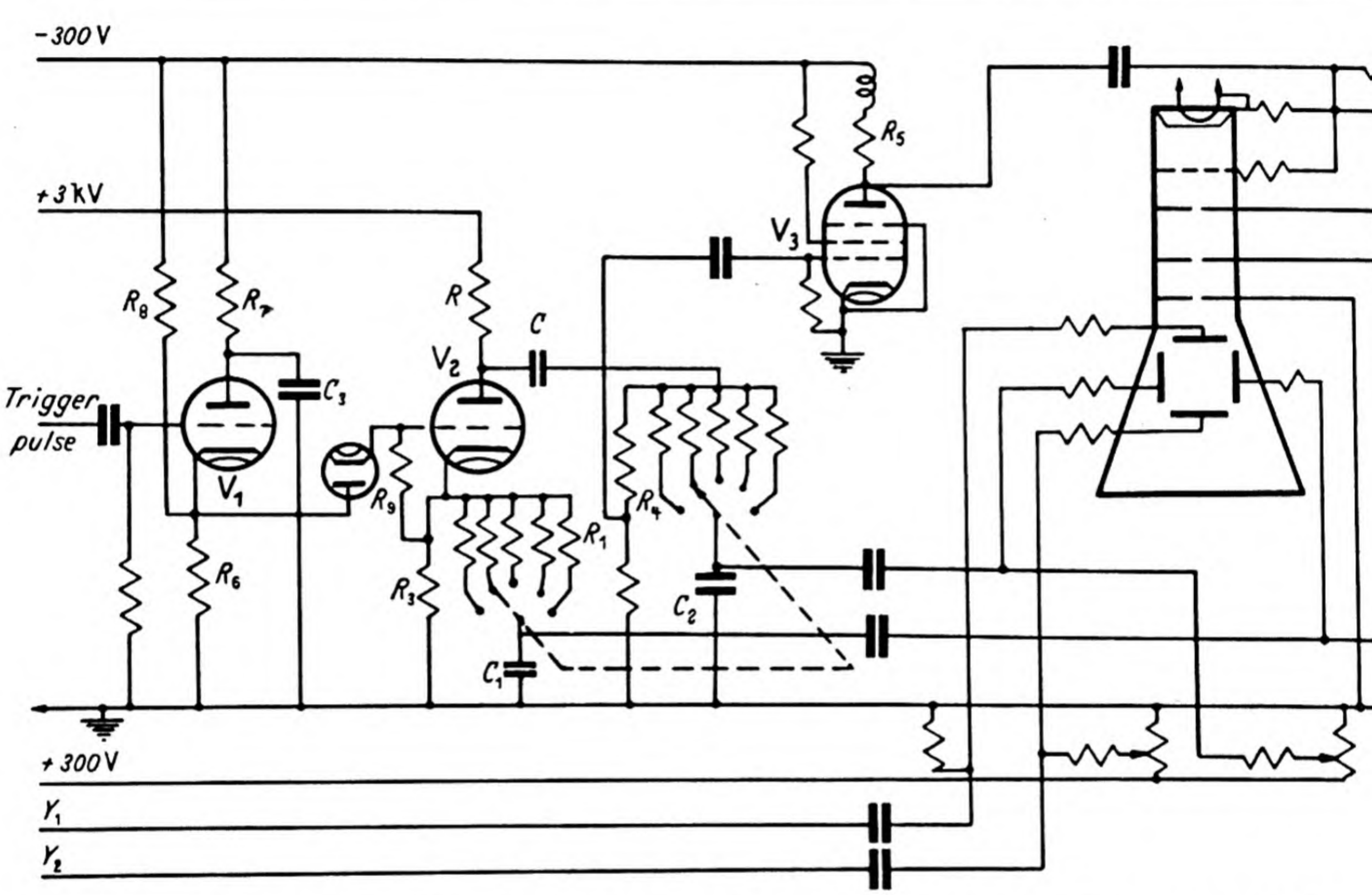

Figure 315. Circuit diagram of oscillograph (Prime and Ravenhill[11], by courtesy, *J. Sci. Instrum.*).

R, 500kΩ, 5 W
R_1 1k, 2kΩ, 4·7kΩ, 10kΩ, 33kΩ
R_2 1kΩ, 2kΩ, 4·7kΩ, 10kΩ, 33kΩ
R_3 10kΩ, 1W
R_4 10kΩ, 1W
R_5 2kΩ, 2W
R_6 10kΩ, ½W
R_7 200kΩ, 1W
R_8 150kΩ, 1W
R_9 1·5kΩ, ½W
C, 0·01μF, 3kV
C_1 0·001μF
C_2 0·001μF
C_3 0·001μF
V_1 2D21 (CV797)
V_2 3C45(CV372)
V_3 EF50(CV173)

Prime and Saxe consider that, whilst the linearity of the fastest (2 μsec) sweep is not good, it is adequate for most work involving times of this order. Faster time sweeps may be used with the 908 tube, but with different circuits as shown later by Hardy[10]. The Y plate sensitivity at 10 kV on the third anode is about 10V/mm.

Prime and Ravenhill[11] have subsequently published details of an improved time-base circuit for use with the G.E.C. 908 tube. They point out that the delay between the application of the trigger pulse, the start of the forward stroke of the time base, and the start of the brightening pulse should be as short as possible. Alternatively, the

signal can be delayed but this may introduce distortion. Further, the amplitude or wave-form of the trigger pulses should not affect the synchronization, and to ensure this a pre-triggering stage may be used.

The circuit, shown in *Figure 315*, was used with the 908 BCC cathode-ray tube, with time-base sweeps varying from 10^{-5} to 5×10^{-7} sec in duration. The time sweep is not strictly linear, as mentioned below. At the highest sweep speeds, peak currents of more than 1A are required to charge up the stray capacitances of the deflector plates, each of which in push-pull deflection must reach a voltage of 800V. A hydrogen thyratron (BTH type 3C45) has been found satisfactory for this purpose. The latter tube has a rated peak current of 35A, with a maximum anode voltage of 3 kV, but a mean anode current of 45 mA should not be exceeded. 150 V are needed,

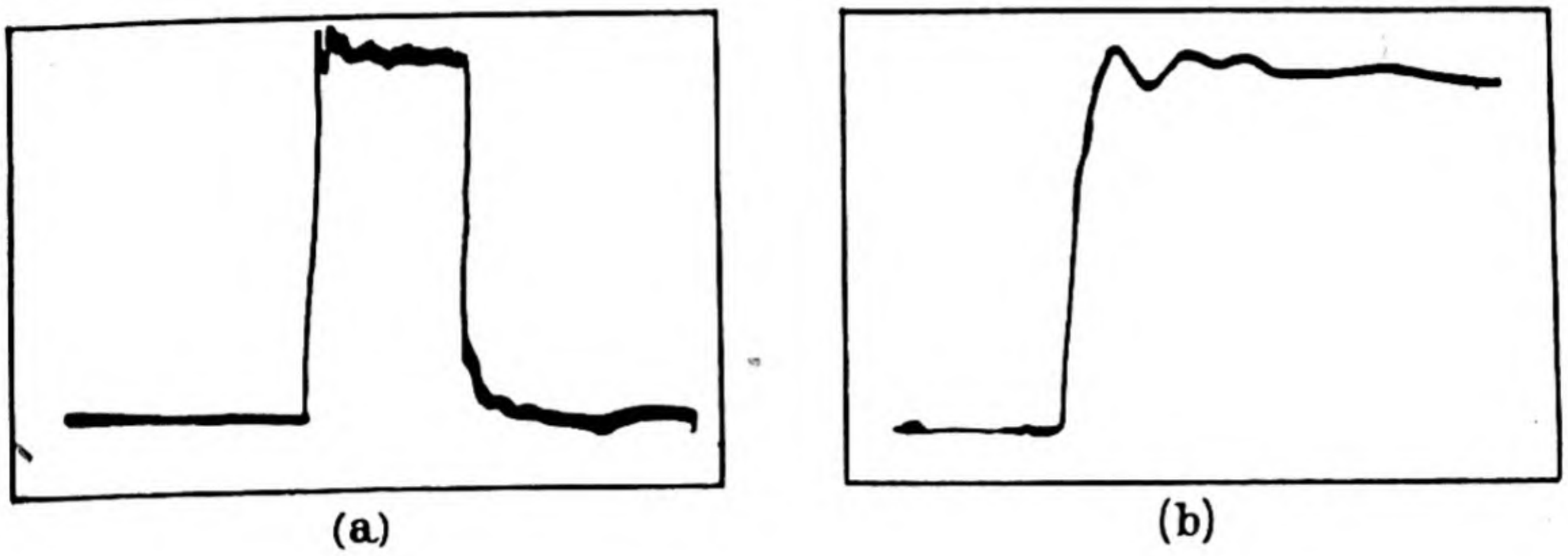

Figure 316. (a) 500 V pulse, 10^{-6}sec duration. (b) Leading edge of pulse shown in (a), time-base duration 5×10^{-7}sec. (c) Output pulse from video-amplifier, gain 1200; input to amplifier a fraction of pulse shown in (a). (Prime and Ravenhill[11], by courtesy, *J. Sci. Instrum.*).

across 1,500 Ω, for triggering the 3C45 thyratron and the delay in establishing conduction in this tube is $\sim 10^{-7}$sec when the grid voltage rises at the rate of 3 kV/μsec.

In the time base circuit of *Figure 315* the capacitor C is charged through R from a $+3$ kV source. When V_2 is triggered, C is discharged through V_2 and the balanced integrating circuits R_1 C_1 and R_2 C_2 in series. The time-base sweep voltage taken across C_1 and C_2 is exponential, but since only 50 per cent. of the whole discharge is needed to give full deflection of the beam, the non-linearity is reduced. However, this non-linearity is one of the defects of the circuit. The switches on R_1 and R_2 control the sweep speeds. R_3 and R_4 serve to discharge C_1 and C_2 during the charging period of C. A fraction of the negative

pulse generated across R_4 drives V_3, which provides the brightening pulse. V_3 has an anode circuit inductance to improve the rate of rise of the brightening pulse so that the early part of the sweep may also be recorded. Hardy[10], see below, has pointed out the limitations to fast recording introduced by this use of V_3. V_1 is a pre-triggering stage, which provides a low impedance source for the triggering voltage, which should have a rapid rate of rise.

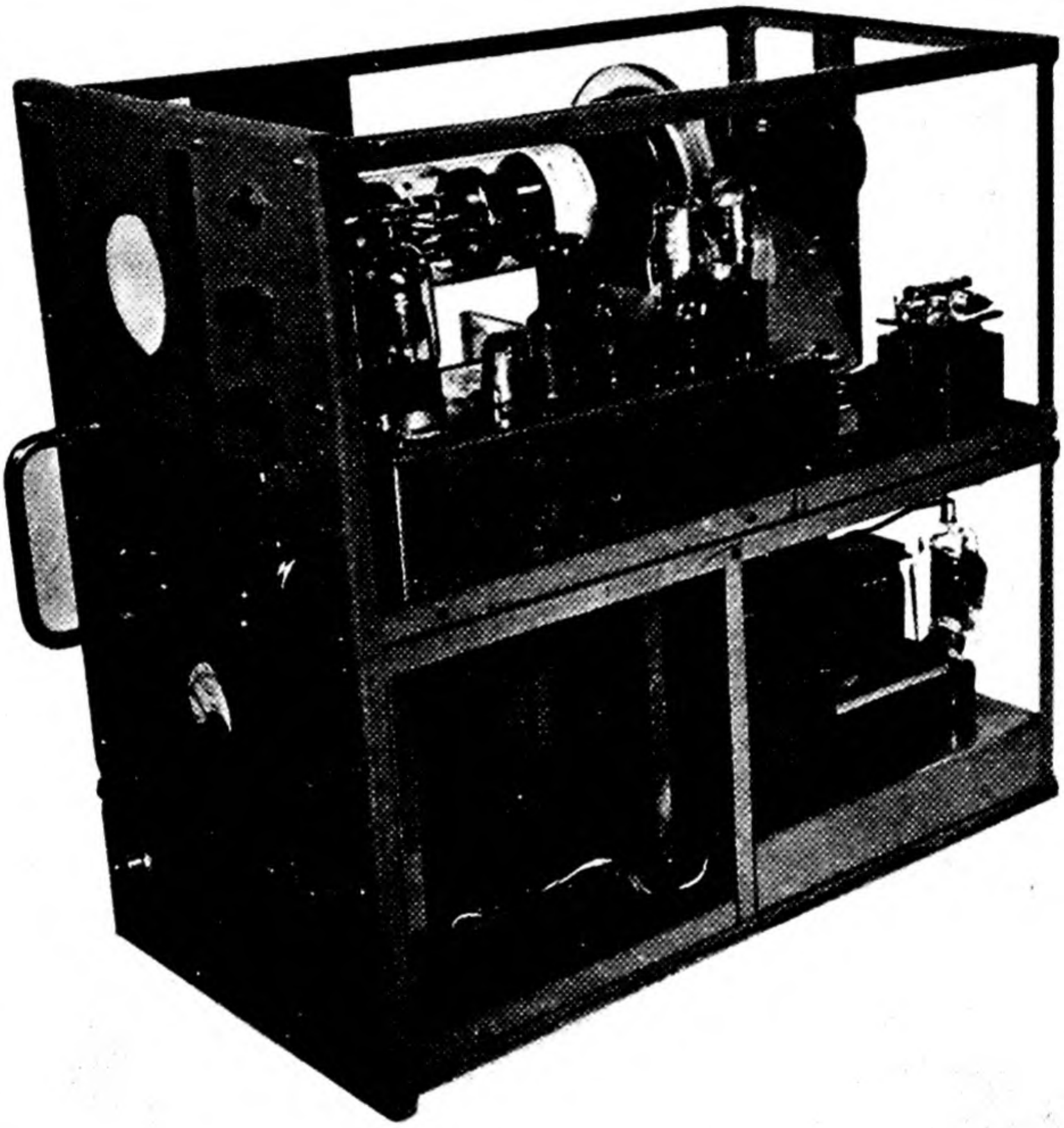

Figure 317. 10 kV sealed-off cathode-ray oscillograph unit.

The high-voltage supply for the cathode-ray tube is obtained from an r.f. source (*see* pages 10–15) in which the oscillator h.t. is stabilized. The shift voltages for the X and Y shifts (*Figure 315*) are also stabilized. The heater transformer for V_2 (*Figure 315*) should be designed with adequate insulation to withstand 1·5 kV pulses.

Typical results obtained with the above oscillograph by Prime and Ravenhill[11] with an F1 lens and Ilford 5G91 film are shown as tracings in *Figure 316*. *Figure 316* a and b show a 1 μsec pulse ; in *Figure 316* c, taken with a video amplifier, 20 traces are superimposed,

again with a 1 μsec pulse, to show the freedom from jitter. The oscillograms showed that the limit of recording was not reached in these experiments. The latest version of this oscillograph, as used at Liverpool, is shown in *Figure 317*.

Hardy[10], who used the above circuits in connection with work on statistical lags in spark break-down, has developed them for faster sweeps. Hardy points out that, due to the time lag in the brightening

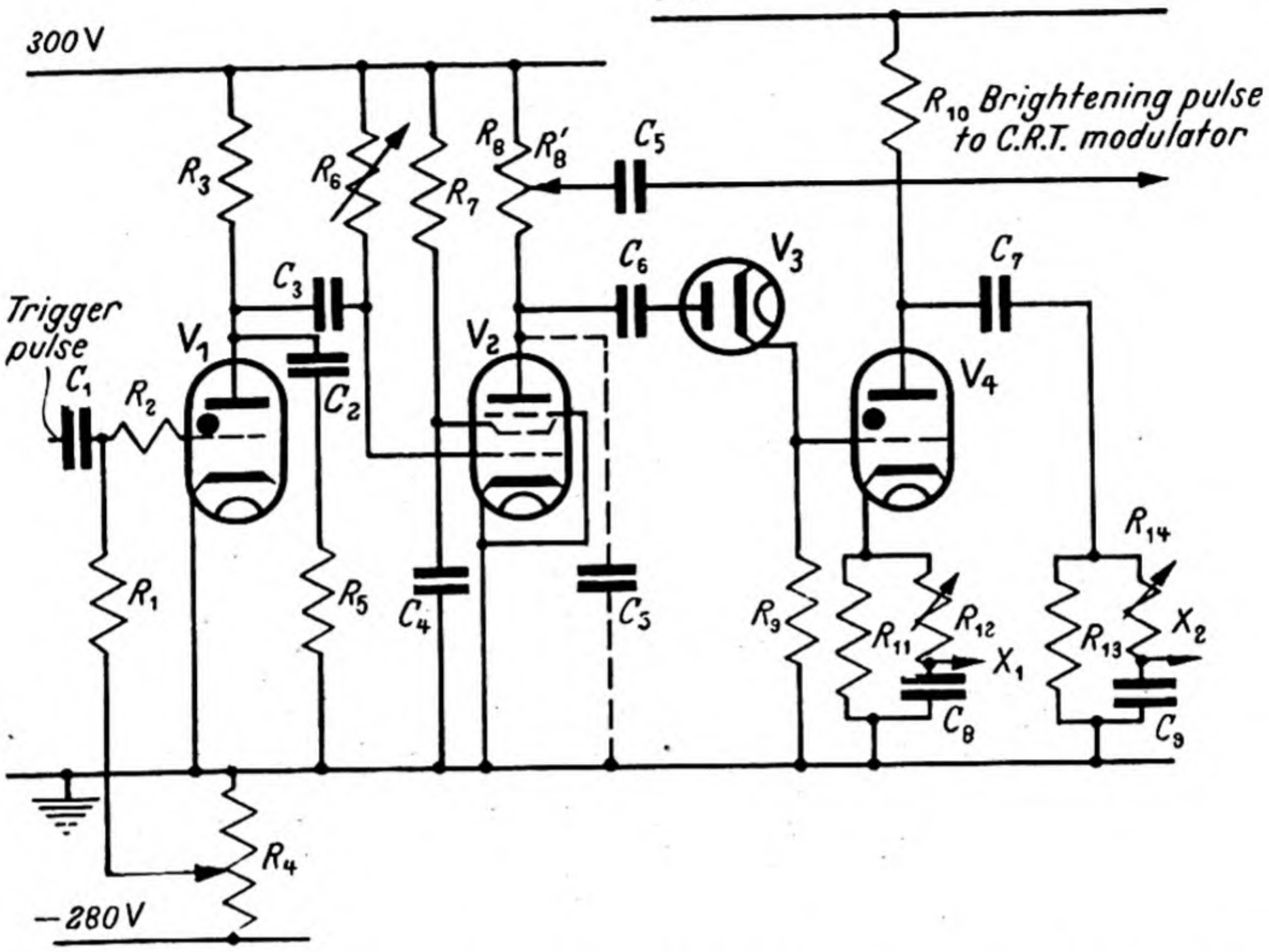

Figure 318. Trigger and time base circuit (Hardy[10], by courtesy, *J. Sci. Instrum.*).

R_1 1MΩ	R_8 10kΩ	C_1 0·1μF	C_8 47pF
R_2 50kΩ	R_9 1MΩ	C_2 0·1μF	C_9 47pF
R_3 220kΩ	R_{10} 470kΩ	C_3 10pF	V_1 GT1C
R_4 500kΩ	R_{11} 10kΩ	C_4 0·1μF	V_2 EF55
R_5 10kΩ	R_{12} 33–100kΩ	C_5 10pF (10kV d.c.)	V_3 U78
R_6 100k–5MΩ	R_{13} 10kΩ	C_6 0·1μF	V_4 BT79
R_7 30kΩ	R_{14} 33–100kΩ	C_7 0·5μF	

pulse amplifier, the latter must be triggered before the time sweep if fast recording is to be obtained. This may be effected by triggering the time sweep from the brightening pulse. The latter, if too short, may result in the later parts of the sweep being insufficiently bright or, if too long, may give appreciable background illumination. For very fast recording the latter is more likely than the former. Indeed, Hardy's new arrangement is especially applicable to very fast sweeps but, it is considered, would not offer much improvement for slower sweeps over the earlier circuits.

Hardy's circuit is shown in *Figure 318*. A positive pulse is applied to the grid of the negative grid control thyratron V_1 and the resulting negative anode pulse cuts off V_2, which in turn provides a positive

anode pulse to trigger the main time base valve V_4 through the diode V_3. The brightening pulse is also taken from the anode of V_2.

Since R_6 is taken to the h.t. line, instead of to earth, the time for which V_2 is non-conducting, determined by the time constant $C_3\,R_6$, is reduced. This is shown schematically in *Figure 319* where the output pulse from V_1 is given with the input pulse to V_2, due to differentiation

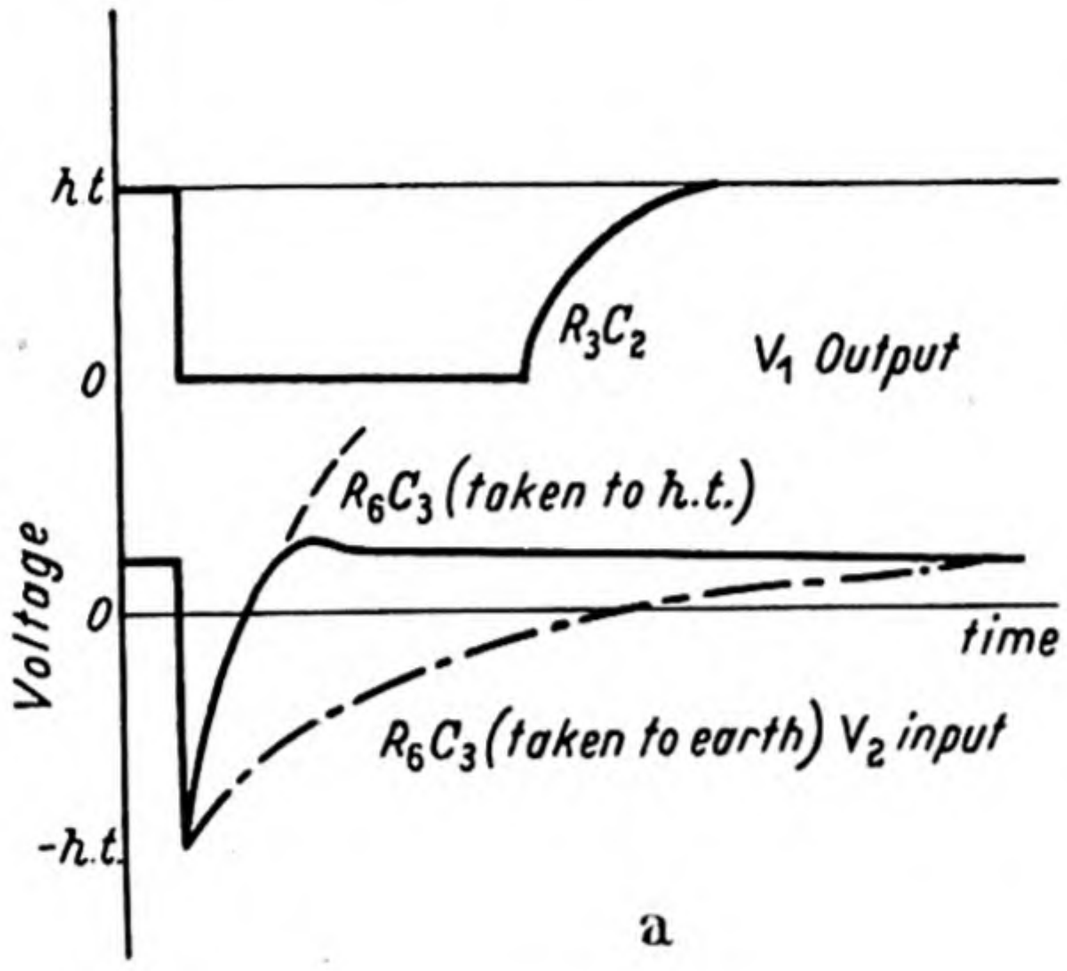

Figure 319. (a) Output from pre-triggering valve, and input to brightening pulse generator. (b) Time base wave-form for the circuit of *Figure 317* (Hardy[10], by courtesy, *J. Sci. Instrum.*).

of the V_1 output. The steep-fronted brightening-pulse is obtained by reducing the time constants $C_s R_8$, CR'_8 as far as possible (C = input capacitance of the cathode-ray tube modulator). Hardy used a short length of 10 kV coaxial cable for C_5. R_8 controls the brightening pulse amplitude.

The diode V_3 holds off the grid voltage, nearly 1·5 kV, of V_4 when the latter fires, and this should be the peak inverse-voltage rating of V_3 which should also have a low inter-electrode capacitance to reduce the amplitude of the pulse fed back through R_8.

The circuit of $V_4\,C_8\,C_9$ (*Figure 318*) is that developed by Prime and Ravenhill[11] but Hardy points out, as had the previous authors, that the stray capacitance in the filament transformer for V_3 and V_4 should

be kept as small as possible. For the fastest sweep, R_{12} and R_{14} must be chosen so that the peak current rating of V_4 is not exceeded. Further[10], the use of bias V_1 on the X plates (*see Figure 319* b which represents the time-base voltage wave-form) enables a more linear sweep to be obtained than with the earlier circuit of Prime and Ravenhill[11]. The published record[10], which is of the same size as the trace on the oscillograph screen, represents a writing speed of about 15,000 km./sec, and a sweep time of about 10^{-8} sec. The linearity is satisfactory and the technique represents probably an approach to the best possible, with the 908 tube. It was taken with a Wray F1 lens and Ilford 5G91 film with a vigorous developer.

MURPHY[12], however, in work on very short pulses ($\sim 10^{-8}$ sec) obtained with certain corona discharges, has found that a long cable, giving about 0·5μsec delay is necessary with circuits such as that of *Figure 318* in order to compensate for the delay in the brightening-pulse time-sweep circuit, notably in the first thyratron of *Figure 315* or *Figure 318*. This delay is necessary with short sweep times. Murphy therefore used hard valve circuits similar to those of Nethercot and his collaborators[1,13] whose work will now be summarized. In these circuits the time lag between the start of the tripping pulse and initiation of the sweep may be only about 5×10^{-8} sec whilst in the above described circuits incorporating two thyratrons the total delay may be about 0·5–1 μsec. In many cases, where delays of this magnitude may be applied to the signal (Y) plate by the use of cable, as for example in the work on corona pulses by GAUNT and CRAGGS[14], the existence of even 1 μsec delay in the firing circuits is not objectionable. BAUER and NETHERCOT[13] also used the G.E.C. 908 B.C.C. 10 kV oscillograph tube and obtained a temporal resolution of about 20,000 km/sec. The sweep times varied from about $2{\cdot}5 \times 10^{-3}$ sec down to 5×10^{-8} sec, with a trigger delay time of not more than 3 or 4×10^{-8} sec. The latter figure should be compared with that given above for thyratron circuits. Since the E.R.A. oscillograph is one of the most successful instruments on which full published data are available, it will be described in detail, following the above account.

The power unit, shown in *Figure 320* supplies 10 kV for the cathode-ray tube, 3 kV for the X-sweep, 500 V for calibration, and 350 V for the multi-vibrator and timing oscillator. The latter supply is stabilized to $\pm 0{\cdot}5$ V for loads varying from 50 to 200 mA. It will be noticed that h.f. rectifier sets are used for the h.t. supplies ; these circuits operate at about 160 kc/s in a voltage doubler for 10 kV and in a half-wave circuit for 3 kV. The earth point on the latter is arranged for a 2·5 kV positive and a 500 V negative line. For moving film recording, without X-deflection, the 3 kV supply is switched off at S_1, and R_1 compensates for the effect of the load reduction on the supply voltage.

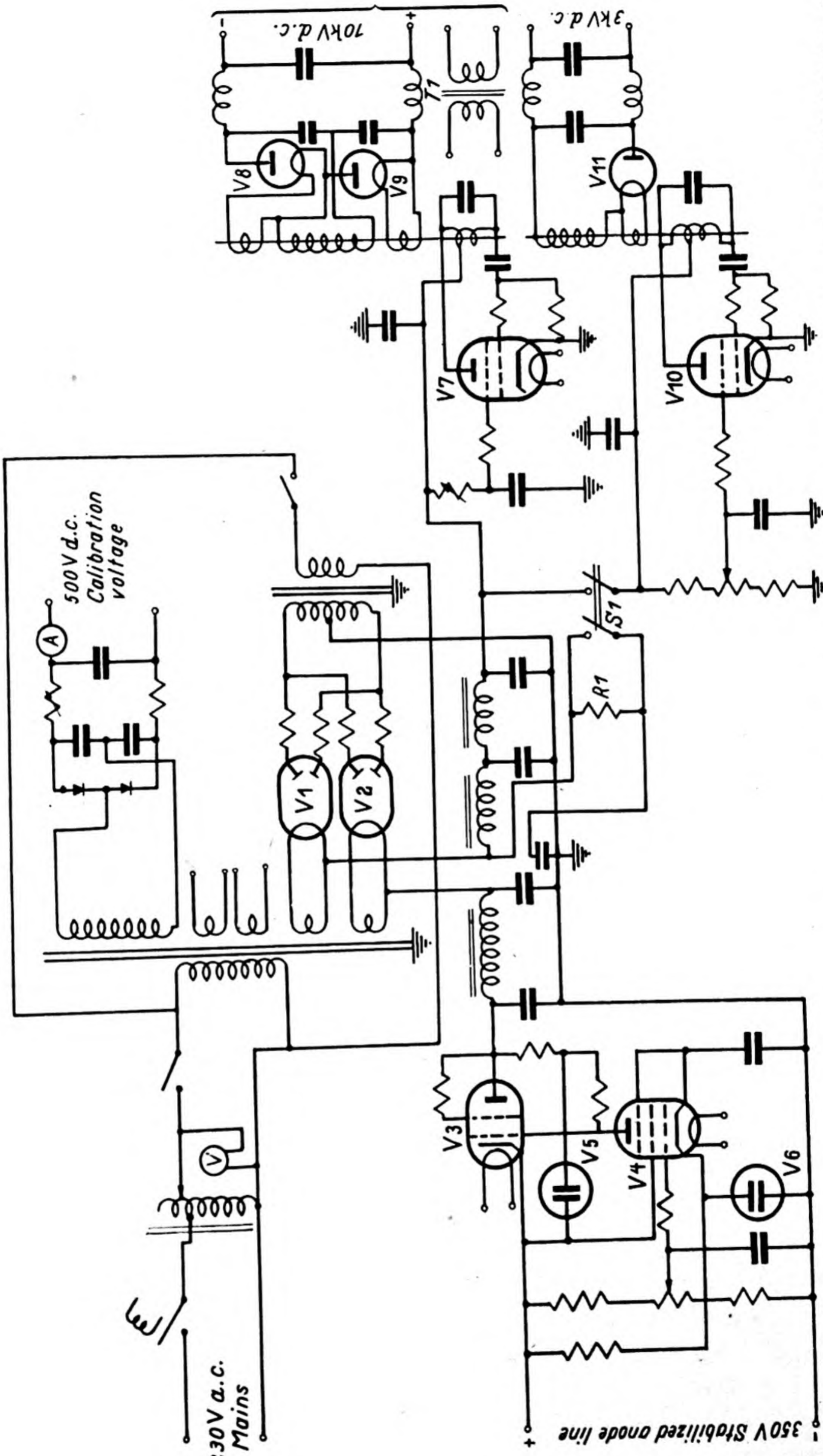

Figure 320. Mains supply unit for a cathode-ray oscillograph (Bauer and Nethercot[13], by courtesy, British Electrical and Allied Industries Research Association).

The transformer T_1 has a secondary insulated for 10 kV. The cathode-ray tube connections are given in *Figure 321*. The diode D_1 prevents the modulator grid from being driven positive. The 200 Ω resistors R_2 and R_3 are inserted to minimize cross coupling at frequencies above 100 Mc/s. Corona from h.t. terminals, which would otherwise occur at voltages > 6–7 kV is prevented by the use of shield electrodes where necessary.

Details of the various supply voltages, namely the potential divider through which the signal is passed, the calibration voltage and the

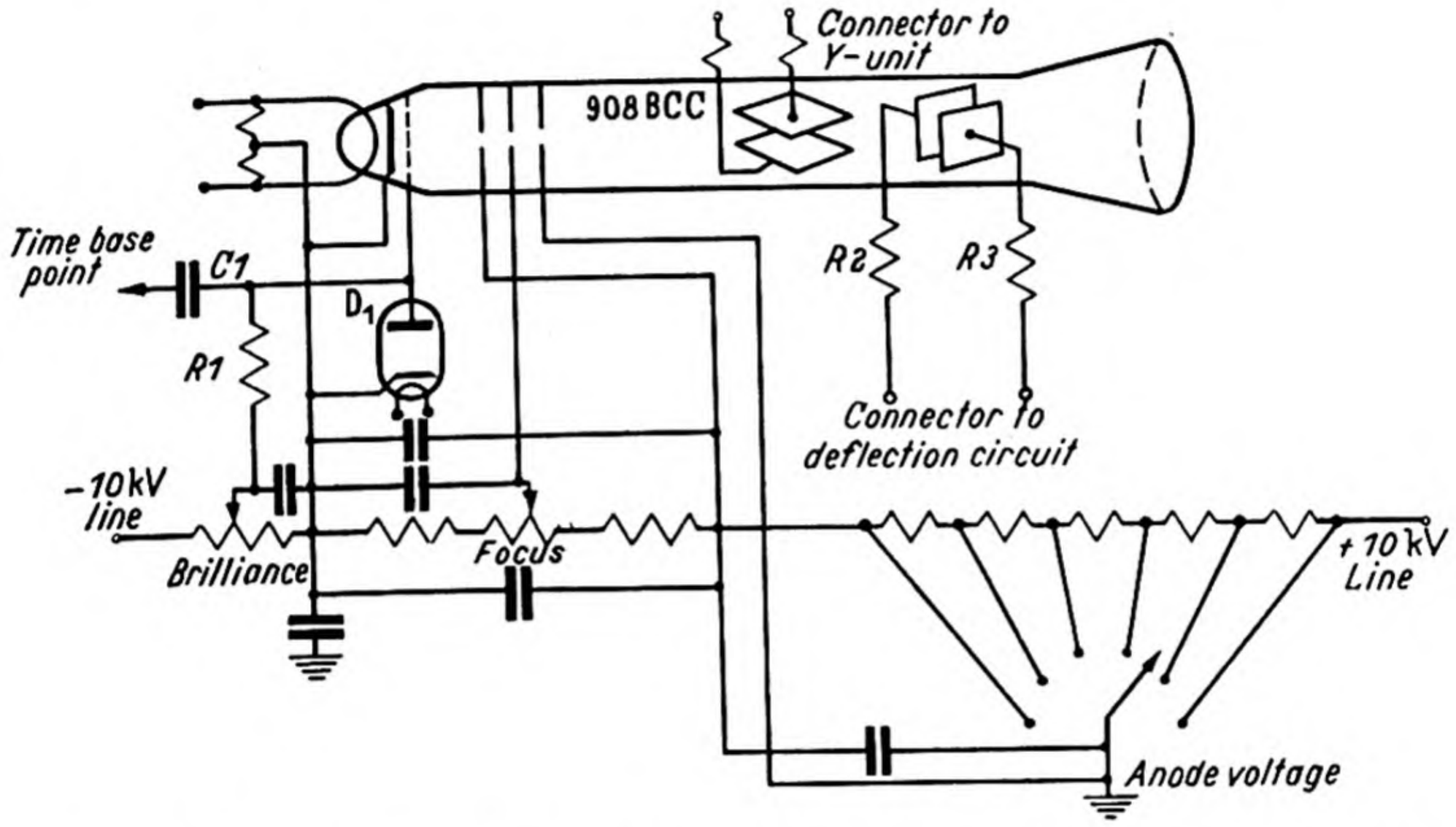

Figure 321. Tube unit for a cathode-ray oscillograph (Bauer and Nethercot[13], by courtesy, British Electrical and Allied Industries Research Association).

oscillator output for time-base calibration, are given in *Figure 322*. 400 V peak, positive or negative, can be applied and will provide at a sensitivity of 0·1 mm./V (10 kV tube voltage) some 8 cm. deflection on the oscillograph screen. This is full screen deflection. The 30 kV potential divider C_1 R_1 is oil-immersed. The potential divider ratios are accurate to within ± 5 per cent. up to 30 Mc/s according to tests made with continuous h.f. voltages.

The main part of the apparatus consists of the multi-vibrator time-base circuit shown in *Figure 323*. This is more complicated than the thyratron time bases described above but gives a more linear sweep with a very short delay in tripping. The multi-vibrator circuit consists of the valves V_1 V_2 and their connections. V_1 is biased almost to cut off, at an anode voltage of 350. V_2 is conducting, with its anode at a fairly low voltage, and if a negative pulse is applied to its grid, the anode current is reduced and the anode potential rises. Thus a positive pulse passes through C_2 to the grid of V_1, which begins to conduct, passing a negative pulse through C_1 to the grid of V_2. The

anode of V_2 then eventually reaches 350 V, giving a square voltage pulse whose duration is determined for the slower sweeps by the time constant $R_2\,C_1$ which sets the time necessary for the grid of V_2 to lose its negative charge. For the faster sweeps R_2 is switched out and replaced by R_1. The anode resistance of V_2 must not exceed 1 kΩ to keep the anode time constant sufficiently small, and for an anode

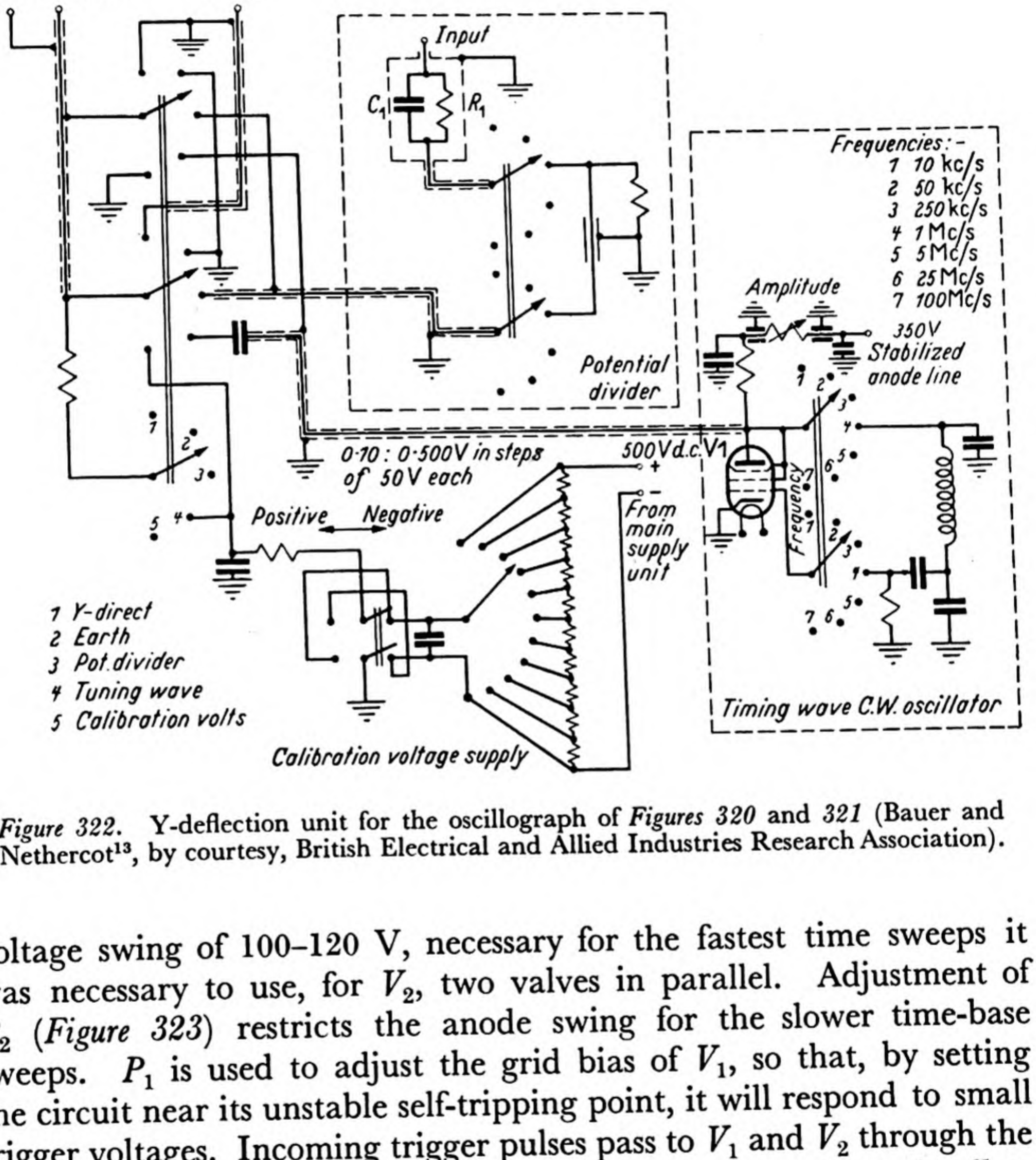

Figure 322. Y-deflection unit for the oscillograph of *Figures 320* and *321* (Bauer and Nethercot[13], by courtesy, British Electrical and Allied Industries Research Association).

voltage swing of 100–120 V, necessary for the fastest time sweeps it was necessary to use, for V_2, two valves in parallel. Adjustment of P_2 (*Figure 323*) restricts the anode swing for the slower time-base sweeps. P_1 is used to adjust the grid bias of V_1, so that, by setting the circuit near its unstable self-tripping point, it will respond to small trigger voltages. Incoming trigger pulses pass to V_1 and V_2 through the diodes D_1 and D_2, which if switched off in turn will respectively allow only positive or negative pulses to reach the grids of V_1 and V_2 respectively.

The square voltage pulse derived from V_2 is used to trip the X-sweep circuit. The square pulse generated across R_3 in the cathode-follower circuit of V_3 which, with V_4, is used to reduce the loading of V_2, is fed through C_3 to the modulator grid of the 908 tube, for spot-brightening.

The time constant R_1 C_1 of *Figure 321* limits the brightening-pulse duration and renders it too short for the slowest sweeps, in the later part of which a decreasing spot brilliance would thus be obtained. Bauer and Nethercot overcame this by applying a part of the rising voltage pulse on the cathode of V_5 to the modulation circuit through R_4 and C_4 (*Figure 323*).

The positive output pulse from V_4 passes through transformer T_1 to the pentode V_5, operated as a constant current tube, and provides the linear symmetrical X-deflection by means of the voltages developed

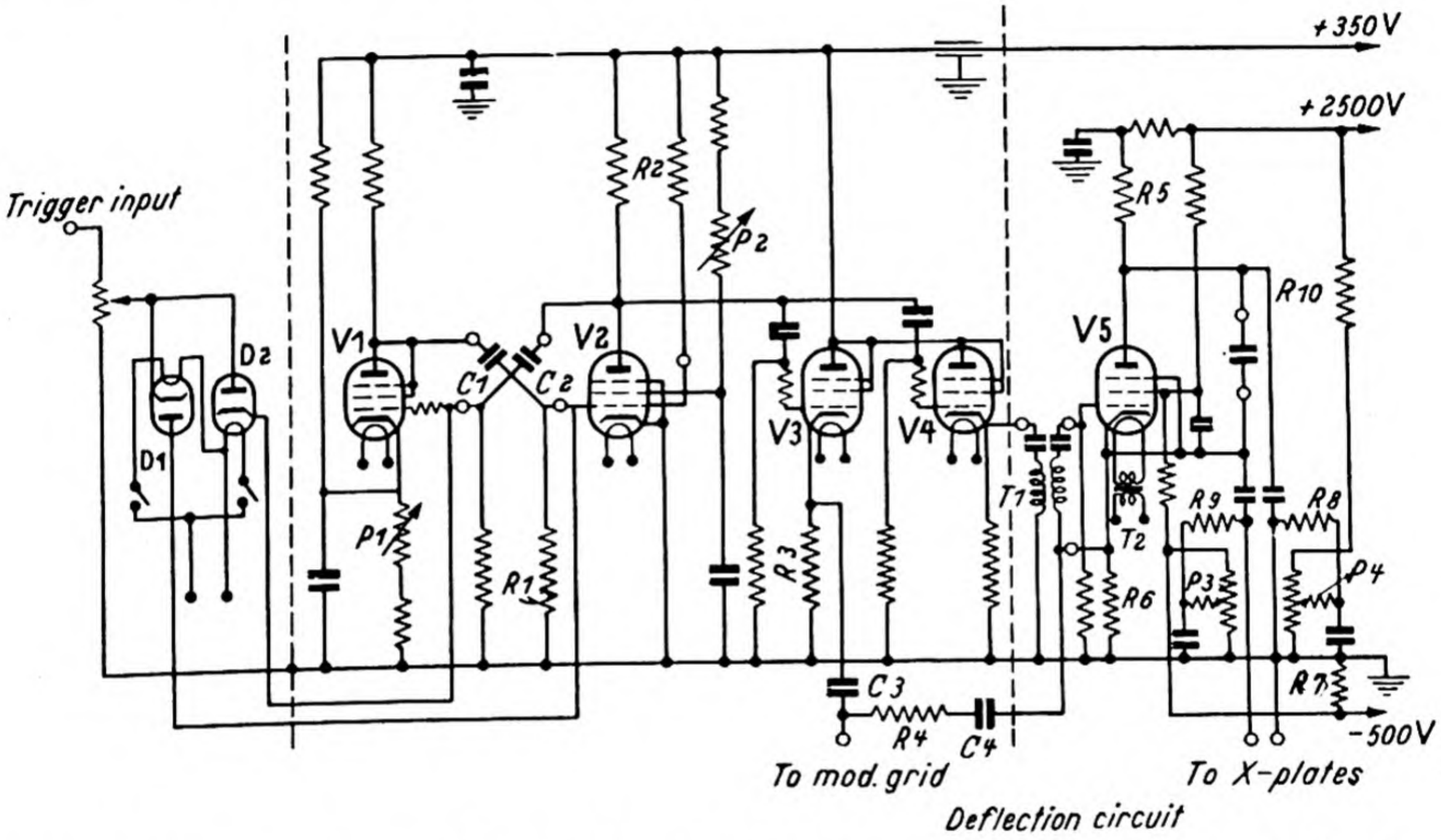

Figure 323. Time-base unit (Bauer and Nethercot[13], by courtesy, British Electrical and Allied Industries Research Association).

across R_5 and R_6. V_5 is, normally, almost cut off with an approximate anode to cathode voltage of 2·5 kV. The symmetrical bias is obtained from R_7 and R_{10} and the ganged potentiometers P_4 and P_3, and is applied to the X-plates through R_8 and R_9. T_2, the heater transformer for V_5, must have a low capacitance since for the fastest sweep only the stray capacitances from anode and cathode of V_5 to earth are used. Three transformers are used at T_1 to give the required range of time-base speeds. Full circuit details are given in the paper[13].

Records taken with a Wray F1 lens are traced in *Figure 324* and show the collapse of the anode voltage of a GTIC thyratron, when suitably pulsed.

Complete details of an oscillograph unit, primarily for nuclear physics, have been given by FITCH and TITTERTON[15] using tubes which were operated at an overall accelerating voltage of 4 kV. The time-sweep speeds varied from 8 inches/μsec, to 1 inch/millisec. The

complete circuits are given in the above paper. The time sweep may be tripped by external or internal trigger pulses, which may be either recurrent or single, and a delay line was included so that the sweep could be made to start before the arrival, at the Y-plates, of the transient to be observed. The circuit includes an amplifier which, with a 1V input signal, would provide a 1·5 inch screen deflection with a minimum rise time of 0·15 μsec. With an F2 lens and suitable film or plates a writing speed of 3 inches/μsec could be obtained.

Two types of high-speed cathode-ray tubes have recently been developed by the DuMont company ; they are the K1030 (30 kV) and the 5RP–A (22 kV). For the latter, a deflectional sensitivity of about

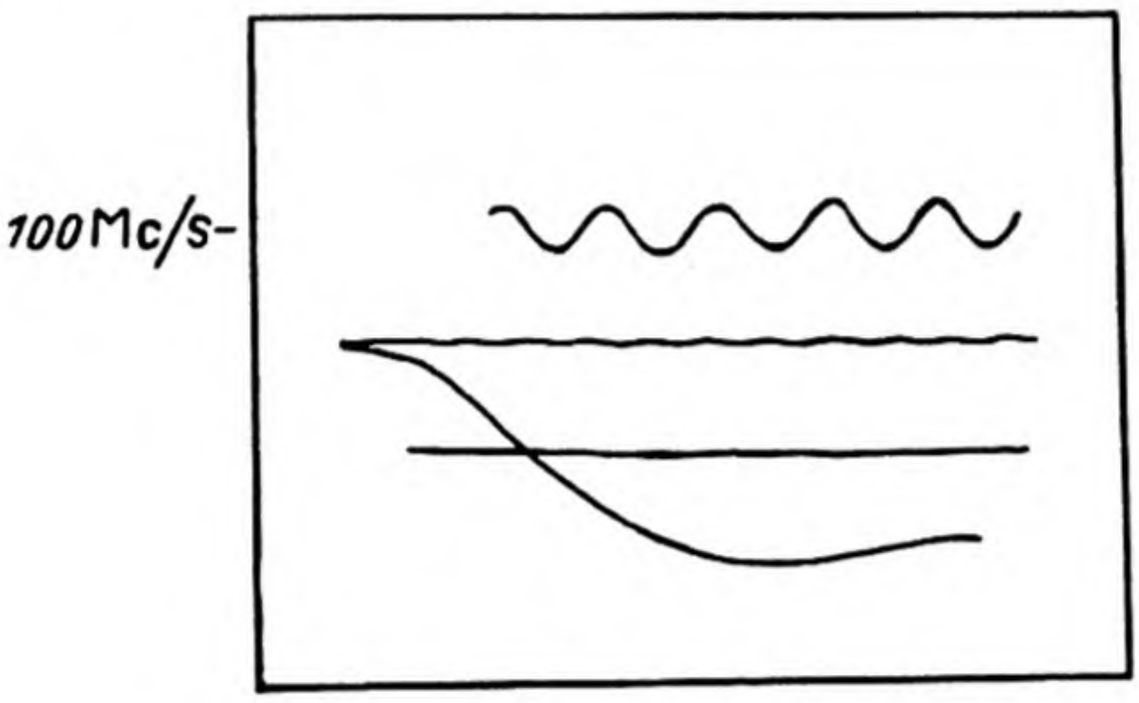

Figure 324. Temporal resolution obtainable with a 10 kV cathode-ray oscillograph (Bauer and Nethercot[13], by courtesy, British Electrical and Allied Industries Research Association).

0·005 inch/V is obtained and the time base sweeps of ~ 100 inches/μsec have been measured[16]. The paper[16] gives details of hydrogen thyratron time bases to give such sweep speeds, with a description of calibration methods. The RCA 912 15 kV oscillograph was used by Hoover[17] in work on transient phenomena, following earlier work by Kuehni and Ramo[18]. In experiments of this kind on recovery transients, following arc-over of a transformer, for example, it is often advantageous to use a recurrent fast sweep, with separation on the Y axis between successive sweeps so that a high resolving time may be maintained. An interesting 4-beam high-voltage oscillograph was described in 1939 by Bigalke[19]. A hot cathode was used as the electron source and cascade acceleration up to 100 kV was obtained by the use of a multi-electrode anode system.

HIGH-SPEED CONTINUOUSLY EVACUATED OSCILLOGRAPHS

The high-speed cathode-ray oscillograph, operated at beam voltages varying up to 100 kV or more and with time-sweep durations of a small fraction of a microsecond has been developed since 1925 by many workers, among whom Rogowski and his collaborators have been pre-eminent[20, 21, 22] and to whom much of the pioneer work is due. A great deal of this development became necessary because of the increasing importance, some 30 years ago, of h.t. transmission and the need for controlled and accurate testing of, for example, cables,

insulators and transformers, and the quantitative observation of break-down voltages in transient conditions.

General reviews of the development of high-speed cathode-ray oscillographs are due to MacGregor Morris and Henley[23], von Ardenne[24], Miller and Robinson[25] and others. Russian work on high-speed oscillography, up to 1937, has been described by Stekolnikov[26]. A convenient introduction to the subject is due to Burch and Whelpton[27] whose oscillograph, following in outline the earlier European models is shown schematically in *Figure 325*. From the

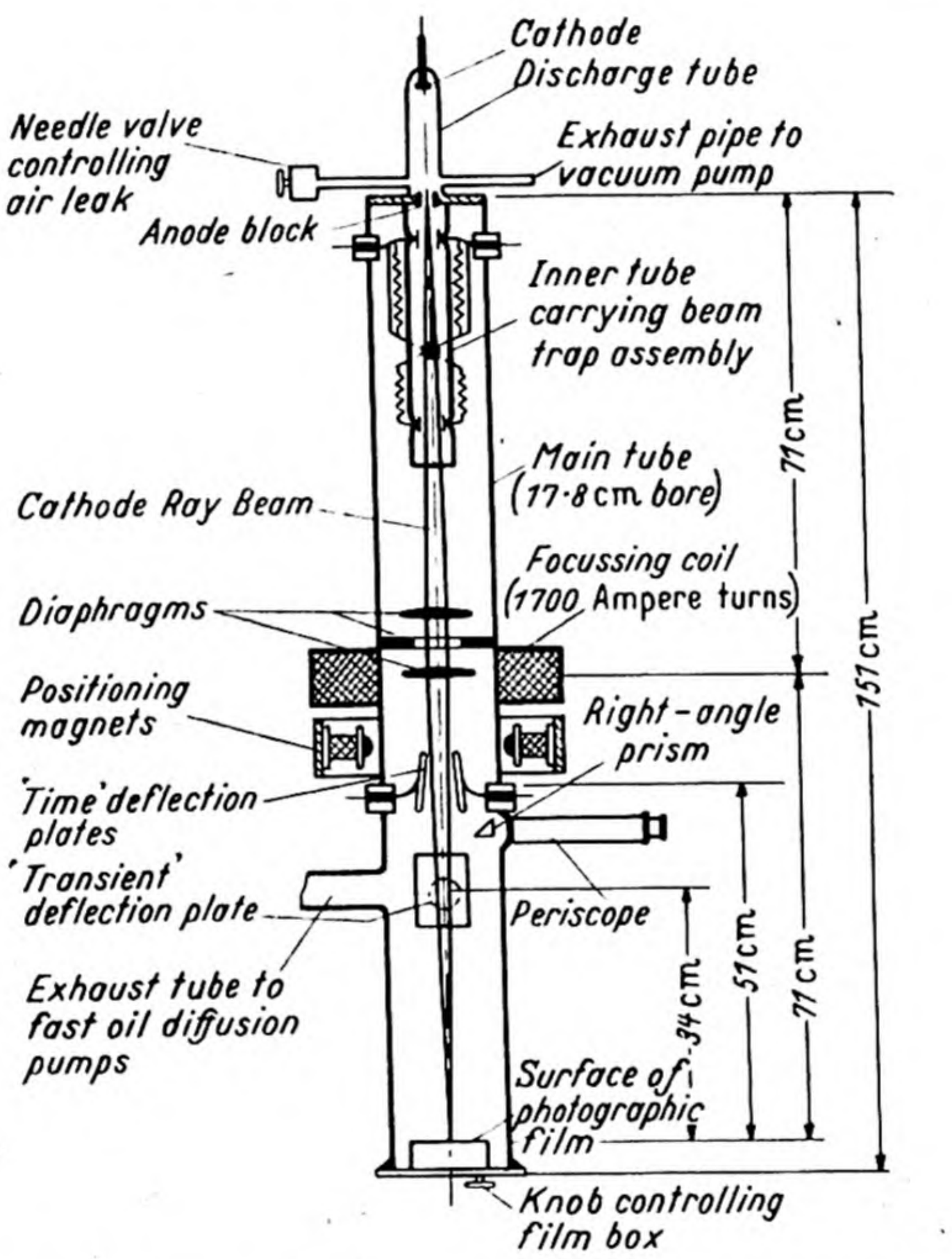

Figure 325. Diagrammatic sketch of continuously evacuated cathode-ray oscillograph (Burch and Whelpton[27], by courtesy, *J. Inst. elect. Engrs.*).

latter it is seen that the main parts of the apparatus are as follows : (*1*) the high-voltage cold cathode discharge tube, which provides, through a perforated anode, the beam of high-velocity electrons necessary to give a sufficiently bright trace on the photographic film or fluorescent screen at the high sweep speeds required, (*2*) a beam trap which, by deflection of the beam until the arrival of the required transient, prevents fogging of the film by a stationary beam impinging on it, (*3*) focusing coils to ensure a small spot size at the screen, (*4*) time deflection plates and transient deflector plates, the latter usually being

the Y plates and (*5*) a photographic film for recording the voltage/time variation for the transient to be observed or a fluorescent screen for visual observation of the transient or for focusing, beam positioning, *etc.* Means of rapidly calibrating the time and voltage axes are usually provided.

Many variations of these component parts are possible, some of which will be briefly described.

The vacuum system consists, typically, of a diffusion pump having a speed of 20–30 l/sec, a suitable rotary pump for backing the diffusion pumps and a needle valve for admitting air to the discharge tube. If required, the diffusion pump may be by-passed to allow the body of the oscillograph to be opened to the atmosphere and roughly evacuated again without the necessity for cooling off the diffusion pump. Some diffusion pump oils may be exposed when hot to the atmosphere without being damaged. Sometimes it is found that a beam of particles, produced in the source, passes without deflection through the beam trap system to the screen or photographic plate, and causes fogging. This phenomenon, mentioned by Burch and Whelpton[27], Whelpton[28], Miller and Robinson[25] and others, appears to be due to negative ions becoming neutralized in the source or the anode canal, and may be

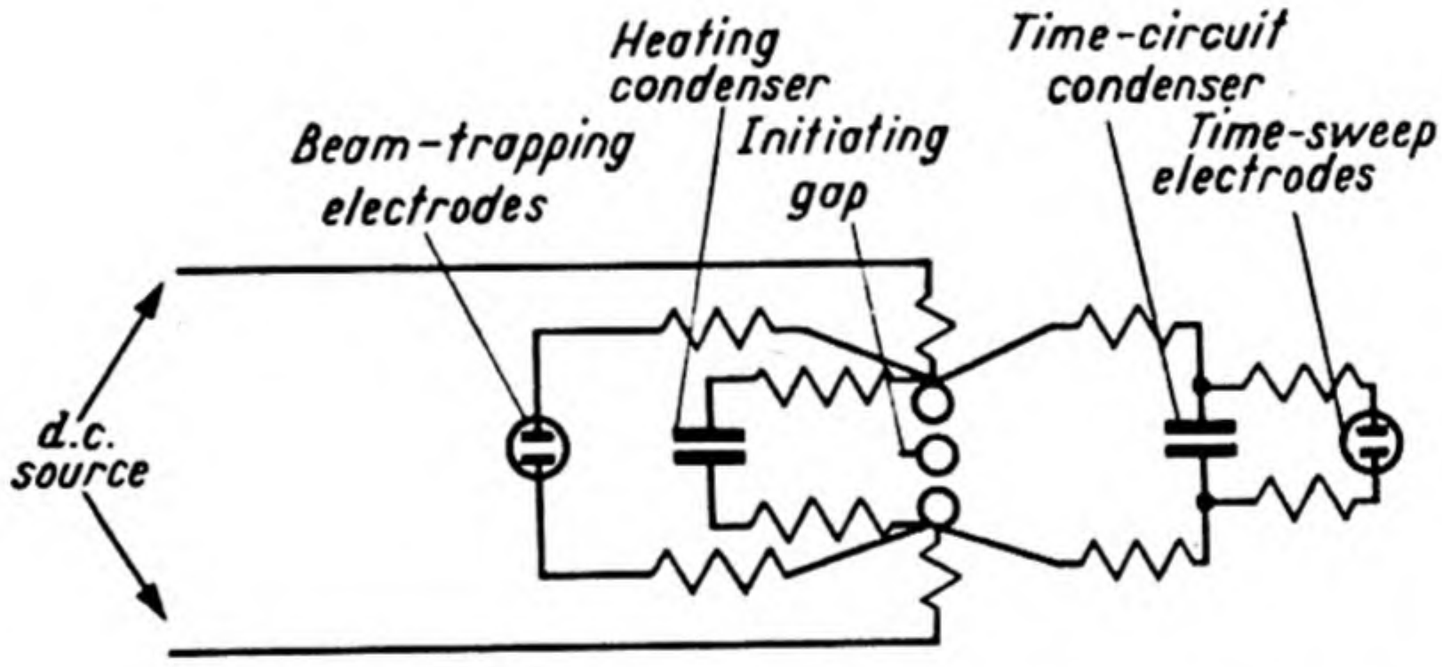

Figure 326. Example of oscillograph auxillary basic circuit (Miller and Robinson[25], by courtesy, *Rep. Progress Phys.*).

overcome by tilting of the source or in other ways. PERRY and his colleagues in their work on lightning discharges in Nigeria had also to overcome this difficulty[29].

The technique of beam-trapping has been used in Europe in preference to the American technique of exciting the source only during the recording time (*see* [27]). In the former, due originally to GÁBOR[30], the source is excited continuously and the beam is allowed to pass to the screen or the photographic emulsion for a short time before the transient appears. The basic circuit, as given by Miller and Robinson[25] is given in *Figure 326* where, it is easily seen, the voltage between the beam trap plates rapidly falls, thus allowing the beam to pass through a suitably arranged aperture, before the time-base plates have

become charged appreciably, when the initiating spark gap conducts on the application of a tripping pulse to the middle sphere. Burch and Whelpton's arrangement of Gábor's beam trap system is shown in *Figure 327* which shows the complete circuit for beam trapping and time sweeping.

The discharge tubes have usually been of the cold cathode type but, very recently, hot cathode sources similar to those developed for high-voltage electron microscopes by HAINE and his collaborators[31] and

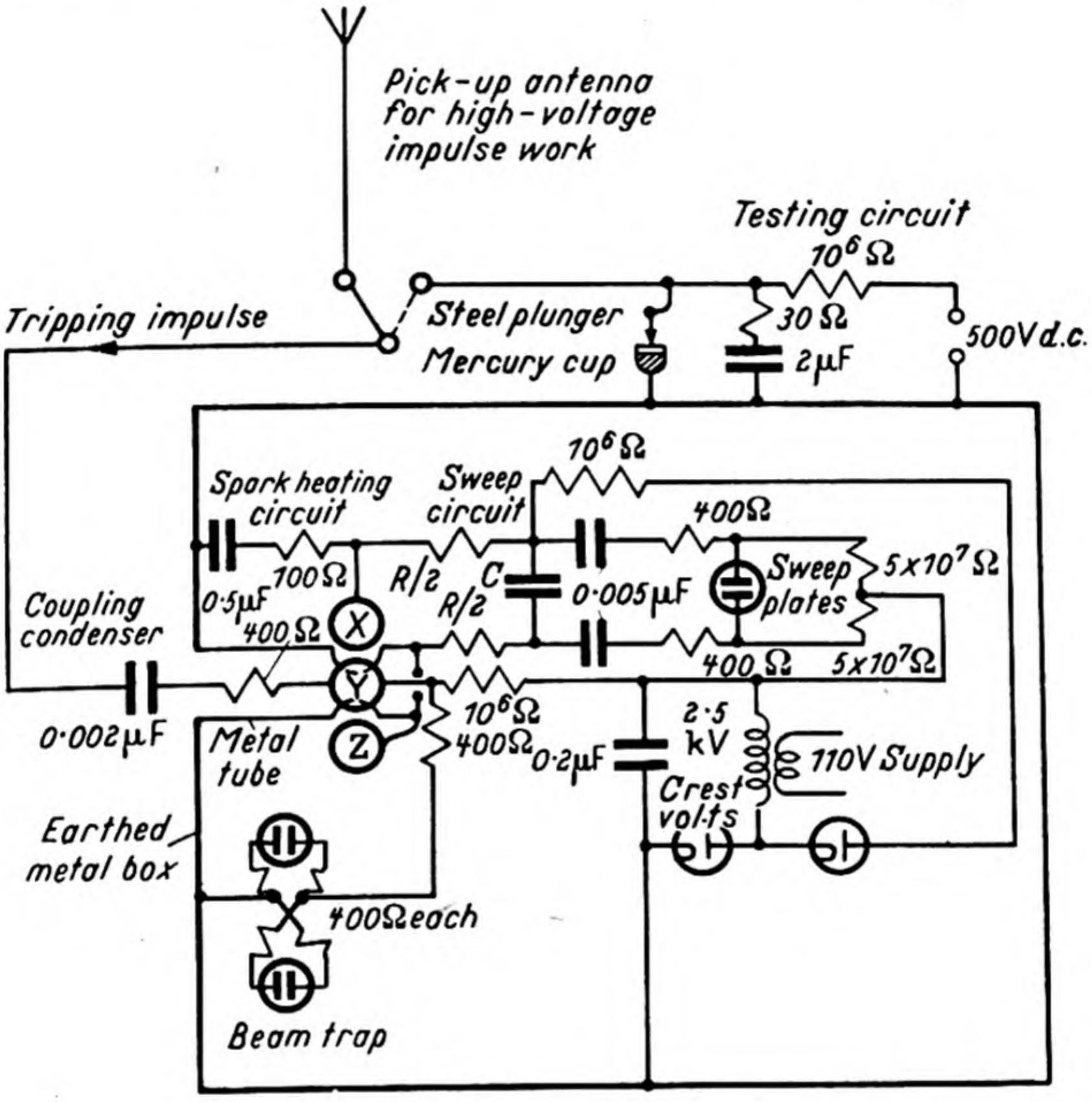

Figure 327. Complete sweep circuit for continuously evacuated oscillograph (Burch and Whelpton[27], by courtesy, *J. Inst. elect. Engrs.*).

others, have become available (earlier work with hot cathodes is briefly mentioned by Miller and Robinson[25]). Burch and Whelpton[27] tried a long discharge tube, in which the electron beam was focused on to the anode hole by means of a coil (see also ROGOWSKI, FLEGLER and TAMM[32]), and operated this source at about 1 mA, 40–45 kV. They later adopted a simpler discharge tube, without pre-anode focusing. There appears to be no general agreement on the best source to use and, indeed, many examples have given satisfactory results. Miller and Robinson give a selection of five types in their paper[25]. Rogowski's group at Aachen was responsible for many publications on this subject[33, 34, 35]. It appears advisable to reduce insulating surfaces, if exposed to the

discharge, to a minimum as in the Burch and Whelpton source to reduce flickering of the beam. When this is done, the source stability may be such as to allow the use of three sources in parallel as in Whelpton's 3-phase oscillograph[28].

Figure 327 also includes the time sweep circuit, which will now be considered, and which is usually initiated in continuously-evacuated high-speed oscillographs by means of the pulse which also untraps the beam, as shown simply in *Figure 326*. The trip arrangement should (*see* Burch and Whelpton[27]) be sensitive, and should work with pulses

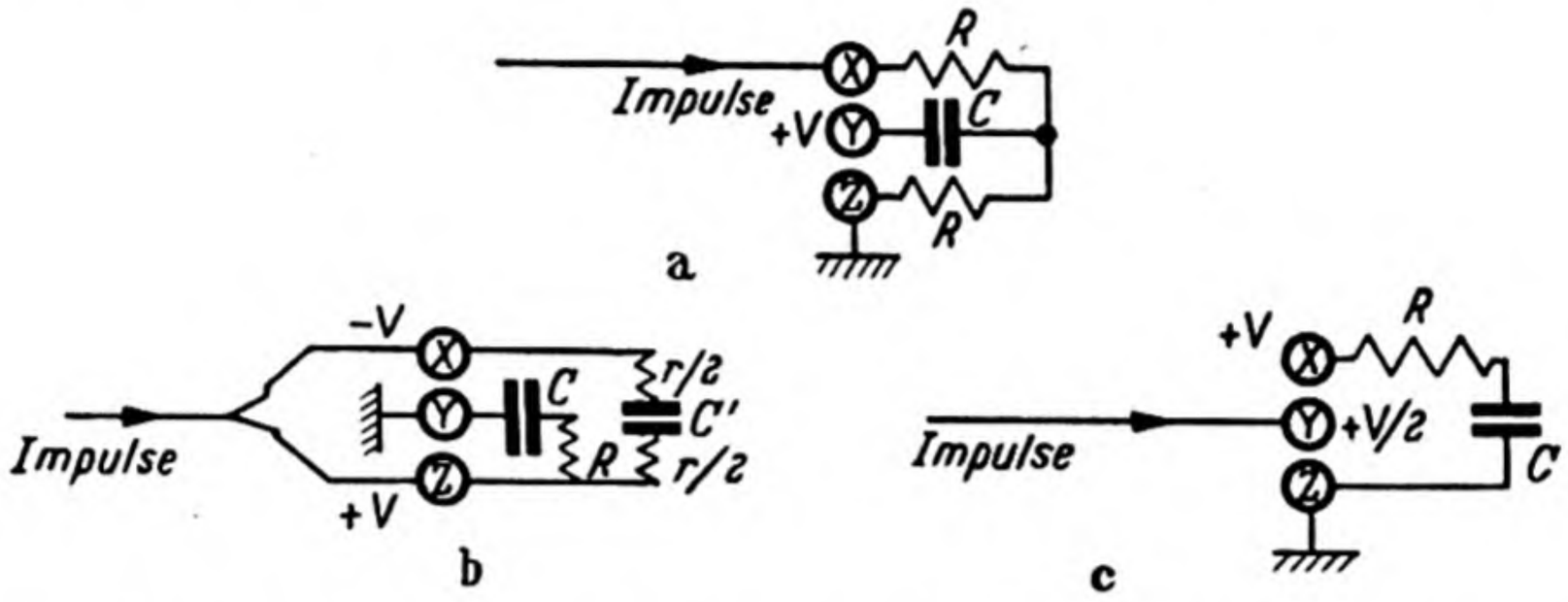

Figure 328. Amphipolar trip circuits (Burch and Whelpton[27], by courtesy, *J. Inst. elect. Engrs.*).

of either polarity. It should be as free as possible from the effects of interaction caused by pick-up between trip and sweep circuits which usually gives distortion of the time scale. Symmetrical deflection on the time sweep and on the beam trap plate system is also desirable since excessive deflection with asymmetric deflection, *i.e.*, with one deflector plate earthed, often gives defocusing. The fly-back of the spot on the film should not appear in the photographic record, unless specially required as a zero line.

Amphipolar tripping is provided by the circuits of *Figure 328* in which $\pm V$ is a steady potential. In *Figure 328* only one gap fires,

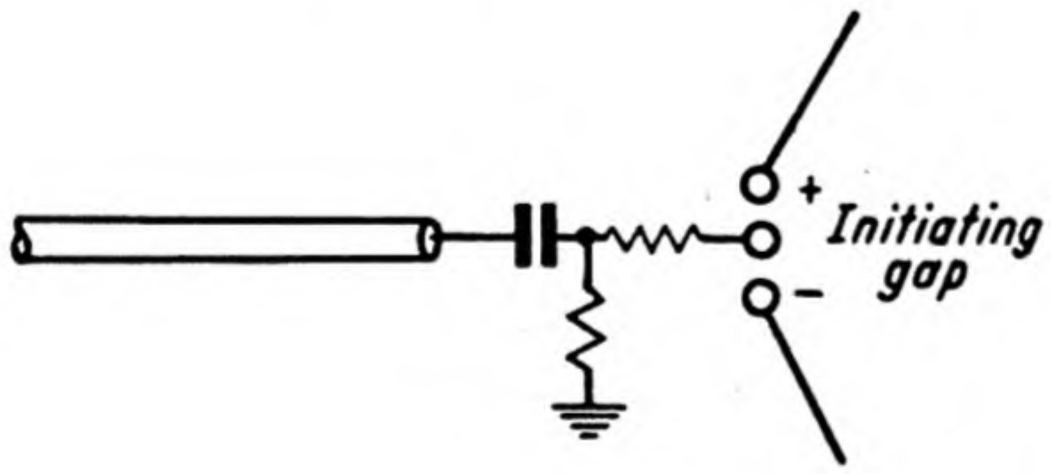

Figure 329. Three-ball gap for tripping of oscillograph circuits (Burch and Whelpton[27], by courtesy, *J. Inst. elect. Engrs.*).

and current flows to earth through the resistance R and C, the sweep condenser, thus increasing the probability of pick-up effects. In *Figure 328* b and c the gaps are in parallel with respect to the tripping impulse voltage. The three-ball gap system is shown also in *Figure 329*. The tripping voltage fires one of the gaps, when the other gap, heavily overvolted, breaks down quickly (*see* pages 146, 266).

There are many possible alternatives to this simple system, for various special purposes, and some of them are discussed, for example, by Miller and Robinson in their review paper[25], by MacGregor Morris and Henley[23] and by von Ardenne[24]. Burch and Whelpton preferred the circuit of *Figure 328* c for impulses with slow rates of rise and it is used in *Figure 327* in which Z is the earthed sphere of the trip gap. On firing of the latter, the common potential of the sweep plates, originally 2·5 kV, falls to zero; at the end of the time sweep the plate potentials are ± 2·5 kV. Thus the time scale is nearly linear since the full spot deflection is much greater than the screen or film width. Often, the operation of circuits such as *Figure 327* in impulse work is difficult because of a common current flowing in different circuits. Burch and Whelpton discuss some effects of this kind, such as those caused by

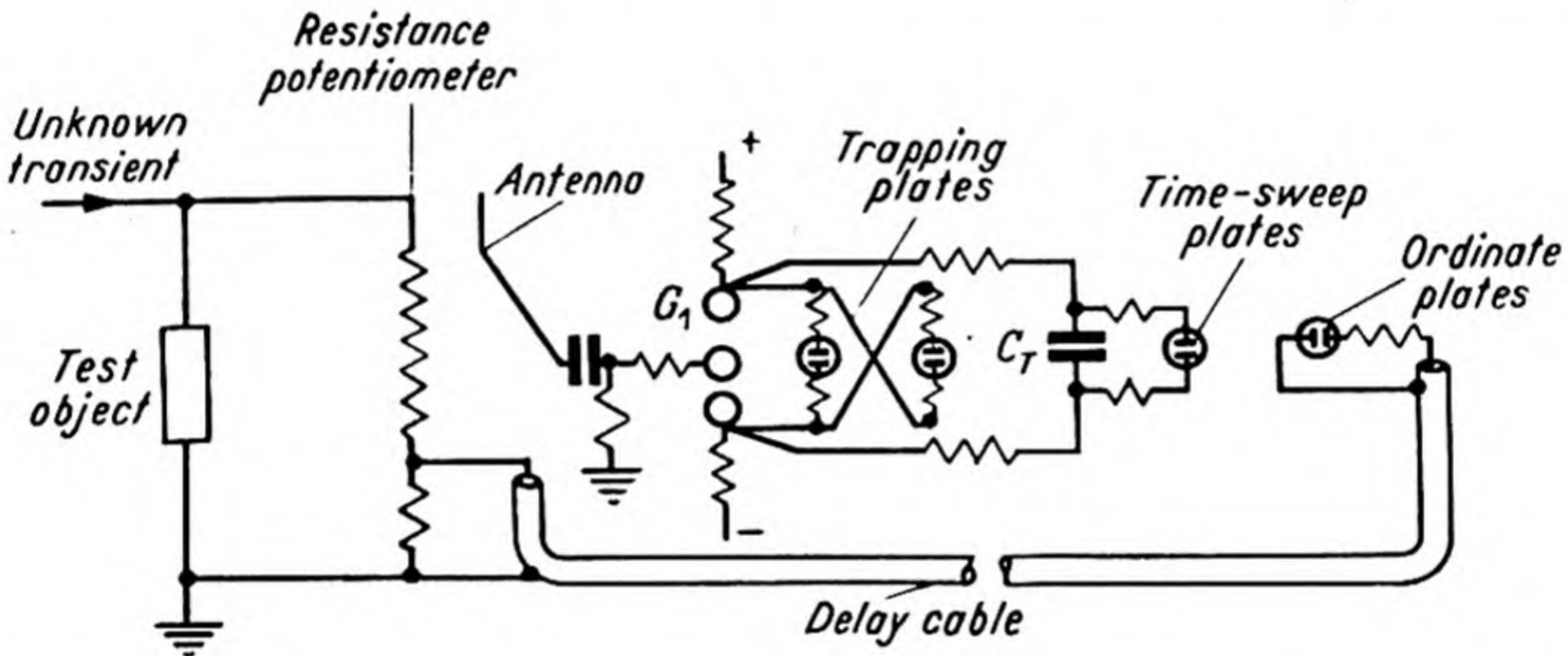

Figure 330. Typical circuit for measurement of uncontrolled impulses with continuous cathode energization (Miller and Robinson[25], by courtesy, *Rep. Progress Phys.*).

oscillatory discharges in the trip circuits. The fly-back can be eliminated by connecting the beam trap across XZ and using a small condenser (0·05 μF) in the spark-heating circuit, so that the sparks can be extinguished when the condensers have discharged to a voltage still sufficiently high to trap the beam. Burch and Whelpton's system is shown in *Figure 327*. The beam trap is then connected across YZ and, on extinction of the spark, the beam trap recharges before the potentials of the sweep plates have changed appreciably. Boekels[36] describes other methods of eliminating the fly-back.

In a trip system[25] widely used in the U.S.A. for controlled surge work the oscillograph discharge tube is energized only during the recording interval.

Miller and Robinson[25] also give the circuits of *Figures 330* and *331*. The former is used for the measurement of random impulses such as those provided by the break-down of a transmission line. When the gap G_1 fires, the beam is untrapped and the time sweep begins. After a suitable interval, set by the delay cable, the impulse

arrives at the Y plates and is recorded, thus ensuring that the front of the impulse is not obscured by the initial part of the sweep (by spot halation or other effects). A resistance or capacitance potentiometer

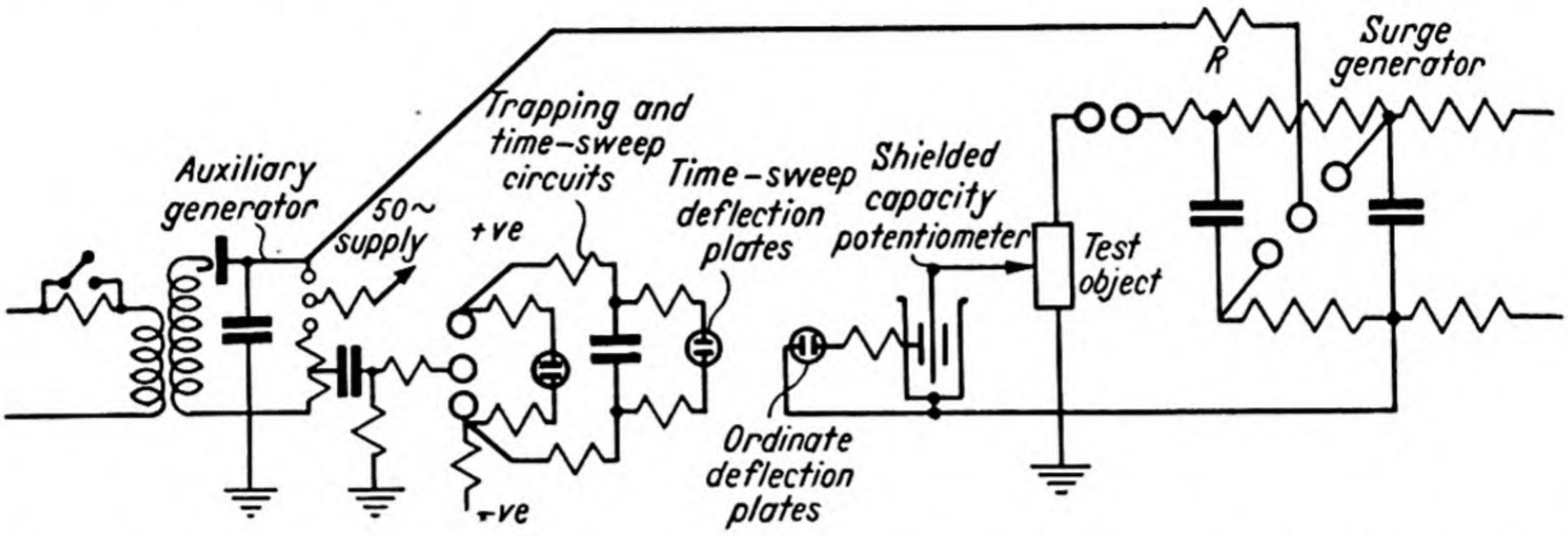

Figure 331. Typical circuit for measurement of controlled impulses without cable delay in the measuring circuit (Miller and Robinson[25], by courtesy, *Rep. Progress Phys.*).

(*see* pages 300–324) may be employed to provide an impulse, at the Y plates, of a suitable size (*Figure 331*). The delay cable is replaced by a suitable resistance *R* (*Figure 331*).

The use of delay cables in oscillography has been reviewed by Miller and Robinson[25] with some consideration of different types of capacitance potential dividers. In some cases, as in the work of BINDER[37],

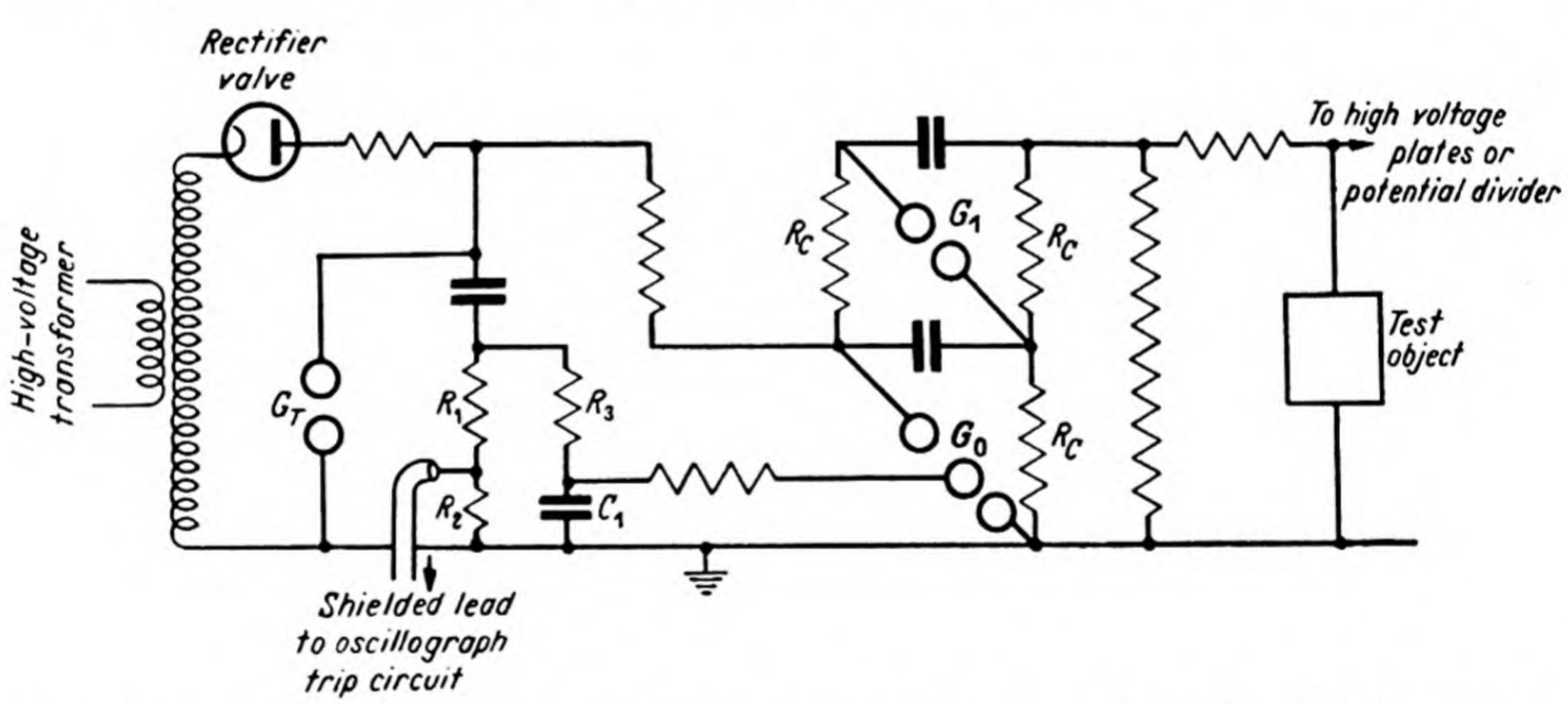

Figure 332. Circuit for generation of delayed high-voltage impulses (Nuttall[39], by courtesy, *J. Inst. elect. Engrs.*).

MESSNER[38] and NUTTALL[39], direct reading of transients having peak values up to 100 or 200 kV was achieved. The various difficulties encountered with potential dividers (pages 309, 311) are thus avoided. Nuttall used the circuit of *Figure 332* to provide delayed high-voltage surges. Hergenrother and Rudenberg[85] have recently described a sealed-off 18 kV cathode-ray oscillograph with a special electrostatic deflector system which allows direct recording of 100 kV transients.

The circuit (*Figure 332*) is supplied from a 100 kV rectifier which charges the 2-stage impulse generator whose spark gaps are G_0 and G_1 through charging resistances R_c. The gap G_T is set to spark over at a voltage slightly lower than G_0. When G_T breaks down a surge is generated across R_1 and R_2, opposite in polarity to the charging voltage of the impulse generator, part of the surge being fed through the cable shown to the oscillograph trip circuit. G_0 is fired by means of the voltage appearing across C_2 when G_T sparks over; the rate of rise of this impulse is set by the values of R_3 and C_2 and further adjustment of the generator may be provided by the setting of the gaps G_T and G_0.

Many other papers have appeared on the technique of recording fast transients with continuously-evacuated high-voltage oscillographs and a selection of a few is included in references[40–44].

Since sealed-off oscillographs are now readily available in Britain for 10–20 kV, and an American DuMont tube may be operated at about 30 kV, there seems to be little need, in general, for the slightly faster sweeps which higher source voltages (50–100 kV) can give. However, it would appear from the available published work that the precision of measurement of time or voltage reached with continuously evacuated oscillographs in the years 1930–1939 (*see* for example the work of ALLIBONE, HAWLEY and PERRY[45]) has not yet been surpassed,

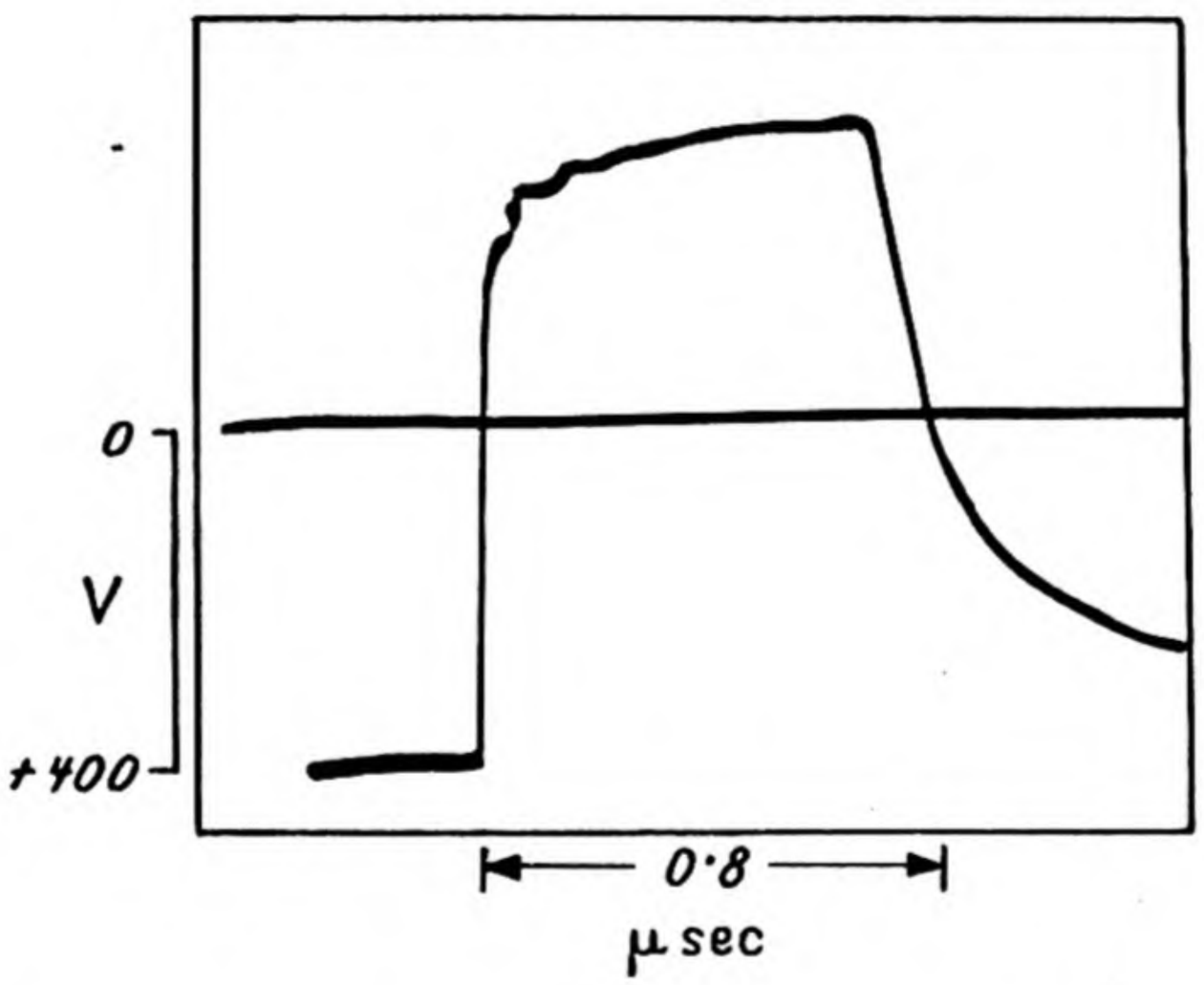

Figure 333. Cable discharge wave (Burch and Whelpton[27], by courtesy, *J. Inst. elect. Engrs.*).

or perhaps even equalled, with sealed-off tubes which tend to give thicker traces and, probably, rather more deflectional distortions and errors. Sealed-off tubes are more convenient and cheaper, are improving continually, and in the future will probably replace the more complicated continuously-evacuated oscillographs for nearly all surge measurements.

An early high-speed record due to Burch and Whelpton[27] is traced in *Figure 333*. Recording speeds of about one-fifth the velocity of light have been obtained, and indeed speeds of ~60,000–100,000 km/sec were recorded some 20 years ago by ROGOWSKI, FLEGLER and BUSS[46]. KATZ and WESTENDORF have obtained a writing speed of about 5×10^9 cm/sec with a 20 kV sealed-off oscillograph[47].

A typical fast oscillogram, published in 1930 by ROGOWSKI and KLEMPERER[48] and which was taken in studies of break-down characteristics of spark gaps, shows a rise time ~10^{-8} sec. Further and later work on fast recording with a continuously-evacuated oscillograph (writing speed ~3×10^9 cm/sec) is by WADE, CARPENTER and MACCARTHY[49].

MISCELLANEOUS TECHNIQUES FOR THE RECORDING OF VERY SHORT TRANSIENTS OR ULTRA-HIGH-FREQUENCY OSCILLATIONS

Continuously-evacuated oscillographs, with source voltages varying up to 95 kV, and with circuit arrangements as shown on pages 348–353 will provide writing speeds up to 10,000 cm./μsec[50]. The deflectional sensitivity with this type of apparatus is of the order of 200 V/cm. on the oscillograph screen; 2 kV sealed-off tubes may give recordable writing speeds of ~2 cm./μsec, which has been increased by KUEHNI and RAMO[51] with the RCA 912 15 kV tube to ~25 cm./μsec with a deflectional sensitivity of ~200 V/cm. The DuMont 5 RP 25 kV tube, with post-deflection acceleration[52] provides writing speeds ~400 cm./μsec.

PARK[53] has recently described a modified 50 kV cathode-ray oscillograph in which a very large increase (~$\times 50$) in beam current is produced momentarily, for the observing period, by a suitable pulse circuit. The highest writing speed thus obtained was about 23,000 cm./μsec (about three-quarters of the velocity of light).

KELLEY[54] has described in detail an oscillograph for the observation of fast voltage transients using a 20 kV DuMont oscillograph tube, type 5RP or 5XP. The sweep generator gives sweep speeds varying from 30 cm./μsec to 0·05 cm./μsec with total sweep times varying from 0·3 to 200 μsec. The transient amplifier, for the Y deflection, has an overall rise time of 0·0063 μsec with a gain of 1,000. The design of such an amplifier, which is of the distributed amplification type, has been discussed also by GINZTON *et al.*[55] and others[12].

Kelley's oscillograph is capable of being triggered by 0·06 V pulses, with negligible random delays provided that the triggering pulse rise time is not less than 0·03 μsec. The screen is illuminated within 0·01 μsec after the arrival of the trigger pulse. The amplifier circuits are described in detail by Kelley[54] and the practical aspects of distributed amplifier design are taken further by MURPHY[12].

Metropolitan-Vickers have described an ingenious system for displaying very fast recurrent transients on a conventional cathode-ray oscillograph[57]. Wave-forms having component frequencies up to 300 Mc/s are faithfully reproduced. The following details are given in the above source[57]; the apparatus has been exhibited at the Physical Society Exhibition, and a detailed paper by McQueen[84] has recently appeared.

The method consists essentially of measuring the amplitude of the transient at any one instant during any one recurrence and displaying this on the oscillograph screen at an appropriate point along the time axis. Successive recurrences thus each contribute an amplitude at a particular time in the transient wave and these Y-deflections are also displayed at appropriate points, at scaled distances along the X axis. The oscillograph time scale can thus be much longer than the transient, by a known amount. About 100 points are sufficient to give an accurate record, but when the wave-form changes rapidly with respect to time some 200 points may be provided. By using a long afterglow screen, transient recurrence rates as low as 100/sec may be used.

The amplitude at any point of the transient is measured over an interval or gating period of 0·001 μsec. The attenuation for an input voltage having frequency f Mc/s and a gating period T μsec is given by

$$\frac{\text{voltage output at frequency f}}{\text{voltage output at low frequency}} = \frac{\sin \pi f T}{\pi f T}$$

If $f = 300$ Mc/s and $T = 0{\cdot}001$ μsec, this ratio is 0·86, and the attenuation is 1·3db. The gating valve is mounted in a special probe unit, to eliminate cable distortion.

The expansion of the time scale is obtained, in effect, by displaying the time delay between a pulse, fixed in time with respect to the observed transient, and the gating pulse which moves along the transient. The shortest time scale is 0·05 μsec, and accurate measurements of time intervals may be made by the use of a horizontal shift calibrated in 0·01 μsec divisions. Transient amplitudes of less than 0·1 V may be measured, and not more than 0·5 V peak-to-peak signal is required for full deflection on a 5-inch cathode-ray tube screen. The apparatus has been used in the study of short pulses in radar receivers and in the monitoring of T.R. cell voltage spikes.

Time expansion techniques for milli-microsecond pulse work are described also by Moody[58].

The conventional deflector plate system used in cathode-ray oscillographs is not capable of responding faithfully to very high frequency voltages, because of the finite transit time of the electrons through the deflector plates and the resulting effective stiffness of the electron beam.

This effect has been studied by HOLLMANN[59] and by KLEMPERER and WOLFF[60]. Hollmann showed that, with electrostatic deflection, the relative dynamic sensitivity for an angular frequency ω of the deflecting voltage and a deflector plate transit time θ with respect to unit sensitivity when $\omega \longrightarrow 0$ is given by $(\sin \omega\theta/2)/\omega\theta/2$ if the effect of field fringing at the edges of the plate may be ignored. For deflection by a transient voltage of the form

$$E(t) = E(1 - e^{-t/\tau})$$

it can be shown[60] that the ratio of the voltage time constant τ to θ should be at least 5 for accurate recording. HOLLMANN[61] has given a more recent treatment of the dynamic sensitivity of cathode-ray oscillographs, and has applied it to Lee's three-beam micro-oscillograph, now to be described.

LEE[62] has shown that for a 50 kV high-speed oscillograph with a deflector plate length of 5 cm., the reduction in deflection sensitivity is about 5 per cent. at 500 Mc/s, and for the transient case τ should have a minimum value of about 2×10^{-9} sec. This loss in sensitivity is clearly negligible for most work, even with high writing speeds, on transient recording, but the technique may become of greater interest in view of the increasing importance of very short transients in nuclear physics (for example, in scintillation counting techniques), in high-speed computing methods and in other fields.

The technique was due originally, it appears, to von Ardenne[63], and has been developed later by Lee[62], Fletcher[64], Hollmann[65] and others (*see*, for example, the review paper by BARTLETT and DAVIES[56]). This method involves the measurement with a microscope of the very small deflections obtained when the length of the deflector plates is reduced. To obtain a satisfactory ratio of deflection/spot size on the oscillograph screen the spot size must be reduced from its normal value in conventional oscillographs, to give a diameter of 10^{-2}—10^{-3} mm. with a diagram size about 1/100th of normal. Records are taken with the beam impinging directly on the photographic emulsion in order to preserve detail.

Von Ardenne's micro-oscillograph had two beams and Lee[62] developed the technique further, using three beams. Lee's oscillograph which operated at 50 kV is shown in outline in *Figure 334*. A hot cathode source was used, with a total beam current of about 5 mA. The time sweep, and any tripping circuits required for the initiation of the transient to be observed on the Y plates were actuated by a pick-up probe which intercepted part of the beam current in the deflection chamber. The beam itself was switched on only a short time before the tripping system was triggered off. A deflection sensitivity of about 0·001 mm./V, on the photographic emulsion, was obtained. The trace width of 0·01 mm. is equivalent to 10 V deflecting voltage.

It was estimated, from Hollmann's work, that, for a deflector plate length of 0·2 in., the transient time effect would give a reduction in deflectional sensitivity at 3,000 Mc/s of 4 per cent. and 40 per cent. at 10,000 Mc/s. In order to allow for fringing the plate length was increased, for the calculations, by 40 per cent.

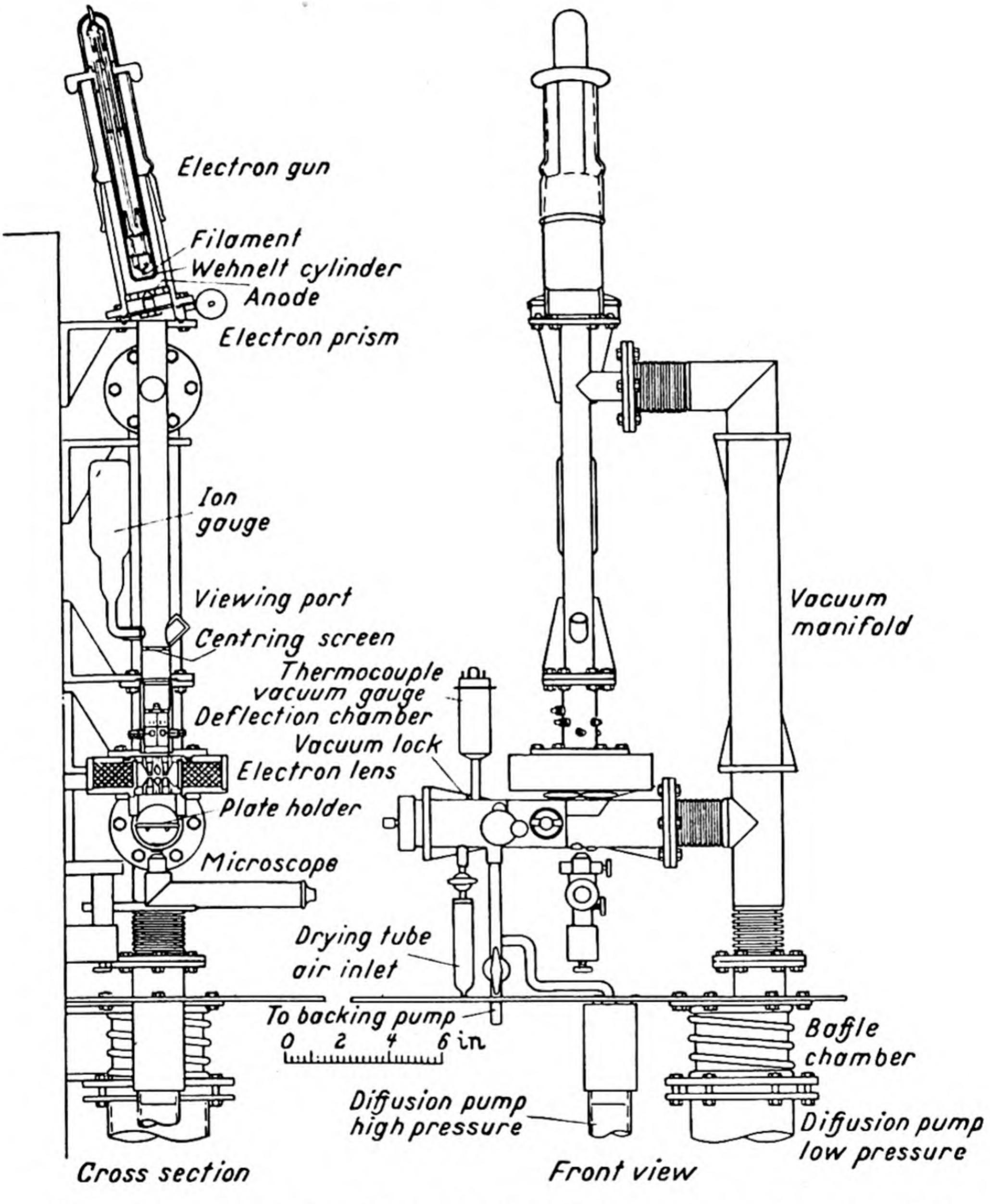

Figure 334. A micro-oscillograph (Lee[62], by courtesy, *Proc. Inst. Rad. Engrs.*).

Figure 335 shows a typical record obtained with Lee's oscillograph ; it represents a record of voltage collapse in a circuit which included a spark gap, the break-down of which produced the transient shown. The range of frequencies which can be investigated with cathode-ray-oscillographs has been increased by approximately a factor of ten with this technique.

The circuit techniques necessary to obtain the full advantages of micro-oscillographic recording have been described more recently by FLETCHER[64] who has studied the formative times of short spark discharges at such high over-voltages that the spark gaps break down in a time $\sim 10^{-9}$sec. The paper describes a sweep circuit, potential

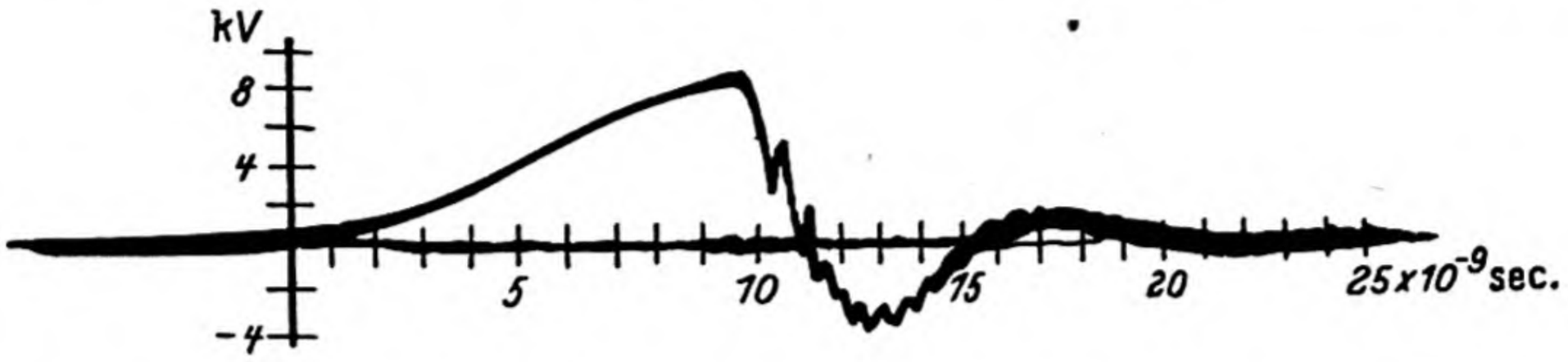

Figure 335. Voltage transient in spark-gap circuit. Enlargement, 50 diameters (Lee[62], by courtesy, *Proc. Inst. Rad. Engrs.*).

dividers and spark-gap switches which may all be used for times $\sim 10^{-9}$sec. In this work, transmission line connections are necessary, to avoid the parasitic oscillations caused by the stray reactances unavoidable in normal wiring methods. With transmission line connection, the effect is not that of lumped inductances and capacitances, but of a resistance with a delay time.

The development of switching circuits, which can be used also for the generation of very short ($\sim 10^{-9}-10^{-10}$ sec) impulses for work on spark-gap break-down, or for other uses, is described in detail by Fletcher, who discusses four types of spark-gap switch. The arrival of the triggering impulse on the middle sphere of a three ball trigger gap causes break-down and an impulse with a rise time of about 20×10^{-9} sec travels down an isolating line to a pulse-sharpening gap. This breaks down very rapidly (perhaps in $0{\cdot}3 \times 10^{-9}$ sec) because of

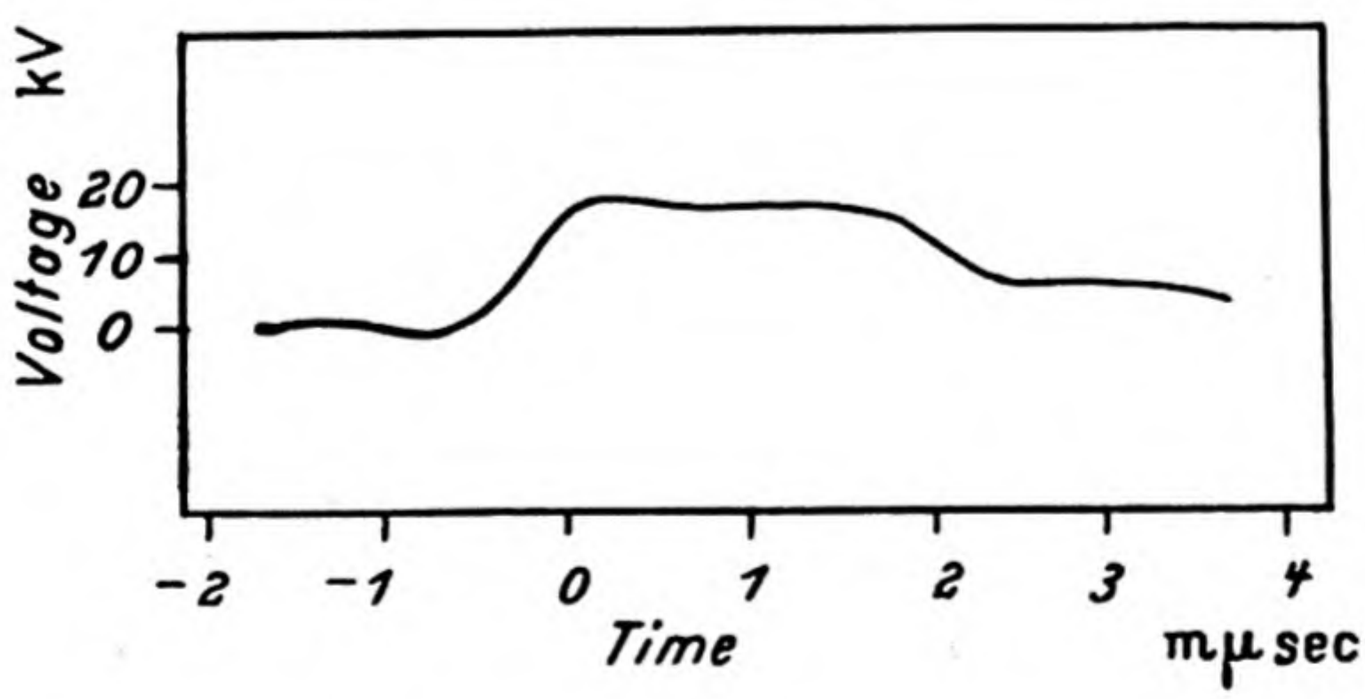

Figure 336. Typical voltage oscillogram showing the arrival of voltage impulse at the left and break-down of spark gap at the right. (The small oscillation in front of the impulse occurs because the voltage is viewed as the reflection from the spark gap superimposed on the incident pulse; the oscillation is on the top of the incident pulse) (Fletcher[64], by courtesy, *Rev. Sci. Instrum.*).

the high overvoltage, provided that its statistical lag (*see* pages 265, 266) is longer than the rise time of the trigger gap break-down; thus the pulse-sharpening effect is produced. It was found, however, that the statistical lag, even without irradiation, of the pulse sharpening gap appeared to be shorter than the rise time of the trigger gap and this led to the use of high-pressure nitrogen gaps (up to 1,500 lb./in.^{2} pressure) with short spacings. Even then the distribution of statistical

lags sometimes gave relatively slow break-down of the pulse sharpening gap, when the statistical lag in the latter was very short, and necessitated the use of another circuit with which pulses with a rise time of about $0{\cdot}4 \times 10^{-9}$ sec could be obtained, as shown in the typical record of *Figure 336*. The above paper[64] should be consulted for further details, and for the detailed design of a three-ball trigger gap working in nitrogen at 600 lb./in.^{2}.

Impulses produced in this manner were $\sim$20 kV, and potential dividers with a ratio of 100 : 1 were required to give reasonable Y-

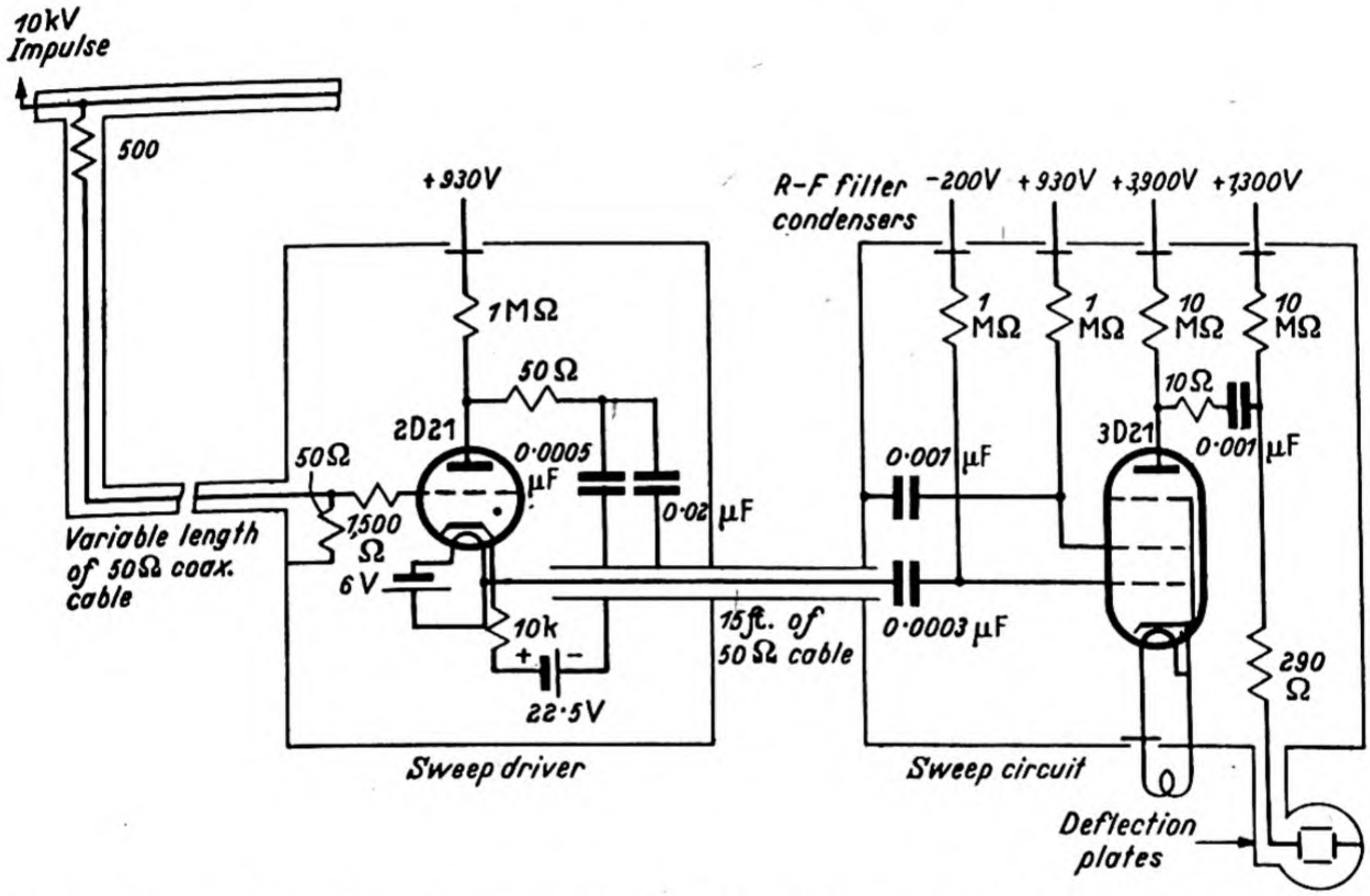

Figure 337. Schematic diagram of ultra-high-speed sweep circuit (Fletcher[64], by courtesy, *Rev. Sci. Instrum.*).

deflections in the oscillograph. The requisite frequency response must extend from 10 to over 3,000 Mc/s. Fletcher[64] describes four novel potential dividers in some detail, all of them involving delay line techniques. The final form of potential divider was such that Fletcher considered that there would be less than 10 per cent. distortion for impulses which were considerably shorter than the $0{\cdot}4 \times 10^{-9}$ sec wave-front used in his work.

The special sweep circuit, developed by Fletcher, is shown in *Figure 337* and provides the 1,000 V necessary for full screen deflection in times varying from 3×10^{-9} sec up to 10^{-6} sec. These times are synchronized with the h.t. impulse to within $\pm 0{\cdot}1 \times 10^{-9}$ sec. The time sweep is produced (*see Figure 337*) by the 3D21 pentode discharging its stray anode capacity. This pentode is driven by a 2D21 gas-filled thyratron which prevents the sweep speed from being affected by the shape of the triggering impulse and prevents the latter also from

causing oscillation effects in the sweep circuit. The 2D21 thyratron was found to have a firing time lag of 51×10^{-9} sec, as compared with the value of 130×10^{-9} sec for the 3C45 tube, and was therefore preferred since the necessary length of delay cable, to obtain satisfactory location of the impulse on the time base, was thereby minimized. The time sweep speed was altered by controlling the filament voltage of the 3D21.

The complete system for observation of spark-gap break-down is shown in *Figure 338*. The cycle of operations is as follows: the oscillograph beam, which is switched on for about a millisecond by means of a mercury pool mechanical switch, is partly intercepted by a probe (as described by LEE[62]) the pulse from which, after amplification,

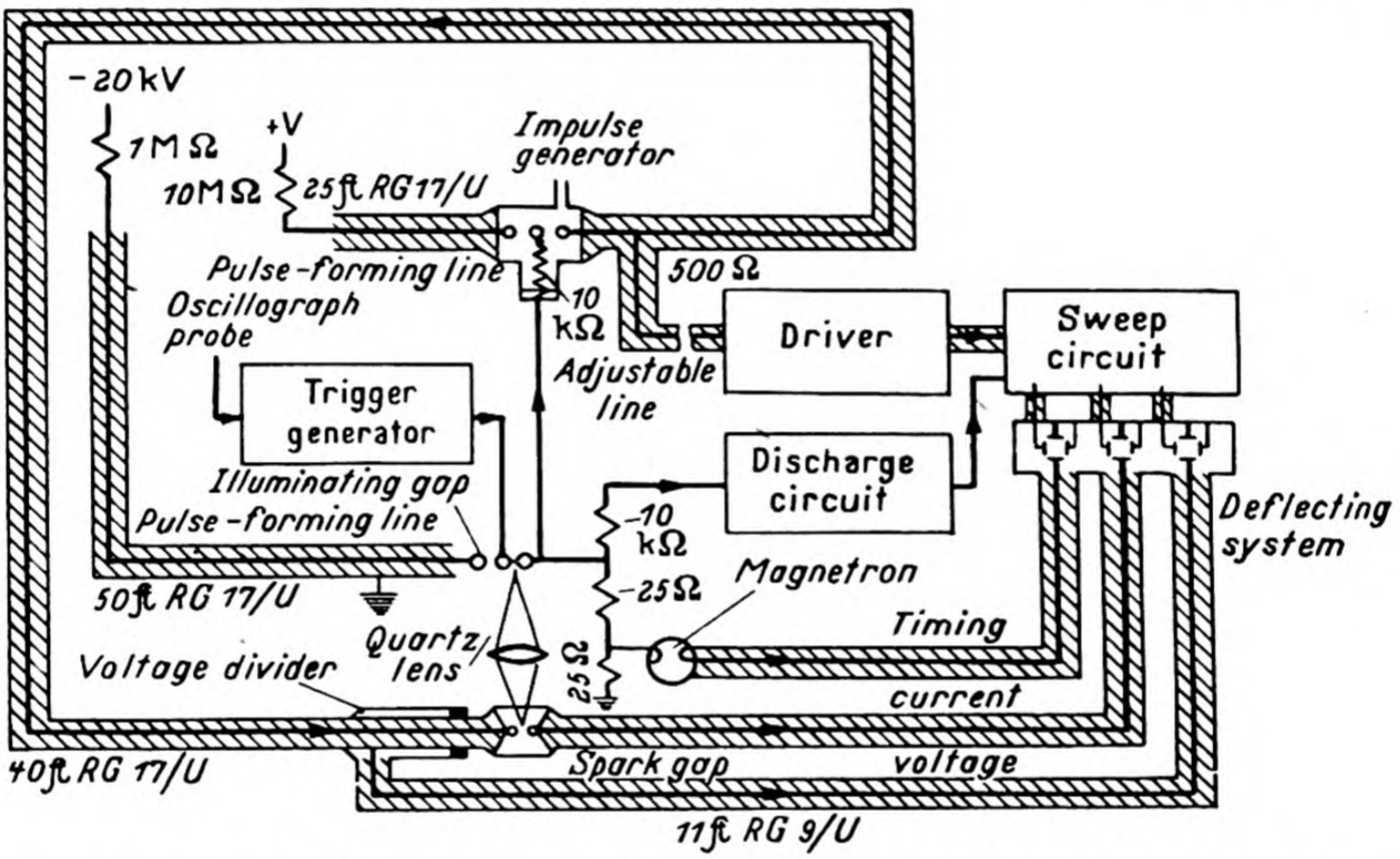

Figure 338. Schematic circuit for testing impulse break-down of air in the 10^{-9}sec region (Fletcher[64], by courtesy, *Rev. Sci. Instrum.*).

trips an ignition coil circuit and triggers a spark gap which illuminates the test gap with ultra-violet light. Simultaneously it sets off a magnetron timing wave, and triggers the high speed impulse generator. A portion of the impulse from the latter is fed into the time sweep driver, thus setting off the time base, whilst a pulse proceeds along a 40 ft. transmission line, through a potential divider, and so to the test spark gap. The current in the latter can be observed with another of the three beams of the oscillograph using another transmission line. The lines from the voltage divider and spark gap are arranged so that signals from them arrive simultaneously at the oscillograph. The adjustable line shown between the impulse generator gap and the driver serves to provide synchronization, with the sweep, of the impulses derived from the voltage divider and the spark gap.

To prevent recharging of the plate circuit of the time-sweep pentode (*Figure 337*) during the millisecond period for which the oscillograph beams are switched on, a thyratron circuit triggered from the illuminating gap was provided. This turned off the supply voltages for the pentode after a single sweep had been obtained.

Moody has described new millimicrosecond circuit techniques in a series of articles[58]. The second of these articles deals with the oscillographic techniques necessary for the recording of pulses lasting $\sim 10^{-9}$ sec. A DuMont 5 XP 11 cathode-ray tube was used, although the G.E.C. 1608 tube will give a similar performance. In the latter, post-deflection-acceleration to a total h.t. of 10 kV gives a relatively high deflectional sensitivity. The time base has durations of 0·1 to 10 μsec and triggers at $5–10 \times 10^{-9}$ sec after arrival of the trigger pulse. Moody and McLusky (*see* [58]) have described the time base and the output (Y plate) trigger circuits in detail; for these circuits distributed amplifiers are used.

The reduction in deflectional sensitivity at very high frequencies due to the finite transit time of the electrons through the deflector plates has been studied by Rudenberg[66] (*see also* the discussion on page 356) who suggests the use of parallel wire deflection systems, such as that shown in *Figure 339*. Here, the transit time and the input

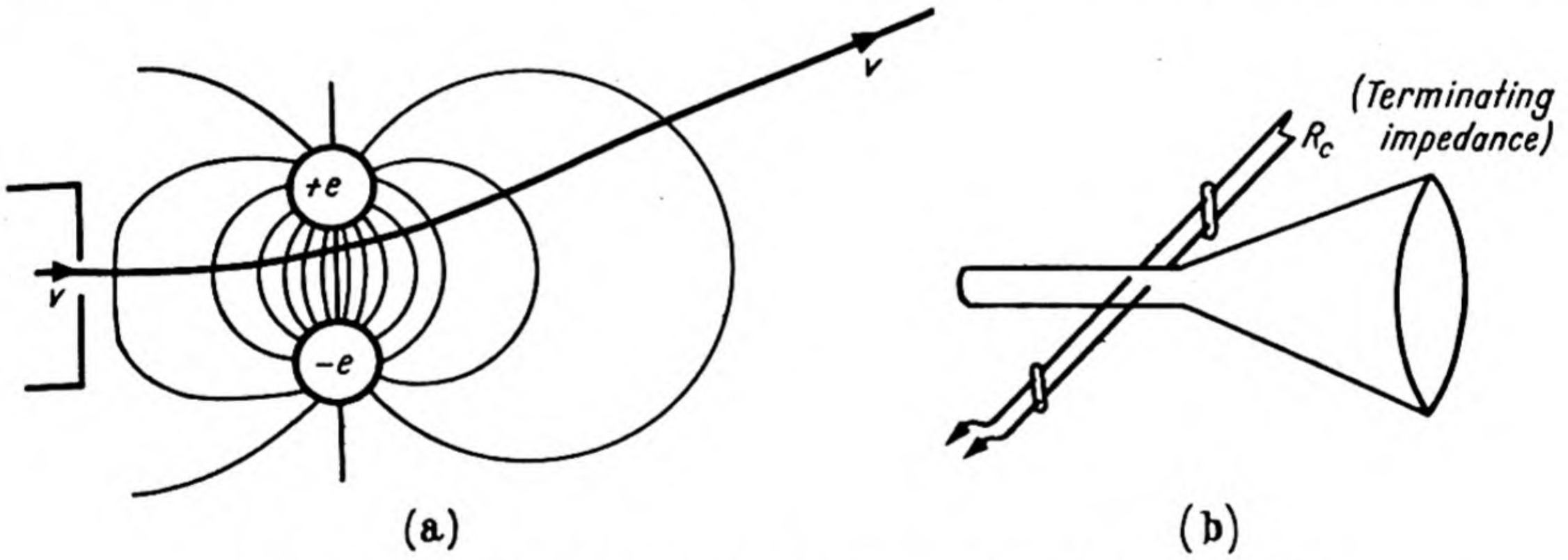

Figure 339. Parallel-wire deflection system (Rudenberg[66], by courtesy, *J. appl. Phys.*).

capacitance of the deflector system could be reduced below the value associated with normal deflector plates. Since the capacitance/unit length of a parallel wire line is

$$C = \pi K / \cosh^{-1}(d/2r)$$

where r = wire radius, d = wire spacing, centre to centre, K = permittivity of free space, then it can be shown (Rudenberg[66]) that the angle θ through which the beam is deflected, is given by

$$\theta = \frac{E}{2V} \frac{\pi}{\cosh^{-1}(d/2r)} \simeq \frac{E}{2V} \cdot \frac{\pi}{\ln (d/r)}$$

if d/r is large. Here E is the deflector plate voltage and V is the

voltage through which the electrons are accelerated. The significant part of the transit time is that required by the beam to pass through a distance approximately equal to the wire spacing. The corresponding formula for using a parallel plate deflector system without edge effects is

$$\theta = El/2Vd$$

where the plates have length l and separation d. Rudenberg[66] discusses the effects of fringing fields and the calculation of deflectional sensitivities at low frequencies in some detail.

The sensitivity of a parallel wire system (*Figure 339*) was compared by Rudenberg, with that of a conventional pair of deflector plates (*Figure 340*). For wires having a diameter of 3 mm. separated by

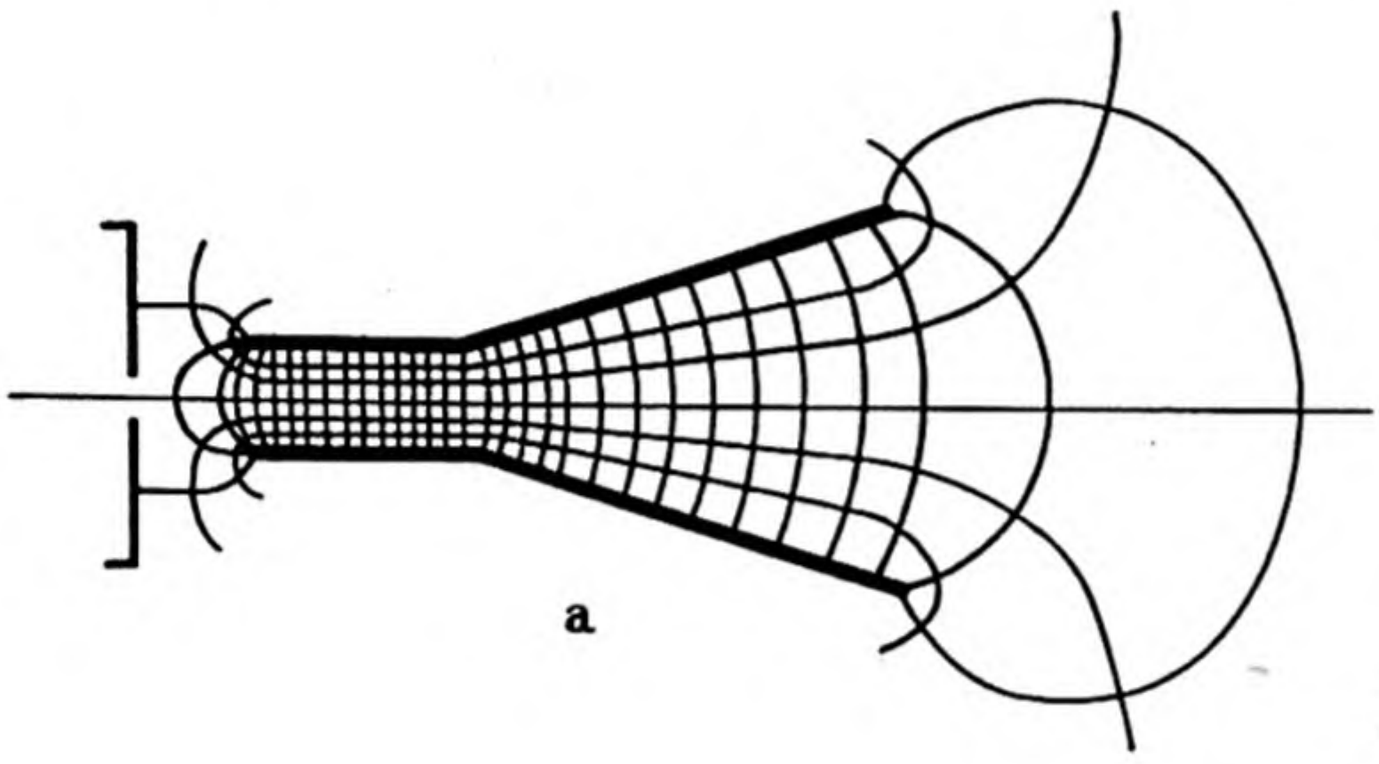

Figure 340. (a) Electrostatic field of deflection plates; (b) dimensions of the above plates in centimetres (Rudenberg[66], by courtesy, *J. appl. Phys.*).

3 mm., $d = 6$ mm. and $\cosh^{-1}(d/r) = 1{\cdot}32$. For $V = 1$ kV, a sensitivity at a screen distance of 250 mm. of 0·3 mm. kV/V should be obtained, whilst the comparable quantity for the system of *Figure 339* was 0·63 mm. kV/V.

The parallel wire system may be terminated with its characteristic impedance R_c and will thus behave as a resistance at all frequencies, where

$$R_c = 120 \cosh^{-1}(d/2r)\ \Omega$$

MACKAY[67] has also discussed transit time effects in cathode-ray oscillograph deflector systems and, independently, has used parallel wire deflector fields. Also, a new travelling wave system for deflection is briefly described (*Figure 341*) in which the deflecting signal operates

several times on the beam at intervals, set by the length of conductor between successive segments of the deflector plates, such that the beam and the signal maintain the correct phase relation. The main part of

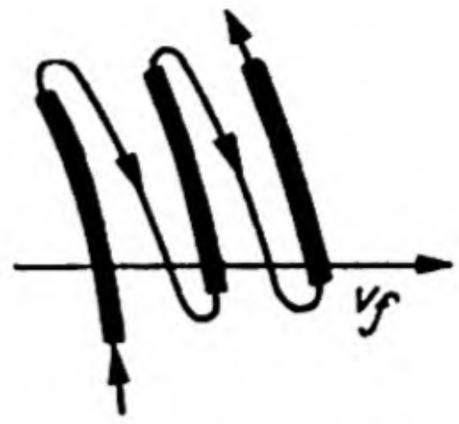

Figure 341. Illustrative of a system of deflection due to Mackay[67] (by courtesy, *Proc. Phys. Soc.*).

Mackay's paper, however, consists of a theoretical treatment of a new form of deflection system in which, say, the Y plates are shaped (*as* in *Figure 342*a) so that the electrons leaving the X plates (*Figure 342*b) at an appreciable angle to the axis $A'A$ and travelling along $B'B$, and

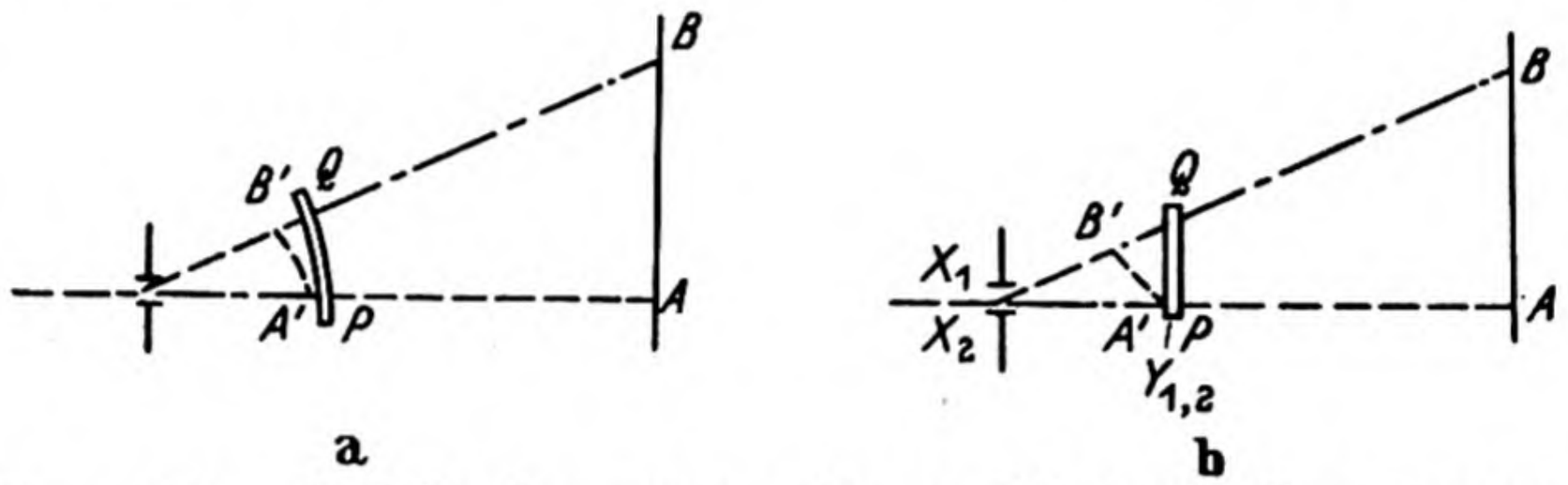

Figure 342. A deflection system due to Mackay[67] (by courtesy, *Proc. Phys. Soc.*).

which would normally arrive at the Y plates PQ later than the axial electrons, will now arrive at almost the same time as the latter at PQ. In this way, Mackay shows that an expanded time scale may be obtained. The original paper[67] should be consulted for further details.

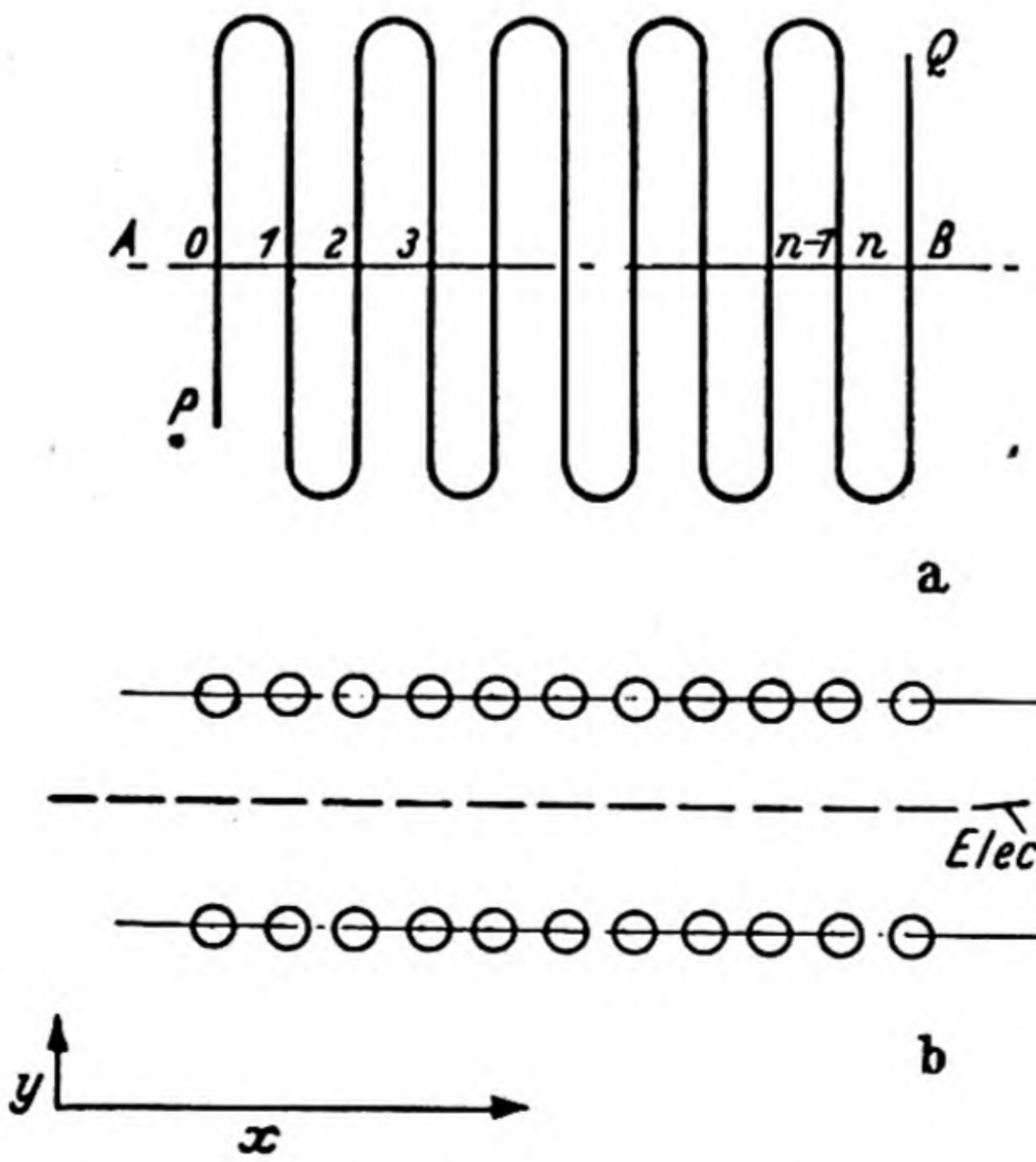

Figure 343. Diagrammatical illustration of a deflecting system. (a) View of the folded parallel transmission lines from above; (b) Side view (Owaki *et al.*[69], by courtesy, *Proc. Soc. Rad. Engrs.*).

The travelling wave deflector plate system, suggested by Mackay[67], and in a later publication by PIERCE[68], has also been used by OWAKI, TERAHATA, HADA and NAKAMURA[69]. These authors used travelling wave deflection on both X and Y axes with the arrangement shown in *Figure 343*. It is clear that an electron travelling along the axis will be subject to a constant accelerating force if the phase velocity (u) of the electro-magnetic wave along the axis (due to the passage of a wave along the wire PQ) is the same as the velocity (v_o) of the electron beam. A theoretical investigation of the deflection shows that when the wave along PQ, caused by the application thereto of a voltage wave, $V\ (x, t) = V_m \cos\ \omega\ (t - \frac{x}{u})$ is not reflected at Q, the beam deflection angle α is given by

$$\tan \alpha_1 = \frac{2\,ekV_m u}{mDv_o\omega} \frac{1}{(u - v_o)} \frac{\sin\ an\omega\ (u - v_o)}{2\,uv_o} \cos\left(wt - \frac{an\omega\ (u + v_o)}{2uv_o} \right)$$

and if $u = v_o$

then $$\tan \alpha_2 = \frac{ek\,V_m\,an}{m\,Dv^2{}_o} \cos\left(\omega t - \frac{an\omega}{v_o}\right)$$

so that the sensitivity varies little over a wide range of frequencies. In the above formula D is the distance between the parallel deflecting wires and k is the ratio of the electric field between the wires and that between

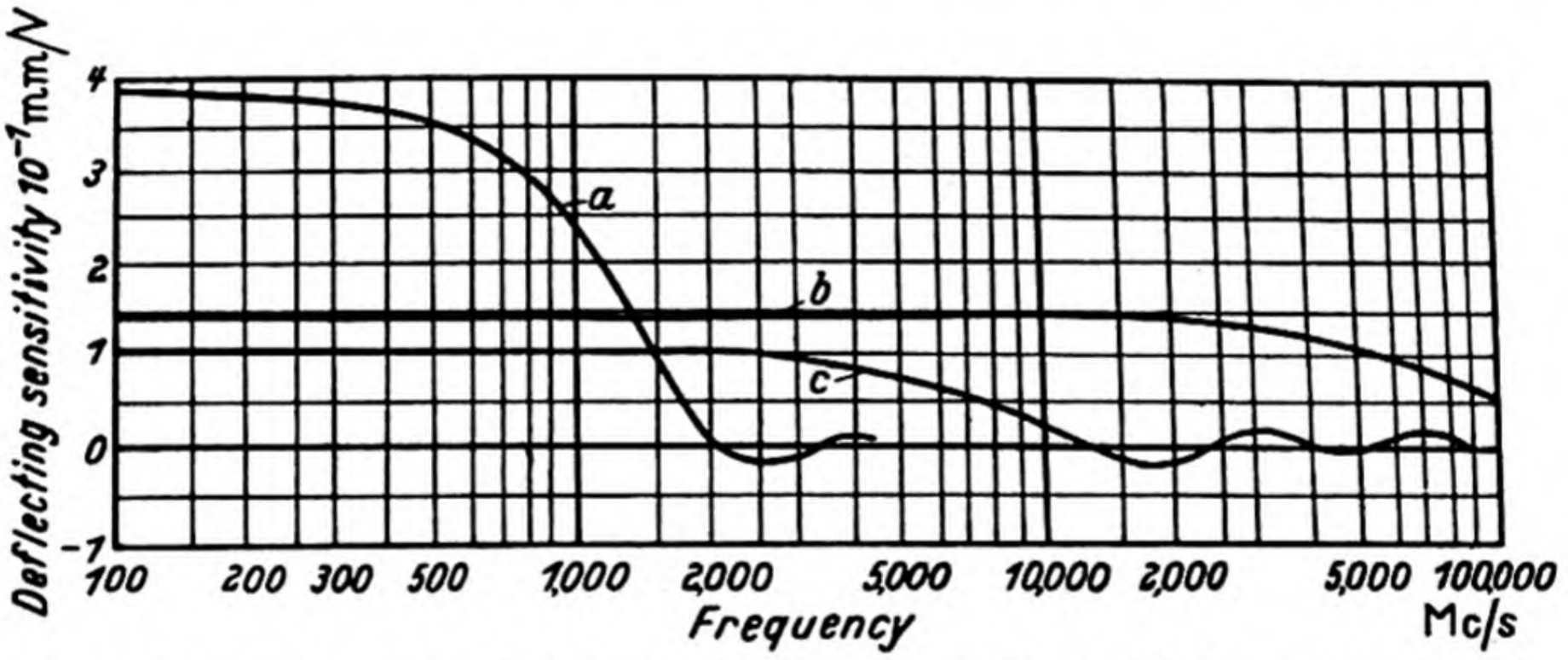

Figure 344. Relation between frequency and sensitivity of an oscillograph when electromagnetic wave and electron travel in same direction. (*a*) Accelerating voltage, 900 V; (*b*) 2,500 V; (*c*) 3,025 V. (Owaki *et al.*[69], by courtesy, *Proc. Inst. Rad. Engrs.*).

two parallel infinite plates with the same spacing, e and m are the electronic charge and mass and $an = (t - t_o)\ v_o$ if t_o is the time of departure of an electron from A in *Figure 343*.

When $u \gg v_o$ we have

$$\tan\ \alpha_3 = \frac{2\ ek\ V_m}{m\ D\omega v_o} \sin \frac{an\omega}{2\,v_o} \cos\left(\omega t - \frac{an\omega}{2\,v_o}\right)$$

which is the expression for the deflection in a normal oscillograph where the transit time effect is negligible.

The relation between frequency and sensitivity is shown in *Figure 344* for $u = 2{\cdot}93 \times 10^9$ cm./sec again when reflection does not

occur. *Figure 344 a* gives results for an accelerating voltage of 900 V so that $v_o = 1{\cdot}78 \times 10^9$ cm./sec. For *Figure 344 b*, $v_o = 2{\cdot}95 \times 10^9$ cm./sec so $v_o \simeq u$ and finally in *Figure 344 c*, where the voltage was 3,025 V, $v_o > u$ since v_o then was $3{\cdot}245 \times 10^9$ cm./sec.

It was not possible for Owaki and his collaborators to study the response of their oscillographs with recurrent or single sweep saw-tooth time sweeps, but they carried out experiments with Lissajous' figures.

GANSWINDT has reported on the recording of magnetron oscillations, with frequencies up to 10^9 c/sec, using a 20 kV cathode-ray oscillograph[70]. Writing speeds of ~ 50,000 Km/sec were attained.

Recent work on travelling wave deflector systems in cathode-ray tubes is described by SMITH, TALBOT and SMITH[71] who give references

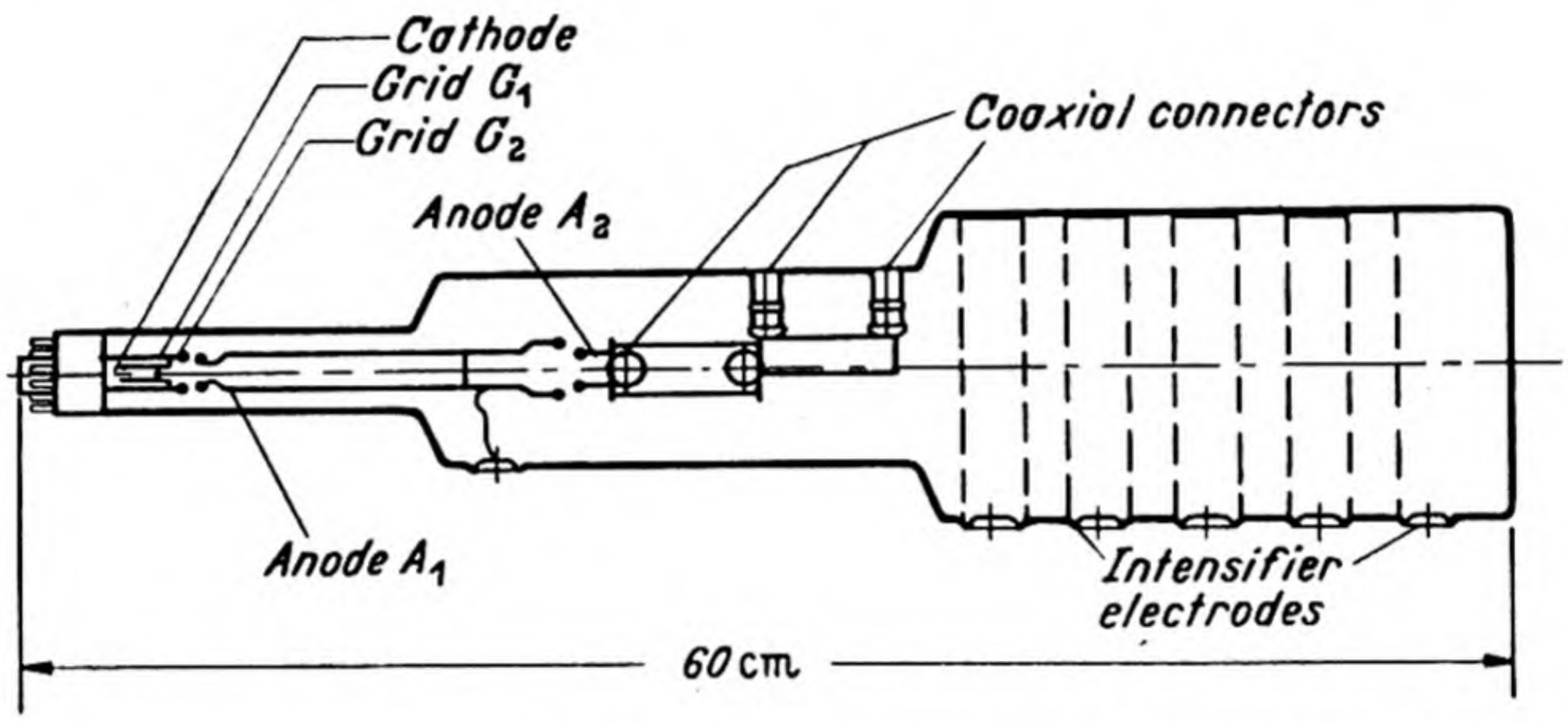

Figure 345. Diagram of a cathode-ray tube with a travelling wave deflector system (Smith *et al.*[71], by courtesy, *Proc. Inst. Rad. Engrs.*).

to earlier work in this field, such as that of Lee[62] which has been described above. The tube developed by Smith *et al.*[71] is shown in *Figure 345*. The beam passes through the deflectors at 10 kV and is then accelerated on its passage through the intensifier electrodes in which it reaches a final energy of about 35 kV. The deflector chambers contain helices, of such dimensions that the phase velocity of the signals along the axis of each helix (impedance 50 Ω) is equal to the beam velocity. The transit time through each helix is $1{\cdot}7 \times 10^{-10}$ sec. and so the reduction in sensitivity at 940 Mc/s is about 4 per cent. The remarkable performance of this tube is illustrated in *Figure 346* which shows a single pulse with a rise time of $0{\cdot}5 \times 10^{-9}$ sec and 5×10^{-9} sec in length. The calibration wave has a frequency of 1,000 Mc/s.

THE PHOTOGRAPHY OF CATHODE-RAY OSCILLOGRAPH SCREEN TRACES

The photography of high-speed single traces on the screens of sealed-off oscillographs has been the subject of much study since it is sometimes necessary to record traces where the brightness is little above that due to stray electrons striking the screen, or to light from the filament.

The Wray F.1 2-inch copying lens is often used in British oscillograph cameras and provides probably the greatest speed available at a reasonable cost. It is convenient to use with the G.E.C. 908 and 1608 oscillographs for recording on 35 mm. films, and is designed for a reduction ratio of 4 to 1. The Dallmeyer F. 1·5 lens is also very convenient for high-speed recording.

The techniques of photography provide many alternatives, and a special study of several of them has been made by Nethercot and his colleagues[72]. Although panchromatic emulsions do not usually give

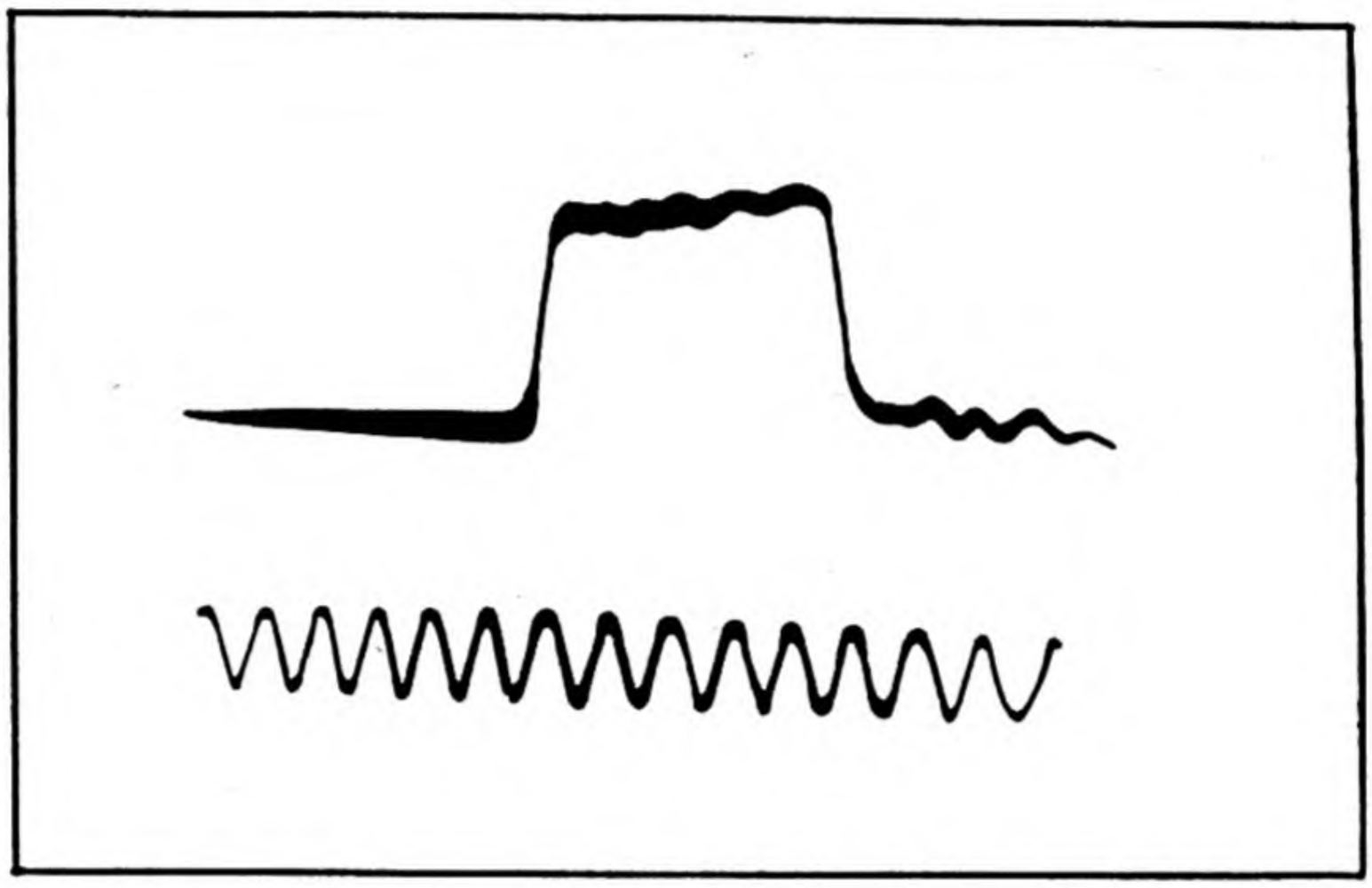

Figure 346. Upper trace shows photograph of a single pulse with $0{\cdot}5 \times 10^{-9}$ seconds rise time and 5×10^{-9} seconds duration taken with the oscillograph of *Figure 345*. Lower trace displays a single trace of 1,000 Mc/s sine wave on the same time base for calibrating purposes. Sine-wave amplitude, 0·18 cm, peak to peak. Pulse amplitude, 0·53 cm. Horizontal deflection, 2·3 cm (Smith *et al.*[71], by courtesy, *Proc. Inst. Rad. Engrs.*).

greater speeds for blue light than those obtainable with the orthochromatic emulsions, Ilford HP3 film may be used since it can be developed to give a very clear background, which is an advantage when intensification is required. Kodak O/Hα1 emulsion is another suitable panchromatic emulsion. Ilford ID2 developer is usually satisfactory with these emulsions. Various intensifiers are available and Nethercot[73] has used a quinone/thiosulphate solution[72] which was found superior to the more usual uranium intensifier. Hendry[74] gives full details for mercuric iodide and silver intensifiers, and Hercock[75] has also given relevant information.

Goldstein and Bales[52] have described in detail the measurement of writing speed of the 5CP11 cathode-ray oscillograph working at about 5·8 kV maximum third anode voltage. At this voltage the deflectional sensitivity was about 36 V/cm., and taking Feldt's definition[76] of the maximum writing speed, *i.e.* that speed at which the

density of the trace on the photographic film is 0·1 above the fog level, the data of *Table XXXI* for various American emulsions were obtained.

TABLE XXXI

Film	*Maximum writing speed cm./μsec*
Aero Tri X Pan	24
Recording Negative, Ortho	24
Super XX	23
Aero Tri X, Ortho	20
Recording Negative Fine Grain Ortho ..	8

The method used was as follows (*see also* [83]). A rectangular voltage pulse whose rise time was measured and found to be about 0·15 μsec., and whose amplitude could be varied without affecting the rise time, was applied to the Y plates of the oscillograph. Photographs were then taken, with a particular lens and emulsion, for various pulse heights, and the maximum writing speed was determined by examination of the leading edge of the pulse. Kodak D19 developer (8-12 mins. at 72°F.) was found to be the best medium for the film processing.

An Eastman-Kodak F 1·6 50 mm. lens was used to give the results of the table. Now putting the lens aperture as f, the maximum writing speed V is given, in terms of the maximum writing speed V_o with a lens aperture equivalent to F 1, and for unit magnification, by the relation $V = 4\,V_o/f^2\,(1 + m)^2$ where the magnification is M.

The paper by Goldstein and Bales[52] gives information on various high-speed cameras which may be used in oscillographic work.

An interesting symposium on photographic recording of cathode-ray tube traces was held in London in 1946 and the proceedings were published as four papers in the *Photographic Journal*. Hercock[77] discussed the general problems associated with screen colours and emulsion sensitivity, recording speeds, and the processing of various emulsions in different conditions. The relative speeds of various recording materials are given in *Table XXXII*.

TABLE XXXII

Development: 5 mins. in ID 33 (an active oscillograph developer) at 65°F.
Relative speeds in units of 1·5 km./sec at F/1 and a 1 : 1 reproduction with a 20μA, 20 kV beam:—

Emulsion	*Screen colour*		
	Blue	*Green*	*Yellow Green*
5R101	4	2	3
5G91	4	2	2
5B52	1	—	—
BP1	2	—	—

Relative speeds of various emulsions as a function of development time are also tabulated[77] and the data show that a fine grain developer such as ID11 will not give maximum speed even after prolonged development, whilst other developers will give maximum speed in much shorter times (4 mins.). . With certain emulsions rapid development, at high temperatures (80–100°F) is possible, for example in 5–20 secs.

HOPKINSON[78], in the same symposium, discussed the luminous efficiency of screens, the spectral distribution of the emitted light and the quantitative response of photographic emulsions to these radiations. Detailed tables of, for example, photographic performance of many emulsions with various screen phosphors are also given by Hopkinson. BERG[79] dealt with various aspects of photographic response, such as reciprocity failure. Finally Nethercot[80] gave results obtained with sealed-off oscillographs working at 5–10 kV. Hopkinson has also published similar accounts of cathode-ray tube screen response in the Proceedings of the I.E.E. Radiolocation Convention[81] where the properties of screen phosphors are discussed by GARLICK and his collaborators[82].

REFERENCES

1 WHITE, E. L., and NETHERCOT, W., *J. Inst. elect. Engrs.*, Pt. II, **96** (1949) 269.
2 ROHATS, N. *Gen. Elec. Rev.*, **39** (1936) 146.
3 WILKINSON, K. J. R. *B.T.H. Activities*, **12** (1936) 64.
4 SCOLES, G. J. *J. Sci. Instrum.*, **25** (1938) 201
5 WILKINSON, K. J. R. *J. Inst. elect. Engrs.*, **83** (1938) 663.
6 WHITE, E. L. *J. Sci. Instrum.*, **20** (1943) 125.
7 MCGILLEWIE, K. I. *J. Inst. elect. Engrs.*, **83** (1938) 657.
8 PRIME, H. A., and SAXE, R. F. *Proc. Inst. elect. Engrs.*, Pt. II, **96** (1949) 662.
9 WILLIAMS, F. C. *J. Inst. elect. Engrs.*, Pt. IIIa, **93** (1946) 1304.
10 HARDY, D. R. *J. Sci. Instrum.*, **29** (1952) 241.
11 PRIME, H. A., and RAVENHILL, P. *J. Sci. Instrum.*, **27** (1950) 192.
12 MURPHY, B. *Wireless Eng.*, **30** (1953) 39.
13 BAUER, R. E., and NETHERCOT, W. *E.R.A. Technical Report* U/T 115.
14 GAUNT, H. M., and CRAGGS, J. D. *Nature*, **167** (1951) 647.
15 FITCH, V. L., and TITTERTON, E. W. *Rev. Sci. Instrum.*, **18** (1947) 821.
16 DAVIS, N. L., and WHITE, R. E. *Electronics*, **23** (1950) 107.
17 HOOVER, W. G. *Trans. Amer. Inst. elect. Engrs.*, **65** (1946) 1086.
18 KUEHNI, H. P., and RAMO, S. *Trans. Amer. Inst. elect. Engrs.*, **54** (1935) 170.
19 BIGALKE, A. *Arch. Elektrotech.*, **33** (1939) 108.
20 MACGREGOR-MORRIS, J. T., and MINES, R. *J. elect. Engrs.*, **63** (1925) 1056.
21 ROGOWSKI, W., and FLEGLER, E. *Arch. Elektrotech.*, **14** (1925) 529.
22 ROGOWSKI. W., WOLFF, O., and KLEMPERER, H. *Arch. Elektrotech.*, **23** (1930) 667.
23 MACGREGOR-MORRIS, J. T., and HENLEY, J. A. *Cathode Ray Oscillography*. London, 1936.
24 VON ARDENNE, M. *Cathode Ray Tubes*. London, 1939.
25 MILLER, J. L., and ROBINSON, J. E. L. *Rep. Progress. Phys.*, **2** (1935) 259.
26 STEKOLNIKOV, I. S. *C.I.G.R.E. Paper* 129, 1937.

[27] BURCH, F. P., and WHELPTON, R. V. *J. Inst. elect. Engrs.*, **71** (1932) 380.
[28] WHELPTON, R. V. *J. Sci. Instrum.*, **12** (1935) 226.
[29] PERRY, F. R. *J. Inst. elect. Engrs.*, Pt. II, **88** (1941) 69.
[30] GÁBOR, D. *Forschungshefte der Studiengesellschaft für Höchstspannungsanlagen*, No. 1 (1927).
[31] HAINE, M. E., PAGE, R. S., and GARFITT, R. G. *J. appl. Phys.*, **21** (1950) 173.
[32] ROGOWSKI, W., FLEGLER, E., and TAMM, R. *Arch. Elektrotech.*, **18** (1927) 513.
[33] ROGOWSKI, W., and MALSCH, F. *Arch. Elektrotech*, **27** (1933) 131.
[34] MALSCH, F., and WESTERMANN, E. *Arch. Elektrotech*, **28** (1934) 63.
[35] MALSCH, F. *Arch. Elektrotech.*, **27** (1933) 642.
[36] BOEKELS, H. *Arch. Elektrotech.*, **25** (1931) 497.
[37] BINDER, L. *Elektrotech. Z.*, **52** (1932) 735.
[38] MESSNER, M. *Arch. Elektrotech.*, **27** (1933) 335.
[39] NUTTALL, A. K. *J. Inst. elect. Engrs.*, **78** (1936) 229.
[40] KNOLL, M. *Z. tech. Phys.*, **12** (1931) 54.
[41] DODDS, J. M. *Arch. Elektrotech.*, **27** (1933) 531.
[42] FOUST, C. M. *Gen. Elec. Rev.*, **34** (1931) 235.
[43] GÁBOR, D. *Arch. Elektrotech*, **18** (1927) 68.
[44] KNOLL, M., and FREUNDLICH, M. *Elektrotech. Z.*, **53** (1932) 669.
[45] ALLIBONE, T. E., HAWLEY, W. G., and PERRY, F. R. *J. Inst. elect. Engrs.*, **75** (1934) 670.
[46] ROGOWSKI, W., FLEGLER, E., and BUSS, K. *Arch. Elektrotech.*, **24** (1930) 563.
[47] KATZ, H., and WESTENDORF, E. *Z. tech. Phys.*, **22** (1941) 121.
[48] ROGOWSKI, W., and KLEMPERER, H. *Arch. Elektrotech.*, **24** (1930) 127.
[49] WADE, E. J., CARPENTER, T. J., and MACCARTHY, D. D. *Trans. Amer. Inst. elect. Engrs.*, **61** (1942) 549.
[50] ROGOWSKI, W. *Arch. Elektrotech.*, **24** (1930) 563.
[51] KUEHNI, H. P., and RAMO, S. *Elect. Eng.*, **56** (1937) 721.
[52] GOLDSTEIN, H., and BALES, P. D. *Rev. Sci. Instrum.*, **17** (1946) 89.
[53] PARK, J. H. *J. Res. Nat. Bur. Stds.*, **47** (1951) 87.
[54] KELLEY, G. G. *Rev. Sci. Instrum.*, **21** (1950) 71.
[55] GINZTON, E. L., HEWLETT, W. R., JASBERG, J. H., and NOE, J. D. *Proc. Inst. Rad. Engrs.*, **36** (1948) 956.
[56] BARTLETT, J. G., and DAVIES, G. T. *J. Inst. elect. Engrs.*, Pt. IIIA, **93** (1946) 1304.
[57] *Metropolitan-Vickers leaflet*, 652/5–1.
[58] MOODY, N. F. *Electronic Engng.*, **24** (1952) 287, 289.
[59] HOLLMANN, H. E. *Hochfreq. u. Elektroakust.*, **40** (1932) 97.
[60] KLEMPERER, H., and WOLFF, O. *Arch. Elektrotech.*, **26** (1932) 495.
[61] HOLLMANN, H. E. *Proc. Inst. Rad. Engrs.*, **38** (1950) 32.
[62] LEE, G. M. *Proc. Inst. Rad. Engrs.*, **34** (1946) 121.
[63] VON ARDENNE, M. *Hochfreq. u. Elektroakust.*, **54** (1939) 181.
[64] FLETCHER, R. C. *Rev. Sci. Instrum.*, **20** (1949) 861.
[65] HOLLMANN, H. E. *Proc. Inst. Rad. Engrs.*, **28** (1942) 213.
[66] RUDENBERG, H. G. *J. appl. phys.*, **16** (1945) 279.
[67] MACKAY, D. M. *Proc. Phys. Soc.*, **61** (1948) 235.
[68] PIERCE, J. R. *Electronics*, **22** (1949) 97.
[69] OWAKI, K., TERAHATA, S., HADA, T., and NAKAMURA, T. *Proc. Inst. Rad. Engrs.*, **38** (1950) 1172.
[70] GANSWINDT, H. *Hochfreq. u. Elektroakust.*, **57** (1941) 114.
[71] SMITH, S. T., TALBOT, R. V., and SMITH, C. H. *Proc. Inst. Rad. Engrs.*, **40** (1952) 297.
[72] NETHERCOT, W. *Photogr. J.* **86B** (1946) 159.
[73] NETHERCOT, W. *Elect. Times*, **110** (1946) 648; *Electronic Engng.*, **16** (1944) 369.

[74] HENDRY, N. *Electronic Engng.*, **16** (1944) 324.
[75] HERCOCK, R. J. *Ilford Tech. Monograph, No. 1.*
[76] FELDT, R. *Electronics*, **17** (1944) 130.
[77] HERCOCK, R. J. *Photogr. J.*, **86** B (1946) 138.
[78] HOPKINSON, R. G. *Photogr. J.*, **86** B (1946) 142.
[79] BERG, W. F. *Photogr. J.*, **86** B (1946) 154.
[80] NETHERCOT, W. *Photogr. J.*, **86** B (1946) 159.
[81] HOPKINSON, R. G. *J. Inst. elect. Engrs.*, Pt. IIIA, **93** (1946) 779, 795, 808.
[82] GARLICK, G. F. J., HENDERSON, S. T., and PULESTON, R. *J. Inst. elect. Engrs.*, Pt. IIIA, **93** (1946) 815.
[83] FOLKERTS, H. F., and RICHARDS, P. A. *R.C.A. Rev.*, **6** (1941) 234.
[84] MCQUEEN, J. G. *Electronic Engng.*, **24** (1952) 436.
[85] HERGENROTHER, R. C., and RUDENBERG, H. G. Professional groups on electron devices PGED-1. *Trans. Inst. Rad. Engrs.* Nov. 1952 p. 2.

11

MISCELLANEOUS HIGH-VOLTAGE APPARATUS

RESISTORS

A detailed study of wire-wound resistances for high-voltage (d.c.) measurement has been made by TAYLOR at the Bureau of Standards[1]. Units (1 MΩ, 1 W) were made of Ni–Cr wire, specially insulated, wound on 6 spool bobbins made either of Lavite impregnated with paraffin or Isolantite. The bobbin units were almost non-inductive since the wire was wound in reversed directions in alternate spools. The temperature coefficient of resistance was 0·0152 per cent. °C., but this high value was tolerated since manganin or constantan, which have lower coefficients, have low resistivities. The resistance of each unit was measured with a special high-voltage Wheatstone bridge, for operation at 2 kV d.c. with 1 : 1 ratio arms of 5,000 Ω and a variable resistance arm of 0 to 1,111,111 Ω variable in 1 Ω steps. An absolute accuracy of 0·01 per cent. in the resistance measurement was obtainable.

The complete resistance stack for 150 kV consisted of one hundred 1 MΩ resistors, thus carrying 1·5 mA maximum current, arranged in 20 sets of 5 units each (*Figure 347*). Each set was mounted, without oil,

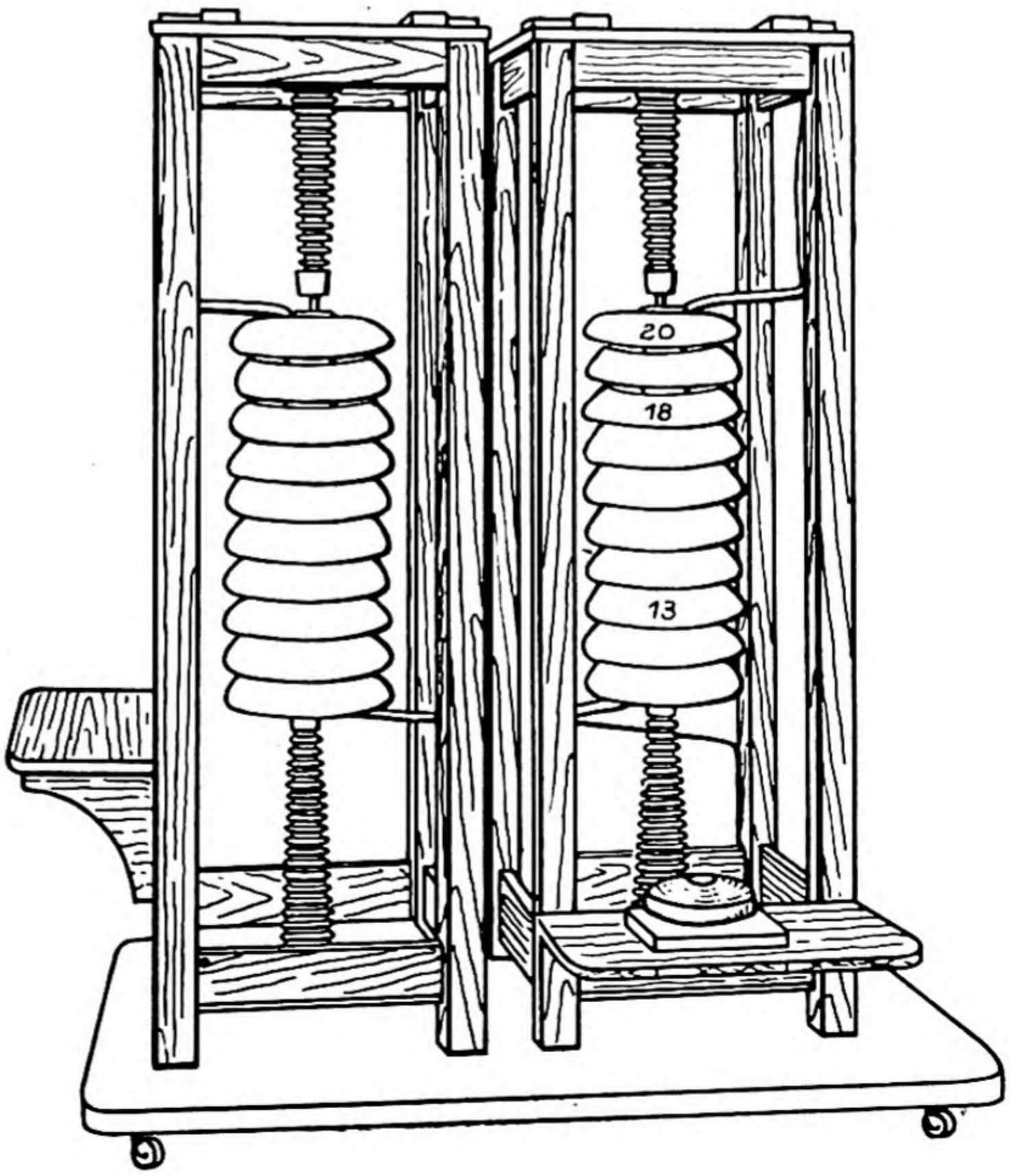

Figure 347. Assembled resistor of 50 MΩ per stack with a microammeter in a grounded circuit dividing the stacks (Taylor[1], by courtesy, *J. Res. Nat. Bur. Stand., Wash.*).

in a spun aluminium corona shield (*Figure 347*) with a hard rubber or Pyrex glass lid. A spring contact through the insulating lid joins each resistance set to the aluminium cover of the next set.

The variation in resistance due to heating is shown in detail in *Figure 348* where the voltage is increased in steps up to 1·3 kV/resistor

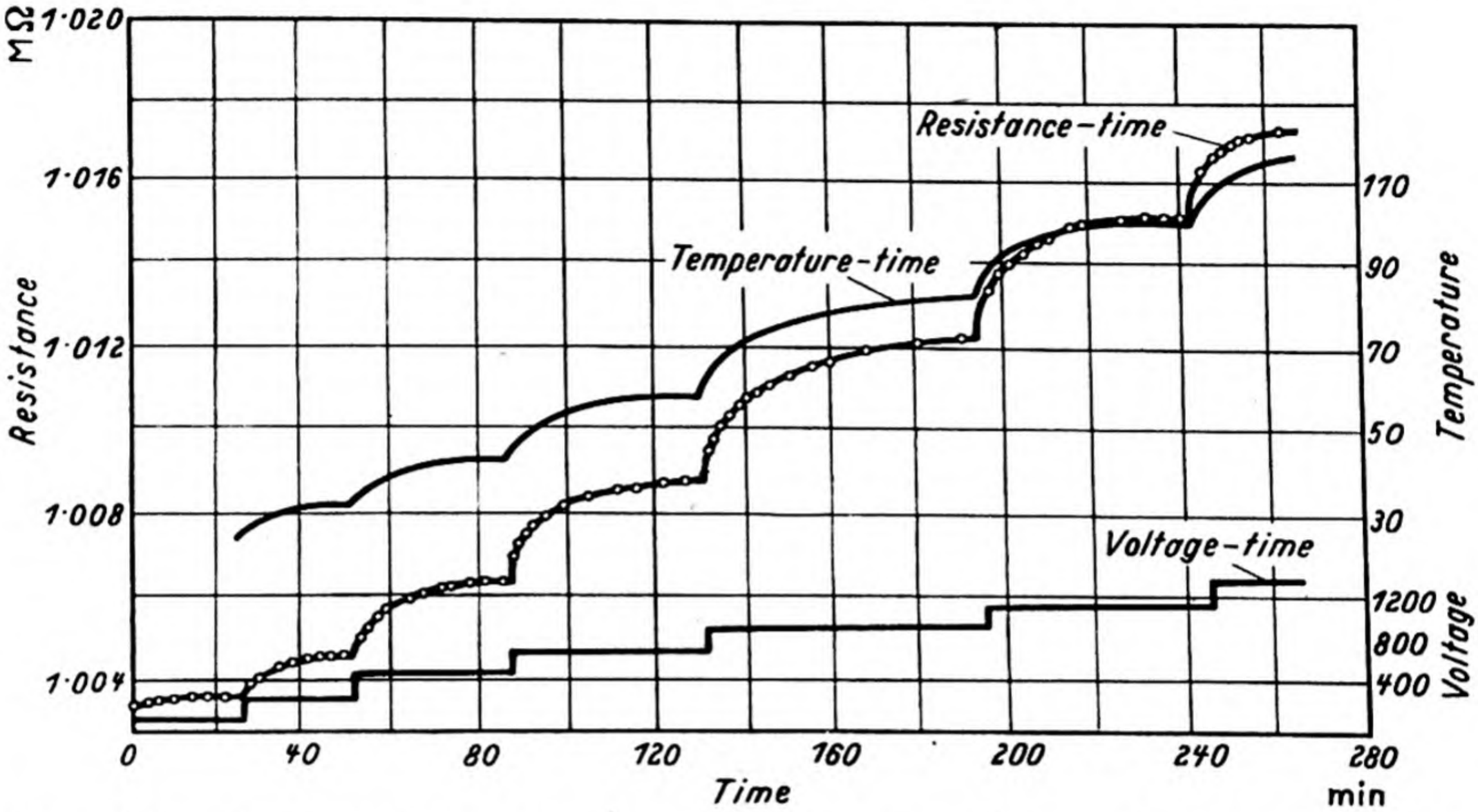

Figure 348. Resistance curves to show effect of heating of the resistors under operating conditions, *i.e.*, heated by the electric current (Taylor[1], by courtesy, *J. Res. Nat. Bur. Stand., Wash.*).

and the resistance and temperature changes during each period, *i.e.*, at any of the test voltages, are plotted. *Figure 349* shows the temperature coefficient for one resistor, heated externally. TAYLOR also gives a curve showing the correction to be made to the resistance value, for 20 minutes operation at any current up to about 1·3 mA when this correction amounts to about 1·5 per cent.

The resistance stack was used at h.t. either by simply measuring the current through it or by connecting an electrometer across the last 1 MΩ resistor, *i.e.* that at the grounded end of the stack. The accuracy of this measurement was limited to that of the electrometer, *i.e.* about 0·1 per cent., but the measurement of current, together with the necessary correction for temperature changes enabled Taylor to claim an accuracy of 0·01 per cent.

Despite the careful design of the corona shields and the limitation of the potential difference between any resistor and its surrounding shield to only 7·5 kV, it would appear from the paper that no tests were made, such as those described by HAFSTAD *et al.*[10] (*see* page 377), for corona at h.t. with the full stack. It is not sufficient, for example, to test each resistor for corona at its rated voltage and then to assume that no corona will be found even at the h.t. end of the resistance assembly.

However, Taylor's corona shields should have been sufficient to suppress corona at 150 kV.

SHALLCROSS[2] has considered in detail the design of electrodes for high-resistance h.t. voltmeters. Earlier relevant work, with special reference to the use of high-resistance voltmeters for high a.c. voltages is described by DAVIS[3].

DEFANDORF[4] states that Taylor has more recently improved these resistors and has used them in the Bureau of Standards 1·4 MV d.c.

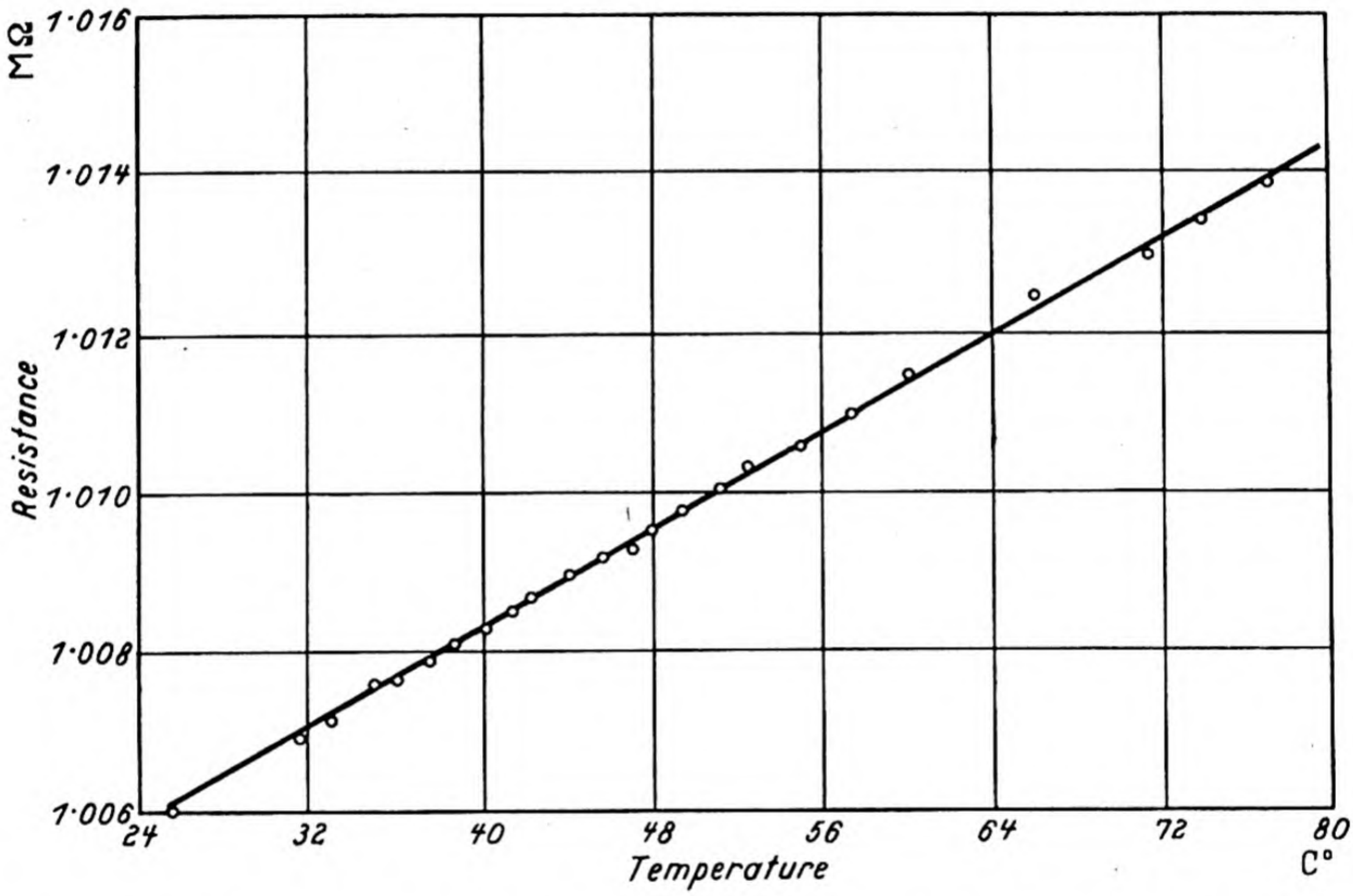

Figure 349. Curve for obtaining temperature coefficient of a single resistor when heated in an oil bath (Taylor[1], by courtesy, *J. Res. Nat. Bur. Stand., Wash.*).

X-ray generator (*see* pages 18, 19). The resistor chain in the latter installation is housed, with its own corona shields, inside another shielding tube, the corona from which does not pass through the measuring chain which is thus virtually provided with a guard electrode system. Manganin resistors, operated at 1 mA, were used because wire-bound resistors tend to be more stable than those of the carbon type, and an accuracy of measurement of 0·1 per cent. or better was possible.

Davis has discussed in detail the theory[3] and construction[5] of a shielded 1·2 MΩ resistor using 0·0076 in. diameter constantan wire for a.c. work at voltages up to 60 kV. In these papers the voltage distribution and divider ratios are calculated in terms of the stray capacitances and all the measurements were made with the greatest care. The accuracy of measurement of the resistance and the error due to

its phase angle were respectively 5×10^{-4} and 2×10^{-4}. An early paper dealing with the measurement of the inductances of resistance coils, of low or high resistance, is that by GROVER and CURTIS[6].

The construction, over several years, of a successful resistance-type substandard d.c. voltmeter for 300 kV has been described by WATERTON[7]. The current through the oil-immersed resistance (about 160 MΩ) is read on an accurate milliammeter. The overall accuracy of

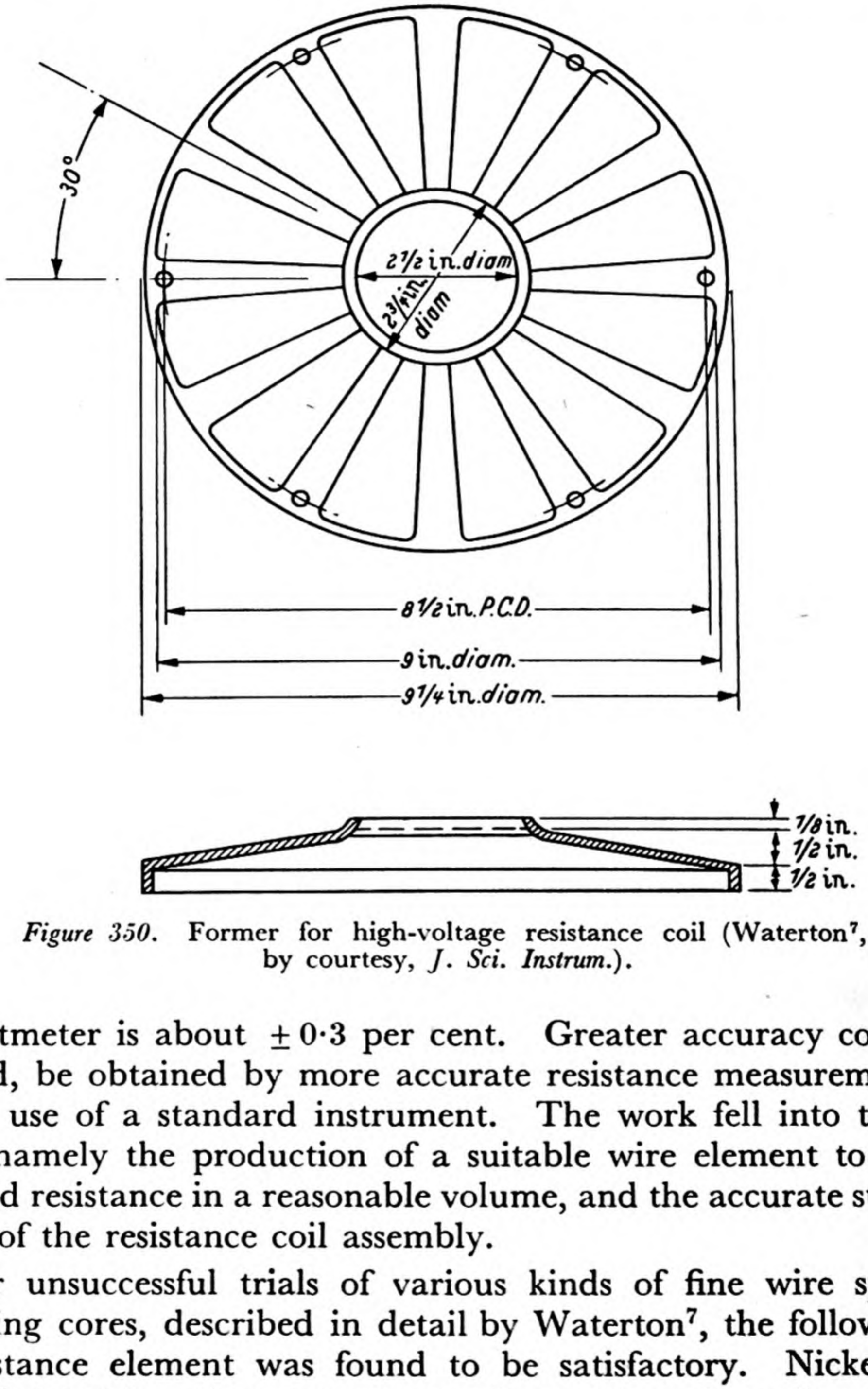

Figure 350. Former for high-voltage resistance coil (Waterton[7], by courtesy, *J. Sci. Instrum.*).

the voltmeter is about ±0·3 per cent. Greater accuracy could, it is claimed, be obtained by more accurate resistance measurements and by the use of a standard instrument. The work fell into two main parts, namely the production of a suitable wire element to give the required resistance in a reasonable volume, and the accurate standardization of the resistance coil assembly.

After unsuccessful trials of various kinds of fine wire spirals on insulating cores, described in detail by Waterton[7], the following type of resistance element was found to be satisfactory. Nickel-chrome wire of 0·002 in. diameter was used, as wire of smaller diameter, *e.g.* 0·0008 in., had proved to be too fragile, and was wound on a

pressboard strip 0·07 in. × 0·01 in. with turns touching. This strip is then wrapped on a second pressboard strip 0·25 in. × 0·017 in. with a spacing between turns of 0·02 in., thus giving a spiral of 10–11 turns per inch. The resistance per yard is about 0·18 MΩ. With a current of 2 mA the voltage between turns of wire on the 0·07 × 0·01 in. strip is ~0·003 V, and between successive turns on the larger strip is 0·91 V. For a complete coil wound on the former shown in *Figure 350* the voltage between turns was 230 V and two sets each of 24 coils formed the complete resistance. (A typical resistance is shown in *Figure 351*.)

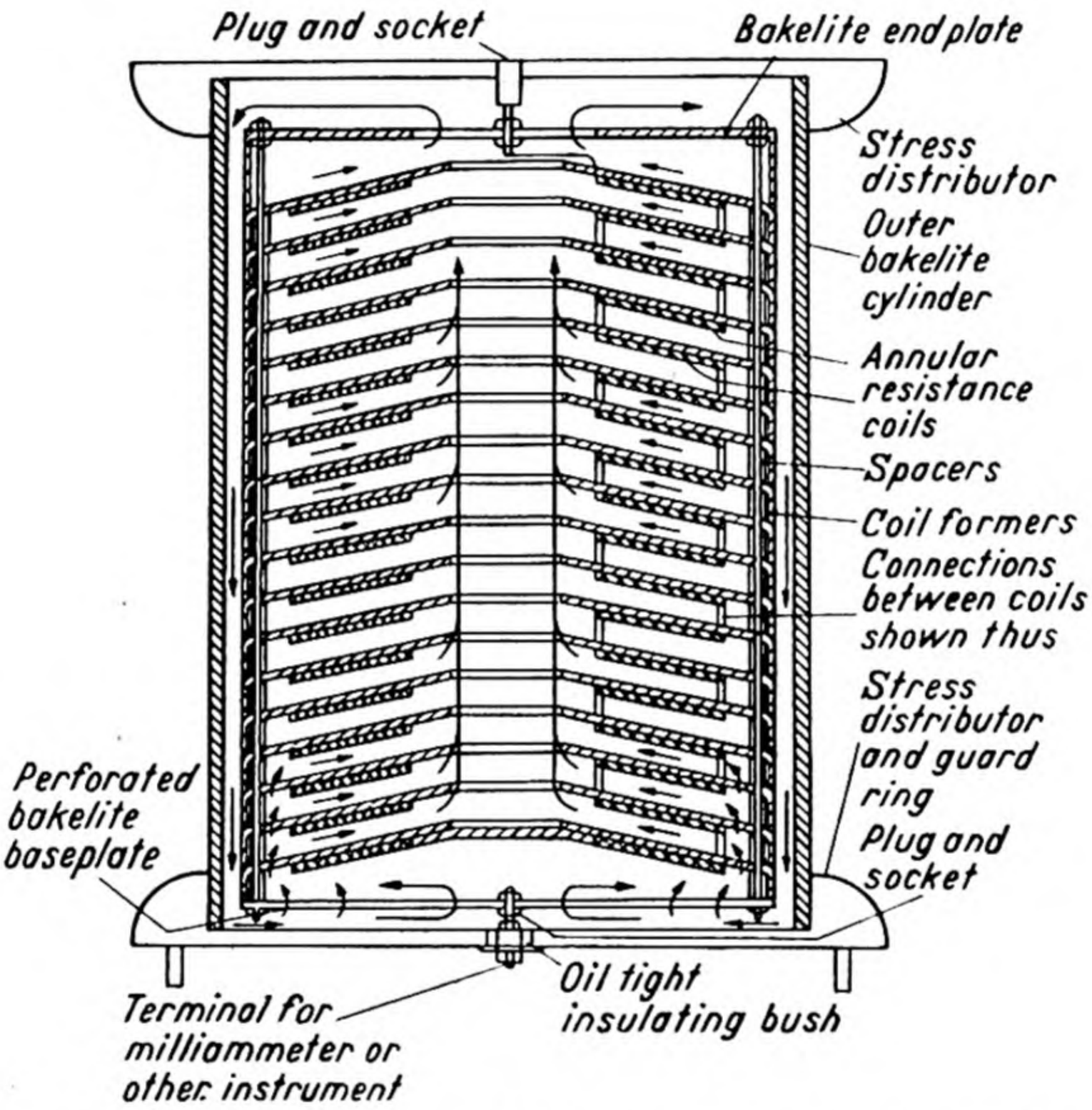

Figure 351. Section through high-voltage resistance, showing oil baffles. The arrows indicate direction of the convective oil flow (Waterton[7], by courtesy, *J. Sci. Instrum.*).

The oxide coating of the wire was sufficient to provide interturn insulation even with the turns touching. The voltage between layers, *i.e.* between the coils of *Figure 351*, which is ~6 kV, did not cause break-down through the wrapping (0·003 in. Kraft paper, $\frac{1}{4}$ in. wide) put on each spirallized spiral of the wire by means of a special wrapping machine. The coil resistance stability was within 0·1 per cent. over long periods.

At 125 kV each unit dissipated 200 W and the container temperature rose 25 °C., corresponding to an oil temperature increase of 40 °C. The oil circulation system is shown in *Figure 351*; the shape of the coil formers shown in *Figure 350* assists in maintaining a steady flow of oil.

The final unit for 150 kV was assembled in a container 18 in. high $\times 10\frac{1}{2}$ in. diameter. The leakage resistance through the oil and the container was $3 \times 10^{12}\ \Omega$ which had a negligible effect on the total resistance of the coils.

The technique of measuring the coil resistance is of interest and involved the use of a Wheatstone bridge with a 120 V supply. This was found to be necessary since the 2 V supply normally used with such a bridge was inadequate to break down the oxide film insulation on the numerous wire joints, *etc.*, in the resistance stack. The bridge ratio was 1,000 : 1 and $10^8\ \Omega$ could be measured in terms of a standard resistance of 100 kΩ adjustable in 1 Ω steps. All the larger resistances used on the bridge were standardized to an accuracy of 1 part in 10^4 and the resistances of the individual coils could be measured to less than 1 part in 10^4. For a stack of 24 coils the maximum total error would be 0·24 per cent. but the stacks were measured as complete units also and were found to have a total resistance equal to that of all the separate coils in them to within < 0·1 per cent. so the final error was assumed to be of this value also. The meter accuracy was less than this, and as mentioned above, the final overall accuracy was about ±0·3 per cent. The temperature coefficient of the nickel-chrome wire was $9{\cdot}8 \times 10^{-5}$/°C. between 20 °C. and 500 °C. and, if necessary, allowance for this must be made. The correction for operation during the first 8 hours, assuming continuous excitation, varies between 0 and 0·4 per cent. depending on the rate of change of temperature. When in use as a standard instrument the units normally pass current for periods of a few minutes and at room temperature, so that the correction for temperature rise is unnecessary.

HANSON's resistance unit[8] for measuring 40 kV d.c. consists of two sets of twenty 1 MΩ Shallcross wire-wound resistors, arranged in a container through which the air is circulated by a fan to equalize the temperatures in the different parts of it. Oil immersion would probably have been more satisfactory in that corona would have been reduced and might have rendered unnecessary the corona shields, shown in *Figure 352*. The Textolite containing-tubes are 7 in. in diameter and 20 in. high. The resistance assembly takes a current of about 1 mA at 40 kV and the heating so caused is sufficient to cause about 1·5 per cent. change in resistance. This effect is eliminated by inserting in the stack of resistors another unit of value about 715 Ω, composed of the same wire and subject to the same temperature changes as the main unit, across which a measuring potentiometer is tapped.

A precision 50 MΩ wire-wound resistance, suitable for work at voltages varying up to 1 MV, has been described by BINDER and HÖRCHER[9].

Hafstad, Heydenburg and Tuve[10] considered that the use of wire-wound resistances was impracticable at 1,000 kV, because of expense and the difficulty of ensuring freedom from corona; Waterton's work[7] (*see* page 374) was not available at the time of the above publication. Hafstad *et al.* therefore proceeded to develop resistance units containing metallized grid-leak resistors, 10 MΩ each and with a current rating of 1 watt. A 10,000 MΩ resistor was made in 50 units each containing 20 resistors connected in series, pushed into rubber tubing and soldered to brass end discs 12 in. diameter which were insulated from each other

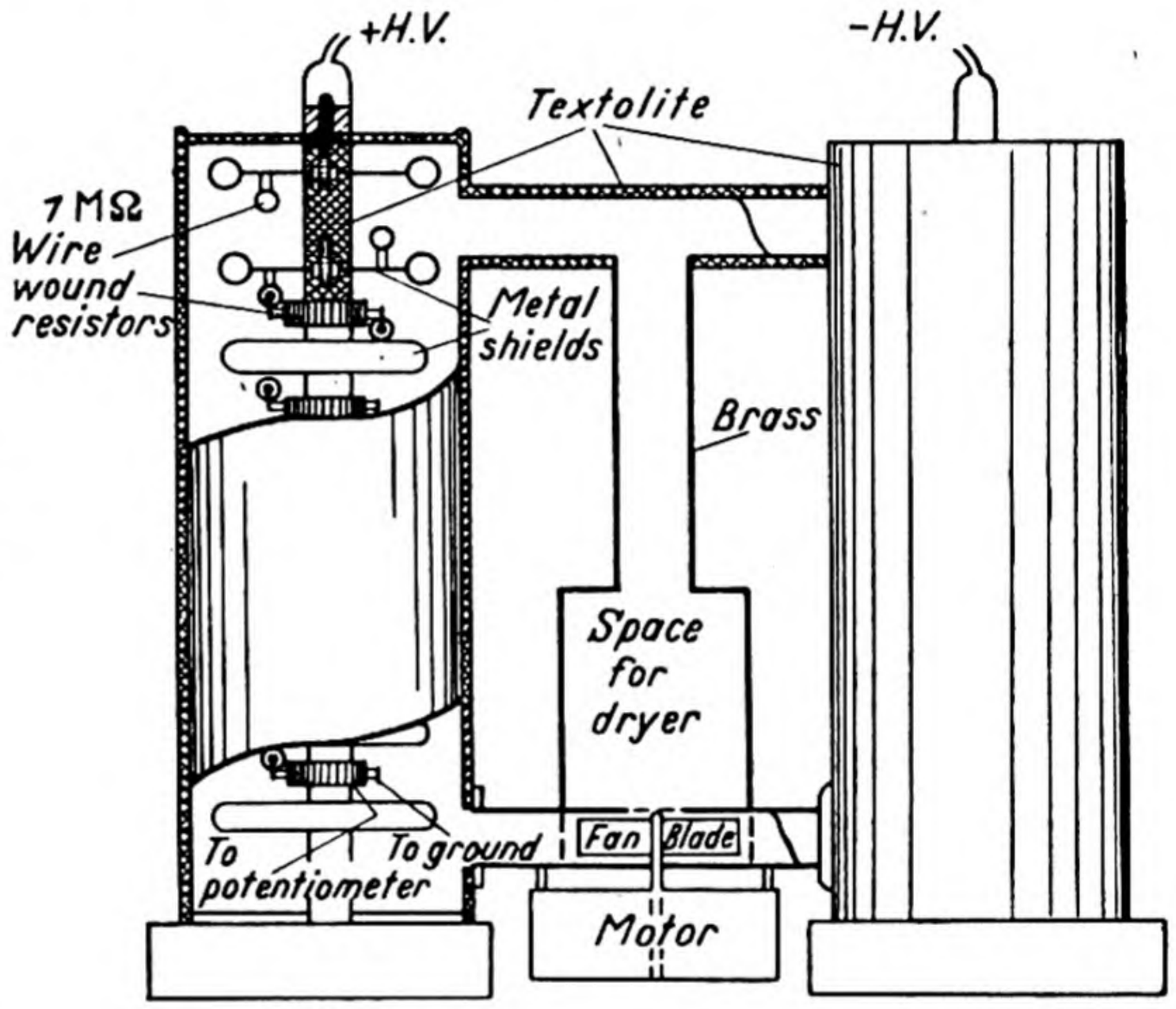

Figure 352. Assembly of a high-voltage air-cooled resistor unit (Hanson[8], by courtesy, *Rev. Sci. Instrum.*).

by Isolantite rods. The brass discs had their edges covered by 3/4 in. copper tubing, to prevent corona discharges. The resistance withstood a voltage gradient of 10 kV/in. without corona; the deposition of dust was prevented by enclosing the stack of 50 units in a Textolite cylinder.

The units were checked in 100 kV sections against standard resistances at the National Bureau of Standards and the measurements were consistent to about 2 per cent. Possible corona effects, which would vitiate the accurate measurement of voltage well above 100 kV with several 100 kV units in series, were eliminated in several ways. Thus, CCl_4 vapour was introduced into the resistance container and was found to have no effect, which would not have been so if corona currents had been appreciable. The linearity of the resistance was checked by observations of the deflection of mass 1 and mass 2 positive ions in the accelerator tube and analyser and, finally, it was found that a 40 per cent. over-voltage on the stack was required before corona was detectable.

A similar resistance unit is described in less detail by ROBERTS[11] who used two hundred 10 MΩ 1 W (*i.e.* about 0·3 mA) resistors wrapped in

a spiral round glass rods supported by a Textolite cylinder. The change in resistance due to heating was found to be negligible up to 250 kV. *i.e.* up to about 0·1 mA, and an accuracy of better than 2 per cent. was claimed for the voltage measurement.

Carbon resistors should be used at currents low compared with their rated values so that heating effects are small but it is often necessary to use currents comparable to the rated maxima in order, for example, to reduce the size of the resistance unit. In this case heating effects cannot be ignored. Data for these conditions have been accumulated by many workers. The following data obtained by CRAGGS (unpublished) refers to two units that were built for 75 and 50 kV. The larger unit was 15 in. long. It was necessary to use robust measuring instruments and 1 mA was chosen as a suitable maximum current. Morganite resistors rated 1 W (50 kV) or 2 W (75 kV) 1 MΩ were used arranged in spirals with 50 and 75 resistors respectively. Preliminary tests showed that a 1 MΩ 1 W Morganite resistor running at 1 mA and at

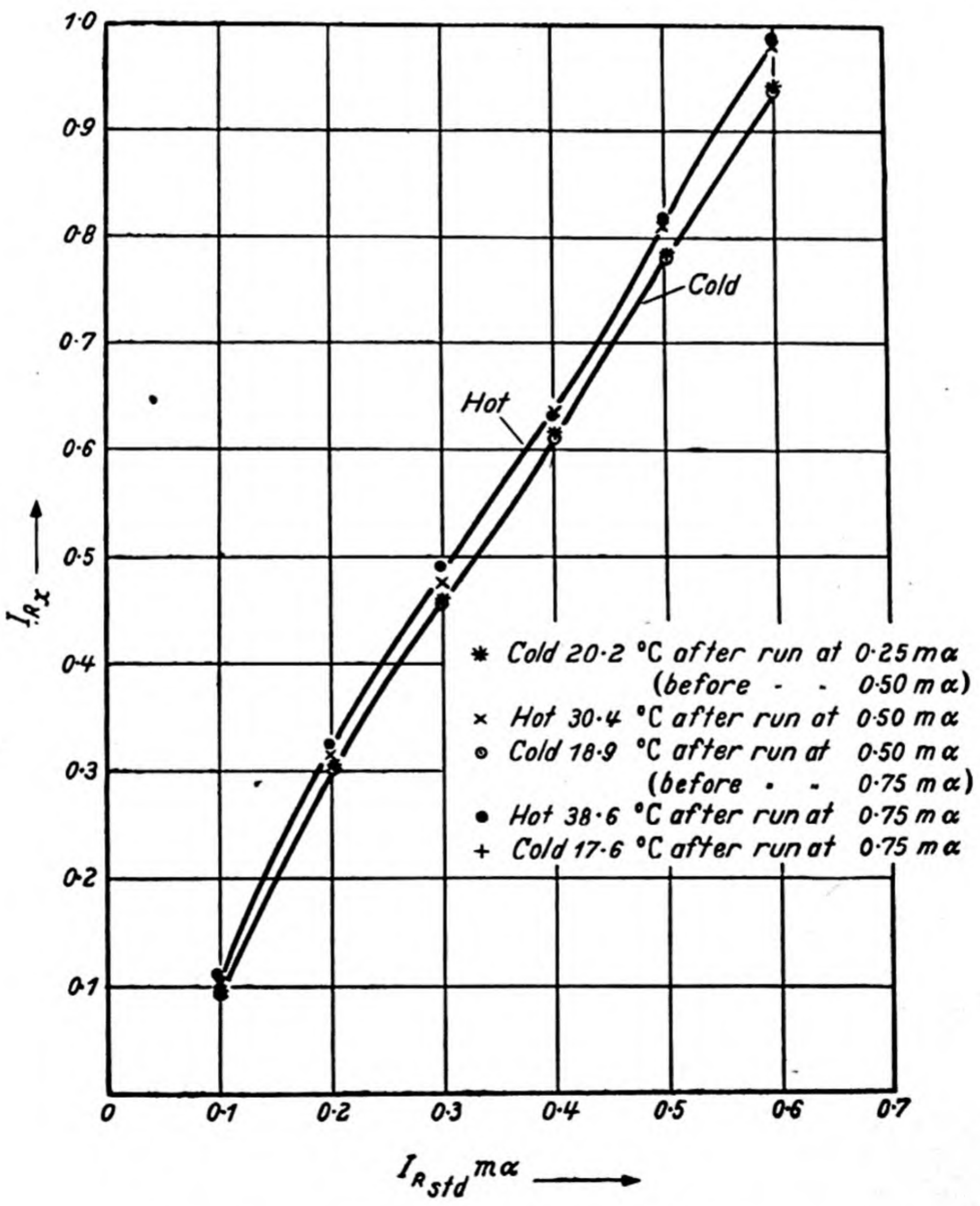

Figure 353. **Calibrations of a 50 MΩ resistance.**

0·55 mA d.c. respectively showed a reduction of 11 per cent. and 7 per cent. in resistance, but in a *large* quantity of oil the change was only about 1 per cent.

The complete 50 kV resistor, at 0·75 mA, changed by about 7 per cent. but returned to its initial value on cooling. The linearity of the current/voltage relation was satisfactory, as shown in *Figure 353*, where $I_{std.}$ is the current through a 78·6 MΩ standard resistance of the wire-wound type (*see* page 374) connected in parallel with the Morganite resistor. The variation of oil temperature and of resistance with time for the 50 kV unit are shown in *Figures 354* a and b. The

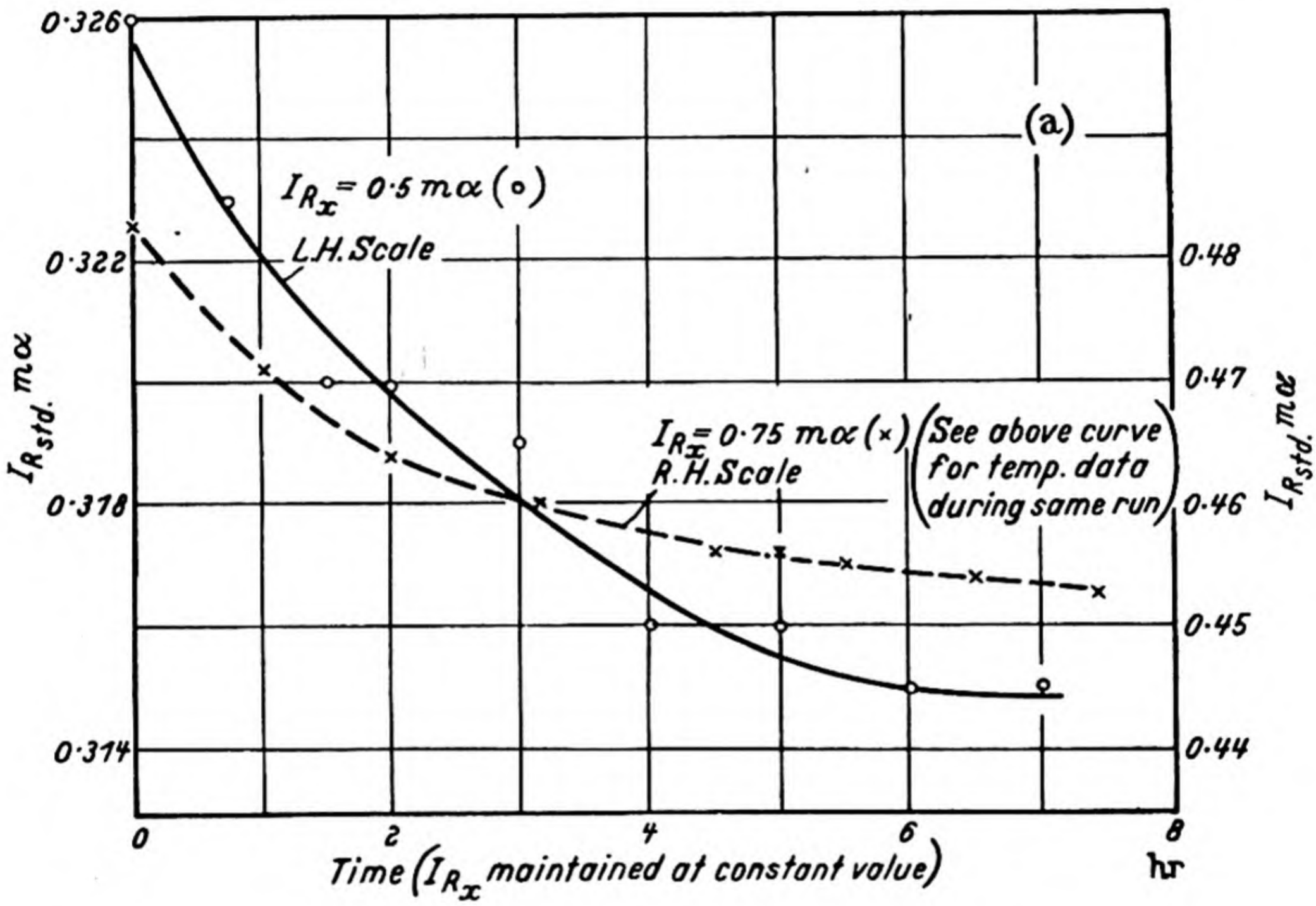

Figure 354. Performance of a 50 MΩ resistance.

variation in the resistance of this unit over 2 months was $< 0{\cdot}5$ per cent. Other data taken with the 75 kV unit, with 2 W 1 MΩ resistors, are given in *Table XXXIII*.

TABLE XXXIII

Current mA	*Temperature rise °C.*	*% change (negative) in resistance*
0·25	2·7	< 0·5
0·5	10·2	2·3
0·75	20·3	6·4
1	29	10

Several runs were necessary at 1 mA to stabilize the resistor. The linearity and constancy of resistance at a given temperature were the same as with the 50 MΩ resistor.

The 10 per cent. change at 1 mA is too high even for most technical work and may be reduced either by thermostatic control or by use of the simple circuit shown in *Figure 355*. Here R_1 is the oil-immersed

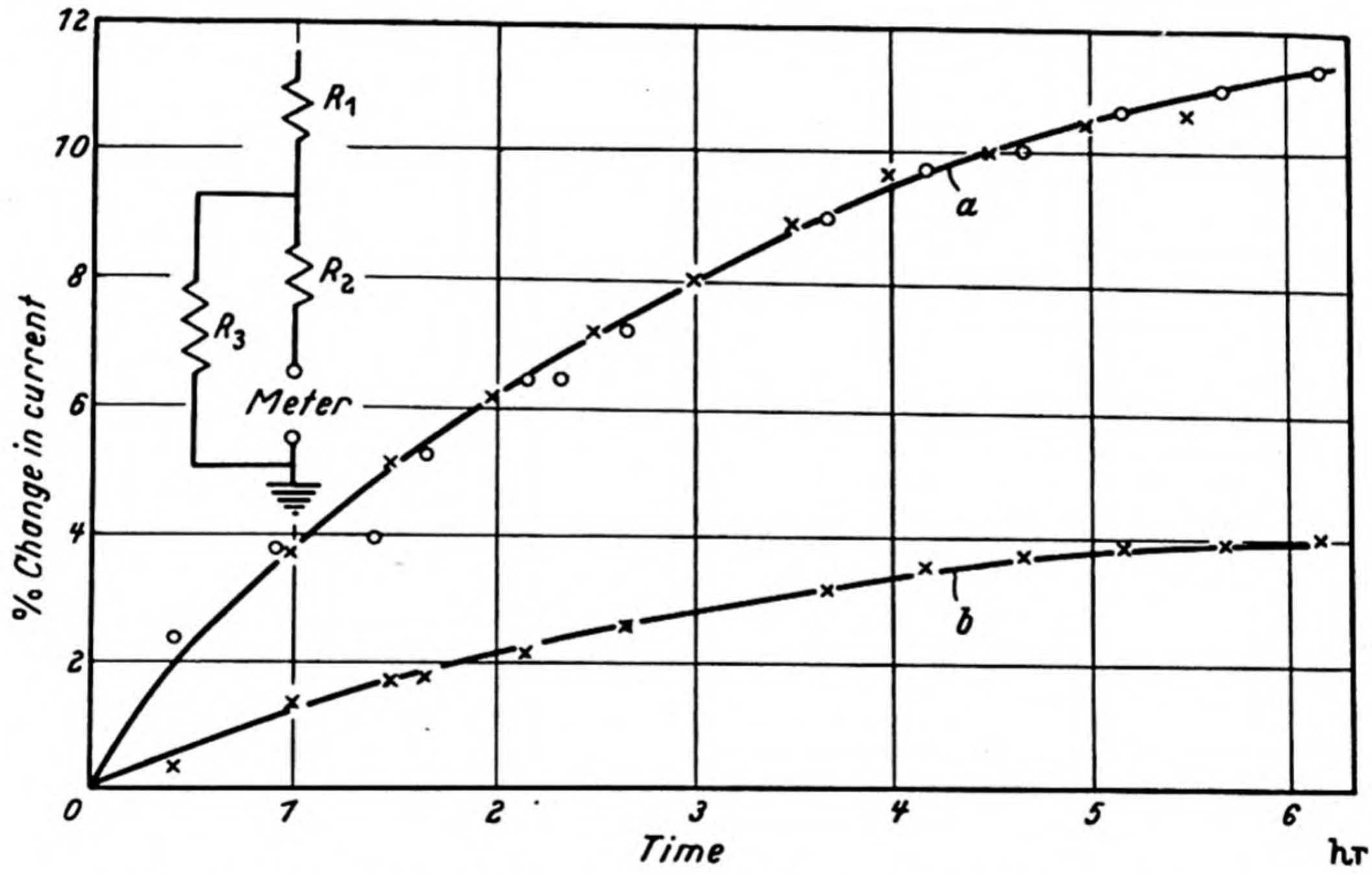

Figure 355. Use of compensating coil in a 70 MΩ resistance.

Morganite resistance and R_2 is a metallic resistance with a high positive temperature coefficient immersed in the same oil. R_3 is a stable resistance of Eureka whose value is independent of the current passed through it and which has a negligible temperature change of resistance. If (R_2 + the meter resistance) = R_3, and a change of R_1 of -10 per cent. is to be compensated, then a positive change of 20 per cent. in R_2 is required for a temperature rise of say 30°.

The relevant constants for the most useful metals of which R_2 may be composed are given in *Table XXXIV*.

TABLE XXXIV

Metal	*Specific resistance at about 20°C. Ω/cm.*[3]	*Temperature coefficient of resistance at about 20°C.*	*% change in resistance for 30°C. rise in temperature*
Drawn copper	$1{\cdot}8\times10^{-6}$	43×10^{-4}	13
97% nickel	12×10^{-6}	62×10^{-4}	19
Pure iron	12×10^{-6}	62×10^{-4}	19
Tungsten	5×10^{-6}	51×10^{-4}	15

The measuring instrument should have a resistance low compared with the metallic coil R_2 in order to avoid swamping the resistance change of the latter, and it is also advantageous to have $R_2 \gg R_3$. The experiments made with this shunt were carried out during the war in conditions where copper was the only metal, of *Table XXXIV*, easily obtainable. The meter resistance was 40 Ω, and R_2 was 1,000 Ω so that $R_3 = 1{,}040\,\Omega$ for equal current division between the two arms of the network. R_2 was wound with 0·0012 in. diameter copper wire. The compensation obtained with the shunt arrangement is shown in *Figure 355* from which it can be seen that a change of −10 per cent. in the resistance was reduced to about −4 per cent. Better compensation could easily be obtained.

Waterton[12] has also described voltmeters of about $1\frac{1}{2}$ per cent. accuracy, for use up to 500 kV, consisting of chains of composition resistors tapped as a potential divider and with an electrostatic voltmeter, or high resistance and microammeter, connected between the tap and earth (*Figure 356*). Waterton found differences in the characteristics of similar resistors made by different manufacturers, or of different resistance values at the same voltage and by the same manufacturer. It is necessary, therefore, to use units of a single make and of the same nominal resistance. Temperature coefficients of standard 5 MΩ 1 W units range up to −0·6 per cent./°C. between 10° and 30 °C. and voltage coefficients up to −0·012 per cent./V for a maximum of 1,000 V across each 1 W unit. More expensive resistors with improved characteristics are now available. The units are clamped between two Bakelite cylinders in a vertical zigzag arrangement (*Figure 356* c) and the bank of resistors is then mounted in an oil-filled Bakelite cylinder with the upper (h.t.) end connected to a smooth metal cap on the cylinder (*Figure 356* c). For 100 kV and 500 kV the containers, both of $6\frac{3}{4}$ in. diameter, are respectively 22 in. and 84 in. high. *Figure 356* shows the circuit arrangements. In *Figure 356* the calibration may be set by altering the number of units in the h.t. part of the stack. The microammeter connection of *Figure 356* b is more accurate;

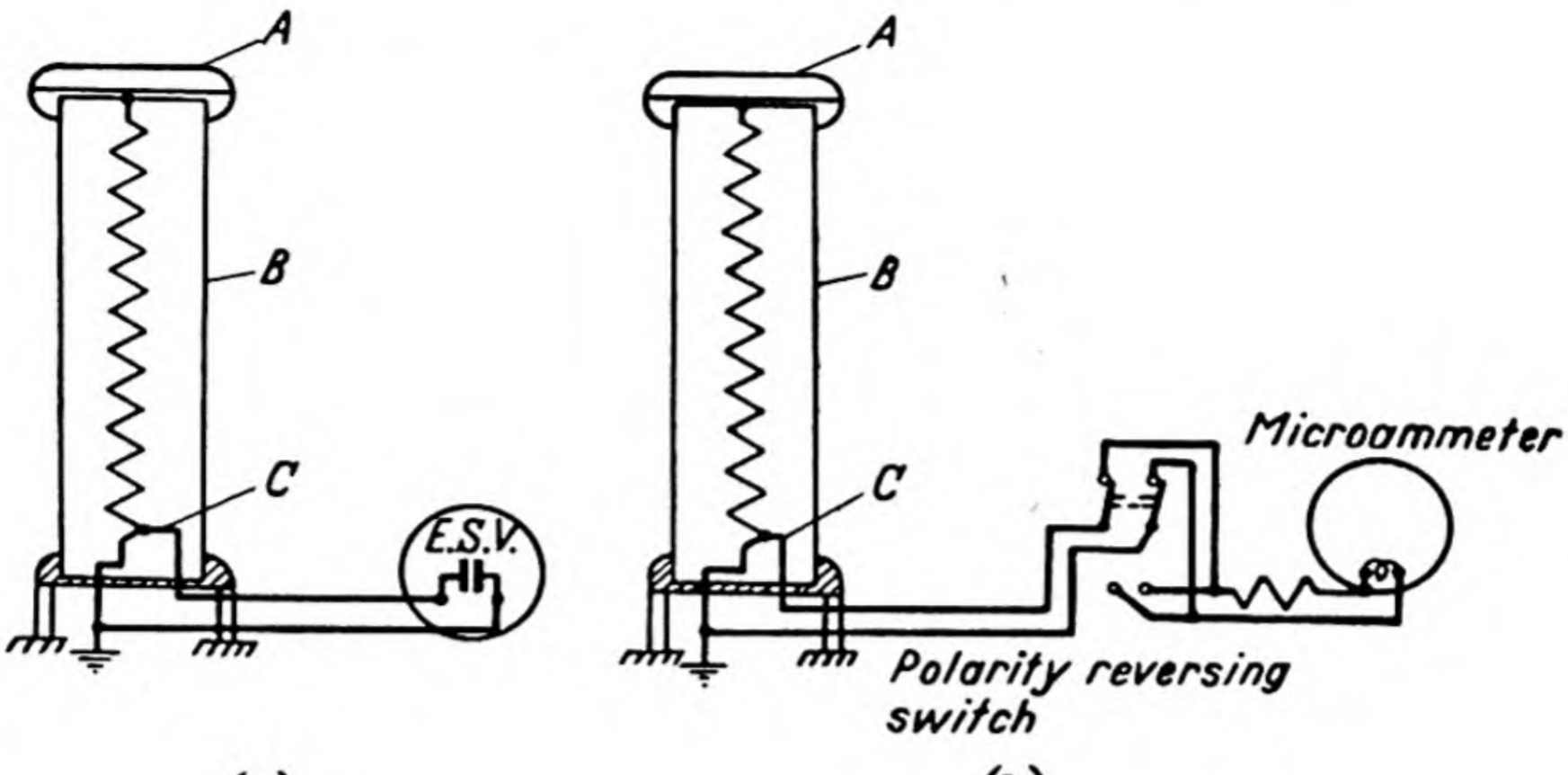

Figure 356. Connections for a high-voltage resistance potentiometer using (a) electrostatic voltmeter as the indicating unit. *A*, high voltage; *B*, potentiometer unit; *C*, tap at 1,000 or 2,000 V. (b) microammeter as the indicating unit. *A*, high voltage; *B*, potentiometer unit; *C*, tap at 1,000 V. (c) Sectional diagram of a high-voltage potentiometer resistance. *A*, stress shield; *B*, resistance support plates; *C*, insulating baffle; *D*, insulating container; *E*, resistance units; *F*, connection to tap (Waterton[12], by courtesy, *J. Sci. Instrum.*).

the current through the meter should be about 10 per cent. of the stack current if errors in the tap indication are to be kept within $\pm 1\frac{1}{2}$ per cent. and a resistance of about 40 MΩ, whose temperature coefficient may have to be allowed for, is connected in series with the meter as shown in *Figure 356* b.

Precision measurements on carbon resistors, made by Siemens and Halske, are due to BOWDLER[13]. These resistors, which had a stability and temperature coefficient comparable with those of wire-wound units, consisted of a porcelain former covered with a thin layer of carbon and for the higher resistances the carbon layer was cut spirally. End contacts consisting of metal clamps were used. The resistor ratings varied from 0·5 to 140 W, 10^2–10^7 Ω; their characteristics are described by HARTMANN and DOSSMANN[45].

Bowdler's measurements on 1 MΩ units showed that their temperature coefficients were reproducible and had the values given in *Table XXXV*.

TABLE XXXV

Nominal resistance	*Temperature coefficient of resistance*
Siemens 50 kΩ	$-3._1 \times 10^{-4}$/°C.
Siemens 2 MΩ	$-3._3 \times 10^{-4}$/°C.
Siemens 4 MΩ	$-3._6 \times 10^{-4}$/°C.
Siemens 4 MΩ	$-4._0 \times 10^{-4}$/°C.
Other makes 3 MΩ	-24×10^{-4}/°C.
Other makes 5 MΩ	-52×10^{-4}/°C.

A 100 MΩ resistor constructed by Bowdler is shown in *Figure 357* a and consists of 4 MΩ, 1 W units. At 100 kV, the test voltage, each unit was required to dissipate 4 W and for this reason the units were immersed in oil. In *Figure 357* a the end-caps of the resistors are pushed on brass sleeves and Bakelite spacing discs are fitted on every fifth joint to locate the resistance string inside the glass containing-tube. The units were each measured, in oil, at 100 V, then at 4 kV, and then at 100 V again and only those whose resistance at 100 V returned to the initial value were used. The average change between 100 V and 4 kV was −2·54 per cent. By various bridge measurements it was shown that no appreciable charge of resistance with voltage occurred for voltages up to 15 kV. The resistance/time and resistance/voltage curves for the complete unit of *Figure 357* a are shown in *Figure 357* b. The resistance/voltage curve was taken in the steady state. Thus the performance of the resistor was shown to be satisfactory in view of the heavy over-running at 100 kV (4 W). At the normal rating of 1 W the change in resistance is seen to be 1 per cent., and, further, to vary by $< 0{\cdot}1$ per cent. after thermal equilibrium had been reached. At 4 kV, the units were near the break-down voltage, when spark-over between adjacent turns of the carbon spiral took place.

Bowdler shows also, for a.c. work, that the effect of stray capacitances is negligible for the above unit. The three cases studied were those of a resistance R with (a) a capacitance C across it (b) a capacitance C to earth, evenly distributed along R and (c) a capacitance C to high-voltage conductors uniformly distributed. These give phase errors (for $\omega = 2\pi \times$ frequency) respectively of $RC\omega$ (current leading), $RC\omega/6$ (current lagging) and $RC\omega/3$ (current leading). For a resistance change of 0·1 per cent., the maximum permissible phase angle is about 0·05 radian and tests with the resistor of *Figure 357* b gave a phase angle of about 0·03 radian at 50 c/s.

Bowdler's studies of carbon resistors[13] for high-voltage measurement have been supplemented by those of many workers. Cooper (unpub-

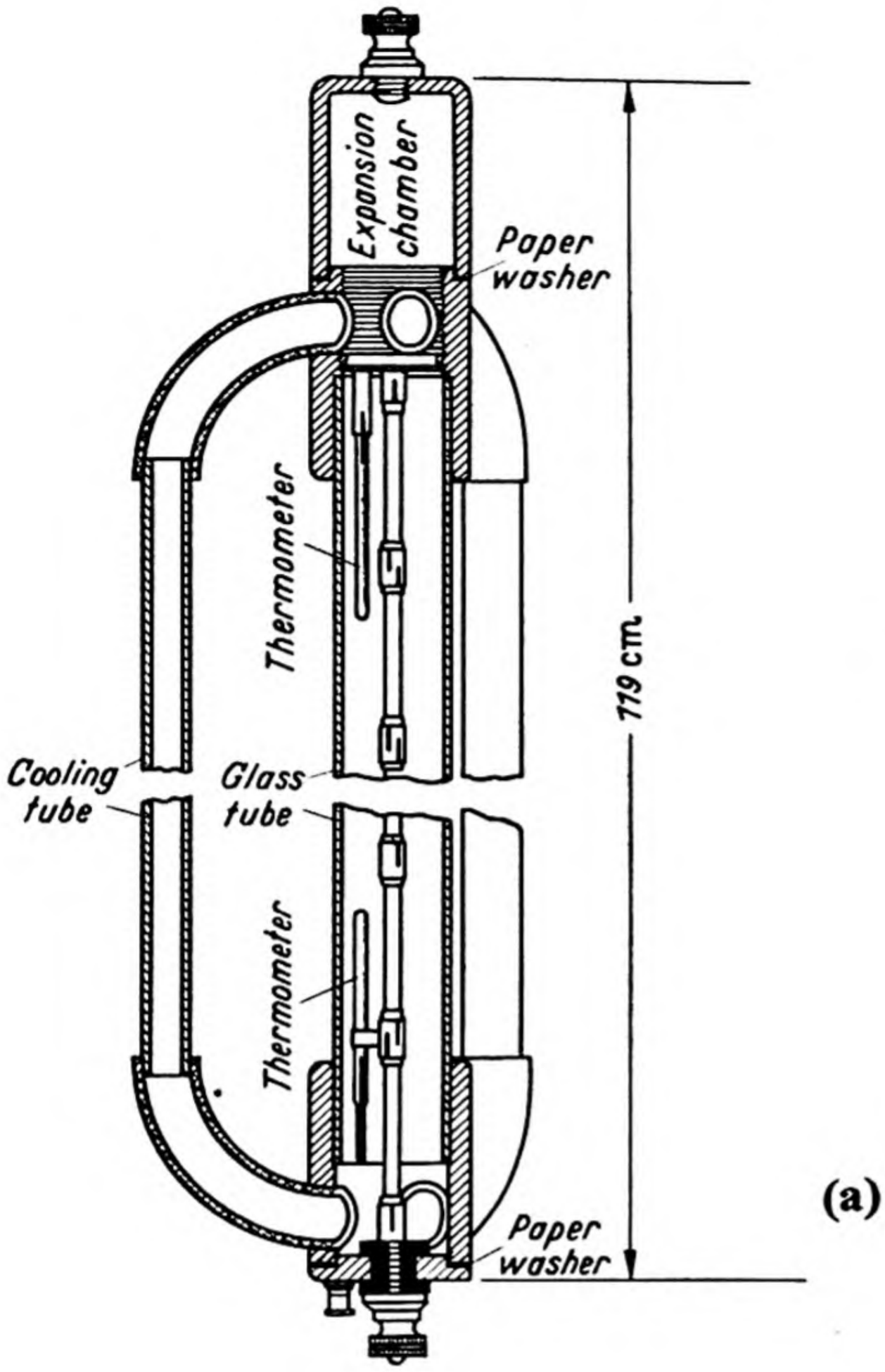

Figure 357. (a) Section of Bowdler's 100 MΩ resistor. (b) Stability tests of Bowdler's[13] resistor (by courtesy, *J. Inst. elect. Engrs.*).

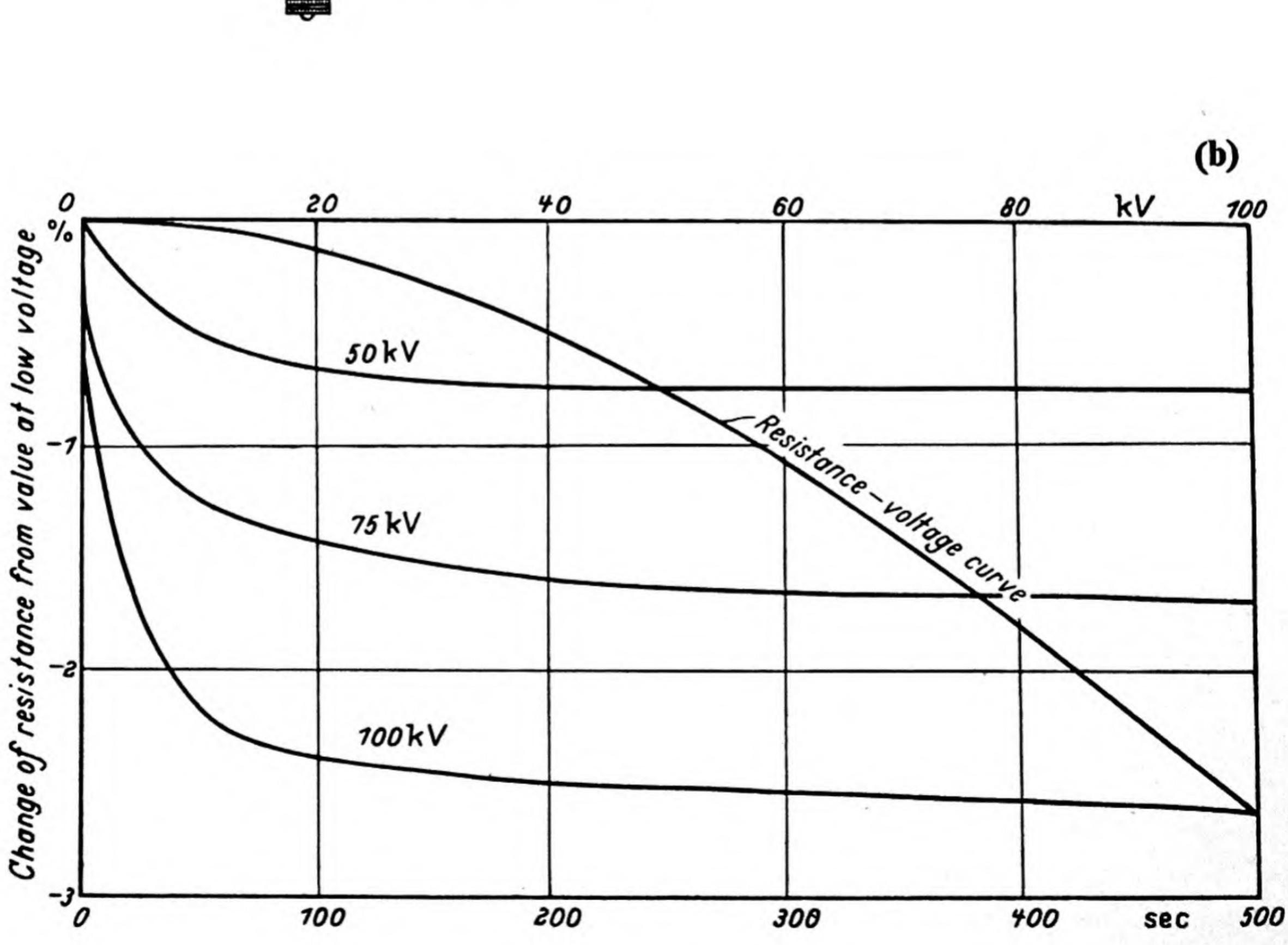

lished) used carbon resistors, made by Siemens-Halske, for d.c. work in the form of units containing ten 5 MΩ resistors. The usual methods for the measurement of resistance are generally applied, at low voltages (10–120 V), and are checked by tests at high voltage to detect corona losses. In the latter case, wire-wound standard resistances of the type described by Waterton[7] are invaluable, or the units may be measured on a high-voltage Wheatstone bridge (*see* page 376).

A brief account of new, high stability, carbon resistors has been published by PLANER and PLANER[14]. These units have a temperature coefficient of resistance of about -3×10^{-4}/°C., as compared with -8×10^{-4}/°C. for graphite and still higher values for carbon layers as normally used in this type of resistor.

Liquid resistances are briefly mentioned on page 324; their use in quantitative work has so far been limited for reasons given in the papers cited.

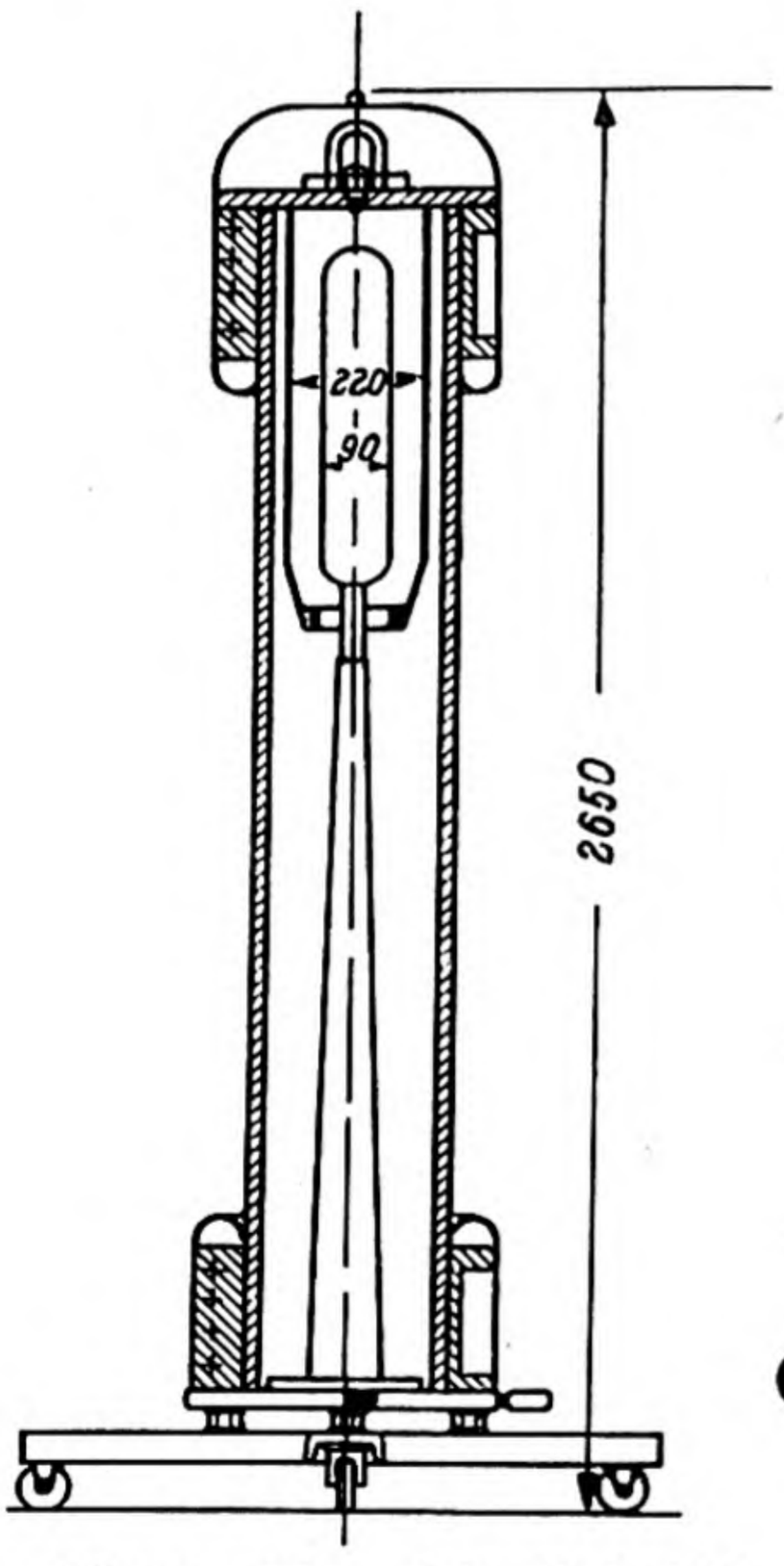

(a)

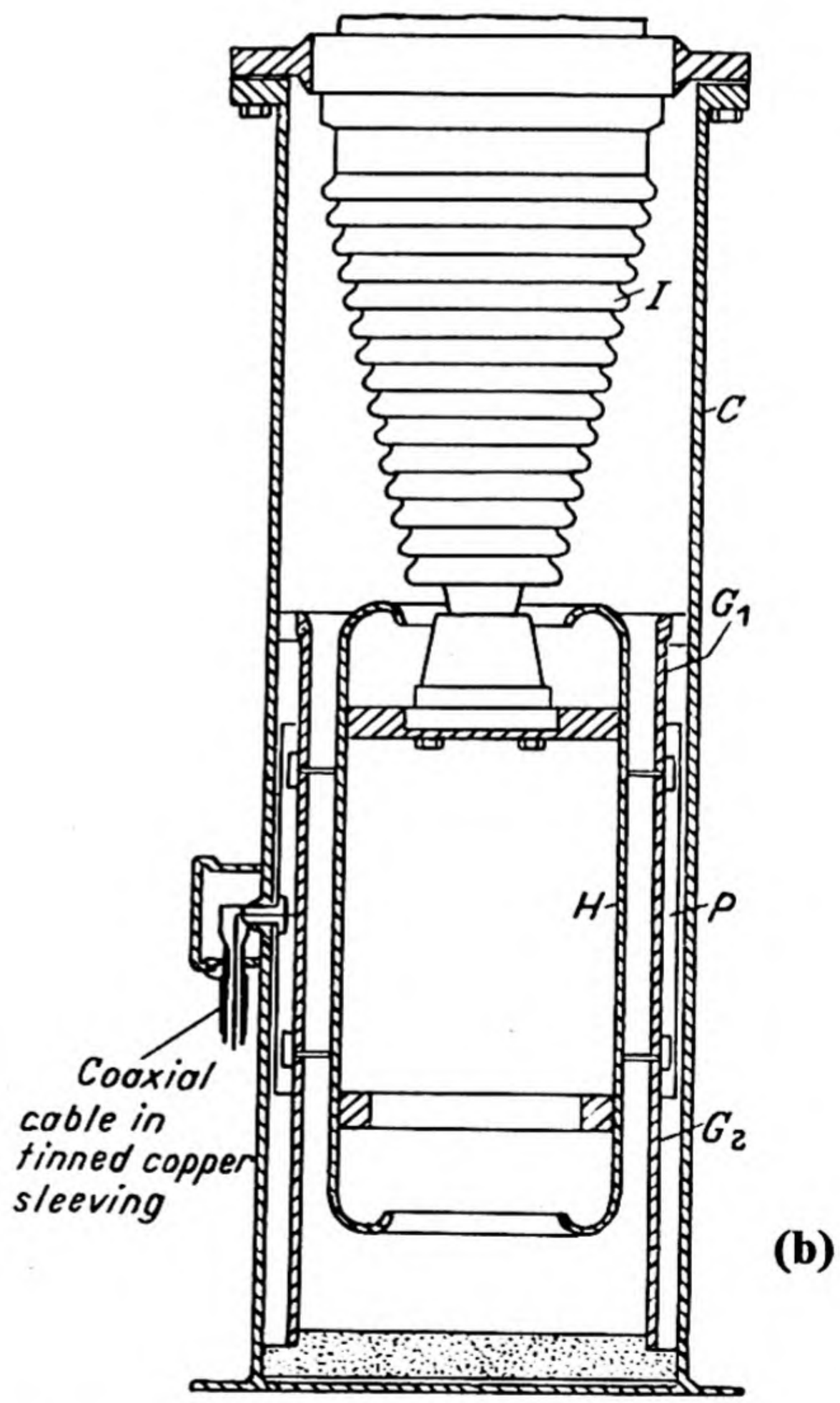

(b)

Figure 358. (a) Palm's[15] 500 kV compressed gas condenser. Dimensions are given in millimetres (by courtesy, *Arch. Elektrotech.*). (b) Compressed gas capacitor. Diagram of Bousman and Ten Broeck capacitor altered to include complete shielding of the working electrode (after Defandorf[4]).

I = Insulator for h.t. electrode
C = Container
P = Low-voltage electrode of the condenser *HP*
G^1, G^2 = Guard electrodes.

CAPACITORS

A study of compressed gas condensers has been made by PALM[15] for operation at voltages varying up to 500 kV, following earlier work[16] by the same author and by SCHERING[17]. Palm's work on the dielectric strength of compressed gases led to the design of a 500 kV condenser, shown in *Figure 358*a[15]. Palm showed, for example, that in nitrogen at 14 atmospheres pressure, the a.c. (low frequency) break-down voltage between 15 and 19·7 cm. diameter concentric cylinders was about 556 kV.

A condenser design, similar to that of Palm, has also been briefly

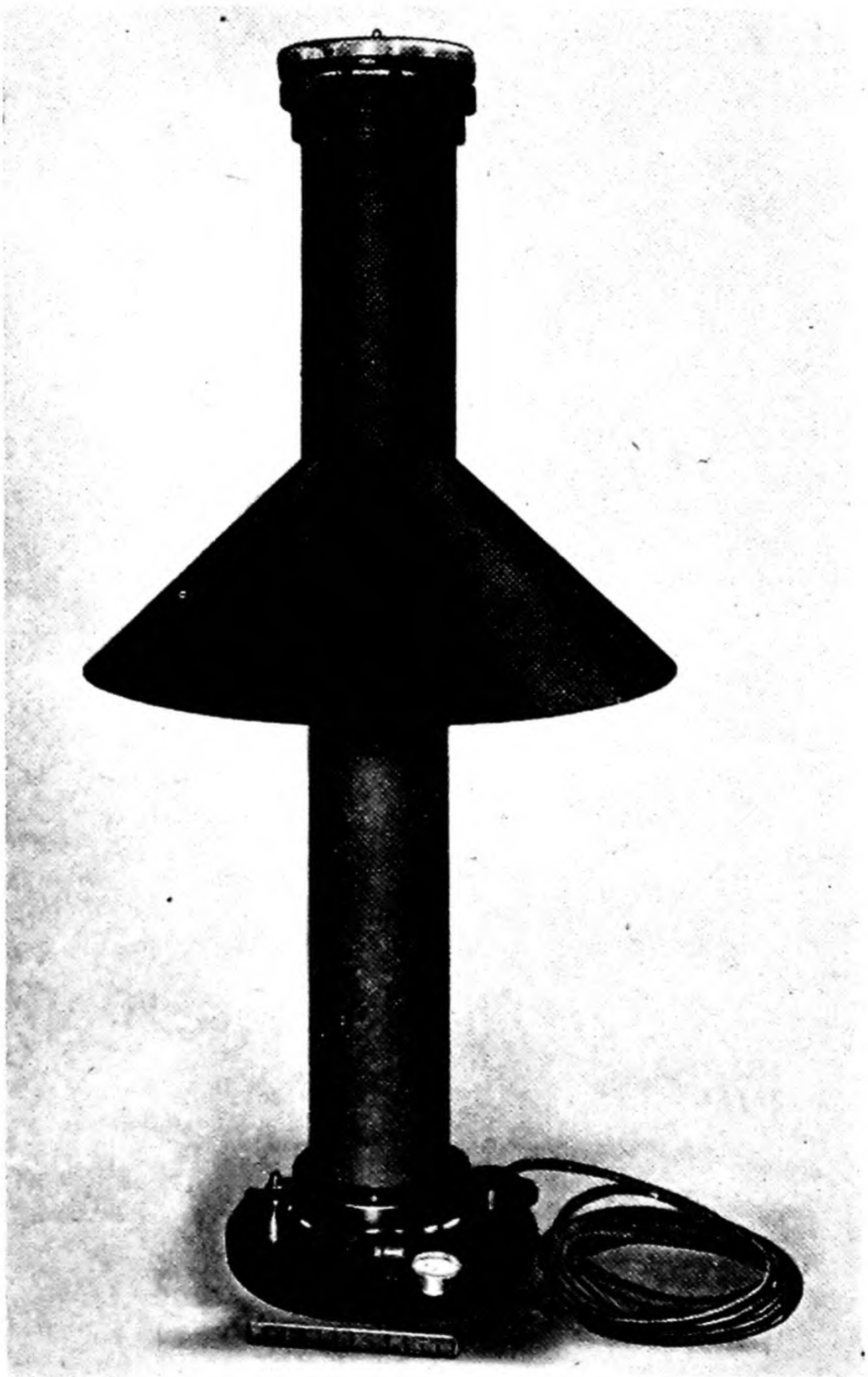

Figure 359. Compressed air standard condenser (by courtesy, Metropolitan Vickers Electrical Co. Ltd.).

described by BOUSMAN and TEN BROECK[18], who used it in modified Schering bridge measurements on the constants (ratio and phase angle) of potential transformers. The condenser, shown in *Figure 358* b in the slightly altered form described by Defandorf[4], was filled with CO_2 to about 100 lb./in.^{2} gauge pressure, had a capacitance of about 50 $\mu\mu$F, and was rated at 300 kV (low frequency a.c.). The internal diameter of the outer cylindrical electrode (*Figure 359*) was 18 inches. Such compressed gas condensers usually have negligible changes of dimension with voltage or temperature and the dielectric loss angle (60 c/s) may be much less than 1 minute. Another type of condenser, filled with compressed air to a maximum pressure of 165 lb./in.^{2}, and rated at 200 kV (r.m.s.) at 50 c/s is shown in *Figure 359* (Metropolitan-Vickers). This unit has a capacitance of 16 $\mu\mu$F (*see* page 386).

A brief discussion of compressed gas condensers (100 $\mu\mu$F, rated up to 300 kV) for Schering bridge work is given by KAPPELER[19]. Gas fillings of CO_2, N_2 or compressed air, to pressures of 10–12 atmospheres gauge pressure, were used.

Measurements of the time constants of high-voltage condensers of various types, rated at voltages varying from 10 to 200 kV (0·004 to 0·1 μF) have been described in detail by Horst[20]. The highest time constants measured were $\sim 10^4$ sec at 5 kV for condensers rated at 30 kV and having capacitances varying between 0·01 μF and about 0·004 μF. The best ratio of time constant (secs)/capacitance ($\mu\mu$F) was about 200. Clearly these ratios will differ greatly for different types of condenser and the above figures are intended only to give the order of time constant to be expected.

THERMIONIC RECTIFIERS

The Philips laboratories have developed various types of high-voltage rectifier valves for use in X-ray apparatus, and cascade d.c. generators. A general review of this work is given by VAN DER TUUK[21]. The use of tungsten filament vacuum rectifiers, which are readily available for voltages up to 125 kV, is limited for some applications by

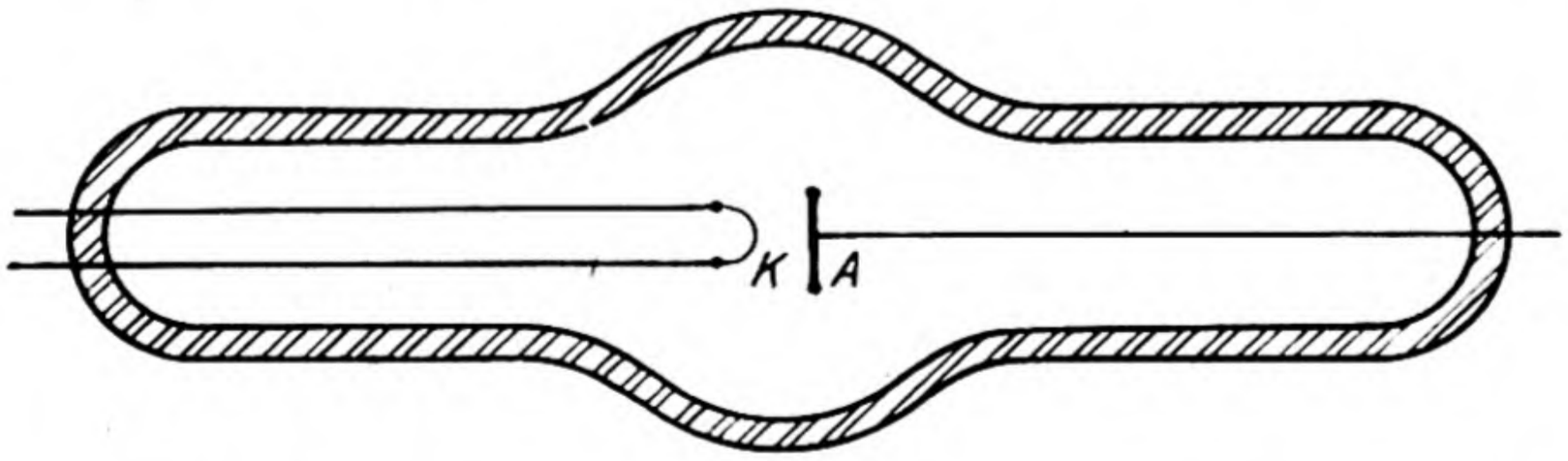

Figure 360. Diagram of the cross-section of a vacuum rectifier valve as used formerly in high-voltage installations. An anode plate *A* is situated at a short distance opposite a tungsten cathode *K* in an evacuated glass tube (van der Tuuk[21], by courtesy, *Philips Tech. Rev.*).

their high impedance. For the simple schematic design of *Figure 360* the voltage drop may be 2·5 kV for 1 A. Even then care must be taken to avoid field emission from the anode in the negative half-cycles, and indeed much of the early work in Britain (by GOSSLING and others) on field currents was stimulated by the need for stable h.t. rectifiers. An improved design of vacuum tube such as the Philips design of *Figure 361* leads to lower voltage drops. Because of the spread of the

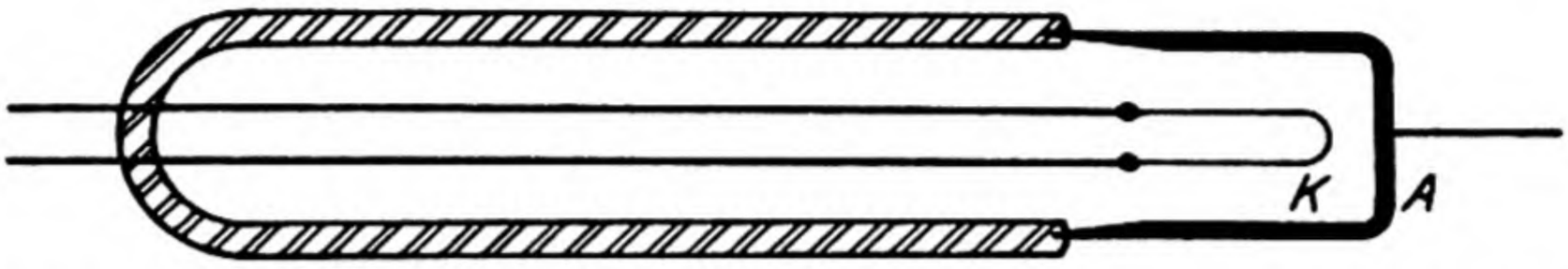

Figure 361. An improved electrode arrangement for a high-voltage vacuum rectifier (van der Tuuk[21], by courtesy, *Philips Tech. Rev.*).

electron stream from the cathode to the anode, due to the large solid angle subtended at the cathode by the anode, the space charge has less effect than in the design of *Figure 360* and the voltage drop is thus reduced to about 650 V at 1 A. The wall-charging effects are also reduced. Finally, the vacuum rectifier of *Figure 362*, using a

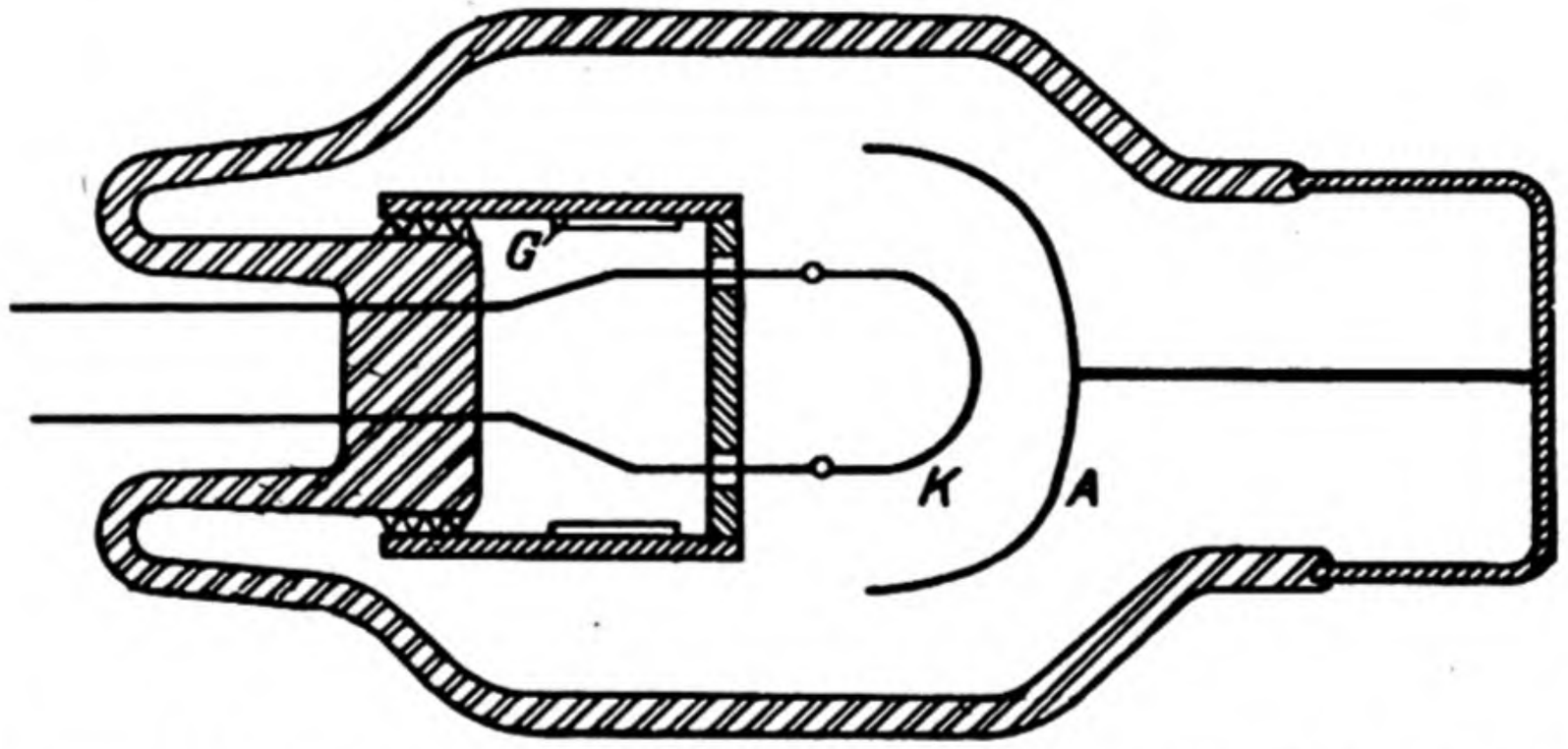

Figure 362. Diagram of a modern vacuum rectifier. The filament *K* is made of thoriated tungsten. The cup-shaped anode *A* no longer forms a part of the (hard-glass) valve wall, which makes it easier to use the valve under oil. *G* is a getter (barium mirror) (van der Tuuk[21], by courtesy, *Philips Tech. Rev.*).

thoriated-tungsten filament, enables the anode *A* to be taken to a higher temperature during the preliminary degassing process and yet ensures that the running temperature of the envelope is low enough to make oil-cooling feasible. A valve of this type for 125 kV now has (van der Tuuk[21]) a length of rather more than 20 cm., with a diameter of 9 cm. and may dissipate 40–50 W.

The Philips mercury vapour h.t. rectifiers, used in the h.t. generators described on pages 30–35, follow the design sketched in *Figure 363* and are virtually cascade tubes. The mercury is confined in a

special reservoir to avoid its contact in the liquid state with the electrodes, and provides a sufficiently high vapour pressure between about 17 and 40 °C. for the discharge to be developed. The voltage drop at 1·5 A may be only 25 V. The cascade principle, and the voltage grading by means of the condensers, indicated in *Figure 363*, which are fitted in mouldings attached to the outside of the tube, enables high total voltages to be applied without the danger of field emission, which occurs at the regions of highly localized electric stress encountered in single stage rectifiers.

The Philips valves used in the modified Cockroft-Walton circuit of *Figure 40*[22] withstand 225 kV peak reverse, strike at 3–4 kV and have a voltage drop of about 50 V in the conducting state. Eight cylinders are used to grade the potential distribution, as in the normal form of high-voltage acceleration tube (*see*, for example, *Figure 4*). This type of valve is also discussed briefly by GRADSTEIN[23].

The Siemens laboratories have developed hot-cathode single-stage rectifiers for 400 kV[24].

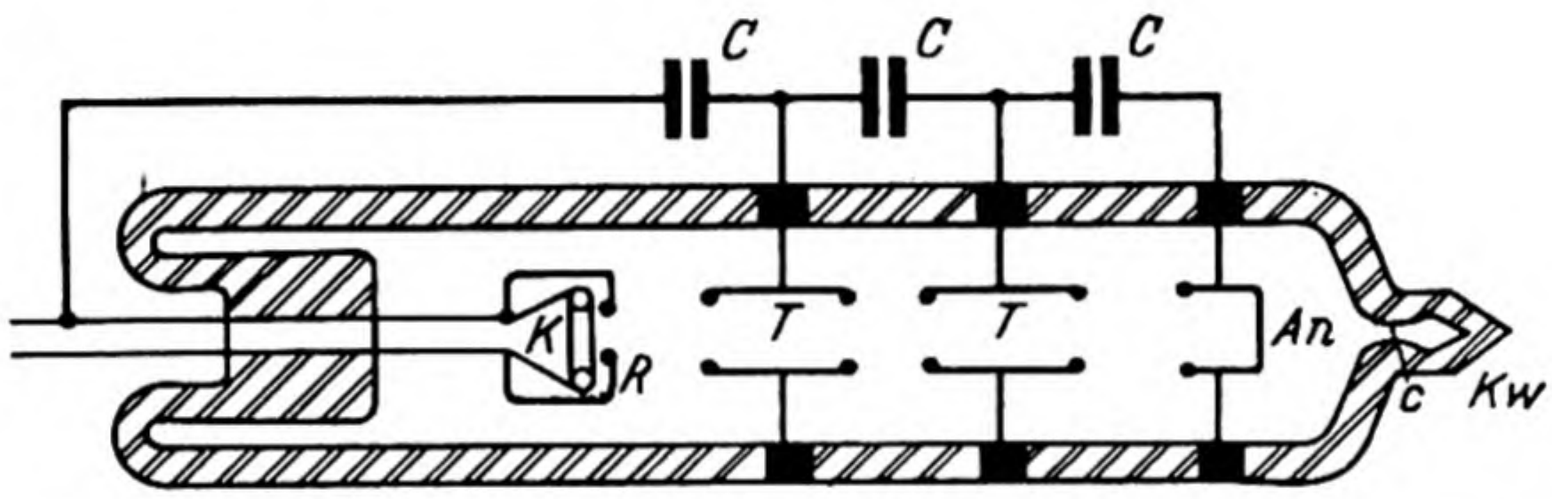

Figure 363. Diagram of a cross-section of a gas-filled rectifier valve (Philips Metalix). The glass envelope is filled with saturated mercury vapour. The distance between the oxide cathode *K* and the anode *An* is divided into three stages by intermediate electrodes *T*, which are connected by the condensers *C* for the sake of a uniform voltage distribution. By a ring *R* placed in front of it the cathode is screened against bombardment by positive gas ions, while the ring at the same time lessens the chance of material from the oxide cathode striking the other electrodes. *Kw* is a mercury reservoir connected with the envelope by a capillary (van der Tuuk[21], by courtesy, *Philips Tech. Rev.*).

Some recent technical developments in high-voltage ignitrons are described by MULHERN[25] who gives details of 50 A, 20 kV and 150 A, 20 kV tubes. The latter is 42 inches in overall height, and 9 inches in diameter and such tubes were used in the assembly of a 17 kV 7·5 MW rectifier set.

The use of ignitrons in pulse circuits at ~20 kV is now established practice for some types of high-energy particle accelerator, and KERST[26] was one of the first to use such techniques in the pulsing of the electron injector gun in a betatron. Later work is due to BOSLEY *et al.*[27].

CORONA RECTIFIERS

BENNETT[28] has described experiments on a cold cathode rectifier tube using a corona discharge in a non-attaching gas where there is a large difference in mobility between the negative (electrons) and positive particles. The current–voltage characteristics for negative and positive corona, using a 1 mil tungsten point discharging in hydrogen at 1 atmosphere pressure, to a plane at a distance of 3 cm. are shown in *Figure 364* and the potentialities of such a system for

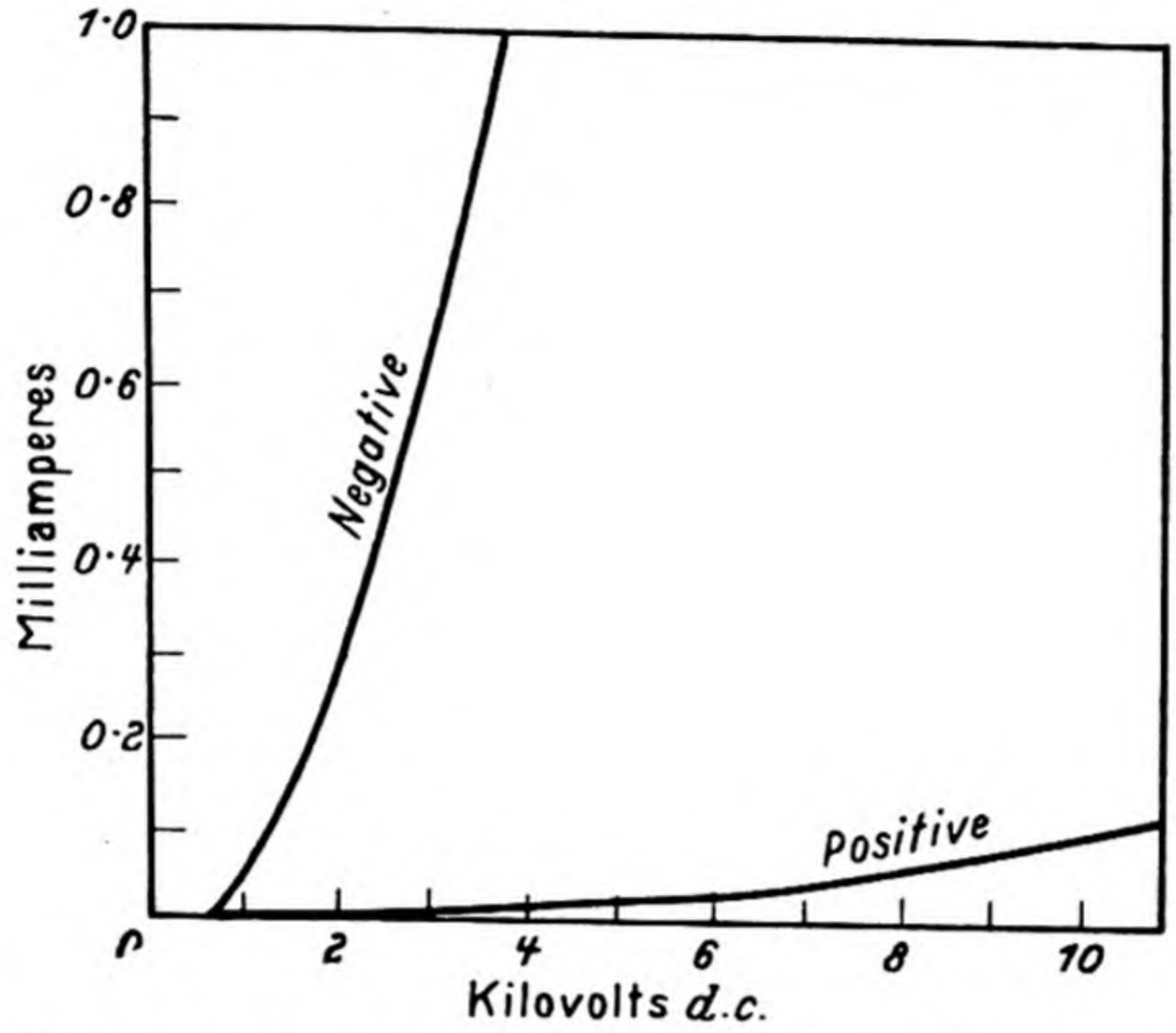

Figure 364. Current-voltage characteristics for negative and positive corona (Bennett[28], by courtesy, *J. appl. Phys.*).

rectification can be immediately appreciated. Bennett states that it is important to eliminate electron-attaching impurities (O_2, CO_2, Cl_2, *etc.*) to less than 1 part in 10^8, so as to avoid the formation of negative ions and to ensure that the large difference in the positive and negative point characteristics (*Figure 364*) may be realized. Corona rectifier tubes may be sealed off and a 100 kV Cockroft-Walton rectifier set using such units is shown in *Figure 365*[28].

Efficiency curves for various gaseous mixtures are given in *Figure 366*. For currents greater than a few mA it is seen that conventional vacuum rectifiers are more efficient, but for lower currents the elimination of filament supplies is an advantage. Bennett also states that the corona rectifiers are more reliable than mercury vapour tubes because of the absence of arcing back. Also, they have a very long life, since the electrode erosion is very small. Bennett's paper[28] gives references to his earlier exhaustive work on corona characteristics.

Corona discharges may also be used, because of their rapid change of current with voltage, in certain stabilizing circuits and have been discussed to this end by, for example, BROWN[29]. Details of the

characteristics of grid controlled corona discharges have been given by ASHBY and HANSON[30]. Special reference is made to the possible

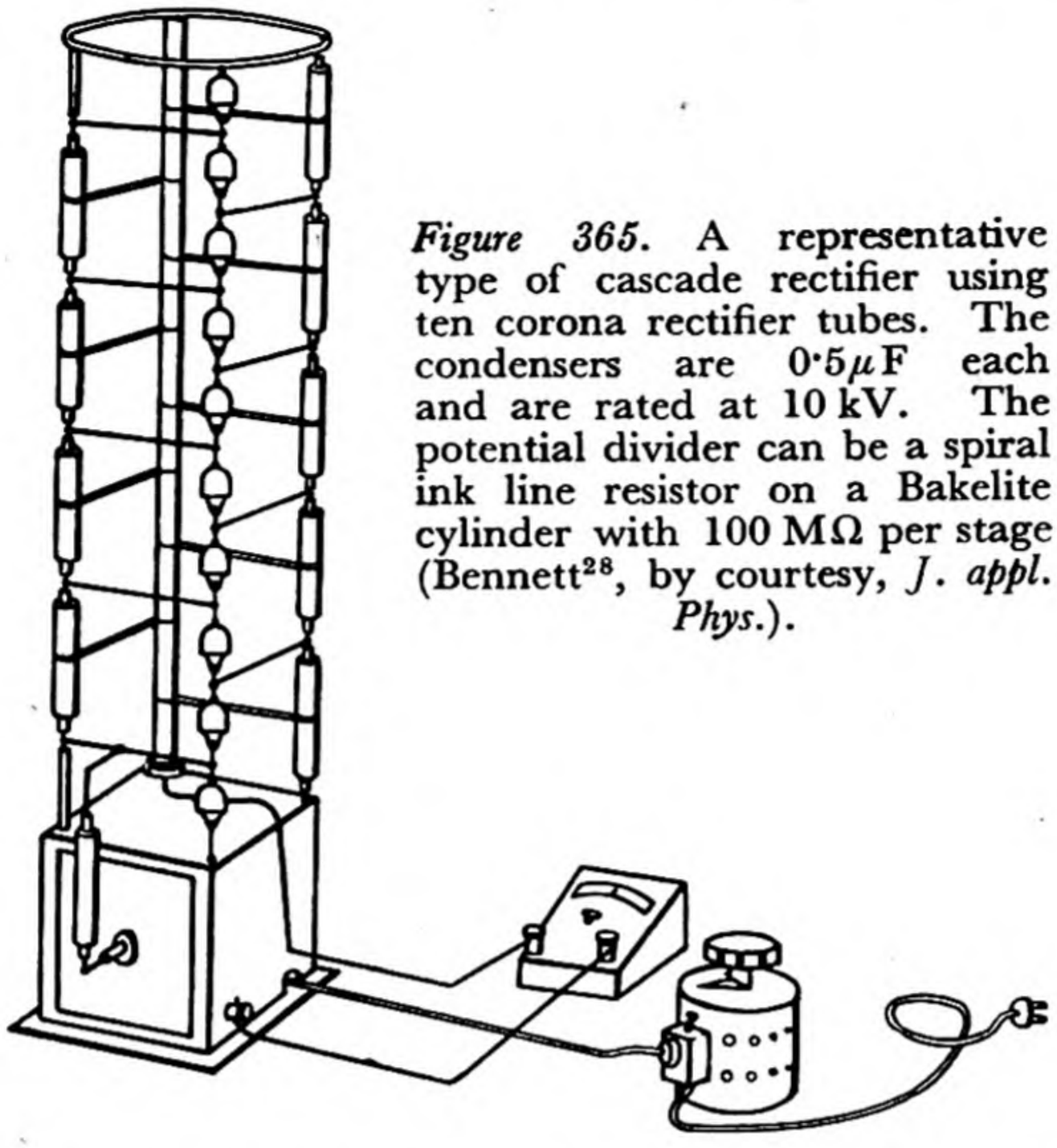

Figure 365. A representative type of cascade rectifier using ten corona rectifier tubes. The condensers are 0·5μF each and are rated at 10 kV. The potential divider can be a spiral ink line resistor on a Bakelite cylinder with 100 MΩ per stage (Bennett[28], by courtesy, *J. appl. Phys.*).

uses of such discharges in the stabilization of corona-fed high-voltage generators.

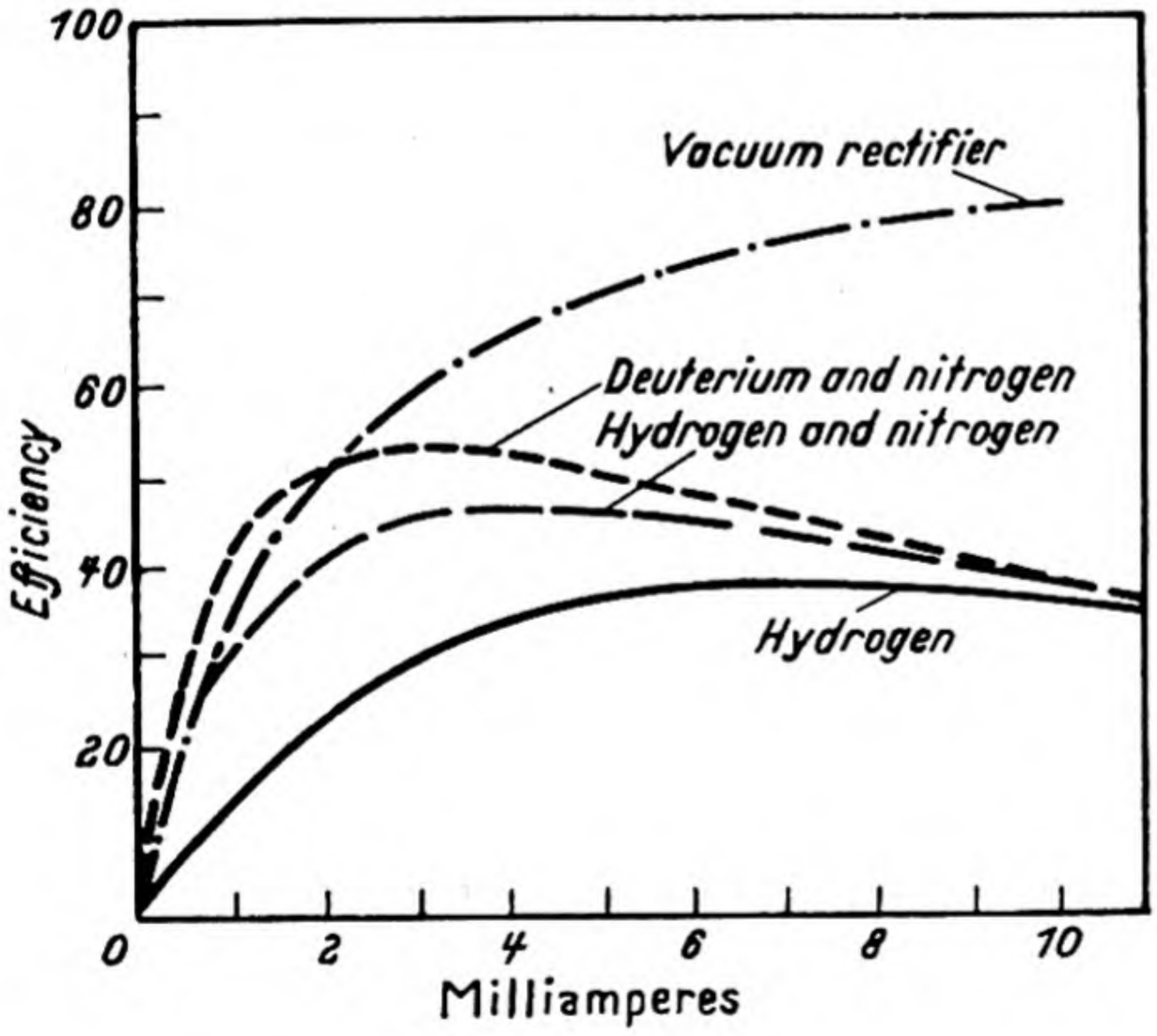

Figure 366. Efficiency, with 20 kV a.c. applied, of various rectifier systems (Bennett[28], by courtesy, *J. appl. Phys.*).

MECHANICAL RECTIFIERS

Mechanical synchronous rectifiers of a new design have been described by IMHOF[31]. High-voltage sets may be made by cascading units of the type shown in *Figure 367*. An assembly of such units is arranged as in *Figure 368* where the rotating needles, one of which is indicated in *Figure 367* at the centre of the toroidal shield, take up

the extreme positions (*a*) and (*b*) for the conducting and isolating periods. For a supply frequency of 50 c/s the needles must revolve at 1,500 r.p.m. The shields, one of which is shown in *Figure 367* serve

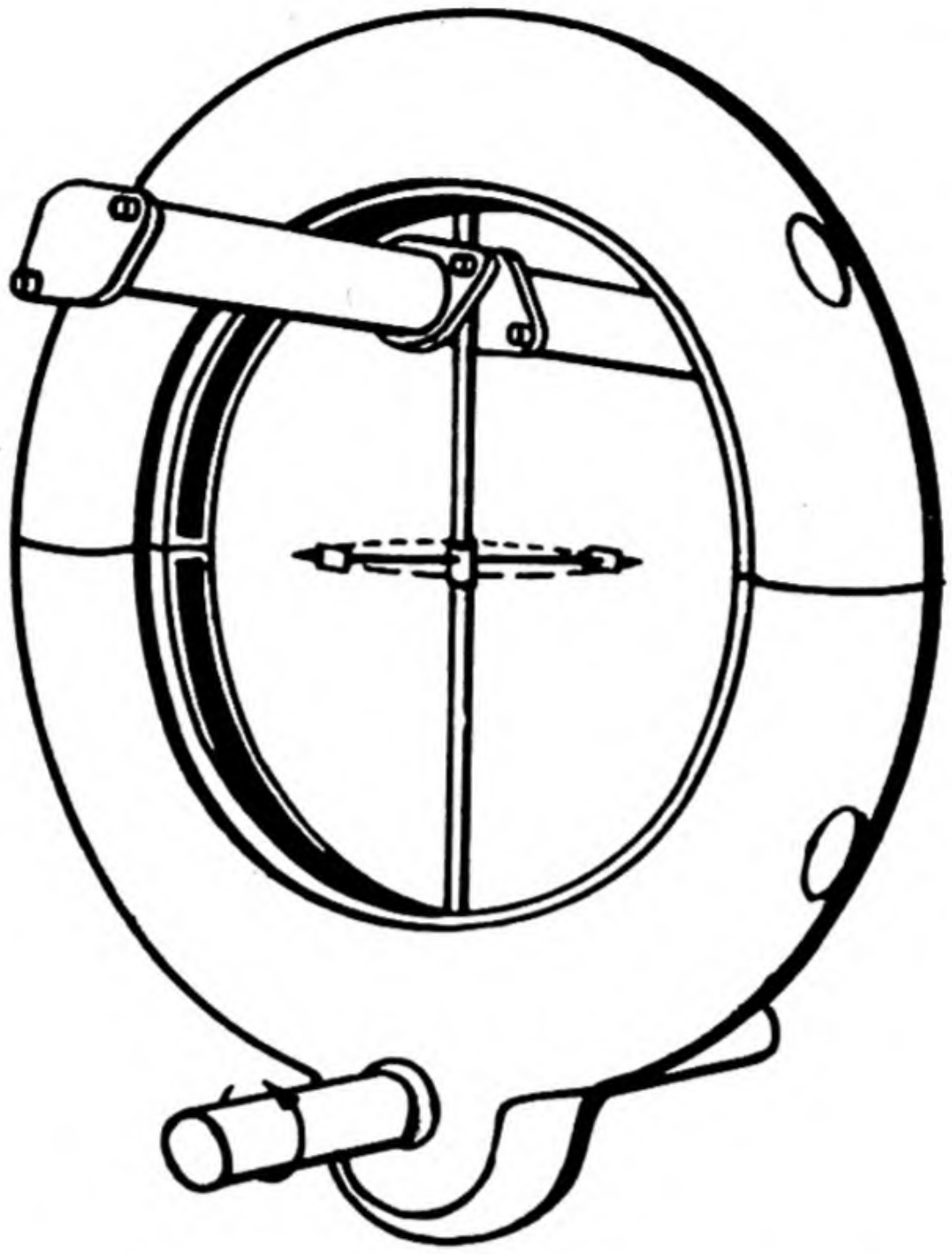

Figure 367. Individual element of a mechanical rectifier (Imhof[31], by courtesy, *Micafil News*).

as potential grading devices and also serve to shield the mechanical parts of each rectifier unit as indicated in *Figure 368*. A 1·2 mV rectifier was constructed of such units; this has 17 stages and is about 30 ft. long and 21 in. in external diameter.

SURGE PROTECTION DEVICES

Apparatus may be protected from overvoltages by the use of sphere gaps, rod gaps or other gaps operating in air and connected in parallel across the apparatus. The gap length is chosen so that the gap does not break down until the voltage on the apparatus is at a suitably defined level above the normal working voltage. When a surge overvoltage occurs it then remains for only a brief time, of the order of 1 μsec or less, across the apparatus before the protective gap breaks down. The break-down of a sphere gap develops more rapidly than for a rod gap with a given overvoltage[32, 33]. The spacings required for a sphere gap or rod gap can be chosen by reference to the calibration tables given in Chapters 7 and 8.

Sealed-off gaps for the protection of circuits against overvoltages have been developed by KNIGHT and HERBERT[34]. These gaps are enclosed

in a glass or ceramic tube containing hydrogen at a pressure up to 2 atm. The electrodes are of sheet nickel, one having a flat face and

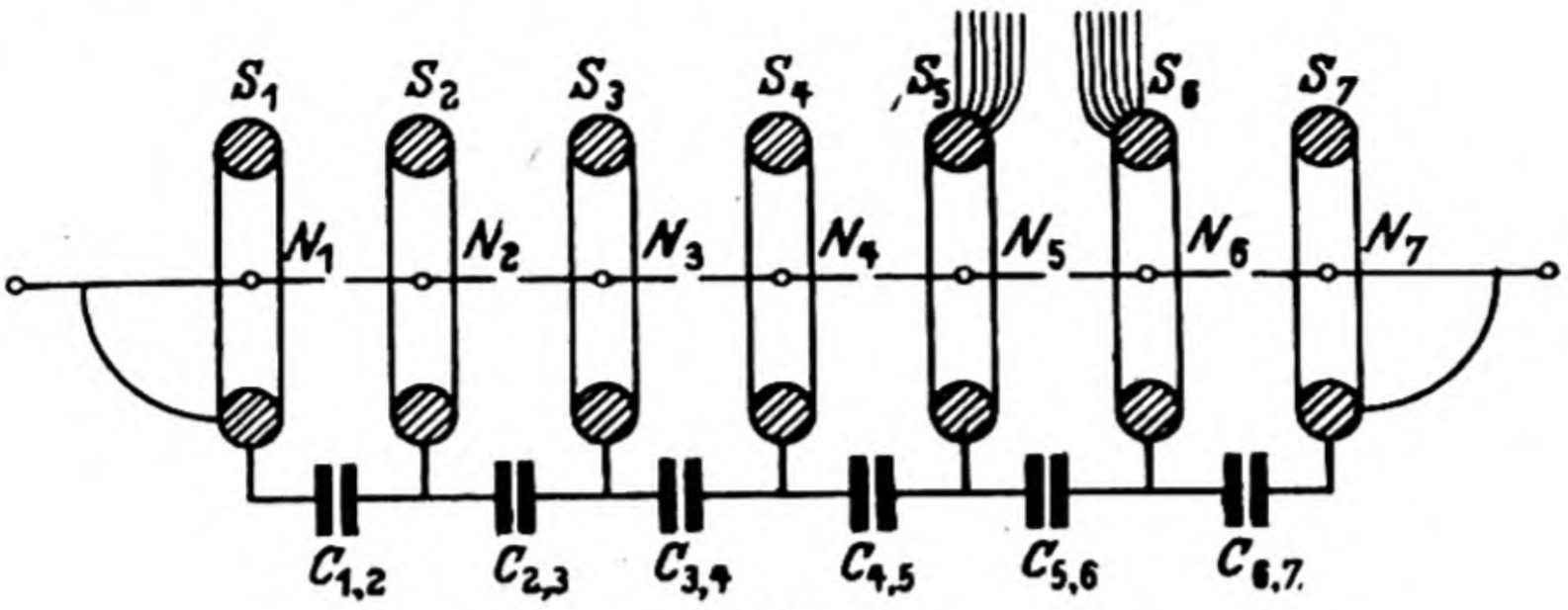

Figure 368. Basic diagrams of a mechanical rectifier assembly (a) at the conducting moment, (b) at the barrier moment. N_1, &c., are the needles (see *Figure 367*), S_1, $_2$, &c., are the h.t. shielding electrodes (Imhof[31], by courtesy, *Micafil News*).

the other a slightly concave face. *Figure 369* shows the break-down voltage as a function of gas pressure for two gap lengths when the gaps

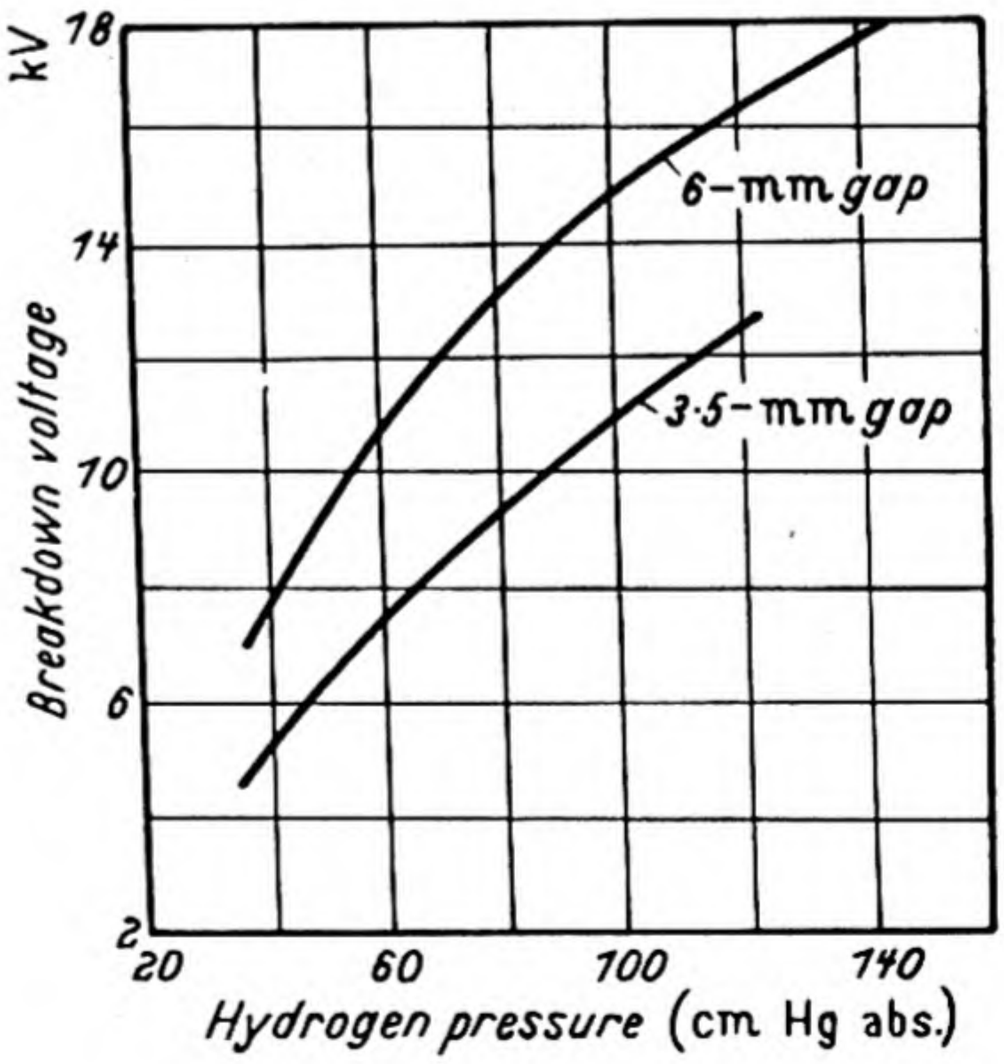

Figure 369. Break-down voltage as a function of gas pressure. Measured on square voltage pulse, having 1 μsec duration, 50–100 kV/μsec front, and repetition rate 500 pulse/sec (Knight and Herbert[34], by courtesy, *J. Inst. elect. Engrs.*).

are broken down with square voltage pulses of 1 μsec duration repeated at 500 pulses/sec. Two types of these tubes have been manufactured, one with a break-down voltage at 16 kV $\pm$ 1 kV and the other at

5 kV ± 0·5 kV. The gap is found to operate on the front of the pulse with no measurable delay. De-ionization of the gap is rapid and the tubes have been used at pulse repetition rates up to 5,000 pulse/sec.

While a parallel-connected gap can protect apparatus against an overvoltage the break-down of the gap may be followed by a power arc which continues across the gap until the power supply is interrupted. To prevent this occurrence protective devices known as surge diverters or lightning arresters have been developed, their main application being in the protection of power transmission systems against overvoltages produced by lightning or other causes[33, 35–40].

A surge diverter usually consists of a spark gap, or a number of spark gaps, in series with a non-linear resistor. As a diverter is normally connected between a high-voltage conductor and earth the spark gap is necessary to prevent current from flowing through the diverter at times when there is no surge on the system. On the occurrence of a surge the voltage rises across the diverter until the spark gap breaks down and the voltage is then limited to a value determined by the surge current and the volt-ampere characteristic of the resistor. After the surge has died away the normal system voltage tends to maintain a small current through the diverter but this follow-current is unstable and is usually interrupted at the first voltage zero following the surge. The residual voltage of a surge diverter, *i.e.* the voltage across it after the spark gap has operated, depends on the surge current but not appreciably on the surge duration.

By the use of a series of gaps rather than a single gap the ability of the diverter to interrupt the follow-current is greatly improved. It is important that the gaps should have a low impulse ratio and for this reason the gaps require to be adequately irradiated to reduce statistical time lags[33, 39]. This irradiation may be provided by the ultra-violet light emitted from surface corona discharges occurring on the insulators between the electrodes[39] (*see* Chapter 8).

The non-linear resistance material used in surge diverters generally contains silicon carbide and is made up in cylindrical blocks. The relation between the current and the applied voltage is of the form

$$V = k\, I^{\beta} \qquad \ldots\ldots(11.1)$$

where the values of k and β depend on the shape and constitution of the block[40].

Among other devices which have been developed for the protection of power transmission lines against surges is the ' expulsion protective gap '[33, 37–44]. This consists of a fibre tube with an open end and with electrodes arranged so that spark break-down occurs within the tube on the application of a surge of sufficient magnitude. Following the spark a power-frequency arc develops within the tube. Because of the

high temperature of the arc, and the rapid vaporization of the organic material forming the tube walls, a high gas pressure is produced in the tube with the result that the hot gases are expelled from the tube. De-ionization of the arc path is sufficiently rapid that the power-frequency follow-current is normally interrupted within the first or second half-cycle.

Methods using a combination of capacitance, inductance and resistance elements have been devised for modifying the wave-form of surges[33]. In general these reduce the steepness of the wave-front of the surge and, to a lesser extent, the amplitude of the surge. The extent to which these methods are successful depends largely on the shape of the surge.

REFERENCES

1 TAYLOR, L. S. *J. Res. Nat. Bur. Stand., Wash*, **5** (1930) 609.
2 SHALLCROSS, P. *J. Frank. Inst.*, **233** (1942) 471
3 DAVIS, R. *J. Sci. Instrum.*, **5** (1928) 305, 354.
4 DEFANDORF, F. M. *J. Wash. Acad. Sci.*, **38** (1948) 33.
5 DAVIS, R. *J. Inst. elect. Engrs.*, **69** (1931) 1028.
6 GROVER, F. W., and CURTIS, H. L. *Bull. Bur. Stds.*, **8** (1912) 455
7 WATERTON, F. W. *J. Sci. Instrum.*, **19** (1942) 105.
8 HANSON, A. O. *Rev. Sci. Instrum.*, **15** (1944) 57.
9 BINDER, L., and HÖRCHER, W. *Z. tech. Phys.*, **19** (1938) 48.
10 HAFSTAD, L. R., HEYDENBERG, N. P., and TUVE, M. A. *Phys. Rev.*, **50** (1936) 504.
11 ROBERTS, R. B. *Phys. Rev.*, **51** (1937) 810.
12 WATERTON, F. W. *J. Sci. Instrum.*, **25** (1948) 304.
13 BOWDLER, G. W. *J. Inst. elect. Engrs.*, **73** (1933) 65.
14 PLANER, G. V., and PLANER, F. E. *Electronic Engng.*, **18** (1946) 66.
15 PALM, A. *Arch. Elektrotech.*, **28** (1934) 296.
16 PALM, A. *Elektrotech. Z.*, **47** (1926) 873, 904.
17 SCHERING, H. *Z. tech. Phys.*, **9** (1928) 442.
18 BOUSMAN, H. W., and TEN BROECK, R. L. *Trans. Amer. Inst. elect. Engrs.*, **26** (1943) 541.
19 KAPPELER, H. *Micafil News*, 1945, p. 30.
20 HORST, E. *Arch. Elektrotech.*, **31** (1937) 827.
21 VAN DER TUUK, J. H. *Philips Tech. Rev.*, **8** (1946) 199.
22 KUNTKE, A. *Philips Tech. Rev.*, **2** (1937) 163..
23 GRADSTEIN, S. *Philips Tech. Rev.*, **1** (1936) 6.
24 MEHLHORN, H. *Siemens Z.*, **18** (1938) 417.
25 MULHERN, M. J. *Trans. Amer. Inst. elect. Engrs.*, Pt. II, **69** (1950) 913.
26 KERST, D. W. *Rev. Sci. Instrum.*, **13** (1942) 387.
27 BOSLEY, W., CRAGGS, J. D., MCEWAN, D. H., and SMEE, J. F. *J. Inst. elect. Engrs.*, Pt. I, **95** (1948) 352.
28 BENNETT, W. H. *J. appl. Phys.*, **18** (1946) 479.
29 BROWN, S. C. *Rev. Sci. Instrum.*, **17** (1946) 543.
30 ASHBY, R. M., and HANSON, A. O. *Rev. Sci. Instrum.*, **13** (1942) 128.
31 IMHOF, A. *Micafil News*, 1945, p. 17.
32 MEEK, J. M., and CRAGGS, J. D. *Electrical Breakdown in Gases*. London, 1953.
33 BRITISH ELECTRICAL AND ALLIED INDUSTRIES RESEARCH ASSOCIATION. *Surge Phenomena*, London, 1941.

[34] KNIGHT, H. DE B., and HERBERT, L. *J. Inst. elect. Engrs.*, Pt. IIIA, **93** (1946) 1058.
[35] Reports on lightning arrester performance characteristics by the A.I.E.E. Lightning Arrester Sub-committee, *Trans. Amer. Inst. elect. Engrs.*, **59** (1940) 347; **60** (1941) 982; **61** (1942) 132; **67** (1948) 520.
[36] JONES, H. F., and GARRARD, C. J. O. *Proc. Inst. elect. Engrs.*, Pt. II, **97** (1950) 365.
[37] LEWIS, W. W. *The Protection of Transmission Systems against Lightning.* New York, 1950.
[38] MONAHAN, T. F. *Proc. Instn. elect. Engrs.*, Pt. II, **98** (1951) 312.
[39] BERKEY, W. E. *Trans. Amer. Inst. elect. Engrs.*, **59** (1940) 429.
[40] ASHWORTH, F., NEEDHAM, W., and SILLARS, R. W. *J. Instn. elect. Engrs.*, Pt. I, **93** (1946) 385.
[41] MCEACHRON, K. B., GROSS, I. W., and MELVIN, H. L. *Trans. Amer. Inst. elect. Engrs.*, **52** (1933) 884.
[42] WISCO, E., and MONTEITH, A. C. *Elect. J.*, **35** (1938) 299.
[43] SPORN, P., and GROSS, I. W. *Trans. Amer. Inst. elect. Engrs.*, **57** (1938) 520.
[44] PETERSON, H. A., RUDGE, W. J., MONTEITH, A. C., and LUDWIG, L. R. *Trans. Amer. Inst. elect. Engrs.*, **59** (1940) 282.
[45] HARTMANN, C. A., and DOSSMANN, H. *Z. tech. Phys.*, **9** (1928) 434.

INDEX OF AUTHORS

Abraham, H., 260
Ackermann, O., 150
Alfvén, H., 222, 223, 260
Allen, J. E., 173
Allibone, T. E., 8, 10, 21, 22, 24, 58, 104, 110, 139, 150, 151, 262, 283, 284, 286, 291, 292, 323–25, 353, 369
Altar, W., 257, 263
Alvarez, L. W., 32, 58
Amstel, J. J. A. P. van, 35, 58
Anderson, M. W., 59
Angelini, A. M., 150
Ardenne, von M., 52, 347, 351, 356, 368, 369
Arnold, A. H. M., 159, 174
Arnold, M., 291
Arnold, W. R., 35, 36, 59.
Ashby, R. M., 84, 88, 391, 395
Ashworth, F., 396
Ashworth, J. A., 63, 87

Babat, G., 54, 59
Baguley, P. W., 174, 288, 292
Bales, P. D., 366, 367, 369
Bancroft, F. E., 21, 24, 58, 110
Bartlett, J. G., 356, 369
Bauer, R. E., 341–346, 368
Beams, J. W., 274, 291
Bedell, F., 77, 88
Beetlestone, A., 8, 58
Bell, E., 174
Bell, G. E., 1, 58
Bellaschi, P. L., 150, 154, 157, 168, 172, 173, 237, 261, 262, 281, 291, 292, 306–309, 317, 318, 325.
Benedict, D. L., 250, 255–257, 263
Benedict, F. R., 150
Bennett, W. E., 86–88, 254, 263
Bennett, W. H., 390, 391, 395
Benson, F. A., 77, 88
Berg, W. F., 368, 370
Berger, K., 150, 174, 287, 290, 292
Berkey, W. E., 274, 280, 290, 291, 396
Bernet, E. J., 88, 262, 263
Bewley, L. V., 309
Bialous, A. J., 260
Bigalke, A., 346, 368
Binder, L., 251, 261, 263, 319, 325, 352, 369, 376, 395
Bjerge, T., 33, 34, 58
Black, H. S., 60, 87
Blumlein, A. D., 188–190
Böcker, H., 215, 219, 220, 260
Boekels, H., 351, 369
Boldingh, H., 150
Bongartz, H., 291
Bonner, T. W., 87, 88, 263
Bosley, W., 110, 389, 395
Bostick, W. H., 177, 210
Bousman, H. W., 241, 299, 325, 385, 387, 395
Bouwers, A., 21, 28, 31–33, 37, 39, 58, 59, 89, 105, 110, 150, 261, 306, 325
Bowdler, G. W., 261, 262, 264, 281, 286, 290, 292, 296, 309–312, 325, 382–384, 395
Bradshaw, E., 224, 261
Brailsford, F., 110
Bramhall, E. H., 59
Breit, G., 109, 110
Brekoo, H. J. P., 59
Brinkman, C., 279, 291
Brooks, H. B., 212–215, 260
Broström, K. J., 33, 58, 82–84, 88
Brown, S. C., 390, 395
Brownlee, T., 157, 158, 173
Bruce, F. M., 223, 224, 233–235, 261, 262
Bryant, J. M., 290, 292
Buechner, W. W., 37, 59, 88
Burch, F. P., 300–306, 311, 318, 325, 347–351, 353, 354, 369
Burcham, W. E., 32, 58
Buss, K., 139, 150, 354, 369

Camilli, G., 92, 93, 110, 262
Candler, J. H., 287, 289, 292
Carpenter, T. J., 354, 369
Castellain, A. P., 261
Cauwenberghe, R. van, 262, 269, 290
Charlton, E. E., 18, 19, 21, 24, 58, 93–99, 101, 110
Chick, D. R., 50
Chubb, L. W., 262, 298, 325
Churcher, B. G., 299, 306, 325
Civilett, J. A., 151
Claussnitzer, J., 229, 261, 291
Clayton, C. G., 190, 210
Clem, J. E., 309
Cloud, R. W., 51, 59
Cochrane, W., 76, 88
Cockcroft, J. D., 20–24, 31–34, 58, 389, 390
Collins, B. G., 257, 263
Collins, G. C., 186
Coltman, J. W., 263
Cooper, R., 261, 320–323, 325, 383
Cox, J. H., 292
Craggs, J. D., 17, 58, 87, 110, 147, 151, 178–184, 186, 187, 193–196, 210, 267, 268, 270, 272–274, 291, 320, 325, 341, 368, 378, 395
Crämer, R., 89, 110, 139, 150
Curran, S. C., 88
Curtis, H. L., 374, 395

Dahl, O., 109, 110
Danforth, W. E., 52
Dannatt, C., 299, 306, 325
Dattan, W., 229, 261, 281, 291
Davies, G. T., 356, 369
Davis, N. L., 368
Davis, R., 174, 261, 262, 264, 281, 286, 290, 296–299, 309–312, 317, 325, 373, 395
Defandorf, F. M., 212, 213, 215, 219, 220, 224, 241, 260, 316, 317, 321, 325, 373, 385, 387, 395
Deighton, M. O., 369
Dempster, A. J., 32, 58
Dempster, L. E., 58, 110
Depp, W. A., 179, 210
Dessauer, F., 90
Devaney, R., 210
Dillon, J. H., 270, 290
Dodds, J. M., 210, 369
Dorsten, A. C. van, 58, 68, 69, 70, 74, 75, 88
Dossmann, H., 382, 396
Douma, T., 59
Dowell, J. C., 306, 325
Doyle, E. D., 297, 325
Drewnowski, K., 224, 261
Duinker, D., 59
Durnford, J., 153, 154, 165, 166, 168–173, 190–192, 210

Eaton, J. R., 114, 118–120, 122, 125–129, 150
Edwards, F. S., 91, 110, 114–117, 131, 133, 135, 139–144, 150, 232, 238–241, 261, 297, 300, 325
Ehrenberg, W., 253. 263

Eklund, S., 222, 223, 260
Elmore, W. C., 87
Elsner, R., 150, 261, 316, 317, 325
England, T. S., 210
Evans, P., 292
Evans, R. D., 63, 87, 270, 290

Fahnestock, J. D., 77, 88
Feldt, R., 366, 370
Felici, M. N., 291
Felici, N. J., 57, 59
Fielder, F. D., 236, 262, 281, 284, 285, 291, 292
Finch, G. I., 76, 88, 109, 110
Fisher, E., 150
Fisher, L. H., 234, 235, 262
Fisk, J. B., 44, 59
Fitch, V. L., 345, 368
Flegler, E., 349, 354, 368, 369
Fletcher, R. C., 356, 358–360, 369
Flowers, J. W., 173, 291
Foitzik, R., 153, 154, 173
Folkerts, H. F., 370
Fortescue, C., 262, 298, 325
Fortescue, R. L., 37, 52, 59
Foust, C. M., 166, 174, 92, 306, 369
Fowler, W. A., 263
Franck, S., 261
Freundlich, M., 369
Frissen, S. von, 84, 88
Froome, K. D., 210
Fry, D. W., 210
Fucks, W., 291

Gábor, D., 300, 302, 303, 306, 325, 348, 349, 369
Gänger, B., 217, 218, 260
Ganswindt, H., 365, 369
Garbuny, M., 263
Gardner, G. F., 166, 174
Garfitt, D. E. M., 261, 269–271, 275, 276, 290
Garfitt, R. G., 10, 58, 369
Garlick, G. F. J., 368, 370
Garrard, C. J. O., 396
Gaster, W., 89, 109, 110
Gaunt, H. M., 341, 368
Gebelein, J. P., 114, 118–120, 122, 125–129, 150
Germeshausen, K. J., 203, 210
Getting, I. A., 39–41, 44, 59
Gilbert, R. W., 84, 88
Gillette, P. R., 210
Gingrich, N. S., 63, 87
Ginzton, E. L., 354, 369
Glasoe, G. N., 175, 207, 210
Gold, G., 233, 261, 291
Goldstein, H., 366, 367, 369
Goodlet, B. L., 105, 107–110, 116, 150
Goossens, R. F., 287, 292
Gorev, A. A., 150, 151, 292
Goss, W. H., 246, 262
Gossling, B. S., 388
Goucher, F. S., 179, 185, 196–199, 201, 202, 210
Gradstein, S., 33, 34, 58, 389, 395
Gray, L. H., 320, 325
Greinacher, H., 10, 21, 33, 34, 58
Griffiths, J. H. E., 202, 210
Gross, I. W., 174, 396
Grover, F. W., 374, 395
Grünewald, F., 114, 150
Grünewald, H., 174
Gugel, H., 151
Guillemin, E. A., 210
Gunn, R., 243, 262
Guth, E., 257, 263

Hada, T., 364, 369
Hafstad, L. R., 77, 78, 88, 254, 263, 372, 376, 377, 395
Hagenguth, J. H., 138, 151, 292, 309, 325
Haine, M. E., 10–12, 17, 58, 67, 87, 147, 151, 178–184, 186, 187, 193–196, 310, 349, 369
Hanson, A. O., 70, 81, 82, 84, 88, 250, 255–257, 263, 376, 377, 391, 395
Hansson, E., 174
Hardy, D. R., 267, 268, 270, 272–274, 291, 338–340, 368
Harnwell, G. P., 1, 58
Harris, J. N., 317, 325
Hartmann, C. A., 382, 396
Hawley, W. G., 151, 292, 323, 325, 353, 369
Haxby, R. O., 78, 80, 88, 243, 255, 262
Haynes, J. R., 179, 210
Henderson, J. E., 246, 262
Henderson, J. T., 174
Henderson, S. T., 370
Hendricks, A. B., 138, 150, 262
Hendry, N., 366, 370
Henkel, R. L., 83–85, 88
Henley, J. A., 347, 351, 368
Herb, R. G., 48, 50–52, 59, 84, 88, 257, 262, 263
Herbert, L., 202, 210, 392, 393, 395
Hercock, R. J., 366–368, 370
Hergenrother, R. C., 352, 370
Hewlett, W. R., 369
Heydenburg, N. P., 77, 78, 88, 254, 263, 376, 395
Heyn, F. A., 33, 37, 58, 59
Hickman, K. W., 60–65, 67, 87
Higham, J. B., 147–149, 151, 324, 325
Hippel, A. von, 292
Hirsch, H., 253, 263
Hobson, J. E., 260
Hochhäusler, P., 109, 110
Höhl, H., 317, 319, 325
Hollmann, H. E., 356, 357, 369
Holtham, A. E. J., 210
Holzer, R. E., 244, 262
Holzer, W., 234–236, 262
Hooker, O. N., 202, 210
Hoover, W. G., 346, 368
Hopkinson, R. G., 368, 370
Hörcher, W., 225, 228, 261, 376, 395
Hornyak, W. F., 263
Horst, E., 291, 387, 395
Hotaling, G., 58, 110
Howard, P. R., 321, 324, 325
Howell, A. H., 291
Hubbard, H. S., 18, 19, 21, 58, 138, 150, 262
Hudson, C. M., 51, 59
Hueter, E., 218, 219, 229, 231, 260, 261
Huggins, L. C., 292
Hunt, F. V., 60–65, 67, 87
Hunt, S. E., 259, 263
Husbands, A. S., 114–117, 131, 133, 140–144, 147-151
Hussain, S. A., 261
Huus, T., 82, 83, 88

Imhof, A., 260, 262, 391–393, 395
Innes, G. S., 8, 21, 24. 58, 110

Jacob, L., 251–253, 263
Jacobi, W., 261
Jacottet, P., 292
Jasberg, J. H., 369
Jennings, B., 47, 48, 59, 79, 86, 88, 250, 257–259, 263
Johnson, R. H., 205, 206, 210
Johnson, T. H., 63, 64, 87
Jones, H. F., 396
Jones, W., 257, 263
Jørgenson, M. O., 229, 261, 291, 292

Kappeler, H., 387, 395
Karsten, O., 173
Katz, H., 354, 369
Kaye, W., 210
Kehse, W., 89, 110
Keinath, G., 262
Kelley, G. G., 354, 369
Kelvin, Lord, 211, 260
Kemppainen, O., 150
Kerkhof, F., 15–17, 58
Kerst, D. W., 50, 59, 110, 389, 395
Kesavamurthy, N., 261

King, R. W., 63, 87
Kirkpatrick, P., 243–246, 262
Klemm, A., 261
Klemperer, H., 354, 356, 368, 369
Knight, H. de B., 202, 204, 210, 392, 393, 395
Knoll, M., 369
Koch, J., 33, 58
Kohler, H. W., 63, 87
Kohlrausch, F., 306, 325
König, H., 262
Kossell, W., 44, 59
Kroemer, H., 292
Krutzsch, J., 315, 317, 325
Küchler, R., 91, 110, 262
Kuehni, H. P., 150, 166, 174, 346, 354, 368, 369
Kuhn, J., 77, 88
Kuntke, A., 21, 30–33, 58, 261, 324, 395

Lampson, C. W., 88
Lauritsen, T., 33, 58, 263
Lebacqz, J. V., 175, 179, 210, 236, 262, 284, 291
Lee, E. S., 292
Lee, G. M., 356–358, 360, 365, 369
Legg, J. W., 292
Lewis, A. B., 150, 261
Lewis, W. W., 174, 292, 396
Liebmann, G., 77, 88
Liechti, A., 137, 315–317, 325
Lindenhovius, H. J., 65–67, 74, 87
Lippert, G. D., 174
Livingood, J. J., 1, 58
Llewellyn Jones, F., 76, 88, 280, 281, 291
Loeb, L. B., 53, 59, 261
Ludlow, J. H., 210
Ludwig, L. R., 396
Lusignan, J. T., 151

McAuley, P. H., 150, 237, 261, 262, 281, 291, 292
McCann, G. D., 166, 167, 174
MacCarthy, D. D., 354, 369
MacLusky, G. J. R., 361
McCormick, N. R., 168–173, 190–192, 210
McEachron, K. B., 152, 154, 173, 292, 396
McEwan, D. H., 110, 395
McGillewie, K. I., 331, 332, 368
MacGregor-Morris, J. T., 347, 351, 368
Mackay, D. M., 362–364, 369
McKenzie, D. B., 139, 150
McKibben, J. L., 52, 53, 86, 88, 268
McMillan, F. O., 261, 281, 291
MacNeice, G. G., 222, 260
McQueen, J. G., 355, 370
Magnusson, C. E., 292
Malpica, J. M., 58, 59, 260
Malsch, F., 369
Mandeville, C. E., 87, 88, 263
Marchal, G., 290
Marchal, Y., 291
Marguerre, W., 151
Marhoefer, C. J., 257, 263
Marshall, F. R., 210
Martin, O., 292
Marton, L., 75, 88
Marx, E., 33, 112, 114–116, 150, 189
Maschkilleison, L. E., 150
Mathews, P., 262
Mautner, R. S., 14, 58
Meador, J. R., 247, 261, 263, 281, 291
Meek, J. M., 17, 58, 147, 151, 178–184, 186, 187, 193–196, 210, 221, 229, 260–262, 265, 267, 271, 272, 275–278, 281–283, 290, 291, 324, 325, 395
Mehlhorn, H., 395
Melville, W. S., 177, 203, 207, 209, 210
Melvin, H. L., 396
Menon, K. B., 261
Merrill, F. H., 43, 59, 292
Messner, M., 250, 251, 263, 319, 325, 352, 369
Metraux, A., 150
Miller, J. L., 320, 325, 347–349, 351, 352, 368
Miner, D. F., 150
Mines, R., 368
Mitchell, R. G., 1–7, 9, 25–28, 58
Miyake, I., 243, 244, 262
Moffatt, J., 58
Monahan, T. F., 396
Monteith, A. C., 396
Moody, N. F., 355, 361, 369
Morand, M., 37, 55, 59
Moreau-Hanot, M., 53–55, 59
Morel, R., 55, 59
Morgan, C. G., 291
Morgan, J. D., 291
Morrison, P., 263
Mortlock, J. R., 262
Mouzon, J. C., 63, 87
Mulhern, M. J., 389, 395
Müller-Hillebrand, D., 180, 210
Mulvey, T., 75, 88
Murphy, B., 341, 354, 368
Myers, F. E., 257, 263

Nacken, M., 216, 217, 260
Nakamura, T., 364, 369
Needham, W., 396
Nethercot, W., 326, 331, 333, 334, 341–346, 366, 368–370
Newman, M., 150, 290, 292
Nieuwdorp, H., 74, 88
Noe, J. D., 369
Nord, G. L., 261, 266, 291
Norinder, H., 173, 300, 325
Norris, E. T., 90, 91, 110
Northrup, D. L., 262
Nuttall, A. K., 319, 325, 352, 369

Oliphant, M. L. E., 33
Onslow, D. V., 59
Oosterkamp, W. J., 33, 58
Owaki, K., 363–365, 369

Paasche, P., 151
Page, R. S., 10, 58, 369
Palm, A., 219, 224, 260–262, 299, 306, 325, 385, 386, 395
Park, J. H., 156–161, 164, 166, 167, 173, 354, 369
Parker, A. B., 76, 88
Parkinson, D. B., 50, 59, 80–83, 88, 243, 248, 262, 263
Pauthenier, M., 37, 53–55, 59
Pedersen, P. O., 292
Peek, F. W., 59, 150
Perrelle, E. T. de la, 291
Perry, F. R., 104, 105, 110, 114–117, 131, 133, 140–144, 150, 151, 174, 288, 292, 323, 325, 348, 353, 369
Peters, J. F., 292
Peterson, H. A., 396
Petree, B., 83–85, 88
Pierce, J. R., 364, 369
Pieri, C. di, 261
Planck, D. W. ver., 261
Planer, F. E., 385, 395
Planer, G. V., 385, 395
Pleasants, J. G., 292
Poole, J. B. le, 33, 58
Powell, J. L., 84, 88, 257, 263
Praetorius, G., 292
Preston, J. S., 324,
Prime, H. A., 149, 151, 210, 335–338, 340, 341, 368
Probst, G., 262
Provoost, P. G., 287, 292
Pugno Vanoni, E., 261
Puleston, R., 370

Quarrell, A. G., 88

Rabov, B., 151
Ramo, S., 260, 346, 354, 368, 369
Raske, W., 315, 317–320, 325

Raskin, A., 59
Ratsey, O. L., 188, 190, 210
Ravenhill, P., 336–338, 340, 341, 368
Rawcliffe, G. H., 150
Read, J., 320, 325
Rebhan, J., 151
Rengier, H., 262
Reynolds, P., 153, 154, 165, 166, 173
Riabov, B. M., 292
Richards, P. A., 370
Ridenour, L. N., 88
Rinia, H., 65–67, 74, 87
Ritz, H., 234–236, 262
Roaf, D., 58
Roberts, R. B., 377, 395
Robinson, B. C., 287, 292
Robinson, J. E. L., 320, 325, 347–349, 351, 352, 368
Rogowski, W., 219, 220, 222, 235, 260, 262, 291, 292, 319, 346, 349, 354, 368, 369
Rohats, N., 150, 151, 154, 173, 326, 327, 368
Rokkaku, H., 150
Roman, W. G., 173
Rorden, H. L., 151, 313, 325
Rose, J. E., 246, 262
Rudenberg, H. G., 352, 361, 362, 369, 370
Rudge, W. J., 396
Rumbaugh, L. H., 88, 263
Rutherglen, J. G., 76, 88
Ryder, E. J., 179, 210
Rymer, T. B., 293–296, 324

Safford, F. J., 43, 59, 249, 262
Sala, O., 88, 257, 263
Sanders, J. H., 58
Sands, M. L., 87
Saxe, R. F., 149, 151, 335, 336, 368
Schade, O. H., 1, 10, 12–17, 58
Schenkel, M., 21, 24, 58
Schering, H., 306, 325, 386, 395
Schmidt, K., 150
Schneeberger, E., 150
Schroeder, R., 260
Schumacher, G., 291
Schumann, W. O., 234, 262
Scoles, G. J., 117, 140, 141, 150, 327, 329–331, 368
Seitz, W., 291
Shallcross, P., 373, 395
Sharp, C. H., 297, 325
Shingu, Y., 150
Shire, E. S., 37, 59
Shoupp, W. E., 88, 257, 262, 263
Siezen, G. J., 15–17, 58
Sillars, R. W., 396
Silsbee, F. B., 158, 159, 173, 212, 213, 215, 241, 260, 317, 325
Slepian, J., 21, 59, 280, 291
Sloan, D. H., 101–104, 110
Smee, J. F., 40, 41, 43, 44, 46, 59, 91, 110, 232, 238–241, 261, 297, 300, 325, 395
Smith, C. H., 365, 369
Smith, S. T., 365, 369
Smuroff, A., 150
Snoddy, L. B., 151, 291
Snow, C., 215, 260
Snowdon, S. C., 88, 257, 263
Solomonov, N. M., 169–171, 173
Sorensen, R. W., 89, 90, 110, 219, 260
Sporn, P., 396
Sprague, C. S., 151, 233, 261, 291
Standring, W. G., 262, 296, 325
Starke, H., 260
Starr, E. C., 261, 281, 291
Stekolnikov, I. S., 148, 151, 154, 166, 173, 174, 347, 368
Stephens, W. E., 88, 262
Stephenson, J. D., 233, 262
Steubing, W., 222, 260
Stoerk, C., 235, 262
Strait, E. N., 88
Street, J. C., 63, 64, 87, 151, 274, 291
Strigel, R., 180, 210, 266, 290, 291, 309, 325
Sutton, R. W., 110

Talbot, R. V., 365, 369
Tamm, R., 349
Tangen, R., 82, 83, 88
Tate, J. T., 88, 263
Taylor, F. W., 90, 91, 110
Taylor, L. S., 371–373, 395
Taylor-Jones, E., 109, 110
Teague, W. L., 292
Ten Broeck, R. L., 241, 299, 325, 385, 387, 395
Terahata, S., 364, 369
Tesla, N., 101, 104–109
Thielen, H., 292
Thomas, H. A., 244, 262
Thomason, J. L., 125, 128, 130, 131, 150, 152, 154, 173
Thompson, W. G., 223, 224, 261
Thomson, G. P., 76, 88
Thonemann, P. C., 33, 58
Thornton, W. M., 223, 224, 261
Titterton, E. W., 345, 368
Toepler, M., 229, 261, 291
Townsend, J. S., 76
Trachmann, H., 151
Tropper, H., 311–315, 325
Trump, J. G., 37, 40–44, 49–51, 53, 55–57, 59, 243, 249, 262
Turner, C. M., 51, 59
Tuuk, J. H. van der, 387–389, 395
Tuve, M. A., 52, 77, 78, 88, 109, 110, 254, 263, 376, 395

Valeev, C., 174
Vallin, G. L., 138, 150, 262
Van Atta, C. M., 59, 246, 247, 262
Van Atta, L. C., 40, 44, 59, 246, 247, 257, 262, 263
Vance, A. W., 71–73, 88
Van de Graaff, R. J., 37, 39, 40–42, 44, 46, 48–51, 53, 55, 57, 59, 70, 78, 80–82, 84, 86, 87, 243, 245, 248–250, 253, 257, 262
Verhoeff, A., 74, 88
Viehmann, H., 251, 263
Vieweg, R., 306, 325
Villard, P., 260
Vogt, H. G., 44, 59
Vollrath, R. E., 54, 59

Wade, E. J., 354, 369
Waghorne, J. H., 292
Wagner, C. F., 166, 167, 174
Waldman, B., 257, 263
Wallraff, A., 291
Waldorf, S. K., 174
Walton, E. T. S., 20–24, 31–34, 58, 389, 390
Wanger, W., 292
Warren, R. E., 51, 59, 84, 88, 257, 263
Waters, M., 224, 261
Waterton, F. W., 45, 59, 69, 88, 221, 260, 374, 375, 377, 381, 382, 385, 395
Watt, B. E., 87, 88, 263
Webster, G. H., 174, 288, 292
Weicker, W., 225, 228, 261
Weller, C. T., 317, 325
Wellings, J. G., 262
Wells, W. H., 88, 262
Westendorf, E., 354, 369
Westendorp, W. F., 58, 94, 110
Westermann, E., 369
Whelpton, R. V., 210, 347–351, 353, 354, 369
White, E. L., 145, 146, 151, 326, 331–334, 368
White, H. J., 179, 210, 291
Whitehead, S., 225–227, 261
Wiedenbeck, M. L., 257, 263
Wilkinshaw, W., 210
Wilkinson, K. J. R., 187–190, 210, 327–329, 331, 368

Williams, F. C., 335, 368
Williams, J. H., 52, 81, 88, 253, 254, 263
Wilman, H., 88
Wilson, R. R., 291
Winand, L., 59
Wingen, H., 222, 260
Winkelbrandt, H., 260
Winz, E., 91, 110
Wirg, E., 262
Wisco, E., 396
Wolff, O., 356, 368, 369
Workman, E. J., 244, 262
Wright, K. H. R., 293–296, 324
Wyatt, J. G., 325
Wynn Williams, C. E., 274, 291

Zaduk, H., 174
Zalesky, A. M., 292
Zarem, A. M., 210
Zdralik, O., 222, 260

INDEX OF SUBJECTS

A.C. generators, 33.
A.C. potential dividers, *see* Potential dividers.
Artificial lines, 175, 176, 178, 179, 182, 183, 189, 190, 194, 195, 198.

Cables for impulse potential dividers, 300–306, 310, 311, 313–315, 320, 323.
Capacitance voltmeters, 237–241, 297–299, 383–387, (*see also* Generating voltmeters).
Capacitors, high-voltage, 237–241, 297–300, 306, 385–387.
Capacitors, non-inductive, 305, 385–387.
Cascade rectifier circuits, 8–10, 16, 18–37, 76, 391.
  theory of, 21–32.
Cathode emission in spark gaps, 265–283.
Cathode–ray oscillographs, high-speed, 326–370.
  continuously-evacuated, 346–354, 356–361.
  high-voltage sources, 10, 332, 338, 342, 343.
  high-voltage measurement with, 251, 319, 321, 323, 352.
  impulse voltage measurement with, 286, 287, 319, 321, 323, 352.
  micro-deflection, 356–361,
  milli–microsecond techniques, 354–365,
  multi-beam, 346, 356, 357,
  photography with, 334, 338, 341, 345, 346, 365–368,
  recurrent surge, 326–334,
  test oscillograms, 334, 337, 346, 353, 358, 366,
  time-base circuits, 326–329, 332, 334–341, 343–346, 348–353, 356, 358–361,
  time-scale expansion, 355,
  transit-time effects, 356–365,
  tripping circuits, 326–328, 334–341, 343–346, 348–353, 356, 358–361,
  using sealed-off tubes, 335–346, 354, 355,
  with impulse generators, 144–149, 154, 162, 166, 167,
  with special deflector systems, (travelling wave, etc.), 361-365,
  writing speeds, 326, 327, 329, 331, 334, 336–338, 341, 345, 346, 353, 354, 356, 357–360, 365.
Corona rectifiers, 390–391.
Corona shields, 20, 36, 38, 43, 371–373, 377, 392.

D.C. sources, *see* Cascade rectifier circuits, *and* Rectifier circuits.
Diverters, surge, 394, 395.
Dividers, potential, *see* Potential dividers.

Electron diffraction camera, 76.
Electronic voltmeters,
  electron and ion beam, 250–253, 255.
  u.h.f. cavity type, 257–259.
Electron microscope, high–voltage source, 10, 33, 68–70, 72, 74–75.
Electrostatic a.c. generators, 55–58
Electrostatic d.c. generators, using dust streams, etc., 37, 53–55.
  see also Van de Graaff generators.
Electrostatic voltmeters, 211–224.
  absolute, 211–216, 218,
  capacitance divider type, 222, 223,
  ellipsoid type, 223, 224,
  in compressed gas, 219, 220,
  in vacuo, 221, 222,
  miscellaneous types, 222, 224.

Gases, insulating, 42, 47–48, 50–52, 93, 96, 99, 101, 219, 220, 299, 300, 306, 385–387.
Geiger counter, high–voltage source, 67.
Generating voltmeters, 79, 81, 82, 241–250.
  calibration of, 242, 244–246,
  for pressure-tank Van de Graaff generators, 243, 245, 248–250,
  oil-immersed, 244.

Ignitrons, 203–205, 389.
Impulse current wave shapes, 152, 153.
Impulse generators,
  circuits, 112–117,
  general design, 131–133,
  high current, 152–173,
  recurrent surge, 326–334,
  spark gaps, irradiation of, 275–279,
  square pulse, *see* Square pulses, production of,
  stray capacitances in, 142–144, 155,
  theory of, 117–131, 152,
  tripping of, 140–141, 144–149, 154–156, 161, 168–173,
  typical types, 133–139, 153,
  voltage distribution in, 141–144.
Impulse ratios of spark gaps, 270, 274.
Impulses, high current, 152–173.
  generator circuit, 152,
  generators, tripping of, 154–156, 161, 168–173,
  magnetic links for measurement of, 166–168,
  shunts for, 154–166,
  typical generators for, 153–155.
Impulses, square, 175–210, *see also* Pulses.
Impulse voltages, measurement of, 264–290.
  by electronic voltmeters, 290,
  by klydonographs, 287–290,
  by oscillographic methods, 286, 287, *see also* Cathode-ray oscillographs
  by peak voltmeters, 290,
  by rod gaps, 283–286,

Impulse voltages, measurement of—*contd.*
by sphere gaps, 264–283, *see also* Sphere gaps.
wave shapes, 111–112, 118–131.
Inductances, high-voltage (r.f.), 12–14, 103, 104, 109.
Inductance voltmeters, 241.
Induction coils, 109.
Ionic wind voltmeters, 224.
Ion sources, 33.

Klydonographs, 287–290.

Lines, artificial, *see* Networks pulse-forming.

Magnetic links, 166–168.
Magnetic pulse generators, 207–209.
Metrosil, 324, 394.
Microsecond switch (Bellaschi's), 168, 169.

Negative ion d.c. high-voltage generator, 32.
Negative ions in corona rectifiers, 390, 391.
Networks, pulse-forming, 175–179, 182, 183, 185, 190–192, 194–196, 198, 206, 208, 209.
Nuclear resonances, etc., 79, 80, 87, 253–257.
tables of, 256, 260.

Oscillographs, cathode-ray, *see* Cathode-ray oscillographs.

Peak voltmeters, 297–299.
Photomultiplier tubes, stabilized high-voltage source for, 67
Potential dividers,
a.c. capacitive, 213, 214, 222, 223, 296–300, 317.
d.c., 293–296,
impulse, 300–324, 343,
capacitive, 300–306, 308, 317–319,
miscellaneous, 307–309, 315–316,
non-linear resistive, 324,
resistive, 300, 306, 309–315, 319–324,
stray impedances in, 297–298, 305–309, 315–317.
Pulsactors, 207–209.
Pulse forming networks, *see* Networks, pulse-forming.
Pulses,
high current, 152–173,
high voltage, 15–17,
square, 175–210, *see also* Impulses.
Pulse transformers, 177, 183, 195, 205, 206, 209.

Radioactive sources, 268–274.
Rectifier circuits,
h.f., 10–15,
l.f., 1–9, 69–70, 74,
pulse generators, 15, 16.
Rectifiers, corona, 390–391,
Rectifiers, mechanical, 391–393.
Rectifiers, metal, 35–37.
Rectifier valves,
continuously evacuated, 9, 10, 24, 34,
sealed-off, 33, 76, 387–389.
Resistances,
carbon and composition, 72, 78, 296, 322, 377–385,
non-inductive, 321,
liquid, 310, 320, 323,
protective, for spark gaps, 231,
very low, 154, 156–166,
wire-wound, 45, 69, 84, 86, 317, 321, 322, 371–377.
Resistance voltmeters, 237, 254, 296, 371–385.
Rod gaps,
for voltage measurement, a.c., 236–237,
tables, 237,
impulses, 283–286,
tables, 285.

Shunts, for high current impulses, 154–166.
Spark gaps, *see also* Sphere gaps,
impulse generator, 140–141, 154–156, 161, 169–173,
irradiation of, 144, 181
multi-electrode, 185, 187, 188, *see also* Spark gaps, three-electrode,
rotary, 177–179,
sealed-off, three electrode, 192–196,
in networks, 194–196,
two electrode, 196–202,
in networks, 198,
three-electrode, 141, 145–148, 161–162, 169–173, 179–190, 192–196, 348–352, 358–360.
triggering of, 180–181, 185, 188, 189, 193–195, 197–202, *see* Cathode ray oscillograph tripping circuits,
uniform field, 233–236.
Sphere gaps, for voltage measurement, *see also* Spark gaps.
d.c. and a.c., 224–233,
effect of humidity, 232,
effect of irradiation, 232, 233,
effect of temperature *etc.*, 231, 232,
geometrical effects, 226–229,
protective resistances for, 231,
tables, 225–231,
impulses, 264–283,
irradiation by discharges, 274–280,
irradiation by radioactive substances, 268–274,
irradiation by ultra-violet light, 266–268,
polarity effects, 281–283,
Square pulses, production of, 175–210, *see also* Pulses.
by chopping circuit, 190–192,
by hard valve circuits, 205–207,
by ignitron circuits, 203–205,
by magnetic circuits, 207–209,
thyratron circuits, 202, 203,
Stabilized high-voltage circuits, 67–87,
measurement of stability, 73–74,
theory of, 60–67.
Surge diverters, *see* Diverters, surge.
Surge protection, 392–395.

Tesla coils, 104–109.

Thyratrons, 202, 203,
in time-base circuits, 326–341, 359–361.
Toepler discontinuity, 229.
Transformers,
cascaded, 33, 89–93, 238, 239,
constant voltage, 76, 77,
h.f., 101–109,
l.f., 19, 20, 33, 89, 238, 239,
peaking, 188,
pulse, 177, 183, 195, 206, 209,
resonant, 93–101,
calibration of, 97–101,
standard voltage, 241,
surge voltage distribution in, 334,
Tesla type, 104–109.
Uniform field spark gaps, 233–236.
Ultra-violet light for spark gap irradiation, 266–268.

Valve rectifier circuits, *see* Rectifier circuits.
Van de Graaff generators,
basic mechanism, 37–39,
in compressed gas, 41, 42, 47–53,
in open air, 40–47, 52,
measurement of beam voltage, 70, 253–260,
stabilization of, 78–87, 257.
Voltmeters electrostatic, *see* Electrostatic voltmeters.

UNIVERSITY
LIBRARY
No 14,019.
Date 20.12.55.
SRINAGAR
ALLAMA IQBAL LIBRARY
14019